Collision and Collapse at the Africa–Arabia–Eurasia Subduction Zone

Edited by

D. J. J. van Hinsbergen, M. A. Edwards and R. Govers

Geological Society
Special Publication 311

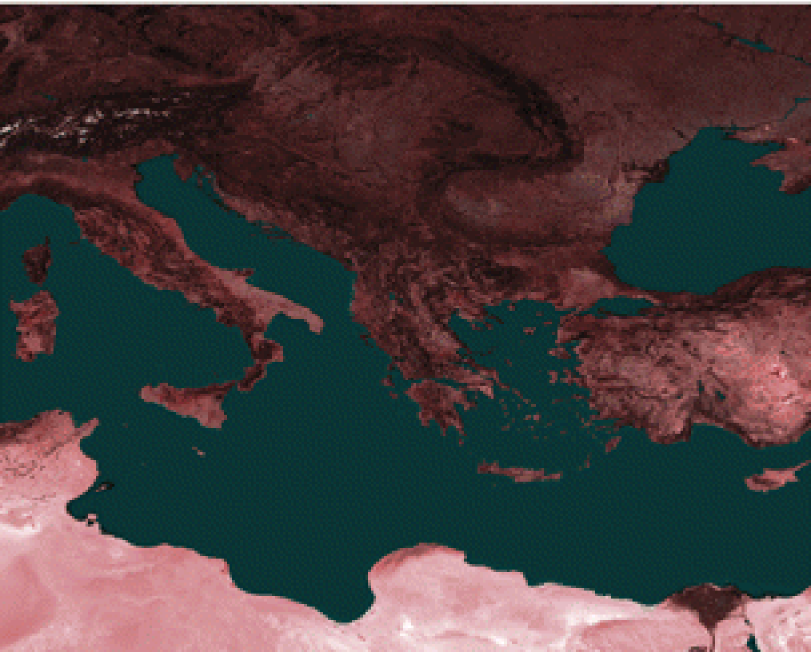

Contents

Collision and Collapse at the Africa–Arabia–Eurasia Subduction Zone

Geological Society books refereeing procedures

The Society makes every effort to ensure that the scientific and production quality of its books matches that of its journals. Since 1997, all book proposals have been refereed by specialist reviewers as well as by the Society's Books Editorial Committee. If the referees identify weaknesses in the proposal, these must be addressed before the proposal is accepted.

Once the book is accepted, the Society Book Editors ensure that the volume editors follow strict guidelines on refereeing and quality control. We insist that individual papers can only be accepted after satisfactory review by two independent referees. The questions on the review forms are similar to those for *Journal of the Geological Society*. The referees' forms and comments must be available to the Society's Book Editors on request.

Although many of the books result from meetings, the editors are expected to commission papers that were not presented at the meeting to ensure that the book provides a balanced coverage of the subject. Being accepted for presentation at the meeting does not guarantee inclusion in the book.

More information about submitting a proposal and producing a book for the Society can be found on its web site: www.geolsoc.org.uk.

It is recommended that reference to all or part of this book should be made in one of the following ways:

Van Hinsbergen, D. J. J., Edwards, M. A. & Govers, R. (eds) 2009. *Collision and Collapse at the Africa–Arabia–Eurasia Subduction Zone*. Geological Society, London, Special Publications, **311**.

Robertson, A. H. F., Parlak, O. & Ustaömer, T. 2009. Melange genesis and ophiolite emplacement related to subduction of the northern margin of the Tauride–Anatolide continent, central and western Turkey. *In*: Van Hinsbergen, D. J. J., Edwards, M. A. & Govers, R. (eds) *Collision and Collapse at the Africa–Arabia–Eurasia Subduction Zone*. Geological Society, London, Special Publications, **311**, 9–66.

GEOLOGICAL SOCIETY SPECIAL PUBLICATION NO. 311

Collision and Collapse at the Africa–Arabia–Eurasia Subduction Zone

EDITED BY

D. J. J. VAN HINSBERGEN
Utrecht University, The Netherlands

M. A. EDWARDS
University of Vienna, Austria

and

R. GOVERS
Utrecht University, The Netherlands

2009
Published by
The Geological Society
London

THE GEOLOGICAL SOCIETY

The Geological Society of London (GSL) was founded in 1807. It is the oldest national geological society in the world and the largest in Europe. It was incorporated under Royal Charter in 1825 and is Registered Charity 210161.

The Society is the UK national learned and professional society for geology with a worldwide Fellowship (FGS) of over 9000. The Society has the power to confer Chartered status on suitably qualified Fellows, and about 2000 of the Fellowship carry the title (CGeol). Chartered Geologists may also obtain the equivalent European title, European Geologist (EurGeol). One fifth of the Society's fellowship resides outside the UK. To find out more about the Society, log on to www.geolsoc.org.uk.

The Geological Society Publishing House (Bath, UK) produces the Society's international journals and books, and acts as European distributor for selected publications of the American Association of Petroleum Geologists (AAPG), the Indonesian Petroleum Association (IPA), the Geological Society of America (GSA), the Society for Sedimentary Geology (SEPM) and the Geologists' Association (GA). Joint marketing agreements ensure that GSL Fellows may purchase these societies' publications at a discount. The Society's online bookshop (accessible from www.geolsoc.org.uk) offers secure book purchasing with your credit or debit card.

To find out about joining the Society and benefiting from substantial discounts on publications of GSL and other societies worldwide, consult www.geolsoc.org.uk, or contact the Fellowship Department at: The Geological Society, Burlington House, Piccadilly, London W1J 0BG: Tel. +44 (0)20 7434 9944; Fax +44 (0)20 7439 8975; E-mail: enquiries@geolsoc.org.uk.

For information about the Society's meetings, consult *Events* on www.geolsoc.org.uk. To find out more about the Society's Corporate Affiliates Scheme, write to enquiries@geolsoc.org.uk.

Published by The Geological Society from:
The Geological Society Publishing House, Unit 7, Brassmill Enterprise Centre, Brassmill Lane, Bath BA1 3JN, UK

(*Orders*: Tel. +44 (0)1225 445046, Fax +44 (0)1225 442836)
Online bookshop: www.geolsoc.org.uk/bookshop

British Library Cataloguing in Publication Data

A catalogue record for this book is available from the British Library.
ISBN 978-1-86239-270-0

Typeset by Techset Composition Ltd., Salisbury, UK
Printed by MPG Books Ltd., Bodmin, UK

Distributors

North America
For trade and institutional orders:
The Geological Society, c/o AIDC, 82 Winter Sport Lane, Williston, VT 05495, USA
Orders: Tel. +1 800-972-9892
Fax +1 802-864-7626
E-mail: gsl.orders@aidcvt.com

For individual and corporate orders:
AAPG Bookstore, PO Box 979, Tulsa, OK 74101-0979, USA
Orders: Tel. +1 918-584-2555
Fax +1 918-560-2652
E-mail: bookstore@aapg.org
Website: http://bookstore.aapg.org

India
Affiliated East-West Press Private Ltd, Marketing Division, G-1/16 Ansari Road, Darya Ganj, New Delhi 110 002, India
Orders: Tel. +91 11 2327-9113/2326-4180
Fax +91 11 2326-0538
E-mail: affiliat@vsnl.com

The Mediterranean and northern Arabian regions provide a unique natural laboratory to constrain geodynamics associated with arc–continent and continent–continent collision and subsequent orogenic collapse by analysing regional and temporal distributions of the various elements in the geological archive. This book combines thirteen new contributions that highlight timing and distribution of the Cretaceous to Recent evolution of the Calabrian, Carpathian, Aegean and Anatolian segments of the Africa–Arabia–Eurasia subduction zone. These are subdivided into five papers documenting the timing and kinematics of Cretaceous arc–continent collision, and Eocene and Miocene continent–continent collision in Anatolia, with westward extrusion of Anatolia as a result. Eight papers provide an overview and new data from stratigraphy, structure, metamorphism and magmatism, covering the geological consequences of the largely Neogene collapse that characterizes the segments of interest, in response to late stage reorganization of the subduction zone, and the roll-back and break-off of (segments of) the subducting slab.

Geodynamics of collision and collapse at the Africa–Arabia–Eurasia subduction zone – an introduction

DOUWE J. J. VAN HINSBERGEN[1]*, MICHAEL A. EDWARDS[2] & ROB GOVERS[3]

[1]*Paleomagnetic Laboratory 'Fort Hoofddijk', Faculty of Geosciences, Utrecht University, Budapestlaan 17, 3584 CD Utrecht, The Netherlands*

[2]*Structural Processes Group, Department of Geological Sciences, University of Vienna, Althanstrasse 14, Vienna A-1090, Austria*

[3]*Tectonophysics Group, Faculty of Geosciences, Utrecht University, Budapestlaan 4, 3584 CD Utrecht, The Netherlands*

**Corresponding author (e-mail: hins@geo.uu.nl)*

Shortly after the recognition of plate-tectonics, Wilson (1966) proposed his now famous cycle describing the creation and demise of ocean basins. His original four stages still form the basis for plate-tectonic discussions today: (1) rifting of a continent; (2) continental drift, sea-floor spreading and formation of ocean basins; (3) subduction initiation and progressive closure of ocean basins by subduction of oceanic lithosphere; and (4) continent–continent collision and final closure of an ocean basin. The Mediterranean basin constitutes the westernmost extremity of the Tethyan domain (e.g. Stampfli & Borel 2002). Here, the last remains of this former oceanic basin have nearly disappeared, thus representing stage (4). This final closure phase is associated with rifting and drifting in the Western Mediterranean (Dercourt *et al.* 1986), and with initiation of the Tyrrhenian–Calabrian and Alboran subduction zones, i.e. all of Wilson's phases are occurring concurrently.

Imprints of previous Wilson stages are preserved in the geological record. Detailed geochemical and metamorphic-petrological study of ophiolites – on-land relics of oceanic crust in mountain belts – (Spadea & D'Antonio 2006; Barth *et al.* 2008), paleogeographic reconstructions (Hall & Spakman 2003), as well as numerical and analogue modeling experiments (Chemenda *et al.* 2001; Toth & Gurnis 1998) have revealed that initiation of oceanic subduction, as the first part of Wilson's phase 3, may start in various ways, e.g. by inversion of a mid-oceanic ridge or fracture zone, or subduction polarity reversal. The subsequent oceanic subduction stage closes the oceanic basin, eventually resulting in the arrival of a continental margin at the trench (Dewey & Bird 1970; Robertson *et al.* 2009). Small continental fragments may subduct entirely (van Hinsbergen *et al.* 2005; Gerya *et al.* 2002, De Franco *et al.* 2008). Subduction of substantially large quantities of continental lithosphere will inevitably lead to break-off of the subducted slab (Wortel & Spakman 2000), relocation of the trench, and possibly a reversal in subduction polarity (Chemenda *et al.* 2001; Kaymakci *et al.* 2009).

Wilson's phase 4 – continent–continent collision – eventually leads to the final arrest of plate convergence. The orogen that formed near the suture zone will be eroded and may experience gravitational orogenic collapse (Dewey 1988; Gautier *et al.* 1999) and the cycle may start again. However, the opposing continental margins are frequently not parallel and irregular, and continent–continent collision may start in one place, while remaining oceanic crust still present laterally along the active margin, forming land-locked oceanic basins (Le Pichon 1982). It is this situation that is presently characterizing the Africa–Arabia–Eurasia subduction zone(s). Whereas continent–continent collision between Arabia and Eurasia was already followed by break-off of the subducted Arabian slab in the Miocene (Keskin 2003; Faccenna *et al.* 2006; Hafkenscheid *et al.* 2006; Hüsing *et al.* 2009), the geodynamic situation in the land-locked oceanic basin of the Mediterranean region yielded is much more complicated. A decrease in convergence rate or a change in the plate motion direction may lead to readjustment in the orientation of the subducted slab with roll-back as a logical consequence (Malinverno & Ryan 1986; Carminati *et al.* 1998; Jolivet & Faccenna 2000; Faccenna *et al.* 2001*a*, *b*). In the Tyrrhenian, Carpathian and Aegean regions, roll-back, slab break-off and activity of Subduction Transform Edge Propagating faults (STEPs; Govers & Wortel 2005) occurred (Le Pichon *et al.* 1979; 1982; van der Meulen 1999; Wortel & Spakman 2000; Faccenna *et al.* 2001*a*; van de Zedde & Wortel

From: VAN HINSBERGEN, D. J. J., EDWARDS, M. A. & GOVERS, R. (eds) *Collision and Collapse at the Africa–Arabia–Eurasia Subduction Zone*. The Geological Society, London, Special Publications, **311**, 1–7.
DOI: 10.1144/SP311.1 0305-8719/09/$15.00

2001; Argnani 2009), as well as lateral extrusion processes, that translate Anatolia westward parallel to the subduction zone along major strike-slip faults, notably the North Anatolian Fault as a result of the Arabia–Eurasia collision (Dewey & Sengör 1979; Sengör *et al.* 1985, 2005; Hubert-Ferrari *et al.* 2002; 2009) These processes, which may be specific for land-locked basins (Edwards & Grasemann 2009) have led to, or were associated with, a complex mosaic of geological terranes, frequently with distinct geological histories of exhumation, deformation, rotation and sedimentation.

The present-day tectonic setting reveals that from east to west along the Africa–Arabia–Eurasia collision zone, a more or less gradual transition exists between two extremities: in the east, continent–continent collision is a fact between Arabia and Eurasia, and Anatolia is still being extruded eastward (McClusky *et al.* 2000; Reilinger *et al.* 2006), whereas in the west, roll-back of the subducted slab below the Tyrrhenian basin has led to oceanization in the backarc. The Aegean and western Anatolian regions form a mid-stage between these two extremes and experience continental extension associated with exhumation of metamorphic core complexes (Lister *et al.* 1984; Gautier *et al.* 1993; Gautier & Brun 1994; Bozkurt & Oberhänsli 2001; Gessner *et al.* 2001; Jolivet 2001; Ring & Reishmann 2002; Jolivet *et al.* 2003; Edwards & Grasemann 2009; Papanikolaou *et al.* 2009; Sen & Seyitoğlu 2009; Tirel *et al.* 2009; van Hinsbergen & Boekhout 2009) and migration and compositional evolution of the associated magmatic/volcanic response (Pe-Piper & Piper 2002; Dilek & Altunkaynak 2009). The exhumation during extension of the overriding plate associated with these retreating subduction zones provides a unique opportunity to study the subduction and exhumation processes within the subduction channel prior to the onset of wide-spread roll-back and stretching of the overriding plate. Jolivet *et al.* (2003) subdivided the exhumation processes of the Mediterranean metamorphic belts into two stages: the syn-orogenic extension phase, in which slices of HP/LT metamorphic rocks travel upward along the subducting slab, either by buoyancy-driven upward flow, or by tectonic extrusion (see e.g. Ring *et al.* 2007), a subject further studied by Vignaroli *et al.* (2009) and the post-orogenic extension phase, which is related to stretching of the lithosphere and exhumation of metamorphic core complexes (see also Tirel *et al.* 2009) upon roll-back or collapse.

To determine the causes and consequences of collision, extrusion and collapse at the Africa–Arabia–Eurasia subduction zone, it is most essential to place all geological elements and processes in time. The contributions in this volume provide essential new time constraints, and further constrain and define the fundamental, and regional processes related to collision and collapse in the Mediterranean and northern Arabian regions.

Research themes

We subdivide this volume into two main parts: collision and collapse. The contributions in these parts (Fig. 1) span a wide range of techniques and processes, and cover a time span from the Cretaceous to the Present, but all contribute to the further detailed understanding and identification of stages 3 and 4 in Wilson's cycle.

Collision

Four papers in this volume provide essential new data that constrain the temporal and spatial evolution of arc–continent and continent–continent collision processes from the Cretaceous to the Present in the Arabia–Anatolia segment of the subduction zone.

Robertson *et al.* document the earliest collision phase in the Anatolian collage, represented by arc–continent collision between the Anatolide–Tauride block and supra-subduction zone ophiolites and volcanic arc-related rocks of the northern part of the Neotethyan ocean, following intra-oceanic subduction. Arc–continent collision in Turkey occurred in the late Cretaceous, with widespread ophiolite emplacement and high-pressure metamorphism. Following this phase of arc–continent collision, the authors suggest that the trench migrated northward, with final continent–continent collision between the Taurides (and overlying ophiolites) and the Eurasia-related Pontides in the Paleocene–Eocene.

Kaymakci *et al.* studied the late Cretaceous to Neogene history of the Çankırı Basin, which nicely documented the post-arc continent collision history described by Robertson *et al.* The authors show that the Çankırı Basin, located on the southern part of the Pontides and straddling the northern part of the Taurides in the Paleogene part of its stratigraphy, has a history that can be subdivided in a late Cretaceous to Paleogene forearc basin stage, and a Paleocene–Eocene foreland basin history. The conclusion of these authors is in line with the conclusions of Robertson *et al.* and shows that arc–continent collision between the Anatolide–Tauride block and the Pontides was followed by relocation of the subduction thrust to the southern margin of the Pontides, leading in the late Paleocene to early Eocene to continent–continent collision between Taurides and Pontides.

Hüsing *et al.* focused their paper on the final continent–continent collision phase that characterizes the Africa–Arabia–Eurasia collision zone, concerning the collision of Arabia with the Anatolide–Tauride block, upon demise of the southern branch of the Neotethys (which is still represented by the eastern Mediterranean basin and for example, the Troodos ophiolite on Cyprus). They studied the foreland basin evolution on northern Arabia and around the Bitlis–Pötürge massif, and found that the youngest foreland basin deposits on Arabia below the southernmost thrust of the Bitlis–Pötürge massif has an age of 11 Ma. They interpret this as the end of regular subduction of the Arabian plate, coinciding with slab break-off and the onset of northward penetration of the Arabian continent into Anatolia, leading to its extrusion, in line with earlier suggestions of Keskin (2003), Sengör *et al.* (2003) and Faccenna *et al.* (2006).

Hubert-Ferrari *et al.* provide essential new $^{40}Ar/^{39}Ar$ age constraints on an offset volcano crosscut by the North Anatolian Fault Zone, and show that the majority of motion along the fault zone occurred after *c.* 2.5 Ma, with a slip rate of approximately 20 mm/a. They argue that the first phase of deformation, which established the present-day 1300 km long fault trace following the onset of its activity around 12–10 Ma ago (in line with the conclusions of Hüsing *et al.*), was associated with a much smaller slip rate of 3 mm/a.

Collapse

Nine papers provide a detailed insight in the geodynamic evolution and the tectonic responses of the Anatolian, Aegean, Carpathian and Tyrrhenian segments of the subduction zone.

Edwards & Grasemann review the geophysical and geological data concerning the evolution of the subducted Tyrrhenian, Carpathian and Aegean slabs and their Neogene history of roll-back. They conclude that upon decrease of the width of a slab as a result of its progressive decoupling, the slab retreat velocity increases and the tectonic response in the overriding plate in terms of extension and exhumation intensify. Their paper provides a new overview of the present-day state of the art of the evolution of the Mediterranean land-locked basin since the Neogene.

Argnani connects the final demise of the Calabrian slab to surface manifestations of these deeper processes in the southern central Mediterranean. He identifies periods of slab break-off and STEP fault activity (Govers & Wortel 2005) that are modulated by the older structural grain in the subducting African lithosphere.

Dilek & Altunkaynak review the post-collisional magmatic response in western Anatolia and propose an elegant scenario placing the migration and compositional variation in post-Eocene magmatism in a timely geodynamic and tectonic scenario. They show that through time since the Eocene, just after continent–continent collision between the Taurides and Pontides (see Robertson *et al.* and Kaymakci *et al.*) volcanism and magmatism in western Turkey has migrated southward, with changing compositions. They suggest that volcanism was initially caused by slab break-off after continent–continent collision, followed by southward migrating volcanism associated with asthenospheric flow due to lithospheric delamination. Middle Miocene volcanism is proposed to result to a large extent from lithospheric extension and formation of the Menderes metamorphic core complex. Finally, Quarternary alkaline volcanism near Kula in central western Anatolia is explained as the result of uncontaminated mantle, which flowed in beneath the attenuated continental lithosphere in the Aegean extensional province.

Vignaroli *et al.* integrate structural, metamorphic and geochronological data into their reconstruction of the Apennine belt of the Central Mediterranean. Tying the plate-tectonic evolution of the region to the geological observations, they track the evolution from oceanic subduction to collision. Principal constraints involve stages when HP rocks were exhumed, followed by continental collision that the authors infer to have occurred simultaneously with orogenic extension in the backarc. Their geodynamic scenario involves a principal role for slab rollback and mantle delamination processes.

Tirel *et al.* provide a new numerical model for the evolution of sequential development of metamorphic core complexes, and a thorough review of the Cycladic metamorphic core complexes as a test case. They conclude that provided the original lithosphere is thick and very hot, a sequence of metamorphic core complexes may develop. The core complexes are characterized by a two-stage development: first a symmetric stage, with graben development at the surface and lower crustal flow in the attenuating crust, followed by an asymmetric stage where one of the graben-bounding faults links up with the opposite lower-crustal flow accommodating shear zone to form an extensional detachment. If, upon cooling of the exhumed metamorphic dome, the crust is still hot and thick enough then a second (or even third) dome may form above the remaining shear zone that accommodated lower crustal flow in the first dome. This scenario is successfully tested in the Cyclades, where such paired belts are formed by e.g. Naxos and Ios, and Syros and Tinos. Tirel *et al.* postulate that the timing of

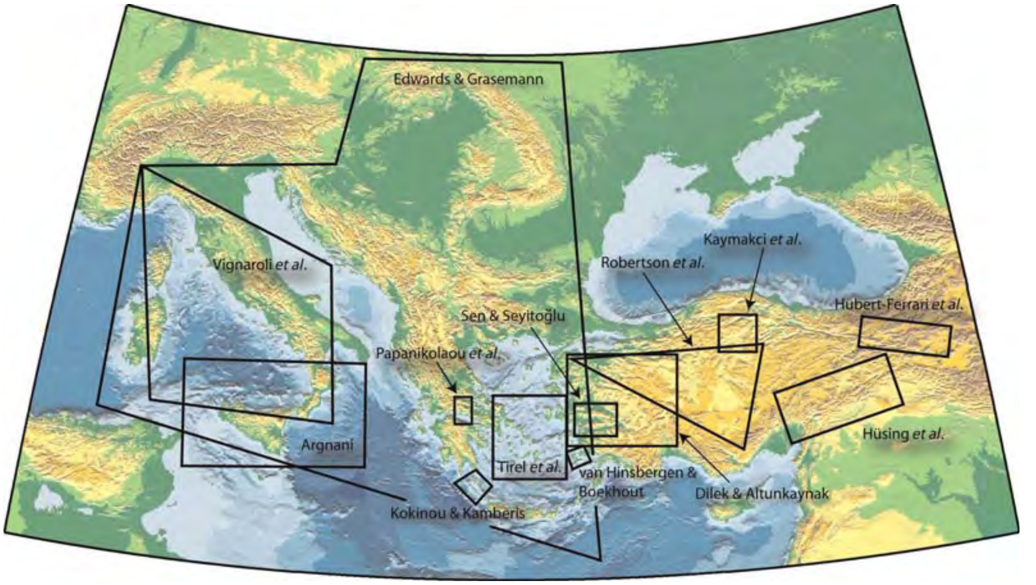

Fig. 1. Topographic and bathymetric map of the Africa–Arabia–Eurasia collision zone, with outlines of the study areas of the papers in this volume.

onset of extension that leads to the formation of a core complex can be approximated by the age of the onset of supra-detachment basin sedimentation.

Papanikolaou *et al.* document the structure of the Itea–Amfissa detachment and the stratigraphy of the lower-upper Miocene supra-detachment basin associated with its activity. They show that this detachment is older than the Gulf of Corinth, and belongs to the East Peloponnesos detachment, which exhumed HP/LT metamorphic rocks. This paper provides essential new age constraints on this detachment fault zone, which, on the Peloponnesos, lacks a well-defined supra-detachment basin stratigraphy. Their new results help to further define the extensional and exhumational history of the external Hellenides and Crete in the Miocene.

van Hinsbergen & Boekhout test a recently postulated scenario for the exhumation of the Menderes core complex. Contrary to the numerical simulations of Tirel *et al.* the Menderes core complex seems to lack an overall asymmetry, and appears to have been exhumed in two symmetric dome stages (e.g. Gessner *et al.* 2001). Recently, Seyitoğlu *et al.* (2004) postulated a southern break-away fault of the Menderes core complex, located in the Lycian nappes, with an Oligocene to early Miocene age. van Hinsbergen & Boekhout tested this postulation on the island of Kos, very close to the postulated break-away fault, and found indeed evidence for an extensional detachment related to the Aegean and Menderes extensional province, but with a much younger age (younger than 12 Ma), and no evidence for pre-12 Ma exhumation as postulated by Seyitoğlu *et al.* (2004). Hence, they conclude that the symmetric bivergent rolling-hinge model of Gessner *et al.* (2001) is a more likely scenario.

Sen & Seyitoğlu provide essential new age constraints on supra-detachment basin evolution associated with the activity of the Alaşehir and Büyük Menderes detachments, that exhumed the second dome-stage of the Menderes core complex. They magnetostratigraphically dated the deposits in these supra-detachment basins, and show an age ranging from 16.6–14.6 Ma, and 16.0–14.9 Ma for the Alaşehir and Büyük Menders supra-detachment basin stratigraphies, respectively. Following the conclusion of Tirel *et al.* this date may coincide with the onset of formation of the second dome of the Menderes, which is in line with this date coinciding with the final cooling of the first dome constrained by fission track analysis (Gessner *et al.* 2001).

Kokinou & Kamberis finally, provide five new seismic profiles of the complex and submerged Kythira Straits, a submerged segment of the external Hellenides between the island of Kythira and Crete. These new data document the complex interactions between arc-normal compression and extension, and arc-parallel extension during the late Neogene outward migration of the Hellenic arc and shed new light on the neotectonic history of the Hellenides.

The contributions of DJJvH and RG were produced within the context of the Netherlands Research School of Integrated Solid Earth Sciences (ISES). DJJvH acknowledges an NWO-VENI grant.

References

Argnani, A. 2009. Evolution of the southem Tyrrhenian slab tear and active tectonics along the western edge of the Tyrrhenian subducted slab. *In*: van Hinsbergen, D. J. J., Edwards, M. A. & Govers, R. (eds) *Collision and Collapse at the Africa–Arabia–Eurasia Subduction Zone*. Geological Society, London, Special Publications, **311**, 193–212.

Barth, M. G., Mason, P. R. D., Davies, G. R. & Drury, M. R. 2008. The Othris Ophiolite, Greece: A snapshot of subduction initiation at a mid-ocean ridge. *Lithos*, **100**, 234–254.

Bozkurt, E. & Oberhänsli, R. 2001. Menderes Massif (Western Turkey): structural, metamorphic and magmatic evolution – a synthesis. *International Journal of Earth Sciences*, **89**, 679–708.

Carminati, E., Wortel, M. J. R., Meijer, P. T. & Sabadini, R. 1998. The two-stage opening of the western-central Mediterranean basins: a forward modeling test to a new evolutionary model. *Earth and Planetary Science Letters*, **160**, 667–679.

Chemenda, A. I., Hurpin, D., Tang, J.-C., Stephan, J.-F. & Buffet, G. 2001. Impact of arc-continent collision on the conditions of burial and exhumation of UHP/LT rocks: experimental and numerical modelling. *Tectonophysics*, **342**, 137–161.

De Franco, R., Govers, R. & Wortel, M. J. R. 2008. Dynamics of continental collision: Influence of the plate contact. *Geophysical Journal International*, **174**, 1101–1120.

Dercourt, J., Zonenshain, L. P. & Ricou, L.-E. 1986. Geological evolution of the Tethys belt from the Atlantic to the Pamir since the Lias. *Tectonophysics*, **123**, 241–315.

Dewey, J. F. 1988. Extensional Collapse of orogens. *Tectonics*, **7**, 1123–1139.

Dewey, J. F. & Bird, J. M. 1970. Mountain belts and the new global tectonics. *Journal of Geophysical Research*, **75**, 2625–2647.

Dewey, J. F. & Sengör, A. M. C. 1979. Aegean and surrounding regions: Complex multiplate and continuum tectonics in a convergent zone. *Geological Society of America Bulletin*, **90**, 84–92.

Dilek, Y. & Altunkaynak, Ş. 2009. Geochemical and temporal evolution of Cenozoic magmatism in western Turkey: mantle response to collision, slab break-off, and lithospheric tearing in an orogenic belt. *In*: van Hinsbergen, D. J. J., Edwards, M. A. & Govers, R. (eds) *Collision and Collapse at the Africa–Arabia–Eurasia Subduction Zone*. Geological Society, London, Special Publications, **311**, 213–233.

Edwards, M. A. & Grasemann, B. 2009. Mediterranean snapshots of accelerated slab retreat: subduction instability in stalled continental collision. *In*: van Hinsbergen, D. J. J., Edwards, M. A. & Govers, R. (eds) *Collision and Collapse at the Africa–Arabia–Eurasia Subduction Zone*. Geological Society, London, Special Publications, **311**, 155–192.

Faccenna, C., Becker, T. W., Pio Lucente, F., Jolivet, L. & Rossetti, F. 2001*a*. History of subduction and back-arc extension in the Central Mediterranean. *Geophysical Journal International*, **145**, 809–820.

Faccenna, C., Funiciello, F., Giardini, D. & Lucente, P. 2001*b*. Episodic back-arc extension during restricted mantle convection in the Central Mediterranean. *Earth and Planetary Science Letters*, **187**, 105–116.

Faccenna, C., Bellier, O., Martinod, J., Piromallo, C. & Regard, V. 2006. Slab detachment beneath eastern Anatolia: A possible cause for the formation of the North Anatolian Fault. *Earth and Planetary Science Letters*, **242**, 85–97.

Gautier, P. & Brun, J.-P. 1994. Ductile crust exhumation and extensional detachments in the central Aegean (Cyclades and Evvia Islands). *Geodinamica Acta*, **7**, 57–85.

Gautier, P., Brun, J.-P. & Jolivet, L. 1993. Structure and kinematics of Upper Cenozoic extensional detachment on Naxos and Paros. *Tectonics*, **12**, 1180–1194.

Gautier, P., Brun, J.-P., Moriceau, R., Sokoutis, D., Martinod, J. & Jolivet, L. 1999. Timing, kinematics and cause of Aegean extension: a scenario based on a comparison with simple analogue experiments. *Tectonophysics*, **315**, 31–72.

Gerya, T. V., Stockhert, B. & Perchuck, A. L. 2002. Exhumation of high-pressure metamorphic rocks in a subduction channel: a numerical simulation, *Tectonics*, **21**(6), 227–236.

Gessner, K., Ring, U., Johnson, C., Hetzel, R., Passchier, C. W. & Güngör, T. 2001. An active bivergent rolling-hinge detachment system: Central Menderes metamorphic core complex in western Turkey. *Geology*, **29**, 611–614.

Govers, R. & Wortel, M. J. R. 2005. Lithosphere tearing at STEP faults: Response to edges of subduction zones. *Earth and Planetary Science Letters*, **236**, 505–523.

Hafkenscheid, E., Wortel, M. J. R. & Spakman, W. 2006. Subduction history of the Tethyan region derived from seismic tomography and tectonic reconstructions. *Journal of Geophysical Research*, **111**, B08401, doi: 10.1029/2005JB003791.

Hall, R. & Spakman, W. 2003. Defining Australia: The Australian Plate as part of Planet Earth. *In*: Hillis, R. & Müller, R. D. (eds) *Geological Society of Australia Special Publication*, **22**, 355–375.

Hüsing, S. K., van Zachariasse, W.-J., van Hinsbergen, D. J. J., Krijgsman, W., Inceöz, M., Harzhauser, M., Mandic, O. & Kroh, A. 2009. Oligocene–Miocene basin evolution in SE Anatolia, Turkey: constraints on the closure of the eastern Tethys gateway. *In*: van Hinsbergen, D. J. J., Edwards, M. A. & Govers, R. (eds) *Collision and Collapse at the Africa–Arabia–Eurasia Subduction Zone*. Geological Society, London, Special Publications, **311**, 107–132.

Hubert-Ferrari, A., Armijo, R., King, G., Meyer, B. & Barka, A. 2002. Morphology, displacement, and slip rates along the North Anatolian Fault, Turkey.

Journal of Geophysical Research, **107**, 2235, doi; 10.1029/2001JB000393.

HUBERT-FERRARI, A., KING, G., VAN DER WOERD, J., VILLA, I., ALTUNEL, E. & ARMIJO, R. 2009. Long-term evolution of the North Anatolian Fault: new constraints from its eastern termination. *In*: VAN HINSBERGEN, D. J. J., EDWARDS, M. A. & GOVERS, R. (eds) *Collision and Collapse at the Africa–Arabia–Eurasia Subduction Zone*. Geological Society, London, Special Publication, **311**, 133–154.

JOLIVET, L. 2001. A comparison of geodetic and finite strain pattern in the Aegean, geodynamic implications. *Earth and Planetary Science Letters*, **187**, 95–104.

JOLIVET, L. & FACCENNA, C. 2000. Mediterranean extension and the Africa–Eurasia collision. *Tectonics*, **19**, 1094–1106.

JOLIVET, L., FACENNA, C., GOFFÉ, B., BUROV, E. & AGARD, P. 2003. Subduction tectonics and exhumation of high-pressure metamorphic rocks in the Mediterranean orogen. *American Journal of Science*, **303**, 353–409.

KAYMAKCI, N., ÖZÇELIK, Y., WHITE, S. H. & VAN DIJK, P. M. 2009. Tectono-stratigraphy of the Çankırı Basin: Late Cretaceous to early Miocene evolution of the Neotethyan Suture Zone in Turkey. *In*: VAN HINSBERGEN, D. J. J., EDWARDS, M. A. & GOVERS, R. (eds) *Collision and Collapse at the Africa–Arabia–Eurasia Subduction Zone*. Geological Society, London, Special Publications, **311**, 67–106.

KESKIN, M. 2003. Magma generation by slab steepening and breakoff beneath a subduction-accretion complex: An alternative model for collision-related volcanism in Eastern Anatolia, Turkey. *Geophysical Research Letters*, **30**, 8046, doi: 10.1029/2003GL018019.

KOKINOU, E. & KAMBERIS, E. 2009. The structure of the Kythira–Antikythira strait, offshore SW Greece (35.7°–36.6°N). *In*: VAN HINSBERGEN, D. J. J., EDWARDS, M. A. & GOVERS, R. (eds) *Collision and Collapse at the Africa–Arabia–Eurasia Subduction Zone*. Geological Society, London, Special Publications, **311**, 343–360.

LE PICHON, X. 1982. Land-locked oceanic basins and continental collision: the Eastern Mediterranean as a case example. *In*: HSÜ, K. J. (ed.) *Mountain Building Processes*. London, Academic Press, 201–211.

LE PICHON, X., ANGELIER, J., AUBOUIN, J., LYBERIS, N., MONTI, S., RENARD, V. *ET AL.* 1979. From subduction to transform motion: a seabeam survey of the Hellenic trench system. *Earth and Planetary Science Letters*, **44**, 441–450.

LE PICHON, X., ANGELIER, J. & SIBUET, J.-C. 1982. Plate boundaries and extensional tectonics. *Tectonophysics*, **81**, 239–256.

LISTER, G., BANGA, G. & FEENSTRA, A. 1984. Metamorphic core complexes of Cordilleran type in the Cyclades. Aegean Sea, Greece. *Geology*, **12**, 221–225.

MALINVERNO, A. & RYAN, W. B. F. 1986. Extension in the Tyrrhenian Sea and shortening in the Apennines as result of arc migration driven by sinking of the lithosphere. *Tectonics*, **5**, 227–245.

MCCLUSKY, S., BALASSANIAN, S., BARKA, A., DEMIR, C., ERGINTAV, S., GEORGIEV, I. *ET AL.* 2000. Global Positioning System constraints on plate kinematics and dynamics in the eastern Mediterranean and Caucasus. *Journal of Geophysical Research*, **105**, 5695–5719.

PAPANIKOLAOU, D., GOULIOTIS, L. & TRIANTAPHYLLOU, M. 2009. The Itea–Amfissa detachment: a pre-Corinth rift Miocene extensional structure in central Greece. *In*: VAN HINSBERGEN, D. J. J., EDWARDS, M. A. & GOVERS, R. (eds) *Collision and Collapse at the Africa–Arabia–Eurasia Subduction Zone*. Geological Society, London, Special Publications, **311**, 293–310.

PE-PIPER, G. & PIPER, D. J. W. 2002. *The igneous rocks of Greece. The anatomy of an orogen*. Berlin-Stuttgart, Gebrüder Borntraeger.

REILINGER, R., MCCLUSKY, S., VERNANT, P., LAWRENCE, S., ERGINTAV, S., CAKMAK, R. *ET AL.* 2006. GPS constraints on continental deformation in the Africa–Arabia–Eurasia continental collision zone and implications for the dynamics of plate interactions. *Journal of Geophysical Research*, **111**, V05411, doi:10.1029/2005JB004051.

RING, U. & REISHMANN, T. 2002. The weak and superfast Cretan detachment, Greece: exhumation at subduction rates in extruding wedges. *Journal of the Geological Society of London*, **159**, 225–228.

RING, U., WILL, T., GLODNY, J., KUMERICS, C., GESSNER, K., THOMSON, S. N. *ET AL.* 2007. Early exhumation of high-pressure rocks in extrusion wedges: The Cycladic blueschist unit in the eastern Aegean, Greece and Turkey. *Tectonics*, **26**, TC2001, doi:10.1029/2005TC001872.

ROBERTSON, A. H. F., PARLAK, O. & USTAÖMER, T. 2009. Melange genesis and ophiolite emplacement related to subduction of the northern margin of the Tauride–Anatolide continent, central and western Turkey. *In*: VAN HINSBERGEN, D. J. J., EDWARDS, M. A. & GOVERS, R. (eds) *Collision and Collapse at the Africa–Arabia–Eurasia Subduction Zone*. Geological Society, London, Special Publications, **311**, 9–66.

SEN, S. & SEYITOĞLU, G. 2009. Magnetostratigraphy of early–middle Miocene deposits from east–west trending Alaşehir and Büyük Menderes grabens in western Turkey, and its tectonic implications. *In*: VAN HINSBERGEN, D. J. J., EDWARDS, M. A. & GOVERS, R. (eds) *Collision and Collapse at the Africa–Arabia–Eurasia Subduction Zone*. Geological Society, London, Special Publications, **311**, 321–342.

SENGÖR, A. M. C., GÖRÜR, N. & SAROGLU, F. 1985. Strike-slip faulting and related basin formation in zones of tectonic escape: Turkey as a case study. *In*: BIDDLE, K. T. & CHRISTIE-BLICK, N. (eds) *Basin Formation and Sedimentation*, Society of Economic Paleontologists and Mineralogists Special Publications, **37**, 227–264.

SENGÖR, A. M. C., ÖZEREN, S., GENÇ, T. & ZOR, E. 2003. East Anatolian high plateau as a mantle-supported, north-south shortened domal structure. *Geophysical Research Letters*, **30**, 8045, doi: 10.1029/2003GL017858.

SENGÖR, A. M. C., TÜYSÜZ, O., IMREN, C., SAKINC, M., EYIDOGAN, H., GÖRÜR, N., LE PICHON, X. & RANGIN, C. 2005. The North Anatolian Fault: a new look. *Annual Reviews in Earth and Planetary Sciences*, **33**, 37–112.

Seyitoğlu, G., Isik, V. & Cemen, I. 2004. Complete Tertiary exhumation history of the Menderes massif, western Turkey: an alternative working hypothesis. *Terra Nova*, **16**, 358–364.

Spadea, P. & D'Antonio, M. 2006. Initiation and evolution of intra-oceanic subduction in the Uralides: Geochemical and isotopic constraints from Devonian oceanic rocks of the Southern Urals, Russia. *Island Arc*, **15**, 7–25.

Stampfli, G. M. & Borel, G. D. 2002. A plate tectonic model for the Paleozoic and Mesozoic constrained by dynamic plate boundaries and restored synthetic oceanic isochrones. *Earth and Planetary Science Letters*, **196**, 17–33.

Tirel, C., Gautier, P., van Hinsbergen, D. J. J. & Wortel, M. J. R. 2009. Sequential development of interfering metamorphic core complexes: numerical experiments and comparison with the Cyclades, Greece. *In*: van Hinsbergen, D. J. J., Edwards, M. A. & Govers, R. (eds) *Collision and Collapse at the Africa–Arabia–Eurasia Subduction Zone*. Geological Society, London, Special Publication, **311**, 257–292.

Toth, J. & Gurnis, M. 1998. Dynamics of subduction initiation at preexisting fault zones. *Journal of Geophysical Research*, **103**(B8), 18063–18067.

van de Zedde, D. M. A. & Wortel, M. J. R. 2001. Shallow slab detachment as a transient source of heat at midlithospheric depths. *Tectonics*, **20**, 868–882.

van der Meulen, M. J. 1999. Slab detachment and the evolution of the Apenninic Arc. *Geologica Ultraiectina*, **170**, 136.

van Hinsbergen, D. J. J., Hafkenscheid, E., Spakman, W., Meulenkamp, J. E. & Wortel, M. J. R. 2005. Nappe stacking resulting from subduction of oceanic and continental lithosphere below Greece. *Geology*, **33**, 325–328.

van Hinsbergen, D. J. J. & Boekhout, F. 2009. Neogene brittle detachment faulting on Kos (E Greece): implications for a southern break-away fault of the Menderes metamorphic core complex (western Turkey). *In*: van Hinsbergen, D. J. J., Edwards, M. A. & Govers, R. (eds) *Collision and Collapse at the Africa–Arabia–Eurasia Subduction Zone*. Geological Society, London, Special Publications, **311**, 311–320.

Vignaroli, G., Faccenna, C., Rossetti, F. & Jolivet, L. 2009. Insights from the Apennines metamorphic complexes and their bearing on the kinematics evolution of the orogen. *In*: van Hinsbergen, D. J. J., Edwards, M. A. & Govers, R. (eds) *Collision and Collapse at the Africa–Arabia–Eurasia Subduction Zone*. Geological Society, London, Special Publications, **311**, 235–256.

Wilson, J. T. 1966. Did the Atlantic colse and then re-open? *Nature*, **211**, 676–681.

Wortel, M. J. R. & Spakman, W. 2000. Subduction and slab detachment in the Mediterranean-Carpathian region. *Science*, **290**, 1910–1917.

Melange genesis and ophiolite emplacement related to subduction of the northern margin of the Tauride–Anatolide continent, central and western Turkey

ALASTAIR H. F. ROBERTSON[1]*, OSMAN PARLAK[2,3] & TİMUR USTAÖMER[4]

[1]*School of GeoSciences, University of Edinburgh, West Mains Road, Edinbugh, EH9 3JW, UK*

[2]*Jeoloji Mühendisliği Bölümü, Çukurova Üniversitesi, 01330-Balcalı, Adana, Turkey*

[3]*Mesleki ve Teknik Eğitim Fakültesi, Adıyaman Üniversitesi, 02040 Adıyaman, Turkey*

[4]*Jeoloji Mühendisliği Bölümü, İstanbul Üniversitesi, 34850-Avcılar, İstanbul, Turkey*

**Corresponding author (e-mail: alastair.robertson@ed.ac.uk)*

Abstract: The Tauride–Anatolide continent, stretching for *c*. 900 km across western and central Turkey, is one of the world's best example of a subducted, exhumed passive margin within a collisional orogen. Twelve widely separated areas were studied and correlated to develop a new plate-tectonic model. A metamorphosed, rifted continental margin of Triassic–Lower Cretaceous age (Tauride–Anatolide platform) is overlain by Upper Cretaceous (Cenomanian-Lower Maastrichtian) pelagic sediments and then by both tectonic melange (subduction complexes) and sedimentary melange (foredeep gravity complexes). The melanges are overthrust by unmetamorphosed ophiolitic rocks, commonly peridotites with swarms of diabase/gabbro dykes, and are underlain by metamorphic soles. New geochemical evidence from basaltic blocks in the melange indicates predominantly subduction influenced, within-plate and mid-ocean ridge-type settings. The dykes cutting the ophiolites were probably intruded during early-stage intra-oceanic arc genesis. The metamorphosed continental margin, melanges and ophiolites in the north (Anatolides) are correlated with unmetamorphosed equivalents in the Taurides further south (e.g. Beyşehir and Lycian nappes).

Oceanic crust of Triassic–Late Cretaceous age formed between the Gondwana-related Tauride–Anatolide continent in the south and the Eurasia-related Sakarya microcontinent in the north. Following Late Triassic–Early Cretaceous passive margin subsidence, the continental margin was covered by Cenomanian-Turonian pelagic carbonates (*c*. 98–90 Ma). Ophiolites formed in an intra-oceanic subduction zone setting in response to northward subduction, probably within a two-stranded ocean, with the Inner Tauride ocean in the SE and the İzmir–Ankara–Erzincan ocean in the north/NW. Metamorphic soles relate to intra-oceanic subduction (*c*. 95–90 Ma). Oceanic sedimentary/igneous rocks accreted to the advancing supra-subduction oceanic slab. The Tauride–Anatolide continental margin then underwent diachronous collision with the trench (*c*. 85 Ma), deeply subducted and metamorphosed at HP/LT (*c*. 80 Ma). Accretionary, ophiolitic and exhumed HP/LT rocks were gravity reworked into a southward-migrating flexural foredeep and progressively overridden (*c*. 70–63 Ma). Slices of the upper part of the platform and its margin detached and were thrust southwards as the (Tauride) Lycian and Beyşehir nappes, together with regional-scale ophiolites. The continental margin and melange were simultaneously exhumed during Maastrichtian–Early Paleocene (70–63 Ma) and transgressed by shallow-water sediments, beginning in the Late Maastrichtian in the east (*c*. 64 Ma) and the Mid?-Late Paleocene (*c*. 60 Ma) further west. Remnant oceanic crust was consumed during Early Cenozoic time, followed by Mid Eocene (45–40 Ma) diachronous continental collision and a second phase of regional deformation. Rather than being progressive there were two stages of collision: first, Upper Cretaceous ophiolite emplacement driven by continental margin-subduction trench collision, and secondly Eocene collision of the Tauride and Sakarya/Eurasian continents.

Supplementary material: Supplementary data are available at: http://www.geolsoc.org.uk/SUP18341.

An early assumption of plate-tectonic theory was that continental crust could not be subducted owing to its thickness and relative buoyancy. More recently it has been accepted that continental crust can be subducted in several tectonic settings, especially where a continental margin collides

From: VAN HINSBERGEN, D. J. J., EDWARDS, M. A. & GOVERS, R. (eds) *Collision and Collapse at the Africa–Arabia–Eurasia Subduction Zone*. The Geological Society, London, Special Publications, **311**, 9–66.
DOI: 10.1144/SP311.2 0305-8719/09/$15.00

with a subduction trench and where continents forcefully collide. Subducted material can be exhumed back to the surface in a geologically short period of time. The Late Cretaceous of Oman is an excellent sample of a subducted, exhumed, passive margin, associated with ophiolite emplacement (Lippard *et al.* 1986; Robertson & Searle 1990; Goffe *et al.* 1988). However, in Oman there is no agreement as to the regional plate-tectonic setting, with subduction away from the passive margin (Searle & Cox 1999; Searle *et al.* 2004, 2005) and towards the passive margin (Gregory *et al.* 1998; Miller *et al.* 1998), both being proposed. Other examples of ophiolites and related melanges that were emplaced onto continental margins related to subduction include the Mid-Jurassic of the Balkans (e.g. Robertson *et al.* 1991; Rassios & Smith 2000; Smith 2006; Robertson 2006) and the Ordovician of Newfoundland (Williams & Stevens 1974).

This paper discusses one of the world's best examples of a subducted, exhumed, passive continental margin associated with regional-scale ophiolite emplacement. Northwestern Turkey is already known to be the site of closure of a Mesozoic oceanic basin associated with high-pressure/low-temperature metamorphism (HP/LT) (Okay & Kelley 1994; Okay *et al.* 1998, 2001; Okay 2002). This classic area has additionally experienced Cenozoic collisional and post-collisional deformation. Here, we present new field-based evidence for a very large area, stretching across central and western Anatolia for *c*. 900 km (Fig. 1). When combined with information from the literature, an extraordinary picture emerges of subduction-accretion, margin subsidence, ophiolite emplacement, exhumation and continental collision.

In Turkey, oceanic lithosphere ('Northern Neotethys') is widely considered to have formed by rifting of a regional microcontinent to the south during the Triassic (Robertson & Dixon 1984; Özgül 1984, 1997; Collins & Robertson 1999; Göncüoğlu *et al.* 2003). Different interpretations of the settings and processes of rifting exist (Stampfli *et al.* 2001; Stampfli & Borel 2002; Göncüoğlu *et al*. 2003; Robertson *et al*. 2005; Okay *et al.* 2006) that are largely outside the scope of this paper. There are also different views concerning the possible existence of only one oceanic suture

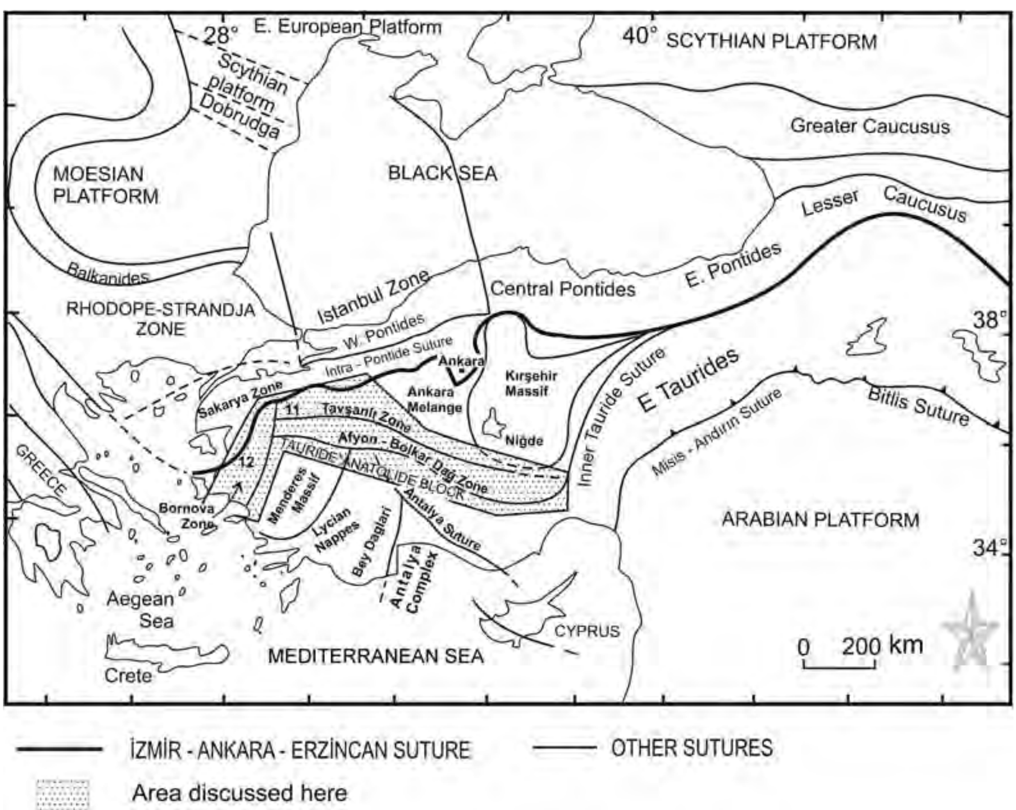

Fig. 1. Regional tectonic divisions of Turkey, as used in this paper (modified from Okay & Tüysüz 1999; Robertson 2002). Note the region studied. See Figure 5 for the locations of the main areas studied during this work (Nos 1–10).

(e.g. Göncüoğlu *et al.* 1996–1997), or several oceanic sutures (Görür *et al.* 1984, 1998) in central and northern Turkey. However, there is general consensus that Tethys in this region was closing during the Late Cretaceous associated with northward subduction and the development of an Upper Cretaceous accretionary prism (Koçyiğit 1991; Rojay *et al.* 2001, 2004; Fig. 2). Intra-oceanic subduction is commonly believed to have triggered the genesis of ophiolites in a supra-subduction zone setting (Collins & Robertson 1998; Parlak *et al.* 2000; Robertson 2002; Yalınız *et al.* 1996, 2000). Subduction culminated in the collision of the subduction trench with the continent to the south and this was the driving mechanism of latest Cretaceous ophiolite emplacement. Final 'hard' collision and suture tightening were delayed for up to 25 Ma, until Mid Eocene.

An advantage of the present study area is that various parts of the continental margin are exposed across the tectonic strike for *c*. 900 kilometres east–west and several hundred kilometres north–south. Near the suture in the north the continental margin and some melanges have been metamorphosed under HP/LT conditions, whereas further south equivalent continental margin units are unmetamorphosed, allowing an overview of the convergent margin evolution.

Tectonic nomenclature

In a classic paper, Ketin (1966) correlated the metamorphic Menderes Massif in the west and the Kırşehir Massif further east (Fig. 1) and collectively termed these the *Anatolides*, in contrast to the unmetamorphosed *Taurides* further south. Şengör & Yılmaz (1981) correlated the regional metamorphosed and unmetamorphosed units as the regional Tauride–Anatolide platform (including the Kırşehir Massif), a terminology broadly followed by many others (Okay 1986; Okay & Tüysüz 1999; Göncüoğlu *et al.* 1996–1997). However, the Menderes Massif and the Kırşehir Massif are commonly considered as palaeogeographically separate units with contrasting geological histories (Robertson & Dixon 1984; Görür *et al.* 1984, 1998; Şengör 1984; Dilek & Whitney 2000).

Here, we follow the traditional usage by referring to the unmetamorphosed units as the *Taurides* and the metamorphosed units as the *Anatolides* (the main subject of this paper), which we correlate as the regional Tauride–Anatolide platform. This includes high-grade metamorphic basement, as exposed in the Menderes Massif. We, therefore, refer to the southerly continental unit as a whole as the Tauride–Anatolide Platform. However, we specifically exclude the Niğde–Kırşehir Massif

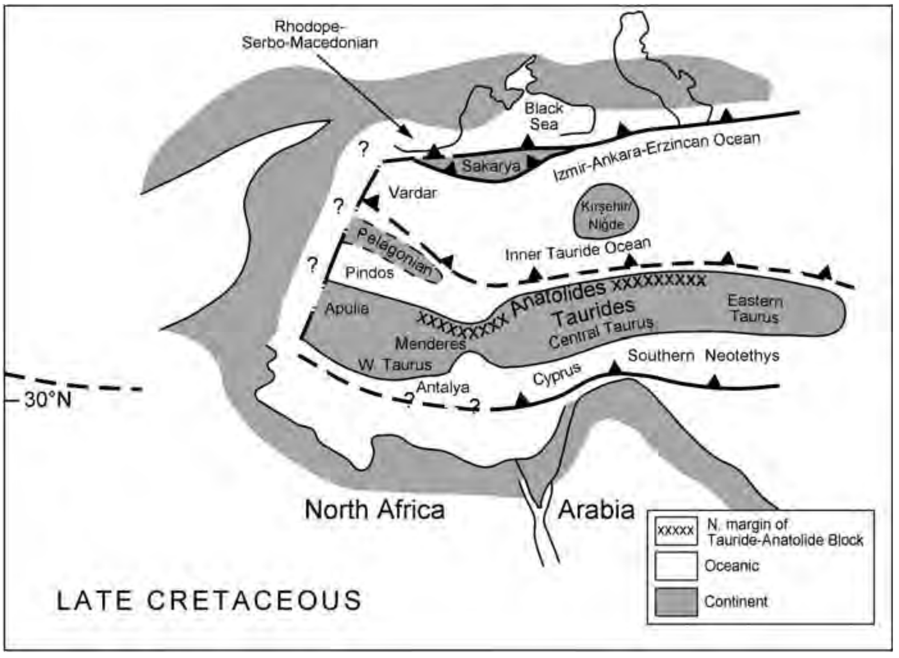

Fig. 2. Plate-tectonic sketch of the Turkish region during the Late Cretaceous, as supported by evidence from this study (modified from Robertson 2002).

(also known as the Central Anatolian Crystalline Complex) from this definition.

The metamorphosed Anatolides were divided into two zones by Okay (1984). A more northerly unit of highly recrystallized HP/LT metamorphic rocks, known as the Tavşanlı zone, is exposed in the NW (Fig. 1). This was reported to be thrust over a more southerly unit of generally lower grade, less recrystallized rocks exposed along the entire length of the Anatolides, known as the Afyon–Bolkardağ zone (or Afyon zone). Okay's (1984) nomenclature is retained here. By contrast, Göncüoğlu *et al.* (1996–1997) used Okay's (1984) definition of the Tavşanlı zone, but named the generally lower grade, less recrystallized rocks to the south, the Kütahya–Bolkardağ zone. The Afyon–Bolkardağ zone, especially the deeper structural levels, has also undergone HP/LT metamorphism, but to a lower grade that the Tavşanlı zone in the north (Blumenthal 1955; Kaaden 1966; Eren 2001; Dilek & Whitney 1997; Candan *et al.* 2005).

In this paper we define the Tavşanlı zone as the very high-grade recrystallized platform carbonates, overlying melanges and ophiolites in the north, and the Afyon–Bolkardağ zone as generally lower-grade, less recrystallized rocks further south, also overlain by melanges and ophiolites. Candan *et al.* (2005) show the Tavşanlı zone as regionally thrust southwards over the Afyon–Bolkardağ zone (e.g. NW of Afyon). Their summary log and section show over-riding slices of Tavşanlı zone platform carbonates, together with melanges and ophiolites. However, we could not confirm the existence of an exposed contact between these two zones, which, if it exists, is likely to underlie younger sediments.

Regional tectonic units

Any tectonic interpretation must take account of other regional units to the north and south of the Anatolides. First, in the south the Tauride–Anatolide continent includes Late Precambrian, Palaeozoic and Mesozoic rocks, well exposed in the Menderes Massif in the west, in the Geyik Dağ in the centre of the area, and in the Bolkardağ in the east (Fig. 1). These regional units are overlain by thrust sheets (Şengör & Yılmaz 1981), which include the Lycian nappes in the west (De Graciansky 1972; Collins & Robertson 1998) and the Beyşehir nappes further east (Özgül 1984, 1997; Monod 1977, 1979; Andrew & Robertson 2002). These allochthonous units were emplaced southwards over the Tauride–Anatolide platform in two phases, during Late Cretaceous and Mid-Eocene time (Andrew & Robertson 2002). The Tauride–Anatolide Platform is bordered to the south by another suture ('Antalya suture'; Fig. 1), which records the demise of an additional Mesozoic oceanic basin, known as the southern Neotethys, but which is outside the scope of this paper (see e.g. Robertson 2000).

We also take account of evidence from the northern margin of the Mesozoic oceanic basin, including the Sakarya zone in the NW. During the Mesozoic the Sakarya zone existed as a continental unit, probably separated from Eurasia by a small oceanic basin that is recorded by the Intra–Pontide suture (Şengör & Yılmaz 1981; Yılmaz *et al.* 1997; Robertson & Ustaömer 2004). The Anatolide melanges and ophiolites come into contact with the Late Mesozoic Ankara Melange in the NE of the area studied (Bailey & McCallien 1954; Koçyiğit 1991; Rojay *et al.* 2004). Limited exposure in the intervening area is discussed in this paper.

Further east, a large continental unit known as the Niğde–Kırşehir Massif, or the Central Anatolian Crystalline Complex (Göncüoğlu *et al.* 1996–1997), includes the large Kırşehir Massif in the north and the smaller, but contiguous Niğde massif in the south. At present, there is no agreement on the Mesozoic tectonic setting of the Niğde–Kırşehir Massif, which is variously seen as part of the Eurasian continental margin (Kazmin & Tikhonova 2006), part of an Anatolide–Tauride continent (Göncüoğlu *et al.* 1996–1997), as a microcontinent within the northerly Neotethys (Görür *et al.* 1984, 1998; Robertson & Dixon 1984; Dercourt *et al.* 1993; Dilek *et al.*, 1999), or even as an allochthonous terrane translated laterally along the orogen to near its present position during Triassic time (Stampfli *et al.* 2001). A possible resolution of this issue is discussed here.

The closure of the main ocean ('northern Neotethys') separating the opposing Tauride–Anatolide and Sakarya continents is marked by the İzmir–Ankara–Erzincan suture zone, which stretches end-to-end across Turkey (Fig. 1). Assuming the Niğde–Kırşehir Massif formed a microcontinent, an additional oceanic suture existed between it and the Tauride–Anatolide continent, known as the Inner Tauride suture (Görür *et al.* 1984, 1988).

We focus here on the northerly, metamorphosed part of the Tauride–Anatolide continent, especially the Afyon–Bolkardağ zone of the Anatolide unit, marked by cross-hatching in Figure 2. Representative cross-sections of the areas discussed here are shown in Figure 3, with stratigraphic columns in Figure 4.

Melange nomenclature, mapping and time scale

Melange is defined as blocks of heterogeneous lithologies set in an incompetent matrix, commonly pelitic or serpentinitic (see Raymond 1984),

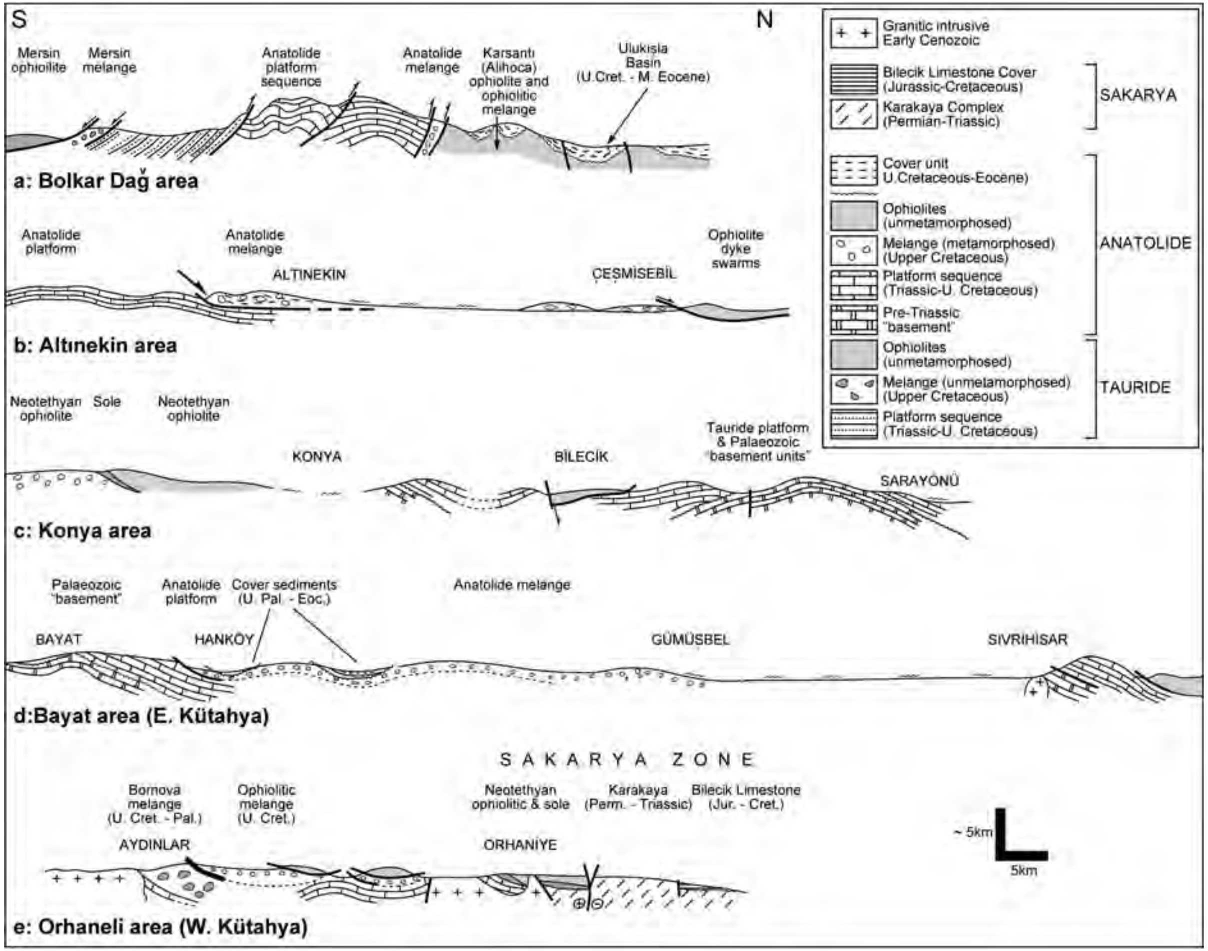

Fig. 3. Summary cross-section of each of the main areas studied during his work. See text for discussion and data sources.

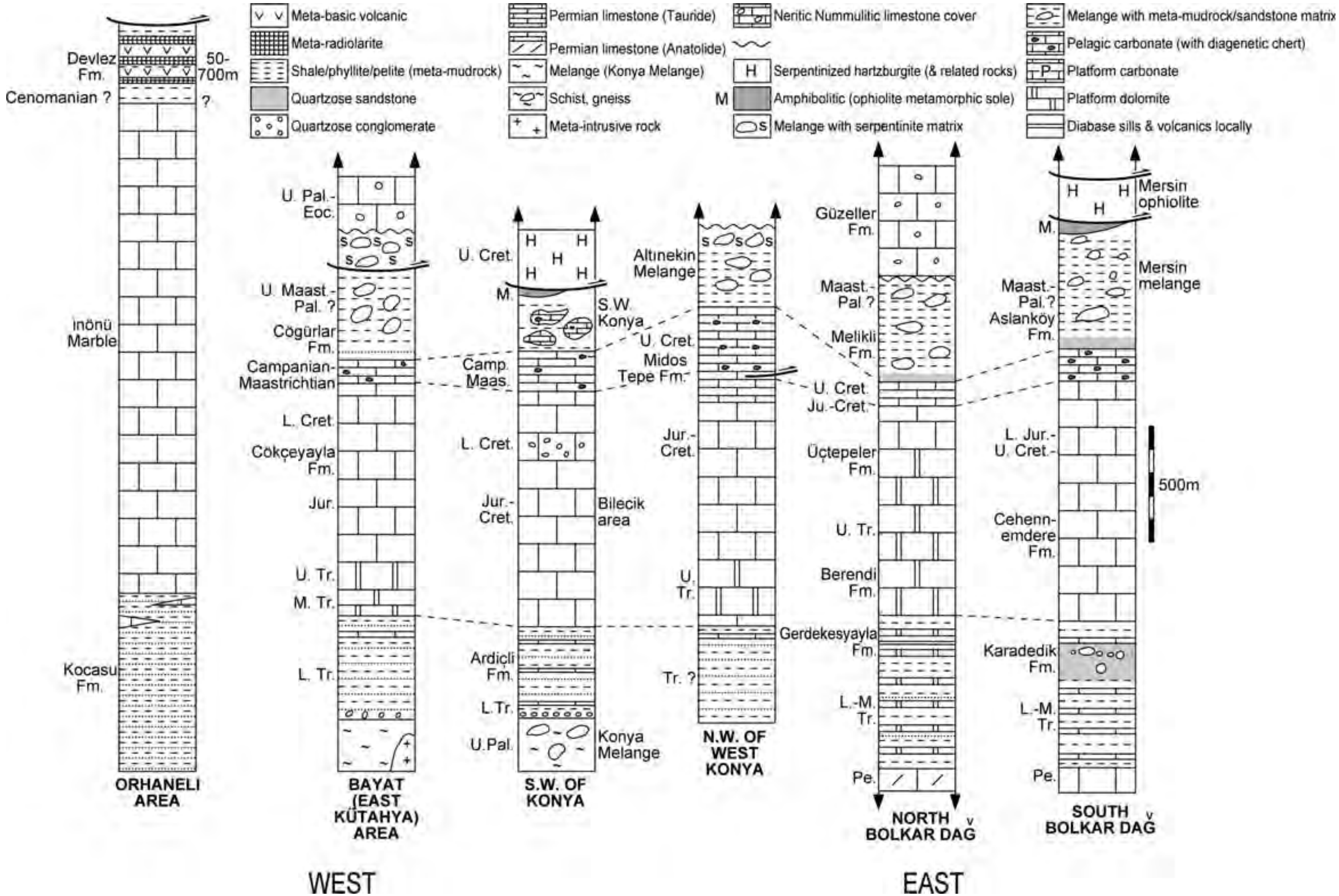

Fig. 4. Summary of the restored stratigraphical succession in each of the main areas studied here. See text for discussion and data sources. Successions 1–5 are from the metamorphic northern margin of the Anatolide unit and succession 6 is from the unmetamorphosed Tauride unit to the south, for comparison. See text for discussion and data sources.

regardless of whether the melange is of sedimentary or tectonic origin, or both. Broken Formation (American Geological Institute 1961) refers to strongly deformed units in which some stratal continuity can still be recognized. Melanges that have formed by tectonic processes are here termed *tectonic melange* and those by sedimentary processes, *sedimentary melange*, broadly equivalent to the classical 'olistostrome'. For several decades now, terms such as 'olistostrome', 'flysch' and 'molasse' have been regarded as redundant in the sedimentological literature as they are hangovers from geosynclinal theory. Olistostromes as nowadays reclassified as large-scale mass-flow features. The melanges studied here show evidence of both tectonic and sedimentary processes.

During this work we have compiled, field checked and added to the available geological maps of the areas studied. The maps are regional-scale and it is not possible to show all the local features. We refer to MTA maps, where available, which potentially allows readers to follow up specific aspects. Dips and strikes in, for example, melange are variable and so it is difficult to show representative data on the scale studied. Also, much of the large-scale deformation is related to Eocene collisional deformation, which post-dates Upper Cretaceous tectonic emplacement and subsequent exhumation, the main topics of this paper. Lineation data shown on some of the maps are summarized and interpreted in the Tectonic processes section.

The timescale used here is that of Gradstein *et al.* (2004).

Afyon–Bolkardağ zone

We now describe each of the areas we have studied from east to west across central and western Anatolia (Figs 1, 5). Colour photographs of field features are shown in the supplementary material. An interpretation is given in the *Tectonic processes* section later in the paper.

Bolkar Dağ (Area no. 1)

The largest exposure area of the metamorphosed Anatolide carbonate platform, together with several different types of melange are in the Bolkar Dağ, which extends east–west for *c.* 100 km and rises to a height of *c.* 3000 m (Fig. 5). The Mesozoic platform in the Bolkardağ is deformed into a mountain-sized, NE–SW trending-anticlinorium (Fig. 3). The meta-platform succession is terminated in the south by a southward-dipping thrust. Unmetamorphosed platform carbonates further south form part of the unmetamorphosed Tauride carbonate platform (Fig. 3). The northern margin of the metamorphosed platform is a regional-scale, high-angle, southward dipping thrust, or reverse fault that separates the platform to the south from melange and ophiolitic units to the north (Demirtaşlı *et al.* 1984; Jaffey & Robertson 2001/2004). The contact zone is cut by generally east–west trending, high-angle down-to-the north, extensional faults (Dilek & Whitney 2000), some of which affect Plio-Quaternary sediments in the area (Jaffey & Robertson 2001, 2004).

Platform. The metamorphosed Bolkar Dağ platform comprises a mainly shallow-water carbonate succession of Late-Permian to Late Cretaceous age (Demirtaşlı *et al.* 1984). Two aspects are highlighted here; first, the presence of extrusive and volcaniclastic rocks within the Early Triassic (Scythian) succession which relate to regional rifting, and second, the transition to ophiolite-derived clastic sediments that relate to Upper Cretaceous ophiolite emplacement.

The meta-platform succession begins with carbonates of inferred Permian age and passes into meta-clastics of Early Triassic (Scythian) age (Fig. 4). We observed a well-exposed relatively unrecrystallized Scythian succession on both limbs of a kilometre-scale, east–west trending (Cenozoic) anticline to the south of Ereğli near Yellice (Fig. 6). A sedimentary log was measured on the north-dipping northern limb of this structure (Fig. 7). Permian meta-carbonates are followed by *c.* 700 m of buff-coloured marls and argillaceous limestones with lenses of quartzitic sandstone, mainly near the base. A flow of altered meta-basaltic rocks (greenschist) appears near the top of the exposed succession. A correlative Lower–Mid Triassic succession on the south-dipping southern limb of the anticline (not measured) passes into Upper Triassic meta-carbonates, including lenses of bioclastic carbonate, interpreted as metamorphosed patch reefs. A succession of inferred Late Triassic age (Berendi Limestones; Demirtaşlı *et al.* 1984) is also exposed *c.* 10 km further west on the northward-dipping limb of the same large-scale anticline (i.e. south of the Ereğli–Ayrancı road, 1 km SE of Böğecik (77215:45531). Thick-bedded marble is overlain by red iron oxide (bauxite), then by marble with calc-schist alternations and medium-bedded dark grey marble with rare diagenetic chert. The Early–Mid Triassic succession is followed regionally by a thick, uniform succession of stratiform marbles representing a carbonate platform succession of Late Triassic–early Late Cretaceous age (e.g. exposed near Yellice; 92694:41784). The shallow-water limestones pass upwards into Upper Cretaceous pelagic carbonates and then into ophiolite-derived debris flows of 'Maastrichtian-Early Paleocene' age (Demirtaşlı *et al.* 1984).

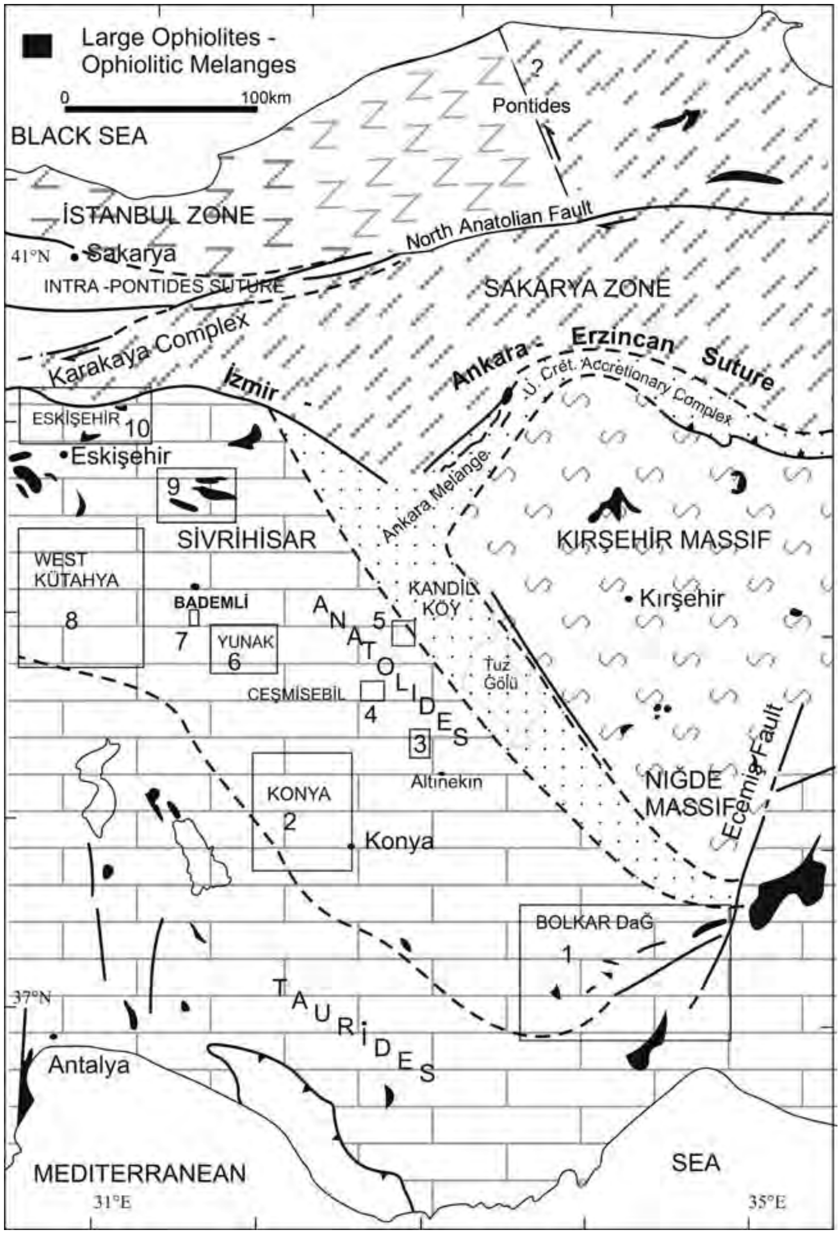

Fig. 5. Outline geological map of the main areas studied during this work. The individual areas (marked as numbered boxes) lie within the Tavşanlı zone and the Kütahya–Bolkardağ zone of the metamorphic northern part of the Tauride–Anatolide Platform. The Ankara Melange is delineated for convenience although it is intergradational with other accretionary melanges in the region. See text for discussion and data sources.

Melanges. Three contrasting types of melange are exposed in different areas of the Bolkar Dağ area.

First, Upper Cretaceous sedimentary melange, composed mostly of mudrocks, sandstone turbidites, multiple debris flows and heterogeneous detached blocks forms the stratigraphical top of the intact Mesozoic carbonate succession, as summarized above. This sedimentary melange relates to collapse of the carbonate platform and gravity emplacement of material derived from accreted oceanic complexes and emplacing ophiolites (see *Tectonic processes*).

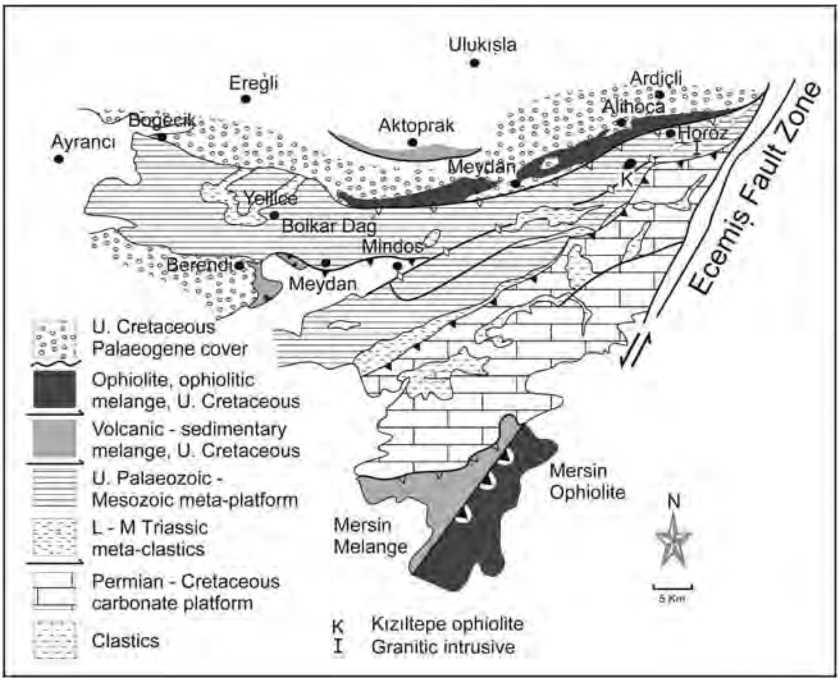

Fig. 6. Outline geological map of the Bolkar Dağ area (No. 1). See Figure 5 for location and the text for discussion. Data from Demirtaşlı *et al.* (1984), the 1:500 000 geological map of Turkey (MTA 2002), Clark & Robertson (2002) and this study. The map details are from the Turkish 1: 100 000 topographical maps Kozan M33 and N33.

Secondly, in the far west, near Berendi (Fig. 6), the Mesozoic platform is locally overlain by serpentinite-rich tectonic melange which contains numerous blocks of crystalline marble (up to 4 m in size), and smaller blocks of limestone, basalt, greenish chert and rare red chert. Both the ophiolitic melange and the Mesozoic platform are unconformably overlain by cream-to buff-coloured flaggy-bedded Nummulitic limestone of Late Palaeocene–Early Eocene age; this provides an upper time limit on ophiolite and melange emplacement in this area. These sediments pass upwards into weakly lithified sandstone, in turn unconformably overlain by the Miocene Mut Formation (MTA 2002).

Thirdly, an elongate exposure of metamorphosed volcanic-sedimentary melange, up to several kilometres wide, is exposed for several tens of kilometres east–west, bordering the northern margin of the metamorphosed Mesozoic carbonate platform. In the east (north of Horoz), the metamorphosed carbonate platform is backthrust directly against ophiolitic lithologies (see below) with, at most, only a thin sliver of melange. Further west (south of Aktoprak) much thicker melange is present in contact with the platform (Figs 3a, 6). This melange, described in some detail here for the first time, is depositionally overlain by an important unit of polymict debris flows, discussed below, and then by Late Maastrichtian–Lower Eocene shallow-marine sediments and volcanics (Demirtaşlı *et al.* 1984; Clark & Robertson 2002, 2004) that, thereby, constrain the timing of emplacement of this melange and related ophiolitic rocks. The melange and the latest Cretaceous–Paleogene Ulukışla Basin lithologies were strongly folded, thrust deformed and juxtaposed with the platform at a high angle during Mid-Eocene time (Clark & Robertson 2002, 2004).

The melange is best exposed within the central part of the outcrop, extending from near Meydan village for *c.* 20 km westwards. It is dominated by large blocks of volcanic rocks of basic to intermediate composition, together with meta-limestones and meta-cherts, set in a sheared sedimentary matrix. Exposures to the north, towards the ophiolitic melange, are more sheared and exhibit a schistose fabric.

Where best exposed, near Meydan, the melange is not greatly recrystallised but is generally reddish, owing to local mineralization (e.g. around Maden). The main types of block are grey marble, green meta-chert, pink pelagic limestone (thin to medium-bedded, with chert lenses) and pink siliceous pelagic limestone (with abundant chert of replacement origin). Volcanic blocks (several metres in size) are mainly relatively unaltered black basalt. There

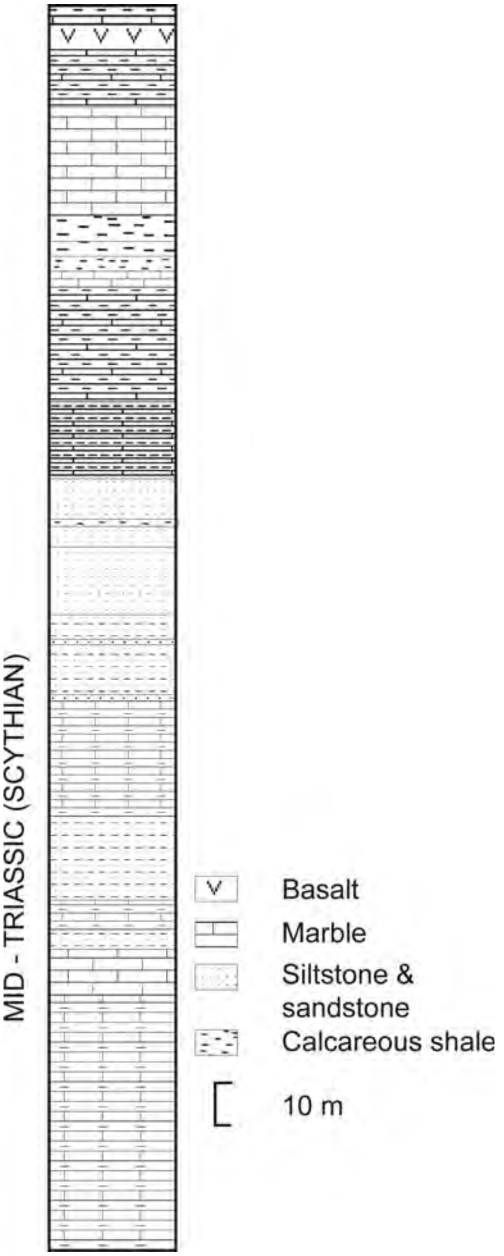

Fig. 7. Measured sedimentary log of the Mid-Triassic succession exposed on the northwestern flank of the Bolkar Dağ near Yellice. Note the presence of volcanic rocks that are believed to relate to rifting (see Fig. 6 for location).

are also rare blocks of basaltic breccia, with angular to sub-angular basalt clasts, up to 15 cm in size, set in a coarse volcaniclastic matrix. These breccias are locally associated with small volumes of recrystallized chert (jasper). The matrix of this melange is mainly dark siliceous mudstone, interbedded with strongly deformed matrix-supported conglomerates, with numerous marble clasts (up to 10 cm in size).

More sheared, schistose melange, generally grey in colour, is well exposed *c.* 20 km further NW (e.g. 3 km east of Karagöl). This melange includes large (up to 20 m) erosionally resistant blocks of basalt and basaltic breccia. The lava blocks range from dark, relatively unaltered, basalt to pale hydrothermally altered lava. In addition, one block (*c.* 4 m in size) is composed of very coarse lava breccia, with clasts up to 40 cm in size.

Associated sedimentary blocks include marble, meta-chert, thin-bedded (<5 cm) siliceous limestone and rare silicified meta-serpentinite. Blocks of tectonically brecciated marble, *c.* 6 m in diameter, show a characteristic jigsaw-type fabric of angular clasts, indicative of *in-situ* brecciation. Schistose matrix sediments include intercalations of coarse sedimentary facies in which locally intact successions, up to several tens of metres thick, are recognized. For example, the pelitic matrix, as exposed along the Meydan–Karagöl road, includes debris flows made up of marble clasts (up to 0.3 m in size), graded calcarenites (up to several tens of cm thick) and sheared calcilutites with calc-schist partings. Clasts, where present, are commonly strongly stretched in the plane of the schistocity. Cleaved, matrix-supported volcanogenic conglomerates are also present, locally with stretched volcanic pebbles set in a sheared volcaniclastic matrix.

Dismembered ophiolitic melange. Unmetamorphosed ophiolitic rocks exposed along the northern flank of the Bolkar Dağ were traditionally known as the Pozantı ophiolite. This was combined with a larger body of ophiolite east of the Ecemiş fault zone (Fig. 6), known as the Karsantı ophiolite, and termed the Pozantı-Karsantı ophiolite (Çakır *et al.* 1978; Juteau 1980; Lytwyn & Casey 1995; Polat *et al.* 1996). The ophiolites to the east of the fault zone are dominated by ultramafic ophiolitic rocks, with a well-developed melange beneath (Tekeli 1981*b*). To the west of the fault zone all parts of a complete ophiolite pseudostratigraphy are present in dismembered form and were termed the Alihoca ophiolite by Dilek *et al.* (1999) after a village in the area (Fig. 6). In many areas the ophiolitic rocks occur as blocks in a sheared pelitic matrix and the unit as a whole has since been termed the Alihoca Ophiolitic Melange (Clark 2002; Clark & Robertson 2002).

The dismembered Alihoca ophiolite and associated Alihoca ophiolitic melange overlies the volcanic-sedimentary melange in the west and is in direct tectonic contact with the Mesozoic platform in the east of the area (Fig. 5). A faulted contact between the platform and the ophiolitic melange in the east, is for example, well exposed *c*. 400 m south of the old Ankara–Adana highway, on the road to Horoz (Fig. 6). Further north (north of the Ankara–Adana highway) most, or all, stratigraphical levels of a complete ophiolite are exposed, albeit dismembered. The ophiolitic rocks range from large (up to kilometre-sized) blocks in a sheared pelitic (locally serpentinitic matrix), to outcrops of ophiolitic broken formation with little sedimentary matrix between ophiolitic blocks and thrust sheets. There are also some areas where the ophiolite is relatively intact, especially basaltic extrusives and sheeted dykes.

Lower levels of the ophiolitic crustal sequence are well exposed as blocks and disrupted thrust sheets in road cuttings along the new Adana–Ankara highway where they are intercalated with sheared dark shales and serpentinite debris flows. Lithologies include cumulate gabbro with pegmatitic layers and pyroxenite, cut by isolated diabase dykes. Higher levels of the ophiolite pseudostratigraphy are exposed as broken formation (with little matrix) further north. For example, where well exposed along the road to Ardıçlı the section begins with coarse-grained gabbro and gabbro pegmatite, cut by thin (0.25–1 m) isolated diabase dykes with chilled margins. Parts of the succession are strongly sheared, brecciated, or epidote rich. After a short break (*c*. 100 m) the section resumes with an interval of dykes with locally preserved chilled margins. After a further short break in exposure, massive and pillowed lavas are exposed (*c*. 200 m thick), with tectonic breccia along cross-cutting shear zones.

In many areas the Alihoca ophiolitic rocks are overlain by an elongate unit, typically several hundred metres thick, composed of sheared pink calcareous mudstones (Çiftehan unit); this was dated as late Campanian–Maastrichtian in age (Demirtaşlı *et al*. 2004; Clark 2002). Terrigenous (e.g. quartz) or deep-level ophiolitic material (e.g. serpentinite) is absent suggesting accumulation in an oceanic setting. The upper and lower contacts of this unit are typically tectonic. However, locally (on the road to Ardıçlı) the hemipelagic sediments overlie ophiolitic extrusives with a contact, which, although faulted, shows a primary stratigraphical relationship. Massive ophiolitic basalt is capped by basaltic breccia (<2 m) which includes reworked sub-rounded clasts, confirming a sedimentary origin as a mass-flow. The breccia is unconformably overlain by silty mudstone and by a single medium-thickness bed of normal-graded volcaniclastic sandstone, followed by homogeneous pink, more or less silty, hemipelagic carbonate. Assuming the contact is stratigraphic, the Çiftehan unit is interpreted as part of an original deep-sea sedimentary cover of the Alihoca ophiolite.

The ophiolitic rocks and the melanges generally are unconformably overlain by Upper Maastrichtian shallow-water carbonates marking the base of the Ulukışla Basin succession (Aktaştepe Formation: Demirtaşlı *et al.* 1984; Clark & Robertson 2002, 2004; Clark 2002). These sediments are critical as they provide an upper age limit for the timing of ophiolite and melange emplacement onto the northern margin of the Bolkar Dağ carbonate platform.

Matrix-supported polymict conglomerates with blocks. Both the mainly sedimentary melange and the dismembered Alihoca ophiolite are locally overlain by a thin, but important, unit of unmetamorphosed matrix-supported debris flows, not observed in any of the other Anatolide areas studied. These sediments have been interpreted as polymict debris flows with outsized detached blocks (Clark & Robertson 2002, 2004).

The matrix-supported conglomerates, estimated as up to several hundred metres thick, were mapped during this study and found to comprise a laterally continuous unit, exposed everywhere beneath the dismembered ophiolite or the volcanic-sedimentary melange and the depositionally overlying Ulukışla Basin. A key observation is that matrix-supported conglomerates in some areas grade upwards into Late Maastrichtian neritic limestones at the base of the overlying Ulukışla Basin. In a well-exposed section (near the top of Aktaş Tepe, along a hilltop pass between Maden and Gümüş villages) typical polymict conglomerates comprise poorly sorted clasts and blocks, ranging up to 10 m in diameter. The clasts are predominantly unmetamorphosed ophiolitic rocks including serpentinite, hartzburgite, dunite, gabbro, diabase and rare basalt, together with red chert and pink pelagic limestone. Other clasts include recycled ophiolite-derived conglomerate, sandstone and shale. Metamorphic clasts include schist, phyllite and rare blueschist (Clark 2002). Many of the clasts are well rounded and are set in a reddish poorly sorted, fine- to coarse-grained matrix. The presence of blueschist clasts is important in helping to constrain the timing of exhumation of HP/LT rocks in the area (i.e. pre-Late Maastrichtian; see *Tectonic processes*).

HP/LT ophiolitic and sole rocks. An important, isolated, klippe of ophiolite-related rocks is exposed near the mountainous crest of the Bolkag Dağ (Kızıltepe ophiolite), an area that was inaccessible during this work. Dilek & Whitney (1997) report that there, the metamorphosed Anatolide platform is overlain by a small outcrop of foliated ophiolite and then by an ophiolitic slice *c*. 300 m thick.

Blueschists were identified within amphibolites at three localities. In two of these, Na-amphiboles (within shear zones) post-date the amphibolite foliation. At a third locality, slightly further east, crossite is associated with chlorite and muscovite. Ar/Ar dating of hornblende yielded an age of 91 Ma (Turonian). The outcrop was interpreted as a fragment of an ophiolite and its metamorphic sole, which both experienced HP/LT metamorphism, in contrast to the dismembered Alihoca ophiolite further north that is unmetamorphosed.

Konya area (Area 2)

To the NW of the Bolkar Dağ area, discussed above, the regional Anatolide meta-carbonate platform extends over a huge area, although largely obscured by a cover of Neogene–Recent deposits (MTA 2002; Figs 3, 4, 5). The Konya area is important for three main reasons. First, pre-Permian 'basement' of the Anatolides is uniquely well exposed there; second, the upper part of the platform succession and a transition to melange are well exposed in a less recrystallized and metamorphosed state than in other areas. Third, little-metamorphosed melange can be traced southeastwards to link up with unmetamorphosed melange and related units associated with unmetamorphosed Tauride units.

Platform and basement. The metamorphosed Mesozoic Anatolide carbonate platform is underlain by a heterogeneous unit, recently renamed the Konya Complex (Robertson & Ustaömer in press), which is largely outside the scope of this paper. In general, this 'basement' includes Silurian-Devonian neritic meta-carbonates, Lower Carboniferous limestones, a melange composed of limestone, volcanics and black chert (lydite) of Silurian–Lower Carboniferous age in a matrix of terrigenous turbidites and debris flows. There is also a thick unit of volcanic rocks that is assigned a Carboniferous age because it lies beneath the regional Permian–Triassic unconformity (Eren 1993; Özcan *et al.* 1988; Eren *et al.* 2004; Göncüoğlu *et al.* 2007). These volcanics and the Konya Complex generally have experienced HP/LT metamorphism of presumed Alpine age (Eren 2001; Eren *et al.* 2004; Candan *et al.* 2005). The Konya Complex is locally overlain by shallow-marine, mixed siliciclastic/carbonate sediments with a rich fauna of inferred late Middle to Late Permian age (Göncüoğlu *et al.* 2003). In the east, the succession passes without a break into siliciclastic and shallow-marine carbonates of Lower Triassic age. Elsewhere, a Triassic succession overlies the Konya Complex unconformably. A siliciclastic succession grades upwards into shallow-water carbonates of Early Triassic age and then passes into thick neritic carbonates of Middle Triassic to Cretaceous age (Berriasian–Lower Maastrichtian; Özcan *et al.* 1988).

Transitional unit. We observed relatively unmetamorphosed Upper Cretaceous transitional facies between the neritic carbonate platform and melange with unusually well-preserved calcareous microfossils (e.g. *Globotrunca* sp.) to the west of Konya (Fig. 8). In this area, the higher, exposed levels of the carbonate platform are finely recrystallized, thick-bedded, shallow-water limestones with abundant shallow-water fossils (e.g. rudist bivalves). These sediments are followed by thin-bedded pelagic limestones, with abundant bedding-parallel lenses and nodules of chert of diagenetic replacement origin (e.g. exposed near the Konya–Seydişehir road). The highest levels of the pelagic limestones and cherts have been redeposited as debris flows, including platy chert clasts in a micritic matrix. Slumped cherts are overlain by *c*. 20 m of sheared shales, marking the base of the melange, in which the matrix has been dated as Middle–Upper Maastrichtian to ?Paleocene (Özcan *et al.* 1988).

Melange. The melange in the Konya region is exposed over a very large area, extending southeastwards from the exposed Mesozoic platform (Fig. 8). Coherent shallow-water carbonates were mapped in this area by MTA (2002). However, we observed only melange dominated by blocks of shallow-water limestone, many of which contain the debris of rudist bivalves. Pelagic limestone blocks include abundant replacement chert with *Globotruncana* sp., similar to the Upper Cretaceous limestones beneath the melange. The neritic limestones typically form trails of elongate blocks ('mega-boudins'), up to several hundred metres long by tens of metres thick. Bedding is well preserved internally and most limestones are relatively undeformed. The pelagic sediments generally comprise smaller blocks ($<$10 m) that include pink and grey pelagic limestone, with or without diagenetic chert, with occasional blocks of red ribbon radiolarite.

The matrix of the melange is both sedimentary (i.e. sheared brown mudstone and local volcaniclastic sandstone) and ophiolitic (i.e. sheared serpentinite) in directly adjacent areas.

Ophiolite and metamorphic sole. Melange exposed near Konya is structurally overlain by serpentinized hartzburgite (Fig. 8); this locally contains abundant hydrothermal magnesite. Along its western margin the melange dips beneath the ophiolite, whereas the eastern margin of the ophiolite is a north–south-trending neotectonic strike-slip fault. In addition, large ophiolitic blocks, mainly serpentinized hartzburgite, are scattered through the melange,

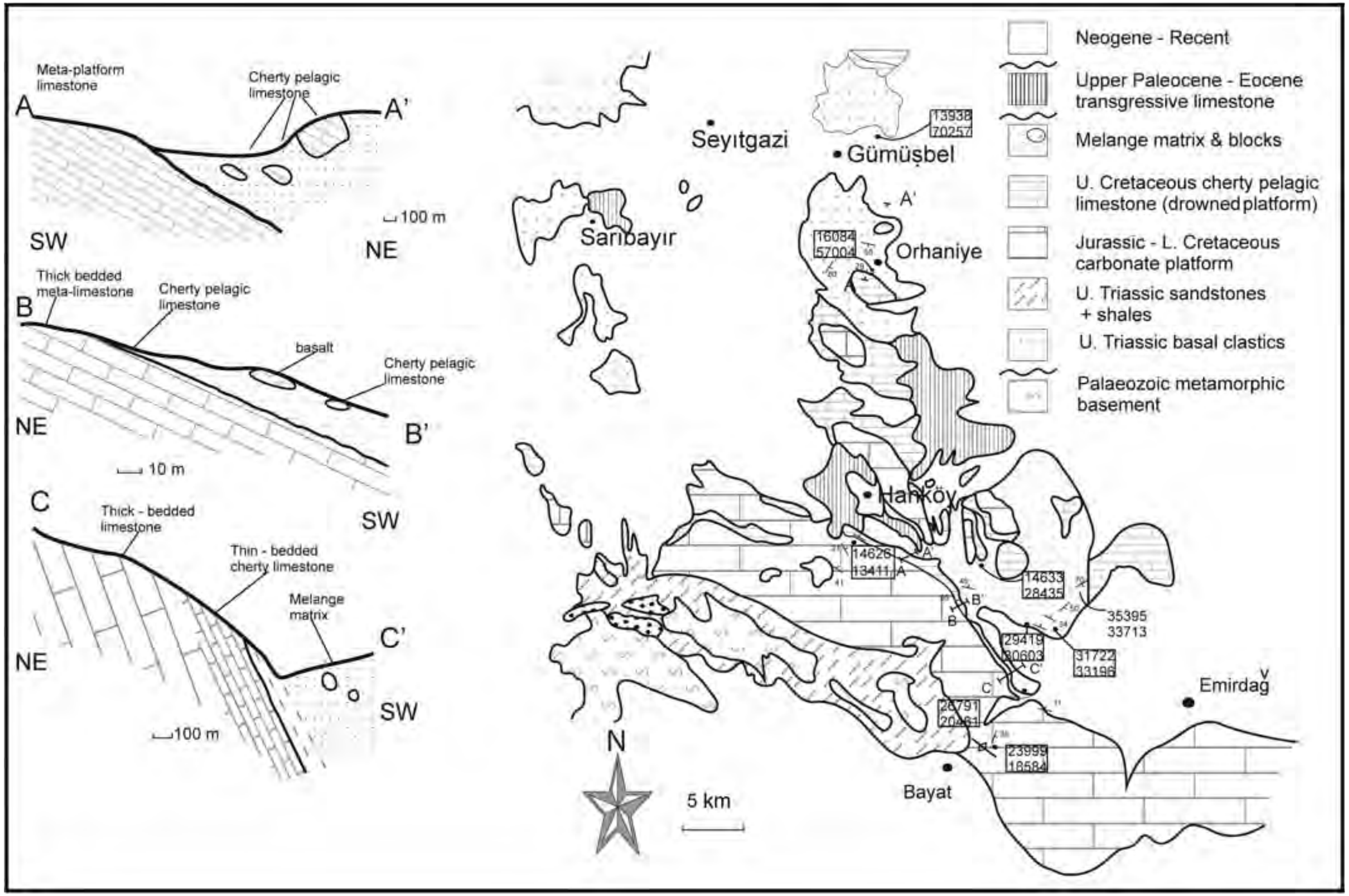

Fig. 8. Outline geological map of the large exposures in the area near Konya (Area no. 2) in which the entire Anatolide platform succession and 'basement' are well exposed. See Figure 5 for location and the text for discussion. Data are the 1:500 000 geological map of Turkey (MTA 2002), Özcan *et al.* (1990), Eren (1993) and this study. The map details are from the Turkish 1:100 000 topographical maps Konya M28 and M29.

together with rare dunite, gabbro, sheeted dykes (commonly rhodingitized) and pillow lava. Hartzburgite blocks, up to several hundred metres in size, locally include an attached metamorphic sole (near Karadiğin; Daşçi 2007). This is *c*. 450 m long by up to 35 m thick and comprises amphibolite, schist and garnet amphibolite, with interlayers of pinkish meta-chert. Several smaller amphibolite blocks (<10 m in size) are found within the adjacent melange.

Altınekin (Area 3)

Lying to the NW of the Konya area, described above, this area is notable because geochemical evidence has been used to argue for a tectonic model in which all of the melange and related units were thrust from a far-distant suture zone (İzmir–Ankara–Erzincan suture zone) hundreds of kilometres away to the north of the Niğde–Kırşehir Massif (Floyd *et al.* 2003).

Platform. There is no direct continuity of outcrop from the metamorphosed Anatolide carbonate platform exposed in the Konya area. However, the platform is likely to be continuous beneath young cover sediments (MTA 2002). The carbonate platform in the Altınekin area is exposed on low hills protruding above a young cover, as seen to the south and SE of Altınekin (Figs 3d, 4 & 9). Thick-bedded meta-platform carbonates are well exposed to the north of the Konya to Aksaray main road. The platform in this area is folded into several large open anticlines and synclines, generally along WNW–ESW axes.

Relatively low stratigraphical levels of the platform succession in the east (e.g. near 05617:23370), of Triassic age (Özcan *et al.* 1990), are dominated by alternating thinner- and thicker-bedded quartz-rich meta-sandstones, locally isoclinally folded. Individual sandstone beds, *c*. 20 cm thick, are interbedded with pelitic sediments (20–40 cm thick). The sandstones exhibit scoured bases and sharp, flat tops, suggestive of traction deposits. Elsewhere (05955:23988), thin- to medium-bedded quartzose sandstones and phyllites, with local nodular chert horizons and lenses of black marble (2 m thick × 6 m long), pass upwards into dark marble, and then into thick-bedded dark dolomite with abundant stromatolites, of inferred Mid-Eocene Triassic age. A transition is well exposed on low hills in this area over *c*. 30 m. Similar dark marble is seen on another low hill *c*. 1 km to the WNW (02829:25610), where a relatively sharp depositional contact exists between dark dolomite below and grey thin-bedded marble above. Further east (e.g. near Kışören 13319:19937) thick-bedded carbonates locally pass upwards into calc-schist and phyllite.

Transitional unit. The meta-platform succession, of Triassic–Early Cretaceous age, is followed northwards by a contrasting sequence of meta-pelagic carbonates, meta-calciturbidites and meta-shales, dated as Late Cretaceous (Özcan *et al.* 1990). Metasediments to the north are folded and reverse faulted. Exposures in this area are again restricted to low hills and ridges surrounded by young sediments. Folded successions of mainly meta-pelagic carbonates are seen on hills to the south of the area shown in Figure 9 (near 32698:90125). Medium- to thick-bedded pinkish marbles *c*. 200 m thick there are overlain by thinner bedded siliceous meta-limestones. Higher levels of the sequence are exposed on the southern limb of a large WNW–ESE-trending anticline; there, cherty meta-pelagic limestones pass upwards into meta-clastic sediment (psammitic schist) *c*. 50 m thick, which exhibits local slump folding. An isolated hill to the SE exposes steeply dipping, very dark-coloured siliceous limestone. Siliceous marble passes depositionally upwards into medium-to thick-bedded, well-laminated meta-sandstones and meta-shales, *c*. 60 m thick. These sediments are cleaved and folded. Within the map area (Fig. 9) the contact with the melange to the north is a normal fault, probably related to later-Cenozoic post-collisional deformation.

The area shown in Figure 9 is folded along nearly east–west axes, such that an original, unfaulted contact is exposed in some areas between the platform and the melange (e.g. SW of Korkayak Tepe). For example, in the east of the area (i.e. NW of Akçasar), thin- to medium-bedded pink siliceous meta-pelagic limestones contain local dark organic-rich layers and pass upwards into calc-schist and epidote-rich greenschist, interbedded with marble. Southwards, this is followed abruptly by sheared serpentinite marking the base of the melange (Fig. 9).

Transitional facies between the carbonate platform and the melange are also locally exposed further NW around Altınekin town (Fig. 9). Well-bedded, folded, quartz-rich meta-sandstones (schists) occur as alternating darker and lighter layers *c*. 1 km south of Altınekin. Slightly further north (north of the road) folded meta-sandstones (up to 60 m thick locally) include an exceptionally thick massive sandstone bed (>8 m thick), interpreted as deposits from a high-density turbidity current. This is overlain by meta-serpentinite marking the base of the melange.

Melange. Two different melanges have been reported from this area: first, ‘Altınekin melange’

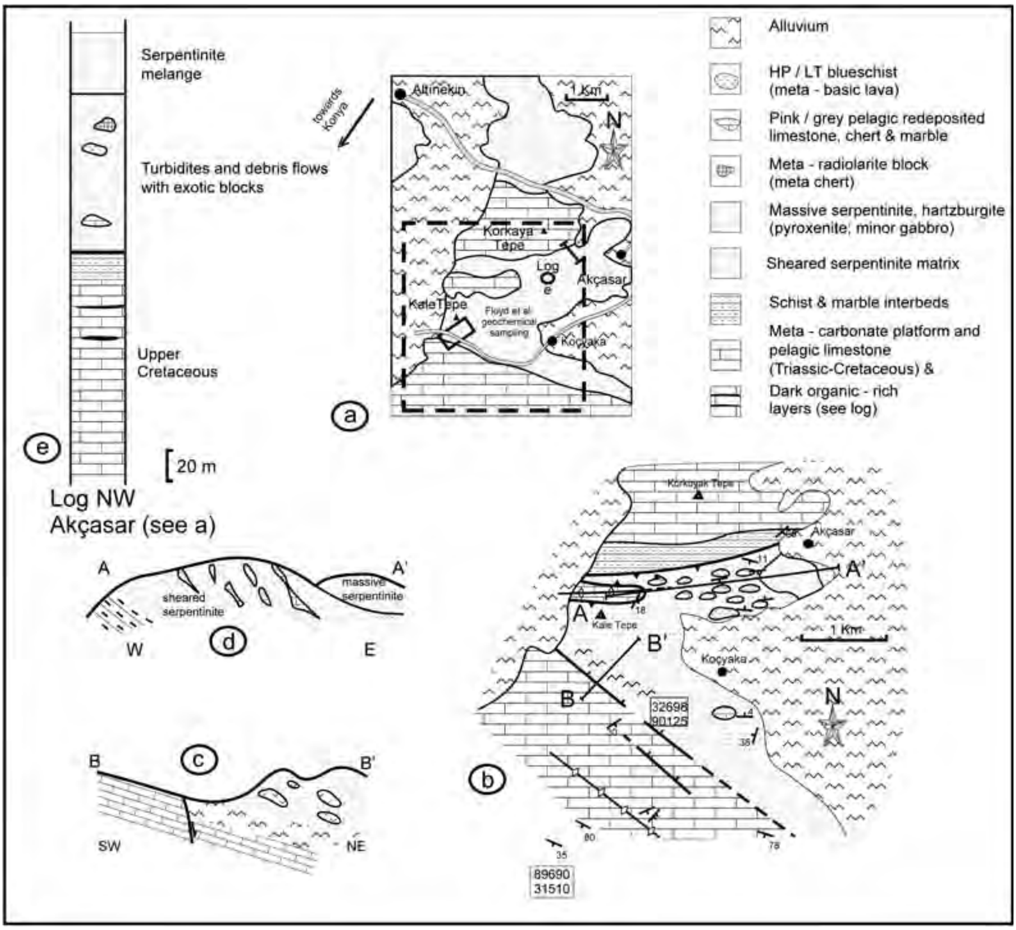

Fig. 9. Outline geological map of exposures in the area near Altınekin (No. 3) where melange is especially well exposed. See Figure 5 for location and text for discussion. Data from Floyd *et al.* (2003) and this study. The map details are from the Turkish 1:100 000 topographical map Ilgın L29.

with a mainly meta-sedimentary matrix; and second, 'Akçasar melange' with a mainly ophiolitic matrix (Özgül & Göncüoğlu 1999; Floyd *et al.* 2003). However, we observed that these two melange types are intergradational. Also, we calculate that the exposed thickness of the melange is only several hundred metres, much less than previously reported (*c.* 3500 m). This is because the regional dips are low and the melange and underlying platform are repeated by folding. The melange is especially well exposed on a vegetation-free ridge between Kale Tepe and Akçasar (Fig. 9). On the west of this ridge the melange (near Kale Tepe) includes blocks of vesicular metabasalt, diabase, gabbro, foliated amphibolite (meta-basalt), marble and also hartzburgite (with minor chromite) and pyroxenite. Locally, the matrix is sheared serpentinite (locally talc-rich) and calc-schist. Meta-basite blocks include blue amphibole (glaucophane), as described by Floyd *et al.* (2003). Larger blocks include much less recrystallized meta-basalt and diabase/microgabbro breccia (up to 80 m thick), with intercalations of well-bedded meta-pelagic limestone and bedded chert. Smaller blocks include recrystallized bioclastic limestone, marble and foliated muscovite schist.

The melange is well exposed *c.* 1 km further SE, towards Koçyaka (Fig. 9), where the matrix is mainly sheared dark phyllite and includes larger (tens of metres) and smaller (metre-sized) blocks of meta-basalt and meta-carbonates. In general, larger blocks (>5 m) retain traces of original bedding, whereas smaller blocks tend to be sub-rounded, structureless and more recrystallized. Local successions of meta-lava, meta-volcaniclastic sediment and meta-carbonate are again visible within larger blocks. The matrix is thin-to medium-bedded lithoclastic sandstone with small exotic clasts (e.g. marble). The melange matrix is variably folded (e.g. isoclinally) on an outcrop scale. Many of the more competent lithologies show a well defined, nearly north–south trending stretching lineation, which is inferred to relate to tectonic exhumation of the melange (see *Tectonic processes section*).

Additional excellent melange exposures are found on a broad ridge SW of Akçasar (Fig. 9), where the matrix is mainly sheared serpentinite containing lenses and blocks of schistose meta-lava (blueschist), marble (up to 4 m in size) and metachert. Relict bedding is strongly extended such that many of the blocks are elongate (i.e. phacoid shaped). The serpentinite matrix encloses elongate slices of calc-schist, which in turn entrain small exotic blocks (e.g. radiolarite).

Where the serpentinite matrix is less highly strained we observed a definite sedimentary fabric; e.g. 0.8 km NW of Koçyaka (Fig. 9b). Strands of sheared serpentinite, typically <1 m thick, incorporate matrix-supported conglomerate with elongate (3×15 cm), to sub-rounded (<15 cm) clasts of lava, ultramafic rocks (e.g. dunite) and marble set in a matrix of sheared clastic serpentinite. Several of the matrix-supported serpentinitic facies are folded disharmonically, probably as a result of syn-sedimentary deformation. The highest structural levels of the melange are exposed in the east near Akçasar, where there is a large body of massive sheared harzburgitic serpentinite (several hundred metres long by tens of metres thick).

Çeşmisebil (Area 4)

An important question is how far north do the regional metamorphosed Anatolide platform and related melanges extend? Where exposed, the platform, overlying melange and ophiolitic units dip regionally northwards at a low angle, with repetitions caused by folding and local faulting. The platform, melange and ophiolitic rocks appear from beneath young cover sediments near Çeşmisebil, further NE (Fig. 10). In this area, the carbonate platform is almost entirely covered by Neogene–Recent sediments but there are small outcrops, most notably in the Cihanbeyli area, near Çeşmisebil village (Figs 5 & 10), where we observed melange, overlying ophiolite and remnants of a metamorphic sole.

The melange is underlain by a coherent unit of thick-bedded, isoclinally folded marble that exhibits a well-developed NNE–SSW-trending stretching lineation (Fig. 10). This limestone is tentatively inferred to be part of the underlying Anatolide carbonate platform, but a large block within the melange cannot be excluded because exposure is very limited. A thin strip of sheared serpentinite separates the thick-bedded marble from *metamorphic* melange above. The melange is characterized by large blocks of meta-carbonate (up to several hundred metres in size), some of which are dark coloured, unaltered and exhibit a fine microbial lamination. The limestone blocks are set in a matrix of poorly exposed, sheared phyllite. Several of the blocks, together form a low hill (Fig. 10). An enclosing shale/schist matrix was later eroded to leave a limestone knoll flanked by scree breccias and immature conglomerates. These carbonates are karstified giving the false impression of the existence of a single much larger limestone block. Slightly further north, the melange includes small (several metre-sized) blocks of recrystallized white limestone rich in nodular chert.

Northwards, the metamorphic melange is overlain by a contrasting *unmetamorphosed* melange. This includes blocks of aphyric and feldspar-pyroxene-phyric basalt, pink pelagic limestone, brecciated limestone, red ribbon radiolarites, dark manganiferous radiolarite (jasper), black pyrolusite, and red/purple mudstone, set in an unmetamorphosed shale matrix.

The unmetamorphosed melange passes northwards into a thin interval of melange with blocks set in a sheared serpentinite matrix. This is structurally overlain (northwards) by a large intact slice of hartzburgite and subordinate dunite. Directly north of Çeşmisebil village (Fig. 10) the ophiolite is underlain by a small slice of brecciated amphibolite, encased in serpentinite; this is interpreted as a fragment of a metamorphic sole. Thin-section examination revealed a texture of coarse, preferentially aligned amphibole crystals imparting the foliation seen in hand specimen. Above this, an extensive ultramafic sheet is cut by numerous diabase and gabbro dykes, similar to those described from the Konya area. Individual dykes, up to 25 m thick individually, exhibit chilled margins and are strongly sheared. We interpret this as an ophiolite slice that was intruded by dykes and later strongly sheared, rather than as serpentinitic melange because exotic units are absent.

Kandil köy (Area 5)

We have investigated the relationship between the Anatolide units and the widely exposed Ankara Melange further north (Fig. 5), mainly to determine whether or not a definite tectonic boundary exists between these two regional tectonic units. Unfortunately, exposures in the intervening area are few and far between because there is an extensive cover of Neogene to Recent sediments. Equivalents of the Anatolide melange of the Afyon–Bolkardağ zone are exposed, but not the HP/LT rocks of the

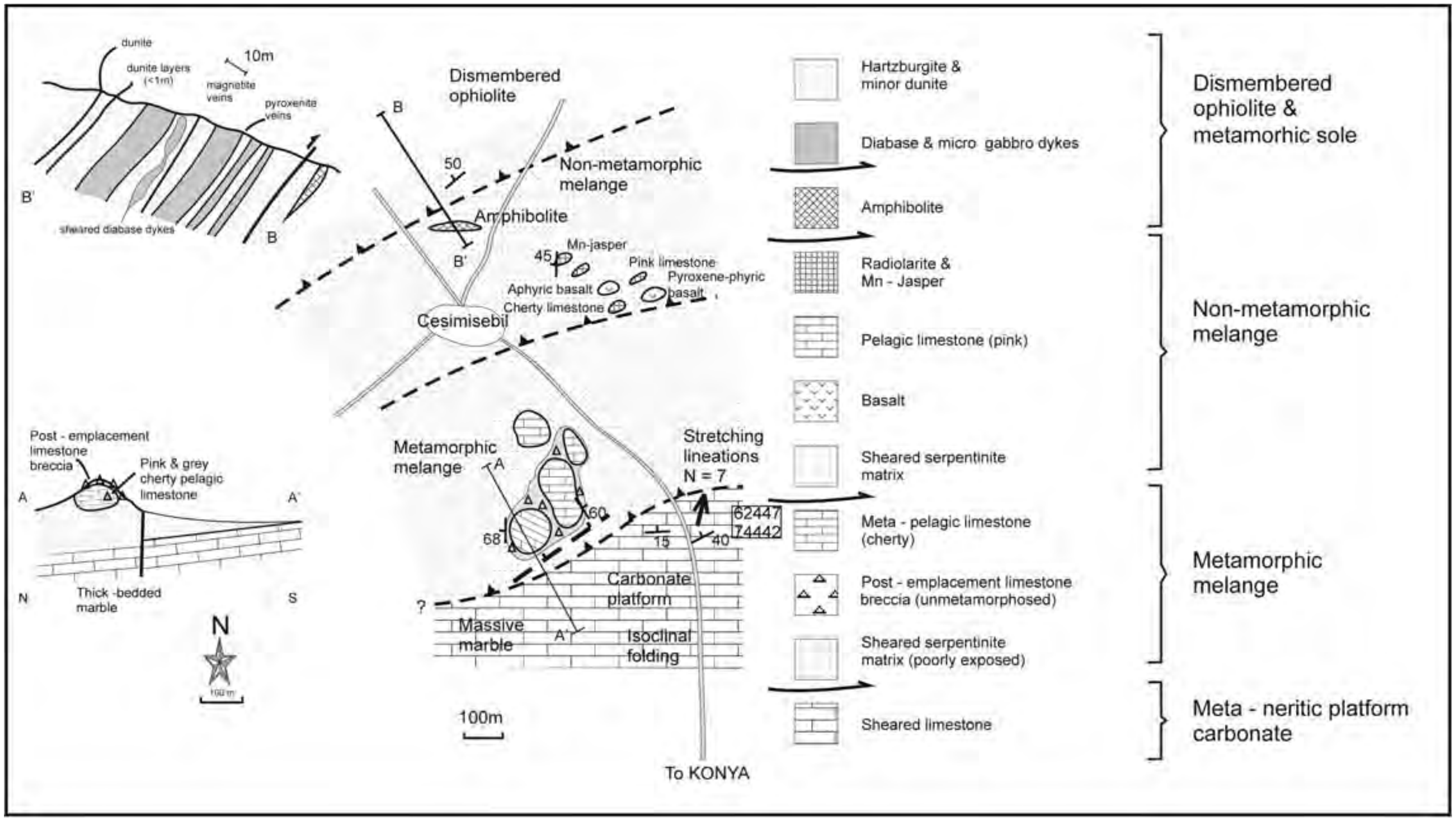

Fig. 10. Outline geological map of limited exposures in the north of the area near Çeşmisebil (No. 4), where a metamorphic sole is locally preserved between melanges below and ophiolites above. See Figure 5 for location and the text for discussion. The map details are from the Turkish 1:100 000 topographical map.

Tavşanlı zone, requiring modification of the regional tectonic map of Okay and Tüysüz (1999).

The best exposed of these areas is a NW–SE trending outcrop near Kandil Tepe (GPS 59758: 11814; Fig. 11) that is controlled by Neogene faulting. The northern slopes of Kandil Tepe are characterized by large elongate blocks of weakly recrystallized fossiliferous neritic limestone in a matrix of sandstone turbidites and shale. Southwards, capping Kandil Tepe, a strip of serpentinite-matrix melange encloses blocks of neritic limestone (up to 6 m across), radiolarian chert, pegmatitic gabbro, cumulate gabbro and massive gabbro; southwards, more homogenous sheared serpentinite with blocks of diabase/gabbros is exposed. The tectonic units and the individual blocks are orientated NW–SE *parallel* to the regional trend of the Anatolide ophiolites and melange further south.

Additional outcrops of melange *c*. 30 km further north, near Yeşilyurt, are dominated by similar blocks of weakly metamorphosed neritic limestone (up to hundreds of metres in size), unrecrystallized radiolarites and local redeposited limestone (calcarenite with volcanic lithoclasts), together with sheared serpentinite, massive basalt, volcanic breccias, gabbro and serpentinite, all set a matrix of volcaniclastic sandstone (turbidites and debris flows) and shale. Large blocks of oolitic and bioclastic limestone, shown on the 1:500 000 geological map of Turkey (MTA 2002), protrude above a young sediment cover with little or no exposed matrix (e.g. Karacadağ–Kozanlı area; GPS 83446: 19120). The lithological assemblage in this more northerly area (near Yeşilyurt) includes large blocks of unmetamorphed Cretaceous neritic limestone as commonly seen in the Ankara Melange further north (Rojay *et al.* 2004). The strike of the blocks and the melange fabric is north–south, *parallel* to the fabric of the Ankara Melange. A contact between the Anatolide-related melange and the Ankara Melange could, therefore, tentatively be placed between Kandil Tepe and Yeşilyurt (beneath a Pliocene basin). However, it is probable that the two melanges are in reality intergradational.

Yunak (Area 6)

The platform, melange and an intact ophiolitic unit are again exposed over a large area further east, near Yunak (Figs 5 & 12). This area has experienced high-angle faulting, of presumed late-collisional or post-collisional age, so that an initial task was to restore the tectono-stratigraphy. West and north of Yunak (e.g. GPS 89732:95726), thick-bedded metacarbonates are in high-angle fault contact with an ophiolitic unit, up to 500 m thick. East of Yunak the carbonate platform is thrust northwards over an ophiolitic unit, as seen near Böğrüdelik, and

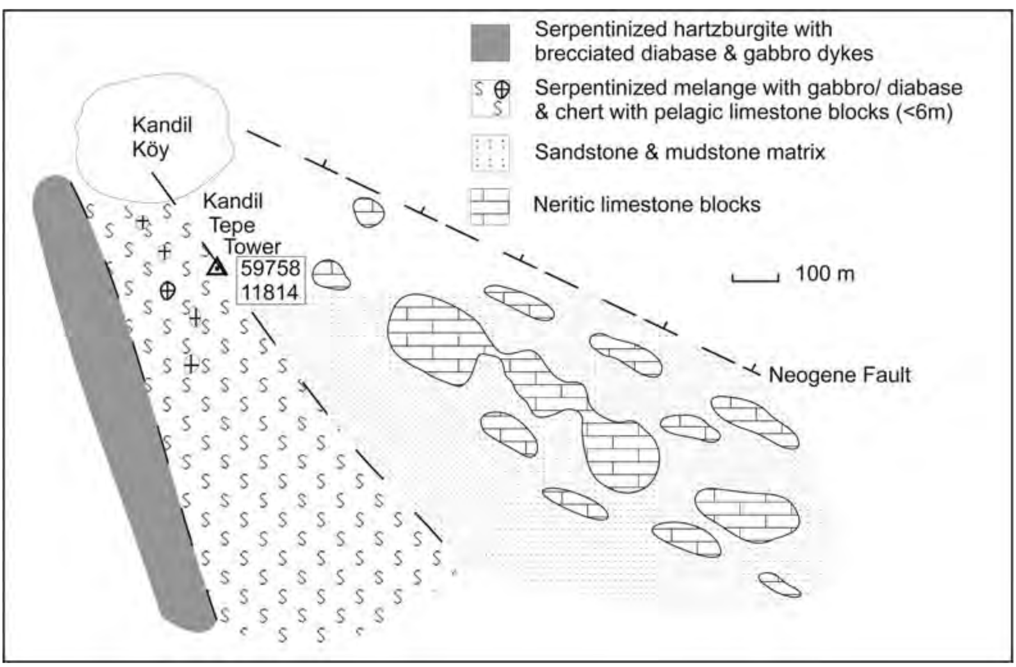

Fig. 11. Outline geological map of the Kandil area (No. 5) between the Kütahya-Bolkardağ zone to the south and the Ankara Melange to the north. See Figure 5 for location and the text for discussion.

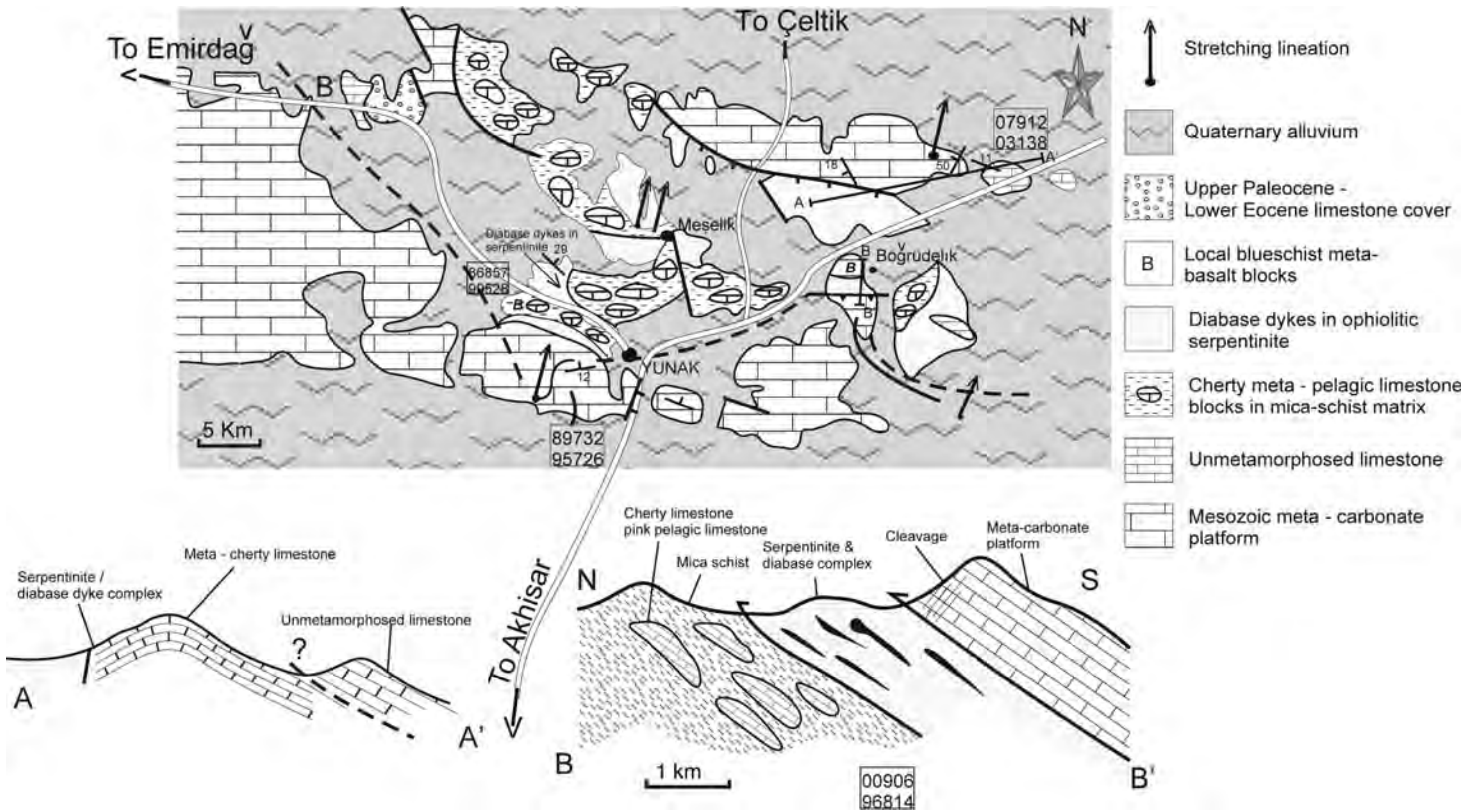

Fig. 12. Outline geological map of the Yunak area (No. 6), a large exposure of the contact between the Anatolide carbonate platform and melange. The map details are from the Turkish 100 000 topographical map Ilgın k27. The data are from this study and the 1:500 000 geological map of Turkey (MTA 2002). See Figure 5 for location and the text for discussion.

this, in turn, is thrust over melange, locally reversing the regional thrust-emplacement stacking order. This deformation probably resulted from collision-related re-thrusting (see *Tectonic processes*).

The Anatolide carbonate platform in this area is highly recrystallized and shows a well-developed cleavage, especially near the top of the succession. The highest levels locally comprise thick-bedded, dark, massive, foliated marble. A regionally consistent nearly north–south, low-angle stretching lineation is well developed in argillaceous facies near the top of the platform succession and is attributed to exhumation (see *Tectonic processes*).

Melange. The melange is dominated by blocks of recrystallized cherty pelagic limestone, or by massive chert-free marble in one local area. Large blocks of altered pink, thin- to medium-bedded recrystallized limestone alternate with bedded replacement chert (up to 30% of the rock by volume) (e.g. near Böğrüdelik, Fig. 12). Blocks are set in a matrix of brown meta-shale and meta-sandstone (phyllite and mica schist). Stretching lineations are locally well developed and C/S fabrics locally indicate top-north transport (e.g. near Meşelik).

Higher levels of the melange are exposed in the NW (locality B on Fig. 13), where detached blocks of glaucophane-bearing blueschist occur within lenticular sheared serpentinite, *c*. 200 m wide.

In addition, a small isolated outcrop of thick-bedded bioclastic limestone with common nodules of replacement chert in the NW of the area is unmetamorphosed and undeformed (07912:03138). This is assumed to be a melange block that escaped metamorphism.

Ophiolite. In the Yunak area the ophiolite is dominated by serpentinized hartzburgite, cut by swarms of diabase and microgabbro dykes that exhibit well-developed chilled margins. Dykes, up to 15 m thick, make up 30–40% of the ophiolitic outcrop. In thin section, chilled margins of the dykes comprise altered diabase, in which altered pyroxene phenocrysts are set in a mesostasis including strongly altered plagioclase microphenocrysts. Locally, ophiolitic dunite is cut by diabase and gabbro dykes, up to 4.5 m thick. Many of the dykes are strongly sheared to form lozenge-shaped blocks or lenses within serpentinite. This unit is classified as dismembered ophiolite rather than ophiolitic melange (as at

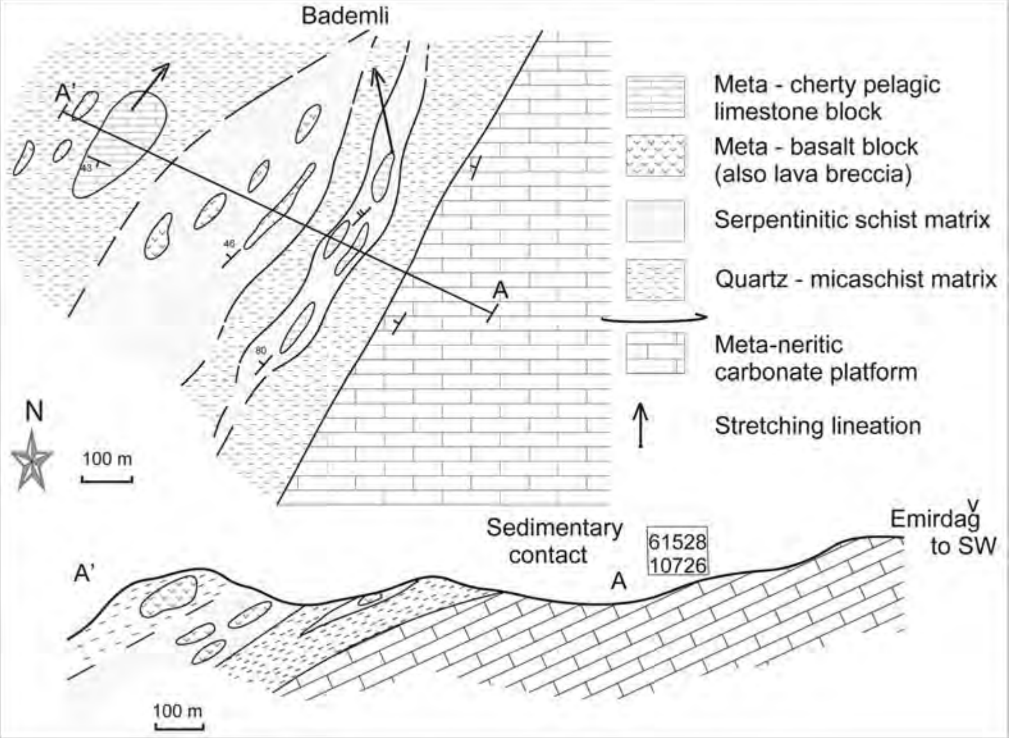

Fig. 13. Outline geological map of the Bademli area (No. 7), which includes a small exposure of the contact between the Anatolide carbonate platform and the Anatolide melange. See Figure 5 for location and the text for discussion. The map details are from the Turkish 100 000 topographical map.

Çeşmisebel; see above). Where the ophiolite/diabase dyke unit is underlain by melange, the contact zone includes purple to green schistose serpentinite with blocks of meta-chert (jasper).

Bademli (Area 7)

This relatively small area along the northern edge of the Emirdağları, near Bademli (south of Davulca; Figs 5 & 13) is important as it demonstrates the presence of 'melange-within-melange' fabrics. These indicate polyphase melange genesis by a combination of tectonic and sedimentary processes. Further south the Anatolide carbonate platform (Emirdağ) is folded on a large-scale. However, in the north, locally, well-bedded meta-platform carbonates dip gently northeastwards beneath the melange. In contrast to areas further east, preserved transitional facies are minimal in this area. Instead, there is a sharp transition over several metres from thick-bedded marble, to buff-coloured phyllitic marble, and then to grey phyllite marking the base of the melange (e.g. 61528:10726).

Melange. Serpentinite melange first appears *c.* 60 m above in the carbonate platform as sheared hartzburgite that encloses blocks of meta-basalt (greenschist). Above, meta-sandstone turbidites envelop lozenge-shaped masses of sheared serpentinite that themselves entrain blocks of metabasalt. Associated dark phyllites contain small marble blocks (<4 m in size). Higher structural levels of the melange are dominated by a broken formation including pink siliceous limestone extending for several kilometres northwards towards Davulca (not studied in detail).

Bayat area (Eastern Kütahya) (Area 8)

This is part of the eastern Kütahya area of Özcan *et al.* (1989), here termed the Bayat area after a local town (Figs 5 & 14). The main importance of this area is that is exposes a pre-Triassic metamorphic basement that contrasts with the Konya area to the west (see above); it also exhibits the most complete Mesozoic cover sequence, well-exposed melange including blueschist blocks and unconformably overlying shallow-water sediments that help constrain the timing of exhumation (see *Tectonic processes*).

Carbonate platform and basement. An intact platform succession unconformably overlies a pre-Triassic metamorphic basement, cut by meta-granitic

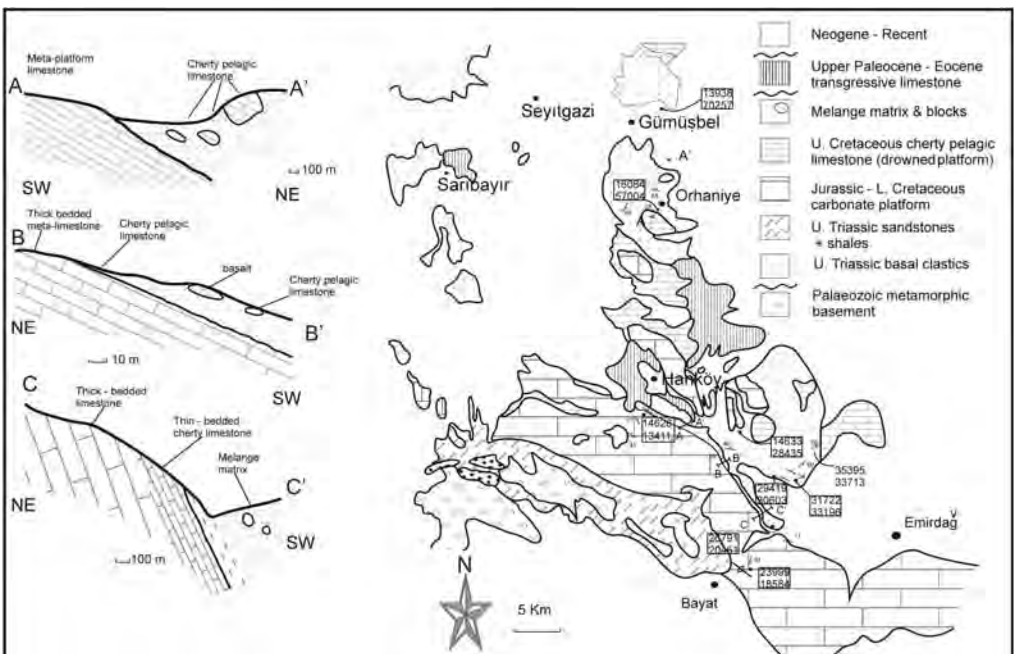

Fig. 14. Outline geological map of the Bayat area (Eastern Kütahya area) (No. 8). See Figure 5 for location. Data from the 1:500 000 geological map of Turkey (MTA 2002), Özcan *et al.* (1988) and this study. See text for discussion. The map details are from the Turkish 1: 100 000 topographical maps Eskişehir J 25 and J 26.

rocks. This has been correlated with the Late Precambrian basement of the metamorphic Menderes Massif (Candan *et al.* 2005; Dora *et al.* 2001). The unconformably overlying succession begins with varicoloured conglomerates, sandstones and shales, followed by dolomitic limestones (wackestones) with fossils of Early Triassic age (Induan–Olenekian) (Özcan *et al.* 1988, 1989; Göncüoğlu *et al.* 2003). We observed that the succession passes conformably upwards into dolomitic carbonates containing large bivalves (Megalodonts) and then into thick-bedded mainly dolomitic meta-carbonates (marbles). The Triassic part of the succession is repeated by a broad NW–SE-trending kilometre-scale anticline (Fig. 14). The southern limb *c.* 4 kilometres north of Bayat (23999:18584) exhibits alternations of thinly bedded, laminated, dolomite, dolomitic limestone, thick-bedded sugary dolomite and local lenses of carbonate conglomerate. Gently northward-dipping dark, well-laminated dolomitic and microbial carbonates platform of Mid-Late Triassic age (Anisian–Norian) are well exposed on the northern limb of the anticline (26791:2046), followed by neritic carbonates of Late Jurassic–Early Cretaceous age.

Transitional facies. Previously, the contact between the Anatolide platform and the melange was reported to be mainly a ductile shear zone in this area (Candan *et al.* 2005). However, we observed the existence of sedimentary transitions, up to several tens of metres thick, from neritic platform carbonates, through pelagic and redeposited facies (e.g. Eskigömü–Bayat road; 22452:26180), to melange (e.g. Sülüklü area; 24133:28435; Fig. 14). Planktonic foraminifera from the transitional units have yielded an Early Maastrichtian age, while the sedimentary matrix of the overlying melange is reported to be of Early Maastrichtian–Early Paleocene age (Özcan *et al.* 1989; Göncüoğlu *et al.* 1992; Göncüoğlu *et al.* 2000; our unpublished data).

The thicknesses of Upper Cretaceous pelagic and redeposited facies above the neritic carbonates vary markedly along strike. For example, several kilometres south of Hanköy (14626:34111) thick-bedded neritic meta-carbonates pass depositionally upwards into thin-bedded cherty pelagic limestone (<5 m thick) and then into grey phyllite with detached blocks of siliceous limestone (up to several metres in size). Some of individual clasts are tectonically brecciated and reworked in a matrix of pink pelagic limestone. Elsewhere, platform carbonates pass upwards into alternations of dark phyllites, thin- to medium-bedded meta-calciturbidites and meta-pelagic carbonates with nodules and lenses of chert of diagenetic origin. Coarse calcarenite, in beds up to 1 m thick, contain numerous shale (phyllite) clasts (<2 cm in size). Local interbeds of limestones conglomerate (up to *c.* 1 m thick) contain flattened limestone clasts (up to 15 cm long × 5 across). Individual sandstone beds near the top of the transitional unit are rich in quartz and muscovite, interbedded with cherty pelagic limestones and form depositional units up to 20 m thick. The highest levels of the transitional interval include quartz-rich turbidites, in beds up to 60 cm thick, often preserved as sheared-out lenses (‘phacoids’). Large subequant blocks (2 m × 6 m) of marble are similar to the underlying platform carbonate facies. Relatively thin-bedded facies are cleaved and isoclinally folded, commonly preserved as small fold cores.

Melange. Melange in the Bayat area overlies the transitional unit with a low-angle thrust contact. In the south the lowest part of the melange is dominated by large, elongate, detached blocks of recrystallized red ribbon radiolarite and marble (Fig. 14), set in a phyllitic matrix. Dark-coloured phyllites are interbedded with matrix-supported conglomerate containing sub-rounded, to elongate, clasts of chert, limestone and siliceous limestone (4 × 28 m). An exotic slab of disrupted pelagic limestone (up to 25 m thick), contains abundant lenticular and nodular chert.

Northwards, the melange is repeated by two WNW–ESE-trending large-scale open anticlines (Fig. 14). On a limb of the southerly of these folds (near Gedikevi köyü: 35395:33713), blocks of relatively unmetamorphosed lava and volcaniclastic sediments occur, together with large limestone blocks (up to several hundred metres long by tens of metres thick), and also smaller blocks of sheared limestone/radiolarite alternations. Meta-lava ranges from aphyric, to feldspar-phyric basalt (greenschists), either vesicular or non-vesicular. Larger blocks preserve short intact successions; e.g. well-bedded volcaniclastic sandstone passing into pink pelagic limestone, with common manganiferous segregations. Primary volcanic textures include dark glassy basalt with rare altered plagioclase phenocrysts and feldspar microphenocrysts in a matrix of dark devitrified glassy basalt. The matrix of the melange in this southerly fold structure includes sheared interbeds of rubbly volcaniclastic, matrix-supported conglomerates with sub-angular clasts. These clasts are mainly pelagic limestone (up to 15 cm in size) with rare lava (both feldspar-phyric and aphyric). In this area, the matrix is dominated by medium-bedded, to thick-bedded quartzose sandstones, with sheared phacoidal fabrics and matrix-supported conglomerates, with sub-rounded clasts, up to 40 in size (e.g. near Kılıçlar village; 31722:33196 and at 29439:30603).

Melange is again exposed in the more northerly fold structure, where it directly overlies well-bedded marble (near Orhaniye: 16084:57004). This is dominated by large blocks (up to 60 × 130 m) of thin-bedded grey pelagic limestone rich in metachert, together with large blocks of pillow lava (up to 30 m in size) within cleaved sandstone turbidites.

The highest exposed levels of the melange are seen further north again (near Gümüşbel 13938:70257), where very hard-weathering blocks of blueschist, up to 5 m in size, are set in a matrix of sheared serpentinite. This area was previously mapped as a coherent ophiolite ('Kınık ophiolite'), with a metamorphic sole (Özcan *et al.* 1989). However, the outcrop is entirely melange, with glaucophane-bearing blueschist blocks in a matrix of sheared serpentinite.

The carbonate platform and melange combined, are unconformably overlain by gently dipping, Nummulitic limestones of Paleocene (Selandian–Thanetian)–Early Eocene age (Özcan *et al.* 1989). Where examined, near Sarıbayır in the west (Fig. 14), poorly exposed melange is directly overlain by unconsolidated conglomerate containing clasts derived from the subjacent melange (e.g. red chert, pelagic carbonate, marble and lavas). Clasts vary from angular, to sub-rounded, to rounded, and up to 40 cm in size. A few thick interbeds of microconglomerate, to coarse sandstone occur, in beds up to 60 cm thick. The succession passes through several metres of pebbly mudstone and marl and then into Nummulitic limestone.

Tavşanlı zone

We have made observations on the melange and related unit in three main outcrop areas of the Tavşanlı zone.

Sivrihisar (Area 9)

The Sivrihisar area (Fig. 5) to the north of the Bayat area, discussed above, is important as it includes well-documented very high-pressure rocks, and also evidence of collision with the Sakarya zone to the north. The Sivrihisar area (Fig. 15) exposes several platform-related units, structurally overlain by a large sheet of ophiolitic peridotite (Gauthier 1984; Monod *et al.* 1991; Whitney *et al.* 2001; Whitney & Davis 2006; MTA 2002).

In the south (Fig. 14, A-A′) an intact succession, shown as Late Palaeozoic in age on the 1:500 000 map of Turkey (MTA 2002) is exposed on both flanks of a NW–SE-trending mountainous ridge, where it comprises a hundreds-of-metres-thick unit of thick-bedded marble and micaschist, folded along east–west axes, with a locally well-developed stretching lineation. On the northern dip slope, this passes upwards, apparently conformably, into an alternating, soft-weathering sequence of schist and pelite, at least several hundred metres thick. These meta-clastic sediments are overlain, apparently conformably by very thick-bedded white sugary marble. On the dip slope of another hill further north this marble is overlain by a thin unit of tectonic melange (*c.* 50 m thick), mainly highly altered serpentinite (rich in hydrothermal magnetite) and green recrystallized chert.

The melange is overlain, above a northward-dipping thrust, by a large thrust sheet of serpentinized ultramafic ophiolitic rock that contains abundant podiform chromite and magnetite. To the east the melange zone thickens and includes basalt, radiolarite serpentinite and Upper Cretaceous pelagic limestone.

Previous studies have shown that the metamorphic sequence is well-foliated, isoclinally folded and contains numerous lenses of meta-basic rocks with a HP/LT mineralogy dated as Late Cretaceous in age (Sherlock *et al.* 1999). Whitney & Davis (2006) have identified numerous small lenses of unusual lawsonite ecologite within lawsonite blueschist, blueschist marble and quartzite within the northern end of the southerly platform-related massif *c.* 40 km NW of Sivrihisar. Lithologies in different parts of the massif suggest lower pressure conditions, however, implying that tectonic breaks are present (D. Whitney, pers. com. 2007). The lawsonite blueschist is indicative of metamorphic conditions of 21–24 kbar and *c.* 422–580 °C (Whitney & Davis 2006). The presence of lawsonite eclogite is witness to very rapid exhumation so as to preserve the mineralogy without retrogression (Whitney & Davis 2006). In the south, the metamorphic massif is intruded by Lower Eocene granites (Okay & Tüysüz 1999).

Additional important outcrops occur to the north of the main ophiolitic peridotite (Fig. 15). Previous studies indicate that, in the north, the ophiolitic peridotite is intersliced with low-grade-metamorphosed clastic sediments and volcanics including exotic blocks of inferred Permo-Triassic age (Gauthier 1984; Monod *et al.* 1991; MTA 2002; Fig. 15). This unit is mapped as overlain along its northern margin by unmetamorphosed neritic limestone of Middle Jurassic–Lower Cretaceous age, culminating in Upper Cretaceous pelagic limestone and sandstone. The low-grade unit and limestones are correlated with the Karakaya Complex and its later-Mesozoic cover, as exposed in the Sakarya zone to the north. In the SE (Fig. 15), the ophiolite is mapped as locally thrust over Lower–Middle Eocene terrigenous sediments and shallow-marine limestones (Monod *et al.* 1991; MTA 2002).

Eskişehir (Area 10)

This area further west (Fig. 5) provides some of the best exposures of well-dated melange, known as the Dağküplü melange (Göncüoğlu *et al.* 2000). Although previously described as a sedimentary

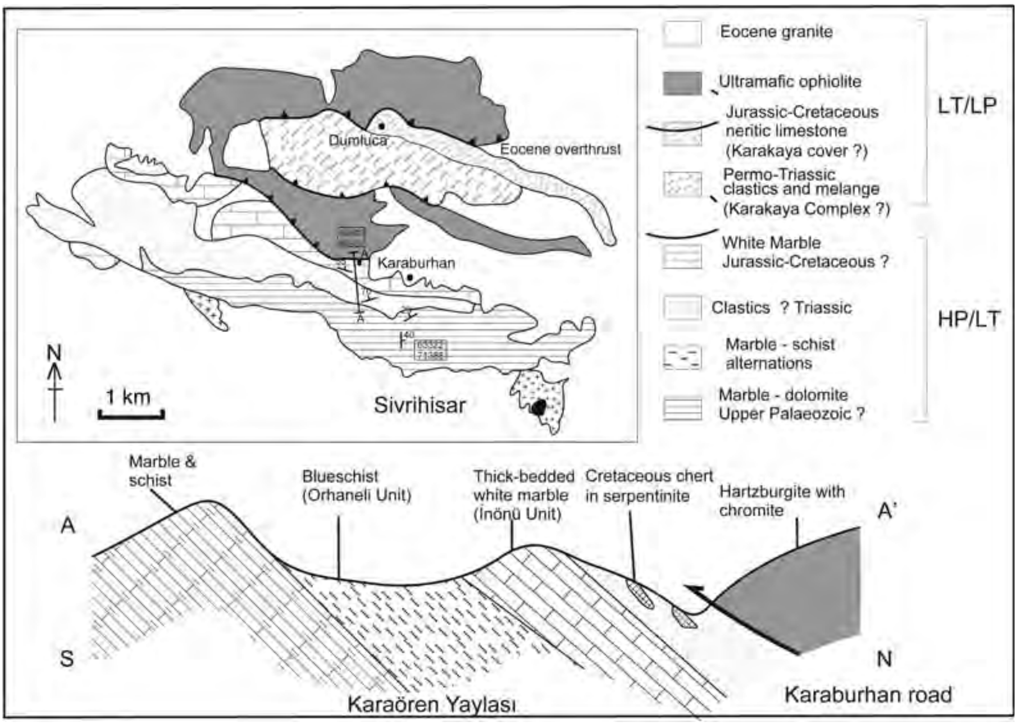

Fig. 15. Outline geological map of the Tavşanlı zone in the Sivrihisar area (No. 9). Data from 1:500 000 geological map of Turkey (MTA 2002) and this study. See Figure 5 for location.

olistostrome, our observations show that this melange should be re-interpreted as tectonic melange (see *Tectonic processes*).

The Dağküplü melange underlies a large sheet of serpentinised hartzburgite, above a regional north-dipping thrust (Fig. 16). The size and abundance of blocks within this melange generally increase towards the over-riding ophiolite. The melange is in faulted contact with metamorphosed carbonates and other less studied metamorphic units to the west. The melange includes blocks of basalt, serpentinite, pelagic limestone, radiolarian chert and

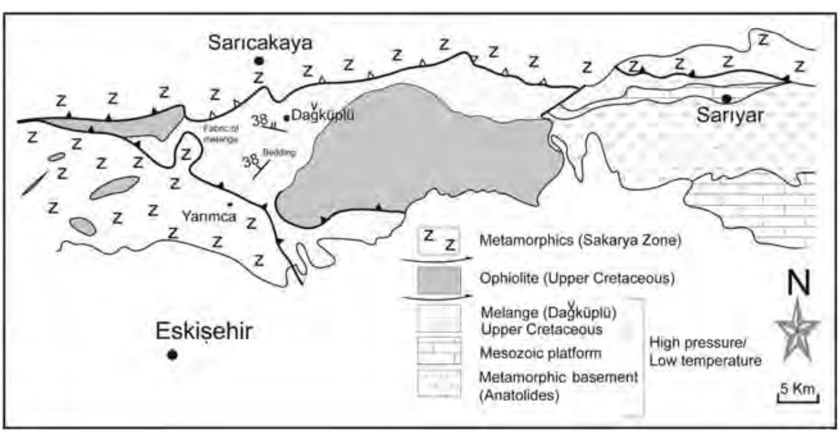

Fig. 16. Outline geological map of the Tavşanlı zone in the Eskişehir area (No. 10). See Figure 5 for location. Data from 500 000 geological map of Turkey (MTA 2002), Göncüoğlu *et al.* (2000) and this study.

blueschists, set in a sandy and shaly matrix (Göncüoğlu *et al.* 2000). The melange matrix and many of the clasts experienced only limited recrystallization allowing radiolarian cherts to be dated as Upper Cretaceous (Göncüoğlu *et al.* 2000). Further east in the same melange outcrop, near Sarıyar, radiolarians of Early Berriasian–Early Hauterivian have been identified within OIB (ocean island basalt)-type basalts, and a Cenomanian age was determined for nearby MOR (mid-ocean ridge)-type basalts (Göncüoğlu *et al.* 2006*a*, *b*).

We observed an excellent section of the melange near the road north of Yarımca (Fig. 16) where the melange matrix is dominated by shales and lithoclastic sandstones that show intense layer-parallel extension. This feature is indicative of assembly by tectonic rather than sedimentary processes. Individual sandstone beds (<1 m thick) show grading, parallel lamination and other features indicative of turbidites. Sandstone/shale melange is cut by serpentinite lenses, which show a pseudo-conglomeratic (i.e. tectonic) fabric.

The melange includes large blocks of exceptionally well-exposed, intact sequences of pillow basalt, massive basalt, red or green ribbon radiolarite and shale, up to several tens of metres thick. The dated Upper Cretaceous radiolarites come from scattered elongate blocks and lenses of red radiolarite exposed near Dağküplü, in close vicinity to larger blocks of volcanic and volcaniclastic rocks (Göncüoğlu *et al.* 2000, 2006). Nearby blocks include well-cemented lava breccia of primary origin, with angular to sub-rounded clasts set in a red shale matrix. There are also several large (80×8 m) tabular blocks of hornblende-phyric andesite and elongate blocks of volcaniclastic sediments, up to several tens of metres long. In addition, large (up to tens of metres in size) blocks of marble, of inferred neritic origin, occur locally. The blocky melange is overlain by thrust slices, which include disrupted slices of red radiolarite, meta-carbonate and basalt, up to several hundred metres long. Sheared serpentinite is locally interleaved.

Structurally above, large bodies of ophiolitic peridotite (Dağküplü ophiolite) cover an area of *c*. 200 km^2; these comprise mantle peridotite, mafic-ultramafic cumulates and plagiogranites, in all *c*. 4 km thick. The mantle peridotite is mainly hartzburgite and subordinate dunite, with interlayered wehrlite, pyroxenite and massive gabbro. Unusually extensive plagiogranites (*c*. 20 km^2) are associated with massive gabbro (Sarıfakoğlu 2006).

Orhaneli (Area 11)

The tectono-stratigraphy of this well-documented area (Figs 1 & 17) comprises a metamorphosed carbonate platform, overlain by melange and then by ophiolitic peridotite, with a locally preserved metamorphic sole. Blueschist metamorphism in this area was dated at *c*. 80 Ma (Campanian) based on $^{40}Ar/^{39}Ar$ dating of phengites (Sherlock *et al.* 1999). Several crosscutting undeformed granodiorites were dated at *c*. 50 Ma (Early Eocene) by the $^{40}Ar/^{39}Ar$ method (Harris *et al.* 1994; Figs 3a & 14). To the north, the large ophiolitic bodies are in strike-slip contact with Permo-Triassic low-grade meta-sediments and meta-volcanics correlated with the Sakarya zone, including the Triassic Karakaya Complex and its Jurassic–Cretaceous carbonate sediment cover.

Carbonate platform. The succession (e.g. Okay 1986) begins with basal metaclastics (Kocasu Formation), overlain by marbles and then by alternations of sodic meta-pelites and meta-psammites, of assumed Early Mesozoic age (Fig. 4). The metaclastics are strongly recrystallized and exhibit a penetrative foliation with no preserved primary sedimentary structures. In addition to ubiquitous quartz and phengite many of the metaclastic rocks contain lawsonite, jadeite, glaucophane and chloritoid (Okay & Kelley 1994; Okay 2002). The mineral assemblages constrain peak pressures to *c*. 24 kbar and temperatures to *c*. 430 °C (Okay & Kelley 1994). The blueschists pass upwards into thick meta-carbonates (İnönü Marble) of inferred Middle Triassic to Early Cretaceous age (Okay 1986). The marbles are overlain by meta-basic igneous rocks and meta-shales that include rare chert intercalations (Devlez Formation). These meta-basic rocks are classic blueschists with sodic amphibole, lawsonite and minor sodic pyroxene, chlorite and phengite (Okay 1986). The metacherts contain quartz, spessartine-rich garnet, hematite, lawsonite and sodic pyroxene. The blueschists are strongly folded, with the axis of mainly isoclinal folds oriented east–west. Fold axial planes are near horizontal, parallel to the foliations and there is a well-developed stretching lineation that is defined by sodic amphibole or calcite (Okay *et al.* 1998).

The top of the carbonate platform has been inferred to be of Cenomanian age (Okay *et al.* 1998) and this was taken as the time of initial collision of the Tauride–Anatolide continent with emplacing ophiolites (Candan *et al.* 2005; Okay & Altıner 2007). However, the Cenomanian age is not constrained by fossil evidence and the youngest age of (pre-collisional) continental margin development is inferred as *c*. 80 Ma (Campanian) from radiometric dating of the HP/LT metamorphic rocks (Sherlock *et al.* 1999).

Melange. The structurally overlying melange, or imbricate slice complex (Ovacık Complex), is generally less recrystallized and less highly deformed;

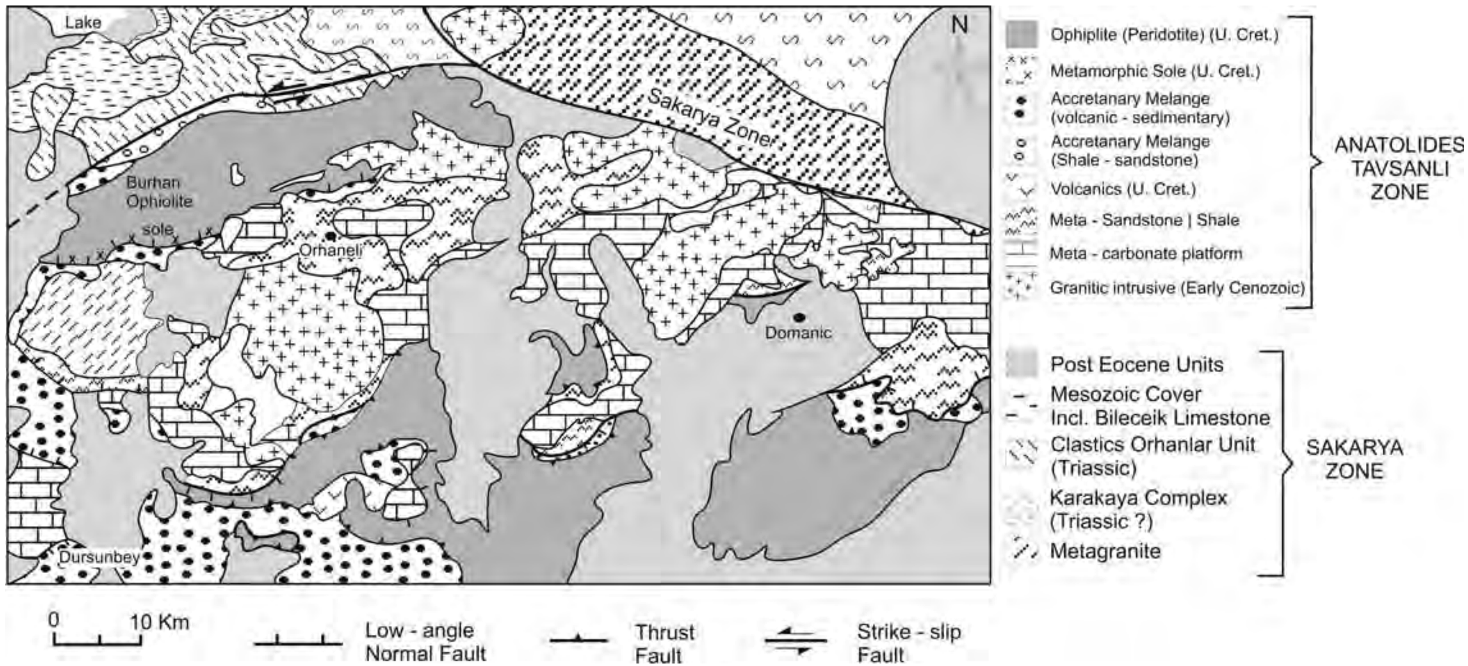

Fig. 17. Outline geological map of the Orhaneli area (Western Kütahya) (No. 11) in the west (Fig. 1). This well-studied area provides a reference for other areas discussed in more detail here. Based on the 1:500 000 geological map of Turkey (MTA 2002) and Okay (1986). See text for discussion.

the rocks including basalt, radiolarian chert, pelagic shale, pelagic limestone and serpentinite (Okay & Kelley 1994; Okay *et al.* 1998). Some lithologies have undergone incipient blueschist facies metamorphism (Okay 1986). HP/LT mineral assemblages (e.g. aragonite, sodic pyroxene and lawsonite) are commonly present in veins and amygdales within basalt. The basalts have experienced Na-metasomatism. Some of the basalts have undergone HP/LT metamorphism, as recorded by augite variably replaced by sodic pyroxene, chlorite, albite and lawsonite. Large units of basaltic agglomerate envelop blocks of recrystallized limestone, up to several hundred metres in size. There are also smaller amounts of red radiolarian chert and pelagic shale, together with subordinate serpentinite, pelagic limestone and greywacke. Sparse fossil evidence indicates Jurassic and Cretaceous ages for some radiolarian cherts and limestones, and an Upper Cretaceous age for pelagic limestone, based on the presence of *Globotruncana* sp. (Özkoçak 1969).

Ophiolite and metamorphic sole. The overlying ophiolitic rocks (Lisenbee 1971) are mainly serpentinised hartzburgite and dunite with rare gabbro and local crosscutting diabase dykes with chilled margins. The ophiolite has not undergone the regional HP/LT metamorphism that affected the underlying units (Önen & Hall 1993). Metamorphic sole rocks at the contact between the ophiolitic peridotites (Kınık ophiolite) and the melange below (Çöğürler complex) range in thickness from 10–300 m and can be traced along strike for *c*. 40 km (Önen & Hall 1993, 2000; Önen 2003). The basal part of the ophiolite is characterized by highly sheared serpentinite in thrust contact with amphibolites. The metamorphic sole (e.g. exposed in road cuts near Kaynarca (Kütahya) shows a classic inverted metamorphic zonation from garnet amphibolites at the thrust contact with the ophiolite, through amphibolites, to greenschists below (Önen & Hall 2000). In detail, the upper part of the section is 34 m thick and consists of steeply dipping, foliated garnet amphibolites with very thin non-garnetiferous amphibolites, and also plagioclase-rich and epidote-rich bands. Below are banded amphibolites with small-scale folding and faulting (122 m), intensely folded amphibole schist, and finally quartz-mica schist at the base of the section (139 m).

Similar relations are exposed in adjacent areas, including the Dağardı melange and the Harmancık ophiolite. The melange in these areas includes blocks of radiolarite, blueschist, greenschist and limestone, together with shale and serpentinite. The lavas include enriched-MORB. The overlying ophiolitic peridotite is cut by swarms of diabase dykes of island arc tholeiite type (Manav *et al.* 2004).

Bornova zone (Area 12)

The importance of the Bornova zone is that it comprises by far the largest single area of melange related to ophiolite emplacement and is also critical to the timing of events as both clasts and matrix are well dated. The Bornova zone (Bornova Flysch Zone of Okay *et al.* 2001), 90 km long by 50 km wide, trends southwestwards from the Kütahya area to near İzmir (Erdoğan 1990; Okay & Siyako 1993; Figs 1 & 18). Okay & Tüysüz (1999) suggested that this zone represents a transform segment of the northern margin of the Tauride–Anatolide Block, linking the Vardar zone of northern Greece. This was mainly because of its unusual NE–SW trend, absence of HP/LT metamorphism (except possibly in the NE), and the presence of continental margin-derived blocks. Here, we interpret the Bornova zone differently, as large-scale mainly sedimentary melanges that were emplaced into a foredeep and then over-ridden by ophiolites (see *Tectonic processes*). No basement is exposed but it is assumed that the Anatolide platform lies beneath.

In the north, the Bornova zone is bordered by the Triassic Karakaya Complex (Nilüfer unit) and Jurassic–Cretaceous limestones (e.g. in the Balıkesir and Balya areas in the NW). In the far NE of the area (near Kepsut), lithologies of the Bornova zone are thrust northwards over the Karakaya Complex and related Triassic clastic sediments of the Sakarya zone (Okay & Siyako 1993).

Our observations show that the Bornova zone comprises two different, but interrelated types of melange. The first, here termed the *Bornova sedimentary-volcanic melange*, has a terrigenous matrix and blocks of mainly sedimentary and occasional volcanic lithologies. This melange varies from essentially unmetamorphosed in the north, to (at least) greenschist facies in the south. The second type of melange, termed the *Bornova ophiolitic melange*, is dominated by ophiolitic and pelagic sedimentary blocks in a matrix of mainly ophiolite-derived clastic sediment. The contacts of the Bornova melange with underlying, and overlying, units are mainly thrusts in the north but high-angle neotectonic faults in the south.

Crucially, in the Karaburun Peninsula in the far SW (Fig. 18) the Bornova sedimentary-volcanic melange overlies an intact unmetamorphosed Tauride-type carbonate platform succession with a transitional sedimentary relationship (Erdoğan *et al.* 1990; Erdoğan & Güngör 1992; Robertson & Pickett 2000). The Bornova melange is extensively exposed around İzmir and areas to the NE, where it

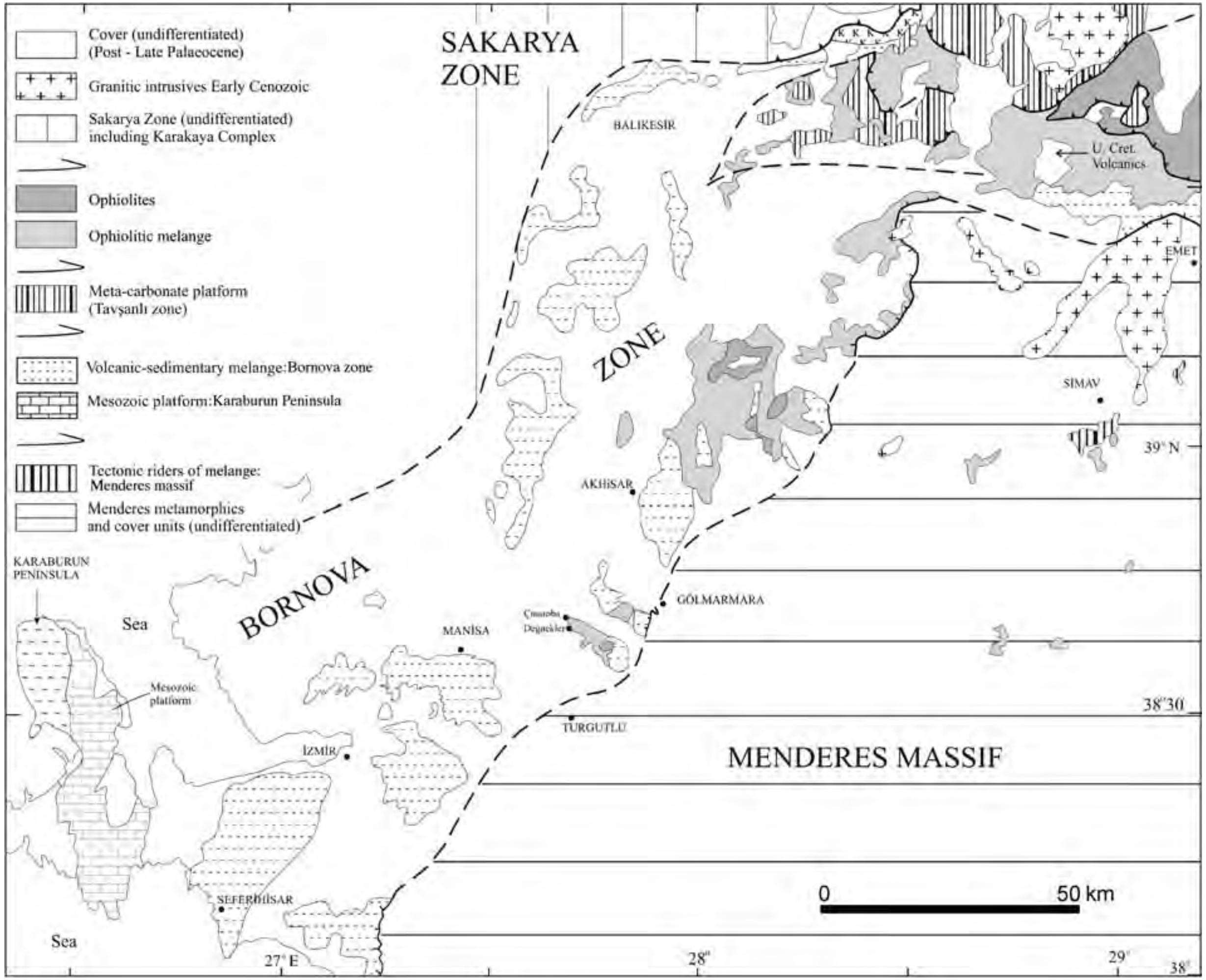

Fig. 18. Outline tectonic map of the Bornova zone (Area no. 12). Simplified from the 1:500 000 geological map of Turkey (MTA 2002). See Figure 1 for location. The map details are from the Turkish 100 000 topographical maps, especially İzmir K 19.

includes kilometre-sized blocks of neritic limestone (Fig. 18). In the Karaburun Peninsula in the far SW (Fig. 1), a Carboniferous melange (Karaburun melange) is unconformably overlain by a Triassic–Early Cretaceous carbonate platform succession. This is transitional upwards into Santonian pelagic carbonates rich in *Globotruncana* sp. and then into shales and sandstones turbidites of Late Maastrichtian age marking the base of the sedimentary-volcanic melange (Erdoğan *et al.* 1990; Robertson & Pickett 2000).

In the İzmir area, the intensity of deformation and metamorphism increases markedly to the SW near the contact with the metamorphic Menderes Massif (Fig. 1). Metamorphosed Bornova melange crops out widely in the Seferihisar area, mapped as ‘clastic and carbonate rocks (flysch)’ overlain by ophiolitic thrust sheets on the 1:500 000 geological map of Turkey (MTA 2002; Fig. 18). Our observations show that the melange is dominated by lenses of well-cleaved phyllites, together with meta-volcanic, meta-volcaniclastic sediments and meta-serpentinite (e.g. in the Doğanbey area). Numerous small asymmetrical folds verge towards the SE. Flattened blocks of volcanic breccia include sub-rounded to sub-angular clasts mainly of extrusive igneous rocks in a volcaniclastic matrix ($<$0.6 m in size). Lenticular blocks of marble (up to 150 m long $\times$ 10 m wide) are mainly composed of meta-conglomerate. Intercalated black phyllites are deformed by east–west trending, upright- to chevron-type folds, with east–west trending axial planes. The meta-sedimentary melange is cut by sheared serpentinite, up to 200 m thick. A small diabase intrusion (probable dyke) with well-preserved chilled margins cuts serpentinite. This melange contains numerous metasomatic quartz veins and generally resembles the metamorphic and deformation state of the upper levels of the Menderes Massif further south (beyond exposures of Neogene volcanics).

Further NE, from near İzmir to the Kütahya area (Fig. 18), the Bornova melange has a very low metamorphic grade and is separated from the Menderes Massif to the south by high-angle neotectonic faults. In general, this melange is dominated by blocks of thick-bedded neritic carbonate and thin-bedded pelagic carbonate (up to several kilometre-sized), together with subordinate basic extrusive rocks set within a terrigenous matrix. Bedding within individual limestone blocks is commonly disrupted and folded. The terrigenous matrix comprises thin, to medium, to locally thick-bedded lithoclastic turbidites and less common matrix-supported conglomerates (debris flows), interbedded with micaceous mudstones. Where exposed, the mudstones are black and clearly rich in organic matter. Lithoclasts are mainly quartzite and phyllite. Associated debris flows contain well-rounded clasts of neritic limestone, radiolarian chert, terrigenous and volcaniclastic sedimentary rocks, cemented by calcite spar.

In the Manisa area (Fig. 18) we observed that the melange is dominated by large (tens of metres) blocks of limestone, especially Upper Cretaceous pelagic limestone (*Globotruncana*-bearing), set in a matrix of terrigenous turbidites and debris flows. Some of the limestone blocks contain rudist bivalve fragments and layers of greenish chert of replacement origin. Successions within several blocks preserve a sedimentary transition from Upper Cretaceous pelagic carbonates (with *Globotruncana*), through white limestones containing large foraminifera, black mudstones (several tens of centimetres thick), into terrigenous sandstones and conglomerates typical of the matrix of the Bornova volcanic-sedimentary melange. These transitions are similar to the transition from the Tauride carbonate platform to the Bornova melange seen in the Karaburun Peninsula. Other blocks up to several kilometres in size include Middle Triassic–Lower Cretaceous shallow-water carbonates (Şahinci 1976; Poisson & Şahinci 1988; Okay & Siyako 1993), as seen north of Manisa. According to Poisson & Şahinci (1988) the terrigenous matrix is at least partially of Paleocene age.

Further north, in the Savaştepe area, the pelagic limestone is reported to be Santonian–Late Campanian (Okay & Siyako 1993). Locally, blocks of platform carbonates as old as Late Triassic (Norian) are reported to be overlain by Upper Cretaceous pelagic carbonates (Poisson & Şahinci 1988), suggesting that the source platform was uplifted and eroded before subsiding and being covered by deep-water carbonates and later being reworked as blocks in the melange. North of Akhisar the melange is unconformably overlain by shallow-water limestones of Lower–Middle Eocene age.

Recently, the geochemistry of blocks of basaltic rocks from the Bornova melange has been studied, indicating the presence of three compositional types: mid-ocean ridge type, within plate (OIB)-type and supra-subduction zone-type (Aldanmaz *et al.* 2007). The three types of basaltic rocks were also identified in the Anatolide melanges studied during this work (see *Tectonic processes*) and in the metamorphic soles of the Tauride ophiolites (Çelik & Delaloye 2003).

In addition, Okay & Altıner (2007) have recently recognized and dated a Mesozoic sedimentary succession in a single block of condensed hemipelagic limestone north of Izmir (near Urbut). Upper Triassic neritic limestones there are unconformably overlain by a discontinuous succession of Tithonian–Middle Albian age, in turn overlain, again unconformably, by Upper Cretaceous (Cenomanian–Turonian) pelagic limestones. The Upper Cetaceous sediments contain detached blocks (<1 m in size) of Upper Triassic, Turonian and Valanginian age. The succession records Late Cenomanian (*c*. 95 Ma) flooding of the shelf, followed by pelagic deposition in an unstable setting, as indicated by input of blocks from the adjacent carbonate platform. The succession overall can be correlated with the Boyalı Tepe unit of the Beyşehir nappes and the Domuz Dağ unit of the Lycian nappes further west (Andrew & Robertson 2002) or the Domuz Dağ unit of the Lycian Nappes (Collins & Robertson 1998). Okay & Altıner (2007) attribute the platform collapse to initial ophiolite obduction onto the northern margin of the Tauride–Anatolide platform. However, we relate the Late Cenomanian event to intra-oceanic subduction, ophiolite and sole formation that preceded ophiolite emplacement by up to 10 Ma (see *Tectonic processes).*

We observed that the Bornova sedimentary-volcanic melange is regionally overlain by the *Bornova ophiolitic melange* with a locally exposed low-angle tectonic contact (e.g. in the Çınaroba area). The ophiolitic melange dominates the outcrop towards the NE and is locally underlain by HP/LT meta-carbonates and meta-clastic sediments that are correlated with the eastern Kütahya zone (Okay & Tüysüz 1999; Fig. 18). Our observations show that the ophiolitic melange includes all the components of an ophiolite, including basalt, diabase, gabbro and various ultramafic rocks, together with numerous sedimentary rocks, especially ribbon radiolarite and pelagic limestone. The basalt ranges from pillowed to massive, vesicular, to non-vesicular and locally includes recrystallized inter-pillow carbonate. Occasional blocks of plagiogranite are also present (e.g. near Çınaroba). Other large (several hundred metres) blocks of intrusive ophiolitic rocks include layered gabbro, dunite and hartzburgite. These occur at a high level and can be correlated with the larger ophiolitic peridotite bodies exposed in the Orhaneli area further NE. Sedimentary blocks within the ophiolitic melange include pink pelagic limestone and radiolarites, massif pelagic limestones with ammonites, limestone with Fe/Mn crusts, green feldspathic volcaniclastic sandstone (*c*. 10 m thick) and recrystallized pink carbonate in a matrix of sheared red shale and sandstone (e.g. Değnekler area).

The matrix of the ophiolitic melange includes thick-bedded, to massive, lithoclastic sandstones that are interbedded with lithoclastic grainstones and pink calcareous mudstones (containing *Globotruncana*). Locally, the matrix-supported conglomerates are nearly monomict, with mainly angular clasts (<20 cm in size) of vesicular basalt set in a matrix of pale volcaniclastic sediments. These conglomerates are interbedded with thin- to medium-bedded volcaniclastic sandstones. Associated matrix-supported conglomerates contain clasts of ophiolitic lithologies (e.g. basalt, diabase, gabbro, serpentinite, pelagic limestone and radiolarite).

Taurides

The mainly metamorphosed melanges and other Anatolide unit are here correlated with unmetamorphosed equivalents in the Taurides further south, as summarized below.

In the SE, the unmetamorphosed Bolkar Dağ carbonate platform is overlain by the Mersin Melange, which is topped by the Mersin Ophiolite with a basal metamorphic sole (Parlak & Robertson 2004; Moix *et al.* 2007). The Mesozoic platform carbonate succession passes through pelagic carbonates and redeposited facies with limestone blocks into ophiolite-derived debris flows dated as Late Campanian–Maastrichtian (Demirtaşlı *et al.* 1984; Özer *et al.* 2004; Taşlı *et al.* 2006). This unit is interpreted to record the break-up and collapse of the Tauride platform associated with ophiolite emplacement (Parlak & Robertson 2004).

Further east, the succession in the relatively autochthonous Mesozoic Geyik Dağ carbonate platform continues into the Eocene (Monod 1977; Özgül 1984, 1997) and is then overthrust by the Beyşehir nappes, restored as part of the rifted northern passive margin of the Tauride–Anatolide platform (Andrew & Robertson 2002). These units were first emplaced onto the northern part of the Tauride platform during the Upper Cretaceous (Campanian–Maastrichtian), associated with the emplacement of large ophiolites (e.g. Şarkikaraağaç ophiolite; Elitok 2002), melanges and fragmentary metamorphic soles (Çelik *et al.* 2006). These units were thrust further south over the Geyik Dağ after the Early Eocene (Mackintosh 2008). The ophiolites are locally underlain, or interthrust with melange, including blocks of neritic limestone (locally with Permian limestone blocks), pelagic limestone (locally dated as Maastrichtian), radiolarian chert, basic volcanic rocks, volcaniclastic sediments, gabbro and serpentinite in a matrix of ophiolite-derived sandstone and mudstone (Andrew & Robertson 2002). The melange largely formed as subaqueous debris flows that were strongly sheared during emplacement. Geochemical studies indicate that the basaltic extrusives were derived from MORB-type and subduction-influenced settings (Andrew & Robertson 2002).

Further east, the Menderes Massif, part of the Tauride–Anatolide Block, has a Late Precambrian high-grade metamorphic 'basement' (e.g. Konak *et al.* 1987; Kröner & Şengör 1990; Dora *et al.* 2001;

Bozkurt & Oberhansli 2001), overlain by meta-shelf-type successions. Shallow-water carbonate deposition persisted until Santonian–Campanian time and was followed by flooding of the platform and the accumulation of pinkish pelagic carbonates of Late Campanian–Late Maastrichtian age. Facies of the Menderes Margin succession pass gradationally upwards through meta-litharenites into melange ('flysch'). Blocks in overlying melange are mainly recrystallized limestone with chert nodules set in a terrigenous matrix, interpreted as turbidites and debris flows (Collins 1997; Collins & Robertson 1998). The matrix has been locally dated as Middle Paleocene and early Middle Eocene in different areas (Özer *et al.* 2001).

Ophiolites and continental margin sediments and volcanics known as the Lycian nappes were emplaced southwards during the latest Cretaceous and re-thrust further south during the Late Eocene–Miocene (Şenel 1991; Collins & Robertson 1998, 1999). The regionally extensive Lycian ophiolite is located at the highest structural levels of the allochthon in the SW of the region and is underlain by a metamorphic sole and several types of sedimentary and ophiolitic melange (Collins & Robertson 1997, 1998; Çelik & Delaloye 2003; Çelik *et al.* 2006). The Mesozoic succession of shallow to deep water, largely carbonate sediments and some volcanics was restored as the north-facing passive margin of the Menderes platform (Collins & Robertson 1999).

Several of the Lycian thrust sheets show upward transitions to Upper Cretaceous convergence-related sediments. The inferred most distal thrust sheet (Köycegiz Thrust Sheet) passes upwards from Cretaceous pelagic carbonates with chert nodules of Cenomanian–Turonian age (De Graciansky 1972). The section grades into litharenenite turbidites and shales of mainly volcaniclastic origin with limestone blocks, followed above this by an incoming of blocks including pelagic limestone, radiolarian chert, basalt and gabbro. A Maastrichtian–Campanian age from one of the limestone blocks implies this ophiolitic melange is of syn-post Maastrichtian age. In one local sequence of the Köycegiz Thrust Sheet (Selimiye Flysch of Ersoy 1992), similar Upper Cretaceous pelagic limestones pass upwards into *c*. 200 m of debris flows and turbidites with clasts of chert, pelagic limestone, redeposited limestone, sandstone and neritic limestones. The clastic sediments contain schist, limestone, black chert and chlorite but *no* ophiolitic material. This is followed by *c*. 100 m of turbidites before the first appearance of ophiolitic clasts and blocks (Collins 1997; Collins & Robertson 1999).

The syn-emplacement sediments, as summarized above, are overlain by several types of melange. The lower Layered Tectonic Melange is dominated by pelagic limestone and chert, intergradational with broken formation and imbricate thrust sheets and shows intense shear deformation. The overlying Ophiolitic Melange includes volcanics, volcaniclastics, peridotites and amphibolitic rocks set in a sheared volcaniclastic matrix, suggesting a sedimentary origin as debris flows for this type of melange (Collins & Robertson 1998). The extrusives include WPB-type lavas of inferred seamount origin (Collins & Robertson 1998). In addition, the northern margin of the Menderes Massif is associated with a melange made up of blocks of limestone and rare ophiolite-related rocks set in a clastic sedimentary matrix. In places, Paleocene neritic limestones unconformably overlie the 'Ophiolitic Melange' (Şenel *et al.* 1989), providing an upper limit for melange emplacement (i.e. Maastrichtian). Locally, Paleocene sediments are intercalated between the Layered Tectonic Melange and the Ophiolitic Melange, giving a minimum age of amalgamation of these melange units. In the southern part of the Menderes Massif the uppermost levels of the succession, of Early Eocene age, are overlain by the 'Menderes Margin Melange'. This shows that the final emplacement of this melange post-dates Early Miocene (Collins 1997; Collins & Robertson 1998, 1999). The Lycian and Beyşehir nappes and related melanges are considered to have a two-stage history i.e. initial Late Cretaceous (Maastrichtian) emplacement onto the Tauride carbonate platform, followed by re-thrusting and further southward translation after the Early Eocene (Collins & Robertson 1997; Andrew & Robertson 2002; Mackintosh 2008).

The northern part of the Menderes Massif is overlain by several different volcanic-sedimentary melanges. These were exposed following Late Oligocene–Early Miocene exhumation (Hetzel *et al.* 1995; Purvis & Robertson 2004). The ophiolites and melanges in this area were detached from underlying basement associated with low-angle extensional faulting, to form tectonic riders within, and around, several Neogene sedimentary basins (Purvis & Robertson 2004). Small isolated bodies of melange (<1 km^2) are exposed within the Selendi Basin. These consist of chert, recrystallized limestone, basalt and serpentinite. Larger outcrops of melange are seen along the western margin of the Gördes Basin (Seyitoğlu *et al.* 1992; Purvis 1998; Purvis & Robertson 2004) including pillow basalt, pelagic limestone and ribbon radiolarite with a shaly matrix. Small outcrops of melange are also exposed around Neogene intrusive rocks in the central part of the Gördes Basin.

Northerly units

Any regional interpretation of the melanges needs to take account of the tectonic development of units to the north, namely the Niğde–Kırşehir Massif

(Central Anatolian Crystalline Complex), the Ankara Melange and the Sakarya zone (Fig. 1). We focused on the nature and timing of the contacts between these units and the Anatolide units to the south.

Niğde–Kırşehir massif. In general, the Niğde–Kırşehir massif has a crystalline core of pre-Triassic basement and a cover of metamorphosed carbonate platform rocks, of inferred Mesozoic age, best exposed in the Niğde massif in the SE (e.g. Göncüoğlu 1986; Whitney & Dilek 1998). The basement and cover experienced relatively high temperature-low pressure type metamorphism during the Late Cretaceous (Fayon *et al.* 2001), and was exhumed from mid crustal to shallow crustal levels. This partially took place by the latest Maastrichtian because part of the Niğde Massif in the SE is transgressed by sediments of the Ulukışla basin (Göncüoğlu *et al.* 2001; Jaffey & Robertson 2001; Clark & Robertson 2002). According to some authors ophiolites of inferred supra-subduction zone type are exposed above the metamorphosed Mesozoic platform of the Niğde–Kırşehir massif (Yalınız *et al.* 1996; Floyd *et al.* 2000). However, these are controversial as they are also interpreted as intrusions into the massif (Kadıoğlu *et al.* 2006). In addition, the Kırşehir Massif is cut by granitic plutons of Late Cretaceous–Early Cenozoic age (see *Tectonic processes*).

Ankara Melange. The regionally extensive Ankara Melange includes radiolarian cherts, pelagic/hemipelagic limestones, alkaline basalts interpreted as Lower Cretaceous seamounts (Rojay *et al.* 2004), and also dismembered mainly ultramafic ophiolitic rocks. Recent radiometric dating of crosscutting plagiogranites (Tankut & Gorton 1990) suggests that some at least of the ultramafic rocks are of pre-Jurassic age (Dilek & Thy 2006). However, at present it seems likely that the ophiolitic rocks of the Anatolides, as studied during this work, are of Cretaceous age, although radiometric dating needs to be carried out of these rocks in the future. Further consideration of the Ankara Melange is outside the scope of this paper.

Sakarya zone. The Sakarya zone in the west documents the northwestern margin of the Mesozoic ocean basin from which the Anatolide and Tauride ophiolites and melanges were derived (Şengör & Yılmaz 1981). A rarely exposed high-grade metamorphic basement is overlain by the Triassic Karakaya Complex, although contact relations are debateable (Tekeli 1981*a*; Pickett & Robertson 1996, 2004; Okay 2000; Okay & Göncüoğlu 2004; Okay *et al.* 2006). The Karakaya Complex is unconformably overlain by conglomerates and sandstones and then by shelf carbonates, ranging from Early Jurassic to mid-Cretaceous age (Bilecik Limestone; Altıner *et al.* 1991).

Successions are reported to differ between the north and south of the Sakarya zone. In the south (Nallıhan area), pelagic carbonates extend to Santonian–Coniacian and pass into Santonian–Middle Maastrichtian sandstone turbidites and pelagic carbonates, then Upper Maastrichtian shallow-marine sandstone and Paleocene non-marine sandstone and conglomerate (Tansel 1980, 1990; Altıner *et al.* 1991). Ophiolite-derived debris flows and ophiolitic thrust slices occur near the suture zone in the south (Yılmaz *et al.* 1997; Okay *et al.* 2001).

In the more northerly part of the Sakarya zone, Jurassic–Lower Cretaceous shelf-type sediments are described as being overlain by Upper Cretaceous tuffs, sandstone turbidites, debris flows and pelagic limestones (e.g. Mudurnu–Göynük area; Saner 1980; Meriç & Şengüler 1986; Altıner *et al.* 1991). These facies may record the development of a volcanic arc and forearc basin related to northward subduction (Şengör & Yılmaz 1981). Clasts in debris flows include Lower Cretaceous neritic limestones and Upper Cretaceous pelagic *Globotruncana*-bearing limestone (Genç 1987). Blocks of serpentinite are reported from Maastrichtian turbidites (Saner 1980). An emergent accretionary wedge to the south was a possible source. Derivation from the Intra–Pontide suture to the north is unlikely because the northern part of the Sakarya zone is free of emplaced ophiolitic rocks.

The southerly part of the Sakarya continental margin exhibits shallowing-upwards and emergence during the Paleocene; it was then detached from its basement and thrust southwards >50 km related to continental collision, probably during Mid-Eocene time (Okay & Tüysüz 1999).

Granitic rocks cut the Sakarya zone and also the suture zone to the south. As summarized by Altunkaynak (2007), an east–west-trending southerly group of medium to high potassic calc-alkaline I-type granite plutons (e.g. Orhaneli, Topuk, Gürgenyayla and Göynükbelen) with ages of *c.* 54–48 Ma (Early–Mid Eocene) cuts the suture zone including the Anatolide blueschists, melange and ophiolitic rocks. The southern plutons are dated as 53–44 Ma and the northern ones as 48–35 Ma (Delaloye & Bingöl 2000; Okay & Satır 2006). A compositionally similar, more northerly group of generally younger (48–36 Ma) plutons (i.e. monzogranite, granodiorite and granite) cuts the Sakarya zone (e.g. in the Marmara Sea area). Geochemical data from both the southerly and northerly granitic plutons suggest the existence of a metasomatized lithospheric mantle source, modified by Late Cretaceous subduction. Mantle-derived melts were modified by crustal contamination, assimilation and fractional crystallization during magma ascent (Altunkaynak 2007). Partial melting of mantle lithosphere was facilitated by asthenospheric upwelling and thermal perturbation, possibly triggered by oceanic slab break-off. However, this alone is unlikely to have been sufficient to generate large-scale pluton intrusion. The main driving force was clearly regional continental collision of the Tauride and Eurasian plates. However, further consideration of this issue is outside the scope of this paper.

Tectonic processes

In this discussion we utilize new and published geochemical analysis of basaltic rocks from the Anatolide and Tauride melanges. Details of sample locations, analytical methods, data tables and geochemical plots confirming the basaltic compositions of the samples studied are given in the supplementary material.

Restoration of rifted margin

The main tectonic units of the continental margin can be restored from south to north as follows: Geyik Dağ (and Hadim/Bolkar nappe); Menderes Massif; Afyon–Bolkardağ zone; Tavşanlı zone; Beyşehir/Lycian nappes and 'sedimentary-volcanic melange' (non-ophiolitic melange). The main considerations are regional stacking order, facies and lithology, metamorphism, recrystallization and deformation, and the timing of emplacement of melange onto platform units. The Geyik Dağ and over-riding Hadim/Bolkar nappe in the south are unmetamorphosed and were never deeply buried. The Mesozoic–Lower Cenozoic sedimentary units of the Menderes Massif were deformed and metamorphosed under HP/LT conditions during the Eocene, but the Precambrian crystalline basement did not undergo this metamorphism (Candan *et al.* 2005). The Afyon–Bolkardağ zone is deformed, metamorphosed under HP/LT conditions but not greatly recrystallized; and the Tavşanlı zone is strongly deformed, recrystallized and metamorphosed under very HP conditions (e.g. Okay & Kelley 1994). The unmetamorphosed Beyşehir and Lycian nappes restore as the rifted northern margin of the Tauride–Anatolide continent. The 'sedimentary-volcanic melange' represents fragments of the rifted margin and more oceanic units (e.g. seamounts; volcanic arc related). Alternatively, Candan *et al.* (2005) suggested that the Afyon–Bolkardağ zone restores as an intra-platform basin between the Menderes Massif to the south and the Tavşanlı zone to the north. Within the Lycian nappes in the south 'flysch' (Karabörtlen unit) of Late Turonian–Early Senonian age (Bernoulli *et al.* 1974) was reported to be older than the Maastrichtian clastic sediments overlying the Afyon–Bolkardağ carbonate platform further north (e.g. in the eastern Kütahya area). The 'flysch' was assumed to record the arrival of allochthonous units; i.e. reaching far south before further north, which would imply the existence of an intra-platform basin which closed by the Late Turonian. However, this reconstruction is problematic for several reasons. First, the Jurassic–Cretaceous sediments of the Lycian nappes are pelagic (Collins & Robertson 1999) and so this interpretation would require the formation of a deep-water basin within the Tauride–Anatolide platform for which there is no independent evidence (e.g. two clastic rifted margins). Second, slices of units similar to the Lycian nappes were not observed overlying the Afyon–Bolkardağ zone, as would be expected for this model. Third, the tectono-stratigraphy and lithology of the Afyon–Bolkardağ zone and the Tavşanlı zone are similar, consistent with them being contiguous platform units. Fourth, the Turonian flysch of the Lycian Nappes (e.g. Köyceğiz Thrust Sheet) comprises lithoclastic turbidites and debris flows, without ophiolite-derived material (Collins & Robertson 1999). This early clastic sedimentation can be related to fault-controlled uplift of the passive margin and related erosion of clastic material. Such erosion reached low stratigraphical levels in the continental margin, as suggested by the presence of schist and black chert (?Carboniferous) clasts. Elsewhere similar faulting and erosion affected inboard parts of the Oman continental margin around Cenomanian time (*c.* 95 Ma) prior to ophiolite emplacement (Robertson 1987).

Triassic rifting and Jurassic-Lower Cretaceous passive margin subsidence

Within the Afyon-Bolkardağ zone ? Late Precambrian basement (Bayat area) and Lower Carboniferous melange (Konya area) are depositionally overlain by mixed shallow-water carbonate-clastic successions of Permian and Early Triassic age in different areas (Özcan *et al.* 1988; Eren 1993, 2001; Göncüoğlu *et al.* 2003; Candan *et al.* 2005). In the Bolkar Dağ area further east the oldest known unit is Upper Permian neritic limestone (Demirtaşlı *et al.* 1984). Comparable facies in the Tavşanlı zone are highly recrysytallized and undated.

Above a regional unconformity (N. Bolkar Dağ, Altınekin, Konya, Bayat areas), the Early Triassic of the Afyon–Bolkardağ zone comprises a generally fining-upward sequence of metamorphosed terrigenous sandstones and shales, interbedded with shallow-water carbonates. Facies evidence and scarce fossils indicate non-marine, to lagoonal (paralic) deposition, passing into a relatively shallow-open marine setting.

The Triassic mixed carbonate-clastic-volcanogenic successions exposed beneath the Mesozoic platform succession (e.g. Bolkar Dağ, Konya and Bayat areas) are considered to record Early Triassic rifting of the Anatolide–Tauride continent followed by spreading prior to or during Late Triassic time. In this interpretation, rifted fragments drifted northwards in front of a newly created Triassic spreading axis and were then subducted or incorporated into an accretionary wedge (Karakaya complex; e.g. Çal unit) bordering the Eurasian margin (Pickett & Robertson 1996, 2004; Robertson *et al.* 2005; Okay *et al.* 2006). The results of this study are consistent with a Triassic extensional setting along the northern margin of the Anatolide-Tauride continent (Robertson & Pickett 2000; Collins & Robertson 1997, 1998; Göncüoğlu *et al.* 2003; Robertson & Ustaömer in press; Mackintosh & Robertson in press) rather than a compressional/collisional setting during Late Triassic time (Stampfli & Borel 2002; Eren *et al.* 2004). The rifted margin was characterized by a mosaic of platforms and basins with considerable palaeogeographic and facies variation along and across the margin (Andrew & Robertson 2002).

The rift-related succession is transitional upwards to a Mid–Late Triassic shallow-marine carbonate platform, commonly dolomitic and stromatolitic (N Bolkar Dağ, Altınekin, Konya and Bayat areas). Shallow-water carbonates accumulated regionally on a subsiding carbonate platform during Late Triassic–Early Cretaceous time. Localized conglomeratic intercalations (e.g. Konya and N Bolkar Dağ) could reflect faulting of the platform, or storm activity.

Regional Upper Cretaceous platform flooding and collapse

The Anatolide–Tauride platform was regionally flooded and overlain by pelagic carbonates beginning in Late Cenomanian time. In the north (e.g. Altınekin) the presence of intercalations of pelagic and redeposited carbonates is suggestive of the development of a slope setting during the Late Cretaceous. In the uppermost levels of the succession dark organic-rich carbonates accumulated locally (e.g. Altınekin area), perhaps within an oxygen minimum zone. Elsewhere (e.g. Yunak, Bademli areas) thick-bedded, neritic, carbonates form the top of the preserved platform succession, probably because pelagic/redeposited facies, as seen elsewhere, were tectonically excised during the emplacement of overlying melanges and ophiolites. The Cenomanian flooding is likely to record a combination of global sea-level high-stand (Hardenbol *et al.* 1998) and regional tectonics related to northward subduction of Neotethyan ocean further north (i.e. *c.* 10 Ma prior to ophiolite obduction).

The submerged platform and /platform slope pass transitionally into Upper Cretaceous (Early Maastrichtian) turbidites and debris flows (e.g. Altınekin; Bayat areas). In places (e.g. Bayat area), the carbonate platform passes transitionally upwards into turbidites and multiple debris flows with a terrigenous clastic matrix and includes clasts probably derived from the subjacent carbonate platform. The terrigenous material is likely to have been derived from an exposed continental hinterland to the south, probably related to regional faulting and flexural uplift of the Tauride–Anatolide Platform that accompanied initial ophiolite emplacement onto the margin. The record is closely comparable with Upper Cretaceous ophiolite emplacement in Oman (Robertson 1987), where fault-controlled upflexure to form an unconformity on the platform (Wasia–Aruma break) was followed by regional subsidence, clastic sediment deposition (Muti Formation) and melange and ophiolite emplacement.

Within the Tavşanlı zone, the uppermost levels of the platform are described as including stratigraphic intercalations of meta-basaltic rock and meta-chert in several areas (e.g. Okay *et al.* 1998). Basaltic lavas are known to have been erupted in comparable settings related to the transition from a carbonate platform to a foredeep associated with ophiolite emplacement, for example in the Oman and Balkan regions (e.g. Robertson 1987, 1991).

Genesis of MOR-type oceanic crust, seamounts and arc-type volcanics

Evidence of the nature and age of oceanic lithosphere and seamounts comes from blocks of extrusive igneous rocks in the melanges of the Anatolides (including the Bornova zone) and Taurides. Presently, only a small number of the exotic units are dated, mainly based on interbedded siliceous or calcareous microfossils. The tectonic settings of the basaltic rocks within the melanges vary considerably, as inferred from geochemical data.

On chondrite-normalized REE (rare earth elements) diagrams and N-MORB (mid-ocean ridge basalt)-normalized multi-element variation diagrams (Figs 19 & 20) the basalts from the Bayat and Bademli areas display flat to slightly LREE (light rare earth element) enriched patterns. Those from the Yunak region show two distinct REE patterns; the first displays LREE-enriched,

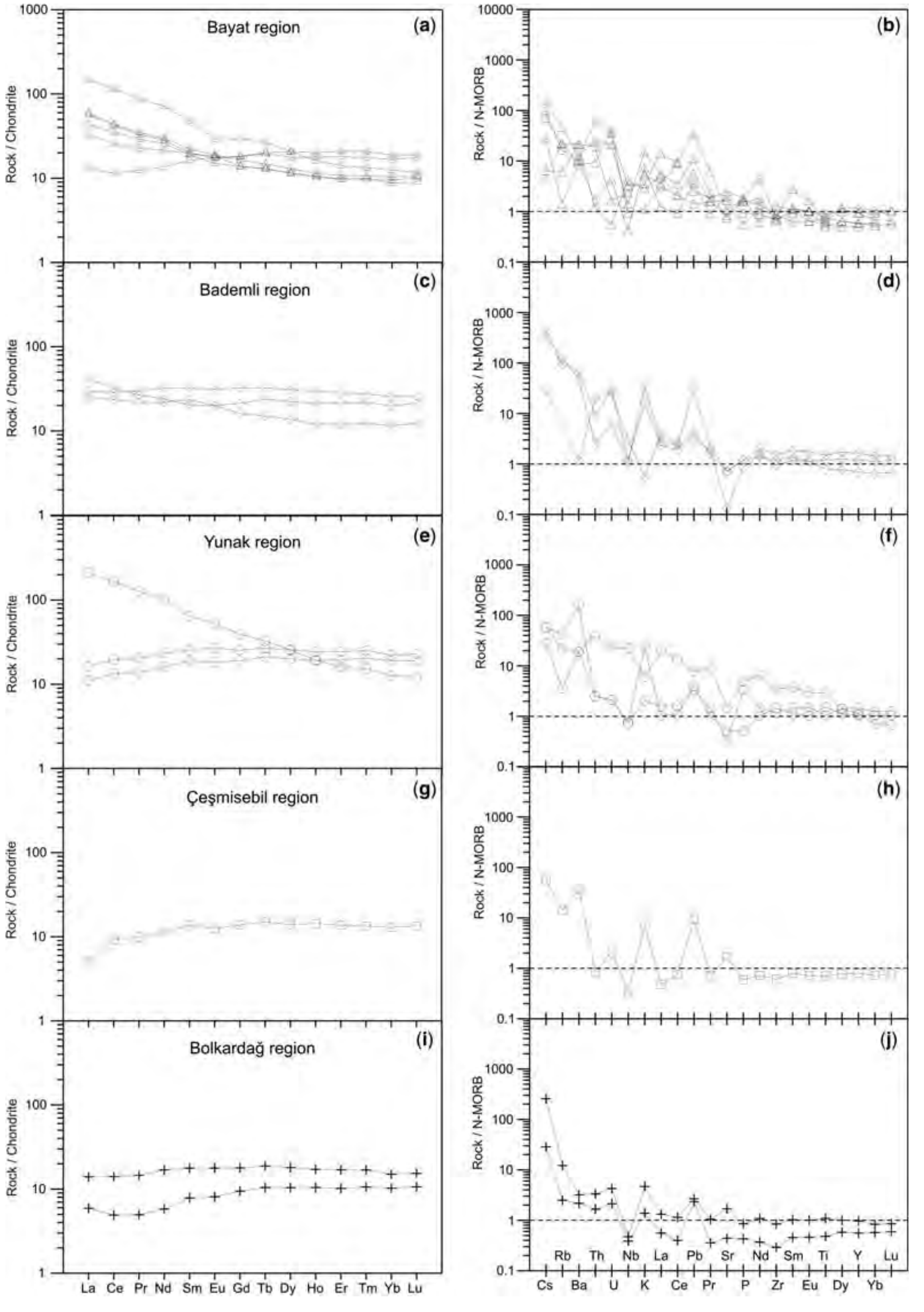

Fig. 19. Chondrite-normalized REE and N-MORB normalized spider diagrams for the volcanics from different localities in Anatolia studied during this work (normalizing values from Sun & McDonough 1989).

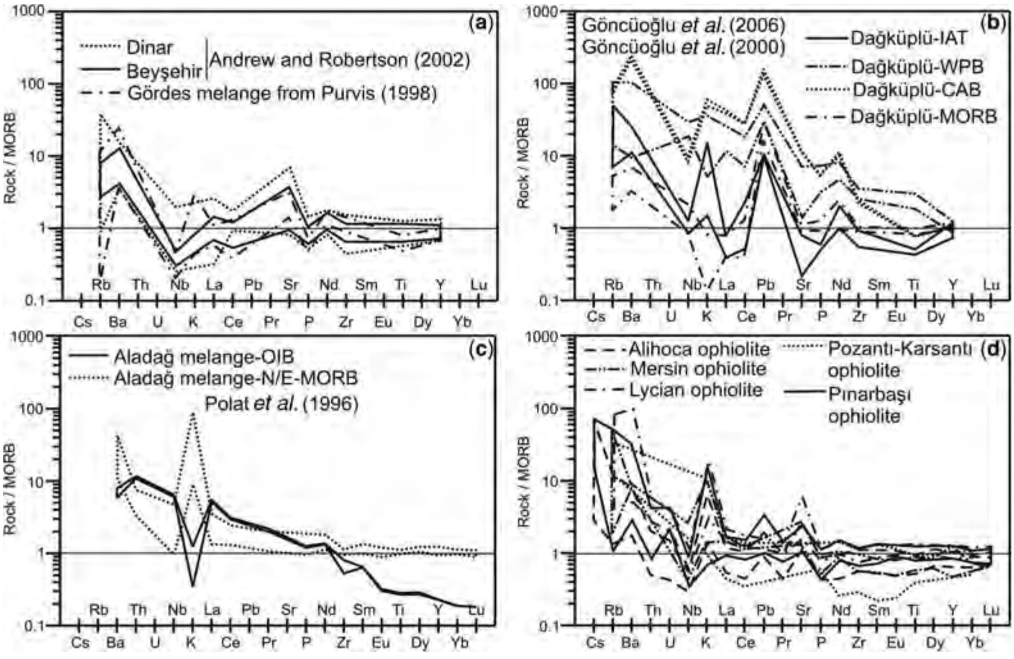

Fig. 20. Chondrite-normalized REE and N-MORB spider diagrams for the volcanics (**a**, **b**, **c**) of different ophiolitic mélanges and isolated dykes (**d**) cutting Tauride ophiolites in Anatolia. (normalizing values from Sun & McDonough 1989). See text for additional data sources.

differentiated patterns, whereas the second exhibits slightly LREE-depleted patterns. The basalt sample from the Çeşmisebil area shows a LREE-depleted pattern. The samples from the Bolkar Dağ region (from the Alihoca volcanic-sedimentary melange) display slightly LREE-depleted to spoon-shaped patterns. All of the samples (except sample 3 from Yunak region) are classified as arc tholeiites and show prominent depletion in high HFSE (high field strength elements) relative to fluid-mobile elements on N-MORB normalized multi-element diagrams (e.g. negative Nb anomaly with respect to the neighbouring incompatible elements). These features typically result from fluid metasomatism in subduction zones (Pearce *et al.* 1995). The basalts are slightly depleted in some HFSE and enriched in LREE with respect to N-MORB, which could reflect melt generation from a source that was depleted by previous melt extraction and subsequently enriched in mobile incompatible trace elements in a subduction zone setting (Pearce 1982; Arculus & Powel 1986; Yogodzinski *et al.* 1993; Wallin & Metcalf 1998; Pearce 2003; Pearce *et al.* 2005).

The trace-element characteristics of many of the basalts exhibit strong similarities with those formed in subduction-related environments elsewhere in the eastern Mediterranean region (Alabaster *et al.* 1982; Yalınız *et al.* 1996; Parlak *et al.* 2000; Al-Riyami *et al.* 2002; Rice *et al.* 2006; Rızaoğlu *et al.* 2006; Parlak 2006). Sample 3 from the Yunak region exhibits relatively enriched multi-element patterns similar to seamount-type alkaline basalts. However, a rift related (WPB) origin cannot be excluded on chemical grounds alone. Jurassic–Cretaceous alkaline-type basalts crop out extensively along the Neotethyan sutures in Turkey (e.g. Floyd 1993; Parlak *et al.* 1995; Lytwyn & Casey 1995; Dilek *et al.* 1999; Parlak 2000; Rojay *et al.* 2001; Çelik & Delaloye 2003; Vergili & Parlak 2005). Basalts from the Eskişehir area (Dağküplü melange) are indicative of a wide range of settings i.e. MORB, WPB and subduction influenced (Göncüoğlu *et al.* 2000, 2006). Based on chemical discrimination, samples of blueschists from the melange in the Altınekin area are suggestive of a subduction-influenced, backarc basin setting (Floyd *et al.* 2003). However, independent geological evidence of a backarc basin is lacking (e.g. related volcanic arc). Samples from unmetamorphosed Tauride-related melanges further south were derived from a comparable range of MORB, WPB and subduction-related settings. These include the Lycian melanges (Collins & Robertson 1997, 1998), the Beyşehir–Hoyran melange (Andrew & Robertson 2002), the Mersin Melange

(Parlak & Robertson 2004), and melange overlying the Menderes Massif (Purvis 1998) (Fig. 20).

Many of the volcanic rocks are interpreted to have come from a depleted mantle source region, modified by the addition of a subduction component. In contrast, the one sample of basalt from melange in the Yunak region is from enriched mantle without a subduction influence. In the Th/Yb vs. Ta/Yb diagram the samples mainly plot with the field of volcanic arc rocks (Fig. 21a). In the ternary element plot, Hf–Th–Nb (Fig. 21b) the volcanics and dykes are classified as volcanic arc and within-plate type (OIB). In the Zr/Y vs Zr diagram (Fig. 21c) these samples plot in the island arc basalt (IAB) and within-plate basalt (WPB) fields.

Summarizing, rare MORB samples are interpreted as oceanic crust. WPB is interpreted as seamount (OIB), rather than rift-related because these lavas are locally interbedded with radiolarite and pelagic carbonates rather than terrigenous sediments, Also, subduction-influenced basalts are surprisingly common in the melange. Subduction related 'volcanic-volcaniclastic rocks' have been reported to be interbedded with radiolarian sediments of Turonian age in central Anatolia, although detailed information on the occurrence is not published (Göncüoğlu *et al.* 2006*a*). It is likely that subduction related basaltic rocks in the Anatolide melange studied here, in the Bornova Melange (Aldanmaz *et al.* 2006) and in the metamorphic soles of the Tauride ophiolites (Çelik & Delaloye 2003) are Late Cretaceous in age.

Several oceanic settings for the subduction-influenced basalts can be considered. First, the arc-type basalts were detached from over-riding ophiolites and incorporated into gravity flows ('olistostromes') as olistoliths (Göncüoğlu *et al.* 2006*b*). However, some of the basalts can be interpreted as accreted thrust slices (e.g. Orhaneli area) rather than gravity blocks (see below). Second, the basalts were derived from an intra-oceanic arc, independent of the supra-subduction zone-type ophiolites. Any such arc would have been located south of the Tauride ophiolites, because the Tauride melanges (e.g. Lycian melange) include these basalts (Çelik & Delaloye 2003). However, independent evidence of an additional southerly subduction zone is lacking. Third, the subduction-influenced basalts might have been erupted associated with early arc magmatism above ophiolitic lithosphere that was created by supra-subduction zone spreading (possibly fed by isolated diabase dykes; see below). During convergence, the leading edge of the supra-subduction zone slab was dismembered and partially transferred to the subducting plate (and partially subducted; see below), allowing ophiolite-related lavas to be initially accreted as melange blocks and later gravitationally reworked in some areas. Fourth, the volcanics are accreted rift-related units (Triassic), in which the subduction component was either coeval or inherited from an earlier subduction event. This is, however, unlikely as these volcanics are not associated with terrigenous rift-related sediments and are locally dated as Late Cretaceous in age.

The third option seems the most plausible. In this case, soon after the ophiolite was created by supra-subduction zone spreading, continuing subduction led to the initial stages of construction of an oceanic volcanic arc. During subduction, or collision with the passive margin the leading edge of the over-riding ophiolite and the arc-type volcanics were detached, over-ridden and dismembered into blocks within the melange. It has commonly been questioned as to what happened to 'missing' forearc-type lithosphere that must have existed between the subduction trench and the finally emplaced ophiolite (e.g. in Oman; Lippard *et al.* 1986). The evidence from Anatolia partially answers this question as 'missing' crustal units can be found within the underlying melange.

The tectonic setting inferred for the basalts can be combined with the known ages of interbedded pelagic sediments to infer the tectonic history of the ocean basin. The available results from the suture zone indicate that deep-water MOR-type volcanism had begun by the Late Triassic (Bragin & Tekin 1996; Tekin *et al.* 2002; Göncüoğlu *et al.* 2006*a*, *b*) and was still forming as late as the Cenomanian (Göncüoğlu *et al.* 2006*a*, *b*). A similar timing has been inferred for Tauride units further south (Collins & Robertson 1998; Robertson & Pickett 2000; Danelian *et al.* 2006). When data from the Ankara Melange are included (Rojay *et al.* 2004) WPB-type basalts were erupted from Late Callovian to Aptian time. However, it should be noted that all of the MOR-type lavas are from blocks in melange and not from coherent ophiolites and so it is impossible to prove that they came from oceanic crust formed by sea-floor spreading although this is the most likely interpretation.

Supra-subduction zone ophiolite genesis

The Anatolide ophiolites (Tavşanlı and Afyon–Bolkardağ zones) are interpreted as exposed remnants of regionally extensive, emplaced oceanic lithosphere. All of the ophiolitic rocks are inferred, based mainly of geochemical evidence, to have formed by supra-subduction zone spreading. None are directly dated and the best indications of their crystallization age come from the metamorphic soles (see below). In contrast to the carbonate platform and much of the overlying melange, the over-riding ophiolites have mostly undergone only very

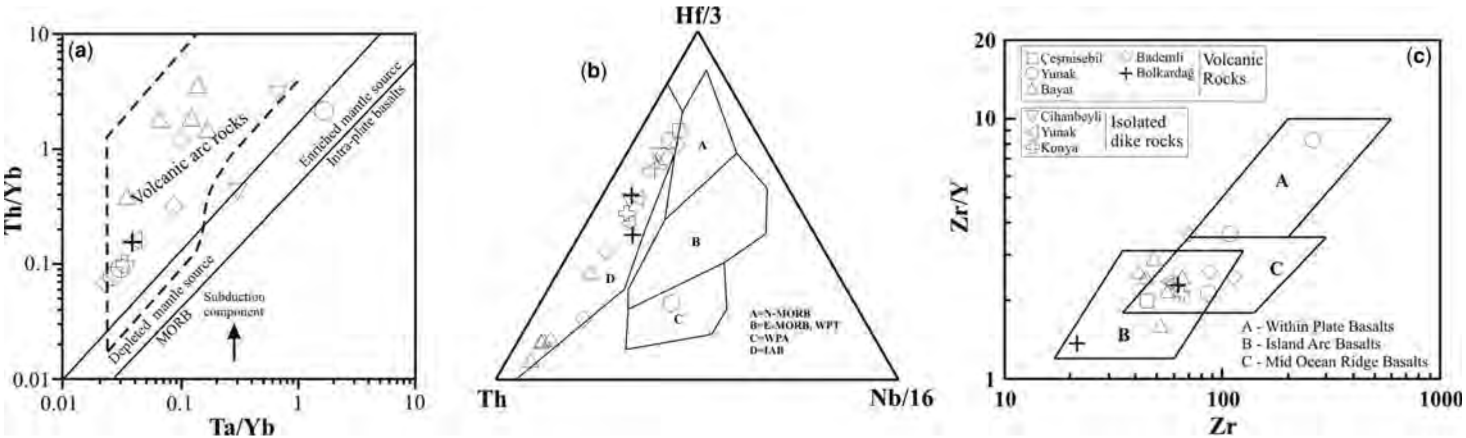

Fig. 21. (**a**) Th/Yb vs Ta/Yb (after Pearce 1982); (**b**) Hf-Th-Nb (after Wood 1980); and (**c**) Zr/Y vs Zr (Pearce & Norry 1979) tectonic discrimination diagrams for the volcanics from various locations in Turkey.

low-grade metamorphism. Many of the ophiolitic bodies are internally coherent; however, the Alihoca (Karsantı) ophiolite in the west is dismembered, transitional to tectonic melange. Within more structurally coherent ophiolitic bodies (e.g. Orhaneli, Eskişehir, Konya, Yunak, Çeşmisebil areas; Fig. 5) only the mantle sequence (e.g. hartzburgite, dunite) and fragments of the lower part of the crustal sequence (e.g. layered gabbros) are exposed. However, the dismembered Alihoca ophiolite includes all parts of a complete ophiolite, including sheeted dykes and basaltic extrusive rocks. This suggests that similar high-level crustal units originally existed in all of the ophiolites.

Isolated diabase dykes cutting ophiolite

The mantle sequences of the Anatolide ophiolites are typically cut by swarms of diabase/gabbro dykes (e.g. Orhaneli, Konya, Yunak, Çeşmisebil and Bolkar Dağ areas). In addition, similar dykes are seen cutting serpentinite in the Bornova zone (Seferihisar area). All of the dykes are basaltic in composition, exhibit flat REE patterns (and are characterized by enrichment of LIL elements (i.e. Rb, Ba, Th, K), Nb depletion, and flat patterns of HFS elements relative to MORB (Fig. 22a, b). Chemically similar dykes cut some of the Tauride ophiolites, including the Mersin ophiolite (Parlak & Delaloye 1996), the Lycian peridotite (Collins & Robertson 1998; Çelik & Delaloye 2003), the Antalya ophiolites (Celik & Delaloye, 2003), the Pozantı-Karsantı ophiolite (Lytwyn & Casey 1995; Dilek et al. 1999; Parlak 2000), the Alihoca ophiolite (Dilek *et al.* 1999) and the Pınarbaşı ophiolite (Vergili & Parlak 2005) (Fig. 20d).

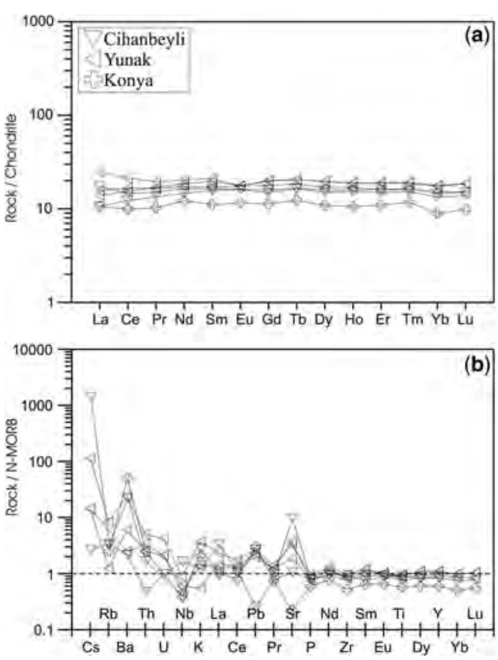

Fig. 22. Chondrite-normalized REE and N-MORB spider diagrams for isolated diabase dykes cutting serpentinized ultramafic rocks (this study).

The chemical evidence indicates that the isolated dykes were intruded in a subduction-related setting. Notably, Th is enriched in the mantle wedges above subduction zones, whereas Ta and Nb show similar degrees of enrichment and depletion in most mantle source regions (Pearce 1982; Alabaster *et al.* 1982). The isolated dykes are believed to reflect the initial stages of ocean arc magmatism (Parlak & Delaloye 1996; Collins & Robertson 1998). Although only rarely preserved within the Tauride and Anatolide ophiolites (i.e. Parsantı ophiolite), chemically similar extrusives form an important part of the Upper Cretaceous ophiolites in southeastern Anatolia (e.g. Göksun or N Berit) ophiolite (Parlak *et al.* 2004). In addition, the dykes are chemically similar to the subduction-influenced basaltic blocks in the melange, as discussed above.

Metamorphic soles

The hartzburgite sheets are locally underlain by amphibolites (e.g. Orhaneli, Konya and Çeşmisebil areas), interpreted as metamorphic soles. The sole-type rocks of the Orhaneli area are attached to the base of over-riding ultramafic ophiolite sheets, whereas the amphibolites in the Çeşmisebil area are encased in serpentinite melange near the base of over-riding ophiolitic peridotite, and those in the Konya area are associated with large hartzburgite blocks in the melange.

Most of the amphibolites show no petrographic evidence of HP/LT metamorphism; these remained attached to the base of the ophiolites when they were emplaced onto the Tauride–Anatolide platform. By contrast, sole-type amphibolites above the metamorphosed Bolkar Dağ platform (Kızıl Tepe) exhibit a HP/LT blueschist mineralogy (i.e. 8–12 Kbar *c.* 24–35 km burial) (Dilek & Whitney 1997) indicating that some ophiolite-related material was subducted, then rapidly exhumed. Also, amphibolites from the sole of the Karsantı ophiolite in the same region are indicative of relatively HP conditions (5–6 Kbar *c.* 15 km burial) based on amphibole geobarometry (Çelik 2007).

The metamorphic soles also provide insights into the nature of oceanic protoliths. Geochemical evidence from amphibolitic sole rocks in the Tavşanlı zone indicates the presence of (at least) alkaline (seamount)-type basalts (Kaynarca area; SW of Kütahya) (Önen & Hall 1993). Amphibolite protoliths in the Afyon–Bolkardağ zone are known to include subduction-influenced (arc) and alkaline (seamount) type basalts (Konya area; Daşçı 2007). There is extensive geochemical evidence of metamorphic soles of the Tauride ophiolites (i.e. not including southern Neotethyan ophiolites that are not discussed here). The protoliths of the Mersin ophiolite sole are of within-plate (seamount)-type (Parlak *et al.* 1995), and those of the Lycian and Beyşehir ophiolites further east record a range of within-plate, mid-ocean ridge and arc-type chemical types (Çelik & Delaloye 2003).

Summarizing, taken together, the metamorphic soles and the basalts in the melanges are chemically indicative of a similar range of seamount-type, arc-type and mid-ocean ridge type tectonic settings.

The metamorphic soles currently give the best estimates of the ages of both the Anatolide and Tauride ophiolites since the primary crystallization age of these ophiolites is yet to be determined. This approach assumes that the metamorphic soles were created related to overthrusting of young, hot oceanic mantle lithosphere, as in other areas (e.g. Oman; e.g. Hacker *et al.* 1996). Accordingly, the Tavşanlı (Kütahya) ophiolites formed around 93 Ma (e.g. Önen 2003), and the Tauride ones around 96–90 Ma; i.e. 91 Ma for the Bolkar Dağ sole (Kızıl Tepe), Dilek *et al.* 1999; 92–90 Ma for the Pozantı-Karsantı sole (Dilek *et al.* 1999; Çelik *et al.* 2006; and 96–91 Ma for the Mersin sole (Parlak & Delaloye 1999).

Ridge subduction or slab break-off?

Lytwyn & Casey (1995) noted the existence of a range of depleted, to enriched-composition, dykes cutting the metamorphic sole and the overlying ultramafic ophiolitic rocks of the Karsantı ophiolite, which were explained by intrusion through an asthenospheric slab window that was created by subduction of a mid-ocean ridge. Chemically depleted crosscutting dykes from the Alihoca (Pozantı) ophiolite further west were dated at *c.* 91 Ma (Dilek *et al.* 1999). The Karsantı ophiolite was later re-interpreted as a typical supra-subduction zone (Parlak *et al.* 2000; Robertson 2002) but this need not preclude the development of a slab window when the SSZ-spreading axis was subducted. Alternatively, Çelik (2007) reported enriched alkaline pyroxenite dykes cutting the metamorphic sole from the Pozantı-Karsantı ophiolite and explained these by a mechanism in which an asthenospheric slab window formed during oceanic slab break-off. However, others propose slab break-off much later in this region during Eocene continental collision (see below). One difficulty with slab break-off prior to emplacement of an ophiolite onto a passive margin is that once detached from its downgoing slab the margin is likely to have become buoyant, effectively preventing ophiolite emplacement onto the continental margin. However, further evaluation of the possibilities of ridge subduction or slab break-off are beyond the scope of this paper.

Melange genesis

The timing of melange genesis is constrained as Upper Cretaceous (mainly Early Maastrichtian–Early Paleocene) from a combination of the youngest ages of the intact pelagic carbonate successions on the drowned carbonate platform beneath the melange (pre-Maastrichtian; e.g. Konya; Bayat areas), the youngest age of oceanic crust obtained from melange blocks (Cenomanian; Eskişehir area), direct dating of the melange matrix (Early Maastrichtian–Early Paleocene; Bayat area), and the Late Maastrichtian or Paleocene–Early Eocene age of local cover sediments (e.g. Bokardağ and Bayat areas; see below). Melange genesis and emplacement were to some extent diachronous along and across the margin (Candan *et al.* 2005; Okay & Altıner 2007).

The melange is interpreted as remnants of Neotethyan oceanic lithosphere, deep-sea sediments, volcanic seamounts, and also of some rift-related and platform units that were emplaced by a combination of tectonic and sedimentary processes. We recognize three main intergradational stages of melange development (excluding the Bornova zone which differs in some respects). First, basaltic rocks (MORB & WPB-type) were accreted to the base of the overlying supra-subduction zone ophiolite (*c.* 100–90 Ma; Fig. 23a). This melange is tectonic in origin, has little evidence of sedimentary reworking, and includes material incorporated from the over-riding ophiolite (e.g. serpentinite) and exhumed blueschists. Examples include relatively thick (10s–100s m) slices of basaltic rocks, radiolarites and pelagic carbonates in the upper levels of the melange in the Tavşanlı zone (e.g. Orhaneli and Eskişehir areas).

Second, when the accretionary complex approached the Tauride–Anatolide continent (Upper Santonian–Lower Maastrichtian) large volumes of terrigenous sediments accumulated in a marginal subduction trench and clastic material began to accumulate as debris flows derived from the advancing accretionary wedge (Fig. 23b). It is important to note that the rifted margin is restored as off-margin platforms and rift basins to the north of the main carbonate platform margin (Andrew & Robertson 2002). Parts of this rifted margin are now preserved in the Taurides, as the Beyşehir nappes (e.g. Boyalı Tepe and Huğlu units), the Lycian nappes (Domuzdağ unit) and the Mersin Melange. Moix *et al.* (2007, 2008) support the

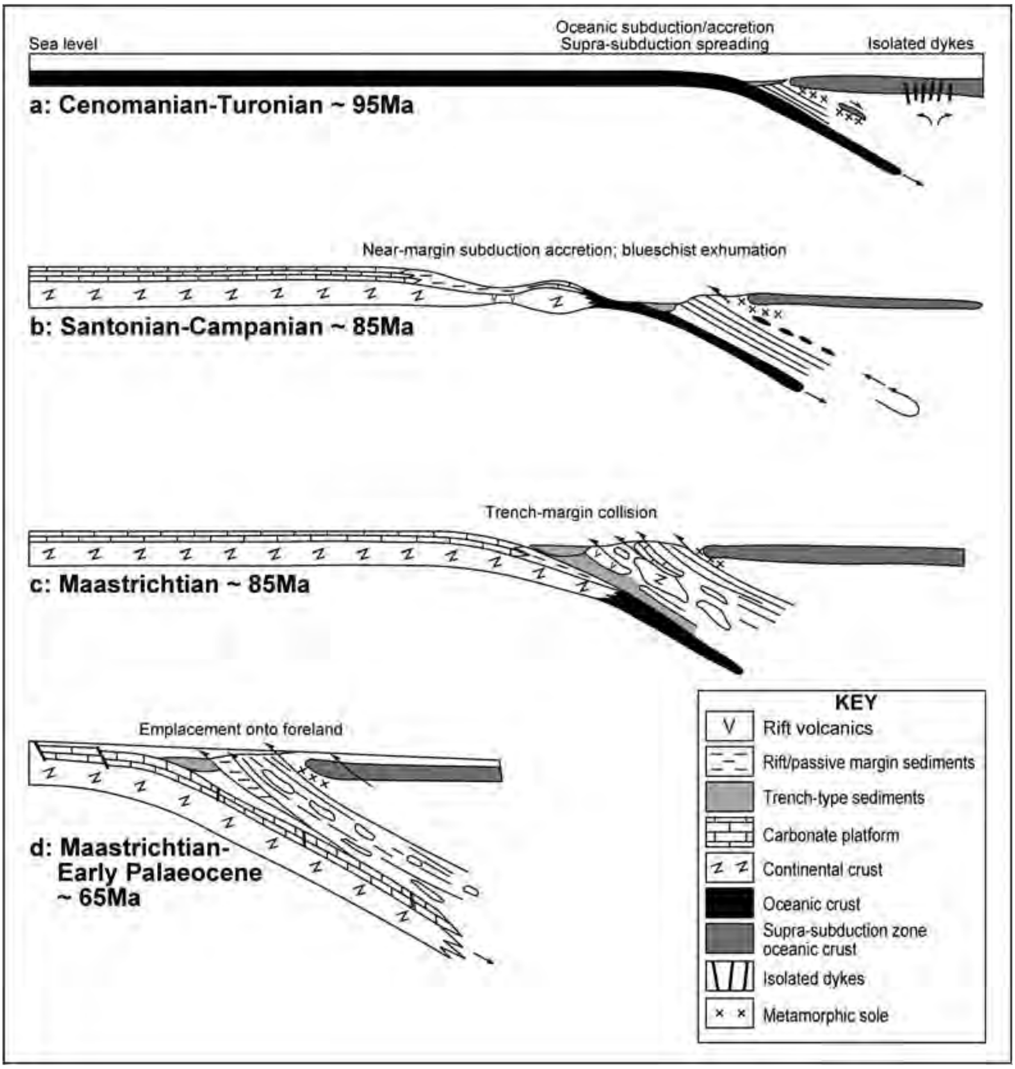

Fig. 23. Stages in the progressive emplacement of melanges from the Neotethyan ocean to the north onto the Anatolide–Tauride continent to the south. See text for explanation.

general correlation of some of the Mesozoic units of the Mersin Melange with the Boyalı Tepe unit of the Beyşehir nappes strengthening the interpretation that these units were thrust far southwards across the Tauride–Anatolide platform (Parlak & Robertson 2004). The platform and rifted margin units collapsed and broke-up when the subduction trench/accretionary wedge collided with the rifted margin. Some material was shed as blocks and debris flows from the collapsing margin (e.g. Bayat area). Fragments of the off-margin platforms were accreted into a matrix of terrigenous trench-type deposits. For example, numerous large blocks and sheets of recrystallized limestones with common nodular chert (e.g. Çeşmisebil; Bayat; Yunak; Bademli areas) were probably accreted from the higher (Upper Cretaceous) levels of subducting marginal platforms or from the regional platform margin. More oceanic-derived material, including subduction-influenced basalts and cherts, became tectonically admixed. Blueschists were exhumed possibly within serpentinite or shale diapirs (e.g. Cloos & Shreve 1988) and emplaced at generally high levels of the melange (e.g. Yunak; Bayat areas). As convergence continued (Late Maastrichtian–Early Palaeocene) accretionary material was mixed, recycled and gravitationally redeposited as multiple debris flows, locally with either a shale or serpentinitic matrix (e.g. Altınekin; Bademli areas). For example, blueschists, massive serpentinized peridotite, marble and meta-chert were gravitationally reworked as blocks within sedimentary serpentinite that was later strongly sheared (Altınekin area). Elsewhere, blocks of pelagic sedimentary rocks and volcanic rocks were incorporated into sedimentary serpentinite and later tectonically mixed with shale in a terrigenous (i.e. near-margin) setting (e.g. Bademli area).

Third, the entire Anatolide–Tauride margin was subducted, associated with the development of a fault-influenced flexural foredeep far to the south (>150 km; Fig. 23c). Accretionary material was reworked southwards from the advancing accretionary wedge by a combination of gravity reworking and bulldozing ahead of the advancing ophiolite. This led to the formation of the sedimentary melanges that are associated with the allochthonous continental margin units (e.g. Beyşehir melange; Maastrichtian–?Paleocene) and with the relatively autochthonous Menderes Massif (Maastrichian–Eocene locally). During the latest stages of convergence large slices of the former rifted margin (e.g. Mersin Melange and the Lycian Layered Tectonic Melange) were overthrust by ophiolite-related melange (e.g. Lycian Ophiolitic Melange) and then by regional-scale ophiolites. These ophiolites include the Lycian and Beyşehir peridotites in the Taurides. The ophiolites of the Anatolides, discussed here, were also emplaced southwards onto the Tauride–Anatolide continental margin during latest Cretaceous time. However, these ophiolites were translated relatively northwards above an extensional detachment as part of an upper plate when the HP/LT-metamorphosed Anatolide continental margin was exhumed from beneath (see below). In contrast, the Tauride ophiolites remained as part of exhuming plate and so ended up relatively far to the south.

Most of the ophiolites in western and central Anatolia lack an upper crustal sequence, including sheeted dykes and overlying extrusive rocks. The Alihoca (Pozantı) ophiolite is an exception because all of the units of an ophiolite are exposed there, albeit dismembered. Indeed, much of the Alihoca ophiolite is made up of blocks in a sheared shaly matrix. The Alihoca ophiolite is likely to have been dismembered during emplacement and is thus intermediate between typically intact over-riding ophiolites and accretionary melange. The break-up of the ophiolites to form blocks in melange is even more pronounced in the Bornova Melange.

One possibility to explain the general absence of upper crustal units is that these ophiolites, like those of the Alps, formed at a rifted spreading axis soon after continental break-up, where sheeted dykes never existed (e.g. Manatschal & Bernoulli 1999; Manatschal *et al.* 2003). However, the Alpine-type ophiolites are compositionally and structurally dissimilar to those of the Taurides–Anatolides. On the other hand, complete ophiolite sequences similar to the Tauride–Anatolide ophiolites, discussed here, do exist on strike to the east, in the Eastern Taurides (Robertson 2002; Parlak *et al.* 2004). The likely explanation of the missing crustal sequences is that they were eroded. The most probable time for this erosion is during the Paleocene–Early Eocene, after initial emplacement onto the Tauride–Anatolide continental margin when ophiolites were located at the highest levels of the regional thrust stack, put prior to continental collision during the Mid-Eocene. During this collision some of the ophiolitic rocks, already lacking crustal sequences (e.g. Dipsiz Göl ophiolite; Central Taurides; e.g. Andrew & Robertson 2002), were incorporated into deeply buried thrust stacks and so were no longer available for erosion at the earth's surface.

The Bornova melange differs from the other melanges because of its huge scale, different regional trend (NE–SW) and the presence of dismembered ophiolites mixed with an ophiolite-derived matrix. The Bornova melange is unlikely to restore simply as a north–south transform-related termination of the Tauride–Anatolide rifted margin (Okay & Tüyşüz 1999) because in this case there would be little reason for large-melange accretion. We restore the Bornova zone as a relatively SW–NE-trending segment of the Anatolide–Tauride continental margin, such that convergence in this area is likely to have been oblique, which may in turn have influenced melange genesis in this area. The generally higher and more northeasterly Bornova ophiolitic melange accreted in an oceanic setting with extensive gravity reworking and mixing of over-riding ophiolites (e.g. Manisa area). The generally structurally lower Bornova sedimentary-volcanic melange records accretion and extensive gravity reworking as gravity blocks and multiple debris flows with a matrix of terrigenous trench-type sediments. However, mixing also resulted from on-going accretion/collision. The blocks include marginal-platform sequences (Okay & Altıner 2007), similar to Tauride thrust units of the Beyşehir nappes (Andrew & Robertson 2002), the Lycian nappes (e.g. Domuz Dağ unit) (e.g. Collins & Robertson 1997, 1998) and the Mersin Melange (Parlak & Robertson 2004). The structurally lowest part of the Bornova melange in the south near the Menderes Massif (e.g. Seferihisar area) is metamorphosed, possibly as a result of deep burial beneath over-riding accretionary and ophiolitic units. The collapsed carbonate platform is exceptionally exposed in the Karaburun Peninsula in the west.

This platform is unmetamorphosed unlike the Anatolide platform, possibly because this segment of the margin was located south of the region of subducted continental margin, similar to the Tauride carbonate platform.

Continental margin subduction and exhumation

The LT/HP metamorphism of both the Tavşanlı zone (e.g. Orhaneli and Sivrihisar areas) and the Afyon–Bolkardağ zone (e.g. Bayat, Altınekin and Bolkardağ areas) resulted from very deep burial of the Mesozoic platform, some of the melange and fragments of ophiolite and metamorphic sole. Geothermobarometry indicates HP/LT metamorphism of the Anatoide platform at 20 ± 2 kbar (*c*. 50–60 km depth) and 430 ± 30 °C (Okay & Kelley 1994), while Ar/Ar isotopic data most recently indicate a Campanian age (*c*. 80 Ma) for blueschist metamorphism (Sherlock *et al.* 1999). Fe-Mg carpholite-bearing assemblages of the Afyon–Bolkardağ zone imply temperatures of *c*. 350 °C and minimum pressures of 6–9 kbar (*c*. 30 km) (Candan *et al.* 2005), but have not yet been accurately dated radiometrically.

Candan *et al.* (2005) envisage that the leading edge of the Tauride–Anatolide platform (Tavşanlı zone) began to collide with obducting ophiolites in the Cenomanian (*c*. 98 Ma) and that the continental margin progressively subducted until around end-Early Paleocene (*c*. 35 Ma). To maintain LT conditions suitable for blueschist preservation (without retrogression) they postulated simultaneous subduction and exhumation (i.e. involving continental slab roll-back). The Tavşanlı zone platform is, indeed, internally imbricated as suggested by local metamorphic grade variations (Whitney & Davis 2006). However, we observed that the Afyon–Bolkardağ platform is relatively intact without e.g. interslicing of melange. Rather than beginning at *c*. 98 Ma we infer that collision and margin subduction began around *c*. 85 Ma (Late Santonian) and ended by *c*. 61 Ma (Middle Paleocene), when the exhumed HP/LT rocks of the Tavşanlı and Afyon–Bolkardağ zones, the Menderes Massif and Tauride units were locally transgressed by shallow-water sediments of ?Mid–Late Paleocene to Early Eocene age. In the northern Bolkar Dağ area exhumation occurred by the Late Maastrichtian when shallow-water limestones began to accumulate unconformably on melange and emplaced ophiolites. The presence of sedimentary melange locally dated as Eocene in the southern Menderes Massif indicates later reworking of accretionary material, but this was possibly related to much-later regional continental collision (see below).

In the east, the thin unit of polymict debris flows with isolated blocks, so far recorded only in the Bolkar Dağ area resulted from gravity reworking of both HP- and LP-metamorphosed accretionary melange and ophiolitic material as multiple debris flows prior to covering by transgressive Maastrichtian shallow-marine sediments. Some of this material was reworked in a high-energy beach or fluvial settings because some of the clasts are very well rounded and water-worn. The polymict debris appear to a have formed actually during exhumation of the Anatolide platform and melange, followed by transgressive shallow-water deposition when this was complete. Further west, exhumation was complete before the Late Paleocene by the time when the melange was covered by shallow-marine Nummulitic limestones (e.g. Bayat and Orhaneli areas).

Our work shows that generally north–south orientated, shallow-dipping stretching lineations are commonly developed within the metamorphosed Anatolide carbonate platform and the metamorphic melange (e.g. the Yunak, Altınekın and Çeşmisebil areas). Stretching lineations are generally most intense near the contact between the carbonate platform and overlying melange. On the other hand, east–west-trending mineral lineations were reported from further west, including Orhaneli (Okay & Tüysüz 1999). Studies of other areas indicate that stretching lineations in similar HP/LT metamorphic rocks may develop either related to exhumation or to deep-burial unrelated to exhumation (see Whitney & Davis 2006). Outcrops studied by us rarely show clear kinematic indicators (e.g. asymmetrical 'wing' structures) and, where present, locally suggest both northward and southward displacement. However, in general, we relate the widely developed north–south stretching lineations to regional exhumation of the Anatolide carbonate platform, metamorphosed melange and related unit, followed by sub-parallel deposition of transgressive sediments (e.g. Bayat area).

In addition, in the east the Ulukışla Basin includes thick volcanic units of Paleocene–Early Eocene age in which basaltic members exhibit 'enriched' patterns of stable major and trace elements, combined with a subduction influence (e.g. negative Nb anomaly). The subduction influence is seen as being inherited from Upper Cretaceous subduction in the region. Further east, the Paleogene cover of the Lycian nappes (Faralya Fomation; Şenel 1991) includes basaltic flows that show mild 'enrichment' and a subduction influence (Collins 1994; Collins & Robertson 1998). The volcanics and the Ulukışla Basin generally are considered to record an extensional or transtensional setting during Palaeogene time (Clark & Robertson 2002, 2004).

The timing of exhumation in the west (e.g. Orhaneli area) is also constrained by the presence of several crosscutting granodiorite plutons of Early Eocene age (52–48 Ma; Harris *et al.* 1994). The plutons cut the metamorphosed platform and ophiolitic peridotite, but pre-date final southward thrusting of the Sakarya zone over the Tavşanlı zone (MTA 2002). In addition, evidence from the Taurides constrains the timing of melange emplacement as mainly Campanian–Maastrichtian–Paleocene in different areas. This is based on a combination of the age of the youngest pelagic sediments above the Tauride carbonate platform (Campanian–Maastrichtian of the Bolkar Dağ), the locally determined age of the melange matrix (Maastrichtian–Paleocene) in the Beyşehir and Lycian Nappes (Andrew & Robertson 2002; Collins & Robertson 1998), and the age of the cover sequence, where exposed (Paleocene for the Lycian Nappes; Şenel, 1991; Collins & Robertson 1998). Summarizing, the ages of emplacement in both the Anatolides and Taurides is broadly similar, suggesting melange was rapidly emplaced over the regional platform (i.e. within *c.* 5 Ma) after initial trench-margin collision (*c.* 85–Ma).

Continental collision

All of the units, including the Anatolide–Tauride continent in the south and the Sakarya zone in the north, experienced pervasive folding and thrusting during Mid–Late Eocene time. The maximum age of this deformation is given by the youngest ages of intact sedimentary sequences overlying exhumed units; i.e. Early Eocene in the Ulukışla Basin and further west (e.g. Bayat and Kütahya areas). The minimum age of deformation is given by the oldest age of unconformably overlying (non-marine) sediments in several areas (i.e. Oligocene in the Ulukışla Basin). We, therefore, infer that continental collision (which was probably diachronous) mainly took place during Mid-Eocene time (*c.* 45 Ma) and was complete by Late Eocene time (*c.* 50 Ma; Bartonian).

In the east, the Mesozoic Bolkar Dağ carbonate platform was internally sliced and back-thrust northwards over melange and the Maastrichtian–Eocene Ulukişla Basin. Less intense reverse faulting also affected the Mesozoic platform and overlying units further west (i.e. in the Altınekin area). Eocene polyphase folding is especially well exposed in the Konya area (Eren 2001). The Beyşehir nappes were thrust southwards, taking with them large slices of the Geyik Dağ platform to form the Hadim Nappe (Özgül 1997; Mackintosh 2008). The Lycian Nappes and related melanges were also rethrust southwards over the Menderes Massif. They were subsequently thrust to their most southerly position during the Mid-Miocene (Langhian, *c.* 15 Ma) (Flecker *et al.* 2005), a later history that is outside the scope of this paper. Mesozoic–Lower Cenozoic clastic meta-sedimentary rocks correlated with the Lycian nappes were imbricated and buried to *c.* 30 km during Middle–Late Eocene (Rimmelé *et al.* 2003, 2006; Candan *et al.* 2005). This implies two stages of continental margin metamorphism in this region, the first during latest Cretaceous–early Cenozoic associated with trench-margin collision which resulted in deep subduction of the Tauride–Anatolide continental margin, and the second during Early–Middle Eocene related to continental collision when a very thick crustal pile was developed on top of the Menderes Massif.

The Sakarya zone was thrust southwards and imbricated with the Tavşanlı zone (e.g. Sivrihisar area) during the Mid-Eocene. However, the contact between the Tavşanlı zone and the Sakarya zone is generally a younger high-angle, strike-slip fault (e.g. Orhaneli area).

Regional palaeogeography: one or several oceanic basins?

Any realistic plate-tectonic reconstruction is critically dependent on determining the number and location of Mesozoic ocean basins between Eurasia and the Tauride–Anatolide continent to the south.

Two main alternatives can be considered (Fig. 24a, b). First, the Niğde–Kırşehir massif formed a promontory of the Tauride–Anatolide microcontinent, with a single Mesozoic ocean, the İzmir–Ankara–Erzican ocean to the north. In this scenario, all of the Anatolide and Tauride ophiolites formed above a single northward-dipping intra-oceanic subduction zone during the Late Cretaceous. The Niğde–Kırşehir promontory later collided with the intra-oceanic subduction zone and ophiolites were emplaced southwards over the Niğde–Kırşehir massif (where present), onto the Tauride–Anatolide continent, reaching as far south as the Mersin ophiolite on the southerly flanks of the Bolkar Dağ (Yalınız *et al.* 1996, 2000; Floyd *et al.* 2000). Remaining ocean to the north of the intra-oceanic subduction zone closed during Early Cenozoic time. In a second alternative the Niğde–Kırşehir massif rifted from the larger Tauride–Anatolide continent during the Triassic, becoming a continental fragment capped by a Mesozoic carbonate platform during later Mesozoic time. The inferred intervening ocean is known as the Inner Tauride Ocean (Görür *et al.* 1984, 1988). During the Late Cretaceous, regional convergence triggered northward subduction within this ocean and Tauride ophiolites (e.g. Mersin; Alihoca; Karsantı; Pozantı) formed by spreading above this southerly subduction zone. Ophiolites were emplaced southwards onto the Anatolide–Tauride continent when the subduction trench collided with the passive margin (Robertson & Dixon 1984; Whitney & Dilek 1997; Robertson 2002). Northward subduction gave rise to Upper Cretaceous arc magmatism within the Niğde–Kırşehir massif (Central Anatolian Crystalline Complex) to the north (Kadıoğlu *et al*. 2006).

An assessment of whether or not the Inner Tauride Ocean really existed is dependent on the analysis of a large body of data from the entire region including northern and eastern Anatolia, areas largely outside the scope of this paper. Unfortunately, the potential Inner Tauride suture is largely covered by the Maastrichtian–Eocene Ulukışla Basin so that the existence of a former southerly margin of a Niğde–Kırşehir microcontinent cannot be confirmed. However, most of the evidence discussed in this paper supports, or is consistent with, the existence of the Inner Tauride ocean. First, the northern margin of the Anatolide–Tauride continent, including the Bolkar Dağ to the south of the inferred Inner Tauride suture experienced regional HP/LT metamorphism (Candan *et al.* 2005), which contrasts with the Niğde–Kırşehir massif that underwent Barrovian metamorphism at up to 5–6 kbar, >700 °C (Whitney & Dilek 1998; Fayon *et al.* 2001). The massif is, therefore, likely to have been located in the over-riding rather than subducting plate, or at least was not buried beyond mid-crustal levels. Second, most of the Anatolide melanges (e.g. Altınekin; Konya and Bayat areas) and some ophiolite-related fragments (e.g. Kızıl Tepe ophiolite and sole of the Bolkar Dağ) also show HP/LT metamorphism. This suggests that the Tauride–Anatolide continental margin. much of the melange and some ophiolite-related fragments were subducted and exhumed together. Third, we observed no structural evidence (e.g. crosscutting structures) to show that the HP/LT melange (e.g. at Altınekin) was emplaced separately from the Antolide carbonate platform beneath. Fourth, the (Tauride) Beyşehir–Hoyran nappes, including melange and ophiolites, form an approximately linear outcrop extending for >500 km east–west, surprising if they were emplaced across a discontinuous Niğde–Kırşehir promontory (Andrew & Robertson 2002). Fifth, assuming a northerly root zone for the ophiolites including the Mersin ophiolite (furthest south) >500 km thrust transport is required, which seems excessive (Andrew & Robertson 2002).

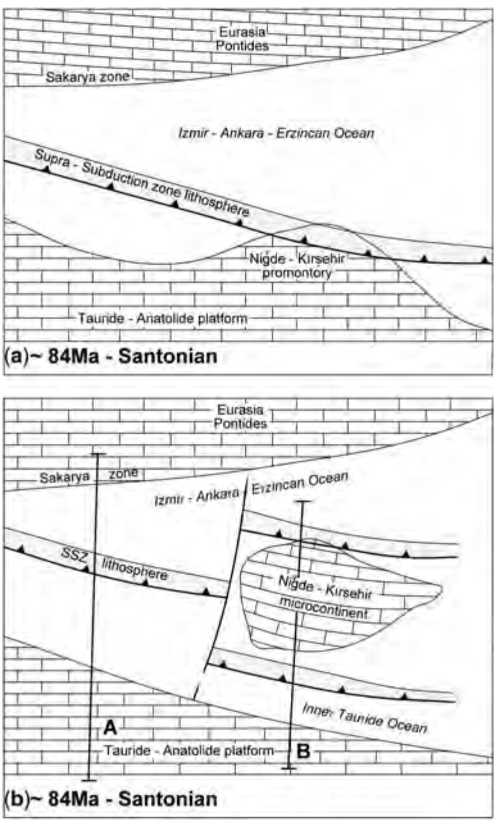

Fig. 24. Alternative regional tectonic models. (**a**) With the Niğde-Kışehir massif as a promontory of the Anatolide–Tauride continent; (**b**) with the Niğde-Kışehir as a microcontinent. A transform fault is tentatively shown terminating the Inner Tauride ocean in the west. Alternatively, the Inner Tauride ocean extended the length of Anatolia. See text for discussion.

In our reconstruction, below, we assume the existence of the Inner Tauride Ocean, but this, in turn, raises several other questions. First, are the Upper Cretaceous granitic rocks cutting the Niğde–Kırşehir massif related to northward subduction of oceanic crust of the Inner Tauride ocean, or are they instead continental collision related? The plutons range in age from 80–70 Ma (Kadıoğlu *et al.* 2006; Göncüoğlu 1986; Yalınız *et al.* 1999) and are classified as of I-, S- and A-type (see Boztuğ 2000; Kadıoğlu *et al.* 2006). The magmas were either derived from subduction-modified, metasomatized mantle, or from an enriched mantle with considerable crustal contamination. Kadıoğlu *et al.* (2006) favour a subduction-related setting related to Upper Cretaceous closure of the Inner Tauride Ocean. In contrast, for Boztuğ (2000) these granitic rocks formed after the collision of the Anatolides and Pontides during Late Cretaceous time. Unfortunately, the Upper Cretaceous granitic plutons lack related extrusive rocks which could help indicate their relationship to the regional stratigraphy (i.e. pre-syn-or post-collisional). Although a generally

NW–SE-trending belt of granitic rocks exists along the western margin of the Kırşehir massif, their overall distribution is patchy, which questions their orgin as a conventional subduction-related magmatic arc (cf. Kadıoğlu *et al.* 2006). On the other hand, their Cretaceous age long predates regional continental collision (i.e. Eocene) of the Eurasian (Pontide) and Tauride–Anatolide continents, and thus the Upper Cretaceous granitic rocks are unlikely to relate to crustal thickening and deep-level anatexis (cf. Boztuğ 2000). Ilbeyli *et al.* (2004) suggested that these Upper Cretaceous granititc rock relate to slab break-off and delamination processes. The Upper Cretaceous Niğde–Kırşehir granitic rocks are therefore likely relate to closure of the Inner Tauride ocean and collision of the Anatolide and Niğde–Kırşehir continental units.

Second, did oceanic crust exist to the north of the Niğde–Kırşehir continental unit during the Mesozoic. For example, Kazmin & Tikhonova (2006) consider Niğde–Kırşehir massif to be part of the Eurasian margin during the Mesozoic. Also, Kadıoğlu *et al.* (2006) dispute the existence of emplaced ophiolites above the Niğde–Kırşehir massif, which they instead interpret as Upper Cretaceous intra-continental intrusions (e.g. gabbros). Related to this controversy is the question of what caused the Upper Cretaceous Barrovian metamorphism of the Niğde–Kırşehir massif (Whitney & Dilek 1998; Fayon *et al.* 2001). Our own unpublished studies of the Çiçekdağ and Sarıkaraman, and other related, mainly igneous units, overlying the Niğde–Kırşehir massif support their interpretation as supra-subduction zone-type ophiolites, emplaced from the İzmir–Ankara–Erzincan ocean to the north (Yalınız *et al.* 1996, 2000; Floyd *et al.* 2000). Despite being dismembered, all of the main components of an originally complete ophiolite are present, including well-dated (Upper Cretaceous) pelagic sediments, basaltic extrusives, sheeted dykes, isotropic gabbro, plagiogranite and layered gabbro. Assuming the existence of a subduction zone dipping northwards from the Niğde–Kırşehir massif, the Upper Cretaceous HT/LP metamorphism of the Niğde–Kırşehir massif might be explained by collision and shallow-level underplating of the microcontinent beneath a forearc to the north.

Assuming the existence of the Inner Tauride Ocean, a remaining question is its original westward (and eastward) extent. One option is that the ocean terminated against a north–south transform near the western margin of the Niğde–Kırşehir microcontinent, in which case only one oceanic basin existed to the west of this, and all of the Anatolide and Tauride ophiolites (west of the inferred transform) represent parts of a single regionally emplaced supra-subduction zone ophiolite. Alternatively, two spreading axes developed the length of Anatolia. In this case, Cretaceous regional compression triggered northward subduction of both of these oceanic domains; the Tauride ophiolites were emplaced from the Inner Tauride ocean, whereas the Anatolide ones were emplaced from the more northerly Izmir–Ankara–Erzincan ocean. In Figure 24b, we suggest a transform termination as two subduction zones are not documented west of the Niğde–Kırşehir massif. Figure 25 shows corresponding plate-tectonic sketches, with a single ocean in the west in (a), and an Inner Tauride ocean to the south of the Niğde–Kırşehir massif in (b).

Plate-tectonic summary

This incorporates our favoured tectonic interpretations and timing of events as above (Figs 25 & 26). Triassic rifting was followed by passive margin subsidence during Jurassic–Early Cretaceous. During Triassic–Late Cretaceous (Cenomanian, *c.* 100 Ma) MOR-type oceanic lithosphere formed at spreading axes, while seamounts formed related to hot-spot activity (Late Jurassic–Early Cretaceous). Common arc-type basalts record an intra-oceanic arc, possibly ophiolite related, and preserved only as accreted blocks in the melange. During the Cenomanian (*c.* 100 Ma) the entire Tauride–Anatolide platform was flooded and covered by pelagic sediments until the Santonian (*c.* 85 Ma). After northward subduction began all of the ophiolites formed by supra-subduction zone spreading. Swarms of subduction-influenced dykes cutting many of the ophiolites reflect incipient arc magmatism, eventually terminated by collision with the continental margin to the south. Metamorphic soles formed during intra-oceanic subduction prior to obduction onto the continental margin (*c.* 100–90 Ma; Cenomanian–Turonian). The soles probably relate to initial displacement of still-hot lithosphere within the ocean (Jones *et al.* 1991; Garfunkel 2006) rather than to steady-state oceanic subduction, or initial obduction onto the margin. Oceanic crust and seamounts, collectively of Late Triassic–Cenomanian age, were accreted in a trench/forearc setting, together with oceanic radiolarites and pelagic limestones. Some of this material was soon exhumed and recycled as multiple debris flows during Upper Maastrichtian–Lower Paleocene in different areas. The subduction trench began to collide with the Anatolide–Tauride continental margin around late Santonian time (*c.* 85 Ma), with regional diachroneity. The platform flexurally up-warped and then collapsed to form a foredeep into which accreted oceanic material was emplaced as gravity flows and thrust units ahead of the advancing ophiolite. The platform then

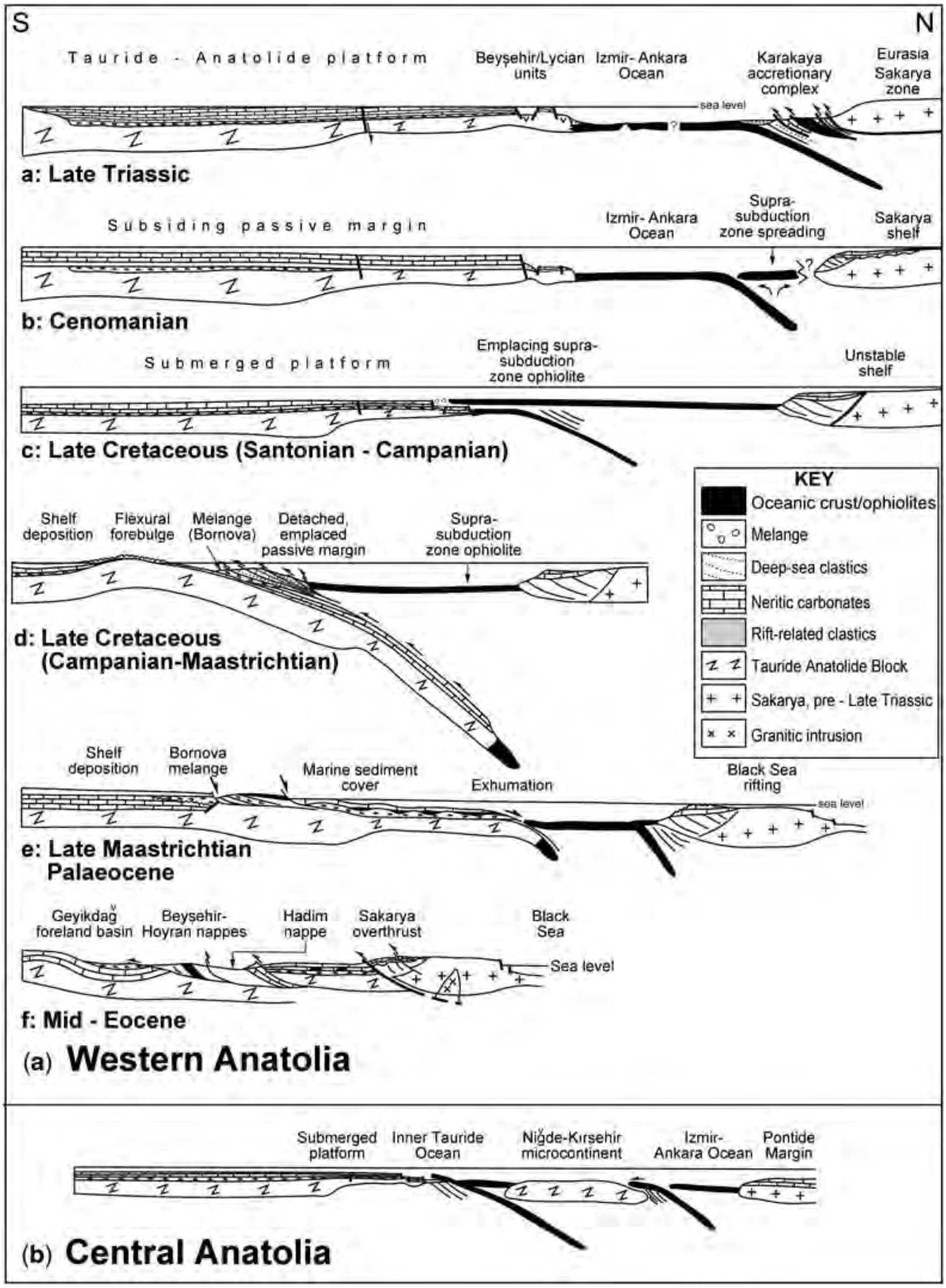

Fig. 25. Reconstruction of the passive margin-subduction/accretion-exhumation history of the metamorphic Anatolides in Turkey based on this study. (**a**) applicable to areas west of the inferred Niğde–Kırşehir microcontinent (see Fig. 23); (**b**) applicable to the Inner Tauride ocean south of the inferred Niğde–Kırşehir microcontinent (see text for discussion of alternatives).

entered the subduction trench, carrying with it some melange and rare ophiolite-related fragments (i.e. serpentinite and metamorphic sole) resulting in HP/LT metamorphism (*c*. 80 Ma for the Tavşanlı zone) at depths down to 50–60 km for the leading edge of the continent (Tavşanlı zone) and *c*. 30 km for the more proximal Afyon–Bolkar Dağ zone (Sherlock *et al.* 1999; Candan *et al.* 2005; Whitney & Davis 2006). Segments of the former rifted margin (e.g. marginal platforms) detached and were thrust southward over the collapsed Tauride–Anatolide platform reaching a far southerly position as the Beyşehir and Lycian nappes. Fragments of the distal rifted margin remained in the north, as seen in the Bornova zone. Subduction halted by Late Maastrichtian time in the east (Bolkar Dağ area) and Paleocene further west, probably because of buoyancy of the thickening crustal wedge as it entered the trench. The Tauride carbonate platform remained south of the subducted continental margin. However, it too collapsed to form a foredeep during Campanian–Maastrichtian time into which several types of accretionary melange were emplaced by thrusting and gravitational processes and then over-ridden by far-travelled continental margin units (e.g. Lycian & Beyşehir nappes) and ophiolites (e.g. Mersin and Lycian ophiolites).

The over-riding plate of the subduction zone was made up of intact ophiolites plus soles, and some underplated (unmetamorphosed) melange. Assuming that all of the ophiolites in the west of the area (west of the Niğde–Kırşehir massif) represent parts of a single supra-subduction zone oceanic slab, the Tauride ophiolites represent the leading edge of the emplaced supra-subduction oceanic slab, whereas the Anatolide ophiolites formed the trailing edge of this oceanic lithosphere. The emplaced ophiolite was probably quite continuous over a vast region, similar for example to the scale of the Oman ophiolite.

In the east, the Niğde–Kırşehir microcontinent collided with the Tauride–Anatolide continent prior Late Maastrichtian closing the Inner Tauride ocean, while oceanic lithosphere remained to the east, west and north. In addition, ophiolites were formed further north within the İzmir–Ankara–Erzincan ocean, also above a northward-dipping subduction zone and emplaced southwards over the Niğde–Kışehir microcontinent prior to Late Maastrichtian time.

The Anatolide continental margin was exhumed during Maastrichtian–Paleocene, as seen in different areas and units, probably owing to buoyancy after northward subduction ended. The Tauride ophiolites and melange remained as part of the lower plate of a regional northward-moving extensional detachment system, as recorded by regionally persistent north–south stretching lineations. In contrast, the Anatolide ophiolites and related melange formed the upper plate of this detachment system, and so ended up directly on the exhumed Anatolide platform. Following exhumation, the Anatolides were locally transgressed by shallow-water carbonates ranging from Maastrichtian–Early Eocene (Bolkar Dağ area), and from Late Paleocene–Early Eocene (i.e. western Anatolides).

Continuing regional north–south plate convergence (e.g. Smith 2006) was accommodated by subduction close to the Eurasian (Sakarya) margin. Similarly, in Oman ophiolites and margin units were emplaced onto the Arabian margin during Late Cretaceous time, whereas remaining oceanic crust remained in the Gulf of Makran and subducted beneath Iran during Cenozoic time (Glennie *et al.* 1990). The direction of the subduction in Turkey is unconstrained in the area studied. Evidence from western Antalolia is consistent with northward subduction as this explains the Eocene southward thrusting of the Sakarya continent over the Tauride–Anatolide Platform. In addition, Early Cenozoic subduction of remnant Neotethyan crust has been inferred for the Central and Eastern Pontides to explain Eocene northward emplacement of ophiolites onto the Eurasian margin (Uştaömer 1993; Okay & Şahintürk 1997; Rice *et al.* 2006, in press).

The Tauride–Anatolide and Sakarya continents underwent diachronous collision during the Eocene. In western and central Anatolia granodiorites intruded the suture zone around 50 Ma (Harris *et al.* 1994; Sherlock *et al.* 1999; Okay & Satır 2006) possibly in response to collision-related slab break-off (Altunkaynak 2007).

Continental collision during Eocene time was associated with marine regression, as documented by a transition from Paleocene shelf-depth sediments to Lower Eocene shallow-water mixed carbonate-clastic and evaporitic sediments in the Ulukışla Basin in the east (Clark & Robertson 2004). During collision, the Sakarya continent was thrust over and interleaved with the Tauride–Anatolide Platform and thick-skinned thrusting internally shortened both of these units. Further south, the Upper Cretaceous Tauride thrust stack (e.g. Lycian and Beyşehir nappes) was re-emplaced southwards over the Tauride–Anatolide Block on a regional scale. The central Tauride Hadim nappe was detached from the relatively autochthonous Geyik Dağ carbonate platform and thrust to its most southerly position, together with the Beyşehir nappes (Mackintosh 2008). In addition, large-scale folding and backthrusting affected many areas (e.g. Bolkar Dağ, Konya area). This deformation was most intense in the east possibly related to reactivation of the Inner Tauride suture and squeezing

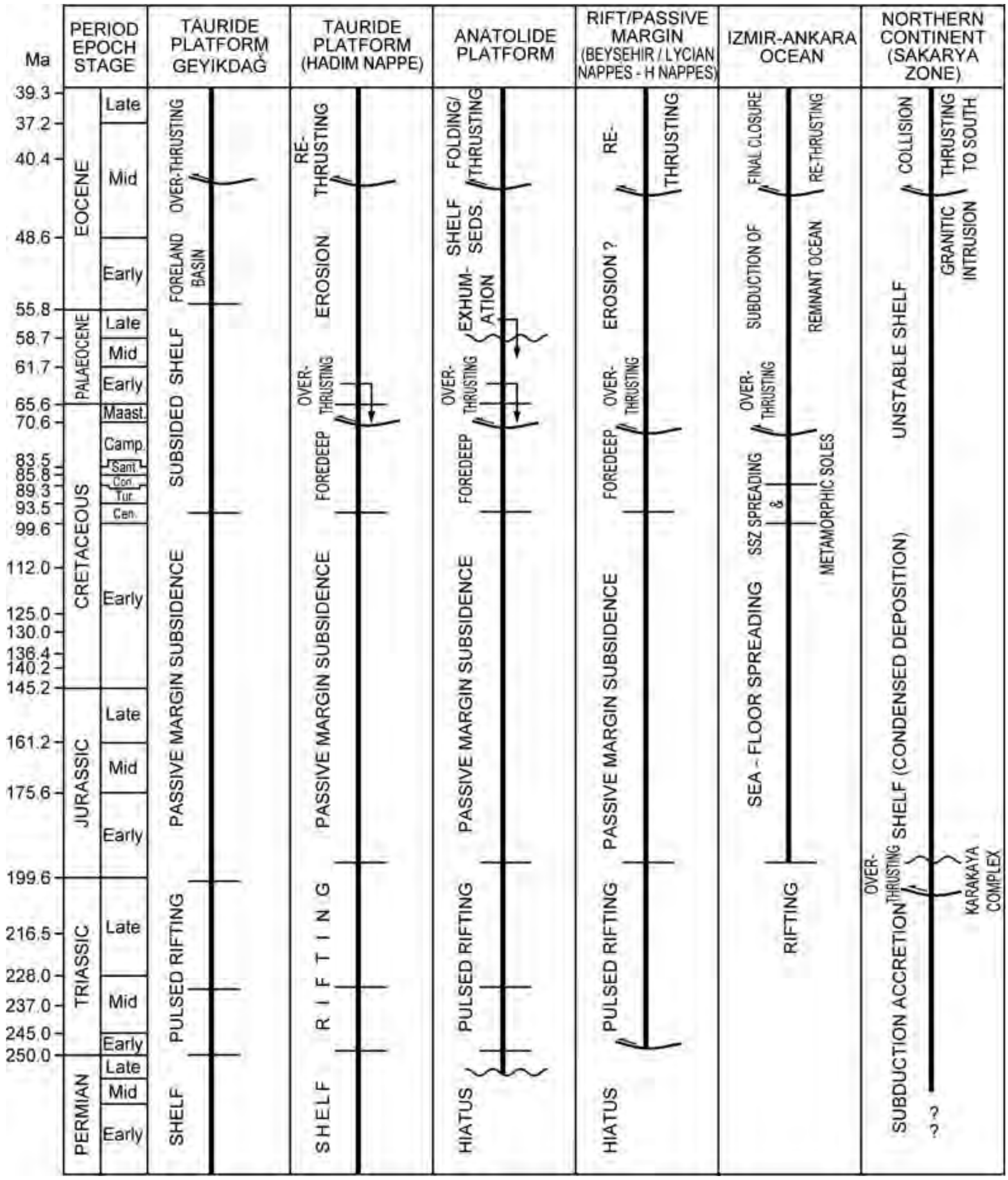

Fig. 26. Time versus geological activity. This is mainly applicable to areas west of the inferred Niğde–Kırşehir microcontinent (see Fig. 23). See text for discussion. Time scale: Gradstein *et al.* (2004).

between the Tauride platform to the south and the Niğde–Kırşehir massif to the north.

Subsequently, the Anatolide–Tauride continent experienced neotectonic deformation, including low-angle to high-angle, extensional faulting in the Menderes Massif, strike-slip between the Tavşanlı zone and the Sakarya zone in the west, extensional faulting along the north margin of the Bolkar Dağ in the east and Plio-Quaternary regional uplift.

Conclusions

- Western and central Turkey provides one of the best examples of the emplacement of ophiolites, related continental margin units and several types of melange onto a collapsed passive continental margin;
- The continental margin rifted during the Triassic followed by passive margin subsidence during

Jurassic–Early Cretaceous, and regional flooding during the Late Cretaceous (Cenomanian–Campanian).

- Four main convergent phases are recorded: intra-oceanic subduction (Cenomanian-Santonian *c*. 95–85 Ma); trench-margin collision leading to ophiolite, rifted margin and melange emplacement (Santonian–Early Paleocene *c*. 85–65 Ma); subduction of remnant oceanic crust (Middle Paleocene–Early Eocene *c*. 60–50 Ma), and final continental collision and crustal thickening (Middle Eocene *c*. 45–40 Ma);
- All of the ophiolites formed by spreading related to northward-dipping subduction;
- Isolated diabase dykes record the earlier stages of oceanic arc magmatism that was halted by obduction,
- Metamorphic soles preserve remnants of seamount, arc-type and rarely mid-ocean ridge type crust;
- Underlying melanges preserve remnants of a similar range of oceanic-derived igneous rocks;
- Subduction influenced tholeiitic basalts of probable Late Cretaceous age record remnants of an oceanic arc that probably began to develop on supra-subduction-type oceanic crust. The arc-type basalts are likely to have been detached from the leading edge of the emplacing ophiolite and emplaced as blocks within the melange beneath;
- Melanges formed by both tectonic and sedimentary processes. Initially-formed oceanic accretionary complexes are mainly tectonic in origin, whereas, at the other end of a spectrum, the farthest-travelled melange on the collapsed platform includes large-scale debris flows;
- Slices of the rifted margin were emplaced large distances (up to several hundred kilometres) onto the continental margin as regional-scale thrust sheets;
- The leading edge of the subducted continental margin in the north underwent high pressure/low temperature metamorphism (i.e. Tavşanlı zone *c*. 80 Ma; Afyon–Bolkardağ zone Maastrichtian–Paleocene), whereas areas further south experienced either low-grade metamorphism (Menderes Massif) or escaped metamorphism altogether (i.e. Taurides).
- The emplacement of ophiolites, continental margin units and melanges was accompanied by exhumation of the HP/LT units, as recorded by transgressive sediments of Maastrichtian–Paleocene age in different areas;
- Remnant oceanic lithosphere was subducted during Paleocene–Early Eocene, followed by continental collision during Mid Eocene;
- Similar Upper Cretaceous supra-subduction zone-type oceanic lithosphere appears to have formed both south and north of a rifted microcontinent, known as the Niğde–Kırşehir Massif (Central Anatolian Crystalline Complex). This implies the near-coeval formation of ophiolites in several oceanic areas with a palaeogeographical complexity similar to the modern SW Pacific region; and
- Finally, rather than progressive collision, a two-stage emplacement model is advocated involving, first latest Cretaceous southward emplacement onto the Tauride–Anatolide continental margin (followed by exhumation of the margin), and second continental collision during the Mid Eocene.

The authors thank the Carnegie Trust for the Scottish Universities for financial assistance for carrying out the fieldwork. We thank Prof. U. Ünlügenç for participating in some of the fieldwork and for assistance with logistical aspects. We thank P. Mackintosh for helpful discussion. The manuscript benefited from helpful reviews by A. Okay and Y. Dilek and the advice of the editor, Dr M. Edwards.

References

ALABASTER, T., PEARCE, J. A. & MALPAS, J. 1982. The volcanic stratigraphy and petrogenesis of the Oman ophiolite complex. *Contributions to Mineralogy and Petrology*, **81**, 168–183.

ALDANMAZ, E., YALINIZ, M. K., GÜCTEKIN, A. & GÖNCÜOĞLU, M. C. 2007. Geochemical characteristics of mafic lavas from the Neotethyan ophiolites in western Turkey: implications for heterogeneous source contributions during variable stages of oceanic crust generation. *Geological Magazine*, **145**, 37–54.

AL-RIYAMI, K., ROBERTSON, A. H. F., DIXON, J. & XENOPHONTOS, C. 2002. Origin and emplacement of the Late Cretaceous Baer-Bassit ophiolite and its metamorphic sole in NW Syria. *Lithos*, **65**, 225–260.

ALTINER, D., KOÇYIĞIT, A., FARINACCI, A., NICOSIA, U. & CONTI, M. A. 1991. Jurassic, Lower Cretaceous stratigraphy, palaeogeographic evolution of the southern part of north-western Anatolia. *Geologica Romana*, **27**, 13–80.

ALTUNKAYAK, D. E. 2007. Collision-driven slab breakoff magmatism in northwestern Anatolia, Turkey. *Journal of Geology*, **115**, 63–82.

American Geological Institute. 1961. *Dictionary of Geological Terms*. New York, Dolphin Books.

ANDREW, T. & ROBERTSON, A. H. F. 2002. The Beyşehir-Hoyran-Hadim Nappes: genesis and emplacement of Mesozoic marginal and oceanic units of the northern Neotethys in southern Turkey. *Journal of the Geological Society, London*, **159**, 529–543.

ARCULUS, R. J. & POWEL, R. 1986. Source component mixing in the regions of arc magma generation. *Journal of Geophysical Research*, **91**, 5913–5926.

BAILEY, E. B. & MCCALLIEN, W. J. 1954. Serpentinite lavas, the Ankara Melange, the Anatolian thrust.

Transactions of the Royal Society of Edinburgh, **62**, 403–442.

BERNOULLI, D., DE GRACIANSKY, P. C. & MONOD, O. 1974. The extension of the Lycian Nappes (SW Turkey) into the southeastern Aegean Islands. *Eclogae Geologicae Helvetiae*, **67**, 39–90.

BLUMENTHAL, M. M. 1955. Geology of the border and westward areas in the north of high Bolkardağ. *MTA Yayınları, Seri D*, **7**, Ankara [in Turkish].

BOZKURT, E. & OBERHANSLI, R. 2001. Menderes Massif (Western Turkey): structural, metamorphic and magmatic evolution–a synthesis. *International Journal of Earth Science*, **89**, 679–708.

BOZTUĞ, D. 2000. S-I-A type intrusive associations: geodynamic significance of synchronism between metamorphism and magmatism in Central Anatolia, Turkey. *In*: BOZKURT, E., WINCHESTER, J. A. & PIPER, J. A. D. (eds) *Tectonics and Magmatism in Turkey and the Surrounding Area*. Geological Society, London, Special Publication, **173**, 441–458.

BRAGIN, N. Y. & TEKIN, U. K. 1996. Age of radiolarian-chert blocks from the Senonian Ophiolitic Melange (Ankara, Turkey). *Island Arc*, **5**, 114–122.

ÇAKIR, U., JUTEAU, T. & WHITECHURCH, H. 1978. Nouvelles preuves de l' écaillage intra-océanique précoce des opiolites téthesiennes: les roches metamorphiques intra-periditiques du massif de Pozanti-Karsantı (Turquie). *Bulletin de la Societé géologique de France*, **20**(1), 61–70.

CANDAN, O., CETINKAPLAN, M., OBERHANSLI, R., RIMMELÉ, G. & AKAL, C. 2005. Alpine high-P/low-T metamorphism of the Afyon Zone and implications for the metamorphic evolution of Western Anatolia, Turkey. *Lithos*, **84**, 102–124.

ÇELIK, Ö. F. 2007. Metamorphic sole rocks and their mafic dykes in the eastern Tauride belt ophiolites (southern Turkey): implications for OIB-type magma generation following slab break-off. *Geological Magazine*, **144**, 849–866.

ÇELIK, Ö. F. & DELALOYE, M. 2003. Origin of metamorphic soles and their post-kinematic mafic dyke swarms in the Antalya and Lycian ophiolites, SW Turkey. *Geological Journal*, **38**, 235–256.

ÇELIK, Ö. F., DELALOYE, M. & FERAUD, G. 2006. Precise Ar-Ar ages from the metamorphic sole rocks of the Tauride Belt Ophiolites, southern Turkey: implications for the rapid cooling history. *Geological Magazine*, **143**, 213–227.

CLARK, M. 2002. *The latest Cretaceous-Early Tertiary Ulukışla Basin, S. Turkey: sedimentation and tectonics of an evolving suture zone*. Unpublished PhD thesis, University of Edinburgh.

CLARK, M. & ROBERTSON, A. H. F. 2002. The role of the Early Tertiary Ulukışla Basin, southern Turkey, in suturing of the Mesozoic Tethys ocean. *Journal of the Geological Society*, **159**, 673–690.

CLARK, M. & ROBERTSON, A. H. F. 2004. Uppermost Cretaceous-Lower Tertiary Ulukışla Basin, south-central Turkey: sedimentary evolution of part of a unified basin complex within an evolving Neotethyan suture zone. *Sedimentary Geology*, **173**, 15–52.

CLOOS, M. & SHREVE, R. L. 1988. Subduction-channel model of prism accretion, melange formation, sediment subduction, and subduction erosion at convergent plate margins: 2. Implications and discussion. *Pure and Applied Geophysics*, **128**, 501–545.

COLLINS, A. S. 1997. *Tectonic evolution of Tethys in the Lycian Taurides, southwestern Anatolia*. Unpublished PhD thesis, University of Edinburgh.

COLLINS, A. & ROBERTSON, A. H. F. 1997. Lycian melange, southwestern Turkey: an emplaced Late Cretaceous accretionary complex. *Geology*, **25**, 25–258.

COLLINS, A. & ROBERTSON, A. H. F. 1998. Processes of Late Cretaceous to Late Miocene episodic thrust-sheet translation in the Lycian Taurides, southwestern Turkey. *Journal of the Geological Society, London*, **155**, 759–772.

COLLINS, A. & ROBERTSON, A. H. F. 1999. Evolution of the Lycian allochthon, western Turkey, as a north-facing Late Palaeozoic-Mesozoic rift and passive continental margin. *Geological Journal*, **34**, 107–138.

DE GRACIANSKY, P. C. 1972. *Recherches géologiques dans le Taurus lycien*. Thèse Université Paris-Sud, Paris.

DANELIAN, T., ROBERTSON, A. H. F., COLLINS, A. S. & POISSON, A. 2006. Biochnonology of Jurassic and Early Cretaceous radiolarites from the Lycian Melange (SW Turkey) and implications for the evolution of the Northern Neotethys ocean. *In*: ROBERTSON, A. H. F. & MOUNTRAKIS, D. (eds) *Tectonic Development of the Eastern Mediterranean Region*. Geological Society of London Special Publication, **260**, 229–236.

DAŞÇI, H. T. 2007. *Origin of amphibolites within the Koyna Melange*. Unpublished MSc thesis, Cükürova University, Adana, Turkey [in Turkish].

DELALOYE, M. & BINGÖL, E. 2000. Granitoids from western and northwestern Anatolia: Geochemistry and modeling of geodynamic evolution. *International Geology Review*, **42**, 241–268.

DEMIRTAŞLI, E., TURHAN, N., BILGIN, A. Z. & SELIM, M. 1984. Geology of the Bolkar Mountains. *In*: TEKELI, O. & GÖNCÜOĞLU, M. C. (eds) *Geology of the Taurus Belt*. Proceedings International Symposium on the Geology of the Taurus Belt, Ankara, Turkey. Mineral Resources and Exploration Institute of Turkey, 12–141.

DERCOURT, J., RICOU, L. E. & VRIELYNCK, B. (eds) 1993. *Atlas Tethys Palaeoenvironmental Maps*. Commission pour le Carte Géologique du Monde/Commission for the Geological Map of the World, Paris.

DILEK, Y. & THY, P. 2006. Age and petrogenesis of plagiogranite intrusions in the Ankara Melange, Central Turkey. *The Island Arc*, **15**, 44–57.

DILEK, Y. & WHITNEY, D. L. 1997. Counterclockwise *P-T*-t trajectory from the metamorphic sole of a Neotethyan ophiolite (Turkey). *Tectonophysics*, **280**, 295–310.

DILEK, Y. & WHITNEY, D. L. 2000. Cenozoic crustal evolution in Central Anatolia: extension, magmatism and landscape development. *In*: PANAYIDES, I., XENOPHONTOS, C. & MALPAS, J. (eds) *Proceedings of the Third International Congress on the Geology of the Eastern Mediterranean*, 183–192.

DILEK, Y., THY, P., HACKER, B. & GRUNDVIK, S. 1999. Structure and petrology of Tauride ophiolites and mafic dyke intrusions (Turkey): implications for the Neotethyan ocean. *Geological Society of America Bulletin*, **111**, 1192–1216.

DORA, O. Ö., CANADAN, O., KAYA, O., KORALAY, E. & DÜRR, S. 2001. Revision of the so-called 'leptite gneisses' in the Menderes Massif: a supra-crustal meta-sedimentary origin. *International Journal of Earth Science (Geologische Rundschau)*, **89/4**, 836–851.

ELITOK, Ö. 2002. Geochemistry and tectonic significance of the Şarkikaraağaç Ophiolite in the Beyşehir-Hoyran Nappes, S.W. Turkey. *In*: Proceedings of 4th International Symposium on Eastern Mediterranean Geology, Isparta, Turkey, 181–196.

ERDOĞAN, B. 1990. Stratigraphic features and tectonic evolution of of the İzmir-Ankara Zone in the region between İzmir and Seferihisar (in Turkish). *Bulletin of Turkish Petroleum Geologists Association*, **2**, 1–20.

ERDOĞAN, B. & GÜNGÖR, T. 1992. Stratigraphy and tectonic evolution of the northern margin of the Menderes Massif. *Turkish Association of Petroleum Geologists Bulletin*, **4**, 9–34.

ERDOĞAN, B., ALTINER, D., GÜNGÖR, T. & ÖZER, S. 1990. Stratigraphy of the Karaburun Peninsula. *Mineral Research and Exploration Institute of Turkey (MTA) Bulletin*, **111**, 1–20.

EREN, Y. 1993. Startigraphy of autochthonous cover units of the Bozdağlar massif, NW Konya) *Geological Bulletin of Turkey*, **36**, 7–23 [in Turkish].

EREN, Y. 2001. Polyphase Alpine deformation at the northern edge of the Menderes-Taurus block, North Konya, Central Turkey. *Journal of Asian Earth Sciences*, **19**, 737–749.

EREN, Y., KURT, H., ROSSELET, F. & STAMPFLI, G. M. 2004. Paleozoic deformation and magmatism in the northern area of the Anatolide block (Konya), witness of the Palaeotethys active margin. *Eclogae Geologicae Helvetiae*, **97**, 293–306.

ERSOY, S. 1992. The stratigraphy and environmental interpretation of the tectonic and neotectonic units Dirmil, Burdur (and its southern side). *Türkiye Jeoloji Bullteni*, **35**, 9–24 [in Turkish].

FAYON, A. K., WHITNEY, D. L., TESSIER, C., CARVER, J. I. & DILEK, Y. 2001. Effects of plate convergence obliquity on timing and mechanisms of exhumation of a mid-crustal terrain, the Central Anatolian Crystalline Complex. *Earth and Planetary Science Letters*, **192**, 191–205.

FLECKER, R., POISSON, A. & ROBERTSON, A. H. F. 2005. Facies and palaeogeographic evidence for the Miocene evolution of the Isparta Angle in its regional Eastern Mediterranean context. *Sedimentary Geology*, **172**, 277–315.

FLOYD, P. A. 1993. Geochemical discrimination and petrogenesis of alkalic basalt sequences in part of the Ankara mélange, central Turkey. *Journal of Geological Society London*, **150**, 541–550.

FLOYD, P. A., GÖNCÜOĞLU, M. C., WINCHERSTER, J. A. & Y YALINIZ, M. K. 2000. Geochemical character of and tectonic environment of Neotethyan ophiolitic fragments and metabasites in the Central Anatolian Crystalline Complex, Turkey. *In*: BOZKURT, E., WINCHESTER, J. A. & PIPER, J. D. A. (eds) *Tectonics and Magmatism in Turkey and the Surrounding Area*. Geological Society, London, Special Publication, **173**, 183–202.

FLOYD, P. A., ÖZGÜL, L. & GÖNCÜOĞLU, M. C. 2003. Metabasite blocks from the Koçyaka HP-LT metamorphic rocks, Konya, Central Anatolia: Geochemical evidence for an arc-back-arc pair? *Turkish Journal of Earth Science*, **12**, 157–174.

GAUTHIER, Y. 1984. *Déformations et métamorphisms associées à la fermeture téthysienne en Anatolie Centrale (Région de Sivrihisar, Turquie)*. PhD thesis, Université de Paris-Sud, Centre d'Orsay.

GARFUNKEL, Z. 2006. Neotethyan ophiolites: formation and obduction within the life cycle of the host basins. *In*: ROBERTSON, A. H. F. & MOUNTRAKIS, D. (eds) *Tectonic Development of the Eastern Mediterranean Region*. Geological Society, London, Special Publication, **260**, 301–326.

GENÇ, Ş 1987. *Geology of the region between Uludağ and Iznik Lake, guidebook for the field excursion along Western Anatolia, Turkey*. Mineral Research and Exploration Institute MTA, Ankara, 19–25.

GLENNIE, K. W., HUGHES-CLARKE, M. W., BOEUF, M. G. A., PILAAR, W. F. H. & REINHARDT, B. M. 1990. Inter-relationship of the Makran-Oman Mountain belts of convergence. *In*: ROBERTSON, A. H. F., SEARLE, M. P. & RIES, A. C. (eds) 1990. *The Geology and Tectonics of the Oman Region*. Geological Society of London, Special Publication, **49**, 773–786.

GOFFE, B., MICHARD, A., KIENAST, J. R. & LE MER, O 1988. A case of obduction-related high-pressure, low-temperature metamorphism in upper crustal nappes, Arabian continental margin, Oman: P-T paths and kinematic interpretation. *Tectonophysics*, **151**, 363–386.

GÖNCÜOĞLU, M. C. 1986. Geochronologic data from the southern part (Niğde area) of the Central Anatolian Massif. *Maden Tetkik ve Arama Derğisi*, **105/106**, 83–96.

GÖNCÜOĞLU, M. C., ÖZCAN, A., TURHAN, N. & IŞIK, A. 1992. Stratigraphy of the Kütahya Region. *ISGB-92. Field Guide Book* **3**, MTA Publications, Ankara, Turkey.

GÖNCÜOĞLU, M. C., DIRIK, K. & KOZLU, H. 1996–1997. Pre-alpine and alpine terranes in Turkey: explanatory notes to the terrane map of Turkey. *Annalles Géologiques des Pays Héllenique*, **37**, 1–3.

GÖNCÜOĞLU, M., TURHAN, N., ŞENTÜRK, K., ÖZCAN, A. & UYSAL, S. 2000. A geotraverse across NW Turkey: tectonic units of the Central Sakarya region and their tectonic evolution. *In*: BOZKURT, E., WINCHESTER, J.A. & PIPER, J.D. (eds) *Tectonics and Magmatism in Turkey and the Surrounding Area*. Special Publication of the Geological Society, London, **173**, 139–162.

GÖNCÜOĞLU, M. C., TURHAN, N. & TEKIN, U. K. 2003. Evidence of Triassic rifting and opening of the Neotethyan İzmir-Ankara Ocean and discussion on the presence of Cimmerian events at the northern edge of the Tuaride-Anatolide Platform, Turkey. *Bolletino della Societa Geologica Italiano Special volume*, **2**, 203–212.

GÖNCÜOĞLU, M. C., YALINIZ, M. K. & TEKIN, U. K. 2006*a*. Geochemical features and radiolarian ages of volcanic rocks from the Izmir-Ankara suture belt, Western Turkey. *In*: GERZINA, N., RESIMIĆ-ŠARIĆ, K., KARAMATA, S., SUDAR, M. & HRVATOVIĆ, H. (eds) International symposium on Mesozoic ophiolite belts of northern part of the Balkan Peninsula, International Symposium, Belgrade-Banja Luka, May 31–June 6, 41–44.

GÖNCÜOĞLU, M. C., YALINIZ, M. K. & TEKIN, U. K. 2006*b*. Geochemistry, tectono-magmatic discrimination and radiolarian ages of basic extrusives from the İzmir-Ankara suture belt (NW Turkey): time constraints for the Neotethyan evolution. *Ofioliti*, **31**, 25–38.

GÖNCÜOĞLU, M. C., ÇAPKINOĞLU, Ş., GÜRSU, S., NOBLE, P., TURHAN, N., TEKIN, U. K., OKUYUCU, C. & GÖNCÜOĞLU, Y. 2007. The Mississippian in the Central and Eastern Taurides (Turkey): constraints on the tectonic setting of the Tauride–Anatolide Platform. *Geologica Carpathica*, **58**, 427–442.

GÖRÜR, N., OKTAY, F. Y., SEYMEN, I. & ŞENGÖR, A. M. C. 1984. Paleotectonic evolution of Tuz Gölü Basin complex, central Turkey *In*: DIXON, J. E. & ROBERTSON, A. H. F. (eds) *The Geological Evolution of the Eastern Mediterranean*. Geological Society, London Special Publication, **17**, 81–96.

GÖRÜR, N., TÜYSÜZ, O. & ŞENGÖR, A. M. C. 1998. Tectonic evolution of the central Anatolian basins. *International Geology Review*, **40**, 831–850.

GRADSTEIN, F. M., OGG, J. G., SMITH, A. G. *ET AL*. 2004. *A Geological Time Scale 2004*. Cambridge University Press.

GREGORY, R. T., GRAY, D. R. & MILLER, J. M. 1998. Tectonics of the Arabian margin associated with the formation and exhumation of high-pressure rocks, Sultanate of Oman. *Tectonics*, **17**, 657–670.

HACKER, B. R., MOSENFELDER, J. F. & GNOES, E. 1996. Rapid emplacement of the Oman ophiolite: thermal and geochronologic constraints. *Tectonics*, **15**, 1230–1247.

HARRIS, N. B. W., KELLEY, S. P. & OKAY, A. I. 1994. Post-collision magmatism and tectonics in northwest Turkey. *Contributions to Mineralogy and Petrology*, **117**, 241–252.

HETZEL, R., RING, U., AKAL, C. & DORA, O. 1995. Bivergent extension in orpgenic belt: the Menderes Massif (Southwestern Turkey). *Geology*, **23**, 455–458.

ILBEYLI, N., PEARCE, J. A., THIRWALL, M. F. & MITCHELL, J. G. 2004. Petrogenesis of collision-related plutonics in Central Anatolia, Turkey, *Lithos*, **72**, 163–182.

JAFFEY, M. & ROBERTSON, A. H. F. 2001. New sedimentological and structural data from the Ecemiş Fault Zone, southern Turkey; implications for its timing and offset and the Cenozoic tectonic escape of Anatolia. *Journal of the Geological Society*, **18**, 367–378.

JAFFEY, M. & ROBERTSON, A. H. F. 2004. Non-marine sedimentation associated with Oligocene-Recent exhumation and uplift of the Central Taurus Mountains, S.Turkey. *Sedimentary Geology*, **173**, 53–89.

JONES, G., ROBERTSON, A. H. F. & CANN, J. R. 1991. Genesis and emplacement of the supra-subduction zone Pindos ophiolite, northwestern Greece. *In*: PETERS, T., NICOLAS, A. & COLEMAN, G. (eds) *Ophiolite genesis and the evolution of oceanic lithosphere*. Proceedings International Conference, Muscat, Sultanate of Oman, 771–800.

JUTEAU, T. 1980. Ophiolites of Turkey. *Ofioliti*, **2**, 199–238.

HARDENBOL, J., THIERRY, J., FARLEY, M. B., JACQUIN, T., DE GRACIANSKY, P.-C. & VAIL, P. R. 1998. Mesozoic and Cenozoic sequence chronostratigraphic framework of European basins. *In*: DE GRACIANSKY, P. C., HARDENBOL, J., JACQUIN, T. & VAIL, P. R. (eds) *Mesozoic and Cenozoic Sequence Stratigraphy of European Basins*. SEPM Special Publication, **60**, Tulsa, Oklahoma, 3–29, plus 8 separate charts.

KAADEN, G. VANDER. 1966. Importance and distribution of glaucophane bearing rocks in Turkey. *MTA Dergisi*, **67**, 38–69 [in Turkish].

KADIOĞLU, Y. K., DILEK, Y. & FOLAND, K. A. 2006. Slab break-off and syncollisional origin of the Late Cretaceous magmatism in the Central Anatolian crystalline complex, Turkey. *In*: DILEK, Y. & PAVLIDES, S. (eds) *Postcollisional Tectonics and Magmatism in the Mediterranean Region and Asia*. Geological America Special Paper, **409**, 381–415.

KAZMIN, V. G. & TIKHONOVA, N. F. 2006. Evolution of early Mesozoic back-arc basins in the Black Sea-Caucasus segment of a Tethyan active margin. *In*: ROBERTSON, A. H. F. & MOUNTRAKIS, M. (eds) *Tectonic Development of the Eastern Mediterranean Region*. Geological Society, London, Special Publication, **260**, 179–200.

KETIN, I. 1966. Tectonic units of Anatolia (Asia Minor). *Bulletin Mineral Research Exploration Institute*, **66**, 23–34.

KOÇYIĞIT, A. 1991. An example of an accretionary forearc basin from North Central Anatolia and its implications for the history of subduction of Neo-Tethys in Turkey. *Geological Society of America Bulletin*, **103**, 22–36.

KONAK, N., AKDENIZ, N. & ÖZTÜRK, E. M. 1987. Geology of the south of the Menderes Massif, I.G.C.P. Project No. 5. *Correlations of Variscan and Pre-Variscan events of the Alpine-Mediterranean mountain belt*. Field Meeting. Mineral Research and Exploration Institute of Turkey (MTA), 42–53.

KRÖNER, A. & ŞENGÖR, A. M. C. 1990. Archean and Proterozoic ancestry in lower Pre-Cambrian to early Palaeozoic crustal elements of southern Turkey as revealed by single zircon dating. *Geology*, **18**, 1186–90.

LIPPARD, S. J., SHELTON, A. W. & GASS, I. G. 1986. *The Ophiolite of Northern Oman*. Geological Society, London, Memoir, **11**.

LISENBEE, A. 1971. The Orhaneli ultramafic-gabbro thrust sheet and its surroundings. *In*: CAMPBELL, A. S. (ed.) *Geology and History of Turkey*. Petroleum Exploration Society of Libya, Tripoli, 349–360.

LYTWYN, J. N. & CASEY, J. F. 1995. The geochemistry of post-kinematic mafic dyke swarms and subophiolitic metabasites, Pozantı-Karsantı ophiolite, Turkey: evidence for ridge subduction. *Geological Society of America Bulletin*, **107**, 830–850.

MACKINTOSH, P. W. 2008. *Tectonic-sedimentary evolution of the northern margin of Gondwana during Late Palaeocene-Early Eocene time in the Eastern Mediterranean region: evidence from the Central Taurus Mountains*. Unpublished PhD thesis, University of Edinburgh.

MACKINTOSH, P. W. & ROBERTSON, A. H. F. Structural and sedimentary evidence from the northern margin of the Tauride platform: testing models of Late Triassic "Cimmerian" uplift and deformation in southern Turkey. *Tectonophysics*, in press.

MANAV, H., GÜLTEKIN, A. H. & UZ, B. M. 2004. Geochemical evidence for the tectonic setting of the Harmancik ophiolites, NW Turkey. *Journal of Asian Earth Science*, **24**, 1–9.

MERIÇ, E. & ŞENGÜLER, İ. 1986. New observations on the stratigraphy of Upper Cretaceous-Paleocene around Göynuk (Bolu, northwest Anatolia). *Jeoloji Mühendisliği*, **29**, 61–64 [in Turkish].

MILLER, J. M., GRAY, D. R. & GREGORY, R. T. 1998. Exhumation of high-pressure rocks of northeastern Oman. *Geology*, **26**, 235–238.

MANATSHAL, G. & BERNOULLI, D. 1999. Architecture and tectonic evolution of non-volcanic margins: present-day Galicia and ancient Adria. *Tectonics*, **18**, 1099–1199.

MANATSCHAL, G., MÜNTENER, O., DESMURS, L. & BERNOULLI, D. 2003. An ancient ocean-continental transition in the Alps: the totalp, Err-Plata, and Malenco units in the Eastern Alps (Graubünden and northern Italy). *Eclogae Geologicae Helvetiae*, **96**, 131–146.

MOIX, P., KOZUR, H. W., STAMPFLI, G. M. & MOSTLER, H. 2007. New palaeontological, biostratigraphic and palaeogeographic results from the Triassic of the Mersin Melange. *In*: LUCAS, S. G. & SPIELMAN, J. A. (eds) The Global Triassic. *New Mexico Museum and Natural History and Science*, **41**, 282–311.

MOIX, P., BECCALETTO, L., KOZUR, H. W., HOCHARD, C., ROSSELET, F. & STAMPFLI, G. M. 2008. A new classification of the Turkish terranes and sutures and its implication for paleotectonic history of the region. *Tectonophysics*, **451**, 7–39, doi: 10.1016/j.tecto.2007.11.044.

MONOD, O. 1977. *Récherches géologique dans les Taurus occidental au sud de Beyşehir (Turquie).* Thèse de Doctorat de Science, Université de Paris-Sud, Orsay, France.

MONOD, O. 1979. *Carte géologique au sud de Beyşehir. 1/100,000.* Editions CNRS, Paris.

MONOD, O., ANDRIEUX, J., GAUTIER, Y. & KIENAST, J. R. 1991. Pontides-Taurides relationships in the region of Eskişehir (NW Turkey). *Bulletin Technical University İstanbul*, **44**, 212–224.

MTA 2002. *Geological Map of Turkey, 1:500,000* (Maden Tektik ve Arama Genel Müdürlüğü) (General Directorate of Mineral Research and Exploration), Ankara.

OKAY, A. I. 1984, Distribution and characteristics of the northwest Turkish blueschists. *In*: DIXON, J. E. & ROBERTSON, A. H. F. (eds) *The Geological Evolution of the Eastern Mediterranean*. Geological Society, London, Special Publication, **17**, 455–466.

OKAY, A. I. 1986. High-pressure/low-temperature metamorphic rocks of Turkey. *Geological Society of America, Memoir*, **164**, 333–347.

OKAY, A. I. 2000. Was the Late Triassic orogeny in Turkey caused by the collision of an oceanic plateau? *In*: BOZKURT, B., WINCHESTER, J. A. & PIPER, J. D. A. (eds) *Tectonics and Magmatism in Turkey and the Surrounding Area*. Geological Society, London, Special Publication, **173**, 25–42.

OKAY, A. I. 2002. Jadeite-chloritoid-glaucophane-lawsonite blueschists in north-west Turkey: unusually high P/T ratios in continental crust. *Journal of Metamorphic Geology*, **20**, 757–768.

OKAY, A. I. & ALTINER, D. 2007. A condensed Mesozoic section in the Bornova Flysch Zone: A fragment of the Anatolide-Tauride carbonate platform. *Turkish Journal of Earth Sciences*, **16**, 257–279.

OKAY, A. I. & KELLEY, S. P. 1994. Tectonic setting, petrology and geochronology of jadeite + glaucophane and chloritoid + glaucophane schists from northwest Turkey. *Journal of Metamorphic Geology*, **12**, 455–466.

OKAY, A. I. & GÖNCÜOĞLU, M. 2004. The Karakaya Complex: A review of data and concepts. *Turkish Journal of Earth Sciences*, **13**, 77–76.

OKAY, A. I. & ŞAHINTÜRK, Ö 1997. Geology of the Eastern Pontides. *In*: ROBINSON, A. G. (ed.) *Regional and Petroleum Geology of the Black Sea and Surrounding Region*. American Association of Petroleum Geologists Memoir, **68**, Tulsa, Oklahoma, 291–311.

OKAY, A. & SATIR, M. 2006. Geochronology of Eocene plutonism and metamorphism in northwest Turkey: evidence for a possible magmatic arc. *Geodinamica Acta*, **19**, 251–266.

OKAY, A. I. & TÜYŞÜZ, O. 1999. Tethyan sutures of northern Turkey. *In*: MASCLE, A. & LOLIVET, L. (eds) *The Mediterranean Basins: Tertiary extension within the Alpine orogeny*. Geological Society, London, Special Publication, **156**, 475–516.

OKAY, A. I. & SIYAKO, M. 1993. İzmir Balıkesir arasında İzmir Ankara Neo-Tetis kenedinin yuni konumu (the new position of the İzmir-Ankara Neo-Tethyan suture between İzmir and Balikesir). *In*: TURGUET, S. (ed.) *Proceedings of the Ozen Sungurlu Symposium, Tectonics and Hydrocarbon Potential of Anatolia*. Akara, 333–354.

OKAY, A. I., HARRIS, N. B. W. & KELLEY, S. P. 1998. Exhumation of blueschists along a Tethyan suture in northwest Turkey. *Tectonophysics*, **285**, 275–299.

OKAY, A. I., TANSEL, I. & TÜYSÜZ, O. 2001. Obduction, subduction and collision as reflected in the Upper Cretaceous-Lower Eocene sedimentary record of western Turkey. *Geological Magazine*, **138**, 117–142.

OKAY, A. I., SATIR, I. & SIEBEL, W. 2006. Pre-Alpide Palaeozoic and Mesozoic orogenic events in Turkey. *In*: GEE, D. G. & STEPHENSON, R. A. (eds) 2006. *European Lithosphere Dynamics, Geological Society Memoir*, **32**, 355–388.

ÖNEN, P. 2003. Neotethyan ophiolitic rocks of the Anatolides of NW Turkey and comparison with Tauride ophiolites. *Journal of the Geological Society, London*, **160**, 947–962.

ÖNEN, P. & HALL, R. 1993. Ophiolites and related metamorphic rocks from the Kütahya region, northwest Turkey. *Geological Journal*, **28**, 399–412.

ÖNEN, P. & HALL, R. 2000. Sub-ophiolite metamorphic rocks from NW Anatolia, Turkey. *Journal of Metamorphic Geology*, **18**, 483–495.

ÖZCAN, A., GÖNCÜOĞLU, M. C., TURHAN, N., UYSAL, S. & ŞENTÜRK, K. 1988. Late Palaeozoic evolution of the Kütahya-Bolkardağ Belt. *METU Journal of Pure and Applied Science*, **21**, 211–220.

ÖZCAN, A., GÖNCÜOĞLU, M. C. & TURHAN, N. 1989. Basic Geology of the Kütahya-Çifteler-Bayat-İhsaniye Regions (in Turkish). *General Directorate of Mineral*

Research and Exploration (MTA), Report, **8118**, 1–142 [unpublished; in Turkish].

ÖZCAN, A., GÖNCÜOĞLU, M. C., TURHAN, N., ŞENTÜRK, K., UYSAL, Ş. & IŞIK, A. 1990. Geology of Konya-Kadınhanı-Ilgın Dolayının Region (in Turkish). *General Directorate of Mineral Research and Exploration (MTA)*, Report **9535**.

ÖZER, S., SÖZBILIR, H., ÖZKAR, I., TOKET, V. & SARI, B. 2001. Stratigraphy of the Upper Cretaceous-Palaeogene sequences in the southern and eastern Menderes Massif (Western Turkey). *International Journal of Earth Science*, **89**, 852–866.

ÖZER, E., KOÇ, H. & ÖZSAYAR, T. Y. 2004. Stratigraphical evidence for the depression of the northern margin of Menderes-Taurus Block (Turkey) during Late Cretaceous. *Journal of Asian Earth Sciences*, **2**, 401–412.

ÖZGÜL, N. 1984. Stratigraphy and tectonic evolution of the central Taurides. *In*: TEKELI, O. & GÖNCÜOĞLU, M. C. (eds) *Geology of the Taurus Belt*. Maden Tetkik ve Arama Derğisi, Ankara, 77–90.

ÖZGÜL, N. 1997. Stratigraphy of the tectono-stratigraphic units in the region Bozkır-Hadim-Taşkent (northern central Taurides). *Maden Tetkik ve Arama Dergisi*, **119**, 113–174 [in Turkish].

ÖZGÜL, L. & GÖNCÜOĞLU, M. C. 1999. Metamorphic evolution of Koçkaya Metamorphic Complex: a HP/LT tectonic slice in west-central Anatolia. *Annual Meeting of Geological Society of Turkey, Proceedings*, **52**, 279–286, [in Turkish].

ÖZKOÇAK, O. 1969. *Etude géologique du massif ultrabasique d'Orhaneli et de sa proche bordure (Bursa, Turquie)*. PhD thesis, Université de Paris.

PARLAK, O. 2000. Geochemistry and significance of mafic dyke swarms in the Pozantı-Karsantı ophiolite (southern Turkey). *Turkish Journal of Earth Sciences*, **24**, 29–38.

PARLAK, O. 2006. Petrology of Neotethyan ophiolites in Turkey: Distinct magma generations and their tectonic significance. *Mesozoic Ophiolite Belts of Northern Part of the Balkan Peninsula*. International Symposium, 31 May–6 June 2006, Belgrade-Banja Luka, 106–109.

PARLAK, O. & DELALOYE, M. 1996. Geochemistry and timing of post-metamorphic dike emplacement in the Mersin ophiolite (southern Turkey): new age constraints from $^{40}Ar/^{39}Ar$ geochronology. *Terra Nova*, **8**, 585–592.

PARLAK, O. & DELALOYE, M. 1999. Precise $^{40}Ar/^{39}Ar$ ages from the metamorphic sole of the Mersin ophiolite (Southern Turkey). *Tectonophysics*, **301**, 145–158.

PARLAK, O. & ROBERTSON, A. H. F. 2004. The ophiolite-related Mersin Melange, southern Turkey: its role in the tectono-sedimentary setting of Tethys in the Eastern Mediterranean region. *Geological Magazine*, **141**, 257–286.

PARLAK, O., DELALOYE, M. & BINGÖL, E. 1995. Origin of subophiolitic metamorphic rocks beneath the Mersin ophiolite, southern Turkey. *Ofioliti*, **20**, 97–110.

PARLAK, O., HÖCK, V. & DELALOYE, M. 2000. Suprasubduction zone origin of the Pozantı-Karsantı ophiolite (southern Turkey) deduced from whole-rock and mineral chemistry of the gabbroic cumulates. *In*: BOZKURT, E., WINCHESTER, J. A. & PIPER, J. D. (eds) *Tectonics and Magmatism in Turkey and the Surrounding Area*. Special Publication of the Geological Society, London, **173**, 219–234.

PARLAK, O., HÖCK, V., KOZLU, H. & DELALOYE, M. 2004. Oceanic crust generation in an island arc tectonic setting, SE Anatolian Orogenic Belt (Turkey). *Geological Magazine*, **141**, 583–603.

PEARCE, J. A. 1982. Trace element characteristics of lavas from destructive plate boundaries. *In*: THORPE, R. S. (ed.) *Andesites*. Wiley, New York, 525–548.

PEARCE, J. A. 2003. Suprasubduction zone ophiolites: The search for modern analogues. *In*: DILEK, Y. & NEWCOMB, S. (eds) *Ophiolite Concept and Evolution of Geological Thought*. Geological Society of America, Special Publication, **373**, 269–293.

PEARCE, J. A. & NORRY, M. J. 1979. Petrogenetic implications of Ti, Zr, Y and Nb variations in volcanic rocks. *Contributions to Mineralogy and Petrology*, **69**, 33–47.

PEARCE, J. A., BAKER, P. E., HARVEY, P. K. & LUFF, I. W. 1995. Geochemical evidence for subduction fluxes, mantle melting and fractional crystallization beneath the South Sandwich arc. *Journal of Petrology*, **36**, 1073–1109.

PEARCE, J. A., STERN, R. J., BLOOMER, S. H. & FRYER, P. 2005. Geochemical mapping of the Mariana arc-basin system: *Implication for the nature and distribution of the subduction component. Geochemistry Geophysics Geosystems*, **6**, Q07006, doi: 10.1029/2004GC000895.

PICKETT, E. A. & ROBERTSON, A. H. F. 1996. Formation of the Late Palaeozoic-Early Mesozoic Karakaya Complex and reltated ophiolites in NW Turkey by Palaeotethyn subduction-accretion. *Journal of the Geological Society London*, **153**, 995–1009.

PICKETT, E. A. & ROBERTSON, A. H. F. 2004. Significance of the volcanogenic Nilüfer Unit and related components of the Triassic Karakaya Complex for Tethyan subduction/accretion processes in NW Turkey. *Turkish Journal of Earth Sciences*, **13**(2), 97–143.

POISSON, A. & ŞAHINCI, A. 1988. La série Mésozoique de Kemalpaşa et le flysch paléocene de Izmir su nord-ouest du Menderes (Anatolie occidentale, Turquie). Un jalon du microcontinent taurique. *Comptes Rendus de l'Academie*. des Sciences, Paris, **307**, 1075–1080.

POLAT, P. A., CASEY, J. F. & KERRICH, R. 1996. Geochemical characteristics of accreted material beneath the Pozantı-Karsantı ophiolite, Turkey: Intra-oceanic detachment, assembly and obduction. *Tectonophysics* **263**, 249–276.

PURVIS, M. 1998. *The Late Tertiary-Recent tectonic-sedimentary evolution of extensional sedimentary basins of the northern Menderes Massif*. Unpublished PhD thesis, University of Edinburgh.

PURVIS, M. & ROBERTSON, A. H. F. 2004. A pulsed extension model for the Neogene-Recent E-W trending Alaşehir (Gediz) Graben and the NW-SE trending Selendi and Gördes Basins, W Turkey. *Tectonophysics*, **391**, 171–201.

RASSIOS, A. & SMITH, A. G. 2000. Constraints on the formation and emplacement of western Greek ophiolites

(Vourinos-Pindos, and Othris inferred from deformation structures in peridotites. *In*: DILEK, T. Y., MOORES, E. M., ELTHON, D. A. & NICOLAS, A. (eds) *Ophiolies and Oceanic Crust: New Insights from Field Studies and Ocean Drilling Program.* Geological Society of America. Special Papers, **349**, 473–483.

RAYMOND, L. A. 1984. (ed.) *Melanges: Their Nature, Origin and Significance.* Geological Society of America. Special Paper, **198**.

RIMMELÉ, G., OBERHÄNSLI, R., GOFFÉ, B., JOLIVET, L., CANDAN, O. & ÇETINKAPLAN, M. 2003. First evidence of high-pressure in the cover series of the southern Menderes Massif. Tectonic and metamorphic implications for the evolution of SW Turkey. *Lithos*, **71**, 19–46.

RIMMELÉ, G., OBERHÄNSLI, R., CANDAN, O, GOFFÉ, B. & JOLIVET, L. 2006. The wide distributon of HP-LT rocks of the Eurasian active margin in the Central and Eastern Pontides, northern Turkey. *In*: ROBERTSON, A. H. F. & MOUNTRAKIS, D. (eds) *Tectonic Development of the Eastern Mediterranean Region*. Geological Society, London, Special Publication, **260**, 447–467.

RICE, S., ROBERTSON, A. H. F. & USTAÖMER, T. 2006. Late Cretaceous-Early Cenozoic tectonic evolution of the Eurasian active margin in the central and Eastern Pontides, Northern Turkey. *In*: ROBERTSON, A. H. F. & MOUNTRAKIS, D. (eds) *Tectonic Development of the Eastern Mediterranean Region*. Geological Society, London, Special Publication, **260**, 413–445.

RICE, S. P., ROBERTSON, A. H. F., USTAÖMER, T., İNAN, N. & TAŞLI, K. in press. Upper Cretaceous–Lower Eocene tectonic development of the Tethyan Suture Zone in the Erzincan area, Eastern Pontides, Turkey. *Geological Magazine*, in press.

RIZAOĞLU, T., PARLAK, O., HÖCK, V. & İŞLER, F. 2006. Nature and significance of Late Cretaceous ophiolitic rocks and its relation to the Baskil granitoid in Elazığ region, SE Turkey. *In*: ROBERTSON, A. H. F. & MOUNTRAKIS, D. (eds) *Tectonic Development of the Eastern Mediterranean Region*, Geological Society, London, Special Publication, **260**, 327–350.

ROBERTSON, A. H. F. 1987. Upper Cretaceous Muti Formation: transition of a Mesozoic carbonate platform to a foreland basin in the Oman Mountains. *Sedimentology*, **34**, 1123–1142.

ROBERTSON, A. H. F. 1991. Origin and emplacement of an inferred late Jurassic subduction-accretion complex, Euboea, eastern Greece. *Geological Magazine*, **128**, 27–41.

ROBERTSON, A. H. F. 2000. Mesozoic-Tertiary tectono-sedimentary evolution of a south-Tethyan oceanic basin and its margins in southern Turkey. *In*: BOZKURT, E., WINCHESTER, J. A. & PIPER, J. D. A. (eds) *Tectonics and Magmatism in Turkey and Surrounding Area*. Geological Society of London, Special Publication, **173**, 97–138.

ROBERTSON, A. H. F. 2002. Overview of the genesis and emplacement of Mesozoic ophiolites in the Eastern Mediterranean Tethyan region, *Lithos*, **65**, 1–67.

ROBERTSON, A. H. F. 2006. Processes of tectonic emplacement of Mesozoic Tethyan ophiolites. *In*: GEE, D. G. & STEPHENSON, R. A. (eds) *European Lithosphere Dynamics*. Geological Society, London, Memoirs, **32**, 235–261.

ROBERTSON, A. H. F. & DIXON, J. D. 1984. Inroduction: aspects of the Geological Evolution of the Eastern Mediterranean. *In*: DIXON, J. E. & ROBERTSON, A. H. F. (eds) *The Geological Evolution of the Eastern Mediterranean*. Geological Society, London, Special Publication, **17**, 1–74.

ROBERTSON, A. H. F. & PICKETT, E. A. 2000. Palaeozoic-early Tertiary Tethyan evolution in the Karaburun Peninsula (western Turkey) and Chios Island (Greece). *In*: BOZKURT, E., WINCHESTER, J. A. & PIPER, J. D. (eds) *Tectonics and Magmatism in Turkey and the Surrounding Area*. Geological Society, London, Special Publication, **173**, 25–42.

ROBERTSON, A. H. F. & SEARLE, M. P. 1990. The northern Oman Tethyan continental margin: stratigraphy, structure, concepts and controversies, *In*: ROBERTSON, A. H. F., SEARLE, M. P. & RIES, A. C. (eds) *The Geology and Tectonics of the Oman Region*. Geological Society, London, Special Publication, **49**, 3–25.

ROBERTSON, A. H. F. & USTAÖMER, T. 2004. Tectonic evolution of the Intra-Pontide suture in the Armautlu Peninsula, NW Turkey. *Tectonophysics*, **381**, 175–209.

ROBERTSON, A. H. F. & USTAÖMER, T. in press. Role of Carboniferous subduction-accretion in tectonic development of the Konya Complex and related units in central and southern Turkey. *Tectonophysics*, in press.

ROBERTSON, A. H. F., CLIFT, P. D., DEGNAN, P. J. & JONES, G. 1991. Palaeogeographical and palaeotectomic evolution of the Eastern Mediterranean Neotethys. *Palaeoceanography, Palaeoclimatology, Palaeoecology*, **87**, 289–343.

ROBERTSON, A. H. F., USTAÖMER, T., PICKETT, E. A., COLLINS, A. S., ANDREW, T. & DIXON, J. E. 2005. Testing models of Late Palaeozoic-Early Mesozoic orogeny in Western Turkey: support for an evolving open-Tethyan model. *Journal of the Geological Society, London*, **161**, 501–511.

ROJAY, B., YALINIZ, M.K. & ATINER, D. 2001. Tectonic implications of some Cretaceous pillow basalts from the northern Anatolian ophiolitic mélange (Central Anatolia-Turkey) to the evolution of Neotethys. *Turkish Journal of Earth Science*, **10**, 93–102.

ROJAY, B., ALTINER, D., ÖZKAN-ALTINER, S., ÖNEN, P. A., JAMES, S. & THIRLWALL, M. W. 2004. Geodynamic significance of the Cretaceous pillow lavas from North Anatolian Ophiolitic Melange Belt (Central Anatolia, Turkey): geochemical and paleontological constraints. *Geodynamica Acta*, **17**(5), 349–361.

SARIFAKOĞLU, E. 2006. Petrology and origin of plagiogranites from the Dağküplü (Eskişehir) ophiolite along the İzmir-Ankara-erzincan suture zone, Turkey. *Ofioliti*, **32**, 39–51.

ŞAHINCI, A. 1976. Le série du Boztepe au nord de Manisa (Anatolie occidentale-Turquie). Norien supérieur néritique et Sénonian inférieur pélagique, *Comptes Rendus de l'Academie des Sciences, Paris*, **283**, 1019–1022.

SANER, S. 1980. Palaeogeographic interpretation of the Jurassic and younger sediments of the Mudurnu-Göynük Basin based on the depositional features of

Jurassic and younger ages. *Türkiye Jeoloji Kurumu Bülteni*, **23**, 39–52 [in Turkish].

SEARLE, M. P. & COX, J. 1999. Tectonic setting, origin and obduction of the Oman ophiolite. *Geological Society of America Bulletin*, **111**, 104–122.

SEARLE, M. P., WARREN, C. L., WATERS, D. J. & PARRISH, R. R. 2004. Structural evolution, metamorphism and restoration of the Arabian continental margin, Saih Hatat region, Oman Mountains. *Journal of Structural Geology*, **26**, 451–473.

SEARLE, M. P., WARREN, C. J. & WALTERS, D. J. 2005. Reply to Comment by Gray, Gregory and Miller on Structural evolution, metamorphism and restoration of the Arabian continental margin, Saih Hatat region, Oman Mountains. *Journal of Structural Geology*, **27**, 375–377.

ŞENEL, Y. M. 1991. Palaeocene-Eocene sediments interbedded with volcanics within the Lycian Nappes: Faralya Formation. *Mineral Exploration Institute of Turkey (MTA), Bulletin*, **113**, 1–14.

ŞENGÖR, A. M. C. 1984. The Cimmeride orogenic system and the tectonics of Eurasia. *Geological Society of America, Special Paper*, **195**.

ŞENGÖR, A. M. C. & YILMAZ, Y. 1981. Tethyan evolution of Turkey, a plate tectonic approach. *Tectonophysics*, **75**, 181–241.

SEYITOĞLU, G., SCOTT, B. C. & RUNDLE, C. C. 1992. Timing of Cenozoic extension in west Turkey. *Journal of the Geological Society, London*, **149**, 533–538.

SHERLOCK, S., KELLEY, S. P., INGER, S., HARRIS, N. & OKAY, A. I. 1999. ^{40}Ar-^{39}Ar and Rb-Sr geochronology of high-pressure metamorphism and exhumation history of the Tavşanli Zone, NW Turkey. *Contributions to Mineralgy and Petrology*, **137**, 46–58.

SMITH, A. G. 2006. Tethyan ophiolite emplacement, Africa to Eurasia motions, and Atlantic spreading. *In*: ROBERTSON, A. H. F. & MOUNTRAKIS, D. (eds) *Tectonic Development of the Eastern Mediterranean Region*. Geological Society of London, Special Publication, **260**, 11–35.

STAMPFLI, G. M. & BOREL, G. D. 2002. A plate tectonic model for the Palaeozoic and Mesozoic constrained by dynamic plate boundaries and restored synthetic oceanic isochrones. *Earth and Planetary Science Letters*, **169**, 17–33.

STAMPFLI, G., MOSAR, J., FAURE, P., PILLEVUIT, A. & VANNAY, J. C. 2001. Permo-Mesozoic evolution of the western Tethys real: the Neotethys East Mediterranean basin connection, *In*: ZIEGLER, P., CAVAZZA, W., ROBERTSON, A. H. F. & CRASQUIN-SOLEAU, S. (eds) *Peri-Tethys Memoir no. 5 Peri-Tethyan Rift/Wrench Basins and Passive Margins*. Memoirs du Museum National D'Histoire Naturelle, 51–108.

SUN, S. S. & MCDONOUGH, W. F. 1989. Chemical and isotopic systematics of oceanic basalts: implications for mantle composition and processes. *In*: SAUNDERS, A. D. & NORRY, M. J. (eds) *Magmatism in the Ocean Basins*. Geological Society, London, Special Publications, **42**, 313–347.

TANKUT, A. & GORTON, M. P. 1990. Geochemistry of a mafic-ultramafic body in the Ankara melange, Anatolia, Turkey: evidence for a fragment of oceanic lithosphere. *In*: MOORES, E. M., MALPAS, J., PANAYIOTOU, A. & XENOPHONTOS, C. (eds) *Ophiolites, Oceanic Crustal Analogues*. Proceedings of the Symposium TROODOS 1987, 339–349.

TANSEL, İ. 1980. Biostratigraphical investigations of the Nallıhan region. *Yerbilmleri*, **5/6**, 31–47 [in Turkish].

TANSEL, İ. 1990. Age of the Balıklıova Formation according to planktonic foraminfera. *Bulletin*, 41–50 [In Turkish with an English summary].

TAŞLI, K., ÖZER, E. & KOÇ, H. 2006. Benthic foraminiferal assemblages of the Cretaceous platform carbonate succession in the Yavça area (Bolkar Mountains, S Turkey): biostratigraphy and palaeoenvironments. *Geobios*, **39**, 521–533.

TEKELI, O. 1981*a*. Subduction complex of pre-Jurassic age, northern Anatolia, Turkey. *Geology*, **9**, 68–72.

TEKELI, O. 1981*b*. The characteristic features of the Aladağ ophiolitic melange (Taurus Mountains). *Bulletin of the Geological Society of Turkey*, **24**, 57–63 [In Turkish with an English summary].

TEKIN, U. K., GÖNCÜOĞLU, M. C. & TURHAN, N. 2002. First evidence of Late Carnian radiolarian fauna from the İzmir-Ankara Suture Complex, Central Sakarya, Turkey: Implications for the opening age of the İzmir-Ankara branch of Neotethys. *Geobios*, **35**, 127–135.

VERGILI, Ö. & PARLAK, O. 2005. Geochemistry and tectonic setting of metamorphic sole rocks and mafic dikes from the Pınarbaşı (Kayseri) ophiolite, Central Anatolia. *Ofioliti*, **30**, 37–52.

WHITNEY, D. L. & DAVIS, P. B. 2006. Why is lawsonite eclogite so rare? Metamorphism and preservation of lawsonite eclogite, Sivrihisar, Turkey. *Geology*, **34**, 473–476.

WHITNEY, D. L. & DILEK, Y. 1998. Metamorphism during Alpine crustal thickening and extension of Central Anatolia, Turkey: the Niğde Massif core complex. *Journal of Petrology*, **39**, 1385–1403.

WHITNEY, D. L., TEYSSIER, C., DILEK, Y. & FAYON, A. K. 2001. Metamorphism of the Central Anatolian Crystalline Complex, Turkey: influence of orogen-normal collision vs. wrench dominated tectonics on P-T-t paths. *Journal of Metamorphic Geology*, **19**, 411–432.

WILLIAMS, H. & STEVENS, R. K. 1974. The ancient continental margin of eastern North America. *In*: BURK, C. A. & DRAKE, C. L. (eds) *The Geology of Continental Margins*. Springer-Verlag, New York, 781–796.

WALLIN, E. T. & METCALF, R. V. 1998. Supra-subduction zone ophiolites formed in an extensional forearc: Trinity Terrane, Klamath Mountains, California. *Journal of Geology*, **106**, 591–608.

WOOD, D. A. 1980. The application of a Th-Hf-Ta diagram to problems of tectonomagmatic classification and to establishing the nature of crustal contamination of basaltic lavas of the British Tertiary volcanic province. *Earth and Planetary Science Letters*, **56**, 11–30.

YALINIZ, K. M., FLOYD, P. & GÖNCÜOĞLU, M. C. 1996. Supra-subduction zone ophiolites of Central Anatolia: geochemical evidence from the Sarikaraman ophiolite, Aksaray, Turkey. *Mineralogical Magazine*, **60**, 697–710.

YILMAZ, Y., TÜYSÜZ, O., YIĞITBAŞ, E., GENÇ, S. C. & ŞENGÖR, A. M. C. 1997. Geology and tectonic evolution of the Pontides. *In*: ROBINSON, A. G. (ed.) *Regional and Petroleum Geology of the Black Sea* *and Surrounding Region*. American Association of Petroleum Geologists Memoir, **68**, 183–226.

YALINIZ, M. K., AYDIN, N. S., GONCUOGLU, M. C. & PARLAK, O. 1999. Terlemez quartz monzonite of Central Anatolia (Aksaray-Sarikaraman): age, petrogenesis and geotectonic implications for ophiolite emplacement. *Geological Journal*, **34**, 33–242.

YALINIZ, K. M., FLOYD, P. & GÖNCÜOĞLU, M. C. 2000. Geochemistry of volcanic rocks from the Çiçekdağ Ophiolite, Central Anatolia, Turkey, and the their inferred tectonic setting within the northern branch of the Neotethyan Ocean. *In*: BOZKURT, E., WINCHESTER, J. A. & PIPER, J. D. A. (eds) *Tectonics and Mangamism in Turkey and the Surrounding Area*. Geological Society, London, Special Publication, **173**, 203–218.

YOGODZINSKI, G. M., VOLYNETS, O. N., KOLOSKOV, A. V., SELIVERSTOV, N. I. & MATVENKOV, V. V. 1993. Magnesian andesites and the subduction component in strongly calc-alkaline series at Piip volcano, far western Aleutians. *Journal of Petrology*, **35**, 163–204.

Tectono-stratigraphy of the Çankırı Basin: Late Cretaceous to early Miocene evolution of the Neotethyan Suture Zone in Turkey

NURETDIN KAYMAKCI[1]*, YAKUP ÖZÇELIK[2], STANLEY H. WHITE[3] & PAUL M. VAN DIJK[4]

[1]*Middle East Technical University, Department of Geological Engineering, 06531-Ankara Turkey; Current address: Utrecht University, Forth Hoofddik Paleomag Lab. Budapestlaan 17, 3584 CD Utrecht, The Netherlands*

[2]*Turkish International Petroleum Company, Sögütözü Cad. No: 27, 06520-Sögütözü/ANKARA, Turkey*

[3]*Faculty of Geosciences, Budapestlaan 4 3584 CD Utrecht, The Netherlands*

[4]*ITC, Hengelosestraat 99, 7514 AE Enschede, The Netherlands*

**Corresponding author (e-mail: kaymakci@metu.edu.tr)*

Abstract: The Çankırı Basin straddles the İzmir–Ankara–Erzincan Suture Zone which demarcates the former position of the northern branch of the Neotethys. It includes more than 3 km of pre-Middle Miocene in-fill related to late Cretaceous to pre-Middle Miocene evolution of the region. The basin has developed on the upper Cretaceous subduction complex and arc related basins of the Neotethys Ocean. The basin fill includes an upper Cretaceous forearc sequence overlain by Paleocene with a local unconformity. The upper Cretaceous configuration of the Çankırı basin is interpreted as a part of a forearc basin. The Paleocene and younger history is interpreted as a foreland sequence dominated by progressively southwards migrated depocenters in front of southward migrating thrust faults upon which a series of piggy-back basins were developed. Termination of the forearc setting and beginning of foreland basin conditions indicates complete subduction of the Neotethyan oceanic crust and onset of collision between the Pontides (Laurasia) and the Taurides (Gondwana) in the Paleocene. Thrusting and related sedimentation continued until the Aquitanian (Early Miocene).

The İzmir–Ankara–Erzincan Suture Zone (IAESZ; Ketin 1966) demarcates the former position of the Northern Neotethys Ocean (Şengör & Yılmaz 1981) along which the Sakarya Continent in the north, and the Anatolide–Tauride block (in the study region represented by the Kırşehir Block, or the Central Anatolian Crystalline Complex; Fig. 1) collided. The subduction history, commencement age and collision history are still under debate.

Along the İzmir Ankara Zone, and to its south, there are two distinct ophiolitic units. The ophiolites exposed in the southern margin of the Çankırı Basin and on the Kırşehir Block are intruded by various upper Cretaceous to lower Cenozoic granitic plutons belonging to various tectono-magmatic settings (Erler & Bayhan 1995; Boztuğ & Jonckhere 2007; Boztuğ *et al.* 2007; Ilbeyli *et al.* 2004). Most of the ophiolites do not contain pillow lavas and have NMORB to supra-subduction zone geochemical signatures (Yalınız & Göncüoğlu 1996; Yalınız *et al.* 1998, 2000). The ophiolites defining the northern margin of the Çankırı Basin (north of the suture zone) generally have NMORB geochemical signatures, are not intruded by granitoids, and have a very well developed epi-ophiolitic cover and associated forearc sequence (Rojay & Süzen 1997; Rice *et al.* 2006). These characteristics, in combination with time-constraints from the stratigraphy associated with the two different ophiolitic belts, suggests a multiphase closure of the Neotethys. The oldest phase is an intra-oceanic subduction along which the southern half of the Neotethys is consumed northwards and gave way to underthrusting of the Kirsehir Block that resulted in metamorphism. Underthrusting and metamorphism of the Kırşehir Block must be older than the granitic intrusions, which range in age from 90 to 57 Ma. (Güleç 1994; Erler Bayhan 1995; Boztuğ & Jonckheere 2007; Boztuğ *et al.* 2007). Following underthrusting, the Kirsehir Block was exhumed possibly during the granitic intrusion history, and came close to the surface some time between 72–57 Ma (Boztuğ & Jonckhere 2007). In the mean time the northern part of the Çankırı Basin was

From: VAN HINSBERGEN, D. J. J., EDWARDS, M. A. & GOVERS, R. (eds) *Collision and Collapse at the Africa–Arabia–Eurasia Subduction Zone*. The Geological Society, London, Special Publications, **311**, 67–106.
DOI: 10.1144/SP311.3 0305-8719/09/$15.00

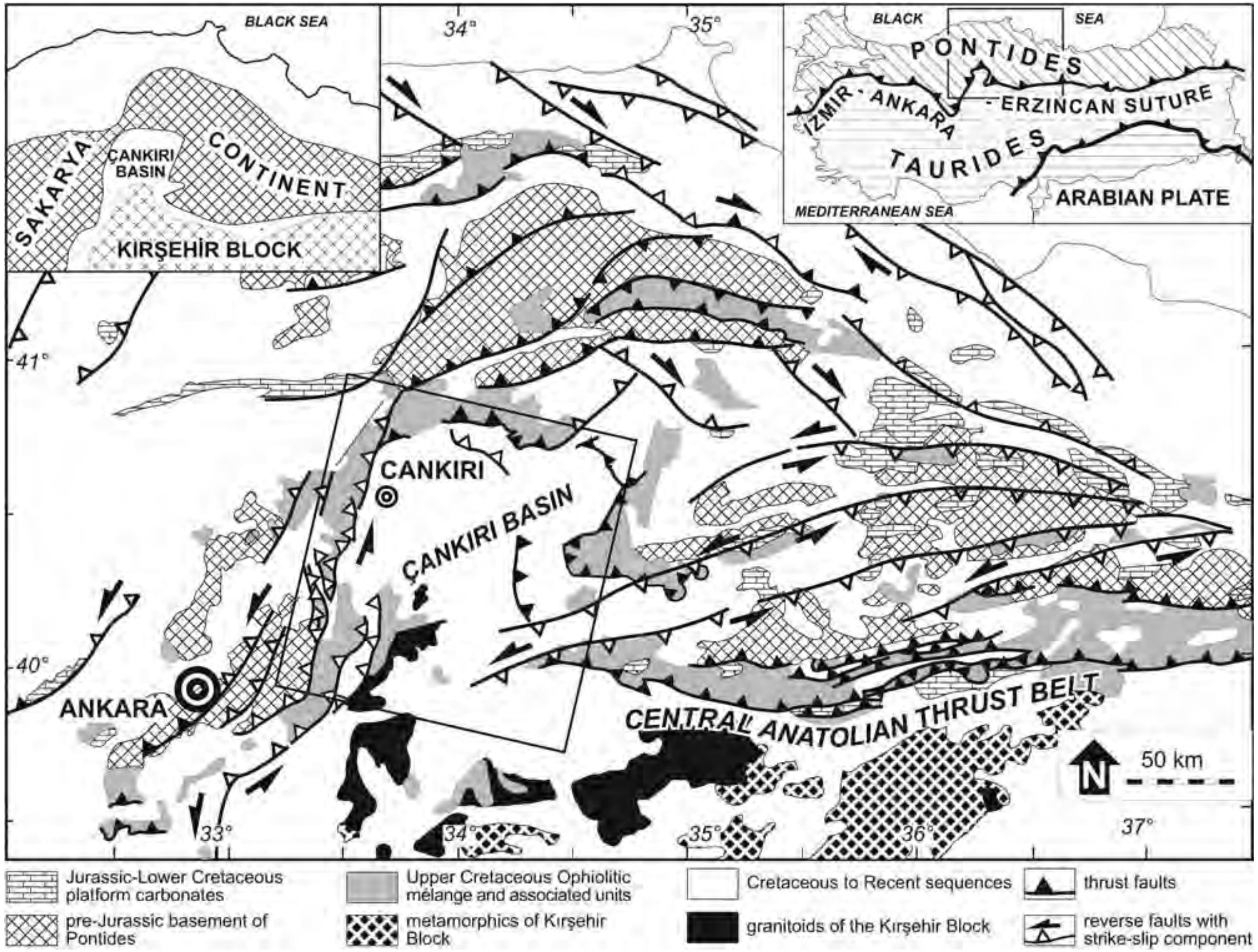

Fig. 1. Tectonostratigraphic map of Central Anatolia. Box shows the location of the Çankırı Basin. Inset maps indicate the major tectonic units in Turkey (modified from Kaymakci *et al.* 2000).

closing under compressional deformation. Recent studies in the southern tip of the Kırşheir Block in Niğde Massif indicates that the exhumation of the Kırşehir Block took place in the early Cenozoic (Whitney *et al.* 2001; Gautier *et al.* 2002). Exhumation of the Kırşehir Block during compressional deformation to its northern margin raises a question whether: (1) there are two different collisional phases separated by a period of extension which exhumed the Kırşehir Block; or (2) exhumation took place during a continuous compressional deformation, due to collision, throughout the Paleocene to earliest Miocene, despite the exhumation of Kırşehir Block. In order to solve this problem, we here study the Çankırı basin, which has a continuous sedimentary history from Campanian to Miocene. Therefore, it has a sedimentary sequence that was deposited during the arc-continent collision, exhumation and final closure of the Neotethys, and may thus provide essential time constraints for the complex closure-history of the Neotethys Ocean. Therefore, the scope of this paper is documenting the tectonostratigraphy of the Çankırı Basin in order to understand its evolution, which will, subsequently, shed light on the terminal subduction of the Neotethys, timing of collision of the Kırşehir Block and the Pontides, and events related to post-collisional convergence in the region.

Geological setting

The Çankırı Basin is located within the İzmir–Ankara–Erzincan Suture Zone and is underlain by an upper Cretaceous ophiolitic mélange and granitoids of the Kırşehir Block (Figs 1, 2).

The ophiolitic mélange can be considered as the subduction complex that resulted from accretion of various lithologies during the subduction of the Neotethys oceanic crust. It includes lithologies derived from both the overriding and subducting plates, together with trench deposits. It also comprises ensimatic island arc and ocean island material embedded within the ophiolitc mélange (Tüysüz *et al.* 1995; Rojay *et al.* 2001, 2004; Rice *et al.* 2006), which formed during the late Cretaceous. Presently, the western, northern and eastern margins of the basin are delimited by the ophiolitic mélange and the Karakaya Complex which belongs to the Sakarya Continent and are collectively called as 'rim' of the basin in an omega shape, while, in the south, it is delimited by the granitoids of the Kırşehir Block (Fig. 1).

In the southern part of the basin, there are isolated outcrops of ophiolite-related rocks which include pelagic limestones, radiolarites and sheeted dyke complexes (Fig. 2), intruded by the granitoids (e.g. Sulakyurt Granitoid) of the Kırşehir Block. Briefly, the basin is floored by the NAOM and the Sulakyurt Granitoid; therefore, they are designated as the basement of the Çankırı Basin in this study.

Stratigraphy

In the Çankırı Basin two depositional sequences are exposed. These sequences are separated from each other with a local unconformity. Stratigraphically, there is no major depositional break between the upper Cretaceous and the Cenozoic units of the Çankırı Basin, despite the fact that the lower to middle Paleocene is missing in its southwestern and eastern margins. In the northwestern and northern parts of the basin, however, local unconformities are very common, the upper Cretaceous and Cenozoic units can be regarded as stratigraphically conformable as biostratigraphically no hiatus can be demonstrated between these sequences (Fig. 3).

Basement

North Anatolian Ophiolitic Mélange (NAOM, upper Cretaceous)

Northern central Anatolia is dominated by a number of ophiolitic belts with various rock constituents. Previous researchers named these ophiolitic units based on their present day geographic locations, the rock constituents and inferred oceanic domain of their origin. Rojay (1993, 1995) proposed a generalized and descriptive nomenclature for all of the ophiolite bearing units in north-central Anatolia without consideration of local constituent lithologies, age and inferred tectonic setting. For simplicity, the nomenclature of Rojay (1995) is adopted in this study.

The NAOM is exposed along all the margins of the Çankırı Basin including the southern margin where it is intruded by the Sulakyurt granitoid and exposed as patchy outcrops overlying the metamorphic continental basement rocks of the Kirsehir Block (see Fig. 2). In the central part of the basin, the NOAM is encountered in an exploration well at a depth of 3566 m (Topuzsaray-I, Fig. 2). Therefore, it is underlying most of the Çankırı Basin. Boundary relationships of the NAOM with other units of the Çankırı Basin are summarized in Figure 4.

Lithologically, the NAOM is composed of a tectonic mixture mainly of spilites, pillow lavas, diabase dykes, red to purple radiolarian chert, cherty limestone, reddish pelagic mudstone and various serpentinized ultramafic rocks including peridotites, harzburgites and pyroxenites. The NAOM also includes layered gabbros, plagiogranites and various limestones derived from nearby

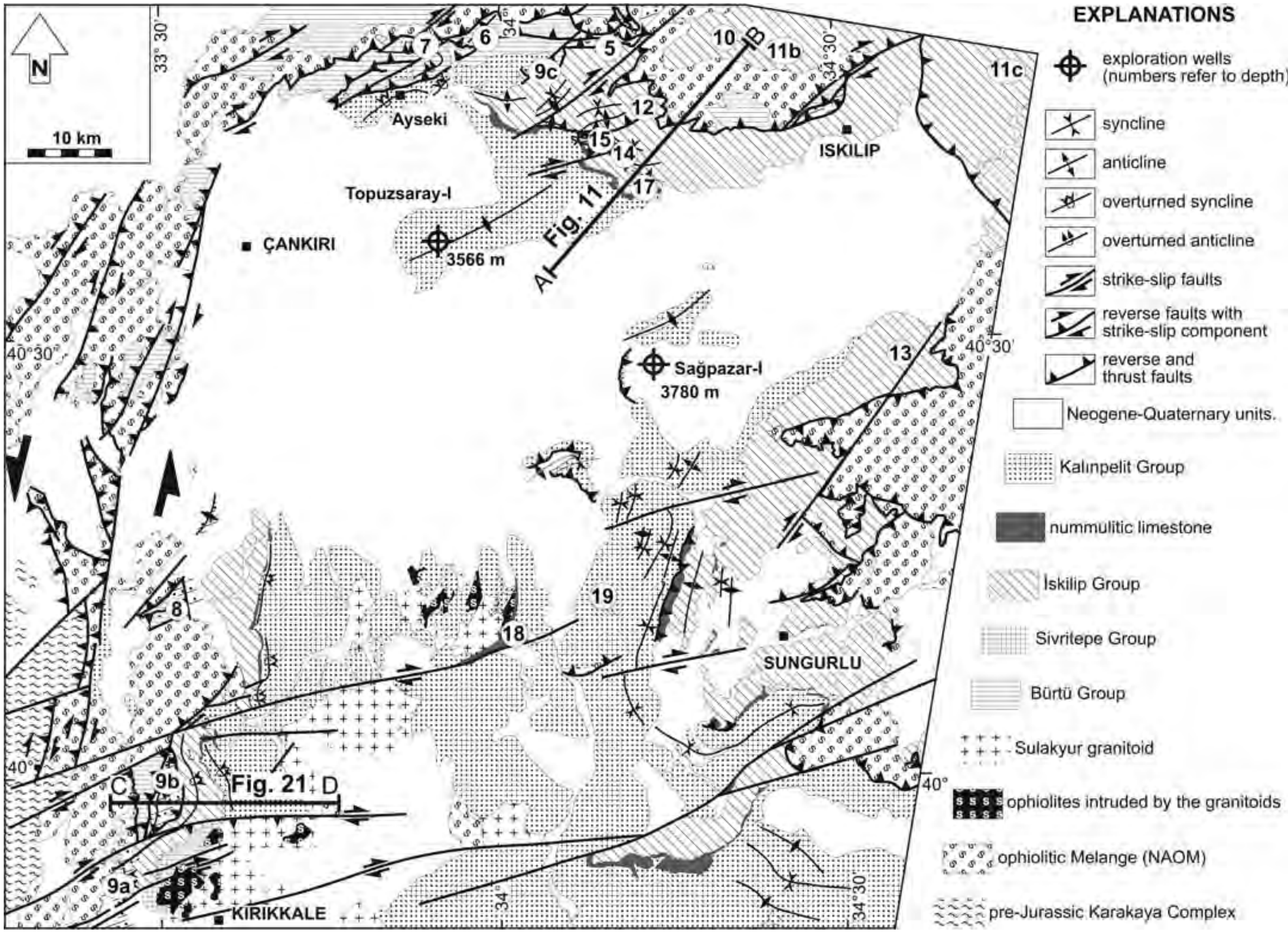

Fig. 2. Geological map of the Çankırı Basin. The numbers in circles refer to the figure numbers of the measured sections.

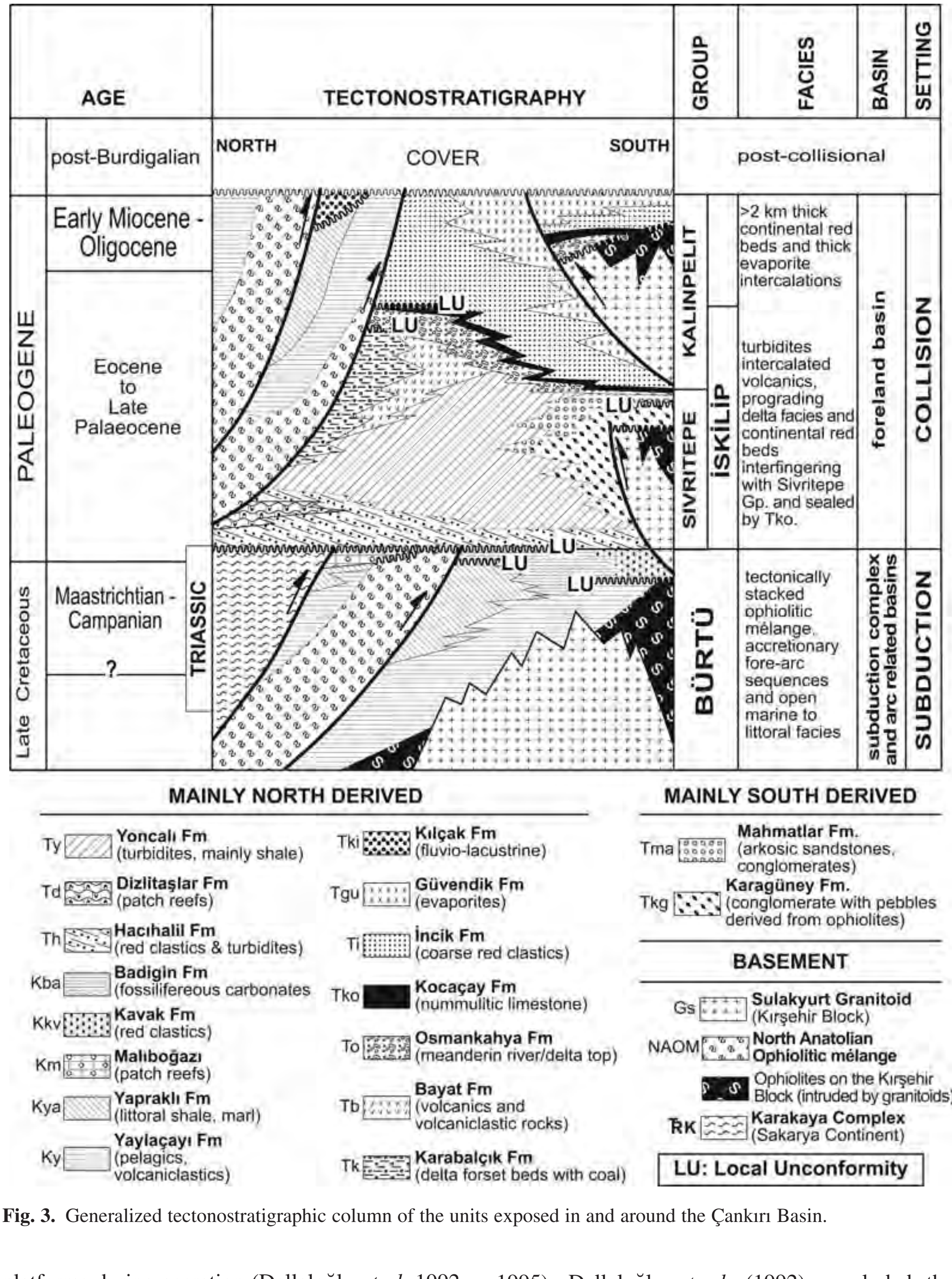

Fig. 3. Generalized tectonostratigraphic column of the units exposed in and around the Çankırı Basin.

platforms during accretion (Dellaloğlu *et al.* 1992; Tüysüz *et al.* 1995; Rojay & Süzen 1997, Rice *et al.* 2006). However, the upper Cretaceous fore-arc deposits (Rice *et al*. 2006) are locally incorporated into the development of the NAOM and locally constitute its matrix. In general, the matrix of the NAOM is missing in most areas (Rojay 1995). Dellaloğlu *et al.* (1992) concluded that NAOM represents a complete ophiolitic sequence, supposedly originated from the northern Neotethys Ocean (Tüysüz *et al.* 1995). Variations occur geographically and the most complete sequence occurs in the western and northern rim of the Çankırı Basin.

(a)	Tkı	Tgu	Ti	Tko	To	Tb	Tk	Ty	Tma	Tkg	Th	Td	Kba	Kkv	Kya	Ky	NAOM	Gs
KILÇAK (Tkı)																		
GÜVENDİK (Tgu)	N/A																	
İNCİK (Ti)	N/A	LVT+U+T																
KOCAÇAY (Tko)	N/A	N/A	LVT+U+T															
OSMANKAHYA (To)	N/A	N/A	U+T	LVT+T														
BAYAT (Tb)	N/A	N/A	U+T	LVT+T	LVT+T													
KARABALÇIK (Kb)	N/A	N/A	U+T	LVT+T	LVT+T	LVT+T+I												
YONCALI (Ty)	N/A	N/A	U+T	LVT+T	LVT+T	LVT+T+I	LVT+T											
MAHMATLAR (Tma)	N/A	N/A	U	LVT+T	LVT+T	N/A	LVT+T	LVT+T										
KARAGUNEY (Tkg)	N/A	N/A	U+T	LVT+T	LVT+T	N/A	LVT+T	LVT+T	LVT									
HACIHALIL (Th)	N/A	N/A	T	N/A	N/A	I+T	LVT+T	LVT+T	LVT?+T	LVT?+T								
DIZILITAŞLAR (Td)	N/A	N/A	U+T	N/A	N/A	N/A	LVT?+T	LVT?+T	LVT?+T	LVT?+T	N/A							
BADIGIN (Kba)	N/A	N/A	U+T	N/A	N/A	N/A	N/A	N/A	N/A	N/A	LVT?	LVT?						
KAVAK (Kkv)	N/A	N/A	U+T	N/A	N/A	N/A	N/A	N/A	N/A	N/A	LVT?	LVT?	LVT					
MALIBOĞAZI (Km)	N/A	N/A	N/A	N/A	N/A	N/A	U+T	N/A	N/A	N/A	U+T	U+T	LVT+T					
YAPRAKLI /Kya)	N/A	N/A	U+T	N/A	U	T+I	T	T	N/A	N/A	U+T	U+T	U+T	U+T				
YAYLACAYI (Ky)	N/A	N/A	U+T	N/A	U+T	T+I	T	T	U	U	U+T	U+T	U+T	U+T	LVT+T			
NAOM	U+T	U+T	U+T	U+T	U+T	T+I	U+T	T	U+T	U+T	U+T	U+T	U+T	U+T	LVT+T	LVT+T		
SULAKYURT GRANITOID (Gs)	N/A	N/A	U+T	U	U+T	N/A	N/A	N/A	U+T	U+T	N/A	N/A	N/A	N/A	N/A	I	I	
KARAKAYA COMPLEX TRk)	U+T	N/A	N/A	N/A	N/A	N/A	N/A	N/A	N/A	N/A	N/A	N/A	N/A	N/A	N/A	T	T	N/A

(b)	a	b	c	d	e
b	U				
c	U+T	LVT			
d	I+T	I	LVT+I		
e	U	N/A	N/A	N/A	
f	N/A	N/A	N/A	N/A	LVT+U

LVT: LATERAL AND VERICAL TRANSITION
U: UNCONFORMABLE
T: TECTONIC
I: INTRUSIVE
N/A: NO CONTACT RELATIONSHIP AVAILABLE

Fig. 4. (**a**) Contact relationships between the pre-Middle Miocene units. (**b**) Conceptual cross-section to explain various contact relationships observed in the Çankırı Basin.

The main difference between the NAOM exposed along the rim and the ophiolitic units intruded by the Sulakyurt granitoid is that the ophiolitic units intruded by the Sulakyurt granitoid lack a melange character and are characterized by a greater abundance of mafic volcanic rocks, gabbros, plagiogranites, various dykes displaying dyke-in-dyke characteristics, dykes with a singe chilled margins and epi-ophiolitic deposits including radiolarites. They are also less deformed compared to the northern ones. These characteristics indicate that the southern ophiolitic units were emplaced as an intact ophiolitic slab and later intruded by the Sulakyurt granitoid, while the northern ones were incorporated into the accretionary wedge of the subducting northern Neotethys. The ophiolites intruded by the Sulakyurt granitoid in the southern margin of the Çankırı Basin have chemical signatures ranging from N-MORB to P-MORB to immature island arc settings contrary to the supra-subduction zone ophiolites exposed further south on the Kırşehir Block (Yalınız & Göncüoğlu 1998; Yalınız *et al.* 1996, 2000). This relationship implies that there are two different tectono-magmatic origins of ophiolitic units on the Kırşehir Block.

Sulakyurt granitoid (pre-late Paleocene)

The geochemical characteristics of the Sulakyurt granitoid vary depending on the wall-rock properties, indicating assimilation of the wall rock. It is composed of intensely altered micro-phanaritic to phanaritic hornblende granite, granodiorite, diorite, syenite, and monzonite (Norman 1972; Akıman *et al.* 1993; Erler & Bayhan 1995; Kuşcu 1997). It also includes various felsic dykes ranging from aplite to vitric rhyolite. The grain size decreases outwards from the pluton interior and is associated with 'chilled margins' and contact metamorphism (Norman 1972). It has not been isotopically dated, however, an indirect pre-late Paleocene age is indicated by the clasts of the granitoid observed within overlying upper Paleocene to middle Eocene units. In the southwestern part of the Çankırı Basin, north of Kırıkkale, the Sulakyurt granitoid intrudes the ophiolitic mélange and associated Campanian–Maastrichtian units (Fig. 1).

Radiometric data from other granitoids of the Kırşehir Block are rather scarce. The radiometric ages of the known granitoids range between 110 ± 14 Ma based on whole rock Rb–Sr isotopes (Güleç 1994) and 54 Ma in the western margin of the Kirsehir block using the total Pb method (Ayan 1969). Boztuğ *et al.* (2007) proposed that the granitoids were emplaced during the late Cretaceous, between 94.9 ± 3.4 to 74.9 ± 3.8 Ma based on $^{207}Pb-^{206}Pb$ single zircon evaporation ages. They suggest that these granites are related to arc–continent collision of the Kırşehir Block with the northern Neotethyan oceanic plate. Based on fission track data, Boztuğ & Jonckheere (2007) proposed that the granitoids exposed in the NW part of the Kırşehir Block were exhumed close to the surface around 62–57 Ma. Based on stratigraphic data, Erler & Bayhan (1995) proposed that most of the granitoids within the Kırşehir Block were exposed prior to Eocene which indicates that the Kırşehir Block consolidated during the development of the Çankırı Basin.

In the Çankırı Basin, the oldest facies in direct contact with the Kırşehir Block is observed only in the southwestern part where generally Kırşehir Block-derived clastics dominate. The age of these deposits is late Paleocene to Eocene and indicates that the granites were exposed before the earliest Eocene, which is consistent with the radiometric data.

Basin sequences

Upper Cretaceous units

The upper Cretaceous units are deposited in a wider basin beyond the Cenozoic configuration of the Çankırı Basin and are developed on and associated with the underlying NAOM). Partly, the upper Cretaceous units including the ophiolitic mélange formed by the Yaylaçayı and Yapraklı formations were previously described by Dellaloğlu *et al.* (1992) as the Kalecik Group. In this study, two different formations of the Kalecik Group are recognized and named for the first time. These include Kavak and Badiğin formations (Fig. 3).

The lower part of this group (Yaylaçayi and Yapraklı formations) was previously interpreted to be associated with accretionary wedge (subduction complex) growth and development of a magmatic arc and arc related basins during the northwards subduction of the Tethys in the late Cretaceous (Tüysüz *et al.* 1995; Kaymakcı 2000; Rice *et al.* 2006).

Bürtü group

The Bürtü group comprises upper Cretaceous to Paleocene units. These include Yaylaçayı, Yapraklı, Malıboğazı, Kavak and Badiğin formations.

Yaylaçayı Formation (Ky, Campanian to Maastrichtian). The Yaylaçayı Formation was first named by Yoldaş (1982). It consists mainly of a volcano-sedimentary sequence (Fig. 5), is exposed at the rim of the Çankırı Basin and is associated with the NAOM. It is regarded as a distinct formation because locally it can be mapped as a separate unit and its internal structure is preserved. Lithologically, the Yaylaçayı Formation exhibits very abrupt lateral facies change. The

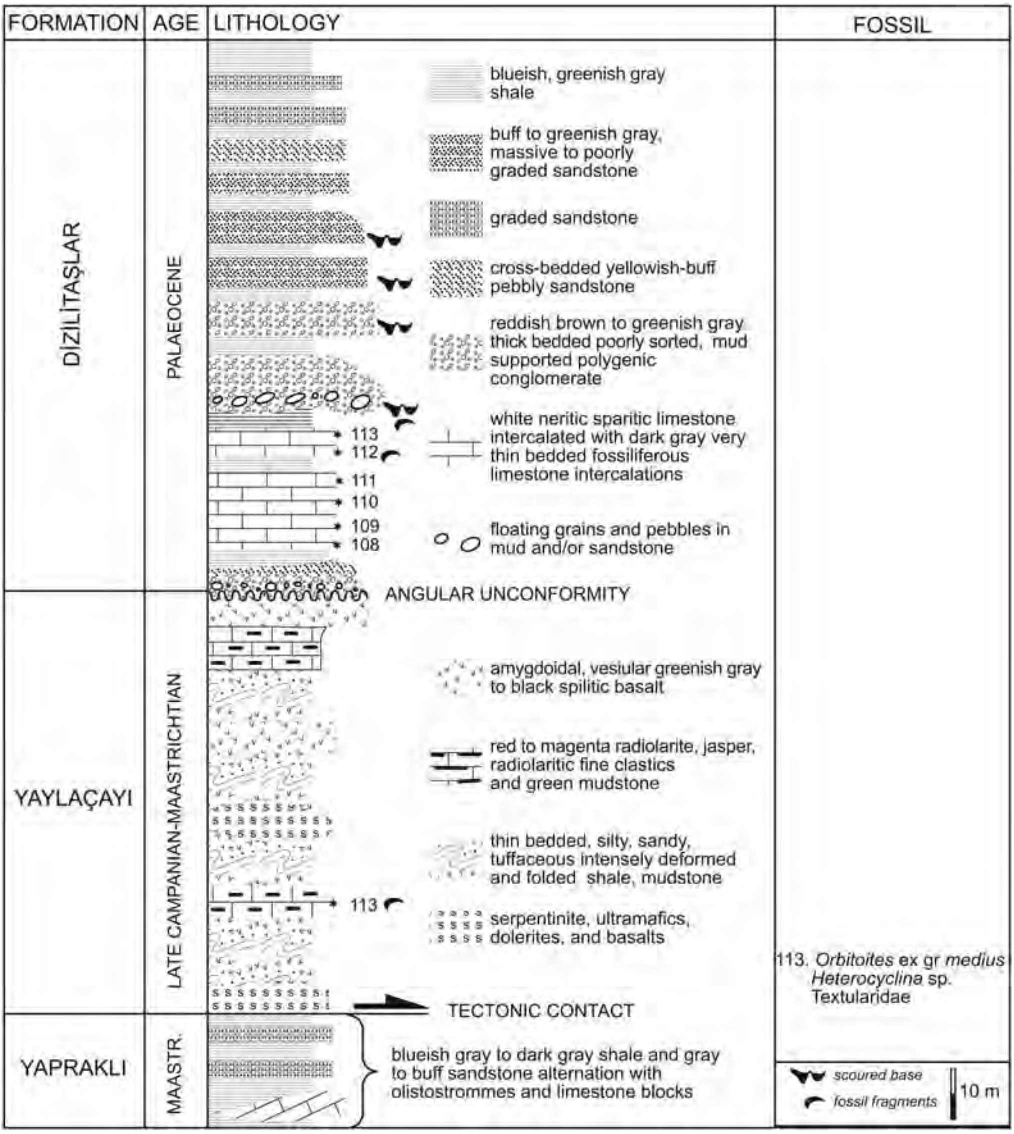

Fig. 5. Measured stratigraphical section for parts of the Yaylaçayı and Dizilitaşlar Formations (its location is indicated with 5 in Fig. 2).

bottom of the formation is well exposed at the south-western part of the Çankırı Basin NW of Kırıkkale (Fig. 2). The dominant character of the unit is the presence of various volcanogenic horizons in which basalts, tuffs and tuffites are intercalated with shales and pelagic marly limestones. In general, it is composed of three distinct lithological associations. From bottom to top these are: (1) red to purple marl, marly pelagic limestone, volcanogenic sandstone, and tuff alternations; (2) pelagic fauna bearing micritic limestone and green shale alternation, intercalated with alternations of spilitic olistostromes and tuff; and (3) turbiditic sandstone and shale alternations intercalated with tuff, agglomerate, beige silty argillaceous limestone, and marl grading upward into a benthic fossil bearing sandy limestone (Fig. 6). Being deposited on top of the ophiolitic mélange and overlain by upper Cretaceous regressive terrigeneous deposits, the Yaylaçayı Formation is inferred to be deposited in a forearc setting (Rojay & Süzen 1997). Tüysüz *et al.* (1995) argue that the Yaylaçayı Formation

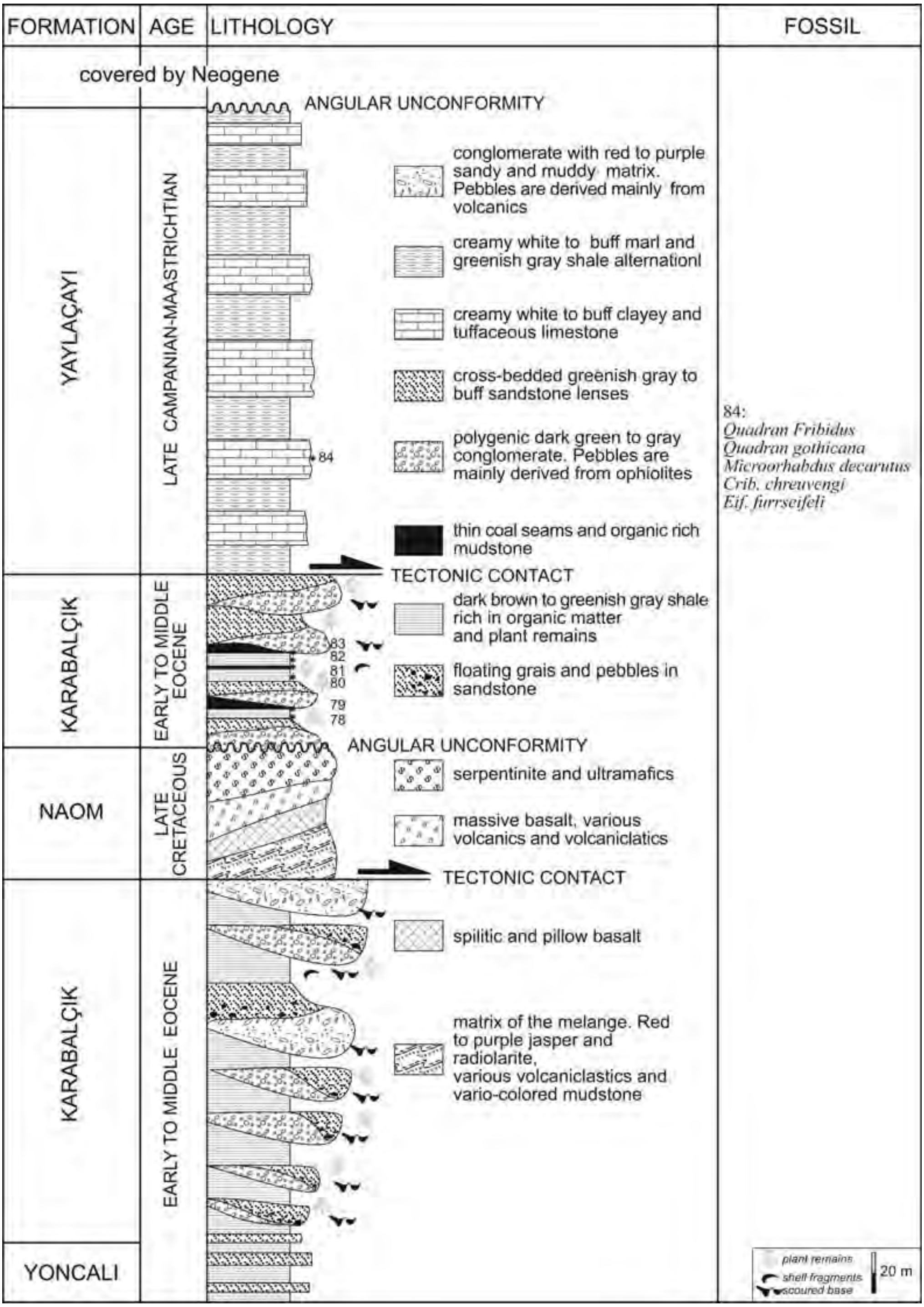

Fig. 6. Measured stratigraphical section for a part of the Yaylaçayı and Karabalçık Formations (its location is indicated with 6 in Fig. 2).

represents an intra-oceanic setting due to the lack of terrigenous material (see also Rice *et al.* 2006).

The age of the unit varies from Maastrichtian (Yoldaş 1982), Cenomanian–Campanian (99–71.3) Ma (Akyürek *et al.* 1984), to Santonian–Campanian (85.8–71.3 Ma) (Tüysüz 1985; Dellaloğlu *et al.* 1992), and Cenomanian–Late Maastrichtian (99–65 Ma) (Tüysüz *et al.* 1995). The following foraminifera fauna have been identified at the base of the Yaylaçayı Formation: *Orbitoides ex gr medius*, *Heterocyclina* sp., Textularidae (Fig. 5) and from the upper part of the formation following nannofossils have been identified: *Quadran fribidus*, *Quadran gothicana*, *Microrhabdus, decarutus*, *crib. chreuvengi, Eif. furrseifeli*, which are of late Campanian to Maastrichtian age (Fig. 6). Considering these ages and those of the above fauna, it is concluded that the Yaylaçayı Formation was deposited in the Santonian to Maastrichtian interval. This time interval corresponds also the onset of volcanic arc development (Yemişliçay Formation, Görür 1997) in the central Pontides north of the Çankırı Basin.

Yapraklı Formation (Kya, Campanian–Paleocene). The Yapraklı Formation was first named by Birgili *et al.* (1974). It is characterized by limestones with macrofossils and fine-grained clastics. The Yapraklı Formation (see Figs 6–8) displays local coarsening-upward sequences and bears evidence for progressive shallowing of the depositional environment, indicated by the transition from fine clastics to neritic limestones. The bottom of the formation is composed of explosive volcanic rocks such as white tuff and agglomerate intercalations. In the middle, it is characterized by turbiditic macrofossil bearing, volcanoclastic conglomerate, sandstone and multicolored shale. Towards the top, limy units and fossiliferous limestones are present. Locally, the unit includes olistostromal horizons. In addition, the unit also includes thick-shelled pelecypoda, wood and plant remains especially in its upper parts, which indicates close proximity to the margin of the basin.

Dellaloğlu *et al.* (1992) have proposed a Senonian to Maastrichtian age for this formation based on planktonic foraminifera, gastropoda and pelecypoda fossils. However, the fossils identified in this study yielded Maastrichtian to Paleocene age in the Malıboğazı section (Fig. 8) and Maastrichtian in Kağnıkonağı section (Fig. 6), and Campanian to Maastrichtian in the Badiğin section (Fig. 7). This age range indicates that the Yapraklı Formation was deposited diachronically in the Campanian(?) to Paleocene interval.

Because the Yapraklı Formation conformably overlies and laterally grades into the Yayalaçayı Formation, we interpret it as partly the proximal equivalent of the Yaylaçayı Formation.

Malıboğazı Formation (Km, upper Cretaceous–Paleocene). The Malıboğazı Formation was previously named by Ayan (1969). It is exposed only in the central southwestern part of the Çankırı Basin. In the Topuzsaray-I well, it is encountered at depths between 2907 to 3090 m. The Malıboğazı Formation comprises approximately 200 m of condensed neritic reefal limestones with rich Rudist, Exogyra, and Orbitoides (Figs 7 & 8) interlayered with spilitic basalts and volcaniclastics. It is conformably deposited on the NAOM as isolated patchy reefs. Similar facies are also reported from elsewhere outside of the Çankırı Basin (see Ünalan 1982; Bingöl 1984; Yazgan 1984; Rojay & Süzen 1997).

Kavak Formation (Kkv, upper Cretaceous–Paleocene). The Kavak formation is informally named in this study. It is exposed only in limited outcrops in the northwestern part of the basin and also encountered in the Topuzsaray-I well at a depth of 3090 m, and is around 150 m thick.

The Kavak formation comprises approximately 15 m of polygenic conglomerates with a limy matrix overlain by a very thickly bedded red to purple conglomerate and sandstone alternation. It laterally grades and overlies the Yapraklı Formation with local unconformities. It includes reworked upper Cretaceous fauna and detritus derived mainly from the basement metamorphic rocks, NAOM, Yaylaçayı and Yapraklı formations (Fig. 7).

Badiğin Formations (Kba, upper Cretaceous–Paleocene). The Badiğin formation is exposed in the northwestern corner of the Çankırı Basin. It is composed of 100 to 200 m thick buff to yellow marl containing gastropoda, exeogyra, worm tracks and pelecypoda fragments and a very thick fossilifereous sandy limestone with intercalations of red sandstone containing fossil fragments and limestone concretions, and of calcite cemented conglomerate (Figs 7 & 8). Like the Kavak formation, it laterally grades into and and overlies the Yapraklı Formation with a local unconformity. It was deposited in near-shore to neritic environments in the latest Maastrichtian to Paleocene.

Cenozoic units

The Cenozoic infill of the Çankırı Basin displays an asymmetrical wedge-like geometry being thicker in the west, north and the east, where it is overthrusted by the northern ophiolites, and become thinner towards the south where it is onlapping onto the Kırşehir Block. The oldest and the thickest deposits lie near the thrust margin and are generally structurally imbricated due to compressional deformation.

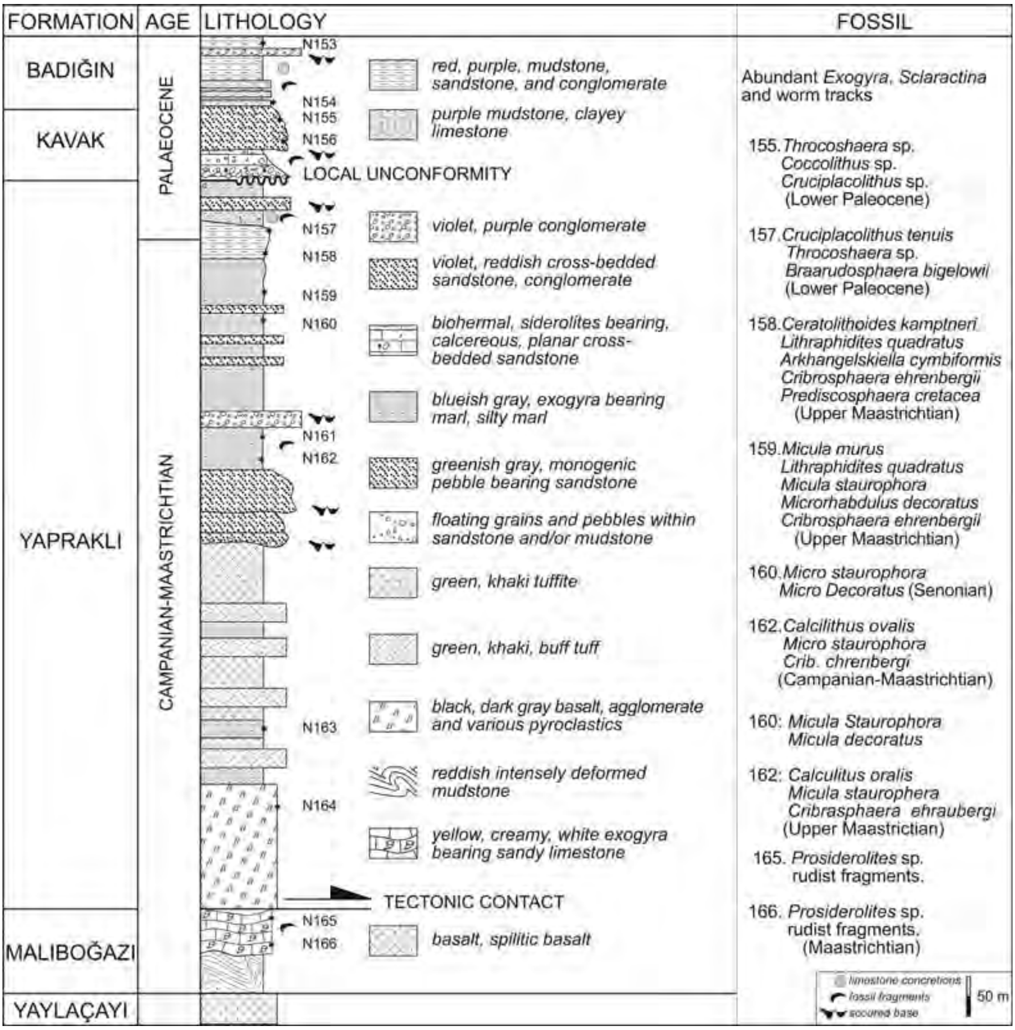

Fig. 7. Measured stratigraphical section for a part of the Yapraklı Formation (its location is indicated with 8 in Fig. 2).

They constitute sedimentologically a proximal facies, which markedly become thinner towards the basin centre. Some of these facies (Karagüney, Mahmatlar, Kocaçay and Incik Formations) progressively onlap on to the Kırşehir Block in the south. Such geometry combined with sedimentological and structural observations will be discussed in the forthcoming sections.

As mentioned above, the basin is structurally delimited along the rim by south-vergent thrust faults which are displaced by multidirectional normal faults of middle Miocene age and later by NE–SE oriented strike-slip faults which developed since the late Miocene. Renewed compression during the post-middle Miocene resulted in coaxial deformation which complicates the lower Cenozoic structures (Kaymakcı *et al.* 2000; 2001*b*; 2003*a* & *b*).

The Cenozoic infill of the Çankırı Basin received detritus mainly from two different sources. The main groups which cover all but the southwestern corner of the basin are devoid of pebbles derived from the granitoids of the Kırşehir Block and their thickness and grain sizes consistently decrease from the rim to the basin center towards the southern margin. Therefore they are described here as the north derived units (see also palaeocurrent data of Norman 1972). On the other hand, the units in direct contact with the Kırşehir Block, along the southern margin of the basin, shed detritus from the granitoids as indicated by granitic pebbles and arkosic sandstones. Therefore, they are categorized here as south derived units.

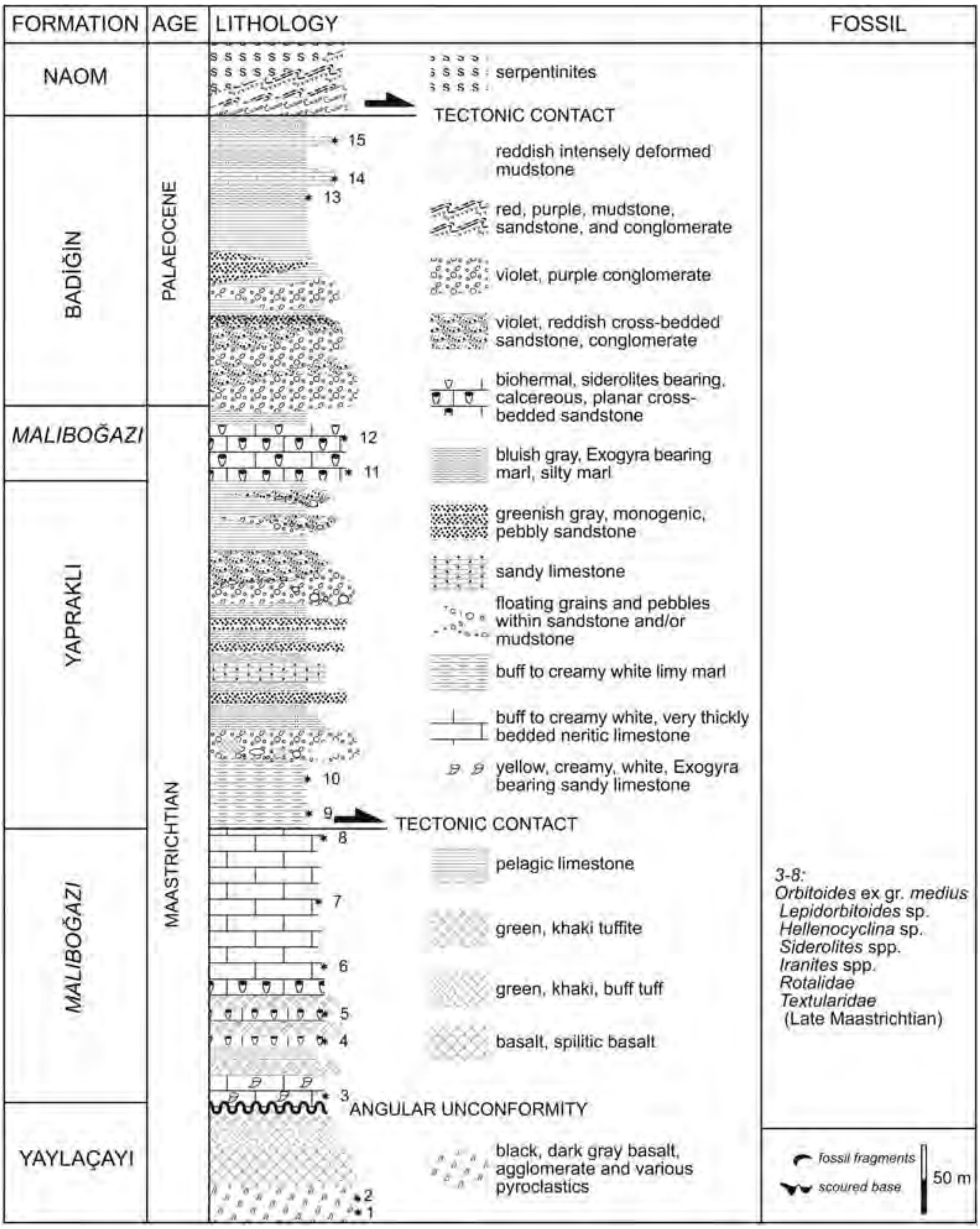

Fig. 8. Measured stratigraphical section for a part of the Malıboğazı, Yapraklı and Badiğin formations (its location is indicated with 8 in Fig. 2).

North derived units

The north derived facies developed in front of the rim and constitute the upper Paleocene to middle Eocene marine flysch to continental molasse successions (Hacıhalil, Dizilitaşlar, Yoncalı, Karabalçık formations), and are associated with middle Eocene volcanic rocks (Bayat Formation) covered by continental red clastics and a nummulitic condensed sequences of middle Eocene age (Osmankahya and Kocaçay formations respectively). Kocaçay Formation is a key horizon in the Çankırı Basin, which together with the Osmankahya Formation, covers both the older basin units and the Kırşehir Block and is the youngest marine deposit within the Çankırı Basin. The Kalınpelit group (informally named in this study) conformably overlies the Kocaçay Formation and comprises a very thick sequence of continental red clastics and evaporites of post-middle Eocene to Oligocene and lower Miocene fluvio-lacustrine deposits. The lower Cenozoic units of the Çankırı Basin were collectively named as the İskilip Group by Dellaloğlu *et al.* (1992). In this study, it is divided into two subgroups while the name 'İskilip Group' is restricted to the lower part of the sequence and is characterized mainly by marine successions while the overlying continental units are informally named as the Kalınpelit group (Fig. 3).

İskilip Group. The İskilip Group was first named by Dellaloğlu *et al.* (1992) and comprised all the lower Cenozoic deposits of the Çankırı Basin. In this study the İskilip Group is restricted only to the upper Paleocene to middle Eocene marine successions of the Çankırı Basin. It includes the Hacıhalil, Dizilitaşlar (Fig. 9), Yoncalı, Karabalçık, Bayat, Osmankahya and Kocaçay formations.

Hacıhalil Formation (Th, upper Paleocene to middle Eocene). This formation was first named by Birgili *et al.* (1974). It is composed of alternations of conglomerates, sandstones and shale (Fig. 10). It is exposed mainly in the southwestern, northern and north-eastern margin of the basin (Fig. 2). Its thickness ranges between 300 to 1360 m.

The Hacıhalil Fm conformably overlies the upper Cretaceous units of the northwestern part of the Çankırı Basin. In the northern part of the basin (Fig. 2), approximately 30 m thick conglomerates rest on the NAOM with an unconformity (Fig. 11b). The individual beds are up to 3 m thick, poorly sorted, generally loosely packed and matrix supported. The matrix consists of sandstones. The largest pebbles are up to 20 cm in diameter and are derived from the NAOM, Yaylaçayı and Yapraklı formations. They are sub-rounded to ellipsoidal, frequently displaying imbrications. The sandstones are up to 2 m thick and locally graded. The shales include widespread bioturbation, floating pebbles, mud-balls, plant and macro fossil fragments and widespread nummulite fossils (Fig. 10). In this area, according to the sedimentological study of Ocakoğlu & Çiner (1997), the Hacıhalil Formation comprises 6 different facies. They are, from north to south: proximal alluvial fan, braided river, meandering river, fan delta and near shore to prodelta/open marine facies. The main sources of sediments are located to the NW, although sediments were also supplied from the SE (Ocakoğlu & Çiner 1997).

The age of the Hacıhalil Formation, as indicated by its fossil contents (Fig. 10), is upper Paleocene to middle Eocene, which has also been reported by Aziz (1975), Yoldaş (1982), Tüysüz (1985), Dellaloğlu *et al.* (1992).

Dizilitaşlar Formation (Td, Paleocene). The name Dizilitaşlar Formation was first used by Norman (1972) for the Paleocene flysch-like conglomerates and sandstones intercalated with neritic limestones (Fig. 9). In the southwestern part of the Çankırı Basin, it is composed of an approximately 60 m thick green, greenish grey medium- to thick-bedded (10–50 cm) shale and thin-bedded (2–5 cm) sandstone alternation at the bottom. This is succeeded by conglomerates, thickly bedded (1–2 m locally) sandstone and shale alternation. The conglomerate pebbles are derived from the NAOM, Yaylaçayı, Yapraklı and Malıboğazı formations and felsic magmatic rocks. The sandstones are locally cross-bedded and graded. It is overlain by an approximately 50 m thick shale sequence alternating with thin-bedded sandstones (Fig. 9).

The central part of the formation (Fig. 9) is constituted by an approximately 100 m thick, buff to dark grey neritic limestone (D3 member of Norman 1972), calcarenite and intercalated pebbly sandstone, boulder-conglomerates and shale. It also includes olistostromal horizons in which limestone blocks are set in a shaly matrix. The limy horizon is followed upwards by an alternation of medium- to thick-bedded shale and thin-bedded sandstone with a cumulative thickness of approximately 200 m. At the western margin of the basin, the Dizilitaşlar Formation is intensely deformed and folded. At the bottom, the Dizilitaşlar Formation is characterized by conglomerates and followed upwards with neritic limestones. At the top part, it is constituted by an approximately 150 m thick lime-cemented sandstones and conglomerates followed upward by, approximately 150 m thick, graded sandstone and thin beds of shale alternation. In the northern margin of the basin, the Dizilitaşlar Formation is represented by thin sandstone-shale alternations at the bottom and a very thick massive neritic limestone followed by a thin alternation of sandstone and shale (Fig. 9).

According to Norman (1972) and Dellaloğlu *et al.* (1992) the age of the Dizilitaşlar Formation is Paleocene. According to Kazancı & Varol (1990), the Dizilitaşlar Formation comprises a mass flow-dominated fan-delta complex (cf. Postma 1983) at the bottom and sand dominated turbidites at the top. The limestones within the Dizilitaşlar Formation were deposited in fringing patch reefs in a regressive setting.

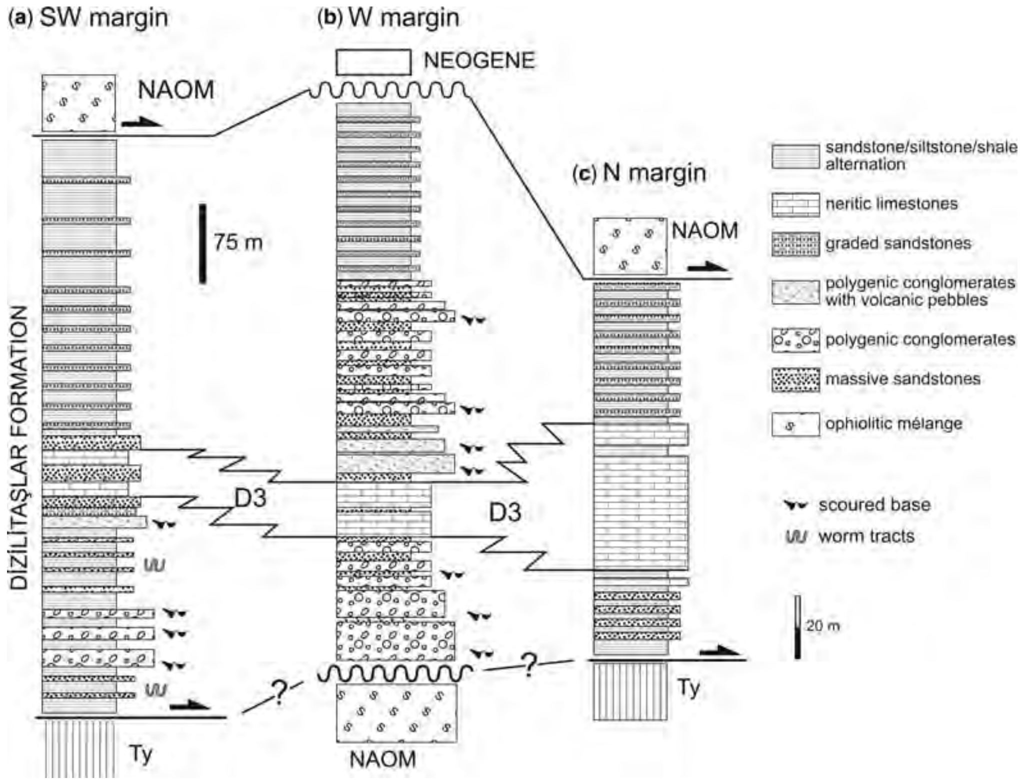

Fig. 9. Generalized columnar sections for the Dizilitaşlar Formation in the southwestern, western and northern margins of the Çankırı Basin (partly modified from Norman 1972; Dellaloğlu *et al.* 1992) (location of the sections are indicated with 9a–c in Fig. 2).

Yoncalı Formation (Ty, upper Paleocene to middle Eocene). The Yoncalı Formation was first named by Aziz (1973). It consists mainly of shale and sandstone alternations (Figs 12 & 13). It is always transitional at the bottom with the Hacıhalil Formation and has lateral and vertical gradations to the Karabalçık, Bayat, Osmankahya and Kocaçay formations. It is unconformably overlain by the Incik and younger formations. It has tectonic boundary relationships with the NAOM and is intruded by generally WNW–ESE orientated feeder dikes of the Bayat Formation (Demirer *et al.* 1992). For example, in the north-eastern part of the area, the thrust contact between underlying Yoncalı Formation and overlying NAOM is intruded by the feeder dikes of the Bayat Formation (Fig. 11c). This relationship indicates compressional deformation and thrusting of the NAOM during or after the deposition of the Yoncalı Formation in the upper Paleocene to middle Eocene.

In the northern part of the basin, the Yoncalı Formation is composed mainly of alternations of shale, sandstone and thin beds of conglomerate. The shales are dark green to dark grey and thin- to thick-bedded (10–100 cm). The sandstones are dark green to buff, fine to medium-grained. They are graded, planar cross-bedded and current ripple-laminated at various levels. The conglomerates are made up of pebbles derived mainly from ophiolitic rocks including radiolarian chert, serpentinite, micritic limestones, basalt, and tuffs. They are subrounded to rounded and the largest clast size is around 5 cm in diameter. The Yoncalı Formation also comprises olistostromes containing pebbles of pelagic limestone, spilitic basalt and serpentinite blocks of various sizes (up to few tens of metres) derived from the ophiolitic units and are enclosed by dark grey shales (Figs 12 & 13).

Along the eastern margin, the Yoncalı Formation is characterized by regular alternations of sandstone, siltstone, shale, and pelagic limestone (Fig. 13). The thickness of the beds ranges between 2 and 10 cm. In this part of the basin, the base of the Yoncalı Formation is not exposed, as it is overthrusted by the NAOM.

The age of the unit is of upper Paleocene to middle Eocene as indicated by its fossil content (Figs 12 & 13).

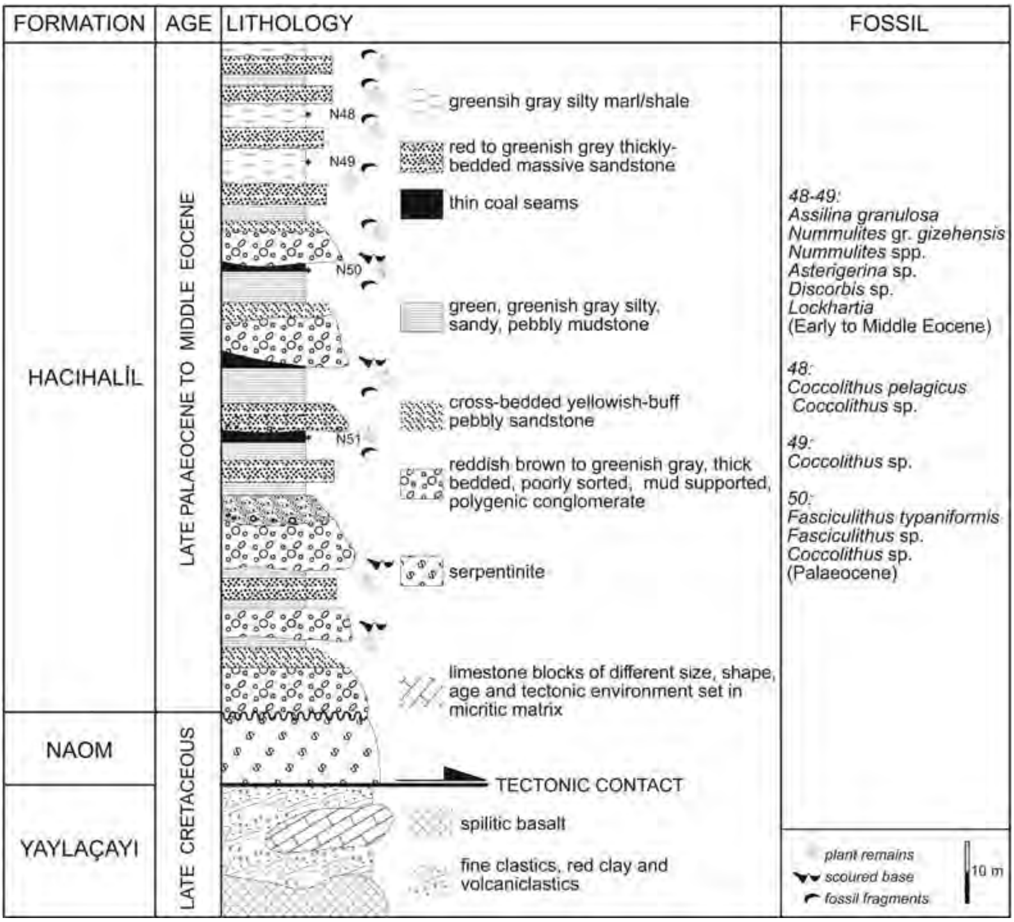

Fig. 10. Measured stratigraphical section for a part of the Hacıhalil Formation (its location is indicated with 10 in Fig. 2).

Karabalçık Formation (Tk, upper Paleocene to middle Eocene). The Karabalçık Formation is named by Dellaloğlu *et al.* (1992) and represented mainly by conglomerates with alternating sandstones and shales and tuff/tuffite intercalations (Figs 12 & 14). It is well developed in the western and northern parts of the basin. In the east it is either not developed or represented by the channel-like patches of conglomerates within the Yoncalı Formation and channel-like conglomerates unconformably resting on the NAOM. In the northern part of the basin, the Karabalçık Formation laterally grades into the Yoncalı, Bayat and Osmankahya formations.

In the northern part of the Çankırı Basin, the Karabalçık Formation is characterized by thick beds of polymict conglomerate containing subrounded to well-rounded pebbles of quartzite, mafic volcanic rocks, vitric tuff, marble, fossiliferous white limestone, micritic limestone, green schist, sandstone and radiolarian chert. These lithologies are derived from the underlying metamorphic rocks, ophiolitic units and other upper Cretaceous units. Some parts of the conglomerates are intensely oxidized and have a clayey and sandy matrix cemented by secondary calcite. Towards the top, the conglomerates are succeeded by an alternation of yellowish grey, medium- to thick-bedded sandstone, greenish grey medium- to thick-bedded shale, and orange to buff thick-bedded conglomerates. Higher up in the section, the Karabalçık Formation is composed of sandstone, siltstone and marl alternations and at least four levels of economic coal horizons (up to 2 m thick). Towards the top, a number of olistostrome levels and very thick (>5 m) cross-bedded conglomeratic sandstones dominate (Fig. 15). The top part includes intercalations of conglomerate and sandstones with fossiliferous horizons characterized

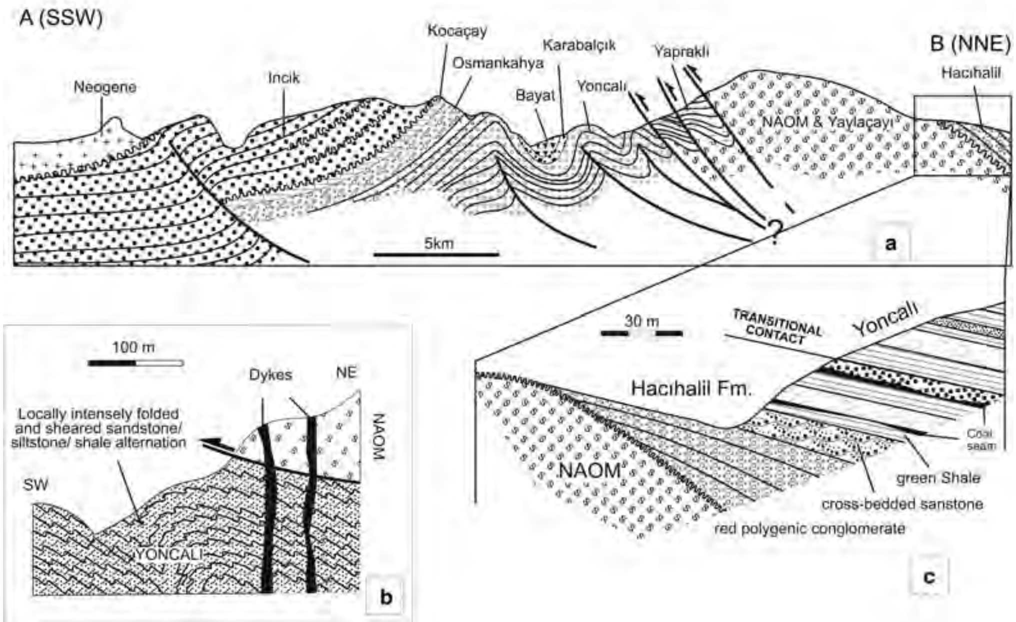

Fig. 11. (**a**) Schematic cross-section along line A–B in Fig. 2. (**b**) Schematic cross-section illustrating how the thrust contact between the North Anatolian Ophiolitic Melange (NAOM) and the Yoncalı Formation is cut by the dykes of Bayat Formation (11b in Fig. 2.) (**c**) Blow-up figure depicting the relation between NAOM, Hacıhalil and Yoncalı formations (11c in Fig. 2).

by imbrication of transported and reworked nummulite fossils (Fig. 14). The orientation of cross beds indicates sediment transport in NW to SE direction.

In the western parts of the basin, the Karabalçık Formation displays a very well developed coarsening upwards sequence starting from the Yoncalı Formation at the bottom and grading into the Osmankahya Formation, which, in turn, grades into Kocaçay Formation that marks the youngest marine unit in the basin. The beds of conglomerates may locally reach up to 5 m thickness. Generally, these are loosely packed, unsorted and lack any internal sedimentary structure, but locally planar cross-bedded and graded horizons are present. The sandstones are medium- to thick-bedded. Age of the formation is early to middle Eocene as indicated by its fossil content (Figs 14 & 17).

Bayat Formation (Tb, upper Paleocene to middle Eocene). This unit was first named by Ayan (1969). It is a widespread unit in the northern and northeastern parts of the study area. It is characterized by a volcano-sedimentary sequence. Its thickness varies from about 300 m in the north to few meters in the eastern part of the basin and it is not developed in the southwestern part of the basin.

Locally, the Kocaçay Formation has an interfingering relationship with the Bayat Formation (Fig. 16). Lithologically, the Bayat Formation comprises two distinct parts (Figs 14, 16 & 17). The lower part is composed of marl, sandstone, conglomerate and tuff intercalations. The marls are green to dark green, medium- to thick-bedded, generally tuffaceous, and locally contain conglomerate lenses of pebbles derived from volcanogenic material. Sandstones are yellowish green, dark grey and generally medium bedded. The grains are medium to coarse in size, sub-angular to sub-rounded and derived from mafic to intermediate volcanic rocks. They also contain wood and plant remains. The conglomerate lenses within the marls and tuffs are green to grey, medium- to thick-bedded. Pebbles are up to 10 cm in diameter, sub-rounded. Tuffs are green, yellowish green, thin- to medium-bedded.

The upper part of the Bayat Formation is mainly composed of various volcanic rocks intercalated with tuffaceous marls. Based on their origin and composition, the volcanic rocks of the Bayat Formation are divided into four categories (Demirer *et al.* 1992): (1) tholeiitic-basalts and tholeiitic-olivine basalt of mantle origin; (2) hornblende-biotite-andesite, biotite-andesite, pumicic biotite-andesite, and hornblende-andesite lavas; (3) basaltic and andesitic

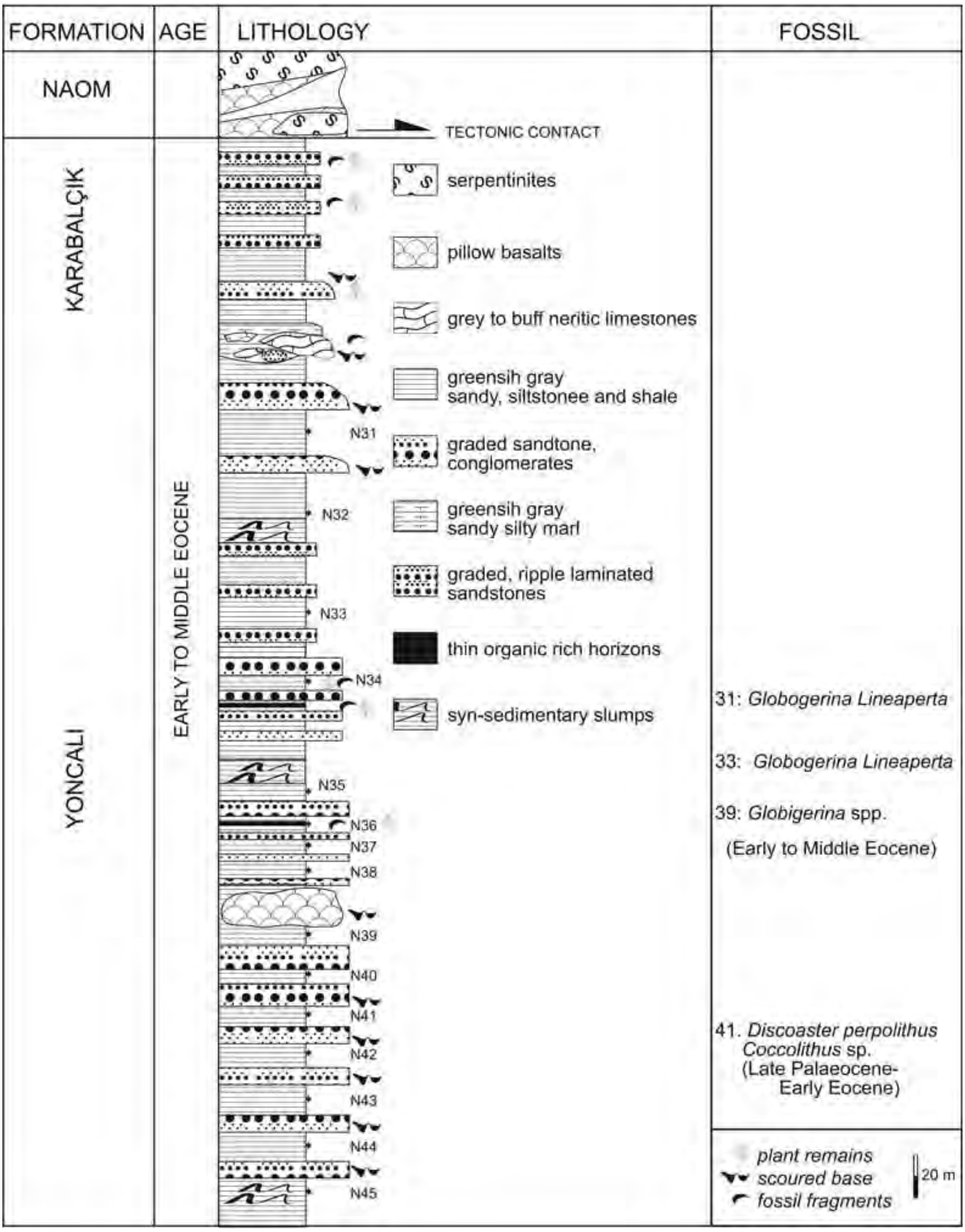

Fig. 12. Measured stratigraphic section for parts of the Yoncalı and Karabalçık formations (its location is indicated with 12 in Fig. 2).

lavas derived from continental crustal setting; and (4) tuffs and agglomerates. In the NE, just outside the studied portion of the Çankırı Basin, a number of generally W–NW to E–SE oriented dykes, which may range up to 10 km in length, have intruded the NAOM, Yoncalı and Karabalçik formations (Fig. 11c). Based on the similarity of their geochemical characteristics and emplacement ages, these dykes were interpreted to be the feeders of the volcanic rocks of the Bayat Formation.

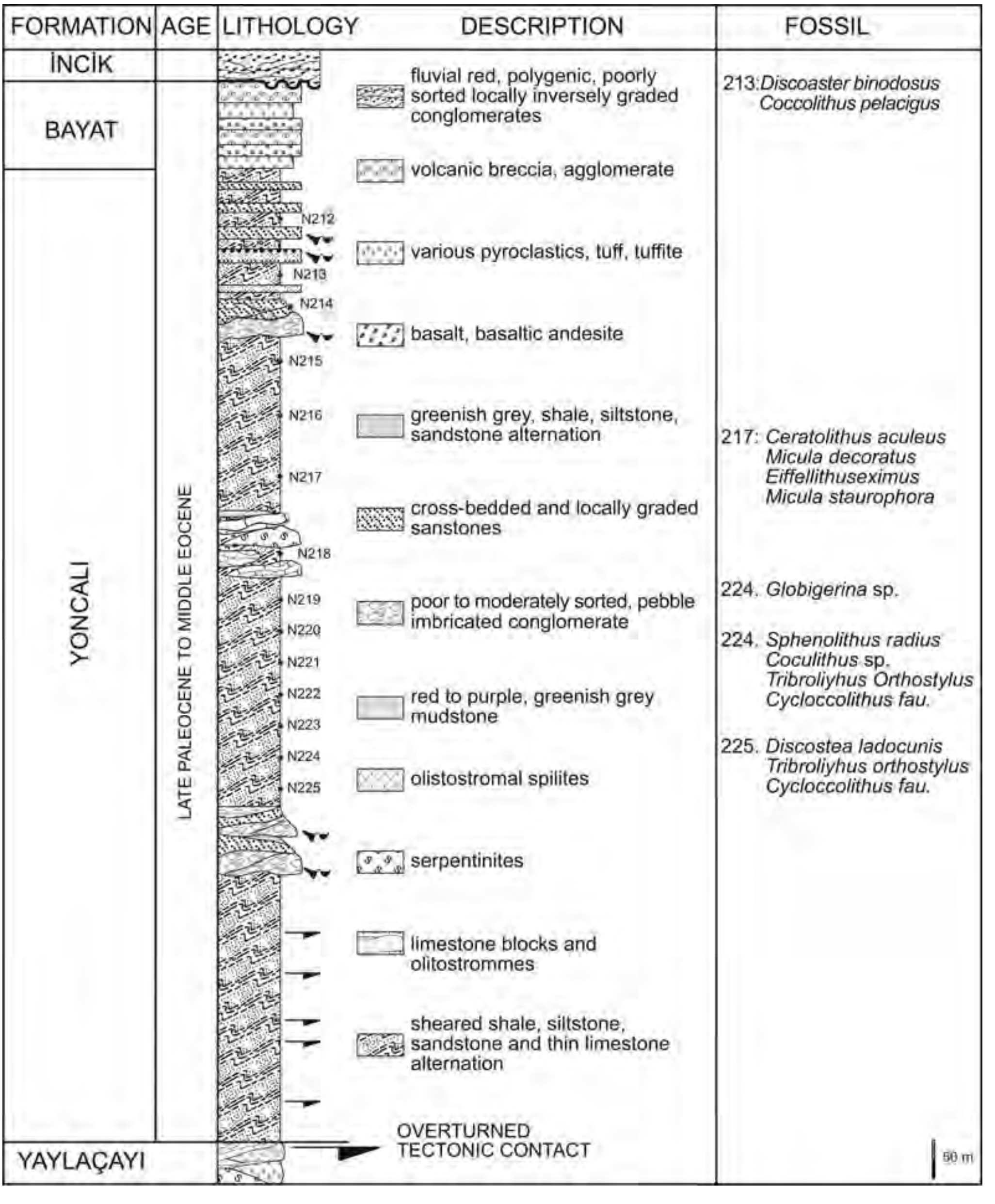

Fig. 13. Measured stratigraphic section for parts of the Yoncalı and the Bayat formations (its location is indicated with 13 in Fig. 2).

In the northeastern part of the Çankırı Basin, the Bayat Formation starts with medium bedded, poligenic conglomerates at the bottom and continues upward with an alternation of green, greenish grey tuffaceous sandstone and marl intercalated with tuff and agglomerates. The age of the Bayat Formation is early to middle Eocene as indicated by its fossil content (Figs 14 & 17).

Osmankahya Formation (To, lower to middle Eocene). The Osmankahya Formation was first named by Birgili *et al.* (1974). It is characterized mainly by continental red clastics. Together with the Kocaçay Formation, it locally covers both the basin in-fill and the basement (Fig. 14).

Lithologically, the Osmankahya Formation is composed of conglomerate, sandstone and mudstone

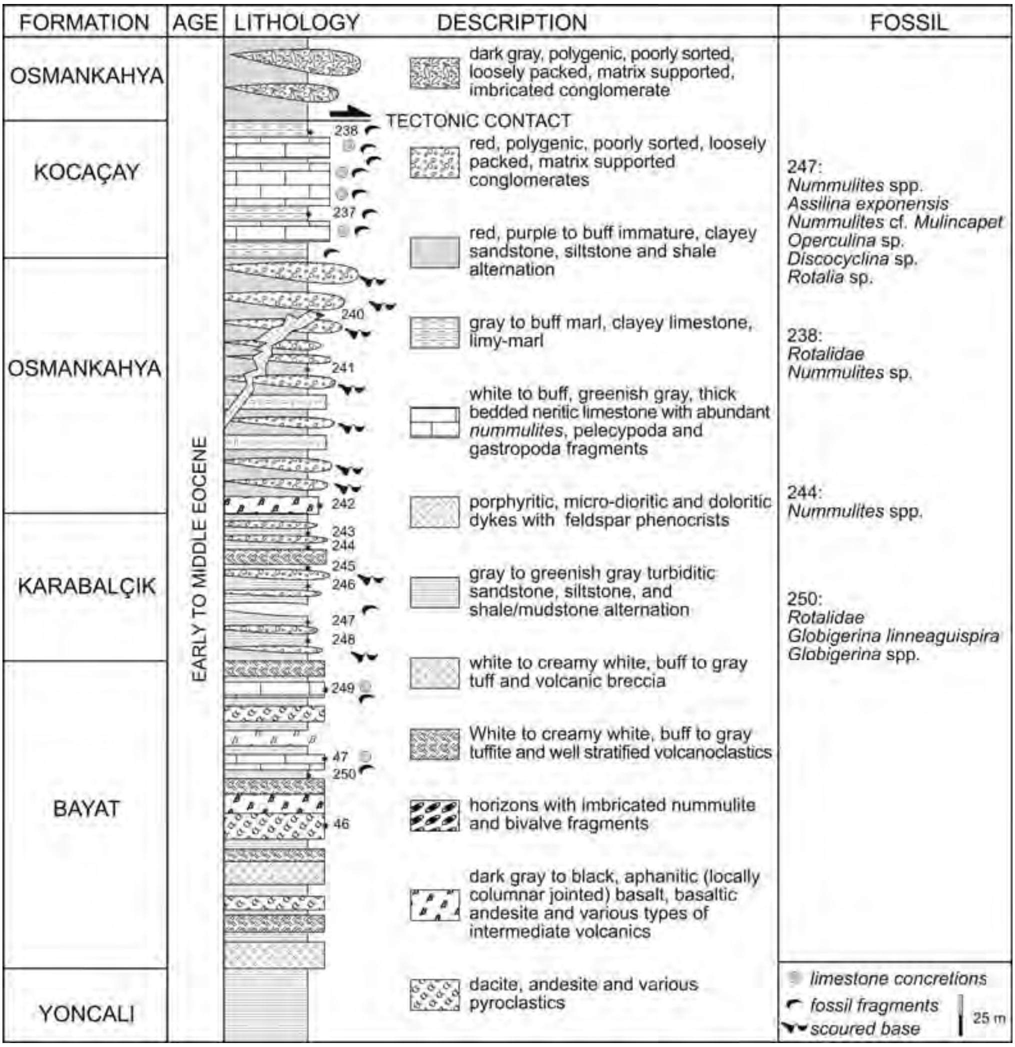

Fig. 14. Measured stratigraphical section for parts of the Bayat, Yoncalı, Karabalçık, and Kocaçay formations. Note that the Bayat Formation underlies the Yoncalı Formation that is generally higher in the stratigraphical position then the Yoncalı and Karabalçık formations (its location is indicated with 14 in Fig. 2).

alternations. In the northern part of the basin, it is characterized by very thick polygenic conglomerates, cross-bedded sandstones and red mudstones intercalated with thin tuffaceous beds. The pebbles of the conglomerates are locally imbricated and sandstones are characterized in some levels by ripple laminations (climbing and symmetrical ripples in places), trough and planar cross bedding and locally by epsilon cross-bedding indicating river channels. The cross-bedded conglomerates may reach up to 20 m in thickness. In the northern part of the basin, west of İskilip (Fig. 2), cross-beds, pebble imbrications and very large-scale cross-bedding indicate an approximate NW to SE transport direction. In the northeastern part of the basin, the Osmankahya Formation includes interfingering of sandstones containing possibly intraformationally reworked and imbricated nummulite fossils.

In the southwestern part of the study area, the Osmankahya Formation laterally grades into the Karagüney and Mahmatlar formations and is characterized by an approximately 100 m thick alternation of red and greenish grey sandy mudstones, sandstones and lens-shaped conglomerate bodies. At the top, the unit is characterized by an

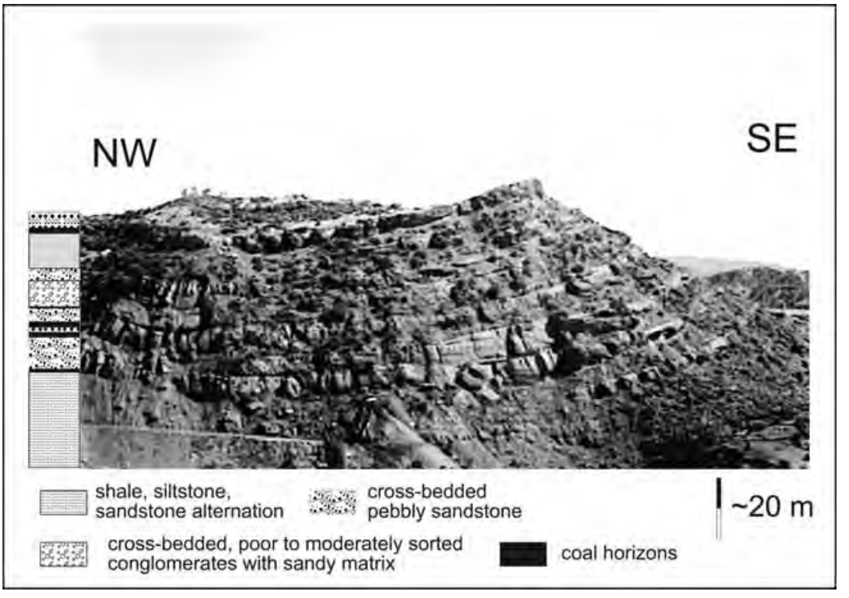

Fig. 15. Photograph of the upper coal bearing parts of the Karabalçik Formation in the northern part of the Çankırı Basin (location is around N:40°43′21″, E:34°08′50.5″, view to NE).

approximately 10 m thick purple to brick-red mudstone that grades into the Kocaçay Formation.

In the central parts of the basin, the Osmankahya Formation always forms an interlayer between underlying Kırşehir Block units and overlying Kocaçay Formation. Osmankahya and Kocaçay formation laterally grade into the Karagüney and Mahmatlar formations where Osmankahya Formation is characterized by red to brick-red mudstones and sandstones (Fig. 18).

The age of the unit, based on its stratigraphical position and pollen analysis, is early to middle Eocene (Ünalan 1982; Yoldaş 1982; Dellaloğlu *et al.* 1992).

Kocaçay Formation (Tko, lower to middle Eocene). This unit was first named by Birgili *et al.* (1974). It is characterized by a few metres to 100 m thick nummulitic and macrofossil dominated fossiliferous limestone and locally conglomeratic limestone with intraformationally reworked nummulites. It is one of the key horizons of the basin as it covers both the basin sequences and the basement. It is a condensed sequence and is the youngest marine deposit in the Çankırı Basin.

The Kocaçay Formation is divided into three distinct lithological levels (Figs 17 & 18). In the northern part of the basin it is composed of brown to dark green, medium bedded, medium to fine-grained tuffaceous sandstone and shale alternation and marl intercalation at the bottom. At the top it is composed of thick-bedded nummulitic limestone (Fig. 17) with thin bedded marl intercalations (Fig. 18). In southeastern part of the study area, it grades into an evaporitic horizon belonging to the Incik Formation. In the southwestern part of the basin, the Kocaçay Formation is exposed in a narrow north-south oriented belt, where it is characterized by nummulites, gastropods and pelecypoda, laterally grading into conglomeratic, nodular limestone levels.

The age of the unit is middle Eocene as indicated by its fossil content (Figs 14 & 16–18).

Kalınpelit Group

The Kalınpelit group comprises the post-middle Eocene to Oligocene Incik, Güvendik and Kılçak formations.

Incik Formation (Ti, middle Eocene to Oligocene). The Incik Formation was first named by Aziz (1975). It is characterized by continental red clastics and it is the most widespread and voluminous units in the basin with thickness of more than 2000 m. In general it conformably overlies the Kocaçay Formation except for local internal unconformable relationships observed in the northern and southwestern part of the basin. Local, internal angular unconformities are also observed within the unit and they are interpreted as syntectonic (progressive) unconformities indicative of syntectonic deposition and synsedimentary deformation of the unit.

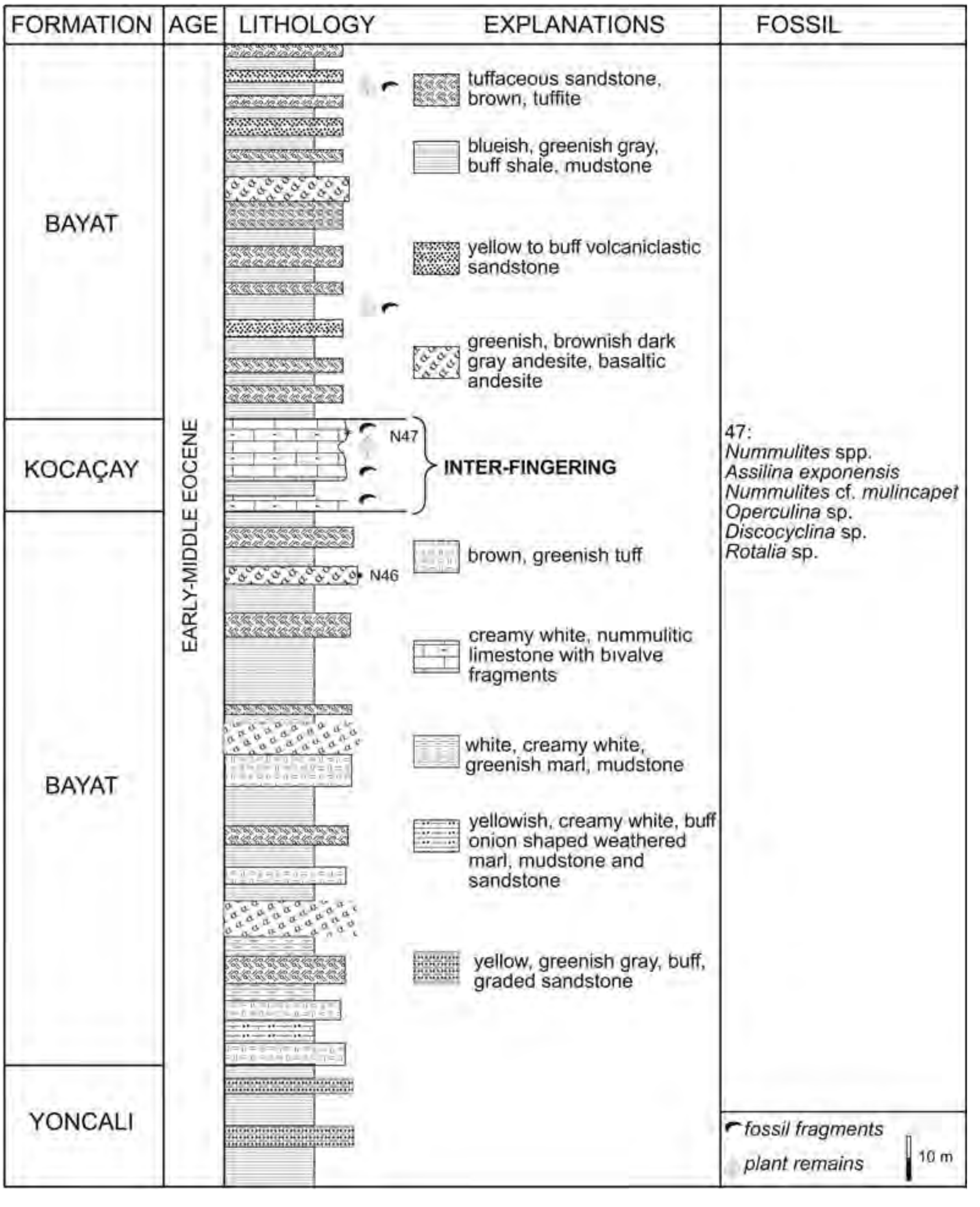

Fig. 16. Measured stratigraphical section for parts of the Bayat and Kocaçay Formations. Note the inter-tonguing of the Kocaçay Formation (its location is indicated with 16 in Fig. 2).

In the northern areas of the basin, the Incik Formation is monotonous with the alternation of very thick-bedded (*c.* 2 m) red conglomerates alternating with very thick-bedded, poorly sorted, immature red sandstones and purple to brick-red, thick- to very thick-bedded mudstones (Fig. 18). The conglomerates and sandstones display lens-shaped patterns which, from north to south, laterally become thinner and finer and finally pinch-out. From north to south, a number of internal angular unconformities coinciding with a number of coarsening upwards sequences are observed in the

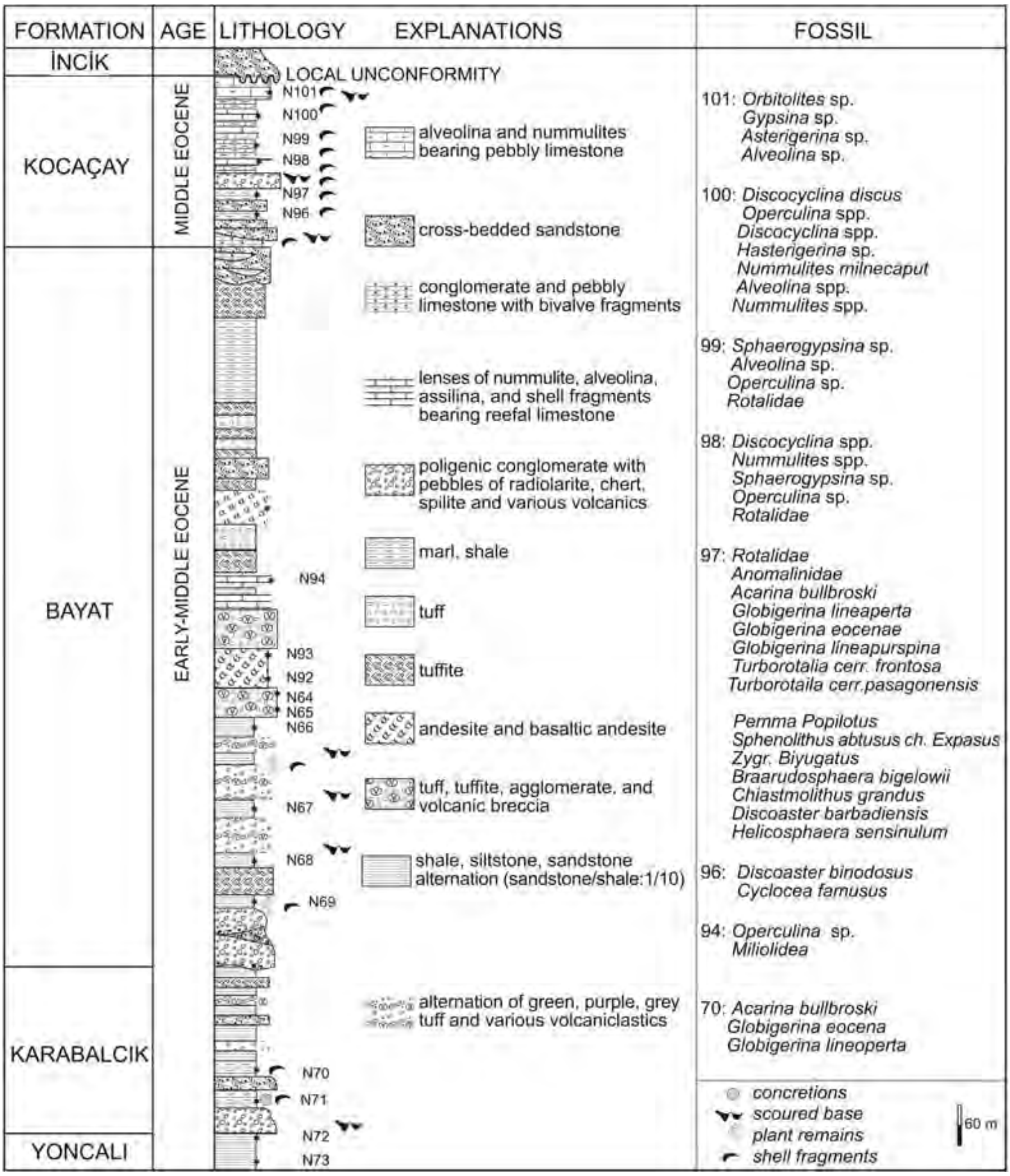

Fig. 17. Measured stratigraphic section for parts of the Karabalçık, Bayat and the Kocaçay Formations (its location is indicated with 17 in Fig. 2).

northern part of the basin. The angular discrepancy between the underlying and overlying sequences of the Incik Formation decreases from north to south. The pebbles are derived mainly from the NAOM and Yaylaçayı Formation, including serpentinites, ultramafics, radiolarites and various volcanic rocks.

In the SW of the basin, the Incik Formation has similar characteristics to its northern counterparts. The grain size, the dips of the bedding, bed thickness and the overall thickness of the unit decrease from west to east and the formation onlap onto the Kırşehir Block (Fig. 19).

It the east, at the bottom it is characterized by yellow to brick-red thinly bedded gypsum, which laterally and vertically grades into green shale and is the oldest gypsum observed in the field. The color of the shale gradually changes from green to red and finally into purple. It is approximately

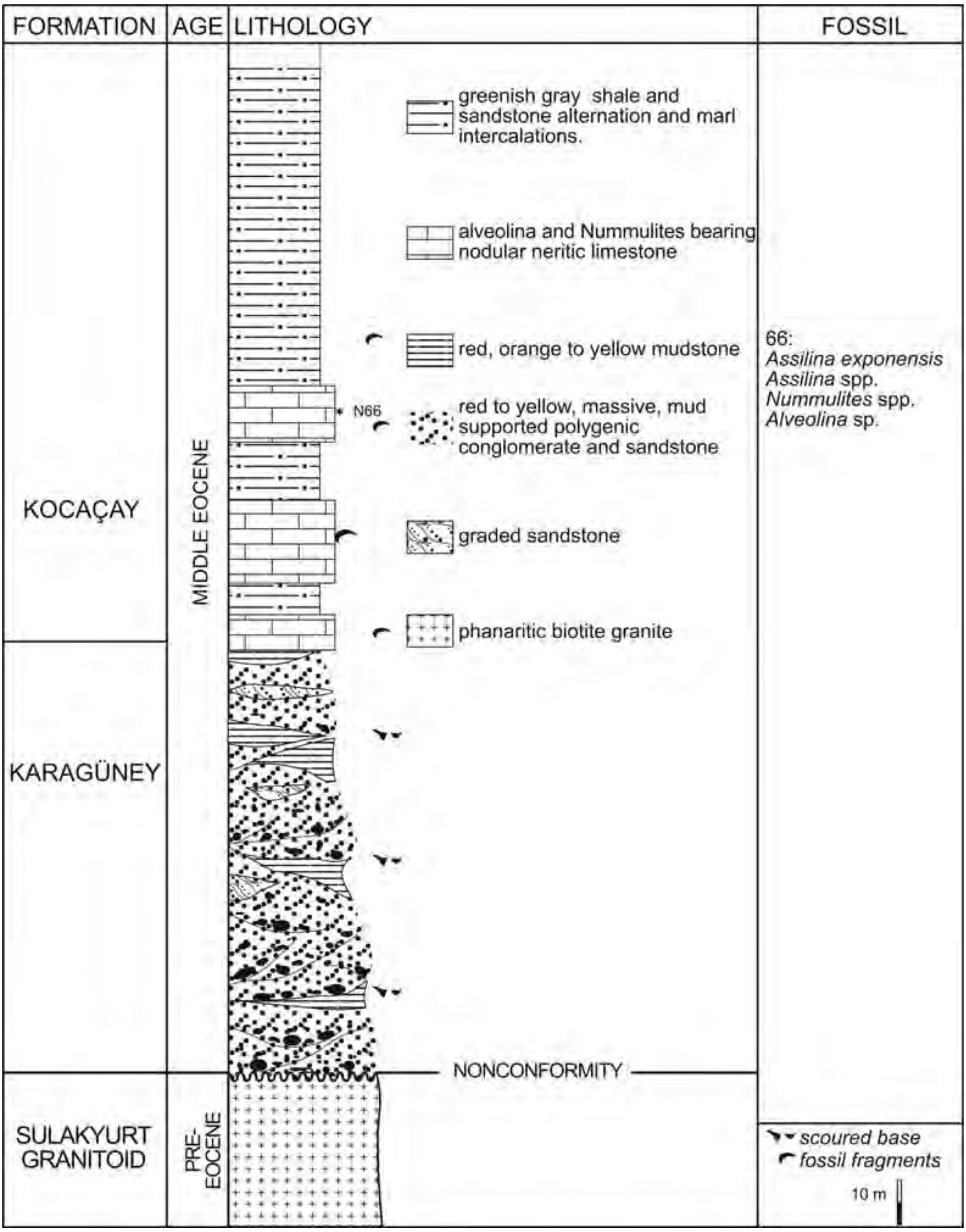

Fig. 18. Measured stratigraphic section for parts of the Osmankahya and the Kocaçay Formations. (its location is indicated with 18 in Fig. 2).

50 m thick. The sequence is followed upwards by thin to medium bedded (10–50 cm), brick-red to purple, ripple laminated, tabular cross-bedded sandstones alternating with red to purple, siltstone and silty-mudstones. Higher up in the section, the sequence is characterized by an alternation of brick-red to purple sandstones, siltstones, shale and greenish grey to bluish grey shale and very thick-bedded (1–2 m) red to orange gypsum horizons. The sequence gradually becomes coarser

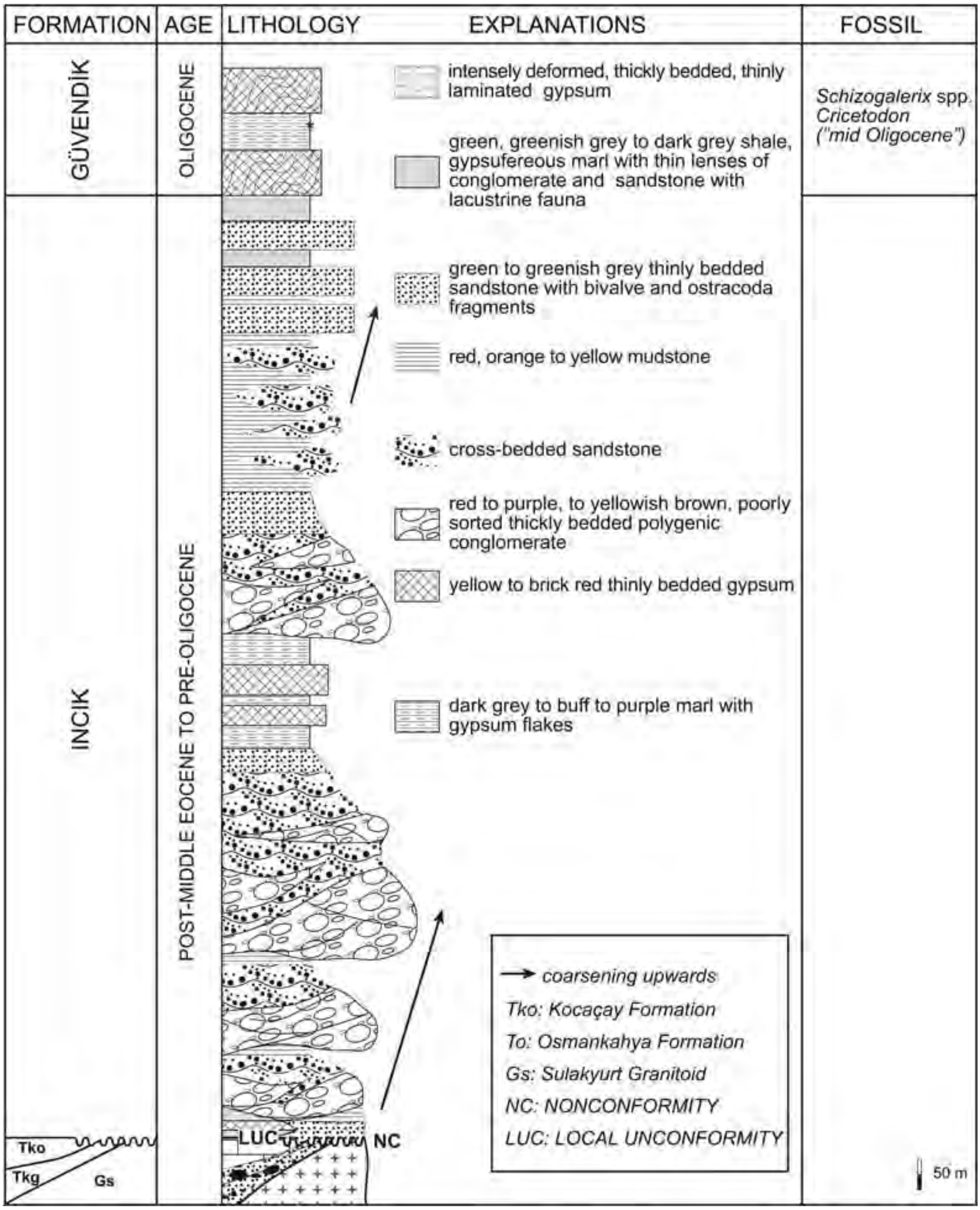

Fig. 19. Generalized stratigraphic section for parts of the İncik and Güvendik formations (İncik formation is partly modified after Dellaloğlu *et al.* 1992).

grained and thicker bedded. In the upper parts, the unit is characterized by approximately 500 m of monotonously alternating thick- to very thick-bedded polygenic conglomerates, and red sandy to silty shales. The overall sequence coarsens upwards and only in the top most 100 m of the unit displays a fining upward sequence. As in the other parts of the basin, internal angular unconformities are frequently encountered in the eastern part of the basin.

In the Sağpazar-1 well (Fig. 2), the Incik and Kocaçay formations interfinger and the Incik Formation is characterized by a very thick sequence of $>$2000 m of evaporites, conglomerates, sandstones and shale alternations. The evaporites include gypsum, anhydrite and rock-salt which are being mined around the town of Çankırı and 20 km SW of Sungurlu.

The age of the Incik Formation is not known precisely, because of a lack of fossils. Based on its relation with the underlying lower to middle Eocene Kocaçay Formation and the Oligocene Güvendik Formation, the age of the formation is middle Eocene to Oligocene.

Güvendik Formation (Tg, Oligocene). The Güvendik Formation was named for the first time by Kaymakcı *et al.* (2001*a*). Although, the Güvendik formation is intensely deformed, three distinct levels can still be recognized (Fig. 19). At the bottom and the top, it is composed of very thick-bedded, finely laminated and intensely deformed gypsum alternating with thin to medium bedded buff to creamy white gypsifereous marls. In the middle, it is composed of greenish grey shales frequently scoured by lenses of micro-conglomerates. In the eastern part of the Çankırı Basin (Fig. 2) the shales include very thin organic horizons with fresh water gastropoda and pelecypoda fragments. In the samples collected from the Güvendik and Gözükızıllı sites (19 in Fig. 2) *Eucricetodon* sp. (only incisors), *Ctenodactylidae*; and *Tataronyinen n.gen.* n.sp. rodent fossils were encountered. Based on these rodents, an Oligocene age is assigned to the Güvendik Formation (Fig. 19).

Kılçak Formation. The Kılçak Formation is the youngest unit related to foreland basin evolution of the Çankırı Basin. It is exposed only in the western margin of the Çankırı Basin. It unconformably overlies all of the older units of the Çankırı Basin and it is tectonically overlain by the NAOM along one of the western boundary-thrust faults of the basin. It is composed of fluvio-lacustrine conglomerate, sandstone, shale and organic rich horizons. According to De Bruijn & Saraç (1992); De Bruijn *et al.* (1992); De Bruijn & Koenigswald (1994); and Ünay (1994) it is of Aquitanian age based on micro-mammals (see Kaymakcı *et al.* 2001*a*, for full account of the unit).

South derived units

Sivritepe group. Outcrops of the south derived units in the southwestern part of the basin contain detritus that was shed mainly from the Kırşehir Block (i.e. Sulakyurt granitoid and the ophiolitic units intruded by the Sulakyurt granitoid) and are interfingering with the North Derived units around NW of Kırıkkale. Their importance is because they record the age of exhumation of Sulakyurt granitoid. The Sivritepe Group comprises the upper Paleocene to middle Eocene Karagüney and Mahmatlar formations.

Karagüney (Tkg) and Mahmatlar Formations (Tma) (upper Paleocene to middle Eocene). The Karagüney and Mahmatlar formations (Fig. 20) are exposed only in the southwestern part of the Çankırı Basin. The stratigraphic position of these two formations is very different from any other unit of the basin sequence of the Çankırı Basin because they are the oldest units which are resting directly on the Kırşehir Block (Figs 2 & 21), and include detritus derived mainly from the Sulakyurt granitoid and the intruded ophiolites. The Karagüney and Mahmatlar formations were first named and described by Norman (1972).

The Karagüney formation (Fig. 20) is composed of reddish conglomerates characterized by sub-angular blocks and boulders derived from ophiolites in a fining upwards sequence. The granitic clasts are observed only in the upper parts of the unit and they reach up to 50 cm in diameter. The boundary relations of the Karagüney Formation with other units are indicated in Figure 4. The thickness of the unit is about 100 m.

The Mahmatlar Formation (Fig. 20) is characterized mainly by detritus derived from the granitoids. It includes sub angular to ellipsoidal granite and ophiolite related boulders and blocks at the bottom. The grain size rapidly decreases and the matrix becomes more limey and nummulite fossils become dominant from bottom to top and from north to south. In the upper parts of the formation, arkosic sandstones dominate. The thickness of the unit is variable and reaches a maximum of about 200 m.

The sub-angular blocks and boulders indicate that they were not transported over long distances and were more likely derived from the underlying nearby ophiolitic units that are associated with the Kırşehir Block, rather than the ophiolites at the rim of the basin. The presence of mainly ophiolite pebbles in the Karagüney Formation and granitic pebbles in the overlying Mahmatlar Formation indicate an inverse stratigraphical relationship during the erosion and transportation processes; such that, first the ophiolitic cover was eroded away, followed by the underlying granitoids (i.e. progressive unroofing) (Fig. 21b).

In the study area, no fossils have been recovered from the Karagüney and Mahmatlar formations within the studied portion of the Çankırı Basin, although very wide spread *Nummulites* sp. and *Assilina* sp. fossils were encountered south of Kırıkkale (Fig. 2). In addition, these two units laterally grade into the upper Paleocene to middle Eocene İskilip Group (Fig. 21a) which allows correlation between the two areas. Based on this relationship, the Karagüney and Mahmatlar formations are interpreted to have been deposited in the late Paleocene to middle Eocene.

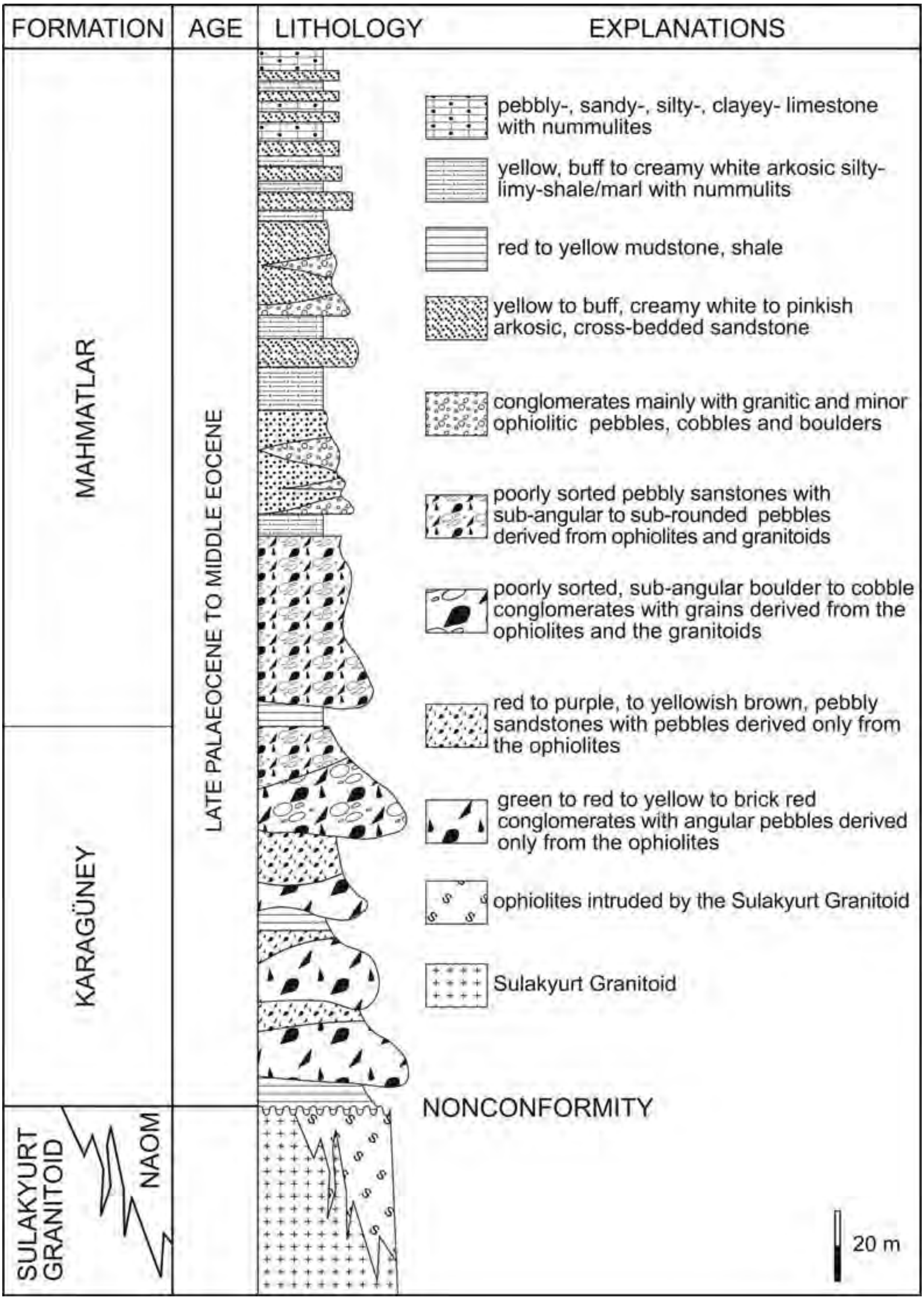

Fig. 20. Generalized stratigraphical section for parts of the Karagüney and Mahmatlar Formations (modified after Norman 1972).

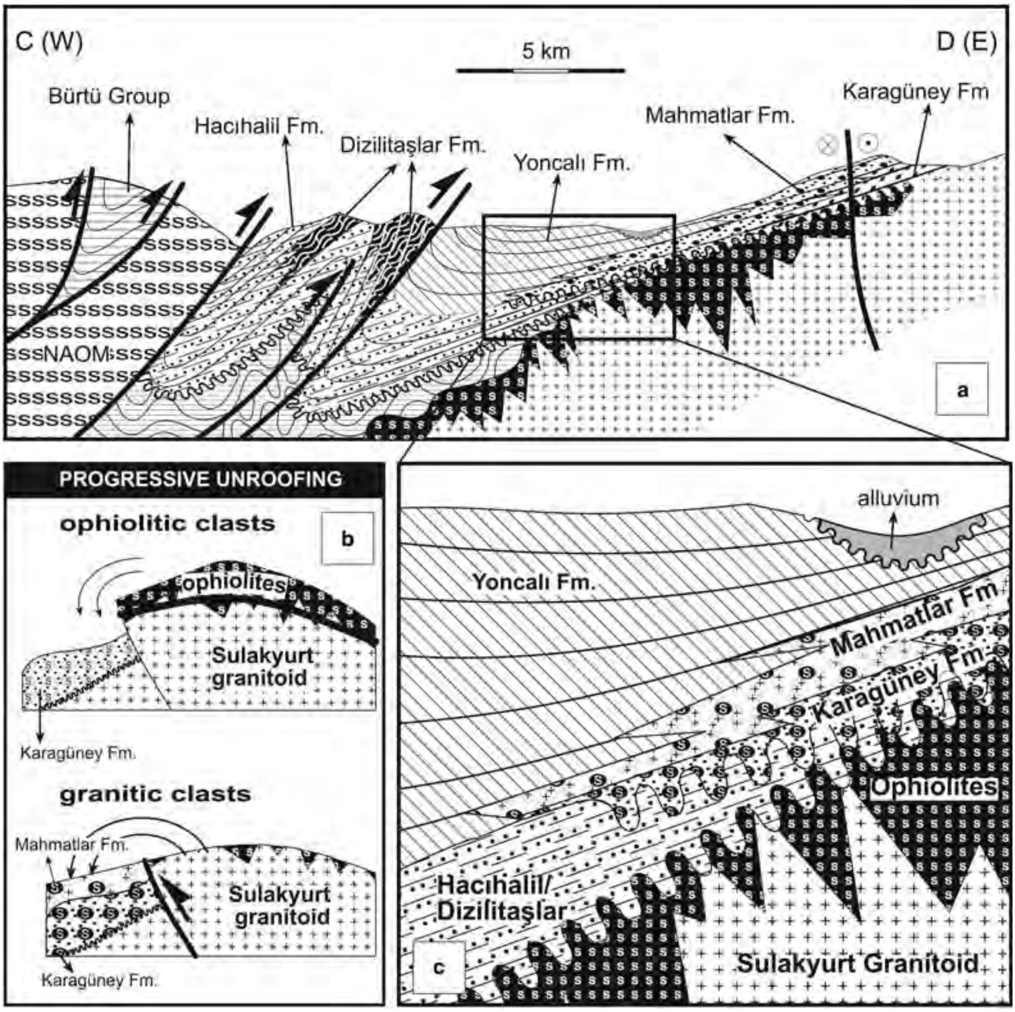

Fig. 21. (**a**) Sketch cross-section along the line C–D (in Fig. 2). (**b**) Conceptual cross-sections illustrating the progressive un-roofing of the granites of the Kırşehir Block and its reflection in the Karagüney and Mahmatlar Formations. (**c**) Blow-up figure depicting the relation between some of the north derived units (Hacıhalil, Dizlitaşlar and Yoncalı formations) and the south derived units (Karagüney and Mahmatlar formations).

Discussion

Temporal relationships

A correlation chart for pre-middle Miocene of the Çankırı Basin is presented in Figure 22. Due to repeated tectonic activity, which is characterized by two distinct thrusting events in the late Cretaceous to early Miocene and later by extensional (middle Miocene) and, finally, by regional transcurrent tectonics (late Miocene to recent) (see Kaymakcı *et al.* 2000, 2001*b*, 2003*a*), the boundary relationships and lateral continuity between individual formations are partly obliterated. The most noticeable boundary relationships observed, in relation to the evolution of the Çankırı Basin, are the syntectonic unconformities between different formations and frequently within the same formation (e.g. Incik Formation). The types of unconformities encountered in the field are depicted in Figure 23 and are reflecting tectonic activity during deposition.

The oldest syntectonic unconformities are observed between the Yaylaçayı (Ky) and the Malıboğazı formations (Km; indicated by 1 in Fig. 22) and between the Yapraklı and Kavak formations (indicated by 2 in Fig. 22) in the northwestern part of the Çankırı Basin. This unconformable

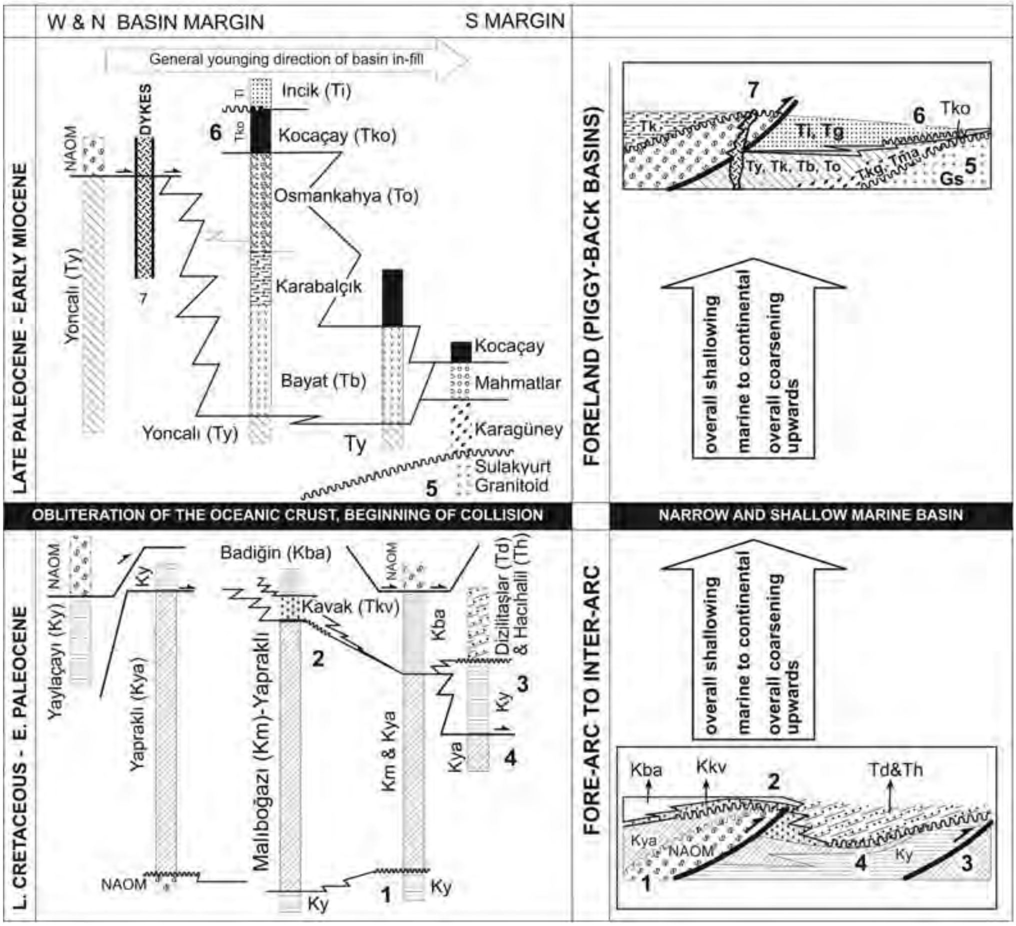

Fig. 22. Correlation chart for pre-middle Miocene formations of the Çakırı Basin (see text for discussion).

boundary in turn is angular unconformably overlain by the Incik Formation (Fig. 23a). The Kavak Formation unconformably overlies the thrust contact between Yapraklı and Yaylaçayı formations (indicated by 3 in Fig. 22) and Yaylaçayı and Yapraklı formations are unconformably overlain by the Hacıhalil and Dizlitaşlar Formations (indicated by 4 in Fig. 22). These relationships are interpreted as the indication of syn-depositional thrusting during the deposition of the Yapraklı and Kavak formations in which general tectonic transport direction occurred from NW to SE (in present day orientations) (Figs 2 & 22).

The same relations are also observed in the upper Paleocene to lower Miocene units. The oldest unconformity is observed between the Sulakyurt granitoid and the upper Paleocene–middle Eocene units in the southwestern part of the basin (5 in Fig. 22). A very well developed syntectonic unconformity is also observed within the Incik Formation itself and between Incik and the formations of the İskilip Group (6 in Figs 22 & 23b & c). These relationships are indicative of differential uplift due to tectonic activity and contemporaneous sedimentation during the late Paleocene to middle early Miocene. Having syntectonic unconformities within the İskilip and Kalınpelit Groups near the rim of the Çankırı Basin and onlap of these units onto the basement indicate progressive migration of the depocenter southwards onto the Kırşehir Block from the late Paleocene onwards.

The most evident boundary relationship with respect to timing of thrusting is observed in the northeastern corner outside of the study area (11c in Fig. 22). There, a number of North–NWto South–SWoriented feeder dykes for the volcanic rocks of the Bayat Formation cut the thrust contact between the underlying Yoncalı Formation and the overlying NAOM (Fig. 11c). This indicates that thrusting occurred before and/or during the deposition of the Bayat Formation in the early to middle Eocene.

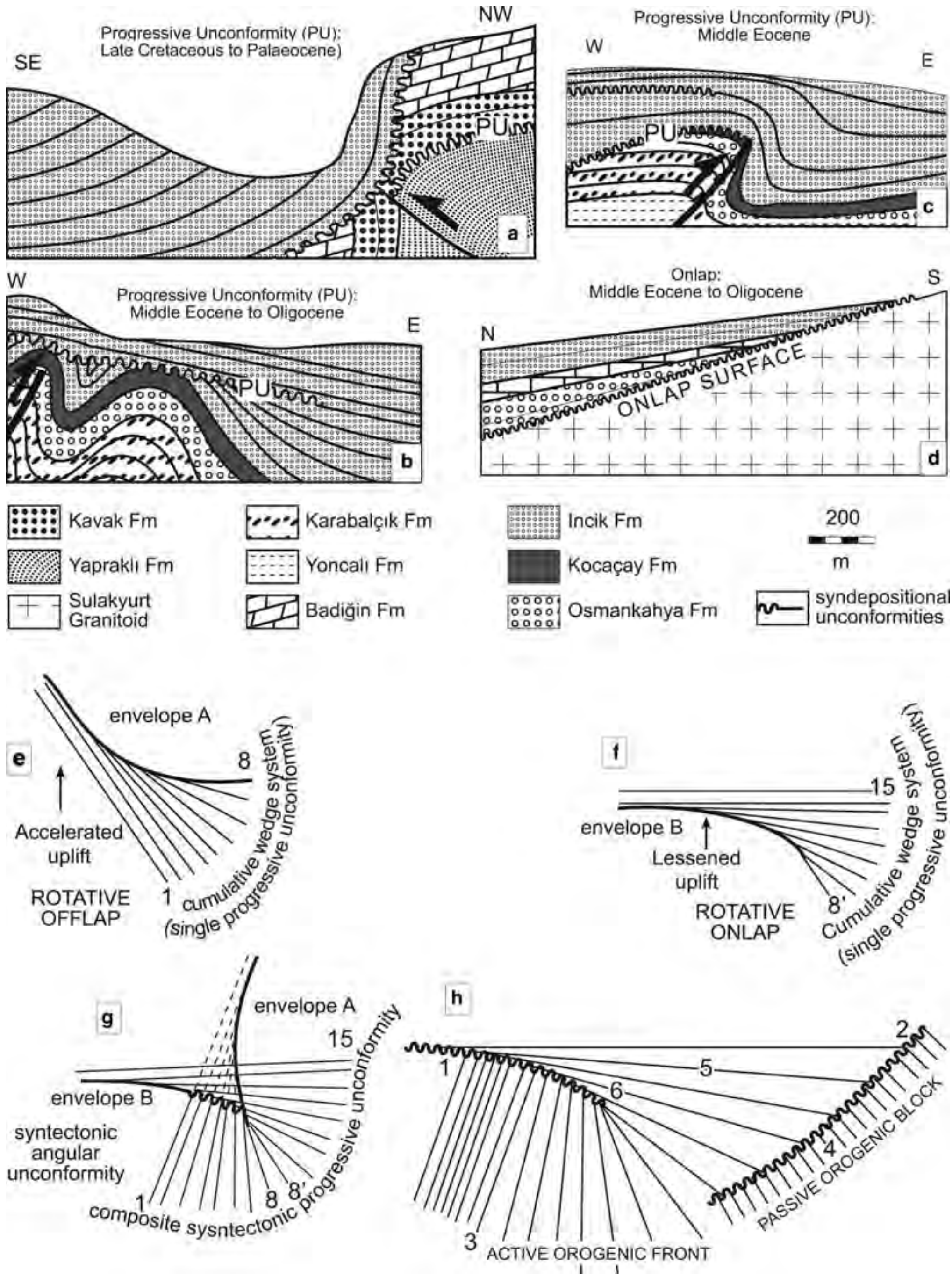

Fig. 23. (**a**–**d**) Sketch cross-sections illustrating the various types of syntectonic unconformities observed during the field studies. (**e**–**h**) Conceptual development of syntectonic unconformities in areas where deformation and deposition are coupled. The numbers 1–15 are the time lines (adopted from Riba 1976).

Although, it is tectonically disturbed by thrust faults, the contacts between the upper Cretaceous and upper Paleocene to Eocene units is locally unconformable, not only in the Çankırı Basin but also further SW outside of it (Norman 1972; Görür *et al.* 1984). This relationship is very important regarding the tectonic evolution of the basin. It infers that the tectonism and accompanying sedimentation was continuous from the late Cretaceous to Eocene. However, the southwestern reworked upper Cretaceous to Paleocene fauna in the Yoncalı and Karabalçık formations in the southwestern part of the basin implies that the boundary between the upper Cretaceous to Paleocene formations and the upper Paleocene to middle Eocene formations must at least be a local unconformity as depicted in Figures 21–23. This relationship implies two possibilities. The first one was that there is no major change in the style of tectonics but the local unconformable relationship between the upper Cretaceous and upper Paleocene to Eocene units is a syntectonic unconformity and, consequently, thrusting and sedimentation were coeval but the unconformably relationship is enhanced due to local uplifts related to ongoing thrusting. The second possibility is that the local unconformable relationship between the upper Cretaceous to lower Cenozoic units indicates a major and complete change in the style of tectonic activity. The second option seems to be the more likely considering: (1) the major change in the palaeostress configurations (radial compression) (Kaymakcı *et al.* 2000, 2003*a*); (2) Palaeomagnetic constraints (oroclinal bending during the early Cenozoic, Kaymakcı *et al.* 2003*b*); (3) and the regional tectonic scheme as evidenced by widespread un-roofing of granitoids and exhumation of metamorphic rocks in the Kırşehir Block (Erler & Bayhan 1995; Whitney *et al.* 2001; Boztuğ & Jonckheere 2007; Boztuğ *et al.* 2007); (4) the youngest age obtained from the ophiolitic mélange as being late Maastrichtian which implies an end of ophiolitic mélange formation; and (5) termination of arc volcanism in the Maastrichtian (Tüyüz *et al.* 1995; Sunal & Tüysüz 2002; Rice *et al.* 2006). Based on these relationships, it is concluded that lower Paleocene marks the end of subduction, obliteration and complete subduction of the Neotethyan oceanic crust and collision of the Kırşehir Block and the Sakarya Continent. Therefore, collision of the Kırşehir Block and the Sakarya Continent took place at the end of late Cretaceous.

Depositional environments and lateral gradations

The Yaylaçayı Formation is locally incorporated into the NAOM, which indicates that deposition of the Yaylaçayı Formation and generation of mélange (NAOM) were contemporaneous. The Yaylaçayı Formation was deposited within forearc to interarc environments and includes volcanic rocks and volcanoclastic rocks derived from the arc and seamount setting (Tüysüz *et al.* 1995; Rojay *et al.* 2001, 2004; Rice *et al.* 2006). The Yapraklı Formation is time equivalent of the Yaylaçayı Formation deposited in shallower and proximal depositional settings (for alternative explanation, see Rice *et al.* 2006). Lateral gradation of the Malıboğazı Formation with the Yapraklı Formation and the presence of rudist fossils indicate that the Malıboğazı Formation was deposited in areas where the water depth was shallow enough for rudists and other benthic fauna to survive and which indicates gradual shallowing of depositional environments due to differential uplift. The rudist bearing units, in the Ankara region, were deposited at the crest of an accretionary wedge (Rojay & Süzen 1997), which was locally and intraformationally deposited uplifted and eroded to supply detritus, together with the NAOM, to the other proximal units including the Kavak and Badiğin formations.

The Kavak and Badiğin formations laterally grade and overlie the Yapraklı Formation with a local unconformity. They were deposited in a transitional continental to marine (mixed) environment in which the proximal facies are categorized as Kavak and distal facies are categorized as Badiğin formation (Fig. 22). The presence of sub-angular blocks and boulders derived from the NAOM and from the other upper Cretaceous units indicate that the Kavak formation was deposited close to its source whence the NAOM, Yaylaçayı and Yapraklı formations must have been exposed and eroded locally. A local unconformable relationship between the Kavak and Yapraklı formations indicates ongoing sedimentation and tectonic activity that resulted in contemporaneous local uplift due to thrusting. A similar relationship is also observed between the Yapraklı and Hacıhalil formations (Figs 5 & 22). These observations indicate that thrusting occurred along with thrust-related sedimentation during the Paleocene. The presence of plant remains and dominance of terrigeneous material in the Yapraklı Formation and in the other Paleocene units, the dominance of continental settings in many areas of Turkey (Gökten 1983; Görür *et al.* 1984, 1998; Okay *et al.* 1996; Gürer & Aldanmaz 2002) indicates that the depositional environments were bordered by land masses and marine areas were restricted.

The İskilip Group comprises mainly marine formations and has lateral gradations with each other. Among these, the lower part of the Hacıhalil Formation is deposited in a continental setting and gradually becomes marine as it grades into the Yoncalı Formation. The Yoncalı Formation represents the more basinal facies of the group and is characterized by a turbiditic sequence and deeper marine shales and clays. The Karabalçık Formation is represented by conglomerates with local coarsening upwards sequences. The Osmankahya Formation overlies the Karabalçık Formation and was deposited mainly in continental settings interfingering with marine settings. The Kocaçay Formation covers all of these units and is characterized by a condensed sequence of nummulitic limestones. The Bayat Formation is represented mainly by volcanic and volcanogenic units embedded within the İskilip Group (upper Paleocene to middle Eocene). The Incik Formation is characterized mainly by continental deposits that laterally grades and overlies all the other formations of the İskilip Group. It also includes local unconformities developed progressively during the activity along the thrust faults and is associated with coarsening upwards sequences. The Güvendik formation was deposited within lacustrine settings as evidenced by the presence of lacustrine fauna. The Kılçak Formatin is deposited in fluvio-lacustrine settings.

The organization of facies and structures indicate presence of thrust regime in the early Cenozoic. These include mezoscopic syn-sedimentary thrust faults (Kaymakcı *et al*. 2000, 2003*a*), wedge-like infill patterns which contain progressive syntectonic unconformities, facies and major thrust faults become younger from the basin rim towards the centre, and southwards migrated depocenters.

Based on the information discussed above, in association with seismic data (see Kaymakcı 2000), the depositional environments of the lower Cenozoic in-fill of the Çankırı Basin has been reconstructed (Fig. 24). It has already been discussed that the palaeocurrent directions in the Hacıhalil sector of the Çankırı Basin indicates mainly southeastward, with minor northward, sediment transport directions, which indicate that the basin rim was exposed locally in the northeastern part of the Çankırı Basin (11c in Fig. 2) during the deposition of the Hacıhalil Formation. The local unconformities, southward transport of the thrusts, which was accompanied by deposition both in the front and the rear of the thrust faults, indicates that the Çankırı Basin evolved within a thrust regime with associated piggy-back basins (terminology after Ori & Friend 1984), in the late Paleocene to early Miocene (Fig. 24).

Evolutionary scenarios of the Çankırı Basin

As discussed previously tectonically there are two distinct episodes in the evolution of the region. The first one took place in the Late Cretaceous to Paleocene interval and related to the subduction of the Neotethys oceanic crust, whilst the second one belongs to collision and post-collisional convergence period in the late Paleocene to early Miocene.

Late Cretaceous to middle Paleocene

Northward subduction of the Neotethys oceanic crust below the Pontides commenced earlier than Cenomanian (Saner 1980; Şengör & Yılmaz 1981; Okay 1984; Dellaloğlu *et al.* 1992; Okay *et al.* 1994, 1996, 2001; Tüysüz *et al.* 1995; Kaymakcı 2000; Robertson 2002; Clark & Robertson 2005; Rice *et al.* 2006), possibly in the early Cretaceous regarding the opening of the Western Black Sea as a backarc basin (Görür 1988, 1997; Okay *et al.* 1994, 2006; Robinson *et al.* 1997; Tüysüz 1999; Tüysüz & Tekin 2007). The subduction occurred along two trenches (Fig 25a–c). The southern one is an intra-oceanic subduction zone associated with an ensimatic arc (Fig 25a & b). During the Turonian, obduction of the N-Morb ophiolitic crust commenced during which supra-subduction zone ophiolites begin to form (Yalınız *et al.* 2000) while the ensimatic arc split and rifted away (Fig. 25c). Supra-subduction zone ophiolite generation is thought to be the consequence of decrease in convergence rates of Taurides (including the Kırşehir Block) and the Pontides (including the Sakarya Continent) and possibly slab roll-back. These processes may also account for the backarc extension and opening of the western Black Sea Basin. During the end of the Santonian (83.5 Ma), a new northwards subduction started (Fig. 25d) in the north along which the supra-subduction zone ophiolitic crust was consumed and later obducted on to the Kırşehir Block (Fig. 25 d & e) (Yalınız *et al.* 1996). This new subduction event might have given way to formation of an ensialic arc development (Yemişliçay Formation of Tüysüz *et al.* 1995, and Tüysüz 1999) and formation of a forearc basin south of it (Rice *et al.* 2006), in which the Yaylaçayı and Yapraklı formations were deposited. The Yapraklı Formation represents the proximal facies of the forearc basin as implied by neritic carbonates and terrigeneous clastics, while the Yaylaçayı Formation represents more basinal facies (Figs 25a–c).

In the Campanian, the supra-subduction zone ophiolites obducted onto the Kırşehir Block and gave rise to the thickening and main metamorphism in the Kırşehir Block crust during which oldest granitoids in the Kırşehir Block intruded (Akìman *et al.* 1995; İlbeyli *et al.* 2004; Boztuğ *et al.* 2007), while in the north, around the Çankırı Basin and its western (towards the Tuzgölü Basin) and eastern extensions (towards the Sivas Basin) the basin narrowed and deep sea conditions were progressively replaced by shallower conditions along the

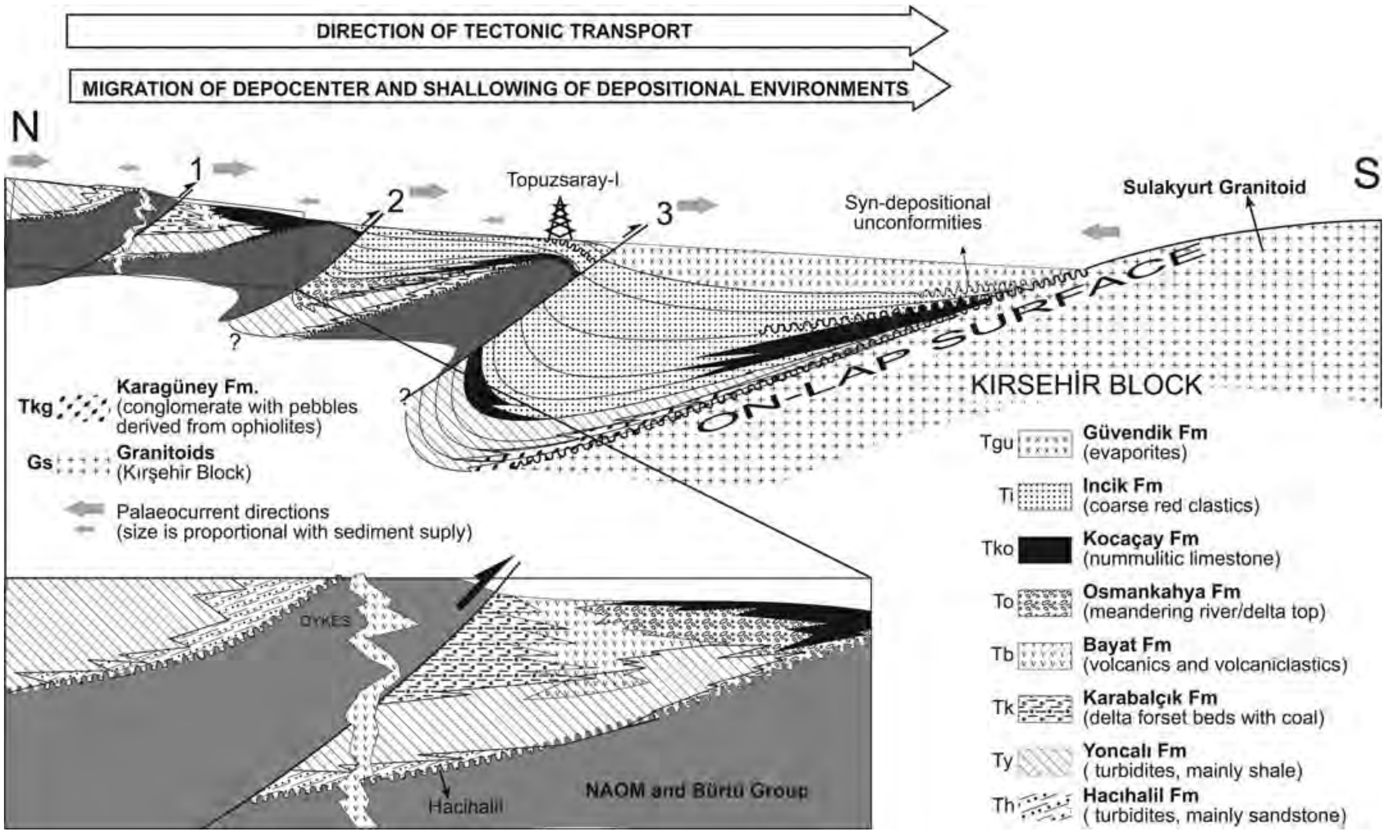

Fig. 24. A conceptual cross-section illustrating early to middle Eocene to early Miocene coupling between thrusting and coeval deposition. Numbers 1–3 are the sequences of thrusts, which developed during the kate Paleocene to early Miocene. Note that the dykes of the Bayat Formation cross-cut the thrust contact between the NAOM and the Yoncalı Formation.

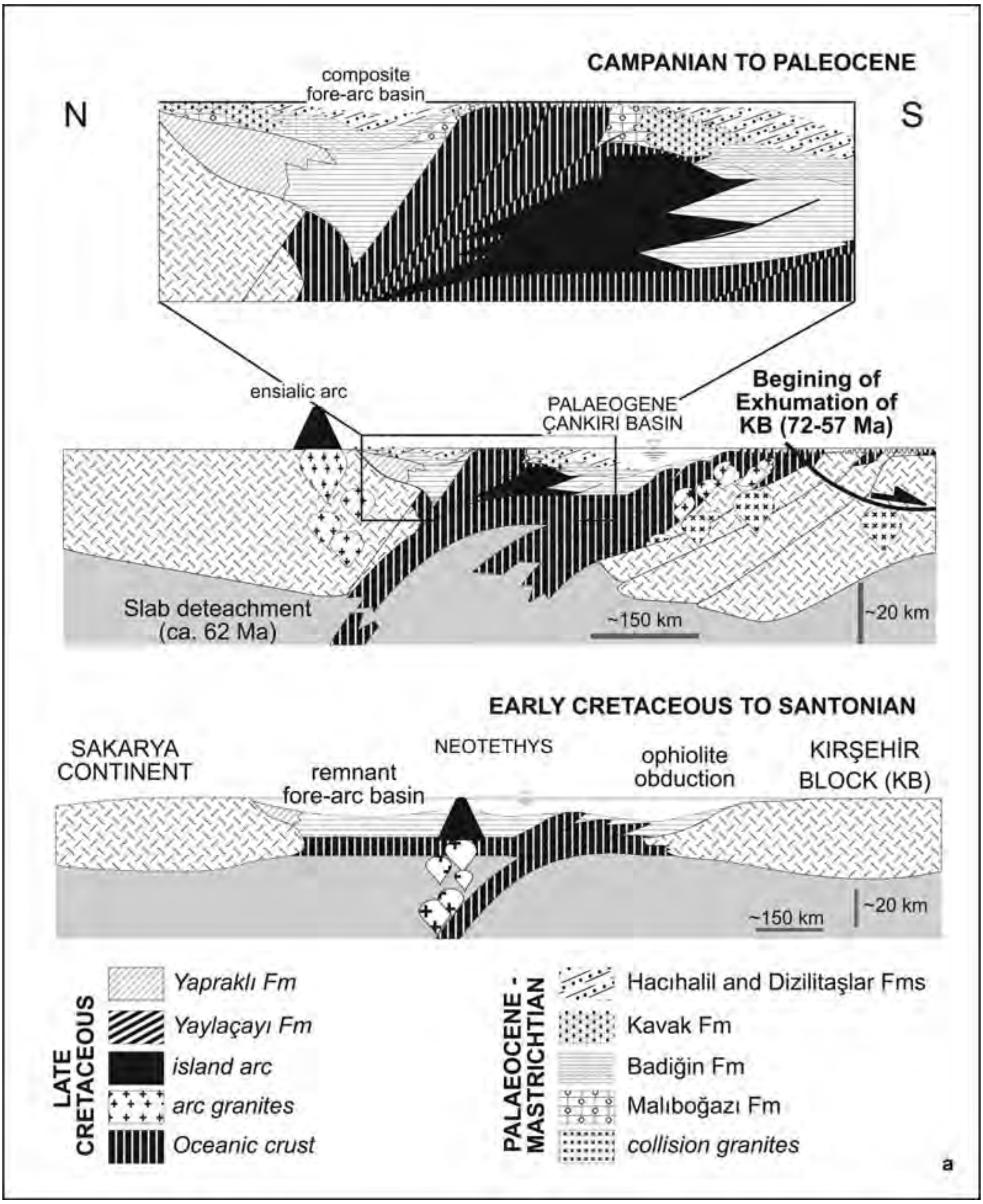

Fig. 25. Conceptual evolutionary scenarios. (**a**) cross-sections for the early Cretaceous to Paleocene.

margins of the basin (Fig. 25 d & e). Due to thrust stacking in the margins of the Çankırı Basin, ophiolitic units (rim) were uplifted and sub-aerially exposed, and supplied detritus to the Yapraklı Formation, and later to the Kavak and Badiğin formations. In the shallower settings of the rim the Malıboğazı Formation is deposited as isolated patch reefs (Fig. 25e).

Obliteration of the intervening oceanic crust gave way to termination of subduction and collision of the Kırşehir Block and the Sakarya Continent at the end of the Maastrichtian (Fig. 25e). This in

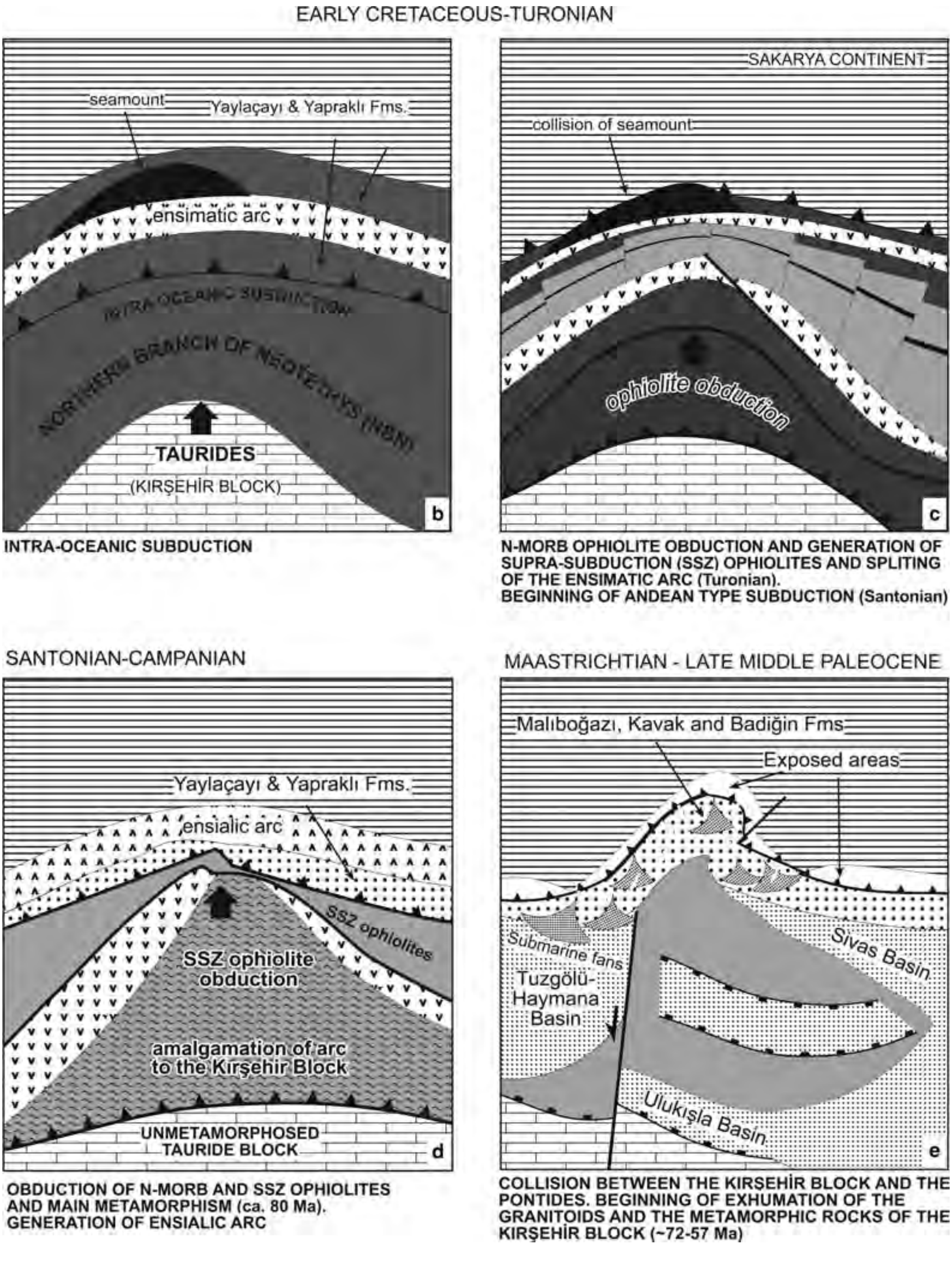

Fig. 25. (**b**–**e**) palaeogeographial scenarios for the early Cretaceous to Maastrichtian interval.

turn, gave way to disruption of the forearc basin which was extending almost all along the subduction front (i.e. İzmir–Ankara–Erzincan Suture Zone). During the end of the late Cretaceous to Paleocene, deposition partly continued only in the deeper parts of the Çankırı Basin. Therefore, the early Cenozoic configuration of the Çankırı Basin is superimposed on a part of the upper Cretaceous

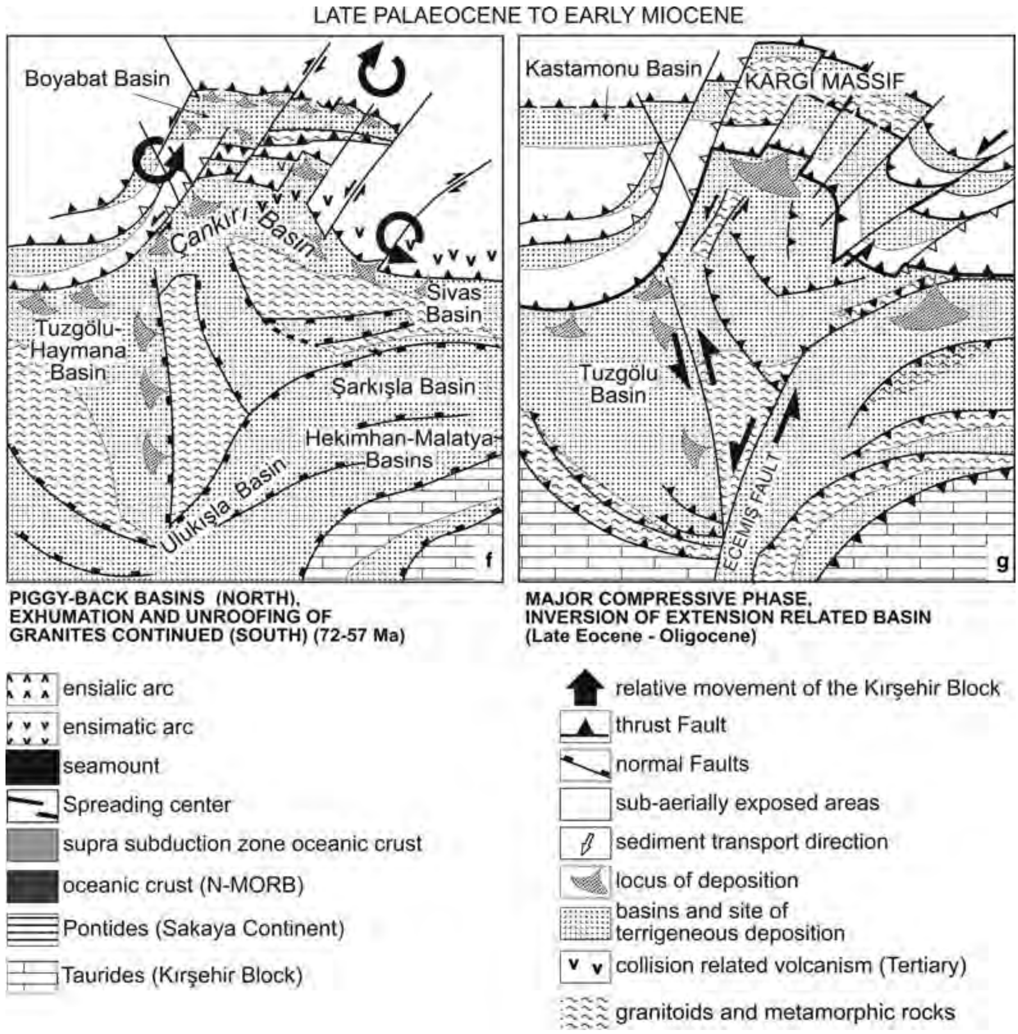

Fig. 25. (**f–g**) palaeogeographial scenarios for the Paleocene to early Miocene interval.

fore-arc basin (Figs 25 & 26) without a major depositional break.

By the end of the Maastrichtian, the oceanic domains were completely consumed, ophiolitic mélange generation and volcanism ceased due to collision of the Kırşehir Block with the Sakarya Continent (continent–continent collision) (Fig. 25f). We speculate that this gave way to detachment of the slab which in turn resulted in a rapid uplift and decrease in the convergence rates between the Pontides and the Kırşehir Block. This might have resulted in extension and exhumation of metamorphic rocks and the granitoids of the Kırşehir Block (Boztuğ *et al.* 2007; Boztuğ & Jonckheere 2007). Extension in the Kırşehir Block continued until the middle Paleocene during which the Çankırı Basin was uplifted and still under slight compression as evidenced indirectly by erosion of the upper Cretaceous units, onset of continental to shallow marine conditions and relatively limited amount of deposition (Kavak and Badiğin formations). From the late Paleocene onwards, metamorphic rocks and granitoids of the Kırşehir Block were subjected to erosion (Erler & Bayhan 1995; Çemen *et al.* 1999; Gautier *et al.* 2002; Boztuğ & Jonckheere 2007).

Late Paleocene to early Miocene evolution of the Çankırı Basin

The late Paleocene to early Miocene evolution of the Çankırı Basin is characterized by foreland

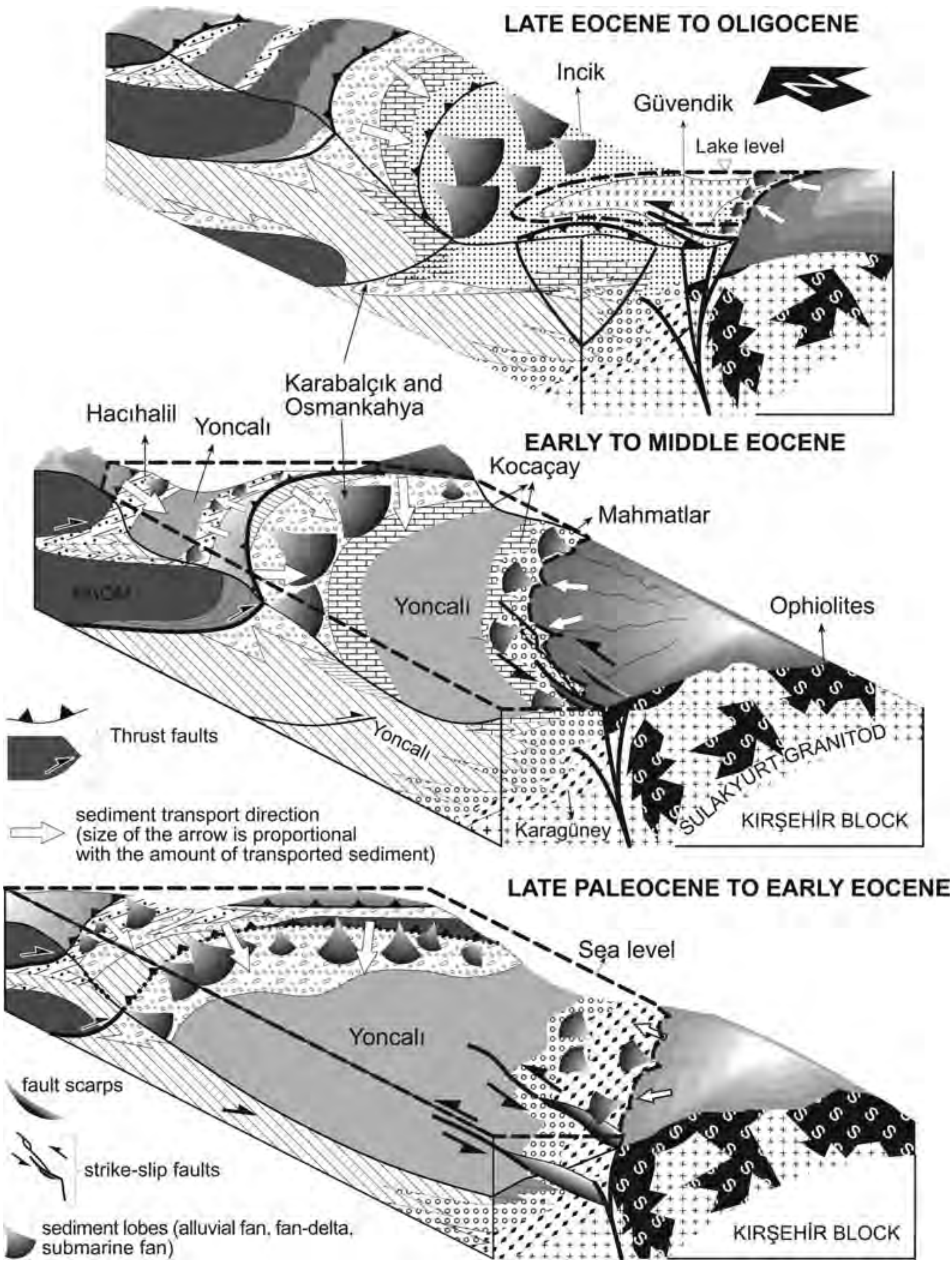

Fig. 26. Block diagrams illustrating the late Paleocene to early Miocene evolution of the Çankırı Basin (see text for discussion).

basin deposition due to collision and further convergence of the Sakarya Continent and the Kırşehir Block (Figs 25f, g & 26). The reconstruction of the depositional environments for the upper Paleocene to lower Miocene sequences of the Çankırı Basin is illustrated in Figure 26. The upper Paleocene to Eocene is characterized by very rapid lateral and vertical facies changes, a consistent relative younging of units from the rim towards the basin centre which onlap progressively onto the flexurally subsiding Kırşehir Block. Deposition of the Hacıhalil and Dizlitaşlar Formations continued during the late Paleocene and they display facies associations ranging from proximal alluvial fan, to braided river, to meandering river, to fan delta, to near shore and to prodelta/open marine facies (Ocakoğlu & Çiner 1997). The Hacıhalil Formation is laterally transitional and always underlies the Yoncalı Formation. This relationship may indicate a gradual relative rise of the sea level (Weijers *et al.* 2007) that caused fining upwards sequences and a relative deepening of depositional environments from continental to a deeper marine facies. Alternation of graded sandstone, siltstone, shale and the presence of current ripples indicate that the Yoncalı Formation was deposited by turbidity currents. Considering its position relative to the Karabalçık and Osmankahya formations, it may represent prodelta clays, near shore clastic settings to deep marine settings (cf. Reading & Collinson 1996). The presence of benthic fauna, plant remains and coal seams indicate that the Karabalçık Formation was deposited in relatively shallow marine conditions, which laterally and/or temporally changed into marshy conditions. The large-scale cross-bedding and the presence of boulders and blocks within the conglomerates, as well as the presence of channels of conglomerates of the Karabalçık Formation within the Yoncalı Formation indicates that the Karabalçık Formation constitutes the foreset beds of a south facing delta. The channels in the Yoncalı Formation may indicate a distributary channel system of this delta (cf. Postma & Roep 1985; Johnson & Baldwin 1996; Reading & Collinson 1996). The Osmankahya Formation was deposited in a prograding near shore setting where fluvial deposition was the dominating agent. The Kocaçay Formation laterally grades over, and covers all the Eocene units. The presence of benthic foraminifera (e.g. nummulites, alveolinae etc.) and bivalves and locally presence of conglomerates and sandstones indicates that the Kocaçay Formation was deposited in a very shallow water conditions. The Incik Formation is deposited in continental settings. Its lateral gradation to the Kocaçay Formation and the presence of greenish grey shale with marine fauna indicate a continental to marine transition (mixed environment). The presence of evaporates indicates arid climate conditions.

The youngest depositional unit related to post-collisional convergence and hence foreland basin development is continued until the Aquitanian and is represented by the Kılçak Formation.

Conclusions

The tectonostratigraphical evolution of the Çankırı Basin occurred mainly in two main episodes. The first one took place in the late Cretaceous to Paleocene and the second in the late Paleocene to earliest Miocene.

The late Cretaceous to Paleocene evolution of the basin was associated with the northwards subduction of the northern Neotethys under the Sakarya Continent. Two different subduction events took place in the region. The oldest event is an intra-oceanic subduction that resulted in an ensimatic arc and supra-subduction zone ophiolite generation that in turn obducted onto the Kırşehir Block. The second subduction event took place during the Santonian–Maastrichtian interval and produced an ensialic arc on the Sakarya Continent. The earliest sub-aerial emergence of the rim occurred in the Maastrichtian. It is thought that the emergence of the rim was associated with the accretionary wedge growth enhanced by collision of the sea mount with the Sakarya Continent. In the south of the sea mount, the Çankırı Basin continued to its evolution as a remnant basin which was relatively narrowed due to subduction. During the Maastrichtian, in the periphery of the emergent areas, the Malıboğazı, Kavak and Badiğin formations were deposited while in the relatively deeper parts, deposition of Yaylaçayı and Yapraklı formations continued. Rapid uplift and emergence occurred during the Paleocene which gave way to increased sediment supply and development of turbiditiy currents.

By the beginning of the Paleocene, the overthickened Kırşehir Block due to obduction and nappe stacking, began to collapse which subsequently gave way to un-roofing of the granitoids and exhumation of the metamorphic rocks of the Kırşehir Block. Un-roofing and exhumation is evidenced by presence of granitic and metamorphic pebbles in the Paleocene deposits in the Çankırı Basin and elsewhere.

By the late Paleocene, indentation of the Kırşehir Block into the Sakarya Continent began (Kaymakcı *et al.* 2003*b*). This gave way to development of a foreland basin system characterized by a series of piggy-back basins. Due to southwards migration of the thrust faults and the depocenters, the depositional environments became shallower and finally passed into continental settings by the end of the middle Eocene. During the post- middle Eocene to early Miocene, the basin became completely restricted and the sea withdrew perpetually from the region. Since the end of the middle Eocene continental conditions have been prevailing in the region. The collision and indentation related convergence and basin development in the Çankırı Basin lasted until the Aquitanian (early Miocene, *c*. 20 Ma). From the Burdigalian onwards a new tectonic regime established in the Çankırı Basin (see Kaymakcı *et al.* 2001*b*).

We thank D. J. J. Hinsbergen, S. Rice and O. Tüysüz for critical reviews. This study is supported by Turkish Government under YLS – grant and Turkish Petroleum Co. The authors would like to thank Y. Öztaş for field support. H. de Bruijn, E. Unay and G. Saraç are acknowledged for micro-mammal sampling and identifications.

References

AKIMAN, O., ERLER, A., GÖNCÜOĞLU, M. C., GÜLEÇ, N., GEVEN, A., TÜRELI, T. K. & KADIOĞLU, Y. K. 1993. Geochemical characteristics of granitoids along the western margin of the Central Anatolian Crystalline Complex and their tectonic implications. *Geological Journal*, **28**, 371–382.

AKYÜREK, B., BILGINER, E., AKBAŞ, B., HEPSEN, N., PEHLIVAN, S., SUNU, O., SOYSAL, Y., DAĞER, Z., ÇATAL, E., SÖZERI, B., YILDIRIM, H. & HAKYEMEZ, H. 1984. The geology of the Ankara-Elmadağ-Kalecik region. *Chamber of Geological Engineers of Turkey Bulletin*. **20**, 31–46.

AYAN, T. 1969. *Çankırı-Yerköy havzası petrol imkanları: Jeolojik ve Tektonik etüdü*. Egeran Müşavirlik Mühendislik Firması. TPAO Rap. No: **469** (unpublished).

AZIZ, A. 1975. *İskilip civarı ile güney ve güneybatısının detay jeolojisi ve petrol olanakları*. M.T.A. Arş. Rap. No: **6132** (unpublished).

BINGÖL, A. F. 1984. Geology of the Elazig area in the Eastern Taurus Region. *Proceed. of the Geology of the Taurus Belt*, MTA, Ankara, 209–216.

BIRGILI, S., YOLDAŞ, R. & ÜNALAN, G. 1974. *Çankırı-Çorum havzası jeolojisi ve petrol olanakları ön raporu*. TPAO Rap. No: **1216** (unpublished).

BOZTUĞ, D. & JONCKHEERE, R. C. , 2007. Apatite fission-track data from central-Anatolian granitoids (Turkey: constraints on Neo-Tethyan closure. *Tectonics*, **26**, TC3011, doi:10.1029/2006TC001988.

BOZTUĞ, D., TICHOMIROWA, M. & BOMBACH, K. 2007. ^{207}Pb–^{206}Pb single-zircon evaporation ages of some granitoid rocks reveal continent-oceanic island arc collision during the Cretaceous geodynamic evolution of the central Anatolian crust, Turkey. *Journal of Asian Earth Sciences*, **31**, 71–86.

ÇEMEN, İ., GÖNCÜOĞLU, M. C. & DIRIK, K. 1999, Structural Evolution of the Tuzgölü Basin in Central Anatolia, Turkey. *Journal of Geology*, **107**, 693–706.

CLARK, M. & ROBERTSON, A. 2005. Uppermost Cretaceous–Lower Cenozoic Ulukışla Basin, south-central Turkey: sedimentary evolution of part of a unified basin complex within an evolving Neotethyan suture zone. *Sedimentary Geology*, **173**, 15–51.

DE BRUIJN, H. & SARAÇ, G. , 1992. Early Miocene rodent faunas from eastern Mediterranean area. Part II. *Mirabella* (Paracricetodontinae, Muroidea). *Proceedings of the Koninklijke Nederlandse Akademie Van Wetenschappen, Amsterdam*, **B95**, 25–40.

DE BRUIJN & KOENIGSWALD, W. 1994. Early Miocene rodent faunas from eastern Mediterranean area. Part V. The genus *Enginia* (Muroidea) with a discussion of the structure of the incisor enamel. *Proceedings of the Koninklijke Nederlandse Akademie Van Wetenschappen, Amsterdam*, **B97**, 381–405.

DE BRUIJN, H., DAAMS, R., DAXNER-HÖCK, G., FAHLBUSCH, V., GINSBURG, L., MEIN, P. & MORALES, J. 1992. Report of the RCMNS Working Group on fossil mammals. Reisensburg 1990. *Newsletter on Stratigraphy*, **26**, 65–118, Berlin, Stuttgart.

DELLALOĞLU, A. A., TÜYSÜZ, O., KAYA, O. H. & HARPUT, B. 1992. *Kalecik (Ankara)-Eldivan-Yapraklı (Çankırı)-İskilip (Çorum) ve Devrez Çayı arasindaki alanın jeolojisi ve petrol olanakları*. TPAO Rap. No. **3194** (unpublished).

DEMIRER, A., ÖZÇÉLIK, Y. & ÖZKAN, R. 1992. *Çankırı-Çorum basenindeki Eosen volkanitlerinin petrografisi.* TPAO Rap. No. **1810** (unpublished).

DICKINSON, W. R. & SEELY, D. R. 1979. Structure and stratigraphy of forearc regions. *AAPG Bulletin*, **63**, 2–31.

DIRIK, K., GÖNCÜOĞLU, M. C. & KOZLU, H. 1999. Tectonic evolution of the southwestern part of the Sivas Basin. *Geological Journal*, **34**, 303–319.

ERLER, A. & BAYHAN, H. 1995. Orta Anadolu Granitoidleri'nin genel değerlendirilmesi ve sorunları. *Hacettepe Üniversitesi Yerbilimleri*, **17**, 49–67.

GAUTIER, P., BOZKURT, E., HALLOT, E. & DIRIK, K. 2002. Pre-Eocene exhumation of the Niğde Massif, Central Anatolia, Turkey. *Geological Magazine*, **139**, 559–576.

GÖKTEN, E. 1983. Şarkışla (Sivas) ğuney-güneydoğusunun stratigrafisi ve jeolojik evrimi. *Türkiye JeolojiKurumu Bülteni*. **26**, 167–176.

GÖRÜR, N. 1988. Timing of opening of the Black Sea Basin. *Tectonophysics*, **147**, 247–262.

GÖRÜR, N. 1997. Cretaceous syn- to postrift sedimentation on the southern continental margin of the western Black Sea Basin. *In*: ROBINSON, A. G. (ed.) *Regional and Petroleum Geology of the Black Sea and Surrounding Region.* American Association of Petroleum Geologists, Memoir, **68**, 227–240.

GÖRÜR, N., TÜYSÜZ, O. & ŞENGÖR, A. M. C. 1998. Tectonic evolution of the central Anatolian basins. *International Geological Review*, **40**, 831–50.

GÖRÜR, N., OKTAY, F. Y., SEYMEN, I. & ŞENGÖR, A. M. C. 1984. Palaeotectonic evolution of the Tuzgölü basin complex, Central Turkey: Sedimentary record of a neotethyan closure. *In*: DIXON, J. E. & ROBERTSON, A. H. F. (eds) *The Geological Evolution of the Eastern Mediterranean*. Blackwell Publishing, Oxford, London.

GÜLEÇ, N. 1994. Rb-Sr isotope data from the Ağaçören Granitoid (East of Tuz Gölü): geochronological and genetical implications. *Turkish Journal of Earth Sciences*, **3**, 39–43.

GÜRER, Ö. F. & ALDANMAZ, E. 2002. Origin of the Upper Cretaceous-Cenozoic sedimentary basins within the Tauride-Anatolide platform in Turkey. *Geological Magazine*, **139**, 191–197.

ILBEYLI, N., PEARCE, J. A., THIRLWALL, M. F. & MITCHELL, J. G. 2004. Petrogenesis of collision-related plutonics in Central Anatolia, Turkey. *Lithos*, **72**, 163– 182.

JOHNSON, H. D. & BALDWIN, C. T. 1996. Shallow clastic seas. *In*: READING, H. G. (ed.) *Sedimentary Environments: Process, Facies and Stratigraphy*. Blackwell Publishing, Oxford. 232–280.

KAYMAKCI, N. 2000. *Tectono-stratigraphical evolution of the Çankiri Basin (Central Anatolia, Turkey).* Ph.D Thesis, Geologica Ultraiectina. No. 190, Utrecht University Faculty of Earth Sciences, The Netherlands.

KAYMAKCI, N., WHITE, S. H. & VAN DIJK, P. M. 2000. Paleostress inversion in a multiphase deformed area: kinematic and structural evolution of the Çankiri Basin (central Turkey), Part 1. *In*: BOZKURT, E., WINCHESTER, J. A. & PIPER, J. A. D. (eds) *Tectonics and Magmatism in Turkey and the Surrounding area.* Geological Society, London, Special Publication, **173**, 445–473.

KAYMAKCI, N., WHITE, S. H. & VAN DIJK, P. M. 2003*a*. Kinematic and structural development of the Çankiri Basin (Central Anatolia, Turkey): a paleostress inversion study. *Tectonophysics*, **364**, 85–113.

KAYMAKCI, N., DE BRUIJN, H., WHITE, S. H., VAN DIJK, M., SARAÇ, G. & UNAY, E. 2001*a*. Tectonic implications of the Neogene stratigraphy of the Çankiri basin with special reference to the Çandir locality (North-Central Anatolia, Turkey). *In*: GÜLEÇ, E., BEGUN, D. R. & GERAADS, D. (eds) *Geology and Vertebrate Paleontology of the Miocene hominoid locality of Çandir. Courier Forschugsinstitut Senckenberg*, **240**, 9–28.

KAYMAKCI, N., OZÇELIK, Y., WHITE, S. H. & VAN DIJK, P. M. 2001*b*. Neogene Tectonics of the Çankiri Basin (north Central Turkey), *Turkish Association of Petroleum Geologists Bulletin*, **13**, 27–56.

KAYMAKCI, N., DUERMEIJER, C. E., LANGEREIS, C., WHITE, S. H. & VAN DIJK, P. M. 2003*b*. Oroclinal bending due to indentation: a paleomagnetic study for the early Cenozoic evolution of the Çankiri Basin (central Anatolia, Turkey). *Geological Magazine*. **140**, 343–355.

KAZANCI, N. & VAROL, B. 1990. Development of a mass flow-dominated fan-delta complex and associated carbonate reefs within a transgressive Paleocene succession, Central Anatolia, Turkey. *Sedimentary Geology*, **68**, 261–278.

KETIN, İ. 1966. Anadolu'nun tektonik birlikleri. *Maden Tetkik ve Arama Enstitüsü Dergisi*, **66**, 20–34.

KUŞCU, İ. 1997. *Mineralogical and geochemical comparison of skarns in the Akdağmadeni, Akçakışla and Keskin districts, Central Anatolia, Turkey*. Ph.D. Thesis, Middle East Technical University, Ankara (unpublished).

NORMAN, T. 1972. Ankara doğusunda Yahşihan bölgesinde Üst Kretase-Alt Tersiyer yaşlı arazinin jeolojisi. *Maden Tetkik ve Arama Enstitüsü Dergisi*, Ankara.

OCAKOĞLU, F. & ÇINER, A. 1997. Fay denetimli bir havzada sedimanter dolgunun niteligi ve evrimi: Çankırı havzası kuzeyinden Lütesiyen yaşlı bir örnek. *Hecettepe Üniversitesi Yerbilimleri*, **19**, 89–108.

OKAY, A. I. 1984. Distribution and characteristics of the northwest Turkish blueschists, *In*: DIXON, J. E. & ROBERTSON, A. H. F. (eds), *The Geological Evolution of the Eastern Mediterranean*, Blackwell Publishing, Oxford, London.

OKAY, A. I., TANSEL, İ. & TÜYÜSZ, O. 2001. Obduction, subduction and collision as reflected in the Upper Cretaceous–Lower Eocene sedimentary record of western Turkey. *Geological Magazine*, **138**, 117–142.

OKAY, A. I., ŞENGÖR, A. M. C. & GÖRÜR, N. 1994. Kinematic history of the opening of the Black Sea and its effect on the surrounding regions. *Geology*, **22**, 267–270.

OKAY, A. I., SATIR, M., MALUSKI, H., SIYAKO, M., MONIE, P., METZGER, R. & AKYÜZ, S. 1996. Paleo- and Neo-Tethyan events in northwest Turkey: geological and geochronological constraints. *In*: YIN, A. & HARRISON, M. (eds) *Tectonics of Asia*. Cambridge University Press, 420–441.

OKAY, A. I., TÜYSÜZ, O., SATIR, M., ÖZKAN-ALTINER, S., ALTINER, D., SHERLOCK, S. & EREN, R. H. , 2006. Cretaceous and Triassic subduction-accretion, high-pressure–low-temperature metamorphism, and continental growth in the Central Pontides, Turkey. *Geological Society America Bulletin*, **118**, 1247–1269.

ORI, G. G. & FRIEND, P. F. 1984. Sedimentary basins formed and carried piggyback on active thrust sheets. *Geology*, **12**, 475–478.

POSTMA, G. 1983. Water escape structures in the context of depositional model of a mass-flow dominated conglomeratic fan delta (Abrioja Formation, Pliocene, America basin, SE Spain). *Sedimentology*, **30**, 91–104.

POSTMA, G. & ROEP, T. B. 1985. Resedimented conglomerates in the bottom set of a Gilbert-type gravel delta. *Journal of Sedimentary Petrology*, **55**, 874–885.

READING, H. G. & COLLINSON, J. D. 1996. Clastic coasts. *In*: READING, H. G. (ed.) *Sedimentary Environments: Process, Facies and Stratigraphy*. Blackwell Science, Oxford, 154–231.

RIBA, O. 1976. Syntectonic unconformities of the Alto Cardener, Spanish Pyrenees: a genetic interpretation. *Sedimentary Geology*, **15**, 213–33.

RICE, S. P., ROBERTSON, A. H. F. & USTAÖMER, T. 2006. Late Cretaceous-Early Cenozoic tectonic evolution of the Eurasian active margin in the Central and Eastern Pontides, northern Turkey. *In*: ROBERSTON, A. H. F. & MOUNTRAKIS, D. (eds) *Tectonic Development of the Eastern Mediterranean Region.* Geological Society, London, Special Publications, **260**, 413–445.

ROBERTSON, A. H. F. 2002. Overview of the genesis and emplacement of Mesozoic ophiolites in the Eastern Mediterranean Tethyan region. *Lithos*, **65**, 1–67.

ROBINSON, A. 1997. Introduction: Tectonic elements of the Black Sea region. *In*: ROBINSON, A. (ed.), *Regional and petroleum geology of the Black Sea and surrounding region*. American Association of Petroleum Geologists Memoir, **68**, 1–6.

ROJAY, B. F. 1993. *Tectonostratigraphy and neotectonic characteristics of the southern margin of Merzifon-Suluova basin (Central Pontides, Amasya)*. Ph.D. Thesis, METU Geological Engineering Department (Ankara, Turkey), (unpublished.)

ROJAY, B. F. 1995. Post-Triassic evolution of central Pontides: Evidence from Amasya region, Northern Anatolia. *Geologica Romana*, **31**, 329–350.

ROJAY, B. F. & SÜZEN, L. 1997. Tectonostratigraphic evolution of an arc-trench basin on accretionary ophiolitic melange prism, Central Anatolia, Turkey. *Turkish Association of Petroleum Geologist Bulletin*, **9**, 1–12.

ROJAY, B., ALTINER, D., ÖZKAN ALTINER, S., ÖNEN, P., JAMES, S. & THIRWALL, M. 2004. Geodynamic significance of the Cretaceous pillow basalts from North Anatolian Ophiolitic Mélange Belt (Central Anatolia, Turkey): geochemical and paleontological constrains. *Geodinamica Acta*, **17**, 349–361.

ROJAY, B., YALINIZ, K. & ALTINER, D. 2001. Age and origin of some pillow basalts from Ankara melange and their tectonic implications to the evolution of northern branch of Neotethys, Central Anatolia. *Turkish Journal of Earth Sciences*, **10**, 93–102.

SANVER, M. & PONAT, E. 1981. Kırşehir ve dolaylarina iliskin paleomagnetik bulgular. Kirsehir Masifinin rotasyonu. *İstanbul Yerbilimleri*, **2**, 2–8.

ŞENGÖR, A. M. C. & YILMAZ, Y. 1981. Tethyan evolution of Turkey: a plate tectonic approach. *Tectonophysics*, **75**, 181–241.

SUNAL, G. & TÜYSÜZ, O. 2002. Palaeostress analysis of Tertiairy post-collosional structures in the Western Pontides, northern Turkey. *Geological Magazine*, **139**, 343–359.

TÜYSÜZ, O. 1985. *Kargı Masifi ve dolayındaki tektonik birliklerin ayırdı ve araştırılması (petrolojik inceleme)*. Istanbul Univ. Jeoloji Mühendisliği Bölümü, Doktora Tezi. (unpublished PhD Thesis)

TÜYSÜZ, O. 1999. Geology of the Cretaceous sedimentary basins of the Western Pontides, *Geological Journal*, **34**, 75–93.

TÜYSÜZ, O. & TEKIN, U. K. 2007. Timing of imbrication of an active continental margin facing the northern branch of Neotethys, Kargı Massif, northern Turkey. *Cretaceous Research*, **28**, 754–764.

TÜYSÜZ, O., DELLALOGLU, A. A. & TERZIOGLU, N. 1995. A magmatic belt within the Neo-Tethyan suture zone and its role in the tectonic evolution of northern Turkey. *Tectonophysics*, **243**, 173–191.

ÜNALAN, G. 1982. Ankara Güneyindeki Ankara Melanjinin stratigrafisi. *In*: Proceedings of the Symposium on the Geology of Central Anatolia, Geological Society of Turkey, 35th Annual Meeting, 46–52 [in Turkish with English abstract].

ÜNAY, E. 1994. Early Miocene rodent faunas from eastern Mediterranean area. Part IV. The Gliridae. *Proceedings of the Koninklijke Nederlandse Akademie Van Wetenschappen, Amsterdam*, **B97**, 445–490.

WEIJERS, J. W. H., SCHOUTEN, S., SLUIJS, A., BRINKHUIS, H. & DAMSTÉ, J. S. S. 2007. Warm arctic continents during the Paleocene–Eocene thermal maximum. *Earth and Planetary Science Letters*, **261**, 230–238.

WHITNEY, D. L., TEYSSIER, C., DILEK, Y. & FAYON, K. 2001. Metamorphism of the Central Anatolian Crystalline Complex, Turkey: influence of orogen-normal collision vs. Wrench-dominated tectonics on P-T-t paths. *Journal of Metamorphic Geology*, **19**, 411–432.

YALINIZ, K. & GÖNCÜOGLU, M. C. 1998. General geological characterictics and distribution of Central Anatolian Ophiolites. *Hacettepe University Earth Science Bulletin*, **19**, 1–15.

YALINIZ, M. K., GÖNCÜOĞLU, M. C. & ÖZKAN-ALTINER, S. 2000. Formation and Emplacement Ages of the SSZ-type Neotethyan Ophiolites in Central Anatolia, Turkey: Paleotectonic Implications. *Geological Journal*, **35**, 53–68.

YAZGAN, E. 1984. Geodynamic Evolution of the eastern Taurus Region (Malatya-Elazığ area, Turkey). *In*: *Geology of Taurus Belt*, Proceedings of International Symposium, Mineral Research and Exploration Institute, (MTA, Ankara) Publication, 199–208.

YOLDAŞ, R. 1982. *Tosya (Kastamonu) ile Bayat (Çorum) arasındaki bölgenin jeolojisi*. Doktora Tezi. Istanbul Universitesi Fen Fakültesi, Genel Jeoloji Kürsüsü, (unpublished).

Oligocene–Miocene basin evolution in SE Anatolia, Turkey: constraints on the closure of the eastern Tethys gateway

SILJA K. HÜSING[1]*, WILLEM-JAN ZACHARIASSE[2], DOUWE J. J. VAN HINSBERGEN[1], WOUT KRIJGSMAN[1], MURAT INCEÖZ[3], MATHIAS HARZHAUSER[4], OLEG MANDIC[4] & ANDREAS KROH[4]

[1]*Paleomagnetic Laboratory "Fort Hoofddijk", Department of Earth Sciences, Utrecht University, Budapestlaan 4, 3584 CD Utrecht, The Netherlands*

[2]*Stratigraphy and Paleontology Group, Department of Earth Sciences, Utrecht University, The Netherlands*

[3]*Department of Geology, Fırat University, Elazığ, Turkey*

[4]*Natural History Museum Vienna, Austria*

**Corresponding author (e-mail: huesing@geo.uu.nl)*

Abstract: The Oligocene–Miocene was a time characterized by major climate changes as well as changing plate configurations. The Middle Miocene Climate Transition (17 to 11 Ma) may even have been triggered by a plate tectonic event: the closure of the eastern Tethys gateway, the marine connection between the Mediterranean and Indian Ocean. To address this idea, we focus on the evolution of Oligocene and Miocene foreland basins in the southernmost part of Turkey, the most likely candidates to have formed this gateway. In addition, we take the geodynamic evolution of the Arabian–Eurasian collision into account.

The Muş and Elazığ basins, located to the north of the Bitlis–Zagros suture zone, were most likely connected during the Oligocene. The deepening of both basins is biostratigraphically dated by us to occur during the Rupelian (Early Oligocene). Deep marine conditions (between 350 and 750 m) prevailed until the Chattian (Late Oligocene), when the basins shoaled rapidly to subtidal/intertidal environment in tropical to subtropical conditions, as indicated by the macrofossil assemblages. We conclude that the emergence of this basin during the Chattian severely restricted the marine connection between an eastern (Indian Ocean) and western (Mediterranean) marine domain. If a connection persisted it was likely located south of the Bitlis–Zagros suture zone. The Kahramanmaraş basin, located on the northern Arabian promontory south of the Bitlis–Zagros suture zone, was a foreland basin during the Middle and Late Miocene, possibly linked to the Hatay basin to the west and the Lice basin to the east. Our data indicates that this foreland basin experienced shallow marine conditions during the Langhian, followed by a rapid deepening during Langhian/Serravallian and prevailing deep marine conditions (between 350 and 750 m) until the early Tortonian. We have dated the youngest sediments underneath a subduction-related thrust at *c*. 11 Ma and suggest that this corresponds to the end of underthrusting in the Kahramanmaraş region, i.e. the end of subduction of Arabia. This age coincides in time with the onset of eastern Anatolian volcanism, uplift of the East Anatolian Accretionary Complex, and the onset of the North and East Anatolian Fault Zones accommodating westward escape tectonics of Anatolia. After *c*. 11 Ma, the foreland basin south of the Bitlis formed not (or no longer) a deep marine connection along the northern margin of Arabia between the Mediterranean Sea and the Indian Ocean. We finally conclude that a causal link between gateway closure and global climate change to a cooler mode, recorded in the Mi3b event ($\delta^{18}O$ increase) dated at 13.82 Ma, cannot be supported.

Tectonic closure and opening of marine gateways is suggested to have led to substantial reorganization of surface and deep ocean water currents and may have caused important changes in global climate. The closure of the Panama Isthmus between 3.0 and 2.5 Ma has influenced the Gulf Stream, triggering major Northern Hemisphere glaciations (Bartoli *et al.* 2005; Schneider & Schmittner 2006). The opening of the Drake Passage allowed the start of the Antarctic Circumpolar Current which might have initiated the abrupt climate cooling around the Eocene/Oligocene boundary and the extensive growth of Antarctic ice sheets (Livermore *et al.* 2005). The restriction of water exchange across

From: VAN HINSBERGEN, D. J. J., EDWARDS, M. A. & GOVERS, R. (eds) *Collision and Collapse at the Africa–Arabia–Eurasia Subduction Zone*. The Geological Society, London, Special Publications, **311**, 107–132.
DOI: 10.1144/SP311.4 0305-8719/09/$15.00

the former straits between Spain and Morocco resulted in the desiccation of the Mediterranean Sea during its Messinian Salinity Crisis (Hsü *et al.* 1973). Likewise, the disconnection of the Indian Ocean and the Atlantic/Mediterranean water masses has been suggested to have caused a major middle Miocene climate change, widely recognized in both the marine (Woodruff & Savin 1989; Flower & Kennett 1994; Zachos *et al.* 2001; Bicchi *et al.* 2003) and the terrestrial record (Krijgsman *et al.* 1994). It is this disconnection that forms the scope of this paper.

The middle Miocene is a period characterized by major environmental changes during which the Earth's climate gradually progressed into a colder mode (Zachos *et al.* 2001). The Miocene Climate Optimum between 17 to 15 Ma was followed by an interval of global climate variability between 15 and 14 Ma, marked by atmospheric and oceanic cooling, East Antarctic Ice Sheet growth, and carbon cycle variability (Woodruff & Savin 1989; Flower & Kennett 1994; Zachos *et al.* 2001). Seven major $\delta^{18}O$ shifts, Mi1 to Mi7, to higher (= colder) values documented in marine records of the Atlantic reflect brief periods of increased glaciations (Miller *et al.* 1991; Wright *et al.* 1992; Miller *et al.* 2005). The Mi3a, Mi3b and Mi4 events between about 14.5 and 12.5 Ma represent the middle Miocene $\delta^{18}O$ increase, leading the global climate into a colder mode at the same time as the onset of the Antarctic glaciations (van der Zwaan & Gudjonsson 1986; Abels *et al.* 2005; Miller *et al.* 2005).

A direct relationship between the Middle Miocene Climate change, whether recorded in oxygen or carbon isotopes, marine or terrestrial fauna, and the closure of the eastern Tethys gateway has so far never been proven, although many studies suggest a causal link between the two events (e.g. Woodruff & Savin 1989; Rögl 1999; Flower & Kennett 1993). Part of the problem is that the sediments that were deposited in the eastern Tethys gateway have on many occasions not been recognized or properly dated. In addition, the chronological sequence of tectonic processes involved in the convergence of the Eurasia and African–Arabian plates is complex and actively debated (see Garfunkel 1998, 2004; Golonka 2004). To assess the timing of gateway closure along the northern Arabian promontory, the major geodynamic processes of the Arabia–Eurasia collision and their tectonic responses have to be taken into account. According to reconstructions of Jolivet & Faccenna (2000) and Bellahsen *et al.* (2003), Arabia collided first in the eastern Anatolian/western Iranian region around 30 Ma ago. Consequently, it gradually rotated counterclockwise leading to diachronous collision eastward from Southeastern Anatolia towards the Persian Gulf (Hessami *et al.* 2001). Therefore, we decided to study the southernmost flysch deposits in eastern Anatolia (Fig. 1), these being the most likely candidates to represent the youngest sediments deposited just prior to the disconnection of the Indian–Arabian gateway.

Geodynamic and geological context

The continental collision of the African–Arabian plate with the Eurasian plate resulted in a tectonic collage in eastern Anatolia that is generally subdivided into: (1) the eastern Rhodope–Pontide Arc in the north; (2) the East Anatolian Accretionary Complex consisting of an ophiolitic mélange overlain by Paleocene to upper Oligocene sediments; and (3) the Bitlis–Pötürge Massif tectonically overlying the northern part of the Arabian margin (Fig. 1) (Şengör & Yılmaz 1981; Yılmaz 1993; Tüysüz & Erler 1995; Robertson 2000; Şengör *et al.* 2003; Agard *et al.* 2005). As north–south shortening continued between the converging Eurasian and Arabian plate, the relatively soft and irresistant East Anatolian Accretionary Complex took up most of the initial post-collisional convergent strain by shortening and thickening (Yılmaz *et al.* 1998). Around 13–11 Ma, eastern Anatolia underwent rapid uplift and was confronted with onset of widespread volcanism (Dewey *et al.* 1986; Pearce *et al.* 1990; Keskin 2003; Şengör *et al.* 2003), which has been associated with detachment of northward dipping subducted lithosphere (Keskin 2003; Faccenna *et al.* 2006; Hafkenscheid *et al.* 2006). From this moment onward, the ongoing northward motion of Arabia (still continuing today) (McClusky *et al.* 2000; Reilinger *et al.* 2006; Allmendinger *et al.* 2007), and the retreat of the Hellenic subduction zone to the west (Berckhemer 1977; Le Pichon *et al.* 1982; Jolivet 2001) led to westward tectonic escape of Anatolia along the North and East Anatolian Faults (Dewey & Şengör 1979; Şengör *et al.* 1985).

The present-day plate boundary of the African and Eurasian plates is determined by the Bitlis–Zagros suture zone (Robertson 2000 and references therein; Westaway 2003). On the Arabian plate, to the south of the suture zone, Eocene and younger (volcano-) sediments are relatively flat lying. North of the Bitlis–Pötürge zone, Tertiary marine sediments crop out rarely and the geology is dominated by pre-Neogene basement rocks (metamorphic rocks) and Neogene volcanic rocks. The Bitlis–Pötürge Massif itself is characterized by a stack of nappes originated on the Eurasian side of the Neotethys (Robertson 2000; Robertson *et al.* 2004).

The Bitlis–Pötürge Massif runs from southeastern Turkey to the eastern Mediterranean basin into the Cyprus arc, where it meets the East Anatolian

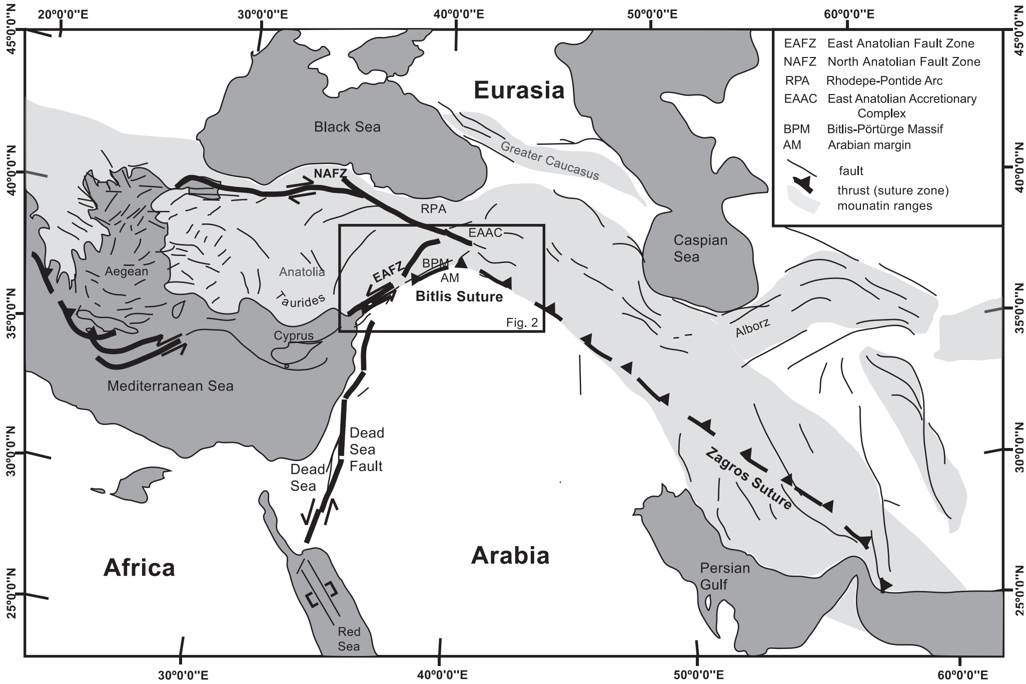

Fig. 1. Outline of tectonic map of the Middle East region, showing major structures such as the Bitlis–Zagros Suture zone, the North and East Anatolian Fault Zones (NAFZ and EAFZ), and mountain ranges related to the convergence of Africa–Arabia and Eurasia (drawn after Geological map of Turkey (Şenel 2002)).

Fault (EAF). Here the structure becomes more complex with several sub-parallel southwestwards running faults and thrusts. The East Anatolian Fault is a 2–3 km wide, active left-lateral strike-slip fault extending from Antakya in the west to Karliova in the NE, where it meets the eastern termination of the North Anatolian Fault (NAF) (Figs 1 & 2; EAFZ and NAFZ). The NAF is a right-lateral strike-slip fault extending over a length of about 1300 km westward. The relative Africa–Arabia motion is taken up by strike-slip displacement along the Dead Sea Fault (Jolivet & Faccenna 2000), while the Africa–Anatolia motion is taken up by subduction south of Cyprus. The overall convergence between Arabia and Anatolia is taken up along the North and East Anatolian fault zones (NAFZ and EAFZ) (Fig. 2) (e.g. McClusky *et al.* 2000; Şengör *et al.* 2005). There is general consensus that the NAFZ and EAFZ had the majority of their displacement in Plio-Pleistocene times (Barka 1992; Westaway 2003, 2004; Hubert-Ferrari *et al.* 2008) although incipient motion may have been as early as late Serravallian/early Tortonian (*c*. 12 to 11 Ma) (Dewey *et al.* 1986; Hubert-Ferrari *et al.* 2002, 2008; Bozkurt 2003; Şengör *et al.* 2005).

The region that comprises the eastern Tethys gateway has thus been subjected to plate convergence and subduction. Şengör *et al.* (2003) suggested that this subduction led to southward migrating accretion of nappes and overlying deep-marine foreland basin deposits, even though individual basins that may reflect such evolution have not been identified in the geological record, which is, at least in part, due to the young volcanic sequences covering a large part of eastern Turkey. If southward accretion of nappes indeed occurred, one should be able to identify southward younging flysch deposits (e.g. van Hinsbergen *et al.* 2005*a*). A foredeep likely remains present until continent–continent collision and subsequent slab break-off stalls convergence and the collision zone is uplifted. Even though small marine basins may remain, the long distance between the Persian Gulf and the Mediterranean Sea makes foredeeps the most promising basins to have formed the gateway between these water masses. In the following paragraphs we will present and discuss the evolution of foredeep basins in SE Turkey in the light of the closure of the eastern Tethys gateway.

Basin evolution

The Arabian foreland is separated from the East Anatolian Accretionary Complex (EAAC) by the Bitlis–Pötürge Massif (Fig. 1). The area of this massif corresponds to the compression zone located

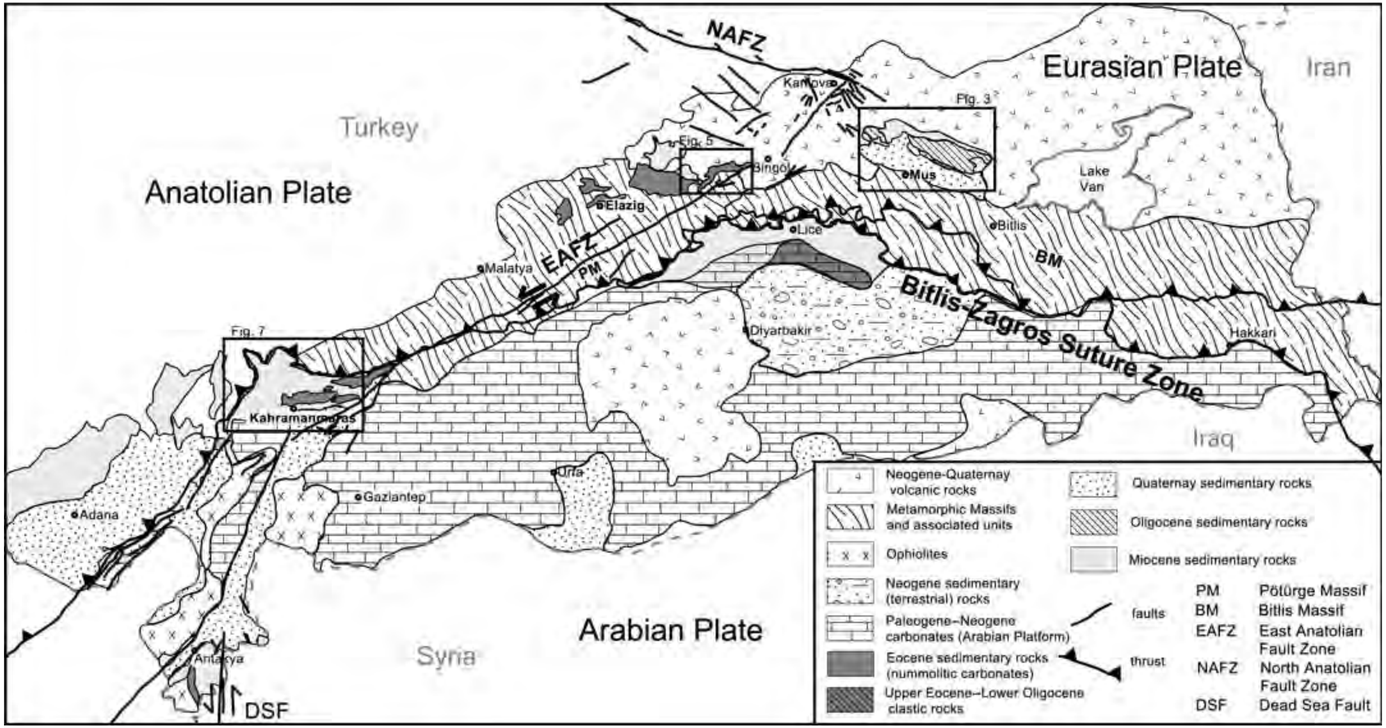

Fig. 2. Outline of schematic geological map of SE Anatolia in Southeastern Turkey with major tectonic structures. Note the three boxes indicating the studied areas: Muş in the easternmost part and Elazığ, both north of the Bitlis–Zagros Suture zone and Kahramanmaraş south of the Bitlis–Zagros Suture Zone (drawn after Geological map of Turkey (Şenel 2002)).

between the two continental crusts, Eurasia and African–Arabian. The massif was stacked to form a nappe complex during the closure of the Neo-Tethys by the middle Miocene (Dewey 1986 and references herein).

We have studied the southernmost flysch deposits in the eastern Anatolian orogenic system. These are found in the Muş and Elazığ basins, both north of the Bitlis–Pötürge Massif, and the Kahramanmaraş basin located south of the Bitlis–Pötürge Massif and near the triple junction of the Arabian, Eurasian and Anatolian plates (Fig. 2).

Geological setting of the Muş basin

The Muş basin is an elongated structure located north of the Bitlis–Pötürge Massif and east of the North and East Anatolian Fault (Figs 2 & 3). According to previous studies (Şaroğlu & Yılmaz 1986; Sancay *et al.* 2006) the basin contains upper Eocene to lower Miocene limestones, marls and turbiditic sandstones with marine sedimentation continuous from the Oligocene to Aquitanian. These deposits overlay an upper Cretaceous ophiolitic mélange. Şaroğlu & Yılmaz (1986) suggested that lower Miocene limestones are widespread in the northern part of the Muş area, while middle Miocene strata were not found. These sequences are unconformably covered by allegedly upper Miocene and younger continental clastics and volcanics (Şaroğlu & Yılmaz 1986; Sancay *et al.* 2006). Detailed biostratigraphy was carried out mainly based on dinoflagellates and palynomorphs yielding a Rupelian (early Oligocene) to Aquitanian (early Miocene) age (Sancay *et al.* 2006). The occurrence of the benthic foraminiferal family of *Miogypsinidae* was interpreted as possible indicator for a connection with the Indo-Pacific during the Oligocene (Sancay *et al.* 2006).

We sampled two sections in the Muş basin (Fig. 3). The eastern transect comprises allegedly Eocene–Oligocene clastics in the northern part of the basin, and Oligocene flysch sediments followed by marine limestones which are covered by volcanics. The second transect in the western part of the basin covers the transition from marls to limestones, assuming it is equivalent to the uppermost part of the eastern succession. The entire succession gently dips towards the NW.

The base of the eastern section (east transect in Fig. 3) is determined by a thrust zone emplacing allegedly Eocene clastic sediments onto Pliocene deposits (see geological map of Turkey, Şenel 2002) (Fig. 3). The first 20 m of the studied section is characterized by an alternation of conglomerates, clays, sands, and silts (Fig. 4). A layer of limestone (1.5 m) with shell fragments and the presence of large gastropods clearly indicate shallow

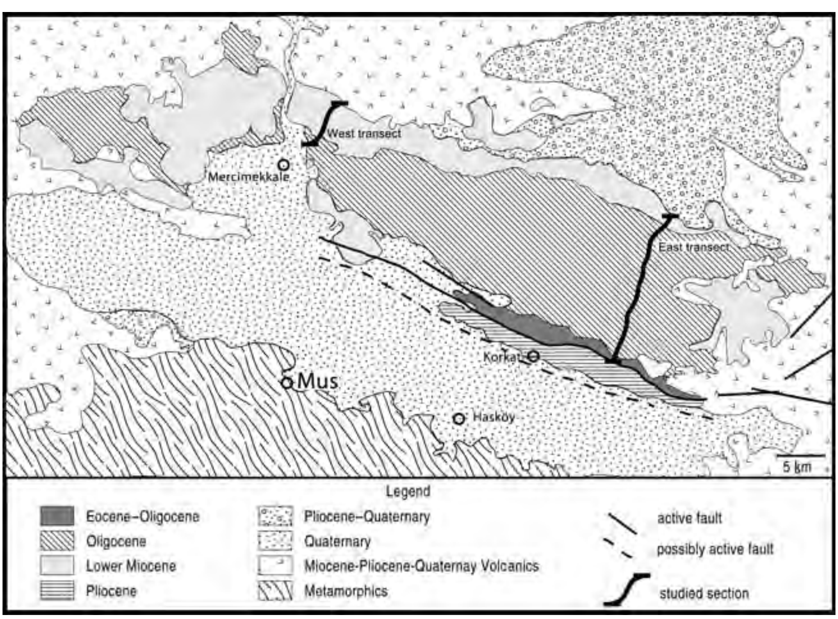

Fig. 3. Simplified tectonic and geological map of the Muş area including the trajectories of the two studied sections: an about 1.4 km long transect in the eastern part of the basin and additionally an about 500 m long transect in the western part of the basin equivalent to the uppermost part of the western transect. Refer to Legend for key to lithology and/or age of outcrops (drawn after Geological map of Turkey (Şenel 2002)).

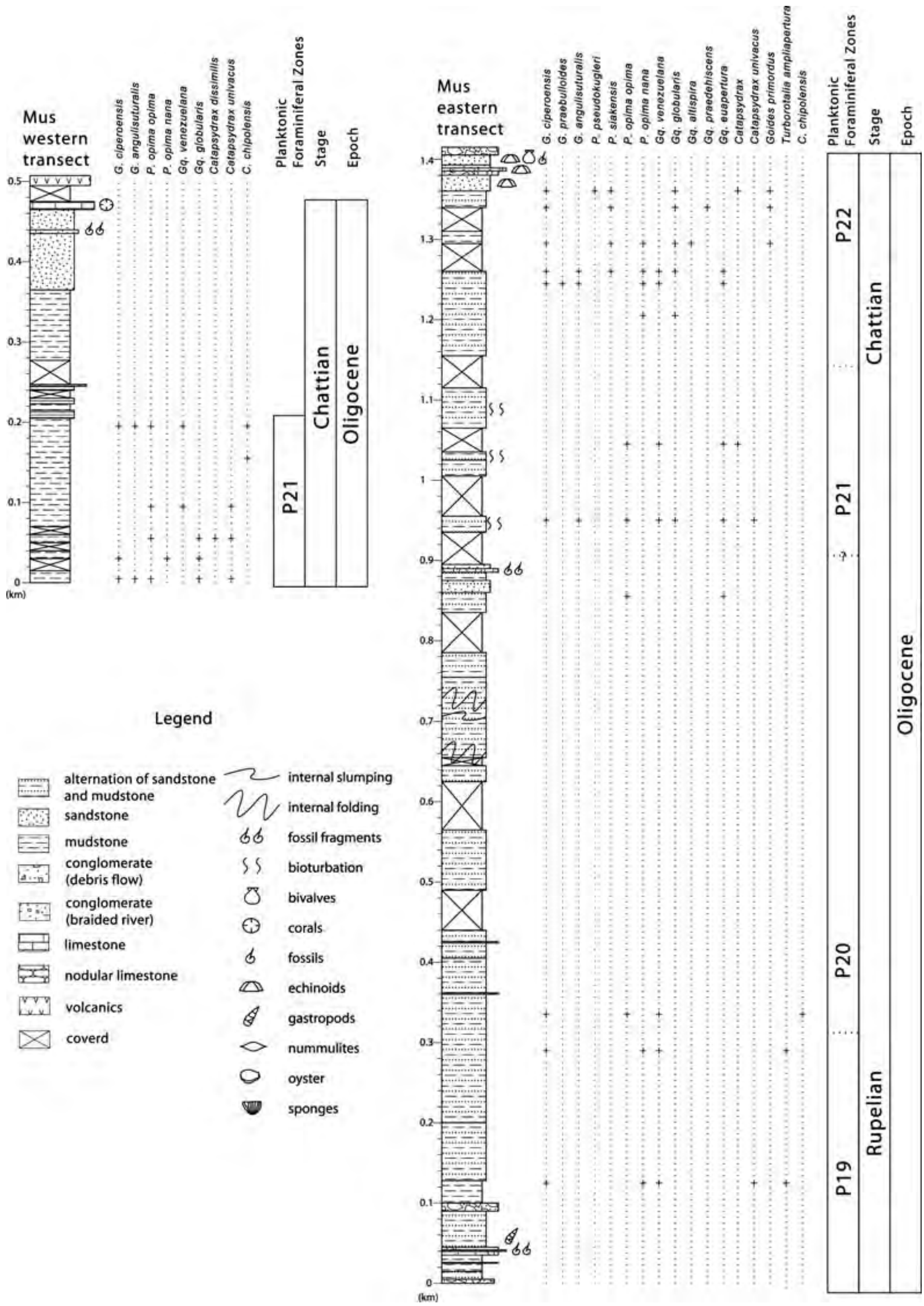

Fig. 4. Lithological column of the studied sections in the Muş basin with the biostratigraphic results. The age model is based on planktonic foraminifer occurrences and the macrofossil assemblage in the uppermost 40 m (mainly limestones and sands) of the stratigraphy. Planktonic foraminifer occurrences have been correlated to planktonic foraminifer zones, which, in turn, are tied to stages during the Oligocene leading to a correlation to the Geological Time Scale. See legend for key to lithologies, structures and fossils.

marine conditions. This sequence is followed by a thick (about 1.3 km) succession of alternating clay and sandstone. Occasionally conglomeratic layers, characterized by angular, unsorted material, occur in the succession. These layers have thicknesses of up to 10 m and are interpreted as debris flows. The sandstone layers show typical transport characteristics such as fining upwards, Bouma sequence, flute casts and fossil fragments indicating a turbiditic origin. These turbidites occur as massive sandstone layers of thicknesses of up to 15 m or as several thinner (up to 50 cm) turbidite layers, probably representing individual events. Only minor slumping, indicating an unstable submarine paleoslope, and folding occur throughout the succession. The upper part of the section shows shoaling characterized by shallow marine limestone, containing echinoderms, bivalves and gastropods, followed by continental clastics.

The western transect (west transect in Fig. 3) is dominated by bluish clay with occasional red sediments. This is followed by a thick, about 100 m, sequence of alternating softer bluish sands, brownish sands and indurate bluish sands, probably all of marine origin. These sediments are overlain by coral limestones, which, in turn, are covered by volcanic rocks, probably of Miocene age. This succession also clearly indicates shoaling towards the top.

Biostratigraphic results of the Muş basin

For biostratigraphy, samples were collected at about every 20 m from both the western and eastern transect (Fig. 3). Not every sample proved to be useful for biostratigraphy or paleobathymetry. The number of foraminifers is extremely variable and most likely fluctuate in pace with changes in terrigenous clastic input. Preservation is generally poor with specimens mostly recrystallized and frequently distorted. Samples from the upper 300 m of the western section are barren in planktonic foraminifers.

The low diversity in planktonic foraminiferal fauna in both sections is dominated by globoquadrinids and catapsydracids with occasional occurrences of *Globigerina ciperoensis* and *Globigerina angulisuturalis* and clearly points to an Oligocene age for the eastern and lower western section (Fig. 4) (Berger & Miller 1988; Spezzaferri & Premoli Silva 1991).

The basal part of the eastern section correlates to planktonic foraminiferal biozone P19 of Berger & Miller (1988) on the basis of trace occurrences of specimens identical to *Turborotalia ampliapertura*. This biozone is Rupelian (early Oligocene) in age (Fig. 4) (Berggren *et al.* 1995). The lowermost occurrence of *Globigerina angulisuturalis* is recorded at 950 m (TR 221) in the eastern section which together with the highest occurrence of *Paragloborotalia opima opima* (at 1045 m (TR222)) indicates that the middle part of the Muş section correlates to planktonic foraminiferal biozone P21 of Blow (1969) and Berger & Miller (1988) which is latest Rupelian to early Chattian in age (Berggren *et al.* 1995). The absence of *Paragloborotalia opima opima* from sample level 1045 m (TR 222) upward in the eastern transect and the occurrence of typical *Paragloborotalia pseudokugleri* and even of forms transitional between *Paragloborotalia pseudokugleri* and *Paragloborotalia kugleri* at the top of the section (1360 m (TR 232)) indicate that the upper part extends upwards into the lower part of planktonic foraminiferal biozone P22 of Berger & Miller (1988) being Chattian in age (Berggren *et al.* 1995). This is confirmed by the presence of *Paragloborotalia siakensis* and *Globigerinoides primordius* in the youngest samples. Both species make their first appearance in the lower part of biozone P22 together with *Paragloborotalia pseudokugleri* (Berger & Miller 1988; Spezzaferri 1994).

In the western section, the co-occurrence of *Globigerina angulisuturalis* and *Paragloborotalia opima opima* at 2 m and 195 m (TR 202 and TR 210) indicates that the lower 200 m correlates to the interval between 900 and 1100 m in the eastern section. Both these intervals belong to biozone P21. This interval is followed by sediments that are barren in planktonic foraminifers but relatively rich in shallow water benthic foraminifers.

The macrofossil assemblage of the uppermost 40 m in the eastern transect comprises bivalves, gastropods and echinoids. The assemblage is diminished by complete aragonite leaching. Nevertheless, the fauna is age indicative and allows palaeoecological interpretations. The mollusc fauna comprises typical Oligocene taxa such as the gastropod *Ampullinopsis crassatina* (Lamarck 1804) and the bivalves *Amussiopecten labadyei* (d'Archiac & Haime 1853) and *Ringicardium buekkianum* (Telegdi-Roth 1914). Some species such as *Dilatilabrum sublatissimus* (d'Orbigny 1852), *Strombus* cf. *praecedens* Schaffer 1912, *Cordiopsis incrassatus* (Nyst 1836), *Amussiopecten subpleuronectes* (d'Orbigny 1852), and *Hyotissa hyotis* (Linnæus 1758) appear during the Chattian and persist into the Miocene.

An important biostratigraphic feature is the co-occurrence of the pectinids *Amussiopecten labadyei* and *A. subpleuronectes* and the occurrence of transitional morphs. This evolutionary phase is recorded so far only from the upper Chattian (Mandic 2000). Especially in the Iranian Qom Basin, this assemblage co-occurs with the larger foraminifera *Eulepidina dilatata*. The last occurrence of *Amussiopecten labadyei* precedes the first occurrence of *Miogypsinoides* which roughly coincides with the base of the early Miocene. The entire mollusc assemblage is therefore pointing to a late Chattian age. This dating is supported by the echinoid fauna. *Parascutella subrotundaeformis* (Schauroth 1865), a sand dollar which occurs most commonly in Northern Italy, is restricted to the Chattian and Aquitanian.

Comparable assemblages are described from the upper Chattian of the central Iranian Qom Formation (Mandic 2000; Harzhauser 2004; Reuter *et al.* 2007) and along the entire northern coast of the Western Tethys (Harzhauser *et al.* 2002). A relation to the Central Paratethys is indicated by the occurrence of *Ringicardium buekkianum*, which is known from the Lower Egerian (Upper Chattian) deposits of Hungary (Báldi 1973). The faunistic relations towards the east are low. Only *Dilatilabrum sublatissimus* (d'Orbigny 1852) reaches to the Zagros Basin and the Arabian shelf during the Aquitanian (Harzhauser *et al.* 2007). The echinoderm *Clypeaster waageni* (Duncan & Sladen 1883), in contrast, represents ties with the echinoid fauna of the Lower Indus Basin.

Numerical ages for the basin fill are provided by three planktonic foraminiferal bioevents. However, equating highest and lowest occurrences (ho and lo) with the Last Occurrence (LO) and First Occurrence (FO) of theses species should be accepted with reservation because the positions are poorly delineated due to large sampling distances in combination with scarcity and poor preservation of the age diagnostic species.

The oldest bioevent in the Muş section is the lowest occurrence of *Turborotalia ampliapertura* some 300 m above the base of the eastern section (TR 190). The LO of this species is calibrated at 30.3 Ma (Berggren *et al.* 1995) providing a minimum age for the base of the Muş section. The age for the top of the eastern section should be slightly younger than the age of 25.9 Ma for the FO of *Paragloborotalia pseudokugleri* (Berggren *et al.* 1995) because of the presence of paragloborotalids being transitional between *Paragloborotalia pseudokugleri* and *Paragloborotalia kugleri*. The ho of *Paragloborotalia opima opima* at 1045 m (TR 222) in the eastern section provides an extra age calibration point of 27.456 Ma being the calibrated age for the LO of *Paragloborotalia opima opima* at ODP Site 1218 (Wade *et al.* 2007). The dating of the top of the section is in accordance with the macrofauna which strongly indicates a late Chattian age for the upper 40 m the eastern transect.

No numerical ages are provided for the western section. However, based on the co-occurrence of *Globigerina angulisuturalis* and *Paragloborotalia opima opima* in the lower 200 m, this interval correlates to the biozone P21. The upper 300 m lack any age diagnostic planktonic foraminifer.

Palaeoenvironmental interpretations for the Muş basin

Benthic foraminifers in the sections were furthermore used to estimate the depositional depth. The commonly used method of calculating depth by determining the ratio between planktonic and benthic foraminifers (van der Zwaan *et al.* 1990; van Hinsbergen *et al.* 2005*b*) is not reliable here due to significant downslope transport (seen in presence of notorious epifytes and shallow water benthic foraminifers such as *Pararotalia* and *Amphistegina*) and poor preservation. Instead, we focus on the deepest water benthic foraminiferal depth markers (for list see van Hinsbergen *et al.* 2005*b*) and the macrofossils. In the eastern section, the depositional environment of the lower 20 m is characterized by shallow marine conditions, indicated by shell fragments in the limestone. However, a rapid deepening trend occurs at about 50 m indicated by the presence of benthic foraminiferal depth markers (typically *Cibicides (pseudo) ungerianus*, *Gyroidina* spp. *Uvigerina* spp. and occasionally *Oridorsalis* spp.), and the absence of markers for deeper water, which points at a depositional depth range of 350 to 750 m (the upper limit is constraint by the occurrence of *Oridorsalis* spp. after van Hinsbergen *et al.* 2005*b*). Towards the top of the eastern section rapid shoaling is evident from the presence of macrofossils. Both the molluscs and echinoderms of the uppermost 40 m indicate a shallow marine, tropical to subtropical, depositional environment with sand bottoms and algal or sea grass patches. Giant conchs such as *Dilatilabrum sublatissimus* (d'Orbigny 1852) are found today in sea grass meadows and sheltered lagoons, where they live partly buried in the soft substrate (Bandel & Wedler 1987). Similarly, the extant representatives of the oyster *Hyotissa hyotis* prefer shallow subtidal habitats where they are attached to rocks and corals (Slack-Smith 1998). Extant *Echinolampas* and *Clypeaste*r, too, occur most commonly on sandy sediments with sea grass patches (Hendler *et al.* 1995).

In the western section a shoaling trend in the upper 250 m is observed by the relatively rich occurrence of shallow water benthic foraminifers and occasional red sediments. The differences between west and east suggest that the western part of the Muş basin shoaled more rapidly or earlier during the Chattian than the eastern part.

Implications for the Muş basin

Based on the occurrence of turbidites, slumping and minor folding, this about 1.5 km thick marine succession is interpreted as deposits of a deep marine basin.

Shallow marine conditions during the Rupelian (P19) were replaced by rapid deepening of the basin during biozone P22, late Chattian. The end of the flysch deposition during the Chattian marks the emergence of the basin which probably remained shallow marine until the late Chattian.

Considering the biostratigraphic ages, a sedimentation rate between 15 and 27 $^{cm}/_{ka}$ is calculated. The constant water depth of 350 to 750 m during deposition indicates approximately 2 km of subsidence throughout the Oligocene, followed by rapid uplift and exposure of the succession after the late Chattian. Our biostratigraphic dates based on planktonic foraminifers in the flysch deposits corroborate the ages published previously based on dinoflagellates and palynomorphs (Sancay *et al.* 2006).

Geological setting of the Elazığ basin

The studied Gevla section is situated in the easternmost part of the Elazığ basin, about 40 km NE of Elazığ (Fig. 2). The basin has been studied by several workers; however, the literature has been published mostly in Turkish (see Aksoy *et al.* 2005) and no detailed information is available for the easternmost part of the basin. At present, the basin fill is exposed in an NE–SW belt in the eastern Taurides of Anatolia. The generalized stratigraphy of the Tertiary sediments has been described as: lower Paleocene continental deposits at the base, followed by upper Paleocene to lower Miocene marine deposits and finally Pliocene to Quaternary continental deposits. The basement of the Elazığ basin is formed by Permo-Triassic metamorphic rocks, namely Keban Metamorphics, which were emplaced over upper Cretaceous magmatic rocks north of Elazığ (Perinçek 1979; Perinçek & Özkaya 1981; Aktaş & Robertson 1984; Bingöl 1984; Aksoy *et al.* 2005).

Detailed stratigraphic, sedimentological and tectonic characteristics of the Elazığ area have been discussed elsewhere (e.g. Perinçek 1979; Perinçek & Özkaya 1981; Aktaş & Robertson 1984; Bingöl 1984; Cronin *et al.* 2000*a*, *b*; Aksoy *et al.* 2005). From the late Paleocene, shallow marine carbonates, deposited in an extensional back-arc setting, were accumulated when the basin further subsided until Middle to Late Eocene (Aksoy *et al.* 2005). During Oligocene to early Miocene, after reaching its maximum extend during the Middle to Late Eocene, deposition was restricted to the N–NW and became progressively shallower, indicated by Oligocene reefal limestones until the final subaerial exposure at the end of Oligocene. Marine Miocene deposits are restricted to small areas in the basin and more widespread north of the basin. From Middle Miocene onwards the basin was affected by a strong, north–south, compression. Later, Pliocene to Pleistocene alluvial fan, fluvial and lacustrine sediments were deposited covering Early Miocene sediments (Cronin *et al.* 2000*a*, *b*; Aksoy *et al.* 2005).

In this setting, we studied a section situated in the easternmost part of the Elazığ basin. According to the geological map of Turkey (Şenel 2002), in the area east of the town Basyurt (Fig. 5), Lower to Middle Eocene continental clastics unconformably overly Mesozoic ophiolitic mélange. These clastic sediments are, in turn, overlain by either Miocene–Pliocene clastic or volcanic rocks.

The basal part of the studied Gevla succession, about 15 km NE of Basyurt, starts with bluish marine clay containing bivalves, followed by an alternation of clay and sandstone (the sandstones are up to 50 cm thick or about 5 m thick with cross bedding) (Fig. 6). A distinct layer with abundant bivalves and gastropods is located at about 50 m stratigraphic position. Three distinct limestone layers occur between about 100 m and 260 m stratigraphic level. The first one, at about 100 m, is a nodular limestone with shell fragments, sponges (up to 30 cm) and corals, followed by two nummulitic limestone horizons, at 244 m and 255 m. This is followed by about 400 m of blue clay grading into a 600 m thick succession of alternating clay and sandstone, whereby the sand layers show typical transport characteristics, such as shell fragments,

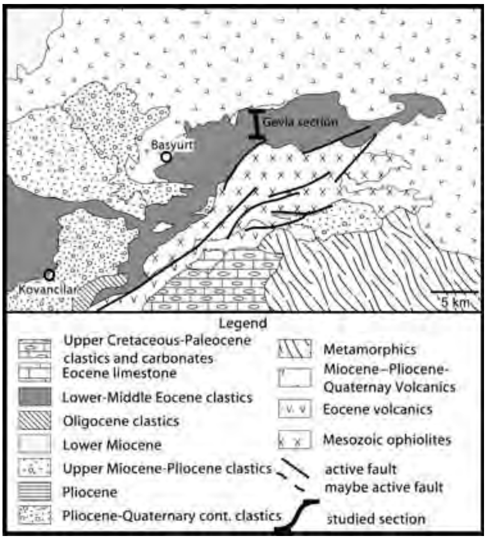

Fig. 5. Simplified tectonic and geological map of the easternmost part of the Elazığ basin. The trajectory of the studied section, called Gevla, is about 15 km NE of the city Basyurt and covers the interval between Eocene limestones and Miocene volcanics to the north. For key to the lithologies and/or ages refer to Legend (drawn after Geological map of Turkey (Şenel 2002)).

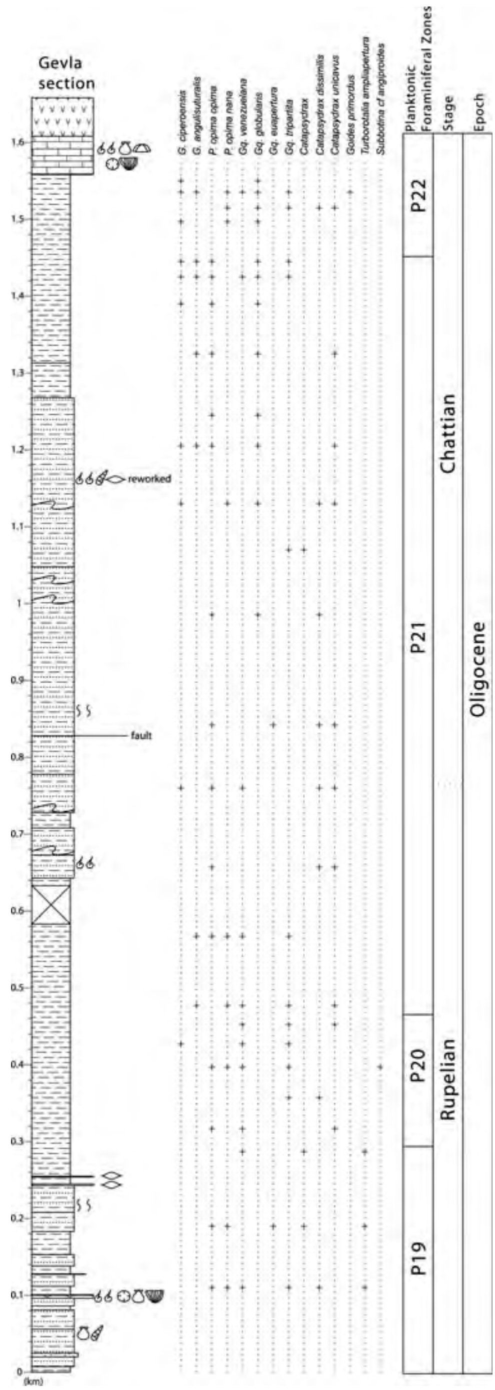

Fig. 6. Lithological column of the studied Gevla section in the Elazığ basin with the biostratigraphic results. The age model is based on planktonic foraminifers and macrofossil assemblage in the 50 m of stratigraphy. Planktonic foraminifer occurrences have been correlated

Fig. 6. (*Continued*) to planktonic foraminifer zones, which, in turn, are tied to stages during the Oligocene resulting into a correlation to the Geological Time Scale. Refer to Legend in Figure 4 for key to lithologies, structures and fossils.

displaced nummulites and gastropods (for instance at 663 m and 1158 m), fining upward sequences and cross bedding. These layers are interpreted as turbiditic in origin. This succession is followed by about 300 m of blue clay, and the section ends with a 50 m thick limestone with bivalves (up to 5 cm), and clayey intervals with well preserved echinoderms, sponges and corals. These limestones, in turn, are covered by Miocene volcanic rocks. In total, the section is about 1.6 km thick.

Slumping at several levels within the succession indicates an unstable submarine slope. Internal folding is not observed within the succession. The entire succession gently dips towards the NW.

Biostratigraphic results of the Elazığ basin

Hand samples were collected from about every 20 m throughout the entire section, but not every sample contained (diagnostic) planktonic and/or benthic foraminifers. The number of foraminifers is extremely variable and most likely fluctuates with changes in terrigenous clastic input. Preservation is generally poor, with specimens mostly recrystallized and frequently distorted. The overall aspects of the planktonic foraminiferal fauna in this section is similar to that of the Muş section, which means that the foraminiferal fauna is dominated by globoquadrinids and catapsydracids with occasional occurrences of *Globigerina ciperoensis* and *Globigerina angulisuturalis* pointing to an Oligocene age for this section (Fig. 6) (Berger & Miller 1988; Spezzaferri & Premoli Silva 1991). The presence of *Turborotalia ampliapertura* up to and including level 287 m (TR 244) provides evidence that the lower part of the section correlates with planktonic foraminiferal biozone P19 of Berger & Miller (1988), which is late Rupelian, early Oligocene, in age (Berggren *et al.* 1995). The lowest occurrence of *Globigerina angulisuturalis* is recorded at 477 m (TR 250) which in terms of the zonal scheme of Berger & Miller (1988) would mark the top of biozone P20 although it should be noted that *Globigerina angulisuturalis* is neither frequent in this section nor does it display very prominent U-shaped sutures. Typical *Paragloborotalia opima opima* is present from level 317 m (TR 245) up to and including level 1445 m (TR 293) indicating that the larger part of the Gevla section correlates with planktonic foraminiferal biozone

P21 of Blow (1969) and Berggren *et al.* (1995) which in terms of chronostratigraphy is latest Rupelian to early Chattian in age (Berggren *et al.* 1995). The top of the section post-dates the highest occurrence of *Paragloborotalia opima opima*, and correlates to the basal part of the late Chattian planktonic foraminiferal biozone P22 (Berger & Miller 1988), which is evidenced by the joint presence of *Paragloborotalia opima nana*, *Globigerina ciperoensis*, *Globigerina angulisuturalis* and *Globigerinoides primordius*.

The macrofossil assemblage from the upper 50 m in this section is similar to the assemblage in the uppermost 40 m of the eastern transect in the Muş basin (Figs 3 & 4). Both assemblages bear a typical late Chattian pectinid fauna with *Amussiopecten labadyei* and *A. subpleuronectes. Pecten arcuatus* (Brocchi 1814), a widespread Oligocene species, a typical Western Tethys element, is present as well, along with the thin-shelled lucinid bivalve *Anodontia globulosa* (Deshayes, 1830). The dominance of such thin shelled species might indicate a slightly deeper environment than in the corresponding section of the Muş basin, yet not deeper than the medium deep sublittoral environment (Mandic and Piller 2001).

The LO of *Turborotalia ampliapertura* has been calibrated to 30.3 Ma within Chron 11r (Berggren *et al.* 1995). The highest occurrence of this species in level 287 m (TR 244) therefore suggests an age older than 30.3 Ma for the bottom of the section. The LO of *Paragloborotalia opima opima* in level 1445 m (TR 293) has been recently recalibrated to 27.456 Ma within Chron 9n at ODP Site 1218 (Wade *et al.* 2007). This age provides a maximum age for the top of the section since the highest occurrence of *Paragloborotalia opima opima* occurs near the top of the section (TR 293). A correlation of the upper 50 m of the section to biozone P22 is supported by the mollusc fauna which indicates a late Chattian age.

Paleoenvironmental interpretations for the Elazığ basin

The depositional environment during the lower Rupelian (biozone P19) was first shallow marine as indicated by the occurrence of limestone with corals, bivalves and gastropods.

However, the depositional environment rapidly deepened as indicated by benthic foraminiferal depth marker species (*Cibicides* (*pseudo-*)*ungerianus*, *Gyroidina* spp. *Uvigerina* spp. and occasionally *Oridorsalis* spp.). Their presence up to the top indicates that the basin was 350 to 700 m deep during much of the Oligocene. The benthic foraminifers do not give any evidence for shoaling, although the limestone deposits at the top of the section and their macrofossils indicates a medium to shallow subtidal environment for the late Chattian.

Implications for the Elazığ basin

The first 260 m of the studied section was deposited under shallow marine conditions during Rupelian (biozone P19). This was followed by a rapid deepening during the Rupelian and the deposition of about 1.3 km in a relatively deep marine (300 to 750 m) environment. During the late Chattian (biozone P22), the basin experienced rapid shoaling to medium deep sublittoral conditions, preferred conditions for echinoids and bivalves. The inferred late Chattian age of the macrofossils in the top of the section indicates that the final emergence of the basin must have occurred shortly after the Chattian followed by widespread Miocene volcanism.

The numerous internal slumping and sandstone layers, referred to as turbidites, indicate a submarine, unstable slope. The entire succession is interpreted as flysch deposited in a deep marine basin, comparable to the Muş basin. Thus, during the Oligocene, rapid (15–30 $^{cm}/_{ka}$) sedimentation of clay and turbidites dominated the basin evolution.

These new biostratigraphic ages differ significantly from the geological map of Turkey (Şenel 2002) where these sediments are indicated as Lower to Middle Eocene. Our data suggests instead that these sediments were deposited under deep marine conditions during the Oligocene, from the Rupelian until the late Chattian, and, additionally, the shallow marine limestones at the top of the section are late Chattian in age. This data also differs from previous studies in the area (e.g. see Aksoy *et al.* 2005 for a compilation of data from the Elazığ basin) where the Eocene time has been identified as the main period of deep marine deposition and in the Oligocene time shallow marine deposits were restricted to the NW of the Elazığ basin. Our data however indicates that at least the eastern part of the Elazığ basin was deep marine throughout the Oligocene and shoaled and emerged only in the late Chattian, latest Oligocene.

Geological setting of the Kahramanmaraş basin

The Kahramanmaraş basin is located near the triple junction of the Arabian, African and Anatolian plates. As a result of the collision of Arabia and Eurasia along the Bitlis Suture a trough formed in front of the thrust sheets and was consequently filled by thick alluvial sediments and thick turbiditic flysch sequences (Lice Formation) (Şengör & Yılmaz 1981; Perinçek & Kozlu 1983; Karig & Kozlu 1990;

Yılmaz 1993). According to several studies (Perinçek 1979; Perinçek & Kozlu 1983), the Kahramanmaraş basin was part of this elongated foreland basin extending from Hakkari in southeastern Turkey, close to the border to Iran and Iraq, to Adana in southern Turkey (Fig. 2). This basin was also called the Lice trough (Dewey *et al.* 1986; Karig & Kozlu 1990; Derman & Atalik 1993; Derman 1999). Eocene deposits in the Kahramanmaraş area are part of the Arabian Platform (Robertson *et al.* 2004). They indicate a shallow marine depositional environment with local terrestrial input followed by allegedly lower to middle Miocene reefal limestone and claystone (Gül *et al.* 2005). Oligocene bioclastic limestones are reported only from the margin of the Kahramanmaraş area (Fig. 7) (Karig & Kozlu 1990). Basal shallow marine red-bed and basalt sequences of the Kalecik Formation have an inferred age of late Burdigalian to Langhian (Karig & Kozlu 1990). The retreat of marine conditions and basin deformation was assumed to have taken place in the late Miocene, although the age control was not documented (Karig & Kozlu 1990).

Three separate sections (Figs 7, 8a & b), all north of the city of Kahramanmaraş, are been studied by us. The lower 200 m were sampled in the hills in the southern part of the main basin (Hill section), the following about 4.6 km along the road north of Kahramanmaraş (Road section) and the upper 1.5 km stratigraphic transect near the village of Avcılar (Avcılar section).

The base of the Hill section consists of nummulitic limestones according to the Geological Map of Turkey (Şenel 2002) of Eocene age, followed by red, conglomeratic sediments with several basalt layers.

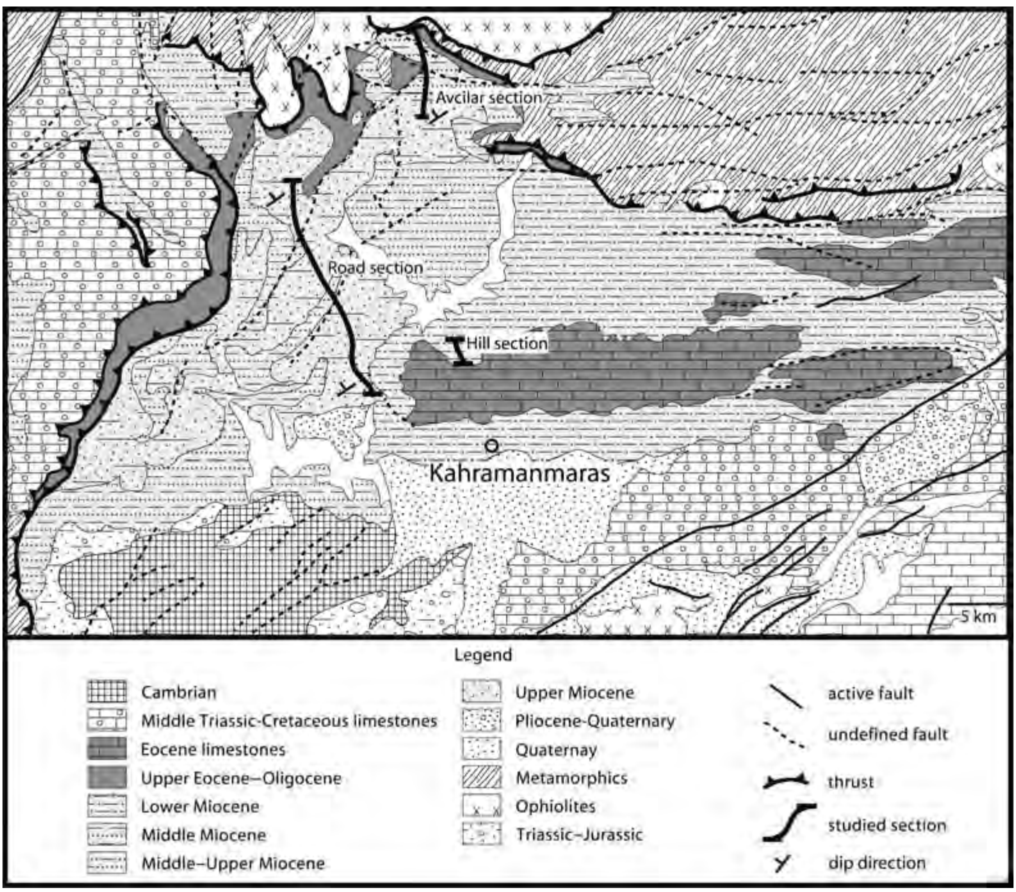

Fig. 7. Simplified tectonic and geological map of the Kahramanmaraş area including the trajectories of the three studied sections north of the city of Kahramanmaraş: (**1**) the lowermost 200 m in the Hill section. (**2**) about 4.6 km of succession along the road (Road section). (**3**) the upper 1.6 km up to the thrust studied in the Avcılar section in the northernmost part of the region. Refer to Legend for key to lithologies and/or ages (drawn after Geological map of Turkey (Şenel 2002)).

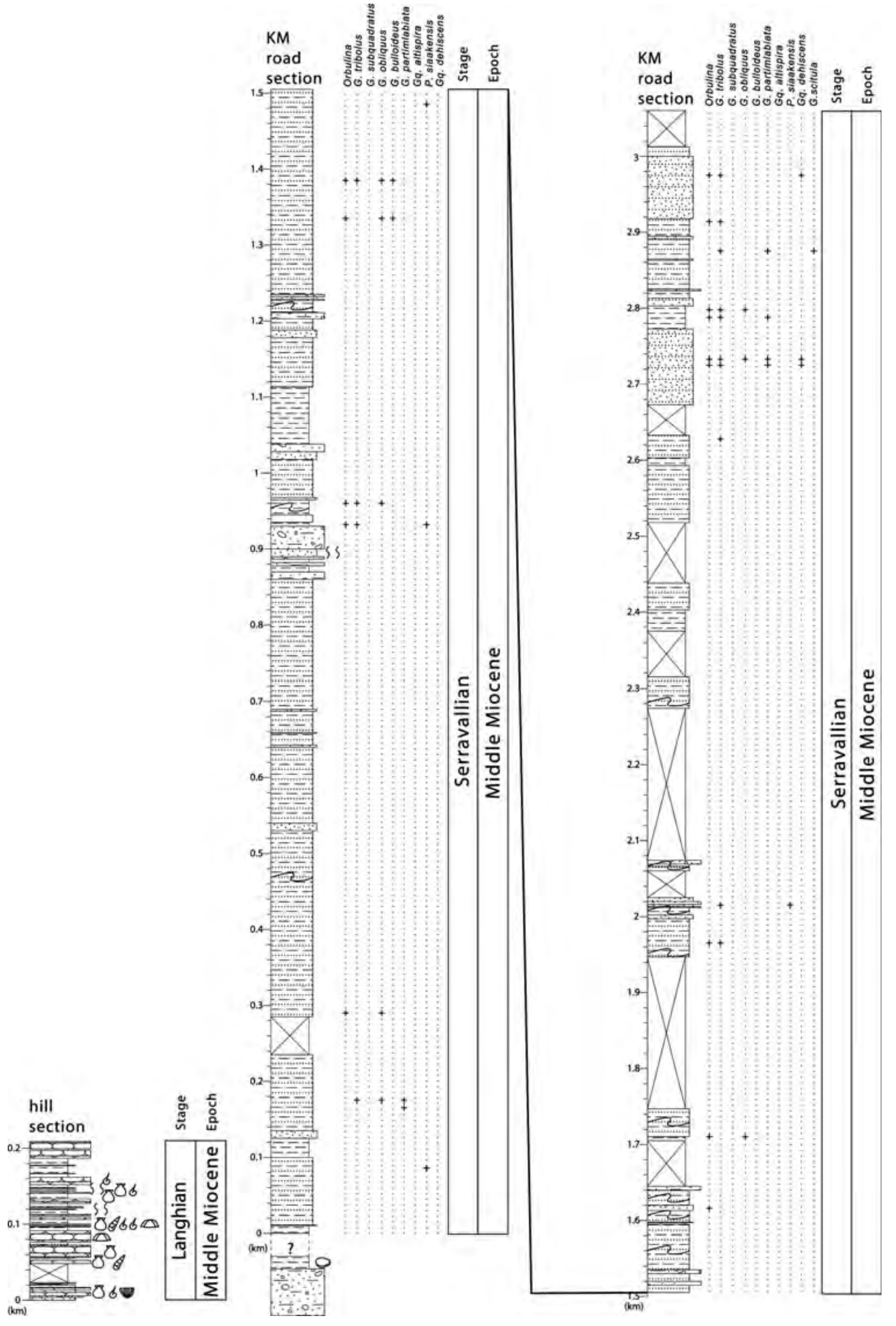

Fig. 8. (**a**) Lithological column of the Hill section and part of the Road section (*c*. 3 km) in the Kahramanmaraş basin with the biostratigraphic results. The age model is based on planktonic foraminifer occurrences, which delineate the correlation of the Hill section to the Langhian and the first *c*. 3 km of the Road section to the Serravallian.

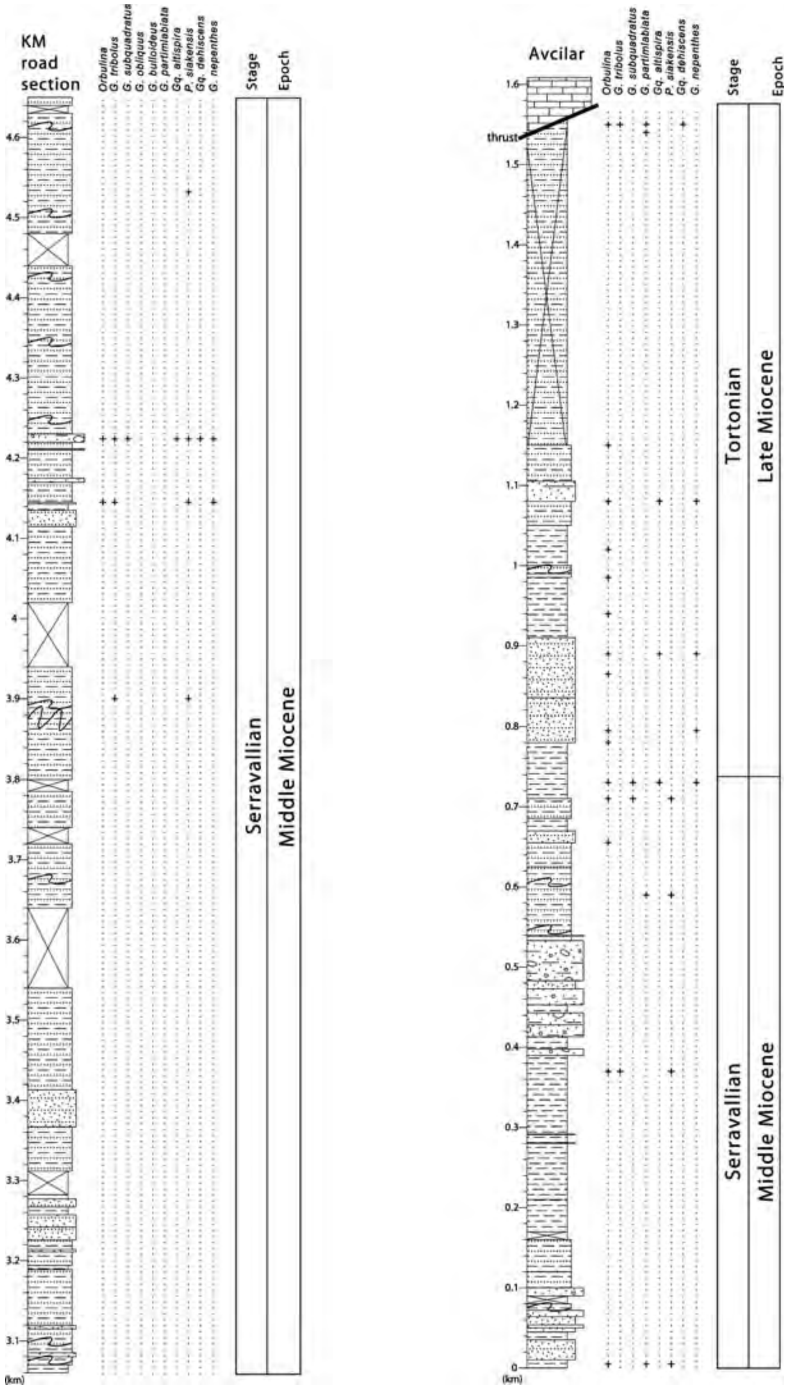

Fig. 8. (*Continued*) (**b**) Lithological column of the upper *c*. 1.6 km of the Road section and the Avcılar section in the Kahramanmaraş basin with the biostratigraphic results. The age model is based on planktonic foraminifer occurrences, which delineate the correlation of the upper *c*. 1.6 km of the Road section to the Serravallian and the lower part of the Avcılar section to the Serravallian, probably overlapping with the Road section, and from *c*. 700 m to the Tortonian based on the LCO 0of *Globigerinoides subquadratus*. Refer to Legend in Figure 4 for key to lithologies, structures and fossils. KM = Kahramanmaraş.

The studied section begins with a 200 m thick succession of nodular limestone (10–15 m thick) alternating with bluish marls. The limestones contain macrofossils such as corals, sponges, echinoderms, bivalves and gastropods, indicating a shallow marine environment. This succession grades into an alternation of marl and sandstones layers, which show typical Bouma sequences and flute casts, which are indicative for a turbiditic origin.

The base of the Road section, however, exposes a strongly different succession, where almost 1 km of the stratigraphy is dominated by large conglomerate lenses. This thick succession of conglomerates contains sand lenses showing cross bedding, indicative of interfingering of braided river channels. This thick fluvial succession probably forms, at least in part, the lateral equivalent of the shallow marine succession in the Hill section. This conglomeratic succession is followed by a level rich in oysters, indicating a transition into shallow marine conditions. This then grades quickly into a very thick succession of alternating marl and sandstone (as mentioned above) with occasional conglomeratic layers, interpreted as debris flows, which cut through the stratigraphy. The sandstones show typical characteristics for turbidites, such as flute casts and Bouma sequences. Some intervals are dominated by massive sandstone layers and/or debris flows, while others are characterized by mainly clay. Slumping can be easily differentiated from (minor) internal folding, both occurring throughout the section. Internal folding, however, does not occur often. The Road section ends at the highest point in the topography along the road going NNW from Kahramanmaraş and since the stratigraphy dips to the NW, a continuation of the stratigraphy was found to the NE, the Avcılar section (Fig. 7). This section was sampled assuming sufficient overlap with the Road section, until the stratigraphy was cut unconformably by carbonates (Figs 8a & b). The stratigraphy of the Avcılar section also consists of a thick succession (about 1.5 km) of mudstone and sandstone with occasional conglomeratic layers, interpreted as debris flows. No shoaling trend based on sedimentological characteristics has been observed towards the top of the section, which ends abruptly with the overthrusting of pre-Neogene carbonates, which were emplaced roughly from North. The upper 400 m were not exposed, except for a few meters just underneath the thrust (Fig. 8b).

Biostratigraphic results of the Kahramanmaraş basin

About every 20 m hand samples were taken for biostratigraphy. Only few samples, however, turned out to be useful for biostratigraphy and/or paleobathymetry. Benthic foraminifers in the lower part of the Kahramanmaraş basin, from the Hill section (Fig. 8a) are dominated by milliolids and representatives of Ammonia, Textularia, Nonion and Elphidium indicating shallow marine (inner shelf) conditions although some samples, at 146, 182 and 198 m (TR 9, 12 and 14), respectively, contain few planktonic foraminifers such as *Globigerinoides trilobus*, *Globigerinoides obliquus* and *Orbulina*. Their presence would indicate that the lower part of the Kahramanmaraş sequence postdates the *Orbulina* datum at 14.74 Ma (Lourens *et al.* 2004). This age assignment is further constraint by the presence of the calcareous nannofossil *Cyclicargolithus abisectus* and rare *Spenolithus heteromorphus* along with the absence of *Helicosphaera ampliaperta*. This assemblage is tentatively assigned to NN5 (Martini 1971) indicating a Langhian age.

Orbulina is common in the samples from the Road section. The rare occurrences of *Globoratalia partimlabiata* in the Road section at 165, 175, 2725, 2788 and 2875 m (TR 20, 21, 71, 73 and 77), respectively, are remarkable because they represent the first recording of this species in Turkey. It has been first described from the middle Miocene of Sicily (Ruggieri & Sprovieri 1970) and since then reported from the Mediterranean (amongst others Foresi *et al.* 1998 and references herein; Hilgen *et al.* 2000; Turco *et al.* 2001; Foresi *et al.* 2002*a*, *b*; Hilgen *et al.* 2003; Abels *et al.* 2005) and adjacent North Atlantic (Chamley *et al.* 1986) and even from the Indian Ocean off NW Australia (Zachariasse 1992). Ages of FO and LO of *Globoratalia partimlabiata* in the Mediterranean have recently been recalibrated at 12.771 and 9.934 Ma (Hüsing *et al.* 2007). Its presence in the basal part of the Road section along with *Globigerinoides subquadratus* at 4224 m (TR 114) indicates that the larger part of the Road section, up to 4200 m, is Serravallian, Middle Miocene, in age, since the base of the Tortonian has been defined at a level close to the Last Common Occurrence (LCO) of *Globigerinoides subquadratus* (Hilgen *et al.* 2000, 2005) with a new astronomical age of 11.625 Ma (Hüsing *et al.* 2007). It cannot be excluded that the Road section terminates into the lowermost Tortonian since *Paragloborotalia siakensis* at 4532 m (TR 120) is the only biostratigraphic marker species present above 4200 m.

In the Avcılar section, the occasional occurrences of *Paragloborotalia siakensis* up to 710 m (TR151) along with *Globorotalia partimlabiata* at 590 m and *Globigerinoides subquadratus* at 710 and 730 m, respectively, (TR 151 and 152) indicate that the lower 700 m of this section is also Serravallian in age. The absence of *Globigerinoides* *subquadratus* and *Paragloborotalia siakensis* in the upper part of the Avcılar section along with the presence of *Globorotalia partimlabiata* near the top of the section (TR 169 and 172) suggests that the section extends up into the Tortonian.

The Avcılar section has been sampled assuming a significant overlap with the Road section and if the uppermost part of the Road section indeed extends into the Tortonian, we might assume an overlap of up to 1 km between these two sections. The maximum age range of the road section and Avcılar section is indicated by the age range of *Globoratalia partimlabiata* of 12.771–9.934 Ma (Hüsing *et al.* 2007).

Paleoenvironmental interpretations for the Kahramanmaraş basin

Deposition of the lower 200 m occurred in shallow marine conditions, as indicated by the occurrence of benthic foraminifers, calcareous nannofossils, poorly preserved echinoderms, gastropods and the large estuarine oyster *Crassostrea gryphoides* (Schlotheim, 1820). This large-sized Oligocene to Miocene species is restricted to brackish water environments with a high nutrient input and prefers building colonies on mud flats of outer estuaries (Slack-Smith 1998). Benthic foraminiferal species of the flysch succession from the road and Avcılar, such as *Cibicides (pseudo-)ungerianus*, *Gyroidina* spp., *Uvigerina* spp., *Oridorsalis* spp. and occasionally *Siphonina reticulata*, suggest water depths between 350 and 750 m during deposition of this section without evidence for shoaling towards the top, which is, in turn, cut by the thrust in the Avcılar section.

Implications for the Kahramanmaraş basin

During the Langhian – early Serravallian, shallow marine conditions prevailed in the Kahramanmaraş basin. The basin deepened during late Langhian/early Serravallian as indicated by the change from limestones and/or conglomerates to an alternation of marl and turbidites. Since neither in the lithology, nor in the biostratigraphic data, a shoaling trend towards the top of the section is observed, deep marine conditions (350–750 m) prevailed in the basin until the early Tortonian.

We interpret the whole section as a characteristic foreland basin flysch succession (as Dewey 1986; Karig & Kozlu 1990; Derman & Atalik 1993; Derman 1999). Assuming the Road and Avcılar sections were sampled with no overlap, the maximum thickness is about 6.1 km, but assuming an overlap of up to 1 km, the maximum thickness is about 5.1 km. It is very difficult to estimate a sedimentation rate for this basin, because three sections were sampled with an unknowing overlap. Secondly the accuracy of the age indicative biostratigraphic events is uncertain due to poor preservation and poor sampling resolution. Furthermore, the age indicative biostratigraphic events, LCO of *Globigerinoides subquadratus* and LO of *Globorotalia partimlabiata* are recorded in different sections, which makes the determination of the sedimentation rate between these two calibration points nearly impossible. The sedimentation rates thus vary much, between 50 and 450 cm/ka, but including slumps, debris flows and turbidites deposited in front of and during the activity of the thrust that now covers the top of the sequence. Taking a conservative estimate of 100 to 200 cm/ka, also because the LO of *Globigerinoides subquadratus* might not correspond to the true LCO, dated at 11.625 Ma (Hüsing *et al.* 2007), but might be higher in the stratigraphy, the age of the youngest flysch is about 11 Ma.

This age range, from Langhian to early Tortonian, differs significantly from the assigned Oligocene age of the open marine flysch and limestone deposits in the Muş and Elazığ basins. The continuous marine sedimentation in the Kahramanmaraş basin from Langhian to early Tortonian at a constant depth indicates that tectonic subsidence, possibly up to the order of 5 km, dominated the evolution of the basin.

Discussion

Evolution of the east Anatolian basins

The stratigraphic results from the east Anatolian basins are summarized in Figure 9, and are correlated to the Geological Time Scale (Gradstein *et al.* 2005). This figure schematically illustrates that the individual basins belong to two different, major basins: (1) a basin north of the Bitlis–Pötürge Massif, encompassing the Elazığ and Muş basins, which was filled with clastic mass flow deposits during the Rupelian and Chattian (Oligocene); (2) a basin south of the Bitlis–Pötürge Massif, a foreland basin which was filled with clastic sediments during the Langhian, Serravallian and early Tortonian (Middle and early Late Miocene).

The Muş and Elazığ basin, both north of the Bitlis–Pötürge Massif, show similar stratigraphic evolution during the Oligocene: Deepening of the basin occurred during the Rupelian and deep marine conditions (350–750 m) prevailed until the Chattian. Both basins evidence a shoaling trend during the Chattian. The macrofossil assemblage in the sandy limestones, such as molluscs and

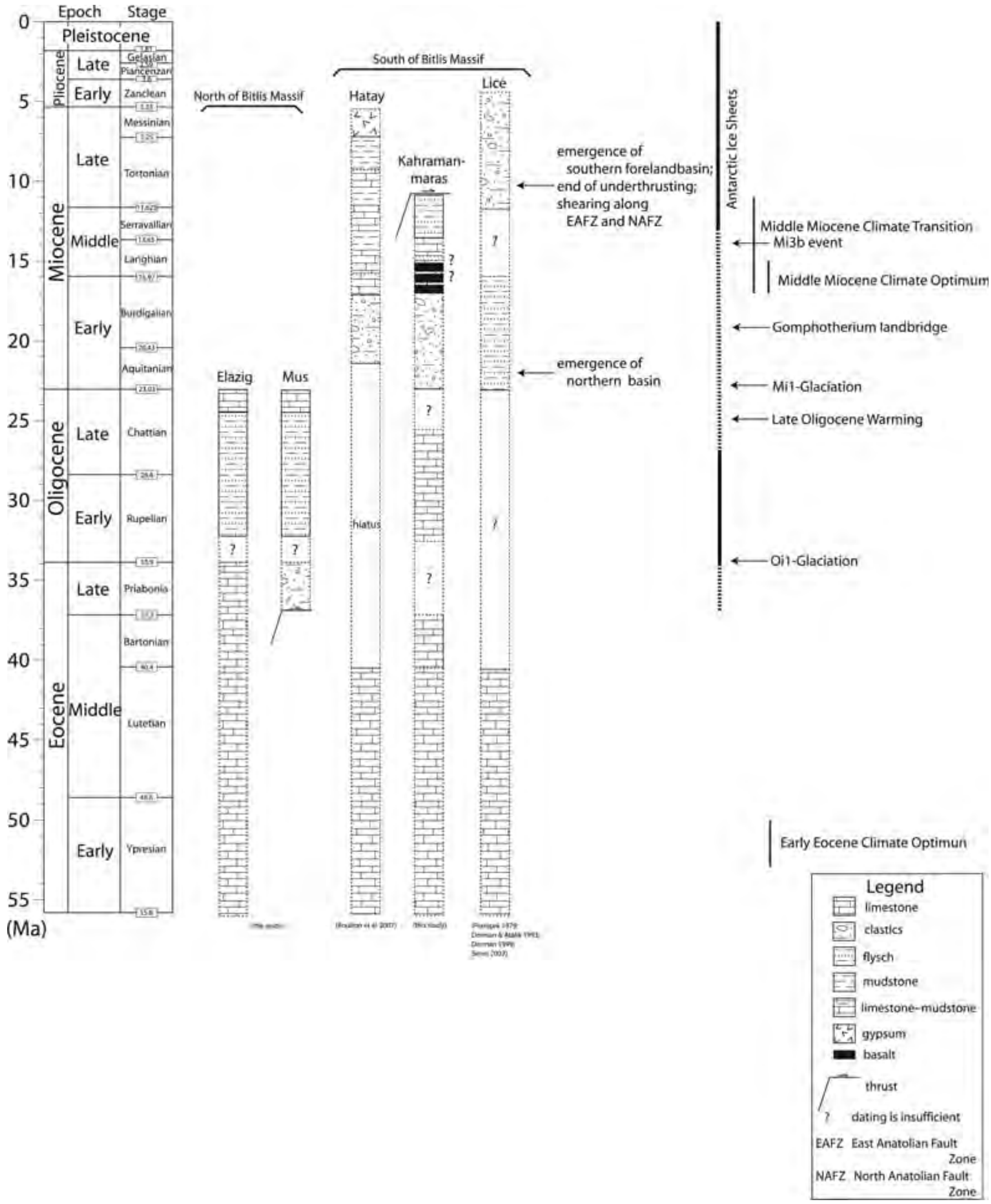

Fig. 9. Chronology of Paleogene–Neogene foreland basin development in Southeastern Turkey. The evolution of the three basins from this study, Muş, Elazığ and Kahramanmaraş, is compared to the Hatay and Lice regions. For purpose of comparison the stratigraphy of all areas has been simplified. Refer to Legend for key to lithologies and structures. Dashed lines of the lithological columns indicate uncertain ages for the section. All ages are given in Ma.

echinoderm, indicates shallow marine, tropical to subtropical deposition, similar to a sheltered lagoon environment, with species preferring subtidal and intertidal environments. In addition, the macrofossil assemblage is comparable to assemblages found in Central Iran, the entire northern coast of the Western Tethys, the Central Paratethys and the lower Indus Ocean, indicating an open marine connection between these marine realms prior to the emergence during the late Chattian. We suggest that the Muş and Elazığ basins were connected forming a large east–west elongated deep marine basin during Rupelian and Chattian.

The rapid deepening of the basin north of the Bitlis Massif may be related either to onset of flexural subsidence associated with (northward) underthrusting within the prevailing overall compressional regime (e.g. for the Elazığ basin Cronin (2000*a*, *b*)) or to the late stages of an extensional deformation period that persisted in the Paleocene and Eocene (e.g. in the Malatya basin (Kaymakçi *et al.* 2006) and in the Muş area (Şengör *et al.* 1985)). These two scenarios are controversial and our data provide age and depth constraints on the Muş and Elazığ basins, which do not allow to eliminate or prefer either of these scenarios.

In the Kahramanmaraş basin, south of the Bitlis–Pötürge Massif, shallow marine sediments were deposited during the Langhian. A rapid deepening during the Langhian to Serravallian indicated by the rapid transition to deep marine (350 to 750 m) flysch deposits, was followed by deposition of continuously deep marine sediments until the early Tortonian. Since no shoaling trend is observed we suggest that the age of the youngest flysch underneath the thrust, biostratigraphically dated as early Tortonian, at about 11 Ma, coincides with the end of underthrusting.

The rapid deepening of the foreland basin south of the Bitlis–Pötürge Massif during the Langhian to Serravallian, followed by the deposition of a thick deep marine flysch succession, can be interpreted as northern Arabia and more specifically the area of the Kahramanmaraş basin, entering into the subduction zone underneath Anatolia. The end of flysch deposition and thus the youngest flysch underneath the thrust of the overriding Bitlis–Pötürge Massif could be envisaged as the end of subduction, thus underthrusting, at about 11 Ma (Tortonian), which is likely followed by rapid uplift in the region. Such episodes of very rapid uplift and folding of foreland basins associated with the stalling of underthrusting is, for example, also well documented in the western Aegean region (Richter *et al.* 1978; van Hinsbergen *et al.* 2005*a*, *c*, *d*).

Our new results of the Kahramanmaraş basin can be compared to previously published data from the Hatay (around Antakya) and Lice regions (see Figs 2 & 9), which have been interpreted as foreland basins related to southward thrusting of the Taurus allochton over the Arabian continental margin belonging to an east–west elongated foreland basin overlying the Arabian promontory (e.g Perinçek 1979; Karig & Kozlu 1990; Derman and Atalik 1993; Derman 1999; Robertson *et al*. 2004).

The stratigraphy and chronology of the Hatay area is very similar to the evolution of the Kahramanmaraş basin. The chronology in the Hatay area has recently been redefined based on micropaleontological dating (Boulton *et al.* 2007) and we can therefore correlate the evolution of the Kahramanmaraş basin to the Hatay area. The stratigraphy in the Hatay area is characterized by a pronounced angular unconformity between middle Eocene and overlying lower Miocene sediments, with a hiatus in the Oligocene (Boulton & Robertson 2007). Sedimentation resumed during the Aquitanian to Burdigalian (Early Miocene) with deposition of conglomerates and mudstones. In the Kahramanmaraş area, Derman & Atalik (1993) and Derman (1999) assigned a lower Miocene age to the about 1 km thick series of fluvial deposits, which precede the thick flysch deposits. We, however, have no age constraints on the fluvial deposits and can therefore not confirm an Early Miocene age. During the Langhian both basins experienced shallow marine limestone deposition and the basin progressively deepened during Serravallian to Tortonian (Boulton *et al.* 2007; Boulton & Robertson 2007). The deposition of shallow marine limestones in the Hatay area have been interpreted to be related to further loading of the lithosphere in response to flexural subsidence and the progressive deepening to flexural control (Boulton & Robertson 2007). Where flexural subsidence exceeded the build up of a carbonate platform hemipelagic sediments were deposited (Boulton *et al.* 2007; Boulton & Robertson 2007). A similar scenario can be envisaged for the Kahramanmaraş basin indicated by coarsening upwards in the thick flysch deposition. In the Hatay area, by the end of the Miocene, the tectonic regime changed and the Pliocene–Quaternary Hatay Graben structure was formed in a transtensional setting related to the EAF (Perinçek & Cemen 1990; Boulton *et al.* 2007; Boulton & Robertson 2007), while deep marine sediments in the Kahramanmaraş basin were overthrusted already during the early Tortonian. This comparison might indicate a diachronous evolution of these two basins with the Kahramanmaraş basin emerging during the Tortonian and the Hatay area remaining open marine until the deposition of Messinian evaporites, or different basin evolutions due to the relatively western position of the Hatay area thus closer to the present-day extent of the eastern Mediterranean.

A comparison to the Lice basin, which is situated to the east of the Kahramanmaraş basin, would evidently give constraints on the syn- or diachronous evolution of the southernmost, Arabian foreland basin. However, the chronology of sediments in the Lice basin is scarcely documented in the literature (e.g. Perinçek 1979; Dewey 1986; Karig & Kozlu 1990; Robertson *et al.* 2004). On the geological map of Turkey (Şenel 2002) shallow marine clastic and carbonatic sediments have been indicated as Early Miocene in age and continental clastic rocks as Middle to Late Miocene in age. This succession would pre-date the flysch deposition in the Kahramanmaraş and Hatay area and would indicate diachronous evolution of the elongated Arabian foreland basin. Other studies assigned, however without documenting an age control, a Tortonian age to the Lice flysch (Dewey 1986). If the flysch deposits in the Lice, Kahramanmaraş and Hatay area are indeed synchronous, we would assume a synchronous evolution of the Arabian foreland basin which emerged during the Tortonian. However since the chronology of the Lice basin is not well documented, firm correlation to the Kahramanmaraş basin and Hatay area remains impossible (see question marks in Fig. 9).

The basin south of the Bitlis–Pötürge Massif including the Kahramanmaraş, Hatay and Lice basins, is interpreted as the southernmost and youngest foreland basin in the east Anatolian fold-and thrustbelt, which formed as a large east–west trending foreland basin on the subducting Arabian plate. The end of underthrusting in the Kahramanmaraş basin is dated at about 11 Ma, but might have been diachronous relative to the emergence of the Hatay and Lice basin.

Tectonic closure of the eastern Tethys gateway

Based on the presented data herein, we envisage the following scenario for the Oligocene to Miocene evolution of the basins north and south of the Bitlis Massif in SE Turkey (Fig. 10). During the early Oligocene, marine sediments were deposited in a large basin to the north of the Bitlis–Pötürge Massif (Fig. 10a). However, our data does not allow us to constrain whether the deepening of

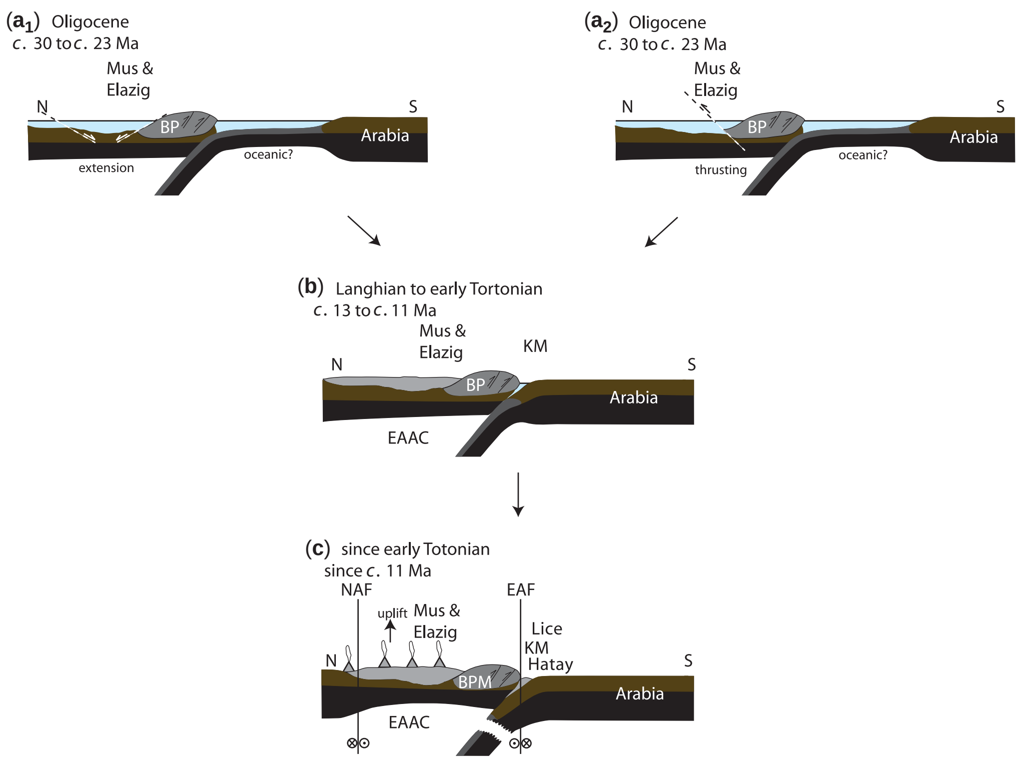

Fig. 10. The evolution of the Oligocene–Miocene basins in SE Turkey are illustrated schematically in three major phases: (**a**) during the Oligocene from *c.* 30 to *c.* 23 Ma: a marine basin was situated north of the Bitlis–Pötürge (BP) until the end of latest Oligocene, Chattian, when this basin emerged; (**a$_1$**) related to extension, (**a$_2$**) related to thrusting. (**b**) during the Langhian to early Tortonian (*c.* 13 to *c.* 11 Ma): areas of present-day northern Arabia enter the position of the foreland basin South of the BP and the northern Arabian promontory was subducted underneath the BP from the Langhian until the early Tortonian, *c.* 11 Ma, and finally. (**c**) since the early Tortonian to Recent: the end of large-scale underthrusting at *c.* 11 Ma in east Anatolia coincides with the onset of collision-related volcanism, uplift of the East Anatolian Accretionary Complex (EAAC), the onset of shearing along the North and East Anatolian Faults (NAF and EAF). Refer to text for further discussion. BP = Bitlis-Pötürge; BPM = Bitlis-Pötürge Massif; NAF = North Anatolian Fault; EAF = East Anatolian Fault; EAAC = East Anatolian Accretionary Complex; KM = Kahramanmaraş.

the basin during the Rupelian was related to either large scale extension (Fig. $10a_1$) or thrusting (Fig. $10a_2$), with the Bitlis–Pötürge Massif situated on the overriding plate. Nevertheless, our data suggest that until the Chattian, flysch was deposited in a deep marine environment, as recorded in the area of Muş and Elazığ. The emergence of the basin north of the Bitlis–Pötürge Massif during the late Chattian (see also Fig. 9) probably coincides with the accretion of the Bitlis–Pötürge Massif to the Anatolian plate.

On the southern side of the Bitlis–Pötürge Massif, oceanic subduction was probably ongoing due to Africa/Arabian's relative distal position (e.g. Besse & Courtillot 2002).

During the Langhian to Serravallian the basin south of the Bitlis–Pötürge Massif deepened rapidly, which might be related to the northern Arabian promontory, the present-day northern margin of the Arabian plate (Kahramanmaraş, Hatay and Lice basins), entering into the subduction zone (Fig. 10b) below the Bitlis–Pötürge Massif. During the Serravallian and early Tortonian, the Kahramanmaraş basins remained deep marine indicated by thick flysch deposition until, at least, the early Tortonian. The youngest flysch underneath the thrust in the Kahramanmaraş area, biostratigraphically dated at about 11 Ma, might be linked to the end of the large-scale underthrusting (subduction) in eastern Anatolia (Fig. 10c). In models proposed by Keskin (2003) and Şengör (2003), it is assumed that the Bitlis–Pötürge Massif was accreted with Arabia during late Eocene, while Robertson *et al.* (2004) suggested Late Oligocene–earliest Miocene time. Our data, on the other hand, indicate the presence of a deep marine realm between the Bitlis–Pötürge Massif and Arabia during Serravallian and early Tortonian, which we suggest is associated with the continuous subduction of Arabia underneath the Anatolian plate.

The timing of the end of thrusting agrees with the onset of the collision-related volcanism at about 11 Ma north of the present-day suture line (Keskin 2003), the uplift of the East Anatolian Accretionary Complex inferred to start around 11 Ma onwards (Şengör *et al.* 2003) and the onset of the North and East Anatolian Fault (Dewey 1986; Hubert-Ferrari *et al.* 2002; Şengör *et al.* 2005) (Fig. 10c). Collision-related volcanism and uplift of the East Anatolian High Plateau despite the relatively thin crust (45 km) has been related to an anomalously hot mantle underneath the eastern Anatolia (Keskin 2003; Şengör *et al.* 2003). This, as well as the onset of westward extrusion of Anatolia and the onset of formation of the North and East Anatolian faults, have been explained by slab detachment at about 11 Ma in eastern Anatolia (Keskin 2003; Şengör *et al.* 2003; Şengör *et al.* 2005; Faccenna *et al.* 2006), which is in line with a recent tomography study of Hafkenscheid *et al.* (2006). Our new results from the Kahramanmaraş area can thus be considered in line with the previously suggested scenarios, the end of underthrusting and the onset of extrusion of Anatolia in the Late Miocene (at about 11 Ma) (Fig. 10c).

Constraints on the closure of the eastern Tethys gateway

The continuous northward migration of the African–Arabian plate led to the disruption of the Tethys seaway and the final closure related to continental collision of Arabia and Eurasia. The paleogeographic extent of the Tethys during the Paleogene and Neogene thus underwent significant changes until the connection was finally closed. Several authors suggested that the final closure of the eastern Tethys gateway may have resulted in significant changes in the paleoceanographic circulation and consequently in a major change in global climate (e.g. Woodruff & Savin 1989, 1991; Jacobs *et al.* 1996; Flower & Kennett 1993; Yılmaz 1993).

Our data from eastern Anatolia indicate that a deep marine connection was present north of the Bitlis–Pötürge Massif from Rupelian to late Chattian. The shoaling of this northern basin during the late Chattian led to severe disruption between an eastern (Indian Ocean) and western (Mediterranean) marine domain; particularly the deep-water circulation was disrupted during the Chattian. The emergence of this basin after the late Chattian resulted in the closure of at least this branch of the southern Neotethys and coincides with the late Oligocene warming, reducing the extent of the Antarctic ice, which was punctuated by the Mi-1 glaciations around the Oligocene–Miocene boundary (Zachos *et al.* 2001).

Other studies suggest that the Tethys seaway was open until the early Miocene and became severely restricted during the Burdigalian (*c.* 19 Ma), when mammal fauna and shallow marine macrofaunal records from the eastern Mediterranean region indicate the existence a landbridge (*Gomphotherium* landbridge) connecting Africa/Arabia and Eurasia (Popov 1993; Rögl 1998, 1999; Harzhauser *et al.* 2002, 2007). These authors claim that, since *c.* 19 Ma, biogeographic separation between the Mediterranean-Atlantic and Indo-Pacific regions persisted; despite some short-lived periodic marine connections between the two domains until the middle Miocene (Rögl 1999; Meulenkamp & Sissingh 2003; Golonka 2004; Harzhauser *et al.* 2007). If a causal link between the closure of the eastern Tethys gateway and global climate cooling exists, a major change in global, or at least local, climate must be expected during the Burdigalian time. The most significant climatic change during the Burdigalian, as evidenced in both the $\delta^{18}O$ and

δ^{13}C record, indicates a change from a cooling to a warming trend which led into the Mid-Miocene Climatic Optimum (Zachos *et al.* 2001).

Our data suggest that if a deep marine connection between the eastern and western marine realm persisted after the late Chattian, it was probably located south of the Bitlis–Pötürge Massif. The studied basins along the south Bitlis suture zone in eastern Anatolia, however, do not comprise the stratigraphic interval between late Chattian and Langhian (25–15 Ma). Consequently, it is not possible to constrain the tectonic evolution and the palaeogeographic extent of the Tethys seaway during this time interval from the stratigraphic record of the east Anatolian basins.

In the context of global climate change, the main oxygen and carbon isotope shift corresponds to the second and major step (Mi3b) of the middle Miocene global cooling, and has recently been astronomically dated at 13.82 Ma, close to the Langhian–Serravallian boundary, in a section on Malta (Abels *et al.* 2005). The middle Miocene decrease in δ^{18}O values was previously attributed, amongst other hypotheses, to a possible local expression of the isolation of the Mediterranean Sea from the Indo-Pacific Ocean (van der Zwaan & Gudjonsson 1986; Jacobs *et al.* 1996). Abels *et al.* (2005), however, show that this event coincides with a period of minimum amplitudes obliquity related to the 1.2-Ma cycle and minimum values of eccentricity as part of both the 400– and 100-ka eccentricity cycle, thus suggesting astronomical forcing (see Abels *et al.* 2005).

If a link between gateway closure and middle Miocene climate change exists, the south Bitlis gateway must have re-opened to finally close in the middle Miocene, which is very unlikely in an overall converging setting. Moreover, our data does not show evidences for a final closure of the seaway in the middle Miocene. In contrast, the data from Kahramanmaraş indicates rapid deepening during the Langhian to Serravallian and prevailing deep marine conditions until the early Tortonian. This has been interpreted as related to continuous northward subduction underneath the Bitlis–Pötürge Massif and finally continental collision during the Serravallian to early Tortonian. Our data suggest that a deep marine connection located between the Bitlis–Pötürge Massif and Arabia, whether periodic or not, was disrupted at latest during the early Tortonian, giving an upper limit of *c.* 11 Ma to the final closure between the Indian Ocean and the Mediterranean along the northern Arabian. The above analysis shows that the end of foreland basin existence in SE Turkey – and therefore the closure of the southern Tethyan gateway – can not straightforwardly be linked to the middle Miocene climate change. Future assessment of the timing of the Tethys gateway closure should focus on detailed stratigraphy of the youngest foreland basins in SE Turkey, NW Iran, Syria and N Iraq, the region of the Bitlis–Zagros suture zone.

Conclusions

The marine basin north of the Bitlis–Pötürge Massif encompassing the Elazığ and Muş basins emerged during Chattian, which was followed by shallow marine limestone deposition during the late Chattian and finally closed after the late Chattian. This marks the disruption of the Tethys gateway north of the Bitlis–Pötürge Massif connecting an eastern (Indian Ocean) and western (Mediterranean Sea) domain.

The Kahramanmaraş basin south of the Bitlis–Pötürge Massif, probably linked to the Hatay and Lice basins, experienced shallow marine conditions during Langhian, rapidly deepened during Langhian to Serravallian and remained deep marine during the Serravallian and early Tortonian. No shoaling trend has been observed in the Kahramanmaraş basin and the age of the youngest flysch underneath the subduction-related thrust has been biostratigraphically dated at early Tortonian, at about 11 Ma. The end of flysch deposition in the Kahramanmaraş area is probably related to the end of subduction, thus the end of underthrusting. The age coincides with the onset of collision-related volcanism, uplift of the East Anatolian Accretionary Complex, and the timing of shearing along the NAF and EAF. Our new results suggest a strong link between the processes outlined above, which have been explained by slab detachment at about 11 Ma in eastern Anatolia.

This age, early Tortonian, about 11 Ma, is the youngest possible age for a deep marine connection between the Mediterranean-Atlantic and Indo-Pacific regions. We can thus constrain the timing of the final closure of a deep marine Tethys gateway to an upper limit of about 11 Ma. The emergence of the basin north of the Bitlis–Pötürge Massif during the late Chattian thus provides a lower limit of the closure of the eastern Tethys gateway.

In the southern basins marine foreland deposition was continuous during Serravallian and early Tortonian and our data does not support a link between the Middle Miocene climate cooling dated at 13.82 Ma and the closure of the eastern Tethys gateway. In contrast, the age of the youngest flysch deposits, thus the youngest foreland basin in SE Turkey is early Tortonian, about 11 Ma.

We thank C. Langereis, N. Kaymakci and E. Yılmaz for their help in the field and M. Triantaphyllou for the determination of nannofossils in the Kahramanmaraş section. We are also grateful for the constructive comments of E. Turco and N. Kaymakci, which led to a significantly improved manuscript. We acknowledge support by the Netherlands Research Centre for Integrated Solid Earth Sciences (ISES) and by the Netherlands Geosciences Foundations (ALW) with financial aid from the Netherlands Organization for Scientific Research (NWO). This work was carried out under the program of the Vening Meinesz Research School of Geodynamics (VMSG) and the Netherlands Research School of Sedimentary Geology (NSG).

References

ABELS, H. A., HILGEN, F. J., KRIJGSMAN, W., KRUK, R. W., RAFFI, I., TURCO, E. & ZACHARIASSE, W. J. 2005. Long-period orbital control on middle Miocene global cooling: Integrated stratigraphy and astronomical tuning of the Blue Clay Formation on Malta. *Paleoceanography*, **20**, 1–17.

AGARD, P., OMRANI, J., JOLIVET, L. & MOUTHEREAU, F. 2005. Convergence history across Zagros (Iran): constraints from collisional and earlier deformation. *International Journal of Earth Sciences*, **94**, 401–419.

AKSOY, E., TÜRKMEN, I. & TURAN, M. 2005. Tectonics and sedimentation in convergent margin basins: an example from the Tertiary Elazig basin, Eastern Turkey. *Journal of Asian Earth Science*, **25**, 459–492.

AKTAŞ, G. & ROBERTSON, A. H. F. 1984. The Maden Complex, SE Turkey: evolution of a Neotethyan active margin. *In*: DIXON, J. E. & ROBERTSON, A. H. F. (eds) *The Geological Evolution of the Eastern Mediterranean*. Blackwell Scientific Publications, Oxford, 375–402.

ALLMENDINGER, R. W., REILINGER, R. & LOVELESS, J. 2007. Strain and rotation rate from GPS in Tibet, Anatolia and the Altiplano. *Tectonics*, **26**, TC3013, doi: 10.1029/2006TC002030.

BÁLDI, T. 1973. *Mollusc fauna of the Hungarian Oligocene (Egerian)*. Budapest, Akadémiai Kiadó.

BANDEL, K. & WEDLER, E. 1987. Hydroid, amphineuran and gastropod zonation in the littoral of the Caribbean Sea, Colombia. *Senckenbergiana maritima*, **19**, 1–130.

BARKA, A. 1992. The North Anatolian fault zone. *Annales Tectonicae*, **6**, 164–195.

BARTOLI, G., SARNTHEIN, M., WEINELT, M., ERLENKEUSER, H., GARBE-SCHÖNBERG, D. & LEA, D. W. 2005. Final closure of Panama and the onset of northern hemisphere glaciation. *Earth and Planetary Science Letters*, **237**, 33–44.

BELLAHSEN, N., FACCENNA, C., FUNICIELLO, F., DANIEL, J.-M. & JOLIVET, L. 2003. Why did Arabia separate from Africa? Insights from 3-D laboratory experiments. *Earth and Planetary Science Letters*, **216**, 365–381.

BERCKHEMER, H. 1977. Some aspects of the evolution of marginal seas deduced from observations in the Aegean region. *In*: MONTADERT, L. (ed.) *Structural History of the Mediterranean Basins*. Technip. Paris, Split, Yugoslavia, 303–313.

BERGER, W. H. & MILLER, K. G. 1988. Paleogene tropical planktonic foraminiferal biostratigraphy and magnetobiostratigraphy. *Micropaleontology*, **34**, 362–380.

BERGGREN, W. A., KENT, D. V., SWISHER III, C. C. & AUBRY, M. P. 1995. A revised Cenozoic Geochronology and Chronostratigraphy. *SEPM Special Publication*, **54**, 129–212.

BESSE, J. & COURTILLOT, V. 2002. Apparent and true polar wander and the geometry of the geomagnetic field over the last 200 Ma. *Journal Geophysical Research*, **107 (B11), 2300**, doi:10.1029/2000JB000050.

BICCHI, E., FERRERO, E. & GONERA, M. 2003. Paleoclimatic interpretation based on Middle Miocene planktonic foraminifera: the Silesia Basin (Paratethys) and Monferrato (Tethys) records. *Paleogeography, Paleoclimatology, Paleoecology*, **196**, 265–303.

BINGÖL, E. 1984. Geology of the Elazig area in the Eastern Taurus region. *In*: *Geology of the Taurus Belt*. MTA (Turkish Geological Survey), Ankara, 209–216.

BLOW, W. H. 1969. Late middle Eocene to Recent planktonic foraminiferal biostratigraphy. *In*: BRONNIMANN, P. & RENZ, H. H. (eds) *Proceedings of the First International Conference on Planktonic Microfossils* (Geneva, 1967), Volume 1: E. J. Brill, Leiden, 199–421.

BOULTON, S. J. & ROBERTSON, A. H. F. 2007. The Miocene of the Hatay area, S Turkey: Transition form the Arabian passive margin to an underfilled foreland basin related to the closure of the Southern Neotethys Ocean. *Sedimentary Geology*, **198**, 93–124.

BOULTON, S. J., ROBERTS, A. H. F., ELLAM, R. M., ŞAFAK, Ü. & ÜNLÜGENÇ, U. C. 2007. Strontium isotopic and micropaleontological dating used to help redefine the stratigraphy of the neotectonic Hatay Graben, Southern Turkey. *Turkish Journal of Earth Sciences*, **16**, 141–179.

BOZKURT, E. 2003. Origin of NE-trending basins in western Turkey. *Geodinamica Acta*, **16**, 61–81.

BROCCHI, G. B. 1814. *Conchiologia fossile subappenina, con osservazioni geologiche sugli Appennini e sul suolo adiacente*. Milano.

CHAMLEY, H., MEULENKAMP, J. E., ZACHARIASSE, W. J. & VAN DER ZWAAN, G. J. 1986. Middle to late Miocene marine ecostratigraphy: clay mineral, planktonic foraminifera and stable isotopes from Sicily. *Oceanological Acta*, **9**, 227–238.

CRONIN, B. T., HARTLEY, A. J., CELIK, H., HURST, A., TÜRKMEN, I. & KEREY, E. 2000*a*. Equilibrium profile development in graded deep-water slopes: Eocene, Eastern Turkey. *Journal of the Geological Society, London*, **157**, 946–955.

CRONIN, B. T., HURST, A., CELIK, H. & TÜRKMEN, I. 2000*b*. Superb exposure of a channel, levee and overbank complex in an ancient deep-water slope environment. *Sedimentary Geology*, **132**, 205–216.

D'ARCHIAC, A. S. & HAIME, J. 1853. *Description des animaux fossiles du groupe nummulitique de l'Inde précédé d'un resumée géologique et d'une monographie de Nummulites*. Gide & Baudry, Paris.

D'ORBIGNY, A. 1852. *Prodrome de Paléontologie Stratigraphique Universelle des Animaux Mollusques & Rayonnés faisant suite au Cours Élémentaire de Paléontologie et de Géologie Stratigraphique*. **2**, Paris, Masson, 1–427.

DERMAN, A. S. 1999. Braided river deposits related to progressive Miocene surface uplift in Kahraman

Maras area, SE Turkey. *Geological Journal*, **34**, 159–174.

Derman, A. S. & Atalik, E. 1993. Sequence Stratigraphic Analysis of Miocene Sediments in Maras Miocene Basin and Effect of Tectonism in the Development of Sequences. *Special Publications Sequence Stratigraphy, Sedimentology Study Group*, **1**, 43–52 [in Turkish].

Deshayes, G.-P. 1824–1837. *Description des coquilles fossiles des environs de Paris. Part I.* Paris.

Dewey, J. F. & Şengör, A. M. C. 1979. Aegean and surrounding regions: Complex multiplate and continuum tectonics in a convergent zone. *Geological Society of America Bulletin*, **90**, 84–92.

Dewey, F. J., Hempton, M. R., Kidd, W. S. F., Şaroğlu, F. & Şengör, A. M. C. 1986. Shortening of continental lithosphere: the neotectonics of eastern Anatolia – a young collision zone, *In*: Coward, M. P. & Ries, A. C. (eds) *Collision Tectonics*, Geological Society, London, Special Publication, **19**, 3–36.

Duncan, P. M. & Sladen, W. P. 1883. The Fossil Echinoidea of Kachh and Kattywar. *Palaeontologia Indica, Ser. XIV*, **1/4**, 1–91.

Faccenna, C., Bellier, O., Martinod, J., Piromallo, C. & Regard, V. 2006. Slab detachment beneath eastern Anatolia: A possible cause for the formation of the North Anatolian Fault. *Earth and Planetary Science Letters*, **242**, 85–97.

Flower, B. P. & Kennett, J. 1993. Middle Miocene Ocean-Climate Transition: High-Resolution Oxygen and Carbon Isotopic Records from Deep Sea Drilling Project Site 558A, Southwest Pacific. *Paleoceanography*, **8**, 811–843.

Flower, B. P. & Kennett, J. P. 1994. The middle Miocene climate transition, East Antarctic ice sheet development, deep ocean circulation and global carbon cycle. *Paleogeography, Paleoclimatology, Paleoecology*, **108**, 537–555.

Foresi, L. M., Iaccarino, S., Mazzei, R. & Salvatorini, G. 1998. New data on calcareous plankton biostratigraphy of the middle-late Miocene (Serravallian/Tortonian) of the Mediterranean area. *Rivista Italiana di Paleontologia e Stratigrafia*, **104**, 95–114.

Foresi, L. M., Bonomo, S., Caruso, A., Di Stefano, E., Salvatorini, G. & Sprovieri, R. 2002*a*. Calcareous plankton high resolution biostratigraphy (foraminifera and nannofossils) of the uppermost Langhian-lower Serravallian 'Ras-il-Pellegrin' section (Malta). *Rivista Italiana di Paleontologia e Stratigrafia*, 337–353.

Foresi, L. M., Caruso, A., Di Stefano, E., Lirer, F., Iaccarino, S., Salvatorini, G. & Sprovieri, R. 2002*b*. High-resolution biostratigraphy of the upper Serravallian/lower Tortonian sequence of the Tremiti Islands. *Rivista Italiana di Paleontologia e Stratigrafia*, **108**, 257–253.

Garfunkel, Z. 1998. Constrains on the origin and history of the Eastern Mediterranean basin. *Tectonophysics*, **298**, 5–35.

Garfunkel, Z. 2004. Origin of the Eastern Mediterranean basin: a re-evaluation. *Tectonophysics*, **391**, 11–34.

Golonka, J. 2004. Plate tectonic evolution of the southern margin of Eurasia in the Mesozoic and Cenozoic. *Tectonophysics*, **381**, 235–273.

Gradstein, F. M., Ogg, J. G. & Smith, A. G. (eds) 2005. *A Geological Time Scale 2004*. Cambridge University Press.

Gül, M., Darbas, G. & Gürbüs, K. 2005. Tectono-Stratigraphic position of Alacik Formation (Latest Middle Eocene – Early Miocene) in the Kahraman Maras Basin. In Turkish with English abstract and summary. *Istanbul University Mühendislik Fakültesi Yerbilimleri Dergisi*, **18**, 183–197.

Hafkenscheid, E., Wortel, M. J. R. & Spakman, W. 2006. Subduction history of the Tethyan region derived from seismic tomography and tectonic reconstructions. *Journal Geophysical Research*, **111**, doi: 10.1029/2005JB003791.

Harzhauser, M. 2004. Oligocene Gastropod Faunas of the Eastern Mediterranean (Mesohellinic Trough/Greece and Esfahan-Sirjan Basin/Central Iran). *Courier Forschungsinstitut Senckenberg*, **248**, 93–181.

Harzhauser, M., Kroh, A., Mandic, O., Piller, W. E., Göhlich, U., Reuter, M. & Berning, B. 2007. Biogeographic responses to geodynamics: A key study all around the Oligo-Miocene Tethyan Seaway. *Zoologischer Anzeiger*, doi: 10.1016/j.jcz.2007.05.001.

Harzhauser, M., Piller, W. E. & Steininger, F. F. 2002. Circum-Mediterranean Oligo-Miocene biostratigraphic evolution – the gastropods' point of view. *Paleogeography, Paleoclimatology, Paleoecology*, **183**, 103–133.

Hendler, G., Miller, J. E., Pawson, D. L. & Kier, P. M. 1995. Sea Stars, Sea Urchins and Allies – Echinoderms of Florida and the Carribbean. Smithonian Institute Press, Washington, London, 1–390.

Hessami, K., Koyi, H. A., Talbot, C. J., Tabasi, H. & Shabanian, E. 2001. Progressive unconformities within an evolving foreland fold-thrust belt, Zagros Mountains. *Journal of the Geological Society, London*, **158**, 969–981.

Hilgen, F. J., Krijgsman, W., Raffi, I., Turco, E. & Zachariasse, W. J. 2000. Integrated stratigraphy and astronomical calibration of the Serravallian/Tortonian boundary section at Monte Gibliscemi (Sicily, Italy). *Marine Micropaleontology*, **38**, 181–211.

Hilgen, F. J., Abdul Aziz, H., Krijgsman, W., Raffi, I. & Turco, E. 2003. Integrated stratigraphy and astronomical tuning of the Serravallian and lower Tortonian at Monte dei Corvi (Middle-Upper Miocene, northern Italy). *Paleogeography, Paleoclimatology, Paleoecology*, **199**, 229–264.

Hilgen, F. J., Abdul Aziz, H., Bice, D., Iaccarino, S., Krijgsman, W., Kuiper, K. F., Montanari, A., Raffi, I., Turco, E. & Zachariasse, W. J. 2005. The Global Boundary Stratotype Section and Point (GSSP) of the Tortonian Stage (Upper Miocene) at Monte dei Corvi. *Episodes*, **28**, 6–17.

Hsü, K. J., Ryan, W. B. F. & Cita, M. B. 1973. Late Miocene desiccation of the Mediterranean. *Nature*, **242**, 240–244.

Hubert-Ferrari, A., Armijo, R., King, G. C. P., Meyer, B. & Barka, A. 2002. Morphology, displacement and slip rates along the North Anatolian Fault

(Turkey). *Journal Geophysical Research*, **107**, 101029–101059.

HÜSING, S. K., HILGEN, F. J., ABDUL AZIZ, H. & KRIJGSMAN, W. 2007. Completing the Neogene geological time scale between 8.5 and 12.5 Ma. *Earth and Planetary Science Letters*, **253**, 340–358.

HUBERT-FERRARI, A., KING, G., VAN DER WOERD, J., VILLA, I., ALTUNEL, E. & ARMIJO, R. 2009. Long-term evolution of the North Anatolian Fault. *In*: VAN HINSBERGEN, D. J. J., EDWARDS, M. A. & GOVERS, R. (eds) *Collision and Collapse of the Africa–Arabia–Eurasia Subduction Zone*. Geological Society, London, Special Publications, **311**, 133–154.

IGRS-IFP, 1966. Étude Géologique de l'Épire (Grèce nord-occidentale). Paris, Institut Francais du Petrol.

JACOBS, E., WEISSERT, H. & SHIELDS, G. 1996. The Monterey event in the Mediterranean: A record from shelf sediments of Malta. *Paleoceanography*, **11**, 717–728.

JOLIVET, L. 2001. A comparison of geodetic and finite strain pattern in the Aegean, geodynamic implications. *Earth and Planetary Science Letters*, **187**, 95–104.

JOLIVET, L. & FACCENNA, C. 2000. Mediterranean extension and the Africa-Eurasia collision. *Tectonics*, **19**, 1094–1106.

KARIG, D. E. & KOZLU, H. 1990. Late Paleogene–Neogene evolution of the triple junction region near Maraş, south-central Turkey. *Journal of the Geological Society, London*, **147**, 1023–1034.

KAYMAKÇI, N., INCEÖZ, M. & ERTEPINAR, P. 2006. 3D-Architecture and Neogene Evolution of the Malatya Basin: Inferences from the Kinematics of the Malatya and Ovacik Fault Zones. *Turkish Journal of Earth Sciences*, **15**, 123–154.

KESKIN, M. 2003. Magma generation by slab steepening and breakoff beneath a subduction-accretion complex: An alternative model for collision-related volcanism in Eastern Anatolia, Turkey. *Geophysical Research Letters*, **30**, doi:10.1029/2003GL018019, 2003.

KRIJGSMAN, W., LANGEREIS, C. G., DAAMS, R. & VAN DER MEULEN, A. J. 1994. Magnetostratigraphic dating of the middle Miocene change in the continental deposits of the Aragonian type area in the Calayud-Terueal basin (Central Spain). *Earth and Planetary Science Letters*, **128**, 513–526.

LAMARCK, J.-B. P. A. DE M. 1804. Suite des mèmoires sur les fossiles des environs de Paris. *Annales de Museum Histoire Naturelle*, **5**, 179–357.

LE PICHON, X., ANGELIER, J. & SIBUET, J.-C. 1982. Plate boundaries and extensional tectonics. *Tectonophysics*, **81**, 239–256.

LINNAEUS, C. 1758. *Systema naturae per regna tria naturae, secundum classes, ordines, genera, species, cum characteribus, differentiis, synonymis, locis. – Editio decima, reformata*. Holmiae.

LIVERMORE, R., NANKIVELL, A., EAGLES, G. & MORRIS, P. 2005. Paleogene opening of Drake Passage. *Earth and Planetary Science Letters*, **236**, 459–470.

LOURENS, L. J., HILGEN, F. J., SHACKLETON, N. J., LASKAR, J. & WILSON, D. 2004. The Neogene Period. *In*: GRADSTEIN, F. M., OGG, J. G. & SMITH, A. G. (eds) *A geological time scale 2004*. Cambridge University Press, 409–440.

MANDIC, O. 2000. *Oligocene to Early Miocene pectinid bivalves of Western Tethys (N-Greece, S-Turkey, Central Iran and NE-Egypt) – taxonomy and paleobiogeography*. Unpubl. PhD thesis, University of Vienna.

MANDIC, O. & PILLER, W. E. 2001. Pectinid coquinas and their paleoenvironmental implications – examples from the early Miocene of northeastern Egypt. *Paleogeography, Paleoclimatology, Paleoecology*, **172**, 171–191.

MARTINI, E. 1971. Standard Tertiary and Quaternary calcareous nannoplankton zonation. *In*: FARINACCI, A. (ed.) Proceedings of the Second Planktonic Conference Roma, Edizioni Technoscienza, Roma. 739–785.

MCCLUSKY, S., BALASSANIAN, S., BARKA, A., DEMIR, A., ERGINTAV, S., GEORGIEV, I. *ET AL*. 2000. Global Positioning System constrains on plate kinematics and dynamics in the eastern Mediterranean and Caucasus. *Journal Geophysical Research*, **105**, 5695–5719.

MEULENKAMP, J. E. & SISSINGH, W. 2003. Tertiary paleogeography and tectonostratigraphic evolution of the Northern and Southern Peri-Tethys platforms and the intermediate domains of the African-Eurasian convergent plate boundary zone. *Paleogeography, Paleoclimatology, Paleoecology*, **196**, 209–228.

MILLER, K. G., WRIGHT, J. D. & FAIRBANKS, R. G. 1991. Unlocking the Ice House: Oligocene–Miocene oxygen isotopes, eustacy, and margin erosion. *Journal Geophysical Research*, **96**, 6829–6848.

MILLER, K. G., WRIGHT, J. D. & BROWNING, J. V. 2005. Visions of ice sheets in a greenhouse world. *Marine Geology*, **217**, 215–231.

NYST, H. 1836. Recherches sur les coquilles fossiles de Kleyn–Spauwen et Housselt (Province du Limbourg). *Messager des Sciences et des Arts de la Belgique, ou Nouvelles Archives Historiques, Litteraires et Scientifiques*, **4**, 139–180.

PEARCE, J. A., BENDER, J. F., DE LONG, S. E., KIDD, W. S. F., LOW, P. J., GUNER, Y., ŞAROĞLU, F., YILMAZ, Y., MOORBATH, S. & MITCHELL, J. G. 1990. Genesis of collision volcanism in Eastern Anatolia, Turkey. *Journal of Volcanology and Geothermal Research*, **44**, 189–229.

PERINÇEK, D. 1979. *The geology of Hazro–Korudag–Cüngüs–Maden–Ergani–Hazar–Elazig–Malatya Area*. The Geological Society of Turkey.

PERINÇEK, D. & CEMEN, I. 1990. The Structural relationship between the Eastern Anatolian and Dead Sea fault zones in southeastern Turkey. *Tectonophysics*, **172**, 331–340.

PERINÇEK, D. & KOZLU, H. 1983. Stratigraphy and structural relations of the units in the Afşin-Elbistan-Doğanşehir region (Eastern Taurus). *In*: TEKELI, O. & GÖNCÜOĞLU, M. C. (eds) Proceedings of the international symposium, Geology of Taurus Belt, MTA, Ankara, Turkey, 181–198.

PERINÇEK, D. & ÕZKAYA, I. 1981. Arabistan Levhasi Kuyzey Kenari Tektonik evrimi. Tectonic evolution of the northern margin of Arabian plate. *Yerbilimleri, Hacettepe Universitesi, Bulletin of Institute of Earth Sciences of Hacettepe University Beytepe Ankara*, **8**, 91–101.

POPOV, S. V. 1993. Zoogeography of the Late Eocene Basins of Western Eurasia Based on Bivalve Mollusks. *Stratigraphy and Geological Correlation*, **2**, 103–118.

REILINGER, R., MCCLUSKY, S., VERNANT, P., LAWRENCE, S., ERGINTAV, S., CAKMAK, R. *ET AL.* 2006. GPS constraints on continental deformation in the Africa–Arabia–Eurasia continental collision zone and implications for the dynamics of plate interactions. *Journal of Geophysical Research*, **111**, V05411, doi:10.1029/2005JB004051.

REUTER, M., PILLER, W. E., HARZHAUSER, M., MANDIC, O., BERNING, B., RÖGEL, F. *ET AL.* 2007. The Oligo-/Miocene Qom Formation (Iran): evidence for an early Burdigalian restriction of the Tethyan Seaway and closure of its Iranian gateways. *International Journal of Earth Sciences*, doi 10.1007/s00531-007-0269-9.

RICHTER, D., MARIOLAKOS, I. & RISCH, H. 1978. The main flysch stages of the Hellenides. *In*: CLOSS, H., ROEDER, D. & SCHMIDT, K. (eds) *Alps, Apennines, Hellenides*. Inter-Union Commission on Geodynamics Scientific Report, **38**, 434–438.

ROBERTSON, A. H. F. 2000. Mesozoic-Tertiary tectonic-sedimentary evolution of a south Tethyan oceanic basin and its margins in southern Turkey. *In*: BOZKURT, E., WINCHESTER, J. A. & PIPER, J. D. A. (eds) *Tectonics and Magmatism in Turkey and the Surrounding Area*. Geological Society, London, Special Publication, **173**, 97–138.

ROBERTSON, A. H. F., UNLÜGENÇ, Ü. C., INAN, N. & TASLI, K. 2004. The Misis-Andirin Complex: a Mid-tertiary melange related to late-stage subduction of the Southern Neotethys in S Turkey. *Journal of Asian Earth Science*, **22**, 413–453.

RÖGL, F. 1998. Paleogeographic considerations for Mediterranean and Paratethys Seaways (Oligocene to Miocene). *Annalen des Naturhistorischen Museums in Wien*, **99**, 279–310.

RÖGL, F. 1999. Circum-Mediterranean Miocene Paleogeography. *In*: RÖSSNER, G. & HEISSIG, K. (eds) *The Miocene Land Mammals of Europe*. Dr. Fritz Pfeil Verlag, München, 39–48.

RUGGIERI, G. & SPROVIERI, R. 1970. I microforaminiferi delle 'marne di S. Cipirello' Translated Title: Foraminifera of the San Cipirello marls. *Lavori Istituto Geologia Palermo*, **10**, 1.

SANCAY, R. H., BATI, Z., ISIK, U., KIRICI, S. & AKCA, N. 2006. Palynomorph, Foraminifera, and Calcareous Nannoplankton Biostratigraphy of Oligo-Miocene Sediments in the Muş Basin, Eastern Anatolia, Turkey. *Turkish Journal of Earth Sciences*, **15**, 259–319.

ŞAROĞLU, F. & YILMAZ, Y. 1986. Geological evolution and basin models during neotectonic episode in the Eastern Anatolia. *Bulletin Mineral Research and Exploration Institute of Turkey*, **107**, 61–83.

SCHAFFER, F. X. 1912. Das Miozän von Eggenburg. Die Fauna der ersten Mediterranstufe des Wiener Beckens und die geologischen Verhältnisse der Umgebung des Manhartsberges in Niederösterreich. Die Gastropoden der Miocänbildungen von Eggenburg. *Jahrbuch der k.k. geologischen Reichsanstalt*, **22**, 127–193.

SCHAUROTH, F. FREIHERR VON, 1865. Verzeichnis der Versteinerungen in Herzoglichen Naturaliencabinett zu Coburg: mit Angabe der Synonyme und Beschreibung Vieler Neuer Arten, Sowie der Letzteren Abbildung auf 30 Tafeln. Coburg, Dietz'sche Hofbuchdruckerei.

SCHLOTHEIM, E. F. von. 1820. Die Petrefactenkunde auf ihrem jetzigen Standpunkte durch die Beschreibung seiner Sammlung versteinerter und fossiler Überreste des Thier-und Pflanzenreichs der Vorwelt erläutert. Gotha, Beckersche Buchhandlung.

SCHNEIDER, B. & SCHMITTNER, A. 2006. Simulating the impact of the Panamanian seaway closure on ocean circulation, marine productivity and nutrient cycling. *Earth and Planetary Science Letters*, **246**, 367–380.

ŞENEL, M. 2002. *Geological Map of Turkey*, Ankara, MTA.

ŞENGÖR, A. M. C. & YILMAZ, Y. 1981. Tethyan evolution of Turkey: a plate tectonic approach. *Tectonophysics*, **75**, 181–241.

ŞENGÖR, A. M. C., GÖRÜR, N. & ŞAROĞLU, F. 1985. Strike-slip faulting and related basin formation in zones of tectonic escape: Turkey as a case study. *In*: CHRISTIE-BLICK, N. (ed.) *Basin Formation and Sedimentation*. Society of Economic Paleontologists and Mineralogists Special Publications, **37**, 227–264.

ŞENGÖR, A. M. C., ÖZEREN, S., GENÇ, T. & ZOR, E. 2003. East Anatolian high plateau as a mantle-support, North–South shortened domal structure. *Geophysical Research Letters*, **30**, doi: 10.1029/2003GL017858.

ŞENGÖR, A. M. C., TÜYSÜZ, O., IMREN, C., SAKINC, M., EYIDOGAN, H., GÖRÜR, N., LE PICHON, X. & RANGIN, C. 2005. The North Anatolian Fault: a new look. *Annual Reviews in Earth and Planetary Sciences*, **33**, 37–112.

SLACK-SMITH, S. M. 1998. Ostreoidea. *In*: BEESLEY, P. L., ROSS, G. J. B. & WELLS, A. (eds) *Mollusca: The southern synthesis*. Fauna of Australia, CSIRO Publishing, Melbourne, **5**, **Part A**, CSIRO Publishing, Melbourne, 268–274.

SPEZZAFERRI, S. 1994. Planktonic foraminiferal biostratigraphy of the Oligocene and lower Miocene in the oceanic record. An overview. *Paleontographia Italica*, **81**, 1–187.

SPEZZAFERRI, S. & PREMOLI SILVA, I. 1991. Oligocene planktonic foraminiferal biostratigraphy and paleoclimatic interpretation from Hole 538A, DSDP Leg 77, Gulf of Mexico. *Paleogeography, Paleoclimatology, Paleoecology*, **83**, 217–263.

TELEGDI-ROTH, K. V. 1914. Eine oberoligozäne Fauna aus Ungarn. *Geologica Hungaria*, **1**, 1–77.

TURCO, E., HILGEN, F. J., LOURENS, L. J., SHACKLETON, N. J. & ZACHARIASSE, W. J. 2001, Punctuated evolution of global climate cooling during the late Middle to early Late Miocene: High-resolution planktonic foraminiferal, oxygen isotope records from the Mediterranean. *Paleoceanography*, **16**, 405–423.

TÜYSÜZ, N. & ERLER, A. 1995. Geology and geotectonic implications of Kazikkaya area, Kagizman-Kars (Turkey). *In*: ÖRCEN, S. (ed.) *Geology of the Black Sea Region*. Proceedings of the International symposium on the Geology of the Black sea Region, 7–11 September 1995, Ankara, Turkey. General directorate of mineral research and exploration and chamber of geological engineering, Ankara, 76–81.

VAN DER ZWAAN, G. J. & GUDJONSSON, L. 1986. Middle Miocene–Pliocene stable isotope stratigraphy and paleoceanography of the Mediterranean. *Marine Micropaleontology*, **10**, 71–90.

VAN DER ZWAAN, G. J., JORISSEN, F. J. & STIGTER, H. C. 1990. The depth dependency of planktonic/benthic foraminiferal ratios: Constrains and applications. *Marine Geology*, **95**, 1–16.

VAN HINSBERGEN, D. J. J., HAFKENSCHEID, E., SPAKMAN, W., MEULENKAMP, J. E. & WORTEL, M. J. R. 2005*a*. Nappe stacking resulting from subduction of oceanic and continental lithosphere below Greece. *Geology*, **33**, 325–328.

VAN HINSBERGEN, D. J. J., KOUWENHOVEN, T. J. & VAN DER ZWAAN, G. J. 2005*b*. Paleobathymetry in the backstripping procedure: Correction for oxygenation effects on depth estimates. *Paleogeography, Paleoclimatology, Paleoecology*, **221**, 245–265.

VAN HINSBERGEN, D. J. J., LANGEREIS, C. G. & MEULENKAMP, J. E. 2005*c*. Revision of the timing, magnitude and distribution of Neogene rotations in the western Aegean region. *Tectonophysics*, **369**, 1–34.

VAN HINSBERGEN, D. J. J., ZACHARIASSE, W. J., WORTEL, M. J. R. & MEULENKAMP, J. E. 2005*d*. Underthrusting and exhumation: A comparison between the External Hellenides and the 'hot' Cycladic and 'cold' South Aegean core complexes (Greece). *Tectonics*, **24**, doi: 10.1029/2004TC001692.

WADE, B. S., BERGGREN, W. A. & OLSSON, R. K. 2007. The biostratigraphy and paleobiology of Oligocene planktonic foraminifera from the equatorial Pacific Ocean (ODP Site 1218). *Marine Micropaleontology*, **62**, 167–179.

WESTAWAY, R. 2003. Kinematics of the Middle East and eastern Mediterranean updated. *Turkish Journal of Earth Sciences*, **12**, 5–46.

WESTAWAY, R. 2004. Kinematic consistency between the Dead Sea Fault Zone and the Neogene and Quaternary left-lateral faulting in SE Turkey. *Tectonophysics*, **391**, 203–237.

WOODRUFF, F. & SAVIN, S. M. 1989. Miocene deepwater oceanography. *Paleoceanography*, **4**, 87–140.

WOODRUFF, F. & SAVIN, S. M. 1991. Mid-Miocene isotope stratigraphy in the deep sea: high resolution correlations, paleoclimatic cycles, and sediment preservation. *Paleoceanography*, **6**, 755–806.

WRIGHT, J. D., MILLER, K. G. & FAIRBANKS, R. G. 1992. Early and Middle Miocene stable isotopes: implications for deepwater circulation and climate. *Paleoceanography*, **7**, 357–389.

YILMAZ, Y. 1993. New evidences and model on the evolution of the southeast Anatolian orogen. *Geological Society of America Bulletin*, **105**, 251–271.

YILMAZ, Y., GÜNER, Y. & ŞAROĞLU, F. 1998. Geology of the quaternary volcanic centers of east Anatolia. *Journal of volcanology and geothermal research*, **85**, 173–210.

ZACHARIASSE, W. J. 1992. Neogene planktonic foraminifers from Sites 761 and 762 off Northwestern Australia. *Proceedings of the Ocean Drilling Program, Scientific Results*, **122**, 665–675.

ZACHOS, J., PAGANI, M., SLOAN, L., THOMAS, E. & BILLUPS, K. 2001. Trends, rhythms, and aberrations in global climate 65 Ma to present. *Science*, **292**, 686–693.

Long-term evolution of the North Anatolian Fault: new constraints from its eastern termination

AURÉLIA HUBERT-FERRARI[1,*], GEOFFREY KING[2], JÉROME VAN DER WOERD[3], IGOR VILLA[4], ERHAN ALTUNEL[5] & ROLANDO ARMIJO[2]

[1]*Section de Sismologie, Observatoire Royal de Belgique, rue circulaire 3, B-1180 Brussels, Belgium*

[2]*Laboratoire de Tectonique, Institut de Physique du Globe de Paris, UMR, 4 place Jussieu, Paris, 75252 Cedex 05, France*

[3]*IPGS-EOST, UMR CNRS/ULP 7516, 5, rue Rene Descartes, Strasbourg, 67084 Cedex, France*

[4]*Institute of Geological Sciences, University of Bern, Baltzerstrasse 1-3, CH-3012 Bern, Switzerland*

[5]*Dept. of Geology, Engineering Faculty, Osmangazi University, Eskisehir, Turkey*

**Corresponding author (e-mail: aurelia.ferrari@oma.be)*

Abstract: The deformation and $^{40}Ar-^{39}Ar$ dating of recent volcanism, that remarkably sits across the North Anatolian Fault eastern termination in Turkey, together with previous studies, put strong constraints on the long-term evolution of the fault. We argue that after a first phase of 10 Ma, characterized by a slip rate of about 3 mm/a, and during which most of the trace was established, the slip rate jumped to about 20 mm/a on average over the last 2.5 Ma, without substantial increase of the fault length. The transition correlates with a change in the geometry at the junction with the East Anatolian Fault that makes the extrusion process more efficient.

The right-lateral North Anatolian Fault (NAF), together with the conjugate East Anatolian Fault (EAF), accommodates the westward extrusion of the Anatolian block toward the Aegean Subduction Zone (Fig. 1; McKenzie 1972; Tapponnier 1977). This process started most probably 12 Ma ago during a late phase of collision between Arabia and Eurasia (Dewey *et al.* 1986; McQuarrie *et al.* 2003) characterized by the uplift of the Anatolian Plateau, the end of marine sedimentation (Gelati 1975; Şengör *et al.* 1985), the onset of volcanism in eastern Anatolia (Yılmaz *et al.* 1987; Pearce *et al.* 1990) and the onset of motion of the North Anatolian Fault (Şengör *et al.* 1985; Barka 1992). Indeed biostratigraphic data unequivocally constrain a Late Miocene age for all basins located along the North Anatolian eastern strand (see Şengör *et al.* (2005) for a review). Some still propose a later initiation time around 5 ± 2 Ma (Barka & Kadinsky-Cade 1988; Bozkurt & Koçyiğit 1996; Bozhurt 2001). The present-day kinematics of the extrusion, constrained by GPS measurements (McClusky *et al.* 2000; Reilinger *et al.* 2006), shows that deformation is localized along a single narrow zone and that the internal deformation of Anatolia though existing (Tatar *et al.* 1996; Gürsoy *et al.* 1997; Jaffey *et al.* 2004) is negligible (Fig. 1). The present geodetic slip rate of the North Anatolian Fault (22 ± 3 mm/a: McClusky *et al.* (2000); 24 ± 1 mm/a: Reilinger *et al.* (2006) is not significantly different from its Holocene slip rate (18.5 ± 3.5 mm/a; Hubert-Ferrari *et al.* (2002)) deduced from offset geomorphological markers. The study of the offset morphology at a wide range of scales (Hubert-Ferrari *et al.* 2002) suggests that deformation has remained localized along the present fault zone for several million years. Barka & Hancock (1984) further suggest that a broad right-lateral shear zone was existing before deformation fully localized in early Pliocene time on the present strand of the North Anatolian Fault. The present North Anatolian Fault has also a nearly uniform total displacement of *c.* 85 km along most of the fault (Armijo *et al.* 1999; Bozkurt 2001; Westaway & Aeger 2001; Hubert-Ferrari *et al.* 2002; Şengör *et al.* 2005) and is thus similar to a transform boundary. The total displacement of the North Anatolian Fault, together with the

From: VAN HINSBERGEN, D. J. J., EDWARDS, M. A. & GOVERS, R. (eds) *Collision and Collapse at the Africa–Arabia–Eurasia Subduction Zone*. The Geological Society, London, Special Publications, **311**, 133–154.
DOI: 10.1144/SP311.5 0305-8719/09/$15.00

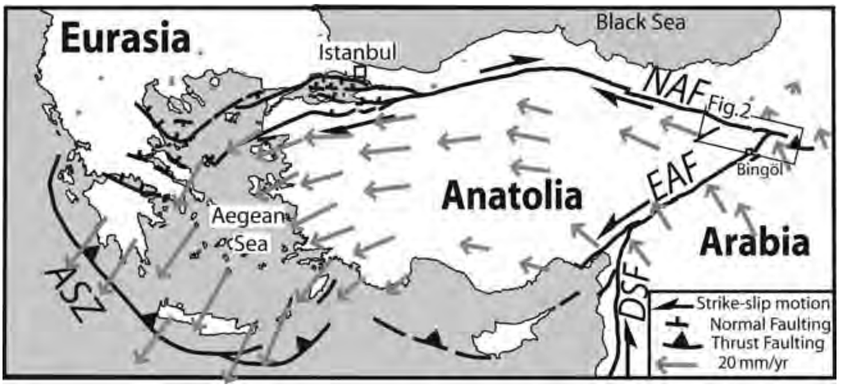

Fig. 1. Continental extrusion of the Anatolian block away from the Arabia–Eurasia collision zone. The current GPS vectors relative to Eurasia are indicated (McClusky *et al.* 2000). NAF, North Anatolian Fault; EAF, East Anatolian Fault; DSF, Dead Sea Fault; ASZ, Aegean Subduction Zone. Box is area of Fig. 2.

age of the fault (12 Ma), yields an average geological slip rate of 7 mm/a.

We focus on the Karliova Triple Junction area, where the eastern extremity of the North Anatolian Fault joins the East Anatolian Fault. This pivotal region marks the transition between the continental shortening to the east and the extrusion regime to the west. In addition recent volcanism covers entirely the region and provides ideal chronological markers to record deformation. By mapping the active faults and their offsets, and by characterizing the relationship between faulting and volcanism, we propose that the extrusion process has evolved with time, with two distinct phases characterized by very different slip rates. Interestingly, the Triple Junction (TJ) evolution can be approximated by a simple plate-tectonic model.

Active faulting at the Anatolia–Eurasia–Arabia triple junction

We have established a detailed map of the three main fault systems (the North Anatolian Fault, the Varto Fault, and the East Anatolian Fault) relevant to the triple junction deformation combining Spot images analysis and fieldwork (Figs 2–5).

At its eastern extremity the North Anatolian Fault can be divided in 4 main segments (Fig. 2). To the west, a first segment of the North Anatolian Fault strikes N125°E and ends at the eastern extremity of the Erzincan basin. This is a complex basin (Barka & Gülen 1989; Fuenzelida *et al.* 1997; Hubert-Ferrari *et al.* 2002), with the left-lateral Ovacık fault terminating southward (Westaway & Aeger 2001). The seismic behavior of the North Anatolian Fault appears to be decoupled on both sides of this major discontinuity (Hubert-Ferrari *et al.* 2002). East of the Erzincan basin a second strait segment extends for 80 km with a N110°E strike to a small pull-apart near Yedisu. East of Yedisu, the faulting geometry is typical of a damage fault pattern occurring at the tip of strike-slip fault with slightly more diffuse deformation combining fault branching, horsetail and reverse faulting (Kim & Sanderson 2006). A third segment of the North Anatolian Fault splits, about 10 km SE of Yedisu, in different curved strands that ruptured in 1949 (Ambraseys 1988). This segment forms a large horsetail with normal faulting deforming the eastern flank of the Turna Mountain until the East Anatolian Fault. Farther NE, a fourth segment extends over 30 km to the Triple Junction and accommodates almost only strike-slip motion as shown in Figure 3 and by focal mechanisms of earthquake of magnitude $M > 5.5$ (Fig. 2). The third and fourth segments form a restraining step-over. Secondary folding parallel to the Periçay River occurs just north of the last segment of the North Anatolian Fault.

East of the Triple Junction the Varto fault system extends over 50 km, forming a large mostly extensional horsetail. Most of the deformation is localized on the Main Varto Fault that is in strait continuation of the fourth segment of the North Anatolian Fault. This main strand, located exactly at the foot of the Bingöl half-caldera, accommodates mostly strike-slip faulting though partly hidden by landslides (Fig. 4). In 1966, the Varto $M = 6.8$ earthquake (Wallace 1968; Ambraseys & Zatopek 1968) ruptured its eastern part with aftershocks having thrusting mechanism. More diffuse strike-slip and normal deformation exists south of the Main Varto Fault, with a clear southward decreasing gradient of deformation. The network of secondary faults in the Varto horsetail is at a slight angle to

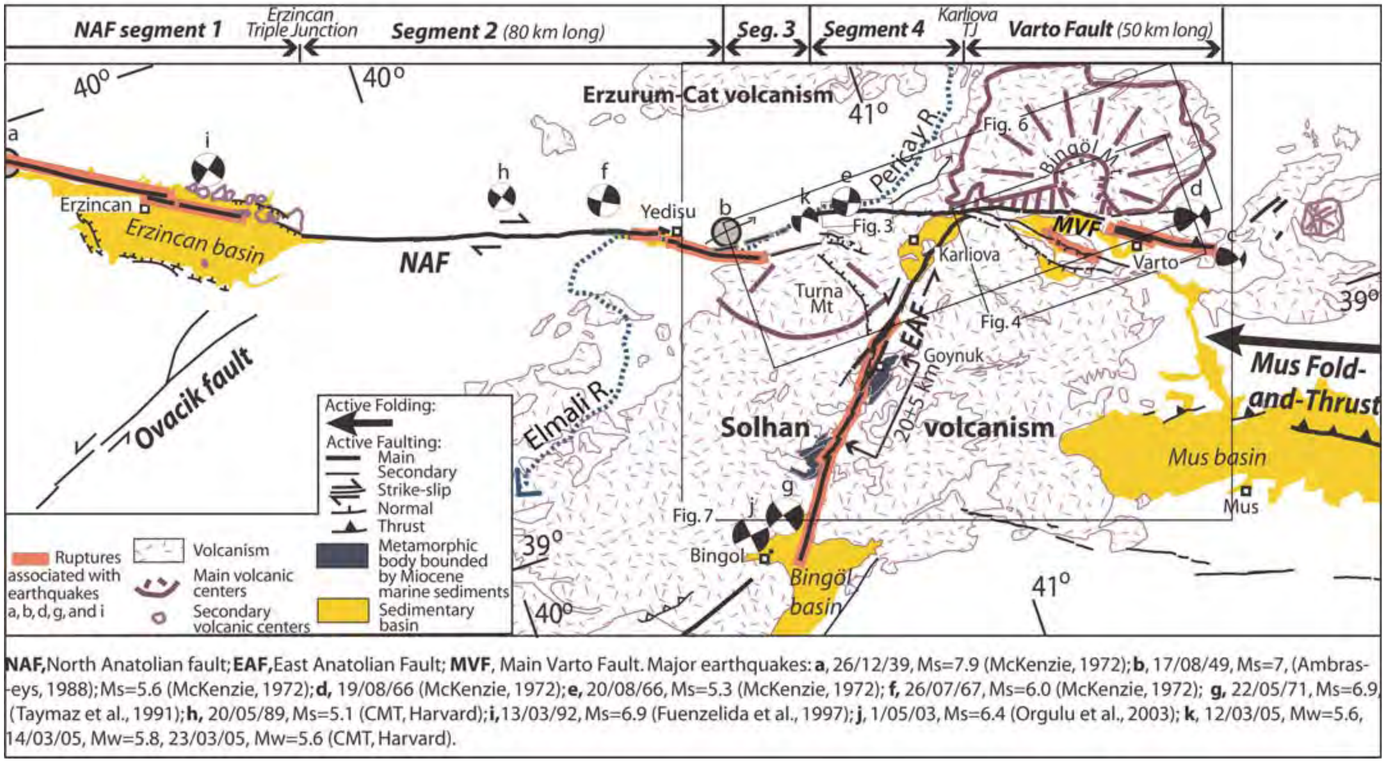

Fig. 2. The Anatolia/Eurasia/Arabia Triple Junction: present fault geometry, seismicity (focal mechanisms and earthquake ruptures), volcanism and sedimentary basins (see location in Fig. 3). Boxes are areas of Figures 3–7. Total offset on the East Anatolian Fault (EAF) constrained by 20 ± 5 km offset of a metamorphic body bounded by Miocene sediments and volcanism (Şaroğlu *et al.* 1992).

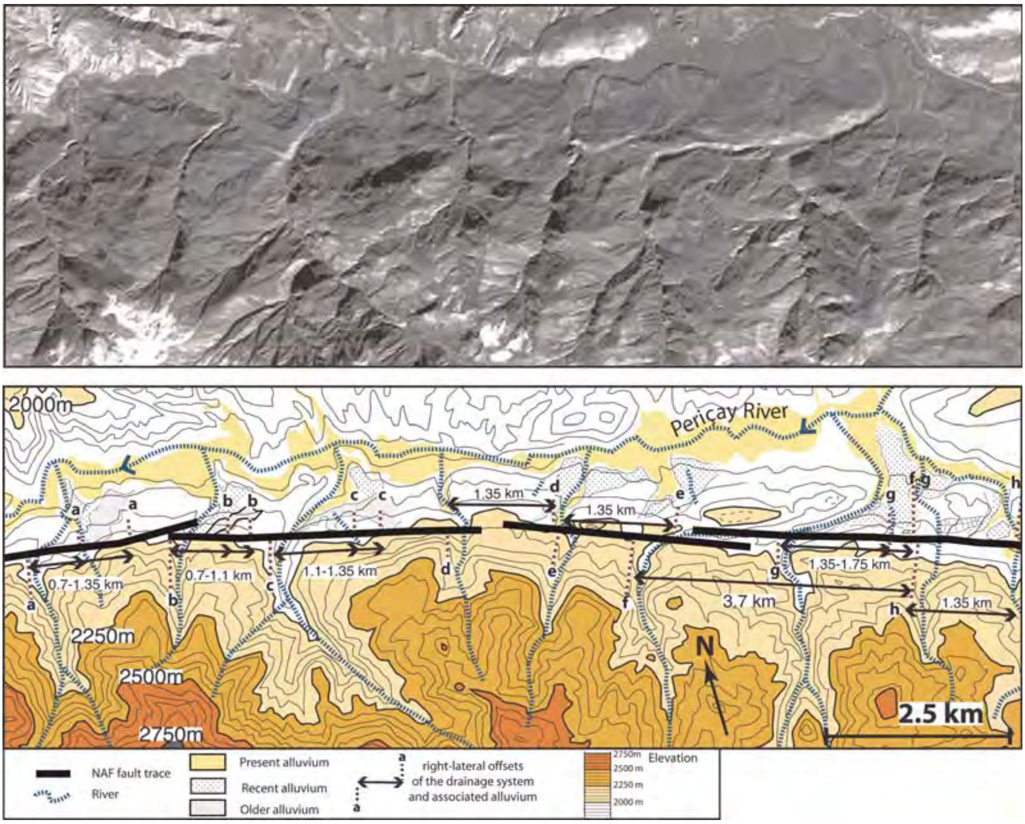

Fig. 3. Right-laterally offset morphology along easternmost segment of the North Anatolian Fault (see location in Fig. 2). Top: Spot image. Bottom: Interpretation confirmed by fieldwork, showing river offsets reaching 3.7 km, and river captures (offsets d and e).

the Main Varto Fault; most splay from the Triple Junction, though some splay from the East Anatolian Fault just SE of the town of Karliova (Fig. 6). The Varto horsetail is also associated with fissure-fed lava flows and intrusion located mostly along faults. The largest intrusions form significant volcanic domes elongated along bounding faults (Figs 4 & 5). South of the town of Varto the fissural volcanism cross-cuts older volcanic product related to the Bingöl half-caldera (Buket & Görmüş 1986; Buket & Temel 1998). Significant shortening in the Triple Junction area occurs only 20 km south of Varto along the Muş fold-and-thrust belt (Fig. 2; Şengör *et al.* 1985; Dewey *et al.* 1986).

At the Triple Junction, the East Anatolian fault ends against the North Anatolian and Main Varto Fault systems. Its last 75 km segment smoothly bends eastward as it approaches the Triple Junction. It ruptured near Bingöl during a $M = 6.9$ earthquake in 1971 (Arpat & Şaroğlu 1972; Seymen & Aydın, 1972). The recent $M = 6.4$ earthquake in May 2003 ruptured a minor conjugate fault (Örgülü *et al.* 2003), probably related to the major change in strike of the East Anatolian Fault near the town of Bingöl (Figs 1 & 4). Near the town of Goynuk the East Anatolian Fault forms a small short-cut pull-apart associated with lacustrine sediments intercalated with lavas of the Turna Mountain and with lignite deposits (Fig. 7).

Recent volcanism at the Anatolia–Eurasia–Arabia Triple Junction

The most salient feature of the Triple Junction is the presence of widespread recent volcanism (Figs 2, 6a; Dewey *et al.* 1986) that has spectacularly recorded the cumulated deformation.

Along the North Anatolian Fault, we are able to reconstruct a single volcanic edifice from two offset structures (Fig. 6). The first structure, neatly cut

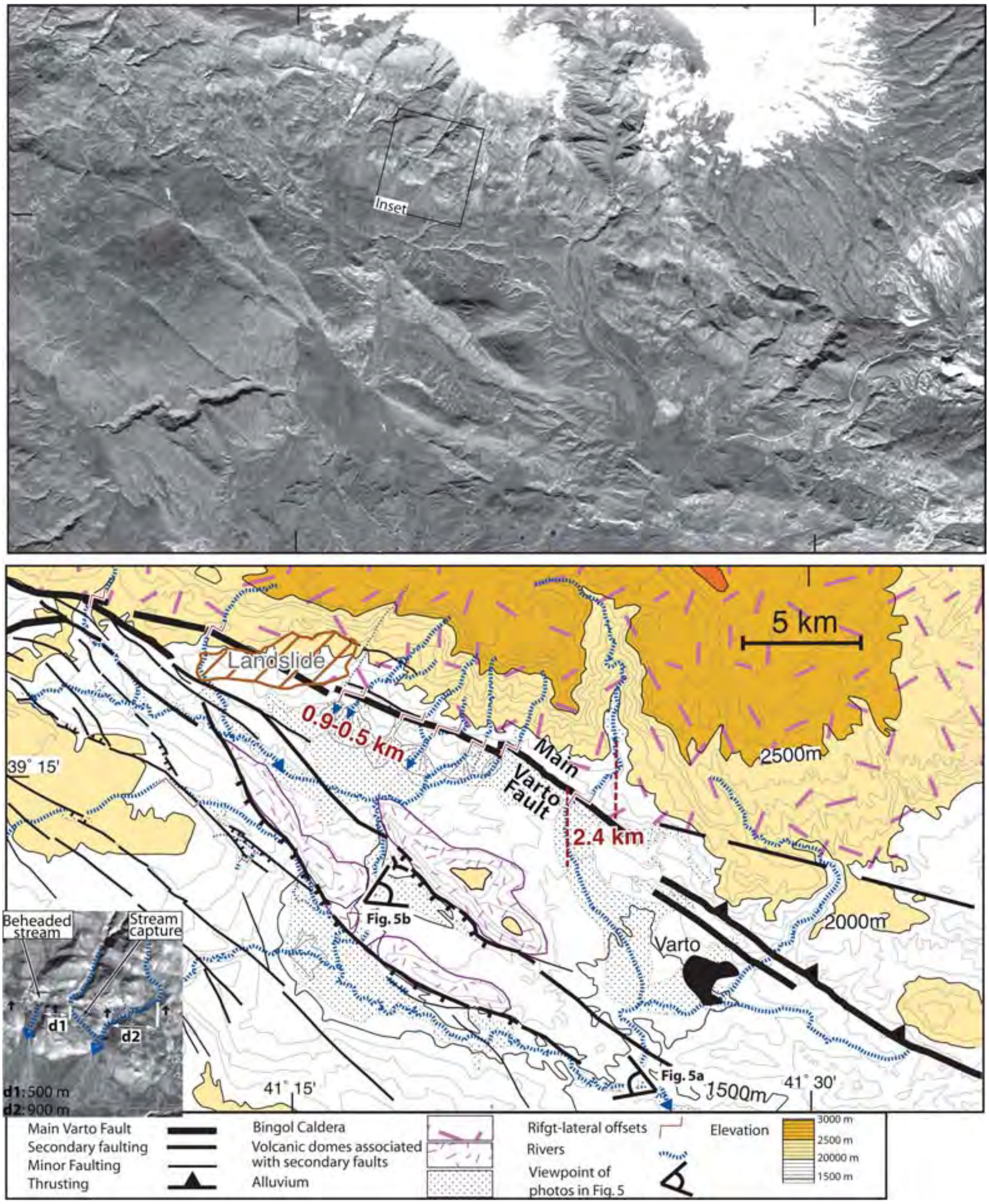

Fig. 4. Deformation splaying east of Karliova Triple Junction forming the large Varto horsetail (see location in Fig. 2). Main Varto Fault at the foot of the Bingöl Caldera accommodates mainly right-lateral deformation with a thrusting component at its eastern extremity. Secondary right-lateral and normal deformation associated with volcanic domes occurs to south. Top: Spot image. Bottom: Interpretation confirmed by fieldwork. Inset: beheaded drainage system along the Main Varto fault confirming right-lateral motion.

to the south by the Main Varto Fault, is the Bingöl half-caldera east of Karliova. The second structure, cut to the north by the North Anatolian Fault, is the semi-circular Turna Mountain west of Karliova. Both structures are composed of volcanic rocks having similar stratigraphic ages (Yılmaz *et al.* 1987; Şaroğlu & Yılmaz 1987, 1991). We can restore the position of the Turna Mountain opposite

Fig. 5. Photos of the volcanic domes associated with the Varto Fault system (viewpoints in Fig. 4).

to the Bingöl half-caldera by a left-lateral displacement of 50 km along the mean direction of the North Anatolian and Main Varto Fault systems (Fig. 6b). As a result a volcano with a nearly conical morphology can be reconstructed. The caldera palaeo-topography along the North Anatolian Fault has been strongly modified by strike-slip faulting and related enhanced erosion. Secondary normal faulting affecting the Turna half-caldera (Fig. 6c) has also altered the initial volcanic structure. Despite the alterated original morphology, the reconstructed volcanic topography excludes any significant relative long-term vertical movement across the North Anatolian Fault. Indeed the topographic profile in Figure 5c across the Turna/Bingöl volcano shows a coherent triangular shape which centre location is nearly identical to the centre location of the Bingöl half caldera as defined by its summital shape.

The age of the volcanism around the Karliova Triple Junction is constrained by $^{40}Ar-^{39}Ar$ dating (Figs 7, 8 & Tables 1 and 2). $^{40}Ar-^{39}Ar$ ages were obtained on groundmass samples of lavas, with K concentrations ranging from 0.8% to 3.3%. As in practically all terrestrial basalts, our samples show variable amounts of aqueous high- and low-temperature alteration, especially of the groundmass. Geologically meaningful results have been reported in spite of the alteration (e.g. Fleming *et al.* (1997) and references therein). In the present work we will show that consistent results can be obtained from whole rock samples by the deconvolution of the least altered Ar-bearing phases from the alteration products using the Ca–K and Cl–K ratios derived from Ar isotope systematic (see Villa *et al.* 2000). To unravel the effects of alteration, the most reliable criterion is a low Cl–K ratio, as Cl is observed to be characteristically high in secondary minerals. Steps having a constant and low Cl/K signature (which usually coincides with a constant and low Ca–K ratio, typical of groundmass) are termed 'isochemical' and used to calculate a weighted average age. In two cases, no constant chemical ratios were obtained, but Cl–K ratios correlate with age, so that we performed a regression to zero chlorine (see Fig. 8).

The fact that lavas forming the Turna Mountains and the Bingöl half-caldera have similar ages (Figs 7 & 8) but distinct from the surrounding volcanism supports the morphological restoration of the

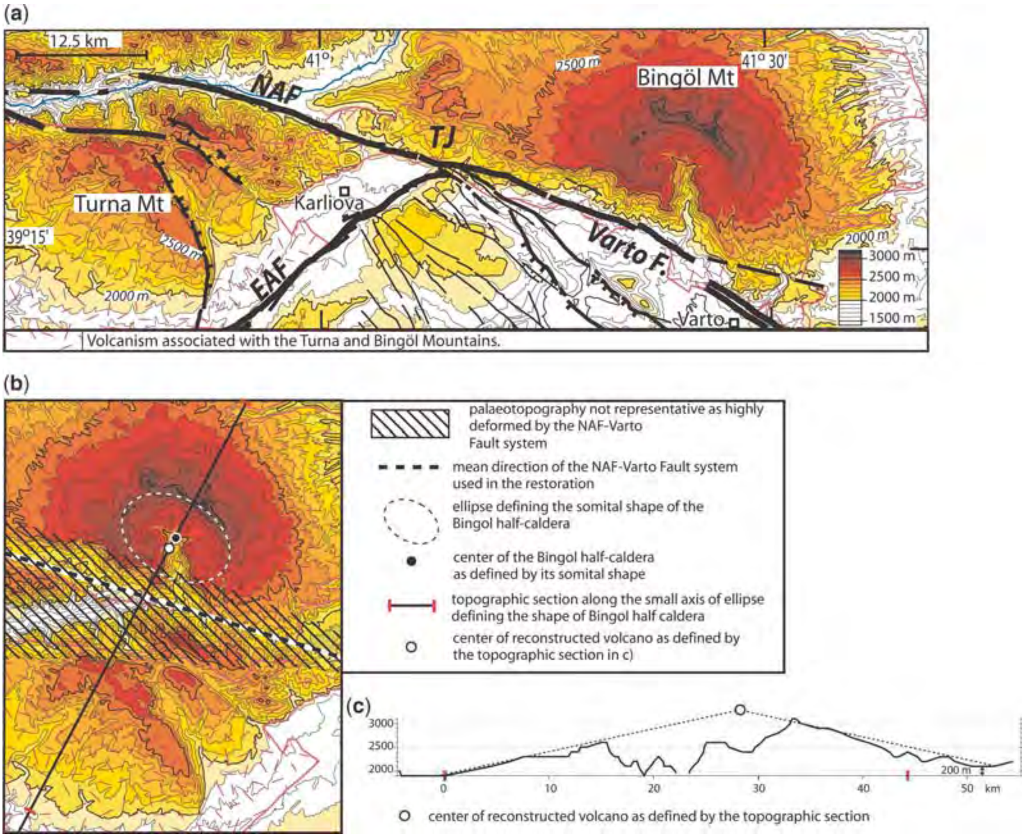

Fig. 6. Volcano reconstruction by a 50 km left-lateral displacement along North Anatolian and Main Varto Fault systems (see location in Fig. 2). (**a**) Present morphology of the junction of the North and East Anatolian Faults with active faults in black and volcanism. Thick lines: main faults; thin lines: secondary faults; lines with ticks: normal motion component. (**b**) After restoration of 50 km, the Turna and Bingöl mountains are put in front of each other, reconstructing a single volcanic edifice. Volcano palaeo-topography is strongly modified along the North Anatolian and Main Varto Fault systems. On its SE flank, normal faulting also deforms the topography. The somital shape of the Bingöl half-caldera has an elliptical shape reflecting a slight elongation of the volcano in a NW–SE direction. (**c**) Topographic profile across the restored volcano. The location of volcano center extrapolating upward the volcano flanks is nearly identical to the one derived from the somital shape of the Bingöl half caldera showing that long-term uplift across the North Anatolian Fault is negligible.

caldera. The Turna Ar–Ar age of 2.85 $\pm$ 0.05 Ma (sample Tu1 in Fig. 8c coherent with sample Tu2 in Figs 8c & d) precisely matches the ages of the Bingöl half-caldera (samples Bi1: 3.13 $\pm$ 0.09 Ma, Bi2: minimum age 3.11 $\pm$ 0.33 Ma, Bi3: 3.1 $\pm$ 0.29 Ma in Figs 8a & b); these ages are coincident with, and are more reliable than, the whole-rock K–Ar ages obtained by Pearce *et al.* (1990) (see Fig. 7). Both half calderas rest on top of older volcanic rocks (Figs 2 & 7). The Turna volcanism lies on the 7.3 to 4.1 Ma old Solhan formation (see Fig. 7, and sample So1 in Fig. 8f). The age of this formation is quite well constrained near the East Anatolian Fault because its volcanism was an obsidian source during prehistoric time (Chataigner *et al.* 1998; Poidevin 1998; Bigazzi *et al.* 1998). The Bingöl half-caldera lies to the NW on the 6.9 to 5.6 Ma old volcanism of the Aras valley (Innocenti *et al.* 1982*a*) and to the NE on the 8.3 to 6.0 Ma old Erzurum volcanism [8.3 $\pm$ 0.1 Ma to 6.0 $\pm$ 0.3 Ma (Innocenti *et al.* 1982*a*); 6.9 $\pm$ 0.32 (Bigazzi *et al.* 1994); 6.83 $\pm$ 0.36 (Bigazzi *et al.* 1997); 8.4 $\pm$ 0.2 Ma (Chataigner *et al.* 1998)]. On the contrary the volcanism south of the Main Varto Fault is more recent than the Bingöl half-caldera as attested by fissure-fed lava flows and fault-related intrusions cross-cutting Bingöl related volcanic products (Buket & Görmüş 1986; Buket & Temel 1998). The latter is also supported by $^{40}Ar–^{39}Ar$ dating

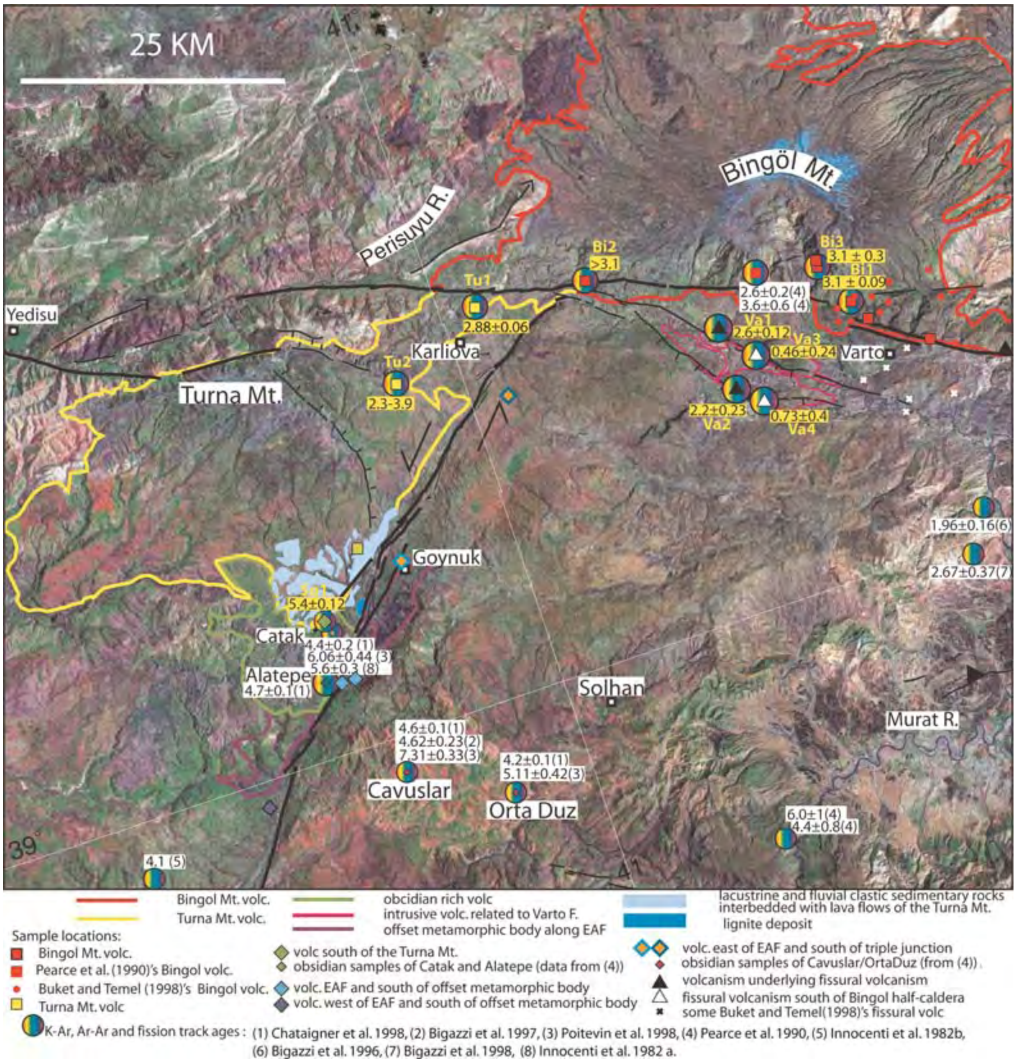

Fig. 7. Detail mapping of volcanism at the triple junction with location of volcanic samples and ages (see location in Fig. 2, age spectra in Fig. 8, and geochemical composition in Table 1). Mapping of the Turna and Bingöl volcanism done combining fieldwork, Landsat images, and reinterpreted published geological maps (Altinli 1961; Bingöl *et al.* 1989; Tarhan 1993, 1994; Buket & Temel 1998; Herece & Akay 2003). Locations of samples of Pearce *et al.* (1990), Buket & Temel (1998), Poitevin (1998) used in Fig. 9 are shown. Samples from Bingöl Mt. (Bi1: 3.1 ± 0.09 Ma; Bi2: min. age 3.1 Ma; Bi3: 3.1 ± 0.3 Ma) and Turna Mt. (Tu1: 2.88 ± 0.06 Ma; Tu2: 2.3 − 3.9 Ma) show similar ^{40}Ar–^{39}Ar ages, while Sohlan volcanism south of Turna Mt. (So1: 5.39 ± 0.12 Ma) is older and fissural Varto volcanism is younger (Va1 and Va2 sampled at the base of the domes along incised river valley have ages of 2.6 ± 0.12, 2.2 ± 0.23 Ma respectively, whereas Va3 and Va4 sampled on the flank of the domes have ages of 0.46 ± 0.24 Ma and 0.73 ± 0.4 Ma respectively). Ages obtained are coherent with other published ^{40}Ar–^{39}Ar, K–Ar, and fission track ages.

(Fig. 8) with samples taken at the base of and on the two main volcanic domes related to the Varto horsetail (Fig. 4). The ^{40}Ar–^{39}Ar ages (Fig. 8), although of lower precision, indicates that volcanism south of the Bingöl half caldera started 2.2 ± 0.23 to 2.6 ± 0.12 Ma ago (Fig. 8e) and that the two main volcanic domes are 0.46 ± 0.24 Ma and 0.73 ± 0.39 Ma old (Fig. 8g and h). Those ages are coherent with ages of fissure volcanisms further south along the Murat river across the Muş fold-and-thrust belt (Fig. 7; Bigazzi *et al.* 1996, 1998).

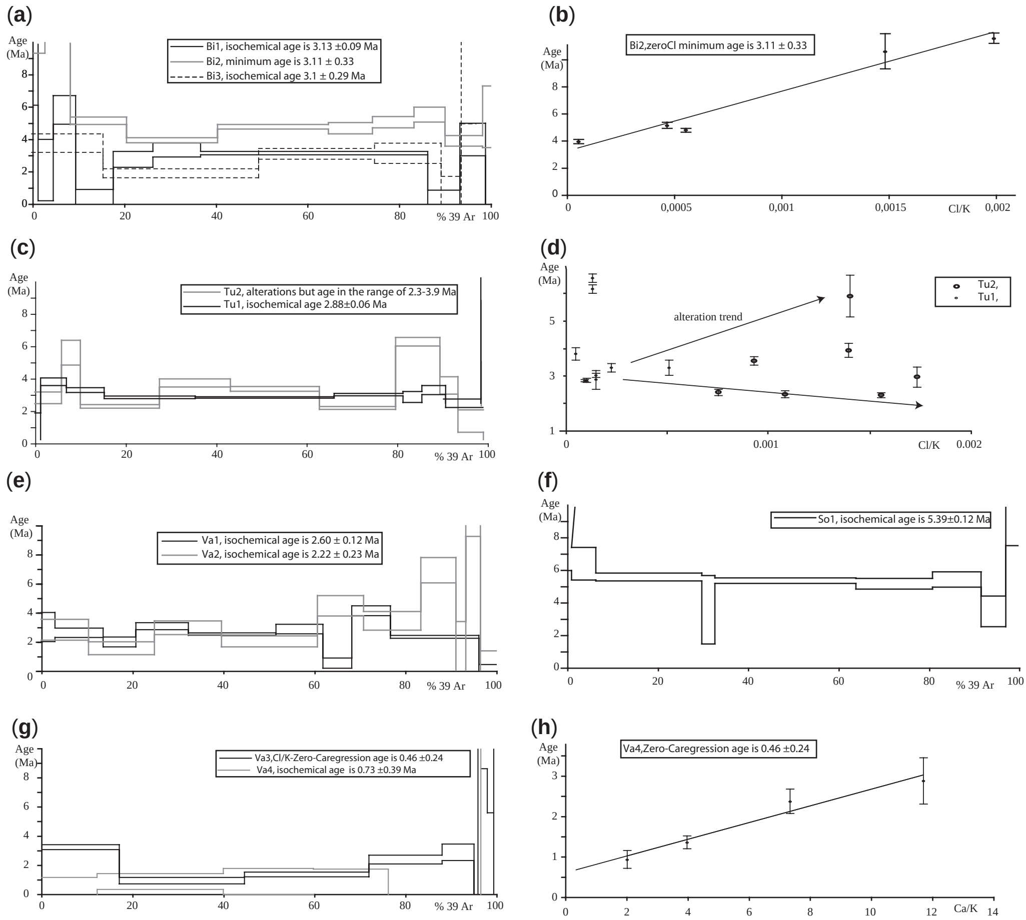

Fig. 8. ^{40}Ar–^{39}Ar dating age spectra for lavas near the triple junction (see sample locations in Fig. 7 and data in Table 2). Analytical procedures of the stepwize heating exactly followed the ones detailed in Villa *et al.* (2000). (**a**) Age spectrum for sample Bi1, Bi2, Bi3; Bi1 isochemical age is 3.13 $\pm$ 0.09 Ma (1 sigma error) using steps 5–7 having Cl–K ratio $<$ 0.0046; Bi2 zero Cl minimum age is 3.11 $\pm$ 0.33 Ma; for Bi3, steps 3 and 4, having Cl–K ratio $<$ 0.0052 and Ca–K ratio $<$ 3, define an isochemical age of 3.11 $\pm$ 0.29 Ma. (**b**) Three-isotope correlation plot for Bi2; the zero-Cl minimum age is 3.11 $\pm$ 0.33 Ma using a regression on steps 1–5. (**c**) Age spectrum for sample TU1 and TU2; TU1 isochemical age is 2.88 $\pm$ 0.06 Ma using steps 4–7 having Cl–K ratio $<$ 0.00015. (**d**) Three-isotope correlation plot for TU1 and TU2. The usual criteria (low Cl–K and Ca–K ratios) produce no simple pattern for TU2. Steps 3–6 with relatively low Cl–K ratio have ages in the range 2.3–3.9 Ma. Comparison with less altered TU1, and with other more altered samples of the North Anatolian Fault suite, suggests that two distinct alteration episodes are recorded, both revealed by high Cl–K ratios. Zero-Cl extrapolations of the two trends are compatible with the 2.85 Ma age of TU1. (**e**) Age spectrum for samples Va1 and Va2. For Va2, the Ca–K ratios are bimodally distributed and require two phases; the isochemical age, calculated on the K-rich steps 1–4, is 2.22 $\pm$ 0.23 Ma. For Va1, the isochemical age on steps 1–6, having Cl–K ratio $<$ 0.008, is 2.60 $\pm$ 0.12 Ma. (**f**) Age spectrum for sample SO1. The isochemical age is 5.39 $\pm$ 0.12 Ma on steps 2–7. (**g**) Age spectrum for samples Va3 and Va4. The Va4 isochemical age is 0.73 $\pm$ 0.39 Ma on steps 1–4. (**h**) Three-isotope correlation plot for sample Va3. The zero-Ca regression age is 0.46 $\pm$ 0.24 Ma using steps 2–5. Both Va3 and Va4 samples robustly define an age $<$ 1Ma for the latest phase of Varto fissural volcanism south of Bingöl half-caldera.

Finally the Bingöl/Turna lavas have an undistinguishable geochemistry considering major or trace elements, quite distinctive from the surrounding volcanism. In total alkali versus SiO_2 diagram (Fig. 9a & Table 1) the Bingöl/Turna volcanic rocks form a well defined trend from basaltic trachy-andesite to the rhyolite field, and can be considered to be transitional between sub-alkaline and mildly alkaline in character. The more recent dyke volcanism just south of the Bingöl Half Caldera is

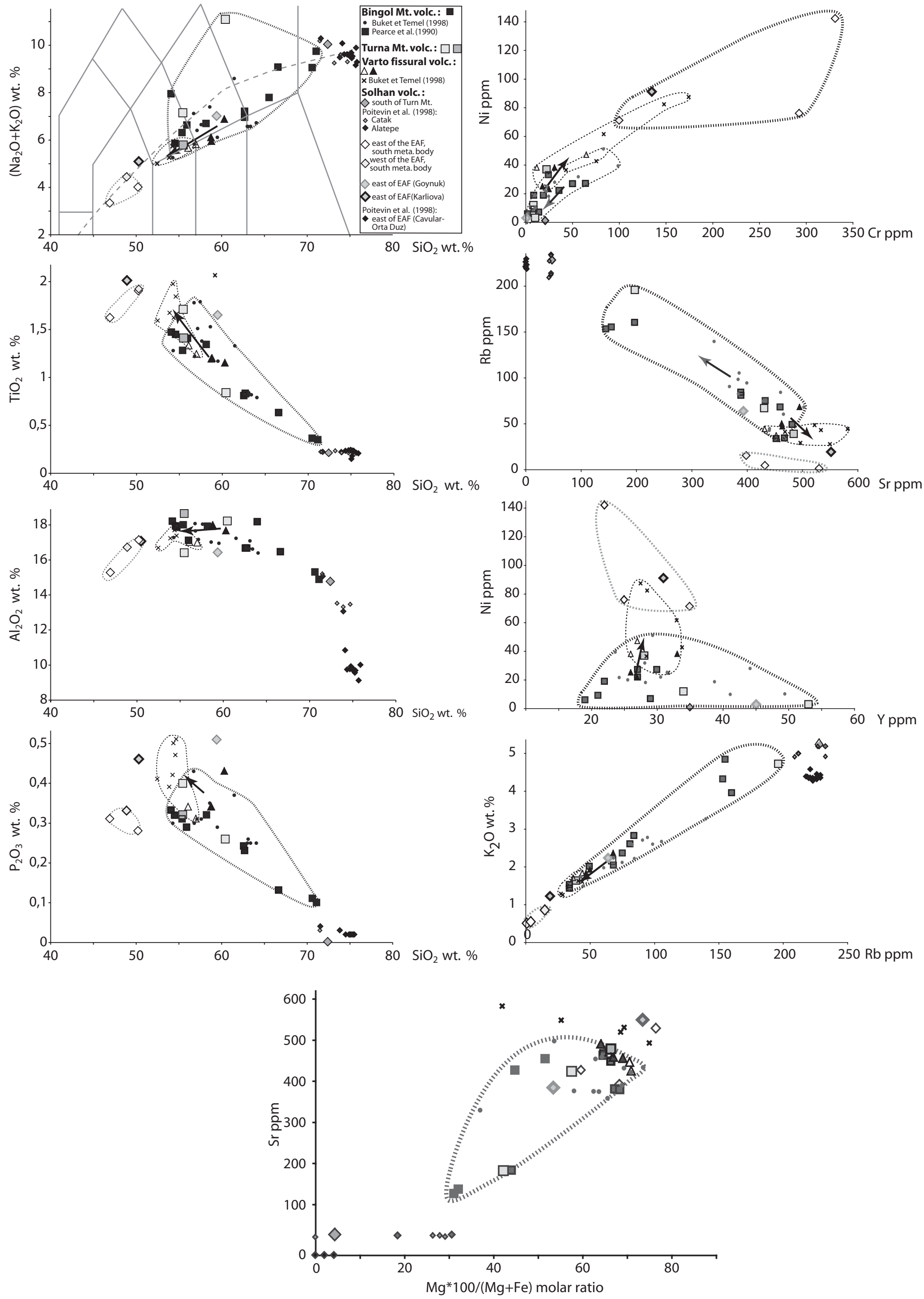

Fig. 9. Plot of some major, minor and trace elements for samples located in Figure 7. Data show that the Bingöl and Turna volcanisms are similar, whereas the volcanisms south of the Bingöl half-caldera and along the East Anatolian Fault have different characteristics. Volcanism south of the metamorphic body mapped in Figure 7 on either side of the East Anatolian Fault is identical confirming a total offset of 20 $\pm$ 5 km on the East Anatolian Fault and an activation

mostly subalkaline but relative to the Bingöl/Turna one it has less alkali, is enriched in K, Ni and Sr and depleted in Rb. Furthermore Buket & Temel (1998) have clearly demonstrated that this volcanism is isotopically distinct from the Bingöl samples. The lavas just south of Turna Mountain, rich in obsidians (Catak-Alatepe sites of the Solhan formation) are rhyolites to be considered transitional between sub-alkaline and mildly alkaline trend. Compared to the Bingöl/Turna volcanism these lavas have more alkali, less Al_2O_3, less TiO_2, a high Rb/Sr ratio, high Ba and low Zn. Other volcanic rocks around the East Anatolian Fault–Solhan Formation are mostly basalts with a transitional character similar to the Bingöl/Turna volcanism but with less alkali, higher Mg, Ti, Ni and Cr content, lower Nb and Zr, and a very low Rb/Sr ratio.

Together with the fact that the two structures are truncated to the south and to the north by a continuous right-lateral fault system, all these observations strongly suggest that the Turna Mountain and the Bingöl half-caldera have a common origin, and are presently offset by about 50 km along the North Anatolian Fault.

Independently, one can also use the volcanism along the East Anatolian fault to further constrain its age and total offset. We estimate the total displacement of the East Anatolian fault by evaluating the offset of a metamorphic/Miocene body surrounded by volcanism (Fig. 2; Şaroğlu *et al.* 1992). A single structure can be reconstructed by a right-lateral displacement of 20 ± 5 km (Arpat & Şaroğlu 1972; Seymen & Aydın 1972; Şaroğlu *et al.* 1992; Westaway 1994, 2003). The Solhan volcanism just south of the so-reconstructed structure has similar age, and undistinguishable geochemistry across the East Anatolian Fault (samples represented with blue diamond in Fig. 7 and in Fig. 9 white and light grey diamonds limited by a thin black line). In addition, the boundary of the single structure so obtained with the surrounding Solhan formation (6–4.1 Ma old) is smooth across the fault: this formation is not related to movement along the East Anatolian Fault and is clearly cross-cut by the later fault (Fig. 7). This shows that the age of the East Anatolian Fault should be less than 4 Ma as already proposed by others (e.g. Şaroğlu *et al.* 1992; Westaway & Aeger 2001). On the contrary, the lacustrine sediments and lignite deposits near Goynuk are most probably related to the extensional step-over of the East Anatolian Fault in that area (Fig. 7). The fact that those sediments are interbedded with the most recent volcanic products of the Turna Mountain suggests that the East Anatolian Fault was active in that area 2.88 Ma ago.

Evolution of the Anatolia–Eurasia–Arabia Triple Junction

The following scenario emerges. The complete Turna–Bingöl caldera was formed from 3.6 to 2.8 Ma ago, before being cut and right-laterally offset 50 km by the North Anatolian Fault. This offset is equal to the Varto fault system total length and is similar to: (1) the geological offset of the North Anatolian Fault near Yedisu – offset of a thrust contact between ophiolitic mélange and volcanoclastic units (Herece & Akay 2003, appendix 13; Şengör *et al.* 2005) and to (2) the offset of the Elmal-Peričay river system (Fig. 2). Fissural volcanism related to the birth of the Varto fault system started 2.6 Ma ago. The volcano offset and volcanism age thus imply that the easternmost segment of the North Anatolian Fault and the present Triple Junction are younger than 2.8 Ma, establishing around 2.6 Ma ago. The deduced average slip rate of the North Anatolian Fault over the last 2.6 Ma of about 20 mm/a roughly corresponds to its present-day rate. The later rate is however a lower bound as secondary deformation exists. With a complete formation of the East Anatolian Fault 2.8 to 3 Ma ago, we get a minimum geological slip rate of the East Anatolian Fault of 7 mm/a, which is comparable to the 9–10 mm/a GPS derived rate (McClusky *et al.* 2000; Reilinger *et al.* 2006) and to the 11 ± 1 mm/a geomorphological rate determined further south (Çetin *et al.* 2003). The main puzzle remains the strong mismatch between the East Anatolian Fault (*c.* 3 Ma) and North Anatolian (12 Ma) ages that we discuss below.

It is well known that a two-phase extrusion process characterizes the India/Eurasia collision (Tapponnier *et al.* 1982). Westaway & Aeger (1996) suggest that a similar scenario is valid for the Anatolia extrusion, with a southward jump of the East Anatolian Fault. The North Anatolian Fault would have kept the same location because the stable Black Sea oceanic lithosphere prevents any new large fault propagation north of its present trace. The Anatolian extrusion would first occur between the North Anatolian Fault and a proto East Anatolian Fault, which can be identified

Fig. 9. (*Continued*) of the East Anatolian Fault after the deposition of the Solhan volcanism that ends 4.4 Ma ago. Varto Fissural volcanism (dark dashed line group) has slightly evolved (see black arrow) through time. Dark filled triangles represent lavas at the base of the fissural volcanism, open triangles lavas of the domes, and black crosses volcanism at the eastern end of the Varto fault system.

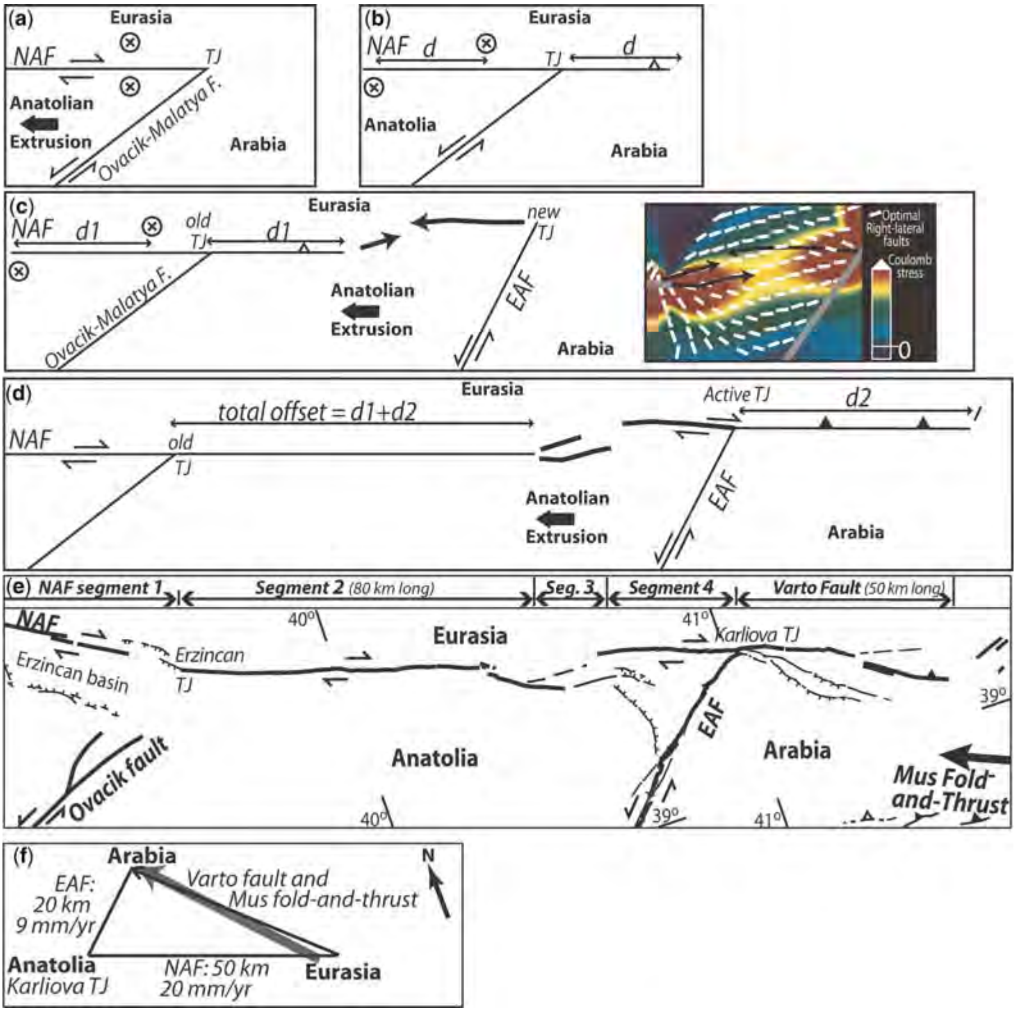

Fig. 10. Possible evolution of the Anatolia/Eurasia/Arabia Triple Junction assuming that faults separate rigid blocks. (**a**) Birth of a triple junction (TJ) in an extrusive plate system where a main left-lateral strike-slip fault meets a main right-lateral strike-slip fault like the North Anatolian Fault. Triple Junction corresponds to Erzincan triple junction. (**b**) Geometry of Transform/Transform/Trench Triple Junction after a North Anatolian Fault total slip of *d*. Triple Junction moves westward at slip rate of the North Anatolian Fault (McKenzie & Morgan 1969). Eurasia/Arabia boundary accommodates both right-lateral and reverse motion and has a length equal to total slip *d* of the North Anatolian Fault. Triple Junction is stable because the North Anatolian Fault and the Eurasia/Arabia boundary are collinear. (**c**) Propagation of new left-lateral strike-slip fault (EAF) into Arabia at a time when $d = d_1$. At eastern extremity of the North Anatolian Fault (NAF) new fault segments are created as a link with East Anatolian Fault and a new triple junction (Karliova TJ) is activated. By this process part of the Arabian plate is accreted to the Anatolian plate. Inset: stress field and optimal failure planes around the North and East Anatolian tips at a time just before establishment of present easternmost North Anatolian segments and creation of Karliova Triple Junction. Gray segments are deep seated localized shear zones representing the North and East Anatolian Faults with a geometry similar to Figure 9c. Optimal right-lateral failure planes for right lateral faulting (white segments) have orientations similar to North Anatolian Fault observed fault geometry west to the present Triple Junction (segments 3 and 4 in 10e represented by bold black segments). (**d**) Geometry after a total slip of $d = d_1 + d_2$ on North Anatolian Fault. Karliova Triple Junction kinematics is identical to Figure 10a, and in particular the total length of the new Eurasia/Arabia plate boundary (d_2) is equal to North Anatolian Fault offset over the last 2.5 Ma. (**e**) Present fault geometry to compare to plate model in d. Structural elements like in Figure 2. (**f**) Triangular vector diagram constrained by strikes of North and East Anatolian Faults, and by slip rates and finite displacement along both faults. Slip rate along the Varto-Muş fault system may be inferred in this way. Gray arrow represents velocity of Karliova derived from an Eulerian vector for Arabia/Eurasia (23.5°N, 23.8°E, 0.5°/Ma) within the errors bounds of the McClusky *et al.* (2000) pole (25.6 ± 2.1°N, 19.7 ± 4.1°E, 0.5 ± 0.1°/Ma).

with the left-lateral Ovacık–Malatya fault, located 110 km more to the west. An old Triple Junction would thus have been located in the Erzincan basin (Fig. 2). Our observations, and in particular the age difference between the North Anatolian Fault (12 Ma), the East Anatolian Fault (2.8–3 Ma) and the present Triple Junction (2.6–2.8 Ma), strongly support this view. Our timing is however different from what Westaway (2004) proposes. The latest extrusion phase would have started about 2.6–3 Ma ago, with the activation of the East Anatolian Fault linked to the Dead Sea Fault and the jump of the Triple Junction to its present location near Karliova. This explains why the easternmost North

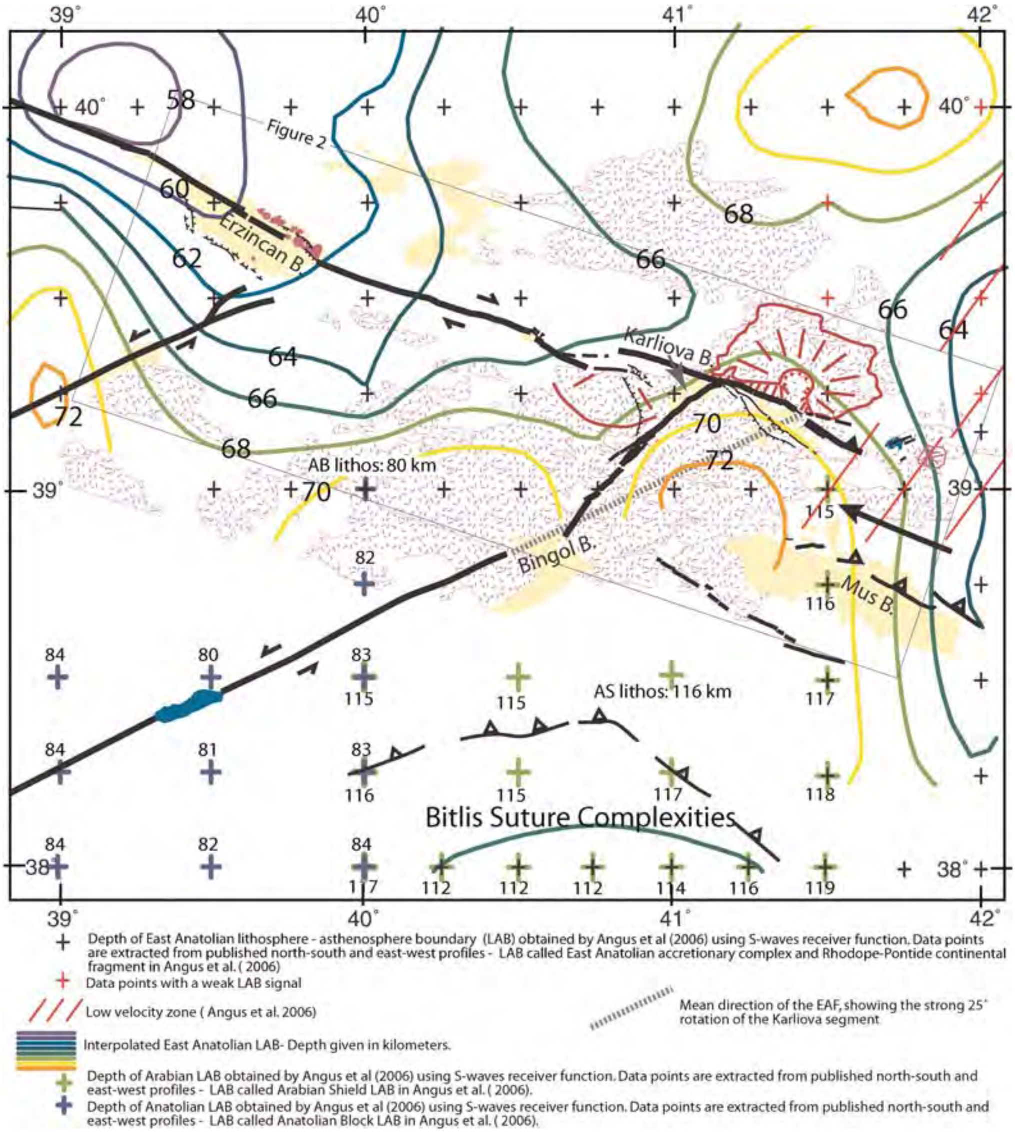

Fig. 11. Lithospheric complexities at the Anatolia/Eurasia/Arabia triple junction. Lithosphere-asthenosphere boundary (LAB) maps obtained from S-wave receiver functions (Angus *et al.* 2006) superimposed on fault map and volcanism as in Figure 2. The North and East Anatolian Faults, and associated structures appear to be rooted deeply in the lithosphere. Note that the 75 km long Karliova segment of the East Anatolian Fault scales exactly with the lithospheric thickness and seems rotated anti-clockwise by 25° with respect to the mean strike of the East Anatolian Fault farther south.

Anatolian Fault must be younger than the North Anatolian segments west of Erzincan, and why the offset of the Bingöl Volcano is significantly smaller than the 85 km total offset of the North Anatolian Fault further west.

The eastward jump of the East Anatolian Fault may have different origins. It occurs at the same time as an increase in deformation and exhumation rates observed in many fold-and-thrust belts (e.g. Axen *et al.* 2001; Morton *et al.* 2003) within the collision zone. The latter has been interpreted as a large scale reorganization of the Arabia-Eurasia collision, 5 $\pm$ 2 Ma ago (Allen *et al.* 2004). An other possible cause is the rapid post-3 Ma change in the Africa/Eurasia motion (Calais *et al.* 2003) directly affecting the Aegean subduction zone and thereby the kinematics of the Anatolian block (Fig. 1). A further possibility would be a direct connection with the arrival of the North Anatolian Fault into the Aegean 3 Ma ago (Gautier *et al.* 1999), which relaxed the elastic strain in the Anatolian lithosphere and transformed the North Anatolian Fault into a transform fault (Armijo *et al.* 2003; Flerit *et al.* 2004). A last cause might be the slab detachment that occurred beneath eastern Anatolia as discussed by Faccenca *et al.* (2006). Whatever its origin, this new set-up would make the extrusion process more efficient, consistently with the substantial increase of the slip rate of the North Anatolian Fault and the localization of deformation on the North Anatolian Fault present strand (Barka & Hancock 1984). Finally it coincides with the recent change in the kinematics in the area around the present intersection between the East Anatolian Fault and the Dead Sea fault (Yürür & Chorowicz 1998; Över *et al.* 2002, 2004).

We have tentatively modelled the overall evolution of Anatolia–Eurasia–Arabia Triple Junction using a plate-tectonic framework where deformation is associated with rigid block motion (Fig. 10). The kinematics of the Karliova and the old Erzincan Triple Junction is modelled as a Transform/Transform/Trench Triple Junction similar to the Mendocino Triple Junction (McKenzie & Morgan 1969). Approximating the behavior of the eastern Turkey continental lithosphere like an oceanic one though subject to caution may still be valid to the first order for the following reasons. First, Jimenez-Munt & Sabadini (2002) have shown that Anatolia had a hard lithospheric rheology. In addition, the eastern crust is only slightly thickened being on average less than 45 km thick so gravitational driving force may be neglected to the first order (Zor *et al.* 2003; Çakir & Erduran 2004). Finally, like oceanic lithosphere eastern Turkey has an anomalously thin (60 to 80 km)

Table 1. *Samples coordinates and geochemical analyses (major and trace elements). Major elements are in % and trace elements in ppm (sample locations are reported in Fig. 7)*

Samples	Bi1	Bi2	Bi3	Bi4	Bi5	Bi6	Tu1	Tu2	So1	So2
Latitude	39.2232	39.307	39.2588	39.2617	39.2034	39.1675	39.3264	39.278	39.1091	39.1562
Longitude	41.4445	41.1756	41.417	41.4169	41.4522	41.5122	41.0522	40.953	40.7818	40.8426
SiO_2	54.59	66.62	62.73	62.62	54.12	55.98	60.45	55.46	72.44	55.5
TiO_2	1.44	0.63	0.83	0.81	1.47	1.41	0.84	1.71	0.21	1.41
Al_2O_3	17.87	16.44	16.66	16.65	18.16	17.12	18.22	16.42	14.75	18.63
Fe_2O_3	8.4	3.58	5.29	5.25	8.47	7.55	5.23	9.17	1.98	6.64
MnO	0.11	0.04	0.09	0.09	0.11	0.11	0.1	0.14	0.01<	0.11
MgO	3.64	0.62	2.49	2.36	3.39	3.22	0.84	2.73	0.02	2.87
CaO	7.8	2.39	5.18	5.2	8.06	7.48	2.44	6.39	0.6	8.06
Na_2O	4.33	5.11	4.36	4.34	6.51	4.61	6.36	4.98	4.8	4.15
K_2O	1.53	3.95	2.82	2.6	1.44	2.01	4.73	2.17	5.23	1.64
P_2O_5	0.32	0.13	0.23	0.24	0.33	0.29	0.26	0.4	0.00<	0.32
H_2O^+	0.76	0.64	0.86	0.08	1.15	1.93	0.89	0.11	0.34	1.48
H_2O^-	0.56	0.73	0.18	0.17	1.08	0.22	0.65	0.44	0.17	0.18
Ba	191	268	322	236	437	438	325	389	207	235
Cr	64	14	9	19	50	36	10	8	21	22
Cu	30	3	14	22	29	66	86	39	−5<	30
Nb	16	16	18	18	19	15	47	21	16	15
Ni	27	7	19	19	27	22	3	12	2<	37
Pb	24	23	20	21	16	28	38	35	34	26
Rb	34	160	84	81	34	49	196	67	228	39
Sr	453	197	389	389	468	481	197	431	48	484
Y	27	29	22	22	30	27	53	34	35	28
Zn	79	62	61	61	82	81	101	90	35	71
Zr	245	430	262	254	263	237	753	312	309	216

lithosphere (Angus *et al.* 2006), with an upper most mantle partly molten and asthenospheric material in close proximity to the base of the crust (Gök *et al.* 2003; Al-Lazki *et al.* 2003; Maggi & Priestley 2005).

Predictions from the above simple model are in good agreement with the observations. The length of the straight segment east of the Erzincan Triple Junction (segment 2 in Fig. 2; $d_1 + d_2$ in Fig. 10d) do match the total offset of the North Anatolian Fault of 85 km. In addition a model of strain distribution (inset in Fig. 10c) resulting from motion along the 'old' North Anatolian Fault (segments 1 and 2) and the 'new' East Anatolian Fault is able to reproduce the non-trivial geometry of the new North Anatolian segments filling the gap between the Erzincan Triple Junction and the northern extremity of the East Anatolian Fault (segments 3 and 4 in Fig. 2; Fig. 10c). It is clearly seen in Figure 10c that the relevant fault segments strikes coincide with the optimum failure planes for right-lateral faulting. A bilateral fault propagation is also favored due to strain increase centred at the extremities of the East Anatolian Fault and 'old' North Anatolian segments. Moreover the 50 km offset of the Bingöl volcano, that records the offset of the North Anatolian Fault over the last 2.5 Ma, is equal to the offsets of the North Anatolian Fault near Yedisu and to the length of the Varto fault corresponding to d_2 in Figure 10d. Finally, the finite displacement vectors associated with the proposed kinematics over the last 2.5 Ma (Fig. 10f) are compatible with present-day motion on the North Anatolian Fault and East Anatolian Fault (McClusky *et al.* 2000; Reilinger *et al.* 2006) and with the predicted plate motion of Arabia relative to Eurasia at this location.

This proposed plate model is only a first estimate of the local kinematics. Our model particularly does not explain the apparent anti-clockwize rotation of 25° of the last 75 km long Karliova segment of the East Anatolian Fault with respect to the mean direction of the East Anatolian Fault further south as well as the related opening of the Bingöl Basin and related shortening which occurred to the north and NW of the Bingöl Basin. In addition our model does not account for secondary deformation that occurs within the plates away from the North Anatolian and East Anatolian Faults (Figs 2–7; Jaffrey *et al.* 2004). For example near the Triple Junction secondary fault systems link the North Anatolian to the East Anatolian Fault. The latter deformation agrees with the first Triple Junction model of Westaway & Aeger (2001). In their model, when the right-lateral and left-lateral faults do not meet at a point like at the present Karliova Junction, a zone of distributed extension accommodates the deformation in between the strike-slip faults and the

Table 1. *Continued*

So3	So4	So5	So6	Ka1	Va1	Va2	Va3	Va4	Va5
39.1347	39.0566	39.0563	38.9729	39.2398	39.2403	39.1814	39.2058	39.169	39.1814
40.8915	40.7836	40.7988	40.6645	41.0558	41.2967	41.2959	41.3226	41.3175	41.2959
59.41	46.96	50.26	48.92	50.32	60.34	58.83	57.03	56.12	58.78
1.65	1.62	1.9	2.01	1.92	1.15	1.2	1.24	1.33	1.19
16.43	15.26	17.12	16.7	17.05	17.65	17.97	16.96	17	17.9
7.95	11.8	12.15	12.11	10.03	4.98	6.25	7.22	7.57	5.85
0.1	0.17	0.16	0.25	0.14	0.06	0.09	0.11	0.12	0.09
2	8.42	3.95	5.68	6.11	1.96	2.78	3.88	3.99	2.87
5.18	12.28	9.72	9.92	8.99	5.94	6.3	7.14	7.83	6.44
4.78	2.83	3.46	3.58	3.87	4.51	4.11	3.97	3.95	4.18
2.23	0.5	0.54	0.85	1.22	2.36	1.83	1.83	1.7	1.92
0.51	0.31	0.28	0.33	0.46	0.43	0.34	0.31	0.34	0.34
0.26	3.16	5.59	3.11	0.89	0.66	1.39	0.49	0.71	1.27
0.70	0.88	1.77	1.06	0.65	0.54	0.69	0.23	0.59	0.49
354	247	112	306	263	286	170	336	242	222
−8<	331	293	100	135	31	18	12	65	25
300	64	121	115	40	27	46	61	31	59
19	12	9	8	15	26	18	14	16	17
3	142	76	71	91	38	25	38	47	23
30	15	14	15	11	35	23	17	20	21
64	2<	4	15	19	68	47	44	37	50
393	531	433	399	552	495	464	432	453	463
45	22	25	35	31	33	26	26	27	27
94	90	92	88	79	81	80	84	71	76
278	124	122	171	218	310	242	229	232	247

Table 2. *Argon–argon stepwise heating results. All isotope concentrations are in millilitres (ml), ages in million years (Ma), and uncertainties are one sigma. In italic are steps used to compute isochemical sample ages. Ca/K and Cl/K ratios are calculated from the total ^{39}Ar, ^{37}Ar and ^{38}Ar, the production ratios and the irradiation times*

Step	T(°C)	$^{40}Ar_{tot}$	^{39}Ar	^{38}Ar	^{37}Ar	^{36}Ar	Ca/K	Cl/K	Age (Ma)
Bi1 – 0.0313 g; J = 0.00104									
1	491	5.3271E-10 ± 5.9E-13	2.3985E-11 ± 3.6E-13	3.8660E-12 ± 1.2E-13	3.94E-10 ± 2.6E-10	1.427E-12 ± 2.2E-13	33.28 ± 22.0	0.03253	11.09 ± 5.00
2	551	9.9629E-08 ± 1.6E-13	6.5078E-11 ± 1.3E-13	5.6149E-12 ± 1.6E-13	1.202E-09 ± 2.2E-10	3.435E-12 ± 2.3E-13	37.42 ± 6.9	0.01568	2.09 ± 1.90
3	608	9.7793E-10 ± 2.7E-13	9.4257E-11 ± 9E-14	4.1216E-12 ± 1.4E-13	1.798E-09 ± 2.3E-10	2.792E-12 ± 1.7E-13	38.65 ± 5.0	0.00691	5.80 ± 0.89
4	676	1.1334E-09 ± 1.4E-13	1.5924E-10 ± 1E-13	5.2275E-12 ± 1.3E-13	4.94E-10 ± 2.1E-10	3.916E-12 ± 2.1E-13	6.22 ± 2.7	0.00392	0.16 ± 0.73
5	*736*	*9.6355E-10 ± 2.8E-13*	*1.6807E-10 ± 1.6E-13*	*5.600E-12 ± 2.3E-13*	*1.031E-09 ± 1.9E-10*	*2.692E-12 ± 1.6E-13*	*12.33 ± 2.3*	*0.00454*	*2.75 ± 0.49*
6	*790*	*9.8799E-10 ± 1.4E-13*	*2.0168E-10 ± 3E-13*	*4.1627E-12 ± 1.5E-13*	*1.888E-09 ± 2.1E-10*	*2.618E-12 ± 1.8E-13*	*18.84 ± 2.1*	*0.00189*	*3.33 ± 0.43*
7	*864*	*5.2624E-09 ± 2.1E-12*	*9.6145E-10 ± 8.7E-13*	*3.2732E-11 ± 9.4E-14*	*1.26E-10 ± 2E-10*	*1.2398E-11 ± 1.7E-13*	*0.26 ± 0.42*	*0.00458*	*3.14 ± 0.10*
8	953	2.1880E-09 ± 4.5E-13	1.3644E-10 ± 2.1E-13	1.7458E-11 ± 9.1E-14	7.56E-10 ± 2.1E-10	7.575E-12 ± 1.8E-13	11.13 ± 3.1	0.02458	0.09 ± 0.76
9	1139	3.9178E-09 ± 2.5E-13	1.0831E-10 ± 1.9E-13	1.8612E-11 ± 1.6E-13	2.196E-09 ± 1.7E-10	1.3051E-11 ± 1E-13	41.11 ± 3.1	0.03252	3.98 ± 1.00
10	1460	9.3376E-10 ± 1.6E-12	2.1946E-11 ± 7.3E-14	3.3444E-12 ± 1.4E-13	6.07E-10 ± 2.7E-10	3.644E-12 ± 2.2E-13	56.37 ± 25.0	0.02642	−8.50 ± −5.70
Bi2 − 0.036 g; J = 0.001042									
1	*490*	*4.9357E-09 ± 2.7E-12*	*1.1306E-10 ± 3.1E-13*	*4.7642E-12 ± 1.4E-13*	*9.39E-11 ± 5.6E-10*	*1.4561E-11 ± 2.3E-13*	*1.66 ± 10.0*	*0.0014853*	*10.60 ± 1.30*
2	*550*	*2.6202E-09 ± 3.7E-13*	*2.2365E-10 ± 2.1E-13*	*4.7725E-12 ± 1.8E-13*	*4.139E-09 ± 2.9E-10*	*5.304E-12 ± 1.8E-13*	*37.48 ± 2.6*	*0.0019923*	*11.56 ± 0.39*
3	*608*	*4.0213E-09 ± 1.8E-12*	*4.9954E-10 ± 7.3E-13*	*8.5184E-12 ± 2.2E-13*	*3.73E-10 ± 4.5E-10*	*9.075E-12 ± 1.7E-13*	*1.50 ± 1.8*	*0.0004678*	*5.13 ± 0.23*
4	*675*	*3.4776E-09 ± 1.1E-12*	*8.0915E-10 ± 7.4E-13*	*1.0675E-11 ± 1.5E-13*	*1.155E-09 ± 5.6E-10*	*6.327E-12 ± 1.9E-13*	*2.86 ± 1.4*	*5.49E-05*	*3.93 ± 0.16*
5	*734*	*4.4085E-09 ± 1.1E-12*	*9.8195E-09 ± 9.4E-13*	*1.4784E-11 ± 1.8E-13*	*2.480E-09 ± 4.7E-10*	*7.128E-12 ± 2.3E-13*	*5.06 ± 0.97*	*0.00055554*	*4.76 ± 0.14*
6	792	2.3159E-09 ± 6E-13	3.9112E-10 ± 3.7E-13	7.0536E-12 ± 2.9E-13	3.40E-10 ± 6.6E-10	4.628E-12 ± 1.8E-13	1.74 ± 3.4	0.0009714	4.67 ± 0.35
7	866	2.4053E-09 ± 4.5E-13	3.7032E-10 ± 3.8E-13	7.7123E-12 ± 2E-13	1.584E-09 ± 5.5E-10	5.176E-12 ± 2.1E-13	8.58 ± 3.0	0.0016704	5.05 ± 0.35
8	953	2.0795E-09 ± 4.9E-13	2.7609E-10 ± 2.4E-13	5.4736E-12 ± 2.3E-13	1.065E-09 ± 6E-10	4.566E-12 ± 1.8E-13	7.74 ± 4.4	0.0013118	5.51 ± 0.46
9	1139	3.0058E-09 ± 2.4E-13	3.3158E-10 ± 4.6E-13	1.1581E-11 ± 1.2E-13	1.169E-09 ± 3.8E-10	8.144E-12 ± 1.8E-13	7.07 ± 2.3	0.0044258	3.89 ± 0.33
10	1460	3.1453E-09 ± 7.6E-13	7.1244E-11 ± 2.5E-13	6.9627E-12 ± 1.2E-13	1201E-09 ± 6.3E-10	1.02664E-11 ± 1.8E-13	34.10 ± 18.0	0.0143146	5.38 ± 1.90
Bi3 − 0.0299 g; J = 0.001046									
1	482	2.6431E-09 ± 6.2E-13	3.1634E-10 ± 3.9E-13	1.4957E-11 ± 1.3E-13	1.219E-10 ± 4.9E-11	6.731E-12 ± 3.3E-13	0.77 ± 0.31	0.007271	3.77 ± 0.57
2	538	5.9564E-09 ± 5.4E-13	6.9031E-10 ± 9.1E-13	3.1622E-11 ± 1.7E-13	3.862E-10 ± 7.6E-11	1.790E-11 ± 3.5E-13	1.12 ± 0.22	0.006740	1.90 ± 0.28
3	*591*	*5.8921E-09 ± 2E-12*	*5.1528E-10 ± 5.1E-13*	*2.0715E-11 ± 1E-13*	*3.383E-10 ± 6.7E-11*	*1.715E-11 ± 3.1E-13*	*1.31 ± 0.26*	*0.005138*	*3.10 ± 0.33*
4	*653*	*4.5199E-09 ± 1.8E-12*	*2.9584E-10 ± 2.6E-13*	*1.1393E-11 ± 1.3E-13*	*4.341E-10 ± 6.3E-11*	*1.374E-11 ± 3.4E-13*	*2.94 ± 0.43*	*0.0042189*	*3.13 ± 0.63*
5	712	2.9816E-09 ± 3.8E-13	8.9764E-11 ± 8.3E-14	4.3703E-12 ± 1E-13	2.797E-10 ± 9.8E-11	1.0207E-11 ± 3.2E-13	6.24 ± 2.20	0.0037398	−0.29 ± −2.0
6	765	4.0522E-09 ± 5.8E-13	6.539E-11 ± 6E-14	5.0164E-12 ± 1E-13	8.202E-10 ± 6.5E-11	1.302E-11 ± 3.3E-13	25.30 ± 2.00	0.0069294	7.75 ± 2.80
7	919	2.0206E-09 ± 1.4E-13	1.6847E-11 ± 1.3E-13	3.2438E-12 ± 1.5E-13	6.013E-10 ± 7.5E-11	6.901E-12 ± 3.2E-13	73.13 ± 9.20	0.025528	3.04 ± 11.0
8	1105	1.7021E-09 ± 3.4E-13	9.250E-12 ± 1.8E-13	3.2880E-12 ± 1.1E-13	2.677E-10 ± 1.4E-10	6.382E-12 ± 3.1E-13	59.03 ± 30.00	0.050651	−34.29 ± −19.0
9	1420	1.8417E-09 ± 2.8E-13	3.6477E-11 ± 1.7E-13	7.5556E-12 ± 7.9E-14	−2.779E-10 ± −4E-11	6.220E-12 ± 3E-13	−15.16 ± −2.00	0.037271	−0.89 ± −4.6
Tu1 − 0.052 g; J = 0.00385									
1	501	5.5254E-10 ± 7.5E-14	2.2207E-10 ± 2.4E-13	3.437E-12 ± 1.5E-13	2.3503E-11 ± 4.8E-13	1.801E-12 ± 1.4E-13	0.21 ± 0.004	0.00050974	0.68 ± 1.20
2	550	9.5506E-10 ± 2.9E-13	1.0121E-09 ± 9.9E-13	1.1955E-11 ± 1.4E-13	8.1834E-11 ± 3.8E-13	1.373E-12 ± 1.2E-13	0.16 ± 0.0008	4.386E-05	3.81 ± 0.23
3	595	1.09768E-09 ± 3.8E-13	1.4909E-09 ± 1.3E-12	1.9194E-11 ± 1.4E-13	9.8085E-11 ± 4.1E-13	1.344E-12 ± 1.2E-13	0.13 ± 0.0006	0.00021925	3.29 ± 0.15
4	*666*	*2.2333E-09 ± 2E-13*	*3.5699E-09 ± 3.2E-12*	*4.4008E-11 ± 1.3E-13*	*2.1511E-10 ± 8.7E-13*	*2.660E-12 ± 1.4E-13*	*0.12 ± 0.0005*	*9.998E-05*	*2.84 ± 0.08*
5	*727*	*3.0321E-09 ± 1.7E-13*	*5.4572E-09 ± 4.9E-12*	*6.6928E-11 ± 1.5E-13*	*3.457E-10 ± 1.2E-12*	*2.795E-12 ± 1.3E-13*	*0.13 ± 0.0004*	*9.566E-05*	*2.84 ± 0.04*
6	*781*	*1.7496E-09 ± 1.6E-13*	*2.6995E-09 ± 2.4E-12*	*3.3763E-11 ± 1.8E-13*	*2.3709E-10 ± 7.7E-13*	*2.007E-12 ± 9E-14*	*0.18 ± 0.0006*	*0.00014257*	*3.02 ± 0.07*

7	852	6.1069E-10 ± 2.3E-13	7.3367E-10 ± 6.8E-13	9.286E-12 ± 1.9E-13	1.0143E-10 ± 5.1E-13	1.069E-12 ± 1.3E-13	0.28 ± 0.0014	0.00014888	2.86 ± 0.34
8	941	7.9474E-10 ± 9E-14	9.2807E-10 ± 8.5E-13	1.3139E-11 ± 2.1E-13	2.0320E-10 ± 8.4E-13	1.248E-12 ± 1.4E-13	0.44 ± 0.0018	0.00050223	3.30 ± 0.28
9	1094	1.2557E-09 ± 1.1E-12	1.4767E-09 ± 1.4E-12	2.4648E-11 ± 1.5E-13	9.7666E-10 ± 2.9E-12	2.806E-12 ± 1.1E-13	1.32 ± 0.0039	0.00108351	2.35 ± 0.13
10	1450	5.5126E-10 ± 1.2E-13	1.7195E-10 ± 2.1E-13	3.777E-12 ± 1.4E-13	1.5488E-09 ± 4.5E-12	1.473E-12 ± 9.9E-14	18.12 ± 0.05	0.00237236	9.37 ± 0.82
Tu2 − 0.0406 g; J = 0.00385									
1	474	1.1370E-09 ± 1.9E-13	4.0374E-10 ± 3.6E-13	8.343E-12 ± 1.2E-13	3.9899E-10 ± 1.4E-12	3.3657E-12 ± 7.7E-14	1.98 ± 0.007	0.00173186	2.97 ± 0.36
2	538	5.1626E-10 ± 1.6E-13	2.8439E-10 ± 2.5E-13	5.221E-12 ± 1.6E-13	2.3475E-10 ± 8.8E-13	9.889E-13 ± 1.2E-13	1.65 ± 0.006	0.00140355	5.91 ± 0.76
3	590	1.4812E-09 ± 5.5E-13	1.1934E-09 ± 1.1E-12	1.8491E-11 ± 1.3E-13	8.5452E-10 ± 2.4E-12	3.8275E-12 ± 6E-14	1.43 ± 0.004	0.00075112	2.41 ± 0.11
4	654	3.1119E-09 ± 1.8E-13	1.0703E-09 ± 9.6E-13	2.0587E-11 ± 1.6E-13	6.6416E-10 ± 1.9E-12	8.645E-12 ± 1.4E-13	1.24 ± 0.004	0.00139792	3.94 ± 0.25
5	720	1.5036E-09 ± 4.7E-13	1.3489E-09 ± 1.2E-12	2.1714E-11 ± 1.6E-13	8.7786E-10 ± 2.4E-12	2.974E-12 ± 1.1E-13	1.30 ± 0.004	0.00093016	3.55 ± 0.15
6	780	1.5989E-09 ± 2.9E-13	1.1495E-09 ± 9E-13	2.1945E-11 ± 1.9E-13	8.0299E-10 ± 2.2E-12	4.3182E-12 ± 5.5E-14	1.40 ± 0.004	0.00155413	2.32 ± 0.09
7	858	1.0462E-09 ± 3E-13	6.7236E-10 ± 6.2E-13	2.563E-11 ± 1.4E-13	6.1734E-10 ± 1.7E-12	1.5265E-12 ± 9E-14	1.84 ± 0.0051	0.00600419	6.62 ± 0.26
8	944	7.947E-10 ± 1.3E-14	2.6783E-10 ± 2.5E-13	2.9391E-11 ± 1.8E-13	4.0985E-10 ± 1.3E-12	2.300E-12 ± 7.8E-14	3.06 ± 0.0095	0.02223124	3.78 ± 0.54
9	1135	1.3789E-09 ± 2.7E-13	3.8622E-10 ± 4.1E-13	7.834E-11 ± 2.5E-13	3.3413E-09 ± 9.4E-12	5.245E-12 ± 1.6E-13	17.40 ± 0.05	0.04373908	1.45 ± 0.69
10	140	8.4245E-10 ± 1.7E-12	6.2037E-11 ± 2.5E-13	9.589E-12 ± 2.1E-13	1.0156E-09 ± 5.5E-12	3.116E-12 ± 1.7E-13	33.10 ± 0.18	0.03140179	− 0.21 ± 5.00
So1 − 0.0246 g; J = 0.001045									
1	476	2.1956E-9 ± 7.2E-12	3.4016E-11 ± 3E-13	2.133E-12 ± 1.6E-13	3.199E-10 ± 9E-11	6.825E-12 ± 3.3E-13	18.93 ± 5.40	0.00350279	11.27 ± 5.30
2	*536*	*2.0008E-09 ± 6E-13*	*1.7478E-10 ± 3.4E-13*	*3.608E-12 ± 1.9E-13*	*−2.355E-10 ± −7.8E-11*	*4.699E-12 ± 3.2E-13*	*−2.69 ± −0.90*	*0.00082852*	*6.39 ± 1.00*
3	*589*	*5.5684E-09 ± 1.9E-12*	*7.6315E-10 ± 6.7E-13*	*1.2048E-11 ± 2.2E-13*	*−1.23E-10 ± −1.5E-10*	*1.1152E-11 ± 3.3E-13*	*−0.32 ± −0.39*	*0.00028994*	*5.58 ± 0.24*
4	*651*	*6.1286E-10 ± 7.4E-13*	*9.4087E-11 ± 3.8E-13*	*1.752E-12 ± 1.9E-13*	*5.13E-11 ± 3.5E-11*	*1.484E-12 ± 3.6E-13*	*1.09 ± 0.76*	*0.00092354*	*3.56 ± 2.10*
5	*716*	*7.068E-09 ± 2.8E-12*	*1.0143E-09 ± 9.9E-12*	*1.7242E-11 ± 1.5E-13*	*7.111E-10 ± 7.1E-11*	*1.434E-11 ± 3.1E-13*	*1.40 ± 0.14*	*0.00062668*	*5.35 ± 0.17*
6	*768*	*3.0615E-09 ± 1.6E-12*	*5.5307E-10 ± 5.7E-13*	*8.509E-12 ± 8.4E-14*	*7.44E-12 ± 5.5E-11*	*5.226E-12 ± 3.3E-13*	*0.03 ± 0.20*	*0.00042703*	*5.16 ± 0.33*
7	*846*	*2.9442E-09 ± 1E-12*	*3.5003E-10 ± 3.2E-13*	*8.147E-12 ± 9.5E-13*	*4.32E-10 ± 1.1E-10*	*6.660E-12 ± 3E-13*	*2.47 ± 0.64*	*0.00188378*	*5.42 ± 0.47*
8	930	2.9733E-09 ± 6E-14	1.7696E-10 ± 2.3E-13	7.645E-12 ± 1.1E-13	1.203E-10 ± 3.98E-11	8.992E-12 ± 3E-13	1.36 ± 0.45	0.00507631	3.46 ± 0.94
9	1107	2.8361E-09 ± 8E-13	8.9163E-11 ± 2E-13	8.530E-12 ± 9.4E-14	1.3385E-10 ± 7.1E-11	8.074E-12 ± 3.5E-13	3.01 ± 1.60	0.01547108	9.70 ± 2.20
Va1 − 0.0521 g; J = 0.00385									
1	*476*	*4.1123E-09 ± 3.5E-13*	*2.7587E-10 ± 3.8E-13*	*1.3810E-11 ± 1.9E-13*	*1.6954E-10 ± 7.2E-13*	*1.355E-11 ± 1.5E-13*	*1.230 ± 0.005*	*0.00672298*	*3.02 ± 1.00*
2	*537*	*3.3554E-09 ± 1.8E-13*	*9.6741E-09 ± 9.6E-13*	*3.0551E-11 ± 2E-13*	*5.2401E-10 ± 1.6E-12*	*1.025E-11 ± 1.6E-13*	*1.084 ± 0.003*	*0.00412594*	*2.63 ± 0.32*
3	*590*	*1.3742E-09 ± 4.4E-13*	*6.5686E-10 ± 7.7E-13*	*1.6628E-11 ± 1.1E-13*	*3.9576E-10 ± 1.3E-12*	*4.110E-12 ± 1.2E-13*	*1.206 ± 0.004*	*0.00287396*	*2.00 ± 0.34*
4	*655*	*2.7328E-09 ± 3.5E-13*	*1.0463E-09 ± 9.8E-13*	*2.6358E-11 ± 2.9E-13*	*9.1875E-10 ± 2.6E-12*	*7.910E-12 ± 1.3E-13*	*1.757 ± 0.005*	*0.00280181*	*3.08 ± 0.24*
5	*721*	*2.2897E-09 ± 6.3E-13*	*1.7597E-09 ± 1.6E-12*	*5.8743E-11 ± 1.9E-13*	*2.0564E-09 ± 5.8E-12*	*6.0904E-12 ± 8.6E-14*	*2.339 ± 0.007*	*0.00487459*	*2.54 ± 0.09*
6	*784*	*1.4824E-09 ± 5.5E-13*	*9.3566E-10 ± 8.6E-13*	*4.3197E-11 ± 2.5E-13*	*1.1651E-09 ± 3.3E-12*	*3.995E-12 ± 1.7E-13*	*2.492 ± 0.007*	*0.00777998*	*2.89 ± 0.33*
7	857	9.9981E-09 ± 3.6E-13	5.7502E-10 ± 5.1E-13	3.8874E-11 ± 2.2E-13	4.7856E-10 ± 1.4E-12	3.354E-12 ± 1.1E-13	1.665 ± 0.005	0.01262894	0.54 ± 0.35
8	943	1.2837E-09 ± 2.4E-13	7.7540E-10 ± 7.2E-13	6.1423E-11 ± 2E-13	4.4596E-10 ± 1.3E-12	2.891E-12 ± 1.4E-13	1.151 ± 0.003	0.01537829	4.14 ± 0.34
9	1135	3.3116E-09 ± 3.9E-13	1.7695E-09 ± 1.6E-12	1.4359E-10 ± 2.7E-13	2.1638E-09 ± 6.1E-12	9.730E-11 ± 9E-14	2.448 ± 0.007	0.01577531	2.35 ± 0.09
10	1440	1.2619E-09 ± 4.5E-13	3.5072E-10 ± 3.3E-13	2.5186E-11 ± 1.4E-13	1.3200E-09 ± 3.6E-12	4.755E-12 ± 8.7E-14	7.547 ± 0.021	0.01339295	0.00 ± 0.45
Va2 − 0.035 g; J = 0.001041									
1	*435*	*4.7683E-09 ± 5.7E-13*	*1.861E-10 ± 2.1E-13*	*3.1868E-11 ± 1E-13*	*3.20E-10 ± 2.8E-10*	*1.5265E-11 ± 2.3E-13*	*3.44 ± 3.00*	*0.03322171*	*2.84 ± 0.72*
2	*471*	*3.3180E-09 ± 1.3E-12*	*2.585E-10 ± 2.7E-13*	*3.9314E-11 ± 6E-14*	*1.65E-10 ± 2.5E-10*	*1.0538E-11 ± 1.9E-13*	*1.28 ± 1.90*	*0.03054676*	*1.57 ± 0.44*
3	*523*	*3.2725E-09 ± 9.4E-14*	*2.640E-10 ± 3.4E-13*	*2.9075E-11 ± 1.9E-13*	*2.93E-10 ± 4.1E-10*	*9.731E-12 ± 1.9E-13*	*2.23 ± 3.10*	*0.02109570*	*2.98 ± 0.47*
4	*586*	*4.1167E-09 ± 3.9E-12*	*3.773E-10 ± 4.2E-13*	*2.1307E-11 ± 1.6E-13*	*1.316E-09 ± 3.6E-10*	*1.2879E-11 ± 2.5E-13*	*7.00 ± 1.90*	*0.00896829*	*2.04 ± 0.38*
5	645	4.6309E-09 ± 1.8E-12	1.8211E-10 ± ±2E-13	9.112E-12 ± 2.3E-13	1.671E-09 ± 3.1E-10	1.4632E-11 ± 2.2E-13	18.46 ± 3.40	0.00575046	4.48 ± 0.70
6	695	2.4965E-09 ± 3.6E-13	2.246E-10 ± 2.1E-13	8.844E-12 ± 2.4E-13	1.740E-09 ± 3.4E-10	7.497E-12 ± 2.6E-13	15.58 ± 3.00	0.00525596	3.46 ± 0.64

(Continued)

Table 2. *Continued*

Step	T(°C)	$^{40}Ar_{tot}$	^{39}Ar	^{38}Ar	^{37}Ar	^{36}Ar	Ca/K	Cl/K	Age (Ma)
7	761	2.3558E-09 ± 4E-13	1.3736E-10 ± 1E-13	7.140E-12 ± 1E-13	4.7E-10 ± 2.5E-10	6.376E-12 ± 2.1E-13	6.93 ± 3.60	0.00740599	6.93 ± 0.87
8	844	1.4566E-09 ± 1.6E-14	3.8899E-11 ± 1.5E-13	5.346E-12 ± 2.1E-13	1.350E-09 ± 2.5E-10	5.246E-12 ± 2.1E-13	71.11 ± 13.00	0.02462937	0.41 ± 3.00
9	1015	2.5307E-09 ± 3.2E-13	5.7919E-11 ± 1.4E-13	1.3127E-11 ± 1.5E-13	2.789E-12 ± 4.6E-13	7.396E-12 ± 1E-13	0.10 ± 0.02	0.04393355	11.15 ± 1.90
10	1350	2.6138E-09 ± 4.6E-13	6.1881E-11 ± 9.8E-14	6.794E-12 ± 1.1E-13	3.655E-12 ± 5.9E-13	8.881E-12 ± 1.9E-13	0.12 ± 0.02	0.01638137	−0.31 ± −1.70
Va3 − 0.032 g; J = 0.00105									
1	465	6.4998E-09 ± 8.9E-12	2.8268E-10 ± 4.3E-13	4.9246E-11 ± 2.1E-13	1.5024E-10 ± 1.7E-12	2.0403E-11 ± 8.8E-14	1.06 ± 0.01	0.03428325	3.23 ± 0.17
2	*531*	*2.0470E-09 ± 1.2E-11*	*4.5213E-10 ± 4.7E-13*	*6.9342E-11 ± 3.2E-13*	*4.5743E-10 ± 2.2E-12*	*6.292E-12 ± 1.8E-13*	*2.02 ± 0.01*	*0.03201413*	*0.93 ± 0.22*
3	*588*	*1.5274E-09 ± 1.5E-12*	*4.4878E-10 ± 3.9E-13*	*5.2868E-11 ± 9.6E-14*	*8.275E-10 ± 3.4E-12*	*4.312E-12 ± 1.4E-13*	*3.98 ± 0.02*	*0.02406281*	*1.35 ± 0.16*
4	*654*	*1.1603E-09 ± 1.1E-12*	*2.6381E-10 ± 4.3E-13*	*1.8469E-11 ± 1.5E-13*	*9.673E-10 ± 3.7E-12*	*3.058E-12 ± 1.5E-13*	*7.35 ± 0.03*	*0.01306567*	*2.37 ± 0.30*
5	*718*	*8.9877E-10 ± 2.8E-14*	*1.1567E-10 ± 1.9E-13*	*9.516E-12 ± 1.7E-13*	*6.7488E-10 ± 2.7E-12*	*2.621E-12 ± 1.3E-13*	*11.71 ± 0.05*	*0.01549824*	*2.87 ± 0.57*
6	775	3.300E-10 ± 2.3E-13	1.4425E-11 ± 2.3E-13	2.339E-12 ± 1.3E-13	1.0758E-10 ± 2.3E-12	1.277E-12 ± 1.3E-13	15.17 ± 0.32	0.03166962	−5.24 ± −5.10
7	850	2.0291E-09 ± 4E-13	1.0611E-11 ± 1.4E-13	3.586E-12 ± 2.6E-13	6.1884E-11 ± 1.9E-12	5.8689E-12 ± 5.6E-14	11.71 ± 0.36	0.05149839	52.90 ± 2.90
8	934	7.0896E-10 ± 3.1E-13	2.2283E-11 ± 1.5E-13	9.716E-12 ± 1.2E-13	1.5877E-10 ± 2.2E-12	2.292E-12 ± 1E-13	14.32 ± 0.20	0.09347200	3.71 ± 4.90
9	1116	5.6148E-10 ± 9.1E-13	2.4415E-11 ± 1.6E-13	5.563E-12 ± 1E-13	7.8419E-10 ± 6E-12	1.989E-12 ± 1.4E-13	65.65 ± 0.50	0.04759723	2.58 ± 3.00
10	1427	1.0101E-08 ± 6.3E-13	8.660E-12 ± 1.9E-13	8.114E-12 ± 1.8E-13	8.288E-10 ± 1.9E-11	3.278E-11 ± 2.7E-13	206.06 ± 4.70	0.05464390	109.04 ± 18.00
Va4 − 0.0295 g; J = 0.001044									
1	*451*	*3.3452E-09 ± 1.1E-12*	*1.4714E-10 ± 1.9E-13*	*2.2616E-11 ± 9E-14*	*2.013E-10 ± 3.8E-11*	*1.1358E-11 ± 2E-13*	*2.74 ± 0.52*	*0.02938744*	*0.05 ± 1.10*
2	*515*	*6.8434E-09 ± 1.8E-12*	*3.3312E-10 ± 3.5E-13*	*4.5567E-11 ± 8.2E-14*	*7.612E-10 ± 2.8E-11*	*2.3834E-11 ± 3.3E-13*	*4.58 ± 0.17*	*0.02590818*	*0.87 ± 0.55*
3	*568*	*6.4424E-09 ± 3.9E-12*	*2.3675E-10 ± 2.6E-13*	*2.5357E-11 ± 1.6E-13*	*6.620E-10 ± 5.2E-11*	*2.1601E-11 ± 3.9E-13*	*5.60 ± 0.44*	*0.01812829*	*0.87 ± 0.90*
4	*640*	*6.7912E-09 ± 1.8E-12*	*1.9689E−10 ± 2E-13*	*1.4609E-11 ± 9E-14*	*8.440E-10 ± 5.7E-11*	*2.297E-11 ± 3.8E-13*	*8.60 ± 0.58*	*0.0095314*	*0.62 ± 1.10*
5	695	1.0633E-08 ± 1.4E-12	1.7221E-10 ± 2.5E-13	1.9399E-11 ± 8.5E-14	1.3184E-09 ± 4E-11	3.708E-11 ± 3.2E-13	15.39 ± 0.47	0.01428134	−2.47 ± −1.00
6	749	5.0164E-09 ± 1.1E-12	3.1425E-11 ± 2.6E-13	7.198E-12 ± 1.3E-13	4.622E-10 ± 1E-11	1.781E-11 ± 3.1E-13	29.71 ± 0.66	0.02625874	−12.87 ± −5.60
7	821	4.2803E-09 ± 1.3E-12	2.0292E-11 ± 8.5E-14	8.4503E-12 ± 8.8E-14	2.446E-10 ± 4.4E-11	1.5039E-11 ± 3.2E-13	24.31 ± 4.40	0.06173873	−13.66 ± −9.00
8	912	4.5570E-09 ± 3.1E-12	2.2315E-11 ± 1.7E-13	1.2373E-11 ± 9.3E-14	3.45E-11 ± 2.9E-11	1.782E-11 ± 3.4E-13	3.10 ± 2.60	0.09055042	−60.78 ± −8.90
9	1094	4.3489E-09 ± 2.2E-12	3.3112E-11 ± 9.9E-14	1.1047E-11 ± 8.7E-14	7.237E-10 ± 4.2E-11	1.603E-11 ± 3.1E-13	44.36 ± 2.60	0.0541744	−19.41 ± −5.30
10	1424	1.3444E-09 ± 1.5E-13	5.3609E-12 ± 1.2E-13	2.0981E-12 ± 9.1E-14	8.908E-10 ± 7.4E-11	5.3108E-12 ± 3.3E-13	374.01 ± 31.00	0.0519913	−63.50 ± −39.00

opening of the Karliova Basin. This situation may have prevailed just before the creation of the Karliova Triple Junction (Fig. 10c), and the observed normal faults and Karliova basin may be inherited from that time. Finally a unique trench system as modelled in Figure 10 does not exist. The deformation is partitioned with mostly right-lateral deformation along the Main Varto Fault and shortening to the south along the Muş fold-and-thrust belt. Present active shortening is attested in the field by uplifted alluvial fans and thrust fault scarps. Recent seismicity does not show any thrusting events despite the dense coverage of the temporary seismic network (Örgülü *et al.* 2003), but the critical factor remains the short period of observation compared to the seismic cycle.

Finally to fully understand for the Triple Junction evolution one must account for the lithospheric complexities existing at the boundaries between the Arabian, Eurasian and Anatolian blocks (Fig. 11). S-wave receiver functions (Angus *et al.* 2006) have shown that near the triple junction the signatures of at least three or four lithosphere-asthenosphere boundaries (LAB) can be found: the LAB of East Anatolian Accretionary Complex and Rhodope-Pontide continental fragment (called here 'East Anatolian' LAB), the LAB of Anatolian Block (called here 'Anatolian' LAB) and the LAB of the Arabian Shield (called here 'Arabian' LAB). The Anatolian Faults and associated structures all have deep lithospheric signatures: along the North Anatolian Fault, an apparent lithospheric right-lateral offset corresponds to the Turna/Bingöl offset (see the isothickness line: 66 km in Fig. 11); across the East Anatolian Fault until, Bingöl Basin, a lithospheric step exists between the northern 70 km deep 'East Anatolian' LAB, and the southern 80 km deep 'Anatolian' and 115 km deep 'Arabian' LAB. The Erzincan Basin, Bingöl Basin and Muş Basin are also deeply rooted: major lithospheric thinning is found in the Erzincan area, the location of the former triple junction; lithospheric thickening exists north and NW of the Bingöl Basin where shortening occurred due to the 25° change in strike of the East Anatolian Fault; the Bingöl Basin and Muş-basin-and-thrust-zone form at the junction between the 'Arabian' LAB and the 'East Anatolian' LAB, the Muş thrust zone being also limited to the north by a low velocity zone. A three dimensional mechanical model including fault discontinuity affecting the whole lithosphere is thus needed to understand in details the kinematics at the junction between Arabia, Anatolia and Eurasia.

Conclusion

The availability of a set of relevant data, together with the relative simplicity of the Anatolian fault system makes it a unique laboratory to study the long-term evolution of major strike-slip fault. Interestingly, the resulting picture is reminiscent of smaller scale faults or cracks evolution, as described in Hubert-Ferrari *et al.* (2003). The history of the North Anatolian Fault propagation is particularly rich and can be summarized as follows. From 12 Ma to 2.5 Ma, it has grown in length westward over 1300 km from Erzincan in eastern Turkey to the Aegan Sea with a slip rate of 3 mm/a, and a propagation speed of 120 mm/a (Armijo *et al.* 2003; Flerit *et al.* 2004). A similar propagation speed was computed for the Altyn Tagh fault, a main strike-slip fault in the extrusion system related to the India–Eurasia collision (Meyer *et al.* 1998; Métivier *et al.* 1998). Rift propagation can also have speed exceeding 100 mm/a (e.g. Wilson & Hey 1995; Manighetti *et al.* 1997), as well as the lateral propagation of the Himalaya front (Meigs *et al.* 1995; Husson *et al.* 2004). This propagation phenomenon is consistently associated with different ages of the fault (Şengör *et al.* 2005): *c.* 12 Ma in the east (Şengör *et al.* 1985; Barka 1992), *c.* 8.5 to 5 Ma in its central part (Hubert-Ferrari *et al.* 2002), *c.* 5 Ma in the western Marmara sea (Straub *et al.* 1997; Armijo *et al.* 1999), *c.* 3 Ma in the Aegean Sea (Gautier *et al.* 1999), *c.* 1 Ma in the Gulf of Corinth at the westernmost end of the fault (Armijo *et al.* 1996). The most dramatic event in this long history is described in the present paper: 2.5 to 3 Ma ago, the slip rate along the North Anatolian Fault suddenly increases from about 3 mm/a averaged in 10 Ma to about 20 mm/a, at a time when part of the Arabian plate was accreted to Eurasia with the initiation of a new East Anatolian Fault. The Whakatane Graben (New Zealand) behaved in a similar way, fault growth was first characterized by tip propagation and relatively slow displacements, and then after fault linkage the average fault increased by almost threefold (Taylor *et al.* 2004).

Swiss National Science Foundation Grant, No. 21-65197.01 funded this work. The data bank of INSU-CNRS gave us access to the satellite imagery. V. Serneels (University of Fribourg, Switzerland) did XRF element analyses. Field work was successfully conducted with the help of M. Burkhard and A. Devrim. We thank P. Claeys for fruitful discussions. Reviews from C. Şengör and another anonymous reviewer improved the manuscript.

References

Allen, A., Jackson, J. & Walker, R. 2004. Late Cenozoic reorganization of the Arabia–Eurasia collision and the comparison of short-term and long-term deformation rates. *Tectonics*, **23**, TC2008, doi:10.1029/2003TC001530.

Al-Lazki, A. I., Seger, D., Sandvol, E., Turkelli, N., Mohamad, R. & Barazangi, M. 2003.

Tomographic Pn velocity and anisotropy structure beneath the Anatolian plateau (eastern Turkey) and the surrounding regions. *Geophysical Research Letters*, **30**, 8043, doi:10.1029/2003GL017391.

ALTINLI, E. 1961. *Geological map of Turkey, Erzurum Quadrangle*, General Directorate of Mineral Research and Exploration (eds.), Ankara.

AMBRASEYS, N. N. & ZATOPEK, A. 1968. The Varto Ustukran earthquake of 19 August 1966. *Bulletin of the Seismological Society of America*, **58**, 47–102.

AMBRASEYS, N. 1988. Engineering seismology. *Journal of Earthquake and Engeneering and Structural Dynamics*, **17**, 1–106.

ANGUS, D. A., WILSON, D. C., SANDVOL, E. & NI, J. F. 2006. Lithospheric structure of the Arabian and Eurasian collision zone in eastern Turkey from S-wave receiver functions. *Geophysical Journal International*, **166**, 1335–1346 doi: 10.1111/j.1365–246X.2006.03070.x.

ARMIJO, R., MEYER, B., KING, G. C. P., RIGO, A. & PAPANASTASSIOU, D. 1996. Quaternary evolution of the Corinth rift and its implications. *Geophysical Journal International*, **126**, 11–53.

ARMIJO, R., MEYER, B., HUBERT-FERRARI, A. & BARKA, A. A. 1999. Propagation of the North Anatolian Fault into the Northern Aegean: Timing and Kinematics. *Geology*, **27**, 267–270.

ARMIJO, R., FLERIT, F., KING, G. C. P. & MEYER, B. 2003. Linear elastic fracture mechanics explains the past and present evolution of the Aegean. *Earth and Planetary Science Letters*, **217**, 85–95.

ARPAT, E. & ŞAROĞLU, F. 1972. The East Anatolian Fault system: thoughts on its development. *General Directorate of Mineral research and Exploration (MTA) Bulletin*, **78**, 33–39.

AXEN, G. J., LAM, P. S., GROVE, M., STOCKLI, D. F. & HASSANZADEH, J. 2001. Exhumation of the west-central Alborz Mountains, Iran, Caspian subsidence, and collision-related tectonics. *Geology*, **29**, 559–562.

BARKA, A. A. & HANCOCK, P. L. 1984. Neotectonic deformation patterns in the convex-northwards arc of the North Anatolian fault. *In*: DIXON, J. G. & ROBERTSON, A. H. F. *The Geological Evolution of the eastern Mediterranean*. Geological Society, London, Special Publication, **17**, 763–773.

BARKA, A. A. & KADINSKY-CADE, K. 1988. Strike-slip fault geometry in Turkey and its influence on earthquake activity. *Tectonics*, **7**, 663–684.

BARKA, A. A. & GÜLEN, L. 1989. Complex evolution of the Erzincan basin (eastern Turkey). *Journal of Structural Geology*, **11**, 275–283.

BARKA, A. A. 1992. The North Anatolian fault zone. *Annales Tectonicae (Supplement)*, **6**, 164–195.

BIGAZZI, G., YEGINĞIL, Z., ERCAN, T., ODDONE, M. & OZDOĞAN, M. 1994. Provenance studies of prehistoric artefacts in Eastern Anatolia: first results of an interdisciplinary research. *Mineralogica et Petrographica Acta*, **XXXVII**, 17–36.

BIGAZZI, G., YEGINĞIL, Z., ERCAN, T., ODDONE, M. & OZDOĞAN, M. 1996. The Pisa-Adana joint project of prehistoric obsidian artifacts; first results from eastern Anatolia using fission track dating method: an overview. *In*: DIMIRCI, S., ÖVER, A. M. & SUMMERS, G. D. (eds) *Proceedings of the 29th symposium on Archaeometry*. Ankara, 9–14, May 1994, 521–528.

BIGAZZI, G., YEGINGIL, Z., ERCAN, T., ODDONE, M. & OZDOGAN, M. 1997. Age determination of obsidian bearing volcanics in Eastern Anatolia using the fission track dating method. *Geological Bulletin of Turkey*, **40**, 57–72.

BIGAZZI, G., POUPEAU, G., YEGINĞIL, Z. & BELLOT-GURLET, L. 1998. Provenance studies of obsidian artefacts in Anatolia using the fission track dating method. An overview. *In*: GOURGAUD, A., GRATUZE, B., POUPEAU, G., POIDEVIN, J. L. & CAUVIN, M. C. (eds) *L'Obsidienne au Proche et Moyen Orient, du Volcan à l'Outil*. BAR International Series Hadrian Books, **738**, 69–89.

BINGÖL, E., BAL, I. & CAN, N. (eds) 1989. *Geological map of Turkey*, scale 1:2000000, General Directorates of Mineral Research and Exploration, Ankara, Turkey.

BOZKURT, E. & KOÇYIĞIT, A. , 1996. The Kazova Basin: an active flower structure on the Almus Fault Zone, a splay fault system of the North Anatolian Fault Zone, Turkey. *Tectonophysics*, **265**, 239–254.

BOZKURT, E. 2001. Neotectonics of Turkey—a synthesis. *Geodinamica Acta*, **14**, 3–30.

BUKET, E. & GÖRMÜŞ, S. 1986. Varto (Muş) havzasındaki Tersiyer yaşlı istifin stratigrafisi. *Yerbilimleri* **13**, 17–29 [in Turkish with English abstract].

BUKET, E. & TEMEL, A. 1998. Major-element, trace element, and Sr-Nd isotopic geochemistry and genesis of Varto (Muş) volcanic rocks, Eastern Turkey. *Journal of Volcanology and Geothermal Research*, **85**, 405–422.

ÇAKIR, Ö. & ERDURAN, M. 2004. Constraining crustal and uppermost mantle structure beneath station TBZ (Trabzon, Turkey) by receiver function and dispersion analyses. *Geophysical Journal International*, **158**, 955–971.

CALAIS, E., DEMETS, C. & NOCQUET, J.-M. 2003. Evidence for a post-3.16-Ma change in Nubia-Eurasia-North America plate motions? *Earth and Planetary Science Letters*, **216**, 81–92.

ÇETIN, H., GÜNEYLI, H. & MAYER, L. 2003. Paleoseismology of the Palu-Lake Hazar segment of the East Anatolian Fault Zone, Turkey. *Tectonophysics*, **374**, 163–197.

CHATAIGNER, C., POIDEVIN, J. L. & ARNAUD, N. O. 1998. Turkish occurrences of obsidian and use by prehistoric peoples in the Near East from 14,000 to 6000 BP. *Journal of Volcanology and Geothermal Research*, **85**, 517–537.

DEWEY, J. F., HEMPTON, M. R., KIDD, W. S. F., ŞAROĞLU, F. & ŞENGÖR, A. M. C. 1986. Shortening of continental lithosphere: the neotectonics of eastern Anatolia-A young collision Zone. *In*: COWARD, M. P. & RIES, A. C. (eds) *Collision Tectonics*. Geological Society of London, Special Publication, **19**, 3–36.

FACCENNA, C., BELLIER, O., MARTINOD, J., PIROMALLO, C. & REGARD, V. 2006. Slab detachment beneath eastern Anatolia. *Earth and Planetary Science Letters*, **242**, 85–97.

FLEMING, T. H., HEIMANN, A., FOLAND, K. A. & ELLIOT, D. H. 1997. Ar-40/Ar-39 geochronology of Ferrar Dolerite sills from the Transantarctic mountains, Antarctica: Implications for the age and origin of the

Ferrar magmatic province. *Geological Society of America Bulletin*, **109**, 533–546.

FLERIT, F., ARMIJO, A., KING, G. & MEYER, B. 2004. The mechanical interaction between the propagating North Anatolian Fault and the back-arc extension in the Aegean. *Earth and Planetary Science Letters*, **224**, 347–362.

FUENZELIDA, H., DORBATH, L., CISTERNAS, A., RIVERA, L., EYIDOĞAN, H., BARKA, A. A., HAESSLER, H., PHILIP, H. & LYBÉRIS, N. 1997. Mechanism of the Erzincan earthquake and its aftershocks, tectonics of the Erzincan basin and decoupling on the North Anatolian Fault. *Geophysical Journal International*, **129**, 1–28.

GAUTIER, P., BRUN, J.-P., RICHARD, M., DIMITRIOS, S., MARTINOD, J. & JOLIVET, L. 1999. Timing, kinematics and cause of Aegean extension: a scenario based on a comparison with simple analogue experiments. *Tectonophysics*, **315**, 31–72.

GELATI, R. 1975. Miocene marine sequence from lake Van eastern Turkey. *Rivista Italiana di Paleontologia e stratigraphia*, **81**, 477–490.

GÖK, R., SANDVOL, E., TÜKELLI, N., SEBER, D. & BARAZANGI, M. 2003. Sn attenuation in the Anatolian and Iranian plateau and surrounding regions. *Geophysical Research Letters*, **30**, 8042, doi:10.1029/2003GL018020.

GÜRSOY, H., PIPER, J. D. A., TATAR, O. & TEMIZ, H. 1997. A palaeomagnetic study of the Sivas basin, Central Turkey: Crustal deformation during lateral extrusion of the Anatolian block. *Tectonophysics*, **271**, 89–105.

HERECE, E. & AKAY, E. 2003. *Kyzey Anadolu Fayi (KAF) Atlasi/Atlas of North Anatolian Fault (NAF).* Özel Yayın. Ser. 2, Maden Tetk. Arama Genl Müdürlügü, Ankara, [IV], 61 pp. + 13 appendices as separate maps.

HUBERT-FERRARI, A., ARMIJO, R., KING, G. C. P., MEYER, B. & BARKA, A. 2002. Morphology, displacement and slip rates along the North Anatolian Fault (Turkey). *Journal of Geophysical Research*, **107**, 101029–101059.

HUBERT-FERRARI, A., KING, G. C. P., MANIGHETTI, I., ARMIJO, R., MEYER, B. & TAPPONNIER, P. 2003. Long-term Elasticity in the Continental Lithosphere; Modelling the Aden Ridge Propagation and the Anatolian Extrusion Process. *Geophysical Journal International*, **153**, 111–132.

HUSSON, L., MUGNIER, J.-L., LETURMY, P. & VIDAL, G. 2004. Kinematics and sedimentary balance of the Subhimalayan range, W. Nepal. *In*: MACCLAY, K. (ed.) *Thrust Tectonics and Hydrocarbon Systems*. AAPG Memoir, **82**, 115–130.

INNOCENTI, F., MAZZUOLI, R., PASQUARE, G., RADICATI DI BROZOL, F. & VILLARI, L. 1982*a*. Tertiary and Quaternary volcanism of the Erzurum-Kars area Eastern Turkey: geochronological data and geodynamic evolution. *Journal of Volcanology and Geothermal Research*, **13**, 223–240.

INNOCENTI, F., MANETTI, P., MAZZUOLI, R., PASQUARE, G. & VILLARI, L. 1982*b*. Anatolia and North-western Iran. *In*: THORPE, R. S. (ed.) *Andesites; orogenic andesites and related rocks*. John Wiley and Sons, 327–349.

JAFFEY, N., ROBERTSON, A. & PRINGLE, M. 2004. Latest Miocene and Pleistocene ages of faulting, determined by ^{40}Ar-^{39}Ar single-crystal dating of air fall tuff and silicic extrusives of the Erciyes Basin, central Turkey: evidence for intraplate deformation related to the tectonic escape of Anatolia. *Terra Nova*, **16**, 45–53.

JIMENEZ-MUNT, I. & SABADINI, R. 2002. The block-like behavior of Anatolia envisaged in the modeled and geodetic strain rates. *Geophysical Research Letters*, **29**, doi: 10.1029/2002GL015995, 2002.

KIM, Y.-S. & SANDERSON, D. J. 2006. Structural similarity and variety at the tips in a wide range of strike-slip faults: a review. *Terra Nova*, **18**, 330–344, doi: 10.1111/j.1365–3121.2006.00697.x.

MANIGHETTI, I., TAPPONNIER, P., COURTILLOT, V., GRUSZOW, S. & GILLOT, P. 1997. Propagation of rifting along the Arabia-Somalia plate boundary: the Gulfs of Aden and Tadjoura. *Journal of Geophysical Research*, **102**, 2681–2710.

MAGGI, A. & PRIESTLEY, K. 2005. Surface waveform tomography of the Turkish-Iranian plateau. *Geophysical Journal International*, **160**, 1068–1080.

MCCLUSKY, S., BALASSANIAN, S., BARKA, A., DEMIR, C., ERGINTAV, S., GEORGIEV, I. *ET AL.* 2000. GPS constraints on plate motion and deformation in the eastern Mediteranean: Implication for plate dynamics. *Journal of Geophysical Research*, **105**, 5695–5719.

MCKENZIE, D. P. & MORGAN, W. J. 1969. Evolution of triple junctions. *Nature*, **224**, 125–133.

MCKENZIE, D. P. 1972. Active tectonics of the Mediterranean region. *Geophysical Journal of the Royal Astronomical Society*, **30**, 109–185.

MCQUARRIE, N., STOCK, J. M., VERDEL, C. & WERNICKE, B. P. 2003. Cenozoic ecolution of neotethys and implications for the causes of plate motions. *Geophysical Research Letters*, **30**, 2036, doi:10.1029/2003GL017992.

MEIGS, A. J., BURBANK, D. W. & BECK, R. A. 1995. Middle-late Miocene (>10 Ma) formation of the Main Boundary Thrust in the western Himalaya. *Geology*, **23**, 423–426.

MÉTIVIER, F., GAUDEMER, Y., TAPPONNIER, P. & MEYER, B. 1998. Northeastward growth of the Tibet plateau deduced from balanced reconstruction of two depositional areas: The Qaidam and Hexi Corridor basins, China. *Tectonics*, **17**, 823–842.

MEYER, B., TAPPONNIER, P., BOURJOT, L., METIVIER, F., GAUDEMER, Y., PELTZER, G. *ET AL.* 1998. Crustal thickening in Gansu-Qinghai, lithospheric mantle subduction and oblique, strike-slip controlled growth of the Tibetan Plateau. *Geophysical Journal International*, **135**, 1–47.

MORTON, A., ALLEN, M., SIMMONS, M., SPATHOPOULOS, F., STILL, J., HINDS, D. *ET AL.* 2003. Provenance patterns in a neotectonic basin: Pliocene and Quaternary sediment supply to the South Caspian. *Basin Research*, **15**, 321–337.

ÖRGÜLÜ, G., AKTAR, M., TÜRKELLI, N., SANDVOL, E. & BARAZANGI, M. 2003. Contribution to the seismotectonics of Eastern Turkey from moderate and small size events. *Geophysical Research Letters*, **30**, 8040.

ÖVER, S., OZDEN, S. & UNLUGENC, U. C. 2004. Late Cenozoic stress distribution along the Misis Range in the Anatolian, Arabian, and African Plate intersection region, SE Turkey. *Tectonics*, **23**, TC3008, doi:10.1029/2002TC001455.

ÖVER, S., UNLUGENC, U. C. & BELLIER, O. 2002. Quaternary stress regime change in the Hatay region (southeastern Turkey). *Geophysical Journal International*, **148**, 649–662.

PEARCE, J. A., BENDER, J. F., DE LONG, S. E., KIDD WILLIAM, S. F., LOW, P. J., GÜNER, Y. *ET AL.* 1990. Genesis of collision volcanism in eastern Anatolia, Turkey. *Journal of Volcanology and Geothermal Research*, **44**, 189–229.

POIDEVIN, J. L. 1998. Provenance studies of obsidian artefacts in Anatolia using the fission track dating method. An overview. *In*: GOURGAUD, A., GRATUZE, B., POUPEAU, G., POIDEVIN, J. L. & CAUVIN, M. C. (eds) *L'Obsidienne au Proche et Moyen Orient, du Volcan à l'Outil*. BAR International Series Hadrian Books, **738**, 105–156.

REILINGER, R., MCCLUSKY, S., VERNANT, P., LAWRENCE, S., ERGINTAV, S., CAKMAK, R. *ET AL.* 2006. GPS constraints on continental deformation in the Africa–Arabia–Eurasia continental collision zone and implications for the dynamics of plate interactions. *Journal Geophysical Research*, **111**, B05411, doi:10.1029/2005JB004051.

ŞAROĞLU, F. & YILMAZ, Y. 1987. Geological evolution and basin models during neotectonic episode in the eastern Anatolia. *Bulletin Mineral Research and Exploration*, **107**, 61–83.

ŞAROĞLU, F. & YILMAZ, Y. 1991. Geology of the Karliova region: intersection of the North Anatolian and East Anatolian Transform Faults. *Bulletin of the Technical University of Istanbul*, **44**, 475–493.

ŞAROĞLU, F., EMRE, Ö. & KUŞÇU, I. 1992. The east Anatolian fault zone of Turkey. *Annales Tectonicae, Special Issue*, **6**, 99–125.

ŞENGÖR, A. M. C., GÖRÜR, N. & ŞAROĞLU, F. 1985. Strike-slip faulting and related basin formation in zones of tectonic escape: Turkey as a case study. *In*: BIDDLE, K. T. & CHRISTIE-BLICK, N. (eds) *Strike-slip faulting and Basin formation*. Society of Economic Paleontologists and Mineralogist, Special Publication, **37**, 227–267.

ŞENGÖR, A. M. C., TÜYSÜZ, O., İMREN, C., SAKINÇ, M., EYIDOĞAN, H., GÖRÜR, N. *ET AL.* 2005. The North Anatolian Fault: A new look. *Annual Review of Earth and Planetary Science*, **33**, 1–75.

SEYMEN, İ. & AYDIN, A. 1972. The Bingöl earthquake fault and its relation to the North Anatolian Fault Zone. *General Directorate of Mineral research and Exploration (MTA) Bulletin*, **79**, 1–8 [in Turkish with English abstract].

STRAUB, C., KHALE, H. G. & SCHINDLER, C. 1997. GPS and geological estimates of the tectonic activity in the Marmara Sea region, NW Anatolia. *Journal Geophysical Research*, **102**, 27587–27601.

TAPPONNIER, P. 1977. Evolution tetonique du Système Alpin en Méditerranée: poinçonnement et écrasement rigide-plastique, *Bulletin de la Sociéte Géologique de France*, **7**, 437–460.

TAPPONNIER, P., PELTZER, G., LE DAIN, A. Y., ARMIJO, R. & COBBOLD, P., 1982. Propagating extrusion tectonics in Asia: new insights from simple experiments with plasticine. *Geology*, **10**, 611–616.

TARHAN, N. 1993. *Geological Map of the Erzurum.* General Directorate of Mineral Research and Exploration, Ankara, **G32 Quadrangle**.

TARHAN, N. 1994. *Geological Map of the Erzurum.* General Directorate of Mineral Research and Exploration, Ankara, **G31 Quadrangle**.

TATAR, O., PIPER, J. D. A., GÜRSOY, H. & TEMIZ, H., 1996. Regional significance of neotectonic anticlockwise rotation in central Turkey. *International Geology Review*, **38**, 692–700.

TAYLOR, S. K., BULL, J. M., LAMARCHE, G. & BARNES, P. M. 2004. Normal fault growth and linkage in the Whakatane Graben, New Zealand, during the last 1.3 Myr. *Journal of Geophysical Research*, **109**, B02408, doi:10.1029/2003JB002412.

VILLA, I. M., HERMANN, J., MÜNTENER, O. & TROMMSDORFF, V. 2000. ^{39}Ar-^{40}Ar dating of multiply zoned amphibole generations (Malenco, Italian Alps). *Contributions to Mineralogy and Petrology*, **140**, 363–381.

WALLACE, R. E. 1968. Earthquake of august 19, 1966. Varto Area, Eastern Turkey. *Bulletin of the Seismological Society of America*, **58**, 11–45.

WESTAWAY, R. 1994. Present-day kinematics of the Middle East and eastern Mediterranean. *Journal of Geophysical Research*, **99**, 12071–12090.

WESTAWAY, R. & AEGER, J. 1996. The Gölbasi basin, Southern Turkey: a complex discontinuity in a major strike-slip fault zone. *Journal Geological Society of London*, **153**, 729–744.

WESTAWAY, R. & AEGER, J. 2001. The kinematics of the Malatya-Ovacik Fault zone. *Geodinamica Acta*, **14**, 103–131.

WESTAWAY, R. 2003. Kinematics of the Middle East and Eastern Mediterranean Updated. *Turkish Journal of Earth Sciences*, **12**, 5–46.

WESTAWAY, R. 2004. Kinematic consistency between the Dead Sea Fault Zone and the Neogene and Quaternary left-lateral faulting in SE Turkey. *Tectonophysics*, **391**, 203–237.

WILSON, D. S. & HEY, R. N. 1995. History of rift propagation and magnetization intensity for the Cocos-Nazca spreading center. *Journal of Geophysical Research*, **100**, 10041–10056.

YILMAZ, Y., ŞAROĞLU, F. & GÜNER, Y. 1987. Initiation of the neomagmatism in East Anatolia. *Tectonophysics*, **134**, 177–199.

YÜRÜR, M. T. & CHOROWICZ, J. , 1998. Recent volcanism, tectonics and plate kinematics near the junction of the African, Arabian and Anatolian plates in the eastern Mediterranean. *Journal of Volcanology and Geothermal Research*, **85**, 1–15.

ZOR, E., SANDVOL, E., GÜRBÜZ, C., TÜRKELLI, N., SEBER, D. & BARAZANGI, M. 2003. The crustal structure of the East Anatolian plateau (Turkey) from receiver functions. *Geophysical Research Letters*, **30**, 8044, doi:10.1029/2003GL018192.

Mediterranean snapshots of accelerated slab retreat: subduction instability in stalled continental collision

M. A. EDWARDS* & B. GRASEMANN

Structural Processes Group, Dept. of Geodynamics and Sedimentology, University of Vienna, Althanstrasse 14, Vienna A-1090, Austria

**Corresponding author (e-mail: michael.edwards@univie.ac.at)*

Abstract: This review of Mediterranean geodynamics highlights that the Mediterranean region captures at a fortuitous moment in time, a picture of the fate of foundering, old, cold oceanic lithosphere of limited area due to being landlocked in an all-but-stalled continental collision (Africa with Europe). We synthesize the geological spatial and temporal data for stretched crust as well as the 3D distribution of old abyssal plains and new oceanic lithosphere segments in concert with heat flow, palaeomagnetic data, geodetic velocity data, earthquake hypocentre distributions and seismic tomography. We use three Mediterranean subduction system settings (the western Mediterranean, the Hellenic and the Pannonian–Carpathian) that nicely reflect the slab instability and retreat. We assume that mantle slab dynamics best explains the observations. The dispersal and segmentation of the foundering landlocked ocean results in a series of discontinuous subduction zones whose individual lengths gradually diminish while retreat accelerates as slab progressively narrow and tear (i.e. along-strike laterally-propagating slab break-off) due to imminent total consumption of available oceanic lithosphere. We suggest that the Mediterranean region offers a lucid series of snapshots of accelerated slab retreat that, additionally, is globally unique as the only present day example of what we term intra-collisional landlocked ocean subduction.

This contribution focuses on three examples of subduction–collision boundaries (which we will term 'snapshots') in the Mediterranean and surrounding regions. It starts with an overview of the orogen at large. It then examines the role of mantle dynamics in slab and subduction zone evolution to outline those key processes that we will attempt to highlight for the snapshot examples. Highlighting of these key processes then underpins, for each snapshot example, a synthesis of observations of, and interpretations concerning, known subduction geodynamics elements. This then additionally provides the reader with a more general review of each snapshot area. All these then further serve to illustrate the snapshots' active and young (largely Oligo-Miocene) histories.

This contribution is, in part, motivated by recent work (Gemmer & Houseman 2007; Houseman & Gemmer 2007) that seeks to explain observations surrounding subduction geodynamics via numerical experiments which show the theoretical feasibility of mantle lithosphere downwelling ('drip off') that is engendered by lower lithosphere instability (with the notable absence of any subducting lithosphere). While this intriguing hypothesis offers a non-plate-tectonic based alternative (initially mainly applicable to the Carpathian–Pannonian snapshot), we keep with the hitherto postulated idea (e.g. Wortel & Spakman 2000) that subducting slab mantle dynamics provide the most elegant explanation (the simplest hypothesis that simultaneously accounts for the majority of the observations) for the actively migrating and evolving Mediterranean subduction–collision boundaries. Many of the ideas that we present here are hinted at or otherwise partly implicit in earlier reviews, syntheses or overview articles on the greater Mediterranean region (e.g. Dercourt *et al.* 1986; Jolivet & Faccenna 2000; Wortel & Spakman 2000; Cavazza *et al.* 2004). We build on these, incorporating knowledge that has subsequently emerged to provide a new review of Mediterranean subduction zone geodynamics for this volume that also serves to highlight two key themes: firstly, the fortuitous status quo of the greater Mediterranean; that each of the three snapshots captures at a different moment in time (and for slightly differing conditions) the fate of one of a handful of subduction zones that have developed due to the foundering and consumption of oceanic crust trapped in an (almost) stalled continental collision ('landlocked' of Le Pichon 1982) and, secondly, that this landlocked setting for actively evolving subduction zones represents a situation that would appear to be presently globally unique yet must be extremely common through geological time; the foundering of a landlocked basin before the complete closure of

From: VAN HINSBERGEN, D. J. J., EDWARDS, M. A. & GOVERS, R. (eds) *Collision and Collapse at the Africa–Arabia–Eurasia Subduction Zone*. The Geological Society, London, Special Publications, **311**, 155–192.
DOI: 10.1144/SP311.6 0305-8719/09/$15.00

the associated ocean and corresponding wholesale collision of the two attendant major converging continental plates (in this case, Africa and Europe while viewing the Mediterranean as part of the Eurasian greater orogenic belt).

The Eurasian greater orogenic belt

Over geological time, continental collision as part of the global scale Wilson-cycle (Wilson 1966) has repeatedly generated major collisional belts (1000s km in length) that arise from the complete collision and suturing together of two or more major (10^6) continents. This is evident both in not-yet-fully-dissected belts like the >5000 km long Palaeozoic Appalachians of North America (e.g. Cloos 1940) as well as in Archean and Proterozoic lower crustal roots such as those seen in multiple instances in the North American Shield (e.g. Hoffman 1988). We focus here on the Eurasian greater orogenic belt.

The greater orogenic belt system that is being generated from the continental collisional of the Eurasian plate with the partnership of the African, Arabian and Indian plates (Fig. 1) provides the Earth Science community with *the* state of the art natural laboratory in which to observe active or only recently terminated crustal and mantle geodynamics processes associated with converging continental lithosphere (Argand 1924). In addition to profiting from the often very complete preservation of rocks spanning a range of conditions and settings from unconsolidated recent sediments to exhumed ultra high pressure suites (that, moreover, are frequently within the framework of a coherent tectono-/metamorpho-stratigraphic architecture), the region encompassing the greater orogenic belt also profits immensely from the immediate traces and residual evidence that are attendant to the collisional processes (that are otherwise quickly removed from the geological record with the procession of time). For example, recent kinematics and tectonic boundary conditions of the colliding plates are well constrainable through both: (1) ocean floor magnetic anomaly data plus palaeomagnetic/stratigraphic studies that afford palinspastic/palaeogeographic reconstructions (e.g. Achache *et al.* 1984; Patriat & Achache 1984; Dercourt *et al.* 1986; Dewey *et al.* 1989*a*; Garfunkel 1998; Stampfli & Borel 2002; Kissel *et al.* 2003; Robertson *et al.* 2004; Schmid *et al.* 2004; van Hinsbergen *et al.* 2005*b*): and (2) consumed surface lithosphere magnitudes that may be derived from subducted slab down-dip (or palaeo-convergence direction) lengths as well as overall post- (or inter-) collisional consumed surface lithosphere geometries and associated mantle flow patterns (in their wake) – all of which are increasingly better imaged through upper mantle seismic tomographic and shear wave anisotropy models (e.g. Spakman *et al.* 1988; Kosarev *et al.* 1999; Duermeijer *et al.* 2000; Wortel & Spakman 2000; Kind *et al.* 2002; Faccenna *et al.* 2003; Sandvol *et al.* 2003; Tilmann *et al.* 2003; Piromallo & Faccenna 2004; Pondrelli *et al.* 2004; Wittlinger *et al.* 2004; van Hinsbergen *et al.* 2005*b*; Hafkenscheid *et al.* 2006; Sol *et al.* 2007) as well as through geochemical evidence of subducted slab/mantle relationships from young volcanism (e.g. Csontos 1995; Turner *et al.* 1996; Schiano *et al.* 2001). Meanwhile, at the other end of the system, exogenic signatures such as sedimentary processes often provide such extremes as: (1) comprehensive chemo-sedimentary records of the material eroded from regions of active shortening, surface uplift, topographic ruggedness, and enhanced precipitation that may accompany mountain building, stored in the form of orogen-adjacent basins such as the Bengal and Indus fans sourced from the Himalaya (e.g. Copeland & Harrison 1990; Burbank *et al.* 1992; France-Lanord *et al.* 1993; Einsele *et al.* 1996; Galy *et al.* 1996); or contrastingly (2) in portions of the active orogen where while climate-quiescent exogenic signatures of long periods of sedimentary process inactivity or insignificance (e.g. low erosion and deposition conditions) have prevailed, information can be preserved regarding, for example, the governing role of subduction-dynamics on exhumation with convergence, in the absence of extreme topography and enhanced sedimentary processes such as the late Miocene of the Cycladic extended continental lithosphere (Jolivet & Faccenna 2000; Vanderhaeghe *et al.* 2003*b*; Kuhlemann *et al.* 2004).

Within this above outlined textbook catalogue of first rate Earth Science research opportunities afforded by the composite Eurasian greater orogenic belt active collisional system, there exist a number of first order differences over the entire stretch (from the outboard Atlantic exposure at the western extremes of the European portions (e.g. the Rif) through the Arabian blocks, Makran subduction and Himalayas to the continental block escape, displacement and shuffling out into SE Indochina – Fig. 1). Of key relevance to this synthesis on Mediterranean geodynamics is the first order observation that this area (the Africa–Europe collision) preserves a far more piecemeal and, at first glance, less straightforward collisional orogenic belt than its along-strike associates; the Arabia–, and India–Asia portions.

Mediterranean snapshots

Philosophically, our Mediterranean snapshots thesis adopts the idea that, viewed from the global Wilson cycle of total collision and unequivocal suturing

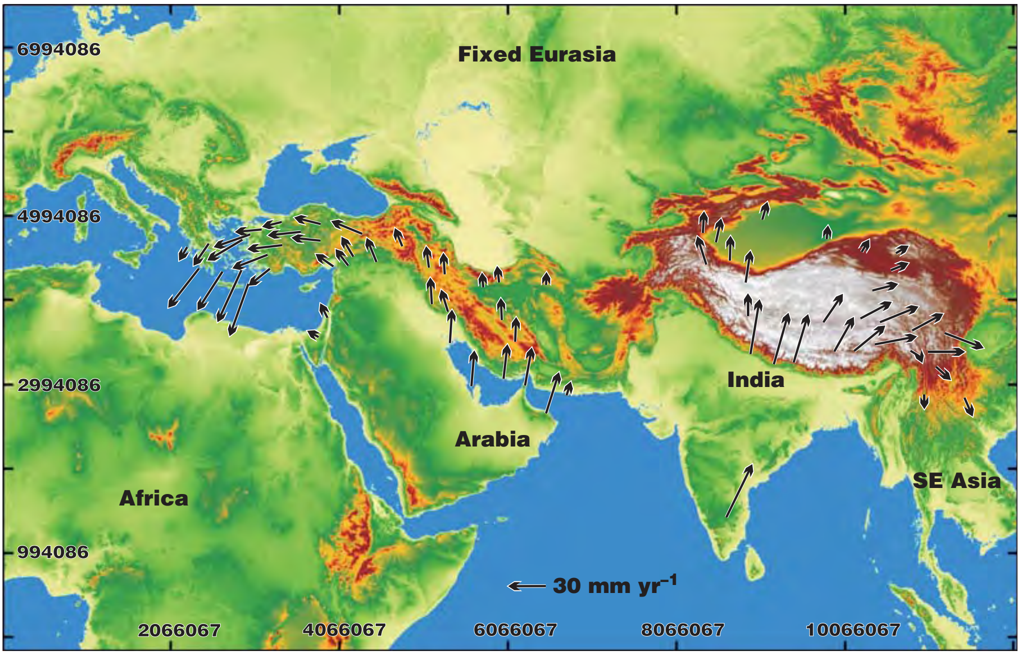

Fig. 1. Overview of greater orogenic belt system being generated from continental collisional of Eurasian plate with partnership of the African, Arabian, and Indian plates. Large arrows, approximate principal surface displacement directions relative to fixed Eurasia for two selected regions; southeast Europe/Arabia and Tibet/SE Asia. Areas selected exhibit strongest known vorticity patterns of any continental crust (see text). Topographic data is Universe Transverse Mercator gridded projection of GTOPO – SRTM30 (Shuttle-borne Radar Topography Mission of NASA, USA) digital elevation data sampled at 30 arc seconds pixel spacing, co-processed with András Jeno Zámolyi (Budapest & Vienna). Geodetic data incorporated from (Chen *et al.* 2000; McClusky *et al.* 2000; Shen *et al.* 2000; Nyst & Thatcher 2004; Zhang *et al.* 2004; Shen *et al.* 2005; Sol *et al.* 2007) and layout after Vernant *et al.* (2004). All residuals/confidence ellipses omitted.

together of major continents, three stages of the Eurasian greater collisional system exist. Each of these corresponds to an increased stage of maturity or advanced intensity of continental collisional convergence. From east to west: (1) the greater Indo–Asian collision; (2) the system of Arabia colliding into Iran and surrounding regions; and (3) the Africa-Europe collisional system. Whereas >1000 km of Indian plate collision into the southern Asian margin have now been accommodated via spectacular deformation (e.g. Patriat & Achache 1984), and at the same time, a less advanced (e.g. Berberian & King 1981) but enhanced velocity (e.g. Vernant *et al.* 2004) collision is well underway at the Arabian collision, the collision of Africa into Europe is comparatively still very incomplete; there arguably remain 100s to >1000 km of convergence before collision is advanced (whether the all-but-stalled collision will in fact persist to this point in the future is moot). We recognize that advanced stages of collision *sensu stricto* have occurred within numerous portions of the Mediterranean (e.g. the ‘post-orogenic’ collapse in many parts of the Alps and Hellenides). We emphasize, therefore that this notion of a very incomplete collision for the Mediterranean is only with respect to the idealized total collision of major continents that we discuss above. We return to the three stages of the Eurasian greater collisional system, and the role of the Mediterranean therein, in the discussion sections below.

Foundering of a landlocked ocean in a stalled collision

African convergence into Europe has slowed dramatically from velocities of a few cm/a to $\ll 1$ cm/a (Dewey *et al.* 1989b; Reilinger *et al.* 2006). Compared to the rapid Miocene to Recent subduction zone migration (retreat) velocities of our snapshots examples (Fig. 2) whose values range from a few to several cm/a (e.g. Schellart *et al.* 2007, and see below) we can, for the purposes

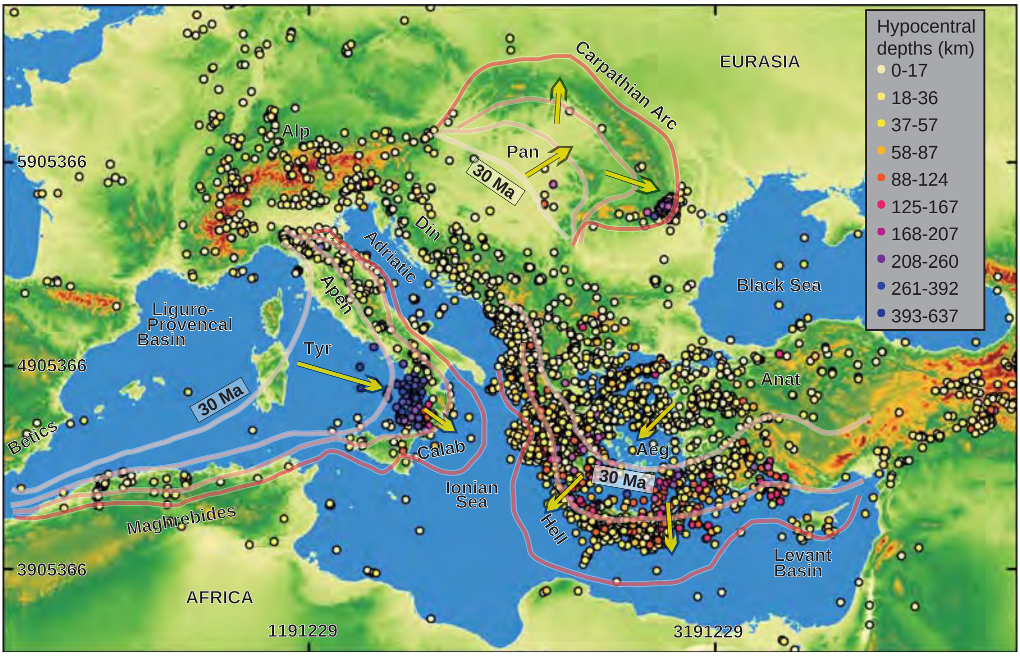

Fig. 2. Overview of retreating slab geodynamics of the Mediterranean region. Seismicity data (hypocentres) depict zones of active plate boundaries (*sensu lato*) where convergence is being accommodated within arc &/or trench systems by well-imaged subducting lithosphere. Note that in all cases, plate boundary lengths are short, especially with respect to slab extent at depth (see Figs 3 to 5) and are all close to their point of final cessation and extinction, thereby offering snapshots in time of the ongoing Africa–Eurasian collision. Historical traces of active plate (subducting slab intersection with surface) boundaries are approximate and based on the general consensus as shown in Cavazza *et al.* (2004) with minor modifications for Aegean from our own unpublished data. Tyr. is Tyrrhenian Sea; Cal. is Calabria (on and offshore); Apen. is Apennines; Alp. is Alphides; Pan. is Pannonian Basin; Din. is Dinarides; Hell. is Hellenides; Aeg. is Aegean; Anat. is Anatolia. Topographic base is Universal Transverse Mercator gridded projection of GTOPO – SRTM30 (full details see Fig. 1). Selected earthquakes, data courtesy: http://neic.usgs.gov/neis/epic/ (Earthquake Hazards Program, National Earthquake Information Center of the United States of America Geological Survey) and Russian public domain catalogue (Moscow 1994), corrected after Engdahl *et al.* (1998).

of this review, regard the Africa–Europe collision as effectively stalled, at least for the present point in geologic time. The piecemeal, or disjointed and not so straightforward nature of the Africa–Europe collisional orogenic belt that was noted above can be seen to be a product of this stalled collision, as in the following.

For the circum Mediterranean (including the palaeo- or 'nascent' Mediterranean (Scalera 2006)), Cavazza & co-workers (2004) amongst others, have summarized the character of a currently discontinuous chain of 100s km long segments of what we might term 'mature orogenesis'; isolated local sections like the Alps and Hellenides that involved high pressure genesis and/or later stage high temperature collapse. These mature orogenesis segments co-exist with accretionary orogen (à la Royden 1993*b*; Royden 1993*a*; Collins 2002) collisional segments (e.g. the central Apennines, Carpathians), and accretion-starved sections of subduction zones, as well as a patchwork or piecemeal distribution of residual ancient (?Mesozoic) and newly created (<30 Ma) oceanic lithosphere. As others have at least partly noted (e.g. Le Pichon 1982; Morley 1993; Royden 1993*b*; Jolivet & Faccenna 2000), the recalcitrance of the African plate to persevere on its collisional path has resulted in one or more spatially-limited, landlocked ancient oceanic lithosphere fragments. The idea of 'landlocked' was first introduced by Le Pichon (1982). We use this term here to mean a limited total available area of original, pre-collision oceanic lithosphere that is (being) wholly enclosed between two continental masses. For the nascent Mediterranean, the original colliding margin(s) were presumably quite uneven and likely comprised embayments and promontories associated with 100s km of amplitude. Old, cold oceanic lithosphere fragments thereby passively foundered and sank under their own weight into the aesthenospheric mantle as part of the progression to imminent total consumption of the steadily diminishing oceanic lithosphere (portions). Of relevance to the (nascent) Mediterranean is that the landlocked segment was (is) trapped between two *slowly* converging (or in this case effectively stalled) continental masses thereby enabling the original oceanic lithosphere sufficient time to steadily founder (i.e. expire via sinking into the aesthenosphere under its own unstable mass). In the absence of superior plate kinematic forces, this foundering causes subduction zone retreat via the mantle dynamics of slab rollback (e.g. Andrews & Sleep 1974; Royden 1993*b*; Funiciello *et al.* 2003; Husson 2006).

For the three snapshot examples and indeed for all the Mediterranean and surrounding region subduction zones (including ancient subduction zone, now-collided continental mass type convergent boundaries), we propose the term '*Intra-Collisional Landlocked Ocean Subduction*', or ICLO subduction. This discriminates such subduction from (e.g.) SW Pacific-type, purely intra oceanic (and/or Andean-arc collision) settings; although both types involve mantle dynamics associated with small area oceanic plate segments whose plate boundary lengths are short (commonly <1000 km), the circumstances differ greatly. Complete consumption of a small (e.g. $<1 \times 10^5$ km^2) portions of oceanic lithosphere is expected to occur for both scenarios. In SW Pacific-type settings, however, such a piece of small oceanic lithosphere is likely to be bounded on many, if not all, sides by plates also composed (mostly) of more oceanic lithosphere. The collision then comprises of piling up of island arc(s) whose preservation is determinate upon accretion to continental material. Accreted Pacific-type terranes such as those of the North American Pacific margin are expected to be relatively straightforward to identify; in addition to differences identifiable via geochemical discrimination of volcanics, a key difference is that for accreted Pacific-type terranes, accretions may repeatedly occur, and so accumulate over long periods such that their number is virtually 'unlimited'. ICLO subduction is by definition limited; restricted in space and time. Identification of fossil examples of ICLO subduction in ancient orogens may indeed be difficult. This theme is considered further in the discussion.

Mantle dynamics of slab rollback and subduction zone retreat

The phenomena of mechanisms associated with, and interactions between, slab retreat, break-off and tearing emerge in numerous references and for purely oceanic settings even emerge quite early in the literature (e.g. Barker 1970; Andrews & Sleep 1974; Karig 1974). The instability potential of the descending slab in the situation of ICLO subduction, like the Mediterranean, obviates the need to drive the evolution of the Mediterranean via plate kinematic forces alone (e.g. Mantovani *et al.* 2000; Mantovani *et al.* 2001) or self-instigated downwelling or 'drip off' of the mantle lithosphere (Gemmer & Houseman 2007; Houseman & Gemmer 2007). As we noted above, we regard the dynamics of slab involvement in the aesthenospheric mantle as the critical mechanism at large in the Mediterranean (e.g. Le Pichon 1982; Wortel & Spakman 2000) and keep with this for our situation of a landlocked ocean.

Key characteristics that we will highlight from our snapshot examples are: (1) that all are characterized by short (which we define as typically <1000 km but cf. ≤ 1500 km in Schellart *et al.* 2007 define as ≤ 1500 km) plate boundary length; (2) the arcuate geometry of the active convergent boundary becomes more pronounced as it matures (as noted by numerous authors – see specific snapshot examples below); (3) the slab retreat does seem to accelerate with decreasing slab width (which we define as the measurement roughly perpendicular to the slab dip direction, not always equivalent to subduction zone length); and (4) that there is some association with slab break-off and/or tearing. This is all suggestive of the instability of foundering ancient oceanic lithosphere. Many authors have noted that a narrow slab (where width is typically less than length) is more susceptible to instability. For example, Dvorkin *et al.* (1993) remarked that the hydrodynamic suction created by the downdip motion of a wide slab is sufficient to balance the downward pull of gravity (that exists due to the great density of the slab). However for a narrow slab, sideways asthenospheric flow into the slab/overriding plate corner effectively eliminates the suction, which results in the rapid sinking of the slab. The corner flow notion is more recently taken up by Govers & Wortel (2005). The extreme length/width proportions were noted for marginal basins of large oceans (Karig 1971; Sleep & Toksoz 1971; Karig 1974). The notion of short plate boundary length instability to explain very long ($\gg 1000$ km) transform boundary margins of these back-arc spreading basins/marginal sea portions was entertained by Andrews & Sleep (1974), as well as Uyeda & Kanamori (1979), while the general, more critical thermal situation for microplates in a convecting mantle was noted by Parsons & McKenzie (1978) and, in a more complete summary, by Taylor & Karner (1983). The South Sandwich Islands island arc and the long tongue of rapidly retreating subducting slab that is generating the Scotia Plate backarc spreading has long drawn much attention, not least due to the intriguing geochemistry of sub-slab mantle flow around the subducting slab edge (e.g. Barker 1970;

Royden 1993*b*; Leat *et al.* 2004). This is also true to some extent for the Caribbean plate (e.g. Mann & Burke 1984; Pindell *et al.* 1988).

For the Mediterranean and surrounding area, it is frequently recognizable that subduction zones (or specifically, their traces) have, over time, developed a pronounced curvature with segments dramatically rotating as they have migrated and retreated. The approximate historical and present day traces of the Mediterranean convergent boundaries are shown on Fig. 2. The ensuing convergent plate boundary retreat and rearrangement that was (and is still being) attained generates thereby an ever-more irregular and discontinuous chain (or series) of classical plate-tectonic boundaries (as per Isacks *et al.* 1968; Dewey & Bird 1970); i.e., subduction zones plus, locally, accretionary orogenesis or continental crust collision that we noted above. During migration, the subduction zone portions of the plate boundaries may temporarily lengthen, but at one point the length of the subduction zone in question will begin to progressively shorten as original oceanic lithosphere is increasingly spent. As a result, continental crust will frequently begin to enter part of the subduction system giving rise to local orogenesis. The nature of orogenesis may attain various levels of intensity (i.e. thin-skinned folding with thrusting lower temperature accretion, or high pressure genesis and exhumation, or even high grade metamorphism with anatexis, plus collapse before convergence becomes arrested, or becomes greatly attenuated with respect to the neighbouring, along-strike oceanic subduction).

Typically, breaking-off or tearing of the slab can be expected at such continental to oceanic subduction transitions either with break-off progressively propagating laterally along strike or with the development of a tear in the approximate downdip direction, possibly even giving rise to a STEP fault type architecture (Gîrbacea & Frisch 1998; Nemcok 1998b; Wortel & Spakman 2000; Funiciello *et al.* 2003; Govers & Wortel 2005; Faccenna *et al.* 2006). Tear off can also, of course, occur in the absence of any continental crust (e.g. the catastrophic slab loss of Levin *et al.* 2002). We expect that tearing of the slab, whether as a steep downdip oriented feature or laterally progressing, along-strike break-off, is expected to enhance the rollback velocity and the extremity of subduction zone curvature. This type of association has been partly illustrated by Schellart *et al.* (2007) as part of a global database of length – curvature versus retreat (also advance) velocity for oceanic subduction zones along with numerical representations. These authors note that trench migration rate is inversely related to slab width and curvature intensity is dependent on proximity to a lateral slab edge, where narrow slabs ($\leq$1500 km) retreat fastest and develop curved geometries. Although these authors' models cannot incorporate specifics such as the repeated piecemeal arrival of continental margin into the system that is highly likely in a ICLO subduction setting such as the Mediterranean, it gives a strong indication of the likelihood for slab rollback. Subduction zone retreat is thereby seen to be a key phenomenon in the Mediterranean and surrounding area that is not only engendered by the very nature of foundering of the instable ancient oceanic lithosphere but that, moreover, is predicted to accelerate as the most recently subducted slab increments widths become progressively narrower and slabs tear and/or break-off. We then have a picture where the width of subducting oceanic lithosphere is an ever narrowing tongue – probably either due to the progression towards complete consumption of oceanic lithosphere and tearing, or simply due to increased extremity of curvature for a very narrow (few 100 km) slab – as would be predicted by Schellart *et al.* (2007). Because the near-surface slab width is less than the slab width at depth, there is an 'apron' (or concave up, beheaded triangular surface) geometry. This geometry imposes great concentration of slab pull. With the ever smaller slab width, asthenospheric flow around the sides becomes easier and so diminishes the suction force noted above (Dvorkin *et al.* 1993). This is further diminished as the slab becomes even steeper (frequently approaching vertical, as we will vividly see in the snapshot examples below). The result is an ever accelerating retreat as the point of final expiration of the slab approaches.

The three snapshot examples

One of the many attractions of the Mediterranean and surrounding region is that the plate evolution boundary conditions are relatively- to very-well known (e.g. Jolivet & Brun 2008). For each of the three snapshot areas, decades of geological study in the Mediterranean, in concert with modern geophysics including heat flow, gravity & Moho depth studies, surface displacement geodesy (Fig. 1), distributions of moment tensors from, as well as surface or depth localization of, seismicity (Fig. 2), and upper mantle seismic tomography all beautifully reveal the active geodynamic processes associated with, and the immediate results of: (1) the piecemeal slab detachment with (2) general slab retreat that (3) over time becomes more localized and (4) in many cases significantly accelerated, and that is (5) synchronous with local convergence plus 'back-arc' extension. As we will see for the three snapshot areas, back-arc extension is very common and, at critical periods, is often notably intense in the wake of enhanced (and frequently late stage accelerated) subduction zone retreat. Back-arc extension may be associated with either extreme thinning such as the Pannonian or Aegean, or entire rupture of continental lithosphere with new oceanic lithosphere production such as the Ligurian–Provençal and Tyrrhenian basins.

The various collisional products of the Mediterranean and surrounding regions include: the Betics, the Maghrebides, the Apennines, the Alps, the Carpathians, and the Dinarides-Rhodopes-Hellenides (including the 'Balkides'). Their young back-arc basins include: the Alboran Sea, the Aegean, the Pannonian, and the Ligurian–Provençal plus Tyrrhenian basins (notable for their Oligocene to Recent oceanic lithosphere production). The third piece to the landlocked hypotheses is the now segmented abyssal plain, represented by lingering ancient (?Mesozoic) oceanic lithosphere remnants that include: the Ionian Sea, the Hellenic abyssal plain, and the Levantine Basin (although for the Ionian Sea remnant cf. Hieke *et al.* (2005) versus Catalano *et al.* (2001)). These abyssal plain remnants represent the last intact vestiges of the foundering of the land-locked ancient oceanic lithosphere region(s) and are awaiting the final consumption into the aesthenosphere. Taken together, all these elements equate to three or four discrete settings, or snapshots, that capture different moments in the final stages of accelerated slab retreat where subduction has ceased (or all but ceased) as most available oceanic lithosphere has been completely, or all but completely, consumed. We review three of these: the western Mediterranean, the Hellenic subduction zone system, and the Pannonian–Carpathian system. For the western Mediterranean we exclude the Betics/Rif/Western Maghrebides – Alboran Sea area and concentrate our focus on the Calabrian–Apennine accretionary belt and its back-arc, the Ligurian–Provençal plus Tyrrhenian basins. As discussed by many authors (e.g. Morley 1993; Royden 1993*b*; Platt *et al.* 1996; Lonergan & White 1997; Faccenna *et al.* 2004; Serpelloni *et al.* 2007), there is ample convincing evidence that a great deal of the tectonic evolution (e.g. convergence, deep exhumation, thickening and later collapse) of the two opposing-vergence orogenic pair portions of the Betics vis à vis the Rif/Western Maghrebides can be adequately explained by slab rollback dynamics (e.g. Wortel & Spakman 2000; Cavazza *et al.* 2004). In comparison to our three chosen snapshot areas, however, the story is less elegant and, particularly for the Miocene and younger history, the story is significantly more up for discussion. We therefore choose to omit the Betics/Rif/Western Maghrebides – Alboran Sea area from the snapshots examples.

The western Mediterranean

In the western Mediterranean (Fig. 3), our focus is the Calabrian–Apennine accretionary belt and its backarc, the Ligurian–Provençal plus Tyrrhenian basin(s). As noted above, we exclude the Betics/Rif – Alboran Sea to facilitate the snapshot example. This area offers an exciting example of continental lithosphere that has been stretched and failed completely leading to widespread new oceanic lithosphere production as the backarc spreading system of a convergence zone (e.g. Malinverno & Ryan 1986). The subducting slab, at least up until recently, has rapidly retreated, accelerated while progressively narrowing, with subduction gradually terminating ($\pm$ slab tear-off – see below) and thus the length of the active plate boundary continually diminishing. This is borne out by (1) the migration pattern revealed by the distribution of young back-arc oceanic crust production as well as (2) the spatio-temporal distribution of both subduction related volcanism & active versus historical faulting trends, and (3) seismicity surface and depth distributions – see below). This is all reflected in Figure 2 as part of the broadly agreed consensus of a west to east retreat of the subduction zone/convergent plate boundary over the last 30 Ma. Overall calculations suggest a total of *c*. 775 km of 'eastward' migration of the convergence zone from Oligocence to Present (Gueguen *et al.* 1998). Since latest Eocene time (Beccaluva *et al.* 1981; and see also Rossetti *et al.* 2004), Adria oceanic lithosphere (also called the Apennine Slab) has subducted westwards (or NW- or SW-wards) beneath Italy, culminating in the Apennines and being associated with 80 to 200 km of shortening that is largely Neogene–Quaternary (Malinverno & Ryan 1986; Giuseppe *et al.* 1997; Gueguen *et al.* 1998; Galadini & Galli 1999). Palaeomagnetic data and historical stress field rotations indicate that the Apennines have rotated anticlockwise from originally NE- trending (Scheepers *et al.* 1993; Mattei *et al.* 1995; Muttoni 1998; Hippolyte 2001) growing as an accretionary wedge plus fragments ripped off the Main Alpine chain, to finally collide into the Adrian continental lithosphere platform (see extensive references in Cavazza *et al.* 2004). This final stage collision modified the original fold and thrust belt geometry of the Apennines (albeit mainly only in the south) to become more complex and out-of-sequence, coinciding also with the steady southwards younging termination of volcanics. The collision has not been intense; deformation is mainly thin-skinned and heat flow values in the Adriatic continental crust (away from volcanic centres) rarely exceed 50 mW/m^2. Total exhumation is estimated at 2.5 km and up to 5 km subsidence in foredeeps such as the Po basin (e.g. Cloetingh *et al.* 2007). Loading of the Adriatic continental promontory via the Apennines on the (south) west side and the Dinarides on the (north) east causes a bowing up of the plate and shallowing in the Adriatic Sea.

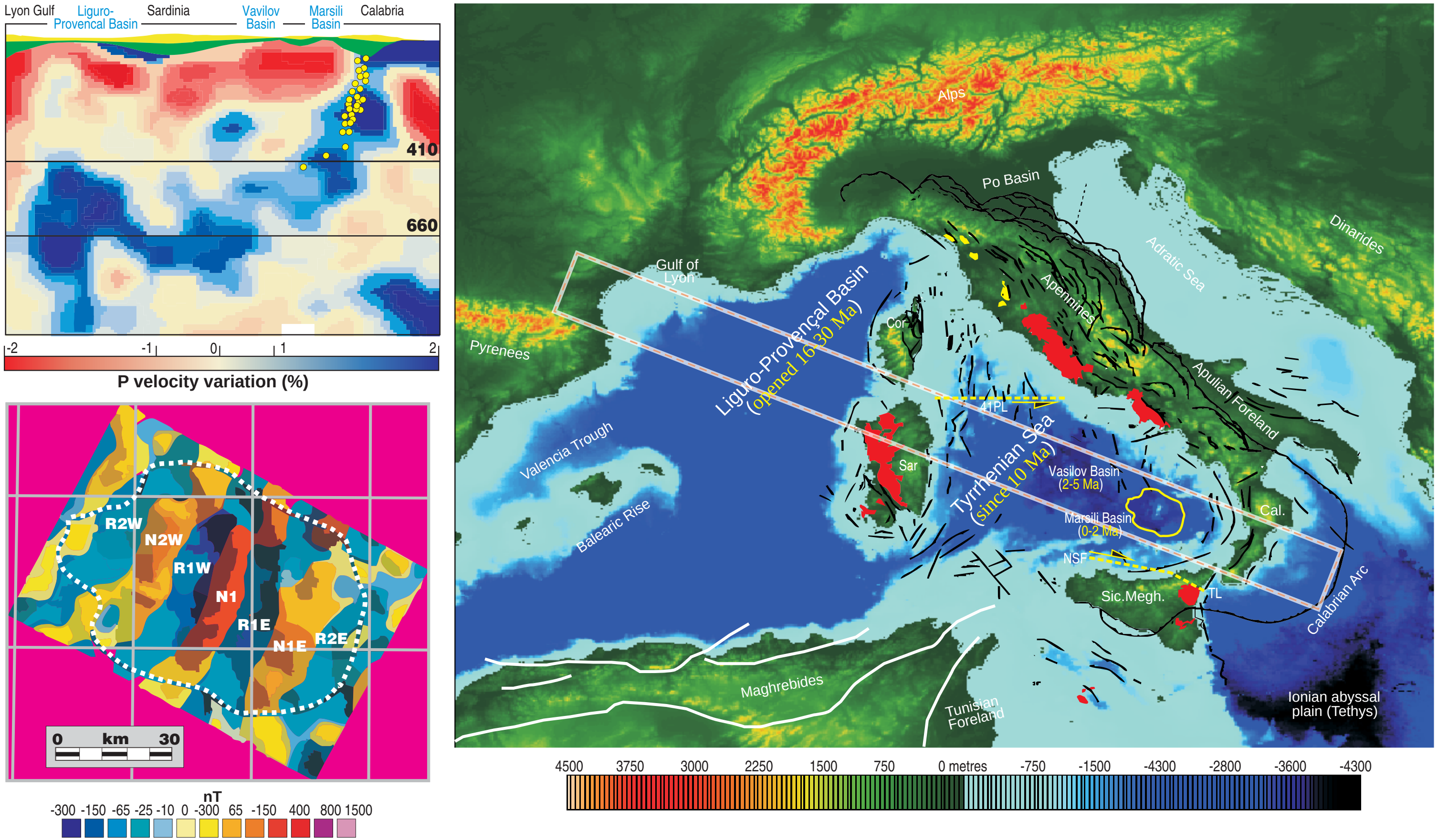

Fig. 3. Main figure: principal (neo)tectonic and historical features of central Mediterranean region related to slab retreat and migration/development/interaction of Apennine/Calabria system with Apulian and N. African plates. Barbed black lines, principal fault traces for Apennine/Calabria system; white lines, principal fault traces for N. African Maghrebides; red, volcanics related to mid-late Cenozoic slab retreat and mantle melts. Fault traces for Alps, Dinarides, Pyrenees and beyond are omitted for clarity. Note contrasting sea floor geometry between Liguro–Provençal Basin (even, flat) and Tyrrhenian Sea (heterogeneity in loci of deeper basins including Vavilov and Marsili basins). Sic. Magh. is Sicilian Maghrebides; Cal. is Calabria. Yellow dashed lines 41PL (41st Parallel North line), NSF (North Sicilian Fault) and TL (Taormina Line) are proposed geodynamic

Within the Western Mediterranean, back-arc extension, crustal stretching and ocean opening were, of course, associated with this system of Apennines rotation and convergence throughout their existence. Backarc extension began in Variscan basement that was already rifted (and thus presumably sufficiently weakened; rifts offering preferred loci for rift fault nucleation and linkage) via a series of wrench fault systems, part of a western Europe-wide process. This is evidenced by syn-rift deposits in basins related to such wrench fault systems at *c*. 35 Ma (e.g. Jolivet & Faccenna 2000; Lacombe & Jolivet 2005 and references therein). Ligurian–Provençal basin opening proper initiates about 30 Ma and proceeds to *c*. 16 Ma, as evident from the ages of syn-rifting sedimentation in the Gulf of Lyon and volcanism and rift flank uplift cooling ages from the Corsica–Sardinia block (Martini *et al.* 1992; Sowerbutts 2000). Helbing *et al.* (2006) similarly draw attention to reactivation of Palaeozoic basement structures in Sardinia that give evidence for a transtensional back-arc setting during Ligurian–Provençal opening and related western Mediterranean subduction rollback. That this is a back-arc system is attested to the presence of the basaltic-andesitic chemistry volcanics – the volcanic arc to the (presumably) NW dipping Oligocene slab (e.g. Faccenna *et al.* 1997 and references therein). Faccenna *et al.* (1997) draw attention to the point that the Ligurian–Provençal Basin (conspicuous for its very even bathymetry – as visible in Fig. 3) is due to rifting of a cold, not relatively weakened continental crust with a shallow Moho (Tirel *et al.* 2009 and see discussion). Although this notion is credible, the thermal state of the pre-rifted continental crust is not completely clear; in Corsica, Danisik and co-workers (2007) note evidence for a pre-Jurassic to early Cretaceous long-lived Tethyan thermal event related to rifting and the early stages of Jurassic opening of the Ligurian-Piedmont Ocean. Moreover, Fellin and co-workers (2006) observe Oligocene collapse of the Alpine nappe stack and rifting prior to opening of the Ligurian-Provençal Basin. They interpret a zircon fission-track age population of *c*. 24 Ma to indicate some cooling after Tertiary thermal events that can be associated with the main Alpine metamorphism and the opening of the Ligurian–Provençal basin. Such incomplete Alpine orogenesis overprint of original Variscan deformed and metamorphosed continental crust is typical of much of the nascent Mediterranean (e.g. Zentralgneiss of Austria, Tatricum of Slovakia, etc). The Corsica–Sardinia block is however both the margin of the Faccenna *et al.* (1997) 'cold' Ligurian–Provençal Basin system and the margin of their 'warm' Tyrrhenian Basin system and thus is likely to record some signature of crustal stretching already at its Oligocene initiation – albeit that the only complete lithospheric failure at this time is West of the Corsica–Sardinia block in the form of the Ligurian–Provençal Basin. Either way, the Corsica–Sardinia block is a key source of evidence for the entire evolution of the Western Mediterranean ICLO subduction system. The crustal fragments of the main Alpine event in the Corsica–Sardinia block are famous (e.g. Mattauer *et al.* 1981; Faccenna *et al.* 2002; Lacombe & Jolivet 2005; Rosenbaum *et al.* 2005; Fellin *et al.* 2006; Molli *et al.* 2006; Danisik *et al.* 2007). These and various other authors have documented that the main Alpine event was followed by a period of core-complex generation. As noted by Rosenbaum & Lister (2005), however,

Fig. 3. (*Continued*) accommodators of Rosenbaum & Lister (2004) see text. Red dashed on white line forming box is approximate trace of swath of seismic tomography profile (see inset). Irregular closed shape yellow line labelled Marsili Basin is location of lower inset (to left of main figure) and area of Chiappini *et al.* (2000) seafloor magnetic survey. Shallow area in centre of this marked region (identifiable by paler blue bathymetric scale tone) is bathymetric high of Marsili Seamount, and represents mid-ocean ridge segment associated with sea-floor spreading since late Pliocene. Topographic and bathymetric data from SRTM30 V.2 (topopography) with Smith and Sandwell global 2-minute grid (bathymetry) processed (with András Jeno Zámolyi of Budapest & Vienna) from: ftp://topex.ucsd.edu/pub/srtm30_plus and www.ngs.noaa.gov. Features drawn after Jolivet *et al.* (2000; 2003), Faccenna *et al.* (1997; 2001; 2003; 2004), Rosenbaum & Lister (2004) and own data.

Upper left inset: Tomographic profile model (PM 05) from Piromallo and Morelli, (2003) redrawn from Faccenna (2003; 2004) and Lucente *et al.* (2006). Subsurface position and continuity of remaining portion of Tethyan lithospheric slab is clearly visible from rapid P-wave velocity (blue) region. Depth scale is given by 410 and 660 km acoustic transitions (discontinuities). (Note contrast between steep upper portion of slab (in wake of rapidly-opened Tyrrhenian Sea) and deeper, more distal portions of slab (now bottoming out and rotating over on 660 discontinuity). At surface of profile, yellow (crust) and green (mantle) lithosphere thicknesses are freely interpreted from gravity and Moho depth data summarized in Cavazza *et al.* (2004). Yellow dots, hypocentres are selected earthquakes (note persistence as far as 410 discontinuity – some events omitted for clarity) from: http://neic.usgs.gov/neis/epic/ (Earthquake Hazards Program, National Earthquake Information Center of the United States of America Geological Survey) and Russian public domain catalogue (Moscow 1994), corrected after Engdahl *et al.* (1998).

Lower left inset: Detail of Marsili Basin magnetic survey data (from Chiappini *et al.* 2000), re-drawn after Nicolosi *et al.* (2006). Identification of chrons symmetry provides further snapshot of ultra fast ocean spreading (up to 19 cm/a) during 0–2 Ma pulse of slab retreat (see text).

this cannot be large, may simply be gravitational collapse of the Alpine over-thickened body, and so might not be a true part of the mantle dynamics associated with slab rollback and arc spreading mechanisms (but see also Jolivet *et al.* 1998). In stark contrast then, to the Pannonian and to the Attic Cycladic – western Turkey and Rhodope systems (see below), here in the Western Mediterranean, complete lithospheric failure with break-up and drift apart of continental blocks and fragments have prevented the distributed shear and extreme crustal stretch that is associated with major sedimentary basin development or core complex-bearing extended terranes. The Corsica–Sardinia block, in addition gives us key rotation evidence. Palaeomagnetic data (e.g. Scheepers *et al.* 1993; Vigliotti & Langenheim 1995; Rosenbaum & Lister 2004; Cifelli *et al.* 2007; Gattaccecaa *et al.* 2007) show that the block more or less rotated in tandem with the central Apennines by as much as 45° anticlockwise up until 10–15 Ma, at which time the two rift apart to create the Tyrrhenian Basin(s) (e.g. Malinverno & Ryan 1986). Jolivet & Goffe (2000) note a pre-rift thickness of *c.* 50 km for the now disbursed Alpine orogenic pile of Corsica, Calabria (Peloritani) and Tuscany.

Geodynamic phenomena in the Tyrrhenian, as well as their interpretations, are a bit livelier than for the Ligurian–Provençal. The Tyrrhenian Sea has more complex bathymetry (Fig. 3) characterized by shallower depths and lower heat flow values in the northern Tyrrhenian Sea Basin that contrasts with deeper basin depths and higher heat flow values for the southern Tyrrhenian Sea Basin (up to 120 mW/m^2 – see e.g. Cavazza *et al*. 2004 for reviews). The southern Tyrrhenian Sea Basin is further composed of two distinct basins; the Vavilov (which opened between 2 and 5 Ma) and the Marsili (which opened between 0 and 2 Ma). In addition, there are a range of volcanics (e.g. the Pliocene of Sardinia in Lustrino *et al.* 2000) and onshore and offshore geometrical features (open to interpretation as to fault type, e.g. Helbing and co-workers (2006) propose the left-lateral Nuoro Fault in central Sardinia as initially being a radial transfer between the west Sardinian rift and northern Tyrrhenian basin which thereafter contributed to extension gash pattern opening of the southern Tyrrhenian basin). More comprehensive overviews of these (with varying perspectives) are offered by Rosenbaum & Lister (2004) and Faccenna *et al.* (2004). Differences between the Vavilov and Marsili have led to various remarks and conclusions; the persistence of mid-ocean ridge back-arc spreading only in the southern Tyrrhenian Sea is certainly coupled to the reduction of the active subduction zone length as part of the gradual move southward of termination of deep active subduction along the Apennines. There is debate as to their degree of significance, but processes including: (1) a horizontal N(NW) to S(SE) laterally propagating tearing – i.e. migrating slab breakoff such as Wortel & Spakman (2000) or Govers & Wortel (2005) as part of the complete consumption of cold, heavy oceanic lithosphere; (2) subduction zone lockup caused by an incoming carbonate platform at 6–7 Ma (Rosenbaum & Lister 2004); and (3) eastward and northeastward mantle flow as part of a more global regime (e.g. Doglioni *et al.* 1999) may all have played some role in the evolution of the active arc and slab to its restricted final position around Calabria.

As well as this west to east retreat of the subduction zone/convergent plate boundary, Figure 2 shows the present distribution of hypocentres. For the northern and central Apennines, it is clear that there is shallow seismicity (<40 km) typical of fold and thrust belt behaviour with only a small portion of the seismicity at intermediate depth (80–110 km); significant seismicity in the accretionary wedge is not present down through to mantle depths. Models for seismic tomography (e.g. Lucente *et al.* 1999; Wortel & Spakman 2000; Piromallo & Morelli 2003; Montuori *et al.* 2007) across this portion of the belt (data not reproduced in this review) differ on whether or not there is a discontinuity from the deeper slab to the upper surface i.e. no connection between high velocity regions in the uppermost aesthenospheric mantle and the larger layer of slab (high velocity) material accumulating onto the 660 km global discontinuity. Slab break-off would be the generally interpreted status quo (e.g. Spakman & Wortel 2003). In contrast, across the Calabrian portion, Figure 2 shows the 'shotgun' distribution of hypocentres from 100 to 400 km depth defining a more or less vertical Benioff–Wadati Zone (Anderson & Jackson 1987). This seismicity partly reflects that the Calabrian arc is the only part of the collisional belt where arc-related volcanism has not ceased. The Benioff Zone is more clearly seen on the display of earthquake source points on the lower left inset in Figure 3, rendered on top of the seismic tomogram reproduced from Faccenna *et al.* (2003) after Piromallo & Morelli (2003). Although there is some uncertainty (see Wortel & Spakman 2000 for further discussion), there is good evidence for an intact lithospheric slab (one that has not yet experienced break-off) continuing from the surface all the way to the 660 km accumulation. Our snapshot here the captures the moment just before (or in the act of) break(ing)-off. The Adriatic continental lithosphere is just entering the system here (whereby it has already collided further NW up the Apennines) and the last vestiges of old Mesozoic oceanic lithosphere (manifest as the abyssal plain beneath the Ionian Sea on Fig. 2) are not yet consumed.

Crucially, we now have dramatic evidence from Nicolosi and co-workers (2006) of very fast backarc spreading above the slab in the form of the Marsili Basin in the Southern Tyrrhenian Sea (Fig. 2, main field) of up to 19 cm/a that has been calculated from the magnetic patterns associated with new oceanic lithosphere production (from the Chiappini *et al.* 2000 seafloor magnetic survey). This would seem to require at least an equivalent magnitude of velocity for slab retreat-engendered trench migration (during the final intensification of the arcuate geometry of the present Calabrian plate boundary). More than this, however, to add to our captured-in-time aspect is that this pulse or period of accelerated retreat has now mostly ceased. Geodetic motion observations (e.g. Oldow *et al.* 2002; Serpelloni *et al.* 2005; D'Anastasio *et al.* 2006; Serpelloni *et al.* 2006) and seismic moment studies (Pondrelli *et al.* 2004) of the Calabria orogenic belt with respect to Sardinia/Corsica and Franco–Iberia show that the belt (i.e. southern Italian mainland with Sicily) closely tracks North Africa (<1 cm/a), has only a minor eastwards component and, importantly, that the Corsica–Sardinia block moves according to Eurasian Plate motions. There appears to be no currently resolvable divergence between Corsica–Sardinia and peninsular Italy and there is no indication that the opening of the Tyrrhenian is still active (Serpelloni *et al.* 2005). More critically Pondrelli *et al.* (2004) show that the Tyrrhenian Basin has now a north–south compressional stress state. It really would then appear that via the various geophysical, structural and volcanic rocks datasets we have captured the final moments of ICLO subduction.

Hellenic subduction zone system

On the eastern side of the Adriatic Sea (the Adriatic promontory or platform) facing the Western Mediterranean theatre, is a fairly continuous and throughgoing orogenic chain arising from Tertiary collision of the Adriatic promontory into Eurasia. From the eastern Alps, the chain comprises (from NW to SE) the Dinarides (including the external Dinarides or Balkanides), Albides & Rhodopes (also Serbo-macedonian-rhodope block) and the Hellenides. Figure 2 shows the active seismicity defining the NE- to North-dipping Benioff–Wadati zone portion of subducted slab architecture for much of this system. Figure 4 highlights the key elements of the active and recent processes in the greater area of the Hellenic subduction zone system (including the surrounding mainland areas), the focus of our second snapshot.

Active geodynamics

The active geodynamics of this region are impressive. They comprise: (1) by far the highest present-day seismic activity in Europe (e.g. Papazachos 1973; Mercier 1979; Ambraseys & Jackson 1990; Taymaz *et al.* 1991; Jackson *et al.* 1992; Baker *et al.* 1997; Giardini 1999; Hatzfeld 1999; Papaionnou & Papazachos 2000; Bohnhoff *et al.* 2004); (2) surface displacement kinematics identified from SLR/GPS-data (Fig. 4) that have some of the highest vorticity expressions known for any continental crust (comparable only to the Eastern Himalayan syntaxis) and that constrain the present day, relative to Eurasia westward movement 'escape' plus rotation of the Anatolian region, and southward extension of the Aegean region, (Noomen *et al.* 1996; Reilinger *et al.* 1997; Clarke *et al.* 1998; Cocard *et al.* 1999; Briole *et al.* 2000; McClusky *et al.* 2000; Ayhan *et al.* 2002; Meade *et al.* 2002; Nyst & Thatcher 2004; Reilinger *et al.* 2006); (3) dramatically extended/thinned lithosphere of the back-arc that is associated with heat flow values of up to 100 mW/m^2, Moho depths as shallow as 24 km, and extension at the Gulf of Corinth rift that is the fastest known spreading for any continental crust (Makris 1978; Bohnhoff *et al.* 2001; Li *et al.* 2003; Bohnhoff *et al.* 2004; Tirel *et al.* 2004; Endrun *et al.* 2005); (4) the association of these plate kinematics with active subduction and widely-recognized dramatic slab retreat of African lithosphere beneath the Aegean (micro)-plate at the Hellenic trench system (e.g. McKenzie 1972; Le Pichon & Angelier 1979; Angelier *et al.* 1982; Papazachos *et al.* 2000); (5) present day mantle dynamics and subduction history of the slab over time that is strikingly evident from the lucid slab architecture portrayed via Benioff–Wadati surface geometry (seen dipping NNE to *c.* 180 km in Fig. 4) and via seismic tomography models with definitive imagery (Fig. 4) showing deep mantle architecture down to 1200 km for the entire SE European region (e.g. Makropoulos & Burton 1984; Spakman *et al.* 1988; Taymaz *et al.* 1991; Hatzfeld 1994; Papazachos *et al.* 1995; Hatzfeld 1999; Karason & van der Hilst 2000; Wortel & Spakman 2000; Faccenna *et al.* 2003; Piromallo & Morelli 2003; Bohnhoff *et al.* 2004; Faccenna *et al.* 2004; Endrun *et al.* 2005; van Hinsbergen *et al.* 2005*b*; Bohnhoff *et al.* 2006); and (6) calc-alkaline volcanism most prominently represented by the island volcanoes of Milos, Santorini, and notably Kos. As is visible on Figure 2, the island area of Kos plus 10–20 km surrounding radius is, furthermore, spatially associated with deeper (non Benioff-Wadati zone) seismicity down to 150 km (Zellmer *et al.* 2000; Mocek 2001; Bohnhoff *et al.* 2006; Coban 2007).

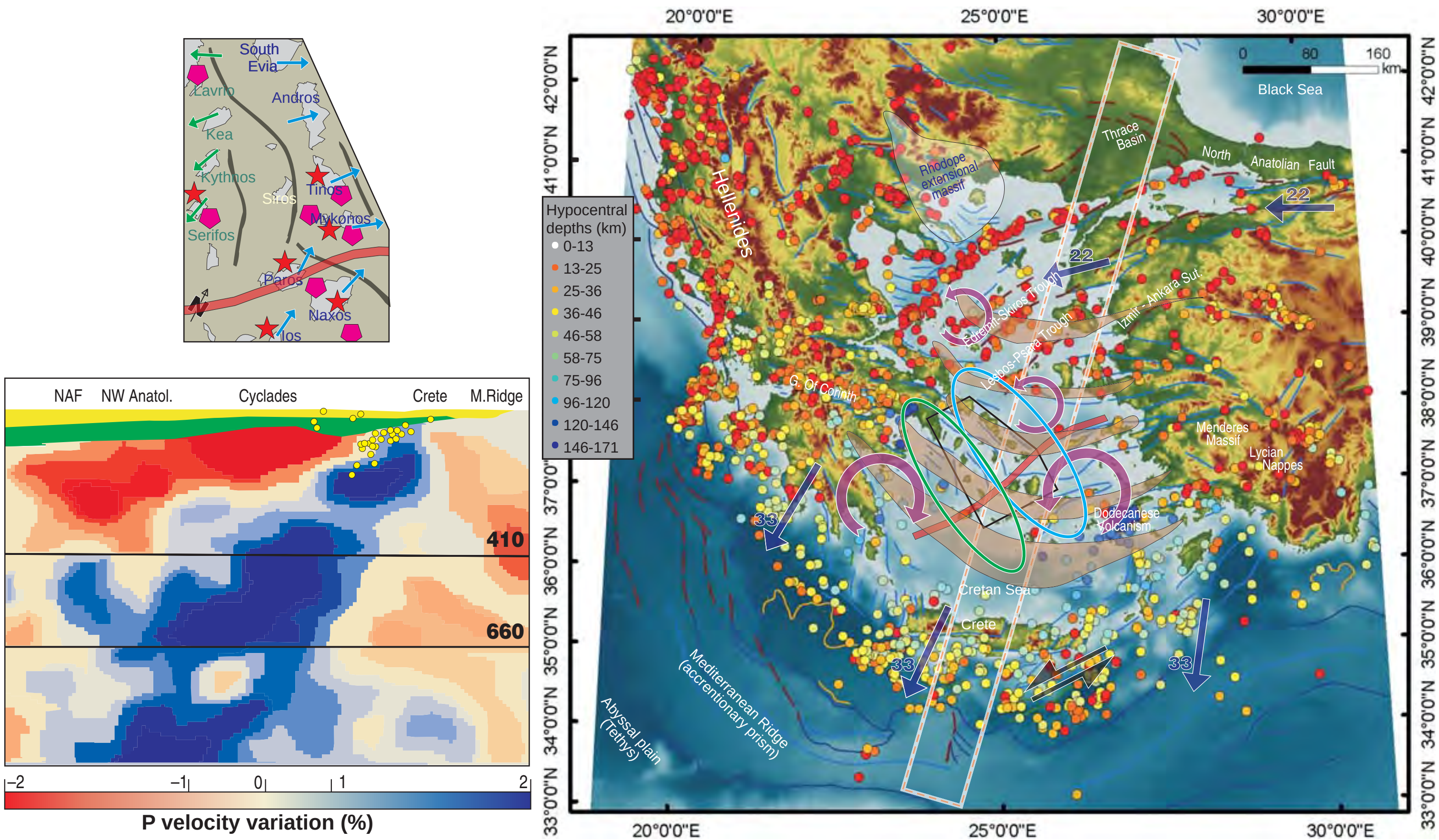

Fig. 4. Overview of Aegean, W. Anatolian and Hellenic Trench region. Straight arrows are geodetically determined surface displacement velocities (see Fig. 1 for sources). Note Anatolia is ‘escaping’ at ‘only’ 22 mm/a while the Hellenic Trench is retreating southward at 33 mm/a. Route of actively westward propagating North Anatolian Fault is well delineated by <25 km depth seismicity. Two large ellipses represent approximate respective regions of SW, and NE-directed late Miocene to Recent vergence of extensional kinematics (see inset). Circular motion arrows represent proposed block rotation directions and amounts (bigger is more, data from van Hinsbergen *et al.* 2005 synthesis). These partly correlate with rotating, breaking ‘slats’ in the model of Taymaz *et al.* (1991) and partly rigid blocks of Goldsworthy *et al.* (2002). Note series of NE–SW trending trough areas

Historical geodynamics

The historical geodynamics are dominated by major thinning and extension of the continental lithosphere that has co-existed with orogenic collisional convergence since at least the Eocene (Brun & Sokoutis 2007; Grasemann & Petrakakis 2007). The main evidence comes from core complex development and associated melting and mid- to lower-crustal metamorphism products. This extension has focussed in the Rhodope, Cyclades and Menderes Massif-Lycian Nappes areas, migrating later to the Crete region where extension thereafter persisted – albeit switching to arc-parallel at *c*. 9 Ma (e.g. van Hinsbergen & Meulenkamp 2006); the velocity arrows on Figure 4 show that the Aegean arc is moving 20% faster than (and thus away from) the Anatolian block (30 mm/a versus 24 mm/a) (Noomen *et al.* 1996; McClusky *et al.* 2000; Wortel & Spakman 2000; Nyst & Thatcher 2004). Extension in the Rhodope Massif was between 26 and 13 Ma (Dinter & Royden 1993; Sokoutis *et al.* 1993; Wawrzenitz & Krohe 1998), possibly as early as 50 Ma in the SW and N margins (Brun & Sokoutis 2007). In the Menderes, extension began around the Oligo-Miocene (Hetzel *et al.* 1995; Collins & Robertson 2003; Gessner *et al.* 2004; Jolivet *et al.* 2004*a*). In the Cyclades, extensive research provides a more comprehensive picture, and we focus on this further (Fig. 4 inset, upper).

Cycladic Islands

Central Cyclades studies have established key geodynamic events in space and time by constraining pressure–temperature–time–deformation (*P–T–t–d*) paths that identify two key Cenozoic components (M1, M2). M1, Cycladic blueschist formation (well-constrained on Tinos, Syros, Naxos and Sifnos) was a, for the most part, discrete, largely early Tertiary, decompression deformation at 40–80 km depth (i.e. 0.8–1.5 GPa) (e.g. Altherr *et al.* 1982; Okrusch & Bröcker 1990; Wijbrans *et al.* 1990; Avigad & Garfunkel 1991; Avigad 1993; Bröcker *et al.* 1993; Patzak *et al.* 1994;

Fig. 4. (*Continued*) that are identifiable from bathymetry contrasts and are also strikingly delineated by lines of dense upper crustal (<25 km depth) seismicity (these are proposed anti-clockwise rotating eastern half of the (broken) slats and also partly correlate to the localized deformation zones of Armijo *et al.* (1996) within their linear elastic fracture mechanics model for present deformation transfer between the North Anatolian Fault and the Gulf of Corinth Rift – see discussion in text). Approximately crescent-shaped brown areas are historical progressive loci of 'geological extension' proposed by Armijo *et al.* (2003). Also shown is proposed 'mid-cycladic lineament' of Walcott & White (1998). Not yet subducted Mesozoic oceanic lithosphere is identifiable from abyssal plain just south of southern subduction zone boundary. NNE-dipping Benioff zone geometry is clear from surface distribution of hypocentres. Inside of this arc is volcanic arc, picked out by mantle seismicity (typically >100 km), most conspicuous in the SE Dodecanese. Cyclades are otherwise aseismic. Box in centre shows area of upper inset map. Red dashed on white line forming box is approximate trace of swath of seismic tomography profile (see inset). Topographic and bathymetric data are Mercator SRTM 30 gridded in degrees, coloured for 1500–2500 m relief emphasis (otherwise as per Fig. 1). Active and young faults summarized from Morelli & Barrier (2004. *Geodynamic map of the Mediterranean.* Commission for the Geological Map of the World, Limoges, France), Athanassios Ganas (pers. comm) and our own data. Modern Greek coastline provided by: Athanassios Ganas (National Observatory, Athens, Greece). Selected earthquakes, data courtesy: http://neic.usgs.gov/neis/epic/ (Earthquake Hazards Program, National Earthquake Information Center of the United States of America Geological Survey), Russian public domain catalogue Moscow (1994), and Endrun *et al.* (2005); Bohnhoff *et al.* (2006), corrected after Engdahl *et al.* (1998).

Upper left inset: Lithotectonic summary map of Cyclades and greater extended lithospheric region of central Aegean. Data compiled from Lister *et al.* (1984); Altherr *et al.* (1988); Henjes-Kunst *et al.* (1988); Wijbrans & McDougall (1988); Buick & Holland (1989); Urai *et al.* (1990); Avigad (1993); Gautier *et al.* (1993); Pe-Piper *et al.* (1997); Avigad *et al.* (1998); Jolivet & Faccenna (2000); Pe-Piper (2000); Altherr & Siebel (2002); Pe-Piper & Piper (2002); Jolivet *et al.* (2004b). Red stars are S-type plutonism; Red pentagons are I-type plutonism; Arrows show principal lineation orientations and sense of shear directions (for low angle displacement/detachment structures) only for those of main tectonic fabrics generated under Greenschist facies conditions dynamic recrystallization ('M2'). Symbols are ommitted for those islands with strong principal lineation fabrics developed at higher P & T conditions, reflecting at least in part a non-sub horizontal, probably non-2D resolvable kinematics associated only with deep burial and exhumation to mid-crustal levels (see text). Black lines are major steep (offshore) faults of the horst and graben systems that are associated with the Cyclades (summarized from Morelli & Barrier (2004)).

Lower left inset: Seismic tomographic profile model (PM 05) from Piromallo & Morelli (2003) redrawn from Faccenna *et al.* (2003; 2004). Position and continuity of forerunner portion of African (Tethyan) lithospheric slab is clearly visible from rapid P-wave velocity (blue) region. Depth scale is given by 410 and 660 km acoustic transition (discontinuities). Slab persists to >1000 km. Note that tomographic mantle model profile compares well with first order features of Wortel and Spakman (2000) above 660 acoustic transition. Yellow (crust) and green (mantle) are freely interpreted from crust/mantle lithosphere thickeness data (mainly Moho depths, some gravity data) from Cavazza *et al.* (2004); Tirel *et al.* (2004); Endrun *et al.* (2005); Bohnhoff *et al.* (2006). Yellow dots: hypocentres for selected earthquakes. Some events omitted for clarity (Benioff–Wadati Zone geometry is well depicted by map view distribution of hypocentral depths in main figure), otherwise seismic data sources as per main figure.

Avigad *et al.* 1997; Bröcker & Franz 1998; Ring & Layer 2003; Bröcker *et al.* 2006; Bröcker & Pidgeon 2007; Tirel *et al.* 2009). The M1 metamorphic fabric is on many islands conspicuously overprinted by M2, a late Oligocene/early Miocene extension, typically at mid-crustal conditions (i.e. greenschist facies, 200–700 MPa but locally of sufficiently high grade to generate migmatite, e.g. Naxos) that is well constrained on the islands of Tinos, Naxos, Ios and Mykonos (e.g. Jansen 1973; Lister *et al.* 1984; Feenstra 1985; Wijbrans & McDougall 1988; Urai *et al.* 1990; Buick 1991*a*; Gautier *et al.* 1993; Gautier & Brun 1994; Jolivet *et al.* 1994; Forster & Lister 1999; Jolivet & Patriat 1999; Keay *et al.* 2001). M2 is typically associated with mid-late Miocene, predominantly I-type granitoid plutonism on several of the islands (pink pentagons on Figure 4 inset, upper left) whose final intrusion stages are syn- to post-kinematic with respect to the pervasive deformation fabric (e.g. Dürr *et al.* 1978; Andriessen *et al.* 1979; Altherr *et al.* 1982; Bröcker *et al.* 1993; Bröcker & Franz 2000). A tight pan-Cycladic discrimination of M1 from M2 is not always forthcoming; temporal overlaps between the two ('M1.5') have been entertained by various of the above authors, depending on the tectonic significance attributed to the relevant various radiogenic isotope system(s) employed.

Cyclades deformation and core complex genesis

On many of the Cycladic islands (Tinos, Mykonos, Naxos, Paros, Ios), the regional deformation fabric is focused into large (often island-wide), low-angle, extensional, mylonitic high strain zones (termed by several authors 'detachments') of several 10s to 100s m thickness that are frequently syn-magmatic and domed. These high strain zones are associated with progressive footwall cooling, retrograde P–T paths, and ductile to brittle changes in deformation, as well as in some cases, juxtaposition of overlying low-grade sedimentary rocks (corresponding to a large metamorphic gap that indicates excision of a major [10s km] crustal section). This key suite of relationships, together with the above noted strong geodynamic expression of present day extension, has led workers to attribute the M2 metamorphic event to late Alpine exhumation via lithospheric-scale high strain zone accommodation of the back arc extension of the retreating Hellenic subduction zone. Recognized thereby are 'metamorphic core complex' (MCC) province settings for these islands, similar to the dozens of examples in the 1000s km long extensional province of the western North American continent (Dürr *et al.* 1978; Coney 1980; Altherr *et al.* 1982; Lister *et al.* 1984; Buick & Holland 1989; Buick 1991*a*, *b*; Pe-Piper *et al.* 2002). Relevant to the accelerated (or at least enhanced) slab retreat setting is that the rapid exhumation required to expose the MCC's seems to have been entirely related to crustal stretching dynamics (no glacial 'sculpting' etc. has prevailed in contrast to the exhumation in the Himalaya, Aleutians, Cascadia, Andes, etc). On Naxos, sedimentologic features suggest a transition from marine deep turibiditic to continental environment during Miocene (Vanderhaeghe *et al.* 2003*b*) and Kuhlemann *et al.* (2004) note clastic debris indicate a depositional environment and provenance of significant persistence. From these, we see that there were no long lasting highland areas in the Cyclades and the exhumation process is effectively due to mantle dynamic processes alone.

Deformation fabric trends

The prevailing deformation (and metamorphic) fabric on the islands where M2 is well developed is typically a homogeneously dynamically recrystallized mylonitic foliation that is ubiquitous for crustal scale shear zones associated with ductilely deformed mid-crustal rocks. Preferred ('stretching') mineral orientations in the studied Cycladic MCC's define a lineation that, on any given island, typically is spatially strongly uniform in orientation and direction for much of the rocks of M2 deformation. This is despite frequently spanning large intervals of deformation temperatures that often persist to temperatures well below (i.e. depths well above) the mid-crustal realm (e.g. $\ll 200\,^{\circ}$C). Using these fabric, Jolivet *et al.* (2004*b*) have proposed a further classification of the Cycladic core complexes into two classes of domes (A and B) based upon the presence or absence of lower crustal rocks and the geometrical relationship of the domal long axis to the principal (usually M2 and usually greenschist facies deformation conditions) stretching lineation, i.e., parallel with or perpendicular to. Although this seems to not be universally true (e.g. Kea and Kythnos, discussed below, would be A-type domes but incorporate no significant lower crust material), something mechanistic to the process of Cycladic MMC genesis in Hellenic back arc extension is certainly lurking in the observation that the domes have a prevailing lineation either quite parallel with or quite perpendicular to the island long axis (and rarely something in-between).

It is important to separate M2 at large from the earlier high pressure – low temperature fabric of M1. M2 fabrics in some cases fully transpose/re-crystallize and retro-metamorphose M1 fabrics, in other cases they deform new material (migmatite, granitiods, vein systems, etc.). A strong sense of shear associated with the prevailing M2 lineation together with a shallow plunge allows allocation of an overall 'tectonic shear direction' for each island. This is highlighted for key islands in Figure 4 (inset, upper). Our recent work (Iglseder *et al.* 2008; Zamolyi 2006; Grasemann & Petrakakis 2007; Rambousek 2007; Petrakakis *et al.* 2008) has obtained equivalent M2 datasets for the western Cyclades that newly identify a realm of S–SW directed crustal extension that (1) was coeval with local anatexis and (2) included more than one episode of crustal failure apparently protracted from Eocene to late Miocene (Grasemann *et al.* 2006) perceptibly much earlier than for the central and western Cyclades. We have constrained this for Serifos island; P/T conditions (from petrology and deformation mechanisms), zircon U–Pb TIMS crystallization ages, Rb–Sr cooling ages and structural surveying reveal that a major granodiorite intrusion syn- to post-dates a top-to-SSW, mid-upper crustal, mylonitic lithospheric-scale extensional low angle shear zone. This entire package further cross-cuts an earlier top-to-SSW, lower-mid crustal, high strain zone that mylonitises an S-type granite whose zircons yield an ion microprobe U–Pb late Eocene crystallization age (probably broadening the interval of known Cycladic granitic plutonism to Eocene – Grasemann *et al.* 2006). A further top-to-SW high-strain low angle fabric discovered on Kea and Kithnos and consistent kinematics from compiled data for Lavrio reveal that the entire western Cyclades are a hitherto unrecognised, roughly 200 × 100 km in area, lithospheric extension region. It appears that this discrete region was persistent in space and time since the Eocene and, critically, has opposing vergence to the NNE-directed Hellenic nappe stacking and detachment kinematics of the E-Cyclades region (arrows in Fig. 4 inset, upper right). These two realms of apparently fundamentally opposing kinematics would seem to render illusive (or at least over interpretatory) the proposal of Walcott & White (1998) for a mid-Cycladic lineament that runs right through the north of Paros (thick orange line in Fig. 4 inset, upper right) to explain two groups of 'lineation' orientations between the northern and southern Central Cyclades. We suggest that there is some confusion of true M2 fabric with incompletely transposed M1 fabric. Even if this is not so, and all prevailing lineations that are typically reported (or reproduced) are true M2 deformation conditions stretching lineations, the differences in vergence direction (NNE versus ENE) between the northern and southern Central Cyclades are now seen to be minor in comparison to our new western Cyclades results. Palaeomagnetic data supporting island rotations (Kissel & Laj 1988; e.g. Morris & Anderson 1996; Morris 2000; van Hinsbergen *et al.* 2005*a*) is most simply interpreted as a Lagrangian reference frame local view ('rigid block behaviour') of a non-rigid block continuum in the Eulerian reference frame. The Eulerian viewer sees the strain patterns for the Hellenic back arc extension (and the expanding arc, and south- and southwestward retreating trench) whereby stretching regions must gradually rotate to accommodate the increasingly arcuate form of the Hellenic Trench. Of use in constraining this back arc extension evolution are those islands where the M2 fabric incorporates elements formed at significantly lower temperatures (i.e. formed below the Curie temperature of the mineral at hand). Such excludes the possibility of transposition of an early-in-M2 fabric and provides a critical constraint on rotations; either the far field strain pattern (in the Eulerian reference frame) has rotated throughout the M2 genesis or the rotation identified through palaeomagnetic data predates the M2 lineation. It is in the last instance worth keeping in mind that the M1, M2 characteristics recorded on the Cycladic islands may not be a fair representation of the tectonic history. The majority of the islands are updomed areas of enhanced stretching and thinning, akin to the co-location of metamorphic domes and focused tectonics with high topography in more lofty orogenic belts like the Nyainqentanghla, Nanga Parbat, the Shuswaps, (e.g. Pan & Kidd 1992; Schneider *et al.* 1999; Vanderhaeghe *et al.* 2003*a*; Brown 2007); in the absence of water and sedimentary cover, both the palaeomagnetic (rigid block) picture as well as the overall tectonic picture might look very different.

Present day deformation

Figure 4 also shows some of the key geodynamic elements proposed by various workers to explain the more recent history. Early geodynamic models seeking to explain the Cenozoic collisional/extensional history of the greater Aegean region use a thin viscous sheet lithosphere type approach that later integrate rigid internal small blocks involving diffuse, bookshelf or 'broken slat' intra-block plate deformation (e.g. McKenzie 1972; McKenzie 1978; Le Pichon & Angelier 1979; Taymaz *et al.* 1991; Jackson *et al.* 1992; Le Pichon *et al.* 1995). Modern geodetic (SLR & GPS) and improved elastic deformation tensor constraints from dense seismicity measurement data continue to refine such (semi)-continuum type models (e.g. the Skiros 2001 event refining the Taymaz *et al.* 1991 broken slat model). Competing alternatives further include: completely rigid lithosphere/microplate to fit block models (Noomen *et al.* 1996; McClusky *et al.* 2000), thin elastic shell type (e.g. Meijer & Wortel 1997), distributed crack tip strain linear elastic fracture (e.g. Armijo

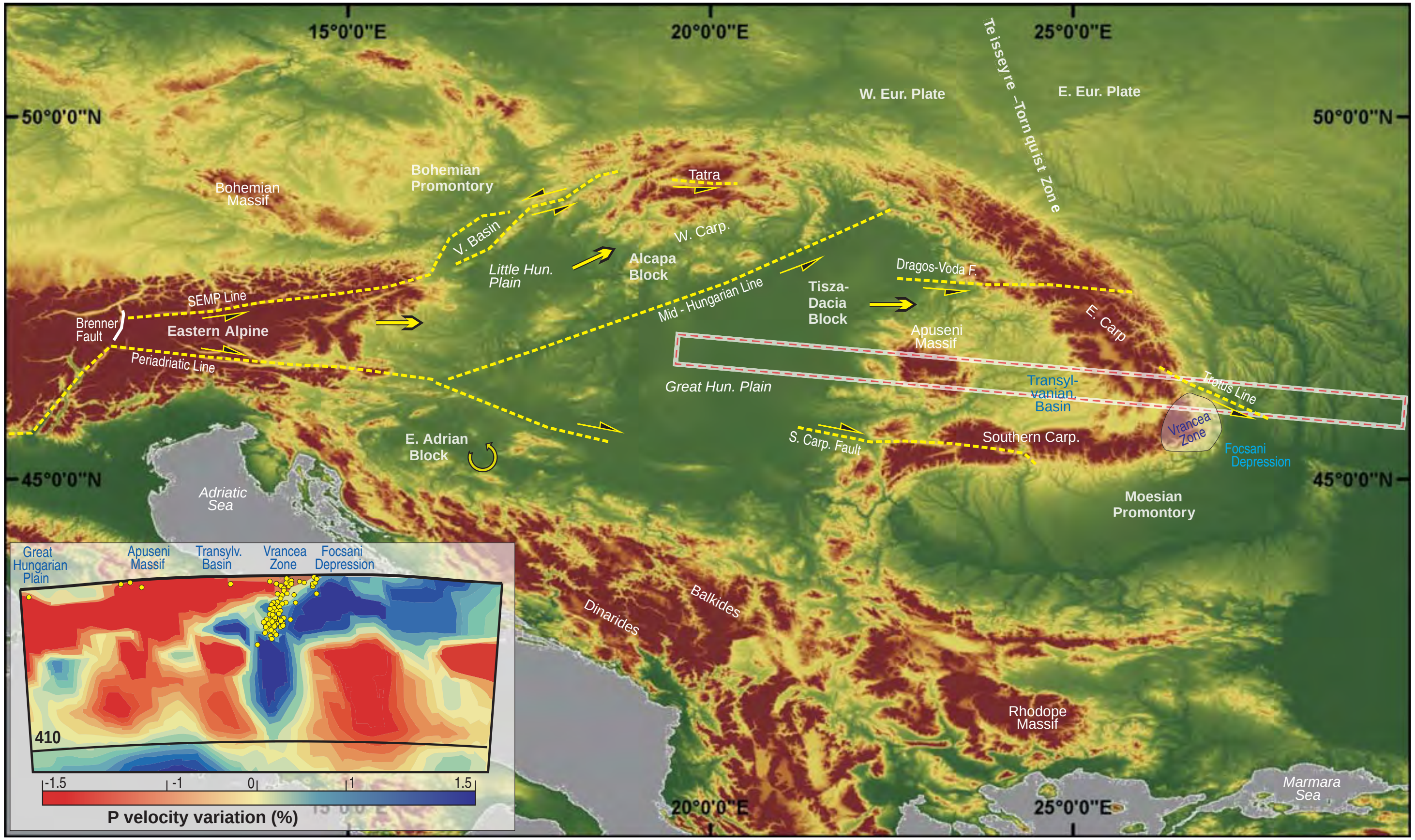

Fig. 5. Mercator SRTM 30 (see Fig. 1) gridded in degrees, coloured for 1500–2500 m relief emphasis. Shown is Pannonian Basin/Carpathian Orogen system. Key event final portion of subducting oceanic lithosphere was trapped in embayment flanked by major promontories (Bohemian and Moesian) causing accelerated retreat with relocation and thinning of major blocks (Tisza, Alcapa). Extreme flatness of Great and Little Hugarian Plains is testimony to extreme local back-arc basin stretch (β ≤ 30 and lithospheric thickness of ≥60 km). Progressive SE- and eastward (with respect to present day orientation) younging and narrowing of volcanism and deformation front is schematically shown. Last 'gasp' of subduction is captured by Vrancea snapshot where seismicity (to 200 km depth) and seismic tomography (lucid near vertical slab tongue geometry of high P-wave velocity region to 410 km depth), and see text. Bold letters, major plate-tectonic units. Italics, geographic distinction; blue - Vrancea area slab dynamics features (see text). Narrow font,

et al. 2003), or, separate from these, divergent free southward flow of the Aegean (Gautier *et al.* 1999). Most of the rigid block models however omit the elegance of linear elastic fracture mechanics approaches in incorporating tips of deforming zones where displacement dies out. The rigid block proponents instead require non- model-able 'hit and miss' zones of distributed deformation between the blocks (best fit scenarios). This approach does provide solutions for the present day instantaneous geodynamics but these models cannot usefully be played back elegantly through time (i.e. they cannot make predictions regarding specific spatio-temporal historical deformation). For example, the youngest historical interval between the present day and the post-M2 (mid-Miocene) is a critical period of change in the governing kinematics of the greater Hellenic subduction zone system. In this period, the North Anatolian Fault, initiating from deep within eastern Turkey, propagates to the site of the Marmara Sea by *c.* 5 Ma thereby beginning the imposition of escaping Anatolia upon the extensional regime of the greater Aegean (Okay *et al.* 1994; Armijo *et al.* 1996; Armijo *et al.* 1999). The northernmost branch of the north Anatolian fault becomes thereafter the (micro) plate boundary of the Hellenic system with fixed Eurasia (Armijo *et al.* 2003; van Hinsbergen *et al.* 2006). Although the detailed datasets on individual slip rates and ages for the myriad of Aegean faults are still relatively few, it appears that the increasing westward impingement of the North Anatolian Fault caused stepwise (re)activation of deformation localization (or significantly increased displacement) at the successive trough regions of the North Aegean Trough, the Skiros Trough, the Lesbos–Psaras Trough, and later the North Evvia Basin and the Evvia Graben and then finally the Gulf of Corinth Rift at *c.* 1 Ma (see Armijo *et al.* 1996 for a review). It therefore becomes clear that, despite the appealing instantaneous rotating block type geometries suggested by the bathymetry, seismicity and geodetic displacement, the snapshot of the evolution of the Hellenic back-arc requires the longer view.

A snapshot of accelerated retreat

In summary, we can see that the Hellenic subduction zone system has, for most of the Cenozoic, been associated with a dynamic backarc system related to the persistent convergence of the subducting African lithosphere that has experienced significant (if not continuous) rollback since the Oligocene. The pulses of back (or within) arc extension related to the enhanced periods of exhumation in the Rhodopes, followed by the Cyclades–Menderes, then Crete and finally the present day Peleponese with Corinth in the West and the Dodecanese in the East testify to periods of enhanced rates of rollback (albeit not as convincing as our other snapshots of clear acceleration with time). Good evidence for tearing (and thereby narrowing) of the slab that is likely associated with enhanced rates of rollback (particularly in the Miocene) is seen in the Dodecanese (the seismic moment and depths of seismicity, the volcanic chemistry, and the tomographic contrast) as well as (to a lesser degree) Peleponese and Corinth, although the signature here is very much defocused by the recent propagation of the North Anatolian Fault. The present day migration velocity of the Hellenic Trench towards the SSW at 3.3 cm/a is, albeit rapid, much less than is likely to have prevailed for the major extensional phases in the past. This fits well with the observations from (for example) modern cross section across the Hellenic Trench (Papanikolaou *in* Jolivet & Brun 2008); the arrival of the Mediterranean Ridge at the Hellenic Trench is the beginning of the end of the available oceanic crust – our snapshot.

Pannonian–Carpathian system

The Carpathians

The Carpathian Mountains (Fig. 5) comprise (1) an outer portion of largely later Cretaceous and Cenozoic age nappes assembled from predominantly thin-skinned fold and thrust belt type deformation of flysch and molasse which arose through accretionary orogenesis, and (2) an inner portion, which

Fig. 5. (*Continued*) names of geodynamic discontinuities (faults, lines, etc); no font emphasis – orogen (range) portions. Red dashed on white line forming box is trace of swath of tomographic profile (see inset). Trace of tomographic profile swath is approximate; continues approximately 200 km to east beyond limit of map. Patch labelled 'Vrancea zone', surface location of hypocentres displayed on tomographic profile on inset; yellow dashed lines, geodynamic discontinuities; arrows, general block motion direction or relative fault displacement (half arrows).

Inset: Tomographic profile re-drawn after Wortel & Spakman 2000. Yellow (crust) and green (mantle) lithosphere thickness are freely interpreted via Moho depth, basin fills, etc. from Royden *et al.* (1983*b*); Lillie *et al.* (1994); Bertotti *et al.* (2003); Cloetingh *et al.* (2004, 2005*a*). Depth scale is given by 410 km acoustic transition. Yellow dots: hypocentres from selected earthquakes, data courtesy: http://neic.usgs.gov/neis/epic/ (Earthquake Hazards Program, National Earthquake Information Center of the United States of America Geological Survey) and Russian public domain catalogue (Moscow 1994), corrected after Engdahl *et al.* (1998).

consists of crystalline basement nappes plus Mesozoic sedimentary cover and whose deformation is predominantly Alpine of Cretaceous age; the composite architecture of both portions (3) interrupted by widespread volcanics of andesitic and other chemistry (e.g. Jirícek 1979; Royden *et al.* 1983*a*; Zweigel *et al.* 1997; Pecskay *et al.* 2006; Kovacs & Szabo 2008), as well as local Cenozoic reworked crystalline massifs that are also present (e.g. Pana & Erdmer 1994; Dallmeyer *et al.* 1996; Faryad & Henjes-Kunst 1997; Schmid *et al.* 2004; Fügenschuh & Schmid 2005). The Carpathians are noteworthy for being a long (>1000 km) yet coherent throughgoing orogenic belt that all the while exhibits a >190 degree strike rotation (termed a 'double loop' by some authors), the foreland of which forms an embayment of >300 km amplitude (labelled Bohemian Promontory, Eur. Plate and Moesian Promontory in Fig. 5). Nested behind the Carpathians is the Pannonian Basin, effectively Europe's largest modern sedimentary basin that is not part of the Atlantic break-up rifted continental margin network (e.g. Stegena *et al.* 1975). The Carpathian fold and thrust kinematics (Jirícek 1979; Decker & Peresson 1996; Linzer 1996; Linzer *et al.* 1998; Nemcok 1998*a*, *c*; Sperner *et al.* 2002) record propagation towards the convex-out direction of the Carpathian loop (i.e. in the North, towards the North; in the NE, towards the NE, etc.) with accretionary thrust wedge growth terminating (in a steady progression to the east and SE) as the thrust wedge was ultimately emplaced (overthrust) in stepwise fashion onto the foreland (the continental passive margin of European platform) in the Mio-Pliocene. This gives a critical insight into the overall north-, then southeastward migration of, along with reduction in the length of, the subduction accretion wedge thrust front. The 190° bend and 300 km embayment additionally gives a nice indication of the nature of the pre-existing European margin geometry and the potential that existed to isolate a landlocked piece of oceanic lithosphere. This pre-existing geometry has been dictated since the end of the Cretaceous by the Moesian and Bohemian promontories (Fig. 5) and has changed little, as indicated by absence of significant Cenozoic deformation within these portions of the European margin both in the surface (e.g. Hamilton *et al.* 1990; Linzer *et al.* 1998; Haas *et al.* 2000) and the subsurface – as reflected (!), e.g. in the CELEBRATION results (e.g. Grad *et al.* 2006).

Volcanism

It is generally held that the Carpathian accretionary fold and thrust belt and volcanic interludes were built from east and southeast retreating oceanic lithosphere subduction that dominated since the Oligo–Miocene (e.g. Royden 1983*a*, *b* and several of the other above noted authors) although there are variants and other ideas (see below). Oddities such as the absence of ophiolitic assemblages have prompted some debate on indeed whether or not during the Cenozoic, the majority of the forearc (i.e. incoming crust that in present day co-ordinates would be north and east of the Carpathians) to the growing Carpathian Arc was indeed ever a truly oceanic (or maybe 'sub-oceanic') crust composed embayment (Gîrbacea & Frisch 1998; Linzer *et al.* 1998; Sperner *et al.* 2004; Tischler *et al.* 2007). As these and numerous other studies discuss, however, there is much evidence that the Carpathian–Pannonian system does indeed represent an accretionary wedge born of a rapidly retreating (foundering) slab of old oceanic lithosphere flysch basin that was an embayment in the Alpine (*sensu lato*) collision. Observed (Fig. 5) is the trend of andesitic (i.e. arc-associated) volcanism whose ages range from the Miocene up to the present day and whose individual instances were local occurrences of short-lived duration. These represent a progressive (south)eastward migration that thereby constrains the historical retreat and/or progressive lateral tearing away of the slab (e.g. Jirícek 1979; Royden *et al.* 1983*a*; Csontos 1995; Zweigel *et al.* 1997; Linzer *et al.* 1998; Pecskay *et al.* 2006; Kovacs & Szabo 2008). Although the tracking of the (south)eastward advance of arc-associated volcanism is impressive, the spatial as well as temporal precision of the volcanism timetable that emerges from the present state of knowledge is insufficient (especially along the southern Carpathians) to exclude variants on our preferred theme of the accelerated retreat of an ever-narrowing slab width. Some version of the step faulting notion (Govers & Wortel 2005) or an obliquely propagating slab tear-off could (also) have operated for either the eastern or, even more so, for the southern Carpathians. In addition, for the calc- alkaline transition described by the various studies noted above, the geochemical characteristics to discriminate volcanism related to standard subducting oceanic lithosphere-engendered melting of aesthenosphere above the slab versus melting of aesthenospheric material related to a tear or partial break-off are, for the so far obtained Carpathians volcanic rocks database, insufficiently discrete. This is in many instances thought to be due to complex contamination of continental crust that has already experienced portions of multiple volcanism episodes due to late Cretaceous or other rifting (e.g. above studies and see also Kozur 1991; Channell & Kozur 1997) followed by overlap with one or both of the above melting phenomena. Further complicating the issue, albeit mainly in more central portions of the Pannonian Basin network, is the aesthenospheric melting and upwelling (whether related to a plume, deep diapirism, or other – see below) that is associated with lithospheric stretch plus accompanying thermal subsidence and corresponding basin growth.

Pannonian basin sedimentation and subsidence history

The Pannonian basin network (including the Vienna Basin, the Little & Great Hungarian Planes and the Transylvanian Basin – see Fig. 5) attests to severely stretched ($\pm$ wrench offset) and thinned continental lithosphere with β factors of typically around 3 but locally as high as 30 (below the key depocentres of the Little and Great Hungarian Planes); this is most vividly expressed by the contrasts between the ancient European Margin (Bohemian and Moesian platforms) and within the Pannonian basin network that are seen in (1) values of lithosphere thickness (150–200 km versus 60–80 km) and (2) Moho depths ($\leq$45 km beneath Polish Trough or $\leq$40 km beneath Carpathians versus $\geq$27 km beneath the Pannonian basin), as well as (3) heat flow (55 mW/m^2 versus 90 mW/m^2), and (4) the basin network 'syn- to post-rift' sedimentation history revealed by the various gravity, seismology (reflection profiling, velocity & receiver function forward modelling), and subsidence & back-stripping studies (e.g. Sclater *et al.* 1980; Royden *et al.* 1983b; Tari *et al.* 1992; Lillie *et al.* 1994; Meulenkamp *et al.* 1996; Hauser *et al.* 2001; Huismans *et al.* 2001; Sachsenhofer 2001; Sperner *et al.* 2004; Cloetingh *et al.* 2005*a*; Bielik *et al.* 2006; Grad *et al.* 2006; Sroda *et al.* 2006; Szafian & Horvath 2006; Cloetingh *et al.* 2007; Matenco *et al.* 2007). In keeping then with the widely held hypotheses that the Carpathian–Pannonian system owes is existence to an east and SE retreating oceanic lithosphere subduction setting, the Pannonian basin network is correspondingly seen to be the backarc basin area to the eastward retreating (or retreated, van der Hoeven *et al.* 2005) slab. It is noteworthy that although parts of the Pannonian basin networks have sediment thicknesses of up to 6–8 km (e.g. Transylvanian Basin), the deepest basin is outwith the Pannonian; the Focsani Depression is a >10-km-thick foredeep basin formed in Tertiary to Quaternary times in the SE foreland and frontal thrust piggy-back basins to the Carpathians. Focsani subsidence is still active (Bertotti *et al.* 2003; van der Hoeven *et al.* 2005) and has been intimately associated with the Vrancea seismogenesis zone (be this a vertical slab tongue or lithospheric downwelling and/or delamination – see Fig. 5 and below).

A number of studies contribute to the present knowledge on the Pannonian basin network sedimentation history (e.g. Royden *et al.* 1983*b*; Tari *et al.* 1992; Meulenkamp *et al.* 1996; Csontos & Nagymarosy 1998; Cloetingh & Lankreijer 2001; Huismans *et al.* 2001; Szafian & Horvath 2006). As these authors show, the sedimentation history is typically identifiable as a 2-stage affair: the initial Early-Middle Miocene syn-rifting phase is associated with a brief, rifting-active subsidence period that can be broadly correlated with the beginnings of acceleration of foredeep depocentre migration in the latest early Miocene. Basin geometries that develop at this stage are very much non-2D. This is, at least in part, the result of heterogeneously distributed extension that was accommodated by transfer faults. Evolution of a network of transfer and accommodation faults as well as the creation of associated basins with their characteristic triangular (*sensu lato*) geometries is seen to be a condition of the stretching, rotation, and re-ordering of the composite microplate amalgamation in the Carpathian backarc. This is indicated in Figure 5 in the present position of the Alcapa (or North Pannonian), and the Tisza- (or Tisia-) Dacia blocks (or microplates). These converged and were differentially displaced about the Mid-Hungarian Line as part of the backarc basin evolution to the south-, and eastward migrating Carpathian Arc. This can be regarded as the 'passive extension' phase in terms of basin evolution mantle dynamics. The subsequent late Miocene to Pliocene post-rifting phase is associated with a protracted subsidence history whose progress is complicated by perturbation of the thermal boundary layer, 'active' aesthenospheric mantle thinning and convective (or buoyancy-induced flow, or diapiric, or other) upwelling along with widespread Pannonian region volcanism including that related to shallow mantle decompression ('fertile'), as well as late regional doming, and flank uplift (possibly due to aesthenospheric mantle flow to the margins of the thinned lithosphere).

Plumes and aesthenospheric upwelling

Because (1) the upwelling magnitude is greater than that expected by, and (2) the volcanic rocks have a geochemistry that in many cases is inconsistent with, the straightforward rollback pursuant to a subducting slab model, we require a more complex geodynamic explanation or, at minimum, some modification to the foundering, subducting slab model. In addition to the andesitic Carpathian arc-related volcanics noted above, felsic to intermediate calc-alkaline volcanics are distributed throughout much of the Pannonian. Respectively, these are generally inferred to be associated with the initial- to advanced-stages of backarc extension (and associated initial decompression melting of fertile mantle that has welled up via some mechanism). Furthermore, various alkali basaltic magmatism products are present that contain, amongst others, ultramafic (e.g. spinel peridotite) mantle xenoliths. The latter have LREE-depleted bulk-rock compositions and have been one source for mantle plumes theories (via, e.g. noble gas and Pb–Sr–Nd isotopes as well as the rare earth element compositions (e.g. Rosenbaum *et al.* 1997; Buikin *et al.* 2005)) although continental lower crust contaminated by tectonically emplaced oceanic crust can also explain the LREE trends to some degree (e.g. Dobosi *et al.* 2003). The debate and distinctions between mantle upwelling, mantle diapirism, and a shallow or even deep (?core-mantle boundary) mantle-sourced plume lie well outside the scope of this paper – but see Lustrino & Wilson (2007) concerning this issue expressly for the Mediterranean back-arc snapshot settings. It seems, however that mantle plume type hypotheses are not required; Kovacs & Szabo (2008), for example, note that although the spatio-temporal distribution of (amongst others) granulite and clinopyroxenite xenolith-bearing mid-Miocene intermediate calc-alkaline volcanics that straddle the Mid-Hungarian Line cannot be (solely) related to a modified (e.g. metasomatized) mantle via the southward directed subduction (e.g. Kovacs & Szabo 2008), they can be convincingly explained via crustal composition that is modified by the incorporation of either the Budva-Pindos or Vardar (also Meliata) Ocean during the Mesozoic–Paleogene plus (any) related minor subduction volcanism during the evolution of the Alcapa block. They further note that this is consistent with the emerging geophysical evidence (e.g. Grad *et al.* 2006) and provides an alternative to plume models.

Tectonic block and microcontinent motions

The translation and re-ordering of the Alcapa and Tisza–Dacia blocks as well their neighbours, the Eastern Alps and the East Adrian block (Fig. 5) are an integral part of the initial history and the progressive migration of the Carpathian Accretionary Belt, as well as the attendant growth of the Pannonian Basin, and thereby retreat of the slab. The Mid-Hungarian Line is the subsurface tectonic contact where the Alcapa and Tisza–Dacia blocks are joined via a wrenching plus thrusting (largely southwards) history whose age should be late Eocene to no later than Oligocene (see Csontos 1995; but also Csontos & Nagymarosy 1998). Rotations were large as these two blocks moved around the European platform promontories (i.e. Moesian, Bohemian) into their present position. The Alcapa block rotated 5 to 15° anticlockwise during the Miocene while the Tisza–Dacia block, initially having rotated as much as 120° rotated anticlockwise in the Oligocene, rotated 40–60° clockwise during the Miocene – in part responding to the northwestwards, then northwards convergence of the (still) rotating Adria block (Kovac *et al.* 1993; Csontos 1995; Linzer 1996; Fodor *et al.* 1998; Plasienka & Kovac 1999; Márton *et al.* 2000; Márton *et al.* 2003; Márton & Fodor 2003; Sperner *et al.* 2004; van der Hoeven *et al.* 2005; Kovac *et al.* 2007; Lesic *et al.* 2007; Márton *et al.* 2007). These and other (Dupont-Nivet *et al.* 2005; Tischler *et al.* 2007) studies show that the Carpathians themselves also rotated and bent, starting at least in the Miocene, seen (e.g.) as *c.* 30° clockwise rotation between 5–13 Ma in the southern Carpathian. The last 5 m/a have been the exclusive focus of rotation (and also volcanism, as well as present day seismicity - see below) located at the 'bend' of the Carpathian arc between the Vrancea Zone (Fig. 5) and the Transylvania Basin, south of the Trotus Line (Linzer *et al.* 1998; Dupont-Nivet *et al.* 2005)

Another key player in the tectonic block re-ordering phenomenon is the westernmost block to the system, the Eastern Alps (Fig. 5). This block is bounded by the Brenner normal fault, the Periadriatic and the SEMP Lines and represents the hypothesized Miocene (possibly up to present day) 'escape' off to the east of the collapsing, gravitationally unstable, over-thickened Austrian Alps (riding above flowing crystalline basement) as a result of the free margin (within the main alpine collisional system) offered by the Carpathian retreat and/or as a result of the northward indenter push of Adria (Ratschbacher *et al.* 1990, 1991; Fodor *et al.* 1998; Nemcok 1998*a*; Grenerczy *et al.* 2000; Haas *et al.* 2000; Linzer *et al.* 2002; Sperner *et al.* 2002). Note that the role of the mechanism of indenter Adria's push in to East Alps is sometimes cast as a 'chicken-and-egg' question – as is also sometimes done for Anatolia (i.e. 'forced' escape of Anatolia due to indenter push of Arabia versus 'attracted' Anatolia escape towards the free margin created by the Hellenic slab rollback and thus the collapse of the Anatolian plateau).

Basin inversion

The translation and re-ordering of the microblocks also must play some role in the phenomenon of basin inversion. All of the basins in the Pannonian basin network (to a greater or lesser degree) are modified by a locally Miocene but largely Plio-Pleistocene (and even Holocene) 'inversion' with shortening in various forms (amongst others: (1) local reverse reactivation of earlier normal faults that originally grew during mainly the Miocene syn- and post-rift phases; (2) basin-wide buckling;

(3) Holocene landform flank uplift; and even (4) local reactivation of original Alcalpa against Tisza–Dacia thrust (or oblique wrench) displacement systems along the Mid-Hungarian Line) that is evident on exposed basin margins and seismic reflection profiles, and is further revealed by a present day compressive stress regime that is observed in borehole and other *in-situ* stress data (Peresson & Decker 1997; Csontos & Nagymarosy 1998; Nemcok 1998*a*; Bada *et al.* 1999; Fodor *et al.* 2005; Plasienka & Kovac 1999; Bertotti *et al.* 2003; Cloetingh *et al.* 2005*a*, *b*; Bada *et al.* 2007; Matenco *et al.* 2007). These studies generally interpret the inversion to be due to the compressive stress regime engendered by the final cessation of back-arc extension to the Carpathians that is concomitant with the corresponding halt of the eastward retreat of the Carpathian subduction zone while the Pannonian region is simultaneously exposed to the continued anti-clockwise rotation and north-NE-directed indentation of the Adriatic microplate (push of Adria) against the (Eastern) Alps and the dextral 'transpressional' inner Dinaride zone (Fig. 5). Modern differential GPS surface displacement studies both at the east Carpathians and around the Dinarides are consistent with this notion (e.g. van der Hoeven *et al.* 2005; Vrabec & Fodor 2006). The dominant style of deformation gradually changes from pure contraction, through some type of transpression to strike-slip faulting from west to east. The magnitude of the contribution to the compressive stress regime related to the basin-wide inversion that can be imparted by the continued eastward escape of the collapsing Eastern Alpine over-thickened lithosphere is probably not large. Nevertheless, the stress trajectories from the Eastern Alps out to the east in the Pannonian Basin must play some significant role and at least locally modify those of the push of Adria. The stress conditions that provide this basin-wide inversion have also been attributed, by some, to be associated with folding of the lithosphere (e.g. Cloetingh *et al.* 2005*a*, *b*) albeit it is unclear how the lithosphere can support the elastic stresses necessary for folding.

Geophysical constraints

The preferred model of a now almost totally retreated, very narrow slab is very well supported by the geophysics. Figure 5, inset, shows a reproduction of a seismic tomography model profile from Wortel & Spakman (2000) that vividly images a high velocity anomaly directly below the Vrancea zone which is readily interpreted as the downgoing slab (with a vertical tongue geometry). Notable is the fairly convincing continuity in the anomaly architecture (cold lithosphere) from the surface down to >400 km depth suggesting that the slab is intact throughout this depth interval. Moreover, the distribution of earthquake hypocentres (almost vertical, down to 200 km depth) within the Vrancea zone provides critical detail to the notion of the continuity in the high velocity architecture; an equivalent continuity is shown by mechanical coupling all the way up to the (near-) surface; most focal mechanisms for intermediate and deep events have downward oriented extension axes (Oncescu 1987). Contrastingly, seismic tomography profiles that cross the Carpathians <150 km further north (where there is no active seismicity) show a clear depth interval gap in the high velocity structure that is present within the uppermost 100 km of the Earth (Spakman & Wortel 2003; Cloetingh *et al.* 2004) suggesting that the slab in these areas is now broken- or torn-off. Of further importance to the subduction retreat hypothesis is that the constrainable distances/depths of subducted slab that can be inferred from the tomographic model velocity anomaly architecture require 100s km (West–East) of oceanic lithosphere to have been trapped in the original embayment loop, at least by the end of the Cretaceous.

Retreating subduction models caveats and alternatives

Despite the powerful support to the accelerated retreating slab hypothesis that is provided by the sub-surface geophysical data, there are a few caveats arising from the Vrancea slab (or Vrancea 'feature'). Sperner *et al.* (2004) note the lack of co-location between the (present day) Vrancea slab seismicity (plus high velocity tomography anomaly) and the Tisia–Dacia Miocene 'suture' (and arguable volcanic arc). They propose various models to explain this, one of which includes a persistence since the Miocene of the present day position of subduction below the Focsani foredeep. They note that because this cannot explain the location ($\leq$100 km to the West) of the accretionary wedge (lacking as it does the otherwise necessary system of backthrusts), the only reasonable model involves post-Miocene lower lithospheric (presumably mantle) delamination, an idea also raised by Knapp *et al.* (2005). Delamination and downwelling are also the processes in the Houseman group's (Gemmer & Houseman 2007; Houseman & Gemmer 2007) lithospheric instability model(s) to explain the Vrancea observations. This model simultaneously can elegantly account for the above discussed phenomena of inversion, mid-basin aesthenosphere upwelling with melting and suspect plume-type chemistry. We note, however, this model does not exclude that the Carpathian–Pannonian system owes its existence to accelerated retreat of an east and SE retreating oceanic lithosphere subduction setting.

Accelerated retreat snapshot

With the exception of the Houseman group drip-off model, the aggregate picture that emerges for the Pannonian–Carpathian system spectacularly illustrates a caught-in-the-last-moments snapshot of retreated subduction, the likelihood of which is diminished neither by the Sperner *et al.* (2004) delamination nor by the various geochemical complexities of the volcanics and back-arc aesthenospheric upwelling. Moreover, the key historical evidence for a retreat that has accelerated over time as the length of the subduction zone has lessened, while the slab has narrowed and steepened, is nicely recorded by the above discussed spatio-temporal distribution of the (southeastward migrating) andesitic volcanics as well as the accelerated eastward migration of the sedimentation depocentres of the Pannonian Basin network. Similar to the other two snapshots, we see here an along-strike lateral propagation of the termination of active collision that is almost certainly associated with a gradual horizontal tearing off of the slab as the last portions of the foundering, heavy, Mesozoic age oceanic lithosphere are progressively consumed; the final narrow vertical tongue of subducting lithosphere at Vrancea is caught as a snapshot of the accelerated subduction retreat within ICLO subduction.

Other mechanisms

Doglioni & colleagues (e.g. Doglioni 1994; Doglioni *et al.* 1991, 1999) emphasise that 'eastward (and NE) mantle flow can account for the main tectonic directions of compression or extension for many of the (nascent) Mediterranean convergence systems, whereby the main tectonic regime is considered to be more east–west rather than north–south. These authors have gone on to compile an impressive dataset to make a global case for an eastward mantle flow (and adopt a simple fluid-model for the entire planet). As these authors note, 'the numerous extensional basins with very high heat flow, and sometimes oceanization, are difficult to explain in the classical scheme of north–south compression.' If such a phenomenon as globally active eastward mantle flow does exist, it is conceivable that this would influence the ultimate geometry of ICLO subduction for a setting like the Mediterranean, and we find the idea intriguing.

Mantovani and colleagues (Mantovani *et al.* 2000, 2001, 2002) tend to disregard slab pull and mantle dynamics at large, appealing instead to plate–kinematically induced forces to explain all Mediterranean regional tectonics. We prefer our model.

Discussion

Three stages of continent-continent collision

As we noted, our Mediterranean snapshots thesis philosophically adopts the idea that three basic levels of this collision exist, when the entire collisional system of Eurasia with Africa/Arabia/India is considered in the broad scale. Each of these corresponds to an increased stage of maturity or advanced intensity of continental collisional convergence: (1) the greater Indo–Asian collision: (2) the system of Arabia colliding into Iran and surrounding regions; and (3) the Africa–Europe collisional system. We do not urge that the Arabia– and Africa–Eurasia collisional portions must proceed to Himalaya levels but suggest this is highly probable.

In stage one, the Indo–Asian collision includes the Himalaya, Tibet (a stack of pre-Indian plate collided terranes) & surrounding belts (Hindu Kush & Pamir, Tien Shan), and SE China plus greater Indochina. Here, it has long been known (e.g. Argand 1924; Tapponnier *et al.* 1981; Allegre *et al.* 1984; Tapponnier *et al.* 1986; Coward *et al.* 1988; Dewey *et al.* 1988; Kidd *et al.* 1988; Yin & Harrison 2000) that full collision is underway and the orogen enjoys an advanced state of convergence between two major continental plates. Plate kinematic evolution restorations (as Wortel & Spakman 2000 note, often called tectonic reconstructions) have shown us, for some decades now, the Cenozoic progress of $\gg$1000 km of the Indian plate ploughing into the southern Asian margin (e.g. Patriat & Achache 1984), wracking up a high plateau, pushing up ranges on the far sides of rigid blocks like the Tien Shan and Altai and driving off crustal blocks on the eastern free margin in its path and wake. Although this region benefits from the insight into collisional geodynamics afforded by active and recent orogenesis as we noted above, there remain key uncertainties that may profit from comparison with the Mediterranean. The interpretation of mapped ophiolitic material, blueschists, interarc- or forearc-like flysch or molasse deposits, and other potential indicators of 'sutures' between, or local instances of rifting and oceanic crustal production within, the collage of accreted terranes is not always unambiguous. The otherwise strikingly west to east cylindrical and 2D-redenderable coherency (often $>$2000 km) in the terrane collage tectono-stratigraphy has discouraged (in most cases thankfully) less elegant plate kinematics interpretations that require a myriad of piecemeal sutures, small basins, and brief openings and closings, local meltings, late flare-ups and so on. But despite this cylindrical style, it may well be that the geometry of the pre-collisional margin(s) was (highly) irregular and consisted of 100s km amplitude embayments and promontories that have now been all but transposed into the governing fabric of the orogen. And indeed, there may be instances, especially within the pre-India collided blocks of Tibet (i.e. Lhasa, Qiangtang), where a 'Mediterranean solution' (local instances of rifting and oceanic crustal production) are preferable to models invoking many 100s km long cylindrical, 2D-redenderable collision phases. For example, the California Franciscan-influenced model for the Qiangtang terrane blueschists (Kapp *et al.* 2000) requires that the Qiangtang was always a single block. Although intriguing, this model is not supported by tectonostratigraphic evidence (e.g. Zhang 2001; Zhang *et al.* 2006) and thus a less spectacular interpretation involving some type of rifting and re-convergence with high pressure exhuming subduction zone processes is maybe more likely. Indeed, a Mediterranean setting at least for the northern Qiangtang Block has recently been suggested (Pullen *et al.* 2008). We re-emphasize, however, that the dramatic (with respect to the Africa plate) velocity of the Indian plate from at least the mid-Cretaceous to the onset of collision and even thereafter (e.g. Patriat & Achache 1984) left little time for sluggish foundering with collapse and consumption of significant volumes of oceanic lithosphere. We accordingly advocate for the India–Asia system neither the existence of widespread trapped orogenic lithosphere pieces nor significant ICLO subduction in contrast to our three Mediterranean snapshots illustrated here.

Stage two, the system of Arabia colliding into Iran and surrounding regions, is characterized by an actively and rapidly growing frontal fold and thrust belt (the Zagros) responding to the incoming colliding Nubian plate which is presently moving with a lively pace (e.g. Gansser 1955; Stöcklin 1968; Berberian & King 1981; Sella *et al.* 2002; McClusky *et al.* 2003; Vernant *et al.* 2004; Masson *et al.* 2005; Reilinger *et al.* 2006). These geodetic data (and models) and seismicity hypocentre distributions (e.g. Jackson & McKenzie 1988; Tatar *et al.* 2005; Jackson *et al.* 2006; Hollingsworth *et al.* 2007) show an actively deforming region that comprises the Caucasus, Zagros, Makran (and historically, Oman), Talesh, Alborz and Kopet Dagh ranges (and any sub-blocks of the Iran collage). Like in the India-Asia collision (the Gangdese), a fossil Andean arc with flysch and ophiolite-bearing suture elements is present (e.g. Gansser 1955; Stöcklin 1968), but not (yet) significantly dissected, in contrast to the India-Asia collision (e.g. Schärer *et al.* 1984). A similar comparison exists within evidence for some lithospheric mantle delamination in eastern Anatolia (e.g. Barazangi *et al.* 2006) in contrast, again, to the more advanced stage of this state under the Tibet plateau (e.g. Kosarev *et al.* 1999). Furthermore, there are various rigid blocks and deforming 'boundaries' and local instances of ophiolitic rocks and possible candidate sutures within the eastern portions of the, relatively little investigated, 'Iranian Plateau', and again this may be seen as a forerunner to attaining a high plateau region (albeit for a smaller geographic region than that of Tibet). Parallels such as these have led many to propose that this system is a good analogue (albeit of shorter orogen length) for the earlier stages of the India collision. Once again, it may or may not be that local land-locked oceanic lithospheric segments had sufficient time to founder and generate significant ICLO subduction belts (that would now be transposed into the Arabia collisional belt). The historical velocity of the Nubian plate was also fairly rapid (Dewey *et al.* 1989*b*; Allen 2004), however, and, at least for the Zagros belt, significant ICLO subduction belt incorporation is not so likely.

Stage three, the Mediterranean, includes of course the 'palaeo-Mediterranean' e.g. the last-stage Tethys ocean closures of the Pannonian – Carpathian system. Once the presently recalcitrant Africa does fully collide into Europe, the current preservation of those last vestiges of intra-convergence oceanic lithosphere awaiting subduction will be obliterated. Once stage three goes to completion, it might well be difficult to identify fossil examples in the future exposed roots of the by-that-time transposed to orogen-parallel, spatially and heterogeneously restricted, short duration, intra-orogenic piecemeal collision (e.g. along-strike restricted, across-strike repeated local orogenesis events such as the Apennines piled up behind the Dinarides, or scattered, short (≤ 50 km) belts with blueschist occurrences (such would be the future equivalent to that which is currently beneath the Calabrian subduction) to become underplated, exhumed once the system is shutoff, and transposed and incorporated somewhere between collided Africa and Europe). ICLO subduction in ancient orogens may indeed only be resolvable through a dense network of basement geochronology and thermochronology. In the Variscan Sudetes, for example, multiple sequential collisions (a discrete history of burial followed by exhumation in each instance) within a spatially limited row of rock packages (<100 km swath – effectively a 'spot') are recorded by successively younger discrete $P-T$ loops (Matte 2001; Franke & Zelazniewicz 2002; Schneider *et al.* 2006). The lack of any along strike continuity for each of these sequential collisions excludes simple interpretation through the application of classical 2D cylindrical orogenesis aggregation of terranes (e.g. Tibet plateau). Applying ICLO subduction (as seen in the Mediterranean) as a modern analogue provides a tangible and elegant mechanism by which the otherwise confusing geometries of numerous local collisions within such a short section of orogen can be explained.

The fact that Africa may or may not collide into Europe as discussed above is not important for the snapshot thesis. Afar mantle plume theories notwithstanding, it is not clear why Africa has stalled (or slowed), but it has, and we are fortunate to gain this insight into ICLO subduction and therefore to have captured these snapshots that would otherwise be unlikely to survive.

Collapse as a competing model

As noted by various authors over the last few years (e.g. Jolivet & Faccenna 2000; Wortel & Spakman 2000), it is important to separate the larger scale (upper mantle) process of slab foundering, retreat, and piecemeal breakup, from the more general, now well-established phenomenon of extensional syn-convergence (or 'post-orogenic') collapse. We keep the term syn-convergence (e.g. Burg 1983; Pêcher *et al.* 1991; Edwards *et al.* 1996) rather than 'post-orogenic' collapse for our large scale consideration of the major collision of Europe and Africa, in view of the fact that the collision is still ongoing, if albeit stalled. We recognize that, at least for the circum-Mediterranean, multiple mature orogenic elements exist (e.g. Alps, Hellenides, etc.) where there has been a protracted sequence of syn-thickening high pressure exhumation followed by post-thickening collapse (on this topic see also Tirel *et al.*, 2009). Collapse in thickened crust in mature portions of orogens such as the now classic syn-convergence, syn-thrust vergence normal faulting in the Himalaya (southern Tibet detachment system, e.g. Burg *et al.* 1981; Burg 1983; Burchfiel *et al.* 1992; Edwards *et al.* 1996) with accompanying (typically high temperature) events such as core complex formation, operation of a widespread crustal scale detachment (system), mid-crustal melting, etc., are attributable to various mechanisms that are not directly related to upper mantle slab dynamics (e.g. enhanced slab pull, accelerated retreat). Numerous authors have highlighted, for example, the roles of collapse-engendering, gravitational body forces that may be stored in the over-thickened crust (e.g. Dewey 1988; Platt & Vissers 1989), with the possible additional roles of, for example, mid-lower crustal weakening with attendant flow, sudden break-off/delamination or convective removal of lithospheric mantle, etc. In a general sense, the process of syn-convergence collapse clearly has been, or still is, in operation in our three snapshot examples (irrespective of which mechanisms are dominant, be it mantle lithosphere removal and/or aesthenospheric upwelling, mid/lower crustal flow, etc.), and this is clearly evident both in the heart of the retreating system – the locus of core complex & detachment systems of the Attic–Cycladic massif (Cyclades, Menderes/Lycian) or Main Alpine (Sardinia/Corisca, Calabria for the Liguro–Provençal–Tyrrhenian setting) as well as at the margins of the retreating system (the escape kinematics of the 'collapse' of the Anatolian or Eastern Alps crustal blocks). Certainly the various differences in character between our three snapshot settings, and more so between specific portions (in space and or time) within the settings, reflect differing mixtures of influences by these processes (e.g. the intensity and overall quantity (and quality!) of blueschists and other high pressure exhumation products, chemistry and relative timing of plutonism and volcanism, etc.). We re-emphasise however, that the range of options and variants of syn-convergence collapse mechanisms are not competing models to upper mantle slab dynamics pursuant to a single process that explains all of our Mediterranean snapshot settings. Competing models that exist would include, for example Mantovani *et al.* (2000).

Stretched continental lithosphere versus rifted continental lithosphere

Of considerable interest for backarc extension within the continental lithosphere is the question of why in some cases there is complete rifting and new oceanic lithosphere creation while in others there is extreme stretching. For each of our three snapshots the main features arising from slab rollback are very similar yet each experienced a different back arc extension phenomenon: (1) for the Tyrrhenian/Ligurian–Provençal system, back arc extension fully rifted the continental lithosphere and proceeded almost solely via oceanization; (2) for the Hellenic subduction system, back arc extension massively stretched, but did not split, the continental lithosphere and proceeded via (a) widespread system(s) of throughgoing crustal high strain zones, detachments, metamorphic core complex development, and relative rock uplift; and (3) for the Pannonian–Carpathian subduction system, back arc extension rifted (but not to failure), and massively stretched, the continental lithosphere resulting in basin subsidence and upwelling of the aesthenospheric mantle. What are the parameters, for example, surrounding the alternative scenarios that dictate whether stretching will lead to extreme ductile flow but not rifting and so extensional failure will take the form of neither oceanisation nor major basin growth but (networks of) detachment-type systems ($\pm$ magmatism) as typified by core-complex rich extended settings (such as the Basin and Range or Aegean-Menderes)?

For scenarios whose boundary conditions incorporate high velocities (several cm/a) applied to limited along strike distances (a few 100 km) such as the Western Mediterranean and the Hellenic Arc, this critical issue is a surprisingly little addressed question – mainly in model studies (e.g. Buck *et al.* 1988; Faccenna *et al.* 1997; Rosenbaum *et al.* 2005; Tirel *et al.* 2007, 2009). It would appear that, in addition to the rollback velocity (and its variation through time), of key importance for the original continental crust (and mantle lithosphere) is: (1) the initial thickness; and (2) the initial thermal condition. Pre-existing tectonic fabric may also play an important role. Particularly when the age of the original fabric is young relative to the initiation of stretching, the orientation of the fabric can be key (i.e. if the trench migration and slab retreat vector(s) are close to perpendicular to the strike of the main orogenic belt (if indeed any is present). Platt (2007) interestingly, suggests that thickened, warm hinterland plateaus (future back arc) could ultimately evolve into oceanic back-arc basins.

For the Pannonian Basin, widespread syn-extensional sedimentary cover upon the pre-existing continental crust renders difficult an extraction of detailed P–T–t–d (pressure, temperature, time, deformation) history as has been possible in the Tyrrhenian/Ligurian–Provençal and Hellenic back arc systems. For the comparison of these two latter systems, it would appear that the initial distribution ratio of landlocked oceanic lithosphere to segments of collided continental lithosphere (and thereby orogen pieces, i.e. thickened, weakened, thermally perturbed) contrasts greatly between these two snapshots. As we noted above, the total volume of scraps of ripped-off Alpine orogen that are identifiable in the otherwise low-grade Western Mediterranean collisional products (portions of Corsica, Calabria and Tuscany) is small and most of the parturient un-rifted continental crust was thermally stable (Tirel *et al.* (2007), for example, allow in this case 30 km initial crustal thickness and a Moho temperature of only 500 °C). Meanwhile the Hellenides owe much of their history to collision with a significant promontory of, or terrane in front of, Africa (and are the aggregate of at least two additional terrane collisions) and the thickening, weakening, and thermal upheaval are attested to by the pressure and temperature conditions recorded by, for example, the world class blueschists (and here for example, Tirel *et al.* (this issue) allow 45 km initial crustal thickness and a Moho temperature of $\leq$1000 °C). Moreover, Hellenic trench retreat velocities seem to have been somewhat lower than for the Tyrrhenian (cf. Schellart *et al.* 2007) and have enjoyed, for much of the time, a high angle to much of the orogenic fabric (see van Hinsbergen (2005*b*) for an overview of all these key conditions). As we noted, Pannonian Basin pre-existing continental crust conditions are less clear. There was certainly thickening due to the Alpine (*sensu lato*) events and tectonic block aggregation but to what extent this engendered a widespread temperature elevation throughout the entire crustal thickness (à la the Cyclades) is elusive. Additionally, the trench retreat direction seems to have varied significantly (from northwards to southeastwards) over the oceanic lithosphere consumption history and thus the system has only partially benefited from a retreat direction orientation that was at a high angle to main the orogenic fabric. Heat input related mantle convection has clearly played a key role in the enhancing lithospheric stretch and suppressing oceanization, but it is unclear how soon in the back-arc extension history anomalous aesthenospheric mantle convection (assuming this was not pre-existing) might have been operational.

Conclusions

1. The Mediterranean region offers a possibly unique series of snapshots of the accelerated retreat that accompanies geodynamic instability of narrowing slab widths fostered via the piecemeal subduction of oceanic lithosphere that has been landlocked between stalled or slowed continental orogenesis; and
2. ICLO – Subduction (‘Intra-Collisional Landlocked Ocean’ subduction) is a key part of the plate-tectonic cycle that must be very frequent over geological time but is uniquely represented on the Earth at present by the Mediterranean.

This research is partly supported through an FWF (Fonds der Wissenschaft – Austrian Research Council) research grant (Project ACCEL). We thank G. Vignaroli, G. Bada and D. van Hinsbergen for reviews and Zámolyi András for help with GIS processing. Numerous of our Vienna EGU 2007 special session conveners and participants provided discussion and feedback. Kostas Petrakakis first introduced us to Mediterranean geodynamics, beginning with a small island south of the Greek mainland.

References

ACHACHE, J., COURTILLOT, V. & ZHOU YAO, X. 1984. Paleogeographic and tectonic evolution of southern Tibet since Middle Cretaceous time; new paleomagnetic data and synthesis. *Journal of Geophysical Research*, **B89**, 10311–10339.

ALLEGRE, C. J., COURTILLOT, V., TAPPONNIER, P., HIRN, A., MATTAUER, M. & COULON, C. *ET AL*. 1984. Structure and evolution of the Himalaya-Tibet orogenic belt. *Nature*, **307**, 17–22.

ALLEN, M. B. 2004. Late Cenozoic reorganization of the Arabia-Eurasia collision and the comparison of short-term and long-term deformation rates. *Tectonics*, **23**, doi:10.1029/2003TC001530.

ALTHERR, R. & SIEBEL, W. 2002. I-type plutonism in a continental back-arc setting: Miocene granitoids and monzonites from the central Aegean Sea, Greece. *Contributions to Mineralogy and Petrology*, **143**, 397–415.

ALTHERR, R., KREUZER, H., WENDT, I., LENZ, H., WAGNER, G. A., KELLER, J., HARRE, W. & HOHNSDORF, A. 1982. A Late Oligocene/Early Miocene high temperature belt in the Attic-Cycladic crystalline complex (SE Pelagonian, Greece). *Geologisches Jahrbuch*, **E23**, 97–164.

ALTHERR, R., HENJES-KUNST, F., MATTHEWS, A., FRIEDRICHSEN, H. & TAUBER HANSEN, B. 1988. O-Sr isotopic variation in Miocene granitoids from the Aegean: evidence for an origin by combined assimilation and fractional crystallization. *Contributions to Mineralogy and Petrology*, **100**, 528–541.

AMBRASEYS, N. N. & JACKSON, J. A. 1990. Seismicity and associated strain of central Greece between 1890 and 1988. *Geophysical Journal International*, **101**, 663–708.

ANDERSON, H. & JACKSON, J. 1987. The deep seismicity of the Tyrrhenian Sea *Geophysical Journal of the Royal Astronomical Society*, **91**, 613–637.

ANDREWS, D. J. & SLEEP, N. H. 1974. Numerical modelling of tectonic flow behind island arcs. *Geophysical Journal of the Royal Astronomical Society*, **38**, 237–251.

ANDRIESSEN, P. A. M., BOELRIJK, N. A. I. M., HEBEDA, E. H., PRIEM, H. N. A., VERDURMEN, E. A. T. & VERSCHURE, R. H. 1979. Dating the events of metamorphism and granitic magmatism in the Alpine Orogen of Naxos (Cyclades, Greece). *Contributions to Mineralogy and Petrology*, **69**, 215–225.

ANGELIER, J., LYBERIS, N., LE PICHON, X., BARRIER, E. & HUCHON, P. 1982. The tectonic development of the Hellenic Arc and the Sea of Crete: a synthesis. *Tectonophysics*, **86**, 159–163.

ARGAND, E. 1924. Le tectonique de L'Asie. *Comptes Rendus, Congrès Internationale Geologique*, **(session. XIII 922)**, 171–372.

ARMIJO, R., MEYER, B., KING, G. C. P., RIGO, A. & PAPANASTASSIOU, D. 1996. Quaternary evolution of the Corinth Rift and its implications for the Late Cenozoic evolution of the Aegean. *Geophysical Journal International*, **126**, 11–53.

ARMIJO, R., MEYER, B., HUBERT, A. & BARKA, A. 1999. Westward propagation of the North Anatolian fault into the northern Aegean: timing and kinematics. *Geology*, **27**, 267–270.

ARMIJO, R., FLERIT, F., KING, G. & MEYER, B. 2003. Linear elastic fracture mechanics explains the past and present evolution of the Aegean. *Earth and Planetary Science Letters*, **217**, 85–95.

AVIGAD, D. 1993. Tectonic juxtaposition of blueschists and greenschists in Sifnos Island (Aegean Sea); implications for the structure of the Cycladic blueschist belt. *Journal of Structural Geology*, **15**, 1459–1469.

AVIGAD, D. & GARFUNKEL, Z. 1991. Uplift and exhumation of high-pressure metamorphic terrains: the example of the Cycladic blueshist belt (Aegean Sea). *Tectonophysics*, **188**, 357–372.

AVIGAD, D., GARFUNKEL, Z., JOLIVET, L. & AZANON, J. M. 1997. Back arc extension and denudation of Mediterranean eclogites. *Tectonics*, **16**, 924–941.

AVIGAD, D., BAER, G. & HEIMANN, A. 1998. Block rotations and continental extension in the central Aegean Sea: palaeomagnetic and structural evidence from Tinos and Mykonos (Cyclades, Greece). *Earth and Planetary Science Letters*, **157**, 23–40.

AYHAN, M. E., DEMIR, C., LENK, O., KILICOGLU, A., ALTINER, Y., BARKA, A. A., ERGINTAV, S. & OZENER, H. 2002. Interseismic strain accumulation in the Marmara Sea region. *Bulletin of the Seismological Society of America*, **92**, 216–229.

BADA, G., HORVATH, F., GERNER, P. & FEJES, I. 1999. Review of the present-day geodynamics of the Pannonian basin: progress and problems. *Journal of Geodynamics*, **27**, 501–527.

BADA, G., HORVATH, F., DOVENYI, P., SZAFIAN, P., WINDHOFFER, G. & CLOETINGH, S. 2007. Present-day stress field and tectonic inversion in the Pannonian basin. *Global and Planetary Change*, **58**, 165–180.

BAKER, D., HATZFELD, D., LYON-CAEN, H., PAPADIMITRIOU, E. & RIGO, A. 1997. Earthquake mechanisms of the Adriatic Sea and western Greece: implications for the oceanic subduction-continental collision transition. *Geophysical Journal International*, **131**, 559–594.

BARAZANGI, M., SANDVOL, E. & SEBER, D. 2006. Structure and tectonic evolution of the Anatolian plateau in eastern Turkey. *In*: DILEK, Y. & PAVLIDES, S. (eds) *Postcollisional Tectonics and Magmatism in the Mediterranean Region and Asia*. Geological Society of America, **409**, 463–473.

BARKER, P. F. 1970. Plate Tectonics of the Scotia Sea Region. *Nature*, **228**, 1293–1296.

BECCALUVA, L., CHIESA, S. & DELALOYE, M. 1981. K/Ar age determinations on some Tethyan ophiolites. *Rendiconti della Società Italiana di Mineralogia e Petrologia*, **37**, 869–880.

BERBERIAN, M. & KING, G. C. P. 1981. Towards a paleogeography and tectonic evolution of Iran. *Canadian Journal of Earth Sciences*, **18**, 210–265.

BERTOTTI, G., MATENCO, L. & CLOETINGH, S. 2003. Vertical movements in and around the south-east Carpathian foredeep: lithospheric memory and stress field control. *Terra Nova*, **15**, 299–305.

BIELIK, M., KLOSKA, K., MEURERS, B., SVANCARA, J., WYBRANIEC, S., FANCSIK, T. *ET AL*. 2006. Gravity anomaly map of the CELEBRATION 2000 region. *Geologica Carpathica*, **57**, 145–156.

Bohnhoff, M., Makris, J., Papanikolaou, D. & Stavrakakis, G. 2001. Crustal investigation of the Hellenic subduction zone using wide aperture seismic data. *Tectonophysics*, **343**, 239–262.

Bohnhoff, M., Rische, M., Meier, T., Endrun, B., Becker, D. & Harjes, H.-P. 2004. CYC-NET: a temporary seismic network on the Cyclades (Aegean Sea, Greece). *Seismological Research Letters*, **75**, 352–359.

Bohnhoff, M., Rische, M., Meier, T., Becker, D., Stavrakakis, G. & Harjes, H.-P. 2006. Microseismic activity in the Hellenic Volcanic Arc, Greece, with emphasis on the seismotectonic setting of the Santorini-Amorgos zone. *Tectonophysics*, **423**, 1–4.

Briole, P., Rigo, A., Lyon-Caen, H., Ruegg, J. C., Papazissi, K., Mitsakaki, C., Balodimou, A. *et al.* 2000. Active deformation of the Corinth rift, Greece: results from repeated Global Positioning System surveys between 1990 and 1995. *Journal of Geophysical Research*, **105**, 25605–25626.

Bröcker, M. & Franz, L. 1998. Rb-Sr isotope studies on Tinos Island (Cyclades, Greece): additional time constraints for metamorphism, extent of infiltration-controlled overprinting and deformational activity. *Geological Magazine*, **135**, 369–382.

Bröcker, M. & Franz, L. 2000. The contact aureole on Tinos (Cyclades, Greece): tourmaline-biotite geothermometry and Rb-Sr geochronology. *Mineralogy and Petrology*, **70**, 257–283.

Bröcker, W. S. & Pidgeon, R. T. 2007. Protolith Ages of Meta-igneous and Metatuffaceous Rocks from the Cycladic Blueschist Unit, Greece: results of a Reconnaissance U-Pb Zircon Study. *The Journal of Geology*, **115**, 83–98.

Bröcker, M., Kreuzer, H., Matthews, A. & Okrusch, M. 1993. $^{40}Ar/^{39}Ar$ and oxygen isotope studies of polymetamorphism from Tinos Island, Cycladic blueschist belt, Greece. *Journal of Metamorphic Geology*, **11**, 223–240.

Bröcker, W. S., Cker, M. & Keasling, A. 2006. Ion-probe U-Pb zircon ages from the high-pressure/low-temperature melange of Syros, Greece: age diversity and the importance of pre-Eocene subduction. *Journal of Metamorphic Geology*, **24**, 615–631.

Brown, M. 2007. Metamorphic conditions in orogenic belts: A record of secular change. *International Geology Review*, **49**, 193–234.

Brun, J.-P. & Sokoutis, D. 2007. Kinematics of the Southern Rhodope Core Complex (North Greece). *International Journal of Earth Sciences*, **96**, 1079–1099.

Buck, W. R., Mertinez, F., Steckler, M. S. & Cochran, J. R. 1988. Thermal consequences of lithospheric extension: pure and simple. *Tectonics*, **7**, 213–234.

Buick, I. S. 1991*a*. Mylonitic fabric development on Naxos. *Journal of Structural Geology*, **13**, 643–655.

Buick, I. S. 1991*b*. The late Alpine evolution of an extensional shear zone, Naxos, Greece. *Journal of the Geological Society, London*, **148**, 93–103.

Buick, I. S. & Holland, J. B. 1989. The P-T-t path associated with crustal extension, Naxos, Cyclades. *In*: Daly, J. S., Cliff, R. A. & Yardley, B. W. D. (eds) *Evolution of metamorphic belts*. Geological Society London, Special Publications, **43**, 365–369.

Buikin, A., Trieloff, M., Hopp, J., Althaus, T., Korochantseva, E., Schwarz, W. H. & Altherr, R. 2005. Noble gas isotopes suggest deep mantle plume source of late Cenozoic mafic alkaline volcanism in Europe. *Earth and Planetary Science Letters*, **230**, 143–162.

Burbank, W. D., Derry, L. A. & France-Lanord, C. 1992. Reduced Himalayan sediment production 8 Myr ago despite an intensified monsoon. *Nature*, **364**, 48–50.

Burchfiel, B. C., Zhiliang, C., Hodges, K. V., Yuping, L., Royden, L. H., Changrong, D. & Jiene, X. 1992. The south Tibetan detachment system, Himalayan orogen: extension contemporaneous with and parallel to shortening in a collisional mountain belt. *Geological Society of America Special Paper*, **269**, 1–41.

Burg, J.-P. 1983. *Tectogénèse comparée de deux segments de chaîne de collision: le Sud du Tibet (suture du Tsangpo); la chaîne hercynienne en Europe (suture du Massif-Central).* PhD Thesis, Université Montpellier, France.

Burg, J.-P., Brunel, M., Chen, G. M. & Liu, G. H. 1981. Deformation of the leucogranites of the Crystalline Main Central Thrust sheet in southern Tibet (China). *Mitteilungen aus dem Geologischen Institut der Eidgenössischen Technischen Hochschule und der Universität Zürich, Neue Folge*, **239a**, 49–51.

Catalano, R., Doglioni, C. & Merlini, S. 2001. On the Mesozoic Ionian Basin. *Geophysical Journal International*, **144**, 49–64.

Cavazza, W., Roure, F., Spakman, W., Stampfli, G. M. & Ziegler, P. A. 2004. *The TRANSMED atlas – the Mediterranean region from crust to mantle geological and geophysical framework of the Mediterranean and the surrounding areas*. Springer-Verlag Berlin, Heidelberg, New York, NY.

Channell, J. E. T. & Kozur, H. W. 1997. How many oceans? Meliata, Vadar, and Pindos oceans in Mesozoic Alpine paleogeography. *Geology*, **25**, 183–186.

Chen, Z., Burchfiel, B. C., Liu, Y., King, R. W., Royden, L. H., Tang, W. *et al.* 2000. Global Positioning System measurements from eastern Tibet and their implications for India/Eurasia intercontinental deformation. *Journal of Geophysical Research*, **105**, 16215–16227.

Chiappini, M., Meloni, A., Boschi, E., Faggioni, O., Beverini, N., Carmisciano, C. & Marson, I. 2000. Shaded relief magnetic anomaly map of Italy and surrounding marine areas. *Annali Geofisicae*, **43**, 983–989.

Cifelli, F., Rossetti, F. & Mattei, M. 2007. The architecture of brittle postorogenic extension: results from an integrated structural and paleomagnetic study in north Calabria (southern Italy). *Geological Society of America Bulletin*, **119**, 221–239.

Clarke, D. B., Henry, A. S. & White, M. A. 1998. Exploding xenoliths and the absence of "elephants' graveyards" in granite batholiths. *Journal of Structural Geology*, **20**, 1325–1344.

Cloetingh, S. & Lankreijer, A. 2001. Lithospheric memory and stress field controls on polyphase deformation of the Pannonian basin-Carpathian system. *Marine and Petroleum Geology*, **18**, 3–11.

Cloetingh, S., Burov, E., Matenco, L., Toussaint, G., Bertotti, G., Andriessen, P. A. M. *et al.* 2004. Thermo-mechanical controls on the mode of continental collision in the SE Carpathians (Romania). *Earth and Planetary Science Letters*, **218**, 57–76.

Cloetingh, S., Matenco, L., Bada, G., Dinu, C. & Mocanu, V. 2005*a*. The evolution of the Carpathians-Pannonian system: interaction between neotectonics, deep structure, polyphase orogeny and sedimentary basins in a source to sink natural laboratory. *Tectonophysics*, **410**, 1–14.

Cloetingh, S., Ziegler, P. A., Beekman, F., andriessen, P. A. M., Matenco, L., Bada, G. *et al.* 2005*b*. Lithospheric memory, state of stress and rheology: neotectonic controls on Europe's intraplate continental topography. *Quaternary Science Reviews*, **24**, 241–304.

Cloetingh, S., Ziegler, P. A., Bogaard, P. J. F., andriessen, P. A. M., Artemieva, I. M., Bada, G. *et al.* 2007. TOPO-EUROPE: the geoscience of coupled deep Earth-surface processes. *Global and Planetary Change*, **58**, 1–118.

Cloos, E. 1940. Crustal shortening and axial divergence in the Appalachians of southeastern Pennsylvania and Maryland. *Geological Society of America Bulletin*, **51**, 845–872.

Coban, H. 2007. Basalt magma genesis and fractionation in collision- and extension-related provinces: a comparison between eastern, central and western Anatolia. *Earth-Science Reviews*, **80**, 219–238.

Cocard, M., Kahle, H. G., Peter, Y., Geiger, A., Veis, G., Felekis, S. *et al.* 1999. New constraints on the rapid crustal motion of the Aegean region: recent results inferred from GPS measurements (1993–1998) across the West Hellenic Arc, Greece. *Earth and Planetary Science Letters*, **172**, 39–47.

Collins, W. J. 2002. Nature of extensional accretionary orogens. *Tectonics*, **21**, no.4, 12.

Collins, A. S. & Robertson, A. H. F. 2003. Kinematic evidence for Late Mesozoic-Miocene emplacement of the Lycian Allochthon over the Western Anatolide Belt, SW Turkey. *Geological Journal*, **38**, 295–310.

Coney, P. J. 1980. Cordilleran metamorphic core complexes; an overview. *In*: Coney, P. J. & Reynolds, S. J. (eds) *Cordilleran metamorphic core complexes and their uranium favorability*. US Department of Energy Open-File Report GJBX-258(80), 25–64.

Copeland, P. & Harrison, T. M. 1990. Episodic rapid uplift in the Himalaya revealed by $^{40}Ar/^{39}Ar$ analysis of detrital K-feldspar and muscovite, Bengal fan. *Geology*, **18**, 354–357.

Coward, M. P., Kidd, W. S. F., Pan, Y., Shackleton, R. M., Zhang, H., Chang, C., Dewey, J. F. & Yin, J. 1988. The structure of the 1985 Tibet Geotraverse, Lhasa to Golmud. *Philosophical Transactions of the Royal Society of London*, **A327**, 307–336.

Csontos, L. 1995. Tertiary tectonic evolution of the Intra-Carpathian area: a review. *Acta Vulcanologica*, **7**, 1–13.

Csontos, L. & Nagymarosy, A. 1998. The mid-Hungarian line: a zone of repeated tectonic inversions. *Tectonophysics*, **297**, 51–71.

D'Anastasio, E., De Martini, P. M., Selvaggi, G., Pantosti, D., Marchioni, A. & Maseroli, R. 2006. Short-term vertical velocity field in the Apennines (Italy) revealed by geodetic levelling data. *Tectonophysics*, **418**, 219–234.

Dallmeyer, R. D., Neubauer, F., Handler, R., Fritz, H., Müller, W., Pana, D. & Putis, M. 1996. Tectonothermal evolution of the internal Alps and Carathians: evidence from $^{40}Ar/^{39}Ar$ mineral and whole-rock data. *Eclogae Geologicae Helvetiae*, **89**, 203–227.

Danisik, M., Kuhlemann, J., Dunkl, I., Szekeley, B. & Frisch, W. 2007. Burial and exhumation of Corsica (France) in the light of fission track data. *Tectonics*, **26**.

Decker, K. & Peresson, H. 1996. Tertiary kinematics in the Alpine-Carpathian-Pannonian system: link between thrusting, transform faulting and crustal extension. *In*: Wessely, G. & Liebl, W. (eds) *Oil and Gas in Alpidic Thrustbelts and Basins of Central and Eastern Europe*. EAGE Special Publication, **5**, 69–77.

Dercourt, J., Zonenshain, L. P., Ricou, L. E., Kazmin, V. G., Le Pichon, X., Knipper, A. L. *et al.* 1986. Geological evolution of the tethys belt from the atlantic to the pamirs since the Lias. *Tectonophysics*, **123**, 241–315.

Dewey, J. F. 1988. Extensional collapse of orogens. *Tectonics*, **7**, 1123–1139.

Dewey, J. F. & Bird, J. M. 1970. Mountain belts and the new global tectonics. *Journal of Geophysical Research*, **75**, 2625–2647.

Dewey, J. F., Shackleton, R. M., Chenfa, C. & Yiyin, S. 1988. The tectonic evolution of the Tibetan plateau. *Philosophical Transactions of the Royal Society of London*, 379–413.

Dewey, J. F., Cande, S. & Pitman III, W. C. 1989*a*. Tectonic evolution of the India/Eurasia Collision Zone. *Eclogae geologicae Helvetiae*, **82**, 717–734.

Dewey, J. F., Helman, M. L., Turco, E., Hutton, D. H. W. & Knott, S. D. 1989*b*. Kinematics of the western Mediterranean. *In*: Coward, M. P., Dietrich, D. & Parker, R. G. (eds) *Alpine Tectonics*. Geological Society, London, Special Publication, **45**, 265–283.

Dinter, D. A. & Royden, L. 1993. Late Cenozoic extension in northeastern Greece; Strymon Valley detachment system and Rhodope metamorphic core complex. *Geology*, **21**, 45–48.

Dobosi, G., Kempton, P. D., Downes, H., Embey-Isztin, A., Thirlwall, M. & Greenwood, P. 2003. Lower crustal granulite xenoliths from the Pannonian Basin, Hungary, Part 2: Sr-Nd-Pb-Hf and O isotope evidence for formation of continental lower crust by tectonic emplacement of oceanic crust. *Contributions to Mineralogy and Petrology*, **144**, 671–683.

Doglioni, C. 1994. Foredeeps versus subduction zones. *Geology*, **22**, 271–274.

Doglioni, C., Moretti, I. & Roure, F. 1991. Basal lithospheric detachment, eastward mantle flow and mediterranean geodynamics – a discussion. *Journal of Geodynamics*, **13**, 47–65.

Doglioni, C., Harabaglia, P., Merlini, S., Mongelli, F., Peccerillo, A. & Piromallo, C.

1999. Orogens and slabs vs. their direction of subduction. *Earth-Science Reviews*, **45**, 167–208.

DUERMEIJER, C. E., NYST, M., MEIJER, C. G., LANGEREIS, C. G. & SPAKMAN, W. 2000. Neogene evolution of the Aegean arc: paleomagnetic and geodetic evidence for a rapid and young rotation phase. *Earth and Planetary Science Letters*, **176**, 509–525.

DUPONT-NIVET, G., VASILIEV, I., LANGEREIS, C. G., KRIJGSMAN, W. & PANAIOTU, C. 2005. Neogene tectonic evolution of the southern and eastern Carpathians constrained by paleomagnetism. *Earth and Planetary Science Letters*, **236**, 374–387.

DÜRR, S., ALTHERR, R., KELLER, J., OKRUSCH, M. & SEIDEL, E. 1978. The Median Aegean Crystalline belt:stratigraphy, structure, metamorphism, magmatism. *In*: CLOOS, H., ROEDER, D. & SCHMIDT, K. (eds) *Alps, Appenines, Hellenides*. Schweitzerbart, 455–477.

DVORKIN, J., NUR, A., MAVKO, G. & BEN-AVRAHAM, Z. 1993. Narrow subducting slabs and the origin of backarc basins. *Tectonophysics*, **227**, 63–79.

EDWARDS, M. A., KIDD, W. S. F., LI, J., YUE, Y. & CLARK, M. 1996. Multi-stage development of the southern Tibet detachment system near Khula Kangri. New data from Gonto La. *Tectonophysics*, **260**, 1–19.

EINSELE, G., RATSCHBACHER, L. & WETZEL, A. 1996. The Himalaya-Bengal Fan Denudation-Accumulation System during the past 20 Ma. *Journal of Geology*, **104**, 163–184.

ENDRUN, L. T. C., MEIER, M., BOHNHOFF, M. & HARJES, H.-P. 2005. Modeling the influence of Moho topography on receiver functions: a case study from the central Hellenic subduction zone. *Geophysical Research Letters*, L12311.

ENGDAHL, E. R., VAN DER HILST, R. & BULAND, R. 1998. Global teleseismic earthquake relocation with improved travel times and procedures for depth determination. *Bulletin of the Seismological Society of America*, **88**, 722–743.

FACCENNA, C., MATTEI, M., FUNICIELLO, R. & JOLIVET, L. 1997. Styles of back-arc extension in the Central Mediterranean. *Terra Nova*, **9**, 126–130.

FACCENNA, C., FUNICIELLO, F., GIARDINI, D. & LUCENTE, P. 2001. Episodic back-arc extension during restricted mantle convection in the Central Mediterranean. *Earth and Planetary Science Letters*, **187**, 105–116.

FACCENNA, C., SPERANZA, F., CARACCIOLO, F. D., MATTEI, M. & OGGIANO, G. 2002. Extensional tectonics on Sardinia (Italy): insights into the arc-back-arc transitional regime. *Tectonophysics*, **356**, 213–232.

FACCENNA, C., JOLIVET, L., PIROMALLO, C. & MORELLI, A. 2003. Subduction and the depth of convection in the Mediterranean mantle. *Journal Geophysical Research*, **108**, 2099, doi:10.1029/2001JB001690.

FACCENNA, C., PIROMALLO, C., CRESPO-BLANC, A., JOLIVET, L. & ROSSETTI, F. 2004. Lateral slab deformation and the origin of the western Mediterranean arcs. *Tectonics*, **23**.

FACCENNA, C., BELLIER, O., MARTINOD, J., PIROMALLO, C. & REGARD, V. 2006. Slab detachment beneath eastern Anatolia: a possible cause for the formation of the North Anatolian fault. *Earth and Planetary Science Letters*, **242**, 85–97.

FARYAD, S. W. & HENJES-KUNST, F. 1997. Petrological and K–Ar and ^{40}Ar–^{39}Ar age constraints for the tectonothermal evolution of the high-pressure Meliata unit, Western Carpathians (Slovakia). *Tectonophysics*, **280**, 141–156.

FEENSTRA, A. 1985. *Metamorphism of bauxites on Naxos, Greece*. offsetdrukkerij Kanters B.V., Alblasserdam, Netherlands.

FELLIN, M. G., VANCE, J. A., GARVER, J. I. & ZATTIN, M. 2006. The thermal evolution of Corsica as recorded by zircon fission-tracks. *Tectonophysics*, **421**, 299–317.

FODOR, L., JELEN, B., MARTON, E., SKABERNE, D., CAR, J. & VRABEC, M. 1998. Miocene-Pliocene tectonic evolution of the Slovenian Periadriatic fault: implications for Alpine-Carpathian extrusion models. *Tectonics*, **17**, 690–709.

FODOR, L., BADA, G., CSILLAG, G., HORVATH, E., RUSZKICZAY-RUDIGER, Z., PALOTAS, K. *ET AL*. 2005. An outline of neotectonic structures and morphotectonics of the western and central Pannonian Basin. *Tectonophysics*, **410**, 15–41.

FORSTER, M. A. & LISTER, G. S. 1999. Detachment faults in the Aegean core complex of Ios, Cyclades, Greece. *In*: RING, U., BRANDON, M. T., LISTER, G. S. & WILLET, S. D. (eds) *Exhumation Processes: Normal Faulting, Ductile Flow and Erosion*. Geological Society, London, Special Publication, **154**, 305–323.

FRANCE-LANORD, C., DERRY, L. & MICHARD, A. 1993. Evolution of the Himalaya since Miocene time: isotopic and sedimentological evidcncc from the Bengal fan. *In*: TRELOAR, P. J. & SEARLE, M. P. (eds) *Himalayan Tectonics*. Geological Society, London, Special Publication, **74**, 605–622.

FRANKE, W. & ZELAZNIEWICZ, A. 2002. Structure and evolution of the Bohemian Arc. *In*: WINCHESTER, J. A., PHARAOH, T. C. & VERNIERS, J. (eds) *Paleozoic Amalgamation of Central Europe*. Geological Society, London, Special Publication, **201**, 279–293.

FÜGENSCHUH, B. & SCHMID, S. M. 2005. Age and significance of core complex formation in a very curved orogen: evidence from fission track studies in the South Carpathians (Romania). *Tectonophysics*, **404**, 33–53.

FUNICIELLO, F., FACCENNA, C., GIARDINI, D. & REGENAUER-LIEB, K. 2003. Dynamics of retreating slabs: 2. Insights from three-dimensional laboratory experiments. *Journal of Geophysical Research B: Solid Earth*, **108**.

GALADINI, F. & GALLI, P. 1999. The Holocene paleoearthquakes on the 1915 Avezzano earthquake faults (central Italy): implications for active tectonics in the central Apennines. *Tectonophysics*, **308**, 143–170.

GALY, A., FRANCE-LONARD, C. & DERRY, L. A. 1996. The Late Oligocene-Early Miocene Himalayan belt constraints deduced from isotopic compositions of Early Miocene turbidites in the Bengal Fan. *Tectonophysics*, **260**, 109–118.

GANSSER, A. 1955. New Aspects of the Geology of Central Iran. *4th World Petroleum Congress*. C. Colombo, Rome, 279–300.

GARFUNKEL, Z. 1998. Constrains on the origin and history of the Eastern Mediterranean basin. *Tectonophysics*, **298**, 5–35.

GATTACCECAA, J., DEINO, A., RIZZO, R. *ET AL*. 2007. Miocene rotation of Sardinia: new paleomagnetic and geochronological constraints and geodynamic implication. *Earth and Planetary Science Letters*, **258**, 359–377.

GAUTIER, P. & BRUN, J.-P. 1994. Crustal-scale geometry and kinematics of late-orogenic extension in the central Aegean (Cyclades and Ewia Island). *Tectonophysics*, **238**, 399–424.

GAUTIER, P., BRUN, J.-P. & JOLIVET, L. 1993. Structure and kinematics of upper Cenozoic extensional detachment on Naxos and Paros (Cyclades Islands, Greece). *Tectonics*, **12**, 1180–1194.

GAUTIER, P., BRUN, J.-P., MORICEAU, R., SOKOUTIS, D., MARTINOD, J. & JOLIVET, L. 1999. Timing, kinematics and cause of Aegean extension: a scenario based on a comparison with simple analogue experiments. *Tectonophysics*, **315**, 31–72.

GEMMER, L. & HOUSEMAN, G. A. 2007. Convergence and extension driven by lithospheric gravitational instability: evolution of the Alpine-Carpathian-Pannonian system. *Geophysical Journal International*, **168**, 1276–1290.

GESSNER, K., COLLINS, A. S., RING, U. & GUNGOR, T. 2004. Structural and thermal history of poly-orogenic basement: U-Pb geochronology of granitoid rocks in the southern Menderes Massif, Western Turkey. *Journal of the Geological Society*, **161**, 93–101.

GIARDINI, D. 1999. The Global Seismic Hazard Assesment Program (GSHAP); 1992–1999. *Annali Geofisicae*, **42**, 957–974.

GÎRBACEA, R. & FRISCH, W. 1998. Slab in the wrong place: lower lithospheric mantle delamination in the last stage of the Eastern Carpathian subduction retreat. *Geology*, **26**, 611–614.

GIUSEPPE, C., MAZZOLI, S., TONDI, E. & TURCO, E. 1997. Active tectonics in the central Apennines and possible implications for seismic hazard analysis in peninsular Italy. *Tectonophysics*, **272**, 43–68.

GOLDSWORTHY, M., JACKSON, J. & HAINES, A. J. 2002. The continuity of active fault systems in Greece. *Geophysical Journal International*, **148**, 596–618.

GOVERS, R. & WORTEL, M. J. R. 2005. Lithosphere tearing at STEP faults: response to edges of subduction zones. *Earth and Planetary Science Letters*, **236**, 505–523.

GRAD, M., GUTERCH, A., KELLER, G. R., JANIK, T., HEGEDUS, E., VOZAR, J. *ET AL*. 2006. Lithospheric structure beneath trans-Carpathian transect from Precambrian platform to Pannonian basin: CELEBRATION 2000 seismic profile CEL05. *Journal of Geophysical Research-Solid Earth*, **111**.

GRASEMANN, B. & PETRAKAKIS, K. 2007. Evolution of the Serifos Metamorphic Core Complex. *In*: LISTER, G., FORSTER, M. & RING, U. (eds) *Inside the Aegean Metamorphic Core Complexes*. Journal of the Virtual Explorer, **28**, Paper 2.

GRASEMANN, B., EDWARDS, M. A., SCHNEIDER, D. A. *ET AL*. 2006. *A newly-identified, opposite sense Aegean crustal block persistent since the Eocene requires key revisions to Eastern Mediterranean Geodynamics model*. Geological Society of America Abstracts with Programs, Vol. 38, 238.

GRENERCZY, G., KENYERES, A. & FEJES, I. 2000. Present crustal movement and strain distribution in Central Europe inferred from GPS measurements. *Journal of Geophysical Research*, **105**, 21835–21846.

GUEGUEN, E., DOGLIONI, C. & FERNANDEZ, M. 1998. On the post-25 Ma geodynamic evolution of the western Mediterranean. *Tectonophysics*, **298**, 259–269.

HAAS, J., MIOC, P., PAMIC, J., TOMLJENOVIC, B., ARKAI, P., BERCZI-MAKK, A., KOROKNAI, B., KOVACS, S. & FELGENHAUER, E. R. 2000. Complex structural pattern of the Alpine-Dinaridic-Pannonian triple junction. *International Journal of Earth Sciences*, **89**, 377–389.

HAFKENSCHEID, E., WORTEL, M. J. R. & SPAKMAN, W. 2006. Subduction history of the Tethyan region derived from seismic tomography and tectonic reconstructions. *Journal of Geophysical Research-Solid Earth*, **111**.

HAMILTON, W., JIRICEK, R. & WESSELY, G. 1990. The Alpine-Carpathian floor of the Vienna Basin in Austria and CSSR. *Festive Volume: Thirty Years of Geological Cooperation between Austria and Czechoslovakia.* Ust Ustav Geol Prague, 23–32.

HATZFELD, D. 1994. On the shape of the subducting slab beneath the Peleponnese, Greece. *Geophysical Research Letters*, **21**, 173–176.

HATZFELD, D. 1999. The present-day tectonics of the Aegean as deduced from seismicity. *In*: DURAND, B., JOLIVET, L., HORVATH, F. & SERANNE, M. (eds) *The Mediterranean basins: tertiary extension within the Alpine orogen*. Geological Society, London, Special Publications, **156**, 415–426.

HAUSER, F., RAILEANU, V., FIELITZ, W., BALA, A., PRODEHL, C., POLONIC, G. & SCHULZE, A. 2001. VRANCEA99—the crustal structure beneath the southeastern Carpathians and the Moesian Platform. *Tectonophysics*, **340**, 233–248.

HELBING, H., FRISCH, W., BONS, P. D. & KUHLEMANN, J. 2006. Tension gash-like back-arc basin opening and its control on subduction rollback inferred from Tertiary faulting in Sardinia. *Tectonics*, **25**.

HENJES-KUNST, F., ALTHERR, R., KREUZER, H. & TAUBER HANSEN, B. 1988. Disturbed U-Th-Pb systematics of young zircons and uranothorites: The case of the Miocene Aegean granitoids (Greece). *Chemical Geology*, **73**, 125–145.

HETZEL, R., RING, U., AKAL, C. & TROESCH, M. 1995. Miocene NNE-directed extensional unroofing in the Menderes Massif, southwestern Turkey. *Journal of the Geological Society of London*, **152**, 639–654.

HIEKE, W., HIRSCHLEBER, H. B. & DEHGHANI, G. A. 2005. The Ionian Abyssal Plain (central Mediterranean Sea): morphology, subbottom structures and geodynamic history an inventory. *Marine Geophysical Researches*, **24**, 279–310.

HIPPOLYTE, J.-C. 2001. Palaeostress and neotectonic analysis of sheared conglomerates: Southwest Alps and Southern Apennines. *Journal of Structural Geology*, **23**, 421–429.

HOFFMAN, P. F. 1988. United plates of America, the birth of a craton; early Proterozoic assembly and growth of Laurentia. *Annual Review of Earth and Planetary Sciences*, **16**, 543–603.

Hollingsworth, J., Jackson, J., Alarcon, J. E., Bommer, J. J. & Bolourchi, M. J. 2007. The 4th February 1997 Bojnurd (Garmkhan) earthquake in NE Iran: field, teleseismic, and strong-motion evidence for rupture directivity effects on a strike-slip fault. *Journal of Earthquake Engineering*, **11**, 193–214.

Houseman, G. A. & Gemmer, L. 2007. Intra-orogenic extension driven by gravitational instability: Carpathian-Pannonian orogeny. *Geology*, **35**, 1135–1138.

Huismans, R. S., Podladchikov, Y. Y. & Cloetingh, S. 2001. Dynamic modeling of the transition from passive to active rifting, application to the Pannonian basin. *Tectonics*, **20**, 1021–1039.

Husson, L. 2006. Dynamic topography above retreating subduction zones. *Geology*, **34**, 741–744.

Iglseder, C. 2005. Fold-structures in the tectono-metamorphic evolution of the Serifos Metamorphic Core Complex, Cyclades, Greece. Pages 130. University of Vienna, Vienna.

Iglseder, C., Grasemann, B., Schneider, D. A., Petrakakis, K., Miller, C. & Klötzli, U. 2008. Tertiary I and S-type plutonism on Serifos (W. Cyclades, Greece). *In*: Robertson, A. H. F., Parlak, O. & Koller, F. (eds) *Tectonics of the Eastern Mediterranean*. Tectonophysics Special Volume, Elsevier, in press, doi:10.1016/j.tecto.2008.09.021.

Isacks, B., Oliver, J. & Sykes, L. R. 1968. Seismology and the New Global Tectonics. *Journal of Geophysical Research*, **73**, 5855–5899.

Jackson, J. & McKenzie, D. 1988. The relationship between plate motions and seismic moment tensors, and the rates of active deformation in the Mediterranean and Middle-East. *Geophysical Journal-Oxford*, **93**, 45–73.

Jackson, J., Bouchon, M., Fielding, E., Funning, G., Ghorashi, M., Hatzfeld, D., Nazari, H., Parsons, B., Priestley, K., Talebian, M., Tatar, M., Walker, R. & Wright, T. 2006. Seismotectonic, rupture process, and earthquake-hazard aspects of the 2003 December 26 Bam, Iran, earthquake. *Geophysical Journal International*, **166**, 1270–1292.

Jackson, J. A., Haines, J. & Holt, W. E. 1992. The horizontal velocity field in the deforming Aegean Sea region determined from the moment tensors or earthquakes. *Journal of Geophysical Research*, **97**, 17657–17684.

Jansen, J. B. H. 1973. *The geology of Greece, Island of Naxos*. Institute for Geology and Mineral Exploration, Athens, Greece.

Jirícek, R. 1979. Tectogenetic development of the Carpathian arc in the Oligocene and Neogene. *Tectonic profiles of the West Carpathians. Geologický Ústav Dionýza Štúra, Bratislava*, 205–214.

Jolivet, L. & Patriat, M. 1999. Ductile extension and the formation of the Aegean Sea. *In*: Durand, B., Jolivet, L., Horvath, F. & Seranne, M. (eds) *The Mediterranean Basins; Tertiary Extension within Alpine Orogen*. Geological Society of London, Special Publication, **156**, 427–456,

Jolivet, L. & Faccenna, C. 2000. Mediterranean extension and the Africa-Eurasia collision. *Tectonics*, **19**, 1095–1107.

Jolivet, L. & Goffe, B. 2000. Les dômes métamorphiques extensifs dans les chaînes de montagnes: extension syn-orogénique et post-orogénique. *Comptes Rendus de l'Academie des Sciences (D)*, **330**, 739–751.

Jolivet, L. & Brun, J.-P. 2008. Cenozoic geodynamic evolution of the Aegean. *Austrian Journal of Earth Sciences*, in press.

Jolivet, L., Brun, J. P., Gautier, P., Lallemand, S. & Patriat, P. 1994. 3D Kinematics of extension in the Aegean from the early Miocene to the Present, insights from the ductile crust. *Bulletin de la Societe Geologique de France*, **165**, 195–209.

Jolivet, L., Faccenna, C., Goffé, B. *et al.* 1998. Midcrustal shear zones in post-orogenic extension: example from the northern Tyrrhenian Sea (Italy). *Journal of Geophysical Research*, **103**, 12123–12160.

Jolivet, L., Faccenna, C., Goffe, B., Burov, E. B. & Agard, P. 2003. Subduction tectonics and exhumation of high-pressure metamorphic rocks in the Mediterranean orogen. *American Journal of Science*, **303**, 353–409.

Jolivet, L., Rimmelé, G., Oberhänsli, R., Goffé, B. & Candan, O. 2004*a*. Correlation of syn-orogenic tectonic and metamorphic events in the Cyclades, the Lycian Nappes and the Menderes Massif: Geodynamic implications. *Bulletin de la Societe Geologique de France*, **175**.

Jolivet, L., Famin, V., Mehl, C., Parra, T., Aubourg, C., Hebert, R. & Philippot, P. 2004*b*. Progressive strain localization, boudinage and extensional metamorphic complexes: the Aegean Sea case. *In*: Whitney, D. L., Teyssier, C. & Siddoway, C. S. (eds) *Gneiss Domes in Orogeny*. Geological Society of America, Special Publication, **380**, 185–210.

Kapp, P., Yin, A., Manning, C. E., Murphy, M., Harrison, T. M., Spurlin, M., Lin, D. *et al.* 2000. Blueschist-bearing metamorphic core complexes in the Qiangtang block reveal deep crustal structure of northern Tibet. *Geology*, **28**, 19–22.

Karason, H. & van der Hilst, R. D. 2000. Constraints on mantle convection from seismic tomography. *In*: Richards, M. R., Gordon, R. & van der Hilst, R. D. (eds) *The history and dynamics of global plate motion*. American Geophysical Union, **121**, 277.

Karig, D. E. 1971. Origin and development of marginal basins in Western Pacific. *Journal of Geophysical Research*, **76**, 2542-&.

Karig, D. E. 1974. Evolution of arc systems in western pacific. *Annual Review of Earth and Planetary Sciences*, **2**, 51–75.

Keay, S., Lister, G. & Buick, I. 2001. The timing of partial melting, Barrovian metamorphism and granite intrusion in the Naxos metamorphic core complex, Cyclades, Aegean Sea, Greece. *Tectonophysics*, **342**, 275–312.

Kidd, W. S. F., Pan, Y., Chang, C., Coward, M. P., Dewey, J. F., Gansser, A. *et al.* 1988. Geological mapping of the 1985 *Chinese*-British Tibetan (Xizang-Qinghai) Plateau geotraverse route. *Philosophical Transactions of the Royal Society of London*, **A327**, 287–305.

Kind, R., Yuan, X., Saul, J., Nelson, D., Sobolev, S. V., Mechie, J. *et al.* 2002. Seismic Images of Crust and Upper Mantle Beneath Tibet: evidence for Eurasian Plate Subduction. *Science*, **298**, 1219–1221.

Kissel, C. & Laj, C. 1988. The Tertiary geodynamical evolution of the Aegean arc: a paleomagnetic reconstruction. *Tectonophysics*, **146**, 183–201.

Kissel, C., Laj, C., Poisson, A. & Gorur, N. 2003. Paleomagnetic reconstruction of the Cenozoic evolution of the Eastern Mediterranean. *Tectonophysics*, **362**, 199–217.

Knapp, J. H., Knapp, C. C., Raileanu, V., Matenco, L., Mocanu, V. & Dinu, C. 2005. Crustal constraints on the origin of mantle seismicity in the Vrancea zone, Romania: the case for active continental lithospheric delamination. *Tectonophysics*, **410**, 311–323.

Kosarev, G., Kind, R., Sobolev, S. V., Yuan, X., Hanka, W. & Oreshin, S. 1999. Seismic Evidence for a Detached Indian Lithospheric Mantle Beneath Tibet. *Science*, **283**, 1306–1309.

Kovac, M., Nagymarosy, A., Sotak, J. & Sutovska, K. 1993. Late Tertiary paleogeographic evolution of the western Carpathians. *Tectonophysics*, **226**, 401–415.

Kovac, M., andreyeva-Grigorovich, A., Bajraktarevic, Z., Brzobohaty, R., Filipescu, S., Fodor, L. *et al.* 2007. Badenian evolution of the Central Paratethys Sea: paleogeography, climate and eustatic sea-level changes. *Geologica Carpathica*, **58**, 579–606.

Kovacs, I. & Szabo, C. 2008. Middle Miocene volcanism in the vicinity of the Middle Hungarian zone: evidence for an inherited enriched mantle source. *Journal of Geodynamics*, **45**, 1–17.

Kozur, H. W. 1991. The evolution of the Hallstatt ocean and its significance for the early evolution of the Eastern Alps and western Carpathians. *Palaeogeography Palaeoclimatology Palaeoecology*, **87**, 109–135.

Kuhlemann, J., Frisch, W., Dunkl, I., Kazmer, M. & Schmiedl, G. 2004. Miocene siliciclastic deposits of Naxos Island: geodynamic and environmental implications for the evolution of the southern Aegean Sea. *In*: Bernet, M. & Spiegel, C. (eds) *Detrital thermochronology – Provenance analysis, exhumation, and landscape evolution of mountain belts*. Geological Society of America, **378**, 51–65.

Lacombe, O. & Jolivet, L. 2005. Structural and kinematic relationships between Corsica and the Pyrenees-Provence domain at the time of the Pyrenean orogeny. *Tectonics*, **24**.

Le Pichon, X. 1982. Land-locked oceanic basins and continental collision; the eastern Mediterranean as a case example. *In*: Hsu, K. J. (ed.) *Mountain building processes*. Academic Press, 210–211.

Le Pichon, X. & Angelier, J. 1979. The Hellenic arc and trench system; a key to the neotectonic evolution of the eastern Mediterranean area. *Tectonophysics*, **60**, 1–42.

Le Pichon, X., Chamot-Rooke, N., Lallemant, S., Noomen, R. & Veis, G. 1995. Geodetic determination of the kinematics of central Greece with respect to Europe: implications for eastern Mediterranean tectonics. *Journal of Geophysical Research*, **100**, 12675–12690.

Leat, P. T., Pearce, J. A., Barker, P. F., Millar, I. L., Barry, T. L. & Larter, R. D. 2004. Magma genesis and mantle flow at a subducting slab edge: the South Sandwich arc-basin system. *Earth and Planetary Science Letters*, **227**, 17–35.

Lesic, V., Marton, E. & Cvetkov, V. 2007. Paleomagnetic detection of Tertiary rotations in the Southern Pannonian Basin (Fruska Gora). *Geologica Carpathica*, **58**, 185–193.

Levin, V., Shapiro, N. M., Park, J. & Ritzwoller, M. H. 2002. Seismic evidence for catastrophic slab loss beneath Kamchatka. *Nature*, **418**, 763–766.

Li, X., Bock, G., Vafidis, A., Kind, R., Harjes, H.-P., Hanka, W. *et al.* 2003. Receiver function study of the Hellenic subduction zone: imaging crustal thickness variations and the oceanic Moho of the descending African lithosphere. *Geophysical Journal International*, **155**, 733–748.

Lillie, R. J., Bielik, M., Babuska, V. & Plomerova, J. 1994. Gravity modelling of the lithosphere in the Eastern Alpine-Western Carpathian-Pannonian region. *Tectonophysics*, **231**, 215–235.

Linzer, H. G. 1996. Kinematics of retreating subduction along the Carpathian arc, Romania. *Geology*, **24**, 167–170.

Linzer, H.-G., Decker, K., Peresson, H., Dell'Mour, R. & Frisch, W. 2002. Balancing lateral orogenic float of the Eastern Alps. *Tectonophysics*, **354**, 211–237.

Linzer, H.-G., Frisch, W., Zweigel, P., Girbacea, R., Hann, H.-P. & Moser, F. 1998. Kinematic evolution of the Romanian Carpathians. *Tectonophysics*, **297**, 133–156.

Lister, G. S., Banga, G. & Feenstra, A. 1984. Metamorphic core complexes of Cordilleran type in the Cyclades, Aegean Sea, Greece. *Geology*, **12**, 221–225.

Lonergan, L. & White, N. 1997. Origin of the Betic-Rif mountain belt. *Tectonics*, **16**, 504–522.

Lucente, F. P., Chiarabba, C., Cimini, G. B. & Giardini, D. 1999. Tomographic constraints on the geodynamic evolution of the Italian region. *Journal of Geophysical Research-Solid Earth*, **104**, 20307–20327.

Lucente, F. P., Margheriti, L., Piromallo, C. & Barruol, G. 2006. Seismic anisotropy reveals the long route of the slab through the western-central Mediterranean mantle. *Earth and Planetary Science Letters*, **241**, 517–529.

Lustrino, M. & Wilson, M. 2007. The circum-Mediterranean anorogenic Cenozoic igneous province. *Earth Science Reviews*, **81**, 1–65.

Lustrino, M., Melluso, L. & Morra, V. 2000. The role of lower continental crust and lithospheric mantle in the genesis of Plio-Pleistocene volcanic rocks from Sardinia (Italy). *Earth and Planetary Science Letters*, **180**, 259–270.

Makris, J. 1978. The crust and upper mantle of the Aegean region from deep seismic soundings. *Tectonophysics*, **46**, 269–284.

Makropoulos, K. C. & Burton, P. W. 1984. Greek tectonics and seismicity. *Tectonophysics*, **106**, 275–304.

Malinverno, A. & Ryan, W. B. F. 1986. Extension in the Tyrrhenian Sea and shortening in the apennines as result of arc migration driven by sinking of the lithosphere *Tectonics*, **5**, 227–245.

MANN, P. & BURKE, K. 1984. Neotectonics of the Caribbean. *Reviews of Geophysics & Space Physics*, **22**, 309–362.

MANTOVANI, E., VITI, M., ALBARELLO, D., TAMBURELLI, C., BABBUCCI, D. & CENNI, N. 2000. Role of kinematically induced horizontal forces in Mediterranean tectonics: insights from numerical modeling. *Journal of Geodynamics*, **30**, 287–320.

MANTOVANI, E., VITI, M., BABBUCCI, D., TAMBURELLI, C. & ALBARELLO, D. 2001. Back arc extension: which driving mechanism? *Journal of the Virtual Explorer*, **3**, 17–44.

MANTOVANI, E., ALBARELLO, D., BABBUCCI, D., TAMBURELLI, C. & VITI, M. 2002. Trench-Arc-BackArc systems in the Mediterranean area: Examples of Extrusion Tectonics. *In*: ROSENBAUM, G. & LISTER, G. (eds) *Reconstruction of the evolution of the Alpine-Himalayan Orogen. Journal of the Virtual Explorer*, **8**, 131–147.

MARTINI, I. P., OGGIANO, G. & MAZZEI, R. 1992. Siliciclastic-carbonate sequences of Miocene grabens of northern Sardinia, western Mediterranean Sea. *Sedimentary Geology*, **76**, 63–78.

MÁRTON, E. & FODOR, L. 2003. Tertiary paleomagnetic results and structural analysis from the Transdanubian Range (Hungary): rotational disintegration of the Alcapa unit. *Tectonophysics*, **363**, 201–224.

MÁRTON, E., KUHLEMANN, J., FRISCH, W. & DUNKL, I. 2000. Miocene rotations in the Eastern Alps – palaeomagnetic results from intramontane basin sediments. *Tectonophysics*, **323**, 163–182.

MÁRTON, E., DROBNE, K., COSOVIC, V. & MORO, A. 2003. Palaeomagnetic evidence for Tertiary counterclockwise rotation of Adria. *Tectonophysics*, **377**, 143–156.

MÁRTON, E., TISCHLER, M., CSONTOS, L., FUEGENSCHUH, B. & SCHMID, S. M. 2007. The contact zone between the ALCAPA and Tisza–Dacia megatectonic units of Northern Romania in the light of new paleomagnetic data. *Swiss Journal of Geosciences*, **100**, 109–124.

MASSON, F., CHERY, J., HATZFELD, D., MARTINOD, J., VERNANT, P., TAVAKOLI, F. & GHAFORY-ASHTIANI, M. 2005. Seismic versus aseismic deformation in Iran inferred from earthquakes and geodetic data. *Geophysical Journal International*, **160**, 217–226.

MATENCO, L., BERTOTTI, G., LEEVER, K., CLOETINGH, S., SCHMID, S. M., TARAPOANCA, M. & DINU, C. 2007. Large-scale deformation in a locked collisional boundary: interplay between subsidence and uplift, intraplate stress, and inherited lithospheric structure in the late stage of the SE Carpathians evolution. *Tectonics*, **26**.

MATTAUER, M., FAURE, M. & MALAVIEILLE, J. 1981. Transverse lineation and large-scale structures related to Alpine obduction in Corsica. *Journal of Structural Geology*, **3**, 401–409.

MATTE, P. 2001. The Variscan collage and orogeny (480–290 Ma) and the tectonic definition of the Armorica microplate: a review. *Terra Nova*, **13**, 122–128.

MATTEI, M., FUNICIELLO, R. & KISSEL, C. 1995. Paleomagnetic and structural evidence for neogene block rotations in the central Apennines Italy. *Journal of Geophysical Research-Solid Earth*, **100**, 17863–17883.

MCCLUSKY, S. C., BALASSANIAN, S., BARKA, A., DEMIR, C., ERGINTA V, S., GEORGIEV, I. *ET AL.* 2000. Global Positioning System constraints on plate kinematics and dynamics in the eastern Mediterranean and Caucasus. *Journal of Geophysical Research*, **105**, 5695–5719.

MCCLUSKY, S., REILINGER, R., MAHMOUD, S., BEN SARI, D. & TEALEB, A. 2003. GPS constraints on Africa (Nubia) and Arabia plate motions. *Geophysical Journal International*, **155**, 126–138.

MCKENZIE, D. P. 1972. Active tectonics of the Mediterranean region. *Geophysical Journal of the Royal Astronomical Society*, **30**, 109–185.

MCKENZIE, D. P. 1978. Active tectonics of the Alpine-Himalayan belt: the Aegean Sea and surrounding regions. *Geophysical Journal of the Royal Astronomical Society*, **55**, 217–254.

MEADE, B. J., HAGER, B. H., MCCLUSKY, S. C., REILINGER, R., ERGINTAV, S., LENK, O. *ET AL.* 2002. Estimates of seismic potential in the Marmara Sea region from block models of secular deformation constrained by global positioning system measurements. *Bulletin of the Seismological Society of America*, **92**, 208–215.

MEIJER, P. T. & WORTEL, M. J. R. 1997. Present-day dynamics of the Aegean region: A model analysis of the horizontal pattern of stress and deformation. *Tectonics*, **16**, 879–895.

MERCIER, J.-L. 1979. Signification neotectonique de l'Arc Egeen; une revue des idees. A review of the neotectonic significance of the Aegean Arc. *Revue de Geographie Physique et de Geologie Dynamique*, **21**, 5–15.

MEULENKAMP, J. E., KOVAC, M. & CICHA, I. 1996. On Late Oligocene to Pliocene depocentre migrations and the evolution of the Carpathian-Pannonian system. *Tectonophysics*, **266**, 301–317.

MOCEK, B. 2001. Geochemical evidence for arc-type volcanism in the Aegean Sea: the blueschist unit of Siphnos, Cyclades (Greece). *Lithos*, **57**, 263–289.

MOLLI, G., TRIBUZIO, R. & MARQUER, D. 2006. Deformation and metamorphism at the eastern border of the Tenda Massif (NE Corsica): a record of subduction and exhumation of continental crust. *Journal of Structural Geology*, **28**, 1748–1766.

MONTUORI, C., CIMINI, G. B. & FAVALI, P. 2007. Teleseismic tomography of the southern Tyrrhenian subduction zone: new results from seafloor and land recordings. *Journal of Geophysical Research-Solid Earth*, **112**.

MORELLI, A. & BARRIER, E. 2004. *Geodynamic map of the Mediterranean.* Commission for the Geological Map of the World, Limoges, France.

MORLEY, C. K. 1993. Discussion of origins of hinterland basins to the Rif-Betic Cordillera and Carpathians. *Tectonophysics*, **226**, 359–376.

MORRIS, A. 2000. Magnetic fabric and palaeomagnetic analyses of the Plio–Quaternary calc–alkaline series of Aegina Island, South Aegean volcanic arc, Greece. *Earth and Planetary Science Letters*, **176**, 91–105.

MORRIS, A. & ANDERSON, M. 1996. First palaeomagnetic results from the Cycladic Massif, Greece, and their implications for Miocene extension directions and tectonic models in the Aegean. *Earth and Planetary Science Letters*, **142**, 397–408.

MUTTONI, G. 1998. Paleomagnetic evidence for Neogene tectonic rotations in the northern Apennines, Italy. *Earth and Planetary Science Letters*, **154**, 25–40.

NEMCOK, M. 1998*a*. Tertiary extension development and extension/compression interplay in the West Carpathian mountain belt. *Tectonophysics*, **290**, 137–167.

NEMCOK, M. 1998*b*. Tertiary subduction and slab break-off model of the Carpathian-Pannonian region. *Tectonophysics*, **295**, 307–340.

NEMCOK, M. 1998*c*. Strain partitioning along the western margin of the Carpathians. *Tectonophysics*, **292**, 119–143.

NICOLOSI, I., SPERANZA, F. & CHIAPPINI, M. 2006. Ultrafast oceanic spreading of the Marsili Basin, southern Tyrrhenian Sea: Evidence from magnetic anomaly analysis. *Geology*, **34**, 717–720.

NOOMEN, R., SPRINGER, T. A., AMBROSIUS, B. A. C., HERZBERGER, K., KUIJPER, D. C., METS, G.-J. ET AL. 1996. Crustal deformations in the mediterranean area computed from SLR and GPS observations. *Journal of Geodynamics*, **21**, 73–96.

NYST, M. & THATCHER, W. 2004. New constraints on the active tectonic deformation of the Aegean. *Journal of Geophysical Research*, **109**.

OKAY, A. I., SENGÖR, A. M. C. & GÖRÜR, N. 1994. Kinematic history of the opening of the Black Sea and its effect on the surrounding regions. *Geology*, **22**, 267–270.

OKRUSCH, M. & BRÖCKER, M. 1990. Eclogites associated with high-grade blueschists in the Cyclades archipelago, Greece: a review. *European Journal of Mineralogy*, **2**, 451–478.

OLDOW, J. S., FERRANTI, L., LEWIS, D. S., CAMPBELL, J. K., D'ARGENIO, B., CATALANO, R., PAPPONE, G., CARMIGNANI, L., CONTI, P. & AIKEN, C. L. V. 2002. Active fragmentation of Adria, the north African promontory, central Mediterranean orogen. *Geology*, **30**, 779–782.

ONCESCU, M. C. 1987. On the stress tensor in Vrancea region. *Journal of Geophysics*, **62**, 62–65.

PAN, Y. & KIDD, W. S. F. 1992. Nyainqentanglha shear zone; a late Miocene extensional detachment in the southern Tibetan Plateau. *Geology*, **20**, 775–778.

PANA, D. & ERDMER, P. 1994. Alpine crustal shear zones and pre-Alpine basement terranes in the Romanian Carpathians and Apuseni Mountains. *Geology*, **22**, 807–810.

PAPAIONNOU, C. & PAPAZACHOS, C. B. 2000. Time-independent and time-dependent seismic hazard in Greece based upon seisomogenic sources. *Bulletin of the Seismological Society of America*, **90**, 22–33.

PAPAZACHOS, B. C. 1973. Distribution of seismic foci in the Mediterranean and surrounding area and its tectonic implication. *Geophysical Journal of the Royal Astronomical Society*, **33**, 419–428.

PAPAZACHOS, B. C., HATZIDIMITRIOU, P. M., PANAGIOTOPOULOS, D. G. & TSOKAS, G. N. 1995. Tomography of the crust and upper mantle in southeast Europe. *Journal of Geophysical Research*, **100**, 12405–12422.

PAPAZACHOS, B. C., KARAKOSTAS, V. G., PAPAZACHOS, C. B. & SCORDILIS, E. M. 2000. The geometry of the Wadati-Benioff zone and lithospheric kinematics in the Hellenic arc. *Tectonophysics*, **319**, 275–300.

PARSONS, B. & MCKENZIE, D. 1978. Mantle convection and thermal structure of plates. *Journal of Geophysical Research*, **83**, 4485–4496.

PATRIAT, P. & ACHACHE, J. 1984. India-Eurasia collision chronology has implications for crustal shortening and driving mechanism of plates. *Nature*, **311**, 615–621.

PATZAK, M., OKRUSCH, M. & KREUZER, H. 1994. The Akrotiri unit on the island of Tinos, Cyclades, Greece: witness of a lost terrane of Late Cretaceous age. *Neues Jahrbuch für Geologie und Palaeontologie*, **194**.

PE-PIPER, G. 2000. Origin of S-type granites coeval with I-type granites in the Hellenic subduction system, Miocene of Naxos, Greece. *European Journal of Mineralogy*, **12**, 859–875.

PE-PIPER, G. & PIPER, D. J. W. 2002. *The igneous rocks of Greece*. Borntraeger, Berlin.

PE-PIPER, G., KOTOPOULI, C. N. & PIPER, D. J. W. 1997. Granitoid rocks of Naxos, Greece; regional geology and petrology. *Geological Journal*, **32**, 153–171.

PE-PIPER, G., PIPER, D. J. W. & MATARANGAS, D. 2002. Regional implications of geochemistry and style of emplacement of Miocene I-type diorite and granite, Delos, Cyclades, Greece. *Lithos*, **60**, 47–66.

PÊCHER, A., BOUCHEZ, J. L. & LE FORT, P. 1991. Miocene dextral shearing between Himalaya and Tibet. *Geology*, **19**, 683–685.

PECSKAY, Z., LEXA, J., SZAKACS, A., SEGHEDI, I., BALOGH, K., KONECNY, V. ET AL. 2006. Geochronology of Neogene magmatism in the Carpathian arc and intra-Carpathian area. *Geologica Carpathica*, **57**, 511–530.

PERESSON, H. & DECKER, K. 1997. Far-field effects of Late Miocene subduction in the Eastern Carpathians: E-W compression and inversion of structures in the Alpine-Carpathian-Pannonian region. *Tectonics*, **16**, 38–56.

PETRAKAKIS, K., ZAMOLYI, A., IGLSEDER, C., RAMBOUSEK, C., GRASEMANN, B., DRAGANITS, E. & PHOTIADIS, A. (eds) 2008. Geological Map of Greece: Serifos Island in IGME *1:50 000 Cycladic maps*.

PINDELL, J. L., CANDE, S. C., PITMAN, W. C., ROWLEY, D. B., DEWEY, J. F., LABRECQUE, J. & HAXBY, W. 1988. A plate-kinematic framework for models of Caribbean evolution. *Tectonophysics*, **155**, 121–138.

PIROMALLO, C. & MORELLI, A. 2003. P wave tomography of the mantle under the Alpine-Mediterranean area. *Journal of Geophysical Research-Solid Earth*, **108**.

PIROMALLO, C. & FACCENNA, C. 2004. How deep can we find the traces of Alpine subduction? *Geophysical Research Letters*, **31**, L06605, doi:10.1029/2003GL019288.

PLASIENKA, D. & KOVAC, M. 1999. How to loop Carpathians – An attempt to reconstruct Mesocenozoic palinspastic history of the Carpathian orocline. *Geologica Carpathica*, **50**, 163–165.

PLATT, J. P. 2007. From orogenic hinterlands to Mediterranean-style back-arc basins: a comparative analysis. *Journal of the Geological Society*, **164**, 297–311.

PLATT, J. P. & VISSERS, R. L. M. 1989. Extensional collapse of thickened continental lithosphere – a working hypothesis for the alboran sea and Gibraltar Arc. *Geology*, **17**, 540–543.

PLATT, J. P., SOTO, J. I. & COMAS, M. C. 1996. Decompression and high-temperature-low-pressure metamorphism in the exhumed floor of an extensional basin, Alboran Sea, western Mediterranean. *Geology*, **24**, 447–450.

PONDRELLI, S., PIROMALLO, C. & SERPELLONI, E. 2004. Convergence vs. retreat in Southern Tyrrhenian Sea: Insights from kinematics. *Geophysical Research Letters*, **31**, L06611, doi:10.1029/2003GL01922.

PULLEN, A., KAPP, P., GEHRELS, G. E., VERVOORT, J. D. & DING, L. 2008. Triassic continental subduction in central Tibet and Mediterranean-style closure of the Paleo-Tethys Ocean. *Geology*, **36**, 351–354.

RAMBOUSEK, C. 2007. Low temperature deformation of a detachment on Serifos Metamorphic Core Complex, Cyclades, Greece. Pages 140. University of Vienna, Vienna.

RATSCHBACHER, L., BEHRMANN, J. H. & PAHR, A. 1990. Penninic windows at the eastern end of the Alps and their relation to the intra-Carpathian basins. *Tectonophysics*, **172**, 91–105.

RATSCHBACHER, L., FRISCH, W. & LINZER, H. G. 1991. Lateral extrusion in the Eastern Alps. Part 2: structural analysis. *Tectonics*, **10**, 257–271.

REILINGER, R. E., MCCLUSKY, S. C., ORAL, M. B., KING, R. W. & TOKSOZ, M. N. 1997. Global positioning systems measurements of present-day crustal movements in the Arabia-Africa-Eurasia plate collision zone. *Journal of Geophysical Research*, **102**, 9983–9999.

REILINGER, R., MCCLUSKY, S., VERNANT, P., LAWRENCE, S., ERGINTAV, S., CAKMAK, R. *ET AL*. 2006. GPS constraints on continental deformation in the Africa-Arabia-Eurasia continental collision zone and implications for the dynamics of plate interactions. *Journal of Geophysical Research-Solid Earth*, **111**.

RING, U. & LAYER, P. W. 2003. High-pressure metamorphism in the Aegean, eastern Mediterranean: Underplating and exhumation from the Late Cretaceous until the Miocene to Recent above the retreating Hellenic subduction zone. *Tectonics*, **22**.

ROBERTSON, A. H. F., USTAOMER, T., PICKETT, E. A., COLLINS, A. S., ANDREW, T. & DIXON, J. E. 2004. Testing models of Late Palaeozoic Early Mesozoic orogeny in Western Turkey: support for an evolving open-Tethys model. *Journal of the Geological Society*, **161**, 501–511.

ROSENBAUM, G. & LISTER, G. S. 2004. Neogene and Quaternary rollback evolution of the Tyrrhenian Sea, the Apennines, and the Sicilian Maghrebides. *Tectonics*, **23**.

ROSENBAUM, J. M., WILSON, M. & DOWNES, H. 1997. Multiple enrichment of the Carpathian-Pannonian mantle: Pb-Sr-Nd isotope and trace element constraints. *Journal of Geophysical Research-Solid Earth*, **102**, 14947–14961.

ROSENBAUM, G., REGENAUER-LIEB, K. & WEINBERG, R. 2005. Continental extension: from core complexes to rigid block faulting. *Geology*, **33**, 609–612.

ROSSETTI, F., GOFFÉ, B., MONIÉ, P., FACCENNA, C. & VIGNAROLI, G. 2004. Alpine orogenic P-T-t-deformation history of the Catena Costiera area and surrounding regions (Calabrian Arc, southern Italy): the nappe edifice of north Calabria revised with insights on the Tyrrhenian-Apennine system formation. *Tectonics*, **23**, 1–26.

ROYDEN, L. H., HORVATH, F. & RUMPLER, J. 1983*a*. Evolution of the Pannonian basin system, 1: tectonics. *Tectonics*, **2**, 63–90.

ROYDEN, L. H., HORVATH, F., NAGYMAROSY, A. & STEGENA, L. 1983*b*. Evolution of the Pannonian basin system, 2: subsidence and thermal history *Tectonics*, **2**, 91–137.

ROYDEN, L. H. 1993*a*. The steady state thermal structure of eroding orogenic belts and accretionary prism. *Journal of Geophysical Research*, **98**, 4487–4507.

ROYDEN, L. H. 1993*b*. Evolution of retreating subduction boundaries formed during continental collision. *Tectonics*, **12**, 629–638.

SACHSENHOFER, R. F. 2001. Syn- and post-collisional heat flow in the Cenozoic Eastern Alps. *International Journal of Earth Sciences*, **90**, 579–592.

SANDVOL, E., TURKELLI, N., ZOR, E., GOK, R., BEKLER, T., GURBUZ, C. *ET AL*. 2003. Shear Wave Splitting in a Young Continent-Continent Collision: An Example from Eastern Turkey. *Geophysical Research Letters*, **30**, 8041 – doi:10.1029/2003*GL*018912.

SCALERA, G. 2006. The Mediterranean as a slowly nascent ocean. *Annals of Geophysics*, **49**, 451–482.

SCHÄRER, U., HAMET, J. & ALLÈGRE, C. J. 1984. The Tans-Himalaya (Gangdese) plutonic belt in the Ladakh region: a U-Pb and Rb-Sr study. *Earth and Planetary Science Letters*, **67**, 327–339.

SCHEEPERS, P. J. J., LANGEREIS, C. G. & HILGEN, F. J. 1993. Counter-clockwise rotations in the southern Apennines during the Pleistocene - paleomagnetic evidence from the Matera area. *Tectonophysics*, **225**, 379–410.

SCHELLART, W. P., FREEMAN, J., STEGMAN, D. R., MORESI, L. & MAY, D. 2007. Evolution and diversity of subduction zones controlled by slab width. *Nature*, **446**, 308–311.

SCHIANO, P., CLOCCHIATTI, R., OTTOLINI, L. & BUSA, T. 2001. Transition of Mount Etna lavas from a mantle-plume to an island-arc magmatic source. *Nature*, **412**, 900–904.

SCHMID, S. M., FÜGENSCHUH, B., KISSLING, E. & SCHUSTER, R. 2004. Tectonic map and overall architecture of the Alpine orogen. *Eclogae geologicae Helvetiae*, **97**, 93–117.

SCHNEIDER, D. A., EDWARDS, M. A., KIDD, W. S. F., KHAN, A. M., SEEBER, L. & ZEITLER, P. K. 1999. Tectonics of Nanga Parbat, western Himalaya: Synkinematic plutonism within the doubly vergent shear zones of a crustal-scale pop-up structure. *Geology*, **27**, 999–1002.

Schneider, D. A., Zahniser, S. J., Glascock, J. M., Gordon, S. M. & Manecki, M. 2006. Thermochronology of the west Sudetes (Bohemian Massif): rapid and repeated eduction in the eastern Variscides, Poland and Czech Republic. *American Journal of Science*, **306**, 846–873.

Sclater, J. G., Royden, L., Horvath, F., Burchfiel, B. C., Semken, S. & Stegena, L. 1980. The formation of the intra-Carpathian basins as determined from subsidence data. *Earth and Planetary Science Letters*, **51**, 139–162.

Sella, G. F., Dixon, T. H. & Mao, A. L. 2002. REVEL: A model for Recent plate velocities from space geodesy. *Journal of Geophysical Research-Solid Earth*, **107**.

Serpelloni, E., Anzidei, M., Baldi, P., Casula, G. & Galvani, A. 2005. Crustal velocity and strain-rate fields in Italy and surrounding regions: new results from the analysis of permanent and non-permanent GPS networks. *Geophysical Journal International*, **161**, 861–880.

Serpelloni, E., Anzidei, M., Baldi, P., Casula, G. & Galvania, A. 2006. GPS measurement of active strains across the Apennines; Frontiers in earth sciences; new ideas and new interpretations. *Annals of Geophysics*, **49**, 319–329.

Serpelloni, E., Vannucci, G., Pondrelli, S., Argnani, A., Casula, G., Anzidei, M., Baldi, P. & Gasperini, P. 2007. Kinematics of the Western Africa-Eurasia plate boundary from focal mechanisms and GPS data. *Geophysical Journal International*, **169**, 1180–1200.

Shen, Z. K., Zhao, C. K., Yin, A., Li, Y. X., Jackson, D. D., Fang, P. & Dong, D. N. 2000. Contemporary crustal deformation in east Asia constrained by Global Positioning System measurements. *Journal of Geophysical Research-Solid Earth*, **105**, 5721–5734.

Shen, Z. K., Lu, J. N., Wang, M. & Burgmann, R. 2005. Contemporary crustal deformation around the southeast borderland of the Tibetan Plateau. *Journal of Geophysical Research-Solid Earth*, **110**.

Sleep, N. & Toksoz, M. N. 1971. Evolution of Marginal Basins. *Nature*, **233**, 548–550.

Sokoutis, D., Brun, J. P., van den Driessche, J. & Pavlides, S. 1993. A major Oligo-Miocene detachment in southern Rhodope controlling north Aegean extension. *Journal of the Geological Society*, **150**, 243–246.

Sol, S., Meltzer, A., Burgmann, R., van der Hilst, R. D., King, R., Chen, Z. *et al.* 2007. Geodynamics of the southeastern Tibetan Plateau from seismic anisotropy and geodesy. *Geology*, **35**, 563–566.

Sowerbutts, A. 2000. Sedimentation and volcanism linked to multiphase rifting in an Oligo-Miocene intra-arc basin, Anglona, Sardinia. *Geological Magazine*, **137**, 395–418.

Spakman, W. & Wortel, M. J. R. 2003. A tomographic view on Western Mediterranean geodynamics. *In*: Cavazza, W., Roure, F., Spakman, W., Stampfli, G. M. & Ziegler, P. A. (eds) *The TRANSMED atlas – the Mediterranean region from crust to mantle: geological and geophysical framework of the Mediterranean and the surrounding areas*. Springer-Verlag Berlin, Heidelberg, 31–52.

Spakman, W., Wortel, M. J. R. & Vlaar, N. J. 1988. The Hellenic subduction zone: a tomographic image and its geodynamic implications. *Geophysical Research Letters*, **15**, 60–63.

Sperner, B., Ratschbacher, L. & Nemcok, M. 2002. Interplay between subduction retreat and lateral extrusion: Tectonics of the Western Carpathians. *Tectonics*, **21**.

Sperner, B., Ioane, D. & Lillie, R. J. 2004. Slab behaviour and its surface expression: new insights from gravity modelling in the SE-Carpathians. *Tectonophysics*, **382**, 51–84.

Sroda, P. *et al.* 2006. Crustal and upper mantle structure of the Western Carpathians from CELEBRATION 2000 *profiles CEL*01 and CEL04: seismic models and geological implications. *Geophysical Journal International*, **167**, 737–760.

Stampfli, G. M. & Borel, G. D. 2002. A plate tectonic model for the Paleozoic and Mesozoic constrained by dynamic plate boundaries and restored synthetic oceanic isochrons. *Earth and Planetary Science Letters*, **196**, 17–33.

Stegena, L., Geczy, B. & Horvath, F. 1975. Late Cenozoic evolution of the Pannonian basin. *Tectonophysics*, **26**, 71–90.

Stöcklin, J. 1968. Structural history and tectonics of Iran: a review. *Bulletin of the American Association of Petroleum Geologists*, **52**, 1229–1258.

Szafian, P. & Horvath, F. 2006. Crustal structure in the Carpatho-Pannonian region: insights from three-dimensional gravity modelling and their geodynamic significance. *International Journal of Earth Sciences*, **95**, 50–67.

Tapponnier, P., Mercier, J.-L., Proust, F., andrieux, J., Armijo, R., Bassoullet, J. P. *et al.* 1981. The Tibetan side of the India-Eurasia collision. *Nature*, **294**, 405–410.

Tapponnier, P., Peltzer, G. & Armijo, R. 1986. On the mechanics of the collision between India and Asia. *In*: Coward, M. P. & Ries, A. C. (eds) *Collisional Tectonics*. Geological Society, London, Special Publications, **19**, 115–157.

Tari, G., Horvath, F. & Rumpler, J. 1992. Styles of extension in the Pannonian basin *Tectonophysics*, **208**, 203–219.

Tatar, M., Hatzfeld, D., Moradi, A. S. & Paul, A. 2005. The 2003 December 26 Bam earthquake (Iran), Mw 6.6, aftershock sequence. *Geophysical Journal International*, **163**, 90–105.

Taylor, B. & Karner, G. D. 1983. On the evolution of marginal basins. *Reviews of Geophysics*, **21**, 1727–1741.

Taymaz, T., Jackson, J. A. & McKenzie, D. 1991. Active tectonics of the north and central Aegean Sea. *Geophysical Journal International*, **106**, 433–490.

Tilmann, F., Ni, J. & INDEPTH III Seismic Team. 2003. Seismic Imaging of the Downwelling Indian Lithosphere Beneath Central Tibet. *Science*, **300**, 1424–1427, http://pangea.stanford.edu/research/groups/crustal/docs/Tilmann.IN3tomography.science.2003.pdf.

Tirel, C., Gueydan, F., Tiberi, C. & Brun, J. P. 2004. Aegean crustal thickness inferred from gravity inversion. Geodynamical implications. *Earth and Planetary Science Letters*, **228**, 267–280.

TIREL, C., WORTEL, M. J. R., BRUN, J. B., GOVERS, R. & BUROV, E. 2007. *Back-arc extension in the Aegean Sea*. EGU2007-A-09683; TS10.5/GD12/SM19-1WE4P-0967.

TIREL, C., GAUTIER, P., VAN HINSBERGEN, D. J. J. & WORTEL, M. J. R. 2009. Sequential development of interfering metamorphic core complexes: numerical experiments and comparison with the Cyclades, Greece. *In*: VAN HINSBERGEN, D. J. J., EDWARDS, M. A. & GOVERS, R. (eds) *Geodynamics of collision and collapse at the Africa–Arabia–Eurasia subduction-zone*. Geological Society, London, Special Publications, **311**, 257–292.

TISCHLER, M., GROGER, H. R., FUGENSCHUH, B. & SCHMID, S. M. 2007. Miocene tectonics of the Maramures area (Northern Romania): implications for the Mid-Hungarian fault zone. *International Journal of Earth Sciences*, **96**, 473–496.

TURNER, S., ARNAUD, N., LIU, J., ROGERS, N., HAWKESWORTH, C., HARRIS, N., KELLEY, S., VAN CALSTEREN, P. & DENG, W. 1996. Post-collision, shoshonitic volcanism on the Tibetan Plateau: implications for convective thinning of the lithosphere and the source of ocean island basalts. *Journal of Petrology*, **37**, 45–71.

URAI, J. L., SCHUILING, R. D. & JANSEN, J. B. H. 1990. Alpine deformation on Naxos (Greece). *In*: KNIPE, R. J. & RUTTER, E. H. (eds) *Deformation mechanisms, rheology and tectonics*. Geological Society, London, Special Publications, **54**, 509–522.

UYEDA, S. & KANAMORI, H. 1979. Back-arc opening and the mode of subduction. *Journal of Geophysical Research*, **84**, 1049–1061.

VAN DER HOEVEN, A. G. A., MOCANU, V., SPAKMAN, W., NUTTO, M., NUCKELT, A., MATENCO, L. *ET AL*. 2005. Observation of present-day tectonic motions in the Southeastern Carpathians: results of the ISES/CRC-461 GPS measurements. *Earth and Planetary Science Letters*, **239**, 177–184.

VAN HINSBERGEN, D. J. J. & MEULENKAMP, J. E. 2006. Neogene supradetachment basin development on Crete (Greece) during exhumation of the South Aegean core complex. *Basin Research*, **18**, 103–124.

VAN HINSBERGEN, D. J. J., LANGEREIS, C. G. & MEULENKAMP, J. E. 2005*a*. Revision of the timing, magnitude and distribution of Neogene rotations in the western Aegean region. *Tectonophysics*, **396**, 1–34.

VAN HINSBERGEN, D. J. J., HAFKENSCHEID, E., SPAKMAN, W., MEULENKAMP, J. E. & WORTEL, R. 2005*b*. Nappe stacking resulting from subduction of oceanic and continental lithosphere below Greece. *Geology*, **33**, 325–328.

VAN HINSBERGEN, D. J. J., VAN DER MEER, D. G., ZACHARIASSE, W. J. & MEULENKAMP, J. E. 2006. Deformation of western Greece during Neogene clockwise rotation and collision with Apulia. *International Journal of Earth Sciences*, **95**, 463–490.

VANDERHAEGHE, O., TEYSSIER, C., MCDOUGALL, I. & DUNLAP, W. J. 2003*a*. Cooling and exhumation of the Shuswap Metamorphic Core Complex constrained by Ar-40/Ar-39 thermochronology. *Geological Society of America Bulletin*, **115**, 200–216.

VANDERHAEGHE, O., DUCHÊNE, S., HIBSCH, C., MARTIN, L., MALARTRE, F., AISSA, R. *ET AL*. 2003*b*. Tectonic evolution of Naxos (Cyclades): a record of heat and mass transfer during orogeny. *European Geophysical Society Geophysical Research Abstracts*, **5**, 05015.

VERNANT, P., NILFOROUSHAN, F., HATZFELD, D., ABBASI, M. R., VIGNY, C., MASSON, F. *ET AL*. 2004. Present-day crustal deformation and plate kinematics in the Middle East constrained by GPS measurements in Iran and northern Oman. *Geophysical Journal International*, **157**, 381–398.

VIGLIOTTI, L. & LANGENHEIM, V. E. 1995. When did Sardinia stop rotating – new paleomagnetic results. *Terra Nova*, **7**, 424–435.

VRABEC, M. & FODOR, L. 2006. Late cenozoic tectonics of slovenia: structural styles at the northeastern corner of the adriatic microplate. *In*: PINTER, N. & GYULA, G. (eds) *The Adria Microplate: GPS Geodesy, Tectonics and Hazards*, Springer, Netherlands, 151–168.

WALCOTT, C. R. & WHITE, S. H. 1998. Constraints on the kinematics of post-orogenic extension imposed by stretching lineations in the Aegean region. *Tectonophysics*, **298**, 155–175.

WAWRZENITZ, N. & KROHE, A. 1998. Exhumation and doming of the Thasos metamorphic core complex (S Rhodope, Greece): structural and geochronological constraints. *Tectonophysics*, **285**, 301–332.

WIJBRANS, J. R. & MCDOUGALL, I. 1988. Metamorphic evolution of the Attic Cycladic metamorphic belt on Naxos (Cyclades, Greece) utilizing ^{40}Ar/^{39}Ar age spectrum measurements. *Journal of Metamorphic Geology*, **6**, 571–594.

WIJBRANS, J. R., SCHLIESTEDT, M. & YORK, D. 1990. Single grain argon laser probe dating of phengites from the blueschist to greenschist transition on Sifnos (Cyclades, Greece). *Contributions to Mineralogy and Petrology*, **104**, 582–593.

WILSON, J. T. 1966. Did the Atlantic close and then re-open? *Nature*, **211**, 676–681.

WITTLINGER, G., FARRA, V. & VERGNE, J. 2004. Lithospheric and upper mantle stratifications beneath Tibet: new insights from Sp conversions. *Geophysical Research Letters*, **31**.

WORTEL, M. J. R. & SPAKMAN, W. 2000. Subduction and Slab Detachment in the Mediterranean-Carpathian Region. *Science*, **290**, 1910–1917.

YIN, A. & HARRISON, T. M. 2000. Geologic Evolution of the Himalayan-Tibetan Orogen. *Annual Review of Earth and Planetary Sciences*, **28**, 211–280.

ZAMOLYI, A. 2006. Geomorphological signal of the Serifos Metamorphic Core Complex, Cyclades, Greece. University of Vienna, Vienna.

ZELLMER, G., TURNER, S. & HAWKESWORTH, C. 2000. Timescales of destructive plate margin magmatism: new insights from Santorini, Aegean volcanic arc. *Earth and Planetary Science Letters*, **174**, 247–263.

ZHANG, K. J. 2001. Blueschist-bearing metamorphic core complexes in the Qiangtang block reveal deep crustal structure of northern Tibet: Comment and Reply: COMMENT. *Geology*, **29**, 663–664.

ZHANG, P. Z., SHEN, Z., WANG, M., GAN, W. J., BURGMANN, R. & MOLNAR, P. 2004. Continuous deformation of the Tibetan Plateau from global positioning system data. *Geology*, **32**, 809–812.

ZHANG, K. J., ZHANG, Y. X., LI, B., ZHU, Y. T. & WEI, R. Z. 2006. The blueschist-bearing Qiangtang metamorphic belt (northern Tibet, China) as an in situ suture zone: Evidence from geochemical comparison with the Jinsa suture. *Geology*, **34**, 493–496.

ZWEIGEL, P., RATSCHBACHER, L. & FRISCH, W. 1997. Kinematics of an arcuate fold–thrust belt: the southern Eastern Carpathians (Romania). *Tectonophysics*, **297**, 177–207.

Evolution of the southern Tyrrhenian slab tear and active tectonics along the western edge of the Tyrrhenian subducted slab

ANDREA ARGNANI*

ISMAR–CNR, Sede di Bologna, Via Gobetti 101, 40129 Bologna, Italy

**Corresponding author (e-mail: andrea.argnani@ismar.cnr.it)*

Abstract: The evolution of the southern Tyrrhenian subduction has been possibly controlled by distinct episodes of slab break-off as indicated by a critical review of the geological literature and by the analysis of purposely acquired multichannel seismic profiles. Within the proposed interpretation the first episode occurred from 8.5 to 4.0 Ma and affected the segment of the slab located in the Sardinia Channel, causing the abandonment of the Adventure thrust front in western Sicily. The second episode occurred between 2.5 and 1.6 Ma, affecting the segment of slab located north of Sicily, and was preceeded by rifting in the Strait of Sicily. The space and time location of these episodes appear controlled by discontinuities pre-existing within the subducted African plate that trend at high angle to the advancing subduction front. These discontinuities delimit segment of subducted slab that can be affected by slab break-off and can act as wayouts for magma and mantle derived He. The major of these discontinuities, the Malta Escarpment, has been reactivated in the Quaternary as a trench-perpendicular tear (STEP faults). Ultimately, the hierarchy in strength of these trench-perpendicular features could have affected the timing and amount of trench retreat and backarc opening.

The Africa–Eurasia plate boundary along the southern Tyrrhenian region is characterized by a lateral change from soft-collision in Sicily to oceanic subduction underneath Calabria (Fig. 1). The occurrence of a continent-to-ocean transition within the subducted plate (Africa), where the Ionian oceanic lithosphere passes to the west to the continental lithosphere of Sicily, is responsible for these two different geodynamic regimes being adjacent along the same convergent boundary.

The distribution of seismicity with depth (e.g. Chiarabba *et al.* 2005) and P-wave seismic tomography (Lucente *et al.* 1999; Wortel & Spakman 2000; Piromallo & Morelli 2003; Spakman & Wortel 2004; Montuori *et al*. 2007) support the occurrence of a deep and narrow Ionian slab located beneath Calabria. On the other hand, P-wave seismic tomography suggests that lithospheric slab is absent underneath Sicily and the southern Apennines, to support the occurrence of slab tears affecting the subducted African lithosphere (e.g. Wortel & Spakman 2000), and S-wave propagation from intermediate to deep earthquakes located within the Tyrrhenian slab indicates that S-waves could not efficiently reach many stations located in the Southern Apennines and western Sicily, on either side of the slab, because they were attenuated when travelling through the asthenosphere (Mele 1998). Theoretical work and laboratory models strongly suggest that tears within the subducted lithosphere play a major role in the dynamic behaviour of subducted slab, particularly in controlling the extent and velocity of trench retreat, together with slab width (Dvorkin *et al.* 1993; Kincaid & Griffiths 2003; Funiciello *et al.* 2006; Schellart *et al.* 2007). The conceptual implications of slab tears have been widely applied to the tectonic evolution of the Mediterranean, with the slab window imaged by tomography in the southern Tyrrhenian as a chief example (Carminati *et al.* 1998; Wortel & Spakman 2000; Argnani 2000; Faccenna *et al.* 2004; Goes *et al.* 2004; Rosenbaum & Lister 2004). Moreover, recent studies on SKS splitting in the central Mediterranean show some indication of the toroidal flow that is expected on the western side of the Tyrrhenian slab to compensate for its rollback (Civello & Margheriti 2004; Faccenna *et al.* 2005: Baccheschi *et al.* 2007).

The peculiar tectonic regime resulting from the propagation of a lithospheric tear that cuts a subducted slab has been conceptually explored by Govers & Wortel (2005) who proposed the name Subduction-Transform Edge Propagator (STEP) fault. Their numerical modelling indicates that significant deformation and rotation of the strain axes are expected along such STEP faults, although acknowledging that these processes are geologically poorly documented.

Several lines of evidence suggest that the Ionian lithosphere is passively sinking and torn apart from the buoyant Hyblean–Pelagian lithosphere during the final stage of the southern Tyrrhenian backarc opening (e.g. Gvirtzman & Nur 1999*a*; Argnani 2000; Doglioni *et al.* 2001). In fact, the western

From: VAN HINSBERGEN, D. J. J., EDWARDS, M. A. & GOVERS, R. (eds) *Collision and Collapse at the Africa–Arabia–Eurasia Subduction Zone*. The Geological Society, London, Special Publications, **311**, 193–212.
DOI: 10.1144/SP311.7 0305-8719/09/$15.00

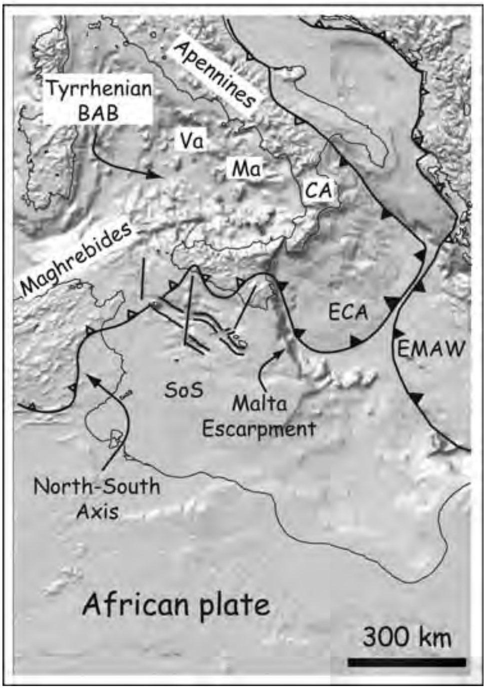

Fig. 1. Main tectonic elements of the central Mediterranean region. Empty triangle along the plate boundary indicate collision (soft collision in the Maghrebides and southern Apennines), whereas filled triangles represent oceanic subduction. Va: Vavilov basin, Ma: Marsili basin, CA: Calabrian Arc, ECA: External Calabrian Arc, EMAW: Eastern Mediterranean Accretionary Wedge, SoS: Strait of Sicily, BAB: backarc basin. In this figure and in the following topography is from ETOPO-2 global dataset.

edge of the Tyrrhenian slab is taken by Govers & Wortel (2005) as a candidate of ongoing STEP with the fault propagating southward along the Malta Escarpment weakness zone.

This contribution aims at addressing two issues. Firstly, the evolution of the slab tear located to the north of Sicily is presented on the basis of a critical review of geological and geophysical data. Secondly, the recent deformation observed along the western edge of the Tyrrhenian slab is illustrated, using recent multichannel seismic marine surveys that have been purposely carried out along the northern part of the Malta Escarpment, in the Messina Straits, and in the central Aeolian Islands.

Geological setting

The geological evolution of the western-central Mediterranean region has been dealt with in several papers (Dewey *et al.* 1973; Horvath & Berckhemer 1982; Rehault *et al.* 1984; Malinverno & Ryan 1986; Le Pichon *et al.* 1988; Dewey *et al.* 1989; Burchfiel & Royden 1991; Patacca *et al.* 1992; Lonergan & White 1997), therefore, only the relevant pieces of evidence will be presented in the followings.

A palaeogeographic reconstruction for the Santonian (Fig. 2; Argnani 2005) illustrates the position of the oceanic and continental domains that are present on the African plate and that will be subsequently subducted underneath the growing Apennine belt. The narrow oceanic branch of the Neotethys, located between the Hyblean and Apulian carbonate platform domains, trends at high angle to the advancing subduction and represents a major control on subduction dynamics.

Sicilian Maghrebides and Southern Tyrrhenian basin

The Sicilian Maghrebides are part of the subduction system that extends from the Southern Apennines to the north African Maghrebides. A thick Mesozoic carbonate platform (the Panormide unit) is encased within the basinal sediments of the Sicilide and Imerese–Sicanian units (Roure *et al.* 1990), where Oligo-Miocene clastic turbidites are widespread (Catalano *et al.* 1996). The thrust stack composed by the Panormide carbonate platform and basinal units was emplaced onto the African foreland, characterized by continental basement, during the late Miocene–early Pliocene (Roure *et al.* 1990; Catalano *et al.* 1996). Thrusting then continued in central-eastern Sicily with the emplacement of the Gela Nappe, the front of which is sealed by the middle Pleistocene sediments of the Gela foredeep (Argnani 1987; Likorish *et al.* 1999; Patacca & Scandone 2004).

The emplacement of the Sicilian Maghrebides occurred with a remarkable clockwise (CW) rotation about vertical axes. In fact, palaeomagnetic data from Sicily indicate that large CW rotation affected the Mesozoic to Pliocene sediments stacked within the fold-and-thrust belt (Channell *et al.* 1990; Speranza *et al.* 1999, 2003). A CW rotation of about 70° occurred between Langhian and Late Tortonian, whereas 30° CW rotation affected the thrust-and-fold belt between Messinian and early Pleistocene. These results support the saloon-door opening of the Tyrrhenian basin, when compared to the coeval counter clockwise rotation of the Southern Apennines (Gattacceca & Speranza 2002). Palaeomagnetic data also show that CW rotations in Sicily increase from west to east (Speranza *et al.* 2003). These data can be tied to the evolution of the Adventure thrust front/foredeep system that is present in the western part of the

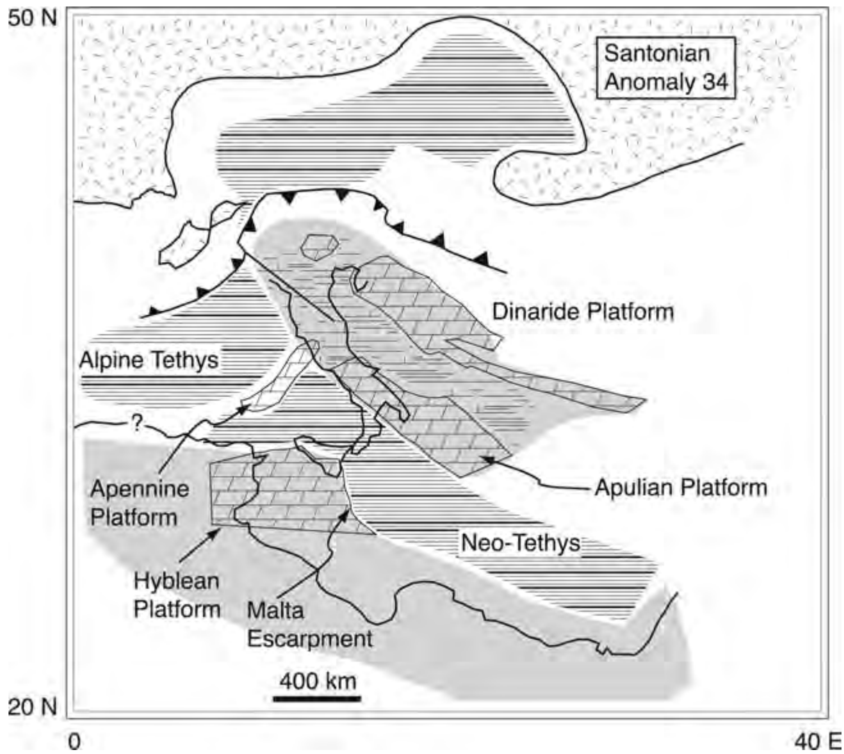

Fig. 2. Palaeogeographic reconstruction for the Santonian time (modified after Argnanic 2005). The oceanic lithosphere subducted beneath the Calabrian Arc has been repositioned on the surface, resulting in a W-ward extension of the Ionian oceanic domain, together with the Alpine Tethys oceanic lithosphere subducted underneath Corsica-Sardinia during Late Oligocene – Early Miocene. The Apennine Platform and the African platforms (Hyblean, Apulian and Dinaride) and pelagic basins of the articulated continental margin are also represented (grey pattern). The present coastline of Italy is for reference and outlines the Adria promontory.

Strait of Sicily (Argnani *et al.* 1987; Argnani1993). A CW rotation of about 70° occurred during the emplacement of the Adventure thrust stack which ended in late Tortonian, as indicated by the Tortonian-early Messinian sedimentary fill of the Adventure foredeep that suffered only little deformation, subsequently. Thrusting continued in central-eastern Sicily, accomplishing a CW rotation of about 30° until the early Pleistocene. Therefore, the Adventure thrust front/foredeep system allows to constrain the position of the Tortonian plate boundary within the African plate.

The thin-crust Vavilov and Marsili sub-basins, that represent the deeper portions of the southern Tyrrenian sea, are filled by 600 m thick sediments and are characterized by large volcanic seamounts, 20–45 km long and elongated roughly north–south (Kastens *et al.* 1988).

The western Tyrrhenian margin shows tilted fault blocks and its thinned crust, resembling a typical stretched passive margin. ODP stratigraphy and stratal relationships within half grabens suggest that stretching occurred from late Tortonian to early Pliocene (Argnani & Savelli 1999). Datings of basalts recovered in the Vavilov sub-basin fall within the same time interval (8 to 4 Ma), indicating that emplacement of MOR-type basalts occurred during extension in the western Sardinia margin (Argnani & Savelli 1999, 2001). This extensional tectonics was followed by some calc-alkaline activity in the central Tyrrhenian arc and, mainly, by within-plate volcanism in Sardinia and in the Magnaghi seamount. A second extensional episode led to the opening of the Marsili sub-basin. Sediments from well ODP 650 (Kastens *et al.* 1988), single-channel seismic profiles (Argnani & Savelli 2001), and work on magnetic anomalies (Nicolosi *et al.* 2006) allow to infer a late Pliocene–early Pleistocene age for the opening of the Marsili basin. As for the Vavilov sub-basin, the stretching in the Marsili sub-basin was followed by major calcalkaline volcanism in the Aeolian arc and by within-plate activity in Sardinia and in the Tyrrhenian basin (Fig. 4).

Focal mechanisms have recently shown the occurrence of a compressional belt located in the southern Tyrrrhenian Sea, north of Sicily (Pondrelli *et al.* 2004, 2006; Vannucci *et al.* 2004; Neri *et al.* 2005). P axes mostly trend North–West to NNW–SSE, except in the central Aeolian Islands, a direction in good agreement with the Nuvel-1 global motion of Africa relative to Europe (DeMets *et al.* 1990). This belt trends roughly wast–west and extends for some 200 km, with an eastern termination near the Island of Salina, in the Aeolian Island. Moreover, GPS data indicate that the convergence between Nubia and Eurasia is absorbed completely, or by a large extent (2.1 mm/a), in the seismic belt located in the southern Tyrrhenian Sea (Hollenstein *et al.* 2003; D'Agostino & Selvaggi 2004; Serpelloni *et al.* 2007), whereas there is no active shortening between the Hyblean plateau and the Aeolian Islands. These pieces of evidence have led to infer the onset of a new tectonic regime, with the young Tyrrhenian lithosphere that has possibly started being subducted to the south, underneath Sicily (Goes *et al.* 2004; D'Agostino & Selvaggi 2004; Faccenna *et al.* 2005).

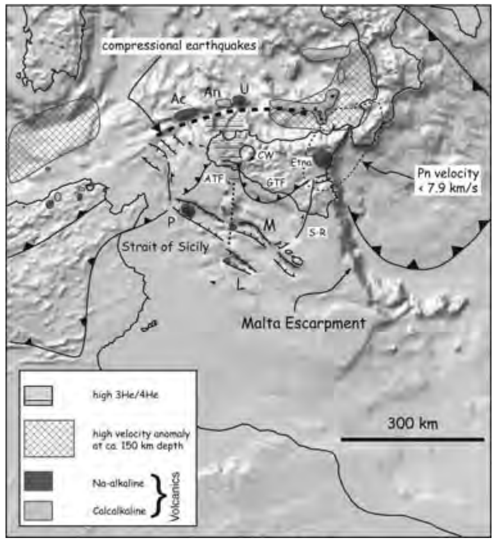

Fig. 3. Map with the main tectonic elements of the southern Tyrrhenian region. ATF: Adventure thrust front, GTF: Gela thrust front, S-R: Scicli–Ragusa fault system, CW: clockwise rotation of thrust sheets, P: Pantelleria trough, M: Malta trough, L: Linosa trough, Ac: Aceste seamount, An: Anchise seamount, U: Ustica Island. The thick dashed line north of Sicily indicates the position of the belt of compressional earthquakes. The thin dashed line in the Strait of Sicily marks the north–south transfer belt that separates the trough of Pantelleria from Malta and Linosa. The regions of high P-wave velocity anomaly at 150 km depth are from Piromallo & Morelli (2003), whereas the field of low Pn velocity of the uppermost mantle underneath Calabria is from Mele *et al.* (1998). The area of He isotopes anomaly in western Sicily is from Caracausi *et al.* (2005) and magmatism is from Argnani & Savelli (2001) and Savelli (2002).

Strait of Sicily and Malta Escarpment

The Strait of Sicily is a shallow sea that stretches from the northern coasts of Africa to Sicily. Three NW–SE elongated troughs, Pantelleria, Malta and Linosa, deeper than 1000 m and about 20 km wide, are present in the centre of the shelf, representing the morphologic expression of a continental rifting episode that affected this portion of African lithosphere in the Neogene (Fig. 3). The main rifting episode occurred in the early Pliocene, thinning the normal thickness continental crust of the Strait of Sicily (*c.* 30 km) to about 10–15 km beneath the rift system (Argnani 1990).

Rift-related volcanism occurred in the Strait of Sicily with both submarine and subaerial activity. The volcanic islands of Pantelleria and Linosa have an age of 300–150 ka to Present, whereas submarine volcanic activity with the same within-plate geochemical characters affected the area since Tortonian (Calanchi *et al.* 1989).

A peculiar feature of the Strait of Sicily is the occurrence of a set of roughly north–south-trending crustal discontinuities (Fig. 3). A roughly north–south-trending belt separating the Pantelleria graben from the Malta and Linosa grabens is characterized by the presence of volcanic activity, ranging from Tortonian to present, and by small Tortonian basins inverted during the Pliocene (Argnani 1990, 1993). Anomalies in He isotope ratio in western Sicily (Caracausi *et al.* 2005), and the Na-alkaline Ustica volcanics, north of Sicily, are located along the northward prolongation of this north–south transfer fault zone of the Strait of Sicily, suggesting the occurrence of deep-seated fractures linked to the mantle (Fig. 3).

Two additional north–south trending tectonic features are present in the African foreland to the west of the Straits of Sicily. One shows a dominant strike-slip motion and limits the northwestern end of the Pantelleria trough (Gamberi & Argnani 1995; Argnani 2003), and the other is the north–south Axis of Tunisia that shows a complex deformation history throughout the Meso-Cenozoic (Burollet 1991). Finally, also the Malta trough appears to be affected in its evolution by the NNE–SSW Scicli-Ragusa strike slip fault that continues northward in the Hyblean Plateau (Gardiner *et al.* 1995).

The steep Malta Escarpment bounds to the east the Strait of Sicily, connecting it to the deep Ionian basin (Scandone *et al.* 1981). This escarpment has long been recognized to be a major tectonic

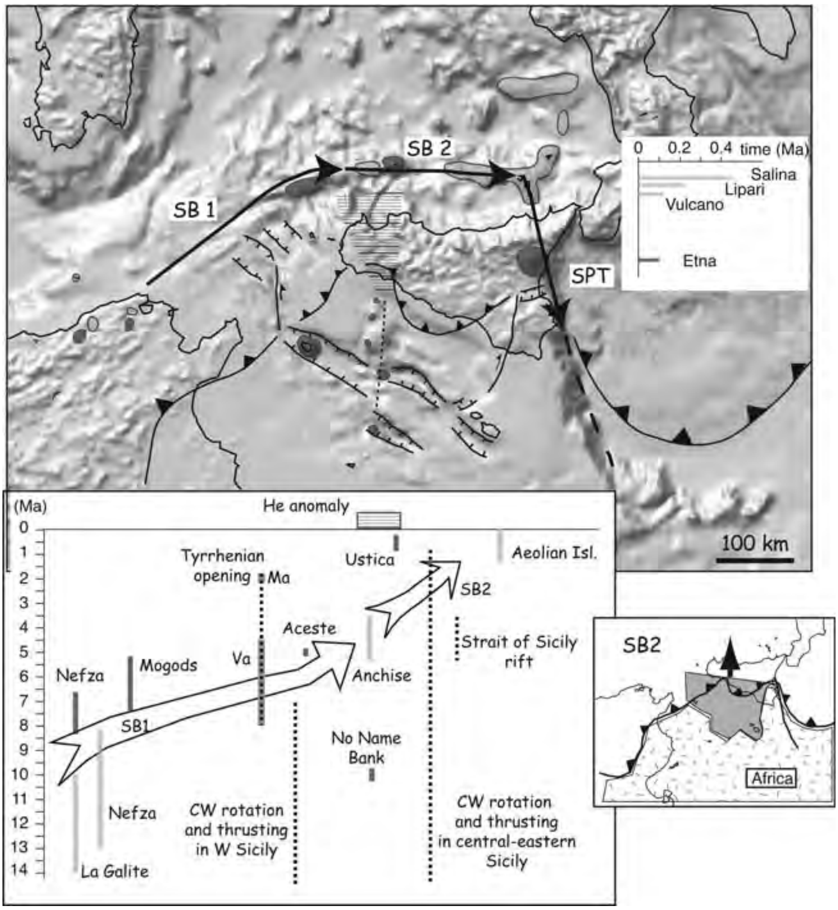

Fig. 4. Map showing the main elements for timing of slab break off. Light grey pattern and bars are calc-alkaline volcanics. Dark grey pattern and bars are Na-alkaline volcanics. The gray bars in the Tyrrhenian opening represents the two major extensional episodes, Vavilov (Va) and Marsili (Ma). SB1: first slab break-off episode, SB2: second slab break-off episode, SPT: trench-perpendicular tear. Inset showing the inferred origin of the Strait of Sicily rift by slab pull force acting during the second episode of slab break-off (SB2); the overall geometry of the grabens and related accommodation/transfer zones defines a small portion of lithosphere that is sliding underneath the Maghrebian front at a rate faster than that of the African plate.

feature of the central Mediterranean although the interpretation of its age, as well as of the age of the adjacent Ionian Basin, is still controversial (e.g. Argnani & Bonazzi 2005 and references therein). The northern part of the Malta Escarpment, the slope of eastern Sicily, is currently the site of a significant seismic activity that has been recorded in the recent instrumental catalogues (Chiarabba *et al.* 2005) and historical chronicles (Boschi *et al.* 1995).

To sum up, it seems that major crustal discontinuities are present within the subducting African plate. Some of them, like the north–south Axis of Tunisia and the Malta Escarpment, have a proven complex and long history of activity; others are less studied, but nevertheless effective in controlling the structural architecture of the Strait of Sicily. These discontinuities trends at high angle to the advancing subduction front and can possibly interfere with subduction dynamics.

Calabrian Arc uplift

Recent uplift characterizes the Calabrian Arc and the adjacent Southern Apennines and Sicily. Several pieces of data suggest that the uplift of this region was mainly accomplished in the last 2 Ma with an acceleration in the last 1 Ma (Ghisetti 1981; Westaway 1993). A critical review of data on marine terraces of Tyrrhenian age shows that the maximum uplift for the past 125 ka has been recorded in Calabria with rates up to 1.2 mm/a that decrease on either side of the Calabrian Arc (Bordoni & Valensise 1998). A late Holocene acceleration in uplift rates, with values over 2.0 mm/a, has been recorded around the Messina Straits from study on uplifted fossil beaches (Antonioli *et al.* 2006).

Earthquake hypocentral distributions and seismic tomography indicate the presence of a steep, deep and narrow slab, dipping NW-wards, underneath the Calabrian Arc (Anderson & Jackson 1987; Selvaggi & Chiarabba 1995; Piromallo & Morelli 2003). The seismic slab reaches a depth of about 500 km and with its 70° slope is one of the steepest observed in subduction zones (Isacks & Barazangi 1977). Although the opening of the Marsili basin have possibly occurred at rates as fast as 19 cm/a (Nicolosi *et al.* 2006), GPS data indicate that roll back of the Tyrrhenian slab is no longer active with significant rates (Hollenstein *et al.* 2003; D'Agostino & Selvaggi 2004; Goes *et al.* 2004; Serpelloni *et al.* 2007).

Evolution of the southern Tyrrhenian slab tear

A note on the terminology used in this paper is required, as similar processes are sometimes described with different names in the literature, and different processes are sometimes given the same name. A slab tear implies a break in the continuity of the slab and can be trench-perpendicular or trench-parallel (Fig. 5). In the first case the break in continuity occurs typically at high angle to the strike of subduction and controls the width of the slab; it cuts the slab at different depths along slope, possibly taking advantage of pre-existing weakness zones within the subducted plate. In the second case the break in continuity is subparallel to the strike of the slab and can occur at different depths which are possibly controlled by the rheology of the subducted slab and by subduction evolution (Yoshioka & Wortel 1995; Wong A Ton & Wortel 1997; van de Zedde & Wortel 2001; Andrews & Billen 2007); to describe this process the term slab break-off is also used throughout this paper, whereas the term slab detachment is often encountered in the literaure (e.g., Wortel & Spakman 2000). Both trench-parallel and trench-perpendicular tears can propagate laterally (e.g. Wortel & Spakman 2000), although it is the trench-perpendicular tear that interferes directly with the plate boundary, representing a typical candidate for STEP faulting; on the other hand, trench-parallel tears occur at depth and affect the Earth's surface only in a complex, indirect way. In this paper the term 'slab decoupling' is used to indicate the decoupling of the subducted oceanic lithosphere from the upper plate during slab steepening. Such process, for instance, has been envisaged to operate beneath Calabria (Fig. 6; Gvirtzman & Nur 1999*b*).

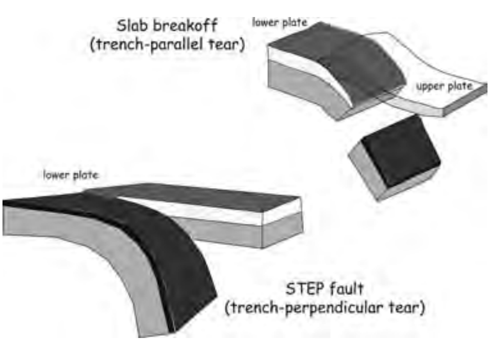

Fig. 5. Simplified sketch showing the difference between the two modes of slab tear discussed in the text: slab breakoff (trench-parallel tear), and STEP fault (trench-perpendicular tear). The STEP fault is after Govers & Wortel (2005). Light grey and dark grey patterns on top of the lower plate represents the continental and oceanic crust, respectively. Note that both slab break-off and STEP faulting take advantage of the mechanical discontinuity represented by the continent–ocean boundary.

Geological and geophysical evidence for a trench-parallel tear offshore northern Sicily

In the region north of Sicily, roughly corresponding to the east–west Aeolian Islands alignment, P-wave tomography suggests the absence of a subducted slab at a depth of *c.* 150 km, showing a low velocity anomaly interposed between the high velocity anomaly of the Tyrrhenian slab, to the east, and the high velocity anomaly located underneath north Africa, to the west (Fig. 3; Wortel & Spakman 2000; Piromallo & Morelli 2003; Montuori *et al.* 2007).

Several lines of geological evidence support the occurence of a trench-parallel tear along the southern Tyrrhenian subduction and allow to detail the timing of the eastward tear progression (Fig. 4).

At the western end of the tomographically imaged lithospheric tear the eastward shift of thrust activity, from the Adventure to the Gela thrust front (Fig. 3) can be related to an episode of slab break-off occurring in the region of the Sardinia Channel at end Tortonian. This slab break-off caused the end of the Adventure thrusting and promoted the 30° CW rotation of the thrust-and-fold belt in central Sicily.

Following the onset of tearing in the Sardinia Channel two major cycles can be identified in the evolution of the Tyrrhenian basin, each composed

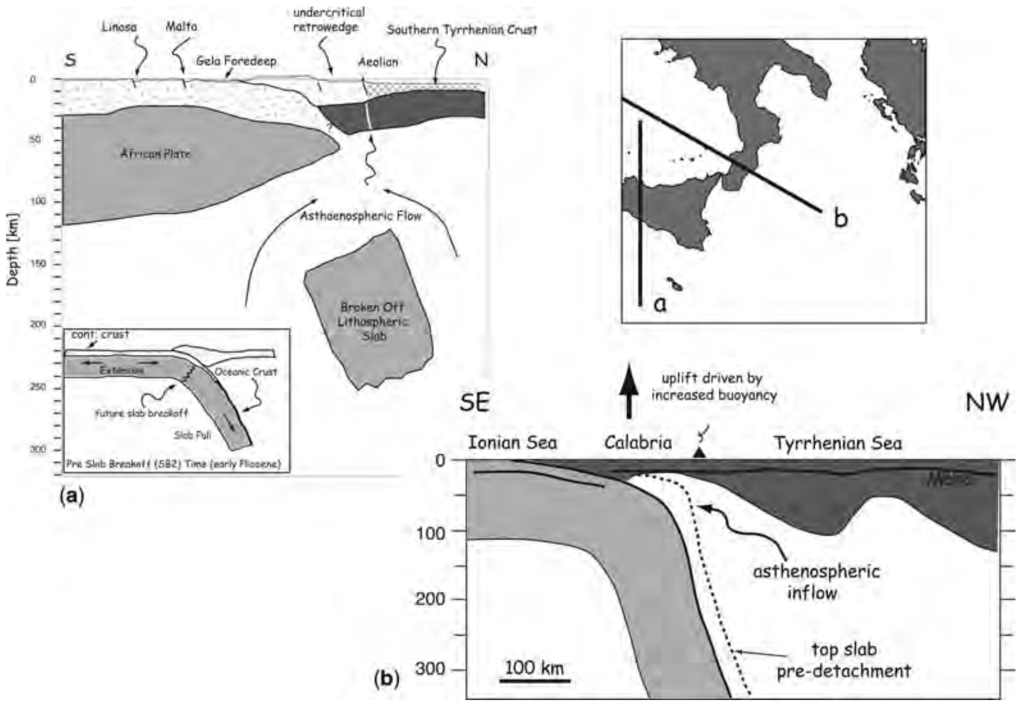

Fig. 6. Simplified lithospheric scale geological sections crossing Sicily (a) and the Calabrian Arc (b). (**a**) illustrates the slab break off north of Sicily and (**b**) the slab decoupling underneath Calabria. Inset in (a) illustrates the inferred situation at about early Pliocene, during rifting in the Strait of Sicily that preceeded the second episode of slab break-off (SB2). Location of cross sections is also shown. Section (b) is modified after Gvirtzman & Nur (1999*a*).

of a stretching dominated episode, with magmatism concentrated mainly in the newly created basin floor, followed by an episode with little extension, calcalkaline volcanism in the arc and within-plate volcanism all over the basin (Argnani & Savelli 1999, 2001). The first cycle occurred from 8.5 to 2.5 Ma (late Tortonian to mid Pliocene), and the second, shorter, lasted from 2.2 Ma (late Pliocene) to the Present (Fig. 4). These cycles reflect the geodynamic evolution of the southern Tyrrhenian backarc basin which is controlled by trench retreat and rolling back of the subducted slab, that becomes progressively steeper in time. The process of roll back appears to be discontinuous in time with episodes of fast trench retreat, and associated backarc basin stretching, alternating with episodes of almost steady trench position, and slab sinking, with associated calc-alkaline and within-plate volcanic activity (Argnani & Savelli 1999, 2001). The extensional episodes within each magmatic cycle can be related to the propagation of a trench-parallel tear, which promotes trench retreat (Dvorkin *et al.* 1993; Wortel & Spakman, 2000; Schellart *et al.* 2007). Therefore, within the uncertainties of the time response to deep lithospheric processes, the evolution of the southern Tyrrhenian basin suggests the occurrence of two major episodes of slab tearing, the first occurring between 8.0 and 4.5 Ma and the second from 2.2 to 1.6 Ma.

The origin of the Strait of Sicily rift is not fully understood, although the roughly north–south extension, about parallel to the coeval strike of the subducted Tyrrhenian slab, suggests the possible activity of a slab pull force (Spence 1987). As the Maghrebian fold-and-thrust belt encroached the continental lithosphere of the African margin, the arrival at the subduction zone of the buoyant continental lithosphere slowed down the subduction rate, maximizing the effect of slab pull on the subducted African lithosphere (Fig. 6a; Argnani 1990 2003). Crustal stretching resulted in faulting and fracturing, originating the system of troughs in the Strait of Sicily and creating potential wayouts for magmas and mantle derived He. Initially, slab pull caused limited extension in the subducted plate, and ultimately led to the break-off of the slab (Argnani 1990, 2003). Assuming this interpretation is correct, rifting in the Strait of Sicily just preceeded the second slab break-off episode that controlled the evolution of the Tyrrhenian basin (Fg. 4).

This interpretation of the Strait of Sicily rifting follows previous work of the Author (Argnani

1990, 1993, 2003) and differs from that proposed by Faccenna *et al.* (2004) who assume that the Strait of Sicily rifting is a direct surface manifestation of a break in the slab. These authors, in fact, envisage a NW–SE-trending trench-perpendicular tear that cuts the slab from the Sardinia Channel to the Strait of Sicily; however, this contrasts with the evolution of the Adventure thrust belt, as previously mentioned, and it is not clear how this tear relates to the Strait of Sicily rifting, which originated by *c.* north–south extension. The geological and geophysical evidence, as discussed below, rather suggests that the tear propagated laterally in a direction parallel to the strike of the slab, to assume its current position north of Sicily.

Although it has been suggested that the young Tyrrhenian lithosphere has started being subducted to the south, underneath Sicily (Goes *et al.* 2004; D'Agostino & Selvaggi 2004; Faccenna *et al.* 2005), geological data in that region give little support to the occurrence of a subduction zone. In fact, both seismic profiles (Fabbri *et al.* 1982; Pepe *et al.* 2000, 2004) and multibeam swath bathymetry (Marani *et al.* 2004) show no obvious trace of a large-scale geological feature indicating subduction, and extensional tectonics has been documented up to late Pliocene – early Pleistocene in the sedimentary basins located along the northern Sicily slope (Fabbri *et al.* 1982; Pepe *et al.* 2000). Trench-parallel tearing is expected to disactivate the slab pull, promoting an increase in compression within the orogen; therefore, a northward shift of compressional tectonics within the accretionary wedge of Sicily could represent an alternative interpretation to the onset of a new subduction. In fact, the retrowedge of the Maghrebain belt of Sicily, that was subject to the Tyrrhenian extension, should restore to its critical taper by compressional deformation (e.g. Willett *et al.* 1993; Fig. 6a). In this event, the compressional belt north of Sicily would not imply any flip in subduction polarity, but rather a complex inversion of pre-existing extensional faults. Eventually, once shortening cannot be accommodated any longer within the orogen, the Tyrrhenian lithosphere will be subducted southward. At present, however, more reliable geological and geophysical data are required in order to properly describe the tectonic regime that is active offshore northern Sicily.

Summary evolution of the southern Tyrrhenian slab tear

As indicated by several lines of geological and geophysical evidence (Fig. 4) the tearing of the African slab started at about 8.5 Ma in north Tunisia, in a location possibly controlled by the north–south Axis discontinuity, and propagated eastward, reaching the Anchise volcanic seamount (roughly the position of the north–south transfer belt in the Strait of Sicily) at about 4 Ma. In the meanwhile, thrusting ended in the Adventure thrust belt of western Strait of Sicily, as the tear progressed eastward. During this time the Vavilov basin opened, with emplacement of MORB-like volcanics. In the Vavilov basin extensional tectonics was followed by calc-alkaline and within-plate volcanism from 4.5 to 2.2 Ma. A second break-off episode, occurring between 2.5 and 1.6 Ma, affected the slab from the Anchise seamount to the central Aeolian Islands (bounded to the east by the Malta Escarpment discontinuity) and was preceeded by slab pull-related rifting in the Strait of Sicily. The Marsili basin openend during this break-off episode. The Aeolian Islands calc-alkaline volcanism developed subsequently, from 1.3 Ma to the present. At about early–middle Pleistocene the Tyrrhenian slab was likely shaped to its present form and horizontal motions were greatly reduced. The pull of the Tyrrhenian slab reactivated the Malta Escarpment discontinuity as a trench-perpendicular tear, and promoted the slab decoupling underneath Calabria that may be responsible for the increased rate of uplit in the Calabrian Arc. In fact, the Calabrian Arc uplift occurred over a broad region, suggesting a geodynamic process that operates at a lithospheric scale. Following Gvirtzman & Nur (1999*b*), it is proposed that the Calabrian Arc (upper plate) detached from the subducted slab and was subject to isostatic rebound as a wedge of asthaenosphere entered underneath the upper plate (Fig. 6b). It is remarkable that the upper mantle Pn velocities present a substantial negative anomaly below a region that extends from southern Calabria to Mt Etna (Mele *et al*. 1998; Fig. 3). Whereas magmatic input can be responsible for the low Pn velocity underneath Mt Etna, the low velocities of southern Calabria may be related to the process of slab decoupling. Moreover, the fact that the two regions are connected may be an indication that the Mt Etna magmatic system is related to the asthenospheric flow induced by slab decoupling.

The role of slab break-off in controlling the evolution of the western-central Mediterranean has been first proposed by Wortel & Spakman (1992), and later developed by Carminati *et al.* (1998) who envisaged a lithospheric tearing that proceeded eastward from north Africa to the Tyrrhenian region, starting in late Langhian. The slab tear evolution presented in this paper is in the line of the broad reconstruction of Carminati *et al.* (1998), although it focuses on the smaller southern Tyrrhenian region and is using more geological data to outline the timing of slab tearing. However, unlike what is proposed by Govers & Wortel (2005), the southern Tyrrhenian tear is not interpreted as a simple STEP fault, but rather as a trench-parallel tear that affected the subducted lithosphere of the Sicilian margin. In fact, no subduction is expected to occur across the STEP fault (Govers & Wortel 2005; Fig. 1), whereas subduction is required to account for the large width and remarkable amount of shortening in the fold-and-thrust belt of Sicily, as well as for the Aeolian arc magmatism. Accordingly, the vertical axis CW rotation in the Maghrebian belt of Sicily is interpreted as due to differential trench retreat and not simply to dextral strike-slip along an east–west-trending STEP fault. In fact, a large post-early Pliocene CW rotation affected the whole of central Sicily, from the northern to the southern coast, suggesting a close relation with the opening of the Tyrrhenian basin (the saloon-door model, e.g. Speranza *et al.* 2003).

The episodes of slab break-off here presented are somewhat different from those proposed by Faccenna *et al.* (2005) who envisaged three episodes of slab deformation (10–8 Ma, 5–4 Ma, and 1–0.8 Ma) which are mostly based on the timing of the change from subduction-related to within-plate magmatism along the subductive boundary. The two slab break-off episodes here presented (8–4 Ma, 2.5–1.6 Ma), that are based on the integration of several pieces of geological evidence, last longer and are followed by an episode of trench-perpendicular tearing affecting the Malta Escarpment (1.6 Ma–Present). Morever, it is considered that the north–south-trending discontinuites that are present in the subducted African plate played a key role in controlling the timing of tear propagation.

Finally, a recent model relating slab tearing and magmatism in the Italian region (Rosenbaum *et al.* 2008) presents a rather complex system of NW-trending lithospheric tear faults affecting the southern Tyrrhenian region since Pliocene and segmenting the slab with a less than 100 km spacing. However, little magmatological evidence is supporting the occurrence of these lithospheric tears, and the inferred kinematic evolution is not really matching the geological observations. In particular, the Adventure (late Tortonian–early Messinian) and Gela (Plio-Quaternary) foredeep basins cannot be easily located within the proposed reconstructions, leaving aside the lack of surface expression of the lithospheric tears.

Deformation along the western edge of the Tyrhhenian slab

A trench-parallel tear along the Aeolian alignment fits the tomographic data and can explain the abundance of volcanic features originated in the last 2 Ma along this trend (De Astis *et al.* 2003). Such a tear progressed eastward, towards the Calabrian Arc, where it may have been intercepted by the major discontinuity represented by the NNW–SSE-trending Malta Escarpment (Scandone *et al.* 1981; Argnani & Bonazzi 2005) which caused a reorientation of the tear from east–west to NNW–SSE, and from trench parallel to trench perpendicular.

A variety of structural features testifies the active deformation occurring along the western edge of the Tyrrhenian slab. These structures are located along the NNW–SSE trend that connects the Malta Escarpment to the central Aeolian Islands. A description of the main features, illustrated by seismic profiles (Fig. 7), will be presented in the following, subdivided into three sectors: Malta Escarpment, Messina Straits and Aeolian Islands.

Multichannel seismic data. The data set consists of multichannel seismic profiles acquired during two surveys carried out during 2001 and 2006 and covering the eastern Sicily offshore, Messina Straits and central Aeolian Islands. Seismic acquisition aimed at obtaining good images of the sedimentary strata and of the recently active tectonic structures, rather than at crustal-scale investigation. Data acquisition has been carried out with 24 to 48-channel Teledyne seismic streamers and a Sodera G.I. gun in harmonic mode (105 + 105 c.i.).

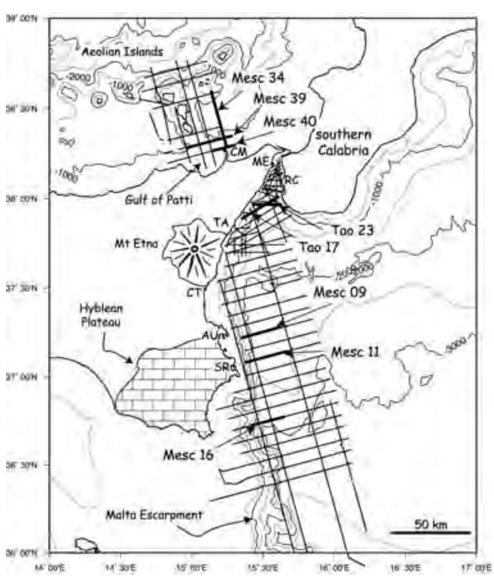

Fig. 7. Grid of multichannel seismic profiles, with location of the lines shown in Figures 9 to 15. Some relevant localities are also indicated. CM: Capo Milazzo, ME: Messina, RC: Reggio Calabria, CT: Catania, AU: Augusta, SR: Siracusa.

Seismic data were digitized and recorded by a Geometric's Stratavisor seismograph, with sampling rate of 1 msec and record length varying from 3 to 12 seconds, and have been processed using a standard sequence up to time migration. Details of seismic acquisition can be found in papers that are specifically dealing with individual parts of these surveys (Argnani & Bonazzi 2005; Argnani *et al.* 2007; Argnani *et al*. 2008).

Seismic units and seismic facies. All over the region, from the Malta Escarpment to the Aeolian Islands, the absence of exploration wells and the limited direct sampling of sediments prevent the establishment of a detailed stratigraphy frame. However, the Plio-Quaternary seismic facies observed throughout the southern Tyrrhenian and Ionian basins (Barone *et al.* 1982; Fabbri *et al.* 1982) can be safely correlated.

Four main seismic facies can be observed in the seismic profiles (Figs 8–14): (a) Plio-Quaternary sediments are characterized by reflections with high to medium amplitude and good continuity. They are resting onto the External Calabrian Arc accretionary prism in the Ionian Sea and on the deformed units of the Calabrian Arc in the Messina Straits and Aeolian Islands; (b) pre Plio-Quaternary units of the Calabrian Arc, present in the Messina Straits and Aeolian Islands and characterized by complex tectonic deformation, are typically poorly resolved. They presents a dominantly chaotic seismic facies, with only small patches with continous and sometimes parallel reflections; (c) the deformed sediments belonging to the External Calabrian Arc accretionary prism, originated by the accretion of the Cenozoic basinal sediments belonging to the Ionian domain and older units, are characterized by a chaotic seismic facies; and (d) the Mesozoic carbonate sediments of the Malta Escarpment are characterized by a package of high-to-medium amplitude and moderate-to-poor continuity reflections; in places this package of reflections can be followed from the Malta Escarpment to the Ionian basin, where they rest underneath the External Calabrian Arc accretionary prism.

Malta Escarpment. Offshore eastern Sicily the Malta Escarpment can be divided into two segments with different tectonic structures (Fig. 8).

The segment of the Malta Escarpment extending north of Siracusa is characterized by the presence of NNW–SSE-trending east-dipping extensional faults located along the morphological escarpment and a few km east of it. Half-graben basin (Fig. 9) are filled with up to 1 s (TWT) of sediment and bounded to the west by extensional faults. Wedging of reflections, identifying growth strata, can be observed within the recent sediments filling the

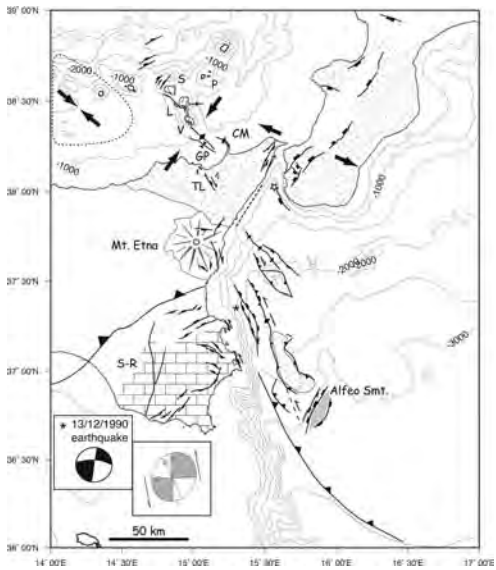

Fig. 8. Main structural features along the Malta Escarpment – central Aeolian trend. Onshore data comes from various sources (Adam *et al.* 2000; Catalano *et al.* 2006; Ghisetti 1979, 1992; Galli *et al*. 2009; Lanzafame & Bousquet, 1997). The field of compressional stress obtained from focal mechanisms (Neri *et al.* 2005), with thick arrows indicating direction of maximum compressional stress, is shown in the upper left. Thick arrows indicate the stress field (Neri *et al*. 2005) also in the Aeolian region and in the Messina Straits. The dashed line near the coast of Sicily north of Etna represent the position of the tilted monocline (Fig. 12). Brick and random dashes patterns represent the Hyblean Plateau and the Calabrian Arc crystalline rocks, respectively. Lines with black rectangles represent extensional faults, whereas lines with black triangles are thrusts and reverse faults. Contractional reactivation occurred where extensional and thrust symbols are present along the same line. Small arrows near a fault line indicates a strike-slip component. The asterisk east of the Hyblean Plateau indicates the epicenter of the 1990 earthquake, the focal mechanism of which is shown in the lower left inset (from Amato *et al.* 1995) together with the fracture pattern expected along a left-lateral strike-slip fault with a Malta Escarpment trend. The open star in the Messina Straits indicate the epicenter of the 1908 Messina earthquake (after Schick 1977). P: Panarea, S: Salina, L: Lipari, V: Vulcano, CM: Capo Milazzo, GP: Gulf of Patti, TL: Tindari–Letojanni fault trend, S-R: Scicli–Ragusa fault system.

half graben which correlate with late Pliocene–Quaternary (Argnani & Bonazzi 2005), although it is well possible that an age younger than late Pleistocene is applicable. In fact, basin sediments are only little affected by motion of the Calabrian Arc accretionary prism, on which they are resting, supporting the younger age.

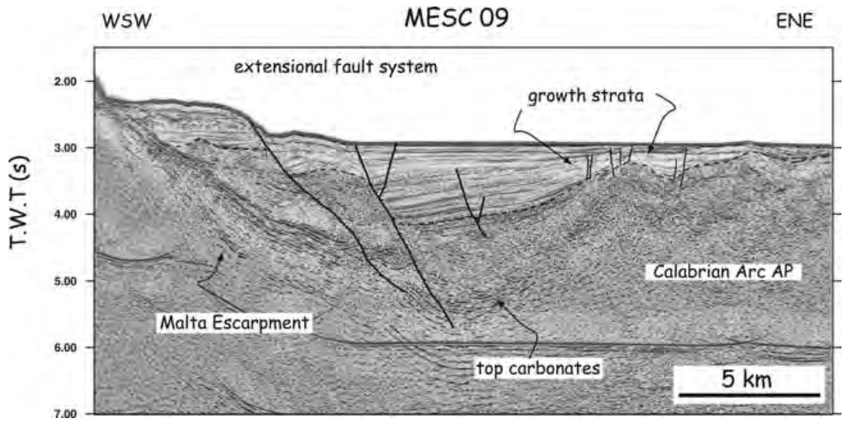

Fig. 9. Seismic profile MESC 09 showing the extensional fault system and the half-graben filled by Plio-Quaternary sediments along the Malta Escarpment. Note the steep eastward-dipping package of reflectors that characterizes the Malta Escarpment. Location in Figure 7.

The extensional fault system dies out both northward and southward (Fig. 8). To the north, the main extensional fault is located further to the east, and it has also been reactivated in contraction (Fig. 8). The small wavelength of the contractional structure suggests that the inverted fault is flattening on the basal detachment of the Calabrian Arc accretionary prism (Argnani & Bonazzi 2005). In fact, the step created by the extensional fault can focus compressional stresses once the accretionary prism moves further, causing a right-lateral transpression.

The Malta Escarpment is not affected by recent faulting in the segment south of Siracusa (Fig. 10). In this part a thick package of reflections is visible along the slope and continues undisturbed further eastward, underneath the chaotic units of the External Calabrian Arc. The recent deformation of this sector is located about 20–30 km eastwards of the morphologic slope and is characterized by a broad area of uplift, trending NNW–SSE, apparently bounded by reverse faults (Fig. 8). The occurrence of deep seated faults seems likely, as the reflection package marking the top of carbonate sediments is also uplifted (Fig. 11).

The Messina Straits. A flight of emergent marine terraces occurs along the coast of Sicily from Taormina to Messina. Although this emergence of marine terraces has been interpreted as due to flexural uplift on the footwall of an offshore fault (Taormina Fault; Catalano & De Guidi 2003), recent data (Argnani *et al.* 2008) led to reconsider this interpretation. In fact, seismic profiles do

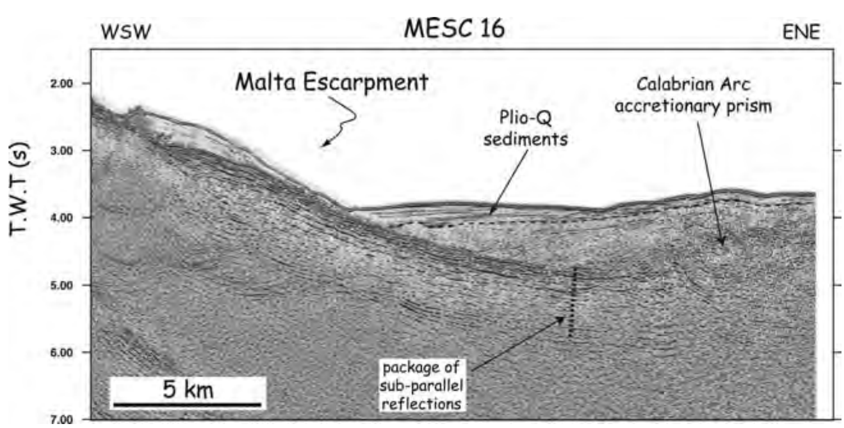

Fig. 10. Seismic profile MESC 16 showing the absence of faults and the continuity towards the Ionian basin plain of the package of reflections that characterizes the Malta Escarpment. See Figure 7 for location.

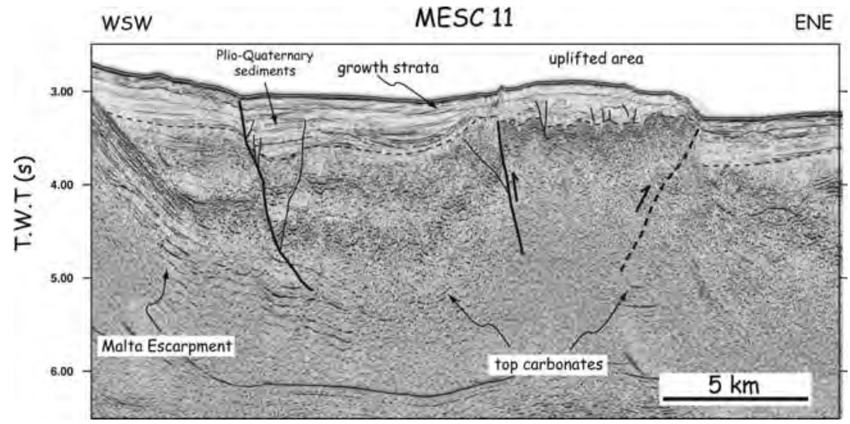

Fig. 11. Seismic profile MESC 11 showing the limited throw of extensional fault. Note the good continuity of the steep reflectors marking the Malta escarpment that continue further to the east underneath the uplifted area bounded by reverse faults. Location in Figure 7.

not image a fault running parallel to the coast; instead, the slope is characterized by a package of sediments originally deposited sub-horizontally and now tilted eastward (Fig. 12). A basal onlap of variable extent characterizes the lower part of this unit, suggesting the occurrence of a pre-existing mild slope to the west. The same relationship can be extended all along the coastline north of Taormina (Fig. 8), suggesting that the whole sector straddling the coastline has been tilted (Argnani *et al*. 2008). The lack of growth strata suggests that the tilting was very recent, as also indicated by the immature drainage pattern characterized by sub-parallel, poorly incised slope channels imaged by multibeam morphobathymetry (Marani *et al.* 2004, and new data currently being processed).

The fault that originated the 1908 Messina earthquake is still unknown, although recent inverse modelling of seismograms and geodetic levelling suggests a 30 km long, E-dipping faults trending about north–south (Amoruso *et al.* 2002, and references therein). However, E-dipping extensional faults that affect the sea-floor have not been clearly detected within the northern part of the Messina Straits (Argnani *et al.* 2008), indicating that the seismogenic fault responsible for the Messina 1908 earthquake is possibly a blind fault (Valensise & Pantosti 1992). On the other hand, seismic profiles offshore SW Calabria show a

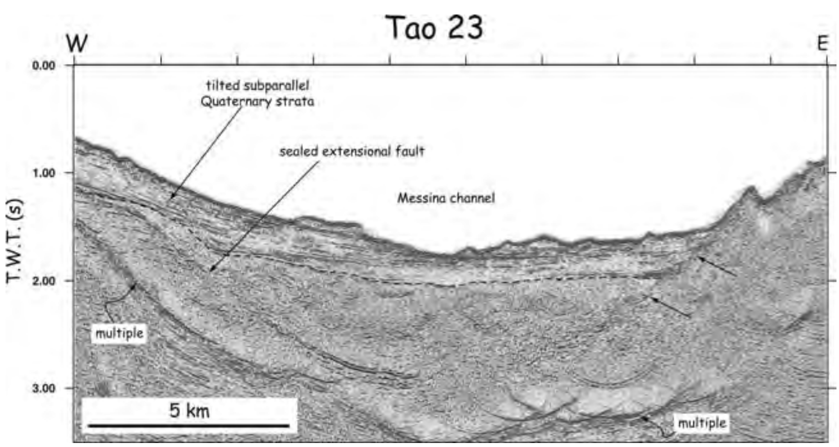

Fig. 12. Seismic profile TAO 23 across the southern part of the Messina Straits showing a thick package of almost parallel strata dipping to the east on the slope, and flattening further to the east. An extensional fault is sealed by these Quaternary sediments at the western end of the profile. The arrows indicate the same fault plane seen on line TAO 17. See Figure 7 for location.

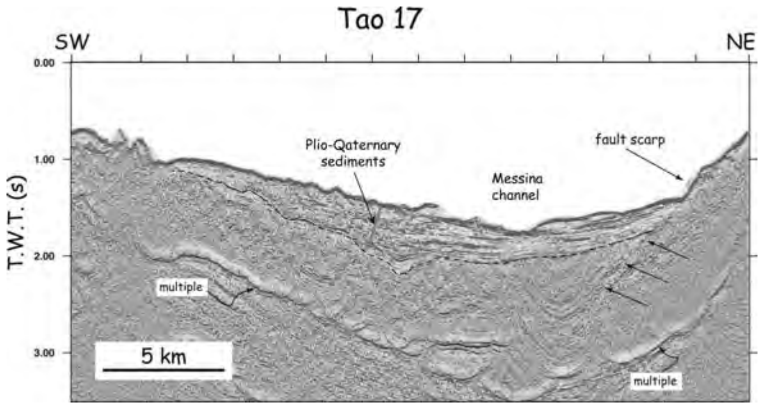

Fig. 13. Seismic profile TAO 17 showing the fault scarp on the Calabrian side (NE) and the fault plane (arrows), whereas no major faulting affects the Quaternary sedimentary package over the rest of the profile. Note the tilted strata along the Sicilian slope, on the western side of the profile. See Figure 7 for location.

20 km-long west-dipping fault that is breaking the sea-floor (Fig. 13). This fault trends NW–SE and represents the longest lineament observed within the Messina Straits (Fig. 8).

Aeolian region. GPS data and earthquake focal mechanisms indicate active NNW–SSE compression in the SW Tyrrhenian region and NW–SE extension in the SE Tyrrhenian and Calabrian region (Hollenstein *et al.* 2003, D'Agostino & Selvaggi 2004; Pondrelli *et al.* 2004, 2006; Neri *et al.* 2005; Serpelloni *et al.* 2007; Argnani *et al.* 2007); the transition between the two domains occurring in the central Aeolian region.

The age of the onset of volcanic activity gets younger along the Salina – Vulcano NNW–SSE alignment (Mazzuoli *et al.* 1995; De Astis *et al.* 2003), with volcanism that started *c.* 450 ka at Salina, 223 ka at Lipari, and 120 ka at Vulcano (Fig. 4). Mt. Etna is located on the same alignment, being the youngest edifice along the trend with its age of *c.* 100 ka (age of the present central edifice).

In the Aeolian Islands several of the faults commonly reported in the literature (see De Astis *et al.* 2003, for a compilation) are not imaged by seismic profiles. In particular, extensional faults are remarkably absent around the central Aeolian Island, and there is no surface evidence of the northern extent of the often reported Tindari–Letojanni fault (e.g. Lanzafame & Bousquet 1997; Billi *et al.* 2006) that should connect the Gulf of Patti with the island of Vulcano (Fig. 8).

A complex NW–SE-trending belt of compressional (or transpressional) structures connects the island of Vulcano with Capo Milazzo, where an uplifted middle-late Pleistocene marine terrace rests on metamorphic units (Lentini *et al.* 2000). Along this belt, seismic profiles show the occurrence of two broad anticlines, partly overlapping: Vulcano fold and Capo Milazzo fold (Fig. 14).

The Plio-Quaternary stratigraphy can be better constrained between Panarea and Sicily where reflections onlap the southern flank of Panarea (Fig. 15). The age of the corresponding sediments, therefore, can be taken as younger than 300 ka, i.e. the age of Panarea. This allows us to infer that folding has occurred since middle Pleistocene. This deformation is superposed on a pre-existing extension, as Pliocene extensional faults are still visible within the folded sediments (Fig. 14).

Transpression along the belt that extends northwestward from Capo Milazzo could also be responsible for the uplift of the islands of Lipari and Salina where marine terraces as old as 124 ka have been continuously uplifted at an average rate of *c.* 0.34 mm/a, suggesting some kind of tectonic process which is independent from shorter term volcano-tectonics fluctuations (Calanchi *et al.* 2002; Lucchi *et al.* 2004).

Recent extensional faults occur only north of the Aeolian Islands, whereas dominant contractional structural features have been observed around the central Aeolian Islands (Argnani *et al.* 2007). This pattern of recent deformation is compatible with GPS-derived strain-rate axes (Serpelloni *et al.* 2007; Argnani *et al.* 2007) and with stress field obtained from focal mechanisms (e.g., Neri *et al.* 2005).

Discussion

Several tectonic features that have been active since the Late Pleistocene are aligned along a NNW–SSE

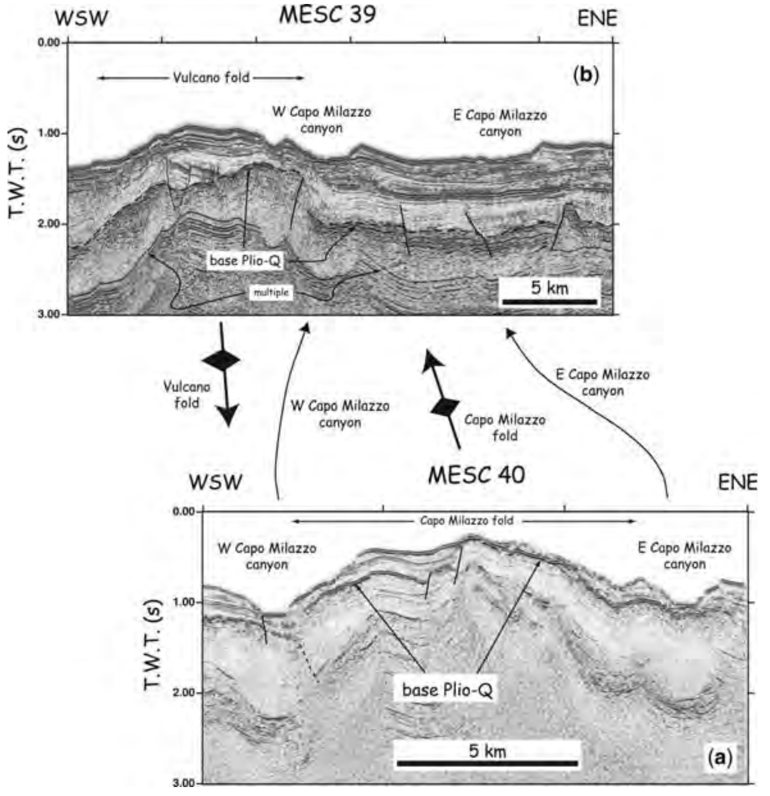

Fig. 14. Upper panel: Part of seismic profile MESC 39 showing the Vulcano fold that dies out southward. Lower panel: part of seismic profile MESC 40 located just north of Capo Milazzo showing the broad Capo Milazzo fold, bounded by two branches of the Stromboli canyon (western and eastern Capo Milazzo canyons), that dies out northward. Note that on both profiles extensional faults affecting Pliocene sediments have been passively involved in the subsequent folding. Location is in Figure 7.

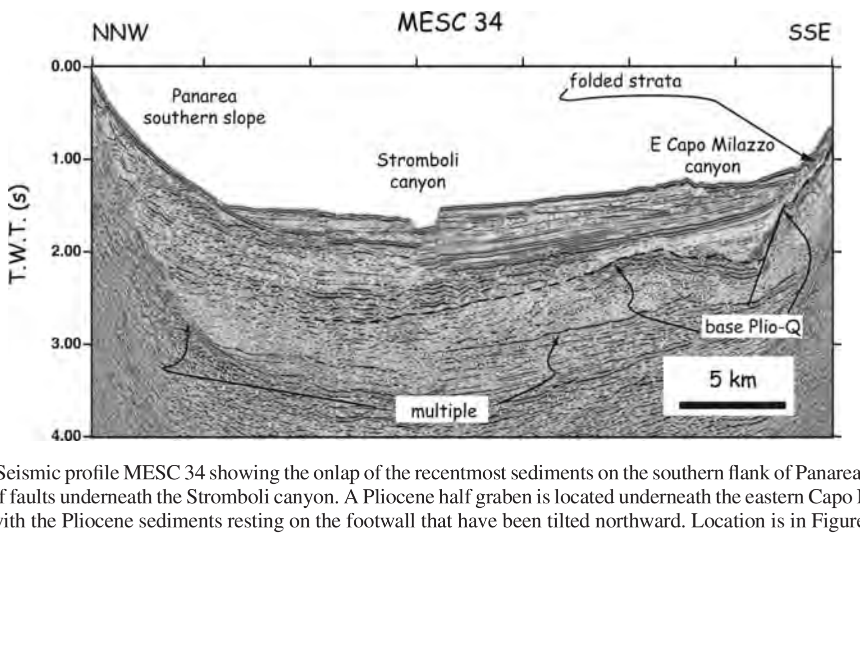

Fig. 15. Seismic profile MESC 34 showing the onlap of the recentmost sediments on the southern flank of Panarea and the absence of faults underneath the Stromboli canyon. A Pliocene half graben is located underneath the eastern Capo Milazzo canyon, with the Pliocene sediments resting on the footwall that have been tilted northward. Location is in Figure 7.

trend for a length of over 150 km (Fig. 8). Independent geophysical evidences, coming from seismology, seismic tomography and S-wave paths indicate the possible occurrence of a lithospheric tear along the same trend. Although a clear tectonic signature of a deep lithospheric tear is difficult to be envisaged, the variety of tectonic response occurring in about the same time span along the Malta Escarpment trend suggests a common origin and supports the occurrence of a trench-perpendicular tear between the Ionian oceanic lithosphere and the continental lithosphere of the Hyblean plateau (Gvitzman & Nur 1999; Argnani 2000; Doglioni *et al.* 2001; Govers & Wortel 2005). Seismic profiles show that Pleistocene deformation affected, in a different way, both the lower plate, along the Malta Escarpment, and the upper plate, in the Messina Straits and Aeolian Islands.

The chief elements in support of a tear along the western edge of the Tyrrhenian slab are discussed in the following paragraph.

Quaternary crustal-scale extensional faults occur along the northern part of the Malta Escarpment but are absent further to the south, indicating a northward increasing vertical throw. The tectonic structures located along the Malta Escarpment present a NNW–SSE orientation and cut through the accretionary prism of the External Calabrian Arc which is encroaching the Malta Escarpment at the latitude of Siracusa (Fig. 8). The NNE-oriented Alfeo Seamount represents an exception to the Malta Escarpment trend (Fig. 8). The pelagic Mesozoic sediments that have been dredged on its scarps (Rossi & Borsetti 1977) suggest that Alfeo can be considered a seamount already separated by the Hyblean plateau at the early stage of passive margin formation.

In spite of the occurrence of large extensional faults, the 13 December 1990 earthquake, the largest event recorded instrumentally along the Malta Escarpment, shows a strike-slip focal mechanism the P-axis of which is compatible with left-lateral strike-slip along the Malta Escarpment trend (Fig. 8; Giardini *et al.* 1995; Amato *et al.* 1995). The earthquake is 15–20 km deep and partitioning between strike-slip and extension can possibly occur as a response to a deep-seated trench-perpendicular tear which would likely have scissor-like motion with large vertical throws (Wortel & Spakman 2000).

Additional indication of left-lateral strike-slip affecting the subducted plate along the Malta Escarpment comes from the slip observed along the Quaternary faults at the eastern border of the Hyblean Plateau (Fig. 8; Adam *et al.* 2000). Within this frame, the broad NNW–SSE-trending uplifted region north of Alfeo Smt. (Fig. 8) can possibly represent a restraining bend of a deep-seated left-lateral tear fault (e.g. McClay & Bonora 2001) that links the extension of the Alfeo Smt. to the faults further north (Argnani & Bonazzi 2005).

Seismic profiles allow us to rule out the hypothesized occurrence of a large extensional fault (Taormina Fault) located offshore along the coastline between Taormina and Messina. An important geodynamic implication is that the extensional faults of southern Calabria (upper plate), and the extensional faults of SE Sicily (lower plate) belong to two different tectonic systems and cannot be physically linked via the Taormina Fault, as previously suggested (e.g. Monaco & Tortorici 2000; Jacques *et al.* 2001). Nevertheless, as suggested by tilting of marine strata along the offshore slope, a long sector of the coastline is actively deforming (Fig. 8). The origin of the observed tilting is difficult to figure out, but it might represent the surface response of the deep tear in the subducted Tyrrhenian slab (Govers & Wortel 2005; Argnani & Bonazzi 2005).

The NNW–SSE-trending Aeolian volcanoes (Vulcano, Lipari and Salina) and Mt Etna are located along a line possibly acting as a guide to magma uprise (Lanzafame & Bousquet 1997). Transpressional deformation affected the central Aeolian Islands since middle Pleistocene, being mostly coeval with volcanic activity. This transpression is superposed to a previous extensional tectonics, suggesting a recent change in tectonic regime. Similarly, the compression currently observed offshore of northern Sicily on the basis of focal mechanisms has been interpreted as the expression of a new tectonic regime that affected the central Mediterranean, possibly in the last 2 Ma (Goes *et al.* 2004: Jenny *et al.* 2006). If compression in the central Aeolian Islands is part of the same process, the onset of the new tectonic regime can be dated around the middle Pleistocene.

A remarkable rotation of structural directions occurs in the region between the central Aeolian Islands and southern Calabria (Fig. 8), and the axes of maximum horizontal compression show a clockwise rotation. These evidences possibly represent the superficial expression of a STEP fault, when compared to numerical modelling prediction (Govers & Wortel 2005). However, additonal complexities are present, that can be attributed to the upper-plate response to deep seated processes.

Conclusions

Several lines of evidence indicate that distinct episodes of slab break-off have possibly occurred during the evolution of the Tyrrhenian subduction. The first episode occurred from 8.5 to 4.0 Ma and affected the segment of the slab located in the

Sardinia Channel. This espisode can be related to the abandonment of the Adventure thrust front and to the opening of the Vavilov basin. The second episode occurred between 2.5 and 1.6 Ma and affected the segment of slab located north of Sicily. This espisode can be related to the opening of the Marsili basin and was preceeded by rifting in the Strait of Sicily. The space and time location of these episodes appear controlled by discontinuities that are pre-existing within the subducted African plate and that trend at high angle to the advancing subduction front. These discontinuities delimit segments of subducted slab that can be affected by slab break-off at different times and, in places, can act as way out for magma and mantle-derived He. Depending upon their degree of weakness they can be activated as trench-perpendicular tear (STEP faults). Several lines of geological and geophysical evidence indicate that the northern part of the NNW–SSE-trending Malta Escarpment, that represents the major discontinuity within the subducted African plate, has been reactivated as a STEP fault since middle Pleistocene. The volcanic activity along the Salina–Vulcano–Etna alignment which becomes younger SE-ward (Mazzuoli *et al.* 1995), the recent NNW–SSE trending extensional faults on the eastern flank of Mt Etna (Lanzafame & Bousquet, 1997), and the Quaternary faulting along the Malta Escarpment, offshore the Hyblean plateau (Argnani & Bonazzi 2005), with their associated earthquakes (Chiarabba *et al.* 2005), all indicate that a reorientation of the lithospheric tear is presently occurring.

Finally, taking into account the evolution of slab tearing along the southern Tyrrhenian subduction, it seems that the hierarchy in strength, of these trench-perpendicular features which are present in the subducted plate, greatly affected the timing and amount of trench retreat and backarc opening.

Discussions with E. Serpelloni, S. Pondrelli and G. Vannucci helped to shape the ideas presented in this contribution. The useful suggestions of A. Billi and an anonymous reviewer helped greatly to improve the manuscript. A special thanks to C. Bonazzi, who carried out the processing of seismic data. Financial support from DPC-INGV project S2, coordinated by G. Valensise and D. Slejko, is kindly acknowledged.

References

ADAM, J., REUTHER, C.-D., GRASSO, M. & TORELLI, L. 2000. Active fault kinematics and crustal stresses along the Ionian margin of the southeastern Sicily. *Tectonophysics*, **326**, 217–239.

AMATO, A., AZZARA, R., BASILI, A., CHIARABBA, C., COCCO, M., DI BONA, M. & SELVAGGI, G. 1995. Main shock and after shocks of the December 13, 1990 Eastern Sicily earthquake. *Annali di Geofisica*, **38**, 255–266.

AMORUSO, A., CRESCENTINI, L. & SCARPA, R. 2002. Source parameters of the 1908 Messina Straits, Italy, earthquake from geodetic and seismic data. *Journal of Geophysical Research*, **107**, 10.1029/2001JB000434.

ANDERSON, H. & JACKSON, J. 1987. The deep seismicity of the Tyrrhenian Sea. *Geophysical Journal Royal Astronomical Society*, **91**, 613–637.

ANDREWS, E. & BILLEN, M. I. 2007. Rheologic controls on the dynamics of slab detachment. *Tectonophysics*, in press.

ANTONIOLI, F., FERRANTI, L., LAMBECK, K., KERSHAW, S., VERRUBI, V. & DAI PRA, G. 2006. Late Pleistocene to Holocene record of changing uplift rates in southern Calabria and northeastern Sicily (southern Italy, Central Mediterranean Sea). *Tectonophysics*, **422**, 23–40.

ARGNANI, A. 1987. The Gela Nappe: evidence of accretionary melange in the Maghrebian foredeep of Sicily. *Memorie della Societá Geologica Italiana*, **38**, 419–428.

ARGNANI, A. 1990. The Strait of Sicily Rift Zone: foreland deformation related to the evolution of a back-arc basin. *Journal of Geodynamics*, **12**, 311–331.

ARGNANI, A. 1993. Neogene basins in the Strait of Sicily (Central Mediterranean): tectonic settings and geodynamic implications. *In*: BOSCHI, E. ET AL. (eds) *Recent Evolution and Seismicity of the Mediterranean Region*. Kluwer Academic Publication, 173–187.

ARGNANI, A. 2000. The Southern Tyrrhenian Subduction System: Recent Evolution and Neotectonic Implications. *Annali di Geofisica*, **43**, 585–607.

ARGNANI, A. 2003. Central Mediterranean evolution and Foreland Tectonics: The Straits of Sicily – Pelagian Sea (North African Continental Margin). *In*: SALEM, M. J., OUN, K. M. & SEDDIQ, H. M. (eds) *The Geology of Northwest Libya, Vol. III*. Second Symposium on the Sedimentary Basins of Lybia, 139–153.

ARGNANI, A. 2005. Possible record of a Triassic ocean in the southern Apennines. *Bollettino della Societá Geologica Italiana*, **124**, 109–121.

ARGNANI, A. & BONAZZI, C. 2005. Tectonics of Eastern Sicily Offshore. *Tectonics*, **24**, TC4009, doi:10.1029/2004TC001656.

ARGNANI, A. & SAVELLI, C. 1999. Cenozoic volcanotectonics in the southern Tyrrhenian Sea: space-time distribution and geodynamic significance. *Journal of Geodynamics*, **27**, 409–432.

ARGNANI, A. & SAVELLI, C. 2001. Magmatic signature of episodic backarc rifting in the southern Tyrrhenian sea. *In*: ZIEGLER, P., CAVAZZA, W., ROBERTSON, A. H. F. & CRASQUIN-SOLEAU, S. (eds) *PeriTethys Memoir 6: Rift/Wrench Basins and Passive Margins.* Memoires du Museum National d'Historie Naturelle, **186**, 735–754.

ARGNANI, A., CORNINI, S., TORELLI, L. & ZITELLINI, N. 1987. Diachronous Foredeep-System in the Neogene-Quaternary of the Strait of Sicily. *Memorie della Societá Geologica Italiana*, **38**, 407–417.

ARGNANI, A., SERPELLONI, E. & BONAZZI, C. 2007. Pattern of deformation around the central Aeolian Islands: evidence from multichannel seismics and GPS data. *Terra Nova*, **19**, 317–323.

Argnani, A., Brancolini, G., Rovere, M., Accaino, F., Zgur, F., Grossi, M. *et al.* 2008. Hints on active tectonics in the Messina Straits and surroundings: preliminary results from the TAORMINA-2006 seismic cruise. *Bollettino di Geofisica Teorica e Applicata*, **49**, 163–176.

Baccheschi, P., Margheriti, L. & Steckler, M. 2007. Seismic anisotropy reveals focussed mantle flow around the Calabrian slab (Southern Italy). *Geophysical Research Letters*, **34**, L05302, doi:10.1029/2006GL028899.

Barone, A., Fabbri, A., Rossi, S. & Sartori, R. 1982. Geological structure and evolution of the marine areas adjacent to the Calabrian arc. *Earth Evolution Sciences*, **3**, 207–221.

Billi, A., Barberi, G., Faccenna, C., Neri, G., Pepe, F. & Sulli, A. 2006. Tectonics and seismicity of the Tindary Fault System, southern Italy: crustal deformations at the transition between ongoing contractional and extensional domains located above the edge of a subducting slab. *Tectonics*, **25**, doi:10.1029/2004TC001763.

Bordoni, P. & Valensise, G. 1998. Deformation of the 125 ka marine terrace in Italy: tectonic implications. *In*: Stewart, I. S. & Vita Finzi, C. (eds) *Coastal Tectonics*. Geological Society, London, Special Publication, **146**, 71–110.

Boschi, E., Guidoboni, E. & Mariotti, D. 1995. Seismic effect of the strongest historical earthquakes in the Syracuse area. *Annali di Geofisica*, **38**, 223–252.

Burchfiel, B. C. & Royden, L. H. 1991. Antler orogeny: A Mediterranean-type orogeny. *Geology*, **19**, 66–69.

Burollet, P. F. 1991. Structure and tectonics of Tunisia. *Tectonophysics*, 359–369.

Calanchi, N., Colantoni, P., Rossi, P. L., Saitta, M. & Serri, G. 1989. The Strait of Sicily continental rift system: physiography and petrochemistry of the submarine volcanic centres. *Marine Geology*, **87**, 55–83.

Calanchi, N., Lucchi, F., Pirazzoli, P. A., Romagnoli, C., Tranne, C. A., Radtke, U., Reyss, J. L. & Rossi, P. L. 2002. Late Quaternary relative sea-level changes and vertical movements at Lipari (Aeolian Islands). *Journal of Quaternary Science*, **17**, 459–467.

Caracausi, A., Favara, R., Italiano, F., Nuccio, P. M., Paonita, A. & Rizzo, A. 2005. Active geodynamics of the central Mediterranean Sea: Tensional tectonic evidences in western Sicily from mantle-derived helium. *Geophysical Research Letters*, **32**, L04312, doi:10.1029/2004GL021608.

Carminati, E., Wortel, M. J. R., Spakman, W. & Sabadini, R. 1998. The role of slab detachment processes in the opening of the western-central Mediterranean basins: some geological and geophysical evidence. *Earth and Planetary Science Letters*, **160**, 651–665.

Catalano, S. & De Guidi, G. 2003. Late Quaternary uplift of northeastern Sicily: relation with the active normal faulting deformation. *Journal of Geodynamics* **36**, 445–467.

Catalano, R., Di Stefano, P., Sulli, A. & Vitale, F. P. 1996. Paleogeography and structure of the central Mediterranean: Sicily and its offshore area. *Tectonophysics*, **260**, 291–323.

Catalano, S., De Guidi, G., Lanzafame, G., Monaco, C., Torrisi, S., Tortorici, G. & Tortorici, L. 2006. Inversione tettonica positiva tardo-quaternaria nel Plateau Ibleo (Sicilia SE). *Rendiconti della Societá Geologica Italiana*, **2**, 118–120.

Channell, J. E. T., Oldow, J. S., Catalano, R. & D'Argenio, B. 1990. Paleomagnetically determined rotations in the western Sicilian fold and thrust belt. *Tectonics*, **9**, 641–660.

Chiarabba, C., Jovane, L. & Di Stefano, R. 2005. A new view of Italian seismicity using 20 years of instrumental recordings. *Tectonophysics*, **395**, 251–268.

Civello, S. & Margheriti, L. 2004. Toroidal mantle flow around the Calabrian slab (Italy) from SKS splitting. *Geophysical Research Letters*, **31**, L10601, doi:10.1029/2004GL019607.

D'Agostino, N. & Selvaggi, G. 2004. Crustal motion along the Eurasia–Nubia plate boundary in the Calabrian Arc and Sicily and active extension in the Messina Straits from GPS measurements. *Journal of Geophysical Research*, **109**, B11402, doi:10.1029/2004JB002998.

De Astis, G., Ventura, G. & Vilardo, G. 2003. Geodynamic significance if the Aeolian volcanism (Southern Tyrrhenian Sea, Italy) in light of structural, seismological, and geochemical data. *Tectonics*, **22**, 1040, doi:10.1029/2003TC001506.

DeMets, C., Gordon, R. G., Argus, D. F. & Stein, S. 1990. Current plate motions. *Geophysical Journal International*, **101**, 425–478.

Dewey, J. F., Pitman, W. C., III, Ryan, W. B. F. & Bonnin, J. 1973. Plate tectonics and the evolution of the Alpine systems. *Geological Society American Bulletin*, **84**, 137–180.

Dewey, J. F., Helman, M. L., Turco, E., Hutton, D. H. W. & Knott, S. D. 1989. Kinematics of the western Mediterranean. *In*: Coward, M. P., Dietrich, D. & Park, R. G. (eds) *Alpine Tectonics*. Geological Society, London, Special Publication, **45**, 265–283.

Doglioni, C., Innocenti, F. & Mariotti, G. 2001. Why Mt Etna? *Terra Nova*, **13**, 25–31.

Dvorkin, J., Nur, A., Mavko, G. & Ben-Avraham, Z. 1993. Narrow subduction slabs and the origin of backarc basins. *Tectonophysics*, **227**, 63–79.

Fabbri, A., Rossi, S., Sartori, R. & Barone, A. 1982. Evoluzione neogenica dei margini marini dell'Arco Calabro-Peloritano: implicazioni geodinamiche. *Memorie della Societá Geologica Italiana*, **24**, 357–366.

Faccenna, C., Piromallo, C., Crespo-Blac, A., Jolivet, L. & Rossetti, F. 2004. Lateral slab deformation and the origin of the western Mediterranean arcs. *Tectonics*, **23**, TC1012, doi:10.1029/2002TC001488.

Faccenna, C., Civetta, L., D'Antonio, M., Funiciello, F., Margheriti, L. & Piromallo, C. 2005. Constraints on mantle circulation around the deforming Calabrian slab. *Geophysical Research Letters*, **32**, L06311, doi:10.1029/2004GL021874.

Funiciello, F., Moroni, M., Piromallo, C., Faccenna, C., Cenedese, A. & Bui, H. A. 2006. Mapping mantle flow during retreating subduction: laboratory models analayzed by feature tracking. *Journal of Geophysical Research*, **111**, B03402, doi:10.1029/2005JB003792.

Galli, P., Scionti, V. & Spina, V. 2007. New paleoseismic data from the Lakes and Serre faults: seismotectonic implications for Calabria (Southern Italy). *Bollettino della Societá Geologica Italiana*, **126**, 347–364.

Gamberi, F. & Argnani, A. 1995. Basin formation and inversion tectonics on top of the Egadi foreland thrust belt (NW Strait fo Sicily). *Tectonophysics*, **252**, 285–294.

Gardiner, W., Grasso, M. & Sedgely, D. 1995. Plio-Pleistocene fault movement as evidence for megablock kinematics within the Hyblean–Malta Plateau, Central Mediterranean. *Journal of Geodynamics*, **19**, 35–51.

Gattacceca, J. & Speranza, F. 2002. Paleomagnetism of Jurassic to Miocene sediments from the Apenninic carbonate platform (Southern Apennines, Italy); evidence for a 60 degrees counterclockwise Miocene rotation. *Earth and Planetary Science Letters*, **201**, 19–34.

Ghisetti, F. 1979. Relazioni tra strutture e fasi trascorrenti e distensive lungo i sistemi Messina-Fiumefreddo, Tindari-Letojanni e Alia-Malvagna (Sicilia nord-orientale); uno studio microtettonico. *Geologica Romana*, **18**, 23–58.

Ghisetti, F. 1981. Upper Pliocene-Pleistocene uplift rates as indicators of neotectonic pattern: an example from southern Calabria (Italy). *Zeitschrift fuer Geomorphologie, Supplementband*, **40**, 93–118.

Ghisetti, F. 1992. Fault parameters in the Messina Strait (southern Italy) and relations with the seismogenic source. *Tectonophysics*, **210**, 117–133.

Giardini, D., Palombo, B. & Pino, N. A. 1995. Long-period modelling of MEDNET waveforms for the December 13, 1990 Eastern Sicily earthquake. *Annali Geofisica*, **38**, 267–282.

Goes, S., Giardini, D., Jenny, S., Hollenstein, C., Kahle, H.-G. & Geiger, A. 2004. A recent reorganization in the south-central Mediterranean. *EPSL*, **226**, 335–345.

Govers, R. & Wortel, M. J. R. 2005. Lithosphere tearing at STEP faults: response to edges of subduction zones. *EPSL*, **236**, 505–523.

Gvirtzman, Z. & Nur, A. 1999*a*. Plate detachment, asthenosphere upwelling, and topography across subduction zones. *Geology*, **27**, 563–566.

Gvirtzman, Z. & Nur, A. 1999*b*. The formation of Mount Etna as the consequence of slab rollback. *Nature*, **401**, 782–785.

Hollenstein, C., Kahle, H.-G., Geiger, A., Jenny, S., Goes, S. & Giardini, D. 2003. New GPS constraints on the Africa–Eurasia plate boundary zone in southern Italy. *Geophysical Research Letters*, **30**, doi:10.1029/2003GL017554.

Horvath, F. & Berckhemer, H. 1982. Mediterranean Backarc Basins. *In*: Berckhemer, H. & Hsu, K. (eds) *Alpine-Mediterranean Geodynamics, AGU Geodynamic Series*, **7**, 141–173.

Isacks, B. L. & Barazangi, M. 1977. Geometry of Benioff zones: lateral segmentation and downwards bending of the subducted lithosphere. *In*: Talwani, M. & Pitman, W. C. (eds) Island arcs, deep-sea trenches and back-arc basins. *A. G. U. Maurice Ewing Series*, **1**, 99–114.

Jacques, E., Monaco, C., Tapponier, P., Tortorici, L. & Winter, T. 2001. Faulting and earthquake triggering during the 1783 Calabria seismic sequence. *Geophysical Journal International*, **147**, 499–516.

Jenny, S., Goes, S., Giardini, D. & Kahle, H.-G. 2006. Seismic potential of Southern Italy. *Tectonophysics*, **415**, 81–101.

Kastens, K., Mascle, J. *et al.* 1988. ODP Leg 107 in the Tyrrhenian sea: Insights into passive margin and back-arc basin evolution. *Geological Society America Bulletin*, **100**, 1140–1156.

Kincaid, C. & Griffiths, R. W. 2003. Laboratory models of the thermal evolution of the mantle during rollback subduction. *Nature*, **425**, p58, 62.

Lanzafame, G. & Bousquet, J. C. 1997. The Maltese escarpment and its extension from Mt. Etna to the Aeolian Islands (Sicily): importance and evolution of a lithosphere discontinuity. *Acta. Vulcanlogica*, **9**, 113–120.

Lentini, F., Catalano, S. & Carbone, S. 2000. *Carta Geologica della provicnia di Messina*. Scale 1:50000, S. E. L. C. A. Firenze.

Le Pichon, X., Bergerat, F. & Roulet, M. J. 1988. Plate kinematics and tectonics leading to the Alpine belt formation; A new analysis. *Geological Society of America, Special Paper*, **218**, 111–131.

Lickorish, W. H., Grasso, M., Butler, R. W. H., Argnani, A. & Maniscalco, R. 1999. Structural styles and regional tectonic setting of the Gela Nappe (SE Sicily). *Tectonics*, **18**, 655–668.

Lonergan, L. & White, N. 1997. Origin of the Betic-Rif mountain belt. *Tectonics*, **16**, 504–522.

Lucchi, F., Tranne, C. A., Calanchi, N., Pirazzoli, P. A., Romagnoli, C., Radtke, U., Reyss, J. L. & Rossi, P. L. 2004. Late-Quaternary ancient shorelines at Lipari (Aeolian Islands). Stratigraphical constraints to reconstruct geological evolution and vertical movements. *Quaternary International*, **115–116**, 105–115.

Lucente, F. P., Chiarabba, C., Cimini, G. B. & Giardini, D. 1999. Tomographic constraints on the geodynamic evolution of the Italian region. *Journal of Geophysical Research*, **104**, 20,307–20,327.

Malinverno, A. & Ryan, W. B. F. 1986. Extension in the Tyrrhenian Sea and shortening in the Apennines as result of arc migration driven by sinking in the lithosphere. *Tectonics*, **5**, 227–245.

Marani, M. P., Gamberi, F., Bortoluzzi, G., Carrara, G., Ligi, M. & Penitenti, D. 2004. Seafloor bathymetry of the Ionian Sea. *In*: Marani, M. P., Gamberi, F. & Bonatti, E. (eds) From seafloor to deep mantle: architecture of the Tyrrhenian backarc basin. *Memorie Descrittive della Carta Geologica D'Italia*, **44**, Plate 3.

Mazzuoli, R., Tortorici, L. & Ventura, G. 1995. Oblique rifting in Salina, Lipari and Vulcano islands (Aeolian islands, southern Italy). *Terra Nova*, **7**, 444–452.

McClay, K. & Bonora, M. 2001. Analog models of restraining stepovers in strike-slip fault systems. *AAPG Bulletin*, **85**, 233–260.

MELE, G. 1998. High-frequency wave propagation from mantle earthquakes in the Tyrrhenian Sea: New constraints for the geometry of the South Tyrrhenian subduction zone. *Geophysical Research Letters*, **25**, 2877–2880.

MELE, G., ROVELLI, A., SEBER, D., HEARN, T. & BARAZANGI, M. 1998. Compressional velocity structure and anisotropy in the uppermost mantle beneath Italy and surrounding regions. *Journal Geophysical Research*, **103**(B6), 12,529–12,543, 1998.

MONACO, C. & TORTORICI, L. 2000. Active faulting in the Calabrian arc and eastern Sicily. *Journal Geodynamics*, **29**, 407–424.

MONTUORI, C., CIMINI, G. B. & FAVALI, P. 2007. Teleseismic tomography of the southern Tyrrhenian subduction zone; New results from seafloor and land recordings. *Journal Geophysical Research*, **112**, B03311, doi:10.1029/2005JB004114, 2007.

NERI, G., BARBERI, G., OLIVA, G. & ORECCHIO, B. 2005. Spatial variations of seismogenic stress orientations in Sicily, south Italy. *Physics of the Earth and Planetary Interiors*, **148**, 175–191.

NICOLOSI, I. F., SPERANZA, F. & CHIAPPINI, M. 2006. Ultrafast oceanic spreading of the Marsili Basin, southern Tyrrhenian Sea: Evidence from magnetic anomaly analysis. *Geology*, **34**, 717–720.

PATACCA, E. & SCANDONE, P. 2004. The Plio-Pleistocene thrust belt – foredeep system in the Southern Apennines and Sicily (Italy). *Bollettino della Societá Geologica Italiana*, **32**, 93–129.

PATACCA, E., SARTORI, R. & SCANDONE, P. 1992. Tyrrhenian basin and Apenninic arcs. Kinematic relations since late Tortonian times. *Memorie della Societá Geologica Italiana*, **45**, 425–451.

PEPE, F., BERTOTTI, G., CELLA, F. & MARSELLA, E. 2000. Rifted margin formation in the south Tyrrhenian Sea: A high-resolution seismic profile across the north Sicily passive continental margin. *Tectonics*, **19**, 241–257.

PEPE, F., BERTOTTI, G. & CLOETINGH, S. 2004. Tectono-stratigraphic modelling of the North Sicily continental margin (southern Tyrrhenian Sea). *Tectonophysics*, **384**, 257–273.

PIROMALLO, C. & MORELLI, A. 2003. P-wave tomography of the mantle under the Alpine-Mediterranean area. *Journal Geophysical Research*, **108**, B2, doi: 10.1029/2002JB001757.

PONDRELLI, S., PIROMALLO, C. & SERPELLONI, E. 2004. Convergence vs. retreat in Southern Tyrrhenian Sea: Insights from kinematics. *Geophysical Research Letters*, **31**, L06611, doi:10.1029/2003GL019223.

PONDRELLI, S., SALIMBENI, S., EKSTRÖM, G., MORELLI, A., GASPERINI, P. & VANNUCCI, G. 2006. The Italian CMT dataset from 1977 to the present. *Physics of the Earth and Planetary Interiors*, doi:10.1016/j.pepi.2006.07.008,159/3–4, pp. 286–303.

REHAULT, J.-P., BOILLOT, G. & MAUFFRET, A. (1984): The western Mediterranean Basin geological evolution. *Marine Geology*, **55**, 447–477.

ROSENBAUM, G. & LISTER, G. S. 2004. Neogene and Quaternary rollback evolution of the Tyrrhenian Sea, the Apennines, and the Sicilian Maghrebides. *Tectonics*, **223**, TC1013, doi:10.1029/2003TC001518.

ROSENBAUM, G., GASPARON, M., LUCENTE, F. P., PECCERILLO, A. & MILLER, S. 2008. Kinematics of slab tear faults during subduction segmentation and implication for Italian magmatism. *Tectonics*, **27**, doi:10.1029/2007TC002143.

ROSSI, S. & BORSETTI, A. M. 1977. Dati preliminari di stratigrafia e di sismica del Mare Ionio settentrionale. *Memorie della Societá Geologica Italiana*, **13**, 251–259.

ROURE, F., HOWELL, D. G., MUELLER, C. & MORETTI, I. 1990. Late Cenozoic subduction complex of Sicily. *Journal of Structural Geology*, **22**, 259–266.

SAVELLI, C. 2002. Time-space distribution of magmatic activity in the western Mediterranean and peripheral orogens during the past 30 Ma (a stimulus to geodynamic considerations). *Journal of Geodynamics*, **34**, 99–126.

SCANDONE, P., PATACCA, E., RADOICIC, R., RYAN, W. B., CITA, M. B., RAWSON, M., CHEZAR, H., MILLER, E., MACKENZIE, J. & ROSSI, S. 1981. Mesozoic and Cenozoic rocks from Malta Escarpment (central Mediterranean). *AAPG Bulletin*, **65**, 1299–1319.

SCHELLART, W. P., FREEMAN, J., STEGMAN, D. R., MORESI, L. & MAY, D. 2007. Evolution and diversity of subduction zones controlled by slab width. *Nature*, **446**, 308–311, doi:10.1038/nature05615.

SCHICK, R. 1977. Eine seismotektonische Bearbeitung des Erdbebens von Messina im Jahre 1908. *Geologisches Jahrbuch. Reihe E: Geophysik*, **11**, 3–74.

SELVAGGI, G. & CHIARABBA, C. 1995. Seismicity and P-wave image of the southern Tyrrhenian subduction zone. *Geophysical Journal International*, **121**, 818–826.

SERPELLONI, E., VANNUCCI, G., PONDRELLI, S., ARGNANI, A., CASULA, G., ANZIDEI, M., BALDI, P. & GASPERINI, P. 2007. Kinematics of the Western Africa-Eurasia plate boundary from focal mechanisms and GPS data. *Geophysical Journal International*, **169**, 1180–1200.

SPAKMAN, W. & WORTEL, M. J. R. 2004. A tomographic view on western Mediterranean geodynamics. *In*: CAVAZZA, W., ROURE, F., SPAKMAN, W., STAMPFLI, G. M. & ZIEGLE, P. A. (eds) *The TRANSMED Atlas – The Mediterranean region from crust to mantle*. Springer Verlag, 31–52.

SPENCE, W. 1987. Slab pull and the seismotectonics of subducting lithosphere. *Review of Geophysics*, **25**, 55–69.

SPERANZA, F., MANISCALCO, R., MATTEI, M., DI STEFANO, A., BUTLER, R. W. H. & FUNICIELLO, R. 1999. Timing and magnitude of rotations in the frontal thrust systems of southwestern Sicily. *Tectonics*, **18**, 1178–1197.

SPERANZA, F., MANISCALCO, R. & GRASSO, M. 2003. Pattern of orogenic rotation in central-eastern Sicily: implications for the timing of spreading in the Tyrrhenian Sea. *Journal of the Geological Society London*, **160**, 183–195.

VALENSISE, G. & PANTOSTI, D. 1992. A 125 Kyr-long geological record of seismic source repeatability: the Messina Straits (southern Italy) and the 1908 earthquake (Ms 7 1/2). *Terra Nova*, **4**, 472–483.

VAN DE ZEDDE, D. M. A. & WORTEL, M. J. R. 2001. Shallow slab detachment as a transient source of heat at midlithospheric depth. *Tectonics*, **20**, 868–882.

VANNUCCI, G., PONDRELLI, S., ARGNANI, A., MORELLI, A., GASPERINI, P. & BOSCHI, E. 2004. An Atlas of Mediterranean Seismicity. *Annali di Geofisica, supplementary*, **47**, 247–306.

WESTAWAY, R. 1993. Quaternary uplift of southern Italy. *Journal of Geophysical Research*, **97**, 15437–15464.

WILLETT, S., BEAUMONT, C. & FULLSACK, P. 1993. Mechanical model for the tectonics of doubly vergent compressional orogen. *Geology*, **21**, 371–374.

WONG, A., TON, S. Y. M. & WORTEL, M. J. R. 1997. Slab detachment in continental collsion zones: an analysis of controlling parameters. *Geophysical Research Letters*, **24**, 2095–2098.

WORTEL, M. J. R. & SPAKMAN, W. 1992. Structure and dynamics of subducted lithosphere in the Mediterranean region. *Proceedings of the Koninklijke Nederlandse Akademie van Wetenschappen*, **95**, 325–347.

WORTEL, M. J. R. & SPAKMAN, W. 2000. Subduction and Slab Detachment in the Mediterranean-Carpathian Region. *Science*, **290**, 1920–1917.

YOSHIOKA, S. & WORTEL, M. J. R. 1995. Three-dimensional numerical modeling of detachment of subducted lithosphere. *Journal of Geophysical Research*, **100**, 20223–20244.

Geochemical and temporal evolution of Cenozoic magmatism in western Turkey: mantle response to collision, slab break-off, and lithospheric tearing in an orogenic belt

YILDIRIM DILEK[1]* & ŞAFAK ALTUNKAYNAK[2]

[1]*Dept. of Geology, Miami University, Oxford, OH 45056, USA*

[2]*Dept. of Geological Engineering, Istanbul Technical University, Maslak 80626, Istanbul, Turkey*

**Corresponding author (e-mail: dileky@muohio.edu)*

Abstract: Post-collisional magmatism in western Anatolia began in the Eocene, and has occurred in discrete pulses throughout the Cenozoic as it propagated from north to south, producing volcano-plutonic associations with varying chemical compositions. This apparent SW migration of magmatism and accompanying extension through time was a result of the thermally induced collapse of the western Anatolian orogenic belt, which formed during the collision of the Sakarya and Tauride–Anatolide continental blocks in the late Paleocene. The thermal input and melt sources for this prolonged magmatism were provided first by slab break-off-generated aesthenospheric flow, then by lithospheric delamination-related aesthenospheric flow, followed by tectonic extension-driven upward aesthenospheric flow. The first magmatic episode is represented by Eocene granitoid plutons and their extrusive carapace that are linearly distributed along the Izmir–Ankara suture zone south of the Marmara Sea. These suites show moderately evolved compositions enriched in incompatible elements similar to subduction zone-influenced subalkaline magmas. Widespread Oligo-Miocene volcanic and plutonic rocks with medium- to high-K calc-alkaline compositions represent the next magmatic episode. Partial melting and assimilation-fractional crystallization of enriched subcontinental lithospheric mantle-derived magmas were important processes in the genesis and evolution of the parental magmas, which experienced decreasing subduction influence and increasing crustal contamination during the evolution of the Eocene and Oligo-Miocene volcano-plutonic rocks. Collision-induced lithospheric slab break-off provided an influx of aesthenospheric heat and melts that resulted in partial melting of the previously subduction-metasomatized mantle lithosphere beneath the suture zone, producing the Eocene and Oligo-Miocene igneous suites. The following magmatic phase during the middle Miocene (16–14 Ma) developed mildly alkaline bimodal volcanic rocks that show a decreasing amount of crustal contamination and subduction influence in time. Both melting of a subduction-modified lithospheric mantle and aesthenospheric mantle-derived melt contribution played a significant role in the generation of the magmas of these rocks. This magmatic episode was attended by region-wide extension that led to the formation of metamorphic core complexes and graben systems. Aesthenospheric upwelling caused by partial delamination of the lithospheric root beneath the western Anatolian orogenic belt was likely responsible for the melt evolution of these mildly alkaline volcanics. Lithospheric delamination may have been caused by 'peeling off' during slab rollback. The last major phase of magmatism in the region, starting *c.*12 Ma, is represented by late Miocene to Quaternary alkaline to super-alkaline volcanic rocks that show OIB-like geochemical features with progressively more potassic compositions increasing toward south in time. These rocks are spatially associated with major extensional fault systems that acted as natural conduits for the transport of uncontaminated alkaline magmas to the surface. The melt source for this magmatic phase carried little or no subduction component and was produced by the decompressional melting of aesthenospheric mantle, which flowed in beneath the attenuated continental lithosphere in the Aegean extensional province. This time-progressive evolution of Cenozoic magmatism and extension in western Anatolia has been strongly controlled by the interplay between regional plate-tectonic events and the mantle dynamics, and provides a realistic template for post-collisional magmatism and crustal extension in many orogenic belts.

Western Anatolia (Turkey) is part of the Aegean extensional province, which is situated in an active convergent zone between the African and Eurasian Plates (Fig. 1a). One of the most seismically active and rapidly deforming domains of the Alpine–Himalayan mountain belt, the Aegean province is also a site of widespread magmatism since the early Eocene (*c.* 54 Ma) although the tectonic

From: VAN HINSBERGEN, D. J. J., EDWARDS, M. A. & GOVERS, R. (eds) *Collision and Collapse at the Africa–Arabia–Eurasia Subduction Zone*. The Geological Society, London, Special Publications, **311**, 213–233.
DOI: 10.1144/SP311.8 0305-8719/09/$15.00

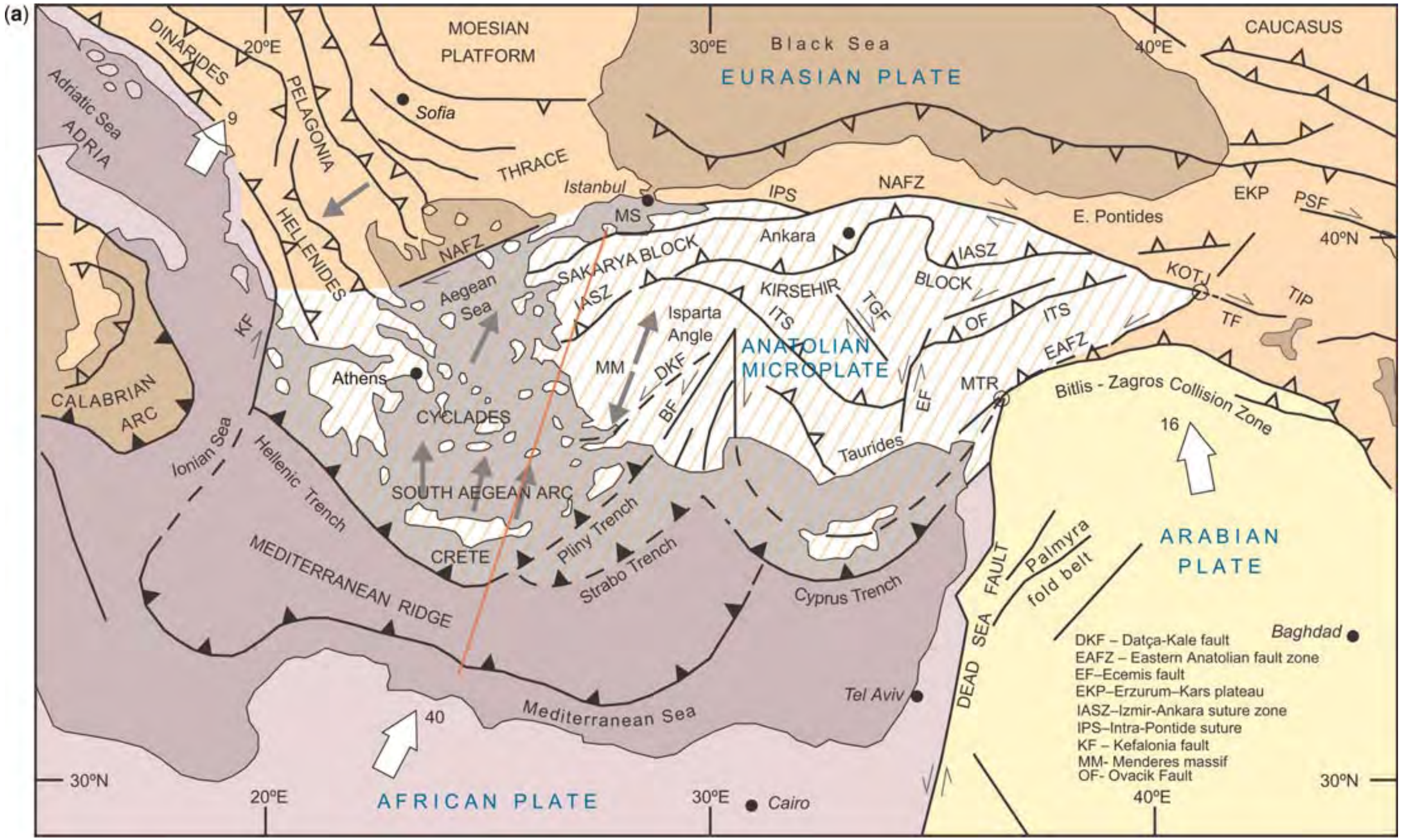

Fig. 1. (**a**) Tectonic map of the Aegean and eastern Mediterranean region, showing the main plate boundaries, major suture zones, and fault systems. Thick, white arrows depict the direction and magnitude (mm/a) of plate convergence; grey arrows mark the direction of extension (Miocene–Recent). Light-grey tone north of the North Anatolian Fault Zone (NAFZ) and west of the Calabrian Arc delineates Eurasian plate affinity, whereas the grey tones south of the Hellenic, Strabo and Cyprus Trenches delineate African plate affinity. KOTJ, Karliova triple junction; MS, Marmara Sea; MTR, Maras triple junction; NAFZ, North Anatolian fault zone; OF, Ovacik fault; PSF, Pampak-Sevan fault; TF, Tutak fault; TGF, Tuz Gölü fault; TIP, Turkish-Iranian plateau (modified from Dilek 2006).

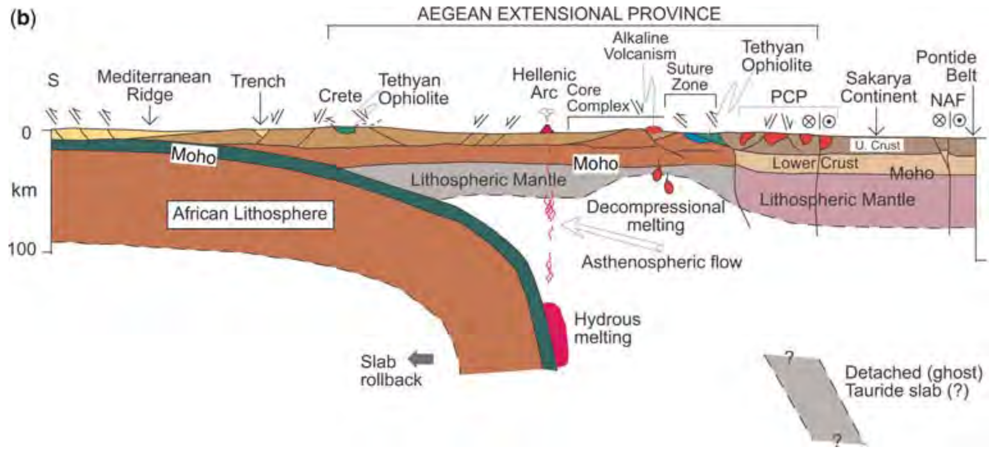

Fig. 1. (*Continued*) (**b**) Interpretative tectonic cross-section along a NNE-SSW-trending profile (straight line in 1a) through the Africa–Eurasia convergence zone and the Aegean extensional province. The Aegean extensional province straddles the Anatolide-Tauride and Sakarya continental blocks, which collided in the Paleocene. The Cretaceous Tethyan ophiolites and blueschist rocks are derived from the suture zone (Izmir-Ankara suture zone) between these two continental blocks. Eocene–Oligocene post-collisional plutons (PCP) north of this suture zone mark the oldest Cenozoic magmatic products in the region. Cenozoic magmatism appears to have migrated southward and to have changed from calc-alkaline to alkaline in composition. Lithospheric-scale necking and decompressional melting associated with aesthenospheric upwelling may have been responsible for Quaternary alkaline volcanism (i.e. Kula region) in the south-central part of the Aegean extensional province.

settings and melt sources of this widespread magmatism appear to have varied through time. The geological record of the Cenozoic magmatic events in the Aegean province is perhaps most complete in western Anatolia, where both the modern landscape and surface rocks are predominantly volcanic (Fig. 1b). Therefore, a systematic documentation of the chronology and the chemical evolution of Cenozoic volcanism in western Anatolia should reveal significant information on the mantle dynamics and its response to lithospheric- and crustal-scale processes during the evolution of an orogenic belt.

For the most part, three major geodynamic processes have been controlling the late Cenozoic evolution of the broader eastern Mediterranean region: subduction of the African/Arabian plate beneath Eurasia along the Hellenic and Cyprus trenches since the late Cretaceous (Westaway 1994; Kreemer *et al.* 2003 and the references therein; van Hinsbergen *et al.* 2005), continental collision of Arabia with Eurasia since the middle Miocene (McKenzie 1978), and the resulting westward escape of the Anatolian block along the North and East Anatolian fault zones away from the Arabia–Eurasia collision zone (Fig. 1; Dewey *et al.* 1986; Barka & Reilinger 1997). Subduction rollback processes along the Hellenic trench since 30 Ma (and potentially since the late Cretaceous) have resulted in upper-plate extension and the gravitational collapse of the Tethyan orogenic crust (Meulenkamp *et al.* 1988; Jolivet 2001; Faccenna *et al.* 2003; van Hinsbergen *et al.* 2005). Both extension and attendant magmatism in the region date back to the late Oligocene (if not older), as evidenced by the existence of metamorphic core complexes (*c.* 26 Ma; Menderes and Kazdag massifs; Fig. 2; Bozkurt & Satir 2000; Okay & Satir 2000; Isik *et al.* 2004) and extensive calc-alkaline to alkaline volcanic rocks (Savaşçin & Oyman 1998; Aldanmaz *et al.* 2000, 2006; Alici *et al.* 2002; Altunkaynak & Dilek 2006, and references therein) in western Anatolia. How the extensional deformation and magmatism started and have varied in time, space, and magnitude since the beginning of the Neogene remain some of the most fundamental questions in the geodynamic evolution of the eastern Mediterranean region and in continental tectonics in general (Dilek 2006).

In this paper we review the nature and geochemical characteristics of Cenozoic magmatism in western Turkey within the framework of its regional tectonics and evaluate the mantle sources and melt evolution of this magmatism. We then discuss the potential links between regional plate-tectonic events and the mantle dynamics that appear to have strongly affected and controlled the evolution of the Cenozoic magmatism in the region. Our model for the western Anatolian Cenozoic tectonics may be applicable to many collisional orogens,

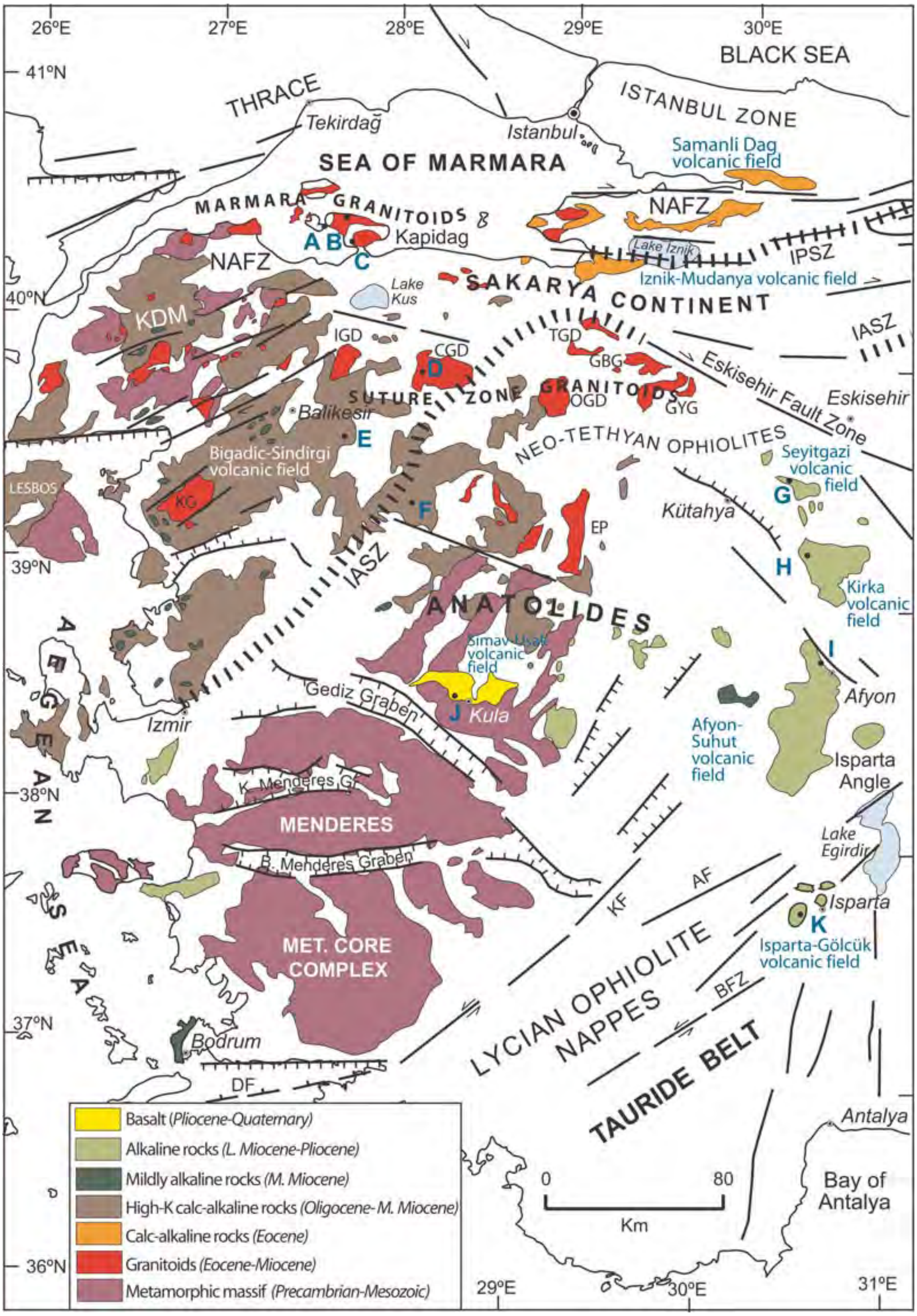

Fig. 2. Simplified geological map of western Anatolia and the eastern Aegean region, showing the distribution of major Cenozoic igneous provinces discussed in this paper and the salient fault systems. Menderes and Kazdag (KDM) massifs represent metamorphic core complexes with exhumed middle to lower continental crust. Izmir-Ankara suture

suggesting that the mode and tempo of post-collisional extension and magmatism in orogenic belts may have a common pathway.

Cenozoic geology and crustal make-up of western Anatolia

The present-day geodynamics of the eastern Mediterranean region is controlled by the relative motions of three major plates (Eurasia, Africa and Arabia) and much of deformation occurs at their boundaries (Fig. 1a; Westaway 1994; Doglioni *et al.* 2002; Dilek 2006). The convergence rate between Africa and Eurasia is greater than 40 mm/a across the Hellenic trench but decreases down to <10 mm/a across the Cyprus trench to the east (McClusky *et al.* 2000; Doglioni *et al.* 2002; Wdowinski *et al.* 2006), most likely as a result of the attempted subduction of the Eratosthenes seamount beneath Cyprus (Robertson 1998). The Arabia–Eurasia convergence across the Bitlis–Zagros suture zone has been estimated to be *c.* 16 mm/a based on global positioning system measurements of present-day central movements in this collision zone (Reilinger *et al.* 1997). These differential northward motions of Africa (<10 mm/a) and Arabia (16 mm/a) with respect to Eurasia are accommodated along the sinistral Dead Sea fault zone (Fig. 1). The Anatolian microplate north of these convergent plate boundaries is moving toward West–SW (with respect to Eurasia) at *c.* 30 mm/a along the North and East Anatolian fault zones (Fig. 1a; Reilinger *et al.* 1997) and is undergoing complex internal deformation via mainly strike-slip and normal faulting. This deformation has resulted in the extensional collapse of the young orogenic crust, which has been developed during a series of collisional events in the region (Dewey *et al.* 1986; Dilek & Moores 1990; Yılmaz 1990), giving way to the formation of metamorphic core complexes and intracontinental basins (Bozkurt & Park 1994; Dilek & Whitney 2000; Jolivet & Faccenna, 2000; Okay & Satir 2000; Doglioni *et al.* 2002; Ring & Layer 2003).

The Aegean province is situated in the upper plate of a north-dipping subduction zone at the Hellenic trench (Fig. 1b) and is considered to have evolved as a backarc environment above this subduction zone (Le Pichon & Angelier 1979; Jolivet 2001; Faccenna *et al.* 2003; van Hinsbergen *et al.* 2005). The slab retreat rate of the subducting African lithosphere has been larger than the absolute velocity of the Eurasian upper plate, causing net north–south extension in the Aegean region since the early Miocene (Fig. 1b; Jolivet *et al.* 1994; Jolivet & Faccenna 2000; Faccenna *et al.* 2003; Ring & Layer 2003). The thrust front associated with this subduction zone and its slab retreat has also migrated from the Hellenic trench (south of Crete) to the south of the Mediterranean Ridge since then (Jolivet & Faccenna 2000; Le Pichon *et al.* 2003). The backarc extension in the Aegean region thus appears to have started *c.*25 Ma, long before the onset of the Arabian collision-driven southwestward displacement of the Anatolian microplate in the late Miocene (Barka & Reilinger 1997; Jolivet & Faccenna 2000).

Timing of the onset, the causes, and the nature of extensional tectonics in western Anatolia are controversial (Seyitoğlu & Scott 1996; Gautier *et al.* 1999; Bozkurt & Satir 2000; Bozkurt 2003; Ring *et al.* 2003; Purvis & Robertson 2004; Catlos & Çemen 2005), although it is commonly accepted that the orogenic crust in western Anatolia and the Aegean area was already thinned significantly by the middle Miocene (Jolivet *et al.* 1994; Ring & Layer 2003, and references therein). Based on zircon fission track ages and radiometric dates from synkinematic granodioritic plutons (i.e. Egrigöz and Koyunoba plutons), some researchers have suggested that tectonic extension and magmatism were synchronous events starting around 25–24 Ma (Isik *et al.* 2004; Ring *et al.* 2003; Thomson & Ring 2006). In addition to slab rollback induced extensional deformation above the Hellenic subduction zone, widespread latest Oligocene–early Miocene magmatism in the region may have been partially responsible for thermally weakening the crust and hence facilitating orogen-wide extension (Thomson & Ring 2006). The timing and the causes of the initial Cenozoic magmatism in western Anatolia have, therefore, significant implications for extensional tectonism and the geodynamic evolution of the region during the late Cenozoic.

The crustal thickness in the Aegean province ranges from *c.* 16 km in the Crete Sea to 25–35 km in the Cyclades and SW Turkey (Makris & Stobbe 1984; Doglioni *et al.* 2002; Faccenna *et al.* 2003; Tirel *et al.* 2004; Zhu *et al.* 2006). These variations

Fig. 2. (*Continued*) zone (IASZ) marks the collision front between the Sakarya continental block to the north and the Anatolide-Tauride block to the south. The Eocene granitoids (shown in red) straddling this suture zone represent the first products of post-collisional magmatism in the region. Much of western Anatolia is covered by Cenozoic volcanic rocks intercalated with terrestrial deposits. Letters A through K mark the type localities of major Cenozoic igneous provinces shown in Figure 3. AF, Acigöl fault; BFZ, Burdur fault zone; DF, Datça fault; IASZ, Izmir-Ankara suture zone; KDM, Kazdag metamorphic massif; KF, Kale fault; NAFZ, North Anatolian fault zone.

in crustal thickness may indicate that extensional thinning has not been uniform in the general north–south direction, assuming that the initial crustal thickness was consistent throughout the region. Recent seismic experiment studies in the region have shown that significant amount of crustal attenuation appears to coincide with the occurrence of the metamorphic core complexes (i.e. Menderes and Cycladic massifs; Figs 1 & 2), in which high-grade intermediate to lower-crustal rocks have been exhumed in the footwalls of large-scale, low-angle detachment surfaces and in the rift shoulders of mostly east–west-trending major grabens (Lister *et al.* 1984; Avigad & Garfunkel 1991; Gautier *et al.* 1999; Bozkurt & Satir 2000; Yılmaz *et al.* 2000; Keay *et al.* 2002; Ring & Layer 2003).

The continental crust making up the upper plate of the Hellenic subduction zone south of the North Anatolian fault is composed of the Sakarya continent and the Anatolide and Tauride blocks (Fig. 2). The Sakarya continent consists of a Palaeozoic crystalline basement with its Permo-Carboniferous sedimentary cover and Permo-Triassic ophiolitic and rift or accretionary-type mélange units (Karakaya complex) that collectively form a composite continental block (Tekeli 1981; Okay *et al.* 1996). These Sakarya continental rocks and the ophiolitic units of the Izmir-Ankara suture zone (IASZ) are intruded by a series of east–west trending Eocene and Oligo-Miocene granitoid plutons (Fig. 2; Altunkaynak 2007). The Kazdag massif within the western part of the Sakarya continent (KDM in Fig. 2) represents a metamorphic core complex, which is inferred to have been exhumed starting at *c.* 24 Ma from a depth of *c.* 14 km along a north-dipping mylonitic shear zone (Okay & Satir 2000).

The western Anatolian orogenic belt consists of, from north to south, two tectonic zones: (1) the Izmir-Ankara suture zone (IASZ); and (2) the Menderes metamorphic core complex. The Menderes metamorphic massif and the IASZ rocks collectively constitute the Anatolide block in western Turkey. The IASZ south of the Sakarya continent includes dismembered Tethyan ophiolites, high-pressure low-temperature (HP/LT) blueschist-bearing rocks, and flysch deposits mainly occurring in south-directed thrust sheets (Figs 1b, 2; Önen & Hall 1993; Okay *et al.* 1998; Sherlock *et al.* 1999). Late-stage diabasic dykes crosscutting the ophiolitic units in the Kütahya area are dated at *c.* 92–90 Ma ($^{40}Ar/^{39}Ar$ hornblende ages; Önen 2003) indicating a minimum late Cretaceous igneous age of the ophiolites, whereas the blueschist rocks along the suture zone in the Tavsanli area have revealed $^{40}Ar/^{39}Ar$ cooling ages (phengite crystallization during exhumation) of $79.7 \pm 1.6 - 82.8 \pm 1.7$ Ma (Sherlock *et al.* 1999) suggesting a latest Cretaceous timing of the HP/LT metamorphism in the region. The Lycian nappes, including the ophiolites, structurally overlie the platform carbonates of the Tauride block farther south (Figs 1b & 2; Collins & Robertson 1999; Ring & Layer 2003) and represent the tectonic outliers of the Cretaceous oceanic crust derived from the IASZ. These Lycian nappes are inferred to have once covered the Menderes metamorphic massif, and then to have been removed due to the tectonic uplift and erosion associated with the exhumation of the Menderes core complex during the late Cenozoic (Ring & Layer 2003; Thomson & Ring 2006).

The Menderes core complex comprises several nappe systems composed of high-grade metamorphic rocks of Pan-African affinity that are intruded by synkinematic granitoid plutons (Hetzel & Reischmann 1996; Bozkurt & Satir 2000; Bozkurt 2004; Gessner *et al.* 2004). Rimmelé *et al.* (2003) estimated the *P-T* conditions of the metamorphic peak for the Menderes massif rocks at >10 kbar and >440 °C. The main episode of metamorphism is inferred to have resulted from the burial regime associated with the emplacement of the Lycian nappes and ophiolitic thrust sheets (Yılmaz 2002). Imbricate stacking of the Menderes nappes beneath the Lycian nappes and ophiolitic thrust sheets appears to have migrated southwards throughout the Paleocene – middle Eocene (Özer *et al.* 2001; Candan *et al.* 2005). The unroofing and exhumation of the Menderes massif may have started as early as in the Oligocene (25–21 Ma) as constrained by the cooling ages of the syn-extensional granitoid intrusions crosscutting the metamorphic rocks (Ring & Collins 2005; Thomson & Ring 2006; Bozkurt & Satir 2000; Catlos *et al.* 2002). This timing may signal the onset of the initial post-collisional tectonic extension in the Aegean region.

The Tauride block to the south consists of Precambrian–Ordovician to Lower Cretaceous carbonate rocks intercalated with volcano-sedimentary and epiclastic rocks (Ricou *et al.* 1975; Demirtasli *et al.* 1984; Özgül 1984; Gürsu *et al.* 2004) that are tectonically overlain by the Tethyan ophiolites (i.e. Lycian, Beysehir-Hoyran, Alihoca and Aladag ophiolites) along south-directed thrust sheets (Collins & Robertson 2003; Dilek *et al.* 1999*a*; Elitok & Drüppel 2008). Underthrusting of the Tauride carbonate platform beneath the Tethyan oceanic crust and its partial subduction at a north-dipping subduction zone in the Inner-Tauride ocean resulted in high-P/low-T metamorphism (Dilek & Whitney 1997; Okay *et al.* 1998). Continued convergence caused crustal imbrication and thickening within the platform and resulted in the development of several major overthrusts throughout the Tauride block (Demirtasli *et al.* 1984;

Dilek *et al.* 1999*b*). The buoyancy of the Tauride continental crust in the lower plate eventually arrested the subduction process and caused the isostatic rebound of the partially subducted platform edge, leading to block-fault uplifting of the Taurides during the latest Cenozoic (Dilek & Whitney 1997, 2000).

Cenozoic magmatism: distribution and geochemistry

The post-collisional Cenozoic magmatism in western Anatolia started after the collision of the Sakarya and Anatolide–Tauride continental blocks in the late Paleocene (Okay *et al.* 1998). The collisional front is today marked by the IASZ (Fig. 2), along which the Upper Cretaceous ophiolites tectonically overlie the high-grade metamorphic rocks of the Anatolides. The earliest products of this post-collisional magmatism are represented by I-type calc-alkaline granitoids that are linearly distributed (*c.* east–west) in a narrow belt along the IASZ. These plutons are intrusive into the Cretaceous ophiolites, the blueschist rock assemblages and the basement rocks of the Sakarya continent and are plastically to brittlely deformed by extensional shear zones and normal faults (i.e. Kapidag and Çataldag plutons; Fig. 3a–d). Those plutons closer to the IASZ (the suture zone granitoids, SZG, of Altunkaynak 2007) range in composition from diorite, quartz diorite, and granodiorite to syenite (Orhaneli, Topuk, Gürgenyayla and Göynükbelen plutons) and have ages around 54–48 Ma (Ataman 1972; Bingöl *et al.* 1982, 1994; Harris *et al.* 1994; Delaloye & Bingöl 2000; Yılmaz *et al.* 2001). The plutons farther north along the Marmara Sea (Marma granitoids, MG, of Altunkaynak 2007) are composed of monzogranite, granodiorite and granite (Armutlu, Lapseki and Kapidag plutons) and have ages around 48–34 Ma (Bingöl *et al.* 1994; Harris *et al.* 1994; Ercan *et al.* 1985; Genç & Yılmaz 1997; Delaloye & Bingöl 2000; Köprübasi *et al.* 2000; Köprübasi & Aldanmaz 2004), slightly younger than the SZGs. Volcanic equivalents of these Marmara granitoids are locally represented by basaltic to andesitic lavas and pyroclastic rocks (Genç & Yılmaz 1997).

Although the geochemical features of the SZG and MG plutons show some similarities, their magmas may have undergone different magnitudes of fractional crystallization and crustal contamination. Both the SZGs and MGs show medium- to high-K calc-alkaline characteristics with their silica contents ranging from *c.* 76 to 64 wt.% (Altunkaynak 2007). Their trace-element abundances exhibit large variations (e.g. Ba: 57–1150 ppm; Th: 2–13 ppm; La: 2.01–57.1 ppm), suggesting that these rocks were moderately enriched in incompatible elements and that their melts were moderately evolved (Pearce 1982). They display enrichment in large ion lithophile elements (LILEs; K, Rb, Ba, Th) over light rare earth elements (LREEs) and medium REEs, and depletion in high field strength elements (Zr, Nb, Ti and P) with respect to the adjacent LILE on MORB-normalized multi-element variation diagrams. Whereas the SZGs show no distinct Eu anomalies (with $Eu^*/Eu = 0.89–0.98$), the MGs display negative Eu anomalies, the magnitude of which increases with increasing SiO_2 contents; the concave upward REE patterns also become more prominent with increasing SiO_2 contents from the SZGs in the south to the MGs in the north, indicating strongly fractionated REE patterns regardless of rock type (Altunkaynak 2007). Stronger depletion of the MG rocks in Eu, Ba, Sr, and P and their higher contents of Pb, K, Ni, and SiO_2 in comparison to the SZG rocks suggest greater amounts of crustal contamination during the ascent of their magmas through the Sakarya continental crust.

The next magmatic pulse in the region is represented by Oligo-Miocene granitoid plutons and volcanic units (ranging from andesite to dacite, rhyodacite and rhyolite) that are overlain by ignimbrite flows, pumiceous air-fall, and mudflow deposits, intercalated with lower to middle Miocene lacustrine rocks and coal seams (Fig. 3e–f; Bingöl *et al.* 1982, 1994; Erkül *et al.* 2005; Yücel-Öztürk *et al.* 2005). These Oligo-Miocene volcanoplutonic complexes have silica contents ranging from 63 to 48 wt.%, medium to high Al_2O_3 abundances, and very low TiO_2 (<1 wt.%), with their MgO contents slightly higher than those of the Eocene volcano-plutonic assemblages. They are made of shoshonitic to high-K calc-alkaline rocks, showing enrichment in the most incompatible elements (Ba, Rb, Th, K, La, Ce) and depletion in Nb, Ta, P, and Ti on MORB-normalized multi-element diagrams (Altunkaynak & Dilek 2006). These features, combined with their LREE enrichment and relatively flat HREE patterns, and minor Eu anomalies ($Eu^*/Eu = 0.75–0.91$) on chondrite-normalized REE diagrams, collectively suggest derivation of their magmas from moderately to strongly evolved melts (Frey *et al.* 1978) with subduction zone geochemical signatures (Thirwall *et al.* 1994; Pearce & Peate 1995).

The ensuing middle Miocene volcanism produced mildly alkaline lavas that are spatially associated with NNE-trending transtensional fault systems (Fig. 2). Volcanic rocks of this phase consist of andesitic, trachy-andesitic and pyroclastic rocks intercalated with mildly alkaline basaltic lavas and have no plutonic equivalents exposed at the surface in the region (Akay & Erdogan 2004). The SiO_2

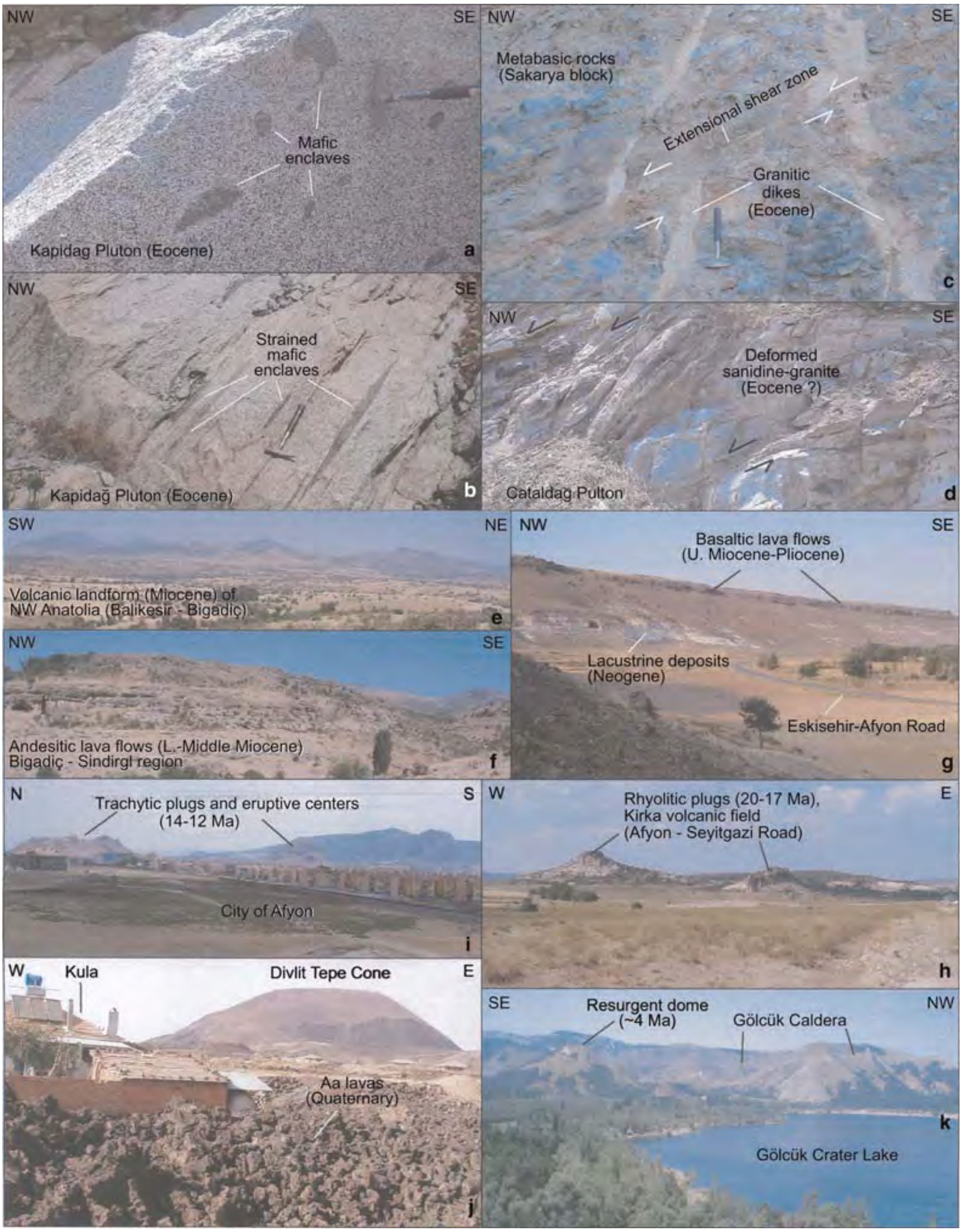

Fig. 3. Products of post-collisional Cenozoic magmatism in western Anatolia as seen in the field (see Fig. 2 for locations). (**a**) Undeformed Eocene Kapidag pluton (with mafic enclaves) as part of the Marmara granitoids in NW Turkey. (**b**) Deformed Kapidag pluton showing L-S tectonite fabric. Highly strained mafic enclaves define a WNW-dipping foliation. (**c**) Eocene granitic-granodioritic dikes intruding the metabasic basement rocks of the Sakarya block displaced along NW-dipping extensional shear zones. (**d**) Eocene Çataldag pluton, a Suture Zone granitoid near the IASZ, showing pervasive brittle-ductile deformation along NW-dipping, subparallel low-angle shear zones. (**e**) Volcanic landform of the Bigadiç-Sindirgi area, consisting mainly of Miocene high-K, calc-alkaline volcanic rocks. (**f**) Lower middle Miocene andesitic lava flows in the Bigadiç-Sindirgi volcanic field. (**g**) Upper Miocene – Pliocene basaltic lava flows and the underlying Neogene lacustrine deposits of the Seyitgazi volcanic field, south of the Eskisehir

contents of these volcanic rocks range from 60 to 46 wt.% (mildly silica-undersaturated), and have moderate to high Al_2O_3 (14.26–19.30 wt.%) and TiO_2 (0.76–2.90 wt.%), and relatively high K_2O and $Na_2O + K_2O$) values for lower SiO_2 contents. These mildly alkaline rocks display less pronounced enrichment trends in Ba, Th, K and weaker Nb and P anomalies on MORB-normalized multi-element diagrams, and lower LREE enrichment patterns on chondrite-normalized REE diagrams, in comparison to the Eocene and Oligo-Miocene igneous assemblages in western Anatolia.

Extensional tectonism was well established in western Anatolia by late Miocene and was accompanied by alkaline magmatism (Dilek & Altunkaynak 2007, and references therein). Mainly basaltic volcanism of this phase with progressively more potassic compositions increased toward south in time (G through K in Figs 2 & 3; Seyitoğlu & Scott 1992; Alici *et al.* 1998, 2002; Savasçin & Oyman 1998; Aldanmaz *et al.* 2000; Innocenti *et al.* 2005; Çoban & Flower 2006). Late Miocene–Pliocene to Quaternary volcanism produced basalts, basanites, and phonotephrites with potassic to ultrapotassic compositions (Richardson-Bunbury 1996; Seyitoğlu *et al.* 1997; Aldanmaz *et al.* 2000; Alici *et al.* 2002; Savasçin & Oyman 1998; Francalanci *et al.* 2000; Innocenti *et al.* 2005) that are commonly spatially associated with major extensional fault systems. Major eruption centers of these potassic-ultrapotassic lavas include the Afyon, Kula, and Isparta-Gölcük volcanic fields in SW Turkey (i, j and k, respectively, in Figs 2 & 3). These alkaline rocks range in age from 8.4 Ma to 0.13 ± 0.005 Ma (Richardson-Bunbury 1996; Aldanmaz *et al.* 2000; Alici *et al.* 2002; Savasçin & Oyman 1998) and have silica-undersaturated (48–41 wt.% SiO_2) compositions with higher Mg numbers (#51–84) and TiO_2 (1.80–3.22 wt.%) contents in comparison to the rocks of the subalkaline and mildly alkaline groups. The potassic-ultrapotassic lavas of the Kula volcanic field (Fig. 3j) have, for example, multi-element patterns similar to those of ocean-island basalts (OIB) with maximum enrichment in the more incompatible elements (from Nd to Cs), and display LILE enrichment (e.g. in Ba and Rb) and HREE depletion relative to the N-MORB (Innocenti *et al.* 2005). They also show LREE enrichment relative to chondrites.

The Isparta–Gölcük volcanic field farther south in the Isparta Angle region (Figs 2 & 3k) contains potassic-ultrapotassic rocks (tephriphonolite, trachyandesite, andesite) with olivine, plagioclase, clinopyroxene, biotite, amphibole and phlogopite phenocryst phases (Alici *et al.* 1998; Çoban & Flower 2006; Kumral *et al.* 2006). These rocks have very low SiO_2 (46.8–49.2 wt.%) and high MgO (10.4–11.6 wt.%) contents and lamproitic affinity, and show high LILE (Ba, Sr, Rb, K) and LREE compared to HFSE. Their depletions in Nb and Ta and high Ba/Nb (>28) ratios are characteristic of subduction zone magmas, and low Sr and high Nd isotopic compositions indicate relatively low degrees of crustal contamination.

The Cenozoic magmatism in western Anatolia appears to have swept across the region, getting younger from north to south and changing its character from calc-alkaline to alkaline over time. We evaluate below first the changing mantle sources and melt evolution of this magmatism in the region, and then the potential links between the regional plate-tectonic events and the mantle dynamics that appear to have strongly affected and controlled this evolutionary path of the Cenozoic magmatism in the region.

Mantle sources and melt evolution

Time-progressive evolution of the Cenozoic magmatism in western Anatolia closely follows the aesthenospheric – lithospheric melting array depicted on the $\varepsilon Nd_{(i)}$ vs. $^{87}Sr/^{86}Sr_{(i)}$ diagram in Figure 4. Eocene volcanoplutonic complexes, upper Oligocene – lower Miocene high-K calc-alkaline to shoshonitic rocks, and middle Miocene mildly alkaline volcanics fall between the MORB and the crustal (Aegean Sea sediments and Aegean metamorphic basement) fields along this array indicating their hybrid compositions. Trace-element and rare-earth element chemistry of these hybrid rocks suggest that the metasomatized lithospheric mantle source contribution to their melt evolution was significant, and that this enriched mantle source was subduction-influenced (Altunkaynak & Dilek 2006, and references therein). The subduction component to the source mantle was most likely introduced by the late Cretaceous subduction of the Neo-Tethyan oceanic lithosphere beneath the Sakarya Continent, as well as by the ongoing subduction at the Hellenic trench in the late Oligocene and later times (van Hinsbergen *et al.* 2005). Earlier Palaeo-Tethyan subduction events affecting the

Fig. 3. (*Continued*) fault zone. (**h**) Lower Miocene rhyolitic plugs in the Kirka volcanic field (Afyon-Seyitgazi Road). (**i**) Middle Miocene trachytic plugs and eruptive centers in and around the City of Afyon in the Afyon-Suhut volcanic field. (**j**) Quaternary basaltic Aa lava flows and a cinder cone in the Kula volcanic field. (**k**) Ignimbrites and a resurgent dome (*c*. 4 Ma) within the Gölcük caldera in the highly alkaline Isparta-Gölcük volcanic field.

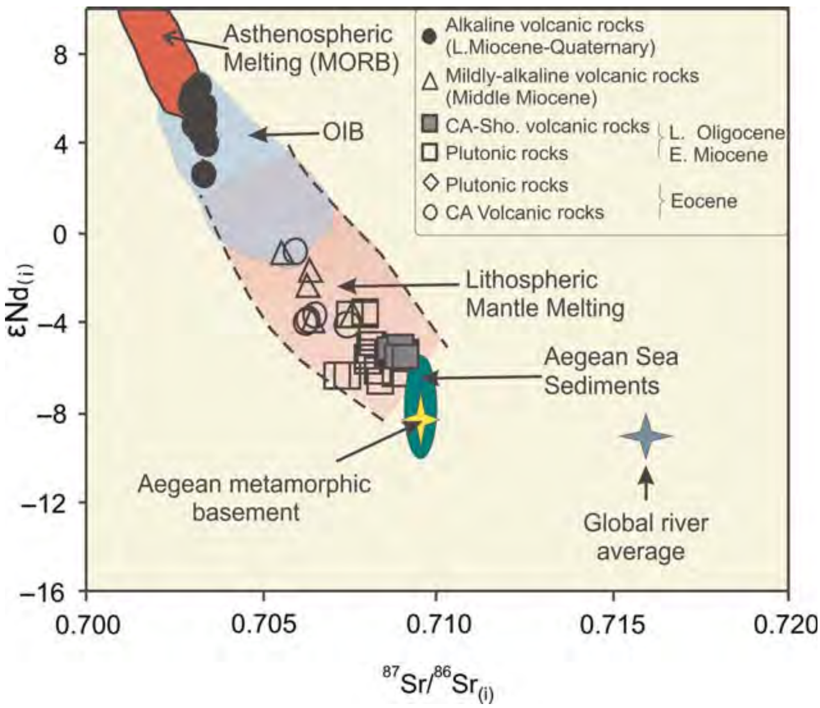

Fig. 4. Epsilon-$Nd_{(i)}$ versus $^{87}Sr/^{86}Sr_{(i)}$ diagram for the Cenozoic magmatic rocks in western Anatolia. Data for aesthenospheric and lithospheric mantle melting array from Davis & Blanckenburg (1995), for Aegean metamorphic basement from Briqueu *et al.* (1986), for Aegean Sea sediments from Altherr *et al.* (1988), and for Global river average from Goldstein & Jacobsen (1988). Modified from Altunkaynak & Dilek (2006).

geodynamic evolution of the Vardar Ocean farther north (Dilek & Thy 2006; Stampfli *et al.* 2001; Okay *et al.* 1996) may have also contributed to the metasomatization and heterogeneity of the continental mantle beneath NW Anatolia.

Geochemical features of the middle Miocene (16–14 Ma) volcanic assemblages in western Anatolia point out a major shift in the nature of the Cenozoic magmatism in the region during this time. Although the negative Ta and Nb anomalies, enriched LREE, and low Rb/Sr ratios of the mildly alkaline middle Miocene volcanic rocks indicate the involvement of a subduction-influenced and incompatible element-enriched mantle source in their magma evolution, their significantly lower La/Nb, Zr/Nb, and $^{87}Sr/^{86}Sr$ ratios, and higher $^{143}Nd/^{144}Nd$ ratios in comparison to the Eocene and Oligo-Miocene igneous assemblages suggest a diminishing effect of subduction influence and possibly a considerable influence of incoming aesthenospheric melts. The $\varepsilon Nd_{(i)}$ vs. $^{87}Sr/^{86}Sr(i)$ values of these middle Miocene volcanics plot in the middle part of the lithospheric-aesthenospheric mantle melting array (Fig. 4) supporting this interpretation.

The upper Miocene–Quaternary alkaline rocks (Fig. 2) plot mainly in the OIB field and partly straddle the MORB-OIB fields (Fig. 4), suggesting an aesthenospheric mantle source for their origin (Aldanmaz *et al.* 2000, 2006; Alici *et al.* 2002; Altunkaynak & Dilek 2006). The lack of negative Ta and Nb anomalies in their trace element patterns and an increase of the Rb/Nb and Ba/Nb ratios with decreasing $^{87}Sr/^{86}Sr$ ratios indicate that subduction contribution to their melt source was non-existent. However, the systematic variation of their εNd values and of Sr–Nd isotope ratios (Fig. 4) suggests a small-scale geochemical heterogeneity in their mantle source.

In line with this evolutionary trend of the mantle melt sources and the diminishing effect of subduction influence, we also see a progressive decrease in the degree of crustal contamination going from calc-alkaline to alkaline compositions starting around 22 Ma (Fig. 5). The lower to middle Miocene (*c.* 22–16 Ma) subalkaline rocks display higher $^{87}Sr/^{86}Sr_{(i)}$ ratios in comparison to the Eocene and Oligo-Miocene subalkaline groups, despite their other geochemical features in common. Therefore, we think of a common melt source for all these

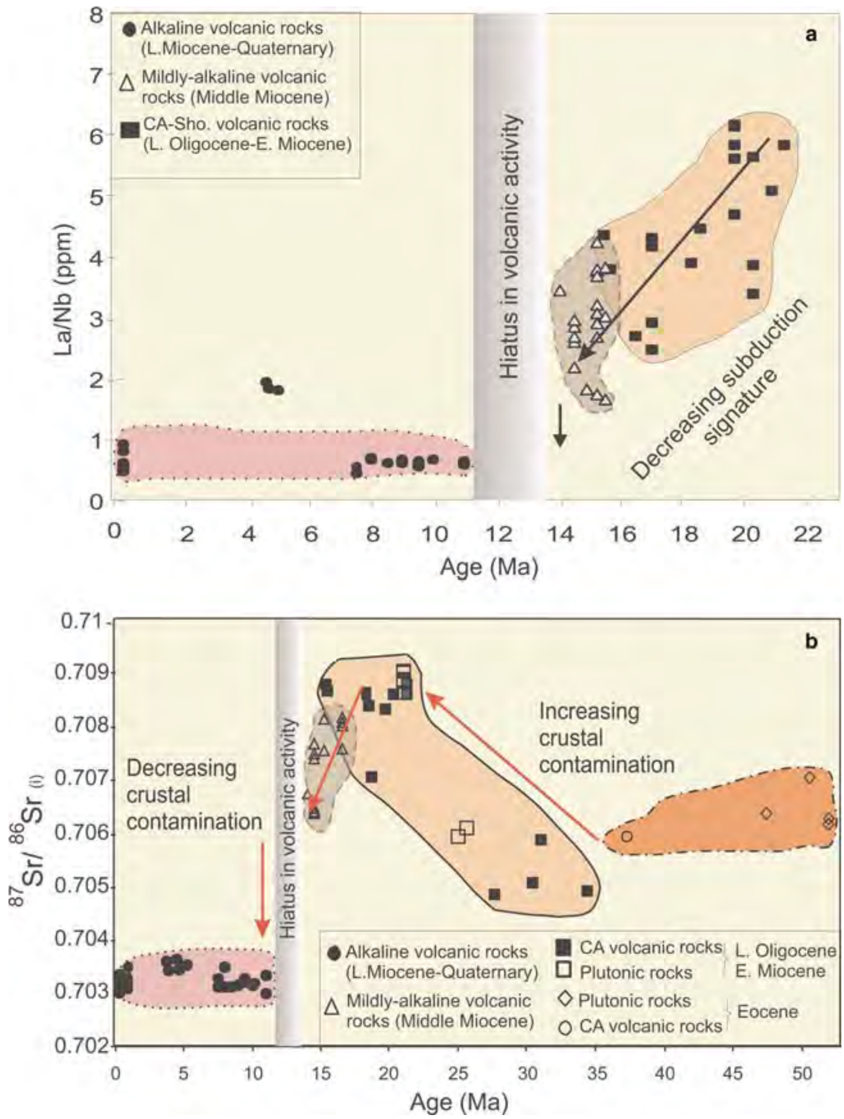

Fig. 5. (**a**) La/Nb versus Age (Ma) diagram, and (**b**) $^{87}Sr/^{86}Sr_{(i)}$ versus Age (Ma) diagram for the Cenozoic magmatic rocks in western Anatolia. See text for discussion.

subalkaline igneous groups but interpret increasing amounts of crustal contamination of the ascending magmas during the period of 22 to 16 Ma, because of their longer residence time in the crust prior to the onset of widespread extensional tectonics in the region. The degree of crustal contamination appears to have decreased rapidly with the eruption of the mildly alkaline lavas during 16–14 Ma (Fig. 5), overlapping with the influence of incoming aesthenospheric melts during their magmatic evolution and with the establishment of the whole-sale lithospheric extension in the region (Ring *et al.* 2003; Çemen *et al.* 2006; Dilek 2006; Dilek & Altunkaynak 2007).

The subsequent apparent abrupt drop in the degree of crustal contamination seems to have coincided with a short hiatus in widespread volcanism in western Anatolia during *c.* 14–11 Ma (Fig. 5). The upper Miocene–Quaternary alkaline lavas have consistently low $^{87}Sr/^{86}Sr$ (0.70302–0.70349) ratios, OIB-like trace-element patterns, high LILE abundances, and high MREE/HREE ratios, characteristic of a garnet-bearing lherzolitic aesthenosphere mantle source (Aldanmaz *et al.*

2000, 2006; Alici *et al.* 2002) for their magmas. Agostini *et al.* (2007) have suggested in the case of the Kula lavas (area j in Figs 2 & 3) the possibility of mixing two isotopically distinct end members of melt sources. The first of these sources is characterized by high $^{143}Na/^{144}Nd$, low $^{87}Sr/^{86}Sr$ ratios, MORB-like Pb isotopic compositions, and low Sr and Nd contents, analogous to the typical geochemical features of a DMM mantle reservoir. The less-depleted second source is characterized by lower $^{143}Nd/^{144}Nd$ and higher $^{87}Sr/^{86}Sr$, Sr and Nd abundances. In the absence of any subduction component in the origin of these melt sources, Innocenti *et al.* (2005) and Agostini *et al.* (2007) have proposed that the Kula lavas were generated from melts that were derived from a heterogeneous, sub-slab mantle source in an intra-plate setting. The geochemical features of the Isparta–Gölcük volcanic rocks in the Isparta Angle area suggest that their magmas were originated from a metasomatized or enriched (in LREE, Ba, Sr) mantle source (Alici *et al.* 1998). The silica-poor leucite lamproites here were likely derived from magmas originated by partial melting of phlogopite-bearing refractory peridotite (spinel-garnet lherzolite transition); aesthenopsheric upwelling, as inferred from melt segregation pressures consistent with shallow aesthenopsheric sources, may also have provided additional heat and melt to this process (Çoban & Flower 2006).

Linking Cenozoic plate-tectonics and mantle dynamics

The apparent causes and mechanisms of the southward propagation of the Cenozoic volcanism in western Anatolia, the changes in its chemical character through time, and the inferred shifts in the mantle source domains (from lithospheric to aesthenospheric domains) are significant questions regarding the Cenozoic chemical geodynamics of the entire Aegean province. We think that the first major post-collisional magmatic pulses in western Anatolia with calc-alkaline geochemical signatures during the Eocene and Oligo-Miocene had a subduction-influenced, lithospheric mantle source. Slab break-off-induced aesthenospheric upwelling was responsible for partial melting of the previously subduction-metasomatized mantle lithosphere beneath the orogenic belt (Figs 6 & 7). The impingement of the upwelling hot aesthenosphere on the overlying metasomatized mantle lithosphere caused its partial melting, producing potassic, calc-alkaline magmas that in turn formed the granitoids and shoshonitic volcanic series (Fig. 6). Geochemical characteristics of the Eocene granitoids and volcanic associations in NW Anatolia are similar to those of other well-documented slab break-off-related igneous suites in various collision zones (von Blanckenburg *et al.* 1992; von Blanckenburg & Davies 1995; Atherton & Ghani 2002). The geological evidence in support of this inferred slab break-off magmatism includes: (1) a linear distribution of the plutons in a narrow belt straddling the IASZ, where ophiolitic and high-P blueschist rocks are exposed (Fig. 7). This spatial pattern suggests focused heat source, limited in space and intensity, that was likely derived from an aesthenospheric window; and (2) continental subduction, evidenced by the latest Cretaceous blueschist rocks of the Tavsanli zone. This attempted subduction of the Anatolide–Tauride continental crust to a depth of $\geq$80 km (Okay *et al.* 1998) is likely to have clogged the subduction zone and caused the detachment of the sinking Tethyan oceanic lithosphere (Fig. 7).

The continued collision of the Sakarya and Anatolide–Tauride continental blocks led into the development of thick orogenic crust, orogen-wide burial metamorphism, and anatectic melting of the lower crust (*c.* 25 Ma, Fig. 7). This episode coincides with bimodal volcanism and widespread ignimbrite flare-up in western Anatolia (Balikesir–Bigadiç, Bigadiç–Sindirgi volcanic fields; e and f in Fig. 3). It was this phase of the post-collisional magmatism that caused thermal weakening of the crust in the western Anatolian orogenic belt leading into its extensional collapse. The Kazdag core complex in NW Anatolia (Fig. 2) began its initial exhumation in the latest Oligocene–early Miocene (Okay & Satir 2000) and the Menderes core complex in Central Western Anatolia (Fig. 2) underwent its exhumation in the earliest Miocene (Fig. 6; Isik *et al.* 2004; Thomson & Ring 2006; Bozkurt 2007). Some of the collision-generated thrust faults may have been reactivated during this time as crustal-scale low-angle detachment faults, (i.e. Simav detachment fault, SW Anatolian shear zone) facilitating the region-wide extension (Thomson & Ring 2006; Çemen *et al.* 2006). In general, tectonic extension also appears to have migrated southward in time; following the exhumation of the Kazdag and Menderes metamorphic core complexes in the Oligo-Miocene, the Tauride block in SW Anatolia was uplifted (Dilek *et al.* 1999*b*) and the blueschist rocks in Crete and the Cyclades in the South Aegean region (Ring & Layer 2003) were exhumed in the Miocene and onwards (Fig. 6).

Starting in the middle Miocene, both lithospheric and aesthenospheric mantle melts were involved in the evolution of bimodal volcanic rocks in western Anatolia with the lithospheric input diminishing in time. This timing coincides with widespread lower crustal exhumation and tectonic extension across the Aegean region (Fig. 6). This extensional phase and the attendant mildly alkaline volcanism were

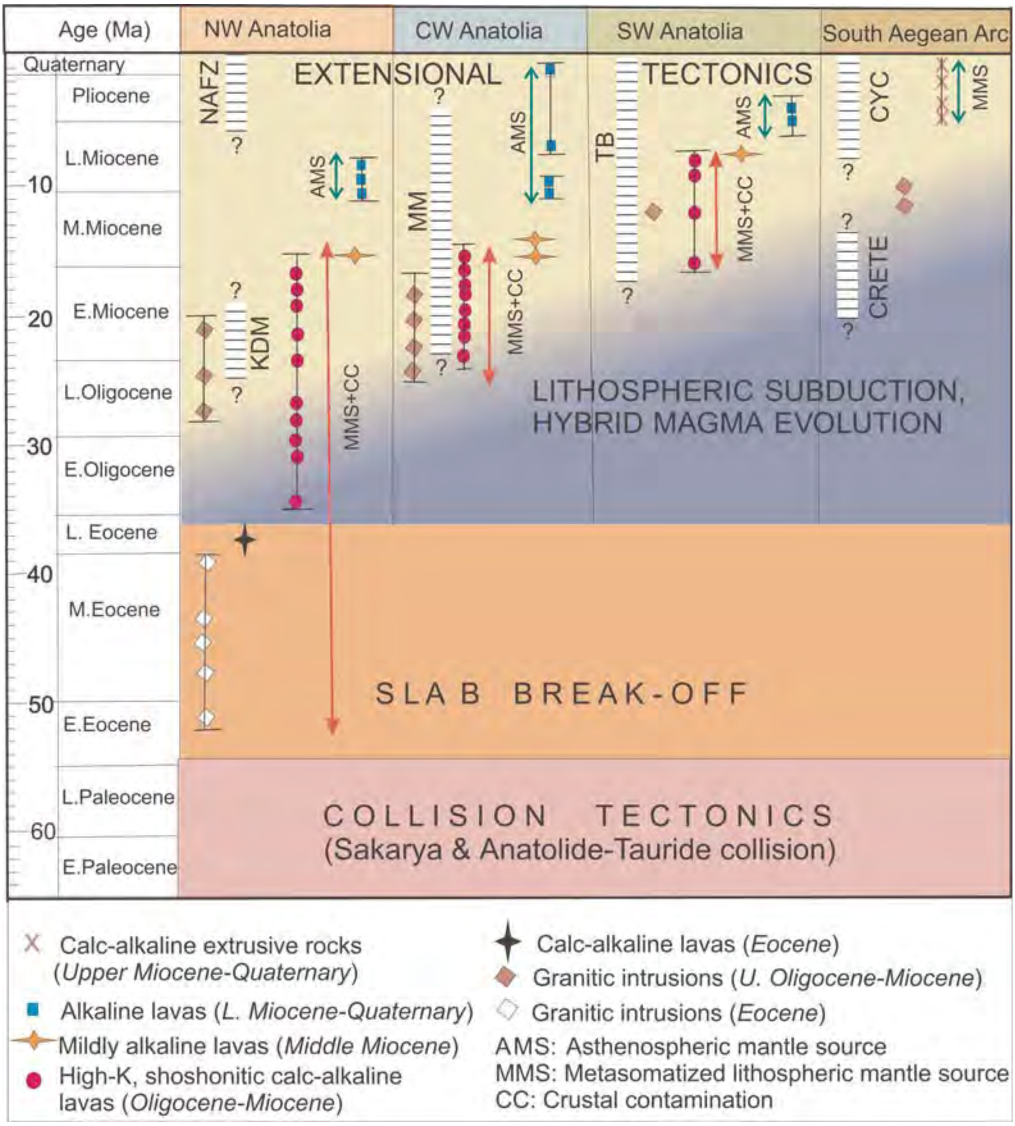

Fig. 6. Geochronology of the Cenozoic tectonomagmatic evolution of western Anatolia and the Southern Aegean Arc. CYC, Cyclades; KDM, Kazdag metamorphic massif; MM, Menderes metamorphic massif; NAFZ, North Anatolian fault zone; TB, Tauride block. See text for discussion.

caused by thermal relaxation associated with possible delamination of the subcontinental lithospheric mantle beneath the northwestern Anatolian orogenic belt (Fig. 7; Altunkaynak & Dilek 2006; Dilek & Altunkaynak 2007, and references therein). Lithospheric delamination might have been triggered by peeling of the base of the subcontinental lithosphere as a result of slab rollback at the Hellenic trench (*c.* 14 Ma in Fig. 7).

Regional graben systems (i.e. Gediz, Büyük Menderes, Fig. 2) developed during the advanced stages of extensional tectonism throughout the late Miocene–Quaternary and further attenuated the continental lithosphere beneath the region (Fig. 7). This extensional phase was accompanied by upwelling of the aesthenospheric mantle and its decompressional melting (Fig. 7). Lithospheric-scale extensional fault systems acted as natural conduits for the transport of uncontaminated alkaline magmas to the surface. The late Miocene and younger (<10 Ma) aesthenospheric flow in the region may also have been driven in part by the extrusion

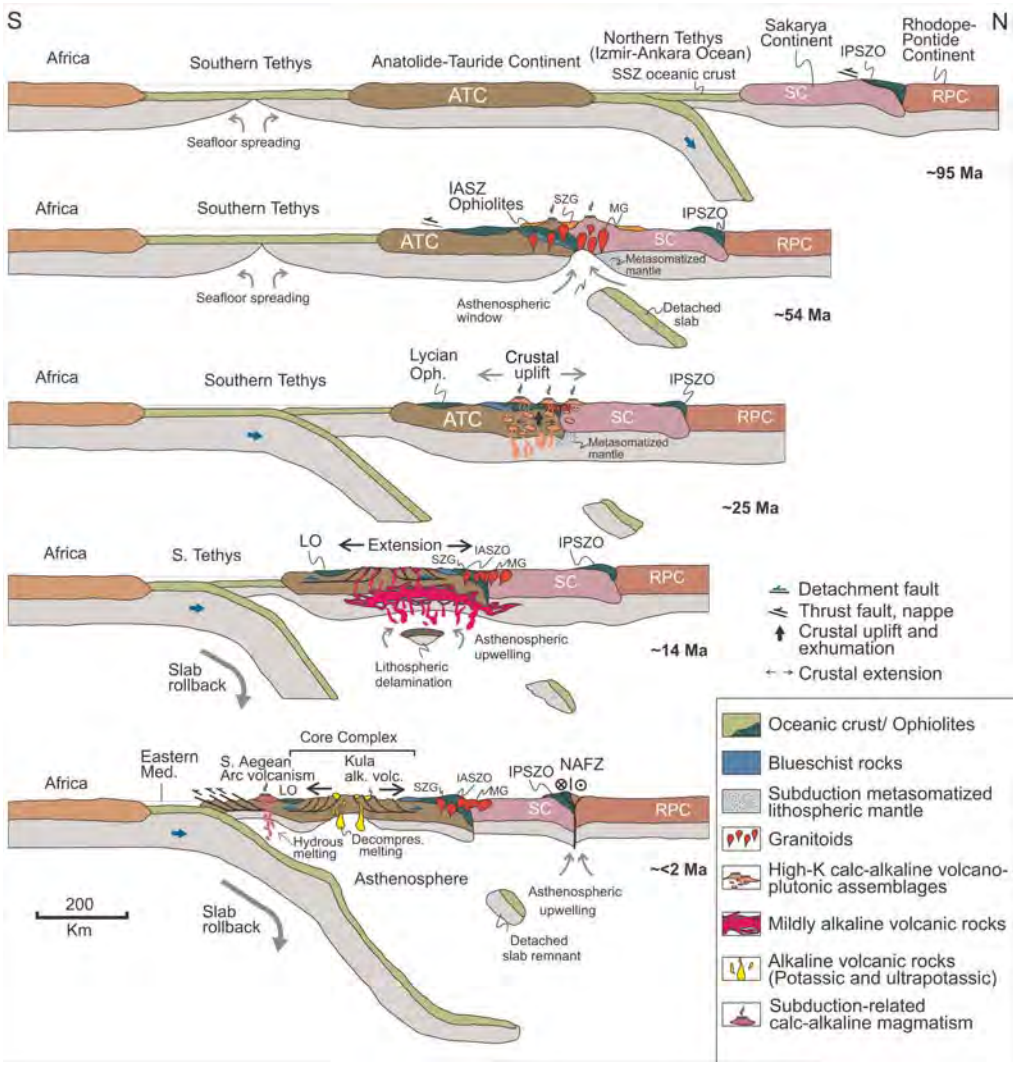

Fig. 7. Late Mesozoic–Cenozoic geodynamic evolution of the western Anatolian orogenic belt through collisional and extensional processes in the upper plate of north-dipping subduction zone(s) within the Tethyan realm. See text for discussion.

tectonics caused by the Arabian collision in the east, as observed by the SW-oriented shear wave splitting fast polarization direction in the mantle parallel to the motion of the Anatolian plate (Sandvol *et al.* 2003; Russo *et al.* 2001). This SW-directed lower mantle flow beneath Anatolia may have played a significant role in triggering intra-plate deformation via extension and strike-slip faulting parallel to the flow direction and horizontal mantle thermal anomalies, which may have facilitated melting and associated basaltic volcanism. This lateral aesthenospheric flow might also have resulted in the interaction of different compositional end-members contributing to the mantle heterogeneity beneath western Anatolia. Similarly, lateral displacement of the aesthenosphere due to the extrusion of collision-entrapped ductile mantle beneath Asia and SE Asia has been suggested to have caused post-collisional high-K volcanism in Tibet and Indo-China during the late Cenozoic (Liu *et al.* 2004; Williams *et al.* 2004; Mo *et al.* 2006).

The apparent SW propagation of both the Cenozoic magmatism and tectonic extension through time was a combined result of the thermally induced collapse of the western Anatolian orogenic belt and the slab rollback associated with the

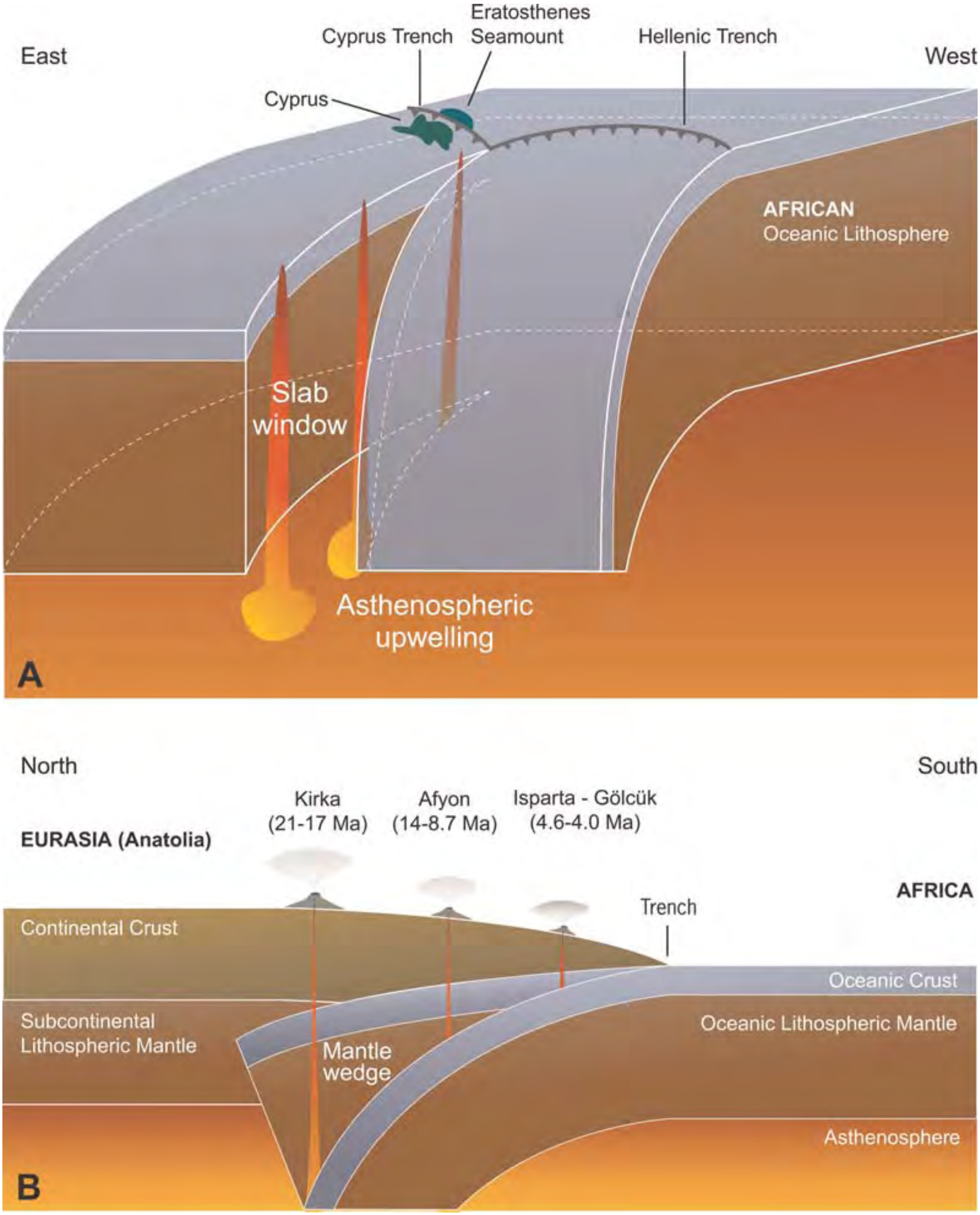

Fig. 8. An interpretive geodynamic model for the evolution of the north–south-trending alkaline volcanic field (from Kirka and Afyon-Suhut to Isparta-Gölcük) in western Anatolia along a Subduction-Transform Edge Propagator (STEP) fault zone, developed in a tear within the northward subducting African lithosphere. The collision of the Eratosthenes Seamount with the Cyprus trench has resulted in slowing down the Africa–Eurasia convergence to <10 mm/a, whereas the convergence between these two plates across the Hellenic trench is *c*. 40 mm/a. This differential motion within the downgoing African plate is interpreted to be responsible for the lithospheric tear. The occurrence of this STEP fault zone coincides with the cusp between the Hellenic and Cyprus trenches.

subduction of the Southern Tethys ocean floor at the Hellenic trench (Figs 6 & 7). The thermal input and melt sources were provided first by slab break-off-generated aesthenospheric flow, then by lithospheric delamination-related aesthenospheric flow, followed by tectonic extension-driven upward aesthenospheric flow and collision-induced (Arabia–Eurasia collision) lateral (westward) mantle flow. The inferred lithospheric delamination around the middle Miocene may have been caused by slab rollback-induced peeling off of the lithospheric root beneath the orogenic belt. The Plio-Quaternary tectonic uplift, crustal exhumation, and young volcanism along the North Anatolian fault zone in the northern Aegean region (Figs 6 & 7; Agostini *et al.* 2007) are most likely associated with transform plate boundary processes and the related aesthenospheric flow.

The subduction zone magmatism related to the retreating Hellenic trench has been responsible for the progressive southward migration of the South Aegean Arc since the late Miocene (Figs 6 & 7; Pe-Piper & Piper 2006). The exhumation of high-P rocks in the Cyclades was likely driven by upper plate extension and channel flow associated with this subduction (Jolivet *et al.* 2003; Ring & Layer 2003). The sharp cusp between the Hellenic and Cyprus trenches (Fig. 1) and the significant differences in the convergence velocities of the African lithosphere at these trenches (*c.* 40 mm/a vs. <10 mm/a at the Hellenic and Cyprus trenches, respectively) are likely to have resulted in a lithospheric tear in the downgoing African plate that allowed the aesthenospheric mantle to rise beneath SW Anatolia (Fig. 8; Doglioni *et al.* 2002; Agostini *et al.* 2007). This scenario is analogous to lithospheric tearing at Subduction-Transform Edge Propagator (STEP) faults described by Govers & Wortel (2005) from the Ionian and Calabrian arcs, the New Hebrides trench, the southern edge of the Lesser Antilles trench, and the northern end of the South Sandwich trench. In all these cases, STEPs propagate in a direction opposite to the subduction direction, and aesthenospheric upwelling occurs behind and beneath their propagating tips. This upwelling induces decompressional melting of shallow aesthenosphere, leading to linearly distributed alkaline magmatism younging in the direction of tear propagation. The north–south-trending potassic and ultra-potassic volcanic fields stretching from the Kirka and Afyon–Suhut region in the north to the Isparta–Gölcük area in the south shows an age progression from 21–17 Ma to 4.6–4.0 Ma that is consistent with this pattern and supports a STEP model for their origin (Fig. 8). Aesthenospheric low velocities detected through Pn tomographic imaging in this region (Al-Lazki *et al.* 2004) support the existence of shallow aesthenosphere beneath the Isparta Angle at present. We infer, therefore, that magmas of the Kirka, Afyon–Suhut, and Isparta–Gölcük fields were produced by melting of the sub-slab (aesthenospheric) mantle, which was metasomatized by recent subduction events in the region (Fig. 8). They were slightly contaminated during their ascent through the crust along the transtensional fault systems within the Kirka–Isparta STEP.

Discussion and conclusions

The geochemical and temporal evolution of the Cenozoic magmatism in western Anatolia clearly shows that plate-tectonic events, mantle dynamics and magmatism are closely linked during the late-stage evolution of orogenic belts. The mantle responds to collision-driven crustal thickening, slab break-off, delamination, and lithospheric tearing swiftly, within geologically short time scales (few million years). This results in lateral mantle flow, whole-sale extension and accompanying magmatism that in turn cause the collapse of tectonically and magmatically weakened orogenic crust. Initial stages of post-collisional magmatism thermally weaken the orogenic crust in continental collision zones giving way into large-scale extension and lower crustal exhumation via core complex formation. These cause-effect relations between magmatism and extension and between the crustal processes and mantle dynamics, and the temporal and chemical evolution of the post-collisional magmatism in western Anatolia, as documented in this study, are common to many orogenic belts (Dilek 2006; Dilek & Altunkaynak 2007, and references therein). This observation suggests to us that the mode and nature of post-collisional magmatism in mountain belts may follow a common pathway with some minor deviations. The existence of active lithospheric subduction and associated slab rollback processes play a significant role, however, in the mode and nature of deformation in orogenic belts that are situated in the upper plates of post-collisional subduction zones (Le Pichon *et al.* 2003).

Slab break-off appears to be the most common driving force for the early stages of post-collisional magmatism in many collisional orogenic belts (Wortel & Spakman 2000; Kohn & Parkinson 2002; Cloos *et al.* 2005). The rocks produced at this stage are represented by calc-alkaline to transitional (in composition) igneous suites. Subsequent lithospheric delamination or partial convective removal of the sub-continental lithospheric mantle in collision-induced, overthickened orogenic lithosphere causes decompressional melting of the upwelling aesthenosphere that in turn results in alkaline basaltic magmatism. Attendant crustal extension and widespread thinning of the lithosphere facilitates rapid ascent of basaltic magmas without much residence time in the crust and hence the eruption of relatively uncontaminated, aesthenosphere-derived magmas at the surface (i.e. Kula lavas in SW Anatolia). Regional geodynamics and other plate boundary processes at work in the vicinity of the collision zones may strongly control, however, the mode and nature of slab break-off and lithospheric delamination events in orogenic belts and hence the suggested pathway of post-collisional magmatism.

This study was supported by research grants from the Scientific & Technical Research Council of Turkey (TUBITAK-CAYDAG-101Y006), Istanbul Technical University, and Miami University Committee on Faculty Research. Constructive and thorough reviews by C. Busby, G. Lister, P. A. Ustaömer, and D. van Hinsbergen helped us improve the paper greatly. We particularly acknowledge our lively discussions and exchange on the Cenozoic geodynamics of the Aegean region with Editor van Hinsbergen during the preparation of this paper.

References

AGOSTINI, S., DOGLIONI, C., INNOCENTI, F., MANETTI, P., TONARINI, S. & SAVASÇIN, M. Y. 2007. The transition from subduction-related to intraplate Neogene magmatism in the Western Anatolia and Aegean area. *In*: BECCALUVA, L., BIANCHINI, G. & WILSON, M. (eds) *Cenozoic Volcanism in the Mediterranean Area*. Geological Society of America Special Paper, **418**, 1–16.

AKAY, E. & ERDOGAN, B. 2004. Evolution of Neogene calc-alkaline to alkaline volcanism in the Aliaga-Foca region (Western Anatolia, Turkey). *Journal of Asian Earth Science*, **24**, 367–387.

ALDANMAZ, E., PEARCE, J. A., THIRWALL, M. F. & MITCHELL, J. 2000. Petrogenetic evolution of late Cenozoic, post-collision volcanism in western Anatolia, Turkey. *Journal of Volcanology & Geothermal Research*, **102**, 67–95.

ALDANMAZ, E., KÖPRÜBASI, N., GÜRER, Ö. F., KAYMAKÇI, N. & GOURGAUD, A. 2006. Geochemical constraints on the Cenozoic, OIB-type alkaline volcanic rocks of NW Turkey: Implications for mantle sources and melting processes. *Lithos*, **86**, 50–76.

ALICI, P., TEMEL, A., GOURGAUD, A., KIEFFER, G. & GÜNDOGDU, M. N. 1998. Petrology and geochemistry of potassic rocks in the Gölcük area (Isparta, SW Turkey): genesis of enriched alkaline magmas. *Journal of Volcanology and Geothermal Research*, **85**, 423–446.

ALICI, P., TEMEL, A. & GOURGAUD, A. 2002. Pb-Nd-Sr isotope and trace element geochemistry of Quaternary extension-related alkaline volcanism: a case study of Kula region (western Anatolia, Turkey). *Journal of Volcanology & Geothermal Research*, **115**, 487–510.

AL-LAZKI, A. I., SANDVOL, E., SEBER, D., BARAZANGI, M., TÜRKELLI, N. & MOHAMMAD, R. 2004. Pn tomographic imaging of mantle lid velocity and anisotropy at the junction of the Arabian, Eurasian and African plates. *Geophysical Journal International*, **158**, 1024–1040.

ALTHERR, R., HENJES-KUNST, F. J., MATTHEWS, A., FIREDRICHSEN, H. & HANSEN, B. T. 1988. O-Sr isotopic variations in Miocene granitoids from the Aegean: evidence for an origin by combined assimilation and fractional crystallization. *Contributions to Mineralogy & Petrology*, **100**, 528–541.

ALTUNKAYNAK, S. 2007. Collision-driven slab breakoff magmatism in northwestern Anatolia, Turkey. *Journal of Geology*, **115**, 63–82.

ALTUNKAYNAK, S. & DILEK, Y. 2006. Timing and nature of postcollisional volcanism in western Anatolia and geodynamic implications. *In*: DILEK, Y. & PAVLIDES, S. (eds) *Postcollisional tectonics and magmatism in the Mediterranean region and Asia*. Geological Society of America Special Paper, **409**, 321–351.

ATAMAN, G. 1972. L'age radiometrique du massif granodioritique d'Orhaneli. *Bulletin of the Geological Society of Turkey*, **15**, 125–130.

ATHERTON, M. P. & GHANI, A. A. 2002. Slab breakoff: a model for Caledonian, Late Granite syn-collisional magmatism in the orthotectonic (metamorphic) zone of Scotland and Donegal, Ireland. *Lithos*, **62**, 65–85.

AVIGAD, D. & GARFUNKEL, Z. 1991. Uplift and exhumation of high-pressure metamorphic terranes: the example of the Cycladic blueschist belt (Aegean Sea). *Tectonophysics*, **188**, 357–372.

BARKA, A. & REILINGER, R. 1997. Active tectonics of the Eastern Mediterranean region: deduced from GPS, neotectonic and seismicity data. *Annali Di Geofisica*, **XL**, 587–610.

BINGÖL, E., DELALOYE, M. & ATAMAN, G. 1982. Granitic intrusions in Western Anatolia: A contribution of the geodynamic study of this area. *Eclogae Geologische Helvetica*, **75**, 437–446.

BINGÖL, E., DELALOYE, M. & GENÇ, S. 1994. Magmatism of northwestern Anatolia. *International Volcanological Congress, IAVCEI 1994, Excursion Guide (A3).*

BOZKURT, E. 2003. Origin of NE-trending basins in western Turkey. *Geodinamica Acta*, **14**, 61–81.

BOZKURT, E. 2004. Granitoid rocks of the southern Menderes Massif (Southwest Turkey): field evidence for Tertiary magmatism in an extensional shear zone. *International Journal of Earth Sciences*, **93**, 52–71.

BOZKURT, E. 2007. Extensional v. contractional origin for the southern Menderes shear zone, SW Turkey: tectonic and metamorphic implications. *Geological Magazine*, **144**, 191–210.

BOZKURT, E. & PARK, R. G. 1994. Southern Menderes Massif: an incipient metamorphic core complex in western Anatolia, Turkey. *Journal of the Geological Society, London*, **151**, 213–216.

BOZKURT, E. & SATIR, M. 2000. The southern Menderes Massif (western Turkey): geochronology and exhumation history. *Geological Journal*, **35**, 285–296.

BRIQUEU, L., JAVOY, M., LANCELOT, J. R. & TATSUMATO, M. 1986. Isotope geochemistry of recent magmatism in the Aegean arc: Sr, Nd, Hf and O isotopic ratios in the lavas of Milos and

Santorini: geodynamic implications. *Earth and Planetary Science Letters*, **80**, 41–54.

CANDAN, O., ÇETINKAPLAN, M., OBERHÄNSLI, R., RIMMELÉ, G. & AKAL, C. 2005. Alpine high-P/low-T metamorphism of the Afyon Zone and implications for the metamorphic evolution of Western Anatolia, Turkey. *Lithos*, **84**, 102–124.

CATLOS, E. J. & ÇEMEN, I. 2005. Monazite ages and the evolution of the Menderes Massif, western Turkey. *International Journal of Earth Sciences*, **94**, 204–217.

CATLOS, E. J., ÇEMEN, I., ISIK, V. & SEYITOĞLU, G. 2002. In situ timing constraints from the Menderes massif, western Turkey. *Geological Society of America Abstracts with Programs*, **34** (6), 180.

ÇEMEN, I., CATLOS, E. J., GÖGÜS, O. & ÖZERDEM, C. 2006. Postcollisional extensional tectonics and exhumation of the Menderes massif in the Western Anatolia extended terrane. *In*: DILEK, Y. & PAVLIDES, S. (eds) *Postcollisional tectonics and magmatism in the Mediterranean region and Asia*. Geological Society of America Special Paper, **409**, 353–379.

CLOOS, M., SAPIIE, B., VAN UFFORD, A. Q., WEILAND, R. J., WARREN, P. Q. & MCMAHON, T. P. 2005. Collisional delamination in New Guinea: The Geotectonics of subducting slab breakoff. *Geological Society of America Special Paper*, **400**, 1–51.

ÇOBAN, H. & FLOWER, M. F. J. 2006. Mineral phase compositions in silica-undersaturated 'leucite' lamproites from the Bucak area, Isparta, SW Turkey. *Lithos*, **89**, 275–299.

COLLINS, A. & ROBERTSON, A. H. F. 2003. Kinematic evidence for Late Mesozoic – Miocene emplacement of the Lycian Allochthon over the Western Anatolide Belt, SW Turkey. *Geological Journal*, **38**, 295–310.

DAVIS, J. H. & VON BLANCKENBURG, F. 1995. Slab breakoff: a model of lithosphere detachment and its test in the magmatism and deformation of collisional orogens. *Earth and Planetary Science Letters*, **129**, 85–102.

DELALOYE, M. & BINGÖL, E. 2000. Granitoids from western and northwestern Anatolia: Geochemistry and modeling of geodynamic evolution. *International Geology Review*, **42**, 241–268.

DEMIRTASLI, E., TURHAN, N., BILGIN, A. Z. & SELIM, M. 1984. Geology of the Bolkar Mountains: *In*: TEKELI, O. & GÖNCÜOGLU, M. C. (eds) *Geology of the Taurus Belt*. Proceedings of the International Symposium, Ankara, 125–141.

DEWEY, J. F., HEMPTON, M. R., KIDD, W. S. F., SAROGLU, F. & SENGÖR, A. M. C. 1986. Shortening of continental lithosphere: the neotectonics of Eastern Anatolia – a young collision zone: *In*: COWARD, M. P. & RIES, A. C. (eds) *Collision Zone Tectonics*. Geological Society, London, Special Publication, **19**, 3–36.

DILEK, Y. 2006. Collision tectonics of the Mediterranean region: causes and consequences. *In*: DILEK, Y. & PAVLIDES, S. (eds) *Postcollisional tectonics and magmatism in the Mediterranean region and Asia*. Geological Society of America Special Paper, **409**, 1–13.

DILEK, Y. & ALTUNKAYNAK, S. 2007. Cenozoic crustal evolution and mantle dynamics of post-collisional magmatism in western Anatolia. *International Geology Review*, **49**, 431–453.

DILEK, Y. & MOORES, E. M. 1990. Regional Tectonics of the Eastern Mediterranean ophiolites. *In*: MALPAS, J., MOORES, E. M., PANAYIOTOU, A. & XENOPHONTOS, C. (eds) *Ophiolites, Oceanic Crustal Analogues*. Proceedings of the Symposium 'Troodos 1987', The Geological Survey Department, Nicosia, Cyprus, 295–309.

DILEK, Y. & THY, P. 2006. Age and petrogenesis of plagiogranite intrusions in the Ankara mélange, central Turkey. *Island Arc*, **15**, 44–57.

DILEK, Y & WHITNEY, D. L. 1997. Counterclockwise *P-T-t* trajectory from the metamorphic sole of a Neo-Tethyan ophiolite (Turkey). *Tectonophysics*, **280**, 295–310.

DILEK, Y & WHITNEY, D. L. 2000. Cenozoic crustal evolution in central Anatolia: Extension, magmatism and landscape development. *In*: PANAYIDES, I., XENOPHONTOS, C. & MALPAS, J. (eds) *Proceedings of the Third International Conference on the Geology of the Eastern Mediterranean*. Geological Survey Department, September 1998, Nicosia – Cyprus, 183–192.

DILEK, Y., THY, P., HACKER, B. & GRUNDVIG, S. 1999*a*. Structure and petrology of Tauride ophiolites and mafic dike intrusions (Turkey): Implications for the Neo-Tethyan ocean. *Bulletin of the Geological Society of America*, **111**, 1192–1216.

DILEK, Y., WHITNEY, D. L. & TEKELI, O. 1999*b*. Links Between Tectonic Processes and Landscape Morphology in an Alpine Collision Zone, South-Central Turkey. *Annals of Geomorphology*, **118**, 147–164.

DOGLIONI, C., AGOSTINI, S., CRESPI, M., INNOCENTI, F., MANETTI, P., RIGUZZI, F. & SAVAŞÇIN, Y. 2002. On the extension in western Anatolia and the Aegean Sea. *In*: ROSENBAUM, G. & LISTER, G. S. (eds) *Reconstruction of the evolution of the Alpine-Himalayan Orogen*. Journal of the Virtual Explorer, **8**, 169–183.

ELITOK, Ö. & DRÜPPEL, K. 2008. Geochemistry and tectonic significance of metamorphic sole rocks beneath the Beysehir-Hoyran ophiolite (SW Turkey). *Lithos*, **100**, 322–353.

ERCAN, T., SATIR, M., KREUZER, H., TÜRKECAN, A., GÜNAY, E., ÇEVIKBAS, A., ATES, M. & CAN, B. 1985. Bati Anadolu Senozoyik volkanitlerine ait yeni kimyasal, izotopik ve radyometrik verilerin yorumu. *Bulletin of the Geological Society of Turkey*, **28**, 121–136 (in Turkish).

ERKÜL, F., HELVACI, C. & SÖZBILIR, H. 2005. Stratigraphy and geochronology of the Early Miocene volcanic units in the Bigadiç Borate Basin, western Turkey. *Turkish Journal of Earth Sciences*, **14**, 227–253.

FACCENNA, C., JOLIVET, L., PIROMALLO, C. & MORELLI, A. 2003. Subduction and the depth of convection in the Mediterranean mantle. *Journal of Geophysical Research*, **108**, 2099, doi:1029/2001JB001690.

FRANCALANCI, L., INNOCENTI, F., MANETTI, P. & SAVAŞÇIN, M. Y. 2000. Neogene alkaline volcanism of the Afyon-Isparta area, Turkey: petrogenesis and geodynamic implications. *Mineralogy & Petrology*, **70**, 285–312.

FREY, F. A., GRENN, D. H. & ROY, S. D. 1978. Integrated models of basalt petrogenesis: a study of Quartz tholeiite to olivine melililites from south eastern Australia utilizing geochemical and experimental data. *Journal of Petrology*, **19**, 463–513.

GAUTIER, P., BRUN, J.-P., MORICEAU, R., SOKOUTIS, D., MARTINOD, J. & JOLIVET, L. 1999. Timing, kinematics and cause of Aegean extension: a scenario based on a comparison with simple analogue experiments. *Tectonophysics*, **315**, 31–72.

GENÇ, S. C. & YILMAZ, Y. 1997. An example of post-collisional magmatim in northwestern Anatolia: the Kizderbent Volcanics (Armutlu Peninsula, Turkey). *Turkish Journal of Earth Sciences*, **6**, 33–42.

GESSNER, K., COLLINS, A. S., RING, U. & GÜNGÖR, T. 2004. Structural and thermal history of poly-orogenic basement: U-Pb geochronology of granitoid rocks in the southern Menderes Massif, western Turkey. *Journal of the Geological Society of London*, **161**, 93–101.

GOLDSTEIN, S. J. & JACOBSEN, S. B. 1988. Nd and Sr isotopic systematics of river-water suspended material: implications for crustal evolution. *Earth and Planetary Science Letters*, **87**, 249–265.

GOVERS, R. & WORTEL, M. J. R. 2005. Lithosphere tearing at STEP faults: Response to edges of subduction zones. *Earth and Planetary Science Letters*, **236**, 505–523.

GÜRSU, S., GÖNCÜOGLU, M. C. & BAYHAN, H. 2004. Geology and geochemistry of the Pre-early Cambrian rocks in the Sandikli area: implications for the Pan-African evolution of NW Gondwanaland. *Gondwana Research*, **7**, 923–935.

HARRIS, N. B. W., KELLEY, S. & OKAY, A. I. 1994. Post-collisional magmatism and tectonics in northwest Anatolia. *Contributions to Mineralogy and Petrology*, **117**, 241–252.

HETZEL, R. & REISCHMANN, T. 1996. Intrusion age of Pan-African augen gneisses in the southern Menderes Massif and the age of cooling after Alpine ductile extensional deformation. *Geological Magazine*, **133**, 565–572.

INNOCENTI, F., AGOSTINI, S., DI VINCENZO, G., DOGLIONI, C., MANETTI, P., SAVASÇIN, M. Y. & TONARINI, S. 2005. Neogene and Quaternary volcanism in Western Anatolia: Magma sources and geodynamic evolution. *Marine Geology*, **221**, 397–421.

IŞIK, V., TEKELI, O. & SEYITOĞLU, G. 2004. The $^{40}Ar/^{39}Ar$ age of extensional ductile deformation and granitoid intrusion in the northern Menderes core complex: implications for the initiation of extensional tectonics in western Turkey. *Journal of Asian Earth Sciences*, **23**, 555–566.

JOLIVET, L. 2001. A comparison of geodetic and finite strain pattern in the Aegean, geodynamic implications. *Earth and Planetary Science Letters*, **187**, 95–104.

JOLIVET, L. & FACCENNA, C. 2000. Mediterranean extension and the Africa-Eurasia collision. *Tectonics*, **19**, 1095–1106.

JOLIVET, L., FACCENNA, C., GOFFÉ, B., BUROV, E. & AGARD, P. 2003. Subduction tectonics and exhumation of high-pressure metamorphic rocks in the Mediterranean orogen. *American Journal of Science*, **303**, 353–409.

JOLIVET, L., BRUN, J. P., GAUTIER, S., LELLEMAND, S. & PATRIAT, M. 1994. 3-D kinematics of extension in the Aegean from the early Miocene to the present: insight from the ductile crust. *Bulletin de la Societe Geologique de France*, **165**, 195–209.

KEAY, S., LISTER, G. & BUICK, I. 2002. The timing of partial melting, Barrovian metamorphism and granite intrusion in the Naxos metamorphic core complex, Cyclades, Aegean Sea, Greece. *Tectonophysics*, **342**, 275–312.

KOHN, M. J. & PARKINSON, C. D. 2002. Petrologic case for Eocene slab breakoff during the Indo-Asian collision. *Geology*, **7**, 591–594.

KÖPRÜBAŞI, N. & ALDANMAZ, E. 2004. Geochemical constraints on the petrogenesis of Cenozoic I-type granitoids in Northwest Anatolia, Turkey: Evidence for magma generation by lithospheric delamination in a post-collisional setting. *International Geology Review*, **46**, 705–729.

KÖPRÜBASI, N., SEN, C. & KÖPRÜBASI, N. 2000. Fistikli (Armutlu-Yalova) granitoinin jeokimyasi [Geochemistry of the Fistikli (Armutlu-Yalova) granitoid]. *Earth Sciences*, **22**, 32–42.

KREEMER, C., HOLT, W. E. & HAINES, A. H. 2003. An integrated global model of present-day plate motions and plate boundary deformation. *Geophysical Journal International*, **154**, 8–34.

KUMRAL, M., ÇOBAN, H., ĞEDIKOGLU, A. & KILINÇ, A. 2006. Petrology and geochemistry of augite trachytes and porphyritic trachytes from the Gölcük volcanic region, SW Turkey: A case study. *Journal of Asian Earth Sciences*, **27**, 707–716.

LE PICHON, X. & ANGELIER, J. 1979. The Hellenic arc and trench system: a key to the evolution of the Eastern Mediterranean area. *Tectonophysics*, **60**, 1–42.

LE PICHON, X., LALLEMANT, S. J., CHAMOT-ROOKE, N., LEMEUR, D. & PASCAL, G. 2003. The Mediterranean Ridge backstop and the Hellenic nappes. *Marine Geology*, **186**, 111–125.

LIU, M., CUI, X. & LIU, F. 2004. Cenozoic rifting and volcanism in eastern China: A mantle dynamic link to the Indo-Asian collision? *Tectonophysics*, **393**, 29–42, doi: 10.1016/j.tecto.2004.07.029.

LISTER, G., BANGA, G. & FEENSTRA, A. 1984. Metamorphic core complexes of Cordilleran type in the Cyclades, Aegean Sea, Greece. *Geology*, **12**, 221–225.

MAKRIS, J. & STOBBE, C. 1984. Physical properties and state of the crust and upper mantle of the eastern Mediterranean Sea deduced from geophysical data. *Marine Geology*, **55**, 347–363.

MCCLUSKY, S., BALASSANIAN, S., BARKA, A., DEMIR, C., ERGINTAV, S. & GEORGIEV, I. 2000. Global Positioning System constraints on plate kinematics and dynamics in the eastern Mediterranean and Caucasus. *Journal of Geophysical Research*, **105**, 5695–5719.

MCKENZIE, D. 1978. Active tectonics of the Alpine-Himalayan belt, the Aegean Sea and surrounding regions. *Geophysical Journal of the Royal Astronomical Society*, **55**, 217–254.

MEULENKAMP, J. E., WORTEL, W. J. R., VAN WAMEL, W. A., SPAKMAN, W. & HOOGERDUYN STRATING, E. 1988. On the Hellenic subduction zone and geodynamic evolution of Crete since the late Middle Miocene. *Tectonophysics*, **146**, 203–215.

MO, X., ZHAO, Z., DENG, J., FLOWER, M., YU, X., LUO, Z., LI, Y., ZHOU, S., DONG, G., ZHU, D. & WANG, L. 2006. Petrology and geochemistry of postcollisional volcanic rocks from the Tibetan plateau: Implications for lithospheric heterogeneity and collision-induced asthenospheric mantle flow. *In*: DILEK, Y. & PAVLIDES, S. (eds) *Postcollisional tectonics and magmatism in the Mediterranean region and Asia*. Geological Society of America Special Paper, **409**, 507–530.

OKAY, A. I. & SATIR, M. 2000. Coeval plutonism and metamorphism in a latest Oligocene metamorphic core complex in northwest Turkey. *Geological Magazine*, **137**, 495–516.

OKAY, A. I., SATIR, M., MALUSKI, H., SIYAKO, M., MONIE, P., METZGER, R. & AKYÜZ, S. 1996. Paleo- and Neo-Tethyan events in northwest Turkey: geological and geochronological constraints. *In*: YIN, A. & HARRISON, M. T. (eds) *Tectonics of Asia*. Cambridge University Press, 420–441.

OKAY, A. I., HARRIS, N. B. W. & KELLEY, S. P. 1998. Exhumatioin of blueschists along a Tethyan suture in northwest Turkey. *Tectonophysics*, **285**, 275–299.

ÖNEN, A. P. 2003. Neotethyan ophiolitic rocks of the Anatolides of NW Turkey and comparison with Tauride ophiolites. *Journal of the Geological Society, London*, **160**, 947–962.

ÖNEN, A. P. & HALL, R. 1993. Ophiolites and related metamorphic rocks from the Kütahya region, northwest Turkey. *Geological Journal*, **28**, 399–412.

ÖZER, S., SÖZBILIR, H., ÖZKAR, I., TOKER, V. & SARI, B. 2001. Stratigraphy of Upper Cretaceous – Palaeogene sequences in the southern and eastern Menderes Massif (Western Turkey). *International Journal of Earth Sciences*, **89**, 852–866.

ÖZGÜL, N. 1984. Stratigraphy and tectonic evolution of the Central Taurides. *In*: TEKELI, O. & GÖNCÜOĞLU, M. C. (eds) *Geology of the Taurus Belt*. Proceedings of the International Symposium on the Geology of the Taurus Belt, 1983, Ankara – Turkey, Mineral Research and Exploration Institute of Turkey, Ankara, 77–90.

PEARCE, J. A. 1982. Trace element characteristics of lavas from destructive plate boundaries: *In*: THORPE, R. S. (ed.) *Andesites*. John Wiley & Sons, 525–248.

PEARCE, J. A. & PEATE, D. W. 1995. Tectonic implications of the composition of volcanic arc magmas. *Annual Review of Earth Planetary Sciences*, **23**, 251–285.

PE-PIPER, G. & PIPER, D. J. W. 2006. Unique features of the Cenozoic igneous rocks of Greece. *In*: DILEK, Y. & PAVLIDES, S. (eds) *Postcollisional tectonics and magmatism in the Mediterranean region and Asia*. Geological Society of America Special Paper, **409**, 259–282.

PURVIS, M. & ROBERTSON, A. H. F. 2004. A pulsed extension model for the Neogene-Recent E-W-trending Alasehir Graben and the NE-SW-trending Selendi and Gördes Basins, western Turkey. *Tectonophysics*, **391**, 171–201.

REILINGER, R. E., MCCLUSKY, S. C. & ORAL, M. B. 1997. Global positioning system measurements of present-day crustal movements in the Arabia-Africa-Eurasia plate collision zone. *Journal of Geophysical Research*, **102**, 9983–9999.

RICHARDSON-BUNBURY, J. M. 1996. The Kula volcanic field, western Turkey: the development of a Holocene alkali basalt province and the adjacent normal-faulting graben. *Geological Magazine*, **133**, 275–283.

RICOU, L. E., ARGYRIADIS, I. & MARCOUX, J. 1975. L'axe calcaire du Taurus, un alignement de fenetres arabo-africaines sous des nappes radiolaritiques, ophiolitiques et métamorphiques. *Bulletin de la Société de Geologie de France*, **16**, 107–111.

RIMMELÉ, G., OBERHANSLI, R., GOFFE, B., JOLIVET, L., CANDAN, O. & ÇETINKAPLAN, M. 2003. First evidence of high-pressure metamorphism in the 'Cover Series' of the Southern Menderes Massif. Tectonic and metamorphic implications for the evolution of SW Turkey. *Lithos*, **71**, 19–46.

RING, U. & COLLINS, A. S. 2005. U-Pb SIMS dating of synkinematic granites: timing of core-complex formation in the northern Anatolide belt of western Turkey. *Journal of the Geological Society of London*, **162**, 289–298.

RING, U. & LAYER, P. W. 2003. High-pressure metamorphism in the Aegean, eastern Mediterranean: Underplating and exhumation from the Late Cretaceous until the Miocene to Recent above the retreating Hellenic subduction zone. *Tectonics*, **22**, 1–23, doi: 10.1029/2001TC001350.

RING, U., JOHNSON, C., HETZEL, R. & GESSNER, K. 2003. Tectonic denudation of a Late Cretaceous-Tertiary collisional belt: regionally symmetric cooling patterns and their relation to extensional faults in the Anatolide belt of western Turkey. *Geological Magazine*, **140**, 421–441.

ROBERTSON, A. H. F. 1998. Tectonic significance of the Eratosthenes Seamount: a continental fragment in the process of collision with a subduction zone in the eastern Mediterranean (Ocean Drilling Program Leg 160). *Tectonophysics*, **298**, 63–82.

RUSSO, R. M., DILEK, Y. & FLOWER, M. F. J. 2001. *Collision-driven mantle flow and crustal response in the eastern Mediterranean region during the late Cenozoic*. 4th International Turkish Geology Symposium, Work in Progress on the Geology of Turkey and Its Surroundings, Adana,Turkey, 24–28 September 2001, p. 98.

SANDVOL, E., TÜRKELLI, N., ZOR, E., GÖK, R., BEKLER, T., GÜRBÜZ, C., SEBER, D. & BARAZANGI, M. 2003. Shear wave splitting in a young continent-continent collision: An example from eastern Turkey. *Geophysical Research Letters*, **30**, DOI: 10.1029/2003GL017390.

SAVASÇIN, M. Y. & OYMAN, T. 1998. Tectonomagmatic evolution of alkaline volcanics at the Kirka-Afyon-Isparta structural trend, SW Turkey. *Turkish Journal of Earth Sciences*, **7**, 201–214.

SEYITOĞLU, G. & SCOTT, B. 1992. Late Cenozoic volcanic evolution of the northeastern Aegean region. *Journal of Volcanology and Geothermal Research*, **54**, 157–176.

SEYITOĞLU, G. & SCOTT, B. 1996. The cause of N-S extensional tectonics in western Turkey: Tectonic escape vs. backarc spreading vs. orogenic collapse. *Journal of Geodynamics*, **22**, 145–153.

SEYITOĞLU, G., ANDERSON, D., NOWELL, G. & SCOTT, B. 1997. The evolution from Miocene potassic to Quaternary sodic magmatism in western Turkey: implications for enrichment processes in the lithospheric mantle. *Journal of Volcanology and Geothermal Research*, **76**, 127–147.

SHERLOCK, S., KELLEY, S. P., INGER, S., HARRIS, N. & OKAY, A. I. 1999. ^{40}Ar-^{39}Ar and Rb-Sr geochronology of high-pressure metamorphism and exhumation history of the Tavşanli Zone, NW Turkey. *Contributions to Mineralogy and Petrology*, **137**, 46–58.

STAMPFLI, G. M., BOREL, G. D., CAVAZZA, W., MOSAR, J. & ZIEGLER, P. A. 2001. *The paleotectonic atlas of the Peritethyan domain* (CD-ROM). European Geophysical Society.

TEKELI, O. 1981. Subduction complex of pre-Jurassic age, northern Anatolia, Turkey. *Geology*, **9**, 68–72.

THIRWALL, M. F., SMITH, T. E., GRAHAM, A. M., THEODORU, N., HOLLINGS, P., DAVIDSON, J. P. & ARCULUS, R. D. 1994. High field strength element anomalies in arc lavas: source or processes. *Journal of Petrology*, **35**, 819–838.

THOMSON, S. N. & RING, U. 2006. Thermochronologic evaluation of postcollision extension in the Anatolide orogen, western Turkey. *Tectonics*, **25**, TC3005, doi: 10.1029/2005TC001833.

TIREL, C., GUEYDAN, F., TIBERI, C. & BRUN, J.-P. 2004. Aegean crustal thickness inferred from gravity inversion. Geodynamical implications. *Earth and Planetary Science Letters*, **228**, 267–280.

VAN HINSBERGEN, D. J. J., HAFKENSCHEID, E., SPAKMAN, W., MEULENKAMP, J. E. & WORTEL, R. 2005. Nappe stacking resulting from subduction of oceanic and continental lithosphere below Greece. *Geology*, **33**, 325–328.

VON BLANCKENBURG, F., FRUH-GREEN, G., DIETHELM, K. & STILLE, P. 1992. Nd-, Sr-, and O-isotopic and chemical evidence for a two-stage contamination history of mantle magma in the central-Alpine Bergell intrusion. *Contributions to Mineralogy and Petrology*, **110**, 33–45.

VON BLANCKENBURG, F. & DAVIES, J. H. 1995. Slab breakoff: A model for syncollisional magmatism and tectonics in the Alps. *Tectonics*, **14**, 120–131.

WDOWINSKI, S., BEN-AVRAHAM, Z., ARVIDSSON, R. & EKSTRÖM, G. 2006. Seismotectonics of the Cyprian Arc. *Geophysical Journal International*, **164**, 176–181.

WESTAWAY, B. 1994. Present-day kinematics of the Middle East and eastern Mediterranean. *Journal of Geophysical Research*, **99**, 12071–12090.

WILLIAMS, H. M., TURNER, S. P., PEARCE, J. A., KELLEY, S. P. & HARRIS, N. B. W. 2004. Nature of the source regions for post-collisional, potassic magmatism in southern and northern Tibet from geochemical variations and inverse trace element modelling. *Journal of Petrology*, **45**, 555–607.

WORTEL, M. J. R. & SPAKMAN, W. 2000. Subduction and slab detachment in the Mediterranean-Carpathian region. *Science*, **290**, 1910–1917.

YILMAZ, Y. 1990. Comparison of young volcanic associations of western and eastern Anatolia under compressional regime; a review. *Journal of Volcanology and Geothermal Research*, **44**, 69–87.

YILMAZ, Y. 2002. Tectonic evolution of western Anatolian extensional province during the Neogene and Quaternary. *Geological Society of America Abstracts with Programs*, **34**(6), 179.

YILMAZ, Y., GENÇ, S. C., GÜRER, O. F. *ET AL*. 2000. When did the western Anatolian grabens begin to develop? *In*: BOZKURT, E., WINCHESTER, J. A. & PIPER, J. A. D. (eds) *Tectonics and Magmatism in Turkey and the Surrounding Area*. Geological Society, London, Special Publication, **173**, 353–384.

YILMAZ, Y., GENÇ, S. C., KARACIK, Z. & ALTUNKAYNAK, Ş. 2001. Two contrasting magmatic associations of NW Anatolia and their tectonic significance. *Journal of Geodynamics*, **31**, 243–271.

YÜCEL-ÖZTÜRK, Y., HELVACI, C. & SATIR, M. 2005. Genetic relations between skarn mineralization and petrogenesis of the Evciler Granitoid, Kazdag, Çanakkale, Turkey and comparison with world skarn granitoids. *Turkish Journal of Earth Sciences*, **14**, 255–280.

ZHU, L., MITCHELL, B. J., AKYOL, N., ÇEMEN, I. & KEKOVALI, K. 2006. Crustal thickness variations in the Aegean region and implications for the extension of continental crust. *Journal of Geophysical Research*, **111**, B01301, doi:10.1029/2005JB003770.

Insights from the Apennines metamorphic complexes and their bearing on the kinematics evolution of the orogen

GIANLUCA VIGNAROLI[1]*, CLAUDIO FACCENNA[1], FEDERICO ROSSETTI[1] & LAURENT JOLIVET[2]

[1]*Dipartimento di Scienze Geologiche, Università Roma Tre, Largo S.L. Murialdo 1, Roma, Italy*

[2]*Laboratoire de Tectonique, Université Pierre et Marie Curie, 4 Place Jussieu, T 26-0 E1, Case 129, UMR CNRS 7072, 75252 Paris Cedex 05, France*

**Corresponding author (e-mail: vignarol@geo.uniroma3.it)*

Abstract: The Apennine belt represents a typical orogenic segment of the western Mediterranean, characterized by the tectonic convergence between European and Africa plates after oceanic subduction. Both oceanic- and continent-derived metamorphic complexes, considered as the remnants of the subduction-exhumation cycle, crop out in the inner sectors of the Apennine belt, where extensional deformation has dominated since the Early Oligocene. We review the available structural, metamorphic and geochronological data coming from these metamorphic complexes in order to provide a kinematics reconstruction accounting for the tectono-metamorphic evolution of the Apennines, from oceanic subduction to final extensional reworking. During the Eocene, oceanic rocks were progressively subducted down to eclogite-facies conditions following a subduction-type metamorphic gradient. The transition from oceanic- to continental-subduction was coeval with a transition from subduction-type to Barrovian-type metamorphic gradient. Continental collision, at the Eocene–Oligocene boundary, post-dated the syn-orogenic exhumation of HP-rocks and was synchronous with the onset of post-orogenic extension in the hinterland domains. Extensional deformation migrated to the east, following the forelandward migration of the thrust system at the trench. The concomitance of extension and compression is here related to fast rollback of the subducting plate and delamination of the lithospheric mantle below the subducted continental crust. Implications on how the subduction tectonics, syn-orogenic exhumation and post-orogenic extension could have controlled the circulation of HP-rocks in the developing Apennines are also discussed.

The Alpine belt, in the western Mediterranean region, results from the Meso-Cenozoic tectonic convergence between the European and African plates (or the Adria promontory), during the consumption of the interposed Liguro–Piedmont oceanic domain (e.g. Dercourt *et al.* 1986; Dewey *et al.* 1989; Platt *et al.* 1989; Stampfli *et al.* 1998; Wortel & Spakman 2000). Presently (Fig. 1), the Alpine belt consists of irregular and arc-shaped orogenic segments (that are, from west to east: Betics, Rif, Atlas, Tell, Calabria–Peloritani Arc, Apennines, Alps, Carpathians) dispersed and fragmented by the occurrence of newly-formed extensional regions (from west to east: Alboran Sea, Algerian Basin, Liguro–Provençal Basin, Tyrrhenian Sea, Pannonian Basin) (e.g. Dewey 1988; Dewey *et al.* 1989; Platt & Vissers 1989; Avigad *et al.* 1997; Jolivet *et al.* 2003; Rosenbaum & Lister 2004*a*).

Focusing our attention on the Tyrrhenian–Apennines system, the subduction process was characterized by Tertiary eastward rollback of the subducting plate and progressive retreat of the trench system (Royden *et al.* 1987; Royden 1993; Faccenna *et al.* 2004; Rosenbaum & Lister 2004*b*) inducing: (i) migration of the thrust front in the eastern external zones (the Adriatic foreland) (e.g. Patacca *et al.* 1990; Massoli *et al.* 2006); (ii) distinct episodes of subduction-related calcalkaline volcanism in the upper plate (e.g. Kastens *et al.* 1988; Argnani & Savelli 1999; Savelli 2002); and (iii) large scale ductile extension in the internal region (Tyrrhenian Sea) (e.g. Malinverno & Ryan 1986; Dewey 1988; Jolivet *et al.* 1998) and its progressive migration toward the Apennine belt (e.g. Lavecchia *et al.* 1994; Pauselli *et al.* 2006). Orogenic construction and deep underthrusting occurred at the expense of both oceanic and continental domains, whose remnants, metamorphosed under high/pressure-low/temperature (HP-LT) conditions are now exposed in the Tyrrhenian Sea margin in the footwall of regional-scale extensional detachment systems (e.g. Jolivet *et al.* 2003, and reference therein). Although detailed works have described both compressional and extensional structures within metamorphic complexes cropping out in the Apennine belt, the published kinematics

From: VAN HINSBERGEN, D. J. J., EDWARDS, M. A. & GOVERS, R. (eds) *Collision and Collapse at the Africa-Arabia-Eurasia Subduction Zone*. The Geological Society, London, Special Publications, **311**, 235–256.
DOI: 10.1144/SP311.9 0305-8719/09/$15.00

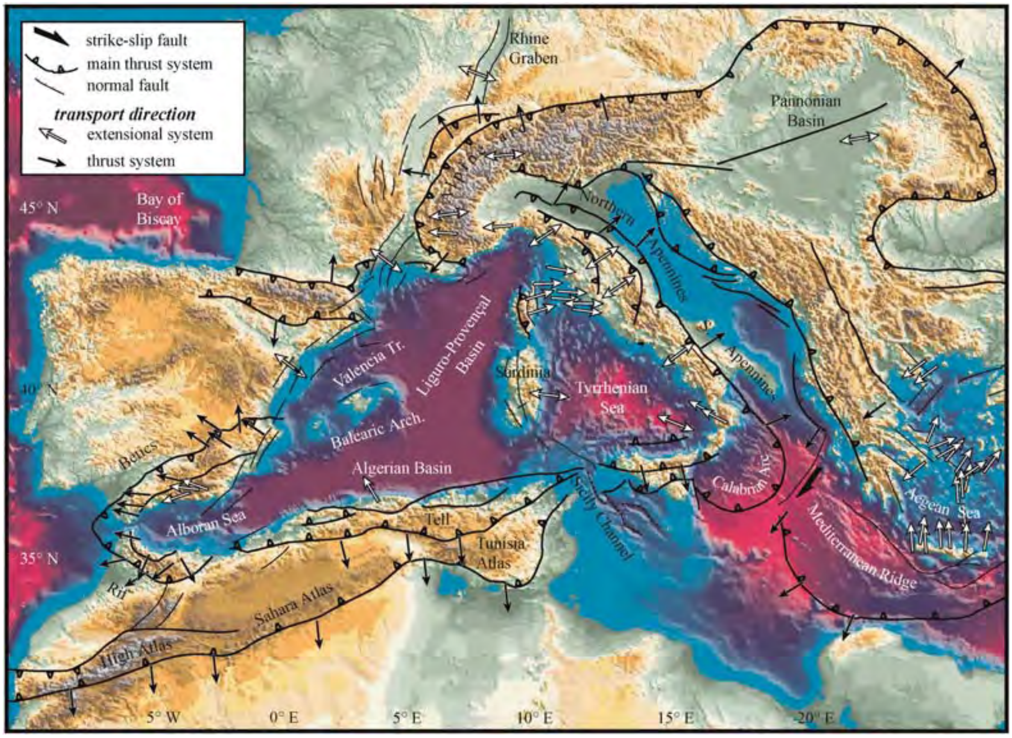

Fig. 1. Tectonic map of the Mediterranean region (after Faccenna *et al.* 2004) showing the trend of the main Alpine orogenic belts and the direction of their tectonic transport. The shear senses of the extensional regions are also reported.

scenarios for the Apennine belt were so far mainly based on palaeogeographic, stratigraphic, magmatic and palaeomagnetism constraints (e.g. Gueguen *et al.* 1998; Bonardi *et al.* 2001; Rosenbaum & Lister 2004*a*) and few considerations have been addressed to the tectono-metamorphic evolution of the belt (e.g. Faccenna *et al.* 2001; Jolivet *et al.* 2003).

This paper represents an attempt to review the existing general dataset (in terms of structures, metamorphism and age of the main tectonic events) recorded by the metamorphic complexes exposed in the Tyrrhenian–Apennines system, with the aim of presenting a synthetic kinematics reconstruction of the whole Apennine belt since the Eocene. The progressive palaeogeographic configuration through time is shown in map view and along two regional cross-sections. The integration of the dataset review and the kinematics reconstruction are finally used to provide insights on the circulation of the exposed HP-rocks (here considered as the path followed by the rocks during their burial and subsequent going back up to the surface, i.e. the subduction-exhumation cycle) inside the Apennine orogenic wedge.

Summary of the geological context

P-wave tomography in the western Mediterranean suggests the presence of west-dipping high seismic velocity anomalies under the Tyrrhenian region, interpreted as the expression of the Apennine subducting lithosphere (e.g. Lucente *et al.* 1999; Wortel & Spakman 2000; Piromallo & Morelli 2003). Seismic data reveal a normal crustal thickness of *c.* 30 km below the Corsica–Sardinia block and a thinned crust in the Tyrrhenian Sea (from 20 km in the northern part to *c.* 10 km in the southern part, e.g. Sartori *et al.* 2001, and references therein; Nicolich 1989). This thinned crust in the Tyrrhenian Sea is characterized by high heat flow values up to 220 mW m^{-2} in the southern portion (Della Vedova *et al.* 2001) and intense magmatism (e.g. Panza *et al.* 2007, and references therein). The highest heat flux values are concentrated under the geothermal areas of Tuscany (up to 1000 mW m^{-2} in the Larderello–Travale–Amiata geothermal fields) (Della Vedova *et al.* 2001). Crustal-scale profiles in the northern and central Apennines indicate that the Adriatic Moho is placed at about 25–30 km and is involved in the fold-and-thrust tectonics (e.g.

Barchi *et al.* 1997; Finetti *et al.* 2001), extensively reworked by low- and high-angle normal faults (e.g. Pauselli *et al.* 2006). The frontal portion of the Apennine belt is characterized by forelandward- (Adriatic-) thrust systems that can be continuously traced from the Northern Apennines, through the Southern Apennines to the Calabria–Peloritani Arc (Bigi *et al.* 1990) (Fig. 2). In both the Northern and Southern Apennines, contractional structures involve Jurassic-to-Pliocene sedimentary sequences to form a fold-and-thrust-belt. Structural evidence and sedimentary constraints suggest the outward progressive migration of the front of compression (e.g. Patacca *et al.* 1990; Cipollari & Cosentino 1995; Elter *et al.* 2003). In the Calabria–Peloritani Arc, pre-Alpine metamorphic and igneous rocks are also piled up in the nappe edifice on top of Adriatic-belonging carbonate sequences (e.g. Amodio-Morelli *et al.* 1976; Bonardi *et al.* 2001 and references therein). The HP-metamorphic rocks are now exposed in the internal zones of the Apennine belt reworked by extension (Fig. 2). In the following paragraphs, we present a review of the main geological features (in terms of kinematics, petrology and geochronology) of the Apennine metamorphic complexes, through the discussion of three representative schematic cross-sections along: (i) the Ligurian Alps; (ii) the northern Tyrrhenian Sea; and (iii) the southern Tyrrhenian Sea (Fig. 3). This dataset is then used to constrain the space-time evolution of the two-stage deformational process affecting the Apennine belt.

The metamorphic complexes exposed along the Tyrrhenian–Apennine system

From the top to the bottom, the Apennine belt consists of the stack of three main groups of units: (i) the European crystalline units in the Ligurian Alps (the Savona Massif), the Corsica–Sardinia block and the Calabride Complex of the Calabria–Peloritani Arc (e.g. the Aspromonte unit) (Fig. 2) and consisting of granitoids of Late Carboniferous-to-Permian age intruding an Early Palaeozoic metamorphic basement (e.g. Amodio-Morelli *et al.* 1976; Durand-Delga 1984; Vanossi *et al.* 1984; Bonardi *et al.* 2001; Renna *et al.* 2007); (ii) ophiolite-bearing units (exposed, from north to south, in the Voltri Massif, Alpine Corsica, Tuscan Archipelago and Calabria; Fig. 2), consisting of Jurassic ophiolites and their Late Jurassic–Early Cretaceous sedimentary cover (e.g. Chiesa *et al.* 1975; Amodio-Morelli *et al.* 1976; Lanzafame *et al.* 1979; Durand-Delga 1984; Vanossi *et al.* 1984; Carmignani *et al.* 1994); (iii) Adriatic crystalline units, cropping out in Tuscany, in Coastal Chain of Calabria and in the Peloritani Mountains, and consisting of Upper Triassic sandstones and limestones (the 'Verrucano Serie' in Tuscany and Coastal Chain; e.g. Amodio-Morelli *et al.* 1976; Carmignani *et al.* 1994) and Palaeozoic basement (e.g. Bonardi *et al.* 2001). All these groups of units experienced Alpine polyphased metamorphism during Tertiary plate convergence (e.g. Hoogerduijn Strating 1994; Jolivet *et al.* 1998; Bonardi *et al.* 2001, and references therein; Franceschelli *et al.* 2004; Rossetti *et al.* 2004; Iannace *et al.* 2007).

Ligurian Alps

The Ligurian Alps define an east–west trending tectonic junction between the west-verging belt of the Western Alps and the east-verging belt of the Northern Apennines (Fig. 2). In the Ligurian Alps, both ophiolitic and continental units are arranged to form a bivergent nappe edifice, on top of which the Oligocene–Pliocene sedimentary deposits of the Tertiary Piedmont Basin lye (e.g. Vanossi *et al.* 1984) (cross-section a–b in Fig. 3). The ophiolitic domain of the Voltri Massif defines the lowermost tectonic domain of the Ligurian Alps. To the west, the Voltri Massif comes into contact with the Savona Massif (the Briançonnais domain), composed by a Hercynian basement (amphibolites, orthogneiss and associated intrusive granites) and its Meso-Cenozoic cover (e.g. Vanossi *et al.* 1984). In the Briançonnais domain, imbrications of units occur along top-to-the-west thrust systems cross-cutting the basement and the cover and also involving the Helmintoïdes Flyschs at the top. To the east, the ophiolitic domain of the Sestri–Voltaggio Zone (e.g. Cortesogno & Haccard 1984) separates the Voltri Massif from the flyschoid units of the Northern Apennines (the Antola Flysch), characterized by an ENE propagation of the imbricate thrust system (Fig. 3a).

Voltri Massif. In the Voltri Massif, eclogitic rocks and the associated serpentinites and metasediments are in tectonic contact with eclogitic-bearing lherzolites (e.g. Hoogerduijn Strating *et al.* 1990) and non-metamorphic units (e.g. Capponi *et al.* 1998), as well as sedimentary deposits of the Tertiary Piedmont Basin. The eclogitic mineralogical assemblage (composed by Ca-rich omphacite and euhedral garnet) was equilibrated at maximum P of 20–22 kbar under relative low T of 500–550 °C (Liou *et al.* 1998; Brower *et al.* 2002; Federico *et al.* 2004; Vignaroli *et al.* 2005) (Fig. 4). Post-eclogitic assemblage is defined by glaucophane-bearing symplectites and then green-amphibole assemblages around garnet and omphacite (e.g. Messiga & Scambelluri 1991). The retrogressive, syn-blueschist, plano-linear fabric shows micro- and meso-scale kinematics

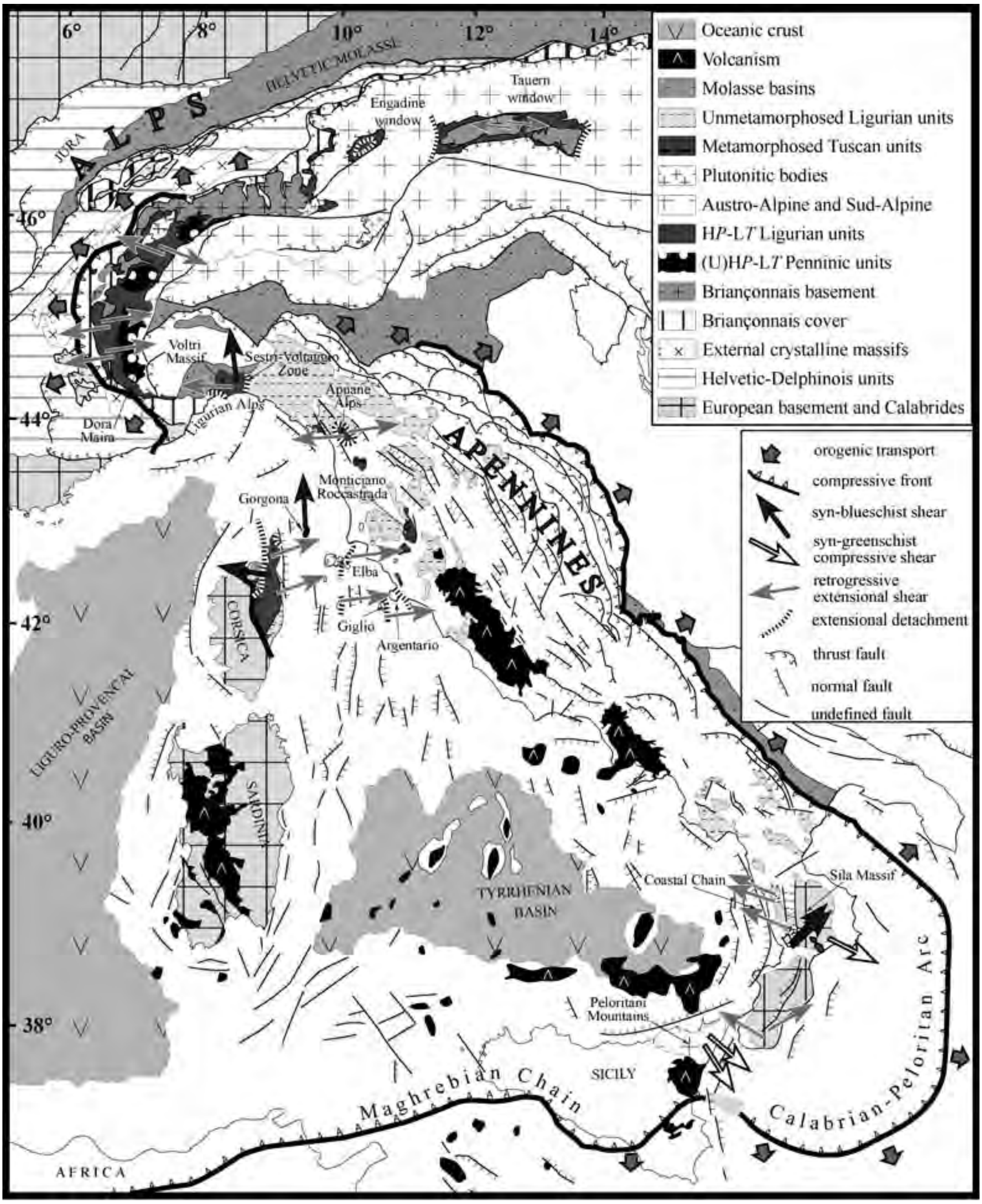

Fig. 2. Tectonic map of the Alps–Apennines belt system (redrawn and modified after Jolivet *et al.* 2003) showing the distribution of the main palaeo-tectonic domains. References for the kinematics data: Choukroune *et al.* (1986); Selverstone (1988); Platt *et al.* (1989); Philippot (1990); Wheeler & Butler (1993); Agard *et al.* (2002); and Reddy *et al.* (2003) for the Alps; Vignaroli *et al.* (2005, 2008*a*) for the Ligurian Alps; Boccaletti *et al.* (1980), Principi & Treves (1984), Storti (1995), Jolivet *et al.* (1998) and Rossetti *et al.* (1999, 2001*a*) for the Northern Apennines; Mattauer *et al.* (1981), Jolivet *et al.* (1990, 1998) and Daniel *et al.* (1996) for the Alpine Corsica; Platt & Compagnoni (1990), Rossetti *et al.* (2001*b*, 2004), Prosser *et al.* (2003), Heymes *et al.* (2008) and Vignaroli *et al.* (2008*b*) for the Calabria–Peloritani Arc.

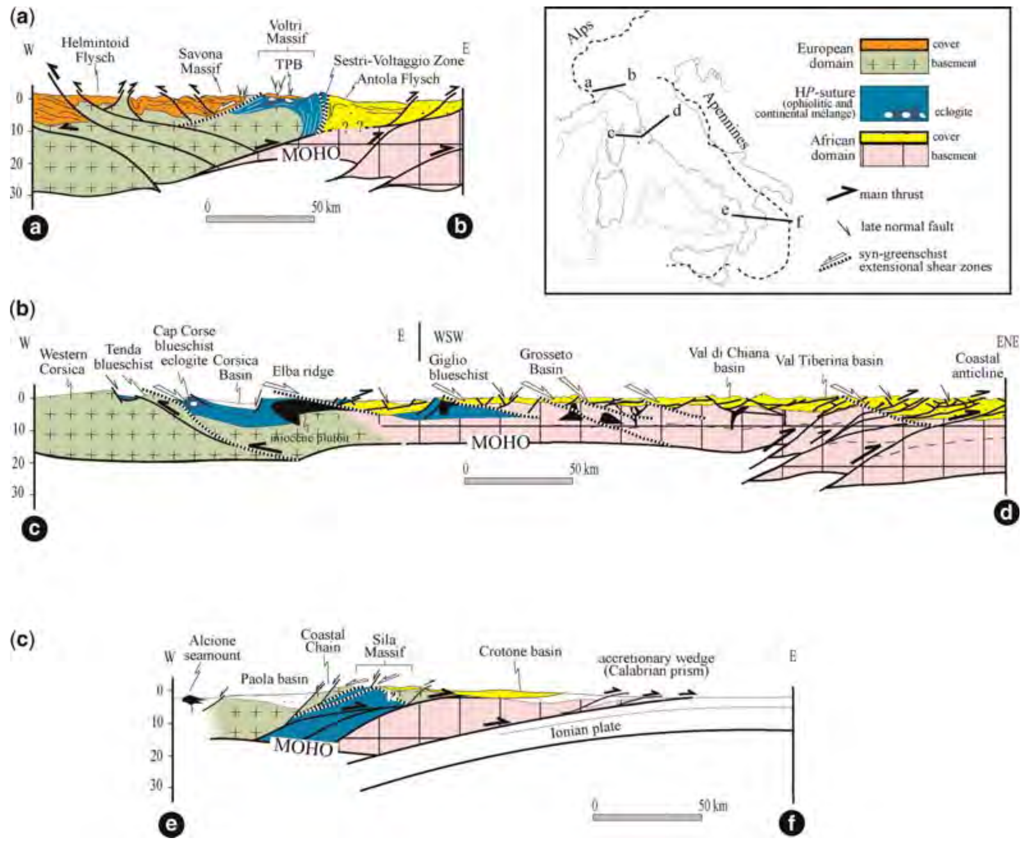

Fig. 3. Crustal-scale cross-sections for (**a**) the Ligurian Alps, (**b**) the Corsica–Apennines system and (**c**) the Calabria–Peloritani Arc. Data are adapted from Hoogerduijn Strating (1994) and Vignaroli *et al.* (2008*a*) for the Ligurian Alps; Jolivet *et al.* (1998, 2003) for the Northern Apennines; van Dijk *et al.* (2000), Jolivet *et al.* (2003) and Rossetti *et al.* (2004) for the Calabria–Peloritani Arc.

indicators pointing to a top-to-the-North–NNW sense of shear (Vignaroli *et al.* 2005). The present-day structure of the massif has been related to the development of the retrogressive ductile-to-brittle fabric, overprinting the HP assemblage (Capponi & Crispini 2002; Federico *et al.* 2007*a*). Compressive structures have been described as responsible for the exhumation of the HP rocks (e.g. Chiesa *et al.* 1975; Brouwer *et al.* 2001; Capponi & Crispini 2002). Hoogerduijn Strating (1994) firstly described the occurrence of extensional detachments inside the contractional nappe edifice as responsible for local pressure gaps. Recently, Vignaroli *et al.* (2008*a*) emphasized the role of top-to-the-West extensional detachment systems as reshaping the previously nappe pile in a dome structure. The age of the eclogitic peak is still under debate. $^{40}Ar/^{39}Ar$ geochronology on phengites from metabasites gives ages spanning from 48 to 43 Ma (Federico *et al.* 2005, 2007*b*). On the other hand, U/Pb SHRIMP dating performed on baddeleyite from eclogites gives younger ages (33.6 $\pm$ 1.0 Ma; Rubatto & Scambelluri 2003). This divergence has been interpreted as indicative of a diachronous eclogitic metamorphism during the subduction process (e.g. Federico *et al.* 2005). Age of the syn-blueschist assemblage is placed at *c.* 40 Ma by $^{40}Ar/^{39}Ar$ dating of phengites in assemblages with glaucophane (Federico *et al.* 2007*b*). The greenschist facies retrogression can be considered to have occurred at 33–35 Ma, based on of $^{40}Ar/^{39}Ar$ geochronology on phengites in association with chlorite and paragonite (Federico *et al.* 2005) and U/Pb SHRIMP dating performed on titanite crystal, pre-to-syn-tectonic with respect to the greenschist retrogressive fabric (Vignaroli 2006).

Sestri-Voltaggio Zone. The Sestri-Voltaggio Zone represents a narrow, north–south striking

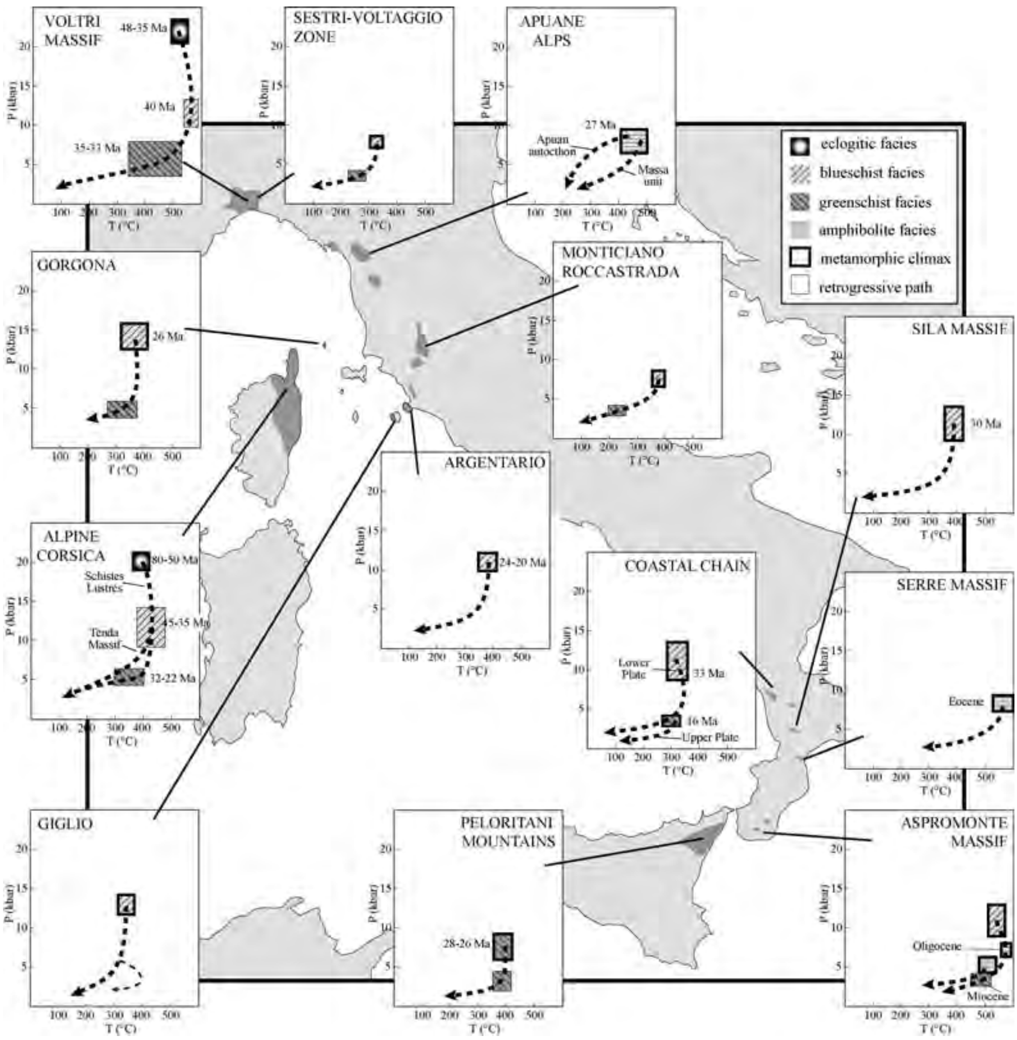

Fig. 4. Synthesis of the *P-T* path followed by the main metamorphic complexes in the Apennine belt. See the text for the data references.

metaophiolitic domain structurally interposed between the Voltri Massif (at the bottom) and the non-metamorphosed units of the Northern Apennines (at the top). Late Triassic–Jurassic dolomitic and carbonate sequences associated with low-grade phyllites, serpentinites, gabbros and metabasites alternating with recrystallized limestones crop out in the Sestri–Voltaggio Zone (e.g. Cortesogno & Haccard 1984; Hoogerduin Strating 1994). Alpine metamorphism has been described for the metabasites. The HP stage is represented by glaucophane-bearing mineralogical assemblages equilibrated under blueschist facies conditions (7–8 kbar over 300–350 °C; Hoogerduijn Strating 1994) (Fig. 4). The subsequent retrogressive evolution is testified by the occurrence of white mica-chlorite-epidote associations, pointing to a low-grade greenschist facies overprint. According to Hoogerduin Strating (1994), the tectonic contact between the Sestri–Voltaggio Zone and the underlying Voltri Massif marks a gap in pressure, indicative of a tectonic excision during the development of an extensional detachment. Presently, there is no constraint on the age of the HP stage recorded in the Sestri–Voltaggio Zone. Nevertheless, structural observations allow us to consider the Sestri–Voltaggio Zone as a higher structural level with respect the exhumation of the Voltri Massif (Cortesogno & Haccard 1984; Hoogerduin Strating 1994; Vignaroli *et al.* 2008*a*), suggesting that its HP stage was older (or coeval) with respect the eclogitic stage in the Voltri Massif itself.

Northern Tyrrhenian

Following the cross-section c–d in Fig. 3b, the ophiolitic units of the Schistes Lustrés in Alpine Corsica are tectonically juxtaposed on top of the Hercynian rocks along a west-verging major thrust system (e.g. Mattauer *et al.* 1981; Fournier *et al.* 1991; Molli *et al.* 2006); on the other hand, the Northern Apennines imbricate thrust systems define an ENE-verging fold-and-thrust-belt involving both the Triassic–Neogene sedimentary sequences and the metamorphic units (e.g. Carmignani *et al.* 1994). The early compressive structures are dissected by ductile-to-brittle, extensional detachments (e.g. Carmignani & Kligfield 1990; Jolivet *et al.* 1990, 1998; Storti 1995; Daniel *et al.* 1996; Rossetti *et al.* 1999), later recognized as responsible for pluton emplacement in the Tuscan Archipelago area (e.g. Keller & Pialli 1990; Rossetti *et al.* 1999).

Alpine Corsica. The structural architecture of Corsica is defined by the superimposition of three major tectonic units, from bottom to the top: the European continental basement of the Tenda Massif, the Schistes Lustrés and the Balagne nappe. The latter represent the HP-LT metamorphosed and non-metamorphosed rocks of the Liguro–Piedmont oceanic domain, respectively. Their present-day stacking form two major north–south trending anticlines exposed in the Tenda Massif and in the Cap Corse region, which tectonic boundaries are controlled by East-dipping low-angle shear zones. Crustal thickening in Alpine Corsica is recorded in the first-phase metamorphic fabric of the Schistes Lustrés and Tenda Massif units (e.g. Daniel *et al.* 1996; Fournier *et al.* 1991; Lahondère 1996; Lahondère & Guerrot 1997; Molli *et al.* 2006). Eclogitic metamorphism in the Schistes Lustrés ($P = 18$–20 kbar and $T = 380$–$400\ ^{\circ}$C) is overprinted by retrogressive metamorphic assemblages equilibrated under the blueschist facies conditions (10–12 kbar and 350–400 °C) typified by carpholite- and/or chloritoid-bearing mineralogical associations (Fournier *et al.* 1991; Jolivet *et al.* 1998) (Fig. 4). The syn-blueschist retrogression is characterized by a plano-linear fabric showing dominant top-to-the-West and subordinate top-to-the-North tectonic transports (e.g. Mattauer *et al.* 1981; Jolivet *et al.* 1990, 1998; Daniel *et al.* 1996). The Tenda Massif provides maximum P–T estimates at about 10 kbar and 450 °C (Molli & Tribuzio 2004; Molli *et al.* 2006) (Fig. 4), whereas the olistostrome below the Balagne nappe, formed during its emplacement onto the Eocene foreland basin (Egal 1992), metamorphosed at 6 kbar and 325 °C (Malasoma & Marroni 2007). The post-orogenic extensional setting pervasively overprints the former HP fabric. The extensional fabric formed under greenschist facies conditions (e.g. Daniel *et al.* 1996) and it is mainly associated with top-to-the-East sense of shear, both in the ductile and brittle enviroments (e.g. Jolivet *et al.* 1990, 1998; Fournier *et al.* 1991; Daniel *et al.* 1996). The brittle deformational structures are represented by east-dipping normal faults cutting the major ductile contacts and partly accommodating the Middle Miocene syn-rift sedimentation (Francardo & Saint Florent basins; e.g. Daniel *et al.* 1996). For the age of tectonic events in the Alpine Corsica, the first order facts are as follows (Brunet *et al.* 2000, and references therein): (i) the eclogitic metamorphism is dated from the Late Cretaceous and Eocene; (ii) the exhumation of the eclogites during top-to-the-West shearing at the blueschist metamorphism occurred at 45–35 Ma; and (iii) the greenschist facies overprint is dated as the Early Oligocene till the Early Miocene.

Tuscan Archipelago. The earlier compressive tectonic event in the Tuscan Archipelago occurred under blueschist metamorphic conditions, as attested by the occurrence of: (i) carpholite-bearing assemblages in metapelites of the Verrucano Group exposed in Giglio Island (12–14 kbar and 350–420 °C; Rossetti *et al.* 1999) and in Monte Argentario Promontory (10–12 kbar and 350–420 °C; Theye *et al.* 1997); and (ii) glaucophane-bearing assemblages in metabasites and carpholite-bearing assemblages in metapelites of Gorgona Island (13–16 kbar and 300–350 °C) (Fig. 4). In Gorgona Island, syn-blueschist *SL*-tectonites show a top-to-the-North sense of shear (Rossetti *et al.* 2001). No HP-minerals have been discovered on Elba Island, probably replaced by HT assemblages during the Miocene–Pliocene pluton emplacement. Structures developed during the second-phase, syn-greenschist metamorphism have been commonly ascribed to an extensional setting based upon metamorphic gaps and progressive brittle deformation overprinting early ductile one moving upward inside the tectonic edifice (e.g. Carmignani & Kligfield 1990; Carmignani *et al.* 1994; Jolivet *et al.* 1998). Ductile shearing is represented by *SL*-tectonites, partitioned into dominant vertical coaxial shortening and localized non-coaxial strain. east–west trending stretching lineation is dominant. Top-to-the-East (top-to-the-ESE in Gorgona Island) sense of shear characterizes the major extensional tectonic contacts, while both top-to-the-East and top-to-the-West sense of shear have been described in the Monte Argentario Promontory (Jolivet *et al.* 1998; Theye *et al.* 1997). Ductile-to-brittle top-to-the-East shearing, developed during the late stage of the extensional regime, controlled the emplacement of pluton intrusions of Elba, Montecristo and Giglio islands (e.g. Jolivet *et al.* 1998, and references therein). Structural analyses indicate that pluton emplacement occurred at shallow depths when the HP rocks were already exhumed to surficial conditions (e.g. Jolivet *et al.* 1998; Rossetti *et al.* 1999; Westerman *et al.* 2004).

Tuscany. The HP-LT metamorphic assemblages have been found in the Mid-Tuscan Ridge (the Monticiano–Roccastrada Ridge), where carpholite-bearing and chloritoid-bearing assemblages are indicative of *P-T* conditions of 8–10 kbar and 350–380 °C (Giorgetti *et al.* 1998) (Fig. 4). In the Apuan Alps, distinct metamorphic signatures have been recognized from the exposed metamorphic sequences. In the lower Apuan Autochthon, the thickening stage was equilibrated under MP-MT metamorphic conditions (390–410 °C and 5–8 kbar; Fig. 4), based on the Mg-content of chloritoid (Franceschelli *et al.* 1997; Jolivet *et al.* 1998). In the upper Massa unit, the presence of kyanite and the higher content of Mg in chloritoid constrain the pressure to 9 kbar and the temperature to 450–480 °C (Molli *et al.* 2000). The retrogressive metamorphic conditions equilibrated under the greenschist facies field (3–4 kbar and 300–350 °C; e.g. Molli *et al.* 2000). A major detachment system, showing both top-to-the-West and top-to-the-East sense of shear and accommodating the exhumation of the previous thrust contacts has been related to this retrogressive metamorphic event (Carmignani & Kligfield 1990; Storti 1995; Jolivet *et al.* 1998). Age of the HP-LT metamorphism is constrained to the Oligocene in the Tuscan Archipelago (synchronous to the extension in the Alpine Corsica) and to the Middle Miocene in Tuscany, whereas the age of the extension-related greenschist metamorphism is placed at the Serravallian in the Tuscan Archipelago and at the Tortonian in the Apuane Alps (e.g. Giglia & Radicati di Brozolo 1970; Kligfield *et al.* 1986; Deino *et al.* 1992; Brunet *et al.* 2000). Brittle extensional structures (high-angle normal faults) also controlled the syn-rift sedimentation since the Late Miocene in Tuscany to the Late Pliocene–Pleistocene (within the Apennine belt) (Bossio *et al.* 1993; Lavecchia *et al.* 1994; Faccenna *et al.* 1997; Bossio *et al.* 1998). Post-orogenic tectonics in Tuscany also played an important role in the development of the Larderello–Travale–Amiata geothermal fields (e.g. Batini *et al.* 2003). Apart from divergent opinions on the role of pre-Alpine metamorphism in the basement rocks hosting the geothermal fields (e.g. Franceschini 1998; Gianelli & Ruggieri 2002; Musumeci *et al.* 2002; Pandeli *et al.* 2005; Bertini *et al.* 2006), the reconnaissance of extensive HT-metamorphism (contact aureoles) is attributed to continuous pluton emplacement between 3 Ma and 0.7 Ma (e.g. Dini *et al.* 2005; Villa *et al.* 2006; Rossetti *et al.* 2008), followed by intense hydrothermal circulation in the host rocks.

Southern Tyrrhenian

The present-day structural arrangement of the Calabria–Peloritani tectonic edifice results from the underplating of Adria-derived units beneath the European margin (cross-section e–f in Fig. 3), with the interposition of oceanic rocks as remnants of the Liguro-Piedmont ocean. Interpretation of the tectonic evolution of the Calabria–Peloritani Arc has been always the subject of continuous debate, particularly for what concerns the palaeotectonic scenario, the kinematics and the timing during the Alpine evolution (Ogniben 1969, 1973; Haccard *et al.* 1972; Alvarez *et al.* 1974; Amodio-Morelli *et al.* 1976; Bouillin 1984; Knott 1987; Dietrich 1988; Bonardi *et al.* 2001; Rossetti *et al.* 2001). Furthermore, both subduction- (Dubois 1970; Piccarreta 1981; Rossetti *et al.* 2001, 2004) and Barrovian-type (Messina *et al.* 1990; Platt & Compagnoni 1990; Bonardi *et al.* 1992; Langone *et al.* 2006) metamorphic gradients are reported for the continent-derived units.

Calabria. In northern Calabria, rocks affected by orogenic metamorphism are constituted by Triassic continent-derived metaclastic and carbonate sequences (Adria margin), oceanic-derived ophiolitic rocks with their associated metamorphosed cover and pre-Alpine basement rocks. Thermobarometric estimates (Fig. 4) fall within the blueschist facies field (330–420 °C over 8–14 kbar in the Sila Massif; 300–370 °C and 8–14 kbar in the Coastal Chain; Dubois 1970; Spadea *et al.* 1976; Piccarreta 1981; Beccaluva *et al.* 1982; Cello *et al.* 1991; Rossetti *et al.* 2001, 2004; Iannace *et al.* 2007). In contrast, continent-derived units of the Calabrian basement nappe exposed in the Serre Massif and the Aspromonte Massif attained metamorphic peak under typical Barrovian conditions transitional from amphibolites-facies (530–600 °C and 5–9 kbar; e.g. Platt & Compagnoni 1990; Langone *et al.* 2006) to HP-stage (510–570 °C and 9–13 kbar; e.g. Cirrincione *et al.* 2008) (Fig. 4). The age of the HP metamorphic stage has been referred to the Eocene–Early Oligocene time, even by using different geochronological methods (Beccaluva *et al.* 1981; Prosser *et al.* 2003; Rossetti *et al.* 2001, 2004). Recently, Iannace *et al.* (2007), working on carbonate tectonic units of the northern Calabria, rejuvenated the age of the metamorphic peak to the Lower Aquitanian. Compressive structures verging towards the Adriatic foreland have been described throughout Calabria. In the Sila Massif, top-to-the-ENE shear sense (developed during blueschist conditions) has been recognized for the Calabride Complex (Rossetti *et al.* 2001). In the Coastal Chain (Dietrich 1988; Rossetti *et al.* 2004; Iannace *et al.* 2007) and in northern Calabria (Wallis *et al.* 1993; Knott 1994), ductile and brittle contractional structures have been described for the oceanic-derived and the Adria-belonging units. In the Serre Massif, tectonic slices of the Hercynian basement are emplaced along top-to-the-SE, ductile-to-brittle thrust system (Langone *et al.* 2006). East-verging thrust systems also controlled the overthrusting of Hercynian basement onto late-orogenic sedimentary deposits, Burdigalian in age, in the eastern portion of the Sila Massif (Bonardi *et al.* 2005). The retrogressive (syn-greenschist) fabric recorded in both the continent- and oceanic-derived rocks shows a top-to-the-WNW sense of shear attributed to extensional deformation (Rossetti *et al.* 2001, 2004). The retrogressive trajectory is characterized by a nearly isothermal decompression path down to the greenschist facies ($P = 3$–5 kbar; $T = 290$–$390\ ^{\circ}$C) and then a rapid cooling towards the surface (Fig. 4). Extensional detachments have been described as responsible for the Neogene architecture of the Calabria tectonic edifice and promoting the final exhumation of the HP units in the Coastal Chain (Rossetti *et al.* 2004), the Sila Massif (Rossetti *et al.* 2001), the Calabrian–Lucanian boundary (Wallis *et al.* 1993) and the Aspromonte Massif (Platt & Compagnoni 1990; Heymes *et al*. 2008). Age of the extension-related fabric has been proposed as spanning from the Late Oligocene to the Langhian (e.g. Rossetti *et al.* 2001, 2004).

Peloritani Mountains. In the Peloritani Mountains, continent-derived metamorphic units from the Africa plate are stacked to form a SE-verging antiformal stack (e.g. Giunta & Somma 1996; Vignaroli *et al.* 2008*b*). Nappe stacking evolved in time and space, as the imbrications of continental material in the accretionary process occurred by incorporating more distal portions of the African margin scraped off from the downgoing subducting plate and accreted under brittle conditions to form a fold-and-thrust belt. A decrease in pressure occurs within this structured belt when moving from the uppermost units facies ($P = 6$–8 kbar; $T = 360$–$430\ ^{\circ}$C) to the lowermost ones ($P = 2.5$–4 kbar; $T = 380$–$440\ ^{\circ}$C) (Vignaroli *et al.* 2008*b*) (Fig. 4). Alternatively, Somma *et al.* (2005) interpreted a gap of metamorphic grade within the tectonic edifice due to the presence of an extensional detachment responsible of thinning the original nappe pile and exhumation of the underlying units. Age of the metamorphic event in the Peloritani Mountains is not well constrained. Geochronological data and fission track analysis constrain the age of the metamorphic climax at *c*. 26 Ma (Atzori *et al.* 1994) and the final exhumation at *c*. 21 Ma (Thomson 1994), respectively.

From metamorphic complexes to kinematics reconstruction

Introducing the kinematics reconstruction

Published kinematics reconstructions for the western Mediterranean (including the Apennines) largely focused on insights coming from seismic refraction data (Gueguen *et al.* 1998), plate motion (Dewey *et al.* 1989; Capitanio & Goes 2006), subduction-related sedimentation (Bonardi *et al.* 2001) coupled with magmatism and palaeomagnetism (Rosenbaum & Lister, 2004*a*, *b*), palaeogeographic configuration (e.g. Golonka 2004, and references therein). In Jolivet *et al.* (2003), the *P*-*T*-t-deformation paths recorded by the metamorphic complexes have been integrated to frame a possible geodynamic scenario of burial and exhumation of the Alpine HP rocks in the Mediterranean region.

Geological features from metamorphic complexes in the Apennines allow us to frame their subduction-exhumation cycle into the tectonic evolution of the belt. From our review it results that: (i) eclogites and blueschists are the most common HP-LT metamorphic rocks, attesting that the stacked units were buried to maximum depths of about 70 km (considering an average rock density of 2.7 g cm^{-3}); (ii) deep underthrusting of subducted material affected the Sardinia–Corsica block in Alpine Corsica, and the Adriatic foreland along the Apennine trench, attesting for a bivergent shape of the orogenic wedge (e.g. Principi & Treves 1984); (iii) the majority of the exhumation of the deep-seated HP-rocks occurred under suppressed geothermal conditions and was particularly efficient during the subsequent activation of extensional (detachment-related) tectonics in the internal zones of the orogenic belt (e.g. Carmignani *et al.* 1994; Jolivet *et al.* 1998; Rossetti *et al.* 2004); (iv) activation of extension occurred during eastward migration of the Apennine trench and accretion in the external zones (e.g. Malinverno & Ryan 1986); and (v) extension direction is near perpendicular to the strike of the trench and sub-parallel to the direction of orogenic transport (e.g. Jolivet *et al.* 1998).

The age of the subduction-related metamorphic climax in the Apennine belt progressively gets younger to the east, Late Cretaceous-to-Eocene in the Alpine Corsica and in the Voltri Massif, Paleocene and Late Eocene in western Calabria (Coastal Chain and Sila Massif), Late Oligocene–Early Miocene in the Peloritani Mountains and Tuscan

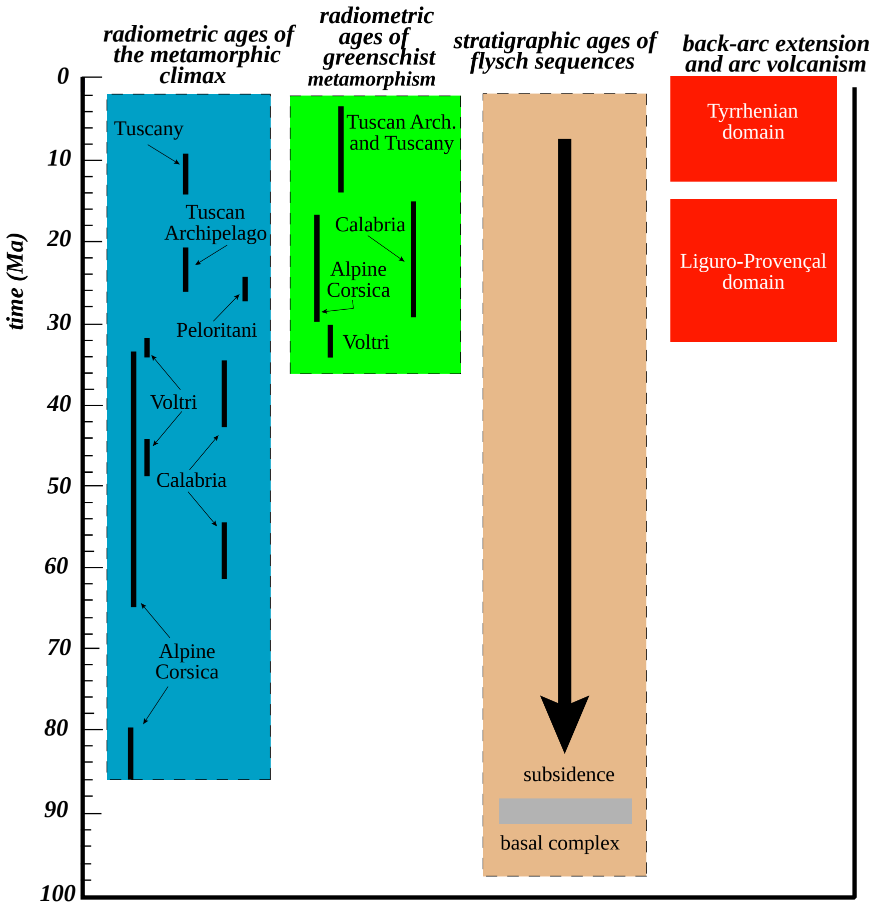

Fig. 5. Summary of the geological data used to constrain the geodynamic evolution of the Apennine belt (after Faccenna *et al.* 2001; modified and re-drawn). Radiometric ages of HP metamorphism from Borsi & Dubois (1968), Schenk (1980) and Rossetti *et al.* (2004) for Calabria; Monié *et al.* (1996), Lahondère & Guerrot (1997), Jolivet *et al.* (1998), Brunet *et al.* (2000) for Northern Apennines and Corsica; Rubatto & Scambelluri (2003) and Federico *et al.* (2005) for the Voltri Massif; Atzori *et al.* (1994) and de Gregorio *et al.* (2003) for the Peloritani Mountains. Radiometric ages of retrogressive metamorphism from Jolivet *et al.* (1998), Kligfield *et al.* (1986), Brunet *et al.* (2000) for Northern Apennines and Corsica; Federico *et al.* (2005) and Vignaroli (2006) for the Voltri Massif; Rossetti *et al.* (2004) for Calabria. Stratigraphic ages of flysch from Principi & Treves (1984), Marroni *et al.* (1992) and Monaco & Tortorici (1995). Radiometric age of magmatism is from Serri *et al.* (1993).

Archipelago, Early Miocene in Tuscany (Fig. 5). This compressional event is also marked by the onset of siliciclastic deposition (Fig. 5), presently cropping out in scattered sites along the Apennine belt (e.g. Principi & Treves 1984; Marroni *et al.* 1992; Cipollari & Cosentino, 1995; Monaco & Tortorici 1995). Similarly, the age of the syn-greenschist retrogression active during extensional reworking shows an eastward rejuvenation, Early Oligocene in the Voltri Massif, Early Oligocene-to-Early Miocene in Alpine Corsica and Calabria, Late Miocene in the Tuscan Archipelago and Tuscany (Fig. 5). Back-arc extension and volcanism in the Liguro–Provençal Basin is coeval with HP-metamorphism in the Tuscan Archipelago and with syn-greenschist retrogression in Alpine Corsica, Voltri Massif and Calabria. In the Tyrrhenian Basin, backarc extension occurred synchronously with retrogressive metamorphism in Tuscany and syn-rifting sedimentation in Calabria (Fig. 5). The space-time evolution of these tectonic processes argues for a westward dipping polarity of the subduction plane during the growth and subsequent collapse of the Apennine belt (Gueguen *et al.* 1997; Jolivet *et al.* 2003; Faccenna *et al.* 2004; Rosenbaum & Lister 2004b).

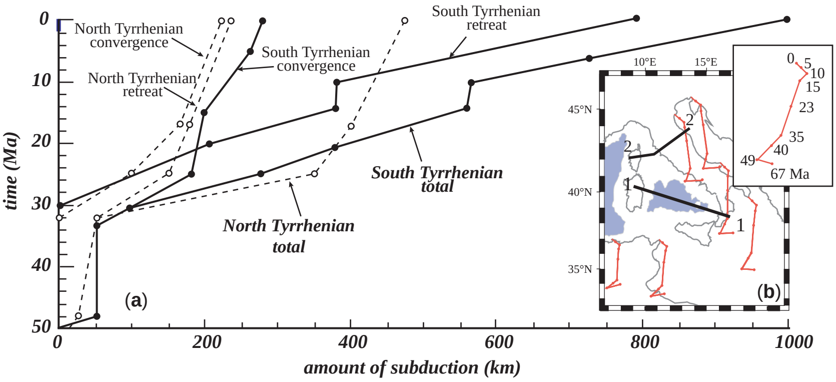

Fig. 6. (**a**) Calculated amount of subduction for the Southern and the Northern Tyrrhenian Sea along cross-sections 1–1 and 2–2 in b), respectively (modified and redrawn after Faccenna *et al.* 2004; Piromallo & Faccenna 2004). (**b**) Tertiary displacement trajectories of Africa with respect to the stable Eurasia from the model of Dewey *et al.* (1989).

In Figure 6a, we plot the total amount of subduction at the Apennine trench obtained by summing up the amount of convergence with the amount of backarc extension during the Tyrrhenian opening (Gueguen *et al.* 1998; Faccenna *et al.* 2001). These calculations have been performed by measuring the component of relative convergence and extension perpendicular to the trench itself during the last 50 Ma. In particular, estimates of the amount of backarc extension are performed by subtracting the oceanic-floored area of each basin and then by restoring the crust to the thickness of stable interior portion of the continental crust (Faccenna *et al.* 2004). According with this scenario, we consider *c.* 275 km of tectonic convergence and *c.* 1000 km of total subduction for the Southern Apennine (section 1–1 in Fig. 6b), and *c.* 225 km of tectonic convergence and *c.* 480 km of total subduction and the Northern Apennine (section 2-2 in Fig. 6b).

Kinematics reconstruction of the Apennine subduction system

The kinematics reconstruction consists of six steps (Fig. 7), in order to depict the evolution of the Apennine belt in the Tyrrhenian area from the HP-event to the syn-orogenic exhumation, to the post-orogenic extension, since the Early Eocene to the Present. Our tectonic scenario follows the reconstruction presented in previous published works (e.g. Bonardi *et al.* 2001; Jolivet *et al.* 2003; Rosenbaum & Lister 2004*a*; Capitanio & Goes 2006), with some modifications about the shape and the extension of the main palaeogeographic (oceanic or continental) domains. We consider the positions of plate boundaries by assuming that Adria plate moved coherently with Africa from the model of Dewey *et al.* (1989). Evolution of the Apennine geodynamics is illustrated in a map sequence integrated with two lithosphere-scale cross-sections, for the Northern and the Southern Apennines, respectively. Within these cross-sections, the structural positions of the Voltri Massif (in the Northern Apennines) and the Peloritani Mountains (in the Southern Apennines) have been projected.

At about 48 Ma (Fig. 7a), during the westward motion of Africa/Adria toward stable Europe, the consumption of the Liguro–Piedmont oceanic domain was still operative. At that time, the subducted oceanic material reached HP-conditions in the Ligurian Alps (e.g. Federico *et al.* 2007) and in Corsica (e.g. Brunet *et al.* 2000) during the progressive growth of the orogenic wedge. Deep underthrusting of ophiolitic units occurred in both the northern and southern portion of the Apennine belt, but only in the Voltri region and Alpine Corsica evidence of the eclogitic metamorphism is preserved. The ophiolitic rocks exposed in Calabria were, probably, subducted at shallower depths within the orogenic wedge (e.g. Rossetti *et al.* 2001*b*). The stacking of ophiolitic rocks in the northern portions of the Apennines (cross-section A–B in Fig. 7a), which partly involved the Tenda Massif continental crust after top-to-the-West shearing (e.g. Mattauer *et al.* 1981; Molli *et al.* 2006). In the Voltri Massif, the kinematics of orogenic transport during this stage is not constrained. In the Southern Apennines (cross-section C–D in Fig. 7a), underthrusting of ophiolitic rocks and slices of European units were buried during top-to-the-East/NE shearing (Rossetti *et al.* 2001*b*). The 40–45 Ma stage (Fig. 7b) was characterized by the northeastern motion of Adria with respect to Eurasia (Fig. 6b). This motion results to

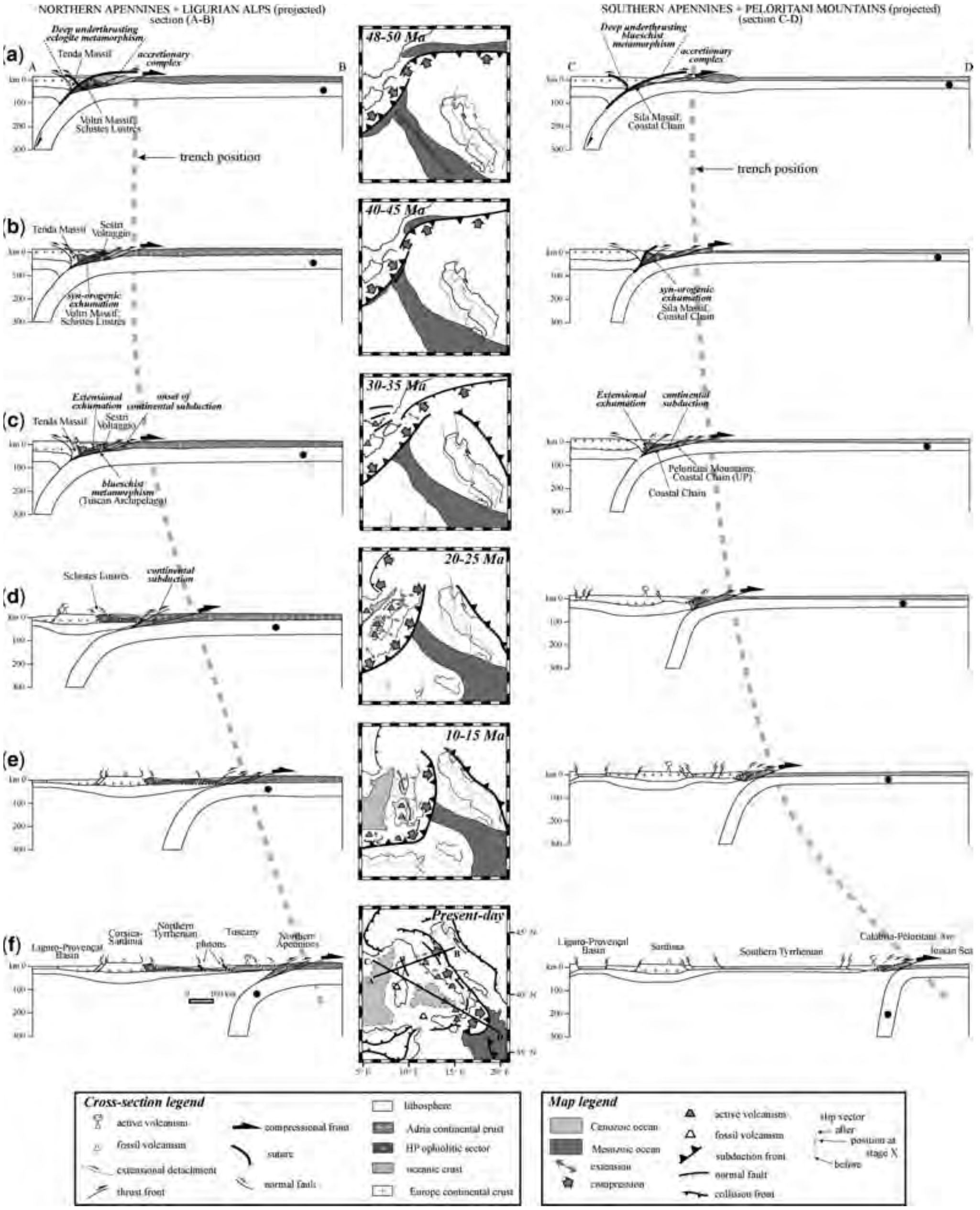

Fig. 7. Possible kinematics reconstruction of the Apennine belt system since the Eocene (details of the a–f stages are reported in the text). Position of the Apennine trench in maps is after Bonardi *et al.* (2001) and Jolivet *et al.* (2003).

be nearly parallel to the strike of the trench (e.g. Jolivet *et al.* 2003), suggesting that a major transpressive kinematics along the trench itself was active. We relate this strike-slip tectonics stage to the syn-orogenic exhumation recorded by eclogites in Corsica and Ligurian Alps during syn-blueschist shearing, as the effect of a forced material convection between the two tectonic plates. In this scenario, the top-to-the-West shearing recorded by some Corsica eclogites, can be tentatively considered as the consequence of partitioning between compression and pure strike-slip during transpressive kinematics. In the 35 Ma stage (Fig. 7c), subduction stopped in the Western Alps and westward migration of the Alpine thrust fronts started. Meanwhile, in the Apennine trench, oceanic subduction was chocked by the entering in subduction of Africa-belonging continental slices (e.g. in Coastal Chain and Peloritani Mountains). The progression of the subduction is attested by calc-alkaline volcanism in Provence and Sardinia regions (e.g. Serri *et al.* 1993; Argnani & Savelli 1999; Savelli 2002) and HP-metamorphism in both oceanic and continental units of Northern Apennines and Calabria (Jolivet *et al.* 1998; Brunet *et al.* 2000; Rossetti *et al.* 2004). From about 30 Ma, eastward trench retreat dominated the Apennine subduction (Faccenna *et al.* 2001). In the Voltri Massif and Alpine Corsica, the opposite migration of the Alpine and Apennine thrust fronts was coeval with the stretching of the domain in between. Blueschists still formed and were exhumed in the frontal accretionary complexes (Tuscany and Calabria), while continental subduction continued in the Peloritani Mountains. The entering in subduction of some continental slices in both the Northern and Southern Apennine trenches (Fig. 7c) seems to coincide with an increase in the retreating velocity of the compressive trench (Fig. 6a) and with the onset of the development of extensional setting in the internal domains in the Apennines (Fig. 5). After this stage, the fast rollback motion of the subducting plate occurred (Fig. 7d) (e.g. Faccenna *et al.* 2004; Rosenbaum & Lister 2004*b*) concomitant with: (i) the eastward drift of the Sardinia-Corsica continental block (e.g. Speranza *et al.* 2002); and (ii) the opening of Liguro–Provençal backarc basin (e.g. Faccenna *et al.* 1997). The extensional setting extensively developed in the inner portions of the Apennines (Fig. 7d), (e.g. Jolivet *et al.* 1998, 2003; Faccenna *et al.* 2001), where syn-greenschist normal-sense detachments induced crustal thinning and post-orogenic exhumation of the HP-rocks from greenschist conditions to the surface. The direction of extension was perpendicular to trenches, except in the Voltri Massif where it trends nearly parallel to the arching of the Western Alps and the Northern Apennines. Concomitant top-to-the-East and top-to-the-West extensional detachments in Alpine Corsica and Calabria, respectively, suggest a crustal-scale pure-shear extensional style. Normal faults accommodated the sedimentation of the oldest syn-rift deposits (10–20 Ma) on the eastern margin of the Sardinia–Corsica block and they get younger towards the east (Sartori 1990).

Meanwhile, in the outer portions of the Calabria–Peloritani Arc (eastern Sila Massif, Serre Massif and Peloritani Mountains), thrusting involved continental units and syn-orogenic sedimentary deposits to form a general East-verging nappe-stack (Bonardi *et al.* 2005; Langone *et al.* 2006; Vignaroli *et al.* 2008*b*). Since 15 Ma (Fig. 7e), as the eastward migration of the Apennine front continued, the Sardinia–Corsica block rotated toward its present-day position and the narrow oceanic part of the Tyrrhenian Sea started to open at very high rates (e.g. Faccenna *et al.* 1997). The velocity of the eastward retreat is not homogeneous all along the Apennine trench. In the southern portions, retreat is at least twice as fast as in the northern part (Fig. 6a), probably due to the drag of the subduction of the Ionian plate. Thrust fronts were still migrating toward the external zones and extension was active in the whole Apennines, as shown by the occurrence of active volcanism in the internal part of the Apennine belt and by the exhumation of HP rocks concomitant with Late Miocene plutonism in the northern Tyrrhenian Sea (e.g. Jolivet *et al.* 1998; Rossetti *et al.* 1999). In Calabria, extensional setting also controlled the evolution of sedimentary basins (e.g. Mattei *et al.* 2002; Cifelli *et al.* 2007). The present-day stage (Fig. 7f) is the result of the continuous eastward migration of the compression–extension system, as oceanic domains of the westernmost part of the Ionian plate are subducting with a westward polarity. Brittle extension propagated all along the Tyrrhenian margin accomplishing for magmatic activity and hydrothermal circulation (Argnani & Savelli 1999; Panza *et al.* 2007) and controlling sedimentation in grabens within the Apennine belt (e.g. Lavecchia *et al.* 1994).

Discussion

Any tectonic reconstruction for the evolution of the Apennine orogenic system has to take into considerations the following major constraints:

- both oceanic- and continent-derived rocks were buried and accreted to form the Apennine orogenic wedge. These rocks reached metamorphic climax at different structural levels, spanning from eclogitic (Schistes Lustrés in Voltri Massif and Alpine Corsica) to LP-greenschist (Coastal Chain and Peloritani Mountains) facies fields, with different P/T ratios. These values, plotted against the major metamorphic facies series in a *P-T* diagram (e.g. Spear 1993), are representative of a progressive transition from subduction- to Barrovian-type metamorphism (Fig. 8) evolving both in space (moving eastward from the internal portions of the orogen) and in time (from the Late Cretaceous in the Alpine Corsica to the Middle Miocene in Tuscany);

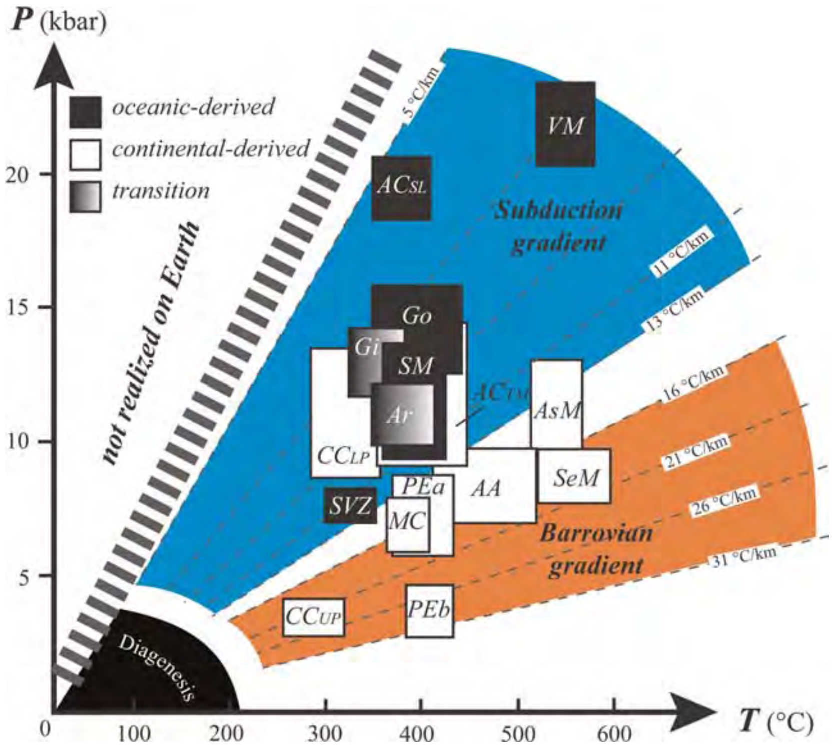

Fig. 8. Metamorphic gradients obtained for the HP-stage of the metamorphic complexes of the Apennine belt. Traces of subduction-type and Barrovian-type gradients are after Spear (1993). AA, Apuane Alps; ACSL, Alpine Corsica (Schistes Lustrés); ACTM, Alpine Corsica (Tenda Massif); Ar, Argentario; AsM, Aspromonte Massif; CCLP, Coastal Chain (lower plate); CCUP, Coastal Chain (upper plate); Gi, Giglio; Go, Gorgona; MC, Monticiano-Roccastrada; PEa, HP, greenschist Peloritani Mountains; LP, greenschist Peloritani Mountains; SM, Sila Massif; SeM, Serre Massif; SVZ, Sestri-Voltaggio Zone; VM, Voltri Massif.

- exhumation occurred during backarc extension and, hence, during the slab rollback; and
- exhumation and backarc extension initiated after the entrance at trench of continental block(s) at Late Eocene–Oligocene times.

Based on the above, we then present a 2D-tectonic scenario (Fig. 9) illustrating the possible paths followed by the HP-rocks (i.e. the subduction-exhumation cycle) exposed in the interior of the Apennine chain during four main steps: (i) oceanic subduction; (ii) syn-orogenic exhumation; (iii) continental collision; and (iv) post-orogenic extension (e.g. Jolivet *et al.* 2003). This reconstruction assumes that: (i) the Apennine belt consists of a bi-vergent (i.e. opposite vergent) orogenic wedge (e.g. Principi & Treves 1984); and (ii) the consumption of the interposed Liguro–Piedmont oceanic domain and the subsequent continental collision were achieved during continuous westward subduction (e.g. Faccenna *et al.* 2001; Rosenbaum & Lister 2004*b*). Discussion of the dynamics of the rollback and the distribution of compression and extension in an orogenic belt is partly based upon published geodynamic models for the Apennines (e.g. Royden *et al.* 1987; Cavinato & De Celles 1999; Pauselli *et al.* 2006).

During oceanic subduction (Fig. 9a), ophiolitic rocks were scrapped off the lower plate and accreted at the bottom of the upper plate. The sinking of highly dense oceanic crust into the mantle during efficient subduction allowed the deep underthrusting of rocks up to final metamorphic equilibration into the eclogitic and/or blueschist facies conditions. A general subduction-type metamorphic gradient is required to obtain such a metamorphism (n°1 and n°2 in Fig. 9a). Considering a near steady-state evolution, the progression of oceanic subduction induced continuous underthrusting of new oceanic material at the bottom of the wedge. Early eclogitized rocks were then forced to move up into the accretionary wedge, re-equilibrating in blueschist facies conditions (n°1 in Fig. 9b). In terms of *P-T* conditions, this early exhumation followed isothermal decompression paths. Jolivet *et al.* (2003) proposed that

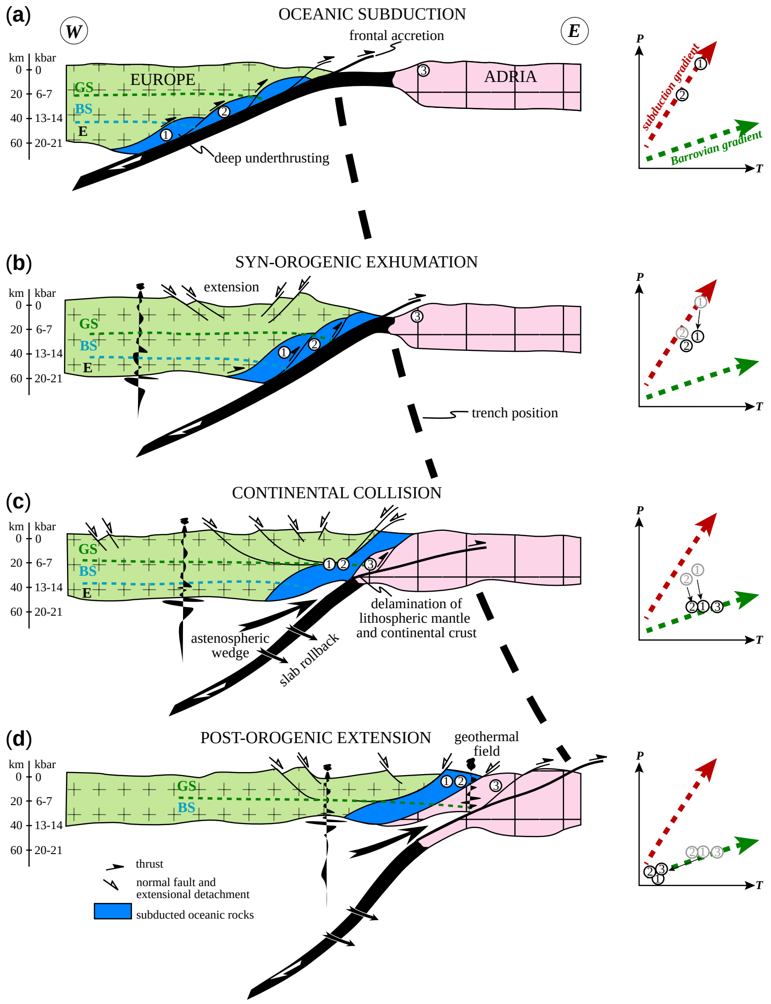

Fig. 9. A 2D-tectonic scenario showing a possible subduction-exhumation dynamic of the Apennine belt as inferred by the *P*-*T* paths experienced by oceanic- and continent-derived metamorphic complexes, see text for details on the a–d stages. Facies fields: GS, greenschist; BS, blueschist; *E*, eclogitic. 1, oceanic eclogitic rocks; 2, oceanic blueschist rocks; 3, continent-derived rocks.

syn-orogenic exhumation occurred within the subduction channel (e.g. Burov *et al.* 2001) at fast rates, depending on the velocity of convergence and slab retreat. Data from the Voltri Massif also suggest that syn-orogenic exhumation of the eclogitic rocks was accomplished by fluid-assisted ductile shearing in conjunction with buoyancy forces (Leech 2001), as documented by the occurrence of exposed eclogite bodies embedded in significantly less dense materials, such as serpentinites and micaschists.

After the consumption of the interposed oceanic domain, continental subduction occurred (n°3 in Fig. 9c). Our dataset reveals that the transition from oceanic to continental subduction at the Apennine trench was characterized by metamorphic gradients progressively moving from subduction- to Barrovian-type (Fig. 8). Different mechanisms can be considered to explain the overprinting of a Barrovian onto early subduction-type metamorphism. One first factor is the heat introduced by magmatism during subduction. As proposed for the Naxos metamorphic core complex in the Aegean Sea (Keay *et al.* 2001), partial melting in the lower crust induced Barrovian metamorphism overprinting HP rocks during extension. Nevertheless, the data presented above show that the Barrovian metamorphism is also recorded as first-phase fabric in subducted rocks. These rocks were thus along a warm gradient when they entered the subduction zone, not during their exhumation path toward the surface. Alternatively, thermomechanical models show that the effect of the lithosphere composition (oceanic and continental) represents a feasible parameter to condition the metamorphic gradient during subduction: less dense continental crust inhibits the deep circulation of the material within the orogenic wedge and, then, the underthrusting of the continental slices works at more superficial levels (e.g. Burov *et al.* 2001; Goffé *et al.* 2003). In our case, the evolution from subduction- to Barrovian-type metamorphism seems to reflect the progressive transition from oceanic to continental subduction at the Apennine trench. The increase of the metamorphic gradient ($<10\ ^{\circ}C\ km^{-1}$ to $21-36\ ^{\circ}C\ km^{-1}$; Fig. 8) may be associated with the difficulty in sinking of less dense continental material (Thompson & England 1984; Goffé *et al.* 2003).

The onset of the continental subduction was synchronous with a dramatic change in dynamics of the Apennine wedge, attested by: (i) eastward retreat of the Apennine front and outward migration of the compressional fronts (n°3 in Fig. 9c); and (ii) pervasive extension in the inner region by means of ductile-to-brittle detachments producing thinning of the previously thickened tectonic edifice and controlling the syn-greenschist exhumation of HP-rocks (n°1 and n°2 in Fig. 9c). The most recurrent models explaining the concomitance of extension in the upper-plate back-arc domains with the burial of significant portions of continental crust at the Apennine trench are: (i) mantle upwelling coming from foundering of thickened lithospheric root without any active subduction (e.g. Decandia *et al.* 1998); (ii) eastward drifting of the compressive thrust system, with subordinate crustal extension (e.g. Finetti *et al.* 2001); (iii) inversion of the subduction polarity (Gueguen *et al.* 1998); and (iv) rollback of the subducting slab (Royden *et al.* 1987; Cavinato & De Celles 1999; Rosenbaum & Lister 2004*b*) accomplished by delamination of the lower crust into the lithospheric mantle (Faccenna *et al.* 2004; Pauselli *et al.* 2006). In agreement with the latter model, we propose that slab rollback and the consequent HP-rock exhumation occurred in response to lithospheric delamination below the accreted orogenic wedge (Bird 1979; Brun & Faccenna 2008) after the entering in subduction of some continental slices (Figs 7c & 9c). In this view, delamination provides an efficient mechanism to decouple the frontal accreting part of the wedge (where thrusting propagates into upper crustal units) and the post-orogenic extensional-hinterland domains (where HP-rocks are progressively exposed at the footwall of ductile-to-brittle detachments) (n°1, n°2 and n°3 in Fig. 9d). Thinning of the previously thickened lithosphere during continuous delamination allows the upward movement of an asthenospheric wedge localized at the base of the crust (see also Pauselli *et al.* 2006). Magmatic underplating induces partial melting in the lower crust generating granitic magmas and hydrothermal circulation inside the stretched upper crust (Rossetti *et al.* 2008). Localization of geothermal fields and volcanism along the Tyrrhenian margin of Italy may reflect the surface manifestation of the edge of the astenospheric wedge under the continental crust (cf. with scenario in Panza *et al.* 2007 for the Central and Southern Apennines).

Conclusions

Geological constraints from the metamorphic complexes outcropping in the Apennines provide insights on the tectono-metamorphic evolution (subduction–exhumation cycle) of the orogenic belt. Metamorphism during oceanic subduction occurred under subduction-type metamorphic gradients and eclogites and blueschists formed. Exhumation of HP-rocks occurred in two main stages: syn-orogenic and post-orogenic. In particular, syn-orogenic exhumation is claimed for explaining the upward movement, under suppressed geothermal conditions, of HP-rocks up to depths corresponding to the greenschist facies field. After the consumption of the interposed oceanic domain, continental subduction occurred and a transition from subduction- to Barrovian-type metamorphic climax was recorded by the metamorphic complexes in the orogenic growth. The entering in subduction of some continental slices was coeval with the onset of post-orogenic extensional setting in the internal domains of the Apennine belt. Delamination of continental crust from the lithospheric mantle accommodates the rollback and contributes to the efficiency of continental subduction and the concomitant extension and magmatism in the hinterland region of the belt. We propose that fast rollback of the subducting plane is partly the consequence of entering of continental crust in the subduction zone.

The authors are grateful to the Editor (R. Govers) and two anonymous reviewers for their comments and suggestions. The manuscript has also benefited from extensive and helpful reviews by R. Vissers.

References

Agard, P., Monié, P., Jolivet, L. & Goffé, B. 2002. Exhumation of the Schistes Lustrés complex: in situ laser probe 40Ar/39Ar constraints and implications for the Western Alps. *Journal of Metamorphic Geology*, **20**, 599–618.

ALVAREZ, W., COCOZZA, T. & WEZEL, F. C. 1974. Fragmentation of the Alpine orogenic belt by microplate dispersal. *Nature*, **248**, 309–314.

AMODIO-MORELLI, L., BONARDI, G., COLONNA, V., DIETRICH, D., GIUNTA, G., IPPOLITO, F. *ET AL*. 1976. L'Arco Calabro-Peloritano nell'orogene Appenninico-Maghrebide. *Memorie della Società Geologica Italiana*, **17**, 1–60.

ARGNANI, A. & SAVELLI, C. 1999. Cenozoic volcanism and tectonics in the southern Tyrrhenian sea: space-time distribution and geodynamic significance. *Journal of Geodynamics*, **27**, 409–432.

ATZORI, P., CIRRINCIONE, R., DEL MORO, A. & PEZZINO, A. 1994. Structural, metamorphic and geochronologic features of the Alpine event in the south-eastern sector of the Peloritani mountains (Sicily). *Periodico di Mineralogia*, **63**, 113–125.

AVIGAD, D., GARFUNKEL, Z., JOLIVET, L. & AZANON, J. M. 1997. Back arc extension and denudation of Mediterranean eclogites. *Tectonics*, **16**, 924–941.

BARCHI, M., MINELLI, G. & PIALLI, G. 1997. The CROP 03 profile: a synthesis of results on deep structures of the Northern Apennines. *Memorie della Società Geologica Italiana*, **52**, 383–400.

BATINI, F., BROGI, A., LAZZARETTO, A., LOTTA, D. & PANDELI, E. 2003. Geological features of the Larderello-Travale and Mt. Amiata geothermal areas (southern Tuscany, Italy). *Episodes*, **26**, 239–244.

BECCALUVA, L., CHIESA, S. & DELALOYE, M. 1981. K/Ar age determinations on some Tethyan ophiolites. *Rendiconti della Società Italiana di Mineralogia e Petrologia*, **37**, 869–880.

BECCALUVA, L., MACCIOTTA, L. & SPADEA, P. 1982. Petrology and geodynamic significance of the Calabria-Lucania ophiolites. *Rendiconti della Società Italiana di Mineralogia e Petrologia*, **38**, 937–982.

BERTINI, G., CASINI, G., GIANELLI, G. & PANDELI, E. 2006. Geological structure of the Larderello geothermal field. *Terra Nova*, **18**, 163–169.

BIGI, G., COSENTINO, D., PAROTTO, M., SARTORI, R. & SCANDONE, P. (eds) 1990. Structural model of Italy and gravity map. Scale 1 : 500,000. Progetto Finalizzato Geodinamica, *Quaderni de 'La Ricerca Scientifica'*, CNR, **114**.

BIRD, P. 1979. Continental delamination of the Colorado Plateau. *Journal of Geophysical Research*, **84**, 7561–7571.

BOCCALETTI, M., COLI, M., DECANDIA, F. A., GIANNINI, E. & LAZZARETTO, A. 1980. Evoluzione dell'Appennino Settentrionale secondo un nuovo modello strutturale. *Memorie della Società Geologica Italiana*, **21**, 359–373.

BONARDI, G., COMPAGNONI, R., MESSINA, A., PERRONE, V., RUSSO, S., DE FRANCESCO, A. M. *ET AL*. 1992. Sovrimpronta metamorfica alpina nell'Unità dell'Aspromonte (settore meridionale dell'Arco Calabro-Peloritano). *Bollettino della Società Geologica Italiana*, **111**, 81–108.

BONARDI, G., CAVAZZA, W., PERRONE, V. & ROSSI, S. 2001. Calabria-Peloritani terrane and northern Ionian Sea. *In*: VAI, G. B. & MARTINI, I. P. (eds) *Anatomy of an Orogen: the Apennines and Adjacent Mediterranean Basins*. Kluwer Academic Publisher, 287–306.

BONARDI, G., DE CAPOA, P., DI STASO, A., PERRONE, V., SONNINO, M. & TRAMONTANA, M. 2005. The age of the Paludi Formation: a major constraint to the beginning of the Apulia-verging orogenic transport in the northern sector of the Calabria–Peloritani Arc. *Terra Nova*, **17**, 331–337.

BORSI, S. & R. DUBOIS, R. 1968. Données géochronologiques sur l'histoire hercynienne et Alpine de la Calabre Centrale. *Comptes Rendus de l'Academie Sciénce, Ser. D*, **266**, 72–75.

BOSSIO, A., COSTANTINI, A., LAZZAROTTO, A., LOTTA, D., MOZZANTI, R., MAZZEI, R., SALVATORINI, G. & SANDRELLI, F. 1993. Rassegna delle conoscenze sulla stratigrafia del neoautoctono toscano. *Memorie della Società Geologica Italiana*, **49**, 17–98.

BOUILLIN, J. P. 1984. Nouvelle interprétation de la liason Apennin-Maghrébides en Calabre: consequences sur la paléogéographie téthysienne entre Gibraltar et les Alpes. *Révue de Géologie Dynamique et de Géographie Physique*, **25**, 321–338.

BROUWER, F. M., VISSERS, R. L. M. & LAMB, W. M. 2002. Metamorphic history of eclogitic metagabbro blocks from a tectonic mélange in the Voltri Massif, Ligurian Alps, Italy. *Ofioliti*, **27**, 1–16.

BRUN, J. P. & FACCENNA, C. 2008. Exhumation of high-pressure rocks driven by slab rollback. *Earth and Planetary Science Letters*, **272**, 1–7.

BRUNET, C., MONIÉ, P., JOLIVET, L. & CADET, J. P. 2000. Migration of compression and extension in the Tyrrhenian Sea, insights from $^{40}Ar/^{39}Ar$ ages on micas along a transect from Corsica to Tuscany. *Tectonophysics*, **321**, 127–155.

BUROV, E., JOLIVET, L., LE LEPOURHIET, L. & POLIAKOV, A. 2001. A thermomechanical model of exhumation of HP and UHP metamorphic rocks in Alpine mountain belt. *Tectonophysics*, **342**, 113–136.

CAPITANIO, F. A. & GOES, S. 2006. Mesozoic spreading kinematics: consequences for Cenozoic Central and Western Mediterranean subduction. *Geophysical Journal International*, **165**, 804–816.

CAPPONI, G. & CRISPINI, L. 2002. Structural and metamorphic signature of alpine tectonics in the Voltri Massif (Ligurian Alps, Noth-Western Italy). *Eclogae Geologicae Helvetiae*, **95**, 31–42.

CAPPONI, G., CRISPINI, L. & FERRARAZZO, I. 1998. New field data on the Case Ferrere area (Voltri Massif, Ligurian Alps). *Bollettino della Società Geologica Italiana*, **117**, 87–92.

CARMIGNANI, L. & KLIGFIELD, R. 1990. Crustal extension in the Northern Apennines: the transition from compression to extension in the Alpi Apuane core complex. *Tectonics*, **9**, 1275–1303.

CARMIGNANI, L., DECANDIA, F. A., FANTOZZI, P. L., LAZZAROTTO, A., LOTTA, D. & MECCHERI, M. 1994. Tertiary extensional tectonics in Tuscany (Northern Apennines, Italy). *Tectonophysics*, **238**, 295–315.

CAVINATO, G. P. & DE CELLES, P. G. 1999. Extensional basins in the tectonically bimodal central Apennines fold-thrust belt, Italy: response to corner flow above a subducting slab in retrograde motion. *Geology*, **27**, 955–958.

CELLO, G., MORTEN, L. & DE FRANCESCO, A. M. 1991. The tectonic significance of the Diamante-Terranova unit (Calabria, southern Italy) in the Alpine evolution of the northern sector of the Calabrian Arc. *Bollettino della Società Geologica Italiana*, **110**, 685–694.

CHIESA, S., CORTESOGNO, L., FORCELLA, F., GALLI, M., MESSIGA, B., PASQUARÉ, G., PEDEMONTE, G. M., PICCARDO, G. B. & ROSSI, P. M. 1975. Assetto strutturale ed interpretazione geodinamica del Gruppo di Voltri. *Bollettino della Società Geologica Italiana*, **94**, 555–581.

CHOUKROUNE, P., BALLÈVRE, M., COBBOLD, P., GUATIER, Y., MERLE, O. & VUICHARD, J. P. 1986. Deformation and motion in the Western Alps. *Tectonics*, **5**, 215–226.

CIFELLI, F., ROSSETI, F. & MATTEI, M. 2007. The architecture of brittle postorogenic extension: results from an integrated structural and palaeomagnetic study in north Calabria (southern Italy). *Geological Society of American Bullettin*, **119**, 221–239.

CIPOLLARI, P. & COSENTINO, D. 1995. Miocene unconformities in the Central Apennines: geodynamic significance and sedimentary basin evolution. *Tectonophysics*, **252**, 375–389.

CIRRINCIONE, R., ORTOLANO, G., PEZZINO, A. & PUNTURO, R. 2008. Poly-orogenic multi-stage metamorphic evolution inferred via P-T pseudosections: an example from Aspromonte Massif basement rocks (Southern Calabria, Italy). *Lithos*, **103**, 466–502.

CORTESOGNO, L. & HACCARD, D. 1984. Note illustrative alla carta geologica della Zona Sestri-Voltaggio. *Memorie della Società Geologica Italiana*, **28**, 115–150.

DANIEL, J. M., JOLIVET, L., GOFFÉ, B. & POINSSOT, C. 1996. Crustal-scale strain partitioning: footwall deformation below the Alpine Oligo-Miocene detachment of Corsica. *Journal of Structural Geology*, **18**, 41–59.

DE GREGORIO, S., ROTOLO, S. G. & VILLA, I. M. 2003. Geochronology of the medium to high grade metamorphic units of the Peloritani Mts, Italy. *International Journal of Earth Sciences*, **92**, 852–872.

DECANDIA, F. A., LAZZAROTTO, A., LIOTTA, D., CERNOBORI, L. & NICOLICH, R. 1998. The CROP03 traverse: insights on post-collision evolution of northern Apennines. *Memorie della Società Geologica Italiana*, **52**, 427–439.

DEINO, A., KELLER, J. V. A., MINELLI, G. & PIALLI, G. 1992. Datazioni ^{40}Ar-^{39}Ar del metamorfismo dell'unità Ortano–RioMarina (Isola d'Elba): Risultati preliminari. *Studi Geologici Camerti, Special Volume*, **2**, 187–192.

DELLA VEDOVA, B., BELLANI, S., PELLIS, G. & SQUARCI, P. 2001. Deep temperatures and surface heat flow distribution. *In*: VAI, G. B. & MARTINI, I. P. (eds) *Anatomy of an Orogen: the Apennines and Adjacent Mediterranean Basins*. Kluwer Academic Publisher, 65–76.

DERCOURT, J., ZONENSHAIN, L. P., RICOU, L. E., KAZMIN, V. G., LE PICHON, X., KNIPPER, A. L. *ET AL*. 1986. Geological evolution of the Tethys belt from the Atlantic to the Pamirs since the Lias. *Tectonophysics*, **123**, 241–315.

DEWEY, J. F. 1988. Extensional collapse of orogens. *Tectonics*, **7**, 1123–1139.

DEWEY, J. F., HELMAN, M. L., TURCO, E., HUTTON, D. H. W. & KNOTT, S. D. 1989. Kinematics of the western Mediterranean. *In*: COWARD, M. P. & DIETRICH, D. (eds) *Alpine Tectonic* Geological Society, London, Special Publication, **45**, 265–283.

DIETRICH, D. 1988. Sense of overthrust shear in the Alpine nappes of Calabria (southern Italy). *Journal of Structural Geology*, **10**, 373–381.

DINI, A., GIANELLI, G., PUXEDDU, M. & RUGGIERI, G. 2005. Origin and evolution of Pliocene–Pleistocene granites from the Larderello geothermal field (Tuscan Magmatic Province, Italy). *Lithos*, **81**, 1–31.

DUBOIS, R. 1970. Phases de serrage, nappes de socle et métamorphisme alpin à la junction Calabre-Apennin: Sur la suture calabro-apenninique. *Révue de Géologie Dynamique et de Géographie Physique*, **12**, 221–254.

DURAND-DELGA, M. 1984. Principaux traits de la Corse Alpine et correlations avec les Alpes Ligures. *Memorie della Società Geologica Italiana*, **28**, 285–329.

EGAL, E. 1992. Structures and tectonic evolution of the external zone of Alpine Corsica. *Journal of Structural Geology*, **14**, 1215–1228.

ELTER, P., GRASSO, M., PAROTTO, M. & MEZZANI, L. 2003. Structural setting of the Apennine-Maghrebian thrust belt. *Episodes*, **26**(3), 205–211.

FACCENNA, C., MATTEI, M., FUNICIELLO, R. & JOLIVET, L. 1997. Styles of back-arc extension in the Central Mediterranean. *Terra Nova*, **9**, 126–130.

FACCENNA, C., BECKER, T. W., LUCENTE, F. P. & ROSSETTI, F. 2001. History of subduction and back-arc extension in the central Mediterranean. *Geophysical Journal International*, **145**, 809–820.

FACCENNA, C., PIROMALLO, C., CRESPO-BLANC, A., JOLIVET, L. & ROSSETTI, F. 2004. Lateral slab deformation and the origin of the western Mediterranean arcs. *Tectonics*, **23**, TC1012, doi:10.1029/2002TC001488.

FEDERICO, L., CAPPONI, G., CRISPINI, L. & SCAMBELLURI, M. 2004. Exhumation of alpine high-pressure rocks: insights from petrology of eclogite clasts in the Tertiary Piedmontese basin (Ligurian Alps, Italy). *Lithos*, **74**, 21–40.

FEDERICO, L., CAPPONI, G., CRISPINI, L., SCAMBELLURI, M. & VILLA, I. M. 2005. ^{39}Ar/^{40}Ar dating of high-pressure rocks from the Ligurian Alps: evidence for a continuous subduction-exhumation cycle. Earth *Planetary Science Letters*, **240**, 668–680.

FEDERICO, L., CRISPINI, L., SCAMBELLURI, M. & CAPPONI, G. 2007*a*. Different PT paths recorded in a tectonic mélange (Voltri Massif, NW Italy): implications for the exhumation of HP rocks. *Geodinamica Acta*, **20**, 3–19.

FEDERICO, L., CRISPINI, L., SCAMBELLURI, M. & CAPPONI, G. 2007*b*. Ophiolite mélange zone records exhumation in a fossil subduction channel. *Geology*, **35**, 499–502.

FINETTI, I. R., BOCCALETTI, M., BOVINI, M., DEL BEN, A., GELETTI, R., PIPAN, M. & SANI, F. 2001. Crustal section based on CROP seismic data across the North Tyrrhenian-Northern Apennines-Adriatic Sea. *Tectonophysics*, **343**, 135–163.

Fournier, M., Jolivet, L., Goffé, B. & Dubois, R. 1991. The Alpine Corsica metamorphic core complex. *Tectonics*, **10**, 1173–1186.

Franceschelli, M., Memmi, I., Carcangiu, G. & Gianelli, G. 1997. Prograde and retrograde chloritoid zoning in low temperature metamorphism, Alpi Apuane, Italy. *Schweizerische Mineralogische und Petrographische Mitteilungen*, **77**, 41–50.

Franceschelli, M., Granelli, G., Pandeli, E. & Puxeddu, M. 2004. Variscan and Alpine metamorphic events in the northern Apennines (Italy): a review. *Periodico di Mineralogia*, **73**, 43–56.

Franceschini, F. 1998. Evidence of an extensive Pliocene–Quaternary contact metamorphism in southern Tuscany. *Memorie della Società Geologica Italiana*, **52**, 479–492.

Gianelli, G. & Ruggieri, G. 2002. Evidence of a contact metamorphic aureole with high-temperature metasomatism in the deepest part of the active geothermal field of Larderello, Italy. *Geothermics*, **4**, 443–474.

Giglia, G. & Radicati di Brozolo, F. 1970. K/Ar age of metamorphism in the Apuane Alps (Northern Tuscany). *Bollettino della Società Geologica Italiana*, **89**, 485–497.

Giorgetti, G., Goffé, B., Memmi, I. & Nieto, F. 1998. Metamorphic evolution of Verrucano metasediments in northern Apennines: new petrological constraints. *European Journal of Mineralogy*, **10**, 1295–1308.

Giunta, G. & Somma, R. 1996. Nuove osservazioni sulla struttura dell'Unità di Alì (M.ti Peloritani, Sicilia). *Bollettino della Società Geologica Italiana*, **115**, 489–500.

Goffé, B., Bousquet, R., Henry, P. & Le Pichon, X., 2003. Effect of the chemical composition of the crust on the metamorphic evolution of orogenic wedges. *Journal of Metamorphic Geology*, **21**, 123–141.

Golonka, J. 2004. Plate tectonic evolution of the southern margin of Eurasia in the Mesozoic and Cenozoic. *Tectonophysics*, **381**, 235–273.

Gueguen, E., Doglioni, C. & Fernandez, M. 1998. On the post-25 Ma geodynamic evolution of the western Mediterranea. *Tectonophysics*, **298**, 259–269.

Haccard, D. C., Lorenz, C. & Grandjacquet, C. 1972. Essai sur l'évolution tectogénétique de la liasion Alpes-Apennines (de la Ligurie a la Calabre). *Memorie della Società Geologica Italiana*, **11**, 309–341.

Heymes, T., Bouillin, J. P., Pêcher, A., Monié, P. & Compagnoni, R. 2008. Middle Oligocene extension in the Mediterranean Calabro-Peloritan belt (southern Italy): Insights from the Aspromonte nappes pile. *Tectonics*, **27**, TC2006, doi: 10.1029/2007TC002157.

Hoogerduijn Strating, E. H. 1994. Extensional faulting in an intraoceanic subduction complex – working hypothesis for the Palaeogene of the Alps-Apennine system. *Tectonophysics*, **238**, 255–273.

Hoogerduijn Strating, E. H., Piccardo, G. B., Rampone, E., Scambelluri, M. & Vissers, R. L. M. 1990. The structure of the Erro–Tobbio peridotite (Voltri Massif, Ligurian Alps); a two day excursion with emphasis on processes in the upper mantle. *Ofioliti*, **15**, 119–184.

Iannace, A., Vitale, S., D'Errico, M., Mazzoli, S., Di Staso, A., Macaione, E. *et al.* 2007. The carbonate tectonic units of northern Calabria (Italy): a record of Apulian palaeomargin evolution and Miocene convergence, continental crust subduction, and exhumation of HP–LT rocks. *Journal of the Geological Society, London*, **164**, 1165–1186.

Jolivet, L., Dubois, R., Fournier, M., Goffé, B., Michard, A. & Jourdan, C. 1990. Ductile extension in Alpine Corsica. *Geology*, **18**, 1007–1010.

Jolivet, L., Faccenna, C., Goffé, B., Mattei, M., Rossetti, F., Brunet, C. *et al.* 1998. Midcrustal shear zones in post-orogenic extension: Example from the northern Tyrrhenian Sea (Italy). *Journal of Geophysical Research*, **103**, 12123–12160.

Jolivet, L., Faccenna, C., Goffé, B., Burov, E. & Agard, P. 2003. Subduction tectonics and exhumation of High-Pressure metamorphic rocks in the Mediterranean orogens. *American Journal of Science*, **303**, 353–409.

Kastens, K., Mascle, J., Auroux, C. A. *et al.* 1988. ODP Leg 107 in the Tyrrhenian sea: insights into passive margin and back-arc basin evolution. *Geological Society America Bulletin*, **100**, 1140–1156.

Keay, S., Lister, G. & Buick, I. 2001. The timing of partial melting, Barrovian metamorphism and granite intrusion in the Naxos metamorphic core complex, Cyclades, Aegean Sea, Greece. *Tectonophysics*, **342**, 275–312.

Keller, J. V. & Pialli, G. 1990. Tectonics of the Island of Elba: a reappraisal. *Bollettino della Società Geologica Italiana*, **109**, 413–425.

Kligfield, R., Hunziker, J., Dallmeyer, R. D. & Schamel, S. 1986. Dating of deformation phases using K–Ar and ^{40}Ar-^{39}Ar techniques: results from the Northern Apennines. *Journal of Structural Geology*, **8**, 781–798.

Knott, S. D. 1987. The Liguride Complex of Southern Italy – a Cretaceous to Paleogene accretionary wedge. *Tectonophysics*, **142**, 217–226.

Knott, S. D. 1994. Structure, kinematics and metamorphism in the Liguride Complex of southern Apennines, Italy. *Journal of Structural Geology*, **16**, 1107–1120.

Lahondère, D. 1996. Les schistes bleus et les éclogites à lawsonite des unités continentales et océaniques de la Corse alpine. *Bur. de Rech. Géol. et Min.*, éans, France.

Lahondère, D. & Guerrot, C. 1997. Datation Sm-Nd du métamorphisme éclogitique en Corse alpine: un argument pour l'existence au Crétacé supérieur d'une zone de subduction active localisée sous le bloc corso-sarde. *Géologie de la France*, **3**, 3–11.

Langone, A., Gueguen, E., Prosser, G., Caggianelli, A. & Rottura, A. 2006. The Curinga-Girifalco fault zone (northern Serre, Calabria) and its significance within the Alpine tectonic evolution of the western Mediterranean. *Journal of Geodynamics*, **42**, 140–158.

Lanzafame, G., Spadea, P. & Tortorici, L. 1979. Mesozoic ophiolites of northern Calabria and Lucanian Apennines (Southern Italy). *Ofioliti*, **4**, 173–82.

Lavecchia, G., Brozzetti, F., Barchi, M., Menichetti, M. & Keller, J. V. A. 1994. Seismotectonic zoning in east-central Italy deduced from an analysis of the Neogene to present deformations and related stress fields. *Geological Society of America Bulletin*, **106**, 1107–1120.

LEECH, M. L. 2001. Arrested orogenic development: eclogitization, delamination, and tectonic collapse. *Earth and Planetary Science Letters*, **185**, 149–159.

LIOU, J. G., ZHANG, R., ERNST, W. G., LIU, J. & MCLIMANS, R. 1998. Mineral parageneses in the Piampaludo eclogitic body, Gruppo di Voltri, western Ligurian Alps. *Schweizerische Mineralogische und Petrographische Mitteilungen*, **78**, 317–355.

LUCENTE, F. P., CHIARABBA, C., CIMINI, G. B. & GIARDINI, D. 1999. Tomographic constraints on the geodynamic evolution of the Italian region. *Journal of Geophysical Research*, **104**, 20307–20328.

MALASOMA, A. & MARRONI, M. 2007. HP/LT metamorphism in the Volparone Breccia (Northern Corsica, France): evidence for involvement of the Europe/Corsica continental margin in the Alpine subduction zone. *Journal of Metamorphic Geology*, **25**, 529–545.

MALINVERNO, A. & RYAN, W. 1986. Extension in the Tyrrhenian sea and shortening in the Apennines as result of arc migration driven by sinking of the lithosphere. *Tectonics*, **5**, 227–245.

MARRONI, M., MONECHI, S., PERILLI, N., PRINCIPI, G. & TREVES, B. 1992. Late Cretaceous flysch deposits of the Northern Apennines Italy: age of inception of orogenesis-controlled sedimentation. *Cretaceous Research*, **13**, 487–504.

MASSOLI, D., KOYI, H. A. & BARCHI, M. R. 2006. Structural evolution of a fold and thrust belt generated by multiple décollements: Analogue models and natural examples from the Northern Apennines (Italy). *Journal of Structural Geology*, **28**, 185–199.

MATTAUER, M., FAURE, M. & MALAVIEILLE, J. 1981. Transverse lineation and large scale structures related to Alpine obduction in Corsica. *Journal of Structural Geology*, **3**, 401–409.

MATTEI, M., CIPOLLARI, P., COSENTINO, D., ARGENTIERI, A., ROSSETTI, F. & SPERANZA, F. 2002. The Miocene tectonic evolution of the southern Tyrrhenian Sea: stratigraphy, structural and palaeomagnetic data from the on-shore Amantea Basin (Calabrian arc, Italy). *Basin Research*, **14**, 147–168, doi: 10.1046/j.1365-2117.2002.00173.x.

MESSIGA, B. & SCAMBELLURI, M. 1991. Retrograde *P-T-t* path for the Voltri Massif eclogites (Ligurian Alps, Italy): some tectonic implications. *Journal of Metamorphic Geology*, **9**, 93–109.

MESSINA, A., COMPAGNONI, R., RUSSO, S., DE FRANCESCO, A. M. & GIACOBBE, A. 1990. Alpine metamorphic overprint in the Aspromonte nappe of the northeastern Peloritani Mts (Calabria-Peloritani Arc, southern Italy). *Bollettino della Società Geologica Italiana*, **109**, 655–673.

MOLLI, G. & TRIBUZIO, R. 2004. Shear zones and metamorphic signature of subducted continental crust as tracers of the evolution of the Corsica/Northern Apennine orogenic system. Alsop. *In*: ALSOP, G. I. (ed.) *Flow processes in faults and shear zones*. Geological Society, London, Special publication, 321–335.

MOLLI, G., GIORGETTI, G. & MECCHERI, M. 2000. Structural and petrological constraints on the tectonometamorphic evolution of the Massa Unit (Alpi Apuane, NW Tuscany, Italy). *Geological Journal*, **35**, 251–264.

MOLLI, G., TRIBUZIO, R. & MARQUER, D. 2006. Deformation and metamorphism at the eastern border of the Tenda massif (NE Corsica) a record of subduction and exhumation of continental crust. *Journal of Structural Geology*, **28**, 1748–1766.

MONACO, C. & TORTORICI, L. 1995. Tectonic role of ophiolite-bearing terranes in the development of the Southern Apennines orogenic belt. *Terra Nova*, **7**, 153–160.

MONIÉ, P., JOLIVET, L., BRUNET, C., TORRES-ROLDAN, R. L., CABY, R., GOFFÉ, B. & DUBOIS, R. 1996. Cooling paths of metamorphic rocks in the western Mediterranean region and tectonic implications. *In*: *The Mediterranean Basins: Tertiary Extension within the Alpine Orogen*. An International Workshop, Abstacts, Université Cergy-Pontoise, Cergy-Pontoise.

MUSUMECI, G., BOCINI, L. & CORSI, R. 2002. Alpine tectonothermal evolution of the Tuscan Metamorphic Complex in the Larderello geothermal field (northern Apennines, Italy). *Journal of the Geological Society, London*, **159**, 443–456.

NICOLICH, R. 1989. Crustal structures from seismic studies in the frame of the European Geotraverse (southern segment) and CROP project. *In*: BORIANI, A., BONAFEDE, M., PICCARDO, G. B. & VAI, G. B. (eds), *The lithosphere in Italy*. Accademia Nazionale dei Lincei, Roma, 41–61.

OGNIBEN, L. 1969. Schema introduttivo alla geologia del confine calabro-lucano. *Memorie della Società Geologica Italiana*, **8**, 453–763.

OGNIBEN, L. 1973. Schema geologico della Calabria in base ai dati odierni. *Geologica Romana*, **12**, 243–585.

PANDELI, E., GIANELLI, G. & MORELLI, M. 2005. The crystalline units of the middle–upper crust of the Larderello geothermal region (southern Tuscany, Italy): new data for their classification and tectonometamorphic evolution. *Bollettino della Società Geologica Italiana, Special Volume*, **3**, 136–159.

PANZA, G. F., PECCERILLO, A., AOUDIA, A. & FARINA, B. 2007. Geophysical and petrological modelling of the structure and composition of the crust and upper mantle in complex geodynamic settings: the Tyrrhenian Sea and surroundings. *Earth-Science Reviews*, **80**, 1–46.

PATACCA, E., SARTORI, R. & SCANDONE, P. 1990. Tyrrhenian basin and Apenninic arcs: kinematic relation since late Tortonian times. *Memorie della Società Geologica Italiana*, **45**, 425–451.

PAUSELLI, C., BARCHI, M. R., FEDERICO, C., MAGNANI, B. & MINELLI, G. 2006. The crustal structure of the Northern Apennines (central Italy): an insight by the CROP03 seismic line. *American Journal of Science*, **306**, 428–450.

PHILIPPOT, P. 1990. Opposite vergence of nappes and crustal extension in the French-Italian western Alps. *Tectonics*, **9**, 1143–1164.

PICCARRETA, G. 1981. Deep-rooted overthrusting and blueschist metamorphism in compressive continental margins: An example from Calabria (southern Italy). *Geological Magazine*, **118**, 539–544.

PIROMALLO, C. & FACCENNA, C. 2004. How deep can we find the traces of Alpine subduction? *Geophysical*

Research Letters, **31**, L06605, doi:10.1029/2003GL019288.

Piromallo, C. & Morelli, A. 2003. P-wave tomography of the mantle under the Alpine-Mediterranean area. *Journal of Geophysical Research*, **108**(B2), 2065, doi:10.1029/2002JB001757.

Platt, J. P., Behrmann, J. H., Cunningham, P. C., Dewey, J. F., Helman, M., Parish, M., Shepley, M. G., Wallis, S. & Weston, P. J. 1989. Kinematics of the Alpine arc and the motion history of the Adria. *Nature*, **337**, 158–161.

Platt, J. P. & Compagnoni, R. 1990. Alpine ductile deformation and metamorphism in a Calabria basement nappe (Aspromonte, South Italy). *Eclogae Geologicae Helvetiae*, **83**, 41–58.

Platt, J. P. & Vissers, R. L. M. 1989. Extensional collapse of thickened continental lithosphere: a working hypothesis for the Alboran Sea and Gibraltar arc. *Geology*, **17**, 540–543.

Platt, J. P., Behrmann, J. H., Cunningham, P. C. et al. 1989. Kinematics of the Alpine arc and the motion history of the Adria. *Nature*, **337**, 158–161.

Principi, G. & Treves, B. 1984. Il sistema corso- appenninico come prisma di accrezione. Riflessi sul problema generale del limite Alpi-Appennini. *Memorie della Società Geologica Italiana*, **28**, 549–576.

Prosser, G., Caggianelli, A., Rottura, A. & Del Moro, A. 2003. Strain localisation driven by marble layers: the Palmi shear zone (Calabria-Peloritani terrane, southern Italy). *GeoActa*, **2**, 155–166.

Reddy, S. M., Wheeler, J., Butler, R. W. H., Cliff, R. A., Freeman, S., Inger, S., Pickles, C. & Kelley, S. P. 2003. Kinematic reworking and exhumation within the convergent Alpine Orogen. *Tectonophysics*, **365**, 77–102.

Renna, M. R., Tribuzio, R. & Tiepolo, M. 2007. Origin and timing of the post-Variscan gabbro–granite complex of Porto (Western Corsica). *Contributions to Mineralogy and Petrology*, **154**, 493–517.

Rosenbaum, G. & Lister, G. S. 2004*a*. Formation of the arcuate orogenic belts in the western Mediterranean region. *Geological Society of America Special Paper*, **383**, 41–56.

Rosenbaum, G. & Lister, G. S. 2004*b*. Neogene and Quaternary rollback evolution of the Tyrrhenian Sea, the Apennines, and the Sicilian Maghrebides. *Tectonics*, **23**, TC1013, doi: 10.1029/2003TC001518.

Rossetti, F., Faccenna, C., Jolivet, L., Funiciello, R., Goffé, B., Tecce, F., Brunet, C., Monié, P. & Vidal, O. 2001*a*. Structural signature and exhumation P-T-t path of the Gorgona blueschist sequence (Tuscan Archipelago, Italy). *Ofioliti*, **26**, 175–186.

Rossetti, F., Faccenna, C., Goffé, B., Monié, P., Argentieri, A., Funiciello, R. & Mattei, M. 2001*b*. Alpine structural and metamorphic signature of the Sila Piccola Massif nappe stack (Calabria, Italy): insights for the tectonic evolution of the Calabrian Arc. *Tectonics*, **20**, 112–133.

Rossetti, F., Faccenna, C., Jolivet, L., Tecce, F., Funiciello, R. & Brunet, C. 1999. Syn- versus post-orogenic extension in the Tyrrhenian Sea, the case study of Giglio Island (Northern Tyrrhenian Sea, Italy). *Tectonophysics*, **304**, 71–93.

Rossetti, F., Goffé, B., Monié, P., Faccenna, C. & Vignaroli, G. 2004. Alpine orogenic P-T-t-deformation history of the Catena Costiera area and surrounding regions (Calabrian Arc, southern Italy): the nappe edifice of north Calabria revised with insights on the Tyrrhenian-Apennine system formation. *Tectonics*, **23**, 1–26.

Royden, L. H. 1993. Evolution of retreating subduction boundaries formed during continental collision. *Tectonics*, **12**, 629–638.

Royden, L., Patacca, E. & Scandone, P. 1987. Segmentation and configuration of subducted lithosphere in Italy: an important control on thrust belt and foredeep-basins evolution. *Geology*, **15**, 714–717.

Rubatto, D. & Scambelluri, M. 2003. U-Pb dating of magmatic zircon and metamorphic baddeleyte in the Ligurian eclogites (Voltri Massif, Western Alps). *Contributions to Mineralogy and Petrology*, **146**, 341–355.

Sartori, R., Carrara, G., Torelli, L. & Zitellini, N. 2001. Neogene evolution of the southwestern Tyrrhenian Sea (Sardinia Basin and western Bathyal plain). *Marine Geology*, **175**, 47–66.

Savelli, C. 2002. Time–space distribution of magmatic activity in the western Mediterranean and peripheral orogens during the past 30 Ma (a stimulus to geodynamic considerations). *Journal of Geodynamics*, **34**, 99–126.

Schenk, V. 1980. U-Pb and Radiometric Dates and their Correlation with Metamorphic Events in the Granulite-Facies Basement of the Serre, southern Calabria (Italy). *Contributions to Mineralogy and Petrology*, **73**, 23–38.

Selverstone, J. 1988. Evidence for east-west crustal extension in the Eastern Alps: implication for the unroofing history of the Tauern Window. *Tectonics*, **7**, 87–105.

Serri, G., Innocenti, F. & Manetti, P. 1993. Geochemical and petrological evidence of the subduction of delaminated Adriatic continental lithosphere in the genesis of the Neogene-Quaternary magmatism of central Italy. *Tectonophysics*, **223**, 117–147.

Somma, R., Messina, A. & Mazzoli, S. 2005. Syn-orogenic extension in the Peloritani Alpine Thrust Belt (NE Sicily, Italy): evidence from the Alì Unit. *Comptes Rendus Geoscience*, **337**, 861–871.

Spadea, P., Tortorici, L. & Lanzafame, G. 1976. Serie ofiolitifere fra Tarsia e Spezzano Albanese (Calabria): Stratigrafia, petrografia, rapporti strutturali. *Memorie della Società Geologica Italiana*, **17**, 135–174.

Spadea, P. 1982. Continental crust rocks associated with ophiolites in Lucanian Apennines (southern Italy). *Ofioliti*, **2**, 501–522.

Spear, F. S. 1993. Metamorphic Phase Equilibria and Pressure-Temperature-Time Paths, 799 p., *Mineralogical Society of America*, Washington, D.C.

Speranza, F., Villa, I. M., Sagnotti, L., Florindo, F., Cosentino, D., Cipollari, P. & Mattei, M. 2002. Age of the Corsica-Sardinia rotation and Liguro-Provençal Basin spreading: new palaeomagnetic and Ar/Ar evidence. *Tectonophysics*, **347**, 231–251.

Stampfli, G. M., Mosar, J., Marquer, D., Marchant, R., Baudin, T. & Borel, G. 1998.

Subduction and obduction processes in the Swiss Alps. *Tectonophysics*, **296**, 159–204.

STORTI, F. 1995. Tectonics of the Punta Bianca promontory: Insights for the evolution of the Northern Apennines-Northern Tyrrhenian Sea basin. *Tectonics*, **14**, 832–847.

THEYE, T., REINHARDT, J., GOFFÉ, B., JOLIVET, L. & BRUNET, C. 1997. Ferro- and magnesiocarpholite from the Monte Argentario (Italy); first evidence for high-pressure metamorphism of the metasedimentary Verrucano sequence, and significance for P-T path reconstruction. *European Journal of Mineralogy*, **9**, 859–873.

THOMPSON, A. B. & ENGLAND, P. C. 1984. Pressure-Temperature-time paths of regional metamorphism II. Their interference and interpretation using mineral assemblages in metamorphic rocks. *Journal of Petrology*, **25**, 929–955.

THOMSON, S. N. 1994. Fission track analysis of the crystalline basement rocks of the Calabrian Arc, southern Italy: evidence of Oligo-Miocene late orogenic extension and erosion. *Tectonophysics*, **238**, 331–352.

VAN DIJK, J. P., BELLO, M., BRANCALEONI, G. P., CANTARELLA, G., COSTA, V. & FRIXA, A. *ET AL.* 2000. A regional structural model for the northern sector of the Calabrian Arc (southern Italy). *Tectonophysics*, **324**, 267–320.

VANOSSI, M., CORTESOGNO, L., GALBIATI, B., MESSIGA, B., PICCARDO, G. & VANNUCCI, R. 1984. Geologia delle Alpi Liguri: dati, problemi, ipotesi. *Memorie della Società Geologica Italiana*, **28**, 5–75.

VIGNAROLI, G. 2006. Structural-metamorphic evolution of the Voltri Massif (Ligurian Alps, Italy). Tectonic Implications for the Alps-Apennines linkage. PhD Thesis Università Roma Tre, 166 pp.

VIGNAROLI, G., ROSSETTI, F., BOUYBAOUENE, M., MASSONNE, H. J., THEYE, T., FACCENNA, C. & FUNICIELLO, R. 2005. A counter-clockwise *P-T* path for the Voltri Massif eclogites (Ligurian Alps, Italy). *Journal of Metamorphic Geology*, **23**, 533–555.

VIGNAROLI, G., ROSSETTI, F. & FACCENNA, C. 2008*a*. Retrogressive fabric development during exhumation of the Voltri Massif (Ligurian Alps, Italy): arguments for an extensional origin and implications for the Alps-Apennine linkage. *International Journal of Earth Sciences*, doi 10.1007/S00531-008-0305-4.

VIGNAROLI, G., ROSSETTI, F., THEYE, T. & FACCENNA, C. 2008*b*. Styles and regimes of orogenic thickening in the Peloritani Mountains (Sicily, Italy): new constraints on the tectono-metamorphic evolution of the Apennine belt. *Geological Magazine*, doi:10.1017/S0016756807004293.

VILLA, I. M., RUGGIERI, G., PUXEDDU, M. & BERTINI, G. 2006. Geochronology and isotope transport systematics in a subsurface granite from the Larderello–Travale geothermal system (Italy). *Journal of Volcanology and Geothermal Research*, **152**, 20–50.

WALLIS, S. R., PLATT, J. P. & KNOTT, S. D. 1993. Recognition of syn-convergence extension in accretionary wedges with examples from the Calabrian Arc and the eastern Alps. *American Journal of Science* **293**, 463–495.

WESTERMAN, D. S., DINI, A., INNOCENTI, F. & ROCCHI, S. 2004. Rise and fall of a nested Christmas-tree laccolith complex, Elba Island, Italy. *In*: BREITKREUZ, C. & PETFORD, N. (eds), *Physical Geology of High Level Magmatic Systems*. Geological Society, London, Special Publications, **234**, 195–213.

WHEELER, J. & BUTLER, R. W. H. 1993. Evidence for extension in the western Alpine orogen: the contact between the oceanic Piemonte and overlying continental Sesia units. *Earth Planetary Science Letters*, **117**, 457–474.

WORTEL, M. J. R. & SPAKMAN, W. 2000. Subduction and slab detachment in the Mediterranean-Carpathian region. *Science*, **290**, 1910–1917.

Sequential development of interfering metamorphic core complexes: numerical experiments and comparison with the Cyclades, Greece

C. TIREL[1,2]*, P. GAUTIER[3], D. J. J. VAN HINSBERGEN[4] & M. J. R. WORTEL[1]

[1]*Department of Earth Sciences, Faculty of Geosciences, Utrecht University, Budapestlaan 4, 3584 CD Utrecht, The Netherlands*

[2]*Current address: Dublin Institute for Advanced Studies, Geophysics Section, 5 Merrion Square, Dublin 2, Ireland*

[3]*Université Rennes 1, Géosciences Rennes UMR 6118 CNRS, Campus de Beaulieu, 35042 Rennes, France*

[4]*Paleomagnetic Laboratory 'Fort Hoofddijk', Faculty of Geosciences, Department of Earth Sciences, Utrecht University, Budapestlaan 17, 3584 CD Utrecht, The Netherlands*

**Corresponding author (e-mail: celine@cp.dias.ie)*

Abstract: The mechanics of metamorphic core complex (MCC) development and the associated process of lower crustal flow have been the topic of several modelling studies. The model setup usually includes a local heterogeneity forcing deformation to localize at a given site, enabling only one MCC to develop. This paper presents numerical lithospheric-scale experiments in which deformation is not *a priori* localized in a specific place, in order to examine whether multiple MCCs could develop during extension, at which conditions, and how. Configurations with either a single MCC or several far-distant MCCs aligned in the section parallel to extension are obtained for a relatively wide range of initial conditions, the only firm requirement being that the lower crust and the sub-Moho mantle both have very low strengths. In contrast, only a narrow range of conditions leads to the development of closely spaced MCCs. In this case, the MCCs interfere with one another (the domes are partly superimposed or/and share a shear zone in common) and develop in sequence. This configuration is compared with the Cyclades archipelago, where closely spaced chains of MCCs have been described in the literature. A review of available data on the islands documents a good agreement with the experiments in terms of final depth of the Moho, geometry and kinematic pattern of the MCCs, and timing of exhumation of the metamorphic rocks. Based on this agreement, we tentatively deduce from the numerical results some of the conditions that prevailed at the initiation of, and during, post-orogenic MCC-type extension in the Cyclades. The most likely initial thickness of the crust is between 40 and 44 km. A thermal lithospheric thickness of only *c*. 60 km is also likely, which might be a condition at the onset of extension or may have been obtained during early stages of extension while the lithosphere was warmed up. Either a backarc subduction setting or a process of mantle delamination may account for this situation. The numerical results also suggest a boundary velocity of 2.0–2.3 cm/a, which should basically reflect the rate at which the South Hellenic subduction zone retreated. Considering *c*. 500 km as an upper bound for the amount of retreat balanced by Aegean extension and assuming that this retreat mostly occurred during MCC-type extension in the Cyclades, we find that the boundary velocity could have been as high as 2.1 cm/a if MCC-type extension lasted 24 Ma, starting at *c*. 30 Ma and finishing at *c*. 6 Ma, as suggested by available geochronological data. A velocity of 2.1 cm/a agrees well with the numerical results.

Metamorphic core complexes (MCCs) are typical structures in regions made up of highly extended continental lithosphere (e.g. Coney 1980; Lister *et al.* 1984; Burg *et al.* 1994; Jolivet *et al.* 1998). They constitute metamorphic domes capped by one or several low-angle normal-sense shear zones (or 'detachment' zones) that separate a highly faulted hanging wall made up of superficial rocks from a footwall made up of rocks exhumed from the middle or lower crust and recording a progressive change from ductile to brittle behaviour (Fig. 1). As such, MCCs reflect highly localized extensional strain on the scale of the crust. As a result, the corresponding region could be expected to show pronounced lateral variations of the Moho depth. Yet, in regions where MCCs are found, the Moho commonly displays a flat geometry, like in the Basin and Range province (Hauser *et al.* 1987;

From: VAN HINSBERGEN, D. J. J., EDWARDS, M. A. & GOVERS, R. (eds) *Collision and Collapse at the Africa–Arabia–Eurasia Subduction Zone*. The Geological Society, London, Special Publications, **311**, 257–292.
DOI: 10.1144/SP311.10 0305-8719/09/$15.00

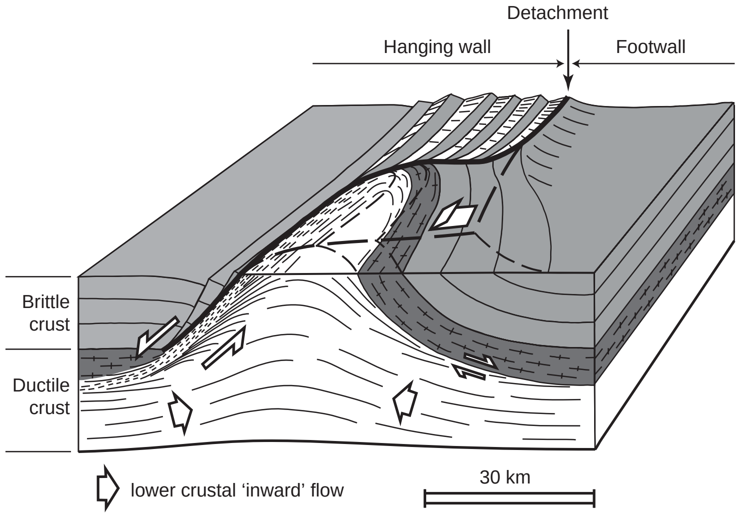

Fig. 1. Simplified sketch showing the main features of a metamorphic core complex, modified after Brun & van den Driessche (1994).

McCarthy & Thompson 1988) and in the Aegean domain (Makris 1978; Sachpazi *et al.* 1997; Tirel *et al.* 2004*b*; Endrun *et al.* 2008). Pervasive flowing of the lower crust, thought to be possible if the rocks are of sufficiently low viscosity, is usually viewed as the most likely mechanism accounting for the flatness of the Moho in such regions (e.g. Block & Royden 1990; Buck 1991; Wernicke 1992; Brun & van den Driessche 1994; McKenzie *et al.* 2000).

The mechanics of MCC development and associated process of lower crustal flow have been addressed in several analytical, numerical and analogue modelling studies so far (Block & Royden 1990; Buck 1991; Wdowinski & Axen 1992; Brun *et al.* 1994; Rosenbaum *et al.* 2005; Wijns *et al.* 2005; Tirel *et al.* 2006; Gessner *et al.* 2007). In these studies, the modelling setup is generally concerned with the crust only; the way extension is accommodated in the underlying mantle is not addressed. More recently, Tirel *et al.* (2004*a*, 2008) have carried out numerical experiments with a setup encompassing the subcrustal mantle. Among these experiments, those involving a very high initial geothermal gradient are characterized by a greater complexity in the development of detachment zones, with commonly several synthetic and antithetic shear zones being formed in sequence during the growth of a single large MCC. In other words, these experiments tend to display strain delocalization during extension. However, for the purpose of a parametric analysis, this study needed to share the same shortcoming as previous studies did: the initial setup included a local heterogeneity forcing deformation to localize at a given site, enabling only one MCC to develop.

In the present study, we have performed new lithospheric-scale experiments in which deformation is not *a priori* localized in a specific place (the initial model is perfectly homogeneous laterally, and the grid is randomly distributed), in order to examine whether multiple MCCs could develop during extension, at which conditions, and how. A relatively wide range of initial conditions produced two-dimensional numerical configurations with either a single MCC or several far-distant MCCs aligned in the section parallel to extension. Extrapolated to a three-dimensional setting, the latter case suggests that distinct subparallel chains of MCCs could be a common situation in nature, provided the appropriate conditions are maintained over a region wide enough. In contrast, only a narrow range of conditions led to the development of closely spaced MCCs. In this case, because of the close spacing, the MCCs interfere with one another (the domes are partly superimposed or/and share a shear zone in common) and develop in sequence. The fact that this configuration is obtained for only a narrow range of conditions suggests that it should be rare in nature. Conversely, if it is observed in a natural setting, some insight may be gained from the experiments about the mechanics of extension and the physical properties of the lithosphere at the onset of the extensional event in the region.

The case of several MCCs aligned in a section parallel to the direction of extension is not uncommon worldwide. Examples may be found in the North American Cordillera (Coney 1980; Wust 1986), especially in the southernmost Basin and Range (Davis 1980) and around the border between USA and Canada (Parrish *et al.* 1988; Vanderhaeghe & Teyssier 2001), also possibly at the latitude of the Snake Range and in the central Basin and Range (Wernicke 1992). The French Massif Central provides another example (Burg *et al.* 1994; Vanderhaeghe & Teyssier 2001). In the Mediterranean area, this situation is encountered in the northern Tyrrhenian domain (Jolivet *et al.* 1998) and, within the Aegean domain, in the Cyclades archipelago (Lister *et al.* 1984; Gautier & Brun 1994*a*, *b*; Jolivet *et al.* 2004) and in the nearby Menderes Massif of western Turkey (Bozkurt 2001; Gessner *et al.* 2001).

The Cyclades archipelago constitutes a particularly interesting example because it has been argued earlier that the islands form closely spaced chains of MCCs that interfere with one another (Gautier & Brun 1994*a*, *b*). In the following, we first describe our numerical experiments, then review the structural and metamorphic evolution of the Cyclades. We subsequently compare the numerical results with the Cyclades. The comparison concerns the final depth of the Moho, the geometry of the MCCs, their kinematic pattern and the timing of exhumation of the metamorphic rocks. Finally, as the natural case and the experiments compare relatively well, we tentatively deduce from the numerical analysis the most likely range of conditions that prevailed in the Cyclades domain at the onset of, and during, Aegean extension.

Numerical modelling

Initial and boundary conditions

Two series of numerical experiments have been carried out to determine the conditions for development of MCCs and particularly sequential development of MCCs, as a function of initial crustal thickness, thermal structure and boundary velocity.

The model geometry consists of a rectangular box (500 × 150 km) composed of a continental crust, a lithospheric mantle and an asthenosphere with brittle–elasto–ductile properties (Fig. 2). The numerical grid consists of 250 × 75 quadrilateral bilinear elements (2 × 2 km). Each element is subdivided into two pairs of triangular sub-elements to avoid meshlocking (Cundall 1989). The mesh is randomly non-regular (random distribution of the nodes) and contains neither an anomaly in structure nor a seed that would force deformation to localize at a given site. The continental crust has an average composition of quartz-diorite with a density of 2800 kg m^{-3} (Table 1). The crust is divided into four colour marker layers to provide for a good visual tracing of the developing structures. The lithospheric mantle and the asthenosphere have an average composition of olivine with a density of 3300 kg m^{-3} (Table 1). Each numerical element is assigned a specific material phase which is defined by density and thermal and rheological parameters.

The initial temperature field is defined by a surface temperature fixed at 0 °C and a temperature of 1330 °C at the base of the lithosphere. The lateral thermal boundary conditions inhibit heat flow across vertical boundaries of the box (no heat exchange with the surrounding region).

Extension of the entire lithosphere is necessarily dependent on displacements applied at plate boundaries. Horizontal displacement with constant velocity is applied to the left boundary of the box (Fig. 2). The opposite boundary is fixed. Other boundary conditions of the numerical box are a free surface at the top of the box and a pliable Winkler basement at the bottom, which supposes free slip along both surfaces. The vertical normal stresses are proportional to the vertical displacement of the bottom boundary (Burov & Cloetingh 1997). Hydrostatic forces ensure local isostatic compensation.

Numerical method

The code PAR(A)OVOZ solves mechanical and thermal equilibrium equations in a large strain mode. This thermo-mechanical code based on

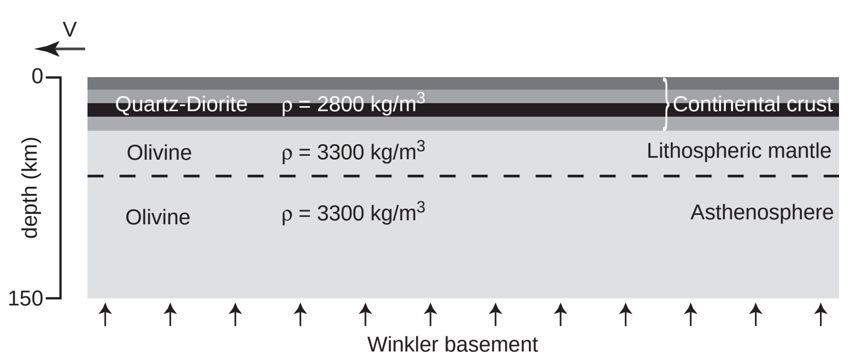

Fig. 2. Model setup used for the numerical experiments.

Table 1. *Variables and parameters used in the experiments*

Variables	Values and Units	Comments
Initial crustal thickness	30, 35, 40, 45, 50, 55, 60 km	Continental crust
Boundary velocity v	1, 1.3, 1.6, 2, 2.3, 2.6, 3 $cm \cdot yr^{-1}$	Applied on left side (see Fig. 2)
Depth of the thermal lithosphere	60, 80, 100, 120 km	Applied geotherms
Parameters	**Values and Units**	**Comments**
Temperature at the base of the lithosphere	1330 °C	
Power law constant A_1	1.26×10^{-3} $MPa^{-n} \cdot s^{-1}$	Quartz-diorite (crust)
Power law constant n_1	2.4	Quartz-diorite (crust)
Creep activation energy E_{a1}	219 $kJ \cdot mol^{-1}$	Quartz-diorite (crust)
Power law constant A_2	7×10^4 $MPa^{-n} \cdot s^{-1}$	Olivine (mantle)
Power law constant n_2	3	Olivine (mantle)
Creep activation energy E_{a2}	520 $kJ \cdot mol^{-1}$	Olivine (mantle)
Density ρ_1	2800 $kg \cdot m^{-3}$	Crust
Density ρ_2	3330 $kg \cdot m^{-3}$	Mantle
Thermal conductivity k_1	2.5 $W \cdot m^{-1} \cdot K^{-1}$	Crust
Thermal conductivity k_2	3.3 $W \cdot m^{-1} \cdot K^{-1}$	Mantle
Coefficient of thermal expansion	3×10^{-5} K^{-1}	
Internal heat production at surface Hs	10^{-9} $W \cdot kg^{-1}$	
Specific Heat Cp	10^3 $J \cdot kg^{-1} \cdot K^{-1}$	

FLAC® and PARAVOZ v3 (Cundall 1989; Poliakov *et al.* 1993) is a mixed finite-difference/finite element, fully explicit, time-marching Lagrangian algorithm, and has been described in several previous publications (Poliakov *et al.* 1993; Burov & Guillou-Frottier 1999, 2005; Burov & Poliakov 2001, 2003; Le Pourhiet *et al.* 2004). The description here will be limited to basic features.

The code solves the conservation equations for energy, mass and momentum:

$$\frac{\partial \rho}{\partial t} + \frac{\partial}{\partial x_i}(\rho v_i) = 0, \tag{1a}$$

where v is velocity and ρ is density, with the Newtonian equation of motion in the continuum mechanics approximation:

$$\frac{\rho \partial v_i}{\partial t} - \frac{\partial \sigma_{ij}}{\partial x_j} - \rho g_i = 0, \tag{1b}$$

$$\frac{D\sigma}{Dt} = F(\sigma, \mathbf{u}, \Delta\dot{\mathbf{u}}, \ldots T \ldots), \tag{1c}$$

where t is time, g is acceleration due to gravity, $\mathbf{u}$ is the displacement vector, T is temperature, F is the functional relationship, D is material derivative and σ is Lagrangian stress. This equation is coupled with constitutive and heat transport equations:

$$k\nabla^2 T - \rho C_p \frac{\rho T}{\partial t} + H_r = \rho C_p \mathbf{v} \cdot \nabla T \tag{2}$$

where $\mathbf{v}$ is the velocity vector, C_p is the specific heat, k is the thermal conductivity and H_r is the internal heat production per unit volume. The Boussinesq approximation is used in the equation of state to account for body forces due to thermal expansion:

$$\rho = \rho_0(1 - \alpha(T - T_0)), \tag{3}$$

where α is the coefficient of thermal expansion (Table 1). Radiogenic heating is taken into account (Table 1). The right-hand side of equation (2) is calculated directly from equation (1), whilst the left-hand side is computed using a separate numerical scheme. A dynamic relaxation technique, based on the introduction of artificial inertial masses in the dynamic system (Cundall 1989), is used to increase the internal time step and accelerate the solution of the governing equations (1).

The Lagrangian method allows the use of a small strain formulation for large strain problems because the mesh is able to move and deform with the material. At each time step, the new positions of the grid nodes are calculated from the current velocity field and updated in large strain mode accounting for the rotation of principal stress axes using Jauman's co-rotational correction:

$$\begin{cases} \omega_{ij} = \frac{1}{2}\left\{\frac{\partial \dot{u}_i}{\partial x_j} - \frac{\partial \dot{u}_j}{\partial x_i}\right\} \\ \sigma_{ij}^{corrected} = \sigma_{ij}^{small\ strain} + (\omega_{ik}\sigma_{kj} - \sigma_{ik}\omega_{kj})\Delta t \end{cases} \tag{4}$$

In quasi-static mode, the algorithm uses artificial inertial masses to suppress inertial effects and accelerate the computations (Cundall 1989). PAR(A)OVOZ also deploys a dynamic remeshing scheme, which makes it possible to model very large displacements.

Each grid element simultaneously handles three rheological terms: brittle, elastic and ductile; thus the local deformation mode may change from dominantly brittle to dominantly ductile or elastic, depending on mechanical and temperature conditions. Material parameters for ductile creep are obtained from Hansen & Carter (1982) for quartz diorite and Goetze (1978) for olivine (Table 1).

The brittle (plastic) behaviour is described by the experimental Byerlee's law (Byerlee 1978) which is reproduced by non-associative Mohr–Coulomb plasticity with a friction angle $\phi = 30^\circ$, cohesion $C_0 = 20$ MPa and dilatation angle $\psi = 0^\circ$ (Gerbault *et al.* 1999):

$$|\tau| = C_0 - \sigma_n \tan\phi, \tag{5}$$

where τ is shear stress and σ_n is normal stress. Plastic failure occurs if the two following conditions are satisfied; shear failure criterion $f = \tau^*_{\mathrm{II}} + \sigma^*_1 \sin\phi - C_0 \cos\phi = 0$ and $\partial f/\partial t = 0$ (Vermeer & de Borst 1984). In 2D formulation, $\tau^*_{\mathrm{II}} = \sqrt{(\tau_{11} - \tau_{22})^2/4 + \tau^2_{12}}$ and $\sigma^*_1 = (\sigma_{11} + \sigma_{22})/2$. In terms of principal stresses, the equivalent of the yield criterion (5) is: $\sigma_1 - \sigma_3 = -\sin\phi\,(\sigma_1 + \sigma_3 - 2C_0/\tan\phi)$.

The elastic behaviour is described by the linear Hooke's law:

$$\varepsilon_{ij} = E^{-1}\sigma_{ij} - \upsilon E^{-1}\sigma_{kk}\delta_{ij}, \tag{6}$$

where repeating indexes mean summation and δ is Kronecker's operator. The values for the elastic moduli are $E = 80$ GPa (Young's modulus) and $\upsilon = 0.25$ (Poisson's ratio) (Turcotte & Schubert 2002).

The viscous (ductile) behaviour is described by an experimental uni-axial power law relationship between strain rate and stress (Kirby & Kronenberg 1987; Ranalli 1987):

$$e^d_{ij} = A(\sigma_1 - \sigma_3)^n \exp(-H/RT), \tag{7}$$

where, $H = E_a + PV$, e^d_{ij} is the shear strain rate tensor, T is the temperature in K, σ_1 and σ_3 are the principal Cauchy stresses (compression is negative), P is the pressure, V is the activation volume. A, H, E_a, and n are the material constants (Table 1) and R is the universal gas constant. The effective viscosity μ_{eff} for this law is:

$$\mu_{eff} = e_{ij}^{d(1-n)/n} A^{-1/n} \exp(H(nRT)^{-1}). \tag{8}$$

For non-uniaxial deformation, the uniaxial relationship (7) is converted to a triaxial form using the invariant of strain rate $e^d_{II} = [Inv_{II}(e_{ij})]^{1/2}$ and geometrical proportionality factors (e.g. Burov *et al.* 2003). This is needed because the rotations due to deformation can be large, and hence the invariant form of strain tensor has to be used:

$$\mu_{eff} = e_{II}^{d(1-n)/n}(A^*)^{-1/n} \exp(H(nRT)^{-1}), \tag{9}$$

where $A^* = \frac{1}{2}A_0 \cdot 3^{(n+1)/2}$.

The general constitutive viscoplastic model of the code is characterized by a visco–elasto–plastic deviatoric behavior and an elasto–plastic volumetric behaviour, with the following strain rate partitioning (M = 'Maxwell', P = 'Plastic'):

$$\dot{\varepsilon}_{ij} = \dot{\varepsilon}^M_{ij} + \dot{\varepsilon}^P_{ij} \tag{10}$$

The visco-elastic and plastic strain-rate components are thus assumed to act in series. The visco-elastic constitutive law corresponds to a Maxwell component, and the plastic constitutive law corresponds to the above-described Mohr–Coulomb model. In this implementation, the new global stress components are calculated, assuming that the principal directions have not been affected by the occurrence of plastic flow.

Numerical experiments

Exploring the conditions for MCC-type extension

To establish the initial and boundary conditions at the onset of extension, a series of experiments has been performed in order to encompass end-member situations of continental extension.

Experiments on the effects of initial crustal thickness and initial geotherms (determining the initial depth of the 1330 °C isotherm) have been carried out. Twenty-eight experiments have been performed with initial crustal thicknesses of 30 to 60 km and initial thermal lithospheric thicknesses of 60 to 120 km (Table 1). A constant horizontal displacement is applied at the left vertical boundary with v = 2.0 cm/a for each of these simulations. Figure 3a shows the initial geotherm and strength profile of the experiments with an initial crustal thickness of 30, 44 and 60 km and an initial depth of the 1330 °C isotherm at 60, 80, 100 and 120 km. The classification of three basic domains (Fig. 3b) has been made on account of the first type of structure observed in the experiments (during the first *c*. 20 Ma of extension). They are characterized by: (i) the formation of ocean floor; or (ii) the development of MCCs (considering that the main features defining a MCC are the exhumation of middle to lower crustal rocks, a detachment zone at the surface, and a flat Moho at depth); or (iii) a combination of these two processes (transitional mode). The experiments identified with

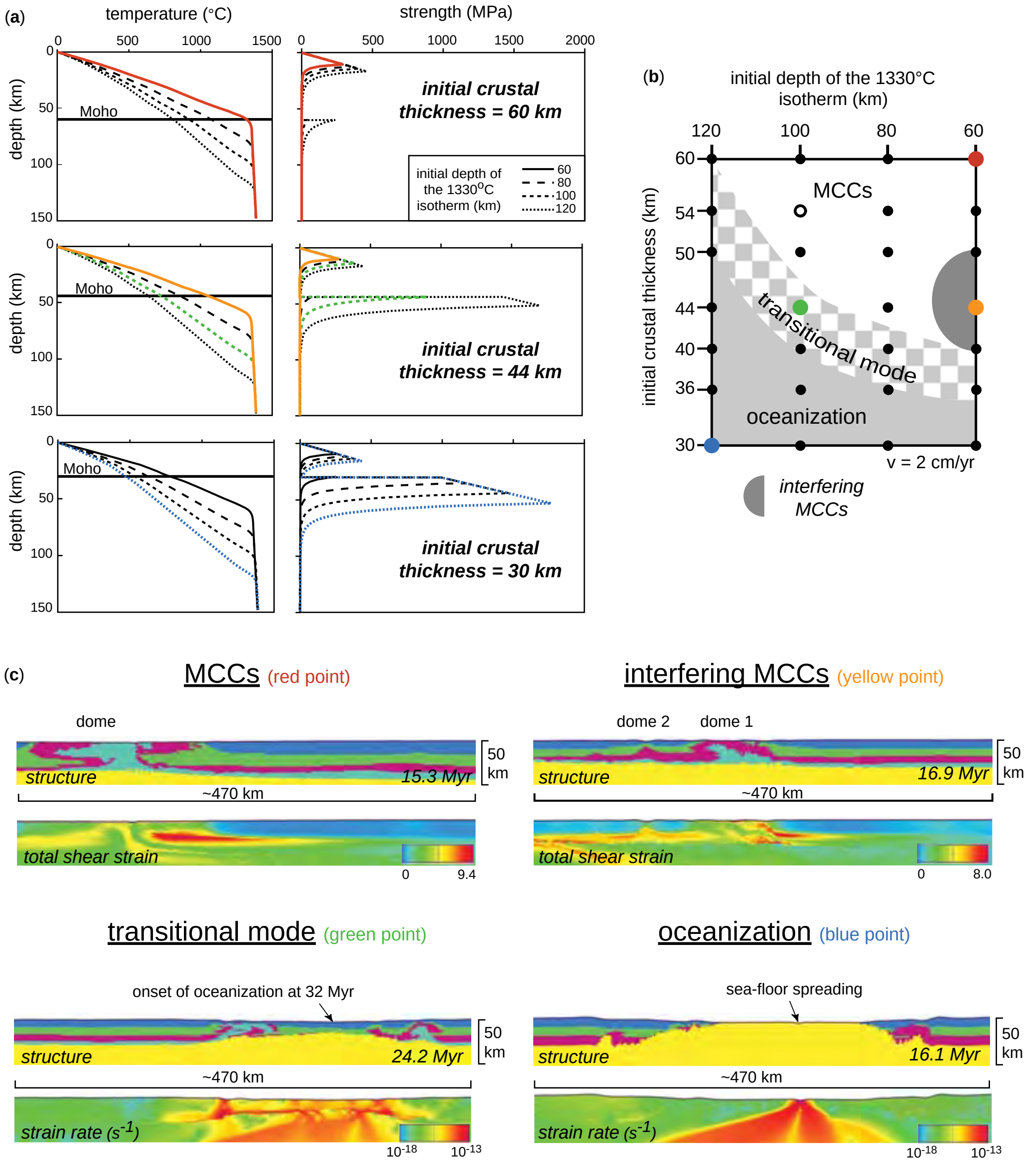

Fig. 3. Main results of the first set of numerical experiments, all performed with a boundary velocity of 2.0 cm/a. (**a**) Initial geotherm and lithosphere strength profile for a selection of experiments with an initial crustal thickness of 30, 44 and 60 km. (**b**) Distribution of the various modes of extension obtained in a series of 28 experiments (large dots) in a graph combining the initial crustal thickness with the initial depth of the thermal lithosphere (depth of the 1330 °C isotherm). (**c**) Snapshots of four experiments illustrating the different modes of extension.

colour dots in Figure 3b are shown with the same colours in Figure 3a. Figure 3c shows snapshots of these specific experiments, illustrating the general MCCs mode, the interfering MCCs mode, the transitional mode and the oceanization mode.

The oceanization mode (blue marker) is characterized by a strong necking of the entire continental crust, which results in sea-floor spreading when break-up occurs (Fig. 3c). This mode implies a high strength of the lithospheric mantle (Fig. 3a).

The MCCs domain identified in Figure 3b displays variable characteristics. Most experiments show the development of several MCCs during extension. Depending on the initial and boundary conditions, the MCCs display a large range in size and amounts of exhumation. This domain can be subdivided into two subdomains, corresponding to two modes of extension, with either independent or interfering domes. The interfering MCCs mode (yellow marker) is obtained for a restricted set of conditions, with an initial thickness of the thermal lithosphere of *c*. 60 km and an initial crustal thickness between 40 and 50 km. A detailed description of this mode is given in the next section.

The non interfering MCCs mode is more common (Fig. 3b). An example is given in Figure 3c (red marker), which shows the development of a single huge dome. Other experiments show the development of several far-distant domes that do not interfere with one another. Such an experiment is illustrated in Figure 4 (identified with an open dot in Fig. 3b). The first timeslice (10.1 Ma) shows the exhumation of a first MCC (dome 1) and the incipient development of a graben (graben 2) which later evolves into a new MCC (dome 2 in timeslices 15.2 and 20.1 Ma). The graben is located away from the first dome (*c*. 165 km) and related shear zones (SZ1 and SZ2). While the second dome develops, new shear zones form (SZ3 and SZ4). The tips of SZ2 and SZ3 are in mutual contact but the two shear zones do not overlap, therefore SZ3 does not reactivate SZ2. Similar features are obtained for the relations between dome 2 and dome 3 and between SZ4 and SZ5 (Fig. 4). We refer to this situation as a case where the MCCs remain independent, in the sense that there is no kinematic interference between them. Nevertheless, a dynamic interference is likely, because the development of a first dome reduces the potential of lower crustal flow, thereby limiting the development of subsequent domes.

The general MCCs mode is obtained for conditions favouring the existence of a weak lower crust, with either a thick crust or a thin lithosphere (both conditions leading to high temperature conditions at the Moho) or both (Fig. 3b). In the extreme case (red marker), a huge MCC is obtained (Fig. 3c). As seen in Figure 3a, a low-strength sub-Moho mantle appears to be another necessary condition for obtaining a MCCs mode of extension with a flat Moho, as already suggested by Buck (1991). This agrees with the results obtained in a different parametric study (with a boundary velocity of 0.66 cm/a) by Tirel *et al.* (2008), who found that the development of MCCs requires an initial Moho temperature of 800 °C or higher. At these temperatures, both the sub-Moho mantle and the lower crust have low strengths and viscosities of the order of 10^{19}–10^{21} Pa.s. Figures 3a and 3b suggest that a sub-Moho mantle with a strength of only *c*. 250 MPa is enough to prevent the formation of MCCs. In addition, to obtain a MCCs mode of extension, an initial crustal thickness of at least 40 km seems required (Fig. 3b). In a thinner crust, lower crustal flow is probably hampered by the limited amount of material able to flow.

Finally, the transitional mode (green marker) is characterized by the development of MCCs of moderate size closely followed by the formation of an ocean floor (Fig. 3c), or by the formation of pseudo-MCCs showing a substantial rise of the Moho, eventually followed by the formation of an ocean.

Experiments with interfering MCCs

The conditions leading to interfering MCCs have been further investigated through a second series of experiments, in order to determine the effects of the initial crustal thickness and the boundary velocity (Table 1) on the three main properties directly comparable with geological and geophysical data;

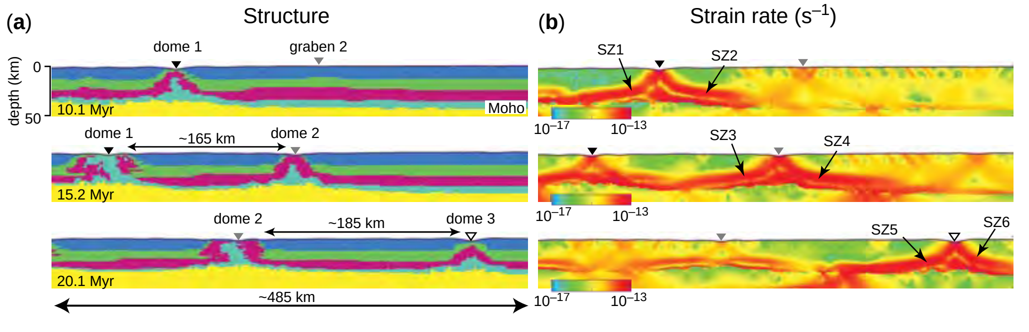

Fig. 4. Results obtained for an experiment with an initial crustal thickness of 54 km, an initial depth of the 1330 °C isotherm at 100 km, and a boundary velocity of 2.0 cm/a (cf. the open dot in Fig. 3b). This experiment illustrates the general MCCs mode of extension, in which several MCCs form but remain far-distant, so that they do not interfere. The successive timeslices are dated with respect to the onset of extension. The triangles above the surface are markers helping to locate structures from one panel to the other.

the width of the dome, the duration of dome development and the final Moho depth. The three first experiments leading to interfering MCCs have been performed with initial crustal thicknesses of 40, 44 and 50 km, an initial thermal lithospheric thickness of 60 km and a boundary velocity of 2.0 cm/a (Table 1) (Fig. 3b). In addition, six experiments have been carried out with an initial crustal thickness of 44 km, an initial thermal lithospheric thickness of 60 km and boundary velocities of 1.0, 1.33, 1.66, 2.33, 2.66 and 3.0 cm/a (Table 1). Three of these experiments show interfering MCCs. In all the experiments displaying interfering MCCs, the domes develop in sequence (one after the other). The results of the two series of experiments are shown and discussed below.

Description of two experiments. The sequential development of interfering MCCs is illustrated in Figure 5 with two experiments having an initial crustal thickness of 44 km, an initial depth of the 1330 °C isotherm of 60 km and a boundary velocity of 2.0 cm/a (Type 1 experiment, corresponding to the yellow marker in Fig. 3) or 2.33 cm/a (Type 2

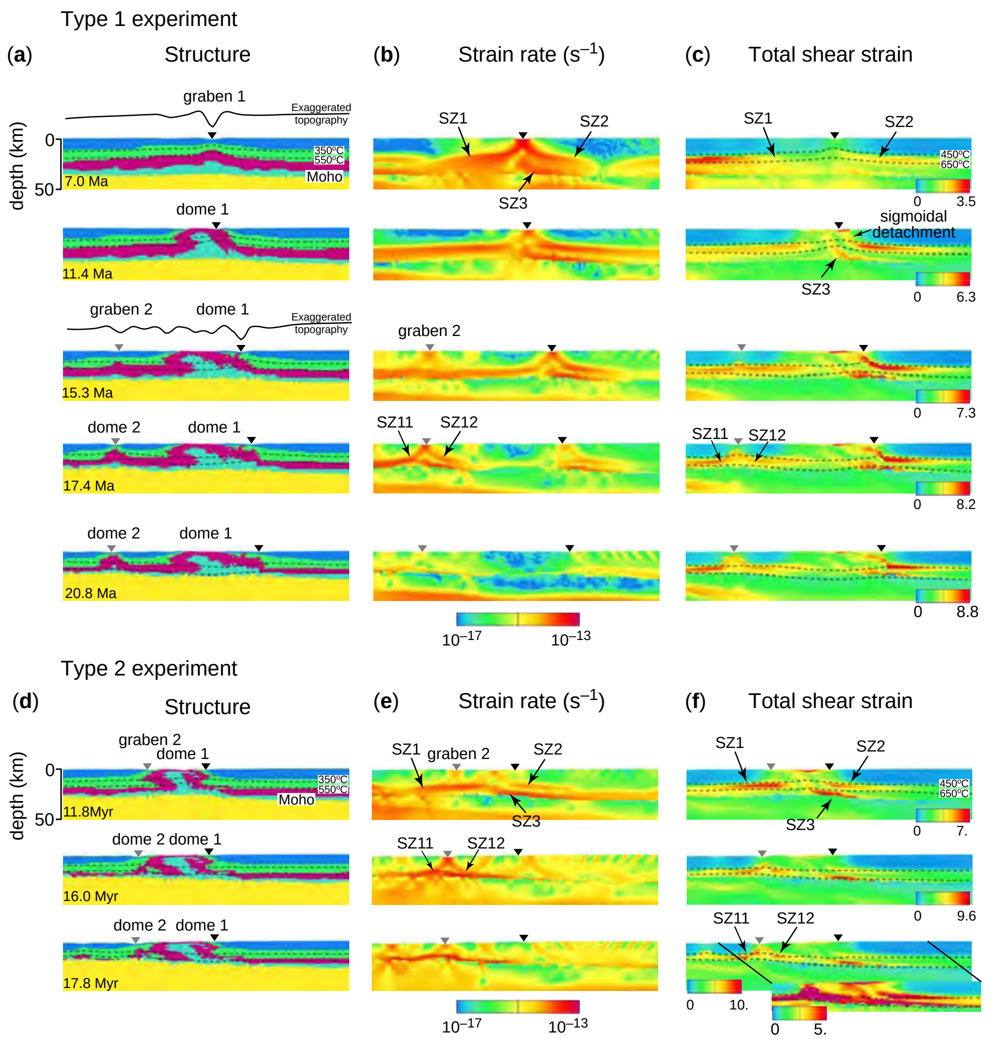

Fig. 5. Results obtained for two experiments with an initial crustal thickness of 44 km, an initial depth of the 1330 °C isotherm at 60 km, and a boundary velocity of 2.0 cm/a (Type 1, cf. the yellow dot in Fig. 3b) or 2.3 cm/a (Type 2). These experiments illustrate the interfering MCCs mode of extension. The successive timeslices are dated with respect to the onset of extension. The triangles above the surface are markers helping to locate structures from one panel to the other. A topographic profile with a vertical exaggeration of 10 is represented in (a) above the timeslices 7.0 and 15.3 Ma.

experiment). These two experiments document a similar process, differing only in terms of distance between adjacent MCCs. The model setup is shown in Figure 2. At the onset of extension, the effective viscosity of the sub-Moho mantle and the lower crust is very low ($10^{19}-10^{20}$ Pa.s) and the two layers are coupled. The experiment of type 1 has been chosen to illustrate the entire process of exhumation. Since the process is the same, only the last stages of the second experiment are shown. The images have been truncated in order to focus on the most important crustal structures. Only a window of 280×50 km is shown. In addition to those visible in Figure 5, other domes are exhumed during each experiment, but do not interfere with one another. These independent MCCs are not shown here, nevertheless, they bear similar characteristics as those seen in Figure 4. The ages are relative to the onset of extension.

The first timeslice of Type 1 experiment, at 7.0 Ma (Fig. 5a, b, c), shows a simultaneous localization of strain in the upper and lower crust. The structure defines a symmetrical graben in the brittle crust (graben 1) and two major conjugate shear zones (SZ1 and SZ2) in the ductile middle crust (Fig. 5b, c). The two shear zones are flat-lying, located at depths around 22–25 km. A third shear zone (SZ3) develops below SZ2 at the Moho interface (Fig. 5b, c). At this stage, the ductile middle-lower crust already rises toward the surface (Fig. 5a).

The second timeslice, at 11.4 Ma, shows the development of an asymmetric dome (dome 1) following the extreme thinning of the upper crust (Fig. 5a). Middle and lower crustal levels have reached the surface and active deformation is localized mainly on the right side of the dome (Fig. 5b, c). SZ2 displays a sigmoidal shape of three parts: flat on the dome top, steeply dipping on the right dome limb and flat again in the lower crust (Fig. 5c). This forms the detachment shear zone observed at the roof of the metamorphic dome. The isotherms rise asymmetrically with respect to the dome apex (Fig. 5a), which confirms the localization of deformation along SZ2. The right side of the dome now forms the zone of lowest topography, and is a likely locus for a supra-detachment basin superimposed on initial graben formation. SZ3 shows a shape similar to SZ2 but does not reach the surface. SZ3 is near-horizontal at the Moho and steeply inclined inside the dome. While still active, SZ1 has not significantly changed in shape or depth since the beginning of deformation.

At 15.3 Ma, dome 1 continues to develop with a recumbent-like fold shape (Fig. 5a). Flattening of this structure is also observed in the shape of SZ2 and SZ3 (Fig. 5c). Nevertheless, the strain rate pattern remains stable (Fig. 5b). Further left, a slight rise of the lower crust is observed (Fig. 5a), accompanied by a slight rise of SZ1 (Fig. 5c). It is related to localization of deformation in the brittle crust leading to formation of a second graben (graben 2, Fig. 5a, b). It is noteworthy that, in this experiment, graben 2 is located right above one of the previously formed shear zones (SZ1), at variance with the situation in those experiments that generated independent MCCs (Fig. 4b). In all the experiments showing a sequential development of domes, the smaller secondary dome originates from necking of the upper crust in a stage where the crustal thickness stands between 28 and 32 km and the Moho temperature is between 750 and 810 °C.

At 17.4 Ma, the shape of dome 1 has not significantly changed and the strain rate pattern indicates that active deformation has strongly decreased there, especially along SZ1 (Fig. 5a, b). A second dome (dome 2) begins to develop symmetrically, dragging SZ1 toward the surface (Fig. 5c). SZ1 is splited into two branches located on both limbs of dome 2 (SZ11 and SZ12, Fig. 5b, c). SZ12 reactivates SZ1 with an opposite, top-to-the-right sense of shear.

At 20.8 Ma, the isotherms have deepened and flattened, documenting advanced cooling of both domes (Fig. 5a). The strain rate pattern indicates an overall strong decrease in active deformation (Fig. 5b).

The initial conditions in Type 2 experiment are the same as before except for the boundary velocity, which is slightly higher. Only the three last stages are shown here (Fig. 5d, e, f). The second dome is smaller and develops closer to the first dome than in the previous experiment. As a result, there is no lid of upper crust left between the two domes. Otherwise the two experiments show similar characteristics. In both cases, the Moho remains sub-horizontal throughout the extensional process and reaches the depth of *c*. 25 km when the exhumation of MCCs has ended.

Analysis of the two experiments. Figure 6 depicts schematically the sequential development of interfering MCCs, based on the results shown in Figure 5. As previously discussed by, for example Tirel *et al.* (2004*a*, 2008), the development of MCCs may be characterized by two main stages: (1) upper crustal necking (graben formation) accompanied by the formation of flat-lying conjugate shear zones in the lower crust (Fig. 6a); followed by (2) exhumation of the dome (amplification and widening) owing to the connection, at mid-crustal depths, of the faulted graben with one of the lower crustal shear zones, forming the main detachment zone (Fig. 6b).

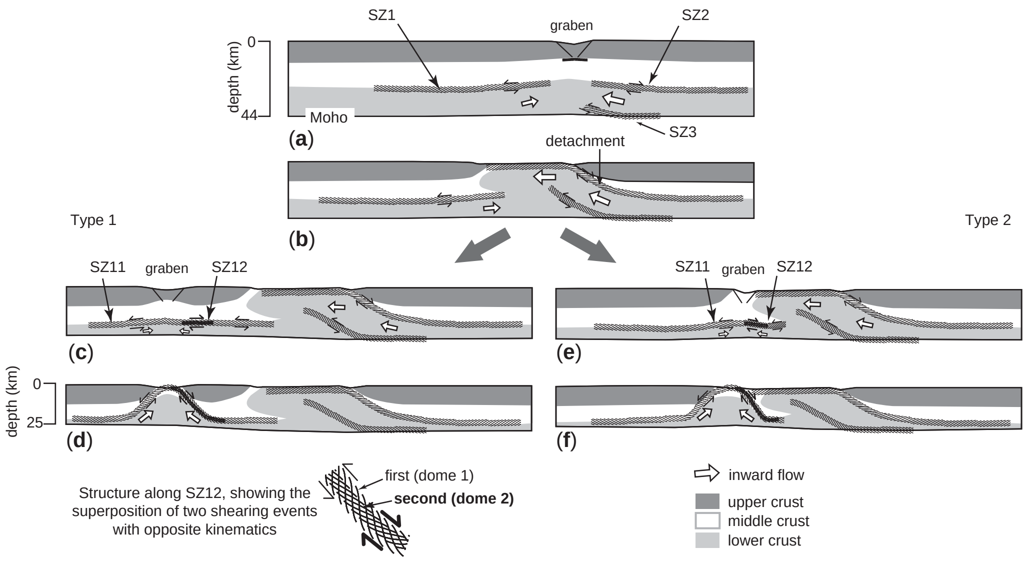

Fig. 6. Sketch based on the results shown in Figure 5, depicting the process of sequential development of interfering MCCs.

Upper crustal necking results in a reduction of the vertical lithostatic load, which induces a horizontal pressure gradient. Due to this gradient, the most ductile material at depth flows horizontally toward the area of necking. We use the term inward flow to describe this feature (cf. Brun & van den Driessche 1994). Inward flow is commonly described in MCC models as a process responsible for a flat Moho geometry (Block & Royden 1990; Wdowinski & Axen 1992; Wernicke 1992; Brun & van den Driessche 1994; Tirel *et al.* 2004*a*, 2008; Gessner *et al.* 2007). In our experiments, horizontal flow of the lower crust occurs over distances several times larger than the width of the dome and is responsible for the development of horizontal shear zones. Two convergent channel flows are systematically obtained, resulting in two conjugate flat-lying shear zones (SZ1 and SZ2; Figs 5 & 6). High strain intensities are also found within SZ3, which follows the Moho but bends upward beneath the dome apex. This particular shape is associated with fast and relatively focused rise of lower crustal material during dome amplification.

Still in the experiments, shearing due to inward flow occurs at the interface between a lower part of the crust where rocks are weak enough to flow pervasively, and an upper part where rocks are too strong to undergo significant deformation (while SZ3, at greater depth, is a mirror effect along the Moho boundary). This interface has a certain thickness, corresponding to the domain where rocks can undergo ductile shearing, in between the isotherms 450 and *c*. 650 °C (Fig. 5c). This thickness depends also partly on the resolution of the experiments. As seen in Figure 3a, we obtain a temperature of the transition between ductile and brittle behaviours of *c*. 300 °C for quartz diorite, which is the rock type we have chosen to represent the crust as a whole (note that, in our experiments, this temperature is not imposed but arises from the combination of the brittle and ductile rheological laws). Thus, in the simulations, shearing due to inward flow occurs at significantly greater depths than the ductile-brittle transition (that is, at temperatures at least *c*. 150 °C higher, corresponding to a difference in depth of about 6 km in the case of Type 1 experiment, cf. the yellow marker of Fig. 3). On the one hand, this difference is consistent with the shape of the strength profiles shown in Figure 3a, in which the brittle–ductile transition coincides with a peak in strength. In this case, shearing along the roof of a lower crustal channel may be expected to occur more readily significantly below the brittle–ductile transition. This agrees with the observation that, in Figure 3a, the temperature of 450 °C coincides with the point of inflexion along the ductile segment of the strength profile, hence marking a relatively abrupt transition between the strong ductile crust, above, and the weak one, below. On the other hand, several authors have argued that rocks immediately beneath the ductile–brittle transition may represent a low in the strength profile of the crust after a certain amount of strain is accumulated, so that this level could be used as a décollement (e.g. Handy

1989; Gueydan *et al.* 2004). If so, then it is conceivable that the roof of the shear zone overlying the lower crustal channel may coincide with the ductile–brittle transition, a situation that our experiments cannot feature. It is also worth stating that our model setup considers the crust as homogeneous; a compositionally layered crust may result in a distinct picture, with a different depth distribution of the shear zones.

In all experiments with interfering MCCs, the second MCC follows the same two-stage development as described above. Figures 6c and 6d and Figures 6e and 6f depict the results obtained in the Type 1 and Type 2 experiments, respectively, the main difference being the distance between the two domes. In both cases, localization of the second graben occurs right above SZ1 which formed during the development of the first dome. This preexisting structure is dragged toward the surface during the amplification stage of the second dome. In addition, renewed inward flow leads SZ1 to be reactivated with a similar sense of shear on the left dome limb (SZ11) but with an opposite sense of shear on the right dome limb (SZ12). This, in turn, hampers inward flow and temperature advection toward dome 1, favouring its cooling and increase in strength (cf. Fig. 5a, b). Widening of the second dome is limited because of the strong crustal thinning already achieved. Since the second dome remains small, shearing along SZ12 probably involves less strain than earlier, kinematically opposite shearing along SZ1 involves (see also Fig. 5b). Hence, relics of the first event should be found along the shear zone. In the end, the strength of the crust is too high to enable lower crustal flow any longer. If extension is to continue due to unchanged boundary conditions, it must proceed without MCCs being further developed. Until that stage, the Moho remains almost flat throughout the exhumation process. This is due to coherent ductile deformation between the lower crust and the sub-Moho mantle (see also Tirel *et al.* 2008).

Role of the initial crustal thickness and the boundary velocity. Figure 7 synthesizes the effects of modifying the initial crustal thickness or the boundary velocity on three measurable aspects of each experiment. The results shown are only for the experiments that yield interfering MCCs. The output parameters are the width of the domes (measured at the surface), the time needed to exhume the first dome (and, combining the domes, the duration of MCC-type extension), and the final depth of the Moho.

The width of the first dome (between 24 and 110 km) and the duration of its exhumation (between 11 and 24 Ma) increase with increasing initial crustal thickness and decreasing boundary velocity (Fig. 7a, b, c, d). Note that the huge dome obtained for an experiment with a 60 km-thick crust (Fig. 3b, c) is consistent with this trend.

The width of the second dome (between 15 and 30 km) and the duration of its exhumation (between 5 and 8 Ma) are much less variable than they are for the first dome. As quoted in the 'Description of two experiments' section, in all experiments, the second dome originates from necking of the upper crust in a stage where the crustal thickness lies in a narrow range, between 28 and 32 km. Hence, the width and timing of exhumation of the second dome are not directly related to the initial conditions of the experiment but to those once the first dome has essentially formed. This is consistent with the view that widening of the second dome, which depends on the possibility of renewed inward flow, is limited by the amount of crustal thinning already achieved during the development of the first dome, which itself is a function of the initial crustal thickness. In other words, the ability of the first dome to absorb a large volume of weak lower crust is proportional to the volume initially available, so that the amount of weak material left for the second dome is always nearly the same.

Combining the timing of exhumation of both domes, a duration of MCC-type extension is obtained, ranging between 16 and 32 Ma (Fig. 7c, d). The width of the whole complex made up of two adjacent domes is not plotted here. This width is related to the width of the domes but also to the distance between them. This distance is variable (cf. the difference between Type 1 and Type 2 experiments) but does not show a clear correlation with the initial crustal thickness or the boundary velocity.

After exhumation of the two domes, the Moho interface is always nearly flat. The final Moho depth (between 22.5 and 29 km) increases with increasing initial crustal thickness and with decreasing boundary velocity (Fig. 7e, f).

Geology of the Cyclades

The above two-dimensional numerical experiments suggest that, for certain conditions, MCCs may develop in sequence during continental lithospheric extension. Extrapolated to a three-dimensional setting, the corresponding region could be characterized by the development of several chains of MCC, each chain trending orthogonal or at a high angle to the direction of extension. Although such a situation may be encountered in several regions worldwide (see Introduction), we will here focus on the Cyclades archipelago because, in our view, this is the area where the existence of subparallel chains of MCC has been best documented so far. In this section, we review the structural and

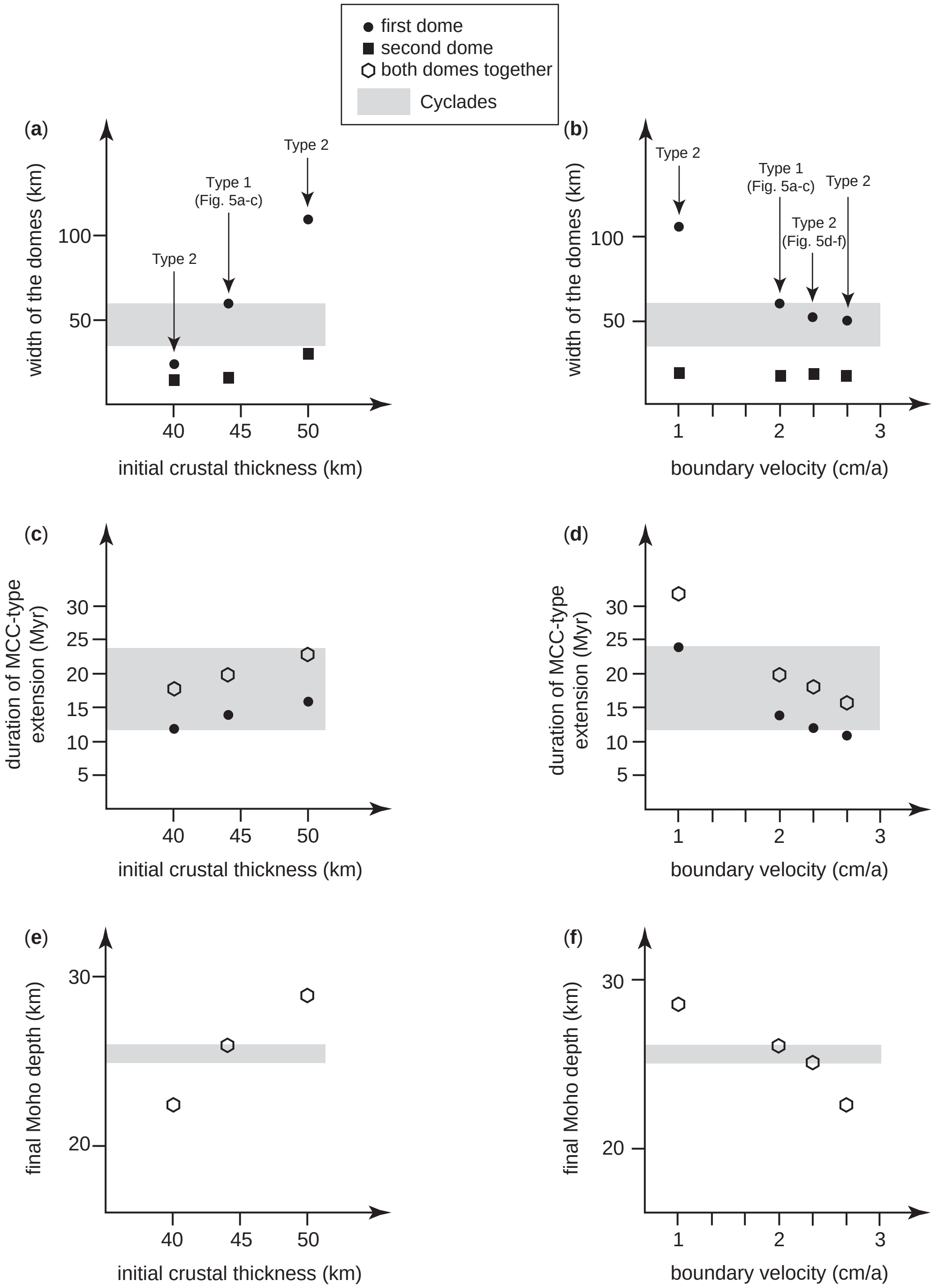

Fig. 7. Series of graphs summarizing the effects of modifying the initial crustal thickness (left) or the boundary velocity (right) on the width of the domes (top graphs), the time needed to exhume the first dome (black dot) and, combining the domes, the duration of MCC-type extension (open symbol) (middle graphs), and the final depth of the Moho (bottom graphs). Grey bands represent the range of values in the Cyclades, as deduced from available geological and geophysical data (see the text). More precisely, the grey band in (**a**) and (**b**) represents the width range for Naxos and Paros first-generation MCCs, to be compared with the numerical results obtained for the first dome only; the grey band in

metamorphic evolution of the Cyclades (see also Fig. 8), focusing on features that allow comparison with our numerical results.

Since the seminal paper of Lister *et al.* (1984), many studies have focused on the identification of extensional detachments and metamorphic core complexes in the Cyclades (e.g. Urai *et al.* 1990; Buick 1991; Gautier *et al.* 1993; Gautier & Brun 1994*a*; Vandenberg & Lister 1996; Forster & Lister 1999; Jolivet & Patriat 1999; Kumerics *et al.* 2005; Iglseder *et al.* 2006; Müller *et al.* 2006). During extension, rocks that previously recrystallized in high-pressure/low-temperature conditions were exhumed from the conditions of a greenschist facies or higher grade overprint to the conditions of brittle deformation. Granitoid intrusions were also emplaced during extension (e.g. Altherr *et al.* 1982). Time constraints indicate that these structures are broadly Miocene in age, most authors agreeing on the view that they formed during Aegean 'backarc' (or post-orogenic/post-thickening) extension. Lister *et al.* (1984) initially proposed that extension was controlled by a single south-dipping detachment zone on the scale of the Cyclades archipelago, however subsequent studies have documented a more complex structural pattern.

The Cyclades as a coherent domain during Miocene extension

Because the orientation of extension-related stretching lineations and subsequent normal faults shows a fairly abrupt change across the archipelago, it is tempting to subdivide the Cyclades into two domains. The direction of maximum stretching is NE–SW to ENE–WSW in the northwestern islands, and north–south in the southeastern islands (Gautier & Brun 1994*a*) as well as on Ikaria (Kumerics *et al.* 2005). The boundary between these two domains coincides with a NE–SW-trending fault zone extending from west of Ikaria to east of Sifnos, with probably a significant wrench (dextral) component of movement along it (Gautier & Brun 1994*a*; Gautier 1995). This fault zone has been named the Mid-Cycladic Lineament (MCL) by Walcott & White (1998). Opposite rotations across the fault zone, as documented by palaeomagnetic data on middle Miocene intrusions on Naxos, Mykonos and Tinos (Morris & Anderson 1996; Avigad *et al.* 1998), confirm the importance of the MCL and are consistent with the view that the divergent pattern of lineations seen on the scale of the Cyclades relates originally to a uniform NNE–SSW direction of stretching (Gautier & Brun 1994*b*; Walcott & White 1998; Gautier *et al.* 1999; Jolivet *et al.* 2004). This view is also consistent with the pattern of rotations on the scale of the whole Aegean region (van Hinsbergen *et al.* 2005*b*). Gautier & Brun (1994*b*) suggested that a rectilinear horst-and-graben system initially occupied the Central Aegean region and underwent progressive bending due to radial spreading of the Aegean lithosphere. Analogue experiments further showed that the presence of a thin layer of sand (simulating the brittle behaviour of the upper crust) at the top of a spreading sheet is a condition sufficient to produce a pattern of oppositely rotated blocks separated by a sharp boundary equivalent to the MCL (Gautier *et al.* 1999). Therefore, the MCL can be seen as a structure accommodating lateral variations in the rotation field of the Central Aegean region during regional extension. In contrast, Pe-Piper & Piper (2006) recently proposed a series of palinspastic reconstructions of the Aegean domain in which they assume *c.* 100 km of sinistral displacement along the MCL during the Miocene (from 17 to 5 Ma, mostly). This would imply that the Central Aegean region actually consists of two domains that were far distant from each other during early stages of core complex-type extension (Pe-Piper & Piper 2006, Figs 2 & 13). However, on account of the similarity of lithologies, tectonometamorphic evolution, and timing of exhumation of rocks on both sides of the MCL, our opinion is that the total offset across the MCL must be minor, in agreement with Walcott & White (1998).

How many MCC and detachment systems in the Cyclades?

A number of observations imply that several MCCs coexist in the Cyclades. Most islands have the geometry of a metamorphic dome defined by the orientation of foliations, occasionally also by lithological contours, and more rarely by a concentric pattern of isograds (Naxos and Paros). On several islands, a

Fig. 7. (*Continued*) (**c**) and (**d**) represents the duration of MCC-type extension in the Cyclades. The time laps for exhuming the first dome and the duration of MCC-type extension are given with respect to the onset of post-orogenic extension. Somehow arbitrarily, the time at which the first dome finishes its exhumation is taken as the time at which the second dome starts to form. Figure 5a–b shows that their developments may slightly overlap in time (i.e. shearing is still active along the frontal detachment of the first dome while the second dome rises) but also that far much of the exhumation of the first dome has occurred before the second dome forms. The time difference between the black dot and the open symbol represents the time laps for exhuming the second dome. It shows little variation, between 5 and 8 Ma.

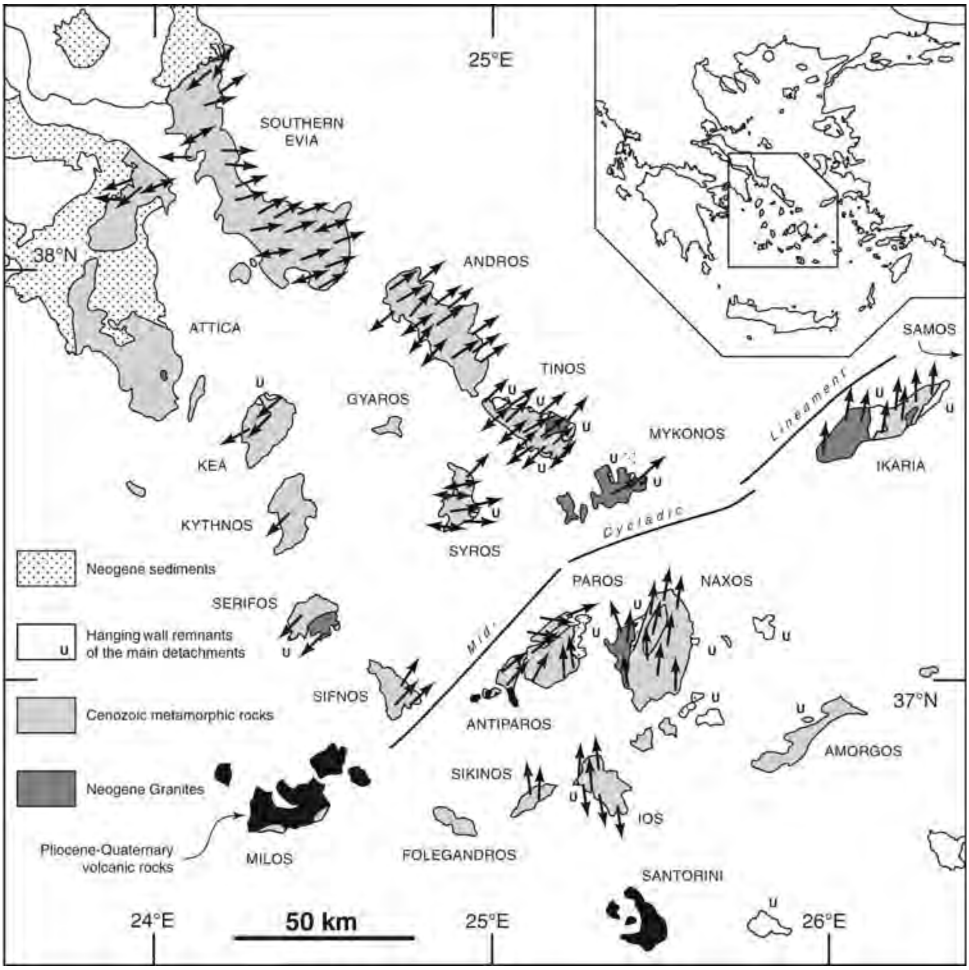

Fig. 8. Simplified geological map of the Cyclades archipelago. Arrows indicate the kinematics of extensional shearing during greenschist facies and locally higher temperature metamorphism, subsequent cooling to the conditions of brittle deformation, and within syn-kinematic intrusions. Data after Buick (1991), Gautier *et al.* (1993), Gautier & Brun (1994*a*, *b*), Gautier (1995), Vandenberg & Lister (1996), Walcott & White (1998), Jolivet & Patriat (1999), Trotet *et al.* (2001*a*), Kumerics *et al.* (2005), Iglseder *et al.* (2006) and Grasemann *et al.* (2007).

composite unit made of rocks that experienced no or limited metamorphism during the Cenozoic, rests upon the flanks of the metamorphic dome. The contact between this unit and the underlying metamorphic rocks usually bears the characteristics of an extensional detachment zone having accommodated the exhumation of the footwall rocks starting from the depths of greenschist facies and locally higher temperature metamorphism (e.g. Lister *et al.* 1984; Urai *et al.* 1990; Gautier *et al.* 1993; Gautier & Brun 1994*a*; Jolivet & Patriat 1999; Jolivet *et al.* 2004; Mehl *et al.* 2005; Müller *et al.* 2006; Grasemann *et al.* 2007). Therefore, each metamorphic dome may be described as a MCC. However, the Cyclades have also experienced Messinian–Quaternary high-angle faulting, with normal faults usually dipping away from the islands (e.g. Angelier 1977*a*, *b*; Gautier & Brun 1994*a*), so that it may be asked whether drag folding along these late faults could alone have produced the dome shape of some of the islands. This is unlikely at least on Naxos, Paros and Ios, where the domes are pronounced and regular (e.g. van der Maar & Jansen 1983; Gautier *et al.* 1993).

Occasionally, low-angle normal faults also dissect the islands and make the identification of a metamorphic dome more difficult, like on Syros (Ridley 1984).

A critical question is whether distinct MCCs found along a section parallel to extension were initially associated with a single detachment zone, as Lister *et al.* (1984) suggested, or formed beneath distinct detachment zones (Gautier & Brun 1994*b*). Gautier & Brun (1994*a*, *b*) and Gautier (1995) argued that, on several islands, a specific distribution of kinematic indicators could be seen, like on Tinos, Andros, central southern Evia, Ios and, to a lesser extent, Syros. They described the ductile deformation associated with greenschist facies metamorphism as non-coaxial, with a top-to-north (or NE) sense of shear in the northern (or northeastern) part of these islands, and a top-to-south (or SW) sense of shear in the southern (or southwestern) part. On Tinos and Andros, the domain with top-to-SW shearing is restricted to a few outcrops along the southwestern coast, so that the corresponding domes appear asymmetric with respect to the shear sense pattern (i.e. top-to-NE shearing dominates). According to Gautier & Brun (1994*a*, *b*), the sense of shear is inverted across a *c*. 1 km-wide zone trending subperpendicular to the mean stretching lineation. Within it, conjugate patterns of shear bands and symmetric boudinage structures dominate, so that this zone may be viewed as a narrow domain of coaxial strain at the transition between two domains with opposite kinematics. Further investigations on Tinos and Andros led Jolivet & Patriat (1999) to modify this description (see also Jolivet *et al.* 2004; Mehl *et al.* 2005). According to these authors, the coastal outcrops showing top-to-SW shearing should not be considered as a distinct entity but belong to a domain of coaxial strain significantly wider than previously presumed, beside the domain showing uniform top-to-NE shearing. Gautier & Brun (1994*a*, *b*) interpreted the above pattern as reflecting the dynamics of the ductile lower crust in response to isostatic rebound and dome amplification beneath a contemporaneous detachment zone (that is, the process of 'inward flow' discussed herein). A different opinion is shared by Jolivet & Patriat (1999) and Jolivet *et al.* (2004), who interpret the juxtaposed domains of coaxial and non-coaxial strain as reflecting the configuration in the middle crust, around the brittle–ductile transition zone, during early stages of extension. With further extension, the main extensional shear zones of the middle crust evolve into typical extensional detachments (Jolivet *et al.* 2004). A potential problem with this interpretation is the presence, in southern Tinos, of a large klippe (or 'extensional allochton') of the same unit that forms the hanging wall of the detachment zone in the northeastern part of the island. This klippe rests entirely onto the domain of coaxial strain defined by Jolivet & Patriat (1999). While this feature is normal in the model invoked by Gautier & Brun (1994*a*, *b*) (see also Brun & van den Driessche 1994), it is unexpected in that of Jolivet & Patriat (1999), even after a large amount of displacement is achieved along the detachment (cf. Jolivet *et al.* 2004, Fig. 13). Because well preserved eclogites and blueschists are found slightly beneath the klippe, and by analogy with the situation on Syros (see next section), Trotet *et al.* (2001*a*) and Mehl *et al.* (2005) suggested that the intervening contact represents an extensional detachment significantly older than that seen in the northeastern part of the island (at a distance of only 5 km). However, since the rocks in between belong to the same footwall unit with low-dipping foliations, this hypothesis does not readily solve the problem: the contact in the south and the northeastern detachment occupy the same structural position, therefore the former should have been reactivated (if not entirely developed) during greenschist facies shearing along the latter and is most probably connected with it. Due to this problematic issue, and on account of the numerical results obtained in this study, our opinion is that the interpretation of Gautier & Brun (1994*a*) remains a viable alternative to the one of Jolivet & Patriat (1999).

Regardless, taking into account the report of top-to-NE/ENE shearing in northern and eastern Syros during greenschist facies metamorphism (Gautier 1995; Trotet *et al.* 2001*a*; Rosenbaum *et al.* 2002), the domain of coaxial strain in southwestern Tinos strongly suggests that Tinos and Syros islands already coincided with distinct metamorphic domes during that stage of the metamorphic evolution. As a consequence, the Tinos detachment and the detachment seen in southeastern Syros, bearing a similar hangingwall rock content (Maluski *et al.* 1987; Patzak *et al.* 1994), were also probably distinct shear zones at that time (Gautier & Brun 1994*b*).

By analogy, it can be proposed that three parallel detachment systems have developed in the northwestern Cyclades during Miocene extension, coinciding with the three NW–SE-trending chains of islands seen at present, namely southern Evia–Mykonos, Gyaros–Syros, and Kea–Sifnos (Gautier & Brun 1994*a*; Jolivet *et al.* 2004). The Evia–Mykonos chain is clearly dominated by top-to-NE ductile to brittle shearing, therefore it was controlled by a NE-dipping detachment zone. In contrast, the kinematics of extensional deformation are not so clearly asymmetric in the case of the Gyaros–Syros chain. While top-to-NE/ENE shearing dominates in the eastern part of

Syros, there is no consensus among authors concerning the island as a whole. According to Trotet *et al.* (2001*a*), a continuum of top-to-ENE shearing is recorded throughout the island from the conditions of high-pressure metamorphism to those of an uneven greenschist facies overprint. A few major shear zones would have localized extensional shearing to the point that interlayered metamorphic subunits record significant differences in their pressure-temperature path (Trotet *et al.* 2001*b*). According to Trotet *et al.* (2001*a*, *b*), the same holds for Sifnos Island. While agreeing with a continuum of extensional deformation from blueschist to greenschist facies conditions, Bond *et al.* (2007) recently questioned the existence of these prominent shear zones on Syros and argued that extensional deformation was dominantly coaxial throughout the synmetamorphic exhumation history. Kinematic data reported by Gautier (1995) and Trotet *et al.* (2001*a*) do not show a dominant sense of shear on the scale of Syros Island (apart from dominantly top-to-NE/ENE shearing in the eastern part), apparently supporting the hypothesis of Bond *et al.* (2007). Finally, the southwestern chain of islands, from Kea to Sifnos, is the least known of the Cyclades (Sifnos excluded). Nevertheless, according to Walcott & White (1998) and recent work by Grasemann *et al.* (2007), Miocene top-to-SW/SSW extensional shearing dominates on Kea, Kythnos and Serifos: these three islands are, hence, probably controlled by a major SW-dipping detachment zone. In contrast, according to Trotet *et al.* (2001*a*), Sifnos displays dominantly top-to-NE extensional shearing, hence it is probably unrelated to this detachment.

In the southeastern Cyclades, no domain of coaxial deformation has been found on Naxos and Paros Islands, where extensional shearing is consistently top-to-north (Urai *et al.* 1990; Buick 1991; Gautier *et al.* 1993). Moving toward northwestern Paros, a strong (*c.* 70°) but progressive clockwise rotation of the stretching lineation is observed (Gautier *et al.* 1993), which is thought to relate to dextral shearing along the Mid-Cycladic Lineament (Gautier & Brun 1994*a*). On Ikaria, almost all kinematic data reported by Kumerics *et al.* (2005) also indicate top-to-north shearing.

In contrast, the case of Ios appears more complex. Lister *et al.* (1984) initially reported mylonitic rocks, with top-to-south kinematic indicators, which they attributed to a ductile extensional detachment named the South Cyclades shear zone. Lister *et al.* (1984) and, more recently, Vandenberg & Lister (1996) and Forster & Lister (1999) have considered that this *c.* 200 m-thick shear zone is the main structure accommodating Neogene extension on Ios. If this hypothesis is correct, then the Ios and Naxos MCCs clearly relate to two distinct (antithetic) detachment zones. However, Gautier & Brun (1994*a*) have shown that large domains with top-to-north kinematic indicators are also found in the northern limb of Ios dome. While acknowledging that the sense of shear is dominantly top-to-south on Ios (at variance with the case on most islands), Gautier & Brun (1994*b*) favoured an interpretation in which the Ios MCC formed in the footwall of a north-dipping detachment. They argued that, even in this case, the Ios and Naxos MCCs are probably related to two distinct (though synthetic) detachments, because: (1) the two domes are well defined, so that drag folding along a late normal fault in between the two islands is unlikely to have produced this division (especially since there is no evidence for such a fault in the bathymetry nor in the Messinian–Quaternary sedimentary record; and (2) pressure conditions associated with greenschist facies metamorphism are similar from southern Naxos to Ios, and are probably even lower on Antiparos, an unexpected feature in the hypothesis of a single north-dipping detachment. Therefore, along a section going from Naxos to Ios, two distinct detachment systems are required. But was Ios truly dominated by non-coaxial deformation during Miocene extension, with either a south-dipping (Lister *et al.* 1984; Forster & Lister 1999) or a north-dipping (Gautier & Brun 1994*b*) main detachment zone? The top-to-north kinematic indicators reported by Gautier & Brun (1994*a*) are associated with high-strain ductile deformation and are found both beneath and above the south-vergent South Cyclades shear zone of Lister *et al.* (1984). Vandenberg & Lister (1996) and Forster & Lister (1999) admit that top-to-north shear zones do exist in northern Ios, associated with mylonitic fabrics. Forster & Lister (1999) report these shear zones as cutting across the South Cyclades shear zone and interpret them as reflecting downdip shearing along the back-tilted flank of the MCC after significant arching of the main shear zone (cf. Reynolds & Lister 1990). This interpretation is questionable, however, because Forster & Lister (1999) indicate that these crosscutting relations are observed within augengneiss that occupy the core of the Ios MCC, in which the main fabric may well relate to pre-extensional events (e.g. Vandenberg & Lister 1996). Conversely, Vandenberg & Lister (1996) suggested that the South Cyclades shear zone cuts across the north-dipping detachment zone of Naxos, yet acknowledging that available geochronological data on synkinematic intrusions do not support this scenario. Altogether, these features suggest that top-to-north and top-to-south extensional shear zones on Ios are broadly contemporaneous, and that there may be no dominant sense of shear on the scale of the island during Miocene extension.

Furthermore, Vandenberg & Lister (1996) and Forster & Lister (1999) mapped a series of low-angle normal faults capping the South Cyclades shear zone, associated with chloritization and brecciation (the Ios Detachment Fault system of Forster & Lister 1999). They consider that this fault system reflects ongoing shearing along the South Cyclades shear zone during cooling and exhumation, so that the faults are reported to have the same top-to-south kinematics. However, field evidence in favour of this interpretation is scarce. The fault system is recognized mainly in the northern limb of the dome, where the normal faults dip northward and are thus assumed to have been tilted into the attitude of apparent thrust faults during subsequent arching. However, if the top-to-north ductile shear zones also developed in response to arching, as argued by Forster & Lister (1999), then arching was already effective while the rocks were still in the conditions of ductile deformation, therefore later brittle normal fault zones could hardly have rotated through the same process. We conclude that further work is needed to check whether the 'Ios Detachment Fault system' is associated with top-to-south or top-to-north kinematics.

Summarizing, like the northwestern Cyclades, the southeastern Cyclades seem to include three parallel detachment systems developed during Miocene extension, coinciding with the three east–west-trending chains of islands seen at present, namely Ikaria–Samos, Paros–Naxos, and Folegandros–Ios (Gautier & Brun 1994*a*). The two northern chains are controlled by a north-dipping detachment zone, while the deformation pattern on Ios suggests that the southern chain has no marked asymmetry. The central chain (i.e. the islands of Naxos and Paros) displays the deepest structural levels of the Cyclades, in the form of two large domes cored with migmatites (e.g. Gautier *et al.* 1993; Jolivet *et al.* 2004).

Interfering detachment systems

Using available pressure estimates for greenschist facies and locally higher temperature metamorphism and taking into account the present geometry and distribution of metamorphic domes in the Cyclades, Gautier & Brun (1994*b*) and Gautier (1995) came to the conclusion that, along at least three transects parallel to stretching (Tinos–Syros, Paros–Sikinos, Naxos–Ios), the different detachment zones and associated MCCs are partly superimposed and, therefore, probably interfere with one another. They discussed two possible evolutionary models incorporating a genetic link between successive synthetic detachment zones. A scenario was finally favoured in which a second detachment develops in the footwall of the first one, giving rise to a secondary MCC formed in the rear flank of the first one (Gautier & Brun 1994*b*, fig. 10). It is worth noting that this scenario bears some resemblance with the numerical simulations obtained in this study. Nevertheless, it has specific aspects that deserve a few comments. Firstly, the second detachment zone was thought to arise from prolonged shearing along a fault zone formed during the development of the first MCC (the 'Listric Accommodation Fault' (LAF) seen in the analogue experiments of Brun *et al.* 1994). As a result, the secondary MCC was expected to show a marked asymmetry. It is not clear whether the present numerical approach is precise enough to feature a LAF in the brittle upper crust, therefore the mechanical background for the development of a secondary MCC in the simulations may be quite different; coincidentally, we obtain no marked asymmetry for the secondary MCC. Secondly, the scenario of Gautier & Brun (1994*b*) incorporated the fact that the two MCCs should interfere, with reference to the three studied transects (for this reason, the LAF was drawn closer to the first detachment than it is in the experiments of Brun *et al.* 1994).

Gautier & Brun (1994*b*) further pointed out that, with ongoing extension, this 'second footwall detachment' scenario may ultimately result in a complete omission of the wedge of upper crustal rocks that initially formed in the rearmost part of the first MCC. They claimed that this feature compares well with the situation in the Cyclades, where no such wedge of upper crustal rocks is exposed on the islands. However, the latter point depends on the interpretation that is made of segments of the metamorphic pile exposing well-preserved eclogites and blueschists, as on Syros and Sifnos. Following the opinion of Avigad (1993) and Wijbrans *et al.* (1993) for the case of Sifnos, Trotet *et al.* (2001*a*) have proposed that high levels of the metamorphic pile on these two islands escaped pervasive retrogression because they were exhumed earlier. An apparent support to this interpretation is the fact that, on Sifnos, radiometric data from these rocks provide significantly older ages than lower levels with intense greenschist facies retrogression (Altherr *et al.* 1979; Wijbrans *et al.* 1990). As a result, high levels of the metamorphic pile may have been part of the upper crust by the time the rest of the pile underwent extensional deformation associated with greenschist facies metamorphism (Avigad 1993; Trotet *et al.* 2001*a*; Parra *et al.* 2002). If so, the claiming of Gautier & Brun (1994*b*) that no wedge of upper crustal rocks exists in the Cyclades is incorrect, and it is not so clear whether adjacent MCCs interfere or not. For instance, much of Syros would represent such upper crustal rocks, and the same may apply to Ios, where high-pressure rocks are relatively abundant in the envelope of the dome, above the South Cyclades shear zone of Lister *et al.* (1984), displaying similarly 'old' ages as on Syros and Sifnos (van der Maar & Jansen 1983). Due to its potential implications, this hypothesis needs to be further discussed.

According to the interpretation of Trotet *et al.* (2001*a*, *b*), important extensional shear zones should exist (and are reported to do so) within the metamorphic pile of Syros and Sifnos (see also Avigad 1993). In addition, the topmost detachment fault seen in southeastern Syros, with Cretaceous metamorphic rocks in the hanging wall (Maluski *et al.* 1987) and well preserved high-pressure rocks in the near footwall, should represent a relatively old structure. However, in the case of Syros, Bond *et al.* (2007) claim that the intermediate extensional shear zones do not exist and, like other authors have argued for Sifnos and Tinos Islands (Schliestedt & Matthews 1987; Bröcker 1990; Ganor *et al.* 1996), consider that the degree of preservation of the high-pressure assemblages reflects primarily the extent of fluid infiltration during greenschist facies retrogression. Limited fluid infiltration and deformation in the least retrogressed rocks may also account for the preservation of older ages by the time rocks passed through P–T conditions of the greenschist facies, as proposed by Wijbrans *et al.* (1990) in the case of Sifnos (see however Wijbrans *et al.* 1993). This is especially clear on Tinos, where the rocks with the best preserved high-pressure assemblages (with ages around 45–37 Ma) lie at the same structural level as those showing a complete greenschist overprint (with ages around 33–21 Ma; Bröcker & Franz 1998; Parra *et al.* 2002). In this particular case, the extent of retrogression is apparently linked with the intensity of shearing during greenschist facies metamorphism (Jolivet & Patriat 1999; Parra *et al.* 2002). The same may hold for Syros (Bond *et al.* 2007) and, eventually, Sifnos (Wijbrans *et al.* 1990). Rosenbaum *et al.* (2002) also consider that, in northern Syros, at high levels of the metamorphic pile, greenschist facies overprint is localized into top-to-NE shear zones that are contemporaneous with Miocene extensional shearing in neighbouring islands. As for the detachment in southeastern Syros, its timing is poorly constrained. Trotet *et al.* (2001a) used a $^{40}Ar/^{39}Ar$ white mica age obtained close to the contact (30.3 $\pm$ 0.9 Ma; Maluski *et al.* 1987) to infer that the detachment was active at that time. Maluski *et al.* (1987) reported this age from an omphacitic metagabbro and pointed out that the obtained spectrum shows evidence for an inherited component. In addition, Trotet *et al.* (2001*a*) indicate that the actual detachment contact is marked by breccias reworking eclogites retrograded into the greenschist facies. This strongly suggests that at least part of the displacement along the detachment occurred significantly later than 30 Ma, that is, at about the same time as in other islands (e.g. Gautier & Brun 1994*a*). Altogether, the above features suggest that, in the Cyclades as a whole, well-preserved high-pressure rock assemblages represent low-strain lenses of variable size embedded into a single layer of greenschist facies metamorphism dating from the late Oligocene–early Miocene. This interpretation may apply to most islands (e.g. Wijbrans *et al.* 1990; Parra *et al.* 2002; Bond *et al.* 2007), Ios included (Forster & Lister 1999). As a result, the inference that no wedge of upper crustal rocks exists in the Cyclades (Gautier & Brun 1994*b*) remains probably valid, which, in turn, supports the view that detachment zones and associated MCCs do interfere with one another in this region. It remains that, on Syros and Sifnos, an upward gradient of preservation of the high-pressure assemblages exists across the *c.* 3 km-thick metamorphic pile (e.g. Wijbrans *et al.* 1990; Trotet *et al.* 2001*a*). We suggest that this gradient reflects the transition from pervasive deformation, below, to more localized deformation, above, within the layer of greenschist facies metamorphism. In other words, greenschist facies metamorphism in the middle crust would coincide with the broad transition from pervasive (ductile) to localized (ductile to brittle) deformation across the thickness of the crust, in good agreement with the views of Jolivet & Patriat (1999) and Jolivet *et al.* (2004).

Post-orogenic versus syn-orogenic extension

The numerical simulations presented in this paper are concerned with the case of whole-lithosphere extension. As stated above, most authors having identified extensional detachments and metamorphic core complexes in the Cyclades interpreted them as resulting from Aegean 'backarc' extension (Lister *et al.* 1984; Buick 1991; Gautier & Brun 1994*b*; Jolivet & Patriat 1999), thus apparently fitting the experimental setup. These structures developed within metamorphic rocks that previously experienced high-pressure/low-temperature conditions, therefore extension may also be described as 'late-orogenic' (Gautier & Brun 1994*b*). However, for the purpose of a comparison with the numerical results, it needs to be discussed whether the extensional structures developed strictly after crustal thickening or/and during ongoing thrusting beneath the locus of extension. In the Aegean, these two cases have been refered to as post vs. syn-thickening, or post vs. syn-collisional, extension (Gautier & Brun 1994*b*), or post vs. syn-orogenic extension/exhumation (Jolivet & Patriat 1999; Trotet *et al.* 2001*a*; Parra *et al.* 2002; Jolivet *et al.* 2003), the latter terminology being now widely accepted. In the following, we prefer to use extension rather than exhumation because exhumation may also result from erosion, eventhough erosion in the Cyclades has probably been limited during the Cenozoic (e.g. Gautier & Brun 1994*a*). We emphasize that extension does not necessarily mean that the whole lithosphere, or even the whole crust, is stretched horizontally. This is obvious in the case of syn-orogenic extension, where plate convergence is the leading process and horizontal shortening the dominant regime on the lithospheric scale. Syn-orogenic extension is sometimes described as corresponding to the development of an extrusion wedge (e.g. Ring & Reischmann 2002; Ring *et al.* 2007*a*).

The distinction between post and syn-orogenic extension is a difficult task, especially because the associated faults and shear zones may have the same kinematics (Jolivet & Patriat 1999; Trotet *et al.* 2001*a*). Gautier & Brun (1994*b*) and Gautier *et al.* (1999) have argued that, because extension with a direction of stretching parallel to plate convergence was active at the same time (i.e. since at least the Aquitanian) across a wide part of the Aegean, from the Rhodope to Crete, this extension was necessarily post-orogenic, based on a comparison with the case of syn-orogenic lateral extension in the Himalaya–Tibet orogen. However, this assessment may be incorrect in the case of a significant retreat of the underthrusted slab during orogeny. As discussed by Jolivet *et al.* (2003), if the dynamics of the orogen is basically that of a retreating subduction, then extension can be everywhere parallel to convergence, including in the area lying above the frontal thrust zone. In a sense, such an orogen is not strictly collisional, therefore the description of extension as post or syn-collisional (Gautier & Brun 1994*b*) is unadapted in this case.

Even if only extensional structures are observed in a late-orogenic setting, it is usually difficult to demonstrate that their formation was strictly post-orogenic, because it can always be argued that coeval thrusting possibly occurred beneath the deepest exposed rocks. Conversely, syn-orogenic extension is demonstrated if a thrust zone can be shown to have been active while extension occurred, or had already started, at shallower levels. Avigad & Garfunkel (1989) and Avigad *et al.* (1997) tentatively argued for the latter case on Tinos and Evia islands, however their arguments have been criticized by Gautier (2000) and Bröcker & Franz (2005). Moreover, in the scenario of Avigad *et al.* (1997) for the Cyclades, coeval thrusting and inferred syn-orogenic extension are restricted to the Oligocene period, while post-orogenic extension started at about 25 Ma, associated with a pervasive greenschist facies overprint, as in the common view (see above). Avigad *et al.* (1997) also acknowledged that the identification of structures associated with the period of syn-orogenic extension is problematic.

The shape of the pressure–temperature path followed by metamorphic rocks may help to decipher between syn-orogenic and post-orogenic extension. Following Wijbrans *et al.* (1993), Jolivet and co-workers have proposed that, among the metamorphic rocks of the Cyclades, those having followed a cold geotherm during exhumation should have done so owing to syn-orogenic extension (Jolivet & Patriat 1999; Trotet *et al.* 2001*a*, *b*; Parra *et al.* 2002; Jolivet *et al.* 2003). A critical question is how cold this geotherm should be, given that exhumation beneath a detachment also helps to prevent heating. The best answer probably comes from the study of Parra *et al.* (2002), showing that, on Tinos, rocks in the footwall of the NE-dipping detachment experienced an episode of isobaric heating (a temperature increase from 400°–550 °C at about 9 kbar) between two episodes of exhumation. Parra *et al.* (2002) convincingly proposed that the first and second episodes reflect syn-orogenic and post-orogenic extension, respectively (see also Jolivet *et al.* 2004). As a result, on Tinos at least, only post-orogenic extension would be recorded since rocks moved out of the conditions of blueschist facies metamorphism. In other words, all the structures developed at greenschist facies and subsequent lower grade conditions are expected to relate to post-orogenic extension, in agreement with earlier proposals (Gautier & Brun 1994*a*; Jolivet & Patriat 1999). There does not seem to be a significant diachronism of greenschist facies metamorphism on the scale of the Cyclades (including at high levels of the metamorphic pile on Syros, see previous section), therefore the whole set of detachment zones and associated MCCs described before have probably developed during post-orogenic extension.

It is difficult to determine when this extension started. Using the data of Bröcker & Franz (1998), Parra *et al.* (2002) have suggested that the beginning of the second episode of exhumation and, therefore, the onset of post-orogenic extension in the Cyclades took place at 30 Ma (see also Jolivet *et al.* 2003, 2004). Based on the data of Wijbrans *et al.* (1990), Wijbrans *et al.* (1993) have proposed a P–T path for lower levels of the metamorphic pile on Sifnos that resembles the one of Parra *et al.* (2002) for Tinos. However, in this case, isobaric heating (at 6.5 kbar) would have occurred from 30 Ma to 22 Ma, so that the second episode of exhumation would start at 22 Ma. Nevertheless, the scenario of Wijbrans *et al.* (1993) assumes that post-thickening extension started at 30 Ma, being first confined to crustal levels beneath the presently exposed rock pile, then migrating into this pile. Therefore, both interpretations (Wijbrans *et al.* 1993; Parra *et al.* 2002) concur in the idea that post-orogenic extension was active in the Cyclades during the earliest Miocene (e.g. Gautier & Brun 1994*a*); they even suggest that it was already active during the late Oligocene.

In contrast, Ring and co-workers have put forward an extreme alternative scenario, in which a context of syn-orogenic extension would have been maintained in the Cyclades until *c.* 21 Ma (Ring *et al.* 2001; Ring & Reischmann 2002; Ring & Layer 2003; Ring *et al.* 2007*a*). This would have been followed by an episode of post-orogenic extension starting later than *c.* 15 Ma (Ring *et al.* 2007*a*), probably at *c.* 12 Ma (Ring & Layer 2003), and resulting from thermal weakening at the time the Aegean magmatic arc would have reached the Cyclades. If this scenario is correct, then extensional structures associated with greenschist facies and higher temperature metamorphism should largely date from an episode of syn-orogenic extension, as, for instance, on Naxos (e.g. Gautier *et al.* 1993; Keay *et al.* 2001), Tinos (e.g. Gautier & Brun 1994*a*; Bröcker & Franz 1998, 2000; Jolivet *et al.* 2004) and Andros (Gautier & Brun 1994*b*; Bröcker & Franz 2006). As a result, our attempt to compare our numerical simulations and the Cycladic case would be questionable.

According to Ring and co-workers, the Central Aegean region is floored by the poorly exposed parautochtonous Basal unit, coinciding with the Almyropotamos unit in central southern Evia (e.g. Dubois & Bignot 1979); this unit would have been underthrusted while extensional shearing developed at higher levels of the metamorphic pile. This interpretation follows Avigad *et al.* (1997) except for the timing of the episode of syn-orogenic extension (before about 25 Ma for Avigad *et al.* as late as 21 Ma for Ring and co-workers). We think that this scenario is unlikely, especially its timing, for the three following reasons:

- Rb–Sr and $^{40}Ar/^{39}Ar$ dating of phengites from samples of the Basal unit has yielded ages mostly between 21 and 24 Ma (Ring *et al.* 2001; Ring & Reischmann 2002; Ring & Layer 2003). While they coincide with the timing of greenschist facies metamorphism in the overlying unit, these ages were interpreted as reflecting high-pressure metamorphism in the Basal unit (hence constraining the age of underthrusting) because the dated phengites have a high Si content ($\geq$3.3 per formula unit). However, as thoroughly discussed by Bröcker *et al.* (2004) and Bröcker & Franz (2005), this interpretation is questionable and the obtained ages are more likely to reflect the timing of post-high-pressure greenschist facies retrogression, as in the overlying unit. Further support to the objections of Bröcker *et al.* (2004) is found in the recent Rb–Sr study of Wegmann (2006) on rocks from southeasternmost Evia, at higher levels of the metamorphic pile, far above the Basal unit. In one rock repeatedly dated with a microsampling method, phengites have a Si content ranging from 3.36 to 3.74 pfu and yield Rb–Sr ages ranging from 21 to 11 Ma. Following the line of reasoning of Ring and co-workers, this would mean that higher levels of the metamorphic pile were still experiencing high-pressure conditions at that time. This is at odds with the report from the neighbouring northwestern Cyclades (Bröcker & Franz 1998, 2006) and from southern Evia itself where, according to Ring *et al.* (2007*a*), such rocks experienced greenschist facies conditions as early as 21 Ma. It should also be stressed that the youngest fossils found so far in the Almyropotamos unit represent the lower or middle Eocene (Dubois & Bignot 1979), not the upper Eocene–Oligocene as commonly reported (e.g. Ring *et al.* 2007*a*), therefore this unit may have started to underthrust as early as during the early Eocene;
- According to the scenario of Ring and co-workers, the Central Aegean region should have been characterized by a depressed geotherm as late as around 21 Ma (i.e. as long as underthrusting and inferred high-pressure metamorphism were developing), and no significant thermal overprint is expected before about 14 Ma, when arc magmatism is considered to have reached the Cyclades. However, this does not take into account the case of the migmatite domes on Naxos and Paros Islands. U–Pb dating of zircons from the migmatitic core of Naxos indicates that partial melting mostly occurred at *c.* 17.5 Ma and was already under way at 20 Ma (Keay *et al.* 2001), in good agreement with time constraints provided by other radiometric methods (e.g. Andriessen *et al.* 1979; Wijbrans & McDougall 1988). This shows that at least part of the Central Aegean region was actually characterized by a high geotherm at about 20 Ma. The Basal unit is unlikely to lie underneath the migmatite domes, because if it had been underthrusted until 21 Ma, migmatization in the hanging wall of this thrust could hardly have been maintained until *c.* 17 Ma (cf. Keay *et al.* 2001). Hence, the migmatite domes probably cut across the contact and, as stated before,

represent the deepest structural levels of the Cyclades. It is not known whether the migmatites seen on Naxos and Paros expand laterally beneath the other islands, although there are chemical data to suggest so (Gautier & Brun 1994*a*). Regardless, the area of Naxos and Paros was hot at 20 Ma, and we do not see how this can be reconciled with the hypothesis of regional underthrusting as late as 21 Ma; and

- Post-orogenic extension is accompanied by the formation of grabens (as also illustrated by our numerical experiments) which may evolve into supra-detachment basins. Thus, the base of the supradetachment basin stratigraphy may provide a minimum age for the onset of post-orogenic extension. The oldest supra-detachment sediments known in the Cyclades, on Naxos and Paros, are Aquitanian (23.0–20.4 Ma; Lourens *et al.* 2004) and form the basis of a nearly continuous stratigraphy reaching the upper Miocene (Angelier *et al.* 1978; Roesler 1978; Sanchez-Gomez *et al.* 2002). This documents continuous formation of accomodation space from the Aquitanian onward, suggesting no fundamental change in the tectonic setting since that time (Gautier *et al.* 1993; Gautier & Brun 1994a; Sánchez-Gómez *et al.* 2002). In addition, the Aquitanian and Burdigalian sediments are marine deposits (e.g. Angelier *et al.* 1978), while it may be argued that sedimentation beneath sea level is unexpected during (or immediately after) an episode of extension coeval with underthrusting, as in the scenario of Ring et co-workers.

To conclude on this part, our opinion is that a context of syn-orogenic extension could hardly have existed in the Cyclades later than about 25 Ma, considering that at least a few million years are necessary to enhance partial melting after underthrusting, whatever the exact origin of the heating event. Syn-orogenic extension finishing at *c*. 37 Ma, as suggested by Parra *et al.* (2002), would fit this condition. We also note that the onset of post-orogenic extension at *c*. 30 Ma in the Cyclades, as suggested by Wijbrans *et al.* (1993) and Parra *et al.* (2002), is fully compatible with the timing of events reported by Thomson & Ring (2006) and Ring *et al.* (2007*b*) in the nearby Menderes massif, where the allochtonous position of the 'blueschist' unit of the Cyclades is well established.

Did extension in the Cyclades significantly deviate from plane strain deformation?

Finally, before comparing the Cyclades and our numerical experiments, we should examine whether crustal extension in the Cyclades closely approximated plane strain deformation, as assumed when extrapolating the two-dimensional simulations to a three-dimensional setting, or not. Based on the presence of folds with axes parallel to the mean stretching lineation on several islands (Naxos, Paros, Tinos and Andros), some authors have argued that a significant component of transverse (*c*. east–west) shortening has accompanied MCC-type extension in the Cyclades (Urai *et al.* 1990; Buick 1991; Avigad *et al.* 2001; Jolivet *et al.* 2004). According to Avigad *et al.* (2001), the magnitude of this lateral contraction was high enough to maintain the thickness of the crust roughly constant despite intense extensional deformation. Transverse shortening may be viewed as a normal response to the three-dimensional displacement field of the Aegean lithosphere during extensional spreading (Gautier *et al.* 1999; Jolivet *et al.* 2004), nevertheless our opinion is that its contribution to crustal strain has never been significant in the Cyclades. Most of the folds taken as evidence for strong lateral shortening are either isoclinal to tight folds with low-dipping axial planes subparallel to the main foliation (therefore they do not properly document horizontal shortening) or upright open folds (documenting limited shortening). On Naxos, which is reported as the island where transverse shortening is best seen, Vanderhaeghe (2004) has shown that subvertical granitic dikes have emplaced throughout the inner envelope of the migmatite dome during extension. About one half of these dikes trend parallel to the *c*. north–south stretching lineation and another half perpendicular to it, therefore bulk flattening strain and horizontal stretching in the east–west direction are actually documented (Vanderhaeghe 2004). The relatively steep attitude of foliations within and around the migmatitic core of the Naxos dome may reflect the diapiric ascent of the migmatites (Vanderhaeghe 2004) rather than folding and horizontal shortening (e.g. Jolivet *et al.* 2004).

In analogue experiments simulating the spreading of a weak lithosphere toward a free boundary, transverse shortening is present but is confined to the inner (northern in an Aegean frame) part of the deforming sheet (Gautier *et al.* 1999). The Cyclades are unlikely to have occupied such a inner position during Aegean extension, at least until the late Miocene, therefore the lack of clear evidence for significant transverse shortening in the ductile record of the islands is not surprising. The situation is possibly different since around the Pliocene (since <3 Ma according to Gautier *et al.* 1999, but more probably since <8 Ma according to the paleomagnetic results of van Hinsbergen *et al.* 2005*b*), when a southward jump of the northwestern tip of the Aegean arc brought the Cyclades in a more inner position than they were before, and when the westward extrusion of Anatolia started to affect the evolution of the Aegean domain. This regional reorganization probably explains the record of WNW–ENE shortening (in the form of tight folds, strike-slip and reverse faults) in Neogene sediments of the Central Aegean region (Angelier 1977*b*), some of which must be younger than 10 Ma (Sánchez-Gómez *et al.* 2002).

We conclude that crustal extension in the Cyclades probably coincided with near-plane strain deformation during much of the period of post-orogenic extension (i.e. except possibly since < 8 Ma), therefore comparing the evolution of the Cyclades with our two-dimensional experiments bears some logic.

Comparison and discussion

Comparison between the numerical experiments and the Cyclades

The previous overview has shown that several aspects of the tectonic evolution of the Cyclades during the Neogene are reminescent of the results of our numerical experiments, especially the coexistence of several MCCs and associated detachment systems along a section parallel to extension ('How many MCC and detachment systems in the Cyclades?' section) and the fact that at least some of these MCCs interfere with one another ('Interfering detachment systems' section). In addition, we have shown that the general kinematic framework that prevailed during the development of these structures is comparable to the one in our experimental setup, that is, a context of whole-lithosphere (i.e. post-orogenic) extension ('Post-orogenic vs. syn-orogenic extension' section) associated with near-plane strain deformation (previous section). We now compare in more detail the results of our numerical experiments with the geological record of the Cyclades. Four essential issues are compared: the final depth of the Moho, the geometry of MCCs, their kinematic pattern, and the amount of time associated with their exhumation:

Moho depth. In the experiments, the Moho interface remains nearly flat throughout the extensional process (Fig. 5). The final Moho depth increases with increasing initial crustal thickness and with decreasing boundary velocity (Fig. 7). Within the range of conditions giving rise to interfering MCCs (see 'Numerical experiments' section), this depth varies between 22.5 and 29 km. In the Cyclades, various geophysical investigations indicate that the Moho is almost flat, lying at depths around 25–26 km (Makris & Vees 1977; Makris 1978; Vigner 2002; Li *et al.* 2003; Tirel *et al.* 2004*b*), well within the expected range of values. According to the experiments, a value of 25–26 km is compatible with an initial crustal thickness (at the onset of post-orogenic extension) of *c.* 43–44 km (Fig. 7e) and a boundary velocity of *c.* 2.0–2.3 cm/a (Fig. 7f).

Geometry of MCCs. Before comparing the geometry (this section) and kinematic pattern (next section) of MCCs in the numerical simulations and in the Cyclades, it must be stressed that, unlike in the experimental setup, the crust of the Cyclades was neither homogeneous nor isotropic at the onset of post-orogenic extension. Most authors agree on the view that crustal thickening during the earlier orogenic period occurred through the operation of dominantly SSW-vergent thrusts (e.g. Bonneau 1982; Jolivet *et al.* 2003; van Hinsbergen *et al.* 2005*a*). It may be suspected that some of these thrusts were later reactivated as normal-sense detachment zones (e.g. Gautier *et al.* 1993; Avigad *et al.* 1997; Trotet *et al.* 2001*a*; Jolivet *et al.* 2003; Ring *et al.* 2007*a*), which may account for the predominance of top-to-NNE shearing during extension on the scale of the Cyclades. However, clear evidence that earlier thrusts have particularly localized later extensional shearing is missing. On Ios Island, Vandenberg & Lister (1996) suggested that the south-vergent South Cyclades shear zone partly reactivates (in extension) a north-vergent Alpine thrust, however the arguments for such a thrust are unclear. It remains that dominantly SSW-vergent Alpine thrusting has certainly produced a broadly north-dipping stack of various lithologies, the weakest of which may have localized later extensional shearing. Thus, not only the predominance of top-to-NNE shearing during extension might be explained by earlier thrusting, so does the spatial distribution of extensional detachments, which could in part reflect the initial geometry of the thrust stack. We are aware of this problem when comparing the Cyclades with the numerical simulations, the problem arising from our deliberate choice of the simplest possible initial conditions in the experimental setup.

Nevertheless, as the simulations compare relatively well with the natural case, our impression is that the role of pre-existing structures has been minor during post-orogenic extension in the Cyclades. We suspect that this arises from the high thermal profile of the crust at, or soon after, the initiation of post-orogenic extension. According to our experiments, at least the lower half of the crust was at temperatures in excess of 550 °C, at which the viscosity contrast between the most common rock types is severely reduced. At these levels, the most significant viscosity drops relate to the progress of anatexis, which depends only partly on the geometry of earlier thrusting.

A number of observations imply that several MCCs coexist in the Cyclades (see 'How many MCC ...' section). Structural data suggest that three detachment systems and associated MCCs have developed in both the northwerstern Cyclades (coinciding with the Evia–Mykonos, Gyaros–Syros and Kea–Sifnos island chains) and the southeastern Cyclades (coinciding with the Ikaria–Samos, Paros–Naxos and Folegandros–Ios island chains). As discussed by Gautier & Brun (1994*b*), the MCCs of at least two of these chains apparently interfere with one another, based on the relationships between Naxos and Ios, Paros and Sikinos, and Tinos and Syros (see 'Interfering detachment systems' section). We now focus on a comparison between the numerical simulations and the Naxos–Ios and Tinos–Syros island pairs, leaving Paros–Sikinos aside because it repeats the case of Naxos–Ios without an equivalent structural or geochronological dataset being available.

We find striking similarities between the simulations and the selected island pairs in terms of geometry (Fig. 9). Naxos constitues a large MCC with a pronounced asymmetry, exhuming high-temperature lower crustal rocks (e.g. Gautier *et al.* 1993). Ios constitutes another MCC (e.g. Vandenberg & Lister 1996) formed in the direction opposite to the slope of the Naxos detachment. The Ios dome seems symmetric (at least, its asymmetry is not as pronounced as on Naxos or Paros). It is appparently narrower than the Naxos dome (although both are partly hidden beneath sea level) and exposes lower grade rocks (e.g. van der Maar & Jansen 1983), indicating that the Ios MCC is less developed. The Ios dome is superimposed on the southern flank of the Naxos dome (Gautier & Brun 1994*b*). Although less clearly expressed, the Tinos–Syros island pair displays a similar geometry. Tinos is an asymmetric MCC exhuming rocks with a pervasive greenschist facies overprint (Gautier & Brun 1994*a*; Jolivet & Patriat 1999; Parra *et al.* 2002). Syros is another MCC formed in the direction opposite to the slope of the Tinos detachment. However, Syros does not show a regular dome, which may be due to the moderate size of the island and to the influence of large normal faults cutting across the metamorphic series (Ridley 1984). It exposes rocks with broadly a less intense greenschist facies overprint than on Tinos (e.g. Trotet *et al.* 2001*a*). We have discussed in the 'Interfering detachment systems' section the possible interpretations of this feature, suggesting that the upward gradient of preservation of the high-pressure assemblages across the metamorphic pile of Syros (and Sifnos) may reflect the transition from pervasive deformation, below, to more localized deformation, above, within a coherent layer of greenschist facies metamorphism. If so, then at least part of Syros exposes rocks of slightly shallower origin than on Tinos. This hypothesis is supported by a comparison of the P–T paths of the deepest rocks on Syros (Trotet *et al.* 2001*b*) and Tinos (Parra *et al.* 2002), showing that, along the greenschist facies segment of the exhumation path, temperatures were $\geq 50^\circ$ higher in the case of

	IOS	NAXOS
shape of the MCC	symmetric dome	asymmetric dome
kinematics of extension	no dominant sense (?)	top-to-north
post-HP highest metamorphic grade	greenschist	anatexis
radiometric record of extension	~ 20-13 Ma	>20-10 Ma
main period of exhumation	?	17-12 Ma

	SYROS	TINOS
shape of the MCC	domal ?	asymmetric dome
kinematics of extension	no dominant sense (?)	top-to-northeast
post-HP highest metamorphic grade	greenschist	greenschist (T>50°C or more / Syros)
radiometric record of extension	~ <30-11 Ma	22-11 Ma
main period of exhumation	?	22-15 Ma (?)

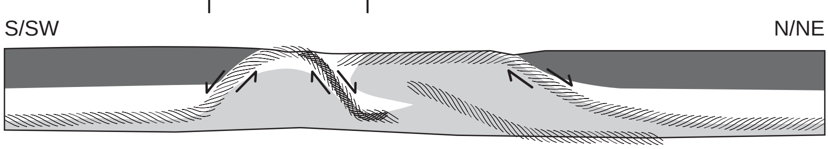

Fig. 9. Comparison between a crustal-scale cross-section showing interfering MCCs, as deduced from the numerical analysis, and relevant data from two transects in the Cyclades showing closely spaced MCCs, as discussed in the text. The comparison reveals a good agreement.

Tinos. In our experiments, the isotherms are carried upward during the earlier stages of MCC development, therefore we expect a rock of deeper origin to experience higher temperatures during exhumation, as also clearly illustrated by the numerical experiments of Gessner *et al.* (2007). Thus, the Tinos MCC has apparently accommodated more exhumation than the Syros MCC has. Note that the same process of upward heat transport during MCC development might also account for the different P–T paths obtained by Trotet *et al.* (2001*b*) across the metamorphic pile of Syros and Sifnos (see e.g. Gessner *et al.* 2007, Fig. 6). As discussed by Gautier & Brun (1994*b*), the Syros MCC is probably superimposed on the southwestern flank of the Tinos MCC.

Summing up, the geometry of MCCs along the Naxos–Ios transect and, to a less extent, the Tinos–Syros transect, compares well with the numerical simulations (Fig. 9). The comparison is more convincing with type 2 experiment, in which the second dome develops in the immediate vicinity of the first dome, so that the two MCCs are partly superimposed (Figs 5d, e, f and 6). In this case, no wedge of upper crustal rock is preserved between the MCCs, a feature that Gautier & Brun (1994b) have claimed to characterize the Cyclades. If, alternatively, higher levels of the metamorphic pile on Syros (and Sifnos) represent rocks that were exhumed to upper crustal conditions before the onset of post-orogenic extension (e.g. Trotet *et al.* 2001*a*; see discussion in 'Interfering detachment systems' section), then the structure is broadly the same, with only the Syros MCC being less developed (i.e., leaving a cap of upper crustal rocks near the apex of the dome).

In addition, special attention should be paid to the width of the two largest MCCs of the Cyclades, on Naxos and Paros. According to the above comparison, these two domes represent MCCs of the first generation. In the experiments, depending on the initial conditions, the width of the first dome is quite variable (Fig. 7a, b). The width of Naxos and Paros domes, measured in the same way as in the experiments (from the front of the detachment, plunging northward, to the rearmost part of the dome, before reaching a wedge of brittle upper crust) is at least 35 km and most probably less than 60 km. This range is compatible with an initial crustal thickness between *c*. 41 and 44 km, and seems to exclude greater values (Fig. 7a). It also seems to exclude a boundary velocity lower than *c*. 2 cm/a (Fig. 7b). Thus, the width of the MCCs of the first generation suggests broadly the same range of initial conditions as the final Moho depth does (see 'Moho depth' section).

Kinematic pattern. Similarities are also found between the simulations and the Naxos–Ios and Tinos–Syros island pairs in terms of kinematic development of the MCCs. However, before attempting a comparison, we should keep in mind the origin of shear zones in the numerical experiments, and address the question whether the same process could have operated in the Cyclades. In the experiments, faulting occurs in the upper crust due to the imposed horizontal stretching; a major fault (i.e., a detachment) ultimately develops at this level if stretching is strong enough (see 'Analysis of the two experiments' section; see also Tirel *et al.* 2004*a*). In the lower crust, ductile shear zones develop as a by-product of the process of inward flow. In the Cyclades, Gautier and Brun (1994*a*, *b*) have interpreted the shear zone pattern of some of the islands (especially Tinos, Andros, Ios) as reflecting such a process of inward flow (see 'How many MCC...' section). On Tinos and Andros, there is good evidence that this shear zone pattern developed during greenschist facies metamorphism and subsequent cooling to conditions corresponding to the transition from pervasive ductile to localized semi-brittle behaviour (Gautier & Brun 1994*a*; Gautier 1995; Jolivet & Patriat 1999; Jolivet *et al.* 2004; Mehl *et al.* 2005). In our experiments, shearing due to inward flow occurs significantly below the ductile–brittle transition (i.e., at temperatures at least *c*. 150 °C higher than the temperature of *c*. 300 °C obtained for the transition), nevertheless it is conceivable that shearing may propagate up to this interface if the ductile–brittle transition is to become a low-strength horizon after a certain amount of crustal extension is achieved (see 'Analysis of the two experiments' section). The structural record on Tinos and Andros shows that this situation may hold in the Cyclades. In addition, as micaschists and marbles dominate among the various rock types found in the islands, shearing due to inward flow may propagate at even shallower depths (that is, along an isotherm of less than 300 °C) if the proper rheological laws were used, instead of that of quartz-diorite. Nevertheless, orthogneisses apparently dominate at lower levels of the Cyclades rock pile, as seen on Naxos, Paros and Ios (e.g. van der Maar & Jansen 1983; Gautier *et al.* 1993), therefore the choice of quartz diorite as the representative rock type for the Central Aegean crust as a whole seems justified (see also Jolivet *et al.* 2003, 2004).

As mentioned before, Naxos and Paros Islands are asymmetric domes that consistently display top-to-north shear criteria. These kinematics are observed from the envelope of the domes (Gautier *et al.* 1993) down to the migmatitic core of Naxos (Buick 1991) and the poorly defined migmatitic domain of Paros (Gautier *et al.* 1993). Hence, in the Cyclades, the largest MCCs, associated with the most pronounced exhumation, do not display evidence of inward flow emanating from the rear part of the dome (that is, inward flow that would produce shearing antithetic to the main detachment zone) whereas, according to the interpretation of Gautier & Brun (1994*a*, *b*), less mature MCCs do so. This may be viewed as a paradox, however, the present experiments show that it is not. As seen on Figure 5, SZ1, which relates to this antithetic inward flow toward the main dome, is pronounced but confined to great depths and, unlike SZ2, never reaches the surface. In contrast, in the case of the secondary dome, the two limbs coincide with antithetic shear zones that extend upward the two flat-lying shear zones (SZ11 and SZ12) developed in response to renewed inward flow. As a consequence, the secondary dome tends to be symmetric, and it can be expected that no dominant sense of shear will be found around its apex. These features compare relatively well with the case of Ios and Syros Islands (see 'How many MCC...' section). As mentioned in 'Analysis of the two experiments' section, SZ12 reactivates SZ1 in opposite sense but with less strain accumulated, therefore it can be expected that relics of the first kinematics will be found along SZ12. While assuming that the Ios MCC was controlled by a north-dipping detachment, Gautier & Brun (1994*b*) suggested that this feature may explain the predominance of top-to-south shearing across the Ios dome (that is, top-to-south shearing would in part reflect early inward flow in the rear flank of the Naxos MCC). However, because the relations between top-to-south and top-to-north shearing are unclear on Ios (see 'How many MCC...' section), we leave it open whether this hypothesis makes sense. The same applies to Syros, which is possibly dominated by coaxial deformation, but where there is no indication of an early top-to-SW shearing event that would be overprinted by top-to-NE shearing (e.g. Trotet *et al.* 2001*a*; see 'How many MCC...' section).

Summarizing, both the geometry (cf. previous section) and the kinematic pattern of MCCs compare well between the experiments and the Naxos–Ios and Tinos–Syros island pairs (Fig. 9). In both cases, the comparison holds for two among three chains of islands, and, thus, seems to ignore the Ikaria–Samos and Kea–Sifnos chains. It should be reminded that, in the experiments with interfering MCCs, additional MCCs do develop (see 'Description of two experiments' section), located at far distance from the MCCs under discussion, so that the former do not interfere with the latter (i.e. they are not superimposed nor they rework earlier shear zones). We tentatively suggest that the Ikaria–Samos and Kea–Sifnos chains, which lie relatively far from the other chains, coincide with these non-interfering MCCs.

Timing of exhumation. The simulations and the Cyclades are now compared in terms of chronology using two approaches. Firstly, the comparison may concern the total time elapsed from the onset of post-orogenic extension until the time the development of all MCCs has reached an end. The latter bound is not equivalent to the end of the extensional process because lithospheric stretching may persist due to unchanged boundary conditions. However, due to crustal thinning, the style of extension is expected to change, and the development of MCCs to be arrested (e.g. Buck 1991), which is indeed what we observe in the experiments (see also Tirel *et al.* 2008). The amount of time defined in this way is here termed the duration of MCC-type extension. In the experiments, within the range of conditions giving rise to interfering MCCs, the duration of MCC-type extension varies between 16 and 32 Ma (Fig. 7). In the Cyclades, it can be estimated as follows: for the onset of post-orogenic extension, following the discussion in 'Post-orogenic vs. syn-orogenic extension' section, we take 30 Ma (e.g. Parra *et al.* 2002; Jolivet *et al.* 2004) as the earliest possible date, which is consistent with the record in the nearby Menderes massif (Thomson & Ring 2006; Ring *et al.* 2007*b*). The latest possible date is *c.* 23 Ma (Gautier & Brun 1994*a*; Bröcker & Franz 1998, 2005, 2006). As for the end of MCC-type extension, a change in structural style seems indeed recorded in the Cyclades during the late Miocene, when regional-scale high-angle faulting, bounding Messinian–Quaternary basins, succeeded to fast cooling of the metamorphic domes, vanishing in the time range *c.* 11–6 Ma (Gautier & Brun 1994*a*; Sánchez-Gómez *et al.* 2002; Hejl *et al.* 2002, 2003; Kumerics *et al.* 2005; Iglseder *et al.* 2006; Brichau *et al.* 2006, 2007). This is in line with the Messinian age for the oldest sediments nonconformably covering the metamorphic series on Milos (van Hinsbergen *et al.* 2004). We thus set the end of MCC-type extension in between 11 and 6 Ma. It is worth noting that the youngest evidence of fast cooling in the footwall of a low-dipping detachment is provided by islands largely made up of a young I-type intrusion, like Ikaria, Serifos, Mykonos and the western part of Naxos (Altherr *et al.* 1982; Hejl *et al.* 2002, 2003; Kumerics *et al.* 2005; Iglseder *et al.* 2006; Brichau *et al.* 2006). It is therefore possible that arc magmatism locally had the capacity of delaying the end of MCC-type extension by a few million years, although Brichau *et al.* (2006) argue that, on Naxos, the intrusion of the *c.* 12 Ma-old granodiorite had a negligible effect on the kinetics of the detachment system. Combining the above dates, the duration of MCC-type extension in the Cyclades is between 12 and 24 Ma, in good agreement with the experimental range. It is compatible with any initial crustal thickness in the range of 40–50 km (Fig. 7c) while it seems to exclude a boundary velocity lower than *c.* 1.7 cm/a (Fig. 7d).

Secondly, the comparison may concern the relative timing of MCC development along a section parallel to stretching, as in the case of the Naxos–Ios and Tinos–Syros island pairs. In the experiments (and in the scenario favoured by Gautier & Brun 1994*b*), the second dome starts to develop once the first dome has achieved much of its exhumation (Fig. 5). This suggests that the period of fastest cooling in the first dome should predate that in the second dome. For instance, in Figure 5a, the first dome experiences fast cooling between the time slices 7.0 Ma and 11.4 Ma, while the second dome does so later, until about 17.4 Ma. At first sight, this relation seems to imply that cooling ages should be older in the first dome. However, this is not necessarily correct, because the amount of exhumation is also different between the two domes. In Figure 5a, at 7.0 Ma, the green layer is approximately bounded by the isotherms 350 and 550 °C, therefore it represents rocks in greenschist facies conditions. Rb–Sr white mica ages from this layer would normally date this stage at 7.0 Ma. Considering the range of estimates for the closure temperature of argon in white mica, between about 330 and 450 °C (e.g. Wijbrans & McDougall 1988; Kirschner *et al.* 1996), $^{40}Ar/^{39}Ar$ white mica ages from this layer should also broadly date the stage at 7 Ma, or possibly the stage at 11.4 Ma, when at least the upper half of the green layer lies above the 350 °C isotherm. In the first dome, the greenschist facies layer, together with deeper rocks, are fastly exhumed within the same time range, from 7.0 to 11.4 Ma. The same relations are observed in Type 2 experiment. At the end of MCC-type extension, especially in Type 2 experiment (Fig. 5d), the second dome exposes only rocks of the greenschist facies layer, therefore white mica ages from this dome are expected to be not significantly different from white mica ages and higher temperature chronometers (e.g. U–Pb on zircon, $^{40}Ar/^{39}Ar$ on hornblende) from the first dome (e.g. in Fig. 5, within the time range from 7.0 to 11.4 Ma, i.e. within ≤ 4.4 Ma). Moreover, Figure 5b shows that, at the same time the second dome rises, shearing is still active along the frontal detachment of the first dome (cf. the stage 17.4 Ma). Hence, cooling ages from this frontal segment of the first dome are expected to be as young as the cooling ages of the second dome. Altogether, these relations suggest that there is not necessarily a significant difference to be expected in the geochronological record of the two domes. The only marked difference should concern the period of fastest cooling, however it is possible that the second dome does not raise enough to allow a proper documentation of this fast cooling period on geochronological grounds.

On Naxos, a period of fast cooling is recorded in the migmatitic core and amphibolite facies inner envelope of the dome in between ca. 16 and 8 Ma (Wijbrans & McDougall 1988; Gautier *et al.* 1993), following an anatectic event that lasted from at least 20 Ma until *c.* 17 Ma (Keay *et al.* 2001). The period of fastest exhumation probably occurred between the end of the anatectic event and the emplacement of the Western Naxos Granodiorite (Gautier *et al.* 1993), that is, beween about 17 and 12 Ma according to the data of Keay *et al.* (2001). S-type granites emplaced in the inner envelope of the dome at 15.5–12 Ma (Keay *et al.* 2001), possibly as a result of decompression melting at deeper levels of the rock pile during fast exhumation. Ongoing core complex development after 12 Ma is indicated by the syn-kinematic character of the Western Naxos Granodiorite with respect to the north-dipping detachment zone, and by the subsequent development of massive cataclasites along the contact between the two (Urai *et al.* 1990; Buick 1991; Gautier *et al.* 1993). A pseudotachylite vein from this contact is dated at 10 Ma (Andriessen *et al.* 1979). According to Brichau *et al.* (2006), brittle shearing along the detachment occurred as late as 8.2 ± 1.2 Ma, based on low-temperature thermochronology. As mentioned above, the intrusion of a large amount of arc-related magma (i.e. the Western Naxos Granodiorite) may have sustained the development of the Naxos MCC for a longer time, although this is not the hypothesis favoured by Brichau *et al.* (2006). As a fact, the two youngest ages obtained by Brichau *et al.* (2006) come from the northern part of the metamorphic dome, seemingly far from the granodiorite. This area also yields the youngest K–Ar and $^{40}Ar/^{39}Ar$ hornblende and biotite ages from the dome (Andriessen *et al.* 1979; Wijbrans & McDougall 1988), a feature that it is tempting to attribute to progressive northward migration of unroofing in the footwall of the detachment (Gautier *et al.* 1993; Brichau *et al.* 2006). However, this could also result from the emplacement of the Western Naxos Granodiorite or an equivalent young intrusion beneath this area, as proposed by Andriessen *et al.* (1979), Wijbrans & McDougall (1988) and Keay *et al.* (2001). Such an intrusion actually exists, as indicated by the local occurrence in northernmost Naxos of a hornblende-bearing I-type granite dated at *c.* 12 Ma (Keay *et al.* 2001). Hence, it is possible that ongoing development of the Naxos MCC after 12 Ma has occurred owing to the emplacement of arc-related magmas.

In the rear part of the dome, rocks that did not experience temperatures higher than 550 °C were at about 500 °C at *c.* 22.5–20 Ma and cooled to about 300 °C at *c.* 14–11 Ma (Andriessen *et al.* 1979; Wijbrans & McDougall 1988; Andriessen 1991).

The cooling history of the Ios MCC is not well constrained. A ^{40}Ar/^{39}Ar white mica pseudo-plateau age at about 20.5 Ma is considered to date shearing along the South Cyclades shear zone (Baldwin & Lister 1998). A Rb-Sr white mica age from a deformed aplitic vein at 13.2 ± 0.4 Ma (Henjes-Kunst & Kreuzer 1982) together with ^{40}Ar/^{39}Ar potassium feldspar minimum apparent ages at about 14 Ma from mylonitic augengneiss (Baldwin & Lister 1998) date another (distinct?) shearing event (vandenberg & Lister 1996; Baldwin & Lister 1998). This second event is suspected to reflect the influence of the mid-Miocene magmatism of the Cyclades, yet, so far, there is no clear evidence for any Miocene intrusion on Ios. Hence, the ages at 13–14 Ma may relate to deformation without a specific thermal event. Apatite fission track ages indicate cooling below about 100 °C between 13.3 ± 1.1 and 8.3 ± 1.1 Ma (Hejl *et al.* 2003). Comparing the geochronological record on Naxos and Ios, we find no significant diachronism. As explained above, because the Ios MCC is associated with much less exhumation, this observation is not incompatible with the Ios dome having formed later.

On Tinos, ^{40}Ar/^{39}Ar and Rb–Sr ages on white mica indicate that greenschist facies top-to-NE extensional shearing occurred at about 24–21 Ma (Bröcker & Franz 1998, 2005). The detachment zone is crosscut by the Tinos composite intrusion and associated thermal aureole (Altherr *et al.* 1982; Avigad & Garfunkel 1989; Bröcker & Franz 2000). Rb–Sr and K–Ar ages from the main I-type granite (Altherr *et al.* 1982; Avigad *et al.* 1998) and its thermal aureole (Bröcker & Franz 2000) suggest an early cooling at 15.5–14 Ma. Whole-rock Rb–Sr dating indicates that marginal S-type intrusions emplaced at the same time (Altherr *et al.* 1982; Bröcker & Franz 1998). Altherr *et al.* (1982) originally argued that the main granite probably emplaced before 17 Ma, however available radiometric data are compatible with the view that it did so at around 15 Ma (see discussion in Bröcker & Franz 2000). Recent U–Pb dating of zircons from the main intrusion has yielded an age of 14.6 ± 0.2 Ma (Brichau *et al.* 2007), supporting the latter view. On the one hand, this indicates that much of the displacement along the detachment zone occurred before 15 Ma. On the other hand, the margins of the plutonic complex show evidence of top-to-NE shearing during and subsequent to emplacement (Gautier & Brun 1994*a*; Bröcker & Franz 1998; Jolivet & Patriat 1999; Brichau *et al.* 2007). A series of subvertical NW–SE-trending dykes dated at 12–11 Ma (Avigad *et al.* 1998) documents ongoing NE–SW stretching once the rocks reached the brittle upper crust (see also Mehl *et al.* 2005). Final cooling at around 12–9 Ma is documented by apatite fission track ages from the main intrusion (Altherr *et al.* 1982; Hejl *et al.* 2002; Brichau *et al.* 2007). It is difficult to establish whether, and when, a period of fastest exhumation occurred on Tinos, especially because it is not clear where the ages of 24–21 Ma should be plotted along the greenschist facies segment of the pressure–temperature path. If, however, a closure temperature of about 500 °C is accepted for the Rb–Sr system in white mica (Bröcker & Franz 1998, 2005), then, using the path obtained by Parra *et al.* (2002), this age range should coincide with pressures around 6 kbar. Pressures associated with the thermal aureole of the *c.* 15 Ma-old Tinos intrusion are around 2–3 kbars (e.g. Bröcker & Franz 2000). Taken together, using a factor of 3.64 to convert pressures (kbar) into depths (km), these values yield a mean exhumation rate around 1.5–2 mm/a during the period from *c.* 22 to 15 Ma. The apatite fission track ages indicate that later exhumation was slower. If the earlier episode of heating at about 9 kbar ended at *c.* 30 Ma, as suggested by Parra *et al.* (2002) (see 'Post-orogenic versus syn-orogenic extension' section), then a mean exhumation rate around 1.4 mm/a is suggested for the period from *c.* 30 to 22 Ma. These estimates are crude, nevertheless they suggest that exhumation proceeded either at constant rate from *c.* 30 Ma to 15 Ma, or was a bit faster during the 22–15 Ma interval.

The cooling history of Syros is very poorly known. At least part of the displacement along the detachment seen in southeastern Syros occurred later than 30 Ma (see 'Interfering detachment systems' section). Zircon fission track ages are around 20 Ma in the hanging wall and around 11 Ma in the footwall, suggesting that the detachment was active at *c.* 11 Ma (Ring *et al.* 2003). All the footwall samples come from northern Syros, so that it is not clear whether the age gap of 9 Ma reflects displacement along the detachment itself or/and along one of the low-angle normal faults that dissect the footwall (Ridley 1984). Summing up, a sound comparison between Tinos and Syros is out of reach so far, nevertheless available radiometric data leave it possible that the Tinos MCC formed earlier.

The above review also indicates that the two island pairs (Naxos–Ios and Tinos–Syros) may have formed contemporaneously. The Naxos MCC experienced its fastest exhumation between *c.* 17 and 12 Ma, while the Tinos MCC may have done so between *c.* 22 and 15 Ma. Thus, the two MCCs could be broadly coeval. In contrast, Jolivet *et al.* (2004) claimed that the Naxos MCC has formed *c.* 5 Ma later than the Tinos MCC has. They further proposed that, in the Cyclades, 'a-type' MCCs (domes with an axis parallel to extension, like on Naxos) are associated with greater exhumation and formed later than 'b-type' MCCs (domes with an axis perpendicular to extension, like on Tinos). This interpretation largely arises from the assumption that the main intrusion on Tinos emplaced as early as 20–19 Ma, as initially proposed by Altherr *et al.* (1982). As stated above, however, available radiometric data make it possible that the whole composite intrusion of Tinos emplaced at *c.* 15 Ma. We also notice that the Ios MCC is clearly a 'a-type' dome (e.g. Gautier & Brun 1994*a*; Vandenberg & Lister 1996), yet, at variance with the hypothesis of Jolivet *et al.* (2004), it did not exhume higher grade rocks than the Tinos MCC did, and recorded extensional shearing as early as *c.* 20.5 Ma (Baldwin & Lister 1998), that is, at the same time as on Tinos.

Implications for the conditions of extension in the Cyclades

Insofar as the numerical experiments presented in this study adequately simulate the process of lithospheric extension, their comparison with the case of the Cyclades suggests a relatively narrow range of conditions for the development of post-orogenic extension in the Central Aegean region during the late Cenozoic. We now review and discuss these conditions.

Conditions at the onset of post-orogenic extension. A first inference concerns the mean thickness of the crust at the onset of post-orogenic extension. The present crustal thickness of 25–26 km in the Cyclades suggests an initial thickness of *c.* 43–44 km (see 'Moho depth' section and Fig. 7e), in line with the range of *c.* 41–44 km suggested by the width of the Naxos and Paros first-generation MCCs (see 'Geometry of MCCs' section and Fig. 7a). These values are consistent with (rough) estimates in the literature (e.g. McKenzie 1978; Le Pichon & Angelier 1979; Gautier *et al.* 1999) and compare well with the current crustal thickness of $\leq$ 46km in the western Hellenides of mainland Greece (Makris 1975), where extension has played only a minor role.

A second inference concerns the thermal state of the lithosphere at the onset of extension. The numerical experiments suggest an initial thickness of the thermal lithosphere of only *c.* 60 km (corresponding to an initial Moho temperature of 1070 °C at 44 km). Measurements of the present heat flow in the Aegean (Jongsma 1974; Erickson *et al.* 1977; Makris & Stobbe 1984) document the presence of a hot lithosphere. Seismic surface-wave data are consistent with a lithosphere-asthenosphere boundary at a depth between 40 and 50 km (Endrun *et al.* 2008) and, thus, with a high thermal profile of the lithosphere at present. As for the thermal state of the Aegean lithosphere at the onset of post-orogenic extension, it may be deduced from the pressure-temperature path of metamorphic rocks involved in the MCCs.

Figure 10 displays the well-documented cases of Naxos (data from the migmatitic core of the MCC) and Tinos. In the latter case, only the second episode of exhumation is considered (cf. Parra *et al.* 2002) as this is the most likely to reflect post-orogenic extension (see 'Post-orogenic *vs.* syn-orogenic extension' section). Figure 10 also displays the geotherm associated with an experiment in which the thermal lithosphere is 60 km-thick. The figure shows that, for Naxos, the conditions at the temperature peak coincide with the numerical geotherm. For Tinos, the 'post-orogenic' exhumation path starts away from this geotherm and crosses it at conditions equivalent to a pressure of 5 kbar. Geochronological constraints (see sections 'Post-orogenic *vs.* syn-orogenic extension' and Timing of exhumation') suggest that this happens at about the same time (*c.* 21 Ma) as the attainment of peak temperatures on Naxos (Fig. 10). Therefore, at this time, Tinos and Naxos plot together along the numerical geotherm. On the one hand, this confirms that a lithosphere only *c.* 60 km-thick is a realistic condition at relatively early stages of post-orogenic extension in the Cyclades. On the other hand, the conditions at the onset of the second episode of exhumation on Tinos (550 °C at 9 kbar; Parra *et al.* 2002) imply a fairly low geothermal gradient (16.8 °C/km) and plot along a numerical geotherm corresponding to a 100 km-thick lithosphere (dashed line in Fig. 10). Insofar as the entire secondary exhumation on Tinos reflects post-orogenic extension, this indicates that the earliest stages of this extension occurred while the lithosphere was still thick. The exhumation paths of both Tinos and Naxos are consistent with the view that this lithosphere has been warmed up until the time it attained the conditions enabling the development of interfering MCCs (i.e. a *c.* 60 km-thick lithosphere), at *c.* 21 Ma. In any case, much of the post-orogenic extensional phase and, within it, the period of development of MCCs occurred while the lithosphere was thin and hot. This is shown by our numerical results and is also in line with several other numerical studies (Block & Royden 1990; Buck 1991; Tirel *et al.* 2004*a*, 2008; Rosenbaum *et al.* 2005; Wijns *et al.* 2005; Gessner *et al.* 2007). In Figure 10, latest stages of the exhumation paths suggest the existence of geotherms even higher than the one associated with a 60 km-thick lithosphere. This may reflect the

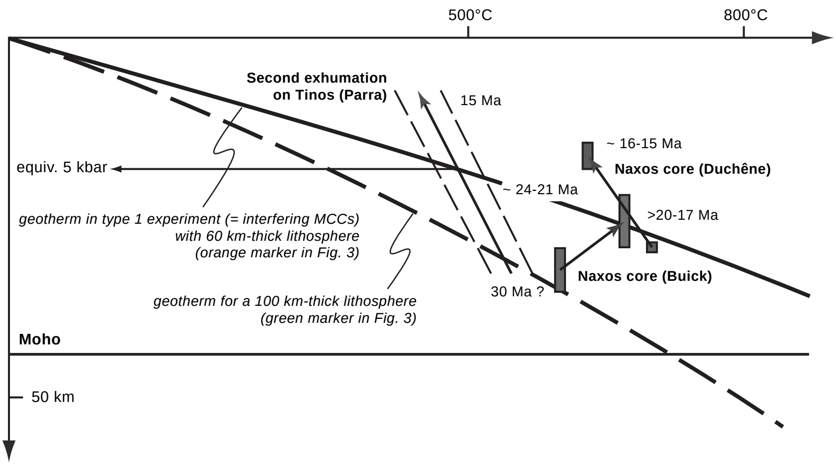

Fig. 10. Comparison between the geotherms associated with two numerical experiments and the exhumation path of metamorphic rocks on Tinos (after Parra *et al.* 2002) and Naxos (after Buick & Holland 1989 and Duchêne *et al.* 2006). A factor of 3.64 was used to convert pressures (kbar) into depths (km). Age constraints are discussed in sections 'Post-orogenic versus syn-orogenic extension' and 'Timing of exhumation'.

ongoing increase of the regional geothermal gradient or/and the local rise of isotherms during MCC development (see 'Geometry of MCCs' section and Gessner *et al.* 2007).

Recently, several studies have shown evidence for a high temperature regime in the shallow mantle and a thin lithosphere (1200 °C at a depth of *c*. 60 km) over widths of 250 to >900 km in several subduction zone back-arc domains unaffected by extensional processes (Currie *et al.* 2004; Hyndman *et al.* 2005; Currie & Hyndman 2006). The authors suggest that heat is rapidly carried upward by vigorous thermal convection in the upper mantle below the overriding plate. This small-scale convection could be promoted by the low viscosities associated with the addition of water, resulting in a reduction of the strength of the base of the lithosphere and its rapid 'erosion' (Arcay *et al.* 2005, 2006). The Cyclades area may have been affected by such processes prior to *c*. 21 Ma (i.e. while warming the lithosphere until its thickness was reduced to *c*. 60 km, cf. Fig. 10) provided it was already lying in the back-arc domain of the South Hellenic subduction zone at that time, which is a matter of debate (e.g. Ring & Layer 2003; Jolivet *et al.* 2004; Pe-Piper & Piper 2006).

Alternatively, the pioneering suggestion of Bird (1978) concerning continental mantle delamination as a cause of strong heating of the crust appears attractive. In the Aegean, this process was first suggested by Zeilinga de Boer (1989) and has been explicitely invoked in a number of recent studies (Thomson *et al.* 1999; Jolivet *et al.* 2003; Faccenna *et al.* 2003; Ring & Layer 2003). Support to this hypothesis is found in a recent review of the late Cenozoic magmatism of the Aegean by Pe-Piper & Piper (2006), as discussed below.

Boundary velocity during MCC-type extension in the Cyclades. In the experiments, the range of boundary velocities which succesfully led to a sequential development of interfering MCCs lies between 1 and 2.7 cm/a. In addition, the present crustal thickness of 25–26 km in the Cyclades suggests a velocity of *c*. 2.0–2.3 cm/a (see 'Moho depth' section and Fig. 7f), while the width of the Naxos and Paros first-generation MCCs (see 'Geometry of MCCs' section) and the duration of MCC-type extension in the Cyclades (see 'Timing of exhumation' section) seem to exclude values lower than *c*. 2 cm/a (Fig. 7b) and *c*. 1.7 cm/a (Fig. 7d), respectively. Hence, the experimental results predict a velocity at the boundary of the stretching domain around 2.0–2.3 cm/a, while lower values seem excluded.

In the case of the Cyclades, this velocity should correspond to the rate at which the South Hellenic subduction retreated during MCC-type extension. In addition, as MCC-type extension in the Cyclades lasted between about 12 and 24 Ma (from 30–23 to 11–6–Ma, see 'Timing of exhumation' section), the associated amount of retreat is predicted to lie between about 240 km (for 12 Ma at 2 cm/a) and 550 km (for 24 Ma at 2.3 cm/a).

These values can be compared with various estimates in the literature. For instance, Faccenna *et al.* (2003) have considered 250 km of retreat during the period from 30 to 5 Ma, hence at a velocity of only 1 cm/a. In contrast, a retreat velocity as high as 3 cm/a has been proposed by Jolivet *et al.* (1998) on the basis of the southward migration of arc magmatism since *c*. 32 Ma (Fytikas *et al.* 1984), assuming the underlying slab kept a constant dip. However, the graph from which this value is deduced (Jolivet *et al.* 1998, Fig. 21b) actually yields a value of about 2.2 cm/a and considers 700 km of migration of arc magmatism, which exceeds by at least 100 km the actual value. Instead, considering about 550 km of migration of magmatism since about 32 Ma (see van Hinsbergen 2004 for a recent compilation) would yield a retreat velocity of 1.7 cm/a, in fair agreement with our numerical analysis. However, among the 550 km of migration, as much as 90 km may be considered as balanced, not by extensional strain but by the lateral extrusion of Anatolia during the last few million years (e.g. Gautier *et al.* 1999), which could lower the boundary velocity of the extensional system to 1.4 cm/a. It is also worth noting that the migration of magmatism is not an ideal mean for quantifying retreat, firstly because the assumption of a constant slab dip may not be valid, and secondly because not every magmatic rock may reflect arc magmatism. Pe-Piper & Piper (2006) recently argued that most Cenozoic magmatic rocks of the Aegean bear petrogeochemical characteristics that are not typical of arc processes and suggest instead that they reflect either slab break-off or delamination of the lithospheric mantle. At first sight, this seems to exclude the migration of magmatism as an appropriate tool to document subduction retreat. However, tomography images of the Aegean mantle are clearly more compatible with progressive delamination of a continuous slab (*sensu* Bird 1978) rather than break-off of several slabs (e.g. Faccenna *et al.* 2003; van Hinsbergen *et al.* 2005*a*). The dynamics of mantle delamination is broadly equivalent to that of a retreating subduction, therefore the migration of delamination-related magmatism may actually be appropriate to quantify retreat (e.g. Zeilinga de Boer 1989).

Another estimate of the amount of retreat may arise from a comparison between the initial and present shape of the Aegean frontal arc. For instance, Gautier *et al.* (1999) suggested a smoothly curved arc at the onset of Aegean extension, which led them to propose about 440 km of retreat (of which 90 km would be balanced by the lateral extrusion of Anatolia, leaving 350 km to be balanced by extensional strain). The end-member case leading to maximum retreat is probably that of an initially rectilinear arc. Using the same arc extremities as in Gautier *et al.* (1999), this case would yield about 600 km of retreat, in reasonable agreement with the value suggested by the migration of magmatism. This would yield about 510 km balanced by extensional strain. If we assume that retreat occurred essentially during MCC-type extension in the Cyclades, then the boundary velocity of the extensional system could have been as high as 2.1 cm/a if extension lasted 24 Ma (starting at *c*. 30 Ma), in good agreement with our numerical analysis, or as high as 4.2 cm/a if extension lasted 12 Ma (starting at *c*. 23 Ma). The latter value is clearly too high and suggests that MCC-type extension in the Cyclades started significantly before 23 Ma or/and that the total amount of retreat has been significantly less than in the above end-member case, or/and that a significant part of the retreat occurred before or/and after MCC-type extension in the Cyclades.

Conclusions

Our numerical analysis suggests that, for certain conditions, MCCs may interfere and develop in sequence during continental extension. Like common claims in the literature, we find that 'inward' flow of an extremely weak lower crust is required for MCCs to develop, while a sub-Moho mantle of very low strength appears to be another necessary condition for maintaining the Moho flat. As a result of lower crustal inward flow, two conjugate flat-lying shear zones form during the early development of the first MCC, one of which later evolves as a typical detachment. In the experiments with interfering MCCs, the second MCC starts to develop right above one of the previously formed shear zones. This shear zone is dragged upward during dome amplification and, due to renewed inward flow, is reactivated with the same kinematics along one dome limb and with the opposite kinematics along the other dome limb.

The Cyclades archipelago is characterized by three closely spaced chains of MCCs developed largely during Miocene extension. We found that the geometry and kinematic pattern of adjacent MCCs along the Naxos–Ios and the Tinos–Syros transects compare well with the numerical experiments. Available geochronological data for these islands are not detailed enough to document a sequential development of MCCs, nevertheless they remain compatible with this hypothesis. We also compared features of the numerical experiments, such as the final Moho depth, the duration of MCC-type extension, and the width of the domes at the end of the exhumation process, to equivalent features in the Cyclades in order to tentatively constrain the initial and boundary conditions suitable to the Aegean case. This comparison leads us to infer a crustal thickness in the range of 40 to 44 km in the Cyclades at the onset of post-orogenic extension. A thermal lithospheric thickness of only *c*. 60 km is also inferred, which might be a condition at the onset of extension or may have been obtained during early stages of extension while the lithosphere was warmed up. Either a backarc subduction setting or a process of mantle delamination may account for this situation.

The experiments also suggest a boundary velocity of 2.0–2.3 cm/a, which should basically reflect the rate at which the South Hellenic subduction zone retreated. Considering *c*. 500 km as an upper bound for the amount of retreat balanced by Aegean extension, and assuming that this retreat mostly occurred during MCC-type extension, in the Cyclades, the boundary velocity could have been as high as 2.1 cm/a (if MCC-type extension lasted 24 Ma, starting at *c*. 30 Ma and finishing at *c*. 6 Ma): this is in good agreement with the numerical analysis.

The post-doctoral grant of C.T. and computational resources were funded by ISES (Netherlands Research Centre for Integrated Solid Earth Science). C.T. thanks E. Burov, Y. Podladchikov and A. Poliakov who have co-developed the kernel of PARAVOZ. D. J. J. v. H. is funded through an NWO-VENI grant. We thank R. Govers, J.-P. Brun and E. Burov for discussions at various stages of the project. We gratefully acknowledge the editor, M. Edwards, and the two reviewers S. Buiter and M. Bröcker for their thoughtful reviews that improved our manuscript.

References

ALTHERR, R., KREUZER, H., WENDT, I., LENZ, H., WAGNER, G. A., KELLER, J., HARRE, W. & HÖHNDORF, A. 1982. A Late Oligocene/Early Miocene high temperature belt in the Attic-Cycladic crystalline complex (SE Pelagonian, Greece). *Geologisches Jahrbuch*, **E23**, 97–164.

ALTHERR, R., SCHLIESTEDT, M., OKRUSCH, M., SEIDEL, E., KREUZER, H., HARRE, W., LENZ, H., WENDT, I. & WAGNER, G. A. 1979. Geochronology of High-Pressure Rocks on Sifnos (Cyclades, Greece). *Contributions to Mineralogy and Petrology*, **70**, 245–255.

ANDRIESSEN, P. A. M. 1991. K-Ar and Rb-Sr age determinations on micas of impure marbles of Naxos, Greece: the influence of metamorphic fluids and lithology on the blocking temperature. *Schweizerische Mineralogische and Petrographische Mitteilungen*, **71**, 89–99.

ANDRIESSEN, P. A. M., BOELRIJK, N. A. I. M., HEBEDA, E. H., PRIEM, H. N. A., VERDURMEN, E. A. T. & VERSCHURE, R. H. 1979. Dating the events of metamorphism and granitic magmatism in the Alpine Orogen of Naxos (Cyclades, Greece). *Contributions to Mineralogy and Petrology*, **69**, 215–225.

ANGELIER, J. 1977*a*. Sur l'évolution tectonique depuis le Miocène supérieur d'un arc insulaire méditerranéen: l'arc égéen. *Revue de Géographie physique et Géologie dynamique*, **XIX**, 271–294.

ANGELIER, J. 1977*b*. Essai sur la néotectonique et les derniers stades tarditectoniques de l'arc égéen et de l'Egée méridionale. *Bulletin de la Societé Géologique de France*, **XIX**, 651–662.

ANGELIER, J., GLACON, G. & MULLER, C. 1978. Sur la présence et la position tectonique du Miocène inférieur marin dans l'archipel de Naxos (Cyclades, Grèce). *Comptes Rendus de l'Académie des Sciences de Paris*, **286**, 21–24.

ARCAY, D., TRIC, E. & DOIN, M.-P. 2005. Numerical simulations of subduction zones. Effect of slab deshydration on the mantle wedge dynamics. *Physics of the Earth and Planetary Interiors*, **149**, 133–153.

ARCAY, D., DOIN, M.-P., TRIC, E., BOUSQUET, R. & DE CAPITANI, C. 2006. Overriding plate thinning in subduction zones: Localized convection induced by slab deshydration. *Geochemistry Geophysics Geosystems*, **7**, doi:10.1029/2005GC0011061.

AVIGAD, D. 1993. Tectonic juxtaposition of blueschists and greenschists in Sifnos Islands (Aegean Sea)—implications for the structure of the Cycladic blueschist belt. *Journal of Structural Geology*, **15**, 1459–1469.

AVIGAD, D. & GARFUNKEL, Z. 1989. Low angle faults above and below a blueschist belt—Tinos Island, Cyclades, Greece. *Terra Nova*, **1**, 182–187.

AVIGAD, D., GARFUNKEL, Z., JOLIVET, L. & AZAÑON, J. M. 1997. Backarc extension and denudation of Mediterranean eclogites. *Tectonics*, **16**, 924–941.

AVIGAD, D., BAER, G. & HEIMANN, A. 1998. Block rotations and continental extension in the central Aegean Sea: palaeomagnetic and structural evidence from Tinos and Mykonos (Cyclades, Greece). *Earth and Planetary Science Letters*, **157**, 23–40.

AVIGAD, D., ZIV, A. & GARFUNKEL, Z. 2001. Ductile and brittle shortening, extension-parallel folds and maintenance of crustal thickness in the central Aegean (Cyclades, Greece). *Tectonics*, **20**, 277–287.

BALDWIN, S. L. & LISTER, G. S. 1998. Thermochonology of the South Cyclades Shear Zone, Ios, Greece: Effects of ductile shear in the argon partial retention zone. *Journal of Geophysical Research*, **103**, 7315–7336.

BIRD, P. 1978. Initiation of intracontinental subduction in the Himalaya. *Journal of Geophysical Research*, **83**, 4975–4987.

BLOCK, L. & ROYDEN, L. H. 1990. Core complex geometries and regional scale flow in the lower crust. *Tectonics*, **9**, 557–567.

BOND, C. E., BUTLER, R. W. H. & DIXON, J. E. 2007. Co-axial horizontal stretching within extending orogens: the exhumation of HP rocks on Syros (Cyclades) revisited. *In*: RIES, A. C., BUTLER, R. W. H. & GRAHAM, R. H. (eds) *Deformation of the Continental Crust: The Legacy of Mike Coward*. Geological Society, London, Special Publication, **272**, 203–222.

BONNEAU, M. 1982. Evolution géodynamique de l'arc égéen depuis le Jurassique supérieur jusqu'au Miocène. *Bulletin de la Societé Géologique de France*, **XXIV**, 229–242.

BOZKURT, E. 2001. Late Alpine evolution of the central Menderes Massif, western Turkey. *International Journal of Earth Sciences*, **89**, 728–744.

BRICHAU, S., RING, U., KETCHAM, R. A., CARTER, A., STOCKLI, D. & BRUNEL, M. 2006. Constraining the long-term evolution of the slip rate for a major extensional fault system in the central Aegean, Greece, using thermochronology. *Earth and Planetary Science Letters*, **241**, 293–306.

BRICHAU, S., RING, U., CARTER, A., MONIÉ, P., BOLHAR, R., STOCKLI, D. & BRUNEL, M. 2007. Extensional faulting on Tinos Island, Aegean Sea, Greece: How many detachments? *Tectonics*, **26**, TC4009, doi:10.1029/2006TC001969.

BRÖCKER, M. 1990. Blueschist-to-greenschist transition in metabasites from Tinos Island (Cyclades, Greece): Compositional control or fluid infiltration? *Lithos*, **25**, 25–39.

BRÖCKER, M. & FRANZ, L. 1998. Rb–Sr isotope studies on Tinos Island (Cyclades, Greece): additional time constraints for metamorphism, extent of infiltration-controlled overprinting and deformational activity. *Geological Magazine*, **135**, 369–382.

BRÖCKER, M. & FRANZ, L. 2000. The contact aureole on Tinos (Cyclades, Greece): tourmaline-biotite geothermometry and Rb-Sr geochronology. *Mineralogy and Petrology*, **70**, 257–283.

BRÖCKER, M. & FRANZ, L. 2005. The base of the Cycladic blueschist unit on Tinos Island (Greece) re-visited: Field relationships, phengite chemistry and Rb–Sr geochronology. *Neues Jahrbuch für Mineralogie, Abhandlungen*, **181**, 81–93.

BRÖCKER, M. & FRANZ, L. 2006. Dating metamorphism and tectonic juxtaposition on Andros Island (Cyclades, Greece): results of a Rb–Sr study. *Geological Magazine*, **143**, 1–12.

BRÖCKER, M., BIELING, D., HACKER, B. & GANS, P. B. 2004. High-Si phengite records the time of greenschist facies overprinting: implications for models suggesting mega-detachments in the Aegean Sea. *Journal of Metamorphic Geology*, **22**, 427–442.

BRUN, J.-P., SOKOUTIS, D. & VAN DEN DRIESSCHE, J. 1994. Analogue modeling of detachment fault systems and core complexes. *Geology*, **22**, 319–322.

BRUN, J.-P. & VAN DEN DRIESSCHE, J. 1994. Extensional gneiss domes and detachment fault systems; structure and kinematics. *Bulletin de la Societé Géologique de France*, **165**, 519–530.

BUCK, W. R. 1991. Modes of continental lithospheric extension. *Journal of Geophysical Research*, **96**, 20161–20178.

BUICK, I. S. 1991. The late Alpine evolution of an extensional shear zone, Naxos, Greece. *Journal of the Geological Society of London*, **148**, 93–103.

BUICK, I. S. & HOLLAND, T. J. B. 1989. The P-T-t path associated with crustal extension, Naxos, Cyclades, Greece. *In*: DALY, J. S., CLIFF, R. A. & YARDLEY, B. W. D. (eds) *Evolution of Metamorphic Belts*. Geological Society, London, Special Publication, **43**, 365–369.

BURG, J. P., VAN DEN DRIESSCHE, J. & BRUN, J.-P. 1994. Syn to post-thickening extension in the Variscan Belt of Western Europe: Modes and structural consequences. *Géologie de la France*, **3**, 33–51.

BUROV, E. & CLOETINGH, S. 1997. Erosion and rift dynamics; new thermomechanical aspects of post-rift evolution of extensional basins. *Earth and Planetary Science Letters*, **150**, 7–26.

BUROV, E. B. & GUILLOU-FROTTIER, L. 1999. Thermomechanical behavior of large ash flow calderas. *Journal of Geophysical Research*, **104**, 23081–23109.

BUROV, E. & POLIAKOV, A. 2001. Erosion and rheology controls on synrift and postrift evolution; verifying old and new ideas using a fully coupled numerical model. *Journal of Geophysical Research*, **106**, 16461–16481.

BUROV, E. & POLIAKOV, A. N. B. 2003. Erosional forcing on basin dynamics: new aspects of syn- and post-rift evolution. *In*: NIEUWLAND, D. A. (ed.) *New Insights into Structural Interpretation and Modelling*. Geological Society, London, Special Publication, **212**, 209–224.

BUROV, E. & GUILLOU-FROTTIER, L. 2005. The plume head-continental lithosphere interaction using a tectonically realistic formulation for the lithosphere. *Geophysical Journal International*, **161**, 469–490.

BUROV, E. B., JAUPART, C. & GUILLOU-FROTTIER, L. 2003. Ascent and emplacement of buoyant magma bodies in brittle–ductile upper crust. *Journal of Geophysical Research*, **108**, 2177–2189.

BYERLEE, J. D. 1978. Friction of rocks. *Pure and Applied Geophysics*, **116**, 615–626.

CHÉRY, J. 2001. Core complex mechanics: From the Gulf of Corinth to the Snake Range. *Geology*, **29**, 439–442.

CONEY, P. J. 1980. Cordilleran metamorphic core complexes: an overview. *In*: CRITTENDEN, M. C., CONEY, P. J. & DAVIS, G. H. (eds) *Cordilleran Metamorphic Core Complexes*. Geological Society of America Memoir, **153**, 7–31.

CUNDALL, P. A. 1989. Numerical experiments on localization in frictional materials. *Ingenieur-Archiv*, **59**, 148–159.

CURRIE, C. A. & HYNDMAN, R. D. 2006. The thermal structure of subduction zone back arcs. *Journal of Geophysical Research*, **111**, B08404, doi:10.1029/2005JB004024.

CURRIE, C. A., WANG, K., HYNDMAN, R. D. & HE, J. 2004. The thermal effects of steady-state slab-driven mantle flow above a subducting plate: the Cascadia subduction zone and backarc. *Earth and Planetary Science Letters*, **223**, 35–48.

DAVIS, G. H. 1980. Structural characteristics of metamorphic core complexes, southern Arizona. *In*: CRITTENDEN, M. C., CONEY, P. J. & DAVIS, G. H. (eds) *Cordilleran Metamorphic Core Complexes*. Geological Society of America Memoir, **153**, 35–77.

DUBOIS, R. & BIGNOT, G. 1979. Présence d'un 'hard ground' nummulitique au sommet de la série cretacée d'Almyropotamos (Eubée méridionale, Grèce). *Comptes Rendus de l'Académie des Sciences de Paris*, **289**, 993–995.

DUCHÊNE, S., AÏSSA, R. & VANDERHAEGHE, O. 2006. Pressure-Temperature-time evolution of metamorphic rocks from Naxos (Cyclades, Greece): constraints from thermobarometry and Rb/Sr dating. *Geodinamica Acta*, **19**, 301–321.

ENDRUN, B., MEIER, T., LEBEDEV, S., BOHNHOFF, M., STAVRAKAKIS, G. & HARJES, H.-P. 2008. *S* velocity structure and radial anisotropy in the Aegean region from surface wave dispersion. *Geophysical Journal International*, **174**, 593–616.

ERICKSON, A. J., SIMMONS, G. & RYAN, W. B. F. 1977. Review of heatflow data from the Mediterranean and Aegean Seas. *In*: BIJU-DUVAL, B. & MONTADERT, L. (eds) *International Symposium on the Structural History of the Mediterranean Basins, Split, Yugoslavia*. Technip, Paris, 263–279.

FACCENNA, C., JOLIVET, L., PIROMALLO, C. & MORELLI, A. 2003. Subduction and the depth of convection of the Mediterranean mantle. *Journal of Geophysical Research*, **108**(B2), 2099, doi:10.1029/2001JB001690.

FORSTER, M. A. & LISTER, G. S. 1999. Detachment faults in the Aegean Core Complex of Ios, Greece. *In*: RING, U., BRANDON, M. T., LISTER, G. S. & WILLETT, S. D. (eds) *Exhumation Processes: Normal Faulting, Ductile Flow and Erosion*. Geological Society, London, Special Publication, **154**, 305–323.

FYTIKAS, M., INNOCENTI, F., MANETTI, P., MAZZUOLI, R., PECCERILLO, A. & VILLARI, L. 1984. Tertiary to Quarternary evolution of volcanism in the Aegean region. *In*: DIXON, J. E. & ROBERTSON, A. H. F. (eds) *The Geological Evolution of the Eastern Mediterranean*. Geological Society, London, Special Publication, **17**, 687–699.

GANOR, J., MATTHEWS, A., SCHLIESTEDT, M. & GARFUNKEL, Z. 1996. Oxygen isotopic heterogeneities of metamorphic rocks: an original tectonostratigraphic signature or an imprint of exotic fluids? A case of study of Sifnos and Tinos islands (Greece). *European Journal of Mineralogy*, **8**, 719–732.

GAUTIER, P. 1995. *Géométrie crustale et cinématique de l'extension tardi-orogénique dans le domaine centre-égéen (îles des Cyclades et d'Eubée, Grèce)*. PhD Thesis, University of Rennes 1, France. Mémoires Géosciences Rennes, **61**, 1–417.

GAUTIER, P. 2000. Comment to "Back-arc extension and denudation of Mediterranean eclogites". *Tectonics*, **19**, 406–409.

GAUTIER, P. & BRUN, J.-P. 1994*a*. Ductile crust exhumation and extensional detachments in the central Aegean (Cyclades and Evvia islands). *Geodinamica Acta*, **7**, 57–85.

GAUTIER, P. & BRUN, J.-P. 1994*b*. Crustal-scale geometry and kinematics of late-orogenic extension in the central Aegean (Cyclades and Evvia Island). *Tectonophysics*, **238**, 399–424.

GAUTIER, P., BRUN, J.-P. & JOLIVET, L. 1993. Structure and kinematics of Upper Cenozoic extensional detachment on Naxos and Paros (Cyclades Islands, Greece). *Tectonics*, **12**, 1180–1194.

GAUTIER, P., BRUN, J.-P., MORICEAU, R., SOKOUTIS, D., MARTINOD, J. & JOLIVET, L. 1999. Timing, kinematics and cause of Aegean extension: a scenario based on a comparison with simple analogue experiments. *Tectonophysics*, **315**, 31–72.

GERBAULT, M., BUROV, E. B., POLIAKOV, A. N. B. & DAGNIÈRES, M. 1999. Do faults trigger folding in the lithosphere? *Geophysical Research Letters*, **26**, 271–274.

GESSNER, K., RING, U., JOHNSON, C., HETZEL, R., PASSCHIER, C. W. & GÜNGÖR, T. 2001. An active bivergent rolling-hinge detachment system: Central Menderes metamorphic core complex in western Turkey. *Geology*, **29**, 611–614.

GESSNER, K., WIJNS, C. & MORESI, L. 2007. Significance of strain localization in the lower crust for structural evolution and thermal history of metamorphic core complexes. *Tectonics*, **26**, TC2012, doi:10.1029/2004TC001768.

GRASEMANN, B., EDWARDS, M. A., IGLSEDER, C., PETRAKAKIS, K., SCHNEIDER, D. & Accel Team. 2007. Tertiary SSW directed crustal extension in the Western Cyclades: A new kinematic domain in the Aegean region (Greece). *Geophysical Research Abstracts*, **9**, SRef-ID: 1607-7962/gra/EGU2007-A-06656.

GOETZE, C. 1978. The mechanisms of creep olivine. *Philosophical Transactions of the Royal Society of London*, **A288**, 99–119.

GUEYDAN, F., LEROY, Y. M. & JOLIVET, L. 2004. Mechanics of low-angle shear zones at the brittle-ductile transition. *Journal of Geophysical Research*, **109**, B12407, doi:10.1029/2003JB002806.

HANDY, M. 1989. Deformation regimes and the rheological evolution of fault zones in the lithosphere: the effects of pressure, temperature, grain size, and time. *Tectonophysics*, **163**, 119–152.

HANSEN, F. D. & CARTER, N. L. 1982. Creep of Selected Crustal Rocks at 1000 MPa. *Eos, Transactions, American Geophysical Union*, **63**, 437.

HAUSER, E., POTTER, C., HAUGE, T., BURGESS, S., BURTCH, S., MURTSCHLER, J. *ET AL.* 1987. Crustal structure of eastern Nevada from COCORP deep seismic reflection data. *Geological Society of American Bulletin*, **99**, 833–844.

HEJL, E., RIEDL, H., SOULAKELLIS, N., VAN DEN HAUTE, P. & WEINGARTNER, H. 2003. Fission-track dating of the south-eastern Bohemian Massif (Waldviertel, Austria); thermochronology and long-term erosionYoung Neogene tectonics and relief development on the Aegean islands of Naxos, Paros and Ios (Cyclades, Greece). *Mitteilungen der Österreichischen Geologischen Gesellschaft*, **93**, 105–127.

HEJL, E., RIEDL, H. & WEINGARTNER, H. 2002. Post-plutonic unroofing and morphogenesis of the Attic-Cycladic complex (Aegea, Greece). *Tectonophysics*, **349**, 37–56.

HENJES-KUNST, F. & KREUZER, H. 1982. Isotopic dating of pre-alpidic rocks from the island of Ios (Cyclades, Greece). *Contributions to Mineralogy and Petrology*, **80**, 245–253.

HYNDMAN, R. D., CURRIE, C. A. & MAZZOTTI, S. P. 2005. Subduction zone backarcs, mobile belts, and orogenic heat. *GSA Today*, **15**, 4–10.

IGLSEDER, C., GRASEMANN, B., PETRAKAKIS, K., EDWARDS, M. A., ZAMOLYI, A., RAMBOUSEK, C., HÖRFARTER, C. *ET AL.* 2006. Multistage Plutonism and the Serifos Detachment System (Cyclades, Greece). *Geophysical Research Abstracts*, **8**, SRef-ID: 1607–7962/gra/EGU06-A-05118.

JOLIVET, L. & PATRIAT, M. 1999. Ductile extension and the formation of the Aegean Sea. *In*: DURAND, B., JOLIVET, L., HORVATH, F. & SÉRANNE, M. (eds) *The Mediterranean Basins: Tertiary Extension within* *the Alpine Orogen*. Geological Society, London, Special Publication, **156**, 427–456.

JOLIVET, L., FACCENNA, C., GOFFÉ, B., MATTEI, M., ROSSETTI, F., BRUNET, C. *ET AL*. 1998. Midcrustal shear zones in postorogenic extension: Example from the northern Tyrrhenian Sea. *Journal of Geophysical Research*, **103**, 12123–12160.

JOLIVET, L., FACCENNA, C., GOFFÉ, B., BUROV, E. & AGARD, P. 2003. Subduction tectonics and exhumation of high-pressure metamorphic rocks in the Mediterranean orogens. *American Journal of Science*, **303**, 353–409.

JOLIVET, L., FAMIN, V., MEHL, C., PARRA, T., AUBOURG, C., HÉBERT, R. & PHILIPPOT, P. 2004. Strain localization during crustal-scale boudinage to form extensional metamorphic domes in the Aegean Sea. *In*: WHITNEY, D. L., TEYSSIER, C. & SIDDOWAY, C. S. (eds) *Gneiss Domes in Orogeny*. Geological Society of America Special Paper, **380**, 185–210.

JONGSMA, D. 1974. Heat flow in the Aegean Sea. *Geophysical Journal of the Royal Astronomical Society*, **37**, 337–346.

KEAY, S., LISTER, G. S. & BUICK, I. 2001. The timing of partial melting, Barrovian metamorphism and granite intrusion in the Naxos metamorphic core complex, Cyclades, Aegean Sea, Greece. *Tectonophysics*, **342**, 275–312.

KIRBY, S. H. & KRONENBERG, A. K. 1987. Rheology of the Lithosphere: Selected Topics. *Reviews of Geophysics*, **25**, 1219–1244.

KIRSCHNER, D. L., COSCA, M. A., MASSON, H. & HUNZIKER, J. C. 1996. Staircase $^{40}Ar/^{39}Ar$ spectra of fine-grained white mica: Timing and duration of deformation and empirical constraints on argon diffusion. *Geology*, **24**, 747–750.

KUMERICS, C., RING, U., BRICHAU, S., GLODNY, J. & MONIÉ, P. 2005. The extensional Messaria shear zone and associated brittle detachment faults, Aegean sea, Greece. *Journal of the Geological Society of London*, **162**, 701–721.

LE PICHON, X. & ANGELIER, J. 1979. The Hellenic arc and trench system: a key to the neotectonic evolution of the eastern Mediterranean area. *Tectonophysics*, **60**, 1–42.

LE POURHIET, L., BUROV, E. & MORETTI, I. 2004. Rifting through a stack of inhomogeneous thrusts (the dipping pie concept). *Tectonics*, **23**, TC4005, doi:10.1029/2003TC001584.

LI, X., BOCK, G., VAFIDIS, A., KIND, R., HARJES, H.-P., HANKA, W. *ET AL*. 2003. Receiver function study of the Hellenic subduction zone: imaging crustal thickness variations and the oceanic Moho of the descending African lithosphere. *Geophysical Journal International*, **155**, 733–748.

LISTER, G. S., BANGA, G. & FEENSTRA, A. 1984. Metamorphic core complexes of Cordilleran type in the Cyclades, Aegean Sea, Greece. *Geology*, **12**, 221–225.

LOURENS, L. J., HILGEN, F. J., LASKAR, J., SHACKLETON, N. J. & WILSON, D. 2004. The Neogene period. *In*: GRADSTEIN, F. M., OGG, J. G. & SMITH, A. G. (eds) *A Geologic Time Scale 2004*. Cambridge University Press.

MAKRIS, J. 1975. Crustal structure of the Aegean Sea and the Hellenides obtained from geophysical surveys. *Journal of Geophysics*, **41**, 441–443.

MAKRIS, J. 1978. The crust and upper mantle of the Aegean region from deep seismic soundings. *Tectonophysics*, **46**, 269–284.

MAKRIS, J. & STOBBE, C. 1984. Physical properties and state of the crust and upper mantle of the eastern Mediterranean Sea deduced from geophysical data. *Marine Geology*, **55**, 347–363.

MAKRIS, J. & VEES, R. 1977. Crustal structure of the Central Aegan Sea and the islands of Evia and Crete, Greece, obtained by refractional seismic experiments. *Journal of Geophysics*, **42**, 329–341.

MALUSKI, H., BONNEAU, M. & KIENAST, J. R. 1987. Dating the metamorphic events in the Cycladic area: $^{39}Ar/^{40}Ar$ data from metamorphic rocks of the island of Syros (Greece). *Bulletin de la Societé Géologique de France*, **3**, 833–842.

MCCARTHY, J. & THOMPSON, G. A. 1988. Seismic imaging of extended crust with emphasis on the western United States. *Geological Society of America Bulletin*, **100**, 1361–1374.

MCKENZIE, D. 1978. Active tectonics of the Alpine-Himalayan belt: the Aegean Sea and surrounding regions. *Geophysical Journal of the Royal Astronomical Society*, **55**, 217–254.

MCKENZIE, D., NIMMO, F., JACKSON, J. A., GANS, P. B. & MILLER, E. L. 2000. Characteristics and consequences of flow in the lower crust. *Journal of Geophysical Research*, **105**, 11029–11046.

MEHL, C., JOLIVET, L. & LACOMBE, O. 2005. From ductile to brittle: evolution and localization of deformation below a crustal detachment (Tinos, Cyclades, Greece). *Tectonics*, **24**, TC4017, doi:10.1029/2004TC001767.

MORRIS, A. & ANDERSON, M. 1996. First paleomagnetic results from the Cycladic Massif, Greece, and their implications for Miocene extension directions and tectonic models in the Aegean. *Earth and Planetary Science Letters*, **142**, 397–408.

MÜLLER, M., GRASEMANN, B., EDWARDS, M. A., VOIT, K., IGLSEDER, C., ZAMOLYI, A. *ET AL*. 2006. Ductile to brittle progressive deformation within crustal-scale shear zones, Western Cyclades, Greece. *Geophysical Research Abstracts*, **8**, SRef-ID: 1607–7962/gra/EGU06-A-06943.

PARRA, T., VIDAL, O. & JOLIVET, L. 2002. Relation between the intensity of deformation and retrogression in blueschist metapelites of Tinos Island (Greece) evidenced by chlorite-mica local equilibria. *Lithos*, **63**, 41–66.

PARRISH, R. R., CARR, S. D. & PARKINSON, D. L. 1988. Eocene extensional tectonics and geochronology of the southern Omineca Belt, British Columbia and Washington. *Tectonics*, **7**, 181–212.

PATZAK, M., OKRUSCH, M. & KREUZER, H. 1994. The Akrotiri unit on the island of Tinos, Cyclades, Greece: Witness to a lost terrane of Late Cretaceous age. *Neues Jahrbuch für Geologie und Paläontologie Abhandlungen*, **194**, 211–252.

PE-PIPER, G. & PIPER, D. J. W. 2006. Unique features of the Cenozoic igneous rocks of Greece. *In*: DILEK, Y. & PAVLIDES, S. (eds) *Postcollisional tectonics and* *magmatism in the Mediterranean region and Asia*. Geological Society of America Special Paper, **409**, 259–282.

POLIAKOV, A. N. B., PODLADCHIKOV, Y. & TALBOT, C. 1993. Initiation of salt diapirs with frictional overburdens: numerical experiments. *Tectonophysics*, **228**, 199–210.

RANALLI, G. 1987. *Rheology of the Earth*. Allen and Unwin, Boston.

REYNOLDS, S. J. & LISTER, G. S. 1990. Folding of mylonitic zones in Cordilleran metamorphic core complexes: evidences from near the mylonitic front. *Geology*, **18**, 216–219.

RIDLEY, J. 1984. Listric normal faulting and the reconstruction of the synmetamorphic structural pile of the Cyclades. *In*: DIXON, J. E. & ROBERTSON, A. H. F. (eds) *The Geological Evolution of the Eastern Mediterranean*. Geological Society of London Special Publication, **17**, 755–761.

RING, U. & LAYER, P. W. 2003. High-pressure metamorphism in the Aegean, eastern Mediterranean: Underplating and exhumation from the Late Cretaceous until the Miocene to Recent above the retreating Hellenic subduction zone. *Tectonics*, **22(3)**, 1022, doi:10.1029/2001TC001350.

RING, U. & REISCHMANN, T. 2002. The weak and superfast Cretan detachment, Greece: exhumation at subduction rates in extruding wedges. *Journal of the Geological Society of London*, **159**, 225–228.

RING, U., LAYER, P. W. & REISCHMANN, T. 2001. Miocene high-pressure metamorphism in the Cyclades and Crete, Aegean Sea, Greece: Evidence for large-magnitude displacement on the Cretan detachment. *Geology*, **29**, 395–398.

RING, U., GLODNY, J., WILL, T. & THOMSON, S. N. 2007*a*. An Oligocene extrusion wedge of blueschist-facies nappes on Evia, Aegean Sea, Greece: implications for the early exhumation of high-pressure rocks. *Journal of the Geological Society of London*, **164**, 637–652.

RING, U., WILL, T., GLODNY, J., KUMERICS, C., GESSNER, K., THOMSON, S. N. *ET AL*. 2007*b*. Early exhumation of high-pressure rocks in extrusion wedges: The Cycladic blueschist unit in the eastern Aegean, Greece and Turkey. *Tectonics*, **26**, TC2001, doi:10.1029/2005TC001872.

ROESLER, G. 1978. Relics of non-metamorphic sediments on central Aegean islands. *In*: CLOSS, H., ROEDER, D. & SCHMIDT, K. (eds) *Alps, Apennines, Hellenides*. Inter-Union Commission on Geodynamics Scientific Report, **38**, 480–481.

ROSENBAUM, G., AVIGAD, D. & SANCHEZ-GOMEZ, M. 2002. Coaxial flattening at deep levels of orogenic belts: evidence from blueschists and eclogites on Syros and Sifnos (Cyclades, Greece). *Journal of Structural Geology*, **24**, 1451–1462.

ROSENBAUM, G., REGENAUER-LIEB, K. & WEINBERG, R. 2005. Continental extension: From core complexes to rigid block faulting. *Geology*, **33**, 609–612. doi: 10.1130/G21477.1.

SACHPAZI, M., HIRN, A., NERCESSIAN, A., AVEDIK, F., MC BRIDE, J., LOUCOYANNAKIS, M. *ET AL*. 1997. A first coincident normal-incidence and wide-angle approach to studying the extending Aegean crust. *Tectonophysics*, **270**, 301–312.

SÁNCHEZ-GÓMEZ, M., AVIGAD, D. & HEIMANN, A. 2002. Geochronology of clasts in allochthonous Miocene sedimentary sequences on Mykonos and Paros Islands: implications for back-arc extension in the Aegean Sea. *Journal of the Geological Society of London*, **159**, 45–60.

SCHLIESTEDT, M. & MATTHEWS, A. 1987. Transformation of blueschist to greenschist facies rocks as a consequence of fluid infiltration, Sifnos (Cyclades), Greece. *Contributions to Mineralogy and Petrology*, **97**, 237–250.

THOMSON, S. N. & RING, U. 2006. Thermochronologic evaluation of post-collision extension in the Anatolide orogen, western Turkey. *Tectonics*, **25**, TC3005, doi:10.1029/2005TC001833.

THOMSON, S. N., STÖCKHERT, B. & BRIX, M. R. 1999. Miocene high-pressure metamorphic rocks of Crete, Greece: rapid exhumation by buoyant escape. *In*: RING, U., BRANDON, M. T., LISTER, G. S. & WILLETT, S. D. (eds) *Exhumation processes: Normal Faulting, Ductile Flow and Erosion*. Geological Society, London, Special Publication, **154**, 87–107.

TIREL, C., BRUN, J.-P. & BUROV, E. 2004*a*. Thermomechanical modeling of extensional gneiss domes. *In*: WHITNEY, D. L., TEYSSIER, C. & SIDDOWAY, C. S. (eds) *Gneiss Domes in Orogeny*. Geological Society of America Special Paper, **380**, 67–78.

TIREL, C., GUEYDAN, F., TIBERI, C. & BRUN, J.-P. 2004*b*. Aegean crustal thickness inferred from gravity inversion. Geodynamical implications. *Earth and Planetary Science Letters*, **228**, 267–280.

TIREL, C., BRUN, J.-P. & SOKOUTIS, D. 2006. Extension of thickened and hot lithospheres: Inferences from laboratory modeling. *Tectonics*, **25**, TC1005, doi:10.1029/2005TC001804.

TIREL, C., BRUN, J.-P. & BUROV, E. 2008. Dynamics and structural development of metamorphic core complexes. *Journal of Geophysical Research*, B04403, doi:10.1029/2005JB003694.

TROTET, F., JOLIVET, L. & VIDAL, O. 2001*a*. Tectono-metamorphic evolution of Syros and Sifnos islands (Cyclades, Greece). *Tectonophysics*, **338**, 179–206.

TROTET, F., VIDAL, O. & JOLIVET, L. 2001*b*. Exhumation of Syros and Sifnos metamorphic rocks (Cyclades, Greece). New constraints on the P-T paths. *European Journal of Mineralogy*, **13**, 901–920.

TURCOTTE, D. L. & SCHUBERT, G. 2002. *Geodynamics*. (2nd ed.) Cambridge University Press, Cambridge.

URAI, J. L., SCHUILING, R. D. & JANSEN, J. B. H. 1990. Alpine deformation on Naxos (Greece). *In*: KNIPE, R. J. & RUTTER, E. H. (eds) *Deformation Mechanisms, Rheology and Tectonics*. Geological Society, London, Special Publication, **54**, 509–522.

VAN DER MAAR, P. A. & JANSEN, J. B. H. 1983. The geology of the polymetamorphic complex of Ios, Cyclades, Greece and its significance for the Cycladic Massif. *Geologische Rundschau*, **72**, 283–299.

VAN HINSBERGEN, D. J. J. 2004. *The evolving anatomy of a collapsing orogen*. PhD Thesis, University Utrecht, The Netherlands. *Geologica Ultraiectina*, **243**, 1–280.

VAN HINSBERGEN, D. J. J., SNEL, E., GARSTMAN, S. A., MARUNTEANU, M., LANGEREIS, C. G., WORTEL, M. J. R. & MEULENKAMP, J. E. 2004. Vertical motions in the Aegean volcanic arc: evidence for rapid subsidence preceding volcanic activity on Milos and Aegina. *Marine Geology*, **209**, 329–345.

VAN HINSBERGEN, D. J. J., HAFKENSCHEID, E., SPAKMAN, W., MEULENKAMP, J. E. & WORTEL, M. J. R. 2005*a*. Nappe stacking resulting from subduction of oceanic and continental lithosphere below Greece. *Geology*, **33**, 325–328.

VAN HINSBERGEN, D. J. J., LANGEREIS, C. G. & MEULENKAMP, J. E. 2005*b*. Revision of the timing, magnitude and distribution of Neogene rotations in the western Aegean region. *Tectonophysics*, **396**, 1–34.

VANDENBERG, L. C. & LISTER, G. S. 1996. Structural analysis of basement tectonites from the Aegean metamorphic core complex of Ios, Cyclades, Greece. *Journal of Structural Geology*, **18**, 1437–1454.

VANDERHAEGHE, O. 2004. Structural development of the Naxos migmatite dome. *In*: WHITNEY, D. L., TEYSSIER, C. & SIDDOWAY, C. S. (eds) *Gneiss Domes in Orogeny*. Geological Society of America Special Paper, **380**, 211–227.

VANDERHAEGHE, O. & TEYSSIER, C. 2001. Crustal-scale rheological transitions during late-orogenic collapse. *Tectonophysics*, **335**, 211–228.

VIGNER, A. 2002. *Images sismiques par réflexions verticales et grand-angle de la croûte en contexte extensif: les Cyclades et le fossé Nord-Egéen*. PhD Thesis, Institut de Physique du Globe de Paris, University Paris 7.

WALCOTT, C. R. & WHITE, S. H. 1998. Constraints on the kinematics of post-orogenic extension imposed by stretching lineations in the Aegean region. *Tectonophysics*, **298**, 155–175.

WDOWINSKI, S. & AXEN, G. J. 1992. Isostatic rebound due to tectonic denudation: a viscous flow model of a layered lithosphere. *Tectonics*, **11**, 303–315.

WEGMANN, M. I. 2006. *Die Entwicklung des Rb/Sr-Isotopensystems in metamorphen Mikrostrukturen in Abhängigkeit von Temperatur, Druck und Mineralkomposition am Beispiel der Hochdruckmetamorphite von Südevia, Griechenland*. Fachbereich Geowissenschaften, Freie University, Berlin, Germany.

WERNICKE, B. 1992. Cenozoic extensional tectonics of the U.S. Cordillera. *In*: BURCHFIELD, B. C., LIPMAN, P. W. & ZOBACK, M. L. (eds) *The Cordilleran Orogen: Conterminous U.S., The Geology of North America*. Geological Society of America, **43**, 553–581.

WIJBRANS, J. R. & MCDOUGALL, I. 1988. Metamorphic evolution of the Attic Cycladic Metamorphic Belt on Naxos (Cyclades, Greece) utilizing $^{40}Ar/^{39}Ar$ age spectrum measurements. *Journal of Metamorphic Geology*, **6**, 571–594.

WIJBRANS, J. R., SCHLIESTEDT, M. & YORK, D. 1990. Single grain argon laser probe dating of phengites from the blueschist to greenschist transition of Sifnos (Cyclades, Greece). *Contributions to Mineralogy and Petrology*, **104**, 582–593.

WIJBRANS, J. R., VAN WEES, J. D., STEPHENSON, R. A. & CLOETINGH, S. A. P. L. 1993. Pressure- temperature-time evolution of the high-pressure metamorphic complex of Sifnos, Greece. *Geology*, **21**, 443–446.

WIJNS, C., WEINBERG, R., GESSNER, K. & MORESI, L. 2005. Mode of crustal extension determined by rheological layering. *Earth and Planetary Science Letters*, **236**, 120–134.

WUST, S. L. 1986. Regional correlation of extension directions in Cordilleran metamorphic core complexes. *Geology*, **14**, 828–830.

ZEILINGA DE BOER, J. 1989. The Greek enigma: is development of the Aegean orogene dominated by forces related to subduction or obduction? *Marine Geology*, **87**, 31–54.

The Itea–Amfissa detachment: a pre-Corinth rift Miocene extensional structure in central Greece

DIMITRIOS PAPANIKOLAOU*, LEONIDAS GOULIOTIS & MARIA TRIANTAPHYLLOU

University of Athens, Faculty of Geology and Geo-environment, Panepistimioupoli Zografou, 15784, Athens, Greece

**Corresponding author (e-mail: dpapan@geol.uoa.gr)*

Abstract: The Itea–Amfissa valley, separating Giona Mountain to the west from Parnassos Mountain to the east, is related to an extensional detachment observed along the eastern slopes of Giona. The detachment is traced for 30 km north of the Corinth Gulf and dips 25°–40° to the east, showing an east–west extension parallel to the Hellenic arc. The lower nappes of Pindos, Penteoria, Vardoussia and mainly the basal thrust of the Parnassos unit form part of the footwall, whereas the upper thrusts of the Parnassos unit and the Western Thessaly–Beotia nappe form part of the hanging wall. The eastern slopes of Giona are controlled by the detachment and several hundred metres of syn-tectonic breccia-conglomerates are observed at the top of the hanging wall rocks and are back-tilt towards the detachment plane. Two conglomeratic sequences are distinguished: the lower one consists of argillaceous matrix and abundant ophiolite detritus whereas the upper one bears carbonate matrix with carbonate detritus together with large olistholites of Mesozoic limestones. Based on calcareous nannofossils a middle Miocene age has been determined for the lower formation and a middle–upper Miocene age is probable for the upper. Planation surfaces cut on top of the sediments rise from south to north starting from sea level at Galaxidi to about 1400 m at Prosilio. The throw of the detachment is about 2.5–4.2 km measured mainly from the structural omission of the Alpine tectono-stratigraphic units. A contrast between the footwall and the hanging wall structure is described, with monoclinic sequence of the Parnassos nappe dipping to the west in the footwall but a complex synsedimentary horst and graben structure of sliding blocks of Alpine formations within the Miocene clastic sequences in the hanging wall. The detachment has been deformed by the east–west-trending steep normal faults that have created the Corinth rift during late Pliocene–Quaternary time showing a north–south extension. The Itea–Amfissa detachment forms the northern tip of the broader East Peloponnesus detachment, observed south of the Corinth rift structure from Feneos to Kyparissi. Similar geodynamic phenomena with large olistholites and breccia conglomerates are known from the Serravalian of Crete, related to the activity of the Cretan detachment.

The two highest mountains of Sterea Hellas in central Greece, north of the Corinth Gulf, are Giona (2507 m) in the west and Parnassos (2455 m) in the east (Fig. 1). They are separated by a narrow morphological valley, covered by alluvial deposits with famous olive groves, cropping from the Itea Gulf in the south to the city of Amfissa in the north. This prominent morphological feature trends north–south at right-angles to the east–west-trending Corinth Gulf, which is well known to be the result of neotectonic activity of east–west-trending normal faults (e.g. Armijo *et al.* 1996). Surprisingly, no tectonic structure or other geodynamic process (e.g. erosion) has ever been reported in the literature to explain this north–south-trending valley. Alpine structures might have produced this morphological feature, parallel to a thrust or a syncline in a north–south direction, which is the general Alpine tectonic trend along central and western Greece. However, both mountains on both sides of the Itea–Amfissa depression are located on the same geotectonic unit of Parnassos (Renz 1955; Papastamatiou 1960; Celet 1962) and no particular thrust or fold has been reported so far that would explain the formation of the valley (Celet 1962; Schwan 1976) (Fig. 1). Interestingly, the existence of post-Alpine clastic sediments of unknown age has been reported in the area of Aghia Efthymia village along the eastern slopes of Giona, capped by a well-developed planation surface at about 350–400 m of elevation and in the area of Prosilio at about 1000–1200 m (Papastamatiou *et al.* 1960, 1962; Celet 1962). This is the most important outcrop of post-Alpine sediments along the northern margin of the Corinth Gulf, in contrast to the southern margin, where post-Alpine sediments crop out almost everywhere along the north Peloponnesus coastline from Corinth to Patras (Fig. 1).

From: van Hinsbergen, D. J. J., Edwards, M. A. & Govers, R. (eds) *Collision and Collapse at the Africa–Arabia–Eurasia Subduction Zone*. The Geological Society, London, Special Publications, **311**, 293–310.
DOI: 10.1144/SP311.11 0305-8719/09/$15.00

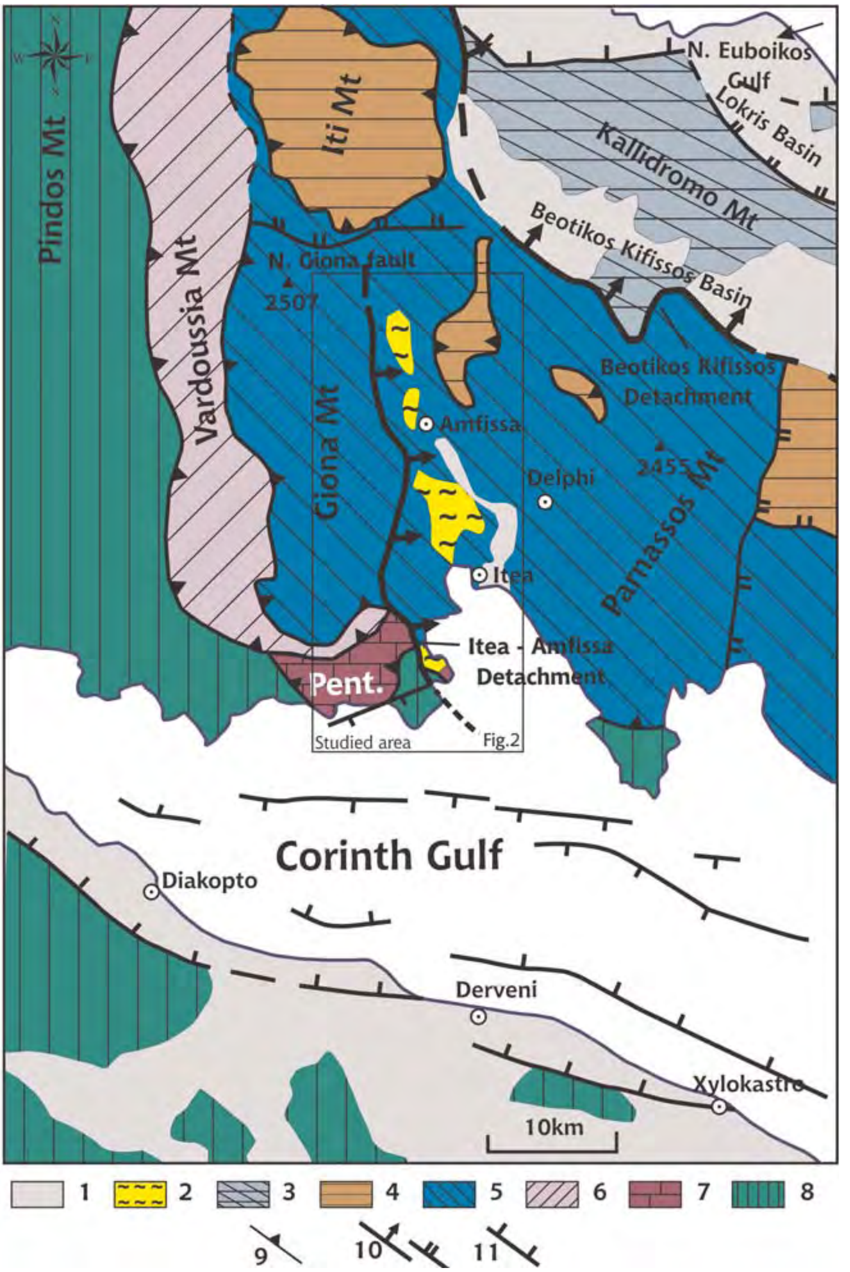

Fig. 1. The studied area within the geographical and geotectonic frame of central Sterea. (1) post-Alpine sediments, mainly Plio-Quaternary; (2) Miocene sediments of the Itea–Amfissa basin; (3) Tectonic units of the Internal Hellenides, mainly SubPelagonian; (4) Western Thessaly–Beotia unit; (5) Parnassos unit; (6) Vardoussia unit; (7) Penteoria unit; (8) Pindos unit; (9) Alpine overthrust; (10) Miocene detachments and normal faults; (11) Plio-Quaternary normal faults.

Our study has shown the existence of a major extensional detachment fault along the eastern slopes of the Giona Mountain, trending in the north–south direction. This Itea–Amfissa detachment has created the Itea–Amfissa depression with clastic sedimentation during Miocene, before the onset of the east–west trending faults of the modern Corinth rift structure.

The geology of the eastern Giona Mountain and the valley of Itea–Amfissa

The Alpine structure of both Giona Mountain and Itea–Amfissa valley comprises a number of thrust units incorporating shallow-water carbonate rocks belonging to the Parnassos platform (Philippson 1898; Renz 1955; Papastamatiou 1960; Celet 1962). At the southern end of Giona Mountain on the Galaxidi peninsula some thrust sheets belonging to the lower parts of the nappe pile show differentiated stratigraphy, with rocks deposited either in slopes or in basinal environments, showing a lateral transition towards the Pindos basin, which forms the next lower nappe cropping out to the west (Celet 1960; Papastamatiou & Tataris 1963; Wiedenmayer 1963; Johns 1979).

Our mapping distinguished four nappes along the southern Giona section (Fig. 2) with: (i) the Pindos nappe at the base, containing Cretaceous pelagic carbonates and Paleocene flysch; (ii) the Penteoria nappe on top of the Pindos, consisting of upper Triassic–middle Jurassic shallow water carbonates overlain by upper Jurassic–Cretaceous pelagic sequences and Paleocene–Eocene flysch; (iii) the Vardoussia nappe overlying the Penteoria nappe, featured by transitional slope facies from the upper Triassic to the Cretaceous and Paleocene–Eocene flysch; and (iv) the Parnassos nappe on top of the previous nappes, containing carbonate platform strata from the upper Triassic to the upper Cretaceous, interrupted by three main bauxite horizons (b_1 in the upper Jurassic, b_2 in the lower Cretaceous and b_3 in the upper Cretaceous) and covered by Paleocene–Eocene flysch deposits.

Internal thrusts are present within each nappe. For example, in the northern part of the Itea–Amfissa valley in the area east of Prosilio, there are two thrust sheets present in the upper part of the Parnassos nappe (Figs 2 and 3, profile A–A′). The highest nappe in this area, the nappe of Western Thessaly–Beotia, lies with a subhorizontal contact above the Parnassos thrust sheets at the western end of the Parnassos Mountain, known as Gerolekas (Fig. 2). This upper nappe is of more internal origin and belongs to the transitional units between the Parnassos platform and the Internal Hellenides (Celet *et al.* 1976; Papanikolaou & Sideris 1979; Papanikolaou 1986). Its main characteristic is that the stratigraphic column is continuous from the Triassic–Jurassic to the Cretaceous–Eocene, with the upper Jurassic–lower Cretaceous flysch type sediments bearing abundant ophiolite detritus marking the vertical transition. In contrast, the units of the Internal Hellenides, like the Subpelagonian, are characterized by a prominent orogenic unconformity in the upper Cretaceous, which covers both the Triassic–Jurassic sediments and the previously emplaced ophiolite nappe. These more internal nappes crop out north of the Parnassos Mountain in the area between the Beotikos Kifisos Basin and Kalidromon Mountain up to the Northern Evoikos Gulf (Fig. 1). The subsidence of the higher nappes and the formation of the Beotikos Kifisos and Lokris post-Alpine basins are due to the activity of the NE-dipping Beotikos Kifisos extensional detachment (Kranis & Papanikolaou 2001) (Fig. 1). Another normal fault trending east–west marks the tectonic boundary of Giona Mountain with Iti Mountain to the north. This fault has subsided the block of Iti Mountain to the north of Giona Mt by more than 1 km of throw. This activity has resulted in the preservation of the outcrops of the Western Thessaly–Beotia nappe in Iti Mt, whereas in Giona Mt this nappe has been eroded.

The Itea–Amfissa north–south-trending extensional detachment system, reported here for the first time, is developed along the eastern slopes of Giona Mountain (Fig. 2). This detachment is first exposed from the south in the area of Galaxidi and can be traced northwards, east of Penteoria and Vounichora villages to further north in the area west of Amfissa and Prosilio.

The overall tectonic structure of the Eastern Giona and the Itea–Amfissa valley is shown in three NE–SW tectonic profiles (Fig. 3). The central and the northern profile (Fig. 3, A–A′, B–B′) show that the footwall of the detachment is made from the lower thrust sheet of the Parnassos nappe, whose carbonate sequence generally dips 15°–30° to the west. This is in agreement with the fact that all along the detachment surface the age of footwall rocks of the platform carbonates is upper Triassic–lower Jurassic and only along the western part of Giona Mountain do the Cretaceous formations crop out. At the southern profile (Fig. 3, C–C′) the upper Triassic base of the Penteoria nappe occurs at the footwall. Small tectonic wedges of the Vardoussia nappe occur along the detachment and below the lower thrust unit of the Parnassos nappe, forming the hanging wall.

In contrast, the structure within the hanging wall of the detachment is complex with a number of thrust sheets belonging to the upper part of the Parnassos nappe, cropping out together with the upper nappe of Western Thessaly–Beotia and the post-Alpine sediments of Aghia Efthymia and Prosilio. The general dip of the thrust sheets in the hanging wall is towards the east, with two distinct thrust sheets of Parnassos unit dipping below the Western Thessaly–Beotia nappe along the Gerolekas slopes. It is noteworthy that only the Ailias tectonic block (Fig. 3, profile C–C′) is made of the lower part of the stratigraphic sequence of Parnassos, incorporating mainly the upper Triassic–middle Jurassic formations, whereas the other blocks of

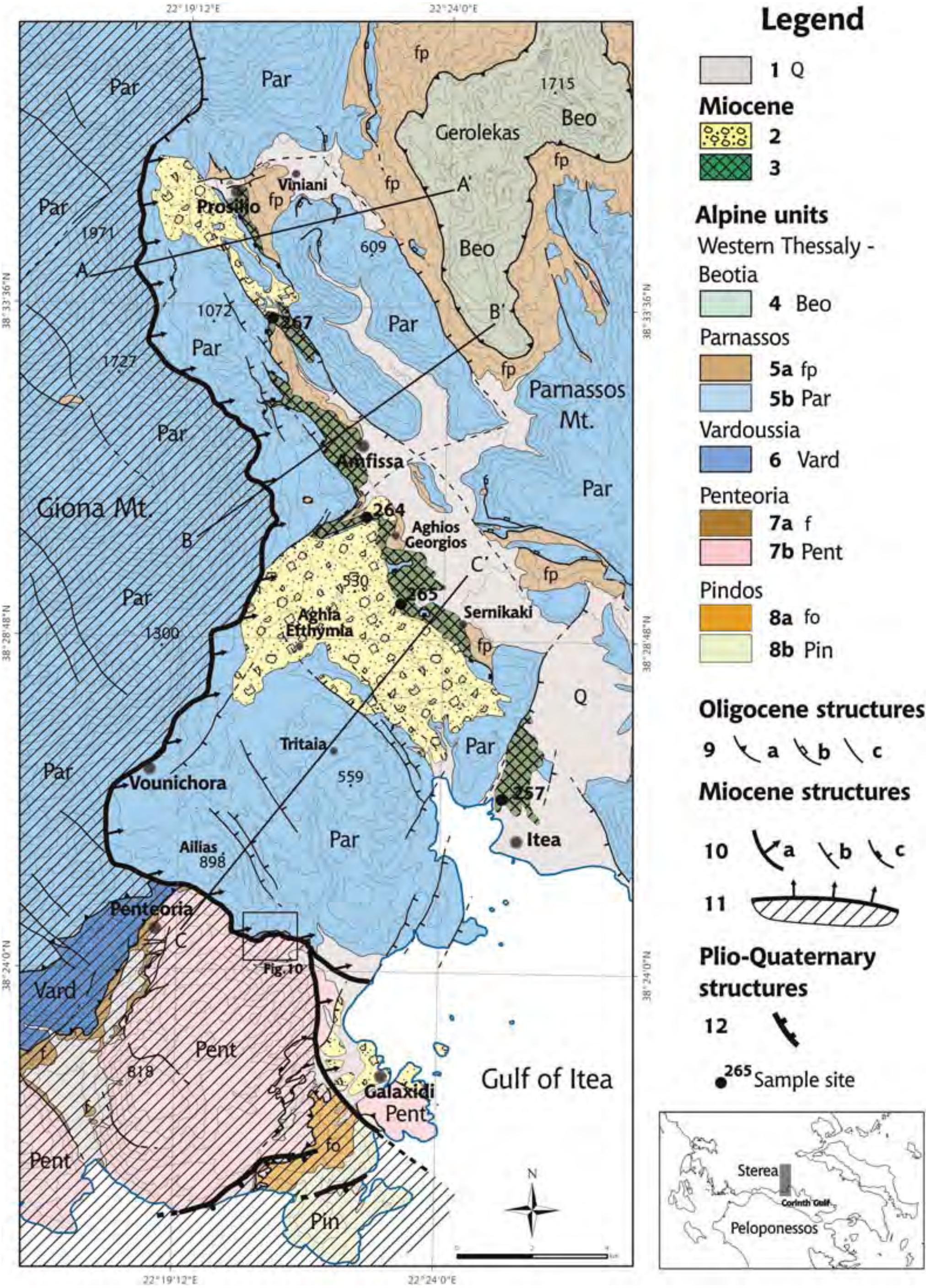

Fig. 2. Simplified geological map of the studied area in the Eastern Giona Mountain and the Itea–Amfissa Valley (based on the maps of Papastamatiou *et al.* 1960, 1962 at scale 1:50 000 and our own mapping at scale 1:10 000). (1) Quaternary deposits; (2) Upper sequence of sediments, middle–upper ?Miocene; (3) Lower sequence of sediments, lower–middle Miocene; (4) Western Thessaly–Beotia nappe; (5a) Parnassos flysch, Paleocene–Eocene; (5b) Parnassos carbonate platform, upper Triassic–upper Cretaceous; (6) Vardoussia nappe; (7a) Penteoria flysch,

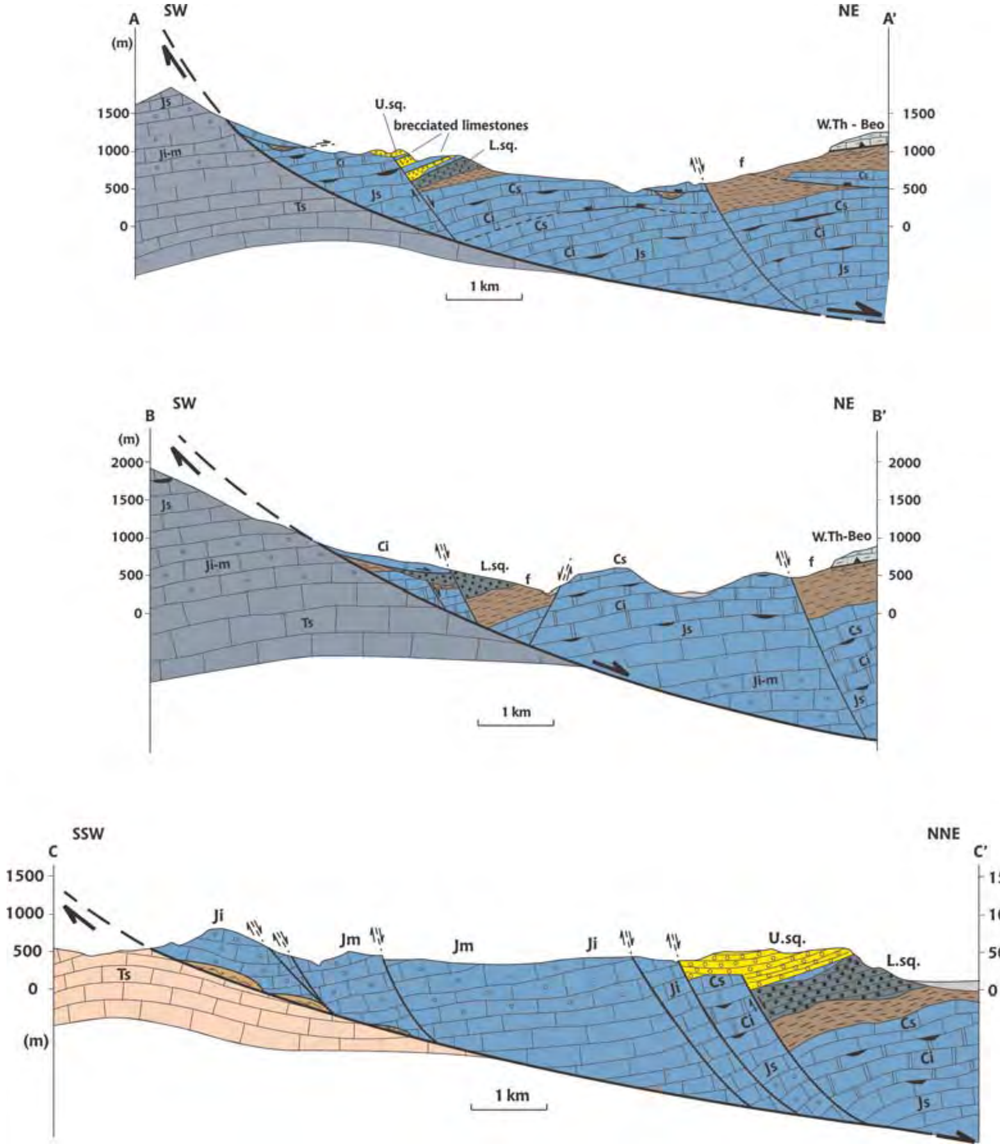

Fig. 3. Tectonic profiles across the Itea–Amfissa detachment. Their location is given on the geological map of Figure 2.

the hanging wall incorporate thrust sheets with upper Jurassic–Eocene formations. The dip of the Aghia Efthymia and Prosilio clastic sediments is usually 10°–30° to the west into the detachment surface. Some steep North–NE–South–SW-trending normal faults are present within the hanging wall rocks close to the detachment.

No other post-Alpine sediments are observed in the area with the exception of some Quaternary scree and alluvium.

Fig. 2. (*Continued*) Paleocene–Eocene; (7b) Penteoria carbonate sequence, upper Triassic–upper Cretaceous; (8a) Pindos flysch, Paleocene–Eocene, (8b) Pindos pelagic sequence, upper Cretaceous; (9) Alpine structures, Oligocene; (9a) overthrust, (9b) thrust, (9c) fault; (10) Miocene structures, (10a) extensional detachment, (10b) normal fault, (10c) gravity nappe, (11) shaded area marks the geological formations of the detachment's footwall; (12) normal faults of the Corinth rift system.

The Itea–Amfissa sedimentary deposits: Tectonostratigraphy and age assessment

Several hundred metres of coarse clastic sediments are observed at the top of the hanging wall succession along the detachment. They generally consist of breccia and conglomerates alternating with sandy and clay layers including smaller pebbles. These sediments represent the remnants of the Itea–Amfissa basin that was formed during the Miocene at the hanging wall of the detachment. The present day Itea–Amfissa valley has been uplifted and incised the Miocene sedimentary basin. Present-day alluvial deposits are observed at altitudes from sea level to 200 m along the valley, whereas the top of the Miocene sedimentary succession is observed several hundred metres higher along the eastern slopes of Giona Mt Outcrops of sediments are traced in Galaxidi, Aghia Efthymia and Prosilio with progressively increasing altitude northwards. Thus, the southern outcrops around Galaxidi are observed at about 0–50 m, the outcrops at the central part around Aghia Efthymia at about 350–500 m and the outcrops at the northern part of the study area around Prosilio at about 800–1300 m (Fig. 2).

Two stratigraphic sequences can de distinguished in the sedimentary deposits of the Itea–Amfissa basin. The lower sequence crops out: (a) on the hillside north of Itea; (b) along the slopes of the cliff separating the Aghia Efthymia planation surface from the alluvial plane of Amfissa in the area of villages Sernikaki, Aghios Konstantinos and Aghios Georgios; (c) in the area of Prosilio; and (d) in narrow outcrops at the base of the limestone cliffs in the area west of Amfissa (Fig. 2). The upper sequence extends over large areas forming a subhorizontal relief in the planation surfaces of Aghia Efthymia and Prosilio (Fig. 2). The main difference of the two sequences is the lithological composition of the clasts in the pebbles and breccia of the conglomerates and the matrix. In particular, the lower sequence comprises mainly sandstones, pelites, ophiolites and radiolarites with minor carbonate rocks within an argillaceous matrix, whereas the upper sequence comprises clasts mainly of dolomite and limestone within a sandy–carbonate matrix. The majority of the carbonate clasts in the upper sequence are of Parnassian origin. On the other hand, the clasts of the ophiolites and the pelagic siliceous sediments characterizing the lower sequence are most likely debris from the upper nappes of the Western Thessaly–Beotia and the more internal ophiolites bearing nappe units. This major difference in the lithological composition of the two sequences indicates that during the deposition of the lower sequence the main sediment supply source was from the upper nappes of Western Thessaly–Beotia and the Internal Hellenides, whereas during the deposition of the upper sequence the carbonate platform of the Parnassos unit was the main supply source.

The transition from the lower to the upper sequence differs significantly from locality to locality along the Itea–Amfissa basin. In the south, in the area of Aghia Efthymia–Sernikaki there is an angular unconformity between the upper and the lower sequence observed along the base of the Aghia Efthymia cliff for more than 4 km. The lower sequence dips 30°–35° to the NW whereas the upper sequence dips 20°–30° to the SW. This is nicely revealed in the area of Portes, near Aghios Nikolaos, where the conglomerate beds of the lower sequence are truncated by the basal conglomerate beds of the upper sequence. The base of the unconformity is marked in the morphology by the cliff, due to the differential erosion of the softer argillaceous lower conglomerate sequence and the much stiffer upper conglomerate sequence, which resembles to a carbonate formation (Fig. 4). The dip of the lower sequence immediately south of Sernikaki is similar to the dip of the basal contact of the lower sequence over its Alpine basement and to the overall dip of the Alpine formations. Thus, the lower sequence forms a triangular outcrop between the Alpine basement in the south and the unconformity of the upper sequence, which in the NW–SE oriented section looks subhorizontal (apparent dip because of the strike-parallel direction; Fig. 5a). The maximum thickness of the lower sequence in the Sernikaki–Aghios Georgios area is estimated to almost 1 km. However, north of Aghios Georgios its thickness decreases abruptly to only a few tens of metres. Herein, it is observed below the subhorizontal

Fig. 4. The cliff of the Aghia Efthymia planation surface on top of the clastic sediments of the upper sequence (U.sq) seen from S–SE. The lower sequence (L.sq) forms the slopes below the cliff. At the back scene the eastern Giona slopes following the detachment plane are also observed with outcrops of upper Triassic (Ts) and lower Jurassic (Ji) limestones.

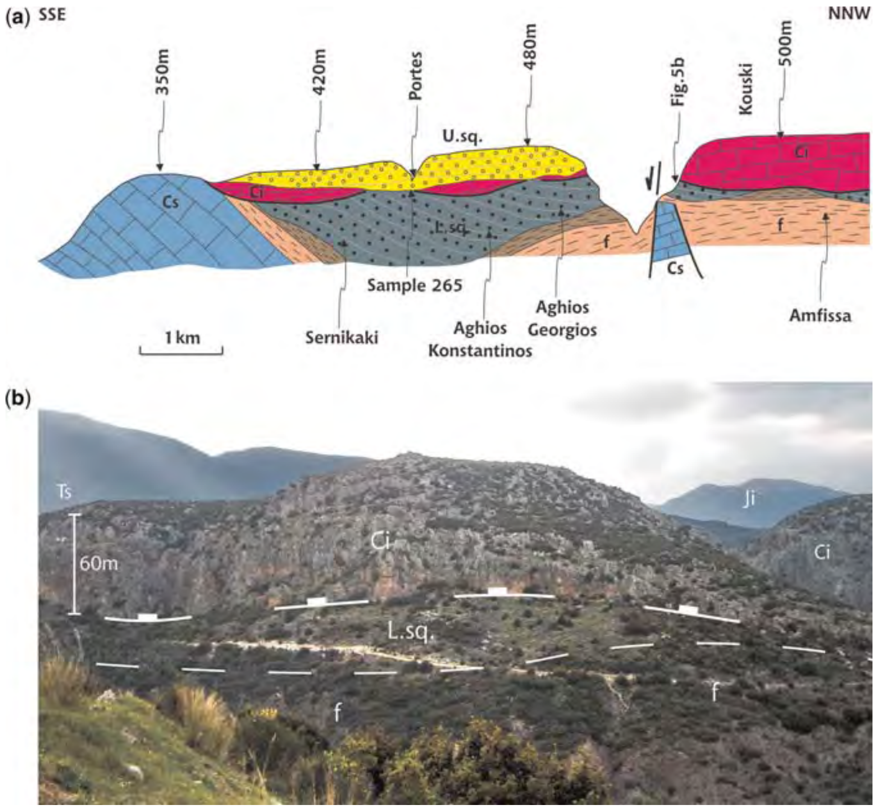

Fig. 5. (**a**) Tectonic sketch showing the angular unconformity between the lower and the upper sequence along the section Sernikaki–Aghios Georgios–Amfissa. Allochthonous Mesozoic limestones are observed at the base of the upper sequence, (**b**) The tectonic block of Cretaceous limestones (Ci) of the Parnassos nappe forming the Kouski hill, on top of the lower sequence sediments (L.sq) and the underlying flysch (f) of the Parnassos nappe between the chapels of Aghia Marina and Aghios Nikolaos.

block of the Mesozoic limestone and above the Eocene flysch (Figs 2 & 5b). Along strike the valley between Aghios Georgios and Amfissa there is a NE–SW trending fault zone, which crosses through the Panaghia, Aghios Nikolaos and Aghia Marina chapels. This fault zone separates the massive limestone klippen unit of Kouski hill to the west of Amfissa resting above the lower sedimentary sequence (Fig. 5b), from the upper sequence cropping out in the southern block all over the planation surface of Aghia Efthymia (Fig. 2). The fault is an oblique-slip normal fault as shown by the slickensides observed in several localities. Subsidence occurred to the southeast as implied by the thickness of the lower sequence. For example, its thickness in the hanging wall is estimated into several hundred metres in contrast to only a few tens of metres in the footwall northwards. A dextral strike-slip component is also traced, but its significance cannot be quantitatively determined. It is remarkable that the altitude of the subhorizontal planation surface of Aghia Efthymia is similar on both sides of the valley following the fault, even though the geological formations are different with outcrops of the upper sequence in the south and block of Mesozoic limestone in the north (Fig. 5a). Additionally, the unconformity of the upper sequence in the south is placed at about the same level with the base of the allochthonous limestone block in the north. Thus, the offset of the basal unconformity of the lower sequence over the Alpine basement on both sides of the NE–SW fault zone along the valley corresponds to the throw of the NE–SW fault zone during the deposition of the lower sequence. An additional throw of 20–30 m was formed during the arrival of the material of the upper sequence and of the emplacement of the allochthonous limestone block. The overall structure indicates a syn-depositional tectonism of the clastic sequences accompanied by the emplacement of olistholites, blocks and small extensional gravity nappes of Mesozoic limestones,

Fig. 6. A characteristic outcrop of the alternation of beds of compact carbonate breccia-conglomerates with loose sandstones-conglomerates marking the transition from the lower to the upper sequence within the Miocene sediments near Prosilio. Sample 267 was taken from the lower soft formation along the level of the road.

sliding from the Itea–Amfissa detachment footwall along the eastern Giona slopes. The upper sequence is 300 m thick, as measured along the Portes–Aghia Efthymia direction, which is perpendicular to the average 30° dip to the SW of the conglomerates (see also Fig. 8b).

On the contrary, no unconformity is traced at the outcrops near Prosilio. Instead, the conglomerates of the lower sequence progressively grade up to those of the upper sequence (Fig. 6). This transition is best observed in the area of Aghios Nikolaos on the road to Prosilio (approaching from the south) where an 8–10 metres thick compact conglomerate bed is formed, marking for the first time the arrival of the carbonate material. A spring (known as Krya Vrisi, which means 'cold spring') is observed at the base of the compact conglomerate bed due to the permeable conglomerates and the underlying impermeable argillaceous matrix. A second compact conglomerate bed with carbonate rocks is observed after an intercalation of several metres of soft conglomerates with sandstones and ophiolites within argillaceous material, similar to the beds of the lower sequence. This soft interval between the two carbonate beds shows an increase to about 40–50% in the content of carbonate clasts from 10–20% at the lower sequence. The following upper conglomerates above the second limestone conglomerate bed turn almost entirely carbonatic with 80–90% of carbonate clasts. The thickness of the two sequences in Prosilio is about 150 m for the lower sequence and 250–300 m for the upper sequence.

Large blocks and olistholites of carbonate rocks are common within the base of the coarse clastic formations of the upper sequence. This is observed almost everywhere even if there is an unconformity between the two sequences or not. Thus, large blocks of limestone are observed at the base of the upper sequence above the villages of Aghios Konstantinos and Aghios Georgios (Fig. 5a) as well as above the village of Prosilio. More spectacular phenomena are observed in the area west of Amfissa, where very large blocks of limestone are emplaced on top of the lower sequence (Fig. 5b). As a result, small-scale nappes are formed, that were emplaced during the sedimentation of the lower sequence and the transition from the lower to the upper sequence. A characteristic outcrop occurs 1 km south of Panaghia, built in the Panaghiorema gorge, where the lower sequence is observed between two blocks of limestone (Fig. 7a). The underlying limestone is of upper Cretaceous age whereas the overlying limestone is of upper Jurassic–lower Cretaceous age. The thickness of the lower sequence conglomerates separating the two limestone units ranges between 20–30 m. In this area the upper conglomerate sequence has not been traced, suggesting that the emplaced limestone blocks are substituting laterally the conglomerates of the upper sequence. The lower sequence conglomerates are deposited in a NW–SE tectonic graben in the area of Koromilies and Papa Lakkos south of Prosilio. This graben structure is filled both by the transitional conglomerate beds from the lower to the upper sequence and by olistholites of Mesozoic limestone in the area towards Prosilio in the north (Fig. 7b). These observations indicate a syn-tectonic sedimentation of the conglomerates with a pronounced activity during the transition from the lower to the upper conglomerate sequence, characterized by the emplacement of allochthonous limestone blocks. Their origin from the footwall carbonate formations of the Itea–Amfissa detachment, demonstrates the genetic relation of the sediments to the detachment. Similar synsedimentary tectonic graben structures occur also within the Aghia Efthymia conglomerates of the upper sequence as observed in a ravine draining the planar area to the SE (Fig. 8a). The synsedimentary character of the normal fault is nicely illustrated by the dragging of the stratification of the conglomerates adjacent to the fault surface and by the gradual overstep sequence which covers the top of the faulted block with the lower Jurassic limestones. This synsedimentary structure corresponds to the southwestern boundary of the tilted block of Aghia Efthymia, whose northeastern boundary is observed in the area of Portes (Fig. 8b). Here, along the Portes–Sernikaki slopes the base of the upper sequence is observed with angular unconformity on top of the lower sequence as described previously (see also Figs 4 and 5a).

The age of the sediments in the Itea–Amfissa depression remained highly controversial, with ages ranging from Neogene to Quaternary

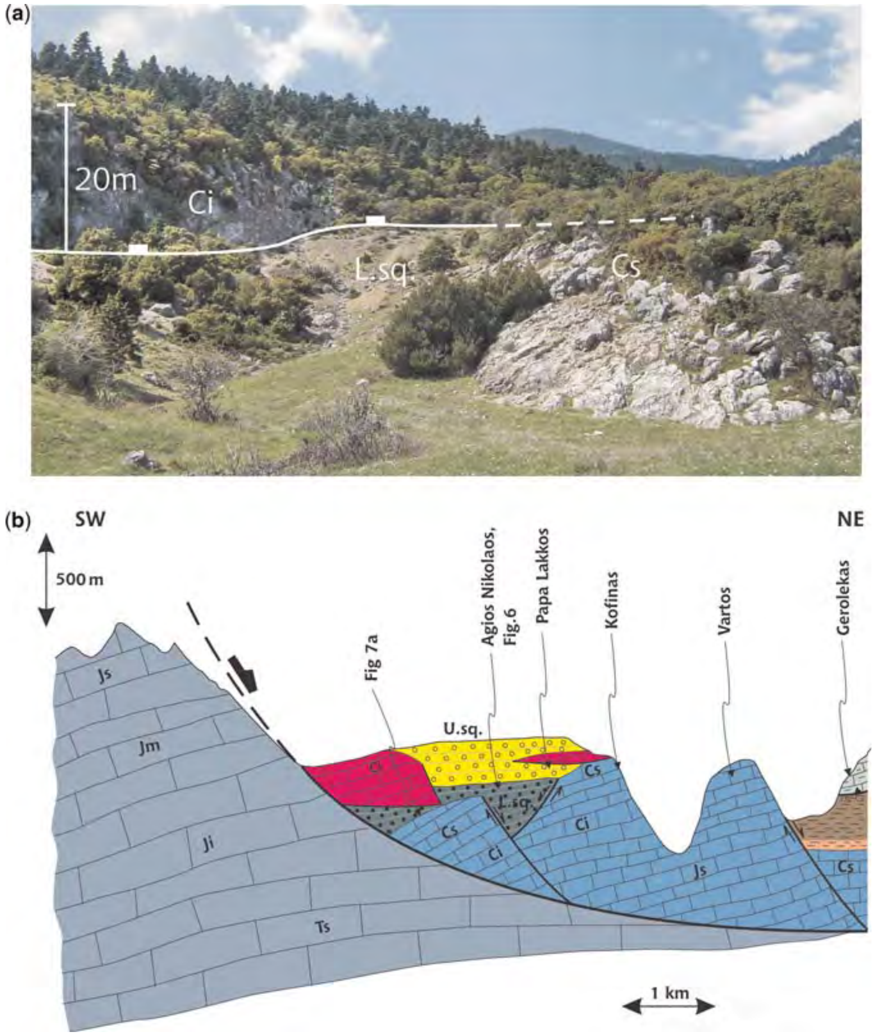

Fig. 7. (**a**) The occurrence of the lower sequence (L.sq) between two limestone blocks of upper Cretaceous (Cs) and upper Jurassic–lower Cretaceous (Ci) in the area southwest of Panaghiorema. (**b**) Schematic representation of the synsedimentary graben of Papa Lakkos south of Prosilio within the hanging wall of the Itea–Amfissa detachment.

without any stratigraphic evidence (Celet 1962; Papastamatiou *et al.* 1960, 1962). This is due to the lack of fossils within the breccia–conglomeratic sediments and the sandy matrix particularly of the upper sequence. In order to resolve this key parameter we sampled from several localities, so as to obtain some age constraints. The material has in general barren, but four sites proved successful in the calcareous nannofossil analysis (their location is indicated on Fig. 2).

The methodology comprised the following: smear slides for calcareous nannofossil analysis have been prepared following the standard preparation technique of Perch-Nielsen (1985). The smear slides preparation in terrigenous material can dilute the concentration of nannofossils that in fact are often only present or rare. In our study area however, we have chosen the simple smear slide preparation technique instead of preparing concentrated samples through settling techniques, which require ultrasonic bath treatment, in order to ensure that the smaller and more delicate forms will remain unbroken. In order to tackle the problem of dilution and search thoroughly for the maker species in the studied clastic deposits, more than one smear slides using different concentrations have been prepared from the same sample. To obtain accurate biostratigraphic estimations, up

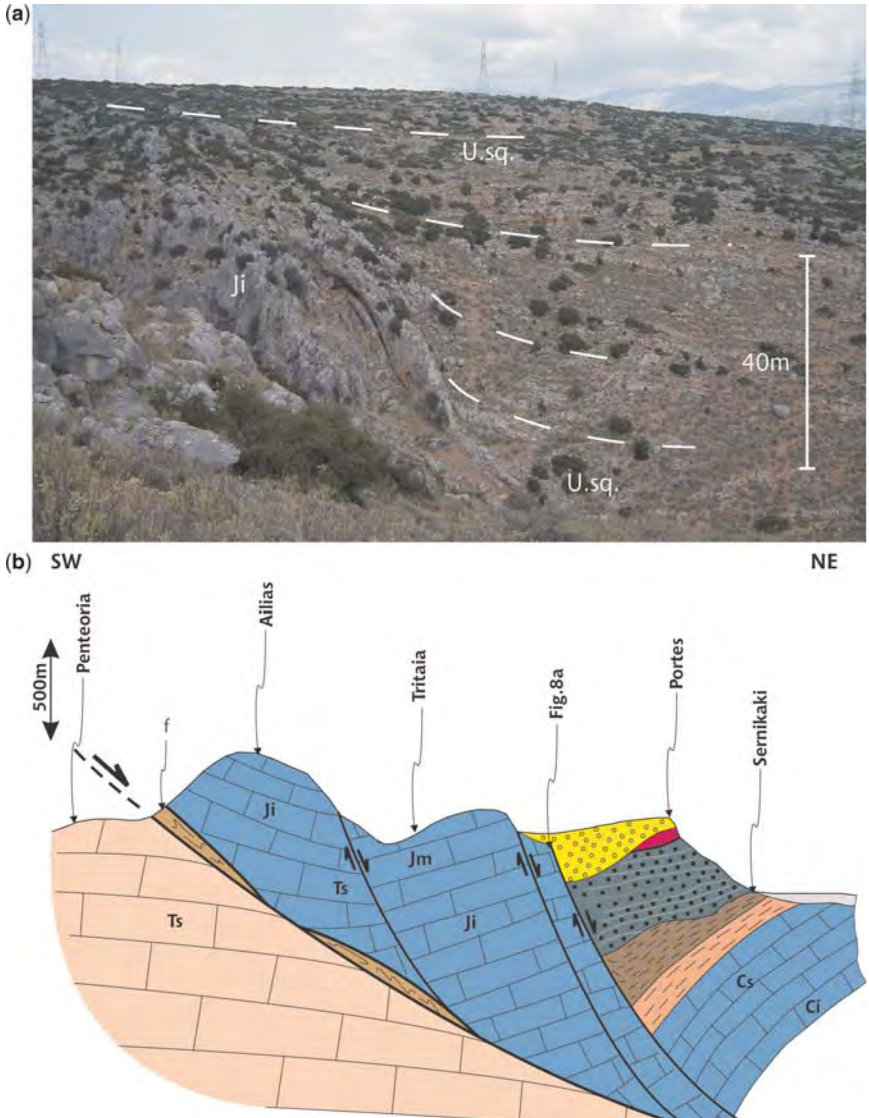

Fig. 8. (**a**) The upper sequence conglomerates (U.sq) overstepping a synsedimentary normal fault in the area east of Aghia Efthymia. Lower Jurassic limestones (Ji) dipping to the NE are observed at the footwall of the fault. (**b**) Back tilt of the upper sequence of Agia Efthymia to the SW from Portes to the detachment.

to 1500 fields of view haven been investigated per slide in longitudinal traverses randomly distributed (15 traverses; 100 fields of view per traverse), counting at least 500 specimens, with a Leica DMLSP optical polarizing light microscope at $\times 1250$. Nannofossil state of preservation is fair, showing evidence of dissolution and/or overgrowth in some specimens, but this did not hinder identifications. Semiquantitative abundances of the taxa encountered were recorded as follows: C, common: 1 specimen/10 fields of view; R, rare: 1 specimen/10–100 fields of view; P, present: 1 specimen/ >100 fields of view; RW, reworked specimens.

The nannofossil biostratigraphic results are based on the biozonal schemes of Martini (1971) and Fornaciari *et al.* (1996), as they have been incorporated in the magnetobiochronological framework of Berggren *et al.* (1995) and revised by Lourens *et al.* (2004). On this basis NN4 and NN6 biozones (Martini 1971) and MNN6b (Fornaciari *et al.* 1996) have been recognized. Numerical ages of biozone boundaries are given according to Lourens *et al*. (2004).

The obtained results are the following:

(a) Sample 265.3 (Fig. 2). The calcareous nannofossil analysis revealed the presence of common *Reticulofenestra pseudoumbilicus* (apart from isolated coccoliths several intact coccospheres have also been observed), *Discoaster variabilis* and *Cyclicargolithus floridanus* along with the absence of *Sphenolithus heteromorphus*, *Discoaster kugleri*, *Calcidiscus macintyrei*, *Helicosphaera stalis* and any trace of Late Oligocene or Pliocene biostratigraphic indices. Rare Cretaceous, common Eocene and Early Miocene reworked species are also present. Some small pennate and concentric diatoms have been detected.

The definition of *R. pseudoumbilicus* is restricted to reticulofenestrids >7 m, following Raffi & Rio (1979). The common and continuous presence of the species is concomitant with the LO of *S. heteromorphus* at the top of NN5 biozone (Fornaciari *et al.* 1996; Raffi *et al.* 1995; Maiorano & Monechi 1998).

Therefore, the nannofossil assemblage of the studied sample implies the presence of NN6 biozone (Martini 1971) or MNN6b (Fornaciari *et al.* 1996) pointing to Serravallian age, ranging between 13.4–11.8 ma.

(b) Sample 264.2 (Fig. 2). The calcareous nannofossil analysis revealed the presence of common *Cyclicargolithus abisectus*, rare forms of *Sphenolithus* cf. *Sphenolithus heteromorphus* and presence of *Helicosphaera ampliaperta*.

The nannofossil assemblage implies the tentative assignment to NN4 biozone (Martini 1971) pointing to Burdigalian-Langhian age, ranging between 18–15 ma.

(c) Sample 257.1 (Fig. 2). Rare overgrown specimens of *Coccolithus pelagicus*, *C. floridanus*, *Ericsonia formosa*, *Sphenolithus heteromorphus*, *Sphenolithus moriformis* have been detected, considered as reworked species. The assemblage does not bear any clear *in-situ* nannofossil index species pointing to an age younger than Langhian.

(d) Sample 267.1 (Fig. 2). Similar nannofossil assemblage with sample 257.1 has been detected, including rare and overgrown specimens of *Coccolithus pelagicus*, *C. floridanus*, *Ericsonia formosa*, *Sphenolithus heteromorphus*, *Sphenolithus belemnos*, *Sphenolithus moriformis*, which are considered as reworked. The assemblage does not bear any clear *in situ* nannofossil index species, pointing to an age younger than Langhian.

In conclusion, the age of the Itea–Amfissa sedimentary deposits is Early to Middle Miocene and more precisely late Burdigalian–Serravalian. Considering that the dated specimens are only extracted from the stratigraphic horizons of the lower sequence a Tortonian age is probable for the upper sequence. Thus, the entire sedimentary history of the Itea–Amfissa basin may comprise the period Late Burdigalian–Tortonian (*c*. 18–8 ma).

The Itea–Amfissa detachment

The Itea–Amfissa detachment is traced for 30 km from the Corinth Gulf in the south to Prosilio and Northern Giona Mountain in the north. It separates the eastern part of the Giona Mountain with altitudes between 1500–2200 m from the Itea–Amfissa valley with altitudes between 0–200 m. Thus, the average difference in topography observed across the detachment in east–west profiles is about 2 km. This difference in altitude is mainly observed within a narrow zone along the eastern slopes of Giona, expressed by a sub-plannar slope dipping to the east with an average dip of 30°. This sub-plannar slope is controlled by the detachment surface that passes below the hanging wall rocks, where it creates a first major break in the slope morphology of about 1200 m topographic difference. A secondary zone of steep morphological slope is developed within the hanging wall formations from the top of the hanging wall to the present day lower level of the Itea–Amfissa valley. This forms a further decrease of topography of several hundred metres expressed by well-defined morphological cliffs (Figs 4 & 9). However, the topographic difference in the Aghia Efthymia cliff is about 350–400 m (Fig. 4) whereas in Prosilio it is about 900–1000 m (Fig. 9). This second step in the Giona slopes is formed by erosional incision of the planation surface at the top of the Miocene clastic deposits occurring in Aghia Efthymia and Prosilio. Considering the difference of elevation of about 1400 m within 30 km distance between the Prosilio, Aghia Efthymia and Galaxidi outcrops of the Miocene clastic formations a general southward tilt of *c*. 3° of the planation surfaces on top of the clastic sediments can be inferred.

The detachment fault plane is exposed in several localities. The best preserved outcrop occurs at the southern part of the detachment in the area east of Penteoria as shown on the detailed geological map of the area (Fig. 10). In this area the fault plane is marked by the existence of some tectonic lenses between the carbonate rocks of the Penteoria nappe in the footwall and those of the Parnassos

Fig. 9. The planation surface above Prosilio on top of the upper sequence (U.sq) as seen from the east and simplified geological sketch. The sediments of the upper sequence are marked by the cliff formed by the erosional incision right above the level of Prosilio village. Below the cliff a triangular outcrop of the lower sequence (L.sq) is formed, bounded to the north by a NE–SW transverse normal fault. Behind the Prosilio planation surface the geometrical eastern slopes of Giona Mountain (shaded in grey) delineate the Itea–Amfissa detachment up to the Reka valley. Note the gradual decrease of the morphological expression of the detachment from left (south) to right (north) along the Giona slopes (indicated by vertical lines).

nappe in the hanging wall. The rocks within the tectonic wedges along the detachment belong to the Eocene flysch (probably belonging to the Penteoria unit) and to the Upper Triassic–Upper Jurassic pelagic carbonates of the Vardoussia unit. The best outcrop of the detachment is observed along the contact of the underlying Upper Triassic carbonates of the Penteoria unit and the overlying Eocene flysch (Fig. 11). This planar contact can be observed for about 500 m length and locally it has a width of about 25–40 m. The dip of the detachment is 30° to N 45° E and the slip direction as deduced from kinematic indicators is slightly oblique in an N 60° E direction.

The throw across the detachment cannot be accurately constrained because there are no outcrops of the same tectono-stratigraphic units on either side of the detachment. As shown in the description of the geological structure of the area there are several thrust sheets within the Parnassos nappe therefore no correlation is feasible on either side of the detachment. Along the southern part of the detachment east of Penteoria the throw incorporates the structural omission of the Jurassic and Cretaceous part of the Penteoria sequence (several hundred metres thick), the whole stratigraphic column of the Vardoussia nappe (exceeding 1 km of thickness) and unknown number of thrust sheets of the Parnassos nappe. The minimum calculated throw, where no thrust sheets of the Parnassos unit are considered, is estimated at several hundred metres, which represents the structural omission of the Upper Triassic platform carbonates of Parnassos. Taking into account the throw inferred from the topography between the Jurassic formations on either side of the detachment, that is more than 800 m, then the overall minimum throw is 2500–2800 m. On the other hand along the northern part of the detachment around Prosilio the minimum throw is 4400 m incorporating: (i) the thickness of the upper thrust sheets of Parnassos (more than 2200 m in thickness); (ii) the overlying nappe of Western Thessaly–Beotia (more than 400 m thick); (iii) the missing Jurassic part of the Parnassos platform (about 800 m thick); and (iv) the topographic difference between the footwall carbonates of Parnassos and the nappe of Western Thessaly–Beotia in Gerolekas at the hanging wall (about 900–1000 m).

Considering an average dip of 30° for the detachment the total displacement in the E–NE direction is more than 9 km. This value is very close to the present width of the Itea–Amfissa Valley measured at the 1000 m contour level between the Eastern Giona and Western Parnassos slopes.

The contrast between the footwall and the hanging wall structure of the detachment is impressive. Thus, a rather rigid structure can be observed all along the footwall with the lower stratigraphic levels of the Parnassos unit (Upper Triassic–Middle Jurassic) dipping 20°–30° to the west. In contrast, the hanging wall is made of a complex

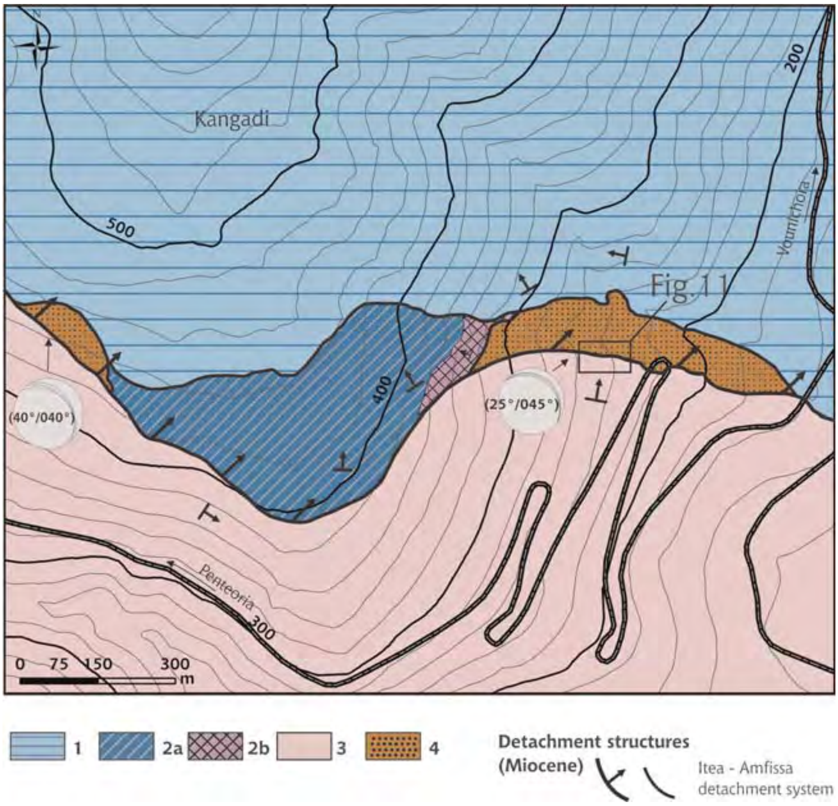

Fig. 10. Detailed geological map of the area on both sides of the detachment at southern Giona between Galaxidi and Penteoria. For location see geological map of Figure 2. (1) Lower Jurassic carbonate rocks of Parnassos nappe; (2a) Jurassic pelagic limestones of Vardoussia nappe, (2b) Upper Triassic pelagic limestones of Vardoussia nappe; (3) Upper Triassic neritic limestones of Penteoria nappe; (4) Eocene flysch of Penteoria nappe.

structure of small-scale blocks of Mesozoic limestones and early Tertiary flysch, which have slided to the E–NE during the sedimentation of the Itea–Amfissa sedimentary deposits (Fig. 12a). The interfingering of the conglomerates with the olistholites and the small gravity nappes along the hanging wall provide a characteristic view of it. This is accentuated during the sedimentation of the upper conglomeratic formation with the carbonate rocks, which are traced both in front and above the sliding blocks.

The faults observed on the hanging wall trend either parallel to the detachment or transverse. In both cases they do not penetrate the footwall rocks, but they are synchronous to the sedimentation of the lower sequence and die out during the sedimentation of the upper sequence. The transverse faults have a general NE–SW direction and they form three distinct fault zones (Fig. 12b). The southern fault zone passes north of Itea, the middle passes south of Amfissa and the northern one passes north of Prosilio (Figs 2 & 12b). These ENE–WSW trending faults have produced a syn-sedimentary tilt to the NW of the lower sequence during middle Miocene and at the same time they bound to the north the outcrops of the upper sequence. The faults parallel to the detachment are forming back tilted blocks within the Alpine formations and syn-sedimentary tectonic grabens filled with clastic sediments similar with the lithologies of the sliding limestone blocks (Fig. 12a). The most characteristic structure is observed in the area of Aghia Efthymia, where the upper sequence dips 30° to the SW against the NW–SE trending fault passing from the Itea harbor and the village of Aghia Efthymia (Figs 2 & 8b). The same tilt to the SW is observed in the sediments of the upper sequence in Prosilio against the detachment surface at 1300 m of altitude (Figs 2 & 7b).

The overall structure within the hanging wall of the Itea detachment is illustrated in two schematic profiles; one across the hanging wall in an east–west direction and the other longitudinal in a north–south direction (Fig. 12). These profiles

Fig. 11. The outcrop of the detachment in the area between Galaxidi and Penteoria. Its location is shown in the geological map of Figure 10. The cliff above the detachment is made of the Vardoussia pelagic Jurassic sediments (2) found in tectonic wedge between the upper Triassic neritic limestones of the Penteoria nappe (1) in the footwall and the lower Jurassic neritic limestones of the Parnassos nappe (3) in the hanging wall. The flat area with the olive trees corresponds to the Eocene flysch (4).

provide the relationship between the sliding of the carbonate units above the detachment together with the sedimentation of the two sequences of breccia–conglomerates. The role of the parallel faults creating the sliding blocks and the resulting horsts and grabens in the north–south trend is illustrated by the transverse section (Fig. 12a), whereas the longitudinal section demonstrates the role of the transverse NE–SW faults that dissect the hanging wall structure in successive blocks along strike (Fig. 12b).

Northwards the detachment can be traced up to the Reka Valley that has an east–west orientation and starts from the area of the Giona summit (2507 m) and ends at the Viniani depression, which occurs below Prosilio at about 7 km north of the Amfissa depression. North of the Reka Valley there is no morphological expression of the detachment but a high-angle normal fault (50°–60° dip to the E–NE) separates the footwall Jurassic carbonates dipping to the west from the hanging wall Cretaceous carbonates dipping to the east (Fig. 13). This fault has a throw exceeding 1200 m, based only from the missing stratigraphic horizons between the footwall and the hanging

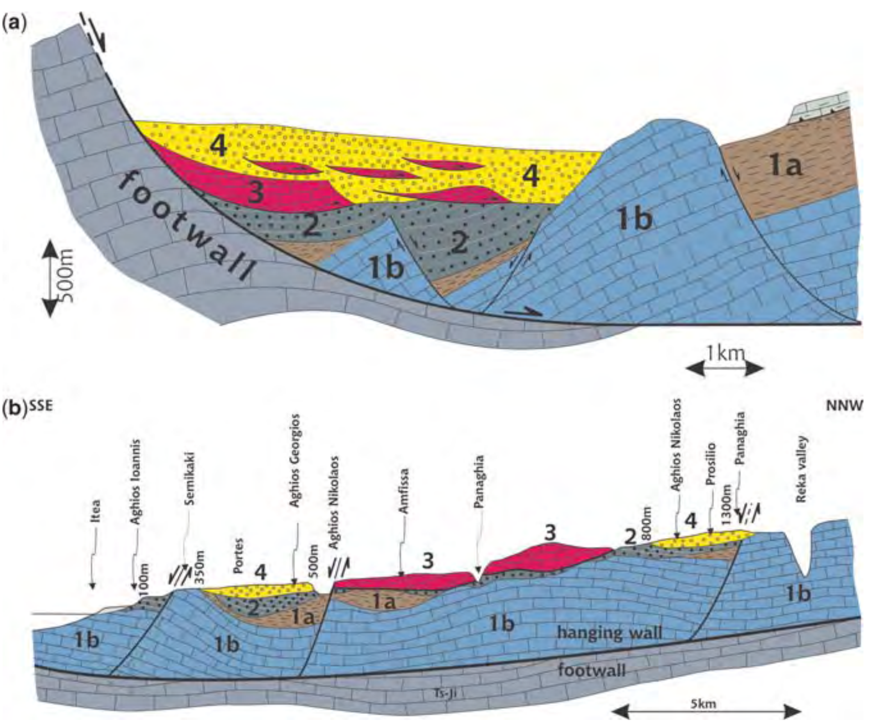

Fig. 12. Schematic profiles of the structure within the hanging wall of the Itea–Amfissa detachment: (**a**) transverse and (**b**) longitudinal. (1) Autochthonous blocks, (1a) Eocene flysch, (1b) Mesozoic limestones; (2) Lower Sequence of Early–Middle Miocene sediments; (3) Allochthonous blocks, mainly of Mesozoic limestones; (4) Upper Sequence of Middle–Late ?Miocene sediments.

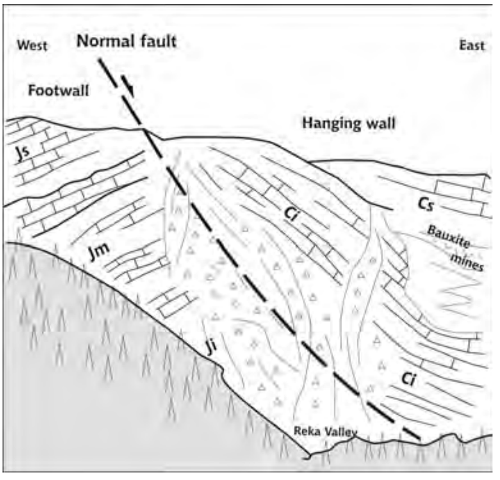

Fig. 13. Panoramatic sketch of the tectonic structure on the northern side of the Reka Valley in Northern Giona as seen from the south in 1400 m of altitude. The Jurassic carbonate rocks in the footwall dip to the west whereas the Cretaceous carbonate rocks in the hanging wall dip to the east. North of the Reka Valley the morphological expression of the extensional structure becomes insignificant, the dip of the normal fault is steep, between 50°–60°, and the throw becomes minimum (a little more than 1 km).

wall. Thus, the extension of the Itea–Amfissa detachment to the north of the Reka Valley is expressed as a high angle normal fault, which terminates along the northern slope of the Giona Mountain that is controlled by a major east–west-trending normal fault – the Northern Giona fault (Fig. 1).

The age of the detachment is indicated by the age of the syntectonic sedimentation of the Itea–Amfissa basin, which is dated as Burdigalian–Serravalian. The probable extension of the upper part of the conglomerates in the Tortonian indicates the most probable time range for the tectonic activity between the late Burdigalian and the Tortonian, which is ranging between 18–8 ma.

The Corinth rift structures

The continuation of the Itea–Amfissa detachment to the south is disrupted by east–west trending steep normal faults present in the area west of Galaxidi (Fig. 14). These faults form part of the Corinth rift system and their throw is in the order of several tens of metres with subsidence occurring of the southern blocks towards the Corinth Gulf. These onshore normal faults are an exception along the southern coast of Sterea Hellas, because the major faults forming the northern margin of

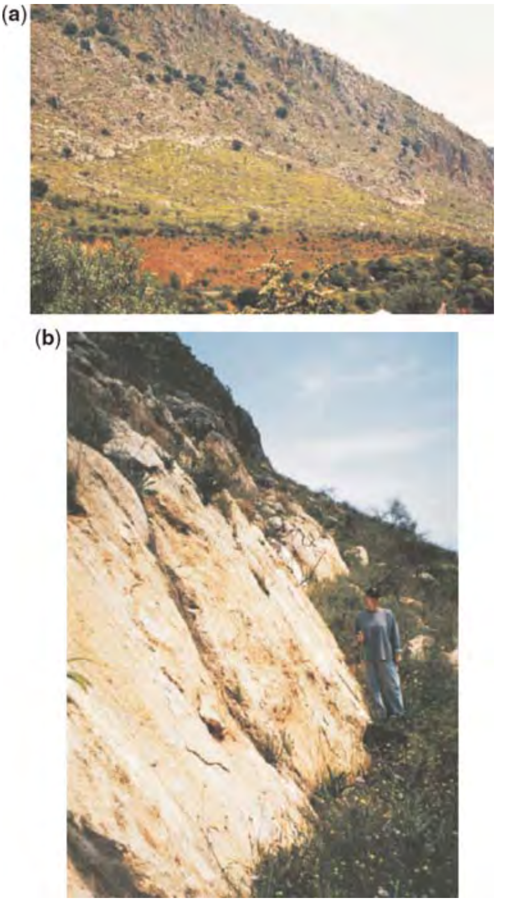

Fig. 14. (**a**) East–ENE–trending normal fault in the area west of Galaxidi near the Corinth coast, alongside the main road Itea–Nafpaktos. (**b**) Close view of the same fault with the Holocene fault scarp, which exceeds 3–4 m in height.

the Corinth Gulf and the rift structure are located offshore several km to the south (Moretti *et al.* 2003). Nevertheless, the characteristics of these faults near Galaxidi show recent activity in the Holocene, as the well-developed post-glacial scarps exceeding 3–4 m of height indicate (e.g. Stewart & Hancock 1991; Roberts 1996). The Itea–Amfissa detachment is expected to continue southwards below the sea bottom of the Corinth Gulf, which has been formed in the late Pliocene–Quaternary, much later than the detachment.

The only east–west fault occurring in the broader area of Parnassos and Giona mountains is the Delphi fault, which runs parallel to the Delphi Valley. However, this fault is a questionable structure, because from one side it shows some recent activity by affecting consolidated scree and slope debris of the Parnassos slopes, but it also exhibits similar geometry to the Alpine structures of the Parnassos unit in the other. Thus, the overall geometry of thrusting and folding from the Parnassos summit to the north up to the Corinth Gulf in the south consists of a number of east–west trending tectonic units-thrusts, incorporating the carbonate platform and the flysch. Especially at the archaeological site of Delphi there is an overturned stratigraphic section placing the Eocene flysch below the upper Cretaceous limestones, resulting in the formation of the famous from the antiquity Kastalia spring. Overall, the Delphi Valley is not a graben-like neotectonic structure and it cannot be explained solely by the activity of the Delphi fault.

Discussion and conclusions

The Itea–Amfissa detachment trending NNW–SSE is a major Miocene extensional structure that followed the co-parallel compressive deformation, which created the nappes, the internal thrusting and the folding of the Alpine units of the area. Thus, the older Alpine deformation of east–west compression was followed by east–west extension. The parallel trend of the detachment with that of the previous compressive structures shows the fundamental change in position of the Giona–Parnassos area from the frontal compressive zone of the evolving orogenic arc of the Hellenides during the Oligocene period, to the co-parallel extensional zone in its backarc area during the Miocene. Thus, when the Itea–Amfissa detachment was formed, the zone of east–west compression had migrated westwards along the Gavrovo and Ionian units of the External Hellenides.

The age of the detachment is Middle–Late Miocene as the dated syn-tectonic sediments of the Itea–Amfissa basin indicates. The end of the east–west extensional phase that produced the detachment cannot be accurately determined, because the higher stratigraphic beds of the upper sequence have not been dated. Thus, the only age constraint can be pre-Late Pliocene that is pre-dating the fossiliferous Late Pliocene and Pleistocene sediments of the Corinth rift structure. Considering the above, the east–west extensional activity occurred in the Middle–Late Miocene, even though a possible extension also into the Early Pliocene cannot be excluded.

Similar geodynamic phenomena with impressive tectono-stratigraphic formations comprising olistholites of Alpine rocks mixed with breccia and conglomerates in the Middle Miocene are known also from the Cyclades and Crete (Fortuin 1978; Dermitzakis & Papanikolaou 1981; Fortuin & Peters 1984). More recently, these formations like the Prina Complex in eastern Crete (Fortuin 1978; Fortuin & Peters 1984) have been related to the activity of the Cretan detachment (van Hinsbergen & Meulenkamp 2006).

The Itea–Amfissa detachment can be traced for about 30 km from the coast of Itea to Prosilio and dies out to the north within the Northern Giona Mountain, where it is substituted by a high angle normal fault with kilometric order of throw. The whole extensional structure does not continue north of the east–west-trending Northern Giona normal fault. In contrast, it expands southwards crossing the Corinth Gulf and is probably linked to the East Peloponnesus detachment, whose length exceeds 150 km from the area of Feneos in Northern Peloponnesus to the area of Kyparissi to the south-east (Papanikolaou & Royden 2007). The age of the East Peloponnesus detachment is not well constrained, but on the basis of the Tortonian sediments on Kythera Island, in the Cretan Basin and on Spetses Island, a Late Miocene–Early Pliocene age has been proposed (Papanikolaou & Royden 2007). Now, in view of the new age constraints in the Itea–Amfissa basin, an older age may be accepted for the East Peloponnesus detachment incorporating also the Middle Miocene.

The throw of the East Peloponnesus detachment has been determined based on the tectono-stratigraphic structural omission of the nappes of the Hellenides on top of the relative autochthon unit of Mani (or metamorphic Ionian). The diagram showing the structural omission along the East Peloponnesus detachment indicates a gradual decrease of the throw towards the north in the area of Itea–Amfissa, where it dies out in the northern Giona area (Fig. 15). Thus, the Itea–Amfissa detachment represents the northern end of the East Peloponnesus detachment.

The disruption of the arc parallel extensional structures, like the Itea–Amfissa detachment, by the transverse extensional structures, such as those of the Corinth rift system, occur within the Central Hellenic Shear Zone (CHSZ), which has been defined on the basis of present day GPS data (Papanikolaou & Royden 2007), but can be probably traced back to initiation in the Late Pliocene. The northern boundary of the CHSZ coincides with the North Aegean Basin, which is interpreted as the western prolongation of the North Anatolian Fault (e.g. Armijo *et al.* 1999). It is remarkable that the timing of the westward propagation of the North Anatolian Fault into the North Aegean Basin is Late Pliocene and this is related to the onset of the recent and active Aegean extension in the north–south direction (Armijo *et al.* 1999; Flerit *et al.* 2004; Papanikolaou *et al.* 2002, 2006). However, the initiation of the CHSZ is probably also related to the change from a former continuous

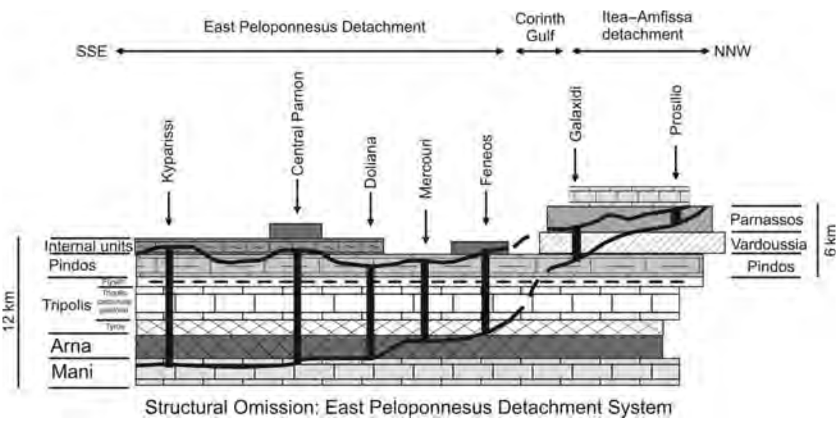

Fig. 15. Diagram of the structural omission along the East Peloponnesus Detachment System based on Papanikolaou & Royden (2007). Units between the upper and lower black lines are missing across the detachment surface; missing sequences at specific localities are indicated by the vertical black bars. The Itea–Amfissa Detachment corresponds to the northern end of the system north of the Corinth rift structure.

Hellenic arc structure until Middle–Late Miocene to the present day Hellenic arc and trench system, which is restricted to the Preveza area by the Kefalonia transform fault (Papanikolaou & Dermitzakis 1981). This younger structure of the Hellenic arc does not extend north of the Kefalonia transform and is related to the onset of the rapid subduction of the oceanic crust of the East Mediterranean Basin that occurred between Late Miocene–Early Pliocene.

In conclusion, the deformation of the Parnassos–Giona area of central Sterea Hellas is characterized by three deformational phases; the first two are arc parallel structures of east–west compression during Oligocene and east–west extension during Miocene, followed by the third deformational phase of north–south extension, which has disrupted the arc since Late Pliocene time.

This is a contribution to the MEDUSA project, funded by the NSF Continental Dynamics Program, grant EAR-0409373. The University of Athens has contributed to some of the field expenses. Constructive comments by M. Edwards, F. Flerit and I. Papanikolaou have significantly improved the manuscript.

References

ARMIJO, R., MEYER, B., KING, G., RIGO, A. & PAPANASTASSIOU, D. 1996. Quaternary evolution of the Corinth Rift and its implications for the late Cenozoic evolution of the Aegean. *Geophysical Journal International*, **126**, 11–53.

ARMIJO, R., MEYER, B., HUBERT, A. & BARKA, A. 1999. Westward propagation of the North Anatolian Fault into the northern Aegean: timing and kinematics. *Geology*, **27**, 267–270.

BERGGREN, W. A., KENT, D., SWISHER, C. C. & AUBRY, M. P. 1995. A revised Cenozoic geochronology and chronostratigraphy. *In*: BERGGREN, W. A., KENT, D. V., AUBRY, M. P. & HARDENBOL, J. (eds), *Stratigraphic Correlation*. Society for Sedimentary Geology (SEPM), Special Publication, **54**, 129–212.

CELET, P. 1960. Observations sur la tectonique de la région côtiere méridionale de massifs du Parnasse – Kiona. *Bulletin de la Societe Geologique de France*, **7/2**, 427–434.

CELET, P. 1962. Contribution a l'étude géologique du Parnasse-Kiona et d' une partie des régions méridionales de la Grèce continentale. *Annales Geologiques des Pays Helleniques*, **13**, 1–446.

CELET, P., CLEMENT, B. & FERRIERE, J. 1976. La zone beotienne en Grece; implications paleogeographiques et structrales. *Eclogae Geologicae Helvetiae*, **69**, 577–599.

DERMITZAKIS, M. & PAPANIKOLAOU, D. 1981. Paleogeography and Geodynamics of the Aegean Region during the Neogene. *VIIth International Congress on Mediterranean Neogene, Athens 1979, Proceedings IV*, 245–288.

FLERIT, F., ARMIJO, R., KING, G. & MEYER, B. 2004. The mechanical interaction between the propagating North Anatolian Fault and the back-arc extension in the Aegean. *Earth Planetary Science Letters*, **224**, 347–362.

FORNACIARI, E., DI STEFANO, A., RIO, D. & NEGRI, A. 1996. Middle Miocene quantitative calcareous nannofossil biostratigraphy in the Mediterranean region. *Micropaleontology*, **42**, 37–64.

FORTUIN, A. R. 1978. Late Cenozoic history of eastern Crete and implications for the geology and geodynamics of the southern Aegean area. *Geologie en Mijnbouw*, **57**, 451–464.

FORTUIN, A. R. & PETERS, J. M. 1984. The Prina Complex in eastern Crete and its relationship to possible Miocene strike-slip tectonics. *Journal of Structural Geology*, **6**, 459–476.

JOHNS, D. R. 1979. The structure and stratigraphy of the Galaxidion region, Central Greece. *VI Colloquium on the Geology of the Aegean Region, Proceedings II*, 715–724.

KRANIS, H. & PAPANIKOLAOU, D. 2001. Evidence for detachment faulting on the NW Parnassos Mountain front (Central Greece). *Bulletin of the Geological Society of Greece*, **34**, 281–287.

LOURENS, L., HILGEN, F., SHACKLETON, N. J., LASKAR, J. & WILSON, D. 2004. The Neogene Period. *In*: GRADSTEIN, F., OGG, J. & SMITH, A. (eds) *A Geologic Time Scale 2004*. Cambridge University Press, 409–440.

MAIORANO, P. & MONECHI, S. 1998. Revised correlations of Early and Middle Miocene calcareous nannofossil events and magnetostratigraphy from DSDP Site 563 (North Atlantic Ocean). *Marine Micropaleontology*, **35**, 235–255.

MARTINI, E. 1971. Standard Tertiary and Quaternary calcareous nannoplankton zonation. *In*: FARINACCI, A. (ed.) *Proceedings of the Second Planktonic Conference*. Roma, Technoscienza, 739–785.

MORETTI, I., SAKELLARIOU, D., LYKOUSSIS, V. & MICARELLI, L. 2003. The Gulf of Corinth: an active half graben? *Journal of Geodynamics*, **36**, 323–340.

PAPANIKOLAOU, D. 1986. Late Cretaceous paleogeography of the Metamorphic Hellenides. Geological and Geophysical Research, IGME, Special issue in honour of Professor Papastamatiou, 315–328.

PAPANIKOLAOU, D. & DERMITZAKIS, M. 1981. *Major changes from the last stage of the Hellenides to the actual Hellenic arc and trench system*. International Symposium on the Hellenic Arc and Trench System (HEAT), Athens 1981, Proceedings II, 57–73.

PAPANIKOLAOU, D. & ROYDEN, L. 2007. Disruption of the Hellenic Arc: Late Miocene Extensional Detachment Faults and Steep Pliocene-Quaternary Normal faults – or – What happened at Corinth? *Tectonics*, **26**, TC5003, doi:10.1029/2006TC002007.

PAPANIKOLAOU, D. & SIDERIS, C. 1979. Sur la signification des zones ultrapindique et beotienne d'apres la geologie de la region de Karditsa: l'Unite de Thessalie Occidentale. *Eclogae Geologicae Helvetiae*, **72**, 251–261.

PAPANIKOLAOU, D., ALEXANDRI, M., NOMIKOU, P. & BALLAS, D. 2002. Morphotectonic structure of the western part of the North Aegean Basin based on swath bathymetry. *Marine Geology*, **190**, 465–492.

PAPANIKOLAOU, D., ALEXANDRI, M. & NOMIKOU, P. 2006. Active faulting in the North Aegean Basin. *Geological Society of America Special Paper*, **409**, 189–209.

PAPASTAMATIOU, J. 1960. La geologie de la region Montagneuse du Parnasse – Kiona – Oeta. *Bulletin of the Society of Geology France, II*, **Paris**, 398–408.

PAPASTAMATIOU, J. & TATARIS, A. 1963. Tectonics of the transitional sediments from the Parnassos-Giona unit to the Olonos-Pindos unit. *Bulletin of the Geological Society of Greece*, **5**, 86–89.

PAPASTAMATIOU, J., VETOULIS, D., MPORNOVAS, J., CHRISTODOULOU, G. & KATSIKATSOS, G. 1960. *Geological map of Greece*. scale 1:50 000. Sheet Amfissa. Institute of Geology and Subsurface Research, Athens.

PAPASTAMATIOU, J., TATARIS, A., KATSIKATSOS, G., MARANGOUDAKIS, N., KALLERGIS, G. & ELEUTHERIOU, A. 1962. *Geological map of Greece*. Scale 1:50 000. Sheet Galaxidion. Institute of Geology and Subsurface Research, Athens.

PERCH-NIELSEN, K. 1985. Cenozoic calcareous nannofossils. *In*: BOLLI, H. M., SAUNDERS, J. B. & PERCH-NIELSEN, K. (eds) *Plankton Stratigraphy*. Cambridge Earth Science Series, 427–554.

PHILIPPSON, A. 1898. La tectonique de l'Egeide. *Annales de Geographie*, **7**, 112–141.

RENZ, C. 1955. *Stratigraphie von Griechenland*. Institute of Geology and Subsurface Research, Athens.

RAFFI, I. & RIO, D. 1979. Calcareous nannofossil biostratigraphy of DSDP Site 132, Leg 13 (Tyrrhenian Sea, Western Mediterranean). *Rivista Italiana di Paleontologia e Stratigrafia*, **85**, 127–172.

RAFFI, I., RIO, D., D'ATRI, A., FORNACIARI, E. & ROCCHETTI, S. 1995. Quantitative distribution patterns and biomagnetostratigraphy of middle and late Miocene calcareous nannofossils from equatorial Indian and Pacific oceans (Leg 115, 130, and 138). *Proceedings ODP Science Results*, **138**, 479–502.

ROBERTS, G. P. 1996. Noncharacteristic earthquake ruptures from the Gulf of Corinth, Greece. *Journal Geophysical Research*, **101**, 25 255–25 267.

SCHWAN, W. 1976. Strukturen, Kinematik und tektonische Stellung des Parnass-Ghiona-Gebirges im Helleniden-Orogen. *Zeitschrift der Deutschen Geologischen Gesellschaft*, **127**, 373–386.

STEWART, I. S. & HANCOCK, P. L. 1991. Scales of structural heterogeneity within neotectonic normal fault zones in the Aegean region. *Journal Structural Geology*, **13**, 191–204.

VAN HINSBERGEN, D. & MEULENKAMP, J. 2006. Neogene supradetachment basin development on Crete (Greece) during exhumation of the South Aegean core complex. *Basin Research*, **18**, 103–124.

WIEDENMAYER, F. 1963. Sur quelques ammonites provenant d'un gisement a cephalopods a Penteoria (Grece). *Bulletin Geological Society of Greece*, **5**, 28–40.

Neogene brittle detachment faulting on Kos (E Greece): implications for a southern break-away fault of the Menderes metamorphic core complex (western Turkey)

DOUWE J. J. VAN HINSBERGEN* & FLORA BOEKHOUT

Palaeomagnetic laboratory 'Fort Hoofddijk', Utrecht University, Faculty of Geosciences, Budapestlaan 17, 3584 CD Utrecht, The Netherlands

**Corresponding author (e-mail: hins@geo.uu.nl)*

Abstract: The southern limit of the Menderes metamorphic core complex has recently been proposed to be formed by an Oligocene–early Miocene top-to-the-north breakaway detachment fault, the Datça–Kahle fault running across the Lycian nappes in southwestern Turkey. Proving a breakaway detachment fault as opposed to a 'simple' local high-angle normal fault is generally hampered by absence of a metamorphic contrast between hanging wall and footwall. The island of Kos lies close to the inferred southern breakaway fault. It exposes Permo- Carboniferous anchi-metamorphic rocks, intruded and contact-metamorphosed at upper crustal levels by a 12 Ma old monzonite during or close to peak-burial conditions. Here, we show that exhumation of these rocks occurred along a top-to-the-north brittle extensional detachment fault underneath upper Mesozoic and Palaeogene non-metamorphic carbonates after 12 Ma, and that any (undocumented) earlier extension did not lead to significant exhumation of the Permo-Carboniferous rocks. Kos should thus be placed within the Cyclades–Menderes extensional province since 12 Ma. The age of exhumation is younger than the proposed activity of the breakaway fault, the existence of which we cannot corroborate. We conclude that the brittle detachment of Kos cannot be straight-forwardly correlated to any ductile-to-brittle detachments of the Menderes or eastern Cycladic metamorphic core complexes further to the north and may represent a relatively isolated structure.

Metamorphic core complexes have since long been recognized to form due to exhumation along low-angle extensional detachment faults that juxtapose high-grade metamorphic rocks in the footwall against upper crustal rocks in the hanging wall (Crittenden *et al.* 1980; Wernicke 1981, 1995; Davis 1983, Lister *et al.* 1984; Lister & Davis 1989; Fig. 1). Recent modelling of formation of metamorphic core complexes suggests that core complexes form in two stages: in the first stage, symmetric boudinage of the crust leads to a graben at the surface and lower crustal flow into the extending region, followed by a second stage where a mid-crustal shearzone at depth links with one of the brittle graben-bounding faults in the upper crust to form an sigmoidal extensional detachment along which a metamorphic dome is exhumed to the surface (Tirel *et al.* 2008, 2009).

Due to the asymmetric structure of a metamorphic core complex, its boundaries on either side are markedly different: on one side they are easily recognizable by the existence of a ductile-to-brittle extensional detachment with a sharp metamorphic contrast between the lower metamorphic grade hanging wall and higher metamorphic grade footwall. On the opposite side, the metamorphic grade of the footwall will more gradually decrease and eventually the detachment will lack a ductile history, juxtaposing only upper crustal, low-grade metamorphic rocks in footwall and hanging wall in an area between the exhumed metamorphic rocks and a break-away fault (Fig. 1). This break-away fault can be considered to be the boundary of the metamorphic core complex (Dorsey & Becker 1995; Otton 1995; van Hinsbergen & Meulenkamp 2006).

The Menderes core complex in western Turkey (Fig. 2) is one of the largest in the world and formed as a result of *c.* north–south extension in the Aegean backarc since the late Oligocene (Bozkurt & Park 1994; Hetzel *et al.* 1995*a*, *b*; Bozkurt & Satir 2000; Bozkurt & Oberhänsli 2001; Gessner *et al.* 2001). Multiple extensional detachment faults with both top-to-the-north and top-to-the-south sense of shear have been recognized in the Menderes massif, and a clear structural asymmetry on the scale of the whole massif is not evident (Hetzel *et al.* 1995*a*; Gessner *et al.* 2001). Recently, however, Seyitoğlu *et al.* (2004) postulated that an Oligocene–lower Miocene 'Kahle–Datça fault zone' in the central part of the Lycian nappes of southwestern Turkey (Fig. 2) formed a break-away fault of the Menderes metamorphic core complex, thus suggesting that in the early

From: VAN HINSBERGEN, D. J. J., EDWARDS, M. A. & GOVERS, R. (eds) *Collision and Collapse at the Africa–Arabia–Eurasia Subduction Zone*. The Geological Society, London, Special Publications, **311**, 311–320.
DOI: 10.1144/SP311.12 0305-8719/09/$15.00

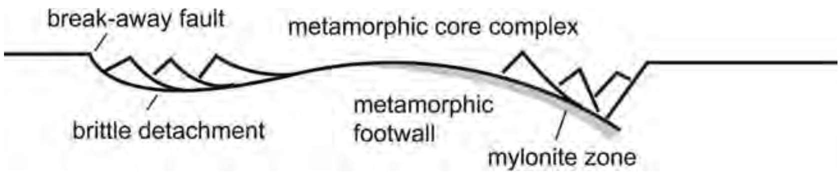

Fig. 1. Schematized cross-section of a metamorphic core complex, indicating the relationship between the break-away fault and the position of the metamorphic core (modified after Lister & Davis (1989)).

stages of exhumation, top-to-the-north unroofing was the dominant process of exhumation. Proving that the Kahle–Datca fault zone is indeed a break-away brittle detachment fault, as opposed to a relatively small-displacement normal fault is difficult, since the most obvious criterion for an extensional detachment fault – a metamorphic contrast between hanging wall and footwall – is absent.

The island of Kos (Fig. 2), however, may provide a case to test the existence of a brittle extensional detachment between the Kahle–Datca fault and the metamorphic complex of the Menderes. Kos is located only about 15 kilometres NW of the Datça fault, and *c.*15 km SW of the Bodrum peninsula, where the southernmost metamorphic rocks flanking the Menderes massif were found (Rimmelé *et al.* 2003). The Dikeos Window in southeastern

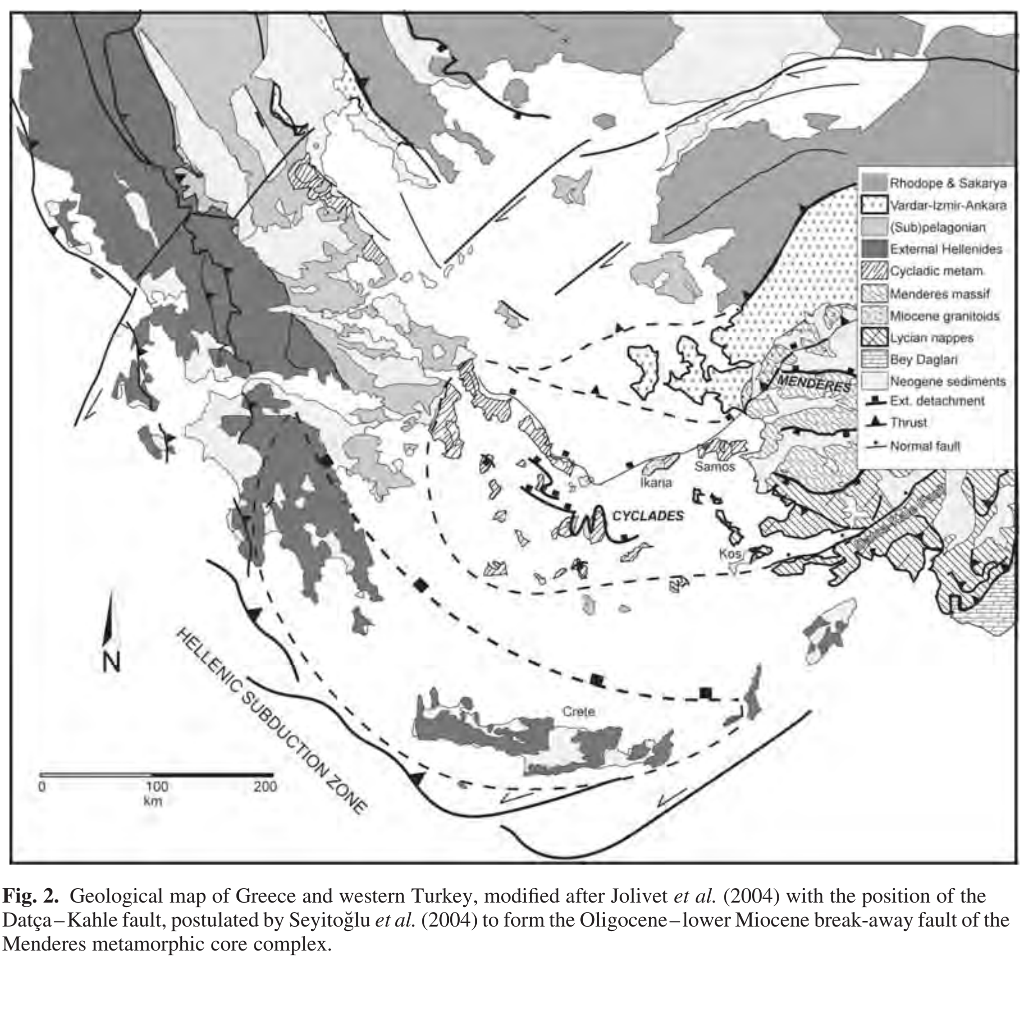

Fig. 2. Geological map of Greece and western Turkey, modified after Jolivet *et al.* (2004) with the position of the Datça–Kahle fault, postulated by Seyitoğlu *et al.* (2004) to form the Oligocene–lower Miocene break-away fault of the Menderes metamorphic core complex.

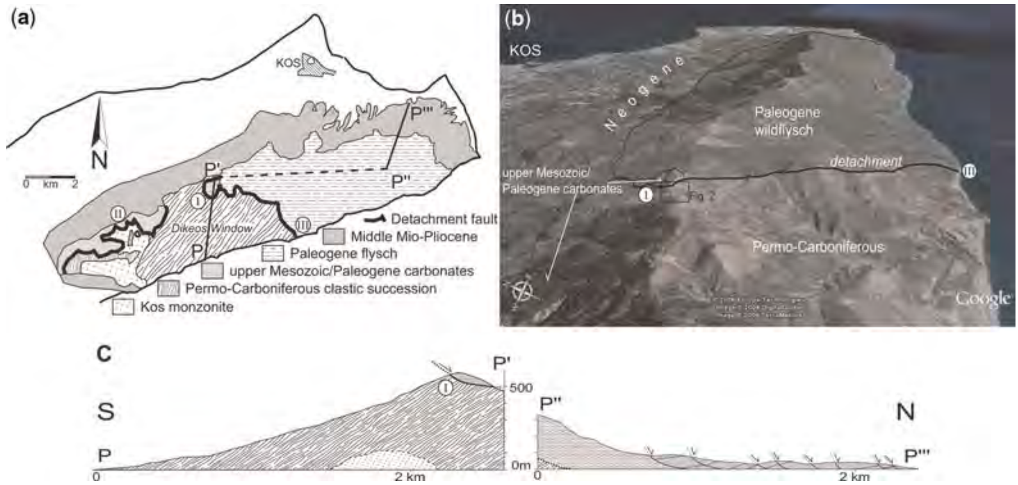

Fig. 3. (**a**) Geological map of eastern Kos, modified after Böger *et al.* (1974) and Altherr *et al.* (1976); Figure 6 shows field photographs of location II near Paleo Pili. (**b**) Google Earth image of the topography and satellite image of eastern Kos looking eastward, with the outline of the Kos detachment. Locations I and III described and discussed in the text are indicated at their field positon. Pictures and drawings in Figure 4 are located at Location I. (**c**) Schematic geological cross-section PP‴, partly modified after Böger *et al.* (1974). For location of cross section see Figure 3a.

Kos exposes Permo-Carboniferous sedimentary rocks which were intruded and metamorphosed at shallow crustal levels by the Kos monzonite around 12 Ma (Altherr *et al.* 1976; Kalt *et al.* 1998). A brittle fault zone separates these rocks from isolated occurrences of upper Mesozoic and lower Cenozoic carbonate units and Palaeogene wildflysch with olistoliths (Desio 1931; Altherr *et al.* 1976, 1982; Gralla 1982; Henjes-Kunst *et al.* 1988; Kalt *et al.* 1998; Papanikolaou & Nomikou 1998; Fig. 3). In this paper we present new information concerning the nature of the contact between the Kos monzonite and surrounding contact-metamorphosed Permo-Carboniferous series, and the overlying upper Mesozoic to Palaeogene carbonates with Palaeogene flysch and discuss these results in light of the kinematic evolution of the Menderes metamorphic core complex and the postulated existence of a southern breakaway fault.

Geological setting

Menderes metamorphic core complex

The Menderes region of western Turkey (Fig. 2) exposes a large-scale complex of Pan-African basement and Palaeozoic to Cenozoic metasedimentary and igneous rocks (Schuiling 1962; Bozkurt & Park 1994, 1999; Hetzel *et al.* 1998; Bozkurt & Oberhänsli 2001; Glodny & Hetzel 2007). It exposes metamorphosed parts of the northern Tauride–Anatolide block that underthrusted below the Izmir–Ankara suture zone during Palaeogene African–Eurasian convergence (Şengör & Yılmaz 1981; Jolivet *et al.* 2004). The protolith of the Menderes basement terrain formed lateral palinspastic units to those of the neighboring Cyclades in central Greece, which share a history of late Palaeozoic to Palaeogene sedimentation and Palaeogene underthrusting and metamorphism (Ring *et al.* 1999; Bozkurt & Oberhänsli 2001; Jolivet *et al.* 2004). To the south, the Menderes Massif is overlain by the Lycian nappes, the northern part of which underwent a HP/LT metamorphic history (Rimmelé *et al.* 2003, 2005). The Lycian nappes consist of thrust sheets of Permo-Triassic clastic sediments and Mesozoic to Palaeogene carbonates and flysch, overthrusted by an ophiolitic mélange and serpentinised peridotites (Bernoulli *et al.* 1974; Okay 1989; Collins & Robertson 1997). Within the Menderes metamorphic core complex, Neogene postorogenic extension was accommodated along several extensional detachments both with top-to-the-north (Hetzel *et al.* 1995*a*; Ring *et al.* 1999*a*; Bozkurt & Sözbilir 2004; Isik *et al.* 2004) and top-to-the-south sense of shear (Bozkurt & Park 1994; Hetzel *et al.* 1995*b*; Bozkurt 2001, 2004, 2007; Gessner *et al.* 2001; Lips *et al.* 2001), which led Hetzel *et al.* (1995*a*) and Gessner *et al.* (2001) to propose bivergent extension of equal importance in the exhumation history of the Menderes region. Low-temperature geochronology has shown that cooling of the metamorphic rocks, attributed to exhumation along the extensional detachments, continued until approximately 8–5 Ma (Gessner *et al.* 2001; Ring *et al.* 2003).

A top-to-the-north break-away fault to the Menderes-Lycian nappes detachment system formed by the Datça–Kahle fault, such as that postulated by Seyitoğlu *et al.* (2004) would however imply that the early Neogene stages of exhumation for the Menderes-Lycian nappes system were accommodated along a dominantly top-to-the-north extensional detachment system.

Geology of Kos

The eastern Greek island of Kos is located only about 15 km NW of the Datça fault (Fig. 2), and *c.*15 km SW of the Bodrum peninsula, where the southernmost HP/LT metamorphic parageneses are found in the Lycian nappes (Rimmelé *et al.* 2003; Fig. 2). It has thus a position in the region where a brittle detachment fault has been postulated by Seyitoğlu *et al.* (2004). In southeastern Kos, the Dikeos window exposes Permo-Carboniferous anchimetamorphic sediments which were folded and then intruded and contact-metamorphosed by the Kos monzonite around 12 Ma (Altherr *et al.* 1976; Gralla 1982; Kalt *et al.* 1998). These are separated by a brittle fault zone from upper Mesozoic and lower Cenozoic carbonate units and Palaeogene wildflysch with olistoliths (Desio 1931; Altherr *et al.* 1976, 1982; Gralla 1982; Henjes-Kunst *et al.* 1988; Kalt *et al.* 1998; Papanikolaou & Nomikou 1998; Fig. 3). The age of folding of the Permo-Carboniferous rocks of Kos cannot be constrained better than between their deposition and the intrusion of the Kos Monzonite, but is likely related to the Alpine folding and thrusting history. Upper Mesozoic recrystallized limestones also occur on the Kefalos peninsula of western Kos (Papanikolaou & Nomikou 1998). The age and lithology of the Kefalos limestones suggest they are correlatable with the limestones overlying the Dikeos window, although the recrystallized nature of the Kefalos limestones led Papanikolaou & Nomikou (1998) to suggest that they may share a burial history with the Dikeos Permo-Carboniferous rocks. Kalt *et al.* (1998) provided Palaeobarometry estimates for the Kos monzonite and surrounding contact-metamorphosed Permo-Carboniferous sediments. Al-in-hornblende barometry yielded pressures of 3.1–5.1 kbar, but Kalt *et al.* (1998) indicated that this is likely an overestimation and render pressure estimates obtained from mineral parageneses in the contact metamorphic aureole of 1.5–2.5 kbar more reliable. The very low metamorphic grade of the Permo-Carboniferous sediments outside the contact metamorphic aureole (Altherr *et al.* 1976; Gralla 1982; Kalt *et al.* 1998) indicate that the Kos monzonite intruded close to or during peak-burial conditions of the Permo-Carboniferous metapelites, corresponding to *c.*1.5–2.5 kbar, or *c.* 5–7.5 km of depth. The anchimetamorphic sediments consist of carbonate, shale and sandstone with sedimentary ages ranging from Ordovician to Permian (Desio 1931; Altherr *et al.* 1976). The clear contact metamorphic aureole in the Permo-Carboniferous rocks is absent in the overlying carbonate succession (Altherr *et al.* 1976; Kalt *et al.* 1998). Altherr *et al.* (1976) therefore suggested that the contact between the Kos monzonite and the upper Mesozoic and Palaeogene carbonates postdates intrusion and cooling of the monzonite and these authors interpreted this contact as a thrust fault. Fission track cooling ages suggest cooling of the monzonite below *c.* 100 °C around 7 Ma (Altherr *et al.* 1982). To date, no structural information has been available for this contact fault zone.

The Neogene sedimentary cover of Kos consists of lower Miocene molassic sediments on western Kos unconformably overlying the Mesozoic carbonates (Papanikolaou & Nomikou 1998), and north of the Dikeos window ranges from middle Miocene to Pleistocene shallow marine to terrestrial deposits (Böger *et al.* 1974; Altherr *et al.* 1976; Willmann 1983). It dips southward as a result of north-dipping normal faults that separate the sediments from the pre- Neogene basement (Böger *et al.* 1974; Fig. 3).

Contact between the Dikeos Permo-Carboniferous and Cretaceous rocks

The contact between the footwall (contact-metamorphosed Permo-Carboniferous clastic sediments and the Kos monzonite) and the hanging wall (non-metamorphosed upper Mesozoic and Palaeogene carbonates and Palaeogene flysch) is exposed in three areas along the northern side of the Dikeos window (Fig. 3). In one of these outcrops clear kinematic criteria have been obtained (location I) at the contact between the contact-metamorphosed Permo-Carboniferous sequence and the non-metamorphic upper Mesozoic and Palaeogene carbonate unit. At location II, near Paleo Pili, the upper Mesozoic and Palaeogene carbonates overlie the Kos monzonite with a brittle fault zone as contact, from which we have not obtained conclusive kinematic criteria. In the east (location III) the Permo-Carboniferous is overlain by the Palaeogene flysch, which forms a chaotic fault zone. In all three cases, the contact is of tectonic origin. The footwall is dome-shaped, and the contact fault zone is dipping northwesterly in the west, and northeasterly in the east (Fig. 3). Upper Mesozoic and Palaeogene carbonates are not laterally continuous, and appear as isolated klippen on

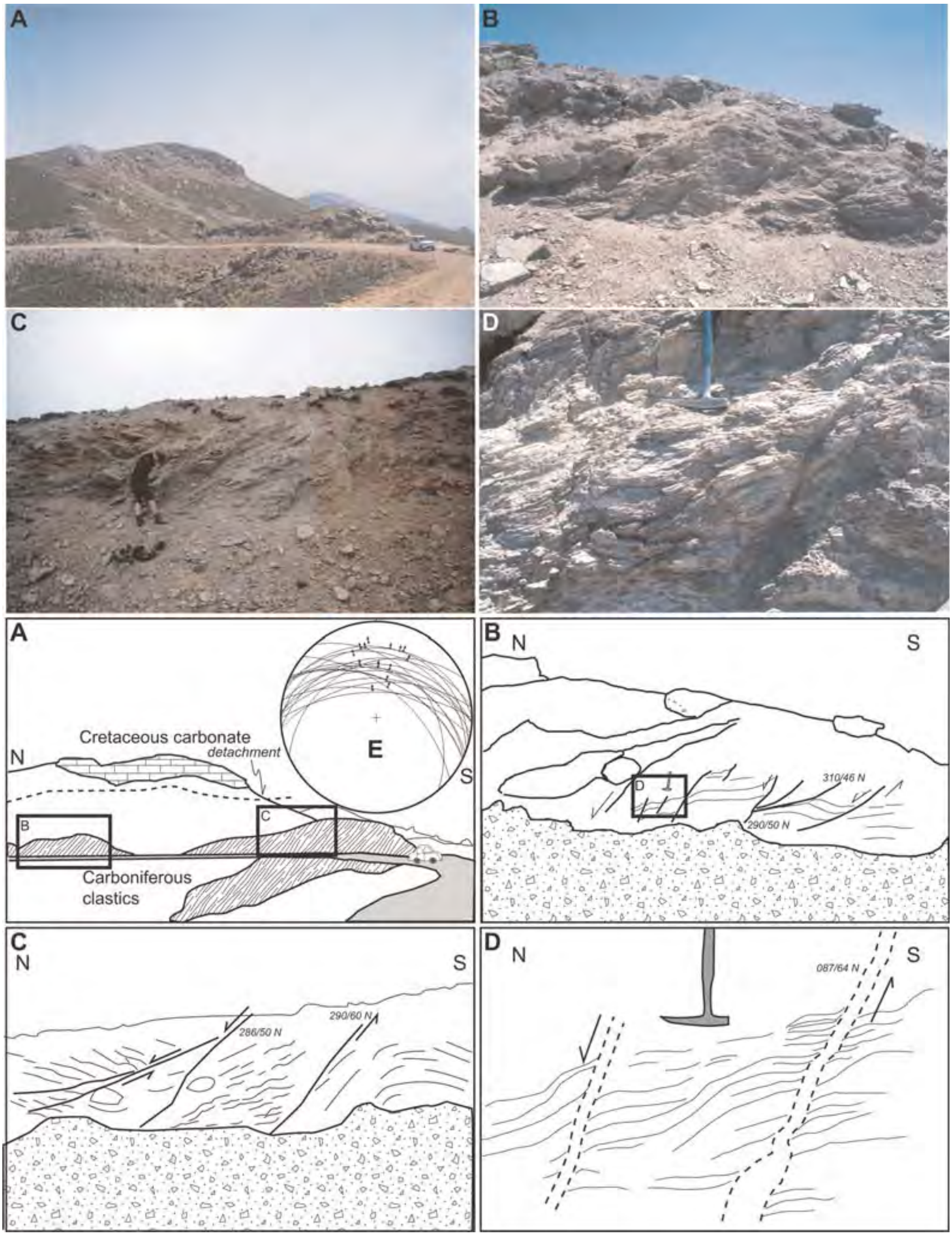

Fig. 4. (**a**–**d**) Photographs and interpretative sketch of location I showing kinematic indicators that give evidence for a top-to-the-north motion along the Kos brittle detachment fault zone. For location, see Figures 3a and b. Figure 4E shows a plot with faults and lineations, with sense of shear indicated, showing that fault zone represents a brittle, top-to-the-north extensional detachment fault. The overall SE dipping main foliation is deflected and deformed by the top-to-the-north normal fault zones that form the detachment. This fault exhumed the Permo-Carboniferous succession and the Kos monzonite from underneath upper Mesozoic and Palaeogene successions and overlying middle Miocene and younger basin sediments since 12 Ma (see text for further details).

top of the Permo-Carboniferous series and the Kos monzonite (Fig. 3). They are heavily brecciated but do not contain clear individual shear zones.

Location I

Location I exposes the contact between the upper Mesozoic and Palaeogene carbonates and the Permo-Carboniferous rocks over a north–south distance of *c*. 200 m (Fig. 4a). The Permo-Carboniferous sequence consists of anchimetamorphic phyllites and quartzites, and minor carbonates. The dominant structure is a foliation which is here southeasterly dipping. The foliation is well developed in phyllitic parts, whereas the quartzites are boudinages within the foliation plane. Some of these boudins show isoclinally folded thin-bedded quartzites and quartz-veins, which provide clear evidence for at least two phases of tight to isoclinal folding (Fig. 5). The fold-axial plane of F2 folds trends subparallel to the enveloping surface of the main foliation, which renders it likely that the latter is an axial plane cleavage.

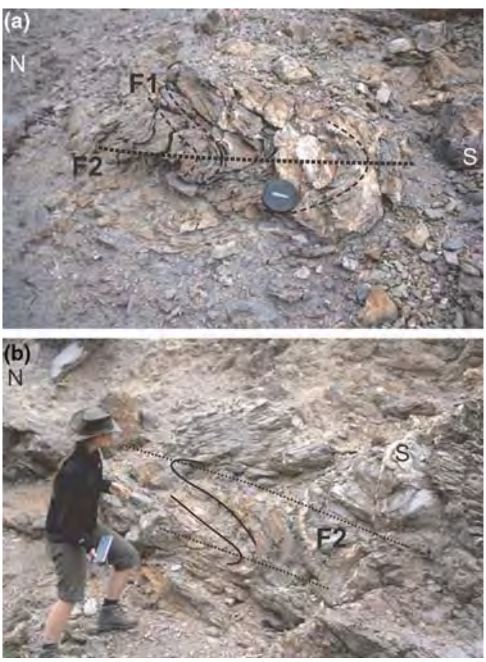

Fig. 5. (**a**) Field photograph at location I showing intensely folded Permo-Carboniferous sandstones, in a boudin within the detachment zone. At least two tight folding phases affected the Permo-Carboniferous rocks in the Dikeos window. (**b**) Tight F2 folds in the Permo-Carboniferous sandstones of location I. Note that the F2 fold axial trace trends subparallel, dipping SE, to the enveloping surface of the main foliation in the outcrops of Fig. 4b and c.

The Permo-Carboniferous series here is crosscut by brittle to semi-brittle north-dipping fault zones, which deflect the foliation to northerly dips (Fig. 4b–d). Slickenside lineations in these fault zones are consistently north-dipping (Fig. 4e) and the asymmetric tectonic fabric formed by beds that are dragged along north-dipping faults. The fabric in tandem with the consistenly north-dipping lineations on the *c*. east–west trending fault surfaces between the north-dipping faults indicates dip-slip, top-to-the-north motion along the fault zone between the Permo-Carboniferous series and the upper Mesozoic and Palaeogene carbonates (Fig. 4). In the next section, we will combine this with the available information on the metamorphic, geochronologic and stratigraphic information to determine the extensional or contractional origin of this fault zone.

Location II

The contact between the Kos monzonite and the upper Mesozoic and Palaeogene carbonates at location I near Paleo Pili is a brittle fault zone of typically 100 m wide, which is developed as north dipping gouge zones in the monzonite (Fig. 6). The deformation zone is several tens of metres thick, below which the monzonite and xenoliths of the Permo-Carboniferous series, here metamorphosed into muscovite-biotite bearing schists is undeformed. The fault zone consists of anastomosing cataclastic zones of typically up to several tens of centimetres wide. These zones are strictly brittle in nature, clearly evidenced by fragmented K-feldspar crystals which are abundant in the monzonite. The cataclasites are furthermore characterized by small dark brown anastomosing bands of typically several millimetres thick consisting of very fine grained fault gouge. We did not observe any slickenside lineations within these cataclastic zones and absence of markers within the monzonite hampers determination of a sense of shear along this fault zone. The cataclasites are generally east–west striking, with highly variable dips varying from shallow northerly dipping to subvertical. The overall enveloping surface determined by the contact between the monzonite and the upper Mesozoic and Palaeogene carbonates can be clearly determined by the 3D exposure in the valley of Paleo Pili and strikes east–west, with a *c*. 40° northerly dip.

Location III

The contact in the east at location II, between the flysch and the Permo-Carboniferous series (Fig. 4) is a mélange of brittly deformed rocks of hundreds of metres thick, dipping at approximately 40° to

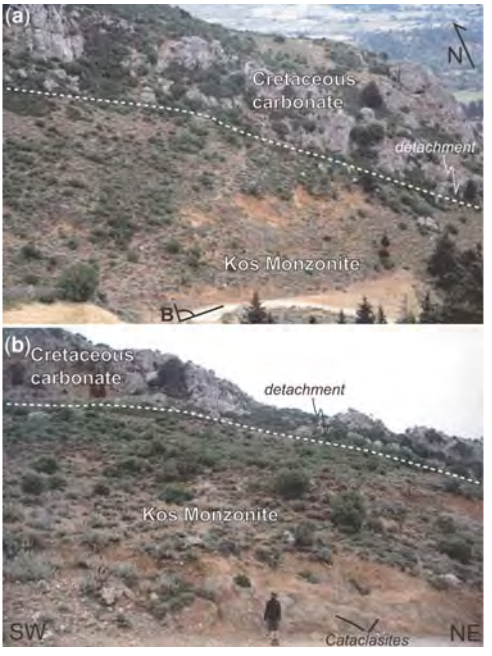

Fig. 6. (**a**) Exposure of the contact between the Kos monzonite and the overlying, non-metamorphosed Cretaceous carbonates at location II, near Paleo Pili. The contact is an anastomosing brittle fault zone developed within the Kos monzonite. This zone is approximately 100 metres thick, below which the monzonite is undeformed. (**b**) Detail of Fig. 6a. Note the cataclastic zones in the monzonite, which are typically *c*. 20 cm wide, and anastomose with an overall enveloping surface with an east–west strike and a *c*. 40° northward dip. Lineations within the cataclastic zones are absent and kinematic indicators are lacking. In conjunction with location I (see Fig. 4), as well as the fact that the Cretaceous carbonates are unconformably overlain in the west of the island by lower Miocene sediments (Papanikolaou & Nomikou 1998), i.e. the same age as the Kos monzonite, we argue that this fault zone accommodated the exhumation of the Kos monzonite and can be regarded as a brittle detachment fault cutting away a vertical crustal section of 5–7.5 km (see text for further explanation).

the NE. The chaotic character of hanging wall and footwall prevails determining a conclusive sense of shear. The flysch is much more deformed than the underlying Permo-Carboniferous unit, although part of this deformation may be the result of a nappe stacking episode and soft-sediment deformation.

Discussion

Six issues are essential in determining the extensional or contractional nature of the fault zone between the non-metamorphosed upper Mesozoic and Palaeogene carbonates and the Kos monzonite and surrounding contact-metamorphosed Permo-Carboniferous series: (1) The hanging wall of the fault zone juxtaposes younger over older; and (2) non-metamorphosed over metamorphosed rocks. (3) The kinematic criteria obtained from location I shows a top-to-the-north normal fault motion, with a comparable shear sense and strike as the basin faults that bound and deform the Neogene stratigraphy (Böger *et al.* 1974). Moreover, (4) the middle Miocene to Pliocene stratigraphy on Kos was deposited during and after intrusion, exhumation and cooling of the Kos monzonite between 12 and 7 Ma (Böger *et al.* 1974; Altherr *et al.* 1976; Willmann 1983), unconformably overlying upper Mesozoic to Palaeogene carbonates on western Kos (Papanikolaou & Nomikou 1998). This, in combination with (5) the pressure conditions of 1.5 to 2.5 kbar during the intrusion of the Kos monzonite (Kalt *et al.* 1998), shows that approximately 5 to 7.5 km of exhumation of the Dikeos window with respect to the sedimentary basins occurred since 12 Ma. Based on these facts we argue that the contact studied in this paper represents a top-to-the-north fault zone that exhumed the Kos monzonite and Permo-Carboniferous series from underneath the upper Mesozoic and Palaeogene series and overlying lower Miocene and younger sedimentary basins. The previously proposed thrust-nature of this contact (Altherr *et al*. 1976) is an unlikely scenario, not in the last part since (6), thrusting of the upper Mesozoic carbonates would require that they formed a coherent block during emplacement, unlike their present-day fragmented nature as isolated klippen on the Dikeos window. It would not be logical to fragment the hanging wall during sediment acquisition on top of it in the Neogene basin. More likely, these isolated blocks form extensional klippen comparable to those observed in the middle to upper Miocene Cretan supradetachment basin (van Hinsbergen & Meulenkamp 2006). This combination of facts strongly supports an extensional nature for the fault zone.

We therefore argue that this fault zone represents a brittle extensional detachment fault that accommodated *c.* 5–7.5 km of exhumation since 12 Ma. Moreover, since the crystallization depth of the Kos monzonite likely corresponds to the maximum burial depth of the surrounding anchimetamorphic Permo-Carboniferous rocks (Kalt *et al.* 1998), any pre-12 Ma extension and basin formation that may have affected Kos (Böger *et al.* 1974; Papanikolaou & Nomikou 1998) did not lead to significant exhumation of the footwall to the Kos detachment.

Placing this interpretation into the regional geological context requires correlation of the pre-Alpine rocks of the Dikeos window to those of the Kefalos peninsula, and the pre-Alpine rocks of Kos to the nappes of Greece and western Turkey, which is not straightforward. The recrystallized limestones of late Cretaceous age on the Kefalos peninsula are unconformably overlain by lower Miocene molassic sediments with olistoliths (Papanikolaou & Nomikou 1998). The recrystallized nature of the limestones led Papanikolaou & Nomikou (1998) to suggest that they may share a burial history with the Dikeos Permo-Carboniferous rocks.

However, the lower Miocene unconformable cover of the Kefalos carbonates shows that the Kefalos Cretaceous carbonates have been near the surface throughout the intrusion and exhumation history of the Kos monzonite, and it supports correlation to the Mesozoic rocks in the hanging wall of the Kos detachment. Two models can be postulated to place the pre-Alpine rocks of Kos in their regional tectonostratigraphic context. The main difficulty in correlation is the old age of the Kos Permo-Carboniferous rocks, which is not known from elsewhere in the Aegean or western Anatolian region (Papanikolaou & Nomikou 1998).

Based on lithology, age and tectonostratigraphic context, they may correspond to either the tectonostratigraphically lowest central Aegean nappe formed by the Tripolitza unit, the Basal Unit and the Phyllite Quartzite, or to the structurally highest Lycian nappes. Blondeau *et al.* (1975) and Papanikolaou & Nomikou (1998) correlated the Mesozoic to Palaeogene carbonates of Kos to the Tripolitza and Pindos nappes of western Greece based on age and sedimentary facies. If this suggestion is correct, the Permo-Carboniferous of Kos could correlate to the HP/LT metamorphic Phyllite Quartzite unit exposed on Crete. Alternatively, the pre-Neogene rocks of Kos may belong to the Lycian nappes, which on nearby Turkish peninsulas expose Permo-Triassic clastic sediments and Mesozoic–Palaeogene carbonates and flysch (Bernoulli *et al.* 1974; Collins & Robertson, 1997). We advocate the latter correlation based on their non- to anchimetamorphic character and their position amidst rocks belonging to the Lycian nappes with comparable age and facies exposed on the Turkish peninsulas north and south of Kos.

The intrusion of the Kos monzonite and associated contact metamorphism provide a unique opportunity to show that in the south of the metamorphic rocks of the Menderes metamorphic core complex, top-to-the-north extensional detachment faulting has been active. This suggests that Kos has been a focused deformation site within the Cyclades–Menderes extensional province since 12 Ma. The top-to-the-north component of shear of the brittle Kos detachment is in line with the scenario of Seyitoğlu *et al.* (2004), which postulates that the Datça fault south of Kos is the Oligocene–lower Miocene break-away fault of the core complex. However, the thermodynamic reconstruction of Kalt *et al.* (1998) shows that the Kos monzonite intruded the Permo-Carboniferous series close to peak burial conditions, indicating that no significant exhumation occurred on Kos prior to 12 Ma. Seyitoğlu *et al.* (2004) suggested that the Datça breakaway fault was active during Oligocene to early Miocene times. This can only be valid if the rocks on Kos belong to the hanging wall of the Oligocene–early Miocene detachment system inferred by Seyitoğlu *et al.* (2004). We cannot corroborate the existence of a Oligocene–early Miocene brittle detachment on Kos and this makes the scenario of Seyitoğlu *et al.* (2004) unlikely. Moreover, seismic profiles of Kurt *et al.* (1999) and Ulug *et al.* (2005) cannot corroborate any on-land continuation of this fault zone and these authors instead suggested a much younger, late Miocene or Pliocene age of the Datça Fault. The existence of a brittle detachment on Kos does show that brittle detachment faulting exhumed upper crustal rocks from mid upper crustal depths south of the Menderes and eastern Cycladic metamorphic core complexes, but the Kos detachment appears to be a relatively isolated structure. Our new data indicate that there is no evidence that the Datca fault forms part of a southerly Oligocene to lower Miocene break-away fault of the Menderes core complex as suggested by Seyitoğlu *et al.* (2004). This renders the bivergent rolling-hinge scenario of Gessner *et al*. (2001) as a better fitting solution for the kinematic evolution of the Menderes core complex.

Conclusions

The Menderes metamorphic core complex western Turkey is clearly defined in the north by extensional detachments along which a sharp metamorphic contrast exists between hanging wall and footwall. The southern limit of the core complex is less well defined. An Oligocene–early Miocene breakaway fault has previously been postulated in the Lycian nappes in southwestern Turkey. Showing the existence of a breakaway detachment fault is difficult due to absence of a metamorphic contrast along the fault for those parts where only upper crustal rocks are exhumed. The island of Kos, just north of the inferred breakaway fault, exposes Permo-Carboniferous anchimetamorphic rocks, intruded and contact-metamorphosed by a 12 Ma old monzonite. Here, we show that exhumation of these rocks was accommodated along a top-to-the-north brittle extensional detachment emplacing them underneath non-metamorphosed upper Mesozoic to Palaeogene carbonates and Neogene basin sediments.

Previously published petrological constraints on the burial history of the Permo-Carboniferous series of Kos has shown that the Kos monzonite intruded close to peak-burial conditions, showing that any pre-12 Ma extension and basin formation on Kos has not led to any detectable exhumation of the Permo-Carboniferous series. We conclude that the island of Kos should be placed within the Cyclades–Menderes extensional province. However, the age of exhumation is younger than the proposed activity of the breakaway of the Menderes metamorphic core complex (Seyitoğlu *et al.* 2004), and the bivergent rolling-hinge scenario of Gessner *et al.* (2001) remains a better fitting solution. We conclude that the brittle detachment of Kos cannot be straightforwardly correlated to any ductile-to-brittle detachments of the Menderes or eastern Cycladic metamorphic core complexes further to the north and may represent a relatively isolated structure.

Research of DJJvH was funded by a Dutch Council for Scientific Research (NWO) 'Veni'- grant. M. Koopman is thanked for the pleasant discussions and her help in the field. E. Bozkurt is thanked for fruitful comments and suggestions on an earlier version of this manuscript. We thank K. Gessner and G. Zulauf for their reviews and M. Edwards for editorial comments.

References

Altherr, R., Keller, J. & Kott, K. 1976. Der jungtertiäre Monzonit von Kos und sein Kontakthof (Ägäis, Griechenland). *Bulletin de la Société Géologique de France*, **18**, 403–412.

Altherr, R., Kreuzer, H., Wendt, I., Lenz, H., Wagner, G. A., Keller, J. *et al.* 1982. A late Oligocene/Early Miocene high temperature belt in the Attica Cycladic crystalline complex (SE Pelagonian, Greece). *Geologisches Jahrbuch*, **E23**, 97–164.

Bernoulli, D., deGraciansky, P. C. & Monod, O. 1974. The extension of the Lycian Nappes (SW Turkey) into the SE Aegean islands. *Eclogae Geologicae Helveticae*, **67**, 39–90.

Blondeau, A., Fleury, J. J. & Guernet, C. 1975. Sur l'existence dans l'île de Kos (Dodécanèse, Grèce), d'une série nétritique surmontée d'un flysch d'âge Cuisien supérieur ou Lutétien inférieur à sa base. *Comptes Rendus Académie Science Paris*, **280**, 817–819.

Böger, H., Gersonde, R. & Willman, R. 1974. Das Neogen im Osten der Insel Kos (Ägäis, Dodekanes) – Stratigraphie und Tektonik. *Neues Jahrbuch Geologie und Palaeontologie Abh.*, **145**, 129–152.

Bozkurt, E. 2001. Late Alpine evolution of the central Menderes Massif, western Turkey. *International Journal of Earth Sciences*, **89**, 728–744.

Bozkurt, E. 2004. Granitoid rocks of the southern Menderes Massif (southwestern Turkey): field evidence for Tertiary magmatism in an extensional shear zone. *International Journal of Earth Sciences*, **93**, 52–71.

Bozkurt, E. 2007. Extensional v. contractional origin for the southern Menderes shear zone, SW Turkey: tectonic and metamorphic implications. *Geological Magazine*, **144**, 191–210.

Bozkurt, E. & Oberhänsli, R. 2001. Menderes Massif (Western Turkey): structural, metamorphic and magmatic evolution – a synthesis. *International Journal of Earth Sciences*, **89**, 679–708.

Bozkurt, E. & Park, R. G. 1994. Southern Menderes Massif: an incipient metamorphic core complex in western Anatolia, Turkey. *Journal of the Geological Society of London*, **151**, 213–216.

Bozkurt, E. 1999. The structure of the Palaeozoic schists in the southern Menderes Massif, western Turkey: a new approach to the origin of the Main Menderes Metamorphism and its relation to the Lycian Nappes. *Geodinamica Acta*, **12**, 25–42.

Bozkurt, E. & Satir, M. 2000. The southern Menderes Massif (western Turkey): geochronology and exhumation history. *Geological Journal*, **35**, 285–296.

Bozkurt, E. & Sözbilir, H. 2004. Tectonic evolution of the Gediz Graben: field evidence for an episodic, two-stage extension in western Turkey. *Geological Magazine*, **141**, 63–79.

Collins, A. S. & Robertson, A. H. F. 1997. Processes of Late Cretaceous to Late Miocene episodic thrust-sheet translation in the Lycian Taurides. SW Turkey. *Geology*, **25**, 255–258.

Crittenden, M. D. Jr., Coney, P. J. & Davis, G. H. 1980. *Cordilleran metamorphic core complexes*. Geological Society of America Memoirs, **153**, The Geological Society of America, Colorado.

Davis, G. H. 1983. Shear-zone model for the origin of metamorphic core complexes. *Geology*, **11**, 342–347.

Desio, A. 1931. Le isole Italiane dell'Egio. *Memoir Carta Geologia d'Italia*, **24**.

Dorsey, R. J. & Becker, U. 1995. Evolution of a large Miocene growth structure in the upper plate of the Whipple detachment fault, north-eastern Whipple Mountains, California. *Basin Research*, **7**, 151–163.

Gessner, K., Ring, U., Johnson, C., Hetzel, R., Passchier, C. W. & Güngör, T. 2001. An active bivergent rolling-hinge detachment system: central Menderes metamorphic core complex in western Turkey. *Geology*, **29**, 611–614.

Glodny, J. & Hetzel, R. 2007. Precise U-Pb ages of syn-extensional Miocene intrusions in the central Menderes Massif, western Turkey. *Geological Magazine*, **144**, 235–246.

Gralla, P. 1982. *Das Präneogen der Insel Kos (Dodekanes, Griechenland)*. PhD Thesis, University of Braunschweig.

Henjes-Kunst, F., Altherr, R., Kreuzer, H. & Tauber Hansen, B. 1988. Disturbed U-Th-Pb systematics of young zircons and uranothorites: the case of the Miocene Aegean granitoids (Greece). *Chemical Geology*, **73**, 125–145.

Hetzel, R., Passchier, C. W., Ring, U. & Dora, Ö. O. 1995*a*. Bivergent extension in orogenic belts: the Menderes massif (southwestern Turkey). *Geology*, **23**, 455–458.

Hetzel, R., Ring, U., Akal, C. & Troesch, M. 1995*b*. Miocene NNE-directed extensional unroofing in the

Menderes Massif, southwestern Turkey. *Journal of the Geological Society of London*, **152**, 639–564.

HETZEL, R., ROMER, R. L., CANDAN, O. & PASSCHIER, C. W. 1998. Geology of the Bozdag area, central Menderes massif, SW Turkey: Pan-African basement and Alpine deformation. *Geologische Rundschau*, **87**, 394–406.

ISIK, V., TEKELI, O. & SEYITOĞLU, G. 2004. The $^{40}Ar/^{39}Ar$ age of extensional ductile deformation and granitoid intrusion in the northern Menderes core complex: implications for the initiation of extensional tectonics in western Turkey. *Journal of Asian Earth Sciences*, **23**, 555–566.

JOLIVET, L., RIMMELÉ, G., OBERHÄNSLI, R., GOFFÉ, B. & CANDAN, O. 2004. Correlation of synorogenic tectonic and metamorphic events in the Cyclades, the Lycian Nappes and the Menderes Massif. Geodynamic implications. *Bulletin de la Société Géologique de France*, **175**, 217–238.

KALT, A., ALTHERR, R. & LUDWIG, T. 1998. Contact metamorphism in pelitic rocks on the island of Kos (Greece, Eastern Aegean Sea): a test for the Na-in-cordierite thermometer. *Journal of Petrology*, **39**, 663–688.

KURT, H., DEMIRBAG, E. & KUSCU, I. 1999. Investigation of the submarine active tectonism in the Gulf of Gökova, southwest Anatolia-southeast Aegean Sea, by multi-channel seismic reflection data. *Tectonophysics*, **305**, 477–496.

LIPS, A. L. W., CASSARD, D., SÖZBILIR, H. & YıLMAZ, H. 2001. Multistage exhumation of the Menderes Massif, western Anatolia (Turkey). *International Journal of Earth Sciences*, **89**, 781–792.

LISTER, G. S. & DAVIS, G. A. 1989. The origin of metamorphic core complexes and detachment faults formed during Tertiary continental extension in the northern Colorado River region, U.S.A. *Journal of Structural Geology*, **11**, 65–94.

LISTER, G. S., BANGA, G. & FEENSTRA, A. 1984. Metamorphic core complexes of Cordilleran type in the Cyclades. Aegean Sea, Greece. *Geology*, **12**, 221–225.

OKAY, A. I. 1989. Geology of the Menderes Massif and the Lycian Nappes south of Denizli, western Taurides. *Mineral Resources Exploration Bulletin*, **109**, 37–51.

OTTON, J. K. 1995. Western frontal fault of the Canyon Range: is it the breakaway zone of the Sevier Desert detachment? *Geology*, **23**, 547–550.

PAPANIKOLAOU, D. J. & NOMIKOU, P. V. 1998. The Palaeozoic of Kos: a low grade metamorphic unit of the basement of the eternal Hellenides terrane. *Special Publications of the Geological Society of Greece*, **3**, 155–166.

RIMMELÉ, G., JOLIVET, L., OBERHÄNSLI, R. & GOFFÉ, B. 2003. Deformation history of the high-pressure Lycian Nappes and implications for the tectonic evolution of SW Turkey. *Tectonics*, **22**, 1007.

RIMMELÉ, G., PARRA, T., GOFFÉ, B., OBERHÄNSLI, R., JOLIVET, L. & CANDAN, O. 2005. Exhumation paths of high-pressure – low-temperature metamorphic rocks from the Lycian Nappes and the Menderes Massif (SW Turkey): a multi-equilibrium approach. *Journal of Petrology*, **46**, 641–669.

RING, U., GESSNER, K., GÜNGÖR, T. & PASSCHIER, C. W. 1999. The Menderes Massif of western Turkey and the Cycladic Massif in the Aegean – do they really correlate? *Journal of the Geologic Society of London*, **156**, 3–6.

RING, U., JOHNSON, C., HETZEL, R. & GESSNER, K. 2003. Tectonic denudation of a Late Cretaceous-Tertiary collisional belt: regionally symmetric cooling patterns and their relation to extensional faults in the Anatolide belt of western Turkey. *Geological Magazine*, **140**, 421–441.

SCHUILING, R. D. 1962. On petrology, age and evolution of the Menderes Massif, W-Turkey: a rubidium/strontium and oxygen isotope study. *Bulletin of the Institute for Mineral Research and Exploration, Turkey*, **58**, 703–714.

ŞENGÖR, A. M. C. & YıLMAZ, Y. 1981. Tethyan evolution of Turkey: a plate-tectonic approach. *Tectonophysics*, **75**, 181–241.

SEYITOĞLU, G., ISIK, V. & CEMEN, I. 2004. Complete Tertiary exhumation history of the Menderes massif, western Turkey: an alternative working hypothesis. *Terra Nova*, **16**, 358–364.

TIREL, C., BRUN, J.-P. & BUROV, E. 1998. Dynamics and structural development of metamorphic core complexes. *Journal of Geophysical Research*, **113**, B04403, doi: 10.1029/2005JB003694.

TIREL, C., GAUTIER, P., VAN HINSBERGEN, D. J. J. & WORTEL, M. J. R. 2009. Sequential development of interfering metamorphic core complexes: numerical experiments and comparison with the Cyclades, Greece. *In*: VAN HINSBERGEN, D. J. J., EDWARDS, M. A. & GOVERS, R. (eds) *Collision and Collapse at the African–Arabia–Eurasia Subduction Zone*. Geological Society, London, Special Publications, **311**, 257–292.

ULUG, A., DUMAN, M., ERSOY, S., ÖZEL, E. & AVCI, M. 2005. Late Quarternary sea-level change, sedimentation and neotectonics of the Gulf of Gökova: Southeastern Aegean Sea. *Marine Geology*, **221**, 381–395.

VAN HINSBERGEN, D. J. J. & MEULENKAMP, J. E. 2006. Neogene supra-detachment basin development on Crete (Greece) during exhumation of the South Aegean core complex. *Basin Research*, **18**, 103–124.

WERNICKE, B. 1981. Low-angle normal faults in the Basin and Range province: Nappe tectonics in an extending orogen. *Nature*, **291**, 645–648.

WERNICKE, B. 1995. Low-angle normal faults and seismicity: a review. *Journal of Geophysical Research*, **100**, B10, 20159–20174.

WILLMANN, R. 1983. Neogen und jungtertiäre Enwicklung der Insel Kos (Ägäis, Griechenland). *Geologische Rundschau*, **72**, 815–860.

Magnetostratigraphy of early–middle Miocene deposits from east–west trending Alaşehir and Büyük Menderes grabens in western Turkey, and its tectonic implications

SEVKET SEN[1]* & GÜROL SEYITOĞLU[2]

[1]*UMR 5143 du CNRS, Muséum national d'Histoire naturelle, Département Histoire de la Terre, 8 rue Buffon, 75005 Paris, France*

[2]*Ankara University, Department of Geological Engineering, Tectonics Research Group, TR-06100 Tandoğan, Ankara, Turkey*

**Corresponding author (e-mail: sen@mnhn.fr)*

Abstract: In western Turkey, the Alaşehir and Büyük Menderes grabens form east–west trending major tectonic structures. Their sedimentary fill is important for regional tectonic models for the late Cenozoic evolution of the Aegean region. These deposits are divided into four units dated between the early Miocene and Quaternary. We studied the magnetostratigraphy of two sections in the Alaşehir graben and one in the Büyük Menderes, partly covering the first and second sedimentary units. Detailed palaeomagnetic analysis allowed us to determine ChRM component for these rocks. The Zeytinçayı river and road sections (Alaşehir graben) record several polarity reversals, which are tentatively correlated to the interval C5Cn.3n–C5ADr (approximately between 14.6–16.6 Ma) of the ATNTS2004. This correlation is also supported by palaeontology and radiometric dating of syn-extensional intrusions. In the Eycelli section (Büyük Menderes graben) only three polarity zones are recorded, and their tentative correlation with the interval of C5Bn.1r–C5Br (14.88–15.97 Ma) is in overall in agreement with the record of Eskihisar sporomorph association in this formation. These results place the initiation of the Alaşehir and Büyük Menderes grabens in the early Miocene. The palaeomagnetic declinations from the Alaşehir graben indicate about 25° anticlockwise rotation, whereas that of the Büyük Menderes graben indicate a clockwise rotation of about 30–40°. These contradictory vertical-axis rotations might be explained by detachment faults in the region. In Tertiary formations of western Turkey, contradictory block rotations are common and likely reflect thin-skinned deformation in the area rather than rigid crustal movements. Therefore, average anticlockwise rotations in western Turkey cannot be used as evidence for the model of back-arc spreading in the Aegean region.

Western Turkey is located in the eastern part of the Aegean region (Fig. 1, inset), one of the highly extended terrains in the world, and consists of metamorphic core complexes (Bozkurt & Park 1994; Hetzel *et al.* 1995; Okay & Satır 2000; Işık & Tekeli 2001). The Menderes core complex covers extensive areas in western Turkey. Recent region-wide tectonic models dealing with the exhumation of the Menderes core complex suggest that vorth–south extensional tectonics initiated in the Oligocene times (Ring *et al.* 2003; Seyitoğlu *et al.* 2004). A symmetrical core complex model has been proposed that the Menderes massif is exhumed along the south dipping Lycian and north dipping Simav detachments (Ring *et al.* 2003). Alternatively, asymmetrical core complex formation is proposed along with the north dipping Datca–Kale main breakaway fault and its northern continuation, the Simav detachment (Seyitoğlu *et al.* 2004). Although these models have different views on the style of Menderes massif's initial exhumation, both models agree that the central Menderes massif is further exhumed along with the north dipping Alaşehir (Kuzey) and south dipping Büyük Menderes (Güney) detachments that border the prominent east–west trending structures (Alaşehir and Büyük Menderes grabens) in western Turkey (Fig. 1).

Even if these recent region-wide models imply that the formation of east–west trending grabens represent an advanced stage of north–south extensional tectonics in western Turkey, initiation and evolution of these structures are still important questions to understand the relationships between extensional tectonics and basin formation.

The views on the initial development of east–west trending grabens can be classified into two groups. One group suggests that east–west trending grabens are younger than late Miocene and they contain trapped fragments of earlier

From: VAN HINSBERGEN, D. J. J., EDWARDS, M. A. & GOVERS, R. (eds) *Collision and Collapse at the Africa–Arabia–Eurasia Subduction Zone*. The Geological Society, London, Special Publications, **311**, 321–342.
DOI: 10.1144/SP311.13 0305-8719/09/$15.00

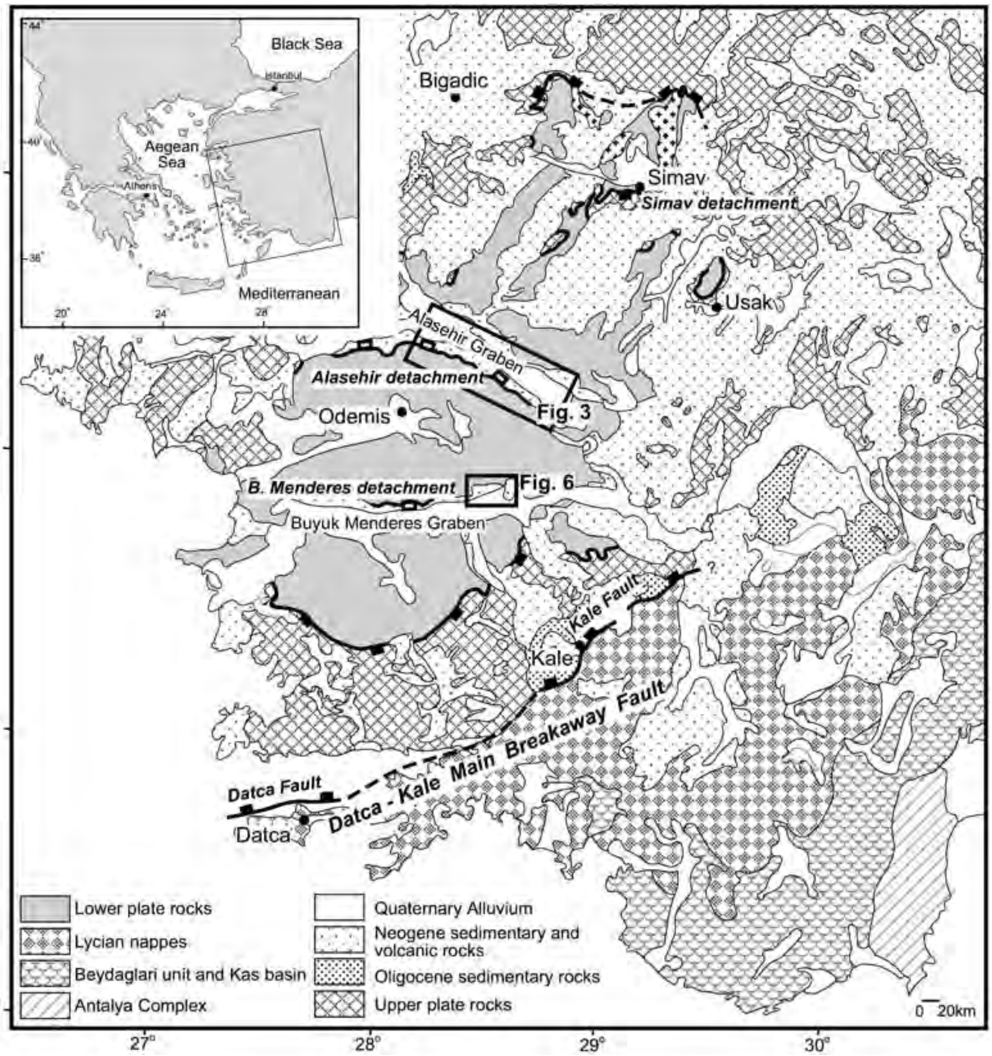

Fig. 1. Simplified geological map of western Turkey (after Seyitoğlu *et al.* 2004). Lower plate rocks are dominantly core rocks of the Menderes massif. Upper plate rocks are composed of mainly cover rocks of the Menderes massif and Lycian nappes. The faults having black rectangles on the downthrown side, Datca–Kale main breakaway fault and its northern continuation, Simav detachment are responsible for the main exhumation of the Menderes massif. The faults with white rectangles are related to the second stage of exhumation process of the central Menderes massif.

North-trending basins. This view was originally proposed by Şengör *et al.* (1985), Şengör (1987) and followed by Yılmaz *et al.* (2000), Gürer *et al.* (2001), and Yılmaz & Gelişli (2003). The second group of researchers proposed that the Alaşehir and Büyük Menderes grabens initiated in the early Miocene and the accumulation of their sedimentary fill is controlled by east–west trending normal faults (Seyitoğlu & Scott 1992, 1996; Cohen *et al.* 1995; Seyitoğlu *et al.* 2002; Purvis & Robertson 2004).

Recently, a substantial amount of age data from both footwall and hanging wall of the east–west trending grabens has been published. Isotopic data from shear zones and syn-extensional granodiorite (Hetzel *et al.* 1995; Lips *et al.* 2001; Gessner *et al.* 2001; Catlos & Çemen 2005; Glodny & Hetzel 2007) indicate that graben-bounding faults were active in the early Miocene. The amount of available age data from the hanging wall of the grabens also increased during the last decade (Seyitoğlu & Scott 1992, 1996; Ünay *et al.* 1995; Emre 1996;

Ediger *et al.* 1996; Şan 1998; Koçyiğit *et al.* 1999; Sarıca 2000). As will be briefly reviewed below, the chronological data are still poor for some sedimentary units; most of them are derived from palynological analyses that give way often to controversial interpretations by different authors. On the other hand, ages based on small mammalian associations reach a more general consensus.

Many formation names have been proposed for the basin fill of the east–west trending grabens; they can be simplified into four sedimentary units. The age of the first and second sedimentary units and their tectonic setting are the main matter of debate among geologists (in particular, see Seyitoğlu & Scott 1992, 1996; Sarıca 2000; Yılmaz *et al.* 2000; Seyitoğlu *et al.* 2002; Bozkurt & Sözbilir 2004). The third sedimentary unit is well dated by micromammalian fossils. The fourth sedimentary unit consists of Quaternary alluvium deposits of these grabens.

Below, the stratigraphy of these deposits and their relationships to major fault systems of the Alaşehir and Büyük Menderes grabens are outlined. We studied the magnetostratigraphy of the first and second sedimentary units in the eastern part of these grabens to provide new chronological data to correlate their stratigraphies to the geomagnetic time scale. This work will eventually have important implications for unravelling the timing of the tectonic evolution of the potentially hydrocarbon bearing graben system in western Turkey.

Stratigraphy

Alaşehir graben

The graben is one of the most prominent east–west extensional structures of western Turkey. Its boundary fault is located on its southern margin (Fig. 1). Constraints on the stratigraphy and age data for the basin's sedimentary fill are summarized in Figure 2. Some of the previous stratigraphic subdivisions are too detailed to use on a regional scale, mainly because of their limited extension and frequent facies changes in these terrestrial deposits. We prefer a generalized stratigraphy, which is composed of the Alaşehir, Kurşunlu and Sart formations and Quaternary alluvium deposits, from the base to the top (Seyitoğlu *et al.* 2002). These are the four sedimentary units mentioned earlier.

The Alaşehir Formation (Iztan & Yazman 1990), the first sedimentary unit, outcrops south and SW of Alaşehir (Figs 2 & 3), and starts with angular boulder conglomerates as seen along the road from Alaşehir to Evrenli village (Fig. 4) (but not seen in the Zeytinçayı section of Fig. 5). These conglomerates accumulated from the south and SW, according to long-axis measurements of the cobbles. The formation continues with alternating yellowish sandstones and mudstones intercalated with approximately 1.5 m thick intervals of angular boulder conglomerates. The upper part of the formation crops out in the valley of Zeytinçayı, east of Çaltılık village (Fig. 4), and is dominantly an organic rich, well-lithified, laminated mudstone, which gradually passes upwards into sandstones with layers of limestones and conglomerates, as seen in Fig. 5 (see also Seyitoğlu *et al.* 2002). The Alaşehir Formation was interpreted as a lacustrine and fan-delta facies by Cohen *et al.* (1995). Ediger *et al.* (1996) were able to date this formation as early–middle Miocene based on their palynological investigation, which recorded an Eskihisar sporomorph association (Fig. 2). This association was initially defined by Benda (1971), and its time range of 20–14 Ma has been constrained by isotopic dating of related volcanic rocks in western Turkey (Benda *et al.* 1974; Benda & Meulenkamp 1979, 1990; Seyitoğlu *et al.* 1994; Seyitoğlu & Benda 1998). The recent regional correlation attempted by Kaya *et al.* (2007) for the Alaşehir Formation was solely based on lithological similarity. They did not provide any first order age data from this formation.

The Kurşunlu Formation, the second sedimentary unit (Seyitoğlu & Scott 1996), is characterized by its dominantly red colour and conformably overlies the Alaşehir Formation. The conformity is supported by the gradual change in colour from grey-green (Alaşehir Formation) to pinkish-red (Kurşunlu Formation) (Fig. 5). The lower boundary of this formation is defined by a dark red angular boulder conglomerate seen SE of Çaltılık (Figs 4 & 5) and south of Acıdere (Fig. 3). The upper part is characterized by an alternation of light red to grey coloured conglomerates and sandstones, as seen SE of Göbekli (Fig. 3). The Kurşunlu Formation has been interpreted as a lateral alluvial fan deposit (Cohen *et al.* 1995). Seyitoğlu & Scott (1996) suggested an early–middle Miocene (20–14 Ma) age based on the record of the Eskihisar sporomorph association (samples analysed by Leopold Benda). However, Yılmaz *et al.* (2000) considered this result invalid and suggested that the lignite samples are reworked; they prefer the results obtained by Ediger *et al.* (1996) who suggest a middle Miocene or late Miocene age based on the determination of the Yeni Eskihisar (14–11 Ma) or Kızılhisar (11–5 Ma) sporomorph associations from the second sedimentary unit (Fig. 2). Koçyiğit *et al.* (1999) also recognized a Yeni Eskihisar sporomorph association within their Göbekli Formation (equivalent to the upper part of the Kurşunlu Formation, Fig. 2) but their species list contains no percentages of taxa which prohibits further evaluation.

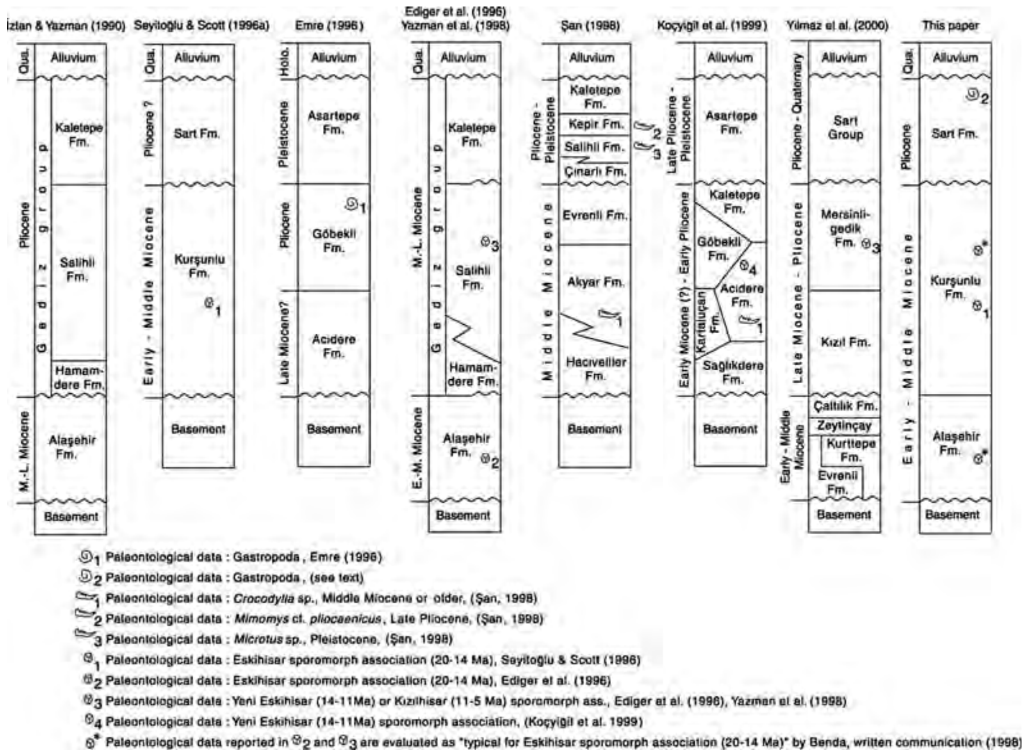

Fig. 2. Stratigraphical correlation of previous studies in the Alaşehir graben.

The overall composition of palynological samples from the second sedimentary unit in Ediger *et al.* (1996) has been evaluated as 'typical for an Eskihisar association' by L. Benda (pers. comm., 1998) who established the sporomorph associations in the Aegean area (see Seyitoğlu *et al.* 2002). This is also supported by the record of a *Crocodylia* sp. tooth (middle Miocene or older) in the second sedimentary unit, as reported by Şan (1998) and Koçyiğit *et al.* (1999). However, it cannot be excluded that the uppermost part of this formation might continue into the upper Miocene, although there is no age data to support this hypothesis. On the other hand, the

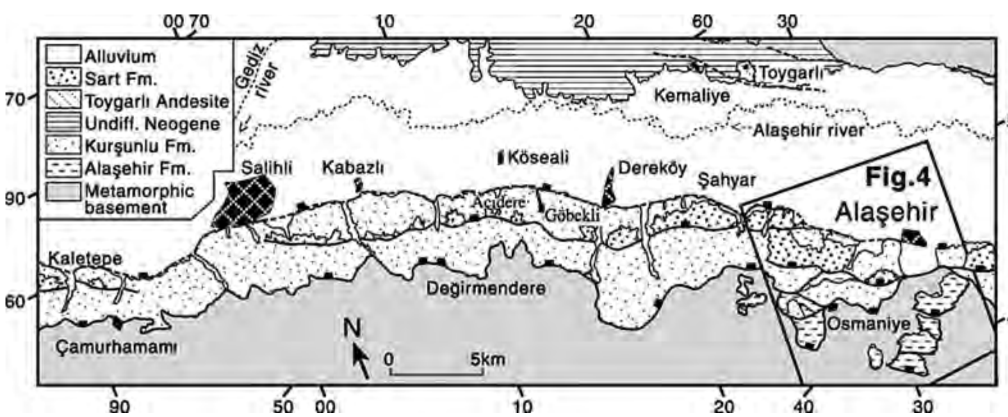

Fig. 3. Geological map of the Alaşehir graben (after Seyitoğlu *et al.* 2000).

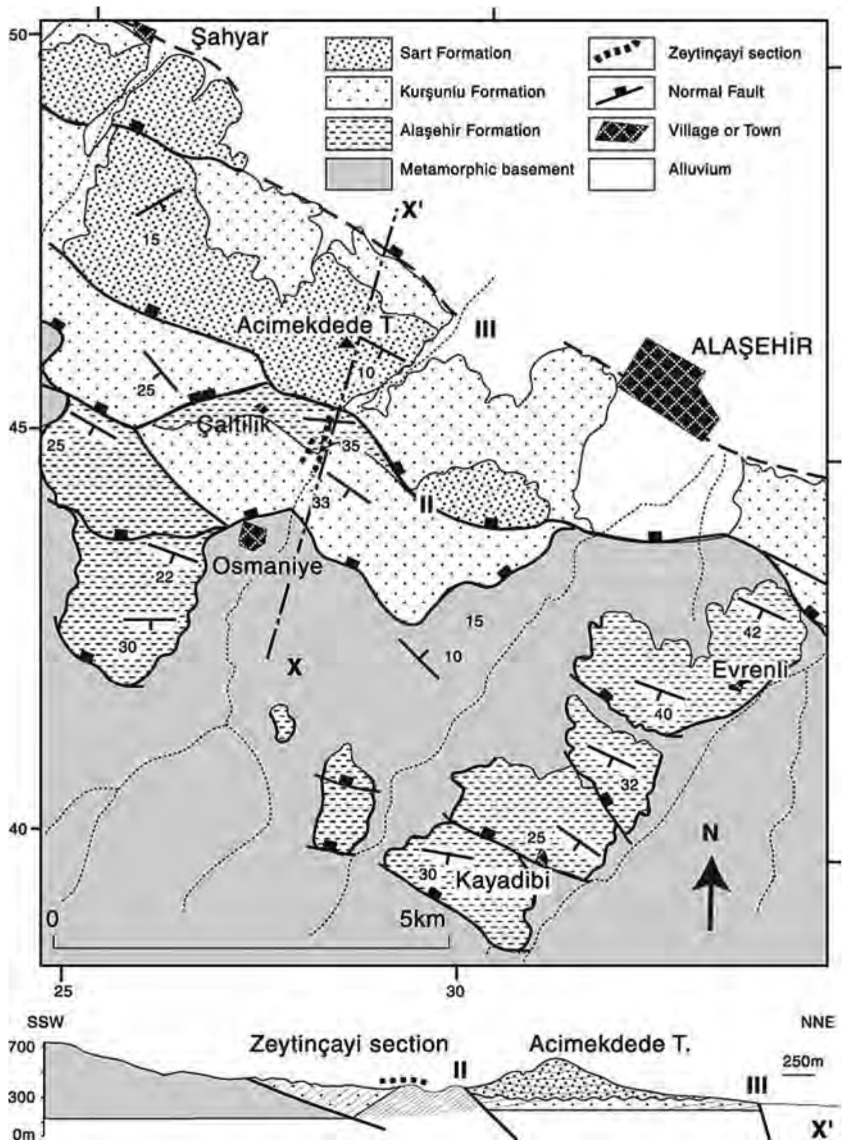

Fig. 4. Geological map of Alaşehir–Osmaniye area and cross section X–X′ in the Alaşehir graben. The sections sampled for magnetostratigraphy (Zeytinçayı-river and Zeytinçayı-road) are indicated by dashed lines.

Pliocene age attributed to the upper part of the formation, based on gastropods, has limited age diagnostic value (Emre 1996) because the list of taxa given is not characteristic enough for biostratigraphy. The recent record of late Pliocene micromammalian fossils at Çaltılı about 8 km west of Salihli (Sarıca 2000), allegedly from the upper part of the Kurşunlu Formation, requires further study such as stratigraphical and structural work in the area from where these fossils come for its correlation with deposits under investigation. The attributed early–middle Miocene age for the lower part of the Kurşunlu Formation will be investigated by means of magnetostratigraphy presented in this study.

The Sart Formation, the third sedimentary unit, is composed of light yellow, semi-lithified conglomerates and sandstones (Seyitoğlu & Scott 1996) and unconformably overlies the Kurşunlu Formation as seen at Kale Tepe (Fig. 3) in the western part of the Alaşehir graben. This formation has been

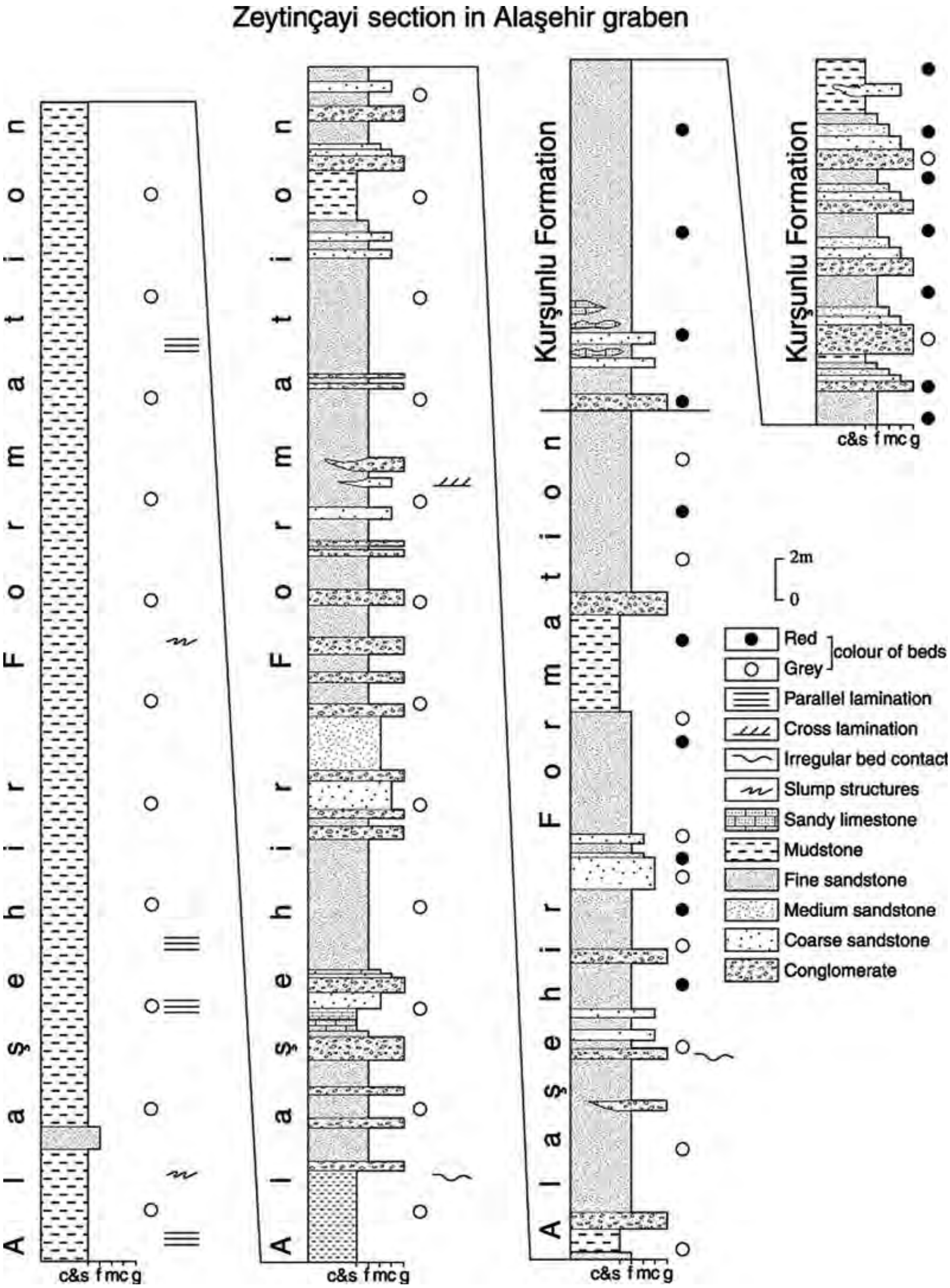

Fig. 5. Measured stratigraphical log (Zeytinçayı section) across Alaşehir and Kurşunlu formations in the Alaşehir graben. See Figure 4 for location.

interpreted as an axial fluvial and lateral alluvial fan facies (Cohen *et al.* 1995). Its age is late Pliocene based on micromammalian fossils (*Mimomys* cf. *pliocaenicus*, *Microtus* sp.) and gastropods (*Pisidium iasiense*, *Valvata (Borysthenia) jelski*, *Valvata (Valvata) sulekina*, *Valvata (Cincinna)* cf. *sibiensis*, *Pisidium* sp.) as reported by Şan (1998) from the area SW of Turgutlu.

Büyük Menderes graben

The graben trends east–west and has a boundary fault along its northern margin (Figs 1 & 6). At the base of the graben, Sözbilir & Emre (1990) described the Hasköy Formation as composed of boulder conglomerates, sandstones and mudstones with lignite layers (Figs 7 & 8). They interpreted the formation to be a fluvio-lacustrine deposit. It contains east–west trending (N 80°E, 30°SE) normal growth faults and the beds thicken towards these faults as observed south of Bayındır (Fig. 6).

This formation is considered an equivalent of the Alaşehir Formation in the Alaşehir graben. The age of the Hasköy Formation is given by Sözbilir & Emre (1990) as middle–late Miocene based on a list of pollen species, although without any name of the sporomorph association that it might represent. On the other hand, L. Benda's palynological determinations for several studies (Becker-Platen 1970; Seyitoğlu & Scott 1992) indicate an Eskihisar sporomorph association (early–middle Miocene: 20–14 Ma) (Fig. 7). In a more recent palynological study, Akgün & Akyol (1999) proposed a middle Miocene age for the sporomorph associations they studied from this formation. Their criteria for age determinations are questioned by Seyitoğlu & Sen (1999).

The Hasköy Formation is conformably overlain by deposits of the Gökkırantepe and Gedik formations belonging to the second sedimentary unit, as distinguished by Sözbilir & Emre (1990) (Fig. 7). We choose not to differentiate the Gedik Formation, which is a local sedimentary unit representing the uppermost levels of the second sedimentary unit. Therefore, all red coloured deposits of the second sedimentary unit are considered here as the Gökkırantepe Formation. Sözbilir & Emre (1990) did not define a type section for this unit. We propose that the section measured along the southern slopes of Kızılcagedik Tepe forms the type section of this stratigraphic unit (Fig. 6).

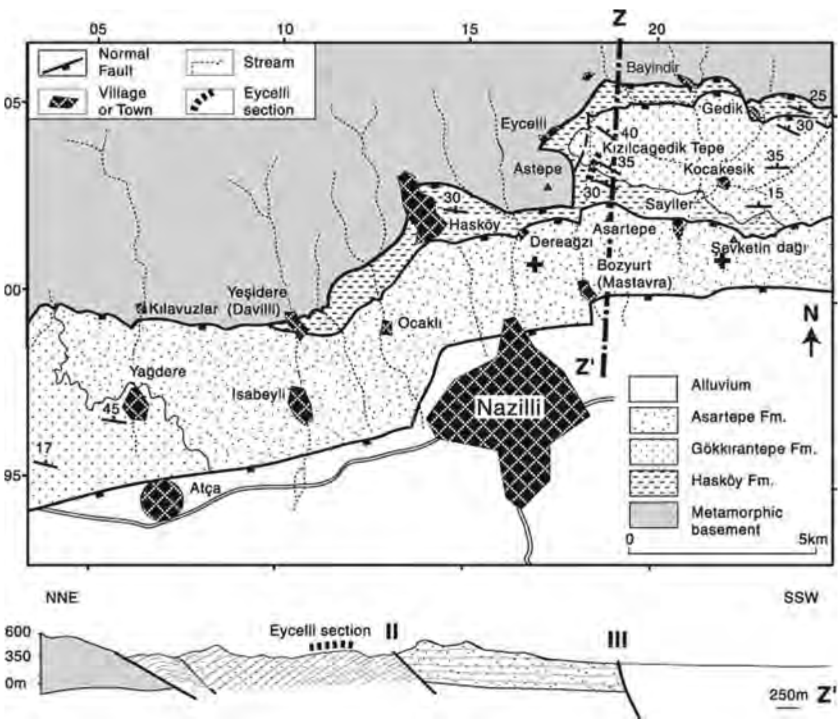

Fig. 6. Geological map of Nazilli area and cross section Z–Z′ in the Büyük Menderes graben. The Eycelli section sampled for magnetostratigraphy is indicated by a dashed line west to the Z–Z′ cross-section.

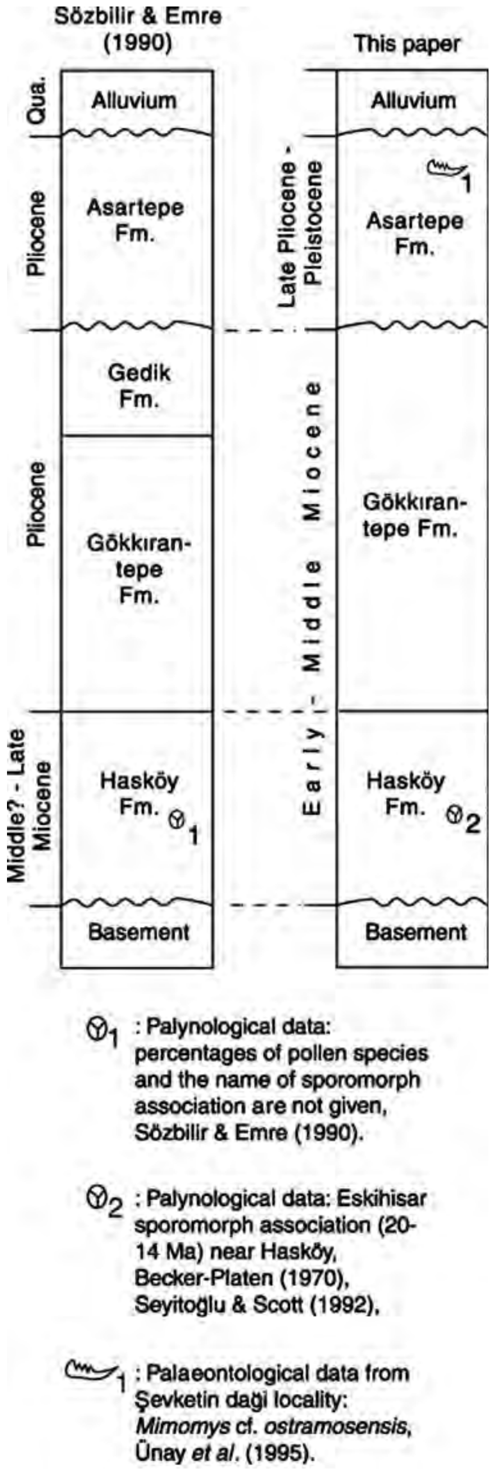

Fig. 7. Generalized stratigraphy of Büyük Menderes graben.

The Gökkırantepe Formation overlies conformably the Hasköy Formation (Fig. 8). It is composed of red conglomerates, sandstones and mudstones. The characteristic red colour of the formation becomes lighter in its uppermost levels and finally pinky-yellowish in sandstones near the top. This formation contains alluvial fan, braid plain, and fluvial facies (Cohen *et al.* 1995).

A Pliocene age for the Gökkırantepe Formation was tentatively proposed by Sözbilir & Emre (1990) based on their middle–late Miocene age attribution to the conformably underlying Hasköy Formation. However, as shown above, the Hasköy Formation is better dated as early–middle Miocene, and consequently the Pliocene age of the Gökkırantepe Formation is unlikely. During our fieldwork, we did not find any fossil to either confirm or contradict earlier attributed ages.

The Gökkırantepe Formation is unconformably overlain by the Asartepe Formation (Sözbilir & Emre 1990) which is composed of alternating yellow conglomerates and sandstones (Fig 7). Deep-cut valleys dominate the land surface of this formation, and the formation contains axial fluvial and coarse alluvial fan facies (Cohen *et al.* 1995). Micromammalian faunas from this formation constrain its age as late Pliocene to Pleistocene (Ünay *et al.* 1995; Sarıca 2000) (Fig. 7).

Bozkurt (2000) mentioned an age controversy in the Nazilli area. He claimed that the palynological age (Eskihisar sporomorph association dated between 20–14 Ma: early–middle Miocene) of Seyitoğlu & Scott (1992) contradicts the late Pliocene–early Pleistocene age given by the micromammalian faunas. The palynological samples were taken from the Hasköy Formation, immediately east of Hasköy, whereas the micromammalian fossils come from the Asartepe Formation at Şevketin dağı (Fig. 6). The geological mapping and stratigraphy showed that the palynological (Hasköy) and micromammalian (Şevketin dağı) sample locations are situated in different sedimentary units. Thus, the apparent controversy has no reason to exist.

Magnetostratigraphy

Sampling and measurements

Cohen *et al.* (1995) examined the facies distribution of the sedimentary fills in the Alaşehir and Büyük Menderes grabens. They concluded that the sedimentary units are syn-tectonic, and that attempts to date them are needed to understand the graben development history. In order to test the published ages and to refine the timing of graben formation, magnetostratigraphic work was undertaken on the

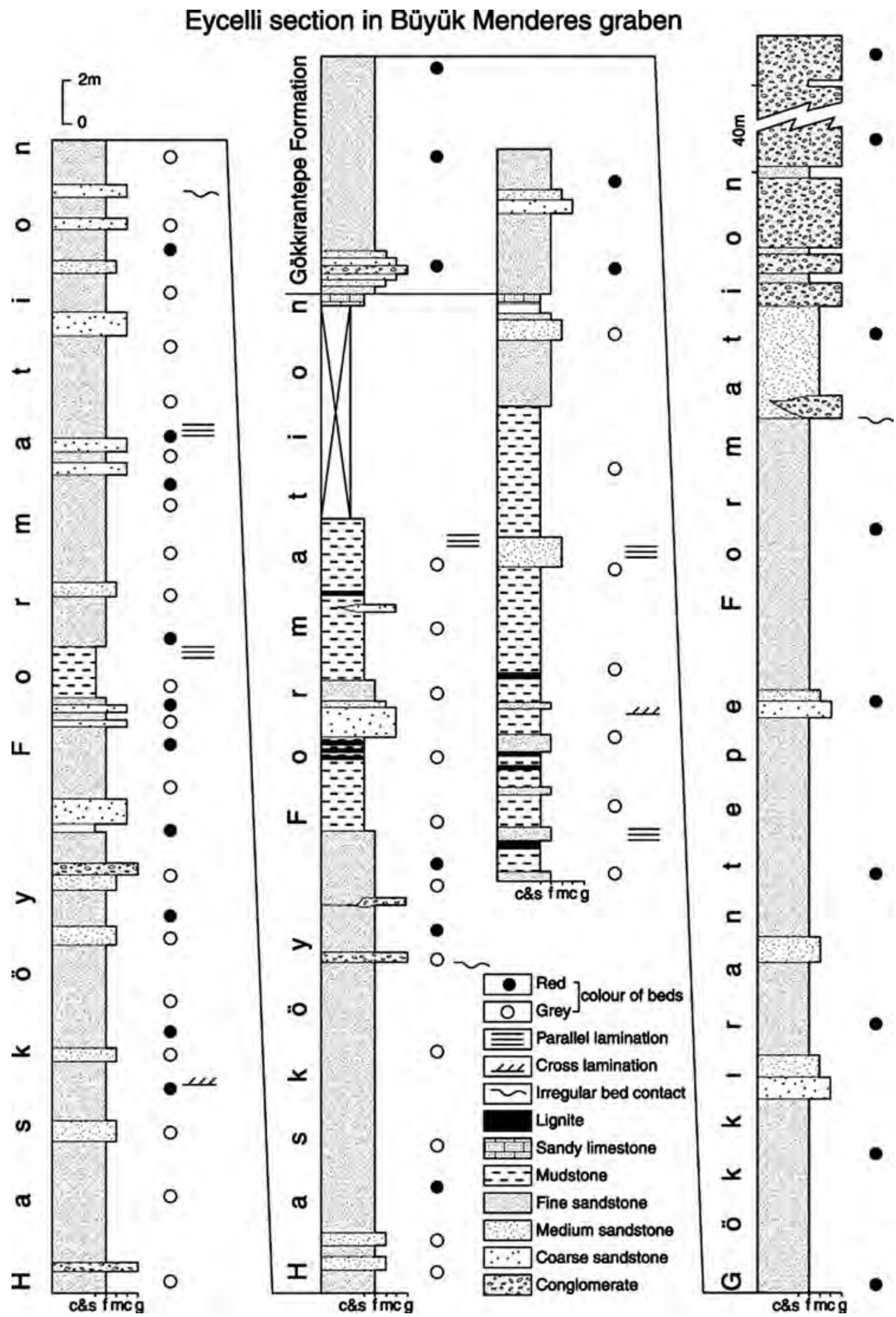

Fig. 8. Measured stratigraphical log (Eycelli section) between Hasköy and Gökkırantepe formations in the Büyük Menderes graben. See Figure 6 for location.

first and second sedimentary units in the Alaşehir and Büyük Menderes grabens (Figs 2 & 7). For these units, the best outcrops were found at the Yılan Çukuru district (Alaşehir graben) and near Eycelli village (Büyük Menderes graben). In addition, the distance between these two districts is less than 50 km, although they are situated North and South, respectively, of the Bozdağ horst that separates these two grabens.

We sampled two sections (Zeytinçayı-river and Zeytinçayı–road sections) in the Alaşehir graben (Fig. 4) and two sections (Eycelli section and Eycelli complementary section) in the Büyük Menderes graben (Fig. 6). Only compass oriented blocks were taken. We preferred this method because the Zeytinçayı outcrops occur in a steep canyon, where stone falls make sampling potentially dangerous, and some parts of the section are difficult to access with drilling equipment. In the case of the Eycelli section the sediments are generally not well consolidated and disintegrate when in contact with water. The sampled sections are limited at the bottom by major faults, and at their top by outcrop exposures. Only sediments unweathered and suitable for palaeomagnetic analyses were sampled; where necessary, the weathered surface was removed to reach fresh rock. Cores were drilled (Ø 25 mm, length 22 mm) from hand samples using compressed water or air as cooler at the Laboratoire de Paléomagnétisme de l'IPG in Paris.

All palaeomagnetic measurements were made in this laboratory. Remanent magnetizations of samples were measured with a three axes CTF cryogenic magnetometer in a magnetically shielded room. For isothermal remanent magnetization (IRM), we used a Drush 1.26 Tesla electromagnet (Fig. 9). Bulk susceptibility was measured with a Bartington susceptibily metre. All samples were demagnetized by stepwise heating from room temperature up to 600 °C in increments of 50 °C (Figs 10 & 11).

Zeytinçayı sections (Alaşehir graben)

The Zeytinçayı sections are situated about 3.5 km WSW of Alaşehir in the Yılan Çukuru district: one in the canyon of the Zeytinçayı river and the other along the road to Osmaniye village (Figs 12 & 13). The river section covers the upper part of the Alaşehir Formation (grey-green laminated clays, mudstones and a few sandstones) and the lower part of the Kurşunlu Formation (mainly pinkish-red clays, sandstones and conglomerates). The road section spans the top of the Alaşehir Formation and part of the Kurşunlu Formation. Both sections are laterally correlated using the formation boundary and also using a palaeosol horizon which is situated at 160–163 m in the river section and at 72–75 m in the road section.

The river section is 195 m thick and was sampled at 86 horizons (ZN1-ZN86) (Fig. 12). The average sampling distance is 2.27 m, including a gap of 10 m toward the top of the section and two 5 m gaps in its middle part. The gaps correspond to mainly coarse sediments unsuitable for palaeomagnetic analysis.

The Zeytinçayı-road section is 83 m thick and 35 horizons were sampled (ZR1-ZR35). The average sampling distance is 2.37 m, with one gap of 10 m (conglomerates) between 42–52 m and another gap of 6 m between 58.5–64.5 m (lack of exposure).

Both magnetic mineralogy and susceptibility analyses are crucial to identify the different components of magnetization in the samples. IRM acquisition was studied in six samples from different lithologies of the Zeytinçayı sections. Samples were magnetized (14 steps) in fields up to 1260 mT, and then thermally demagnetized (11 steps) up to 600 °C. Sample ZN12-1 (Fig. 9a) is from the laminated grey-green clays of the Alaşehir Formation. Its IRM curve is typical of magnetic carriers such as the magnetite. However, its demagnetization curve is more complex and indicates several magnetic carriers. There is a first drop in intensity at 350 °C and a second drop just before 600 °C. These unblocking temperatures are similar to those of pyrrhotite and greigite (320 °C and 360 °C) and of magnetite (580 °C), respectively. Sample ZR27-2 (Fig. 9b) is from red clays of the overlying Kurşunlu Formation. Its IRM acquisition curve increases progressively without reaching saturation, and its thermal demagnetization is not completed at 600 °C. This sample apparently shows the dominance of intermediate to hard coercivity magnetic grains, confirming the presence of an important fraction of hematite as the magnetic carrier. These observations are kept in mind when analysing thermal demagnetization curves of some 166 samples from both Zeytinçayı sections that we analysed for polarity identification.

The variation of susceptibility during stepwise thermal demagnetization was measured in 84 samples from both Zeytinçayı sections (Fig. 10a). Only 6% of the samples display a stable susceptibility up to 600 °C. Ninty-four percent of samples show a sudden susceptibility increase between 400–500 °C. The increase in susceptibility should be attributed to chemical break-down (oxidation) and formation of another magnetic mineral. The chemical break-down step is rather similar to that of pyrite, an iron sulphide, which usually occurs around 420 °C as is actually the case as seen in Figure 10a. The susceptibility increase is stronger in samples from the Alaşehir Formation than in those from the overlying Kurşunlu Formation.

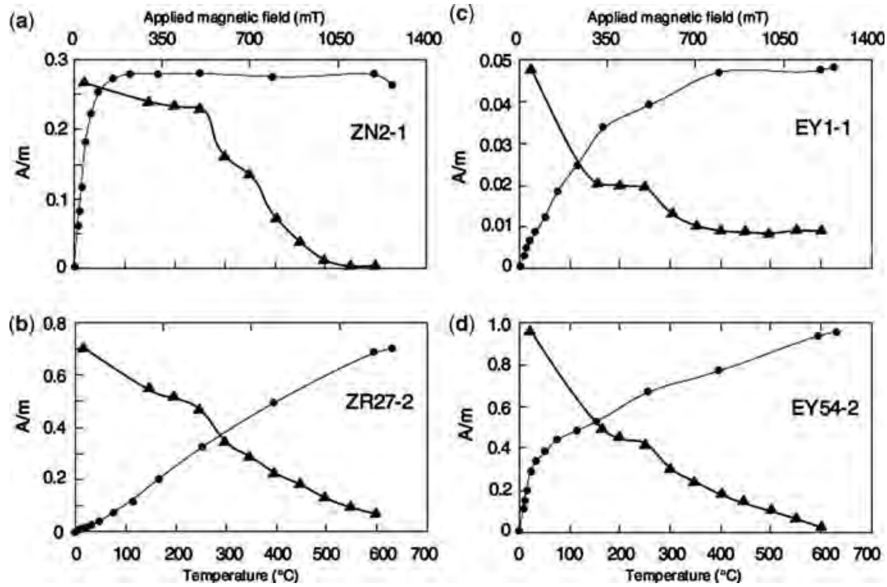

Fig. 9. Diagrams of isothermal remanent magnetization (IRM) (solid circles) and of its thermal demagnetization (triangles) for four samples from Zeytinçayı (ZN and ZR) and Eycelli (EY) sections.

The susceptibility increase generally occurs together with an increase in the intensity of magnetization, and subsequently the directions become random. These random directions are not considered for polarity definition in samples.

To determine the polarity pattern succession, we analysed 128 samples from the Zeytinçayı-river section and 38 samples from the Zeytinçayı-road section. All samples were subjected to stepwise thermal demagnetization up to 600 °C. Along the Zeytinçayı-river section, the intensity of the natural remanent magnetization (NRM) is about 2 mA/m in sediments between 0–60 m, and quite weak (<1 mA/m) between 60–138 m, and rather variable (0.2–4.5 mA/m) in the upper part. The distribution of the intensity variation at the 300 °C step is very similar to that of the NRM; this means that the differences of NRM intensity across the section is not related to a secondary component. In the Zeytinçayı-road section, the NRM intensities are weak (<1 mA/m) up to 55 m, but variable above as in the river section.

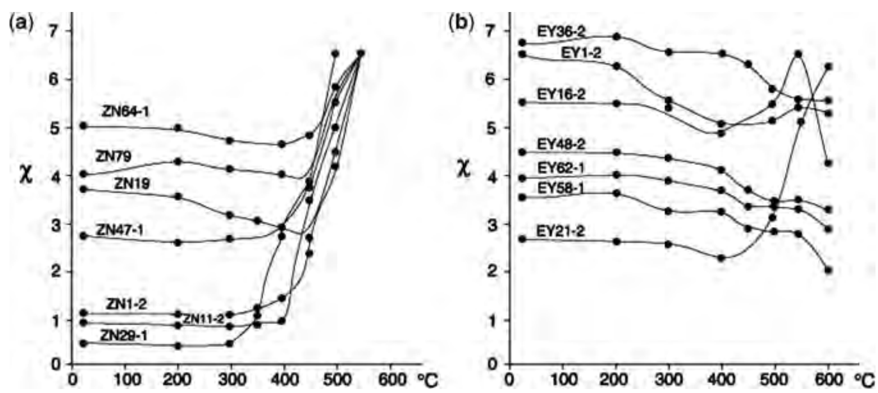

Fig. 10. Diagrams of initial succeptibility variation during thermal demagnetization for characteristic samples from Zeytinçayı-river (**a**) and Eycelli (**b**) sections. For Zeytinçayı-river samples, ZN79 is from the Kursunlu Formation while the others are from the Alaşehir Formation.

The deposits in the Zeytinçayı area are tilted (for 9 measurements, the mean strike = Ø 280° and dip = 33°), and this helps to verify the reliability of the Characteristic Remanent Magnetization (ChRM) component. Before tectonic correction, many samples have random directions and even those with clearly defined polarities are not well grouped on the stereographic diagrams. On the other hand, when the directions are plotted after tectonic correction, most samples are grouped (see below), and the mean normal and reversed polarity directions are quite similar to those directions already recorded in early–middle Miocene deposits of Turkey (Krijgsman *et al.* 1996).

Typical Zijderveld diagrams of samples from the representative lithologies and sedimentary units are shown in Figure 11. As noted above, the increase in susceptibility around 400–500 °C coincides with the occurrence of unstable magnetizations and random directions. This is particularly true for samples from the Alaşehir Formation. Therefore, in such samples the directions of the ChRM were calculated by including the steps between removed overprint component and the susceptibility increase. In 88% of the samples, it was possible to calculate the direction of the ChRM magnetic vector using principal component analysis (PCA). In this analysis, the Fisher's (1953) statistics were applied on line fits with at least three successive steps. For the remaining samples, indicated with open circles in Figures 12 & 13, line fits with only one or two steps are considered as representative of the ChRM based on their similar directions to that of other samples from the same site or from its proximity. All ChRM directions were plotted in stratigraphic order in Figures 12 & 13.

The Zeytinçayı-river section is dominated by reversed polarities but includes at least five normal polarity zones (Fig. 12). At the base, between 0–20 m, three normal polarity zones are interrupted by two reversed polarity zones. They are all well defined by two or more successive sites, except the second reversed zone that is characterized by one site only (ZN12). Between 20–93 m a long reversed zone is identified. However, three sites between 75.8–77.9 m yielded intermediate or poorly defined [i.e. maximum angular deviation (MAD) > 10] normal polarities. The behaviour of samples during thermal demagnetization suggests that a strong secondary magnetization component cannot be removed enough to reveal their ChRM. The following sites between 93–130 m yielded a succession of two normal polarity zones interrupted by a reversed polarity zones. One of the normal polarity zones is defined by two sites while the other normal polarity zones is characterized by seven successive sites. In the interval between 70–130 m, the definition of the ChRM is not always

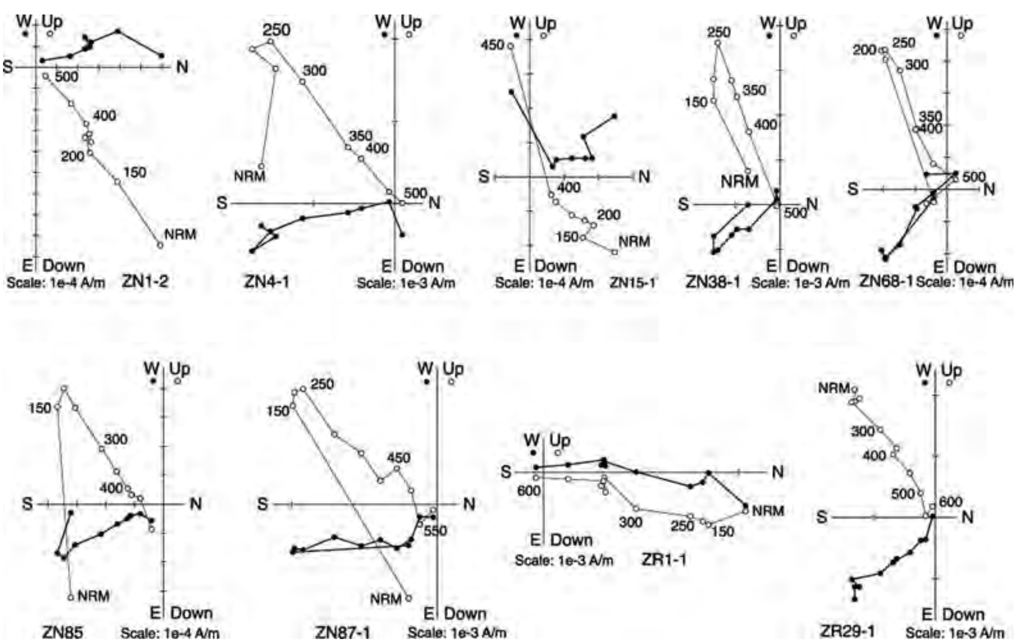

Fig. 11. Typical orthogonal projections diagrams of stepwise thermal demagnetization for selected samples from the Zeytinçayı sections. Closed (open) circles represent the horizontal (vertical) projection. Values indicate temperatures in °C for demagnetizing steps.

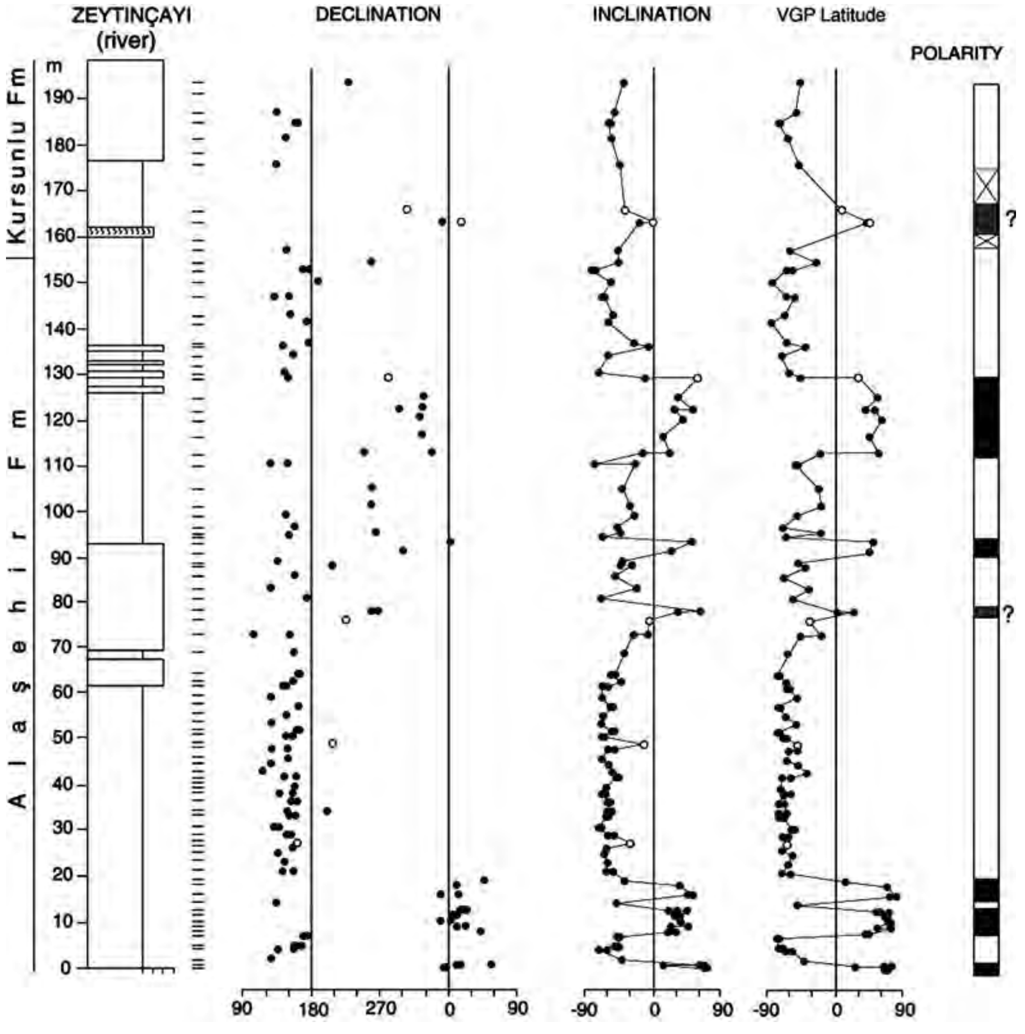

Fig. 12. Declination, inclination and Latitude of virtual geomagnetic pole (VGP) of ChRM versus stratigraphy in the Zeytinçayı-river section. The sampling intervals are shown with short lines right to the lithologic column. The polarity succession along this section is given on the right hand side of the figure. The greyed parts indicate the horizons where the polarity is poorly defined. Open (closed) circles denote sure (unsure) polarity. Black (white) in the polarity column represents normal (reversed) polarity.

satisfactory due to the weak intensities of remanent magnetization as mentioned above. At the upper part of the section, which corresponds to the top of the Alaşehir Formation and the base of the Kurşunlu Formation, the polarities of the ChRM are well defined as reverse, except between 162–166 m where three samples from two successive sites might indicate a normal polarity zone. These samples are taken from the red clastics of the Kurşunlu Formation. Two of them have ChRM values poorly defined (i.e. MAD > 10), and their normal polarity may well be an artefact of a strong secondary magnetization. In addition, this part of the section includes some sampling gaps.

In the Zeytinçayı-road section, the polarity record consists of a succession of three normal and four reversed zones, each recorded in two or more successive sites (Fig. 13). The bottom site (ZR1) also provided a normal polarity direction ($D = 5.3$, $I = 43.4$). This site was taken in yellowish brown sandstones, apparently weathered, and thus probably remagnetized. The upper 47 m of the section is entirely reversed. However, we have to note that some intermediate directions are

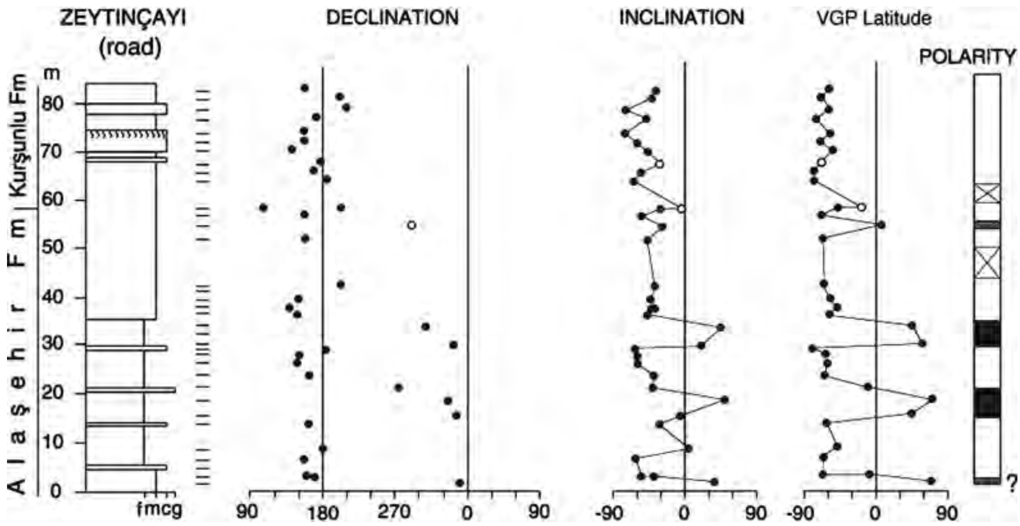

Fig. 13. Declination, inclination and VGP latitude of ChRM versus stratigraphy in the Zeytinçayı-road section. For other explanations, see Figure 12.

recorded at 55 m and 77 m, probably due to the sediments having a strong secondary magnetization. The overall polarity pattern of this section is quite similar and stratigraphically equivalent to that of the upper part of the Zeytinçayı-river section. However, the thickness of polarity zones varies from one section to another. We interpreted this as being due to some variation in sedimentation rate from one section to another, as it is often the case in fluviatile deposits.

Eycelli section (Büyük Menderes graben)

This section is situated between Akkaya Kuyulari and Gökkırantepe Tepe, north of Nazilli (Fig. 6). The sampling covers the upper part of the Hasköy Formation (0–112 m) and the lower part of the Gökkırantepe Formation (112–304 m). An exposure gap between 92 and 112 m in this section has been filled by sampling a supplementary section 200 m apart from the main section. Altogether, 62 levels were sampled taking oriented blocks. The sampled sediments in the Hasköy Formation are fluvio-lacustrine clays, silts and sandstones with the inclusion of a few lignite horizons. The Gökkırantepe Formation sediments consist of pinkish to red mudstones, sandstones and conglomerates. The total thickness of the sampled section is 304 m. Its lower part (0–173 m), which includes the Hasköy Formation and the base of the Gökkırantepe Formation, was sampled at 58 levels with fairly regular spacing (average 2.9 m). The upper part of this section (173–304 m) mainly consists of large conglomerate and sandstone layers which are unsuitable for palaeomagnetic investigation. In that part, only 4 horizons were sampled in thin red clays or silts interbedded with the sandstones and conglomerates.

The IRM coercivity spectra was studied in six samples from characteristic lithologies. In all cases, the IRM curves show a steep rise at low magnetization steps, but saturation is not reached by 1260 mT (Fig. 9c, d), showing that these sediments contain a mixture of soft and hard coercitive magnetic minerals. Sample EY1-1 is from the silty clays of the Hasköy Formation. The demagnetization of the IRM displays a significant unblocking step before 150 °C, probably corresponding to the unblocking of goetite. We note that the magnetization is not completely demagnetized by 600 °C because of the probable contribution of hematite. Sample EY54-2 is from pinkish clays of the Gökkırantepe Formation. The IRM curve for this sample has a steep rise at low steps of magnetization, but the intensity increases progressively up to 1260 mT. Its demagnetization curve displays the same pattern as EY1-1, except that its magnetization is completely cleaned at 600 °C. The main magnetic mineral of this sample is apparently magnetite together with a fraction of goethite which is probably a secondary overprint formed by weathering or diagenesis.

Bulk susceptibility was measured on 60 samples (Fig. 10b), of which 20% show no change in susceptibility during thermal demagnetization and in 22% of the samples susceptibility decreases smoothly, particularly at higher temperatures. In 58% of the samples susceptibility increase begins at about 450 or 500 °C. For the last samples, only steps before the susceptibility increase were used for polarity determination.

Seventy-seven samples were demagnetized stepwise up to 600 °C. The NRM intensity varies across the section between 0.02–5.9 mA/m with a mean of 0.89 mA/m. 26% of the samples show an important intensity drop at 150 °C (interpreted as due to goethite). 36% of the samples were completely demagnetized at 600 °C, while the remaining 64% were not. The first group of samples probably indicates that their main magnetic carrier is a (or several) magnetic mineral(s) with low coercivity, whereas in the second group of samples a high coercivity mineral, such as hematite, prevents total demagnetization at 600 °C step. The latter samples are generally those in which the susceptibility increases around 450–500 °C.

Typical Zijderveld diagrams of samples from this section are given in Figure 14. The polarity of the ChRM component was calculated using the PCA method. Figure 15 shows the declination and inclination of the primary component versus stratigraphy. The section is dominated by reversed polarities except in four successive sites between 136 and 162 m which have normal polarities. As shown in this figure, it is obvious that in particular the declinations and also in some extent the inclinations of the ChRM are not homogenous but rather scattered in their values. This may have several reasons: in some samples this is due to weak remanent magnetization that does not provide stable directions. In other, it is possibly due to insufficient removal of the secondary component of magnetization. In addition, the degree of compaction or diagenesis of sediments is not identical in every part of the section. Therefore, we interpret that this rather scattered state of declinations and inclinations may have several causes. For that reason, we selected 52 samples on 77, those having the best defined ChRM directions, to calculate the mean values of declinations and inclinations for each polarity zone.

Correlation to the Astronomically Tuned Neogene Time Scale (ATNTS2004)

To correlate the polarity sequences from the Zeytinçayı and Eycelli sections, we used the ATNTS2004 of Lourens *et al.* (2004). The polarity patterns documented in the Zeytinçayı and Eycelli sections are not detailed enough to provide direct correlations with the ATNTS2004. Therefore, we need biochronological data to constrain a time interval to

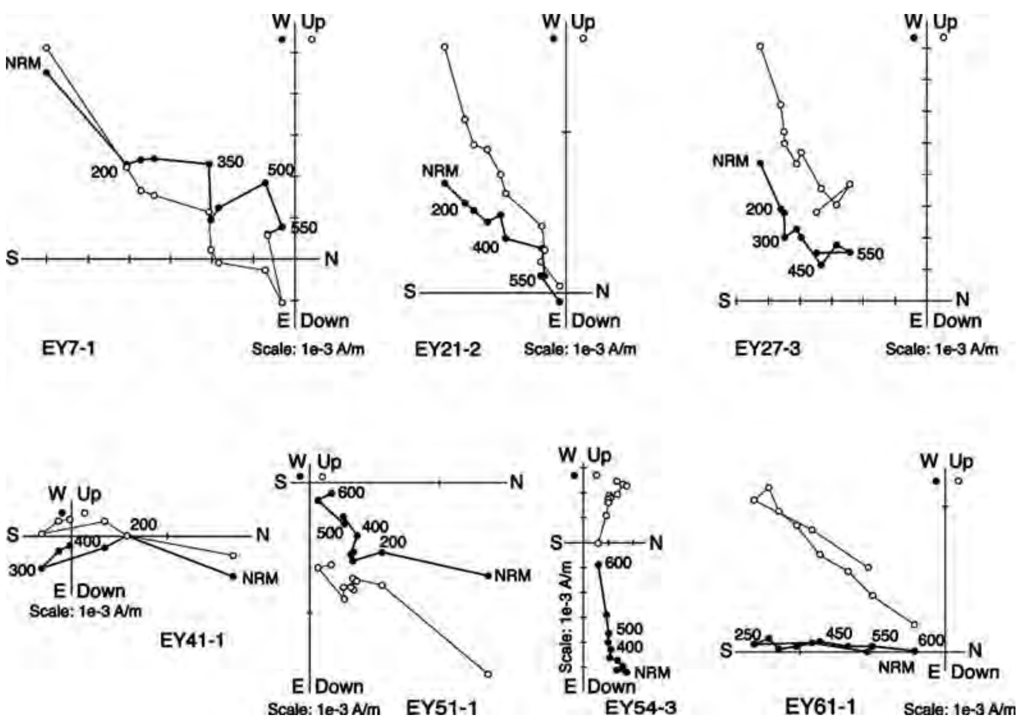

Fig. 14. Typical orthogonal projections diagrams of stepwise thermal demagnetization for selected samples from the Eycelli section. For other explanations, see Figure 11.

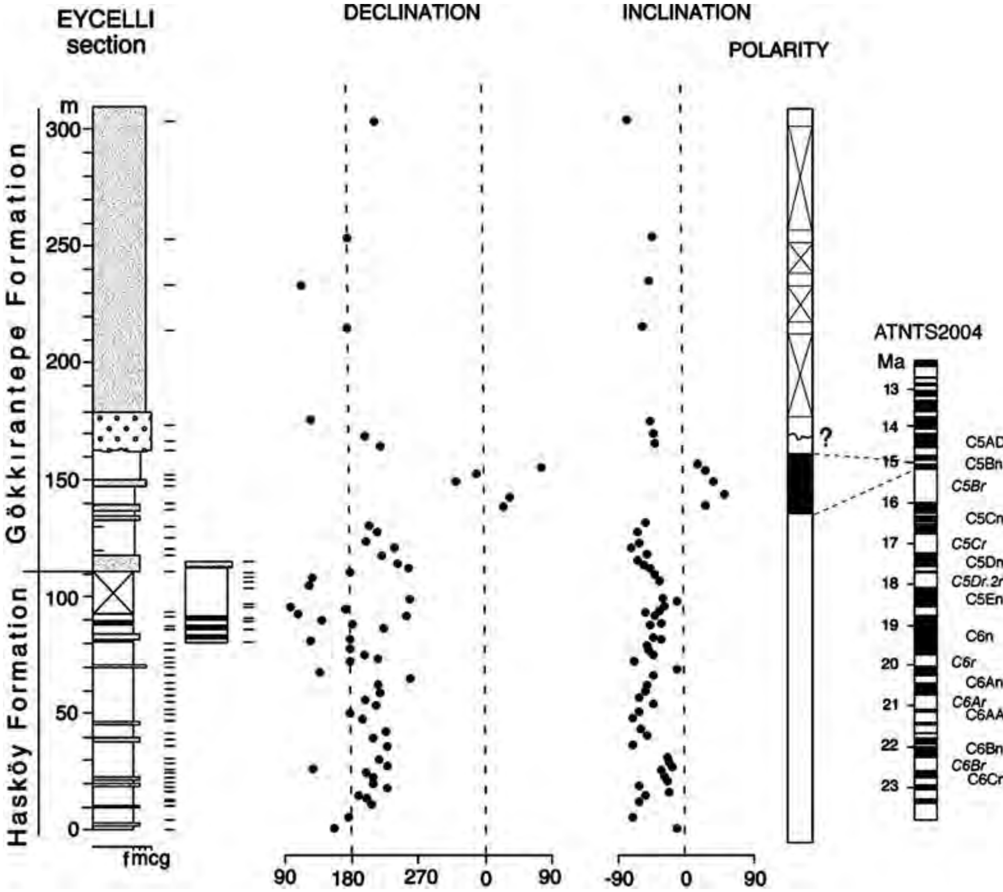

Fig. 15. Declination and inclination of ChRM versus stratigraphy in the Eycelli section. In the lithologic column, the white parts are clays and silts, the greyed parts represent sandstones and conglomerates, and the short black bands are coal intercalations. Note that the top of the Hasköy Formation was sampled in a complementary section which is 200 m apart from the main section. For other explanations, see Figure 12.

compare the polarity pattern of these sections with the ATNTS2004. As discussed above, the time range of the studied deposits is solely given by palynological data. The Alaşehir and Hasköy formations in the Alaşehir and Büyük Menderes grabens, respectively, are dated as early–middle Miocene based on the record of the Eskihisar sporomorph association (Ediger *et al.* 1996). This association is well known in western Turkey, and its age ranges from 14 to 20 Ma (Benda & Meulenkamp 1979). For the overlying Kurşunlu Formation, the palynological data are more abundant but somewhat controversial. Its sporomorph associations were determined as belonging to the Eskihisar or Yeni Eskihisar pollen zones which cover different time intervals, i. e. early–middle Miocene and middle–late Miocene, respectively. However, the identification of these sporomorph associations is difficult in some cases, mainly when characteristic elements are missing or the pollen sampling is poor. The occurrence of *Crocodyla* sp. in the lower horizons of the Kurşunlu Formation brings another age constraint. The last occurrence of crocodiles in northern Mediterranean areas is during the MN5 mammal zone (15–16.5 Ma) or in one case (Sansan, SW France) in MN6 (13–15 Ma) (Pickford & Morales 1994; Steininger *et al.* 1996; Sen 1997). Their extinction is explained by the global mid Miocene cooling event at 14.1 Ma. This record, in combination with palynological data, provides biostratigraphic age control for the studied deposits in the Alaşehir graben, suggesting an early to early middle Miocene age.

As mentioned above, the Zeytinçayı sections are dominated by reversed polarities. Thus, correlation with the dominantly normal polarity interval of the

ATNTS2004 between 18.1–19.7 Ma is unlikely. Combining the resulting magnetostratigraphy of the Zeytinçayı sections with the palaeontological ages results in two possible correlations to the ATNTS2004: one to the C6Bn.2n–C6An.1r interval (approximately between 20.3–22.1 Ma) (Fig. 16a), which is older than the time interval predicted by the palynological ages, and the other to the C5Cn.3n–C5ADr interval (approximately between 14.6–16.6 Ma) (Fig. 16b). Correlating the Zeytinçayi polarity zones to the interval between the C6Bn.2n–C6An.1r of the ATNTS2004 results in a mean sedimentation rate of 10.7 cm/ka (Fig. 16a). Such a sedimentation rate seems too high for the lithified clays of the Alaşehir Formation, but fits with the coarser sediments of the Kurşunlu Formation.

The other potential correlation to the interval between C5Cn.3n–C5ADr is shown in Figure 16b. The three normal zones at the base of the Zeytinçayı section might correlate with chron C5Cn (between 15.97–16.60 Ma, mean sedimentation rate 3.17 cm/ka), the long reversed zone with C5Br (between 15.16–15.97 Ma, mean sedimentation rate 8.76 cm/ka), and the two normal zones between 91–130 m with chron C5Bn (between 14.78–15.16 Ma, mean sedimentation rate 10.37 cm/ka). With this correlation, the top reversed zone at Zeytinçayı would correspond to chron C5ADr (between 14.581–14.784 Ma) and invokes a high sedimentation rate (about 31 cm/a) in that part of the section. The correlation to the C5Cn.3n–C5ADr interval, and the inferred sedimentation rates, fit well with the observed upward coarsening trend of sediments from the mid Alaşehir Formation up to the Kurşunlu Formation. Moreover, the correlation of the Fig. 16b fits better with both palaeontological ages and a U–Pb date of a syntectonic intrusion (16.1 ± 0.2 Ma–15.0 ± 0.3 Ma; Glodny & Hetzel *et al.* 1995). Consequently, this latter correlation is preferred.

The Eycelli section in the Büyük Menderes graben was also dated by pollen as early–middle Miocene, and it was considered equivalent to the Alasehir Formation. There is no possible lithological correlation between the Zeytinçayi and Eycelli sections because their respective basins are separated by the Bozdag horst. One of the initial aims of the present study was to provide an independent correlation between the early–middle Miocene deposits of both Alasehir and Büyük Menderes grabens.

The lower half of the Eycelli section was densely sampled for magnetostratigraphy, and it yielded a

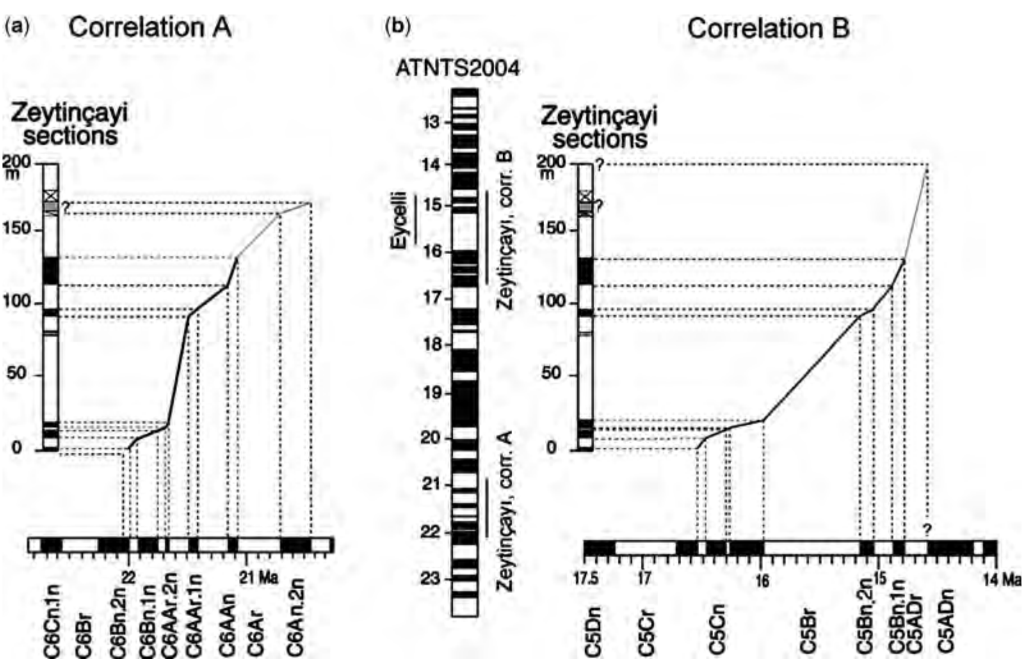

Fig. 16. Two hypotheses of correlation between the Zeytinçayı-river palaeomagnetic reversal stratigraphy and the ATNTS2004 (Lourens *et al.* 2004). The progressive increase of the sedimentation rate upward in the correlation B matches better with the depositional styles recorded along this section. This correlation is also supported by palynologic and radiometric ages. In the middle of the figure, the potential correlations of the Zeytinçayı-river section and the tentative correlation of the Eycelli section reversal stratigraphy to the ATNTS2004 are summarized.

long reversed zone on 136 m (Hasköy Formation + base of the Gökkırantepe Formation), followed by a short normal zone (five sites on 26 m). The upper half of the section is mainly formed of conglomerates in which only seven horizons on 150 m were sampled, and these samples have a reversed polarity. This latter part of the section was possibly deposited in a short time interval, thus the thickness of this part cannot be considered as indicative of a long reverse polarity period.

It should be mentioned that the long reversed zone have declinations and inclinations of the ChRM rather scattered. This is in fact due to poorly defined ChRM components in weakly magnetized sediments of the Hasköy Formation.

The polarity succession recorded in the Eycelli section cannot be correlated with any part of the ATNTS2004. Unfortunately, this section did not yield any biochronological data. However, in other parts of the graben, the palynology of the Hasköy Formation lies within the early–middle Miocene (see above). In this time interval, long reversed periods of the ATNTS2004 occurred between 19.72–20.04 Ma (Chron C6r), 17.74–18.06 (Chron C5Dr.2r), 16.72–17.23 Ma (Chron C5Cr) and 15.16–15.97 Ma (Chron C5Br) (Fig. 15). Other intervals of the Miocene are dominated by normal polarities. These four possibilities can be reduced to two owing to the fact that chrons C6r and C5Cr are followed by long normal chrons and that the short normal zone of the Eycelli section does not fit with these long normal polarity intervals. Consequently, the lower part of Eycelli section might represent either Chron C5Dr.2r or Chron C5Br. The correlation of the long reversed zone of the Eycelli section with Chron C5Br seems more appropriate for two reasons: (i) it fits with palynological ages of the Hasköy Formation; and (ii) the resulting mean sedimentation rate (16.7 cm/ka) for the Hasköy Formation and the base of the Gökkirantepe Formation is in agreement with the sedimentary nature of these deposits. The other reversed chrons of early–middle Miocene are shorter than the Chron C5Br, and a correlation with one of these intervals implies a mean sedimentation rate over 50 cm/ka, too much for lithological characteristics of sediments in this section. Thus, we tentatively correlate the Eycelli section with the C5Bn.1r–C5Br interval (14.88–15.97 Ma) of the ATNTS2004, i.e. late early Miocene–early middle Miocene interval (Figs 15 & 16).

Rotation on vertical axis: regional versus local tectonics

Figure 17 shows stereographic plots of the ChRM after tectonic correction of the three sections. They include only samples with reliable palaeomagnetic directions, i.e. MAD $< 10^\circ$ (Table 1). In the Zeytinçayı-river and road sections, the mean directions of ChRM are not completely antipodal ($\delta = 13.5^\circ$ at Zeytinçayı-river, and $\delta = 11.9^\circ$ at Zeytinçayı-road). Nevertheless, in both sections the directions of the ChRM show that this area undervent a vertical-axis anticlockwise rotation of about 25° since the deposition of these sediments. On the other hand, for the best 52 samples from the Eycelli section, the mean directions of magnetization are not antipodal either ($\delta = 13.1^\circ$). However, both reversed and normal samples indicate a clockwise rotation of about 30–40°. Note that these sections are in two different grabens.

In western Turkey, palaeomagnetic data from early–middle Miocene volcanics show dispersed directions (Kissel *et al.* 1987). The Izmir region is

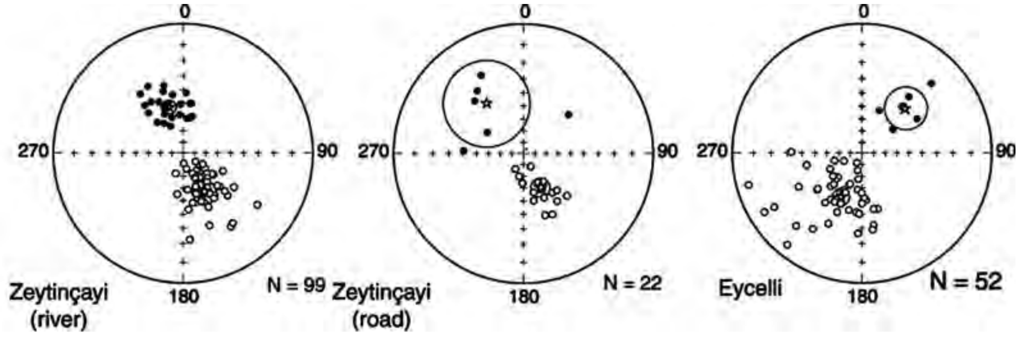

Fig. 17. Stereographic projections of the characteristic remanent magnetization components for the Zeytinçayı (river and road) and Eycelli sections. The stars give the mean values for normal and reversed directions, and the circles indicate Fisher's (1953) α95 confidence interval. Note that they are calculated on most reliable samples given in Table 1. The Zeytinçayı sections provide an anticlockwise rotation of about 25°, while the Eycelli section reveals a clockwise rotation of about 30–40°. The mean values are in Table 1.

Table 1. *Mean values of the characteristic remanent magnetization for samples from the sections of Zeytinçayı (river and road) and Eycelli. The mean values are calculated for each polaritiy zone normal (N) and reverse (R). The head abreviations are: N = number of samples, Dgeogr and Igeogr = declination and inclination without tectonic correction, Dstr and Istr = declination and inclination after tectonic correction, k = precision parametre, α95 = error margin*

Section	Polarity	N	Dgeogr	Igeogr	k	α95	Dstr	Istr	k	α95
Zeytinçayı (river)	N	24	4.7	27.3	32.5	5.1	343.2	49.4	31.8	5.3
Zeytinçayı (river)	R	75	172.2	−32.9	19.7	4.2	149.7	−53.6	21.8	3.6
Zeytinçayı (road)	N	6	325.4	49.8	4.0	38.6	323.3	43.0	5.5	31.4
Zeytinçayı (road)	R	16	173.1	−35.4	25.1	7.3	155.2	−55.3	25.4	7.5
Eycelli	N	6	65.4	17.2	20.3	15.3	43.4	39.4	20.4	15.2
Eycelli	R	46	234.3	−78.9	10.9	6.7	210.2	−48.6	10.6	6.8

characterized by 35° westerly declinations, while the mean declination of three sites south of Bergama is 20° to the east. Volcanic rocks from the Karaburun peninsula, dated between 17–21 Ma, have an average declination of 45° easterly with, however, large variations between sites. In summary, despite an apparent counterclocwise rotation of the Anatolian block during the Neogene times, regional or local variations also exist, probably because of local tectonics while the anticlockwise rotations are related to the general westward extrusion of the Anatolian plate.

Palaeomagnetic and structural data suggest that, in western Anatolia, major fault bounded distinct domains have rotated around vertical axis as partly independent blocks at different rates and in different senses. Unfortunately the palaeomagnetic and chronologic data are too scarce to recover all the Neogene times to enlighten the timing and the speed of rotational motions. However, magnetostratigraphic studies can provide better time constraints to understand the tectonic history of individual continental blocks. The rotations recorded in the Zeytinçayı and Eycelli sections are consistent with the previous observations, and show that Turkey, and especially western Anatolia, has a much more complicated deformation pattern than originally thought (Şengör *et al.* 1985). Westaway (1990) suggested that the extension rate in West Anatolia increases westward, and thus causes a counterclockwise vertical vorticity, hence a counterclockwise rotation around the vertical axis on a regional scale. However, according to him some blocks bounded with major faults may act independently to provide clockwise rotation.

The researchers are also aware of that ‘thin skinned’ extensional tectonics might cause independent rotations in some blocks (Kissel *et al.* 1987; Hakyemez *et al.* 1999). Recent studies (Hetzel *et al.* 1995; Emre 1996; Işık & Tekeli 2001; Işık *et al.* 2003; Seyitoğlu *et al.* 2004) in western Turkey documented that detachment faults play an important role on the thin skinned extensional deformation. The opposing sense of rotations around a vertical axis shown here from the Alasehir and Büyük Menderes grabens, might be attributed to block rotations on detachment faults.

Discussion

As outlined in the introduction part, the region-wide tectonic models agree that the central Menderes massif was exhumed as a symmetrical core complex (Ring *et al.* 2003; Seyitoğlu *et al.* 2004). The Massif was at the surface at the beginning of early Miocene according to apatite-fission track age data of Gessner *et al.* (2001). The dome shaped massif is fragmented by east–west trending, opposite dipping graben bounding faults. Their tectonic development resembles the rolling hinge model. Its footwall (Gessner *et al.* 2001) and hanging wall data (Seyitoğlu *et al.* 2002) are well documented especially in the Alaşehir graben.

The high angle, east–west trending first fault system controlled the accumulation of first and second sedimentary units during early Miocene–late Miocene (?) in the Alaşehir graben (Seyitoğlu *et al.* 2002). When the transition from first sedimentary unit to the second one occurred in the hanging wall of first fault system (14.6–16.7 Ma), as indicated by magnetostratigraphical data of this paper, the ductile Alaşehir shear zone was already developed in the mid-crust as a continuation of the first fault system (see Işık *et al.* 2003). Syn-extensional granodiorite (Hetzel *et al.* 1995; Işık *et al.* 2003), intruded into this shear zone, indicates that the middle crust equivalent of the first fault system, the Alaşehir shear zone, was already active during 16.1 ± 0.2 Ma–15.0 ± 0.3 Ma (Glodny & Hetzel 2007, see also dating in Catlos & Çemen 2005 as 17 ± 5 Ma).

In the Pliocene, the second fault system developed in the hanging wall of the first fault system and it produced the deposition of third sedimentary unit. The first fault system rotated to lower angles;

Seyitoğlu *et al.* (2002) provided field evidence that the first fault system is also active in contrast to the original rolling hinge model (Buck 1988; Wernicke & Axen 1988). This is also supported by isotopic dating of Lips *et al.* (2001; 7 ± 1 Ma) and Catlos & Çemen (2005; 4.5 ± 1.0 Ma). Apatite fission track data of Gessner *et al.* (2001) indicate a rapid exhumation in the footwall of the first fault system following 5 Ma that is accelerated by the initiation of second fault system (see Seyitoğlu *et al.* 2002, Fig. 10).

In the Quaternary, the third fault system becomes operational in the hanging wall of the second fault system and controls the accumulation of fourth sedimentary unit, Quaternary alluvium deposits. The previous fault systems further rotated and graben bounding first fault system becomes a low angle normal fault. In the Quaternary–present day, the high angle fourth fault system cut and displaces all earlier structures (see Seyitoğlu *et al.* 2002, Fig. 10d).

The tectono-sedimentary model supported by magnetostratigraphic and isotopic datings indicates that the east–west trending graben formation in western Turkey is similar to the rolling hinge model until Quaternary–Recent times. However, Bozkurt & Sözbilir (2004) put forward that the high angle normal faults cut and displace the presently low angle first fault system and that this implies that the rolling hinge model is not applicable to the east–west trending graben formation. It should be noted that our model supports the fact that high angle faults cut the low angle normal faults as indicated by fourth fault system in the Seyitoğlu *et al.* (2002, Fig. 10d). The existence of Quaternary–Recent fourth fault system does not affect the earlier (early Miocene–Quaternary) history of the rolling hinge process. All cross cutting relationships documented by Bozkurt & Sözbilir (2004) match the 'fourth fault system'. They can not disprove the rolling hinge model in the Alaşehir graben.

Another important issue discussed in the recent literature is the claim of Yılmaz *et al.* (2000) that the first sedimentary unit, the Alaşehir Formation, was deposited in a North-trending basin and later trapped in the younger east–west trending graben. Several lines of evidence suggest that the Alaşehir Formation was a product of the east–west trending Alaşehir graben. According to the sedimentological work of Cohen *et al.* (1995), all sedimentary deposits within the graben are syn-tectonic, and they can be used to date the graben formation. In the seismic refraction diagrams recorded by Turkish Petroleum Co., the Alaşehir Formation forms a sedimentary wedge that becomes thicker towards the east–west trending fault system, indicating its syntectonic development (Yılmaz & Gelişli 2003). A similar feature was also observed in the Zeytinçayı valley where the wedge of the upper part of the Alaşehir Formation thickens towards the N75W, 42NE oriented syn-sedimentary fault.

Conclusions

Palaeomagnetic analyses show that sediments from the Zeytinçayı (Alaşehir graben) and Eycelli (Büyük Menderes graben) sections are suitable for palaeomagnetic studies. Magnetic properties of the sediments and the behaviour of samples during demagnetization are different in the two areas. This might suggest that the deposits were formed in different sedimentary environments.

This study provides a chronological frame to the first and second sedimentary units in the Alaşehir and Büyük Menderes grabens. Correlation of the recorded polarity zones with the ATNTS2004 (Fig. 16b) indicates that in the studied Zeytinçayı and Eycelli sections, the transition from the first unit to the second unit occurred at about 14.5 Ma in both sections. This provides an age older than this date to the first sedimentary units in the Alasehir and Büyük Menderes grabens that are Alasehir and Hasköy formations, respectively. This result clearly places the initiation of east–west trending graben formation in the early Miocene and is compatible with recent isotopic dating (Catlos & Çemen 2005; Glodny & Hetzel 2007). Consequently, the use of younger ages attributed to the timing of graben formation in western Turkey is misleading (Hakyemez *et al.* 1999; Bozkurt 2000; Yılmaz *et al.* 2000; Bozkurt & Sözbilir 2004).

This paper also provides two more examples to the collection of contradictory rotations around the vertical axes in western Turkey. The local tectonics controlled by the thin skinned extensional deformation due to detachment faults might be the cause of such rotations. Therefore these rotations may not be meaningful evidence for the model of back arc spreading in the Aegean region.

This paper is dedicated to the memory of Leopold Benda (13.1.1933–11.10.1998) who is the founder of late Cenozoic sporomorph chronology in the Aegean region. Nuran Sarıca helped with the sampling. All measurements have been performed in the Laboratoire de Paléomagnétisme et Géodynamique de l'IPG (Paris). Discussions with colleagues from this laboratory, and mainly with M.-G. Moreau, H. Bouquerel and S. Gilder, contributed to a better understanding of palaeomagnetic results. This study was granted by CNRS (France) and the Scientific and Technical Research Council of Turkey-TUBITAK (YDABCAG-424/G). S. Gilder kindly improved the English. Pertinent comments and suggestions of the referees E. Bozkurt and S. Hüsing, and that of the editor D. van Hinsbergen were greatly constructive to improve previous versions of this paper. We are very grateful to them.

References

AKGÜN, F. & AKYOL, E. 1999. Palynostratigraphy of the coal bearing Neogene deposits in Büyük Menderes graben, Western Anatolia. *Geobios*, **32**, 367–383.

BECKER-PLATEN, J. D. 1970. Lithostratigraphisce Untersuchungen im Känozoikum Südwest-Anatoliens (Türkei). *Beihefte zum Geologischen Jahrbuch*, **97**, 1–244.

BENDA, L. 1971. Grundzüge einer pollenanalytischen Gliederung des türkischen Jungtertiärs. *Beihefte Zum Geologischen Jahrbuch*, **113**, 1–46.

BENDA, L. & MEULENKAMP, J. E. 1979. Biostratigraphic correlations in the Eastern Mediterranean Neogene. 5. Calibration of sporomorph associations, marine microfossils and mammal zones, marine and continental stages and the radiometric scale. *Annales Geologiques des Pays Helleniques, (hors ser.)*, **1**, 61–70.

BENDA, L. & MEULENKAMP, J. E. 1990. Biostratigraphic correlations in the Eastern Mediterranean Neogene. 9. Sporomorph associations and event stratigraphy of the eastern Mediterranean. *Newsletters on Stratigraphy*, **23**, 1–10.

BENDA, L., INNOCENTI, F., MAZZUOLI, R., RADICATI, F. & STEFFENS, P. 1974. Stratigraphic and radiometric data of the Neogene in Northwest Turkey. *Zeitschrift der Deutschen Geologischen Gesellschaft*, **125**, 183–93.

BOZKURT, E. 2000. Timing of extension on the Büyük Menderes graben, western Turkey, and its tectonic implications. *In*: BOZKURT, E., WINCHESTER, J. A. & PIPER, J. D. A. (eds) *Tectonics and magmatism in Turkey and the surrounding area*. Geological Society, London, Special Publications, **173**, 385–403.

BOZKURT, E. & PARK, R. G. 1994. Southern Menderes massif: an incipient metamorphic core complex in western Anatolia, Turkey. *Journal of the Geological Society, London*, **151**, 213–216.

BOZKURT, E. & SÖZBILIR, H. 2004. Tectonic evolution of the Gediz Graben: field evidence for an episodic, two stage extension in western Turkey. *Geological Magazine*, **141**, 63–79.

BUCK, W. R. 1988. Flexural rotation of normal faults. *Tectonics*, **7**, 959–73.

CATLOS, E. J. & ÇEMEN, I. 2005. Monazite ages and the evolution of the Menderes Massif, western Turkey. *International Journal of Earth Sciences*, **94**, 204–217.

COHEN, H. A., DART, C. J., AKYUZ, H. S. & BARKA, A. 1995. Syn-rift sedimentation and structural development of the Gediz and Büyük Menderes grabens, western Turkey. *Journal of the Geological Society, London*, **152**, 629–638.

EDIGER, V., BATI, Z. & YAZMAN, M. 1996. Paleopalynology of possible hydrocarbon source rocks of the Alaşehir–Turgutlu area in the Gediz graben (western Anatolia). *Turkish Association of Petroleum Geologists Bulletin*, **8**, 94–112.

EMRE, T. 1996. Gediz grabeni'nin jeolojisi ve tektonigi [Geology and tectonics of the Gediz graben]. *Turkish Journal of Earth Sciences*, **5**, 171–185.

FISHER, R. A. 1953. Dispersion on a sphere. *Proceedings of Royal Society, London*, **A217**, 295–305.

GESSNER, K., RING, U., JOHNSON, C., HETZEL, R., PASSCHIER, C. W. & GUNGOR, T. 2001. An active bivergent rolling-hinge detachment system: central Menderes metamorphic core complex in western Turkey. *Geology*, **29**, 611–614.

GLODNY, J. & HETZEL, R. 2007. Precise U–Pb ages of syn-extensional Miocene intrusions in the central Menderes Massif, western Turkey. *Geological Magazine*, **144**, 235–246.

GÜRER, A., GÜRER, O. F., PINCE, A. & ILKISIK, O. M. 2001. Conductivity structure along the Gediz graben west Anatolia, Turkey: tectonic implications. *International Geology Review*, **43**, 1129–1144.

HAKYEMEZ, H. Y., ERKAL, T. & GOKTAS, F. 1999. Late Quaternary evolution of the Gediz and the Büyük Menderes grabens, western Anatolia, Turkey. *Quaternary Science Reviews*, **18**, 549–554.

HETZEL, R., RING, U., AKAL, C. & TROESCH, M. 1995. Miocene NNE-directed extensional unroofing in the Menderes massif, southwestern Turkey. *Journal of the Geological Society, London*, **152**, 639–654.

IŞIK, V. & TEKELI, O. 2001. Late orogenic crustal extension in the northern Menderes massif (western Turkey): evidence for metamorphic core complex formation. *International Journal of Earth Sciences*, **87**, 757–765.

IŞIK, V., SEYITOĞLU, G. & ÇEMEN, I. 2003. Ductile-brittle transition along the Alaşehir shear zone and its structural relationship with the Simav detachment, Menderes massif, western Turkey. *Tectonophysics*, **374**, 1–18.

IZTAN, H. & YAZMAN, M. 1990. Geology and hydrocarbon potential of the Alaşehir (Manisa) area, western Turkey. *In*: SAVASCIN, M. Y. & ERONAT, A. H. (eds) *Proceedings to International Earth Sciences Congress on Aegean regions, Izmir*, **1**, 327–338.

KAYA, O., ÜNAY, E., GÖKTAS, F. & SARAÇ, G. 2007. Early Miocene stratigraphy of central west Anatolia, Turkey: implications for the tectonic evolution of the eastern Aegean area. *Geological Journal*, **42**, 85–109.

KISSEL, C., LAJ, C., ŞENGÖR, A. M. C. & POISSON, A. 1987. Paleomagnetic evidence for rotation in opposite senses of adjacent blocks in northeastern Aegea and western Anatolia. *Geophysical Research Letters*, **14**, 907–910.

KOÇYIĞIT, A., YUSUFOĞLU, H. & BOZKURT, E. 1999. Evidence from the Gediz graben for episodic two-stage extension in western Turkey. *Journal of the Geological Society, London*, **156**, 605–616.

KRIJGSMAN, W., DUERMEIJER, C. E., LANGEREIS, C. G., DE BRUIJN, H., SARAÇ, G. & ANDRIESSEN, P. A. M. 1996. Magnetic polarity stratigraphy of late Oligocene to middle Miocene mammal-bearing continental deposits in central Anatolia (Turkey). *Newsletters on Stratigraphy*, **34**, 13–29.

LIPS, A. L. W., CASSARD, D., SÖZBILIR, H. & YILMAZ, H. 2001. Multistage exhumation of the Menderes massif, western Anatolia (Turkey). *International Journal of Earth Sciences*, **89**, 781–792.

LOURENS, L. J., HILGEN, F. J., LASKAR, J., SHACKLETON, N. J. & WILSON, D. 2004. Chapter 21: The Neogene Period. *In*: GRADSTEIN, F. M., OGG, J. G. & SMITH, A. G. (eds) *A Geologic Time Scale 2004*. Cambridge University Press, Cambridge, 409–440.

OKAY, A. I. & SATIR, M. 2000. Coeval plutonism and metamorphism in a latest Oligocene metamorphic core complex in northwest Turkey. *Geological Magazine*, **137**, 495–516.

PURVIS, M. & ROBERTSON, A. 2004. A pulsed extension model for the Neogene-Recent East–West trending Alaşehir graben and the NE–SW-trending Selendi and Gordes basins, western Turkey. *Tectonophysics*, **391**, 171–201.

PICKFORD, M. & MORALES, J. 1994. Biostratigraphy and palaeobiogeography of East Africa and the Iberian peninsula. *Palaeogeography, Palaeoclimatology, Palaeoecology*, **112**, 297–322.

RING, U., JOHNSON, C., HETZEL, R. & GESSNER, K. 2003. Tectonic denudation of a late Cretaceous–Tertiary collisional belt: regionally symmetric cooling patterns and their relation to extensional faults in the Anatolide belt of western Turkey. *Geological Magazine*, **140**, 421–441.

ŞAN, O. 1998. *Ahmetli (Manisa) guneyinde Menderes masifi ve Tersiyer ortu kayalarinin jeolojisi [Geology of the basement and Tertiary cover rocks of Menderes massif in the south of Ahmetli (Manisa)]*. MSc thesis, Ankara University.

SARICA, N. 2000. The Plio-Pleistocene age of Büyük Menderes and Gediz grabens and their tectonic significance on N–S extensional tectonics in west Anatolia: mammalian evidence from the continental deposits. *Geological Journal*, **35**, 1–24.

ŞEN, S. 1997. Magnetostratigraphic calibration of the European Neogene Mammal Chronology. *Palaeogeography, Palaeoclimatology, Palaeoecology*, **133**, 181–204.

ŞENGÖR, A. M. C. 1987. Cross-faults and differential stretching of hanging walls in regions of low angle normal faulting: examples from western Turkey. *In*: COWARD, M. P., DEWEY, J. F. & HANCOCK, P. L. (eds) *Continental Extensional Tectonics*. The Geological Society, London, Special Publication, **28**, 575–589.

ŞENGÖR, A. M. C., GORUR, N. & SAROĞLU, F. 1985. Strike-slip deformation basin formation and sedimentation: Strike-slip faulting and related basin formation in zones of tectonic escape: Turkey as a case study. *In*: BIDDLE, K. T. & CHRISTIE-BLICK, N. (eds) *Strike-slip Faulting and Basin Formation.* Society of Economic Paleontologists and Mineralogists, Special Publication, **37**, 227–264.

SEYITOĞLU, G. & SCOTT, B. C. 1991. Late Cenozoic crustal extension and basin formation in west Turkey. *Geological Magazine*, **128**, 155–166.

SEYITOĞLU, G. & SCOTT, B. C. 1992. The age of the Büyük Menderes graben (west Turkey) and its tectonic implications. *Geological Magazine*, **129**, 239–242.

SEYITOĞLU, G. & SCOTT, B. C. 1996. The age of Alaşehir graben (west Turkey) and its tectonic implications. *Geological Journal*, **31**, 1–11.

SEYITOĞLU, G. & BENDA, L. 1998. Neogene palynological and isotopic age data from Selendi and Usak-Güre basins, western Turkey: A contribution to the upper limit of Eskihisar sporomorph association. *Newsletters on Stratigraphy*, **36**, 105–115.

SEYITOĞLU, G. & SEN, S. 1999. Discussion on "Akgün F. and Akyol E. 1999. Palynostratigraphy of the coal bearing Neogene deposits in Büyük Menderes graben, Western Anatolia. Geobios, 32(3), 367–383". *Geobios*, **32**, 934.

SEYITOĞLU, G., BENDA, L. & SCOTT, B. C. 1994. Neogene palynological and isotopic data from Gördes basin, west Turkey. *Newsletters on Stratigraphy*, **31**, 133–142.

SEYITOĞLU, G., CEMEN, I. & TEKELI, O. 2000. Extensional folding in Alaşehir (Gediz) graben. *Journal of the Geological Society, London*, **157**, 1097–1100.

SEYITOĞLU, G., TEKELI, O., CEMEN, I., SEN, S. & ISIK, V. 2002. The role of the flexural rotation/rolling hinge model on the tectonic evolution of Alaşehir graben, western Turkey. *Geological Magazine*, **139**, 15–26.

SEYITOĞLU, G., ISIK, V. & CEMEN, I. 2004. Complete Tertiary exhumation history of the Menderes massif, western Turkey: an alternative working hypothesis. *Terra Nova*, **16**, 358–364.

SÖZBILIR, H. & EMRE, T. 1990. Neogene stratigraphy and structure of the northern rim of the Büyük Menderes graben. *Proceedings to International Earth Sciences Congress on Aegean regions, Izmir*, 314–322.

STEININGER, F. F., BERGGREN, W. A., KENT, D. V., BERNOR, R. L., SEN, S. & AGUSTI, J. 1996. Circum-Mediterranean Neogene (Miocene and Pliocene) marine-continental chronologic correlations of European Mammal Units. *In*: BERNOR, R. L., FAHLBUSCH, V. & MITTMANN, W. (eds) *The Evolution of Western Eurasian Neogene Mammal Faunas*. Columbia University Press, New York, 7–46.

ÜNAY, E., GOKTAS, F., HAKYEMEZ, H. Y., AVSAR, M. & ŞAN, O. 1995. Dating of the sediments exposed at the northern part of the Büyük Menderes graben (Turkey) on the basis of Arvicolidae (Rodentia, Mammalia). *Geological Bulletin of Turkey*, **38**, 75–80.

WERNICKE, B. & AXEN, G. J. 1988. On the role of isostasy in the evolution of normal fault systems. *Geology*, **16**, 848–851.

WESTAWAY, R. 1990. Block rotation in western Turkey. 1. Observational evidence. *Journal of Geophysical Research*, **95**, B12, 19857–19884.

YAZMAN, M., BATI, Z., SAYILI, A., GÜVEN, A. & YILMAZ, M. 1998. *An approach to the tectonostratigraphic evolution and hydrocarbon potential of the Alasehir area in the extensional province of western Turkey*. Africa/Middle East Second International Geophysical Conference & Exposition, Cairo, Egypt. Technical Program Abstracts, 351.

YILMAZ, Y., GENÇ, S. C., GURER, F., BOZCU, M., YILMAZ, K., KARACIK, Z. *ET AL*. 2000. When did the western Anatolian grabens begin to develop? *In*: BOZKURT, E., WINCHESTER, J. A. & PIPER, J. D. A. (eds) *Tectonics and magmatism in Turkey and the surrounding area*. The Geological Society, London, Special Publication, **173**, 353–384.

YILMAZ, M. & GELIŞLI, K. 2003. Stratigraphic-structural interpretation and hydrocarbon potential of the Alaşehir graben, western Turkey. *Petroleum Geoscience*, **9**, 277–282.

The structure of the Kythira–Antikythira strait, offshore SW Greece (35.7°–36.6°N)

ELENI KOKINOU[1]* & EVANGELOS KAMBERIS[2]

[1]*Technological Educational Institute Crete, 3 Romanou Str. Chalepa, Chania, Crete, GR 73133 Greece*

[2]*Hellenic Petroleum (Exploration and Exploitation of Hydrocarbons Division), 199 Kifissias Avenue, 15124 Maroussi, Athens, Greece*

**Corresponding author (e-mail: ekokinou@chania.teicrete.gr)*

Abstract: The Kythira–Antikythira strait, within the SW Hellenic Arc, forms a 100 km long NNW–SSE trending ridge between Peloponnesus and Crete and represents the submarine continuation of the Hellenic Alpine belt. In order to present the shallow as well as the deeper structure of Kythira–Antikythira strait we studied five seismic sections, oriented either parallel or perpendicular to the inner part of the Hellenic Arc. This information was complemented with velocity analyses from a dense network of seismic lines and information concerning the bathymetry.Contractional structures recognized on the seismic profiles indicate that this part of the Gavrovo–Tripolitza geotectonic zone was involved in the Miocene shortening related to the westward propagation of the Hellenic fold-and-thrust system. East-dipping thrust faults which root in the top of the crystalline basement were identified on the seismic profiles. The deepest reflector identified on the profiles corresponds to the crystalline basement. Shallower reflectors include those corresponding to the contacts between the Mesozoic/Miocene, Upper Miocene/Lower Pliocene and Pliocene/Pleistocene sedimentary sequences. The Upper Cenozoic to Quaternary sequence rests unconformably upon Mesozoic carbonates. Messinian intrusions, forming small scale domes, deform the Pliocene–Quaternary sedimentary succession. West- and east-dipping normal faults were also recognised both within the Palaeozoic and Cenozoic successions, and are related to regional extension during sedimentation.

Subduction in the eastern Mediterranean region was governed by the convergence between Eurasia and Africa in an area where continental and oceanic microplates were trapped between the converging continental plates (Jolivet & Faccenna 2000). Characteristic features of this area include the arcuate Calabrian and Hellenic orogenic belts and associated extensional basins, which are generally explained to result from roll-back of subducted slabs and retreating subduction zones, possibly in combination with slab detachment and post-collisional gravitational collapse of the overthickened lithosphere (Gautier *et al.* 1999; Wortel & Spakman 2000; Jolivet 2001; Govers & Wortel 2005). Royden & Burchfiel (1989) proposed that orogenic belts with high topographic elevation were formed where the rate of convergence exceeded the rate of subduction (advancing subduction; e.g. Alps). In contrast, low topographic relief and regional extension in the upper plate are considered to characterize subduction boundaries where the rate of subduction exceeded the rate of overall plate convergence (retreating subduction; e.g. Betics–Alboran–Rif, Apennines, Hellenic and Carpathian thrust belts).

The Hellenic Arc represents the most seismically active area of Europe due to the interaction between Eurasia and Africa plates. Main geotectonic feature of the area is the Hellenic Trench, where the eastern Mediterranean oceanic lithosphere (frontal part of the African plate) is subducted under the Aegean overriding plate. Earthquakes with magnitudes of up to 8.0 have been reported in the literature since the early historic times, (Papazachos 1990; Papazachos & Papazachou 2003) pointing out the great seismogenetic potential of the area. According to Papazachos *et al.* (2000), an ocean–continent interaction occurs on a curved subduction zone, which is characterized by a shallow branch (20.0–100.0 km) of the Wadati–Benioff zone, intersecting the outer side of the sedimentary arc (Western Peloponnesus-west of Kythira-south coast of Crete, east coast of Rhodes) and dips at low angle (*c.* 30°) to the north and NE. Subduction at the Hellenic subduction zone appears to have been operated continuously since the late Cretaceous (Faccenna *et al.* 2003; van Hinsbergen *et al.* 2005).

In the northwestern part of the Aegean region, the boundary between the Aegean and African plates (e.g. Ionian Sea) is of continent–continent

From: van Hinsbergen, D. J. J., Edwards, M. A. & Govers, R. (eds) *Collision and Collapse at the Africa–Arabia–Eurasia Subduction Zone*. The Geological Society, London, Special Publications, **311**, 343–360.
DOI: 10.1144/SP311.14 0305-8719/09/$15.00

type now due to the collision of the Hellenides with the Apulian platform (Le Pichon & Angelier 1979; Lyberis & Lallemant 1985; Finetti 1985; Underhill 1989; van Hinsbergen *et al.* 2006). The boundary between these regions of contrasting subduction style is presently formed by the right-lateral Kefallonia Transform Fault Zone (e.g. Sachpazi *et al.* 2000). The southern part of the Hellenic arc south

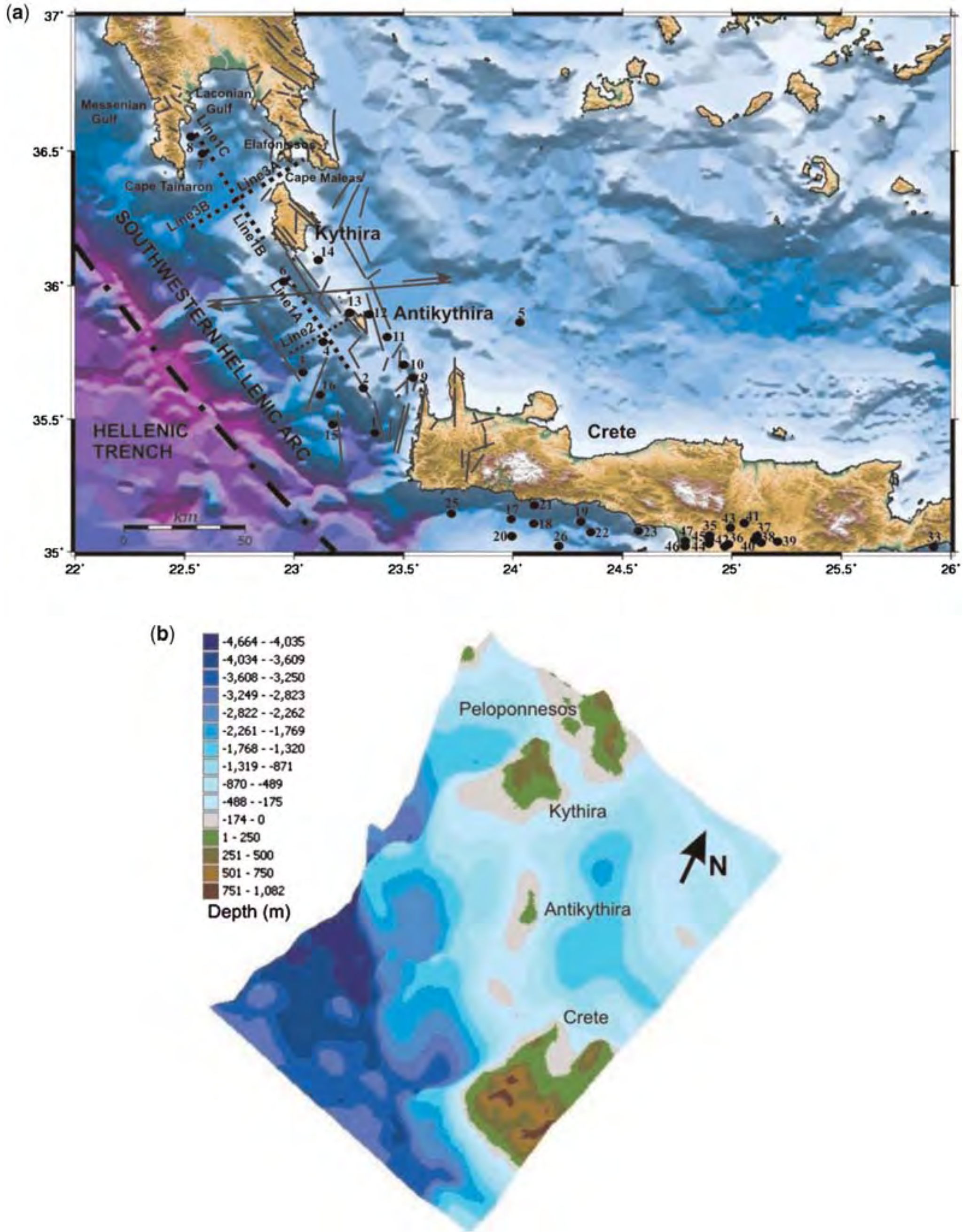

Fig. 1. (**a**) Map of the study area. Thick solid lines represent the active faults (Lyberis *et al.* 1992; Papazachos 1996), dotted lines the seismic lines shown in the present work, bullets show the positions of selected 1D velocity models used for the 3D velocity image; (**b**) the topography of the study area.

of, and including Crete and Rhodos, has since the early Pliocene been associated with left-lateral strike-slip along the Pliny and Strabo trenches (Mascle *et al.* 1999; Fassoulas 2001; ten Veen & Kleinspehn 2003; van Hinsbergen *et al.* 2007). In between these two regions, active NE directed subduction is accommodated along the Hellenic Trench and deformation in the overriding plate on the Peloponnesos, and in the Kythira–Antikythira strait is associated with a complex pattern of arc-parallel and arc-normal extension and strong compression perpendicular to the Hellenic Trench (Fig. 1) (e.g. Papazachos & Kiratzi 1996). Beneath this area, the subduction zone dips gently to the NE, changing to a steeper dip farther NE beneath the Argolikos Gulf (Hatzfeld 1994; Papazachos *et al.* 2000).

The Kythira–Antikythira (KA) strait (Fig. 1a, b) represents a NNW–SSE oriented structural high situated between Peloponnesus and Crete in the southwestern part of the Hellenic Arc. To better constrain the complex tectonic history of this segment of the Hellenic Arc, we here present interpretations of stacked seismic lines (Fig. 1a) located in the western extremity of KA strait. These interpretations have allowed us to establish a model for the crustal structure of the study area and support a geodynamic interpretation for the KA strait.

The seismic sections (Fig. 1a, Line 1A, Line 1B, Line 1C) of Line 1 are parallel to the Hellenic Arc and cross the western part of KA strait in a NW–SE direction. Line 2 is perpendicular to the Hellenic Arc, situated west of Antikythira Island in a NE–SW orientation. Seismic section Line 3A crosses the offshore area west of Elafonissos Island (eastern most peninsula of Peloponnesus) and north of Kythira Island in a NW–SE direction. The seismic segment Line 3B is located in the south-eastern offshore area of the Tainaron cape and it is almost perpendicular to the direction of the Hellenic Arc.

Geological setting of the KA strait

The geotectonic history of KA strait is probably related to the geological development of western Greece. The external Hellenides form a stack of thrust sheets consisting of shallow- and deep marine sediments that were deposited in parallel Mesozoic basins (‘isopic zones’, including from N(E) to S(W) the Pindos deep marine basin, the Gavrovo platform, the Ionian deep marine basin and the pre-Apulian slope of the Apulian platform, which thrusted from N(E) to S(W) during Tertiary subduction and accretion (Aubouin 1959; Jacobshagen 1986, 1994). The youngest and structurally lowest of these nappes is the Pre-Apulian zone, which in the late Miocene–early Pliocene the northwestern External Hellenides to the north, was shortened and uplifted in response to NE–SW compression due to the onset of collision of the west-Aegean nappe stack with Apulia (van Hinsbergen *et al.* 2006). At the same time, in the south the subduction of the oceanic lithosphere of the Ionian basin continued.

The Alpine structure of Kythira consists of two of these nappes: the Tripolitza and Pindos units, underlain by a sequence of metasedimentary rocks of the Phyllite Quartzite unit (Theodoropoulos 1973). Thrusting of the Pindos over the Tripolitza unit occurred largely during the Oligocene, evidenced by a kilometres-thick syn-orogenic clastic sequence on top of the Tripolitza unit of uppermost Eocene to earliest Miocene age (IGRS-IFP 1966; Richter 1976; Peeters *et al.* 1998; Sotiropoulos *et al.* 2003). The Tripolitza nappe is separated from the underlying metasediments of the Phyllite Quartzite unit by an early to late Miocene extensional detachment, which is also identified on Kythira; exhumation of the metamorphosed rocks below the Tripolitza unit occurred largely prior to *c.* 15 Ma (Danamos 1992; Fassoulas *et al.* 1994; Jolivet *et al.* 1996; Thomson *et al.* 1998). Additionally the pre-Neogene formations of Antikythira were also found to comprise elements of the Gavrovo–Tripolitza zone, and some strata of the Pindos nappe are indicated in the neighbouring islet of Pori (Lyberis *et al.* 1982). The Gavrovo–Tripolitza zone is considered a mechanically strong and rigid carbonate sequence which generally is internally deformed by very broad spaced thrust faults (Xypolias & Doutsos 2000; Sotiropoulos *et al.* 2003). At the top of the sequence, a younger post Alpine formation is deposited that is strongly affected by normal faults with a dominant NNW–SSE trend. These faults have affected the upper two tectonic nappes forming blocks that slide over the metamorphic basement forming grabens and horsts (Papanikolaou & Danamos 1991). According to these authors, Neogene sediments (between 13.0 and 2.0 Ma) have been deposited in those grabens, composed mainly of terrestrial deposits followed by marine post alpine sediments originated at the central part of the island.

The KA strait is bounded by fault scarps striking generally north–south to NNW–SSE to the east and NNW–SSE to NW–SE to the west (Fig. 1a, b). These directions are also observed on Kythira and Antikythira where they represent normal faults (Lyberis *et al.* 1982). In the study area the basins and plateaus located in the inner part of the western Hellenic Trench were developed due to the late Cenozoic fault tectonics (Le Quellec *et al.* 1980). The Cretan sea basin located to the east, reveals depths up to 1.3 km, while the Hellenic Trench, forming the western limit of strait, has depths down to 3–5 km. Additionally smaller scarps are present with a NNW–SSE orientation, which were formed due to the activity of extensional faulting that affected the area in the late Cenozoic. Lyberis *et al.* (1982) concluded that the KA segment of the Hellenic Arc acts as a complex zone of transform-extensional motion associated with rotations and translations between two major segments (Peloponnesus and Crete) of the external arc. Faults, parallel to the axis of the arc are well represented and correspond to mainly transverse extension. In addition, the presence of the en echelon normal fault system results in a dextral component of extensional motion parallel to KA axis.

Velocity models of the KA strait and the western part of Crete

The presented seismic lines were acquired during a streamer reflection campaign (Hellenic Petroleum Co.,) in the KA strait many years ago. Western Geophysical Company of America, which towed a high pressure airgun tuned array, produced the seismic signals. The receiver group interval was 25 m and the minimum offset was 250 m. The recording length and the sampling rate were 8 seconds (s) and 4 milliseconds (ms), respectively. The data processing sequence includes geometrical spreading correction, deconvolution, velocity analysis, stacking and time variant filtering.

The interpretation of the seismic segments is based on: (1) bathymetry data; and (2) velocity analysis data occurred for the presented lines. Bathymetry data (www.geomapapp.org) was processed in order to construct a 3D image of the KA strait sea floor, which helps us to trace the main geotectonic features on the seismic sections. Lack of deep borehole data either from deep water or the continental platform of Kythira and Antikythira Islands impedes to calibrate the seismic horizons. Therefore, 1D velocity models deduced from other seismic reflection experiments in the larger study area and in the southern part of Crete were used in order to support our interpretations and to further construct a 3D velocity pseudosection for the study area.

Common Depth Point (CDP) velocity data is used in the present work in order to construct 2D and 3D velocity models for the upper 15.0–20.0 km of the larger study area. The detection of the velocity layers is based on velocity jumps. The detection of the seismic units on the seismic sections has been done by superimposing the velocity models on the stacked sections. The reflection coefficients and the lithoseismic patterns were taken into account. Additionally, onshore and offshore velocity data from the southwestern part of Crete was included in the database aiming at a more complete image of the west Cretan crust. Previous velocity models (Makris & Stobbe 1984; Bohnhoff *et al.* 2001; Makris & Yegorova 2006) were also used in order to correlate our models and to extend them to a depth of 35 km.

Root Mean Square (RMS) velocities were converted to interval velocities according to Dix equation. The 1D velocity models were used for the construction of 2D models. Representative examples of 1D velocity distribution are shown in Figure 2a. Generally, velocity increases with depth, but velocity reversals (Fig. 2a, models 5, 7, 15, 36, 47) are also observed between 2.2 and 5.5 km depth. Velocity reversals at such depths could be caused by intrusions of Messinian evaporites or compressive deformation. Similar velocity reversals were also observed in the seismic line ION-7 (0.0–180.0 km) that crosses the Ionian basin from the deep Ionian abyssal plain up to the gulf of Patras (Kokinou *et al.* 2003, 2005). Thereinafter, a 3D database was created using topographic data, previously available information about velocity distribution and interval velocities for the upper 20.0 km of the Cretan crust derived from reflection experiments. Special emphasis has been given to the upper 15.0–20.0 km of the cover that comprises a seismogenic layer of generally small to moderate earthquakes.

The 3D velocity pseudosections (Fig. 2b) provide a generalized image of the onshore and offshore KA strait and western part of Crete. As shown in Figure 2b the layer thicknesses change not only in east–west direction but also in north–south. We divided the Cretan–Antikythira–Kythira crust in five units. The upper layer, showing a velocity range between 1.5–2.2 km/s, corresponds to the seawater layer and the upper series of the post-Alpine sediments. The second layer has a velocity between 2.3 and 4.4 km/s and could represent the lower post-Alpine sequences and part of the upper Alpine successions. It is followed by a layer showing a velocity range of 4.5–6.0 km/s, which is attributed to the lower successions of the Alpine sediments, mainly consisting of carbonates. The next layer corresponds to a velocity between 6.1 and 6.5 km/s and could be the lowermost part of the carbonate_ succession and the Palaeozoic metamorphosed sequence. The layer corresponding to 6.6–7.9 km/s may represent the lowermost part of the continental crust.

The layers underneath the KA strait are almost horizontal except for some local variations in thickness. The inclination of the layers towards Crete is related to the impressive crustal thickness underneath Crete, as shown in previous studies for the northern and southern offshore part of Crete: Bohnhoff *et al.* (2001) concluded that the crust in the Cretan region is continental with maximum thickness of 32.5 km beneath North and Central Crete and thins towards the north and south to

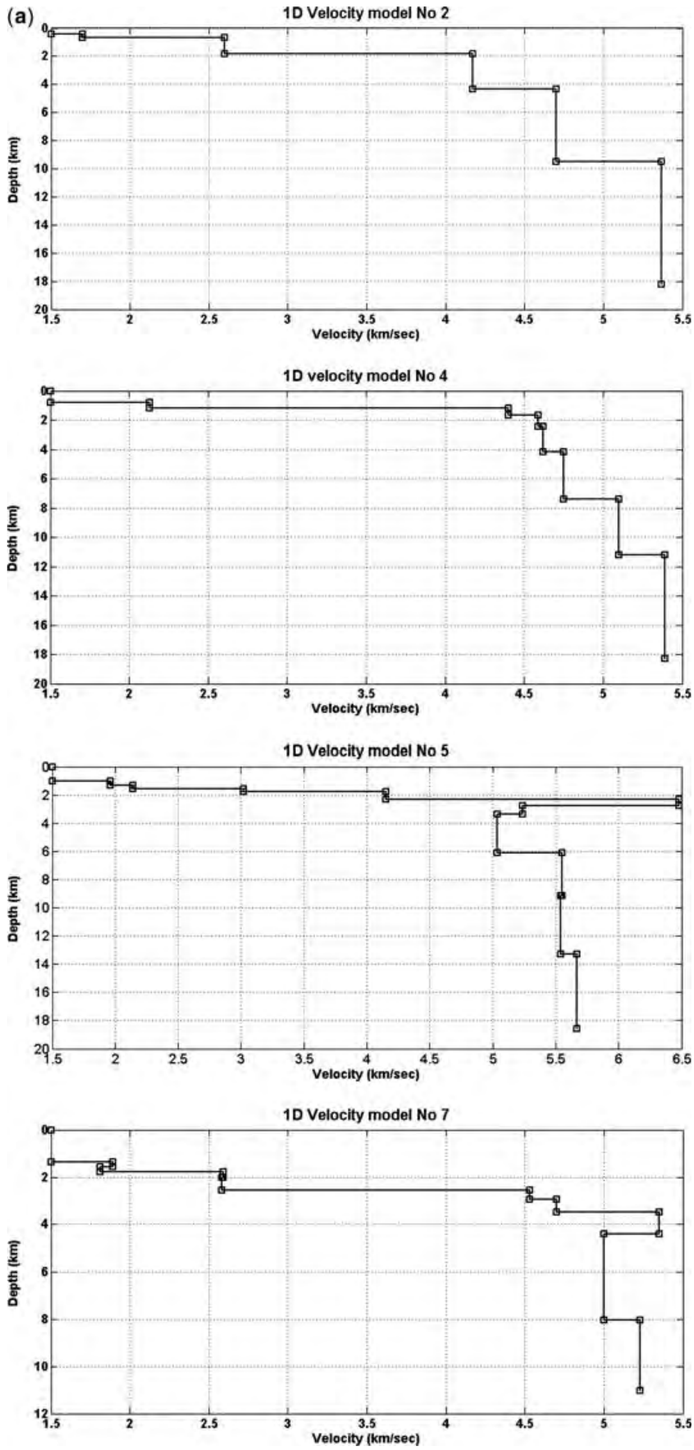

Fig. 2. (**a**) 1D velocity models for the area of KA strait and the western part of Crete. (*Continued*)

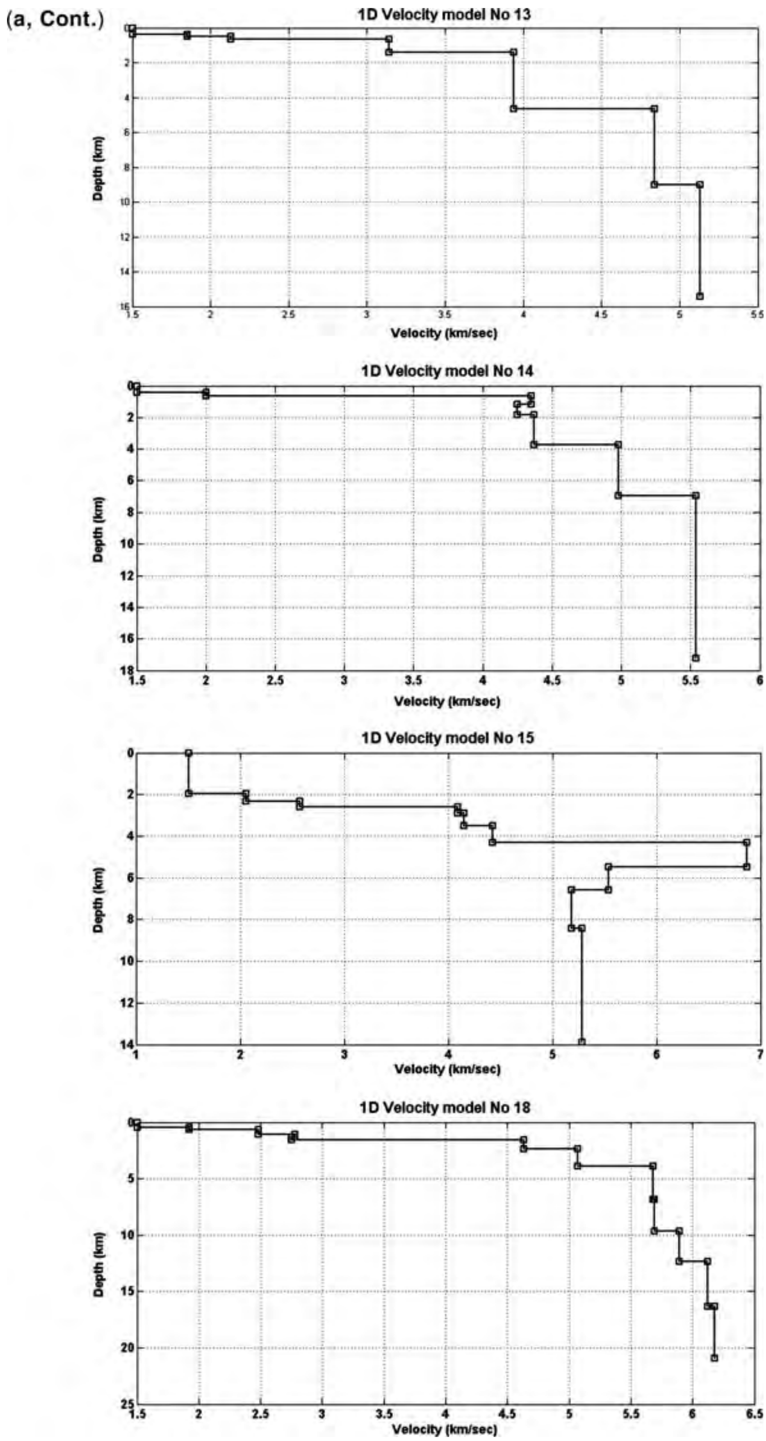

Fig. 2. (*Continued*).

(a, Cont.)

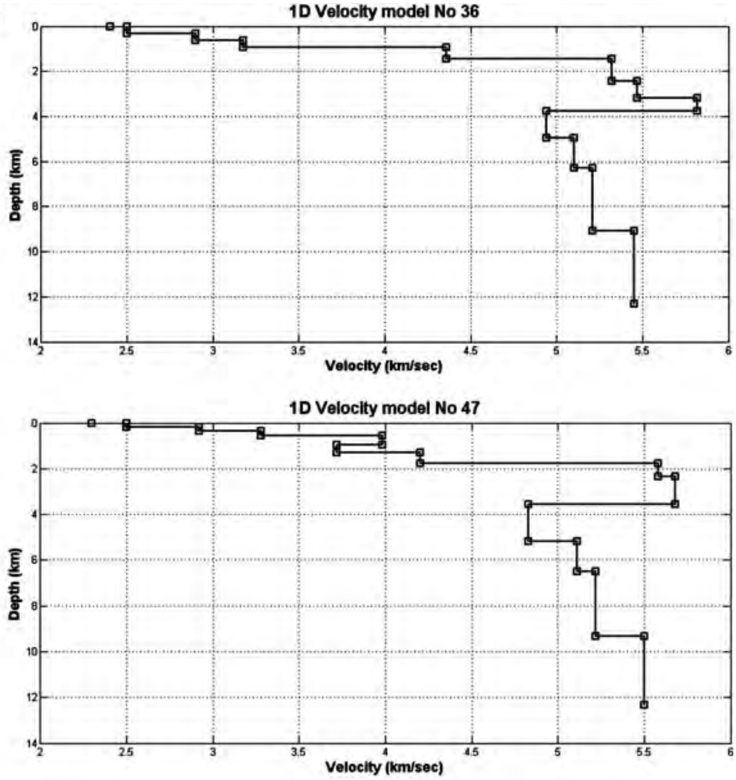

(b)

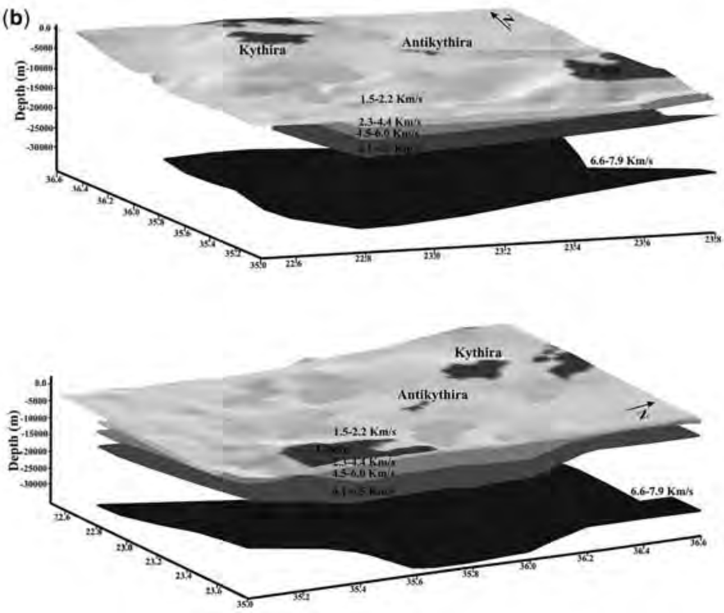

Fig. 2. (**b**) 3D velocity pseudosections showing the velocity structure of the larger study area, top figure: in east–west direction, bottom figure: in north–south direction.

15.0 and 17.0 km, respectively. Additionally, large velocity variations are observed in the upper crust, which are also detected in the models of the present work.

Interpretation of the seismic lines

The seismic segment Line 1A

On this portion of the seismic section (20.0–67.5 km, Figs 1a & 3a–c), the depth to the sea-floor ranges from 0.75–1.0 s two-way travel time (TWT). The topography of the sea-floor and the structure of the upper layers are mainly related to normal faults.

The upper layer corresponds to a velocity range between 1.7–2.3 km/s and is attributed to Pliocene–Quaternary (Pl–Q) sediments, locally deformed by Messinian intrusions, shown as small scale domes at positions 32.5–35.0 km and 56.0–62.0 km of the seismic segment. Similar patterns have also been recognized in the deep reflection profile ION-7 located in Ionian sea (Kokinou *et al.* 2005). Downlap (1a) and onlap (1b) structures are present west of 47.5 km and at depths greater than 1.5 s TWT. At positions between 55.0 and 65.0 km, a layer is detected, which shows a velocity range of 2.5–3.86 km/s and is possibly attributed to the Lower Pliocene (Pli) sedimentary sequence. In the rest of the seismic segment the Pliocene–Quaternary succession is underlain by Messinian (M) sediments with a velocity of about 2.86–4.0 km/s. The maximum values probably relate to the presence of evaporate intercalations.

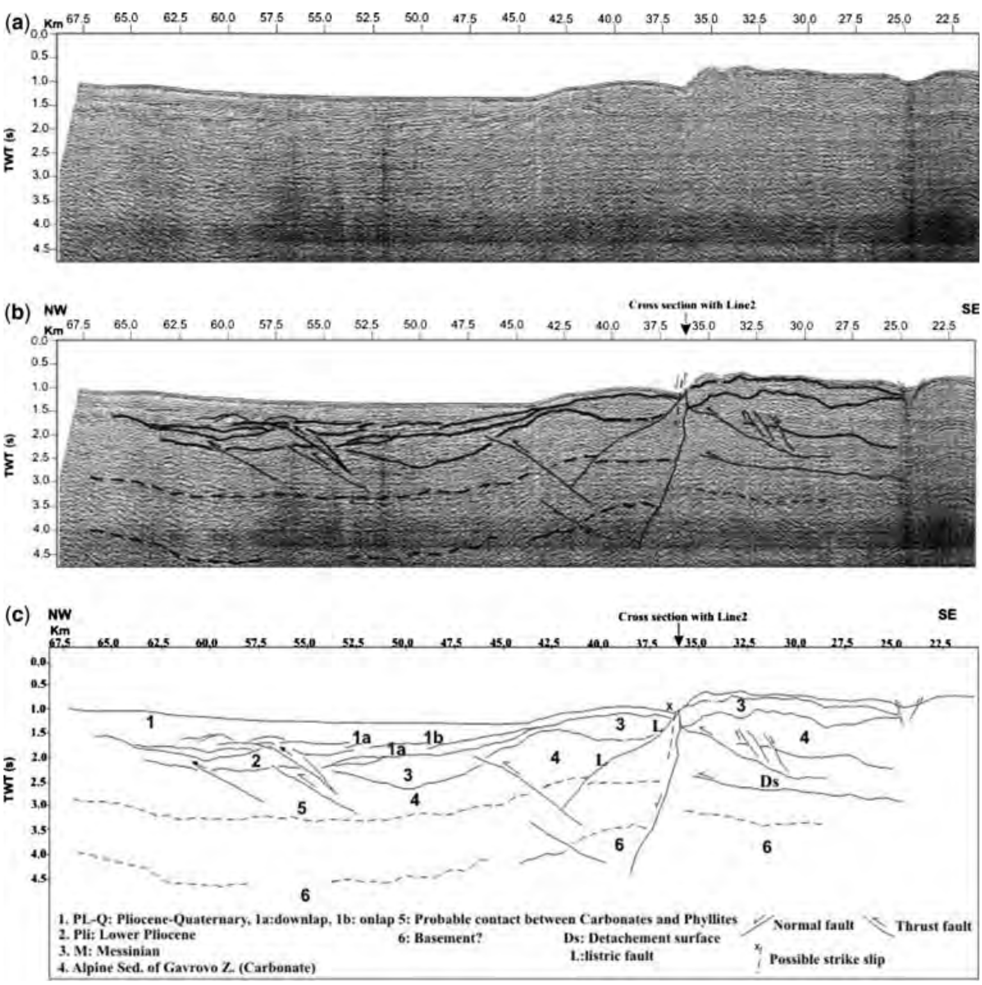

Fig. 3. Stacked section of the Line 1A (**a**) without interpretation; (**b**) the main structures detected; (**c**) the structure deduced from the Line 1A.

The Alpine sediments of Gavrovo–Tripolitza geotectonic zone are present at depths greater than 1.25 s TWT (at the shallower part of the seismic section) and 2.75 s TWT (at the deeper part of the section) showing a velocity range of 3.7–4.7 km/s depending on depth. A probable contact between carbonates and the Phyllite–Quartzite Unit (Phyllites) is detected at about 2.8–3.4 s TWT.

The deeper horizon, with a velocity greater than 5.5 km/s shown in the present seismic section below 3.5 s TWT, possibly represents the top of the crystalline basement. This layer probably corresponds to successions older than the Palaeozoic.

Quaternary extensional faulting deforms the upper sedimentary series and possibly the Alpine carbonates. Detachment surfaces (Ds), of early to late Miocene age (Fassoulas *et al.* 1994; Jolivet *et al.* 1996; Thomson *et al.* 1998), are shown in the southeastern part of the seismic segment between Crete and Antikythira, which separate the upper non metamorphosed units from the lower metamorphosed unit of Phyllite–Quartzite.

Additionally an extensional surface with possible strike slip movement is situated between 35.0 and 37.5 km of the seismic section. The presence of different lithoseismic patterns east and west of the extensional surface and the correlation of the present seismic segment with other seismic lines supports the strike slip movement. However, the vertical offset of Ds is most prominent here. A

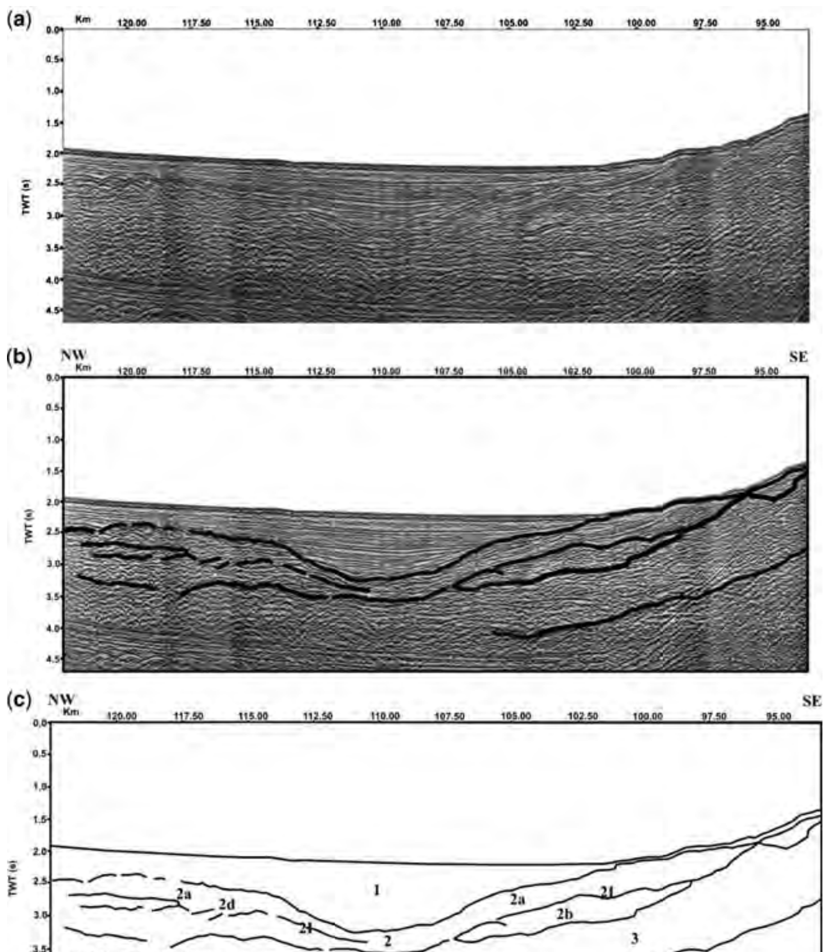

Fig. 4. Stacked section of the Line 1B (**a**) without interpretation; (**b**) the main structures detected; (**c**) the structure deduced from the Line 1B.

large scale listric fault is present between 35.0 and 42.5 km, deforming both the pre- and post Alpine sequences. Thrust faulting seems to have affected the deeper layers up to and possibly including the Lower Pliocene unit of the seismic segment.

The seismic segment Line 1B

A sedimentary basin of possibly Miocene age is situated in the area NW of Kythira (93.0–122.0 km, Figs 1a & 4a–c), affected by extensional tectonics during the late Cenozoic. The present seismic section is characterised by an almost flat sea-floor at about 2 s TWT.

The Pliocene–Quaternary sequence shows an impressive thickness (about 1 s TWT) compared to Line 1A. Small scale channel fill deposits are locally present between 105.0 and 115.0 km at about 2.5 s TWT. The velocity of the pre-mentioned layer ranges between 2.0 and 2.2 km/s. The continuation of the Pliocene–Quaternary base is partly interrupted by small scale intrusions of Messinian evaporates (Upper Miocene). The whole Miocene sequence reveals a thickness of 0.8 s TWT and a velocity range between 2.86 and 4.05 km/s. The top of the Mesozoic carbonates (3.2–4.9 km/s) could be an erosional surface resulting from uplift during the Middle Miocene. According to Xypolias (2007), uplift and doming of the tectonic windows in the Peloponnesus and Crete took place at the Early to Middle Miocene.

The seismic segment Line 1C

Line 1C (124.0–137.5 km) is located in the Laconian gulf (Figs 1a & 5a–c) and crosses the offshore area of the eastern Mani peninsula. According to the geological map of Peloponnesus modified after Bornovas & Rontogianni-Tsiabaou (1983) HP/LT metamorphic Phyllite–Quartzite and Plattenkalk units are present on the Mani peninsula. Under the term Mani unit in the present work we consider the Phyllite–Quartzite and Plattenkalk units.

The depth to the sea-floor ranges from 0.25 s TWT (northwestern part of the seismic section) to 1.75 s TWT (southeastern most part of the seismic section). A zone of east dipping normal faults is present at position between 132.5 and 135.0 km. Because of the pre-mentioned fault zone Mani unit is sinking underneath the Gavrovo–Tripolitza unit. Gavrovo–Tripolitza unit probably constitutes the continuation of the Mani unit to the east. The Pliocene–Quaternary succession shows a thickness of about 0.5 s TWT and it is underlain by the Upper Miocene sequence. The top of the Mesozoic carbonates is detected at 1.5–2.0 s TWT and shows a thickness of about 1.5 s TWT that is in agreement with the seismic Line 1B.

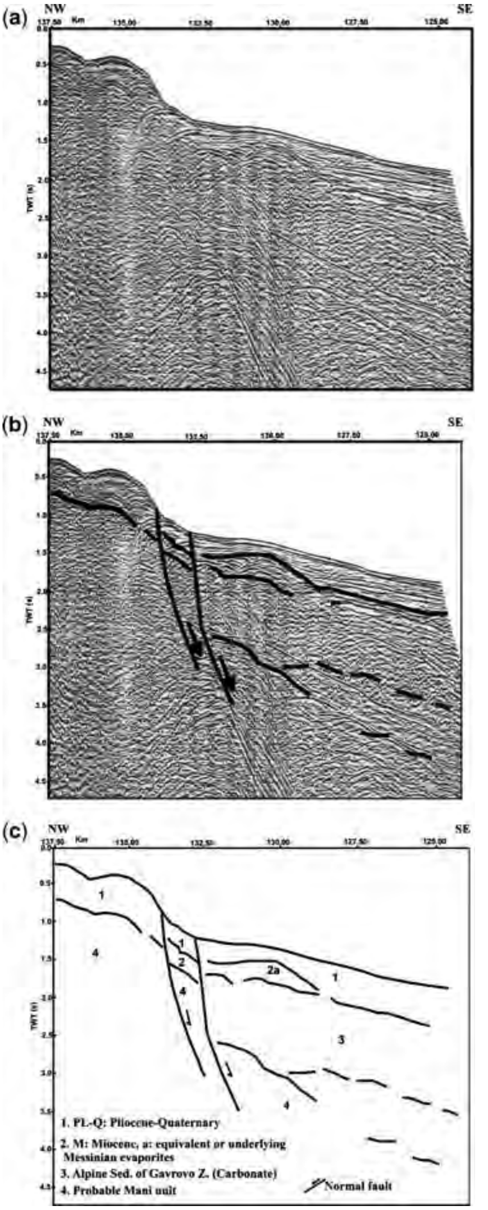

Fig. 5. Stacked section of the Line 1C (**a**) without interpretation; (**b**) the main structures detected; (**c**) the structure deduced from the Line 1C.

The seismic Line 2

This seismic section (4.0–31.0 km, Figs 1a & 6a, b) is almost perpendicular to the orientation of the Hellenic Arc and is situated west of Antikythira. This section is considered the most representative for the crustal structure of the southern KA strait. The tectonic features (A, B) possibly represent large scale thrust faults affecting almost all the sedimentary sequences down to the basement, except the Pliocene–Quaternary succession. The westerly vergence of the Hellenic fold and thrust system is clearly seen in this specific seismic section.

The Pliocene–Quaternary succession follows the shape of the sea-floor topography and it is deformed by recent extensional faulting. Velocity analyses determine the velocity of the pre-mentioned layer between 1.9 and 2.25 km/s at the shallow part of the seismic section and up to 2.38 km/s at greater depths. The underlain Messinian sediments reveal velocities between 2.78 and 4.24 km/s, while the Alpine carbonates show a velocity range between 3.7 and 4.7 km/s. The deeper layers represent the Phyllite-Quartzite unit and the crystalline basement respectively.

Kamberis *et al.* (2005) based on field work in the Gavrovo–Tripolitza and Ionian zones, referred to the existence of several WNW–ESE and ENE–WSW trending, sinistral and dextral strike slip faults, which cut almost perpendicular the previously mentioned thrust zones. These faults are considered as accompanying features, formed as strike slip faults during the westwards thrust propagation in Miocene times (Kamberis *et al.* 2000). The fault, located at about 10 km of the Line 2 presents similar characteristics to those reported by Kamberis *et al.* (2000, 2005) and it is probably an old strike slip fault, reactivated during the latest Cenozoic as normal fault.

The seismic sections of Line 3

Two seismic sections, Line 3A (2.0–22.0 km, Figs 1a & 7a–c) and Line 3B (22.5–51.0 km, Figs 1a & 8a–c) were selected to present the structure south of Peloponnesus in a SW–NE direction. Both seismic sections show a stratigraphic layering similar to that of the already presented seismic sections.

A tectonic high is present in the seismic section of Line 3A (Figs 7a–c), at a position between 2.0 and 8.0 km. We compared the lithoseismic patterns of this structure with that of the Kefallinia diapir (Kokinou *et al.* 2005). Similarities between the two structures can hardly be found. Additionally, a zone of west dipping normal faults (Fig. 7a–c) is present at position west of 17.5 km. All sedimentary successions up to Pliocene–Quaternary and the sea-floor show to be deformed, confirming that this area is still active.

Line 3B (Figs 8a–c) shows the structure south of Tainaron cape. The Tainaron unit gradually dips eastwards. Thrust faults are also present in this seismic section, confirming the westerly vergence of the Hellenic fold- and thrust system. A detachment surface is also detected at position 27.5–32.5 km and at depth of about 3.75 s TWT, separating the upper non metamorphosed units of the Gavrovo–Tripolitza carbonates from the underlying metamorphosed unit of Phyllite–Quartzite.

Discussion

In the context of the present work a detailed interpretation of seismic lines has been performed, which run pararell to and almost perpendicular to the trend of the Hellenic Arc. Velocity models for the KA strait and the western part of Crete suggest the presence of continental crust. Two schematic sections (Fig. 9a, b), orientated perpendicular and parallel to the Hellenic Arc, illustrate the structure of the KA strait. A strong correlation between sea-floor morphology and normal faults exists. The deformation pattern of KA strait, presented in this work, shows pronounced thrusting to the west older than the middle or upper Miocene sediments.

Our results are in line with the pre-Neogene structure of the External Hellenides in northwestern Greece and the northern Peloponnesus, also showing a pronounced west-verging fold- and thrust structure (Skourlis & Doutsos 2003; Sotiropoulos *et al.* 2003; Kokkalas *et al.* 2006). The thrusts exposed on the northwestern Peloponnesus continue further to the south and show a similar vergence. The Phyllite–Quartzite and Plattenkalk units are represented in the seismic sections of the present work by the Mani unit (Fig. 5) which gradually dips eastwards beneath the Gavrovo–Tripolitza carbonates due to the activity of east-dipping normal faults.

A low-angle structure between the Tripolitza and the metamorphic units of the Phyllite–Quartzite and Plattenkalk units has been traced. This structure has previously been identified on Crete and the Peloponnesos as an extensional detachment with a top-to-the-NE sense of shear, and was active until the middle to late Miocene based on thermochronological evidence (Thomson *et al.* 1998) and stratigraphic evidence on Crete (van Hinsbergen & Meulenkamp 2006).

The dominant directions of post-thrusting normal faults have a NNW–SSE to NW–SE orientation in the south Peloponnesus and a NE–SW to NNE–SSW orientation in the westernmost part of Crete. In the south Peloponnesus, NW-trending faults control the accumulation of sediments of post–late Pliocene age (Frydas 1990). They remain active today and divide the area into three peninsulas. To the south, on Kythira island, the oldest marine sediments are of Tortonian age (Meulenkamp *et al.* 1977) and remain active today, as is indicated by prominent and fresh fault scarps (Kokkalas *et al.* 2006). The North–NNE-trending normal and oblique normal faults form young scarps in the southern Peloponnesus and the offshore Kythira area.

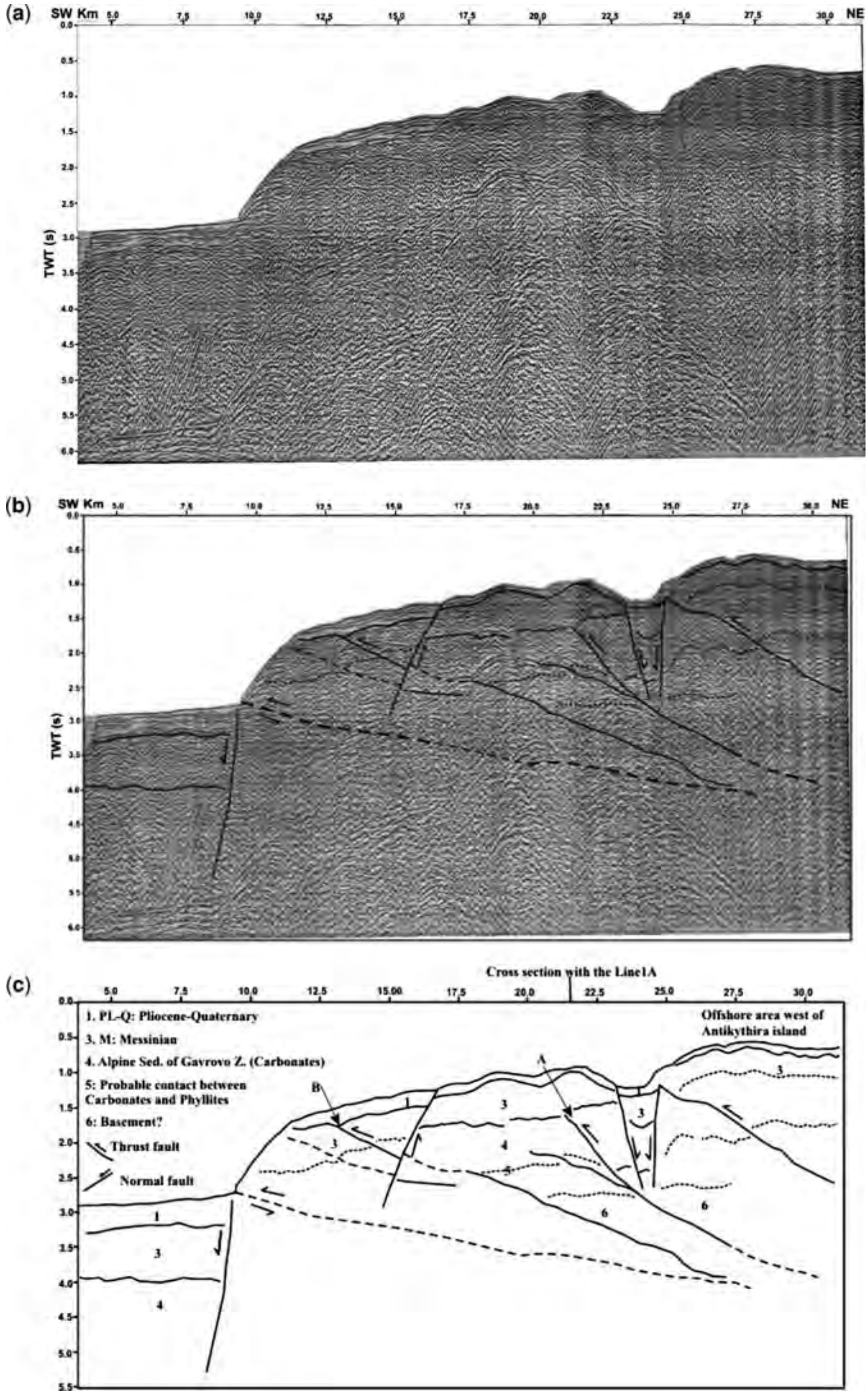

Fig. 6. Stacked section of the Line 2 (**a**) without interpretation; (**b**) the main structures detected; (**c**) the structure deduced from the Line 2.

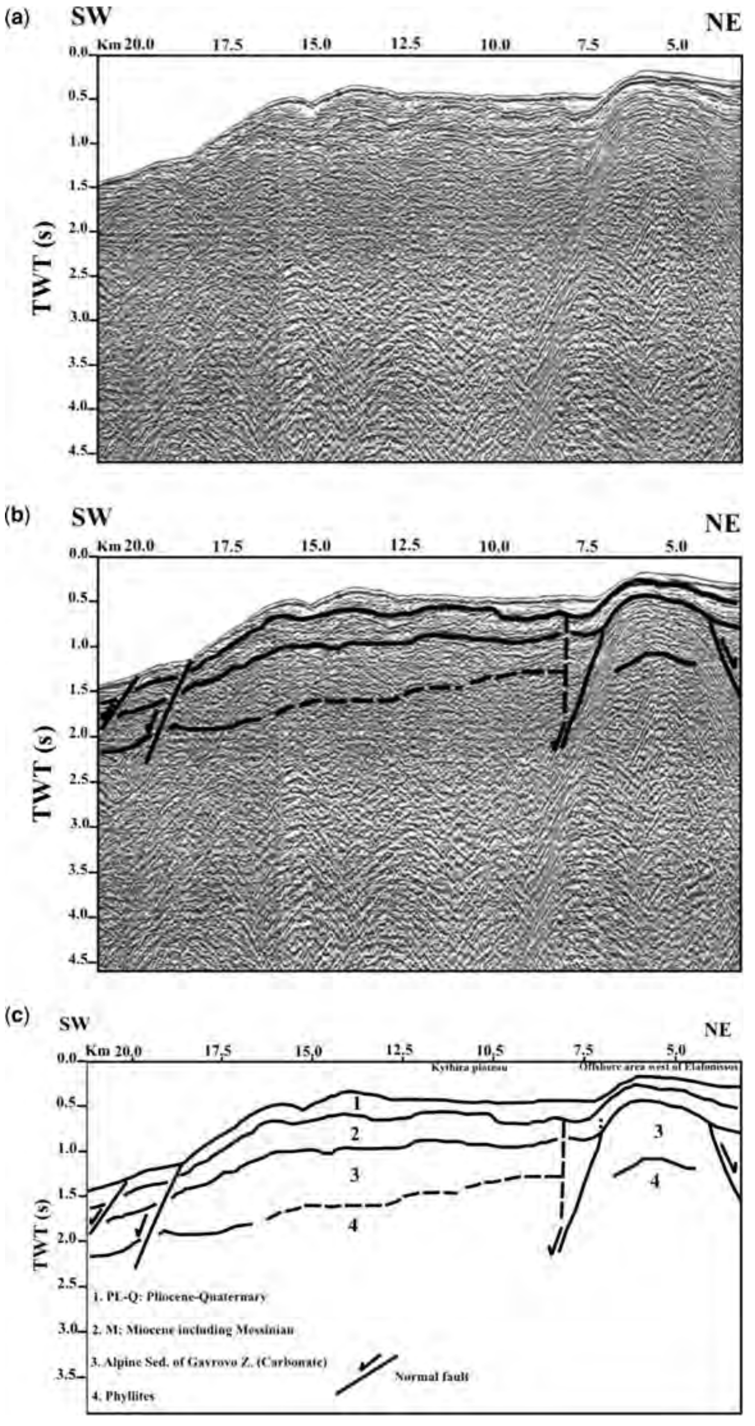

Fig. 7. Stacked section of the Line 3A (**a**) without interpretation; (**b**) the main structures detected; (**c**) the structure deduced from the Line 3A.

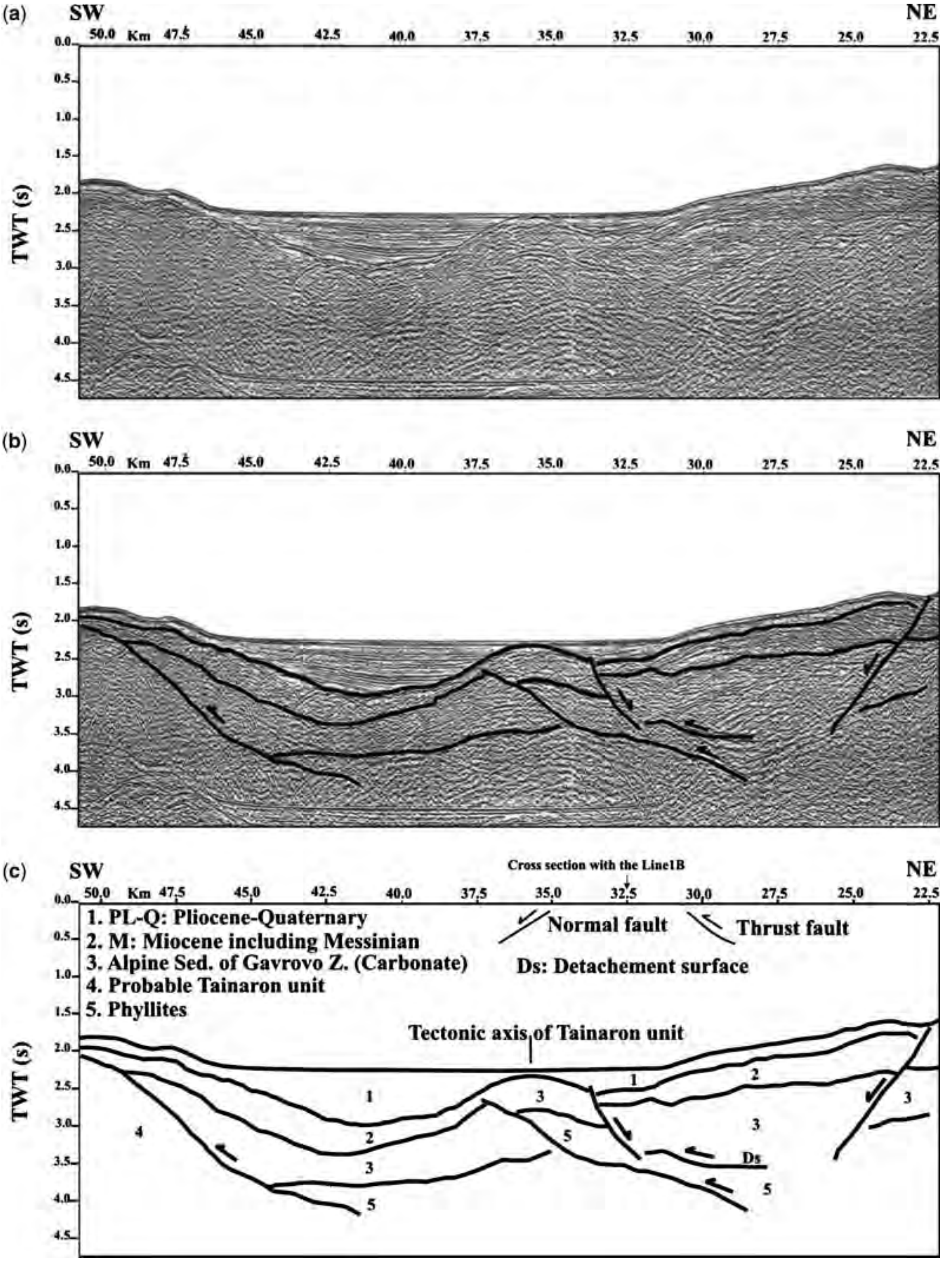

Fig. 8. Stacked section of the Line 3B (**a**) without interpretation; (**b**) the main structures detected; (**c**) the structure deduced from the Line 3B.

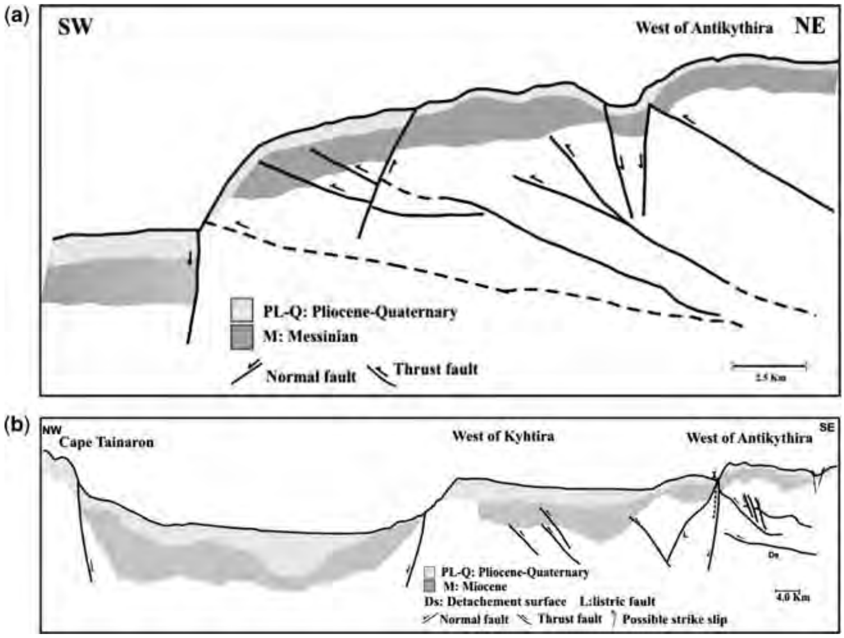

Fig. 9. Schematic sections, not to scale, illustrating the inner part of the Hellenic arc and related features (**a**) perpendicular and (**b**) parallel to the orientation of the Hellenic Arc.

Lyberis *et al.* (1982) suggested that normal faulting prevails in the KA area. According to this author, the first fault family strikes NW–SE to NNW–SSW, parallel to the axis of the submarine ridge and controls the general morphology of the KA strait. The other family strikes north–south to NNE–SSW, oblique to the axis. However, approximately east–west normal faults are also present, especially on Kythira and on western Crete, where they affect Pliocene sediments. These east–west normal faults have been either reactivated as oblique-slip faults compatible with the main ENE–WSW extension or cut by large NW–SE or north–south normal faults. There are also some small strike-slip faults consistent with a compression that trended approximately north–south. The present work can support the presence of east and west dipping normal faults.

Farther southward, in western Crete, NW-trending faults are scarce, whereas NNE-trending faults become more important and have controlled, since the Late Miocene, the evolution of off-shore (Mascle *et al.* 1982) and on-shore basins (Fig. 6). According to ten Veen & Meijer (1998), arc-normal pull is the dominant force that generates the Late Miocene extension in the Cretan segment of the overriding plate, although arc-normal pull in combination with intra-plate spreading forces cannot be excluded. Ten Veen & Kleinspehn (2003) also concluded that outward expansion of the forearc is blocked along western Crete whereas sinistral shear is observed in the expanding Cretan–Rhodes forearc. Additionally the majority of the earthquake events in the brittle upper crust in the western part of Crete, for which fault plane solutions were determined, show a horizontal east-west-trending T axis (Taymaz *et al.* 1990; De Chabalier *et al.* 1992).

Papazachos (1996) proposed a dextral strike-slip fault zone with a reverse component (Fig. 1a), striking in an almost east–west direction for the KA seismogenic zone. This strike-slip fault zone is considered responsible for the shallow (40.0–100.0 km) seismicity of KA strait. Dextral strike-slip movement is also traced on the seismic section Line 1A (Fig. 3), but it is located at shallower depth. This fault could represent the westward continuation of the Mid-Cycladic Lineament postulated by Walcott & White (1998) that accommodates the clockwise rotation in northwestern Greece with respect to the south. However, since it is still active (and the MCL is not), it may alternatively form the northernmost fault associated with the south Aegean strike-slip system, which has been active since the early Pliocene and includes the Pliny and Strabo Trenches (Mascle *et al.* 1999; ten Veen & Kleinspehn 2003; van Hinsbergen *et al.* 2007).

In addition, the post-Alpine and Alpine sedimentary successions reveal an approximate thickness of 15.0–16.0 km. Papazachos *et al.* (2000) used 961 shallow and intermediate earthquakes for the period 1965–1995 to define the geometry of the Hellenic Arc, by constructing three cross sections for the western, central and eastern part. A very intense shallow seismicity ($h < 20.0$ km) is defined in the western part of Cretan crust. Based on this report we traced the shallow seismogenic layer in our profiles located in the northwestern offshore Crete and we detected this layer at an approximate depth from 7.0–18.0 km.

The Gavrovo–Tripolitza zone constitutes a 3 km thick shallow-water carbonate sequence of Mesozoic age and is considered to represent the shelf sediments of the Apulian passive continental margin which passed gradually into the deepwater sedimentary sequence of Pindos to the east (Fleury 1980). According to the present study the thickness of the Gavrovo–Tripolitza zone (carbonate) ranges between 0.5 (intensively eroded) and 0.75 s TWT, namely greater than 2.1 km. A similar study (Sotiropoulos *et al.* 2003) in Etoloakarnania and NW Peloponnesus determined the thickness of Gavrovo–Tripolitza carbonate sequence at about 0.75–1.0 s TWT.

Alves *et al.* (2007) presented seismic reflection sections located in the southern Cretan margin, in order to study the Neogene stratigraphy of the area. Up to 1.2 s TWT of strata, accumulated since the Middle Miocene, in association with extension in the South Aegean region. The seismic segments presented in this work show a thickness of about 0.5–0.75 s TWT for the strata accumulated since the Messinian in the southern part of KA strait, which is in agreement with the study of Alves *et al.* (2007). The strata, accumulated since the Messinian in the northern part of KA strait, show a thickness up to 1.25 s TWT.

Conclusions

The studied seismic lines are located in an active region which represents the transition from extensional backarc to the forearc. The latter shows signs of frontal accretion. Deep compressional structures and shallower extensional structures are present. Later extension is related to structures, showing a predominantly NW–SE orientation. We summarize the interpretation as follows:

1. Strong evidence for SW-verging and NE-dipping thrusts has been found. These are well known from the western Peloponnesos and western Greece and relate to the emplacement of the Pindos zone on top of the Tripolitza zone. This occurred during the Oligocene. The westward increase in thickness of the Alpine sediments of the upper crust is possibly related to the westward migration of the thrust front of the External Hellenides. The thrust front affects the sedimentary sequences up to and including Messinian or Lower Pliocene successions.
2. Detachment surfaces are recognized in the seismic sections situated near to Peloponnesus and Crete but no evidence for such surfaces has been found for the rest of the KA strait.
3. NNE–SSW and *c*. E-W running faults which intersect each other and the sediments in the KA strait have been detected. These sediments likely have an age of Tortonian and younger. The interfering faults structures have been identified earlier on the Peloponnesus. These structures possibly affected the whole of the southeastern Aegean region and remain active today.
4. An *c*. E-W running strike-slip fault is possibly identified. This fault has been postulated before based on seismic evidence.
5. The top of the Gavrovo–Tripolitza sequence (carbonates) is represented by a very strong reflector at 1.5–3.2 s TWT, while the top of the crystalline basement gradually dips westwards with depths ranging from 3.0–4.0 s TWT.

This work was supported by the project ‘Pythagoras’ funded by the EPEAEK, Geophysics Department contribution 689. The authors express their gratitude to Hellenic Petroleum Co. (EL.PE) for making the data available. We wish to thank Dr. ten Veen and Dr. Alves for their constructive criticism, which improved a version of this manuscript. The GMT system (Wessel & Smith 1998) was used to plot part of the figures.

References

Alves, T. M., Lykousis, V., Sakellariou, D., Alexandri, S. & Nomikou, P. 2007. Constraining the origin and evolution of confined turbidite systems: southern Cretan margin, Eastern Mediterranean Sea (34°30–36°N). *Geo-Marine Letters*, **27**, 41–61.

Aubouin, J. 1959. Contribution a l’étude géologique de la Grèce septentrionale: le confins de l’Epire et de la Thessalie. *Annales Géologiques des pays Helléniques*, **10**, 1–484.

Bohnhoff, M., Makris, J., Papanikolaou, D. & Stavrakakis, G. 2001. Crustal investigation of the Hellenic subduction zone using wide aperture seismic data. *Tectonophysics*, **343**, 239–262.

Bornovas, I. & Rontogianni-Tsiabaou, T. 1983. *Geological map of Greece*. Institute of Geology and Mineral exploration, Athens.

Danamos, G. 1992. Contribution to the Geology and Hydrogeology of the island of Kythira. PhD thesis, Athens.

De Chabalier, J. B., Lyon-Caen, H., Zollo, A., Deschamps, A., Bernard, P. & Hatzfeld, D. 1992. A detailed analysis of microearthquakes in western Crete from digital three-component seismograms. *Geophysical Journal International*, **110**, 347–360.

Faccenna, C., Jolivet, L., Piromallo, C. & Morelli, A. 2003. Subduction and the depth of convection of the Mediterranean mantle. *Journal of Geophysical Research*, **108**, 2099.

Fassoulas, C. 2001. The tectonic development of a Neogene basin at the leading edge of the active European margin: the Heraklion basin, Crete, Greece. *Journal of Geodynamics*, **31**, 49–70.

Fassoulas, C., Kilias, A. & Mountrakis, D. 1994. Postnappe stacking extension and exhumation of HP/LT rocks in the island of Crete, Greece. *Tectonics*, **13**, 127–138.

Finetti, I. 1985. Structure and evolution of the central Mediterranean (Palagian and Ionian Seas). *In*: Stanley, D. J. & Wezel, F. C. (eds) *Geological evolution of the Mediterranean Basin*. Springer, New York, 215–230.

Fleury, J. 1980. Les zones de Gavrovo - Tripolitsa et du Pinde - Olonos (Grèce continentale et Pèloponnése du Nord). Évolution d'une plateforme et d'un bassin dans leur carde alpin. *Société Géologique du Nord*, Special Publication, **4**.

Frydas, D. 1990. Plankton-Stratigraphie des Pliozans und unteren Pleistozans des SW-Peloponnes, Griechenland. *Newsletters on Stratigraphy*, **23**, 91–108.

Gautier, P., Brun, J.-P., Moriceau, R., Sokoutis, D., Martinod, J. & Jolivet, L. 1999. Timing, kinematics and cause of Aegean extension: a scenario based on a comparison with simple analogue experiments. *Tectonophysics*, **315**, 31–72.

Govers, R. & Wortel, M. J. R. 2005. Lithosphere tearing at STEP faults: Response to edges of subduction zones. *Earth and Planetary Science Letters*, **236**, 505–523.

Hatzfeld, D. 1994. On the shape of the subducting slab beneath the Peloponnese, Greece. *Geophysical Research Letters*, **21**, 173–176.

IGRS-IFP 1966. *Étude Géologique de l'Épire (Grèce nord-occidentale)*. Institut Francais du Petrol, Paris.

Jacobshagen, V. 1986. *Geologie von Griechenland*. Borntraeger, Berlin-Stuttgart.

Jacobshagen, V. 1994. Orogenic evolution of the Hellenides: new aspects. *Geologische Rundschau*, **83**, 249–256.

Jolivet, L., Goffé, B., Monié, P., Truffert-Luxey, C., Patriat, M. & Bonneau, M. 1996. Miocene detachment on Crete and exhumation P-T-t paths of high-pressure metamorphic rocks. *Tectonics*, **15**, 1129–1153.

Jolivet, L. 2001. A comparison of geodetic and finite strain pattern in the Aegean, geodynamic implications. *Earth and Planetary Science Letters*, **187**, 95–104.

Jolivet, L. & Faccenna, C. 2000. Mediterranean extension and the Africa-Eurasia collision. *Tectonics*, **19**, 1094–1106.

Kamberis, E., Sotipopoulos, S., Aximniotou, O., Tsaila-Monopolis, S. & Ioakim, C. 2000. Late Cenozoic deformation of Gavrovo-Tripolitza zone in NW Peloponnesos (Western Greece). *Annals Geofisica*, **43**, 905–919.

Kamberis, E., Pavlopoulos, A., Tsaila-Monopolis, S., Sotiropoulos, S. & Ioakim, C. 2005. Paleogene deep-water sedimentation and Paleogeography of foreland basins in the NW Peloponnese (Greece). *Geologica Carpathica*, **56**, 503–515.

Kokinou, E., Vafidis, A., Loucogiannakis, M. & Louis, J. 2003. Deep seismic imaging and velocity estimation in Ionian Sea. *Journal of the Balkan Geophysical Society*, **6**, 100–116.

Kokinou, E., Kamperis, E., Vafidis, A., Monopolis, D., Ananiadis, G. & Zelilidis, A. 2005. Deep seismic reflection data from offshore western Greece: a new crustal model for the Ionian sea. *Journal of Petroleum Geology*, **28**, 185–202.

Kokkalas, S., Xypolias, P., Koukouvelas, I. & Doutsos, T. 2006. Postcollisional contractional and extensional deformation in the Aegean region. *Geological Society of America, Special Paper*, **409**, 97–123.

Le Pichon, X. & Angelier, J. 1979. The Hellenic Arc and trench system: a key to the neotectonic evolution of the Eastern Mediterranean area. *Tectonophysics*, **60**, 1–42.

Le Quellec, P., Mascle, J., Got, H. & Vitori, J. 1980. Seismic structure of south-western Peloponnesus continental margin. *Bulletin of the American Association of Petroleum Geology*, **64**, 242–263.

Lyberis, N. & Lallemant, S. 1985. La transition subduction-collision le long de l'arc égéen externe. *Comptes Rendus de l'Académie des Sciences, II*, **300**, 887–890.

Lyberis, N., Angelier, J., Barrier, E. & Lallement, S. 1982. Active deformation of a segment of arc, the strait of Kythira, Hellenic arc, Greece. *Journal of Structural Geology*, **4**, 299–311.

Makris, J. & Stobbe, C. 1984. Physical properties and state of the crust and upper mantle of the Eastern Mediterranean Sea deduced from geophysical data. *Marine Geology*, **55**, 347–363.

Makris, J. & Yegorova, T. 2006. A 3-D density-velocity model between the Cretan Sea and Libya. *Tectonophysics*, **417**, 201–220.

Mascle, J., Le Quellec, P., Leite, O. & Jongsma, D. 1982. Structural sketch of the Hellenic continental margin between the western Peloponnesus and eastern Crete. *Geology*, **10**, 113–116.

Mascle, J., Huguen, C., Benkhelil, J., Chomot-Rooke, N., Chaumillon, E., Foucher, J. P. *et al.* 1999. Images may show start of European-African plate collision. *Eos*, **80**, 421–428.

Meulenkamp, J. E., Theodoropoulos, P. & Tsapralis, V. 1977. Remarks on the Neogene of Kythira, Greece. *Proceedings of the VI Colloqium on the Geology of the Aegean region*, **1**, 355–362.

Papanikolaou, D. & Danamos, G. 1991. The role of the geotectonic location of Kythira and Cyclades in the geodynamic evolution of the Hellenic arc. *Bulletin of the Geological Society of Greece*, **XXV**, 65–79.

Papazachos, B. C. 1990. Seismicity of the Aegean and surrounding area. *Tectonophysics*, **178**, 287–308.

Papazachos, B. C. 1996. Large seismic faults in the Hellenic Arc. *Analli di Geofisica*, **39**, 891–903.

PAPAZACHOS, C. B. & KIRATZI, A. A. 1996. A detailed study of the active crustal deformation in the Aegean and surrounding area. *Tectonophysics*, **253**, 129–153.

PAPAZACHOS, B. C. & PAPAZACHOU, C. B. 2003. *Earthquakes of Greece*. Ziti, Thessaloniki [in Greek].

PAPACHAZOS, B. C., KARAKOSTAS, V. G., PAPAZACHOS, C. B. & SCORDILIS, E. M. 2000. The geometry of the Wadati-Bennioff zone and lithospheric kinematics in the Hellenic arc. *Tectonophysics*, **319**, 275–300.

PEETERS, F. J. C., HOEK, R. P., BRINKHUIS, H., WILPSHAAR, M., DE BOER, P. L., KRIJGSMAN, W. & MEULENKAMP, J. E. 1998. Differentiating glacio-eustacy and tectonics; a case study involving dinoflagellate cysts from the Eocene-Oligocene transition of the Pindos Foreland Basin (NW Greece). *Terra Nova*, **10**, 245–249.

RICHTER, D. 1976. Das Flysch-Stadium der Helleniden-Ein Überblick. *Zeitschrift der Deutschen Geologischen Gesellschaft*, **127**, 467–483.

ROYDEN, L. H. & BURCHFIEL, B. C. 1989. Are systematic variations in thrust belt style related to plate boundary process? (The Western Alps versus the Carpathians). *Tectonics*, **8**, 51–61.

SACHPAZI, M., HIRN, A., CLÉMENT, C., HASLINGER, F., LAIGLE, M., KISSLING, E. *ET AL*. 2000. Western Hellenic subduction and Cephalonia Transform: local earthquakes and plate transport and strain. *Tectonophysics*, **319**, 301–319.

SKOURLIS, K. & DOUTSOS, T. 2003. The Pindos Fold and Thrust Belt (Greece): Inversion kinematics of a passive continental margin. *International Journal of Earth Sciences*, **92**, 891–903.

SOTIROPOULOS, S., KAMBERIS, E., TRIANTAPHYLLOU, M. & DOUTSOS, T. 2003. Thrust sequences at the central part of the External Hellenides. *Geological Magazine*, **140**, 661–668.

TAYMAZ, T., JACKSON, J. A. & WESTAWAY, R. 1990. Earthquake mechanisms in the Hellenic Trench near Crete. *Geophysical Journal International*, **102**, 695–731.

TEN VEEN, J. H. & MEIJER, P. Th. 1998. Late Miocene to Recent tectonic evolution of Crete (Greece): geological observations and model analysis. *Tectonophysics*, **298**, 191–208.

TEN VEEN, J. H. & KLEINSPEHN, K. L. 2003. Incipient continental collision and plate-boundary curvature: Late Pliocene-Holocene transtensional Hellenic forearc, Crete, Greece. *Journal of the Geological Society, London*, **160**, 161–181.

THEODOROPOULOS, K. D. 1973. *Natural Geography of Kythira Island*. Lectureship Thesis, Athens.

UNDERHILL, J. R. 1989. Late Cenozoic deformation of the Hellenide foreland, western Greece. *Geological Society of America Bulletin*, **101**, 613–634.

THOMSON, S. N., STÖCKHERT, B. & BRIX, M. R. 1998. Thermochronology of the high-pressure metamorphic rocks of Crete, Greece: implications for the speed of tectonic processes. *Geology*, **26**, 259–262.

VAN HINSBERGEN, D. J. J. & MEULENKAMP, J. E. 2006. Neogene supradetachment basin development on Crete (Greece) during exhumation of the South Aegean core complex. *Basin Research*, **18**, 103–118.

VAN HINSBERGEN, D. J. J., HAFKENSCHEID, E., SPAKMAN, W., MEULENKAMP, J. E. & WORTEL, M. J. R. 2005. Nappe stacking resulting from subduction of oceanic and continental lithosphere below Greece. *Geology*, **33**, 325–328.

VAN HINSBERGEN, D. J. J., VAN DER MEER, D. G., ZACHARIASSE, W. J. & MEULENKAMP, J. E. 2006. Deformation of western Greece during Neogene clockwise rotation and collision with Apulia. *International Journal of Earth Sciences*, **95**, 463–490.

VAN HINSBERGEN, D. J. J., KRIJGSMAN, W., LANGEREIS, C. G., CORNÉE, J. J., DUERMEIJER, C. E. & VAN VUGT, N. 2007. Discrete Plio-Pleistocene phases of tilting and counterclockwise rotation in the southeastern Aegean arc (Rhodos, Greece): early Pliocene formation of the south Aegean left-lateral strike-slip system. *Journal of the Geological Society, London*, **164**, 1–12.

WALCOTT, C. R. & WHITE, S. H. 1998. Constraints on the kinematics of post-orogenic extension imposed by stretching lineations in the Aegean region. *Tectonophysics*, **298**, 155–175.

WESSEL, P. & SMITH, W. H. F. 1998. New, improved version of the Generic Mapping Tools. Released EOS Trans. *AGU*, **79**, 579.

WORTEL, M. J. R. & SPAKMAN, W. 2000. Subduction and slab detachment in the Mediterranean-Carpathian region. *Science*, **290**, 1910–1917.

XYPOLIAS, P. 2007. Cenozoic tectonics of the external Hellenides. *Geophysical Research Abstracts*, **9**, 1821.

XYPOLIAS, P. & DOUTSOS, T. 2000. Kinematics of rock flow in a crustal-scale shear zone: implication for the orogenic evolution of the southwestern Hellenides. *Geological Magazine*, **137**, 81–96.

Index

Note: Figures are shown in *italic* font, tables in **bold**.